

Millie Pant · Tarun Kumar Sharma ·
Rajeev Arya · B. C. Sahana ·
Hossein Zolfagharinia *Editors*

Soft Computing: Theories and Applications

Proceedings of SoCTA 2019

Advances in Intelligent Systems and Computing

Volume 1154

Series Editor

Janusz Kacprzyk, Systems Research Institute, Polish Academy of Sciences,
Warsaw, Poland

Advisory Editors

Nikhil R. Pal, Indian Statistical Institute, Kolkata, India

Rafael Bello Perez, Faculty of Mathematics, Physics and Computing,
Universidad Central de Las Villas, Santa Clara, Cuba

Emilio S. Corchado, University of Salamanca, Salamanca, Spain

Hani Hagras, School of Computer Science and Electronic Engineering,
University of Essex, Colchester, UK

László T. Kóczy, Department of Automation, Széchenyi István University,
Gyor, Hungary

Vladik Kreinovich, Department of Computer Science, University of Texas
at El Paso, El Paso, TX, USA

Chin-Teng Lin, Department of Electrical Engineering, National Chiao
Tung University, Hsinchu, Taiwan

Jie Lu, Faculty of Engineering and Information Technology,
University of Technology Sydney, Sydney, NSW, Australia

Patricia Melin, Graduate Program of Computer Science, Tijuana Institute
of Technology, Tijuana, Mexico

Nadia Nedjah, Department of Electronics Engineering, University of Rio de Janeiro,
Rio de Janeiro, Brazil

Ngoc Thanh Nguyen, Faculty of Computer Science and Management,
Wrocław University of Technology, Wrocław, Poland

Jun Wang, Department of Mechanical and Automation Engineering,
The Chinese University of Hong Kong, Shatin, Hong Kong

The series “Advances in Intelligent Systems and Computing” contains publications on theory, applications, and design methods of Intelligent Systems and Intelligent Computing. Virtually all disciplines such as engineering, natural sciences, computer and information science, ICT, economics, business, e-commerce, environment, healthcare, life science are covered. The list of topics spans all the areas of modern intelligent systems and computing such as: computational intelligence, soft computing including neural networks, fuzzy systems, evolutionary computing and the fusion of these paradigms, social intelligence, ambient intelligence, computational neuroscience, artificial life, virtual worlds and society, cognitive science and systems, Perception and Vision, DNA and immune based systems, self-organizing and adaptive systems, e-Learning and teaching, human-centered and human-centric computing, recommender systems, intelligent control, robotics and mechatronics including human-machine teaming, knowledge-based paradigms, learning paradigms, machine ethics, intelligent data analysis, knowledge management, intelligent agents, intelligent decision making and support, intelligent network security, trust management, interactive entertainment, Web intelligence and multimedia.

The publications within “Advances in Intelligent Systems and Computing” are primarily proceedings of important conferences, symposia and congresses. They cover significant recent developments in the field, both of a foundational and applicable character. An important characteristic feature of the series is the short publication time and world-wide distribution. This permits a rapid and broad dissemination of research results.

**** Indexing: The books of this series are submitted to ISI Proceedings, EI-Compendex, DBLP, SCOPUS, Google Scholar and Springerlink ****

More information about this series at <http://www.springer.com/series/11156>

Millie Pant · Tarun Kumar Sharma ·
Rajeev Arya · B. C. Sahana ·
Hossein Zolfagharinia
Editors

Soft Computing: Theories and Applications

Proceedings of SoCTA 2019



Springer

Editors

Millie Pant
Department of Paper Technology
IIT Roorkee
Roorkee, India

Rajeev Arya
NIT Patna
Patna, India

Hossein Zolfagharinia
Ryerson University
Toronto, ON, Canada

Tarun Kumar Sharma
Graphic Era Hill University
Dehradun, Uttarakhand, India

B. C. Sahana
NIT Patna
Patna, India

ISSN 2194-5357 ISSN 2194-5365 (electronic)
Advances in Intelligent Systems and Computing
ISBN 978-981-15-4031-8 ISBN 978-981-15-4032-5 (eBook)
<https://doi.org/10.1007/978-981-15-4032-5>

© Springer Nature Singapore Pte Ltd. 2020

This work is subject to copyright. All rights are reserved by the Publisher, whether the whole or part of the material is concerned, specifically the rights of translation, reprinting, reuse of illustrations, recitation, broadcasting, reproduction on microfilms or in any other physical way, and transmission or information storage and retrieval, electronic adaptation, computer software, or by similar or dissimilar methodology now known or hereafter developed.

The use of general descriptive names, registered names, trademarks, service marks, etc. in this publication does not imply, even in the absence of a specific statement, that such names are exempt from the relevant protective laws and regulations and therefore free for general use.

The publisher, the authors and the editors are safe to assume that the advice and information in this book are believed to be true and accurate at the date of publication. Neither the publisher nor the authors or the editors give a warranty, expressed or implied, with respect to the material contained herein or for any errors or omissions that may have been made. The publisher remains neutral with regard to jurisdictional claims in published maps and institutional affiliations.

This Springer imprint is published by the registered company Springer Nature Singapore Pte Ltd.
The registered company address is: 152 Beach Road, #21-01/04 Gateway East, Singapore 189721,
Singapore

Preface

This book focusses on the strides made in the domain of soft computing and its applications to address the key issues plaguing the domains of image and signal processing, supply chain management, computational Biology and Bioinformatics, human resource management, finance and economics. It includes the immaculate works presented during the 4th International Conference on Soft Computing: Theories and Applications (SoCTA 2019), organized by the Department of Electronics and Communication Engineering, National Institute of Patna, Bihar, India from 27th–29th December, 2019. This book stands true to its motive of encouraging young minds and fresh ideas in the field of soft computing.

Roorkee, India
Dehradun, India
Patna, India
Patna, India
Toronto, Canada

Millie Pant
Tarun Kumar Sharma
Rajeev Arya
B. C. Sahana
Hossein Zolfagharinia

Contents

Performance Optimization by MANET AODV-DTN Communication	1
Deepak Choudhary and Roop Pahuja	
Effectiveness of Whale Optimization Based I+PD Controller for LFC of Plug-in Electric Vehicle Included Multi-area System	11
Utkarsh Raj and Ravi Shankar	
Dual Band Printed Rectangular Ring-Shaped Monopole Antenna for Wireless Communication	21
Chandrakant Jatav and Sudhanshu Verma	
Printed U-Shaped Monopole Dual Band Antenna for Wireless Application	29
Vikash Chandra Sharma and Sudhanshu Verma	
IoT-Enabled Early Prediction System for Epileptic Seizure in Human Being	37
Sayali Shinde and Brijesh Iyer	
Effective Author Ranking Using Average of Different h-Index Variants	47
Prabhat Kumar Chandra, Vivekanand Jha, and Kumar Abhishek	
A Survey Report on Recent Progresses in Nearest Neighbor Realization of Quantum Circuits	57
Anirban Bhattacharjee, Chandan Bandyopadhyay, Bappaditya Mondal, and Hafizur Rahaman	
Annual Rainfall Prediction Using Time Series Forecasting	69
Asmita Mahajan, Akanksha Rastogi, and Nonita Sharma	
A Novel Approach for Design 7:3 and 5:3 Compressors	81
Ajay Kumar Kushwaha and Vikas Kumar	

High-Accurate, Area-Efficient Approximate Multiplier for Error-Tolerant Applications	91
M. Parvathi	
Hoax and Faux of Information Credibility in Social Networks: Explored, Exemplified and Experimented	103
Ram Chatterjee, Hardeo Kumar Thakur, Ridhi Sethi, and Abhishek Pandey	
Minimize Power Ratio (PR) in OFDM Using Tone Reservation Method	115
Yogendra Kumar Upadhyaya and Ajay Kumar Kushwaha	
A Single-Phase Multi-level Inverter Using a Lesser Number of Switching Devices	125
Ashutosh Kumar Singh, Ravi Raushan, and Pratyush Gauri	
Symmetric Key Generation and Distribution Using Diffie-Hellman Algorithm	135
Kaustubh Purohit, Avanish Kumar, Mayank Upadhyay, and Krishan Kumar	
Design of Controllers Using PSO Technique for Second-Order Stable Process with Time Delay	143
Satyendra Kumar and Moina Ajmeri	
A Green Dynamic Internet of Things (IoT)-Battery Powered Things Aspect-Survey	153
Nitin B. Raut and N. M. Dhanya	
An Efficient Layout of Single-Layer Full Adder Using QCA	165
Nilesh Patidar and Namit Gupta	
A Review of mm-Wave Power Amplifiers for Next-Generation 5G Communication	173
Pradeep Gorre, R. Vignesh, Rajeev Arya, and Sandeep Kumar	
Vision-Based Automated Traffic Signaling	185
H. Mallika, Y. S. Vishruth, T. Venkat Sai Krishna, and Sujay Biradar	
Performance Comparison of SVM and ANN for Reversible ECG Data Hiding	197
Siddharth Bhalerao, Irshad Ahmad Ansari, and Anil Kumar	
Application of Multi-criteria Decision-Making Method for the Evaluation of Tamilnadu Private Bus Companies	209
S. M. Vadivel, A. H. Sequeira, Sunil Kumar Jauhar, R. Baskaran, and S. Robert Rajkumar	

CNC Machine Shop Floor Facility Layout Design Using Genetic Algorithm	223
S. M. Vadivel, A. H. Sequeira, Sunil Kumar Jauhar, K. S. Amirthagadeswari, and T. Aravind Krishna	
Source of Treatment Selection for Different States of India and Performance Analysis Using Machine Learning Algorithms for Classification	235
Nitima Malsa, Pooja Singh, Jyoti Gautam, Arpita Srivastava, and Santar Pal Singh	
Ant Lion Optimization Technique for Minimization of Voltage Deviation Through Optimal Placement of Static VAR Compensator	247
Stita Pragnya Dash, K. R. Subhashini, and J. K. Satapathy	
On Vector Variational Inequalities and Vector Optimization Problems	257
B. B. Upadhyay and Priyanka Mishra	
Characterizations of the Solution Sets for Constrained Pseudolinear Semi-infinite Programming Problems	269
B. B. Upadhyay and Akriti Srivastava	
Novel Chaotic Elephant Herding Optimization for Multilevel Thresholding of Color Image	281
Falguni Chakraborty, Provas Kumar Roy, and Debasish Nandi	
Forecasting Groundwater Fluctuation from GRACE Data Using GRNN	295
Dilip Kumar and Rajib Kumar Bhattacharjya	
Android Application for Recognition of Indian Origin Agricultural Products	309
Snehal P. Tarale and Veena Desai	
A Fuzzy Logic Based Approach for Prediction of Squamous Cell Carcinoma	325
Saurabh Jha, Ashok Kumar Mehta, and Chandrashekhar Azad	
Investigating Multilevel Hesitated Patterns Using Vague Set Theory	335
Abhishek Dixit, Akhilesh Tiwari, and Rajendra Kumar Gupta	
Six Switch Three Phase Five-Level Inverter with Sinusoidal Pulse Width Modulation	347
Rajesh Kumar Mahto and Ambarisha Mishra	
AI-Enabled Real-Time Sign Language Translator	357
Yash Patil, Sahil Krishnadas, Adya Kastwar, and Sujata Kulkarni	

A Comparative Performance of Sorting Algorithms: Statistical Investigation	367
Priyadarshini and Anchala Kumari	
Evolutionary Computing for Designing Cryptographic Primitives for Block Cipher: Challenges and Opportunities	381
Pratap Kumar Behera and Sugata Gangopadhyay	
A True Event-Based Metaheuristic Algorithm Optimized AGC Mechanism for a Multi-area Power System	391
Sariki Murali and Ravi Shankar	
Wireless Emanation of Braille to Text/Voice and Vice Versa	403
Aishwarya Korde, Omkar Gaikar, Sonam Nikam, and Smita Rukhande	
An Exploratory Analysis Pertaining to Stress Detection in Adolescents	413
Mrinal Pandey, Bharti Jha, and Rahul Thakur	
Load Frequency Control of an Interconnected Multi-source Power System Using Quasi-oppositional Harmony Search Algorithm	423
Abhishek Saxena and Ravi Shankar	
An Extensive Investigation of Wavelet-based Denoising Techniques for Various ECG Signals Utilizing Thresholding Function	433
V. Supraja, P. Nageswara Rao, and M. N. Giriprasad	
Effect of Noise on Segmentation Evaluation Parameters	443
V. Vijaya Kishore and V. Kalpana	
A Review Paper on Feature Selection Techniques and Artificial Neural Networks Architectures Used in Thermography for Early Stage Detection of Breast Cancer	455
Kumod Kumar Gupta, Ritu Vijay, and Pallavi Pahadiya	
An Artificial Neural Network Model for Estimating the Flood in Tehri Region of Uttarakhand Using Rainfall Data	467
B. G. Rajeev Gandhi, Dilip Kumar, and Hira Lal Yadav	
Advanced Virtual Apparel Try Using Augmented Reality (AVATAR)	479
Sourav Shaw, Swapnali Kadam, Shreya Joshi, and Dhanashree Hadsul	
A Novel Fault-Detection Scheme for Nearest-Neighbor-Based Reversible Circuits	489
Anirban Bhattacharjee, Chandan Bandyopadhyay, Bappaditya Mondal, and Hafizur Rahaman	
Automated Railway Gate Control Using Internet of Things	501
B. Arunjyothi and B. Harikrishna	

Contents	xii
Simulated Annealing Based Algorithm for Tuning LDA Hyper Parameters	515
Nikhlesh Pathik and Pragya Shukla	
A Better Group Consensus Ranking via a Min-transitive Fuzzy Linear Ordering	523
Sukhamay Kundu	
A Novel Metaheuristic Approach for Resource Constrained Project Scheduling Problem	535
Bidisha Roy and Asim Kumar Sen	
A Novel Approach to Handle Huge Data for Refreshment Anomalies in Near Real-Time ETL Applications	545
N. Mohammed Muddasir and K. Raghuvir	
Comparison of Photodetection Capability of Spin Coated TiO₂ Thin Film and In₂O₃ Thin Film Devices	555
Rahul Raman, Amitabha Nath, and Mitra Barun Sarkar	
Development of IDS Using Supervised Machine Learning	565
Indrajeet Kumar, Noor Mohd, Chandradeep Bhatt, and Shashi Kumar Sharma	
Automated Traffic Light Signal Violation Detection System Using Convolutional Neural Network	579
Bhavya Bordia, N. Nishanth, Shaswat Patel, M. Anand Kumar, and Bhawana Rudra	
An Enhanced Butterfly Optimization Algorithm for Function Optimization	593
Sushmita Sharma, Apu Kumar Saha, and Sukanta Nama	
Dynamic Analysis of Wind Turbine Drivetrain Under Constant Torque	605
Rishi Kumar and Sankar Kumar Roy	
To Build Scalable and Portable Blockchain Application Using Docker	619
Priyanka Kumar and Maharshi Shah	
Text Summarization: An Extractive Approach	629
Vishal Soni, Lokesh Kumar, Aman Kumar Singh, and Mukesh Kumar	
Clifford+T-based Fault-Tolerant Quantum Implementation of Code Converter Circuit	639
Laxmidhar Biswal, Chandan Bandyopadhyay, and Hafizur Rahaman	

Applying Deep Learning for Discovery and Analysis of Software Vulnerabilities: A Brief Survey	649
Shashank Kumar Singh and Amrita Chaturvedi	
Fuzzy Decision Making System for Better Staff Performance Appraisal in Institutional Organization	659
Soni Sweta and Ajit Kumar Pandey	
A Graph-Theoretic Approach for Sustainable New Product Development (SNPD) in Supply Chain Environment	671
Amit Kumar Sinha and Ankush Anand	
Generalization Performance Comparison of Machine Learners for the Detection of Computer Worms Using Behavioral Features	677
Nelson Ochieng, Waweru Mwangi, and Ismail Ateya	
Fully Annotated Indian Traffic Signs Database for Recognition	695
Banhi Sanyal, R. K. Mohapatra, and Ratnakar Dash	
Streamlining Choice of CNNs and Structure Framing of Convolution Layer	705
Sonika Dahiya, Rohit Tyagi, and Nishchal Gaba	
SNAP N' COOK—IoT-Based Recipe Suggestion and Health Care Application	719
Diksha Mukherjee, Albin Paulson, Shajo Varghese, and Mukta Nivelkar	
Accuracy-Based Performance Analysis of Alzheimer's Disease Classification Using Deep Convolution Neural Network	731
Ketki C. Pathak and Swathi S. Kundaram	
Multiple Information Fusion and Encryption Using DWT and Yang-Gu Mixture Amplitude-Phase Retrieval Algorithm in Fractional Fourier Domain	745
Muhammad Rafiq Abuturab	
Development of Intrusion Detection System Using Deep Learning for Classifying Attacks in Power Systems	755
Ankitdeshpandey and R. Karthi	
An Improved Adaptive Transfer Function for Explosion Spark Generation in Fireworks Algorithm	767
Tapas Si and Amit Mukhopadhyay	
NSE Stock Prediction: The Deep Learning Way	783
Ankit K. Barai, Pooja Jain, and Tapan Kumar	
Recent Development of AI and IoT in the field of Agriculture Industries: A Review	793
Amith A. Kulkarni, P. Dhanush, B. S. Chethan, C. S. Thammegowda, and Prashant Kumar Shrivastava	

Contents	xiii
Optimized Fuzzy Rule-Based System to Measure Uncertainty in Human Decision Making System	799
Soni Sweta and Kanhaiya Lal	
A Review on Detection of Breast Cancer Cells by Using Various Techniques	813
Vanaja Kandubothula, Rajyalakshmi Uppada, and Durgesh Nandan	
Analysis of Security Issues and Possible Solutions in the Internet of Things for Home Automation System	825
P. Sai Ramya and Durgesh Nandan	
Utilization of the Internet of Things in Agriculture: Possibilities and Challenges	837
P. Mani Sai Jyothi and Durgesh Nandan	
Study on Real-Time Face Recognition and Tracking for Criminal Revealing	849
A. Krishna Chaitanya, C. H. Kartheek, and Durgesh Nandan	
Analysis of Precision Agriculture Technique by Using Machine Learning and IoT	859
Y. Sasi Supritha Devi, T. Kesava Durga Prasad, Krishna Saladi, and Durgesh Nandan	
Dispersive Nature of the FEL Amplifiers in the Whistler Mode	869
Ram Gopal, M. Sunder Rajan, Priti Sharma, and Abhinav K. Gautam	
An Improved Energy-Efficient Faulty Information Extraction Scheme Using PFDIAES and PFDIF Algorithms	883
P. T. Kalaivaani and Raja Krishnamoorthy	
Cyber Attacks and Security—A Critical Survey	895
Nithin Kashyap, Hari Raksha K. Malali, and H. L. Gururaj	
A Comparative Study on Different Techniques of Sentimental Analysis	905
K. S. Peeyusha, G. Pooja, S. Shreyas, and S. P. Pavankumar	
An Approach to Select the Proper Combination within Positional and Non-positional Average Values of Features in Protein Classification	913
Suprativ Saha and Tanmay Bhattacharya	
Areca Nut Disease Detection Using Image Processing	925
A. B. Rajendra, N. Rajkumar, and P. D. Shetty	
Simulink Simulation for Predicting Thermodynamic Properties of Water–Lithium Bromide Solution Using ANN	933
Dheerendra Vikram Singh and Tikendra Nath Verma	

A New Bit Plane Specific Longest Repeating Pattern Test for Statistical Analysis of Bit Sequences	943
Bharat Lal Jangid and Ram Ratan	
Intelligent Interference Minimization Algorithm for Optimal Placement of Sensors using BBO	955
Chandra Naik and D. Pushparaj Shetty	
Classification of SOA-Based Cloud Services Using Data Mining Technique	971
Zeenat Parween and R. B. S. Yadav	
A Novel Clustering-Based Gene Expression Pattern Analysis for Human Diabetes Patients Using Intuitionistic Fuzzy Set and Multigranulation Rough Set Model	979
Swarup Kr Ghosh and Anupam Ghosh	
Investigation on HRV Signal Dynamics for Meditative Intervention	993
Dipen Deka and Bhabesh Deka	
A Review on Deep Learning-Based Channel Estimation Scheme	1007
Amish Ranjan, Abhinav Kumar Singh, and B. C. Sahana	
Patient Diabetes Forecasting Based on Machine Learning Approach	1017
Arvind Kumar Shukla	
Pose Invariant Face Recognition Using Principal Component Analysis	1029
Akash Krishna Srivastava, H. Sneha, Diksha, and Koushlendra Kumar Singh	
An Autonomic Resource Allocation Framework for Service-Based Cloud Applications: A Proactive Approach	1045
Tushar Bhardwaj, Himanshu Upadhyay, and Subhash Chander Sharma	
Index Point Detection and Semantic Indexing of Videos—A Comparative Review	1059
Mehul Mahrishi and Sudha Morwal	
Classification of Neuromuscular Disorders Using Machine Learning Techniques	1071
Anuj Singh, Arun Vikram, M. P. Singh, and Sudhakar Tripathi	
Comparative Study of the Ultrasonic and Infrared Person Counter	1081
Ankit Saxena, Swapnesh Taterh, and Nishant Saxena	

Fuzzy Logic Based Improved Control Design Strategy for MPPT of Solar PV Systems	1093
Rahul Bisht, Newton Kumar, and Afzal Sikander	
Evaluation of Soil Physical, Chemical Parameter and Enzyme Activities as Indicator of Soil Fertility with SFM Model in IA-AW Zone of Rajasthan	1107
Jyoti Sihag, Divya Prakash, and Parul Yadav	
Author Index.	1123

About the Editors

Dr. Millie Pant is an Associate Professor, Department of Applied Science and Engineering, IIT Roorkee, India. She has supervised 16 Ph.D.s in the area of numerical optimization, operations research, soft computing and swarm intelligence techniques with applications to various engineering design problems, image processing, computer vision, supply chain management. She has 181 research publications to her credit. She is PI and Co-PI in 2 DST and MHRD sponsored projects. She has edited 7 volumes of Conference Proceedings AISC series of Springer of SoCProfs Conference series since 2017 and 2 volumes of Conference Proceedings AISC series of Springer of SoCTA Conference series. She is an Associate Editor in International Journal of Swarm Intelligence, Inderscience, and Guest Editor in several international journals like International Journal of Memetic Computing, Springer, International Journal of Collaborative Engineering, Inderscience. She is a reviewer in IEEE Transactions on Evolutionary Computation, Applied Soft Computing, Applied Mathematics and Computation, Neural Network Works, Information science. She has acted as General Chair, Program Chair, Session and Track Chair in many national and international conferences. She has delivered Guest Lectures in the field of swarm intelligence, nature inspired computing, computational intelligence in institution of national and international repute like National University of Singapore, Singapore, Liverpool Hope University, Liverpool, UK, Brisbane, Australia, Zakopane, Poland, Graphic Era University, Dehradun, Meerut Institute of Engineering and Technology, ABV-IIITM Gwalior, MANIT, Bhopal, National Institute of Hydrology, Roorkee, NIT, Assam. She has international collaboration with MIRS Lab, USA, Liverpool Hope University, UK, and Université Paris-Est Créteil Val-de-Marne, Paris, France. She is a founder member of SoCProfs, SoCTA, and RAACE Conference series.

Dr. Tarun Kumar Sharma is Professor at Graphic Era Hill University, Dehradun. He worked at Amity School of Engineering and Technology, Amity University Rajasthan, India. He holds Ph.D. in Soft Computing from India Institute of Technology, Roorkee. He has supervised 2 Ph.D.s. He has 77 research publications to his credit. He is one of the founding member of SoCTA series. He acted as

General Chair of RAACE 2017, Program Chair in SoCTA 2016, Organizing Secretary in SoCPROS 2015, and PC member in SoCPROS 2014 and SoCPROS 2013. He has edited 3 volumes of Conference Proceedings published by AISC series of Springer Publication and 2 edited books in Asset Analytics, Springer. He is Guest Editor in several international journals like IJACI, IJAIP, IJSIR, IJAMC, IJAEC, IJISDC, and IJPD. He is a member in the editorial board of national and international journals. He has acted as session and track chair in many national and international conferences. He has delivered Guest Lectures in the field of swarm intelligence, nature inspired computing, and computational intelligence in the institution of national and international repute. He is a founder member of SoCTA and RAACE Conference series. He is a member of IET, IANEG, CSTA, and MIRS Lab.

Dr. Rajeev Arya received the Engineering Degree in Electronics & Communication Engineering from Government Engineering College, Ujjain, (RGPV University, Bhopal) India, and the Master of Technology in Electronics & Communication Engineering from Indian Institute of Technology (ISM), Dhanbad, India. He received the Ph.D. degree in Communication Engineering from Indian Institute of Technology, Roorkee, India. He is currently an Assistant Professor with the Department of Electronics & Communication Engineering at National Institute of Technology, Patna, India. His current research interests are in wireless communication, ant colony optimization & soft computing techniques, cognitive radio, signal processing, communication systems & circuits design. He has published many articles in international journals and conferences. He is a member of the ISRD and the IAENG. He is an active reviewer in many reputed international journals.

Dr. B. C. Sahana is an Assistant Professor, Department of Electronics and Communication Engineering, NIT Patna, India. He has supervised 10 M.Tech. and 32 B.Tech. students in the area of signal processing, optimization, soft computing and swarm intelligence techniques with applications to various engineering design problems, image processing and compression, computer vision, geophysical signal processing, filter design. He has 21 research publications in journals and conferences. He is a reviewer in IEEE access. He has delivered Guest Lectures in the field of geophysical signal processing, nature inspired computing, computational intelligence in the institution of national and international repute.

Dr. Hossein Zolfagharinia is an award-winning Assistant Professor of Operations Management in the Global Management Studies department at the Ted Rogers School of Management, Ryerson University. He received his Undergraduate and Master's Degrees in Industrial Engineering. Following this, he earned his Ph.D. in Operations and Supply Chain Management from the Lazaridis School of Business and Economics at Wilfrid Laurier University. In addition to his academic background, he has more than four years of professional work experience as a business method analyst in the oil and drilling industry. Furthermore, he gained experience in the area of Supply Chain Management through managing several projects in trucking and maritime transportation companies in the past (e.g., Logikor Inc.,

Global Spatial Technology Solutions (GSTS) Inc.). Dr. Zolfagharinia's two main research interests are in: (1) investigating the benefits of collaboration in supply chain management with a focus on logistics and transportation, (2) applying operations management techniques in a healthcare context. He is the author of a book chapter and several top-tier refereed journal articles. These journals include: European Journal of Operational Research, Transportation Research: Part B and Part E, International Journal of Production Economics, and Operations Research for Health Care. He frequently presents his work at scholarly/professional conferences at both the national and international levels (e.g., Institute for Operations Research and Management Sciences (INFORMS), Annual meeting of Canadian Operational Research Society (CORS), and Decision Sciences Institute (DSI)). He is the recipient of the 2017-2018 Dean's Scholarly, Research, and Creative Activity Award. He has received over \$250,000 in the form of research grants, scholarships, and fellowships. These include Natural Sciences and Engineering Research Council of Canada (NSERC), Social Sciences and Humanities Research Council-Institutional Grant (SSHRC-SIG), Ontario Centers of Excellence (OCE), Ontario Graduate Scholarship (OGS), the Best OGS Research Proposal, and the Ontario Institute of the Purchasing Management Association of Canada (OIPMAC) Achievement Excellence, and he is the provisional winner of Supply Chain & Logistics Association of Canada Paper Competition.

Performance Optimization by MANET AODV-DTN Communication



Deepak Choudhary and Roop Pahuja

Abstract Mobile Ad Hoc Network (MANET) has the ability to self-configure and establish a mobile wireless mesh that can be used in extreme conditions, such as in areas affected by disasters. One of the routings in MANET is AODV routing. AODV is one of the reactive routing needed to send data. However, in the implementation of disaster conditions, AODV has weaknesses that are vulnerable to extreme environmental conditions. In this study, communication will be modeled that leads to disruption due to disaster. MANET AODV-DTN is used to improve network performance. With this system, the Probability Delivery Ratio (PDR) parameter value can be increased as evidenced by the variable modification of the number of nodes to be 0.431%, reducing the average delay by 63.525%, and producing the energy consumption increased by 0.170%. Simulation with the variable modification of speed obtained by PDR 0.482%, reducing the average delay by 78.710% and energy consumption increased by 0.167%. Modification of buffer size variables obtained 0.729% PDR results, reducing the average delay of 71.603% and energy consumption increased by 0.161%. From these data, MANET AODV-DTN is better than MANET AODV.

Keywords MANET · AODV · DTN · PDR · Average delay

1 Introduction

Condition in the disaster area will affect the rescue process, therefore communication networks are needed that can survive in these conditions. The design and use of communication network systems for disaster areas must have good Quality of Service values to ensure that data transmission can reach the destination quickly under limited energy. This causes the system performance to be optimal in these conditions.

D. Choudhary (✉) · R. Pahuja

Instrumentation and Control Department, Dr. B.R Ambedkar National Institute of Engineering–Jalandhar, Jalandhar, Punjab, India
e-mail: engg_deepak@yahoo.com

Based on [1, 2], the requirement to design a communication network for use in an emergency is higher redundancy when data sent from source to destination. This high redundancy causes data to be rearranged if the message is damage before reaching the destination, data access is sent quickly, has the capacity to work in emergency conditions and normal conditions. Therefore, in this study, MANET network communication will be designed using AODV-DTN and comparing with MANET AODV.

This paper aims to find out and compare the performance of MANET AODV and MANET AODV-DTN so it can be used in disaster conditions. In this study, three parameters will be tested are Probability Delivery Ratio (PDR), average delay, and energy consumption through three variable modifications, which are speed, number of nodes, and buffer size.

2 Background and Related Network

2.1 Mobile Ad Hoc Networks (MANETs)

Mobile Ad hoc Networks (MANETs) is a network that allows the exchange of information without using infrastructure networks. MANET has a complex distributed system and consists of wireless mobile nodes that can be connected freely and dynamic to the network topology. MANET has a traditional network that can reduce infrastructure costs and easy to implement.

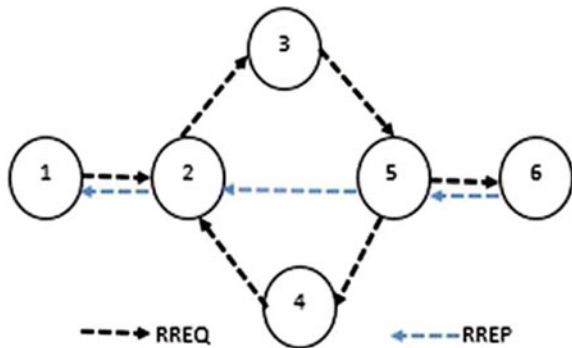
MANET has several networks for different scenarios, a limited structure on MANET means that each node must be a router and responsible for carrying routing packet tasks. Because it uses one or more routing protocols in MANET, it requires a large amount of message storage media and energy where mobile devices in MANET have limited memory as a message storage medium [3, 4].

2.2 Ad Hoc on Demand Distance Vector (AODV) [5]

AODV is a reactive routing protocol that starts working when requests from the source node and find the path will be used to send messages to the destination node. To find the best route, AODV will find Route (Fig. 1) distributing Route Request (RREQ) to all nodes adjacent to source node. At the same time, the broadcast ID and sequence number are sent to avoid sending the same message to a node.

The neighbor node will send RREQ to the next neighbor node until it ends at the destination node. After RREQ reaches the destination node, the node will reply to the RREQ message with Route Reply (RREP). Selected the path is the shortest route with the lowest cost compared to other routes.

Fig. 1 Example of a figure caption [6]



To avoid changing network topology, AODV will send HELLO messages continuously. If during the sending process there is a change in the topology from the source node to the destination node, the node will send the Error Route (RRER) to its neighboring node to the source node. Each node will get the RRER message and the source node will route again to find the route to the destination.

2.3 Delay Tolerant Networks (DTN)

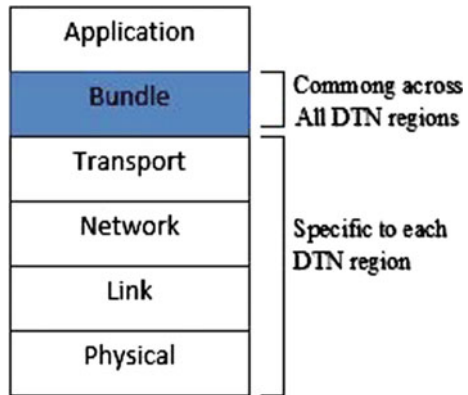
Delay Tolerant Networks (DTN) are not always available end-to-end networks that cause message delays. Even though the network has delays in the network, the DTN can still function then it can work in extreme areas. DTN works using store and forward methods, it means the data packets passing through intermediate nodes will be stored first before being forwarded. This will be anticipated if the next node cannot be reached or die or in other limitations [6].

In DTN, system store and forward processes are performed on an additional layer called a bundle layer. The layer bundle is an additional layer to modify the data package with the facilities provided by DTN, the bundle layer is located below the application layer. In the bundle layer, the data from the application layer will be broken into bundles, the bundle function is to store temporary data (Fig. 2).

3 Simulation Design

Scenarios communication design for disaster area, have no connecting with the internet. All devices designed in this study are mobile nodes with the traffic of all nodes sending and receiving messages. The design is used to compare MANET using AODV and MANET AODV-DTN. The comparison is done by testing two systems based on the simulation results using Network Simulator 2 which takes into account

Fig. 2 Bundle layer in DTN
[7]



Quality of Service in the form of PDR, average delay and energy consumption with changing several variables, namely the number of nodes, speed and buffer size.

In this study, the parameters of the simulation were fixed and used with the same values in different simulations. These parameters can be seen in Table 1.

In Table 2 There are three simulation scenarios that will be used in this study. Scenario 1 modification of variable speed changes is done to test changes in the speed at each node that is used to determine the duration of contacts that occur at each node. Scenario 2 is modified to change the number of node variables to test the effect on the probability of sending to the mobility of each node. Scenario 3 is

Table 1 Design simulation parameters

Parameter	Value
Packet size	512 byte
Dimension	750 m × 750 m
Total number of nodes	50
Speed (m/s)	2
Radio trans range (m)	180
Simulation time (s)	150
Antenna model	Omnidirectional
Propagation model	Free space
Pause time (s)	0
Initial energy	1000
Sleep energy	0.05
Transmit power	1
Receive power	1
Transition power	0.2
Transition time	0.001

Table 2 Design simulation parameters

Parameter	Scenario 1	Scenario 2	Scenario 3
Num of node	50	20, 30, 40, 50, 60, 70, 80	20, 30, 40, 50, 60, 70
Speed (m/s)	2, 4, 6, 8, 10	2	2
Buffer size	50	50	50

modified to change the buffer size to test the effect of the number of queues dropped in the buffer.

4 Result and Analysis

The results of the research based on the design have been done in Sect. 3, this section will discuss the results of the simulation and performance analysis of the two systems MANET AODV and MANET AODV-DTN.

4.1 1st Scenario

In the 1st Scenario, the simulation is designed based on changes in the speed variables of the MANET AODV route and the MANET AODV-DTN system routing. The variable speed is changed by the number of node variables and buffer size which are the same values as the initial specifications.

From Fig. 3, it illustrates the probability of success of the two systems designed. MANET AODV-DTN has an average probability of 0.98 while MANET AODV has an average probability of 0.97. MANET AODV-DTN can increase the success of 0.48% delivery compared to MANET AODV. The routing strategy in MANET AODV-DTN sends more data packets than the MANET AODV package delivery strategy. The MANET AODV-DTN system makes copies of each packet when the

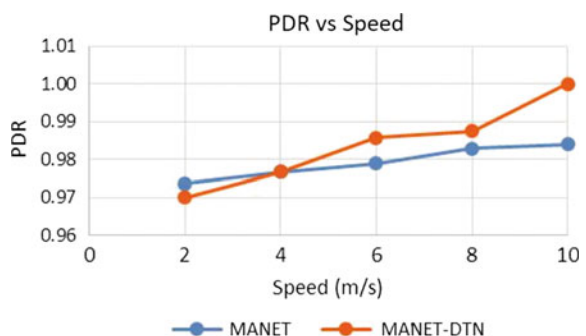
Fig. 3 Graph of simulation results changes in speed variables to PDR

Fig. 4 Simulation results graph variable speed changes to average delay

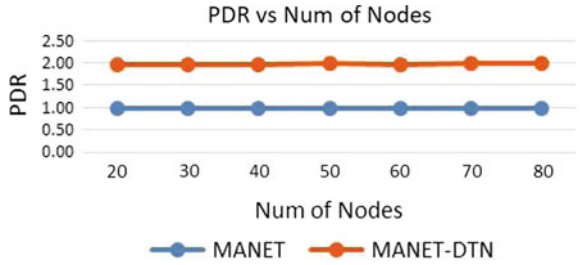
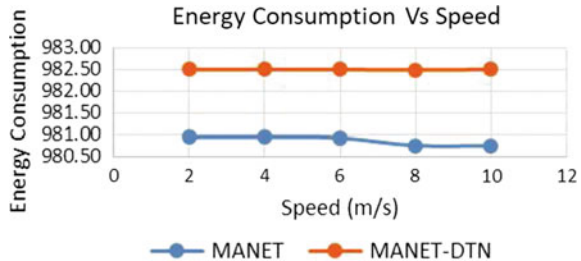


Fig. 5 Simulation results graph variable speed changes to consumption energy



node speed increases, the packet is not easily lost or damaged so it can reach the destination. If the probability of successful package delivery is greater than reduces delay. In MANET AODV-DTN each transmission node will cause increased energy consumption to network while sending, receiving and storing messages (Figs. 4 and 5).

4.2 2nd Scenario

In the 2nd Scenario, the simulation is designed based on changes in speed variables from the MANET routing AODV and MANET AODV-DTN routing systems. Variable node speed is changed with variable speed and buffer size are equal in value to the initial specifications.

The probability of successful delivery (Fig. 6) of MANET AODV-DTN is 0.98 and MANET AODV has an average probability of 0.98 as well. Because of increased traffic on the network to the number of nodes that meet each other, messages will be exchanged between nodes. However, the average delay (Fig. 7) time of MANET AODV is 23.2 ms bigger than MANET AODV-DTN is 8.48 ms. MANET AODV-DTN has a storage capacity of 100,000, while MANET AODV does not. Then the message can make contact between nodes more often until there is no queue and the delay time can be reduced. While the energy consumption used is smaller MANET AODV on average at 980.90 J compared to MANET AODV-DTN at 982.49 J because it requires more energy to send data to the message (Fig. 8).

Fig. 6 Graph of simulation results changes in Num of nodes variables to PDR

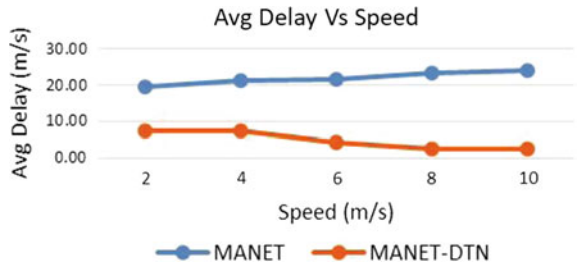


Fig. 7 Graph of simulation results changes in Num of nodes variables to Avg delay

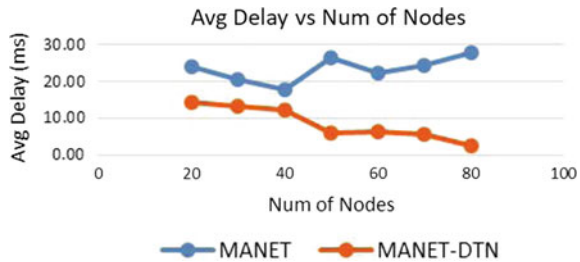
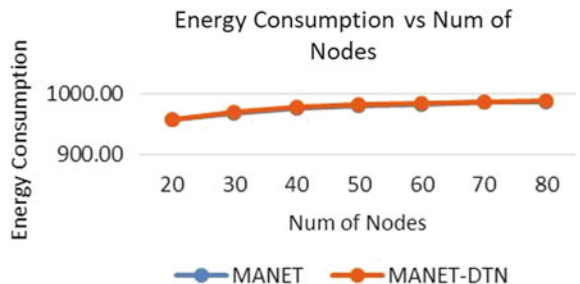


Fig. 8 Graph of simulation results changes in Num of nodes variables to energy consumption



4.3 3rd Scenario

In the 3rd scenario, the simulation is designed based on changes in the buffer size variables of the MANET AODV and MANET AODV-DTN. The variable buffer size is changed by the variable speed and the number of nodes that are the same as the initial specifications.

In the 3rd scenario, simulation MANET AODV has a successful packet delivery probability of an average of 0.96 and MANET AODV-DTN averaging 0.97. To increase holding time, a large buffer capacity is needed, MANET AODV-DTN has sufficient buffer capacity compared to MANET AODV so that the average delay time is better MANET AODV-DTN 7.62 ms while MANET AODV has an average of 25.23 ms. Energy consumption produced, MANET AODV-DTN increased by 0.161% from MANET AODV (Figs. 9, 10, and 11).

Fig. 9 Graph of simulation results changes in buffer size variables to PDR

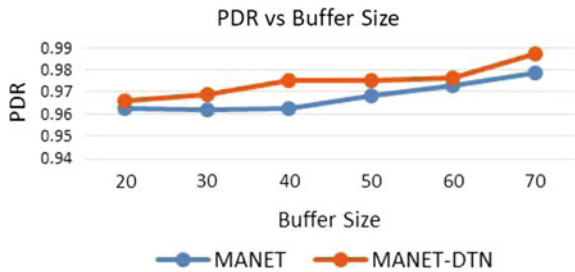


Fig. 10 Graph of simulation results changes in buffer size variables to Avg delay

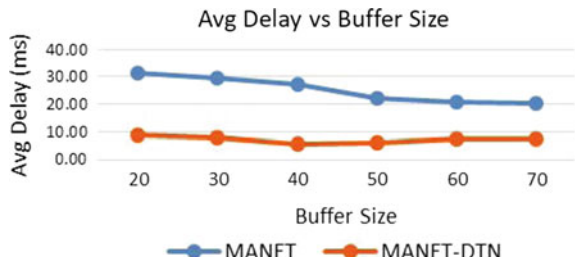
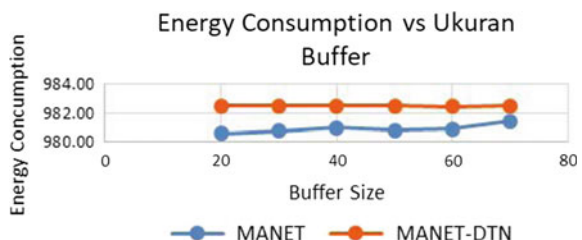


Fig. 11 Graph of simulation results changes in buffer size variables to Avg delay



5 Conclusion

The following can be concluded from the simulation results:

1. The higher number of nodes, the higher the PDR value for MANET AODV and MANET AODV-DTN. In the same condition, MANET AODV-DTN can increase PDR 0.43% compared to MANET AODV. The more messages received by the destination node, the smaller average delay MANET AODV-DTN. MANET AODV-DTN can reduce the average delay of 63.5% compared to MANET AODV. However, the energy consumption of MANET AODV-DTN increased by 0.17% from MANET AODV.
2. The higher the node speed, the higher the PDR value for MANET AODV-DTN and MANET AODV. In the same conditions, MANET AODV-DTN can increase the PDR of 0.48% compared to MANET AODV. The more messages received by the destination node, the smaller average delay value, MANET AODV-DTN

reduces the average delay of 78.71% compared to MANET AODV. However, the energy consumption of MANET AODV-DTN increased by 0.16% compared to MANET AODV.

3. The larger the buffer size, the higher the PDR value for MANET AODV-DTN and MANET AODV. In the same conditions, MANET AODV-DTN can increase the PDR of 0.72% compared to MANET AODV. The more messages the node receives, the smaller average delay value, MANET AODV-DTN can reduce the average delay by 71.6% compared to MANET AODV. However, the energy consumption of MANETAODV-DTN Increased by 0.16% from MANET AODV.
4. From three scenarios designed, MANET AODV-DTN is more suitable for communication for disaster areas because it has a good PDR value and reduces the average delay value even though energy consumption is very limited.

References

1. Premkumar, R.: Wireless networks for disaster relief (2014)
2. Kishorbhai, V., Vasanthbhai, N.: AON: a survey on emergency communication systems during a catastrophic disaster (2014)
3. <https://www.divaportal.org/smash/get/diva2:833565/FULLTEXT01.pdf>
4. Awerbuch, D., Mishra, D.: Ad hoc On Demand Distance Vector (AODV) routing protocol. Cs.jhu.edu (2017) [Online]. <http://www.cs.jhu.edu/~cs647/aodv.pdf>. Accessed 11 Nov 2017 Waktu 7:08
5. Performance analysis Aodv (Ad Hoc On Demand Distance Vector) and Dsr (Dynamic Source Routing) protocol to active attack I Manet (Mobile Ad Hoc Network) in term of network Qos (Quality Of Service). Eproc, 1(1). ISSN: 2355-9365.2014
6. Silaban, R.M., Cahyani, N.D., Suryan, V.: Analisis Perbandingan Performansi Ad Hoc On-Demand Distance Vector (Aodv) Dan Zone Routing Protocol (Zrp) Pada Ad-Hoc Hybrid Jaringan Wireless. Teknik Informatika, Fakultas Teknik Informatika, Universitas Telkom
7. Kharisma, B.: Pengenalan internet berbasis Delay Tolerant Network (DTN) [Blog] (2014)

Effectiveness of Whale Optimization Based I+PD Controller for LFC of Plug-in Electric Vehicle Included Multi-area System



Utkarsh Raj and Ravi Shankar

Abstract This study deals with the load frequency control of multi-area, multi-source system. A re-heat thermal generating unit, a gas unit and a plug-in electric vehicle unit is considered in each area. Some physical constraints like Governor dead band and generation rate constraint non-linearity are examined for the thermal unit. Whale optimization algorithm optimized I+PD controller is employed for the load frequency control of the proposed system. Load disturbance of 1% is considered for studying the system dynamics. To show the superiority of the proposed scheme, its performance is compared with the performance of the system under PIDN controller. Also, the system is tested against variable load to check the robustness of the system.

Keywords AGC · EV · I+PD · LFC · PIDN · WOA

1 Introduction

Modern power systems are subdivided into various areas for control purpose which are themselves interconnected by tie lines. These control areas share power with each other according to the demand on the power system. Due to this, there is fluctuation in the frequency from the nominal value. Also, since the power transfer between the areas is done through the tie lines, hence there is an oscillation in the tie-line power value from the scheduled nominal value. The major purpose of load frequency control (LFC) is: (i) To maintain the area frequency fluctuations within the scheduled nominal values, (ii) To keep tie-line power flow between the areas within the scheduled nominal values [1].

For the better implementation of LFC, extensive research work has been done. Various conventional controllers like Integral (I), proportional-integral (PI), and

U. Raj (✉)
Motihari College of Engineering, Motihari, India
e-mail: utkarshraj18@gmail.com

R. Shankar
National Institute of Technology, Patna, India
e-mail: ravi@nitp.ac.in

proportional-integral-derivative (PID) are employed for LFC [2, 3]. Though various intelligent control techniques like fuzzy logic control, state feedback control, artificial neural network, etc. Upalanchiwar and Sakhare [4], Pal et al. [5] have proposed in recent times, but conventional controllers still remain popular due to their practical utilities. To minimize the drawbacks of conventional controller I+PD is been used for the LFC of the system.

To achieve the best performance from a conventional controller, its settings need to be properly optimized [6]. Various optimization techniques have been proposed in the literature. Genetic algorithm (GA) is being used for controller optimization by Shankar et al. [7]. Other optimization techniques used in the literature are FOA [8], DE [9], PSO [10], O-SFLA [11] and QOHS [12]. Whale optimization algorithm (WOA) is a novel modern optimization technique from the family of population-based evolutionary algorithms. It simulates the bubble-hunting strategy of humpback whales.

Rest of the article has been subdivided into the following sections: Sect. 2 investigates the proposed system and Sect. 3 briefly discusses the WOA. Section 4 shows the simulation results while Sect. 4 culminates the present research work.

2 System Modeling

2.1 Proposed System

The linearized model of the two-area, multi-source system is considered in this study. A thermal generating unit and gas generating unit has been considered in each control area. Physical constraints like G.D.B. and G.R.C. non-linearity are considered for the thermal generating units. The value of GDB is taken as 0.05% and that of GRC as 3% per minute. A linearized model of plug-in electric vehicle (PEV) has also been considered in each area. The power demand between the grid and the load is balanced using PEV, consisting of a battery charger. In this study, the discharging/charging capacity of PEV is considered as ± 5 kW. The transfer function system model of the PEV is taken from Saha and Saikia [13]. The proposed system transfer function model is presented in Fig. 1.

2.2 Proposed Controller

In spite of various drawbacks like slower response speed and poor noise rejection capability, conventional controllers still remain popular due to their practical amenities. The proposed control scheme consists of a sum of integral controller and proportional-derivative controller (I+PD). Based on practical experience, various constraints have been applied to the controller parameters.

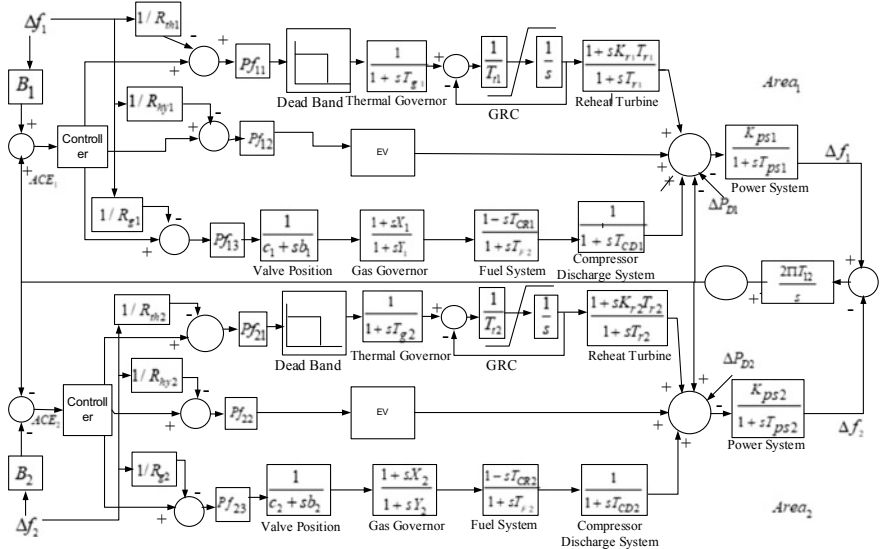


Fig. 1 Transfer function model of proposed power system

$$0 \leq Kp_i, Ki_i, Kd_i \leq 1 \quad (1)$$

where $i = 1, 2$. The block diagram model for the previously discussed proposed controller is shown in Fig. 2.

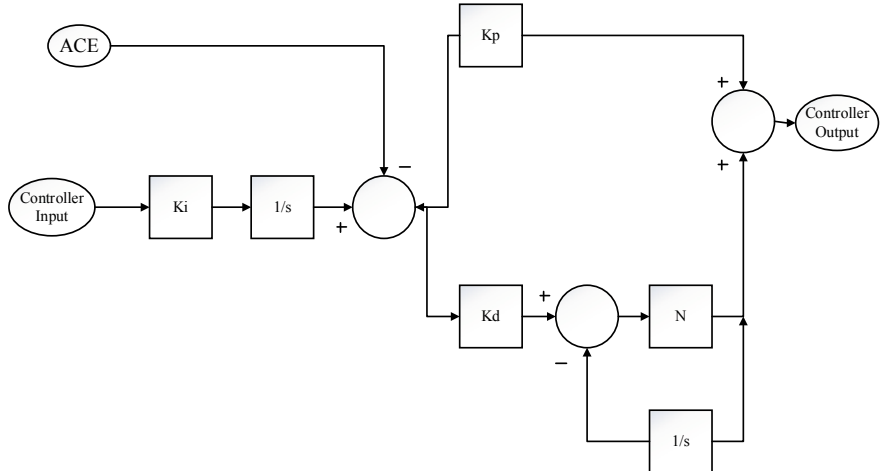
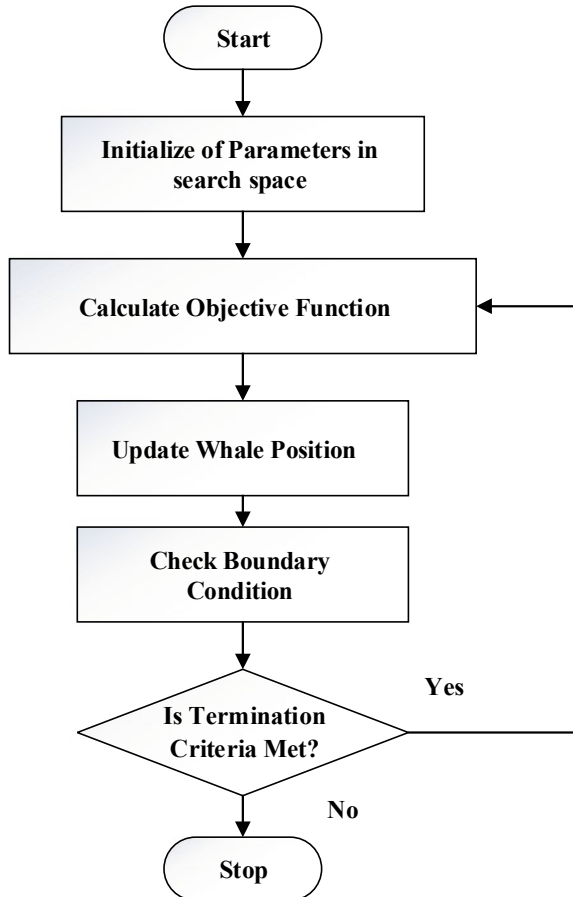


Fig. 2 Block diagram model of the proposed controller

3 Whale Optimization Algorithm

WOA, a new member of population-based evolutionary algorithm technique, has been presented by Mirjalili et al. [14]. In WOA, the unique foraging behavior of humpback whales called ‘bubble-net feeding’ is being reproduced. Humpback whales use this strategy to hunt for their preys like krills or a school of fish [15]. This strategy is formulated in the form of WOA optimization technique whose flowchart is shown in Fig. 3.

Fig. 3 Flowchart of WOA optimisation technique



4 Simulation Results

4.1 Comparison with PIDN Controller

The system proposed in this article has been simulated in the MATLAB® environment. A 1% constant load disturbance is applied to the system initially. The proposed controller parameters are optimized using the WOA technique. To show the advantage of the proposed control technique, the system dynamics with the proposed control scheme is compared with that of PIDN controller. The PIDN controller parameters are also optimized using the WOA technique. The comparison of system dynamics for both the control schemes is shown from Figs. 4, 5 and 6 and tabulated in Table 1. Tables 2 and 3 give the optimized parameter values of proposed controller and PIDN controller, respectively.

Fig. 4 Frequency fluctuation profile in first area

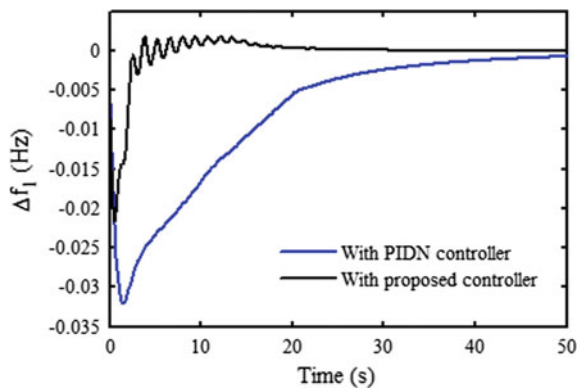


Fig. 5 Frequency fluctuation profile in second area

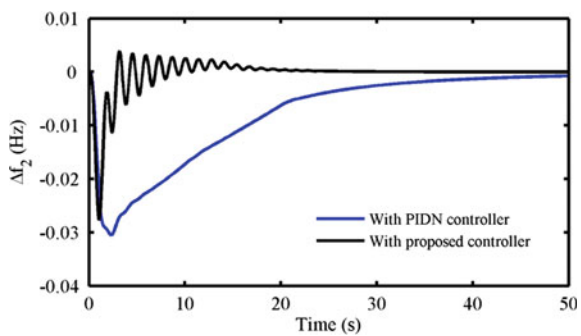


Fig. 6 Fluctuation profile for tie-line power flow

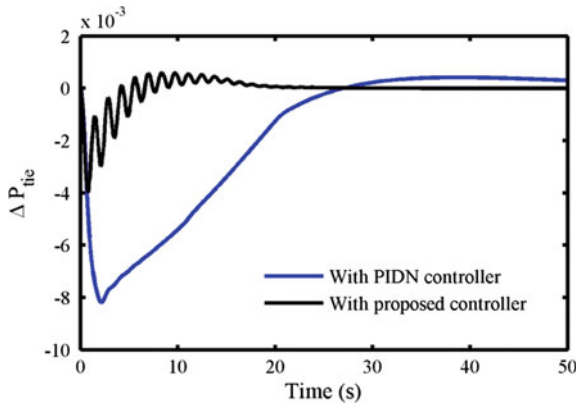


Table 1 Comparison of performance between presented controller and PIDN

	Proposed controller	PIDN controller
$\Delta f_{1\max}$	-0.02172	-0.03215
$\Delta f_{2\max}$	-0.02769	-0.03054
$\Delta P_{\text{tie},\max}$	-0.00397	-0.00819

Table 2 Optimized parameters of proposed controller

Parameter	Optimized value
Kp_1, Kp_2	0.2706, 0.3162
Ki_1, Ki_2	0.2771, 0.3362
Kd_1, Kd_2	0.4378, 0.6671
N_1, N_2	18.9447, 10.8676

Table 3 Optimized parameters of PIDN controller

Parameter	Optimized Value
Kp_1, Kp_2	0.0814, 0.7165
Ki_1, Ki_2	0.9414, 0.1790
Kd_1, Kd_2	0.8205, 0.9651
N_1, N_2	22.8673, 45.9474

4.2 Effectiveness of Proposed Control Scheme Under Variable Load Disturbance

Effectiveness of control schemes are generally tested for constant step load perturbation in the literature. But in practical situations, load disturbances are rarely constant. Hence the proposed control scheme has also been tested under variable load disturbance condition. The graph of load disturbance versus time is shown in

Fig. 7 Graph of load disturbance versus time

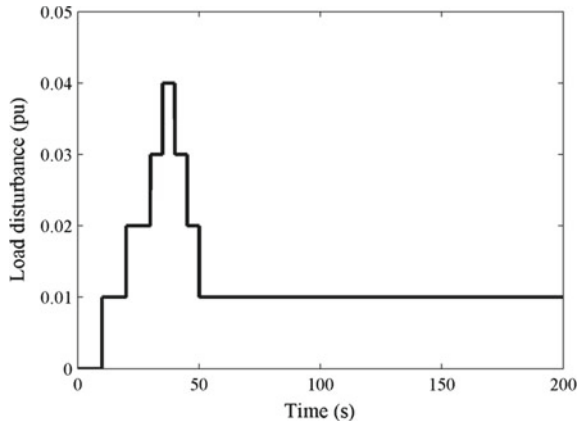


Fig. 8 Frequency fluctuation profile in first area

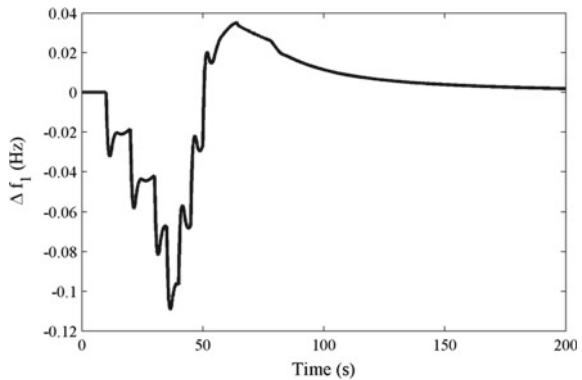


Fig. 7. The WOA-optimized proposed controller is considered for the secondary LFC of the proposed system. The dynamics of the presented system under the variable load condition are shown from Figs. 8, 9 and 10. The WOA-optimized controller parameter values are given in Table 4.

5 Conclusion

In the current research work, a binary-area multi-source system has been considered for LFC study. WOA-optimized I+PD controller has been used for frequency stabilization study. The supremacy of proposed controller has been shown by contrasting it with WOA-based PIDN controller for the same proposed system. Further, the efficacy of the presented control scheme has been shown under variable load conditions.

Fig. 9 Frequency fluctuation profile in second area

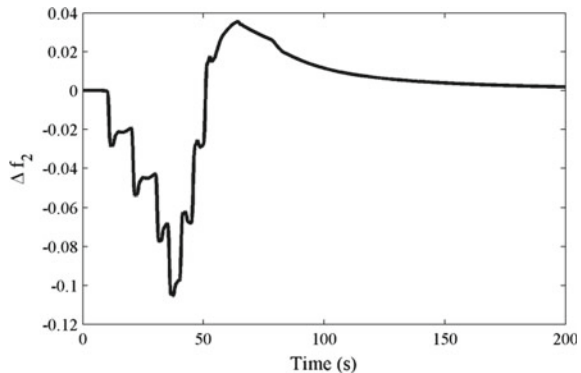


Fig. 10 Fluctuation profile for tie-line power flow

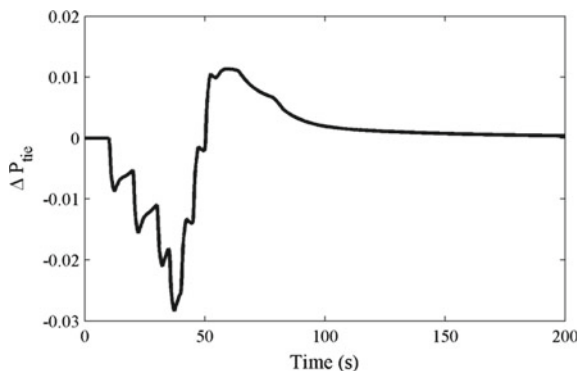


Table 4 Optimized parameters of proposed controller

Parameter	Optimized value
K_{p1}, K_{p2}	0.2847, 0.5972
K_{i1}, K_{i2}	0.2343, 0.5598
K_{d1}, K_{d2}	0.2459, 0.5312
N_1, N_2	27.2613, 23.2915

Appendix

Thermal generating unit: $K_r = 0.3$, $T_t = 0.3$ s, $R_{th} = 2.4$ Hz/pu, $T_r = 10$ s, $T_g = 0.08$ s, GRC = 0.0017pu/MW/s;

Gas generating unit: $X = 0.6$ s, $Y = 1.0$ s, $T_F = 0.23$ s, $b = 0.05$ s, $c = 1$, $T_{CR} = 0.01$ s, $T_{CD} = 0.2$ s, $R_G = 2.4$ Hz/pu MW, $R_{th} = 2.4$ Hz/pu;

Power system: $K_{ps} = 120$ Hz/pu, $T_{ps} = 20$ s;

EV: $K_{EV} = 1$ and $T_{EV} = 1$.

References

1. Shiva, C.K., Mukherjee, V.: A novel quasi-oppositional harmony search algorithm for AGC optimization of three-area multi-unit power system after deregulation. *Eng. Sci. Technol. Int. J.* **19**(1), 395–420 (2016)
2. Parmar, K.P.S., Majhi, S., Kothari, D.P.: Load frequency control of a realistic power system with multi-source power generation. *Int. J. Electr. Power Energy Syst.* **42**(1), 426–433 (2012)
3. Shankar, R., Pradhan, S.R., Chatterjee, K., Mandal, R.: A comprehensive state of the art literature survey on LFC mechanism for power system. *Renew. Sustain. Energy Rev.* **76**(2015), 1185–1207 (2017)
4. Upalanchiwar, T., Sakhare, P.A.V.: Design and implementation of the fuzzy PID controller using MATLAB/SIMULINK model. *3*(3), 369–372 (2014)
5. Pal, A.K., Bera, P., Chakraborty, K.: AGC in Two-area deregulated power system using reinforced learning neural network controller (2014)
6. Bhasin, H., Gupta, N.: Critical path problem for scheduling using genetic algorithm. *Soft Comput.: Theor. Appl. Adv. Intell. Syst. Comput.* 15–24 (2018)
7. Shankar, R., Chatterjee, K., Bhushan, R.: Impact of energy storage system on load frequency control for diverse sources of interconnected power system in deregulated power environment. *Int. J. Electr. Power Energy Syst.* **79**, 11–26 (2016)
8. Shankar, R., Kumar, A., Raj, U., Chatterjee, K.: Fruit fly algorithm-based automatic generation control of multiarea interconnected power system with FACTS and AC/DC links in deregulated power environment. *Int. Trans. Electr. Energy Syst.* e2690 (2018)
9. Mohanty, B., Panda, S., Hota, P.K.: Differential evolution algorithm based automatic generation control for interconnected power systems with non-linearity. *Alexandria Eng. J.* **53**(3), 537–552 (2014)
10. Mohanty, B., Hota, P.K.: A hybrid chemical reaction-particle swarm optimisation technique for automatic generation control. *J. Electr. Syst. Inf. Technol.* 1–16 (2017)
11. Sharma, T.K., Pant, M.: Opposition-based learning embedded shuffled frog-leaping algorithm. *Soft Comput.: Theor. Appl. Adv. Intell. Syst. Comput.* 853–861 (2018)
12. Mukherjee, V., Shiva, C.K.: Automatic generation control of multi-unit multi-area deregulated power system using a novel quasi-oppositional harmony search algorithm. *IET Gener. Transm. Distrib.* **9**(15), 2398–2408 (2015)
13. Saha, A., Saikia, L.C.: Performance analysis of combination of ultra-capacitor and superconducting magnetic energy storage in a thermal-gas AGC system with utilization of whale optimization algorithm optimized cascade controller. *J. Renew. Sustain. Energy.* **10**(1) (2018)
14. Mirjalili, S., Lewis, A.: Advances in engineering software the whale optimization algorithm. *95*, 51–67 (2016)
15. Guha, D., Kumar, P., Subrata, R.: Whale optimization algorithm applied to load frequency control of a mixed power system considering nonlinearities and PLL dynamics. *Energy Syst.* (0123456789) (2019)

Dual Band Printed Rectangular Ring-Shaped Monopole Antenna for Wireless Communication



Chandrakant Jatav and Sudhanshu Verma

Abstract In the present work, printed rectangular ring-shaped antenna with inverted L-shaped strip for dual band wireless communication. Structure of antenna is simple and the size is $34 \times 18 \text{ mm}^2$. This modified inverted L-shape will give the required bandwidth with good return loss. The simulated results show the dual band from (2.5–3.2 GHz) and (5.09–5.83 GHz) with the center operating frequency at around 2.9 and 5.48 GHz having reflection coefficient less than -10 dB for wireless applications.

Keywords Trident shaped antenna · Rectangular ring · Slot antenna

1 Introduction

In the present year, improvement of communication system with wireless services calls for much more frequency band which boosts wideband antenna design. Moreover, the antenna should only have to provide wideband but also it is necessary to have small dimensions. The monopole antenna has the characteristics of low, lightweight, low profile, and easy fabrication. Many structures of dual band or multiband antenna [1–8] proposed to the application of WIMAX and WLAN. Number of structures such as H-shaped, E-shaped, G-shaped, S-shaped, cover only WLAN band [1–3]. Antenna in [4–8] is designed and it satisfies the WLAN and WIMAX application, these designs have drawbacks and these antennas have a relatively larger size. In this letter, a newly rectangular ring-shaped patch antenna introduced for WLAN application. And the proposed antenna size is smallest compared to mentioned above. With introducing rectangular shaped and adding trident shaped inverted L-shaped and defected ground obtained dual band for WLAN applications. The simulated results of the proposed model are discussed in the present work.

C. Jatav (✉) · S. Verma

Department of Electronics and Communication Engineering, Madan Mohan Malaviya University of Technology, Gorakhpur, India

e-mail: chandrakantjatav@gmail.com

S. Verma

e-mail: svermaeecd@gmail.com

2 Antenna Design

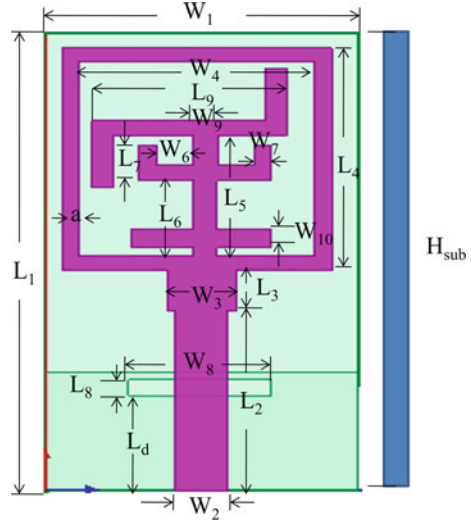
The plan development system for making the proposed antenna is represented in Fig. 2. This simulated on the 1.6 mm thickness of FR4 substrate has permittivity 4.4 and loss tangent is 0.02. The compact radiator is connected with $50\ \Omega$ microstrip which composed of a modified rectangular ring and signal stripe has width 3 mm. This proposed model consists of defected ground and dielectric substrate of FR4 length $L_1 = 34$ mm, width $W_1 = 18$ mm. The antenna is designed on the simulation tool ANSYS HFSS 16.2.

All dimensions introduce in Table 1. On the basis of dimensions antenna design fabricated and measured. The design of the proposed antenna step by step is shown in Fig. 1. Simple antenna structures antenna1, antenna2 and antenna3 are not given the good result shown in comparing graph. By introducing an inverted L-shape on the above trident shape gives better results at 5.48 resonating frequency Optimized

Table 1 Design parameters of proposed antenna

Parameters	Optimized value (mm)
L_1	34
L_2	13.4
L_3	3
L_4	17
L_5	9
L_6	4.4
L_7	2
L_8	1.2
L_9	11.2
L_s	8.7
L_d	6.3
W_1	18
W_2	3
W_3	4
W_4	15.5
W_5	1.4
W_6	1.8
W_7	1
W_8	8.2
W_9	1.15
H	1.6
a	1

Fig. 1 Structure of design antenna



proposed antenna produce dual band (2.57–3.21 GHz) and (5.09–5.83 GHz) applicable for WIMAX and WLAN applications. Optimized dimensions for our proposed model shown below in Table 1 and Fig. 2.

3 Result Discussion

Due to the given dimensions shown in Table 1, a rule for our proposed model antenna was designed and tested. The antenna with the variation in its design is shown in Fig. 1 and the comparison in the outcomes of these designs in terms of refection coefficient are presented in Fig. 3. Simulated results show the required bandwidth with good |S₁₁| of the proposed antenna. Notching at the trident shape and fit two inverted L-shape on the trident shape with the proper selection of the dimensions resonant peak of the proposed antenna4 achieved at 5.48 GHz lower cutoff frequency (f_L) is 5.07 GHz and upper cutoff frequency (f_H) is 5.80 GHz, so calculated bandwidth by a formula with the center operating frequency (f_C). The counterfeit and measured return losses against frequency seen in Figs. 4 and 5.

The surface current density of the proposed model is shown in Fig. 6a, b at 2.9 GHz frequency and 5.80 GHz frequency. The current density is high on the middle radiating element so it observed that the middle radiating element is the most active part of the proposed antenna4. The current density is shown in Fig. 3

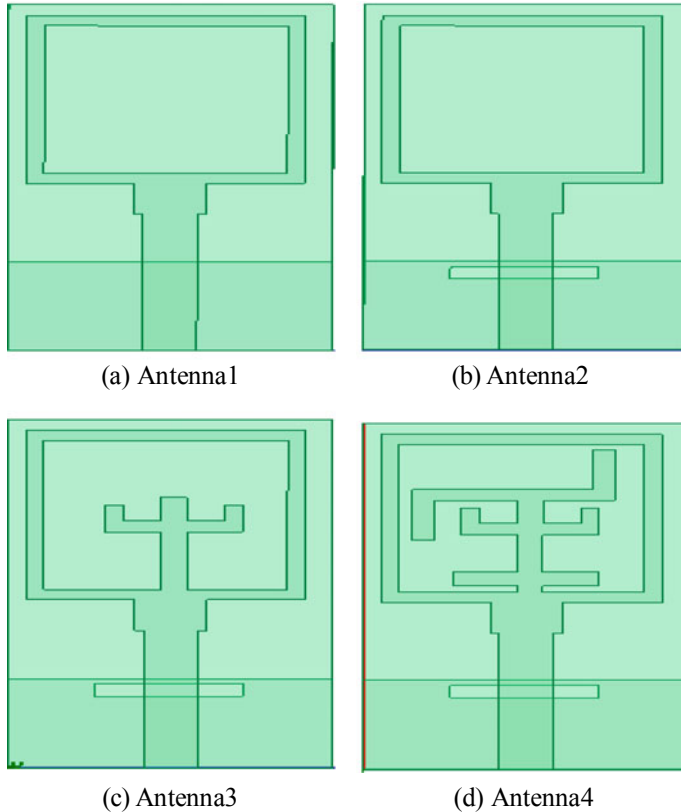


Fig. 2 The proposed antenna design with different shape

at the lower and higher band on the rectangular ring and strip under it that means rectangular ring and strip is very important role generation of two resonant modes lower and higher band.

In dual band operation mechanism, the trident with L-inverted shape monopole antenna is a counterfeit surface at resonant frequency of 2.9 and 5.48 GHz, shown in Fig. 6. Figure 5 shows the gain of dual band modified inverted L-shape antenna is about 4.8 dB.

Proposed antenna4 provided omnidirectional characteristics in Fig. 7, which is shown that simulated radiation patterns at resonant frequencies 2.9 and 5.48 GHz.

4 Conclusion

A dual band rectangular ring-shaped monopole antenna with an inverted L-shape and truncate rectangular slot on the ground plane, have been design successfully to

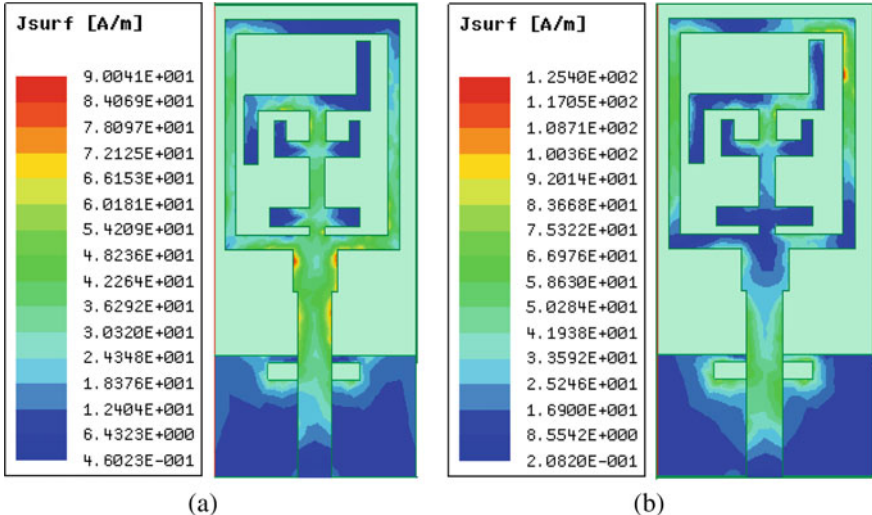


Fig. 3 **a** Current density of proposed antenna at 2.9 GHz. **b** Current density of proposed antenna at 5.4 GHz

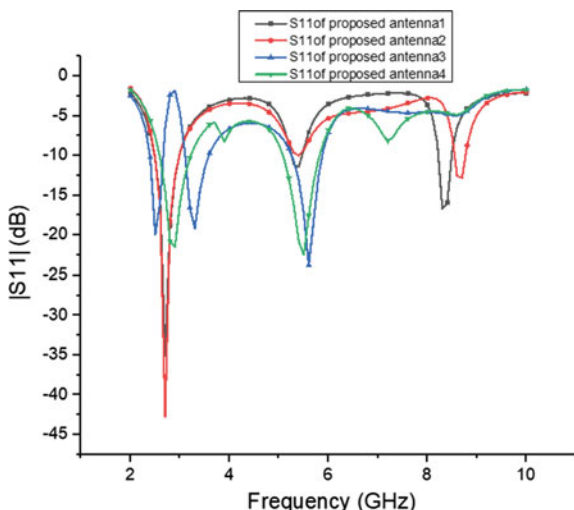


Fig. 4 Comparison results $|S_{11}|$ of different antennas

obtained WLAN and WIMAX applications. Simulated results show that enhancement of bandwidth and gains with introducing inverted L-shapes with trident shape on the patch. The percentage bandwidth of dual band is achieved 24.56 and 13.55% with peak gain 4.8 dB. With the suitable radiation pattern and good gain of the simulated dual band antenna are used for WLAN and WIMAX application.

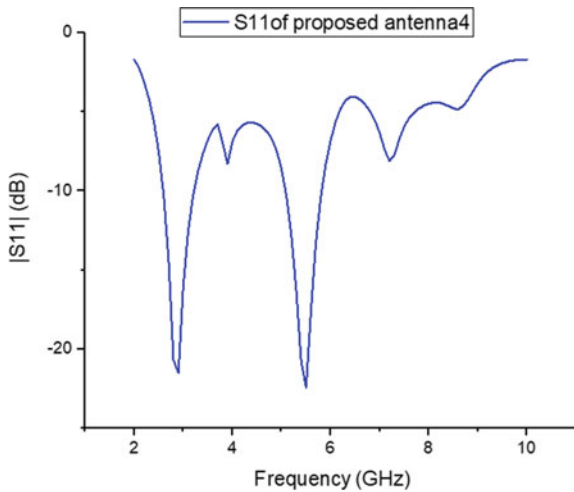
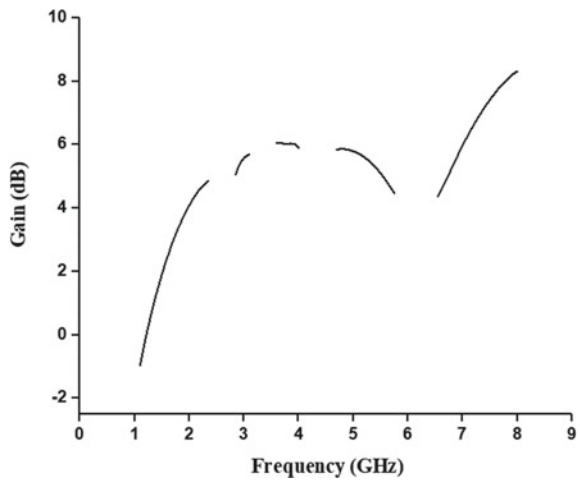


Fig. 5 |S₁₁| result of proposed antenna

Fig. 6 Gain of proposed antenna



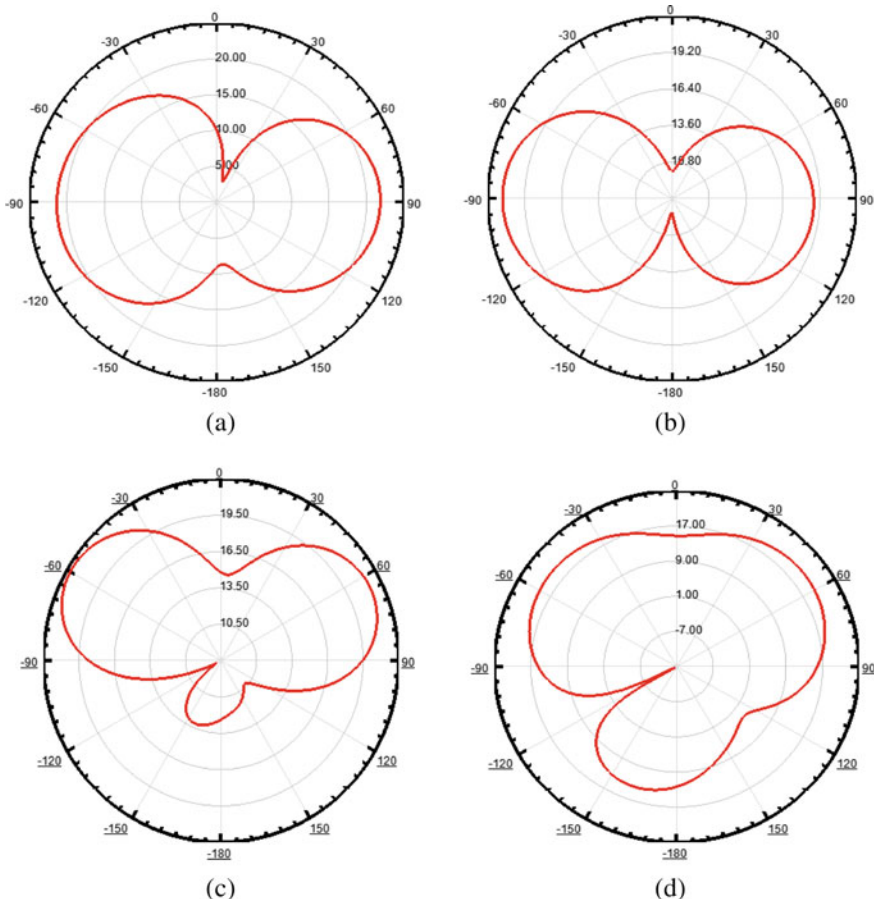


Fig. 7 Radiation pattern at 2.9 GHz (a) E-field & (b) H-field and Radiation pattern at 5.48 GHz (a) E-field & (b) H-field

References

1. Keno, Y.L., Wang, K.L.: Printed double-T monopole antenna for 2.4/5.2 GHz dual-band WLAN operations. *IEEE Trans. Antennas Propagate* **51**(9), 2187–2192 (2013)
2. Yon, J.H.: Fabrication and measurement of rectangular ring with open-ended CPW-fed monopole antenna for 2.4/5.2 GHz WLAN operations. *Microw. Opt. Technol. Lett.* **48**(8), 1480–1483 (2016)
3. Guy, J.-H., Zhen, S.-S., Xue, L.-L., Sun, Z.: Dual-band monopole antenna with L-shaped strips for 2.4/5 GHz WLAN applications. *Microw. Opt. Technol. Lett.* **50**(11), 2830–2833 (2008)
4. Koon, T.W., Kim, D., Rye, J.I., Kim, G.C., Yolk, J.-G.: A coupled dual-U-shaped monopole antenna for WiMAX dual-band operation. *Microw. Opt. Technol. Lett.* **53**(4), 745–748 (2011)
5. Lau, H.W., Kou, C.H., Yang, C.F.: Novel CPW-fed planar monopole antenna for W IMAX/WLAN application. *IEEE Antenna Wirel. Propagat. Lett.* **9**, 240–243 (2010)
6. Chu, Q.X., Yom, LuH: Design of compact dual-wideband antenna with assembled monopoles. *IEEE Trans. Antennas Propagate* **58**(12), 4063–4066 (2010)

7. Chon, H.D., Chen, H.T.: A CPW-fed dual-frequency monopole antenna. *IEEE Trans. Antennas Propagate* **52**(4), 978–982 (2014)
8. Fun, S.T., Yin, Y.Z., Hue, W., Song, K., Li, B.: CPW-fed printed monopole antenna with an n-shaped slot for dual-band operations. *Microw. Opt. Technol. Lett.* **54**(1), 240–242 (2012)

Printed U-Shaped Monopole Dual Band Antenna for Wireless Application



Vikash Chandra Sharma and Sudhanshu Verma

Abstract In this paper, coplanar wave guide (CPW) fed printed U-shaped monopole dual band antenna is introduced. U-shaped monopole antenna presented CPW fed with symmetrical circular and triangular slot on ground plane which is applicable for wide band and wireless application. The simulated result shows that the design of U-shaped symmetrical circular and triangular slot antenna covers with wide band application from 3.76–4.56 to 6.16–9.15 GHz with resonating frequency 4.42 and 8.04 GHz. The second band of the antenna offers the 39.05% bandwidth with less than –10 dB reflection coefficient which is applicable for UWB and wireless application. The overall dimension of the ground plane is $80 \times 101 \times 1.5 \text{ mm}^3$ with substrate material having dielectric constant 2.2 along with loss tangent 0.002 is used. The results of the proposed antenna with inverted L-strip along with radiation patterns, reflection coefficient $|S_{11}|$ in dB and surface current density of antenna is presented and discussed. The distinctive of the proposed antenna has been investigated using software HFSS.

Keywords Slot antenna · Printed antenna · Wide band antenna

1 Introduction

Due to the need for wireless applications, high gain antenna is required on large scale. Here this antenna introduces U-shaped slot comprise with broad main slot. In the last decade mobile and wireless communication system has increased dramatically [1]. This cellular network has required a high data rate. The criteria for (ITMA) international mobile telecommunication, 4G wireless communication systems are designed [2]. In the wireless communication system, the data rate is up

V. C. Sharma (✉) · S. Verma

Department of Electronics and Communication Engineering, Madan Mohan Malaviya University of Technology, Gorakhpur, India

e-mail: vikashchandrasarma94@gmail.com

S. Verma

e-mail: svermaeced@gmail.com

to (1 GB/S) for less mobility and even up to (100 Mb/S) for high mobility for mobile access. In the sequence of solving the problem and satisfaction, high data rate requirement wireless system 5G will develop immediately [3]. In the field of engineering Manufacturing, 5G offers a high quality of services such as electronic transactions, transportation industry, etc. In 5G wireless communication network has been future used by millimeter-wave frequencies. The frequency range of millimeter-wave ranges from 30 to 300 GHz in the electromagnetic spectrum [4]. Ultra-wide bandwidth (UWB) systems have got a large number of engrossment repayable to less power feeding and high data rate ability. In the view, this phenomenon the UWB antennas is the main part and important part of these systems, which promotes and indicated the frequency band by ‘Federal Communication Commission’ (FCC), i.e. 3.1–10.6 GHz have received attention by researchers. Present time the role of coplanar waveguide (CPW) is very important for wireless communication. These days CPW transmission line is used at high level as a feeding network and slot antenna [4]. Coplanar wave guide CPW has a lot of useful design advantages which is like a less dispersion, low radiation leakage, small characteristic impedance on substrate height and uni-planar configuration [4, 5]. Now in Advanced ‘modern wireless systems’ it offers many types of radiofrequency technology such as WiFi, WiMAX and basically Zigbee, 3G, and LTE comes in this category. Last few years ago, in the research field, it has been performed to make many types of design and goals. Many types of ‘wideband low-profile antennas’ have been constructed by utilizing a slot antenna [6, 7] a ‘loop antenna’ [10] and a ‘spiral antenna’ [11, 12]. In the literature, a lot of ‘slot antenna’ element is capable of CPW coplanar wave guide configuration. In the field of research, the main motive of researchers has been to work on the enhancement of bandwidth of microstrip antenna [6–9]. In this paper, the parasitic [11, 12] technique is used for bandwidth enhancement. According to the view, thickness of substrate is increased. When the thickness is increased about $0.05\lambda_0$, the inductance of fed is decreased by 50Ω impedance matching.

2 Antenna Design

For achieving the wide band, here, U-shaped is introduced with two symmetrical triangular and circular slots of radius R_1 and R_2 which is shown in Fig. 2. According to base paper, along with circular slot, an inverted L-strip is introduced which is shown in Fig. 2. U-shaped and symmetric circular and triangular slots are removed from the overall ground plane dimension. For comparison of antenna design, first of all, symmetrical triangular slot is introduced which is shown in Fig. 1a. After that, in the design of antenna2 symmetrical circular slot is introduced which is lower side of U-shaped which is shown in Fig. 1b. In the design of antenna3, both slot triangular and circular slot are introduced together which is shown in Fig. 1c and finally the fourth design of the antenna is introduced, U-shaped inverted L-strip triangular and circular slot which is shown in Fig. 1d because of poor $|S_{11}|$ result of antenna1, antenna2, antenna3 which is present in Fig. 3.

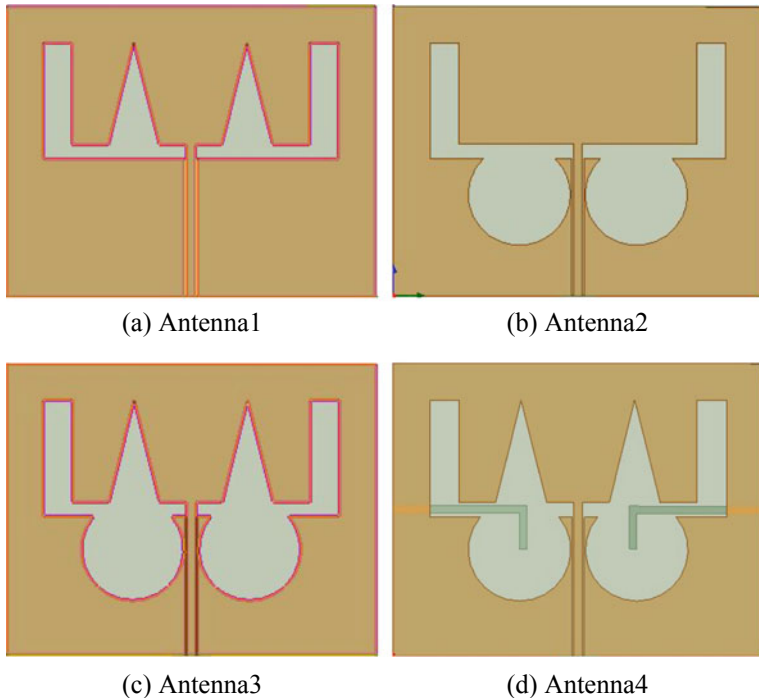


Fig. 1 The proposed antenna design with different shapes

Among these antennas, the good $|S_{11}|$ in dB result and effective bandwidth is achieved by symmetric triangular and circular slot with an inverted L-strip which is applicable for ultra wideband and wireless application. The design model of the antenna is present in Fig. 2 with all dimensions. Design parameters of the proposed antenna and their values are shown in Table 1.

The area of the ground plane is $L \times W \times H$ mm³ with substrate material having a dielectric constant which is 2.2 and loss tangent is 0.002 is used which is corresponding to the ground plane. The fed line is connected with coplanar wave guide CPW which is excites to the ground plan.

3 Result Discussion

The variation in different shapes of proposed antennas is shown in Fig. 1 and the comparison of these designs in the term of reflection coefficient are shown in Fig. 3. Triangular and Circular slot loaded U-shaped inverted L-strip Printed Microstrip ‘patch antenna’ are present in Fig. 2 and the simulated result of these designs in the term of reflection coefficient $|S_{11}|$ are present in Fig. 5. The radius comparison of

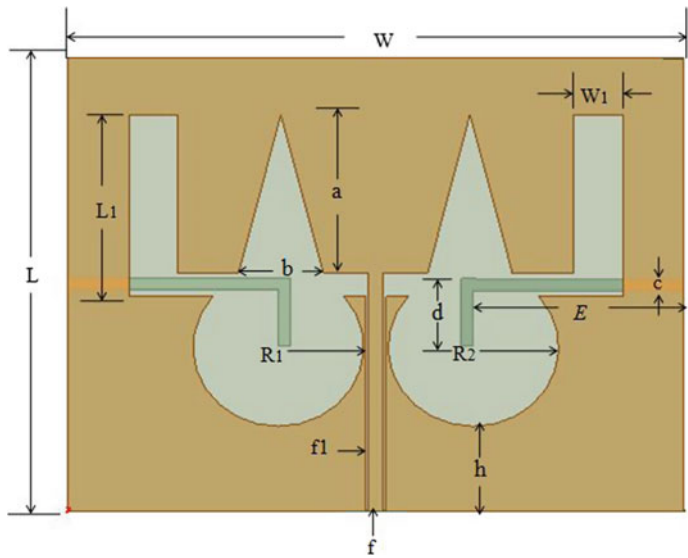
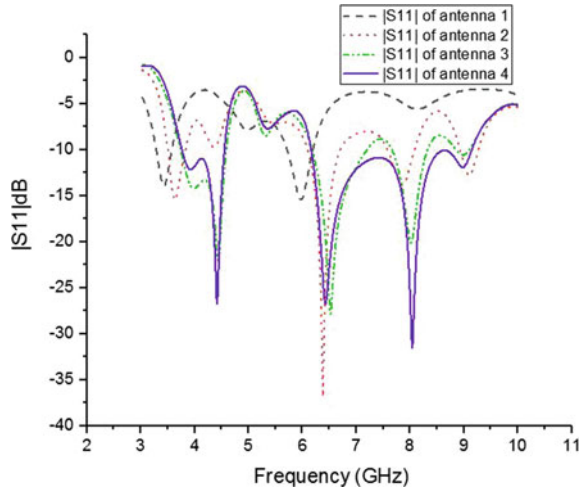


Fig. 2 Structure of design antenna

Table 1 Design parameters of proposed antenna

Parameters	Optimized value (mm)
L	80
L_1	32
W	101
W_1	8
a	28
b	14
c	2
d	11.75
E	34.5
R_1	14
R_2	14
f	2.4
f_1	0.5
h	15
H	1.5

Fig. 3 Comparison results $|S_{11}|$ of different antennas



symmetrical circle of this design in the term of reflection coefficient is presented in Fig. 4. Among these comparisons, the good $|S_{11}|$ result achieved by symmetrical circle radius at 14 mm is applicable for wireless applications.

The proposed antenna gives dual band. The first band range of this antenna 3.76–4.56 GHz with resonating frequency 4.42 GHz which is applicable for WiMAX application and second band range covers from 6.16–9.15 GHz with resonating frequency 8.04 GHz. The total bandwidth is achieved 39.05% which is less than -10 dB reflection coefficient with good return loss -31.51 GHz at centre frequency 6.14 GHz. The current distribution of proposed antenna is achieved at 4.42 GHz frequency and 8.04 GHz frequency which is shown below in Fig. 6.

Fig. 4 Comparison results $|S_{11}|$ of different radius

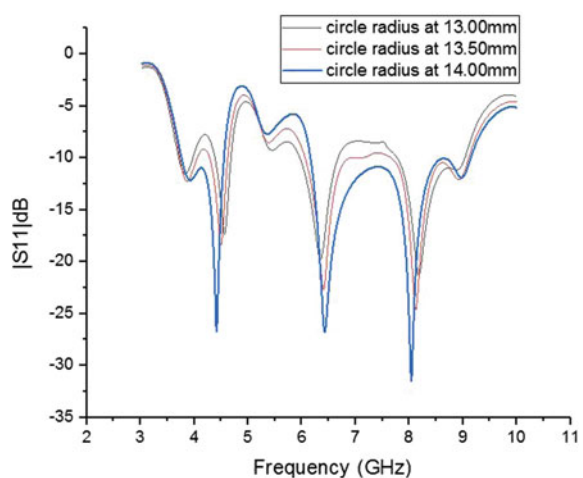
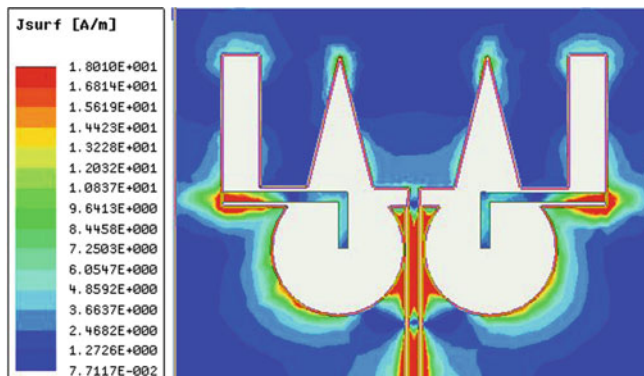
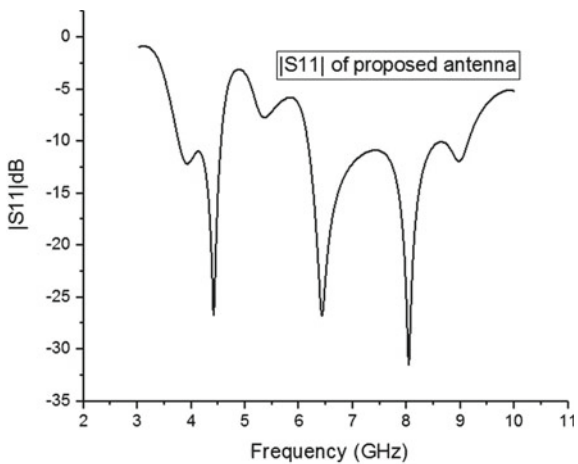
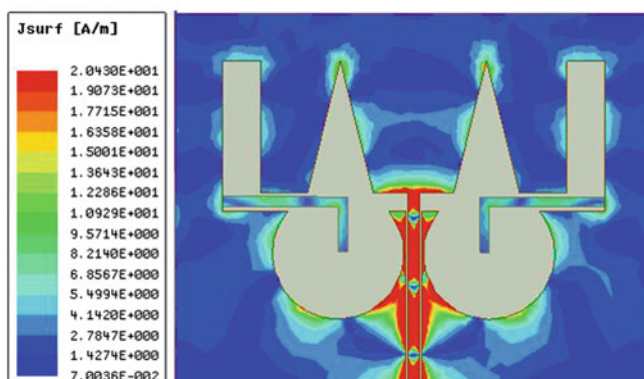


Fig. 5 $|S_{11}|$ result of proposed antenna



(a)



(b)

Fig. 6 **a** Current density of proposed antenna at 4.42 GHz. **b** Current density of proposed antenna at 8.04 GHz

The radiation patterns are achieved of design antenna ‘E-plane’ and ‘H-plane’ at the two resonant frequencies which are 4.42 and 8.04 GHz are shown in Fig. 7 and radiation pattern of the proposed antenna is z-Omni directional.

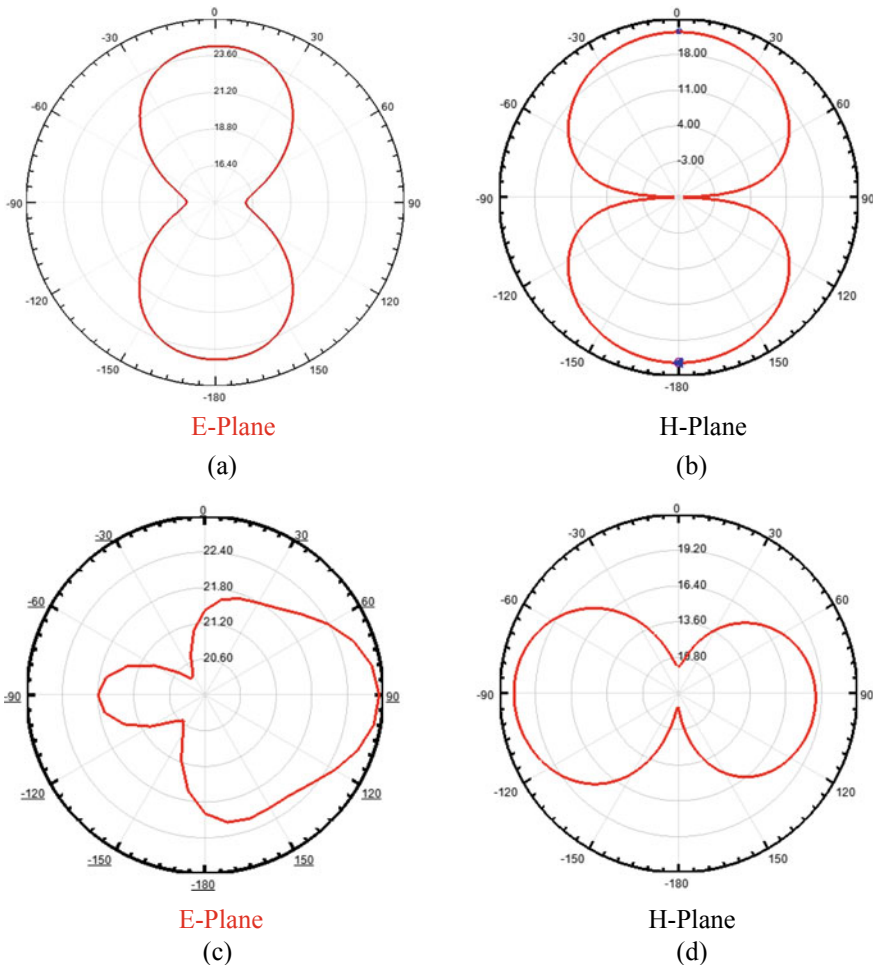


Fig. 7 (a) E-Plane at 4.42 GHz; (b) H-Plane at 4.42 GHz; (c) E-Plane at 8.04 GHz; (d) H-Plane at 8.04 GHz

4 Conclusion

A circular, triangular slot loaded with inverted L-strip U-shaped Printed Microstrip Patch Antenna is fed with coplanar wave guide CPW using two symmetrical triangles and circle with different position on and different radius which are removed from ground plane. The enhanced bandwidth is 39.05% of frequency ranges 6.16–9.15 GHz at resonating frequency 8.04 GHz. This antenna is a smaller radiator and simple in structure and antenna configuration is more in compact size and more coupled electromagnetic energy in the patch for enhancing the bandwidth. The design of the antenna is successfully simulated with the help of HFSS V.16.2 for Wireless applications.

References

1. Goyal, R.K., Sharma, K.K.: T-slotted microstrip patch antenna for 5G WI-FI network. *IEEE Trans.* **16**(4), 2684–2687 (2016)
2. Long Li, J., Hui Luo, M., Liu, H.: Design of a slot antenna for future 5G wireless communication systems. In: Progress in electromagnetics research symposium spring (PIERS), Russia, vol. 65, no. 3, pp. 739–741, March 2017
3. Imran, D., Farooqi, M.M., Khattak, M.I., Ullah, Z., Khan, M.I., Khattak, M.A., Dar, H.: Millimeter wave microstrip patch antenna for 5G mobile communication. *IEEE Trans. Antennas Propag.* (2017)
4. Shahjehan, W., Hussain, I., Khattak, I.M., Asad, R., Iqbal, N.: Multi-band antenna for 5G applications. In: International Conference on Computing, Mathematics and Engineering Technologies (2019)
5. Deng, C., Li, Y., Zhang, Z.: A wideband high-isolated dual-polarized patch antenna using two different balun feedings. *IEEE Antennas Wireless Propag. Lett.* <https://doi.org/10.1109/lawp.2014.2347338,2013>
6. Lin, Y.-F., Liao, P.-C., Cheng, P.-S., Chen, H.-M., Song, C.T.P., Hall, P.S.: CPW-fed capacitive H-shaped narrow slot antenna. *Electron. Lett.* **41**, 17–18 (2005)
7. Mak, K.M., Lai, H.W., Luk, K.M., Ho, K., Lu, L.: Polarization reconfigurable circular patch antenna with a C-shaped. *IEEE Trans. Antennas Propag.* **65**(3), 1388–1392 (2017)
8. Barbuto, M., Trotta, F., Bilotti, F., Toscano, A.: Circular polarized patch antenna generating orbital angular momentum. *Prog. Electromagnet. Res.* **148**, 23–30 (2014)
9. Zosu, S., Li, P., Wang, Y., Feng, W., Liu, Z.: A CPW-fed broadband circularly polarized regular-hexagonal slot antenna with L-shape monopole. *IEEE Antennas Wireless Propag. Lett.* **10**, 1182–1185 (2011)
10. Sharif, B.S., Matin, M.A., Tsimenidis, C.C.: Probe fed stacked patch antenna for wideband applications. *IEEE Trans. Antennas Propag.* **55**(8), 2385–2388 (2007)
11. Park, J., Hyung-gi, N., Seung-hun, B.: Design of modified L-probe fed microstrip patch antenna. *IEEE Antennas Wireless Propag. Lett.* **3**, 117–119 (2004)
12. Mak, C.L., Luk, K.M., Lee, K.F.: Microstrip line-fed L-strip patch antenna. In: IEE Proceedings—Microwaves, Antennas and Propagation, vol. 146, no. 4, pp. 282–284 (1999)

IoT-Enabled Early Prediction System for Epileptic Seizure in Human Being



Sayali Shinde and Brijesh Iyer

Abstract The paper reports a hardware-based system for the prediction of epilepsy in the human subject under test. EEG signals from the dataset are analyzed to predict epilepsy status. The EEG signal database is analyzed with the help of support vector machine and thresholding to classify the human subject under test as normal or else. The reported technique is very simple and demonstrates a reasonable agreement with the existing methodologies.

Keywords DWT · EEG · Epilepsy · Seizure · SVM

1 Introduction

Epileptic seizure is a term that itself introduces two separate terms, i.e. epilepsy and seizure. Epilepsy is a chronic neurological disorder of a cerebral nervous system that affects peoples of all ages, races and ethnic background. Over 50 million patients are reported suffering from epilepsy worldwide with 204 million peoples diagnosed to have epilepsy. Nearly 80% of the people with epilepsy live in low- and middle-income countries [1]. Human brain communicates with different organs with the help of neurons. The neurons transmit electro-chemical signals to produce human thoughts, feelings and actions. However, an electro-chemical storm is resulted in the simultaneous transmission of signals by many neurons. Biochemically, this storm is an intense wave that overwhelms brain function and converges into seizures. If a person has two or more recurrent seizures then he/she is considered to have epilepsy. Hence, seizure is a symptom of epilepsy. However, not everyone who appears to have seizure should have epilepsy.

Epileptic seizure may turnout in six phases such as—*Prodromal phase* (occurs a day or hours before actual seizure), *an aura phase* (occurs few seconds to few minutes before actual seizure), *pre-ictal phase* (occurs immediately before seizure), *ictal*

S. Shinde · B. Iyer (✉)

Department of E&TC Engineering, Dr. Babasaheb Ambedkar Technological University, Lonere 402103, India

e-mail: brijeshiyer@dbatu.ac.in

phase (actual seizure duration), *post-ictal phase* (occurs after seizure immediately) and *inter-ictal phase* occurs before the start of next seizure. Hence, early epileptic seizure prediction is possible by analyzing *inter-ictal* and *pre-ictal* phases of seizures.

Although the main cause of epilepsy remains unknown, its diagnosis can be useful in the treatment. Epilepsy limits the active life span of peoples by imposing restrictions on independent activities and thereby leads to socio-economic issues. Hence, the development of a customer-friendly framework which will help specialists, patients and guardians in regulating the epileptic seizures. This framework will identify epilepsy when the patient isn't having a seizure at that instant.

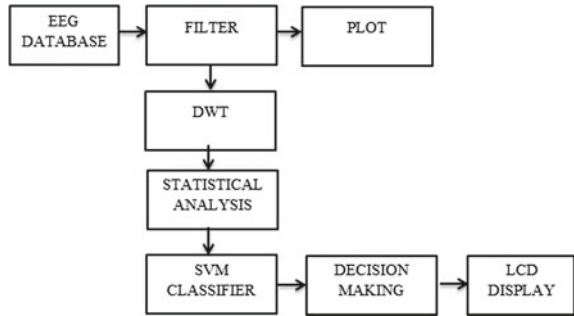
There are different diagnosing techniques such as a neurological exam, blood tests, high-density EEG, Computerized tomography (CT) scan, Magnetic resonance imaging (MRI), Functional MRI (fMRI), Positron emission tomography (PET), Single-photon emission computerized tomography (SPECT), Neuropsychological tests, Statistical parametric mapping (SPM), Curry analysis, Magnetoencephalography (MEG), Electroencephalogram (EEG). Out of all these EEG is preferable because it is having high time resolution and it is simple to use. Further, EEG provides a very high temporal resolution in the order of milliseconds. EEG sensors are simple to handle and it is a very powerful tool tracking the variation in the functioning of the brain [2]. Many notable research works have been reported in the area of epilepsy detection and prediction. A fractal-dimension based algorithm was proposed by K. Devarajan et al. for the detection of epilepsy [3]. Preprocessing and noise removal from EEG signals by machine learning methods, feature selection techniques such as Sequential Forward Selection (SFS), statistical techniques are also used for epilepsy detection[4–6]. Tzallas et al. reported classification of EEG seizure detection methods into pattern recognition, morphological analysis, parametric and decomposition methods, clustering methods and data mining methods [7]. Time domain, frequency domain, wavelet, EMD, PCA and ICA based methodologies were also adopted for the prediction and detection of epilepsy [8–12]. However, none of these methodologies provide early detection of epilepsy. Hence, the paper reports a methodology for early detection of epilepsy and a low-cost, lightweight hardware device for the detection of epilepsy.

The rest of the paper is organized as Sect. 2 discusses the proposed methodology for early detection of epilepsy whereas the discussion on the proposed methodology and its qualitative analysis are presented in Sect. 3. The paper is concluded in Sect. 4.

2 Proposed System

Figure 1 depicts the block diagram for the proposed early detection mechanism of epilepsy. EEG database used for the present analysis consist of 11,500 instances (rows) and 178 data points (columns) recorded at 1 s each. 179th column contains labels either 0 for healthy activity or 1 for seizure activity [13]. EEG signal is decomposed into theta band (4–8 Hz), alpha band (8–14 Hz) and beta band (14–32 Hz) using empirical bandpass filters. DWT is used for extracting features from EEG signals.

Fig. 1 Block diagram of overall system



Various statistical cost functions such as Mean, Variance, Standard deviation, Maximum and minimum amplitude, Power, Energy, Homogeneity (statistics) and Correlation are used for the analysis of the decomposed EEG signal.

Further, the statistically analyzed signals are applied to the support vector (SVM) machine classifier to differentiate between the electrical activity of a healthy subject and an epileptic one. Our data is linearly separable having binary class so SVM is a most suitable classifier because for binary classification its prediction speed is fast and interpretation is also easy. After classification using SVM classifier, a threshold level is set to classify if the subject under test is healthy or will have seizure in the future.

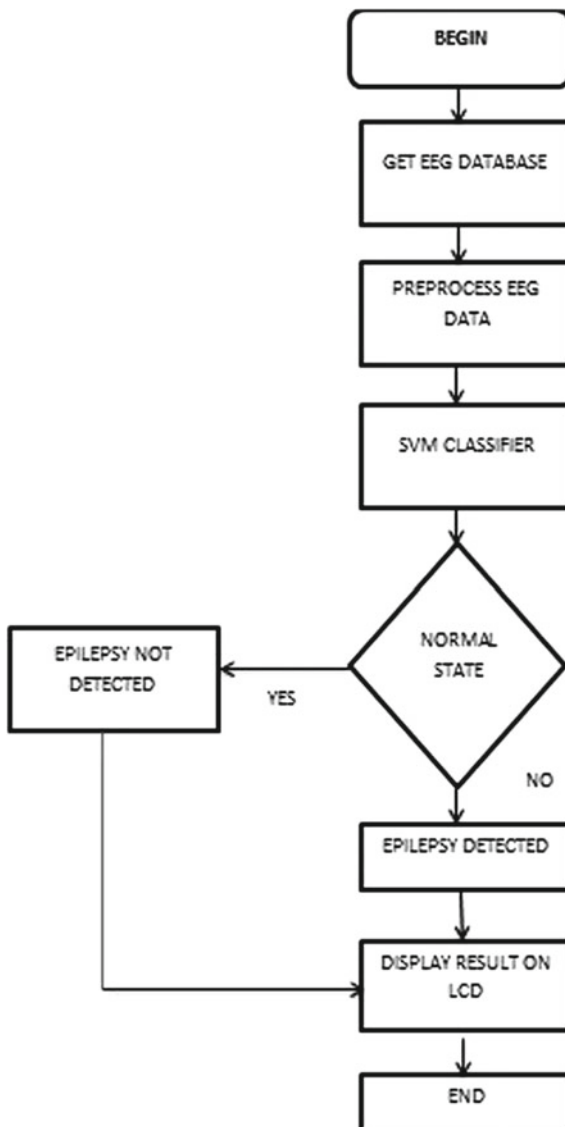
The regularized output is normalized between zero and one and to initiate prediction a threshold 0.5 is selected. The reason for the particular choice of threshold value is that the data is balanced and linearly separable i.e. either 0 or 1. Further, at 0.5 threshold value SVM provides equal error rate (EER). EER is the point where the false positive rate is equal to false-negative rate (hence equal errors), i.e. $FPR = FNR = 1 - TPR$ [14]. The handheld epilepsy prediction device is build up by interfacing LCD display with ARDUINO. Figure 2 depicts the flowchart for the proposed methodology.

3 Results and Discussions

Figure 3 depicts the dataset used in the present analysis. It consists of EEG recordings of 500 peoples for the duration of 23 s. This results in $500 \times 23 = 11,500$ instances (rows) with each instance consist of 178 data points (columns) for a recording after every second. The highlighted column has numbers (labels) 1, 2, 3, 4, 5. Out of them, 1 represents the seizure activity and remaining labels represent the healthy activity. The highlighted column indicates labels associated with each data row.

Figure 4 shows new dataset after assigning labels 2, 3, 4, 5 as ‘0’ for healthy activity while labels 1 is retained ‘1’ for seizure activity.

After assigning the new labels the data set is applied to the bandpass filter for separating the data into different bands such as delta (0–4 Hz), theta (4–8 Hz), alpha

**Fig. 2** System flowchart

-21	-9	2	11	24	29	16	-8	-36	-51	-38	-4	25	16	-16	-74	-101	-89	-49	5
-257	-258	-168	-32	140	277	366	408	416	415	423	434	416	374	319	268	215	165	103	1
-11	-23	-39	-43	-32	-18	-30	-51	-72	-80	-56	-41	-40	-43	-32	-13	-1	-7	-44	3
125	129	121	112	100	83	63	41	-2	-51	-88	-102	-97	-77	-45	-19	13	44	68	4
-13	-13	-4	3	15	19	21	25	29	33	32	35	36	34	32	26	23	18	20	2

Fig. 3 Block out of the total dataset

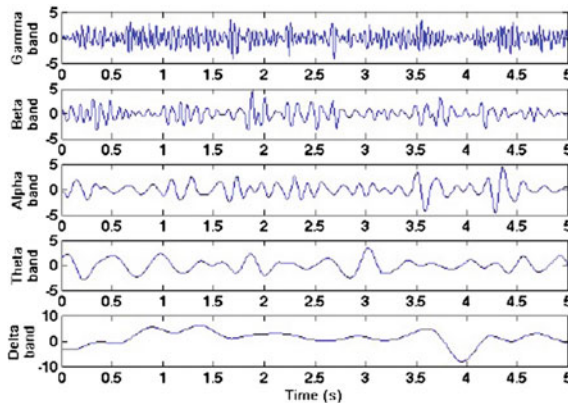
-21	-9	2	11	24	29	16	-8	-36	-51	-38	-4	25	16	-16	-74	-101	-89	-49	0
-257	-258	-168	-32	140	277	366	408	416	415	423	434	416	374	319	268	215	165	103	1
-11	-23	-39	-43	-32	-18	-30	-51	-72	-80	-56	-41	-40	-43	-32	-13	-1	-7	-44	0
125	129	121	112	100	83	63	41	-2	-51	-88	-102	-97	-77	-45	-19	13	44	68	0
-13	-13	-4	3	15	19	21	25	29	33	32	35	36	34	32	26	23	18	20	0

Fig. 4 New dataset after assigning labels ‘0’ & ‘1’

(8–13 Hz), beta (13–32 Hz) and gamma (32–100 Hz) bands. Figure 5 shows the output of the BPF with different bands.

Out of the total dataset, 75% data i.e. 8625 rows we have assigned as a training set. Hence, training set is a matrix of 8625×22 . Figure 6 shows output of feature extraction of a training set. Blue columns indicate feature extracted for THETA band as mean, variance, standard deviation, maximum amplitude, minimum amplitude, power respectively. Followed by red columns indicates feature extracted for ALPHA band and brown columns for feature extracted for BETA band respectively. The green column indicates features values for energy, homogeneity, correlation respectively.

Out of total dataset, 25% data i.e. 2875 rows we have assigned as a testing set. Hence, testing set is a matrix of 2875×22 . Figure 7 shows the output of feature extraction of a testing set. Blue columns indicate feature extracted for THETA band as mean, variance, standard deviation, maximum amplitude, minimum amplitude, power respectively. Red columns indicate feature extracted for ALPHA band and

**Fig. 5** Output of band pass filter

THETA					ALPHA					BETA					ENERGY	HOMO	CORR	0		
MEAN	VAR	STD DEV	MAX	MIN	MEAN	VAR	STD DEV	MAX	MIN	POWER	MEAN	VAR	STD DEV	MAX	MIN	POWER				
-22.9	617.7	24.92	14.28	-109	1141	-24.5	795	28.28	18.81	-124	1397	-21.8	1079	32.94	31.81	-137	1556	0.457	0.862	0.614
38.58	74614	273.9	737.4	-367	76103	41.57	90079	301	816.3	-400	91807	37.78	89902	300.7	836.8	-413	91329	0.423	0.926	0.83
-61.9	6621	81.6	90.52	-278	10458	-66.6	7760	88.34	100.8	-301	12194	-59.8	6779	82.57	104.3	-284	10360	0.628	0.946	0.802
-12.1	3104	55.87	124.7	-136	3250	-13	3942	62.97	144.5	-152	4112	-11.9	4805	69.52	175	-163	4948	0.422	0.901	0.764
-26.8	1047	32.45	34.32	-104	1764	-28.8	1539	35.3	37.38	-115	2067	-25.8	1126	33.65	35.85	-116	1792	0.591	0.975	0.926

Fig. 6 Output after feature extraction of training set

THETA						ALPHA						BETA								
MEAN	VAR	STD DEV	MAX	MIN	POWER	MEAN	VAR	STD DEV	MAX	MIN	POWER	MEAN	VAR	STD DEV	MAX	MIN	POWER	ENERGY	HOMO	CORR
-0.1	553.57	23.59	72.65	-81.6	553.58	-0.09	714.08	26.8	84.22	-93.4	714.09	-0.04	960.65	31.08	102.5	-109	960.65	0.332	0.812	0.57
12.23	25389	159.8	512.1	-302	25539	13.08	31029	176.0	576.7	337	31200	11.47	32313	180.3	631.6	-353	32444	0.437	0.941	0.864
-6.65	162715	404.5	1106	-876	162759	-7.81	198616	446.9	1220	-1011	198677	-9.89	209593	459.1	1255	-1206	209691	0.43	0.926	0.828
13.57	899.86	30.08	68.18	-49.1	1084	14.6	1058.6	32.63	74.55	-52.9	1271.8	13.17	938.1	30.71	73.68	-49.9	1111.6	0.53	0.98	0.95
-10.5	2615.8	51.29	95.68	-139	2725.3	-11.2	3426.5	58.7	113.8	-159	3552.6	-10	4740.9	69.05	150.5	-181	4841.4	0.366	0.857	0.67

Fig. 7 Output after feature extraction of testing set**Fig. 8** Sample number based output prediction

```
Command Window
-0.0004      0.0371      0.0006      0.0
-0.0000      0.0248      0.0005      0.0

The Score of Training is : 97.36 %
Enter the SAMPLE number
the SAMPLE number should be between
1 to 2800
fx 23|
```

brown columns for feature extracted for BETA band and green columns indicate feature values for energy, homogeneity, correlation respectively (Fig. 8).

As soon as a sample number is entered, the designed system alerts either as ‘patient is healthy’ or as ‘patient can get seizure in future’ (Figs. 9 and 10).

Fig. 9 Output of the sample showing patient is healthy

```
Command Window
0.0000      0.2720      0.0017
0.0001      0.0175      0.0004
-0.0004      0.0371      0.0006
-0.0000      0.0248      0.0005

W
The patient is healthy
fx >>
```

Fig. 10 Output of the sample showing patient can get seizure in future

```
Command Window
0.0000      0.2720      0.0017      0.0049      -0.003
0.0001      0.0175      0.0004      0.0011      -0.000
-0.0004      0.0371      0.0006      0.0014      -0.001
-0.0000      0.0248      0.0005      0.0011      -0.001

Q
The patient can get epileptic seizures in future
fx >> |
```

Fig. 11 Hardware prototype of the proposed system



Figure 11 depicts the hardware prototype for the proposed android-based system. The EEG data is applied as the input to the system. Based on the developed algorithm, the system generates alerts about the detection of epilepsy.

Tables 1 and 2 provide the qualitative comparative analysis of the proposed method with the existing ones. These tables clearly indicate that the proposed method is very attractive solution over the existing technologies.

The approaches reported in [15–17] are not attractive due to one or more reasons like the use of complex mechanisms for epilepsy detection or prediction, classifiers, hardware implementation, performance in terms of early detection and prediction, etc.

The proposed method provides 100% detection sensitivity for normal or diseased human subjects. Further, early prediction of convergence of human subjects under test is possible with the proposed methodology as it utilizes the data of *inter-ictal* and *pre-ictal* phases of seizures for the analysis. The detection and hence the prediction sensitivity is 100% due to the fact that the data is balanced and linearly separable, i.e. either 0 or 1 and 0.5 is selected as the threshold for classification. Further, with this threshold value SVM classifier also provides equal EER.

Table 1 Qualitative comparative analysis of the proposed method: technology aspect

Contribution	Method	Classifier	No. of channels	Hardware implementation	Performance metric	Early prediction ability
Rojas et al. [14]	Wavelet-based prediction	No classifier	Single channel	No	100% sensitivity	No
Orosco et al. [15]	EMD based detection	No classifier	Single channel	No	56% sensitivity	No
Yoo et al. [16]	Time, detection	SVM	Multi-channel	Yes	84% accuracy	No
Dalton et al. [7]	Time, detection	Template matching	Single channel	Yes	91% sensitivity	No
Proposed method	Time series based prediction	SVM	Multiple channel	Yes	100% sensitivity	Yes

Table 2 Qualitative comparative analysis of the proposed method: product-based aspect

Contribution	Hardware implementation	Technology	Deployability of the prototype	Cost per unit (Approximate in INR)
Yoo et al. [16]	Yes	CMOS IC	Specialized labs are required for production of chips	Not reported
Dalton et al. [7]	Yes	Accelerometer-based kinematic sensors	Proprietary item with Intel	Not reported
Shoaib et al. [17]	Yes	CMOS IC	Specialized labs are required for production of chips	Not reported
Proposed method	Yes	IoT based	Handy	2000/-

Further, the hardware prototype of the proposed method is also very economical and easy to implement and reproduce (Table 2) as compared to its counterparts. The proposed mechanism collects the decomposed data from EEG sensors and processes it via simple *Raspberry Pi* boards. The processed results can be made available to the health practitioners over distance. This feature will help the patient to receive immediate medical attention in an emergency.

4 Conclusions

Early prediction of seizure is necessary due to three reasons; correctly detection, continuous monitoring and reduce operational cost. The paper reports a system that extracts large number of features from the EEG data after wavelet transformation and performs statistical analysis before applying it to the SVM classifier. This system provides 100% detection and hence the prediction accuracy with a very simple mechanism as compared to the existing mechanisms. Further, a simple android-based hardware prototype increases make its commercial viability. In the future, the reported system can be upgraded to an IoT based system as a pervasive healthcare system.

Acknowledgements This work is partially funded by the “IoT-Based Consumer Behaviour Analytics Project” by DigitalDojo Pvt. Ltd. Mumbai-India.

References

1. WHO report of epilepsy. <http://www.who.int/news-room/fact-sheets/detail/epilepsy>
2. Devarajan, K., Jyostna, E., Jayasri, K., Balasampath, V.: EEG-based epilepsy detection and prediction. IACSIT Int. J. Eng. Technol. **6**(3), 212–216 (2014)
3. Usman, S., Usman, M., Fong, S.: Epileptic seizures prediction using machine learning methods. Comput. Math. Meth. Med. **2017**, 1–10 (2017)
4. Osorio, K., Gonzaiez, J., Santacoloma, G.: Automatic epileptic seizure prediction based on scalp EEG and ECG signals. In: XXI Symposium on Signal Processing, Images and Artificial Vision (STSIVA), 1–7 Sept 2016
5. Ibrahim, S., Majzoub, S.: EEG-based epileptic seizures detection with adaptive learning capability. Int. J. Electr. Eng. Inform. **9**(4), 813–824 (2017)
6. Tzallas, A., et al.: Automated epileptic seizure detection methods: a review study. In: Stevanovic, D. (ed.) *Epilepsy—Histological, Electroencephalographic and Psychological Aspects*, p. 276. InTech Europe, Rijeka (2012)
7. Dalton, A., et al.: Development of a body sensor network to detect motor patterns of epileptic seizures. IEEE Trans. Biomed. Eng. **59**(11), 3204–3211 (2012)
8. Rana, P., et al.: Seizure detection using the phase-slope index and multichannel ECoG. IEEE Trans. Biomed. Eng. **59**(4), 1125–1134 (2012)
9. Zandi, A., et al.: A novel wavelet-based index to detect epileptic seizures using scalp EEG signals. Proc. Eng. Med. Biol. Soc. **3**(2), 919–922 (2008)
10. Alam, S., Bhuiyan, M.: Detection of seizure and epilepsy using higher order statistics in the EMD domain. IEEE J. Biomed. Health Inform. **17**(2), 312–318 (2013)
11. Shih, Y., Chen, T., Yang, C., Chiueh, H.: Hardware-efficient EVD processor architecture in FastICA for epileptic seizure detection. In: Proceedings of the Signal & Information Processing Association Annual Summit and Conference (APSIPA ASC), Hollywood, CA, USA, pp. 1–4, 3–6 Dec 2012
12. EEG Database: <https://archive.ics.uci.edu/ml/datasets/Epileptic+Seizure+Recognition>
13. Litt, B., Echauz, J.: Prediction of epileptic seizures. Lancet Neurol. **1**(1), 223 (2002)
14. Rojas, C.A., Valderrama, M., Witon, A., Navarro, V., Quyen, M.: Probing cortical excitability using cross-frequency coupling in intracranial EEG recordings: a new method for seizure prediction. In: International Conference of the IEEE EMBS, Boston, MA, USA, pp. 1632–1635, Sept 2011

15. Orosco, L., et al.: An epileptic seizures detection algorithm based on the empirical mode decomposition of EEG. In: International Conference of the IEEE EMBS, Minneapolis, MN, USA, pp. 2651–2654, 3–6 Sept 2009
16. Yoo, J., et al.: An 8 channel scalable EEG acquisition SoC with patient-specific seizure classification and recording processor. *IEEE J. Solid State Circuits* **48**(1), 214–228 (2013)
17. Shoib, M., Lee, K.H., Jha, N.K., Verma, N.: A 0.6–107 μ W energy-scalable processor for directly analyzing compressively-sensed EEG. *IEEE Trans. Circuits Syst I. Reg. Papers* **61**(4), 1105–1118 (2014)

Effective Author Ranking Using Average of Different h-Index Variants



Prabhat Kumar Chandra, Vivekanand Jha, and Kumar Abhishek

Abstract In the last few years, it has been noticed that h -index and their variants perceived a lot of attention in scientific world due to some valuable properties (easy to compute, relation between quantity of publications and their significance, and so on). Many other metrics have been proposed in order to enhance and conquer the flaw of the original Hirsch proposal. This paper presents a comprehensive analysis of the h -index and their variants. The initial h -index proposal is studied in detail with its advantages and disadvantages. A brief discussion of many of the h -related indices is discussed along with their mathematical workings and primary characteristics. Some of the major works that analyze and compare them are also presented. The logic of h -index and its variant has been implemented and reviewed to find the author ranking. The results obtained from h -index and its variant are compared using different citation databases (DBLP and ACM library databases). The effect of all the indicators and the variation in the result are analyzed. To find the better and fair result for author ranking, we calculate the average of all the indicators. The results show that averaging h -index variants gives a fair author ranking to compare the works of different authors.

Keywords Citation · h-Index · Average ranking

1 Introduction

The introduction of the Hirsch index (h -index) had a considerable impact and influence on scientometric and bibliometric research. The main part of the concepts building on the Hirsch work is concerned to introduce new variants and generalize

P. K. Chandra (✉)
Gaya College of Engineering, Bihar, India
e-mail: prabhat.bitd@gmail.com

V. Jha
Motihari College of Engineering, Bihar, India

K. Abhishek
National Institute of Technology Patna, Bihar, India

them. *h*-Index is an author level index that quantifies both the citation impact and productiveness of the research publications of a scholar or scientist.¹ This index is based on the collection of most cited papers and the number of citations that they have acquired in other papers or publications.

One of the most important questions in citation networks is author's ranking. Many aspects like conference popularity, university ranking, research funding, and authors authoritative depend on author's ranking and their papers impact. These questions can be paraphrased as (i) Who are the key authors (researchers) in a particular field of research? (ii) Need to check ranking by various metric methods, (iii) What kinds of overtime trends (temporal analysis) are observed in these networks? and (iv) How often do authors publish?

In a center search [1], it was seen that along with *h*-index more than 37 variants were also listed. But finding author ranking through *h*-index and its variant gives inconsistent result. Research into developing of new *h*-index variants or we can say a new bibliometric indicator often proceeds in a somewhat improvised fashion. In general, researchers take an indicator and identify their properties on which they stated their advantages which have some desirable property. The weakness of such method to new indicator development is that in most cases it is heterogeneous and unsystematic. To choose a new indicator is often made in somewhat inconsistent way, we cannot find the appropriate property of the new indicator, and in these cases, the indicators are only compared on the basis of their states and complexities. So, the research on *h*-index and its variants is also analytically oriented.

There exists some more inconsistency in *h*-index method; hence, it is not an appropriate method to quantify the scholar. As *h*-index is totally dependent on a single parameter, i.e., citation of each paper, sometimes, it may happen that more than two scientists get the same *h*-index value. In that situation, it is difficult to give the appropriate rank of those particular scientists. Apart from this, it also violates some of the basic properties like [11]. (a) If two researchers are getting the same relative performance growth, then their rank relative to each other should remain consistent. (b) If two researchers are getting the same absolute work improvement, then their rank relative to each other should remain consistent.

Various indicators show different ranks of the author for the same information or data. When we do ranking for the authors, one major component is weighed in the assessment process, viz. the number of citations received by the papers of the author [10]. This is particularly vital since the quality of a paper is concentrated in general when one or more of its authors are renowned researcher(s) in their domain, in which case it attracts a significant number of citations. Applying various mathematical formulas shows how author rank is changed. Due to fluctuation in ranking, morality of a good author may be down. There are some applications which rely more on performance gradient against time of an author than the absolute score he/she gets at a particular moment. So, our idea is to do the selection process on the basis of average ranking through which young candidates grant the allocation in their domain.

¹<https://en.wikipedia.org/wiki/H-index>.

Motivated by the inadequacy of the existing systems and approaches, this paper focuses on overcoming the above problems. We aim to develop a new proposed model in which rank of an author is calculated through the average of different h -index variants and it will give efficient and better result for an author.

2 Related Work

In 2005, Hirsch [9] introduced a bibliometric parameter, i.e., h -index, which was based on citation, and received tremendous attention from the community of researchers and scientists as both quality and impact of paper were measured on the basis of single parameter, i.e., citation. But, it was later noticed that it only measured the high-quality paper whose h -index value is high. Later, in 2006, Egghe [6]; [5] introduced new index called the g -index which was also based on citation. His contribution was basically improvement in the mathematical formula, where more research papers can be added in the calculation which were discarded in h -index. In 2008, Ronald Rousseau [12] developed two more metrics, i.e., h^2 indices and R indices, which only included more papers to evaluate the ranking of the author. In [3], the authors developed a novel method to evaluate the author ranking. They took the mean of h -index, c -index, and c' -index. But, all these indexes are not based on the single parameter, i.e., the citation of the paper; they considered more parameters to calculate the ranking metric.

3 Dataset

We have [2] used the DBLP dataset of the computer science domain developed by [13]. The dataset was extracted from arnetminer.org, where data was collected specifically from the field of computer science. Mainly, two important sources were selected which were DBLP and ACM library from where more than 21 lakhs data was collected. Each data comprises of the attributes like *paper name*, *author name*, *year*, *conference name*, *citation value*, *index of the paper*, and *paper id*. A sample of the dataset is shown in Fig. 1. The algorithm to cluster the dataset is shown in Fig. 2. All the calculations were performed in *python* platform with version 2.7.

```

2244018
#*OQL[C++]: Extending C++ with an object Query Capability.
#@Jose A. Blakeley
#year1995
#confModern Database Systems
#citation14
#index0
#arnetid2

##Transaction Management in Multidatabase Systems.
#@Yuri Breitbart, Hector Garcia-Molina, Abraham Silberschatz
#year1995
#confModern Database Systems
#citation22
#index1
#arnetid3

##Overview of the ADDS system.
#@Yuri Breitbart, Tom C. Reyes
#year1995
#confModern Database Systems
#citation1
#index2
#arnetid4

##Multimedia Information Systems: Issues and Approaches.
#@Starvrous Christodoulakis, Leonidas Koveos
#year1995
#confModern Database Systems
#citation25
#index3
#arnetid5

```

Fig. 1 An example of raw ACM library dataset

Step 1 : Input folder for file scan
Step 2 : Establish a connection with Database
Step 3 : Repeat steps 4 and 5 for every file in input folder
Step 4 : Prepare Database query with dynamic placeholders
Step 5 : nameTokens = split file name
Step 6 : Obtain conference and year from name Tokens
Step 7 : Repeat steps 8 to 13 for every line of input text
Step 8 : If line contains "."

Step 9 : Tokens = split line by "."

Step 10 : Obtain name, paper and year from tokens

Step 11 : Combine Paper index, Conference, Year and No. of citation, and push to DB

 using dynamic query

Step 12 : end if

Step 13 : Commit database and go to next line

Step 14 : Close Database connection

Fig. 2 Algorithm to cluster the dataset

4 Methods and Model

4.1 Methods

We explore few relevant known metrics to find author ranks based on the selected metrics. The metrics chosen are as follows:

-*h*-Index: *h*-Index is an author-level index that quantifies both the citation impact and productiveness of the research publications of a scholar or scientist. This index is totally based on the collection of most cited papers and the number of citations that they have acquired in other papers or publications. The key point of *h*-index is that a researcher with an index of *h* has published *h* papers, each of which has been cited in other papers at least *h* times. Thus, [8] the *h*-index mirrors both the count of publications and the number of citations per publication. Mathematically, it can be defined as follows:

$$\text{citation}[i] \leq i \quad (1)$$

Then, the value of *i* will give the *h*-index value of that particular author. The *h*-index is cumulative in nature, which means from time to time the value of *h*-index will increase gradually since it is only dependent on the number of citations. So, the time complexity of the *h*-index will be $O(n)$.

-*g*-Index: *g*-Index is a customized version of *h*-index. It is a measure which expresses the comprehensive quality of a journal or of a scientist that deals with the performance of the top articles, and hence, their number of citations should be counted, [7] even when they are declared to be in the top class. So, the *g*-index is the unique largest number such that the top *g*-articles received together should be at least g^2 citations. It can be equivalently defined as the number of highly cited articles, such that each of them has an average of *g* citations [4]. Mathematically, it can be defined as follows:

$$g^2 \leq \sum_{i \leq g} c_i \quad (2)$$

Then, the value of *i* will give the *g*-index value of that particular author. The *g*-index is cumulative in nature, which means from time to time the value of *g*-index will increase gradually.

-*h*²-Index: It is denoted as *k* and defined as the highest rank, such that the first *k* publications each received at least k^2 citations. Mathematically, it can be defined as follows:

$$k^2 \leq x_k, (k+1)^2 > x_{k+1} \quad (3)$$

The *h*² index is also cumulative in nature, which means from time to time the value of *h*² index will increase gradually.

-R-Index: It is defined as square root of the sum of all citations of the article included in the h -core. The R -index is also cumulative in nature. Mathematically, it can be defined as follows:

$$R = \sqrt{\sum_{j=1}^h X_j} \quad (4)$$

4.2 Model

We implement these metrics on the chosen dataset and get the result of each metric index. As expected, the author rank varies in every individual method based on the way it is calculated. Thus, after detailed analysis, we find that calculating the average rank of the author is one of the best solutions to overcome the above problem. The idea is motivated by the fact that after calculating the average rank of the authors, the mean rank of ranks will not vary significantly. So, after fetching all the data of authors and arranging them according to their ranks, we find the ranks of the author based on different ranking methods, and then with the results obtained from the various baselines (different ranking methods here), we find the average of all ranking metric methods.

5 Results and Analysis

Sample result based on the baseline h -index and g -index is given in Table 1a, b, respectively. Table 2 gives the author ranking based on all the baseline metric methods that were chosen. From these tables, it can easily be seen that the rank of a particular author varies in every individual metric method. Different ranking methods show different rank results for each author. For some authors, their ranking is the same, but for most of the authors, their ranking is not the same in other metrics. It has been noticed that for a particular author, in one method, it is showing the highest rank. But at the same time, his/her rank is decreasing by 10. In h -index method, **Jiawei Han** is at rank 3, and in r -index method, he stands at position number 13. Thus, different metrics provide different ways of judging the authors. Due to this, it may happen that the morality of the particular author will be down. Thus, there is no universal metric to judge the quality of authors and their work on common grounds. After implementing the proposed method, we get a better result and way for ranking the authors. Table 3 gives the ranking of the authors based on the proposed average ranking method. With the help of average rank of all the metrics, we compensate the difference in higher and lower values of different metric measures. Figure 3 shows the comparison chart for the several baselines and the proposed method.

Table 1a, b Sample result based on the h-index and g-index

h-Index		g-Index	
Author	h-Index value	Author	g-Index value
Hector Garcia-Molina	50	Rakesh Agarwal	114
Scott Shenker	47	Scott Shenker	93
Jiawei Han	44	Ian T. Foster	93
Christos Faloutsos	43	HariBalkrishnana	88
Rakesh Agrawal	41	Adil Shamir	85
MoniNaor	41	Hector Garcia-Molina	84
Anil K. Jain	40	Robert Morris	82
Thomas A. Henzinger	40	David E. Culler	81
Philip S. Yu	40	Jiawei Han	80
Christos H. Papadimitriou	40	Christos Faloutsos	80
JenifferWidom	40	Anil K. Jain	78
Rajeev Motwani	39	Jon M. Kleinberg	77
DeobrahEstrin	39	Leslie Lamport	77
HariBalakrishnan	38	Rajeev Motwani	76
David J. Dewitt	37	DeobrahEstrin	76
MihirBellare	37	Jitendra Malik	76
W. Bruce Croft	37	MihirBellare	75

6 Conclusion and Future Work

Thus, this paper presents an extensive overview of different methods for calculating the author ranks given their citations and proposes a method to find a fair author ranking by exploiting the existing methods. It was observed that *h*-index and its variant show different ranking results on the same set of data. The inconsistency of the *h*-index ranking system can be overcome by adding additional parameter to evaluate the better ranking. The ranking of authors is calculated based on the average rank of the authors obtained by all the variants of *h*-index to overcome the fluctuation of the result.

Future work includes the implementation of a better ranking algorithm where the ranking is not only dependent on a single parameter but also dependent on others. All these dimensions of work will be addressed in the future.

Table 2 Sample result based on all the baseline metric methods

Rank	<i>h</i> -Index	<i>g</i> -Index	<i>h</i> ² -Index	<i>R</i> -Index
1	Hector Garcia-Molina	Rakesh Agarwal	Rakesh Agarwal	Rakesh Agrawal
2	Scott Shenker	Scott Shenker	Hector Garcia-Molina	Ian T. Foster
3	Jiawei Han	Ian T. Foster	David E. Culler	Scott Shenker
4	Christos Faloutsos	HariBalkrishnana	Robert Morris	HariBalakrishnan
5	Rakesh Agrawal	Adil Shamir	MoniNaor	Ramkrishnan Srikant
6	MoniNaor	Hector Garcia-Molina	Scott Shenker	Adi Shamir
7	Anil K. Jain	Robert Morris	Rajeev Motwani	Robert Morris
8	Thomas A. Henzinger	David E. Culler	Oded Goldreich	Hector Garcia-Molina
9	Philip S. Yu	Jiawei Han	Ian T. Foster	David E. Culler
10	Christos H.Papadimitriou	Christos Faloutsos	Jiawei Han	Leslie Lamport
11	JenifferWidom	Anil K. Jain	Christos Faloutsos	Jitendra Malik
12	Rajeev Motwani	Jon M. Kleinberg	DeobrahEstrin	Christos Faloutsos
13	DeobrahEstrin	Leslie Lamport	Leslie Lamport	Jiawei Han
14	Ian T. Foster	Rajeev Motwani	MihirBellare	DeobrahEstrin
15	Dan Suciu	DeobrahEstrin	Jennifer Widom	Anil K. Jain

Table 3 Sample result for the proposed average ranking method

Author's average rank
Rakesh Agarwal
Scott shenker
Hector Garcia-Molina
Ian T. Foster
Jiawei Han
David E. Culler
Christos Faloutsos
Rajeev Motwani
MoniNaor
Deborah Estrin
Anil K. Jain
HariBalakrishnan
MihirBellare
Jennifer widom
Oded Goldreich

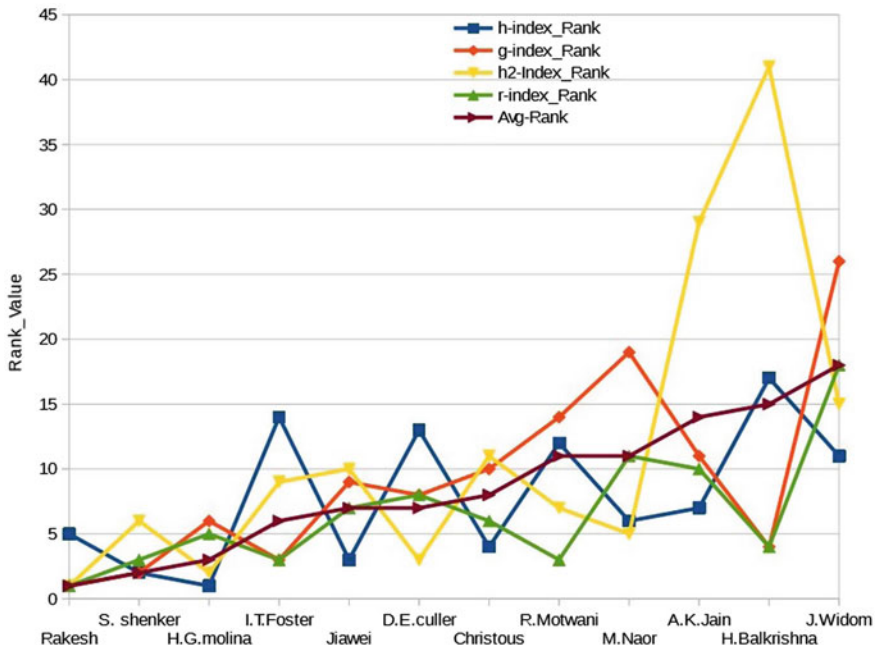


Fig. 3 Comparison chart of different rank metrics with average rank

References

1. Bornmann, L., Mutz, R., Hug, S.E., Daniel, H.D.: A multi level meta-analysis of studies reporting correlations between the h-index and 37 different h-index variants. *J. Inf.* **5**(3), 346–359 (2011)
2. Chakraborty, T., Kumar, S., Reddy, M.D., Kumar, S., Ganguly, N., Mukherjee, A.: Automatic classification and analysis of interdisciplinary fields in computer sciences. In: 2013 International Conference on Social Computing. pp. 180–187. IEEE (2013)
3. Ciaccio, E.J., Bhagat, G., Lebwohl, B., Lewis, S.K., Ciacci, C., Green, H.: Comparison of several author indices for gauging academic productivity. *Inf. Med. Unlocked* **15**, 100166 (2019)
4. van Eck, N.J., Waltman, L.: Generalizing the h- and g-indices. *J. Inf.* **2**(4), 263–271 (2008)
5. Egghe, L.: An improvement of the h-index: The g-index. ISSI (2006)
6. Egghe, L.: Theory and practice of the g-index. *Scientometrics* **69**(1), 131–152 (2006)
7. Egghe, L., Rousseau, R.: An informetric model for the hirsch-index. *Scientometrics* **69**(1), 121–129 (2006)
8. Hirsch, J.: An index to quantify an individual's scientific research output that takes into account the effect of multiple coauthorship. *Scientometrics* **85**(3), 741–754 (2010)
9. Hirsch, J.E.: An index to quantify an individual's scientific research output. In: Proceedings of the National academy of Sciences **102**(46), 16569–16572 (2005)
10. Paul, P.S., Kumar, V., Choudhury, P., Nandi, S.: Temporal analysis of author ranking using citation-collaboration network. In: 2015 7th International Conference on Communication Systems and Networks (COMSNETS). pp. 1–6. IEEE (2015)
11. Prathap, G., et al.: The inconsistency of the h-index. *J. Assoc. Inf. Sci. Technol.* **63**(7), 1480–1481 (2012)

12. Rousseau, R.: Woeginger's axiomatisation of the h-index and its relation to the g-index, the h^2 -index and the R^2 -index. *J. Inf.* **2**(4), 335–340 (2008)
13. Tang, J., Zhang, J., Yao, L., Li, J., Zhang, L., Su, Z.: Arnetminer: extraction and mining of academic social networks. In: Proceedings of the 14th ACM SIGKDD international conference on Knowledge discovery and data mining. pp. 990–998. ACM (2008)

A Survey Report on Recent Progresses in Nearest Neighbor Realization of Quantum Circuits



Anirban Bhattacharjee, Chandan Bandyopadhyay, Bappaditya Mondal,
and Hafizur Rahaman

Abstract The thrive of attending very fast computation has bred the ideas for new computing paradigms like optical computing, quantum computing, and in the last few years, quantum computing has left an impressive footprint before the design industry. Even companies like IBM, Microsoft are claiming the initiation of physical implementation of quantum circuits in on-chip units. But the successful implementation of this circuit needs to satisfy several design constraints and one such constraint is Nearest Neighbor (NN) enforcement. To introduce the reader with the progress made in NN-based implementation of quantum circuits, here, in this survey paper, we have tried to include some of the peer-reviewed works in our content. While describing the works, we have added necessary examples so that it becomes easy to follow for a reader. To this extent, we also have introduced the NN logic and its related cost functions in our survey report.

Keywords Quantum circuit · Quantum gate · Nearest neighbor (NN) · SWAP gate · Quantum cost (QC)

1 Introduction

Emergence of quantum computing has made an alluring effect among the research community due to its proficiency in solving some complicated problems with exponential speedup over conventional computing paradigm. As a result, realization

A. Bhattacharjee (✉) · C. Bandyopadhyay · B. Mondal · H. Rahaman

Department of Information Technology, Indian Institute of Engineering Science and Technology, Howrah, West Bengal 711103, India

e-mail: anirbanbhattacharjee330@gmail.com

C. Bandyopadhyay

e-mail: chandanb.iiest@gmail.com

B. Mondal

e-mail: bappa.arya@gmail.com

H. Rahaman

e-mail: rahaman.h@gmail.com

© Springer Nature Singapore Pte Ltd. 2020

M. Pant et al. (eds.), *Soft Computing: Theories and Applications*,

Advances in Intelligent Systems and Computing 1154,

https://doi.org/10.1007/978-981-15-4032-5_7

towards a highly scalable and fault-tolerant quantum architecture [1] received tremendous attention. However, there exist many difficulties that prevent the practical realization of a real-time quantum computing device. In this conjecture, fault-tolerance behavior is considered as the essential driving factor towards the accomplishments of quantum circuit design. For this purpose, error-correcting codes like surface or steane codes found significant [1]. Moreover, these codes become applicable only for nearest neighbor quantum architecture. In other words, the implementation of error-correcting codes demands the qubits to interact with only adjacent neighbors. In addition to this, such nearest neighbor qubit interaction has also been regarded as the essential design parameter for the physical realization of some quantum technologies like ion-trap [2], quantum dots [3], superconducting qubits [4] and nuclear magnetic resonance [5]. Consequently, ensuring of nearest neighbor architecture is considered as the necessary design issue for quantum circuit synthesis.

Establishment of such nearest neighbor architecture can be acquired by making the nonadjacently placed qubits adjacent with the help SWAP gates. It can be carried out by exchanging the states of the qubits until they become adjacent. Following such a SWAP insertion procedure, in turn, enhances the design overhead of the resultant NN circuit. Optimization of the resultant NN architecture in terms of limited use of SWAP gates has become more challenging for the researchers such that the circuit overhead can be kept under control. In this regard, several research articles related to the efficient realization of NN structures have been discussed whereby the authors considered the SWAP optimization issue using various design algorithms. Here, in this survey paper, we are reviewing the progress made towards the efficient realization of the nearest neighbor quantum circuit.

The rest of the paper is organized as follows. In Sect. 2, we have introduced the preliminaries on the quantum circuit and the nearest neighbor constraint. A survey report on existing works of NN-based design is presented in Sect. 3 and finally, we conclude the paper in Sect. 4.

2 Background

Qubit is considered as the basic quantum information unit which can be modified using a sequence of quantum gates. This quantum unit is similar to bits used in classical computing but unlike bit, qubit has numerous states between 0 and 1-known as a superposition state. This superposition state can be expressed using the following expression:

$$|\Psi\rangle = \alpha|0\rangle + \beta|1\rangle \quad (1)$$

where the terms α and β are the complex probability amplitudes of the respective basis states $|0\rangle$ and $|1\rangle$ provided the condition $\alpha^2 + \beta^2 = 1$ is satisfied.

Basically, quantum gates perform quantum operations on the states of the qubit which can be realized by means of unitary matrices. In other words, quantum computations on an n -qubit system are carried out by multiplying relevant $2^n \times 2^n$ unitary matrices.

Definition 1 Quantum gates are considered as the basic quantum operators used for manipulating qubits and a cascade of such gates along with the set of circuit lines on which they act together forms a quantum circuit.

Quantum gates employed in quantum circuit realization belongs to universal quantum gate libraries. NCV [6, 7] is considered as the most widely used gate library containing basic quantum gates like NOT, CNOT, controlled-V, and controlled- V^\dagger , respectively (the symbolic notation of basic gates has been depicted in Table 1).

For implementing quantum circuit, nearest neighbor qubit interaction condition needs to be preserved. In order to arrive towards such a design constraint, SWAP gates (symbolically represented in Fig. 1) are inserted in front of gates with nonadjacent interacting qubits and interchange their locations till they become adjacent. This procedure of making the interacting qubits adjacent is considered as the Nearest Neighbor (NN) phenomenon.

Definition 2 Nearest Neighbor cost (NNC) is considered as the distance separating the positions of the input qubits (control/target) of any 2-qubit gate and such difference in distance value can be computed as

Table 1 Symbolic representation of some quantum gates

Gates	Symbol	Gates	Symbol
NOT		Controlled-V	
CNOT			
V		Controlled- V^\dagger	

Fig. 1 SWAP gate structure

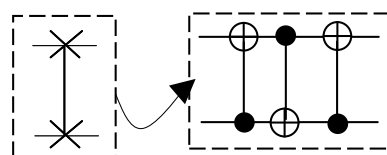
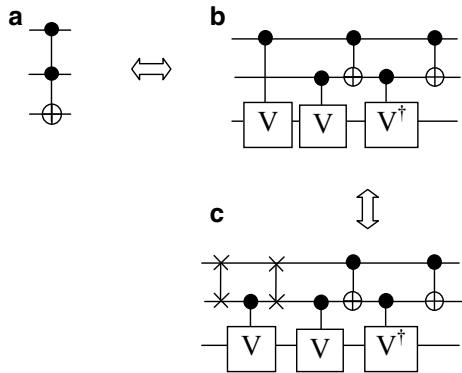


Fig. 2 **a** Toffoli gate Structure. **b** NCV realization of Fig. 2a. **c** NN structure of Fig. 2b



$$\text{NNC}(g) = |c - t| - 1 \quad (2)$$

The expression shown above estimates the nearest neighbor cost of any specific gate g with its control and target qubits placed at locations c and t , respectively. Combining such costs of the individual gates leads to an overall cost ($\text{NNC}(C)$) for the given quantum circuit C and can be expressed as

$$\text{NNC}(C) = \sum \text{NNC}(g) \quad (3)$$

By investigating the above expression it can be inferred that a given circuit satisfies the nearest neighbor property if it either contains 1-qubit gates or having only 2-qubit gates with qubits placed at adjacent positions. More precisely, if the cost estimation expression given in (3) evaluates to zero then the circuit can be considered as NN-compliant.

Example 1 Consider a Toffoli gate shown in Fig. 2a and its equivalent NCV representation. By investigating Fig. 2b, it can be inferred that this NCV structure does not satisfy the nearest neighbor criteria as the NNC of the circuit turns out to be more than zero ($\text{NNC}(C) = 1$). To transform this circuit into its equivalent NN realization SWAP gates are implemented and the resultant circuit is depicted in Fig. 2c.

3 Works on NN-Based Representation

Last couple of years has witnessed several progress in the field of NN-based representation, where the authors have mainly worked towards the efficient realization of such designs. Not only embedding SWAP gates in designs remain the sole objective of these works, but the incorporation of several design strategies like global reordering, local reordering, windowing policy have also been followed to contain the usage of SWAP gates. On the other side, the representation of NN circuit has changed from

1D to 2D and even the concept of n-D has come into the picture. Here, we have tried to include some of the peer-reviewed works and their contributions.

To achieve circuits with linear NN architecture, the existing design workflows have been extended in the article [8]. Here, template matching based post-optimization approach, exact design methods as well as reordering strategies viz. Global and Local are introduced. The existing synthesis algorithms may not generate an optimal circuit with respect to the number of elementary gates used to realize the desired function so the quantum cost of the resultant circuit is not minimal. To simplify the resultant circuits, template-based optimization strategies are applied. Furthermore, the exploitation of such template approaches not only reduces the quantum cost but also realizes optimal NN-compliant circuit thereby several NNC based templates are designed. The idea behind using templates is to replace a set of gates by another set while at the same time preserving the functionality of the circuit. After implementing templates, the circuit is further NN optimized using traditional matching rules like deletion and moving.

For better interpretation, a NN circuit shown in Fig. 3a is considered and the equivalent NN optimal circuit obtained after using template matching rules is represented in Fig. 3b.

Besides using templates, an optimal circuit can also be generated by employing exact design methodology. The purpose of using such exact synthesis approaches is to construct an optimal quantum architecture both in terms of minimal quantum cost as well as NN optimality. To this end, the design problem has been expressed in the form of a SAT solving instance as discussed in the article [8].

Example 2 Consider again the Toffoli gate represented in Fig. 2a and also its corresponding decomposed network as depicted in Fig. 2b. The nonoptimal circuit in Fig. 2b is optimized with respect to NNC using the exact design approach of [9] is shown in Fig. 4b over the one obtained using Naïve approach (see Fig. 4a).

Although an efficient NN quantum architecture is obtained using the previous design strategies, these solutions can be improved further by changing only the initial ordering of the qubits. Qubit reordering techniques reduce some additional NN overhead in the circuit thereby produces better NN structures. To this end, a couple of heuristic design schemes have been employed in [8] of which one of them rearranges the qubits from a global perspective while the other one changes the line order locally.

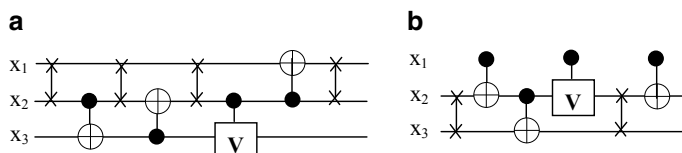


Fig. 3 **a** NN circuit having quantum cost of 16. **b** NN circuit with quantum cost of 10

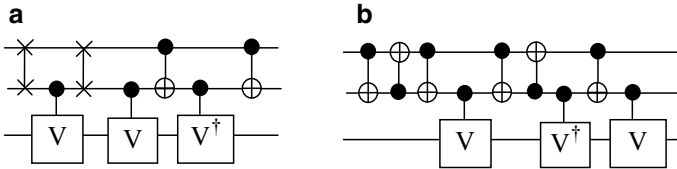


Fig. 4 **a** NN structure using naïve method (quantum cost is 11). **b** Improved NN circuit with quantum cost of 9

To clearly understand the heuristics used for determining an appropriate qubit ordering is illustrated in the example presented next.

Example 3 Considering the circuit shown in Fig. 5a whose original qubit ordering is changed globally. The contribution of each qubit towards NNC in the circuit is computed and based on this estimated value the qubits are reordered accordingly. The resultant reordered circuit after global reordering is depicted in Fig. 5b. However, the application of local reordering strategy on the circuit (see Fig. 5a) produces an equivalent NN-complaint circuit in Fig. 5c).

All the design workflows discussed so far are integrated together and appended to the existing quantum circuit synthesis algorithms so as to explicitly consider the NN restriction into account and such an attempt has been the underlying proposition of the work [8].

The NN design structures obtained using the approaches stated in [8] are not optimal so there exists an opportunity for further improvement. For this purpose, NN optimization of quantum circuits in single-dimensional representation has been addressed in [9]. Here, the nearest neighbor optimization problem has been transformed into a Minimum Linear Arrangement (MINLA) problem. Initially, the optimization problem is represented in the form of an interaction graph for a given circuit. Thereafter, the given circuit is partitioned into sub-circuits where qubits are reordered for each sub-circuits such that a localized circuit with adjacent gates is obtained. For this purpose, SWAP gates are implemented in-between sub-circuits so as to generate the desired qubit ordering for each of them. This has been done by constructing interaction graphs for each sub-circuit and then the MINLA approach is applied to them separately. In other words, each nonadjacent gate in each sub-circuit

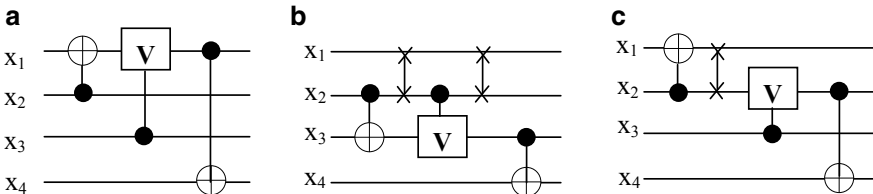


Fig. 5 **a** Sample Circuit. **b** Globally reordered circuit of Fig. 5a. **c** Locally reordered circuit of Fig. 5a

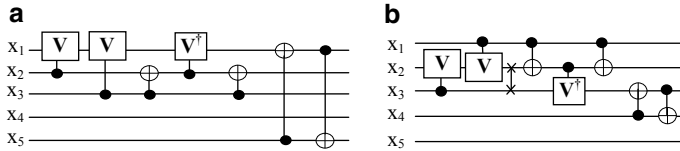


Fig. 6 **a** Nonlocal benchmark circuit (4gt11_84). **b** Local circuit of Fig. 6a obtained using MINLA

needs to be made NN-compliant by locally rearranging the qubits order involved in the sub-circuits. The solutions obtained after solving each sub-circuits may not generate a unique result and to resolve this the one that minimizes the total SWAP gate requirements in-between all the sub-circuits is selected otherwise anyone is chosen randomly. Additionally, a look-ahead strategy is implemented to improve the solutions obtained using MINLA.

For the better realization of the proposed approach, a sample benchmark circuit named 4gt11_84 has been considered as shown in Fig. 6a. From Fig. 6a, it can be discerned that the given circuit contains nonlocal gates (nonadjacent) so to transform it into a local circuit the proposed MINLA approach is implemented and the resultant circuit is depicted in Fig. 6b.

All these existing linear NN design methodologies are based on the heuristic policy which produces suboptimal or near-optimal solutions. An alternative synthesis workflow involving the exact methodology based on constraint solvers has been introduced in [10]. Here, both global and local reordering strategies are discussed determining the best linear qubit order sequence thereby producing an optimal NN circuit.

To find the best global qubit order, the NNC value is recomputed after generating every permutation and comparing it with the one obtained in the previous sequence rather than considering the NNC impact of each qubit as done in [8]. For this purpose, initially, an adjacency matrix of a given circuit is constructed and then a modified cost function presented in [10] is employed for evaluating such qubit sequences.

To have a better interpretation, an example is provided illustrating the realization of globally ordered quantum circuit using the exact NN optimization scheme stated in [10].

Example 4 Consider the quantum circuit represented in Fig. 7a with initial qubit order $\pi(q_0 \ q_1 \ q_2 \ q_3 \ q_4)$. Execution of an exact reordering strategy stated in [10] obtains an optimal NN-based representation requiring only two SWAP gates (see Fig. 7b) compared to the architecture achieved using heuristic method (see Fig. 7c) stated in [8].

Like the global approach, an exact local optimization method based on pseudo-Boolean optimization solvers is discussed in [10] for producing optimal NN solutions. Determining the best local qubit ordering sequence from all possible options can be done by evaluating the cost using inversion vectors. The resultant value obtained after combining the individual entries of the inversion vector corresponds to the amount

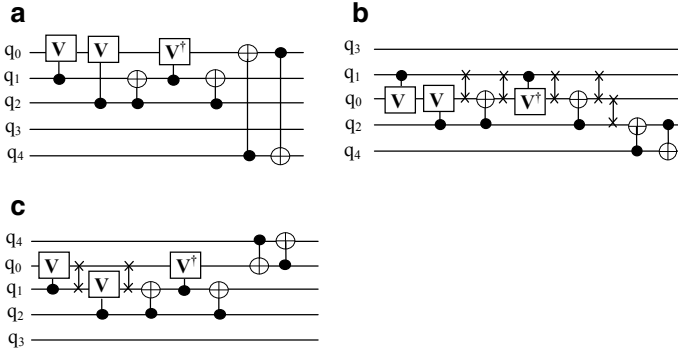


Fig. 7 **a** Input quantum circuit. **b** NN circuit obtained using exact global optimization approach of [10]. **c** NN circuit obtained using heuristic global optimization approach [8]

of SWAP operations needed to create a specific qubit sequence order. However, such estimation procedure does not turn out to be beneficial for qubit rearrangement. Therefore, possible permutation options for all gates in the given circuit are considered and evaluated using the cost function stated in [10]. Finally, the ordering having a least-cost value is implemented. To find such best order within a reasonable time-bound, the design problem has been formulated in the form of Boolean satisfiability representation as discussed in [10].

Although the implementation of exact design methodology produces an optimal NN-compliant circuit such strategies hardly found feasible for circuits with large number of qubits due to huge computational time requirements. For this purpose, an efficient heuristic synthesis workflow based on local reordering approach has been presented in the article [11] that improves the NN architecture in terms of cost reduction and also satisfies scalability. For such efficient NN realization, an N -gate based look-ahead methodology has been employed which makes any nonadjacent gate g adjacent by observing the effect on N following gates and inserts SWAP gates in such a manner so that less SWAP gate is required for the following gates.

However, there can be instances in which change of either control/target qubit positions of any nonadjacent gate may not have any effect on the following gates. All such possible cases are identified and categorized into four different classes based on various gate combinations. These classes are formed estimating the effect of moving the control/target qubit positions of any current gate g_c by considering a pair of each N gates. For each of these classes, control and target qubit positions are permuted in all possible manners so as to obtain the total SWAP count needed to move the control or target qubit of g_c downwards. In this manner, a given circuit is made NN-compliant by scanning it from the left and inserting SWAP gates as needed.

To get a better apprehension of the SWAP cost calculation an illustrative example has been provided next.

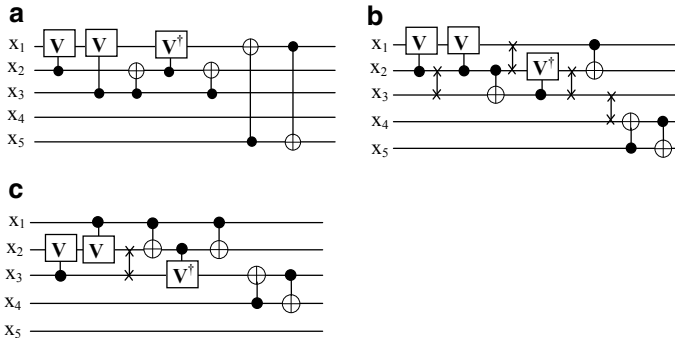


Fig. 8 **a** Benchmark Function (4gt11_84). **b** NN representation using look-ahead on three gates. **c** NN representation using look-ahead only on the next immediate gate or on one gate

Example 5 Consider a benchmark function shown in Fig. 8a which needs to be made NN-compliant using heuristic look-ahead scheme stated in [11]. The equivalent NN design obtained using look-ahead process by considering only three following gates is represented in Fig. 8b. An improved solution with less NNC can be realized when applying look-ahead process considering only a single gate is depicted in Fig. 8c.

All these design approaches transform a given quantum circuit to its equivalent linear NN representations. But such architecture restricts the qubits to have only two adjacent neighbors which in turn increases the design overhead in the resultant NN circuit. However, technological advancements lead to the development of 2D representation whereby the number of interacting neighbors rises from two to four for a qubit. For this purpose, the authors of [12] presented a synthesis automation model that improves the qubit interactions for quantum technologies using 2D representation. To reflect such higher dimensional NN design, some placement procedure needs to be developed for arranging the qubits in 2D structures and an attempt based on Mixed Integer Programming (MIP) is employed in the work [12]. Here, the synthesis workflow uses two methods of which one of them (Method 1) relies only on single grid-based MIP model where SWAP gates are simply added before any nonadjacent gates after initial qubit arrangement. In the other method (Method 2), the mapping problem is solved by partitioning the given circuit into sub-circuits and for each of them qubit mappings are determined and SWAP gates are added in each sub-circuit similar to Method 1. In addition to this, a swapping network is needed to transform the qubit placement derived in one sub-circuit to the placement used in the other one. To realize this swapping between any two consecutive sub-circuits, a bubble sort algorithm is implemented on the 2D structure. The 2D results obtained from the proposed design methods in [12] (Method 1, Method 2) clearly outperforms the best 1D results by reducing the SWAP gate count substantially.

The 2D result obtained in [12] is improved further by employing a fast and efficient qubit mapping scheme which has been the underlying objective of the work [13]. The significance of appropriate grid size along with initial qubit mapping has been

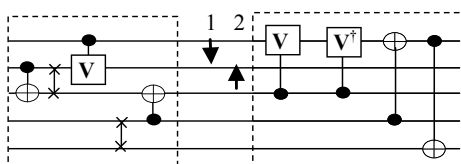
discussed in [13]. In this regard, finding proper grid size is considered as the essential optimization problem and addressed by formulating heuristic estimation models. Following this, the input qubits are arranged on such 2D grid by running an initial qubit mapping algorithm. For this purpose, a priority stack is used defining the order of selecting the qubits and subsequently placed on the grid structure using the corresponding qubits interactions. Finally, SWAP gate insertion process is followed whereby row and column difference of the nonadjacent interacting qubits is computed such that they can be made adjacent by moving them either horizontally or vertically.

The NN results obtained in [13] can be improved further by exploiting an even better qubit mapping approach and this has been addressed in the works [14, 15] whereby the entire process is segmented into three stages of qubit selection, qubit placement, and SWAP insertion. Selection and placement of qubits are conducted based on some metrics developed using the interaction details of the qubits in the given circuits. In [14], qubits are arranged onto a 2D structure using the interaction time of the corresponding qubits while cost factor metric is estimated for qubit mapping purpose discussed in [15]. Finally, SWAP gates are inserted by examining each gate in the given circuit leads to an NN-compliant circuit.

The workflow introduced in [16] discusses an efficient heuristic mapping approach providing better results compared to previous approaches irrespective of any specific dimensional representations. Here, a global reordering scheme is designed using both exhaustive and genetic algorithm-based search procedures. Afterward, a local reordering process considering all possible paths occurring between any two interacting qubits is implemented. Both the reordering schemes employ an improved cost estimation function stated in [16]. Though the use of exhaustive strategy produces optimal results but found infeasible for large circuits and thereby an alternative heuristic-based genetic algorithm is applied. After populating the qubits on given architecture, SWAP gates can be inserted in various ways considering only the one having least-cost value on a path chosen randomly from the available paths. Furthermore, the proposed method can be extended to higher or multidimensional architectures.

Example 6 Consider the circuit shown in Fig. 9 where the dashed region marked on the left side of the circuit designates the set of gates with adjacent interacting qubits after performing SWAP operations while the one on the right represents the gates with nonadjacent qubits. To make these gates adjacent, SWAP gates need to be applied in the best possible manner for a given path. The arrows shown in Fig. 9 indicate that there exist two possible ways in which SWAP gate can be inserted to make the corresponding gate adjacent.

Fig. 9 SWAP insertion process



4 Conclusion

NN constraint is found to be one of the major hindrances towards the physical implementation of the quantum circuit and to highlight the progress made in this field, in this paper, we have surveyed some of the state-of-art design techniques and their contributions. Starting from 1D representation to 2D and in later part, we have surveyed the works on n-D NN architecture as well. Strategies like gate reordering, line reordering, windowing techniques are also included in this review paper.

References

1. Chow, J.M., Gambetta, J.M., Magesan, E., Abraham, D.W., Cross, A.W., Johnson, B., Masluk, N.A., Ryan, C.A., Smolin, J.A., Srinivasan, S.J. et al.: Implementing a strand of a scalable fault-tolerant quantum computing fabric. *Nat. commun.* **5**, (2014)
2. Kielpinski, D., Monroe, C., Wineland, D.J.: Architecture for a largescale ion-trap quantum computer. *Nature* **417**(6890), 709–711 (2002)
3. Taylor, J., Petta, J., Johnson, A., Yacoby, A., Marcus, C., Lukin, M.: Relaxation, dephasing, and quantum control of electron spins in double quantum dots. *Phys. Rev. B* **76**(3), 035315 (2007)
4. Blais, A., Gambetta, J., Wallraff, A., Schuster, D., Girvin, S., Devoret, M., Schoelkopf, R.: Quantum information processing with circuit quantum electrodynamics. *Phys. Rev. B* **75**(3), 032329 (2007)
5. Criger, B., Passante, G., Park, D., Laflamme, R.: Recent advances in nuclear magnetic resonance quantum information processing. *Philos. Trans. R. Soc. London A: Math., Phys. and Eng. Sci.* **370**(1976), 4620–4635 (2012)
6. Barenco, A., Bennett, C.H., Cleve, R., DiVincenzo, D.P., Margolus, N., Shor, P., Sleator, T., Smolin, J.A., Weinfurter, H.: Elementary gates for quantum computation. *Phys. Rev. A* **52**(5), 3457 (1995)
7. Miller, D.M., Wille, R., Sasanian, Z.: Elementary quantum gate realizations for multiple-control Toffoli gates. In: IEEE International Symposium on Multiple-Valued Logic (ISMVL), pp. 288–293, Finland (2011)
8. Saeedi, M., Wille, R., Drechsler, R.: Synthesis of quantum circuits for linear nearest neighborarchitectures. *Quant. Inf. Proc.* **10**(3), 355–377 (2011)
9. Shafaei, A., Saeedi, M., Pedram, M.: Optimization of quantum circuits for interaction distance in linear nearest neighbor architectures. In: 50th Design Automation Conference, USA (2013)
10. Wille, R., Lye, A., Drechsler, R.: Exact reordering of circuit lines for nearest neighbor quantum architectures. *IEEE Trans. on CAD* **33**(12), 1818–1831 (2014)
11. Kole, A., Datta, K., Sengupta, I.: A heuristic for linear nearest neighbor realization of quantum circuits by SWAP gate insertion using N-gate lookahead. *IEEE J. Emerg. Sel. Topics Circ. Syst.* **6**(1), 62–72 (2016)
12. Shafaei, A., Saeedi, M., Pedram, M.: Qubit placement to minimize communication overhead in 2D quantum architectures. In: Proceeding of ASP Design Automation Conference, pp. 495–500, Singapore (2014)
13. Shrivastwa, R. R., Datta, K., Sengupta, I.: Fast qubit placement in 2D architecture using nearestneighbor realization. In: Proceeding of Int'l Symposium on Nanoelectronic and Information Systems, pp. 95–100, 2015
14. Bhattacharjee, A., Bandyopadhyay, C., Wille, R., Drechsler, R., Rahaman, H.: A novel approach for nearest neighbor realization of 2d quantum circuits. *IEEE Comput. Soc. Ann. Symp. on VLSI* (2018). <https://doi.org/10.1109/ISVLSI.2018.00063>

15. Bhattacharjee, A., Bandyopadhyay, C., Biswal, L., Rahaman, H.: A heuristic qubit placement strategy for nearest neighbor realization in 2d architecture. In 22nd International Symposium on VLSI Design and Test, pp. 593–605, Singapore (2018)
16. Kole, A., Datta, K., Sengupta, I.: A new heuristic for n-dimensional nearest neighbour realization of a quantum circuit. IEEE Trans. on Comput.-Aided Des. of Inte. Circ. and Sys. **37**(1), pp. (99) 1–1, (2017)

Annual Rainfall Prediction Using Time Series Forecasting



Asmita Mahajan, Akanksha Rastogi, and Nonita Sharma

Abstract This paper attempts to determine which one of the various univariate forecasting techniques is producing accurate and statistically compelling forecasts for rainfall. The term “univariate time series” is referred as a time series that consists of a sequence of measurements of the same variable collected over regular time intervals. Forecasting techniques to predict rainfall are an important aspect as they are useful for business purposes, to take into account the transportation hazards that is a result of heavy rainfall, also it helps farmers and gardeners to plan for crop irrigation and protection. Most commonly, the techniques for prediction are regression analysis, clustering, autoregressive integrated moving average (ARIMA), error, trend, seasonality (ETS) and artificial neural network (ANN). In this paper, a review is provided based on different rainfall prediction techniques for predicting rainfall as early as possible. This paper has compared the performance of various forecasting techniques such as ARIMA, ANN, ETS based on accuracy measures like mean square error (MSE), root mean square error (RMSE), mean absolute percentage error (MAPE) and mean absolute error (MAE). On comparing these techniques, it is evident that ARIMA is performing well on the given data.

Keywords Forecasting · ARIMA · ETS · NNAR · Annual rainfall prediction · Accuracy measures

1 Introduction

Agriculture is the main and foremost aspect on which the economy of India depends as India is an agricultural country [1]. For the better economic growth of our country, early prediction of rainfall [2] is necessary because the agriculture of India

A. Mahajan (✉) · A. Rastogi · N. Sharma
Dr. BR Ambedkar National Institute of Technology, Jalandhar 144011, India
e-mail: asmita.95mahajan@gmail.com

A. Rastogi
e-mail: arastogi.305@gmail.com

N. Sharma
e-mail: nsnonita@gmail.com

highly depends and is affected by rainfall. In mid-July 2017, [3] a group of farmers in Anandgaon village in Beed district of Maharashtra filed a police complaint [4] against the Indian Meteorological Department (IMD). They accused the department, which forecasts weather, of misleading them. IMD was threatened by the farmers in Maharashtra to shut down their [5] department if they are not able to forecast accurately. This paper tries to assess the error-free forecast of rainfall.

Forecasting as [6] the name suggests is the process of guessing the future accurately with the help of the past and present data and also by [7] analysing any trend associated with the data. For generating an accurate and sensible forecast, there are two simple steps. The first step is to collect the useful data required for forecasting and gather some information that will help to produce an accurate forecast. The second step is choosing a forecasting technique that will use the gathered [8] information to calculate future predictions.

Some of the forecasting techniques that are used to predict data time series having trend and seasonality are ARIMA, ETS and neural network autoregression (NNAR). ARIMA is a forecasting technique that is used to predict [9] the future values of a series based on its own criteria. ARIMA is used on the data that is stationary, i.e. variance and standard deviation exhibited by the data are constant over time. Similar to ARIMA which is superior, the exponential smoothing forecasting method is a linear combination of the past data, each associated with some weights. The weights are assigned giving more importance to [10] the recent observations compared to the past observations. Lastly, to discover patterns from the data, a class of nonlinear models, i.e. neural networks, is useful.

The accuracy measures used in this paper to compare the techniques mentioned above are MAE, MSE, MAPE and RMSE. MAE is the average [11] absolute error value; the forecast with the MAE value close to zero is considered to be an effective forecast. MSE is defined as the mean or average of the squared error values. RMSE is defined [12] as the square root of the mean or average of the squared error values. MAPE is the mean or average of the absolute percentage errors of the forecast. The standards Akaike information criteria (AIC) and Bayesian information criteria (BIC) are also included to compare the models implicitly. The method which [13] will be used for comparison and prediction is the one which gives the best accuracy over the others.

The rest of the paper is arranged as follows: Sect. 2 gives the methodology employed in this paper; Sect. 3 discusses the results and discussions of the finding, and Sect. 4 gives the conclusion. Comparing the different models used in this paper, it is clear that the ARIMA model best predicts the rainfall and provides some good results for the data given.

2 Methodology

This section of the paper is all about defining different forecasting models that are used for annual rainfall prediction. Lets us assume y_1, y_2, \dots, y_T as the past data,

$y_{T+h|T}$ represents forecasted values evaluated from y_1, y_2, \dots, y_T . Different techniques of forecasting are discussed below.

2.1 ARIMA Method

The ARIMA model depicts the stationary data as function of autoregressive and moving average parameter. The AR component performs regression on the data with the use of the past data. The MA component models the error term as a linear combination of the errors occurred in the past time periods. The abstraction of an autoregressive moving average (ARMA) model is called as autoregressive integrated moving average(ARIMA) model. If the series is non-stationary, differencing is done to make the series stationary, and this step is repeated till the data becomes stationary [10, 11]. Given a time series data X_t , when the series is stationary $x_t = X_t$ when series is not stationary, and differencing is required only once $x_t = X_t - X_{t-1}$

And the general equation for the ARIMA model is given as

$$X_t = c + \sum_{i=1}^p \phi_i x_{t-i} - \sum_{i=1}^p \theta_i \epsilon_{t-i} \quad (1)$$

where ϕ_i is the AR parameter, θ_i is the MA parameter, and ϵ_t is the series of random unknown errors.

2.2 Simple Exponential Smoothing Method

In this, the forecast values predicted are the weighted mean of previous knowledge or observations, with the weights inversely proportional to the time at which the data is collected. The range for the value of α is between zero and unity. Each weight associated with an observation shows a decreasing trend. If the value of α is close to zero, we have to give more weightage to past observations. If the value of α is close to unity, we have to give more weightage to immediate observations [9, 10]. The equation is given as follows:

$$y_{t+h|t} = \sum_{j=1}^t \alpha^{t-j} (1 - \alpha)^t l_0 \quad (2)$$

where $(0 \leq \alpha \leq 1)$.

2.3 ETS Method

ETS model, which is also commonly known as state space model, considers the dimensions error, trend and seasonality associated with the time series data. Each dimension error, trend and season is given a type, i.e. additive, multiplicative and none.

ETS (Error, Trend, Season):

Error = (A, M)

Trend = (N, A, M)

Season = (N, A, M)

ETS (A, N, N) denotes simple exponential smoothing with additive errors

Point forecast for the model ETS (M, A, N) is given by:

$$\begin{aligned} y_t &= (u_{t-1} + v_{t-1})(1 + \epsilon_t) \\ u_t &= (u_{t-1} + v_{t-1})(1 + \alpha\epsilon_t) \\ v_t &= v_{t-1} + \beta(u_{t-1} + v_{t-1})\epsilon_t \end{aligned} \quad (3)$$

2.4 Neural Network

Neural network is an iterative learning method in which the time series data is used as an input to the network. Each data point is associated with some weight which is adjusted over time with each iteration [12, 13]. For prediction purposes, the feed-forward neural network with a single hidden layer is used. Basic equation:

$$y_t = \begin{cases} 1 & \text{if } \sum_j w_{ij}x_j - \theta_j > 0 \\ 0 & \text{otherwise} \end{cases} \quad (4)$$

where y_i is output function, x_i is input, and w_{ij} are the weights associated with each input.

NNAR model equation:

$$y_i = f(y_{t-i}) + \epsilon_t \quad (5)$$

where f is the neural network with the hidden nodes in single layer.

2.5 Measures of Accuracy

The techniques discussed so far have to be evaluated on the basis of accuracy based on their prediction. Error is calculated between the predicted values and the actual values of the data. These errors are then compared, and the model with the least error is the best. Let us assume that A_t is the actual data at t th time and F_t is the predicted

value, where $t = 1, 2, \dots, T$. The equations related to various accuracy measures used in this paper are given below.

$$\text{MAE} = \frac{1}{T} \sum_{t=1}^T |A_t - F_t| \quad (6)$$

$$\text{MSE} = \frac{1}{T} \sum_{t=1}^T (A_t - F_t)^2 \quad (7)$$

$$\text{RMSE} = \sqrt{\frac{\sum_{t=1}^T (A_t - F_t)^2}{T}} \quad (8)$$

$$\text{MAPE} = \frac{100}{T} \sum_{t=1}^T \frac{|A_t - F_t|}{A_t} \quad (9)$$

Akaike information criterion (AIC) has been used as a method to choose the best and accurate model, along with the accuracy measures. Distance usually a relative distance is determined between the true plausibility function of the data which is not known and the fitted plausibility function of the model. This distance plus the constant is used to assess the value of AIC. A model having lower AIC is considered to be close to the truth and is taken as the best model.

3 Results and Discussions

This section is divided into three parts. First section explains the job of data collection for annual rainfall from year 2010 to year 2017, from where the data has been taken, what is the data all about, etc. In the second section, the results of various forecasting techniques have been shown with the help of figures. And the last section shows the comparison of these techniques on the basis of their accuracy of predicting the annual rainfall for the year 2018 and hence analysing the most suitable model.

3.1 Annual Rainfall Data

Annual rainfall data set is prepared by assembling annual rainfall data of several areas of India as shown in Fig. 1. Data has been prepared from Climate Change Knowledge Portal (CCKP) and Open Government Data (OGD) Platform India. The annual rainfall data set accommodates 96 observations from January 2010 to December 2017 for rainfall measured in mm (millimetre). To study the pattern and nature the data

exhibits, a plot of the data points with respect to time has been drawn and shown in Fig. 2.

Before performing any preprocessing steps on the data, there is a need to define some observed patterns. A long-term upwards and downwards pattern in the data is referred to as a trend, whose nature can sometimes be nonlinear. Regular periodic fluctuations in data that occur within each 12 month period year after year are referred to as seasonality. When data exhibits ups and downs or movements from peak to contractions to depressions to expansion that are not of the fixed time period, then it is called as cyclic pattern. The residual fluctuations in the data series which exists after considering the unknown events are referred to as irregular pattern. Figure 3 describes graphically all the four fluctuations in the given data.

Figure 4 shows the ACF plot. It is used to analyse the randomness in the data, i.e. how much correlated the past data points are. As it is seen at lag 12, the value in the ACF plot is high, which is a depiction that a strong correlation exists between the successive data values.

▲	Rainfall....MM.	Year	Month	Country	ISO3
1381	7.65333	2016	Jan	India	IND
1382	9.33450	2016	Feb	India	IND
1383	21.29710	2016	Mar	India	IND
1384	21.30670	2016	Apr	India	IND
1385	63.54470	2016	May	India	IND
1386	149.41600	2016	Jun	India	IND
1387	322.16200	2016	Jul	India	IND
1388	235.77400	2016	Aug	India	IND
1389	156.57900	2016	Sep	India	IND
1390	51.03860	2016	Oct	India	IND
1391	8.62107	2016	Nov	India	IND
1392	9.65157	2016	Dec	India	IND
1393	25.45556	2017	Jan	India	IND
1394	9.14722	2017	Feb	India	IND
1395	33.61944	2017	Mar	India	IND
1396	47.88056	2017	Apr	India	IND
1397	77.32778	2017	May	India	IND
1398	232.57500	2017	Jun	India	IND
1399	322.08610	2017	Jul	India	IND
1400	277.41110	2017	Aug	India	IND
1401	191.00830	2017	Sep	India	IND
1402	103.78060	2017	Oct	India	IND
1403	22.35833	2017	Nov	India	IND

Fig. 1 Annual rainfall data set

Fig. 2 Annual rainfall in mm

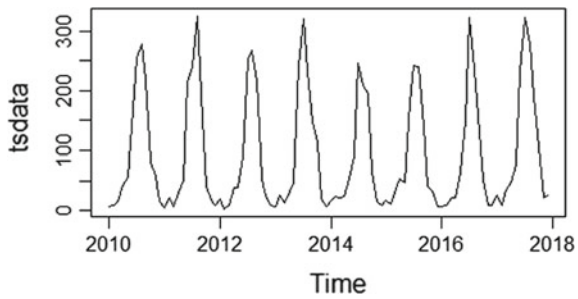


Fig. 3 Trend–seasonality analysis

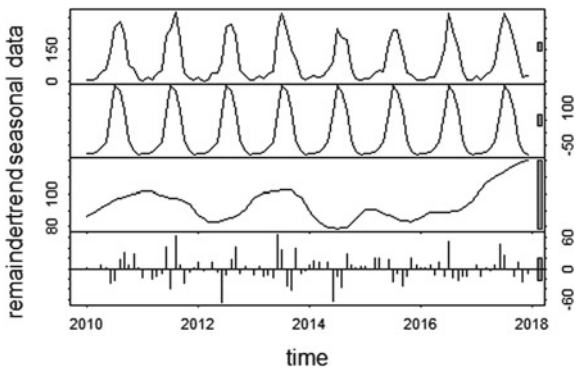
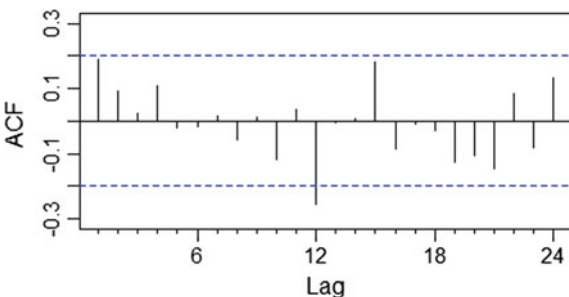


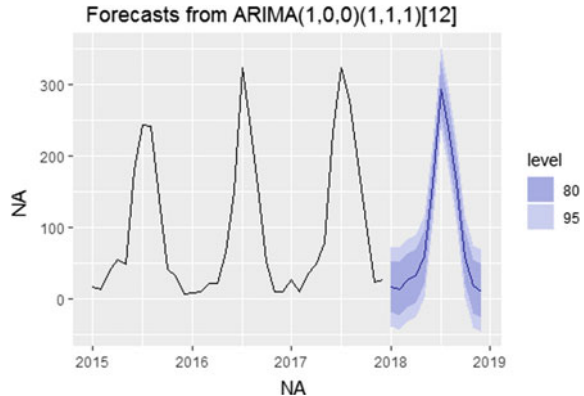
Fig. 4 Autocorrelation plot



3.2 Forecasts of Different Techniques

In this section, the forecasts using different techniques to predict the annual rainfall in India for the year 2018 are shown. The techniques used in this paper for forecasting are ARIMA, ETS and NNAR.

ARIMA uses Hyndman–Khandakar algorithm in the process of forecasting, in which the model which has minimum AIC value is considered to be an appropriate model with p , d and q parameters, where p is known to be the number of autoregressive terms, q represents the number of moving average terms, and d denotes

Fig. 5 ARIMA forecasting

the number of non-seasonal differences needed. ARIMA(p, d, q)(P, D, Q) model depicts seasonal ARIMA model.

In order to determine the best ARIMA model which will fit the data, firstly determine whether or not the difference is needed, i.e. whether the data is stationary or not. After this, apply the ARIMA model directly for forecasting. The ARIMA model selected for the given data to predict the annual rainfall is ARIMA(1,0,0)(1,1,1). In which, $p = 1$ depicts only one AR term, with no difference required as the given data is stationary and with no non-seasonal MA term. As in the given data, seasonality pattern has been observed; therefore, the model has one seasonal AR term and requires seasonal differencing only one time after which the data becomes stationary and one seasonal MA term. In Table 1, the estimated values for the ARIMA method are shown. In Fig. 5, a graphical representation of the predicted rainfall for the year 2018 from ARIMA method has been shown.

Forecasting process of ETS also uses the Hyndman algorithm. ETS(M, N, M) is used for this forecast which means it has multiplicative error level M , with no trend N and multiplicative seasonal component M . The smoothing parameters of fitted

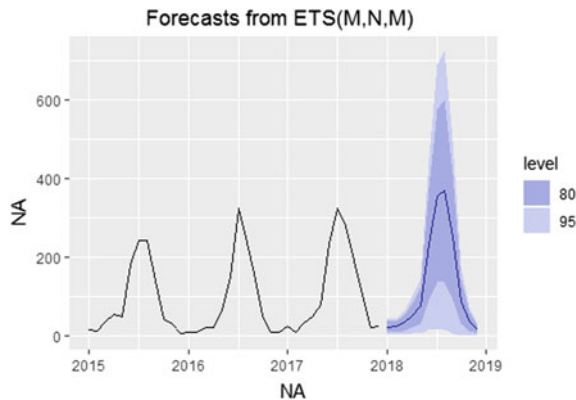
Table 1 Estimated values of ARIMA method

ARIMA(1,0,0)(1,1,1) [12]

Parameter	Estimate	Standard Error
AR1	0.2429	0.1066
SAR1	-0.4546	0.1493
SMA1	-0.4572	0.2006
Variance	810.1	-
AIC	816.07	-
BIC	825.8	-

Table 2 Estimated values of ETS method

ETS(M, N, M)	
Parameter	Estimate
Alpha	0.1734
Gamma	$2e^{-4}$
Sigma	0.4375
AIC	1043.278
BIC	1081.743

Fig. 6 ETS forecasting

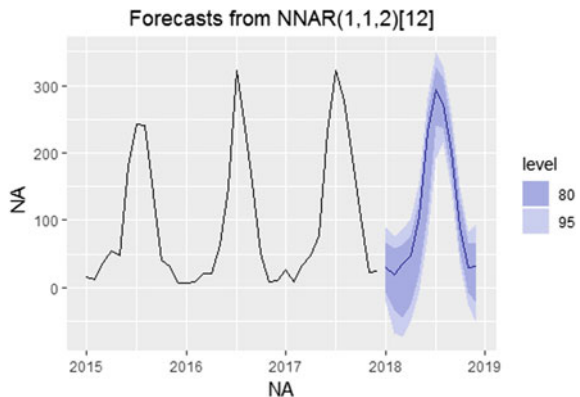
ETS model are $\alpha = 0.1734$ and $\gamma = 2e^{-4}$. Table 2 represents the estimated values of ETS method. The forecasted value from ETS technique is shown in Fig. 6.

A feed-forward network of the NNAR forecast is denoted by $NNAR(p, P, k)$ that indicates p as the number of non-seasonal lags used as inputs, P as the number of seasonal lags used as inputs and k as the number of nodes in the hidden layer. $NNAR(1,1,2)$ model is the one which fits best for the given data and denotes one non-seasonal lag, one seasonal lag and two hidden layers. The mean of 20 (2-2-1) networks with 9 weights is the generated model for the forecasting. The forecasted value from NNAR technique is shown in Fig. 7.

3.3 Error Analysis

The accuracy of each model was then observed based on the accuracy measures such as RMSE, MSE, ME, MAE and MAPE. Table 3 shows the comparison of the three models based on these accuracy measures.

The values for the RMSE accuracy measure turns out to be 26.144, 28.952 and 28.987 for ARIMA, ETS and NNAR, respectively. The values of MAE turn out to be 17.146, 19.545 and 21.408 for ARIMA, ETS and NNAR, respectively. The other error measures can be seen in Table 3. It is evident from the results that ARIMA is

Fig. 7 NNAR forecasting**Table 3** Comparison based on error terms of different models

Measures—Model	ARIMA	NNAR	ETS
MAE	17.14682	21.4089	19.5455
RMSE	26.14477	28.98724	28.95217
MAPE	35.10377	61.92725	41.71262
MASE	0.63795	0.97652	0.72720

the best model for the given data as it has the low error value for all the measures compared to the other two forecasting techniques. The low error value signifies that the predicted values obtained from the ARIMA model are close to the actual values and hence will have better predictions in the future.

4 Conclusion

This paper commenced introducing why rainfall prediction is important in the country like India, what were the shortcomings before and how to tackle these by analysing which is the best method to predict annual rainfall in India. This paper targets to evaluate and collate the forecasting techniques ARIMA, ETS and NNAR to predict the annual rainfall in mm for the year 2018. Error measures such as RMSE, MSE, MAE and MAPE have been used to compare and contrast the three techniques and to come up with the best technique for the prediction. Based on the results and discussions, it can be concluded that the simpler model, i.e. ARIMA always yields a better forecast than the more complex model such as ETS and NNAR. This paper comes up with the conclusion that on the basis of the error inspection, the ARIMA technique has shown less error for all accuracy measures and is considered to be the most accurate model to predict the annual rainfall for the particular data set given.

References

1. Naim, I., Mahara, T.: Comparative Analysis of Univariate Forecasting Techniques for Industrial Natural Gas Consumption. Indian Institute of Technology, Roorkee (2018)
2. Akkurt, M., Demirel, O.F., Zaim, S.: Forecasting Turkey's natural gas consumption by using time series methods. *Euro. J. Econ. Political Stud.* **3**(2), 1–21 (2010)
3. Forecasting Principles and Techniques. <https://otexts.com/fpp2/> Otext.com (2018)
4. Aggregating and Analyzing data with DPLYR. <https://datacarpentry.org/R-genomics/04-dplyr.html> datacarpentry.org (2017)
5. Time Series and Forecasting. <https://www.statmethods.net/advstats/timeseries.html> Statmethods.net (2017)
6. Yadav, S., Sharma, N.: Forecasting of Indian Stock Market using time-series models. In: Computing and Network Sustainability, pp. 405–412. Springer, Singapore (2019)
7. Zhang, J., Lee, G.M., Wang, J.: A comparative analysis of univariate time series methods for estimating and forecasting daily spam in United States. In: Twenty-Second Americas Conference on Information Systems, San Diego (2016)
8. Yusof, F., Kane, I.L.: Modeling monthly rainfall time series using ETS State space and Sarima models. *Int. J. Curr. Res.* **09**, 195–200 (2012)
9. Jain, G., Mallick, B.: A study of time series models ARIMA and ETS. *Int. J. Modern Educ. Comput. Sci. (IJMECS)* **9**(4), 57–63 (2017)
10. Osarumwense, O.-I.: Time series forecasting models: a comparative study of some models with application to inflation data. *Science (IJMECS)* **9**(4), 57–63 (2017)
11. Singh, N., Sharma, N., Sharma, A.K., Juneja, A.: Sentiment score analysis and topic modelling For GST implementation in India. In: Soft Computing for Problem Solving, pp. 243–254. Springer, Singapore (2019)
12. Monthly, seasonal and annual rainfall (in mm) area weighted average for the whole country starting from 1901 onwards. <https://data.gov.in/catalog/all-india-area-weighted-monthly-seasonal-and-annual-rainfall-mm>
13. All historical and future climate data from the Climate Change Knowledge Portal are available for download. <https://climateknowledgeportal.worldbank.org/download-data>

A Novel Approach for Design 7:3 and 5:3 Compressors



Ajay Kumar Kushwaha and Vikas Kumar

Abstract The partial product reduction represents the major bottlenecks for low-power high-performance multiplier design. Conventionally, 3:2 compressor is used to reduce the partial products for binary multiplication. With the increase of input bit length, the complexity of aforesaid task becomes enormous. Use of multi-input compressor is an elegant way of reducing the complexity of partial product reduction especially for higher order multiplication. Two multi-input compressors, namely 5:3 and 7:3 compressors, are widely used for partial product reduction for binary multiplication. However, the performance of multi-input compressors decides the overall performance of the multiplier. This paper presents a new approach to design high-performance low-power 7:3 and 5:3 compressors for efficient multiplication. The proposed circuit has been designed using CMOS 0.18 μm TSMC technology process parameters. The performances of designed circuit are examined with T-Spice Tanner EDA V.13 at 25 °C temperature simulator. The designed circuit based on the proposed strategy outperforms other competitive designs.

Keywords Multi-input compressor • Parallel multiplier • Partial product reduction • Power dissipation • Redundant carry generator

1 Introduction

The performance of today's arithmetic circuits is evaluated in terms of operating speed as well as its power dissipation. Multiplication is one of the most critical arithmetic operations that act as a major bottleneck to improve speed–power performance of the digital system [1–6]. In parallel multiplication, several partial products are required to be added to achieve the final result. The amount of time and power

A. K. Kushwaha (✉)
Government Engineering College Raipur, Raipur, Chhattisgarh, India
e-mail: ajay.igecsagar@gmail.com

V. Kumar
Barat Sanchar Nigam Limited, Patna, India
e-mail: vikaskumarmitpurnea@gmail.com

that it requires to generate the final result is significant with respect to overall system performance [7, 8].

Multiplication process can be broadly divided into three stages: generation of partial products, partial product reduction and the final addition stage. Partial product reduction (PPR) stage consumes most of the power and time for the parallel multiplication. Multi-input compressors [9–11] can effectively reduce the complexity of multiplication. The strategy by which the proposed circuit generates the final result is groupwise addition of input bits to count the number of ones in the given data. In order to implement this strategy, the sequence of input bit is divided into groups. Each group consists of two input bits. The half adder adds the two bits and produces the result in binary form. This result acts as input to the half adder of the next stage, where it is added with the result obtained from the next group. This simple procedure continues till the final result is generated. At some intermediate stages, non-carry generation condition arises. For this specific condition, only XOR gate is used instead of half adder. This strategy of removal of redundant AND gate reduces power dissipation and improves operating speed. The final result is generated in terms of Sum (LSB), Carry1 and Carry2 (MSB).

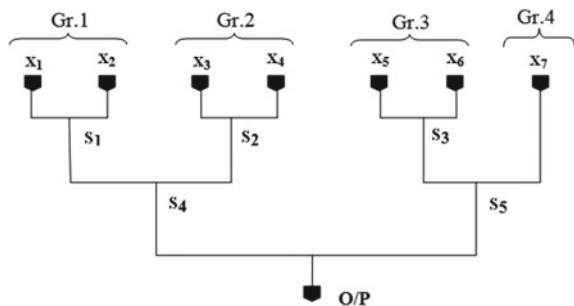
The paper is organized in four sections. This is Sect. 1, where introduction is given. In Sect. 2, the theoretical background and the proposed structure of 7:3 and 5:3 compressors are given. The simulation results of proposed circuits are discussed in Sect. 3 followed by conclusion which is given in Sect. 4.

2 Proposed Method and Circuit Description

The concept of the proposed method for multi-input compression is explained with the help of Fig. 1. Strategy is described for 7 input data X_1 to X_7 (i.e., 7:3 Compressor). In this illustration, only “Sum” results are considered. The same strategy is adopted for carry bits also.

The proposed method as presented in Fig. 1, initially the input bits are divided into groups of two bit. However, for odd number of input bits, the last group consists only one bit. In the case of 7-input, the proposed method divides it into four groups, three

Fig. 1 Proposed method of multi-input



of which consist of two bits each and fourth one consists of one bit. Now, for each group, sum and carry bits are generated using half adder circuit. As, for example, suppose for the group consisting of two bits X_1 and X_2 , the generated sum and carry are:

$$\text{Sum} = X_1 \text{ XOR } X_2$$

$$\text{Carry} = X_1 \text{ AND } X_2$$

Here, in the Figure, “Sum” bit for Gr.1 is represented by S_1 .

Again, the Sum results of each two groups are added using half adder circuit. The same operation is done on the carry bit also. This simple procedure is continued till the final result is obtained. The 7:3 compressor architecture based on aforesaid strategy is shown below in Fig. 2.

As presented in Fig. 2, X_1 to X_7 are the seven inputs to the compressor, whereas SUM, CARRY1 and CARRY2 are the three outputs. The seven input data have been divided into four groups, three of which consist of two input data bit each and the fourth group has only one input data bit. The two input bits of group 1, i.e., X_1 and X_2 , are given as input to half adder HA1. The two bits are added, and the result is generated from HA1 as Sum and Carry. Similar procedure is applied to rest of the

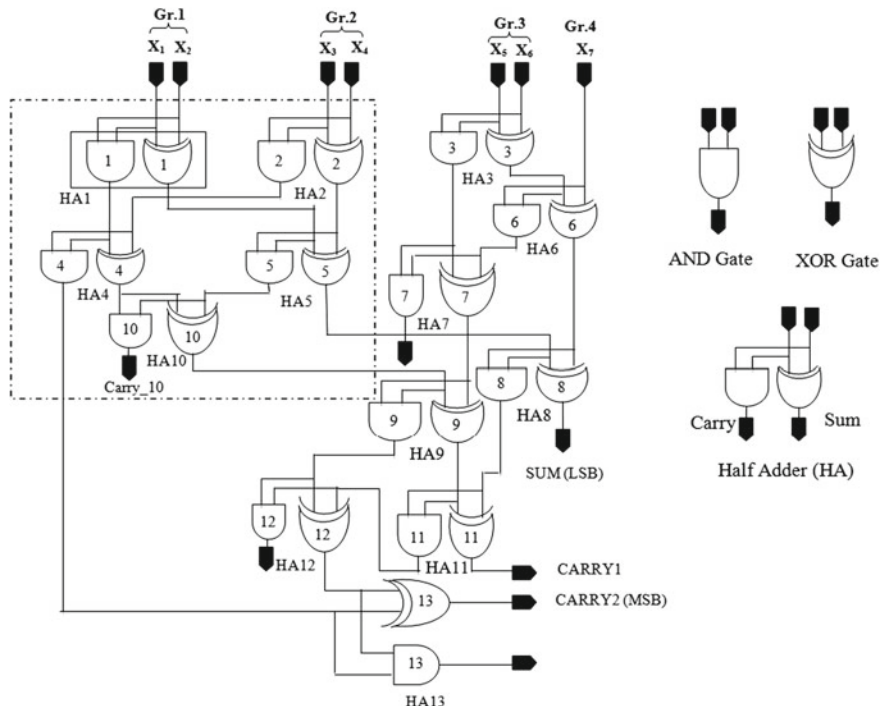


Fig. 2 Architecture for 7:3 compressor

two groups, i.e., group 2 and group 3. The single bit of group 4 is added with the sum bit of HA3 by HA6 (Fig. 2). The Sum bit of HA8 is the least significant bit of the final result of 7:3 compressor denoted as SUM in Fig. 2. The next higher significant bit (CARRY1) is generated by HA11. The most significant bit (CARRY2) of the final result is generated by XOR13.

The next step in the proposed strategy is to detect the half adders for which carry output is always zero and eventually to eliminate the redundant carry generators. To elaborate this, the dotted portion in Fig. 2 is examined and is presented in Fig. 3. In Fig. 3, only XOR gate of HA4 and AND gate of HA5 are considered because we need only Sum bit of HA4 and Carry bit of HA5 to examine carry generation of HA10 (in Fig. 2).

As shown in Fig. 3, suppose four inputs are X_1, X_2, X_3 and X_4 . The output function for the circuit presented in Fig. 3 is “Carry_10”. To examine the function “Carry_10”, the Boolean expression for the function is written first and the expression is:

$$\text{Carry_10} = [(X_1 \oplus X_2) \cdot (X_3 \oplus X_4)] \cdot [(X_1 \cdot X_2) \oplus (X_3 \cdot X_4)] \quad (1)$$

The function “Carry_10” (Eq. 1) is explained with the help of truth table (Table 1). As presented in Table 1, for all input combinations, the function “Carry_10” is becoming zero (i.e., carry is not generated).

Fig. 3 Verification for non-carry generation

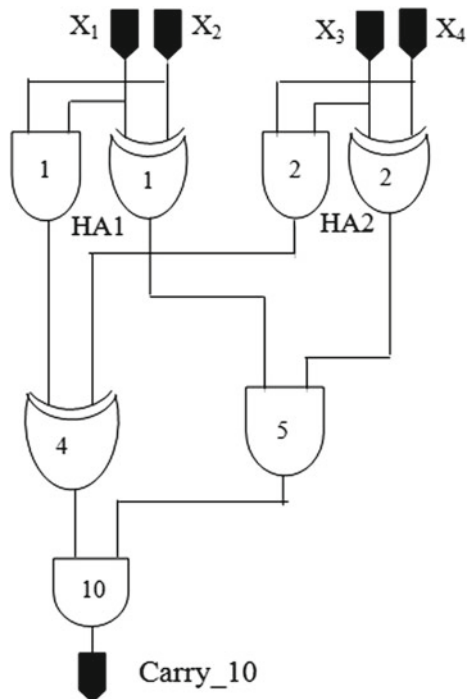


Table 1 Verification for non-carry generation for Carry_10

X_1	X_2	X_3	X_4	$\text{Carry_10} = [(X_1 \oplus X_2) \cdot (X_3 \oplus X_4)] \cdot [(X_1 \cdot X_2) \oplus (X_3 \cdot X_4)]$
0	0	0	0	0
0	0	0	1	0
0	0	1	0	0
0	0	1	1	0
0	1	0	0	0
0	1	0	1	0
0	1	1	0	0
0	1	1	1	0
1	0	0	0	0
1	0	0	1	0
1	0	1	0	0
1	1	0	0	0
1	1	0	1	0
1	1	1	0	0
1	1	1	1	0

So, for this circuit, carry generator is redundant and can be eliminated from the final circuit (Fig. 2) without hampering overall circuit operation. Similar condition arises for HA7, HA12 and HA13 in Fig. 2. In the proposed strategy, all redundant carry generators (AND gates) are removed to improve performance of multi-input compressor. Removal of AND gate makes the final circuit further simple, fast and less power consuming. The proposed structure of 7:3 compressor and 5:3 compressor are shown in Fig. 4 and Fig. 5 respectively.

3 Simulation Result and Discussion

To verify the proposed strategy of the compressors (5:3 and 7:3 compressors) as explained in the previous section are designed and optimized on TSMC 0.18 μm CMOS technology at 25 °C temperature using Tanner EDA V.13. Transient responses are verified and the performances are evaluated. Evaluated simulation results are compared with some other competitive designs with respect to delay and power dissipation. The transient response of designed 5:3 compressor at 500 MHz input is shown Fig. 6. In Fig. 6, five inputs are presented as “Input X_1 ” to “Input X_5 ” all with same weight. Outputs are denoted as “SUM”, “Carry1” and “Carry2”. “SUM” bit has the weight-age of 2^0 , whereas “Carry1” and “Carry2” are having weight-age of 2^1 and 2^2 respectively.

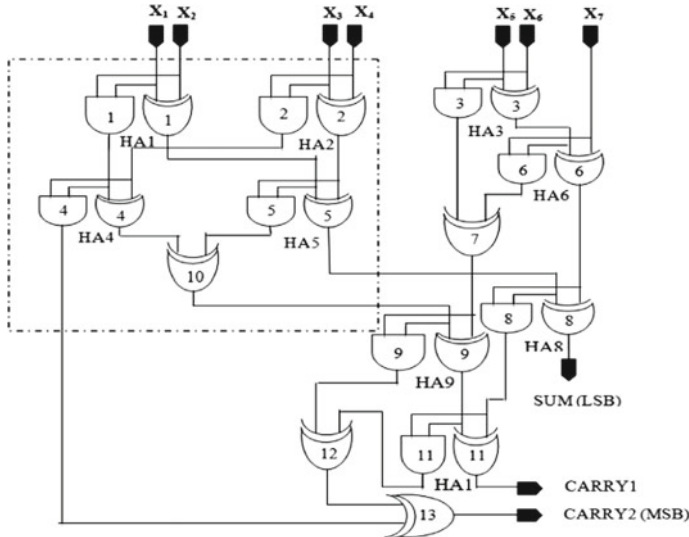


Fig. 4 Proposed 7:3 compressor architecture

Fig. 5 Proposed 5:3 compressor architecture

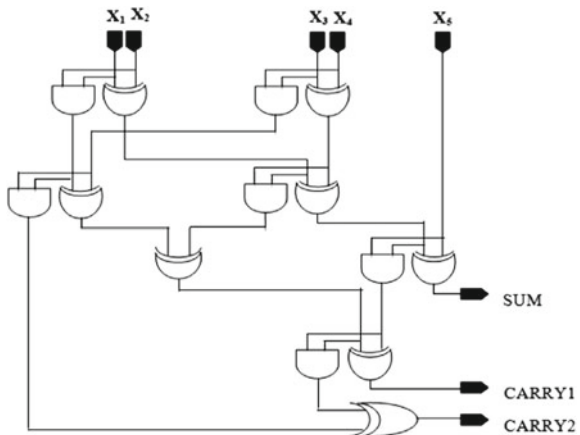


Table 2 summarizes the overall performances of the proposed 5:3 and 7:3 compressors. Table 3 summarizes the power performance of designed 5:3 and 7:3 compressor for different input frequencies with the input data pattern shown in Fig. 6. Table 4 presents the performance comparison of designed 5:3 and 7:3 compressors based on the proposed strategy with the designs presented at 100 MHz input. The 7:3 and 5:3 compressors based on the proposed strategy offer minimum power delay product than the all reported designs. Normalization is done on the power delay product to understand better. The SERF-based 5:3 and 7:3 compressors proposed offer minimum PDP among the presented in circuits. The proposed 5:3 and 7:3 compressors offer PDP of only 22.85% and 50% than the SERF-based design reported.

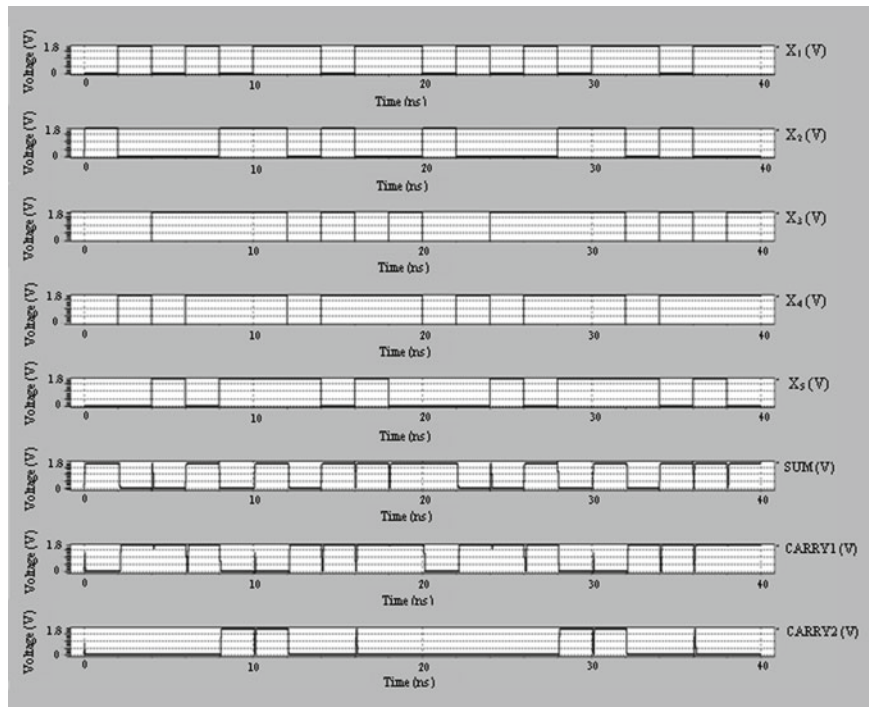


Fig. 6 I/O waveform proposed 5:3 compressor at 500 MHz input

Table 2 Performance of 5:3 and 7:3 compressors

S. No.	Compressor type	No. of active device	Latency (ps)	Power dissipation at 500 MHz (μW)	Power delay product at 500 MHz ($\mu\text{W} \times \text{ns}$)
1	5:3	132	733.02	30.7	22.50
2	7:3	210	964.14	221	213.07

Table 3 Power performance of 5:3 and 7:3 compressors at different frequencies

Supply voltage	Compressor type	1 MHz	10 MHz	50 MHz	100 MHz	500 MHz	1 GHz
1.8 V	5:3	6.16×10^{-8}	6.14×10^{-7}	3.06×10^{-6}	6.17×10^{-6}	3.07×10^{-5}	6.14×10^{-5}
	7:3	3.88×10^{-7}	4.04×10^{-6}	7.65×10^{-5}	2.38×10^{-5}	2.21×10^{-4}	4.44×10^{-4}

Table 4 Performance comparison for the proposed 5:3 and 7:3 compressors with reported in [2] designs at 100 MHz

Design	Tech.	Compressor type							
		5:3				7:3			
		Avg. power (μW)	Delay (ns)	PDP ($\mu\text{W} \times \text{ns}$)	Norm. PDP	Avg. power (μW)	Delay (ns)	PDP ($\mu\text{W} \times \text{ns}$)	Norm. PDP
Transmission gate (TG) CMOS based	90 nm MOSIS	243	1.10	267.3	1	475	1.07	508.25	1
16-Transistor adder based		31.3	0.98	30.67	0.11	73.9	1.05	77.59	0.15
Static energy recovery full adder (SERF) based		19.4	1.02	19.79	0.07	46.2	1.04	48.05	0.09
Proposed	TSMC 0.18 μm	6.17	0.73	4.50	0.016	23.8	0.96	22.85	0.045

4 Conclusion

A novel structure for 5:3 and 7:3 compressors is explained in this paper. In the proposed strategy, compressors are structured based on half adder instead of full adder. To do this, the input bits are divided into groups of two bits each. In case of odd number of inputs, the last group consists of only one bit. Two bits in each group are added with half adder. The same grouping and summing strategy is applied on sum and carry bits separately. After completing the circuits, redundant carry generators are detected and are removed from the circuits. This removal of redundant carry generator improves circuit performance and reduces power dissipation compared to reported competitive designs. All the simulations are done on TSMC 0.18 μm CMOS technology at 25 °C temperature using Tanner EDA V.13.

Acknowledgements This work is supported by the Third Phase of Technical Education Quality Improvement Program (TEQIP-III) under the “TEQIP Collaborative Research Scheme”, National Project Implementation Unit (NPIU), a unit of Ministry of Human Resource Development (MHRD), Government of India, for implementation of World Bank assisted projects in technical education.

References

1. Saha, A., Pal, D., Chandra, M.: Low-power 6-GHz wave-pipelined 8b \times 8b multiplier. *IET Circuits Devices Syst.* **7**(3), 124–140 (2013). <https://doi.org/10.1049/iet-cds.2012.0221>
2. Nirlakalla, R., Rao, T.S., Prasad, T.J.: Performance evaluation of high speed compressors for high speed multipliers. *Serb. J. Electr. Eng.* **8**(3), 293–306 (2011). <https://doi.org/10.2298/SJEE1103293N>

3. Marimuthu, C.N., Thangaraj, P.: Transmission gate based high performance low power multiplier. *J. Appl. Sci.* **10**(23), 3051–3059 (2010). <https://doi.org/10.3923/jas.2010.3051.3059>
4. Baran, D., Aktan, M., Oklobdzija, V.G.: Energy efficient implementation of parallel CMOS multipliers with improved compressors. In: IEEE International Symposium on Low-Power Electronics and Design, pp. 147–152 (2010). <http://doi.org/10.1145/1840845.1840876>
5. Dandapat, A., Ghosal, S., Sarkar, P., Mukhopadhyay, D.: A 1.2-ns 16 × 16-bit binary multiplier using high speed compressors. *Int. J. Electr. Electron. Eng.* **4**(3) (2010)
6. Radhakrishnan, D., Preethy, A.P.: Low power CMOS pass logic 4-2 compressor for high speed multiplication. In: Proceedings of IEEE Midwest Symposium on Circuits and Systems, 3.3.31296–1298 (2000). <http://doi.org/10.1109/MWSCAS.2000.951453>
7. Najafi, A.A., Najafi, A., Mirzakuchaki, S.: Low-power and high-performance 5:2 compressors. In: The 22nd Iranian Conference on Electrical Engineering (ICEE), pp. 33–37 (2014). <http://doi.org/10.1109/IranianCEE.2014.6999498>
8. Kushwaha, A.K., Paul, S.K.: Inductorless realization of Chua's oscillator using DVCCTA. *Analog Integr. Circ. Sig. Process.* **88**, 137–150 (2016). <https://doi.org/10.1007/s10470-016-0746-9>
9. Ramakrishnan, M., Bansal, D., Balamurugan, S., Mallick, P.S.: Design of 8-4 and 9-4 compressors for high speed multiplication. *Am. J. Appl. Sci.* **10**(8), 893–900 (2013). <http://doi.org/10.3844/ajassp.2013.893.900>
10. Menon, R., Radhakrishnan, D.: High performance 5:2 compressor architecture. *IEEE Proc. Circ. Devices Syst.* **153**(5), 447–452 (2006). <https://doi.org/10.1049/ip-cds:20050152>
11. Mishra, N., Sharma, T.K., Sharma, V., Vimal, V.: Secure framework for data security in cloud computing, soft computing: theories and applications. *Adv. Intell. Syst. Comput.* 61–71 (2018). http://doi.org/10.1007/978-981-10-5687-1_6

High-Accurate, Area-Efficient Approximate Multiplier for Error-Tolerant Applications



M. Parvathi

Abstract Due to increased applications of embedded systems, the need for fast and area-efficient components has become essential building blocks in the design phase. Most of the signal processing applications, image processing applications, are using efficient hardware blocks specific to the functionality in the name of error-tolerant blocks while compromising for minute error that may cause negligible deviation from the accurate result. The contemporary basic building blocks that needed for computation are greatly replaced by error-tolerant logic blocks due to the advantage of improvement in design optimization. In this paper, an error-tolerant multiplier is proposed with a new technique for accuracy improvement and area efficiency. The technique involved in this work is reframing the partial products to meet the multiplication product to the nearest accurate value. Simulation results for an 8×8 multiplier are observed and are comparable with greater improvement in the area at sustained delay characteristics. Observations are carried in Xilinx environment and achieved 57% of area improvement within the acceptable accuracy range from 55% to 100% than the existing error-tolerant design.

Keywords Embedded system · Area efficiency · Accuracy · Error-tolerant multiplier

1 Introduction

Abrupt change in the latest technology trends becomes a powerful issue point for the designers with emphasis on low-power battery operated and compact embedded designs. This leads to migration of design emphasis from conventional designs to optimized designs in terms of power dissipation minimization, area and delay while preserving the desired performance. To meet this problem of optimization, some

M. Parvathi (✉)

Professor, ECE Department, BVRIT Hyderabad College of Engineering for Women, Hyderabad, Telangana, India

e-mail: pbmuddapu@gmail.com

applications use small amounts of error-tolerable components. Most of these applications are related to biomedical embedded devices in which the optimization is error tolerant. As an example, human senses corresponding to vision, odor, audible range, feel, these can work with near accurate values. Most of the applications involve adders and multipliers, if the designs are used with accurate multipliers which lead to more area and power consumption. Therefore, it is required to develop a multiplier with attributes like less area and power consumption along with speed efficiency. As a design choice, an error-tolerant multiplier is the best to design with high accuracy compared to the existing one, which works on parallel computing methods.

ETM is a novel technique that brings better results in performance in terms of speed, power against to the affordable percentage of error accuracy [1–4]. Taking error accuracy as design considerations, researchers have come up with various design methods that have huge impending applications where super high speed and ultra low power are required. Most of the digital data is present in upper bit limit rather than the lower; majority of the ETM designs evolved to manipulate data on lower bit length. In precise, MSB part of multiplication follows contemporary procedures, whereas LSB part is a non-multiplication portion which will be left for various design phases.

In error multiplier designs, the difference between accurate product (A_r) and error product (E_r) is called as error difference (ED). Kyaw et al. [5] projected that the majority errors that occur in magnitude are insignificant if it results with comparable hardware within the limited delay. This was achieved by making multiplier into two parts, i.e., multiplication part and non-multiplication part. Mostly, the lower-order bit side will be considered as non-multiplication part, used for manipulation to achieve improvement in performance. Further, the literature shows the design methods that result in low power along with considerable speed improvement compared with the existing designs. For real-time applications such as DCT and iDCT, Bhardwaj et al. [6] proposed an approximate Wallace tree multiplier with its considerable low power and area efficiency. This involves floating multiplication that needs large number of unsigned multipliers. The use of approximate multipliers is more prominent in image processing and DSP applications [7–9] for further improvement in the parameters PSNR and NC. Marimuthu et al. [9, 10] proposed a multiplier in a JPEG encoder application which reveals that the peak signal-to-noise ratio (PSNR) reduction is at most 0.15 dB compared to that of the exact one. It is a boundless challenge for researchers always to come up with new approximate multiplier designs with consumption of lower power and critical paths to be shorter than conventional multipliers especially for high-performance DSP applications. Approximate arithmetic circuits are more prominent components used for low power and lossy applications [11–13]. In the similar way, digital watermarking technology [14] is one of the major application areas in which approximate multiplication method may help in improving performance evaluation calculation fast and efficiently. An approach for new form of fuzzy number using alpha-cut method is proposed in [15] to observe linguistic scale values. This method can be improved further for fast and less number of computations by using error-tolerant multipliers. Similarly, other application area, where

feature extraction method for facial expression recognition [16] may use approximate methods to achieve fast and accurate measurement at the minimal error cost.

In this paper, the proposed method is implemented using 8-bit radix and observed for accuracy, delay and area optimization. Xilinx 10.1i tool is used with Verilog coding for Spartan6 device. Further, hypothetical and realization aspects of contemporary ETM are discussed in Sect. 2. It also covers the proposed multiplication algorithm for 16-bit ETM. Corresponding experimental results are discussed in Sect. 3 along with comparisons that are done using standard parallel multiplier. Further analysis and conclusions are discussed in Sect. 4.

2 Attributes of Contemporary ETM

One can feel less design effort on approximate multipliers due to the freedom in use of various design combinations that results in high accuracy. In general, a traditional multiplier design consists of three phases: partial product generation phase, partial product accumulation phase and a carry propagation adder phase (CPA) at the final stage. However, in ETM designs, most of the manipulation will be done at lower bit length side (LSB) and is called as inaccurate or approximate multiplication part. One of the simplest techniques that can be used in the design phase of approximate partial products is 2×2 multiplier inaccurate block [11]. On the other hand, the accurate part that deals with MSB can be designed in contemporary available methods. The final ETM can be merging of both accurate and inaccurate multiplication parts that can be resulted with design requirements.

For an $m \times n$ multiplier where $m > n$, the most significant product bits are m times of the multiplier bits. The remaining least significant bits are truncated partial products such that the overall design produces an error multiplication with reduced precision. However, to achieve better percentage of accuracy in error average, an error compensation circuit may be added in the last stage of design. However, care must be taken while designing the error compensation circuit that the area overhead must not increase compared to the corresponding truncation part of the partial product bits.

The necessary attributes to be followed to measure the performance of ETM are as follows [13]:

Overall error, $OE = |A_r - E_r|$ where A_r denotes the actual correct result obtained from true multiplication part, and E_r is the result obtained from the partial or truncated part.

Accuracy: It is also known as percent of **error** means that the deviation from exact result. It is a ratio of the difference between the true value and measured value to the true value. This ratio is then multiplied by 100. Hence, % Accuracy (A) = $|1 - (OE/A_r)| \times 100\%$. Its value ranges from 0 to 100%.

Proposed ETM Algorithm

The drawback of the existing algorithm [13] is low accuracy and is found maximum

200	1	1	0	0	1	0	0	0
200	1	1	0	0	1	0	0	0
1	0	0	1	0	0	0	0	a1
					0	0	0	a2
					0	0	0	a3
					0	1	0	a4
1	0	0	1	0	0	0	1	Er

$Ar=1001110001000000(40000)$ $Er=1001000001010101(36949)$ Accuracy= 92.37%

Fig. 1 Example for approximate multiplier with accuracy 92.37%

88.7%. This is because with ‘all’ the bits in its result part towards LSBs are treated as ‘1’s whenever any of the two input sequence bits from LSBs are simultaneously ‘1’s. Due to this compromise in the output bit condition, the method results in poor accuracy. In order to improve the accuracy to a great extent, the proposed multiplier considers the individual bits of ‘a’ and ‘b’ sequences to follow certain conditions. Consider two 8-bit input sequences a and b. After multiplication of a and b, the result bits will be 16-bit sequence. Out of the 16 bits, the error part uses lower 8 bits, and remaining upper 8 bits are used for accurate part calculation. The accurate part of multiplication using MSBs follows regular procedure to generate the accurate result part, whereas error part of multiplication using LSBs will be generated using certain conditions. These conditions for generating error result part are: If either $a[0]$ or $b[0]$ is ‘1’, then equate the least significant two bits of result to ‘01’. Similarly, if either $a[1]$ or $b[1]$ is ‘1’, then equate the least significant four bits to 0101. It will continue in the same way that if $a[2]$ or $b[2]$ is ‘1’, then equate the least significant six bits to 10101. Finally, for either $a[3]$ or $b[3]$ bit is ‘1’, then equate the result bits of error part to 1010101. Few examples are shown in Figs. 1, 2, 3, 4, 5, 6 and 7 by considering error part with all possible bit variation patterns. Table 1 shows error and percentage of accuracy values for few input values, in which accuracy range observed for 8×8 input bits is 55–100%.

3 Experimental Results

The proposed ETM is implemented using Spartan6 low-power device xc3s500e-5fg320 for speed grade of -1L. Design is implemented using Verilog, and simulations were carried for the traditional, existing and proposed multipliers. Traditional multiplication is carried out in two different styles. In the first method, simple assignment notation of $a[n] * b[n]$ is used for the implementation, that results in utilization of

201	1	1	0	0	1	0	0	1
201	1	1	0	0	1	0	0	1
<hr/>								
1	0	0	1	0	0	0	0	a1
					0	0	0	a2
					0	0	0	a3
					0	1	0	a4
1	0	0	1	0	0	0	1	0
					1	0	1	0
					1	0	1	1
								Er

$A_r = 1001110111010001(40401)$ $E_r = 1001000001010110(36950)$ Accuracy=91.45%

Fig. 2 Example for approximate multiplier with accuracy 91.45%

204	1	1	0	0	1	1	0	0
204	1	1	0	0	1	1	0	0
<hr/>								
1	0	0	1	0	0	0	0	a1
					0	0	0	a2
					0	0	0	a3
					0	1	0	a4
1	0	0	1	0	0	0	0	Er
					0	1	1	0
					1	0	1	0
					1	0	1	0

$A_r = 1010001010010000 (41616)$ $E_r = 1001000001101010(36970)$ Accuracy= 88.83%

Fig. 3 Example for approximate multiplier with accuracy 88.83%

embedded multiplier block MULT18X18SIO. However, this technique needs special FPGA devices with such embedded multipliers as built-in parts. This embedded multiplier block uses regular multiplication based on modified Booth algorithm with the multiplicand multiplied by each bit of the multiplier to generate partial products; further, the partial products will be added together to generate the final result. Multiplexers were used in this module to generate partial products. Since this module is used as a primitive, the overall wire length is reduced which in turn reduces the overall delay. In the second method, the multiplication is carried by traditional way, i.e., summing up of all partial products (PP) that are generated. Simulation results for traditional multiplier are observed in Fig. 8. Corresponding technology schematics in which multiplier block MULT18X18SIO are shown in Fig. 9. Since this process follows repeated addition, the hardware requirement is more in this case.

202	1	1	0	0	1	0	1	0
202	1	1	0	0	1	0	1	0
<hr/>								
1	0	0	1	0	0	0	0	a1
						0	0	a2
						0	0	a3
						0	1	a4
1	0	0	1	0	0	0	1	Er

Ar=1001111101100100(40804) Er=1001000001011010(36954) Accuracy= 90.56%

Fig. 4 Example for approximate multiplier with accuracy 90.56%

206	1	1	0	0	1	1	1	0
206	1	1	0	0	1	1	1	0
<hr/>								
1	0	0	1	0	0	0	0	a1
						0	0	a2
						0	0	a3
						0	1	a4
1	0	0	1	0	0	0	0	Er

Ar=1010010111000100 (42436) Er=1001000001101111(36975) Accuracy= 87.13%

Fig. 5 Example for approximate multiplier with accuracy 87.13%

By following the steps discussed in Sect. 2, ETM is designed but using partial product style for both error and accurate parts of multiplication bits. Corresponding pseudocode is shown below, keeping actual part multiplication in its regular style.

//Pseudocode for ETM method-I: using partial product method for both error and accurate parts

//error part (lower 4 bits)

assign a1 = (b[0] == 1'b1)? {16'b0000000000000001}: 16'b0000000000000000;

assign a2 = (b [1] == 1'b1)? {16'b00000000000000101}: 16'b0000000000000000;

assign a3 = (b [2] == 1'b1)? {16'b00000000000010101}: 16'b0000000000000000;

assign a4 = (b [3] == 1'b1)? {16'b0000000001010101}: 16'b0000000000000000;

207	1	1	0	0	1	1	1	1
207	1	1	0	0	1	1	1	1
<hr/>								
1	0	0	1	0	0	0	0	a1 1
					0	0	0	0 1 0 1 a2 5
					0	0	0	1 0 1 0 1 a3 21
					0	1	0	1 0 1 0 1 a4 85
1	0	0	1	0	0	0	0	Er

Ar=1010011101100001 (42849) Er=1001000001110000(36976) Accuracy= 86.29%

Fig. 6 Example for approximate multiplier with accuracy 86.29%

192	1	1	0	0	0	0	0	
192	1	1	0	0	0	0	0	
<hr/>								
1	1	0	0	0	0	0	0	a1
			0	0	0	0	0	0 0 a2
			0	0	0	0	0	0 0 a3
			0	0	0	0	0	0 0 a4
1	1	0	0	0	0	0	0	Er

Ar=1001000000000000 (36864) Er=1100000000000000(49152) Accuracy= 75%

Fig. 7 Example for approximate multiplier with accuracy 75%

```
//accurate (upper 4 bits)
assign a5 = (b[4] == 1'b1)? {4'b0000, a, 4'b0000}: 16'b0000000000000000;
assign a6 = (b[5] == 1'b1)? {3'b000, a, 5'b00000}: 16'b0000000000000000;
assign a7 = (b[6] == 1'b1)? {2'b00, a, 6'b000000}: 16'b0000000000000000;
assign a8 = (b[7] == 1'b1)? {1'b0, a, 7'b0000000}: 16'b0000000000000000;
assign result = a1 + a2 + a3 + a4 + a5 + a6 + a7 + a8;
```

As an experiment, only error part of the proposed ETM is implemented in partial product method, while regular multiplication styles, i.e., $a[n] * b[n]$, are used for accurate part, and corresponding pseudo code is shown below:

//ETM method-II

Table 1 Few example 8-bit numbers with corresponding accurate and approximate values, percentage of accuracies

a[7:0]	b[7:0]	A_r	E_r	E_r [13]	%A [13]	%A of proposed method
3	3	9	6	15	166	66.6
6	6	36	26	60	166	72.2
7	7	49	27	63	128	55.1
14	14	196	111	252	128	56.6
16	16	256	256	511	199	100
24	24	576	469	448	77.7	81.42
46	46	2116	1583	1276	60.3	74.81
77	77	5929	5035	4339	73.18	84.92
126	126	15,876	14,223	12,796	80.5	89.58
200	200	40,000	36,949	28,480	71.2	92.37
243	243	59,049	58,326	7921	13.4	98.77

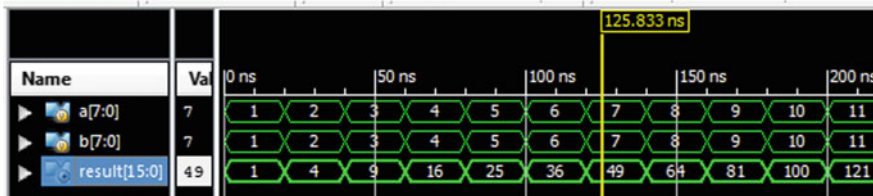


Fig. 8 Simulation results for accurate multiplier

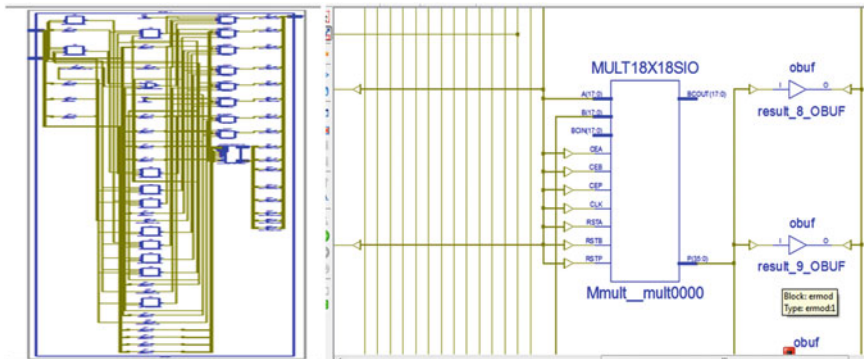


Fig. 9 Technology schematics of traditional multiplier; simulation results shows the utilization of embedded multiplier module MULT18X18SIOs, for regular multiplication expression $a[] \times b[]$

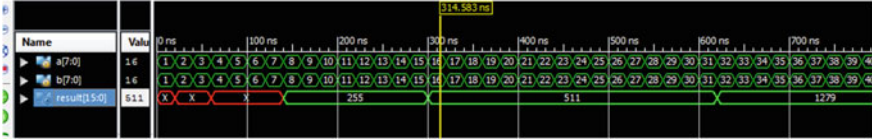


Fig. 10 Simulation results for error-tolerant multiplier [13]

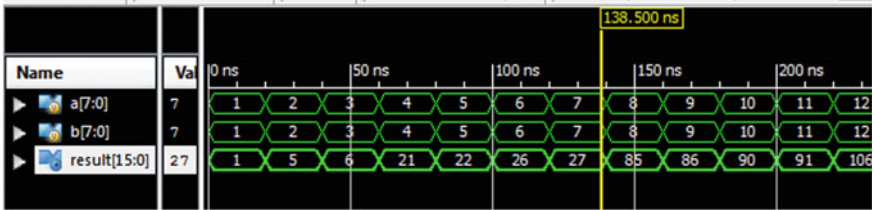


Fig. 11 Simulation results for error-tolerant multiplier, proposed

```
//partial products for error part (lower 4 bits)
assign a1 = (b[0] == 1'b1)? {16'b0000000000000001}: 16'b0000000000000000;
assign a2 = (b[1] == 1'b1)? {16'b00000000000000101}: 16'b0000000000000000;
assign a3 = (b[2] == 1'b1)? {16'b00000000000010101}: 16'b0000000000000000;
assign a4 = (b[3] == 1'b1)? {16'b0000000001010101}: 16'b0000000000000000;
//regular multiplication method for accurate part (upper 4 bits)
assign result[15:8] = a[7:4] * b[7:4]; //regular multiplication expression
assign result[7:0] = a1 + a2 + a3 + a4;
```

In the ETM method-II, due to the regular multiplication expression, the final product uses built-in embedded multiplier MULT18X18SIOs in FPGA. Hence, the overall CLBs would reduce in this case. The existing and proposed ETM simulation results are shown in Figs. 10 and 11. Corresponding technology schematics are shown in Figs. 12 and 13.

Table 2 shows the proposed and existing ETM performance comparisons.

4 Conclusions

This paper proposed a new technique for higher accuracy in error-tolerant multiplier in two design styles. In the first design style, both error and accurate part of multiplier bits are generated using partial product method. Further, all these partial products are summed up for generation of the final multiplication result. In the second design style, only error part uses partial product method, but accurate part uses regular algebraic product expression. Hence, it needs a built-in embedded block of multiplier MULT18X18SIOs in the chosen FPGA. The proposed ETM is simulated for all 256 multiplication combinations using 8-bit input bits and observed the accuracy

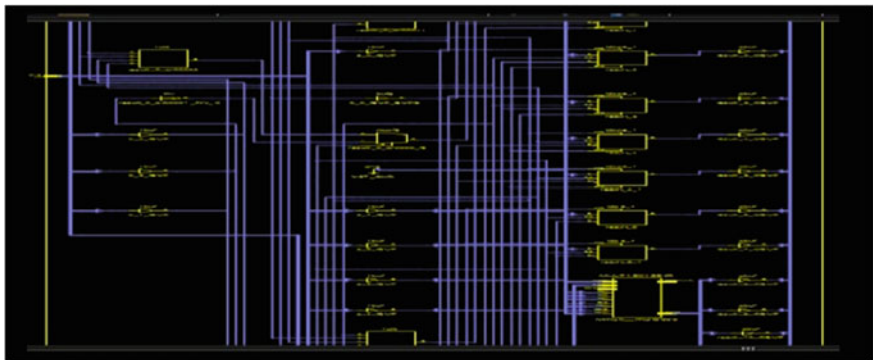


Fig. 12 Technology schematics of error multiplier [13]

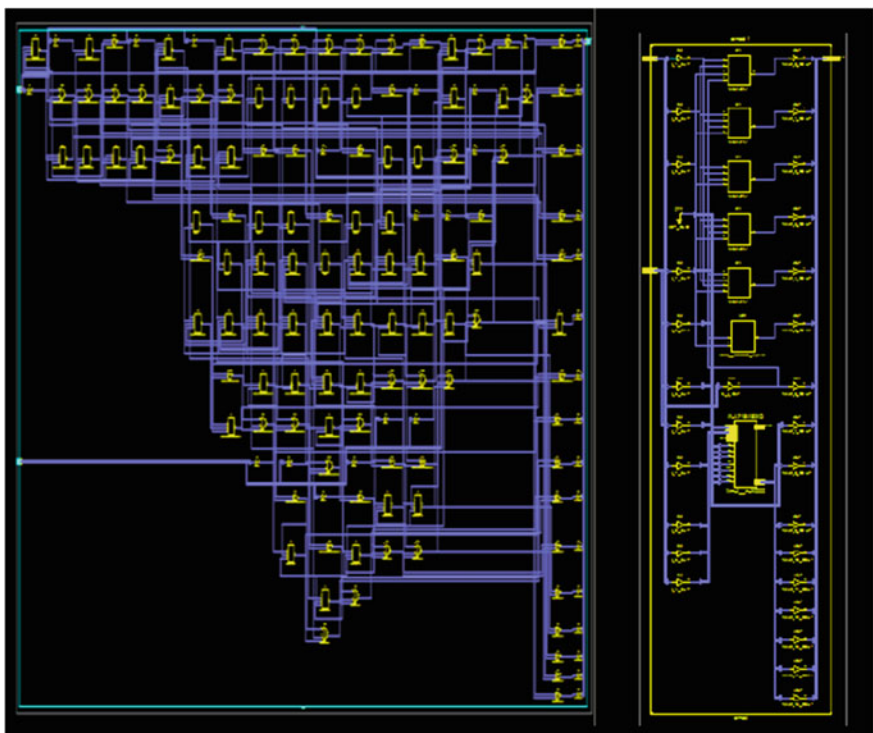


Fig. 13 Technology schematic of proposed error multiplier by methods I and II

Table 2 ETM performance comparisons

Parameter	Traditional multiplier method-I	Traditional multiplier method-II	ETM [13]	Proposed ETM with method-I	Proposed ETM with method-II
Delay (ns)	18.431	9.28	8.85	14.356	8.85
No of slices	63	0	7	32	3
No of 4 I/P LUTs	108	0	12	54	6
Embedded multiplier module MULT18X18SIOs	–	1 out of 20	1 out of 20	–	1 out of 20

improvement ranging from 55% to 100%. In the implementation phase too, the proposed design results in 22.1% of speed improvement under method-I compared with traditional multiplier. When compared with the existing ETM [13], the proposed ETM area overhead is reduced by 57% in terms slice and LUT utilization.

References

1. Anand, S., Saxena, A.K.: Design of approximate multiplier for error-tolerant applications. *Int. J. Eng. Res. Appl.* **3**(3), 880–883 (2013)
2. Juang, T.B., Hsiao, S.F.: Low-error carry-free fixed-width multipliers with low-cost compensation circuits. *IEEE Trans. Circuits Syst. II Express Briefs* **52**(6), 299–303 (2005)
3. Liu, C., Han, J., Lombardi, F.: A low-power, high-performance approximate multiplier with configurable partial error recovery. In: Proceedings of the 2014 Design Automation & Test in Europe Conference & Exhibition (DATE), EDAA, pp. 1–4. IEEE, Dresden, Germany (2014)
4. Varma, S., Jain, R.: Design and verification of truncation-error tolerant 8-bit signed-multiplier. *Int. J. Sci. Res. (IJSR)* **3**(6), 2700–2704 (2014). ISSN (Online): 2319-7064
5. Kyaw, K.Y., Goh, W.L., Yeo, K.S.: Low-power high-speed multiplier for error-tolerant application. In: Proceedings of the International Conference on Electron Devices and Solid-State Circuits (EDSSC), pp. 1–4. IEEE (2010)
6. Bhardwaj, K., Mane, P.S., Henkel, J.: Power-and area-efficient approximate Wallace tree multiplier for error-resilient systems. In: 15th International Symposium on Quality Electronic Design (ISQED), pp. 263–269. IEEE (2014)
7. Kidambi, S.S., El-Guibaly, F., Antoniou, A.: Area-efficient multipliers for digital signal processing applications. *IEEE Trans. Circuits Syst.-IL* **43**(2), 90–95 (1996)
8. Thomas, N.R., Teresa, V.V.: Error tolerant modified booth multiplier for lossy applications. *Int. J. Modern Eng. Res. (IJMER)* **2**(3), 1125–1128 (2012)
9. Marimuthu, R., Elsie Rezinold, Y., Mallick, P.S.: Design and analysis of multiplier using approximate 15-4 compressor. *IEEE Access* **5**(1), 1027–1036 (2017)
10. Jiang, H., Liu, C., Liu, L., Lombardi, F., Han, J.: A review, classification and comparative evaluation of approximate arithmetic circuits. *ACM J. Emerg. Technol. Comput. Syst.* **13**(4), Article 60, 60.1–37 (2017)
11. Kulkarni, P., Gupta, P., Ercegovac, M.D.: Trading accuracy for power in a multiplier architecture. *J. Low Power Electron.* **7**(4), 490–501 (2011)
12. Wang, J.-P., Kuang, S.-R., Liang, S.-C.: High-accuracy fixed-width modified booth multipliers for lossy applications. *IEEE Trans. Very Large Scale Integr. (VLSI) Syst.* **19**(1), 52–60 (2011)

13. Jain, G., Jain, M., Gupta, G.: Design of radix-4,16,32 approx booth multiplier using error tolerant application. In: Proceedings of 6th International Conference on Reliability, Infocom Technologies and Optimization (ICRITO) (Trends and Future Directions), AIIT, Amity University Uttar Pradesh, Noida, India, pp. 314–320 (2017)
14. Abdul, A.M., Cherukuvada, S., Soujanya, A., Sridevi, G., Umar, S.: Watermarking technology in QR code with various attacks. In: Pant, M., et al. (eds.) Proceedings of Soft Computing: Theories and Applications, Advances in Intelligent Systems and Computing, vol. 584, pp. 147–156 (2018)
15. Rajkumar, A., Helen, D.: New arithmetic operations of triskaidecagonal fuzzy number using alpha cut. In: Pant, M., et al. (eds.) Proceedings of Soft Computing: Theories and Applications, Advances in Intelligent Systems and Computing, vol. 584, pp. 125–135 (2018)
16. Rahul, M., Mamoria, P., Kohli, N., Agrawal, R.: An efficient technique for facial expression recognition using multistage hidden Markov model. In: Ray, K., et al. (eds.) Proceedings of Soft Computing: Theories and Applications, Advances in Intelligent Systems and Computing, vol. 742, pp. 33–43 (2019)

Hoax and Faux of Information Credibility in Social Networks: Explored, Exemplified and Experimented



Ram Chatterjee, Hardeo Kumar Thakur, Ridhi Sethi, and Abhishek Pandey

Abstract The ever-evolving ubiquitous online social networks have been witnessing plethora of precarious, enigmatic and flabbergasted information imposing a probe on its credibility, in the recent state of affairs. This has posed interesting challenges in context of research on information credibility, pinpointing the trustworthiness, necessity and influence of privacy and security in online social media. This paper primarily focuses on the increasing inundation of idiosyncrasies in online social media, the significance of ensuring credibility of information, and incidental collated compromises apropos to online reviews. The crux of this paper implicates investigation of the prevalent opinion spammers that distorts the perceived quality of a product via fraudulent reviews. These falsified reviews' progressive proliferation have been explored, exemplified and experimented with the tools, viz. "Fakespot," "ReviewMeta" and "Review Index" demonstrating action, detection and prevention from the coherent and inherent fraud-bots which are intentionally targeted on large online app review databases entailing deceptive and skeptic opinions.

Keywords Information credibility · Online social networks · Opinion spammers · Online social media · Fraud-bots

1 Introduction

The quintessence of privacy and security in online social media connotes to the "information credibility" entailed in the online reviews that drives the customer's

R. Chatterjee (✉) · H. K. Thakur · R. Sethi · A. Pandey
Manav Rachna University, Sector—43, Aravalli Hills, Delhi-Surajkund Road,
Faridabad, Haryana 121004, India
e-mail: ram@mru.edu.in

H. K. Thakur
e-mail: hkthakur@mru.edu.in

R. Sethi
e-mail: ridhisethi20@gmail.com

A. Pandey
e-mail: abhishek.ap.ap@gmail.com

intention and interest toward a product and/or a service. Hence, “information” may be interpreted as the processed data adding meaning to its recipients, which has been communicated and leverages some facts provided or learned about something or someone [1]. On the following note, in line with the context of the discussion, “credibility”, inculcates quality of inspiring belief or trustworthiness about something or someone. Hitherto, “information credibility” can thus be construed on the degree of the validity, correctness and trustworthiness of the information content under context [2].

2 Information Credibility—Corollaries

The customer’s crucial conjecture on the credibility of the online information is available as reviews lie in the ethical practices of postage of online information that should be verifiable in terms of its authenticity. This necessitates on the ability of the customers to validate the reviews and claims, on the product and/or services, posted online. This connotes to “evidence-based practices” as one of the best ways to earn respect [3] for the advertised product and/or service.

2.1 *The Essentiality of Credible Information [4–6]*

The overwhelming fraudulent online information driven by malicious interests of product promotion at the cost of demeaning rival’s product information is penetrating the online social media massively. Hence, to gain and hold on to the trust of its customers and to woo new customers, it has become mandatory for companies to post and verify the genuineness of the online contents and reviews, for the following compelling reasons:

- Overload of options: In the purview of plethora of social media options and fierce competition, the companies are bound to post authentic information to gain trust of the customers on their products/services.
- Existing Niches: “Branding” has been inherent to customer’s choice of product/service. This advocates focused advertisements of products/services to targeted customers/subscribers. Here, the credibility of information influences the customer/subscriber based on the following manner:
 - Reputation building: “Reputation” is the core factor functional in retaining customers/subscribers. Hence, published contents that can be cross-checked, expert quotes on product/service, inspected information, adds to the credibility, building the reputation.
 - Accountability: Admittance to false or wrong information, posted accidentally, lies in the onus of the company concerned, and this ethical practice of “accountability,” adds on to the genuineness of the company, imbibing customer’s trust on company’s reputation.

2.2 The Compromising Contexts of Information Credibility [7]

The eccentricity of fake news, doctored photos have gained sufficient familiarity among customers/subscribers for them to set apart the sham and actual, revealed the study conducted by University of California.

Another evidence in the literature connotes to a Web-based research with moderately high population with ages spanning from adolescent to old, where investigators explored the human ability of correctly identifying fake images, where rating of images' credibility was "fairly low" on a seven-point scale with the first pointer indicating "no reliability" and seventh pointer being "exceedingly realistic." Readers may note that these precisions in the result were observed in the light of the fact where the participants knew the source of information being "The New York Times" or "NPR" or supplementary news groups of repute.

The above-mentioned remarkable demarcation ability of participants between the fake and the real is attributed to their internet skills, social media use, photo-editing experience, as noteworthy predictors for evaluation of even the image credibility, besides information credibility. This manifests the fact that even careless or distracted customers are also skilled enough to spot fakeness in digital images. Nevertheless, the trend of fake posts is leveraged by personal benefits of individuals and/or companies that evokes the provokes of inherent malicious interests.

3 The Nuances of Compromised Credibility—Bulletin Ballots

3.1 Businesses Caught Posting Fake Reviews [8]

This report materialized way back in 2009, where a business that was into aesthetic operations was into limelight for its postage of client-oriented fraudulent feedbacks, triggered by its employee. The company had to pay \$300,000 for settlement as a penalty to the New York state as published in an editorial by the "New York Times." It was mentioned by the then Governor that the company's endeavors for business growth by befooling its clients was distrustful, illegitimate and malicious.

3.2 Postage of Bogus, Bribed Reviews by Amazon Retailer [8]

Yet another hoax was witnessed named as "VIP Deals" where cashback offer was publicized as trade tricks against convincing feedbacks on "Kindle Fire cases." This malevolent deal proposition was soon discovered by Amazon, wherein the company

blocked online access to the superficial reviews, following the guiding principle that restricts any reimbursement against fraud feedbacks.

3.3 The Incident of Blemished Heritage [8]

This event tracks itself a year back where a hefty fine was imposed by the Federal Trade Commission on “Legacy Learning Systems,” on account of having persuaded people to post persuasive reviews on its instrumental training lessons on guitar. The fraudulent disguised themselves as frequent and permanent clients on review URLs that prompted the company to deal with the issue seriously and charge the miscreants for their deceptive marketing and advertising methods.

3.4 Amazon Sues 1,000 ‘Fake Reviewers’ [9]

It has been witnessed recently about Amazon having started legal action against more than 1,000 unidentified people that it claims to be providing fake reviews on the US version of its Web site. The online retailer admitted its image having mottled by fraudsters’ postage of fallacious feedbacks, in the lawsuit. The news manifests having litigated plenty of accused for this hype on the URL—www.fiverr.com—an online platform for availing freelance services at an insignificant cost.

3.5 Falsified Reviews Procures Imprisonment [10]

This evidence talks about an imprisonment of nine months sentenced to a TripAdvisor reviewer on account of doing business of counterfeited feedbacks to similar organizations of hospitality sector, with an objective to popularize itself online. A hefty fine was also imposed on the miscreants. The imprisonment was done to establish an exemplary dictum to curb the menace of falsified feedbacks in exchange of monetary benefits. This judgment by the Italian court proved commendable in the light of the fact that usually under such acts of illegitimacy, the practice of fine or closing the company was the widespread practice normally.

4 The Tools Exposition—Automated Approaches

This section presents the analyzed and self-tested data, preferably in the form of self-explanatory figures (Figs. 1, 2 and 3), which have been arranged logically, as depicted below. These figures with tagged texts evidently serve as guidelines to these tools for a layman’s assistance to ease its usability.

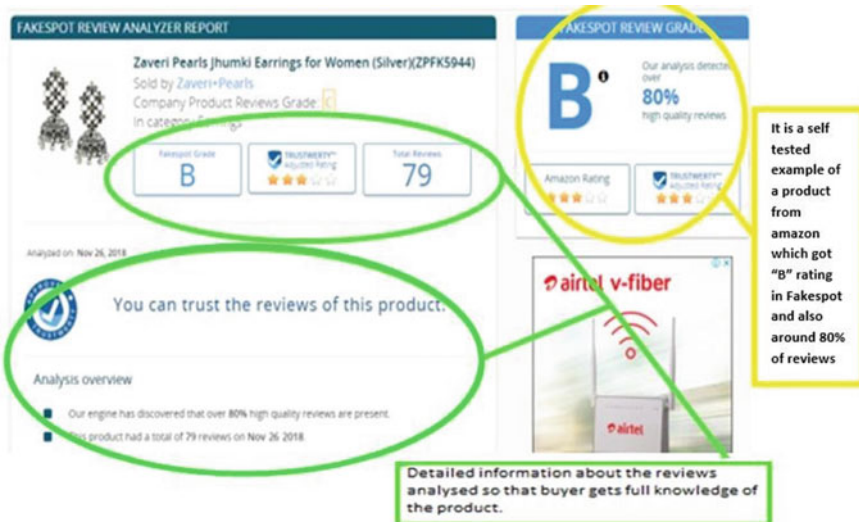


Fig. 1 Fakespot review on a bona fide Amazon product [11]

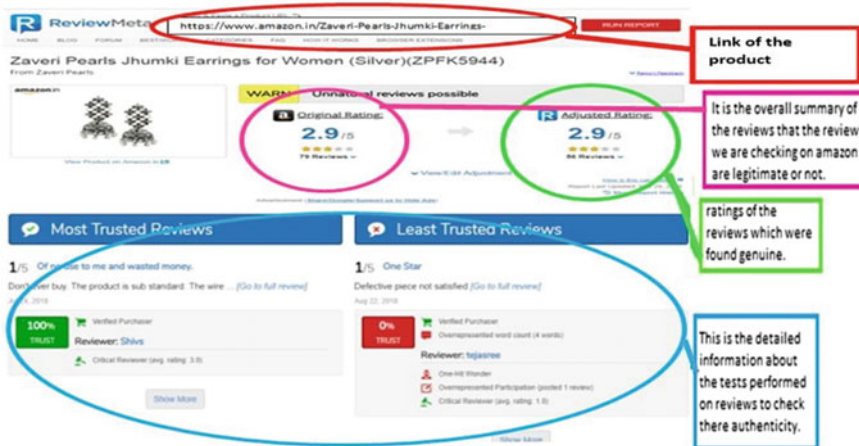


Fig. 2 ReviewMeta review on a bona fide Amazon product [12]

The experiment conducted connotes to a bona fide product that was available for sale on the Amazon Web site. The URL of the product was pasted in the box, as illustrated in the figures, followed by the hit on the “go” button. The product reviews from the Amazon site was analyzed via the “Fakespot,” the “ReviewMeta” and the “Review Index” tools that in juxtaposition revealed the discrimination of fakeness from the reality, apropos to the product review tested for.



Fig. 3 Review Index review on a bona fide Amazon product [13]

The elucidation further materializes in the form of a comparative table represented in Sect. 7, for scholars' suggestion, as ready reference on veracity of diversified tools for one's own predilection of usage and further exploration.

It is for the scholars' interest and further exploration, a comparative analysis has been presented in Sect. 5 that delineates the experimented tools in a lucid manner.

5 Result Analysis—Experiment's Explications

The ramification of the tools experimented above entails few clarifications to highlight the logistics of the output produced for intuitive comprehension of readers. Ardent readers may note the distinguishing aftermaths as follows:

- “Fakespot,” rated the product as “B” grade post analysis of the product review. Here, “B” grade serves as an appraisal for authenticity of the reviews posted.

The tool elucidates and corroborates its grading on the basis of the percentage of reviews that it evaluates as “authentic.”

- “ReviewMeta,” on similar lines distinguishes itself from analogous tools by posting two ratings, viz. overall summary of the reviews and ratings of reviews found genuine. Further, the tool also clarifies in detail the tests performed to check the reviews' legitimacy.
- “Review Index” characterizes and classifies the reviews' realism on different percentages, viz. percentage of—reviews detected, unverified reviews, or old reviews, spam tests and generates a final score as an outcome of all the tests, categorized as “authentic” (denoted by green color) and “fake” (denoted by red color) as depicted in Fig. 3.

6 Intricacies to Interpreting Fakeness—Manual Approaches

This section unearths the manual approaches congenial to revealing and/or spotting fake reviews. The fakeness can be identified on the following parameters [14–16], subjected to their clear and crisp scrutiny apropos to the review.

- Lacking of details: The fake reviews often lack in details in the context of narrating the specifics rather the reviews are stuffed with fancy words of fallacy. To exemplify personnel in hotel business being claimants of better service providers typify hotel reviews with catchy words like “check-in,” “price,” “vacation,” “business trips” and “my husband”, stretching the qualitative aspects out of proportion for customers to believe in them as the best service providers.
- Implication of more first person pronouns: The forged reviews intentionally are populated with words like “I”, “me”, boasting about themselves as genuine with tall claims to lead customers into bewilderment. For example, “Me and my family had a super excellent experience of stay in this hotel. I have no words to describe the services at par excellence like a five star hotel. I must also mention the quality services to be cheap and best. I have no words to describe further.” Here, the underlined words and the repeated usage of “I” connotes to blowing one’s own trumpet and may entail more fakeness than realism.
- Presence of more verbs than nouns: As depicted through the analysis of language usage, bogus reviews implicate more verbs as their authors surrogate more pleasurable or startling stories for factual facets. Genuine reviews are more populated with nouns.
- Inputs on Indicative idiosyncrasies: Language expertise is not enough to master the art and logic of spotting fake reviews. Scrutinizing reviews of varied buyers and mistrustful timestamps of postage of reviews are few articulated tactics to master the art of spotting fakeness than chanced successes. Given below are few nitty-gritty serving as indicators of fakeness.
 - Plenty of positive reviews with similar words and phrases posted within a short time frame.
 - Plethora of reviews with very similar photography, preferably with comparable backgrounds.
 - Adverse comparison with rival’s products.
 - Abundance of five star reviews with short contents.
 - Positive reviews with no admittance of underlying features.
 - Persistent use of product’s qualified full name.
 - Language laxity to promote search engine optimization of the product search.
 - Over praising of the product in its review.
 - Reviews by prominent and frequent positive review writers.
 - Flashing of quick and cozy reviews very soon after a product launch.
 - Reviews that are not traceable to verified purchases.
 - Multiple reviews with similar themes.

STRONG DECEPTIVE INDICATORS

A focus on who they were with

In this example, "My husband;" also words like "family."

Greater use of first-person singular

Fake reviews tend to use "I" and "me" more often.

Direct mention of where they stayed

Hotel and city names were less common in truthful reviews, which focus more on details about the hotel itself, like "small" or "bathroom."

"My husband and I stayed in the [hotel name] Chicago

and had a very nice stay! The rooms were large and comfortable. The view of Lake Michigan from our room was gorgeous. Room service was really good and quick, eating in the room looking at that view, awesome! The pool was really nice but we didn't get a chance to use it. Great location for all of the downtown Chicago attractions such as theaters and museums. Very friendly staff and knowledgeable, you can't go wrong staying here."

SLIGHT DECEPTIVE INDICATORS

High adverb use

"Very" and "really" are both used twice; "here" is used once.

High verb use

"Get", "go", "use", "can't", "didn't", "eating", "had", "looking", "stayed", "was" (three times), "were."

Use of "!" and positive emotion

Deceptive reviews tend to use exclamation points, while truthful reviews used more punctuation of other kinds, including "\$."

Fig. 4 Exemplification of textual propaganda in reviews—demonstrating fakeness [16]

- Untraceable reviewer history, slack/scare ranking of reviewer.

To exemplify and elaborate further, Fig. 4 highlights few more textual tyranny on amplification of fakeness in reviews written by deceiving reviewers.

7 Automated Tools Analysis—Tabulated Transcript

It is for the ardent readers' interest and implementation, a tabulated transcript of automated tools with a preliminary analysis on a vis-à-vis approach is enlisted below for reference (Table 1).

Table 1 Comparative analysis of popular automated tools [17]

Tool	Pros	Cons	Working	Outcome	Methodology
Fakespot	Does not display extra information, just results in grades and is easy and less time consuming to use	Compares the size of reviews. Moreover, algorithm works on sentimental approach, searches for specific sentiments or phrases to get fakeness	A user simply copies a product's link into the site's search engine and, its proprietary technology then analyzes the reviews in order to identify repeated words and phrases, frequency, dates, purchasing patterns and verified purchases to produce a list of reviews which are likely to be fake	Letter grades and detected percentage	This tool implements a plethora of technologies to ascertain the trustworthiness of the reviews.
Accuracy 60–70%	It is free to use via its handy online tool				The appreciation specifics of the tool lies in its ability to analyze the reviewer's dialect, the synopsis of the reviewer, inter-reviewer associations and self improvising machine learning algorithms.
Usage Often					The technologies include: opinion mining, profile clusters, cluster relationships and artificial intelligence entangled
ReviewMeta	It is more helpful and accurate tool than any other tool. More trustworthy as it undergoes 12 tests including sentimental and other aspects to check fakeness	Displays extra information which might not be need of the user. It is not user friendly. Gives a detailed information about the product which is not needed	Pasting the product link into the site's search tool, produces result of 'Pass', 'Warning' or 'Fail' to help guide a buyer's decision. Findings are based on language used within reviews, frequency of reviews, how soon after listing reviews are received and the number of unverified reviews	Number of reviews with recalculated percentage and three outcomes (Fail, Pass and Warn)	Here, 3 out of 12 tests are assessed: Redundancy of phrases, assessment of count of words, and impulse reviews. The remaining tests focus on extraneous data. It shares all the tests performed in the process to check authenticity
Accuracy 70–80%	In order to help you choose which ones to trust				
Usage Often					
ReviewIndex	ReviewIndex is another handy online tool, although a little more basic than Fakespot and ReviewMeta, used for spotting fake reviews	Special thing about review index is that it not only detects reviews of products but of videos tool	Low accuracy and seldom used	The review index analyses a product's link to produce an educated guess of the product's reviews	It produces a scoring of the analyzed reviews out of 10. The authentic and unauthentic reviews are displayed in different colors with percentage
Accuracy 10–20%					
Usage Seldom					

8 Conclusion

The aspect of information credibility of online social reviews is a growing concern in the light of the increasing anticipated hoax and faux implications in the posted reviews. This deliberate practice of deceptive reviews for the purpose of promotion of products and/or services with uncanny or malicious interest needs to be explored and experimented with automated and manual approaches, to evaluate the actual trustworthiness of the information presented, for customers to form informed decisions on purchase/acquiring of products and/or services.

As digital marketing trends are wide spreading and progressively being adapted by customers, the need for clear and crisp, precise and perfect demarcation of online reviews in context of its fakeness and realism is rising steadily. Hence, with a motive to capture the factual details and capitalize on sensitivity and measures on privacy and security of online social media, this paper commences with a prelude on information credibility, its compromises, the real-world incidents, and progresses toward automated and manual approaches to tackle the issues in a correlated, cooperative and coordinated manner.

9 Future Work

The future prospects have few notable dimensions of improvements, one of which entails designing customized tool for online review analysis with best features of automated tools incorporated into a single tool, enhanced with better accuracy and precision measures of trustworthiness of online reviews, justified via machine learning, artificial intelligence and deep learning approaches, for its wide spread acceptability as a standard tool. Another scope connotes to sentiment analysis amplified with text mining approaches with proven techniques of NLP to design a tool with better conceptualization and customization features apropos to the analysis of fakeness in online reviews.

References

1. Information definition. <http://ecomputernotes.com/fundamental/information-technology/what-do-you-mean-by-data-and-information>. Last accessed 21 June 2019
2. Credibility definition. <https://en.oxforddictionaries.com/definition/credibility>. Last accessed 21 June 2019
3. Significance of INFORMATION CREDIBILITY. <https://www.quora.com/Why-is-it-important-to-use-credible-sources-of-information-in-professional-practice>. Last accessed 21 June 2019
4. Information credibility need. <https://www.meltwater.com/blog/the-importance-of-content-authenticity-and-credibility/>. Last accessed 21 June 2019

5. Alexander, J.E., Tate, M.A.: Web Wisdom; How to Evaluate and Create Information Quality on the Webb, 1st edn. L. Erlbaum Assoc. Inc., Hillsdale, NJ, USA (1999)
6. Metzger, M.J., Flanagin, A.J., Eyal, K., Lemus, D.R., McCann, R.M.: Credibility for the 21st century: integrating perspectives on source, message, and media credibility in the contemporary media environment. *Ann. Int. Commun. Assoc.* **27**(1), 293–335 (2016)
7. News article. <https://www.sciencedaily.com/releases/2018/10/181011173106.htm>
8. Information credibility compromises. <https://www.reviewtrackers.com/oops-businesses-caught-posting-fake-reviews-online/>. Last accessed 21 June 2019
9. Amazon fake reviews. <https://www.theguardian.com/technology/2015/oct/18/amazon-sues-1000-fake-reviewers>. Last accessed 21 June 2019
10. News article. <https://www.theguardian.com/world/2018/sep/12/man-jailed-italy-selling-fake-tripadvisor-reviews-promo-salento>. Last accessed 21 June 2019
11. Fakespot tool. <https://www.amzdiscover.com/blog/3-free-fake-reviews-detectors-to-help-you-spot-fake-reviews-on-amazon/>. Last accessed 21 June 2019
12. Steps to use ReviewMeta. <https://www.inc.com/jessica-stillman/heres-how-to-spot-fake-online-reviews-with-90-perc.html>. Last accessed 21 June 2019
13. Steps to use ReviewIndex. <https://thereviewindex.com/in>. Last accessed 21 June 2019
14. Castillo, C., Mendoza, M., Poblete, B.: Information credibility on twitter. In: Proceedings of the 20th International Conference on World wide web (WWW '11), ACM, New York, NY, USA, pp 675–684 (2011)
15. Kwon, S., Cha, M., Jung, K., Chen, W., Wang, Y.: Prominent features of rumor propagation in online social media. In: Proceedings of the IEEE 13th International Conference on Data Mining, IEEE Xplore, pp 1103–1108 (2014)
16. Language analysis. <http://www.modernhoot.com/tag/fake-reviews/>. Last accessed 21 June 2019
17. Tools comparative study. <https://reviewmeta.com/blog/fakespot-vs-reviewmeta-for-analyzing-reviews/>. Last accessed 21 June 2019

Minimize Power Ratio (PR) in OFDM Using Tone Reservation Method



Yogendra Kumar Upadhyaya and Ajay Kumar Kushwaha

Abstract Orthogonal Frequency Division Multiplexing (OFDM) is a spectrally efficient multicarrier modulation technique for high-speed data transmission over multipath fading channels. One the major issues in OFDM is a large ratio between peak and average power, which affects Power Amplifiers in terms of complexity. A lot of techniques have proposed to reduce the power ratio but transmitted power, bit error rate (BER), etc. are so high. In this paper, combined SLM and proposed Tone Reservation methods are performed to reduce for power ratio between peak and average. Proposed Tone Reservation is the best suitable technique, based on BER and CCDF performance of the system.

Keywords Selecting Mapping (SLM) · Bit Error Rate (BER) · Complementary Cumulative Distribution Function (CCDF) · Peak to Average Power Ratio (PAPR)

1 Introduction

A multicarrier system, such as Frequency Division Multiplexing (FDM), distributes the entire offered bandwidth in the spectrum into sub-bands for multiple carriers to transmit parallelly [1]. An overall high data rate is obtained to put the carriers nearly on the spectrum. Nevertheless, inter-carrier interference (ICI) is occurring because of spacing problems between the carriers [2]. To minimize inter-carrier interference, broadbands are required to place between any adjoining carriers, which outcome in terms of low data rate. Orthogonal Frequency Division Multiplexing (OFDM) is a multicarrier digital communication method to resolve the issues. It combines a large number of low data rate carriers to make a high data rate communication system. Orthogonality gives the carriers spaced, with no inter-carrier

Y. K. Upadhyaya (✉) · A. K. Kushwaha
Government Engineering College, Raipur, Chhattisgarh, India
e-mail: yk.upadhyaya@gmail.com

A. K. Kushwaha
e-mail: ajay.igecsagar@gmail.com

interference, long symbol periods is implied each carrier less data rate and inter-symbol interference is diminished [3]. Though, the idea for OFDM is developed in 1960. There is no utilization in the last decade. Multicarrier (MC) transmission is a good technique for high data rate transmission as compared to wireless channels [4, 5] and it is robust to small bands and frequency selective fading interference adopted as wireless mobile communication systems like IEE802.1 Ia, etc.

2 PAPR Reduction Technique Used

2.1 SLM Technique

The selective mapping (SLM) already exists scheme for the less power ratio between peak and average. It is developed for OFDM and also very effective and distortion less methods which is used for the power ratio between the peak to average reduction in OFDM. This technique shows that only one sequence is selected out of number sequences. SLM techniques contain limited to side information and number of phase rotations factors [6].

The input data sequences for QAM is given

$X = [X_0, X_1, X_2, \dots, X_{N-1}]$ with phase $d_v = \exp(j2\pi\Phi)$

the phase sequence (Φ) can be written as

$$\Phi = \Phi = [\Phi_0, \Phi_1, \Phi_2, \dots, \Phi_{V-1}] \quad \Phi \in [0, \Omega] \quad (1)$$

Here, the phase vector is applied to reduce the PAPR and it is multiplied by the subcarrier of OFDM for reducing the peak. Only the phase vector that has less peak is multiplied by subcarriers. Transmitter and receiver know the phase vector. The phase vector circularly rotates. The rotation which has minimum peak is selected and send rotation number as side information. The benefit of this SLM scheme is that there is very less side information is used for reducing PAPR in OFDM systems.

Multiplication of the phase vector is done with subcarrier, after IFFT operation. In SLM, the value of the function is minimized taking the optimize value of the value v or phase vector value d. The maximize value of function is minimized after optimizing the value of phase vector d. The OFDM symbol x_n can be expressed as

$$x_n = \frac{1}{\sqrt{N}} \sum_{k=0}^{N-1} X_k * d_{v,k} e^{j2\pi nk/N} \quad (2)$$

2.1.1 Simulation Results

In simulation of OFDM system, QAM modulation is used for data symbols and there are 64 subcarriers in an OFDM symbol. The selecting mapping is used for decreasing

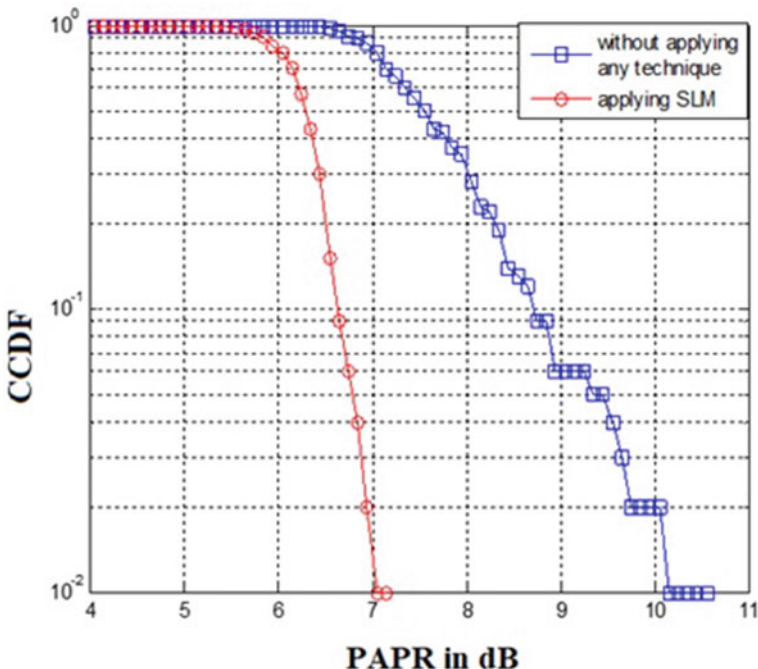


Fig. 1 PAPR versus CCDF plot for SLM

PAPR in OFDM. CCDF curve, CCDF curve shows the occurring of probability greater than a certain threshold value. PAPR is more than 10 dB at probability of 10^{-2} without any technique. PAPR is more than 7 dB at probability of 10^{-2} with selective mapping technique as shown in Fig. 1.

2.2 Tone Reservation

A less number of subcarriers which is not used in Tone Reservation is called Peak reduction Carrier (PRC) or Peak reduction Tone (PRT). It is reserved to minimize the power ratio. The block diagram of Tone Reservation (TR) is shown in Fig. 2 and it is best suitable method to obtain optimal values of the PRC which also reduces power ratio between peak and average value of transmitted OFDM signal. It is a very difficult task to optimize the TR and practical implementation has big issues. Because of some advantage tone reservations can be used to reduce power ratio between average and peak value in OFDM without internal system.

In this scheme, optimization peak of reduction tone is used for reducing the PAPR in OFDM symbols [7, 8]. The benefit of Tone Reservation is that not affecting the internal system. In this scheme selection of high value of reduction tone for reducing PAPR of OFDM signal.

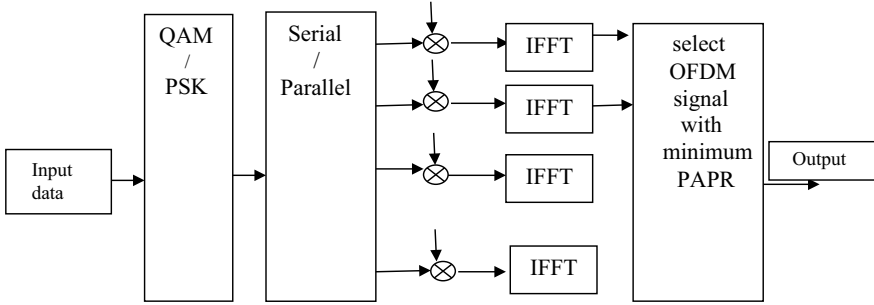


Fig. 2 Block diagram for tone reservation

In order to reduce the PAPR of OFDM signal using TR scheme, some subcarriers are reserved as a PRT set which is used to generate the peak cancelling signal. Let $R = \{i_0, i_1, i_2 \dots i_{w-1}\}$ represent the set of files of PRTs and R_t^c be the supplement of R_t in $N = \{0, 1, 2, \dots N - 1\}$ here width of PRT set is W . Besides the Tone Reservation Rate (TRR) can be written as

$$\text{TRR} = W/N \times 100\% \quad (3)$$

The expression for input symbol $S(n)$ in frequency domain is written as follows:

$$S_n = X_n + C_n = \begin{cases} X_n & n \in R_t^C \\ C_n & n \in R_t \end{cases} \quad (4)$$

Here X_n stands input data symbol and C_n is related to PRT. Assumptions $X_n = 0$ ($n \in R$) and $C_n = 0$ ($n \in R_t^C$). The discrete signal for OFDM signal is written as follow

$$\begin{aligned} s_k &= \frac{1}{\sqrt{N}} \sum_{k=0}^{N-1} (X_n + C_n) e^{j2\pi nk/N} \\ &= \frac{1}{\sqrt{N}} \sum_{k=0}^{N-1} (X_n) e^{j2\pi nk/N} + \frac{1}{\sqrt{N}} \sum_{k=0}^{N-1} (C_n) e^{j2\pi nk/N} \\ s_n &= c_n + x_n \end{aligned} \quad (5)$$

Peak cancelling signal represent $c = [c_0, c_1, c_2, c_3, \dots c_{N-1}]$ for $0 \leq k \geq N - 1$. The peak cancel signal c is designed in proper way to decrease the peak value of OFDM signal x_n competently. Some algorithms is suggested to find the peak cancel signal [7], $p = [p_0, p_1 \dots p_{N-1}]$. The frequency domain kernel $P = [P_0, P_1 \dots P_{N-1}]$ gave time domain kernel through IFFT. 1's and 0's represents PRTs and remaining tones [8]. By using shifting and scaling property, peak cancel signal is found by iteration in the time domain kernel P . The peak cancel signal C'

at the l th iteration is found as

$$C^{i+1} = C^i + \alpha_l p_{\tau_i}$$

where p_{τ_i} is the circulate shift of P by τ_i and α_i is the complex value scaling element which is computed to decrease peaks' value at the l th iteration to preferred threshold level β the circular shift and the scaling element α_i can be found by

$$\tau_i = \operatorname{argmax} |x_k + c_k^{i-1}|$$

$$\alpha_i = -(|x_{\tau_i}| - \beta)e^{j\theta_{\tau_i}}$$

where $\theta_{\tau_i} = \arg(\tau_i)$ since P is not a deltas' function, its side portion because of the magnitude growth of the sample over the PAPR threshold level [9, 10]. Thus we chose the PAPR threshold level β a little bit lower than the target PAPR close to OFDM output. The PAPR of an OFDM signal $s = [s_0, s_1, \dots, s_{N-1}]$ with the TR scheme

$$\text{PAPR} = \frac{\max |x_n + c_n|^2}{E[|x_n|^2]} \quad (6)$$

Minimize the value of s_n in maximum value of x_n by optimize the value of Peak Reduction Tone (PRT) signal in the (7).

2.2.1 Simulation Result

The gain is obtained 2 dB at 10^{-2} probability. Another gain is measured at 10^{-1} probability.

Probability occurring at 10^{-1} probability, PAPR is more than 7 dB with applying Tone Reservation technique. Figure 3 shows the graph between the CCDF versus PAPR with tone reservation technique and without any technique.

3 Combined SLM and Proposed Tone Reservation

The proposed tone reservation technique is applied using SLM technique. The OFDM symbol is obtained by using SLM technique from equation (2).

$$x = [x_0, x_1, x_2, \dots, x_{M-1}] \quad (7)$$

where x is the received OFDM data vector before applying SLM technique and M is the number of OFDM symbol [11].

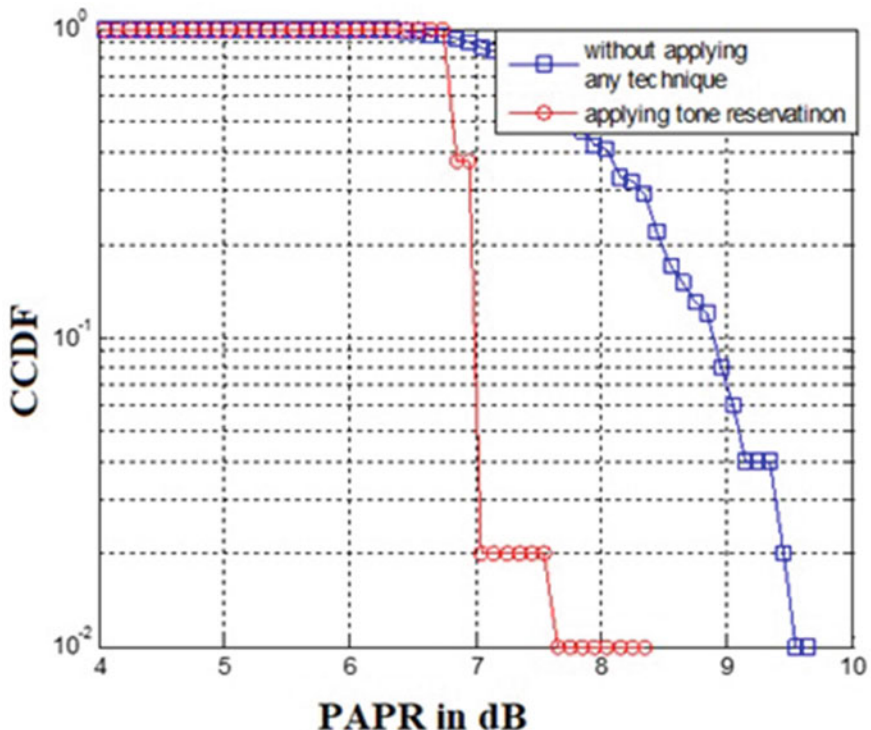


Fig. 3 CCDF versus PAPR plot for Tone Reservation

Peak detection is obtained by using sorting or any other technique

$$x_{\text{peak}} = \max(x_{\text{peak}}) \quad (8)$$

$$x_r = [\text{optimize value of } p_i] + x_{\text{peak}} \quad (9)$$

$$p_i = \alpha_i e^{i2\pi b_i / N}$$

α_i and b_i is the scaling and phase factors.

The value of α_i and b_i shift circularly as given in the lookup table. Both transmitter and receiver have the same look table. The position of the peak and a number of circular shifts are sent as side information.

x_r is the reduced peak. The peak x_{peak} is replaced with x_r until the PAPR reaches a fixed value.

Algorithm

1. IFFT SLM data as a input.
2. Detect the highest peak.
3. Get reduced PAPR by Tone Reservation.

```

If PAPR >  $\beta$ 
  Return to detect the peak value
else
  Signal is transmitted

```

3.1 Simulation and Result

The CCDF versus PAPR curves are shown in Fig. 4 with no applied technique, SLM and proposed Tone Reservation [11, 12]. PAPR is more than 10 dB at the probability of 10^{-2} . PAPR is more than 7 dB at the probability of 10^{-2} using selective mapping. PAPR is more than 5.8 dB at the probability of 10^{-2} with Tone Reservation. The suggested scheme is defined for QAM and the performance analysis showed that in terms of the PAPR and CCDF. A gain of 4.2 dB is attained at the probability of 10^{-2} .

Figure 5 shows the peak detection and remove peak and there is highest peak at position 203 and position 248. The highest peaks has been removed by applying

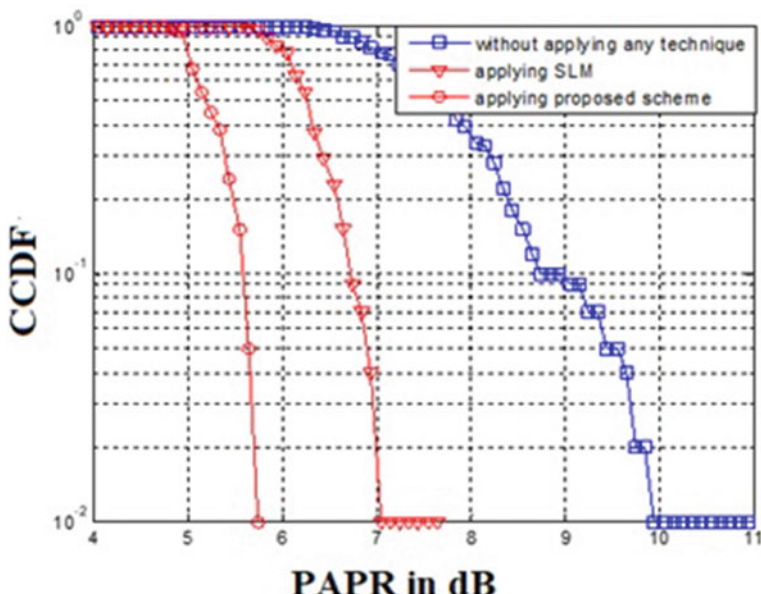


Fig. 4 CCDF versus PAPR plot for proposed scheme

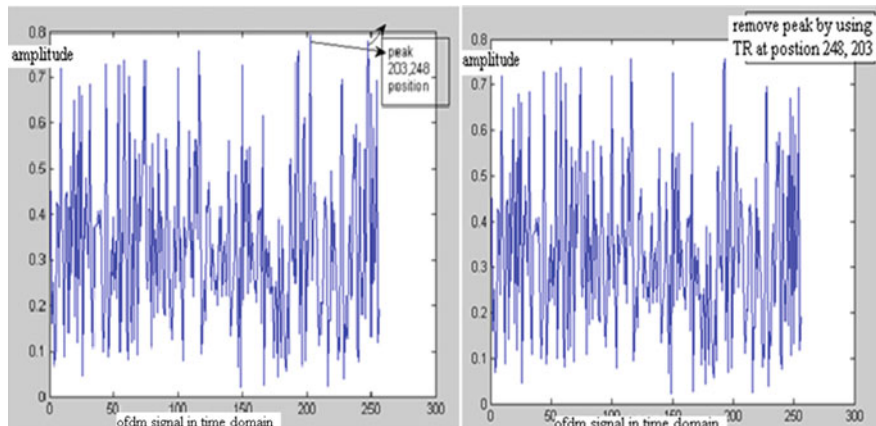


Fig. 5 Peak detection and remove peak

proposed Tone Reservation [13]. CCDF versus PAPR for proposed scheme and TR is shown in Fig. 6. PAPR is more than 6 dB at probability 10^{-2} with proposed Tone Reservation scheme [9, 13] and also get more than 2.3 dB for QAM.

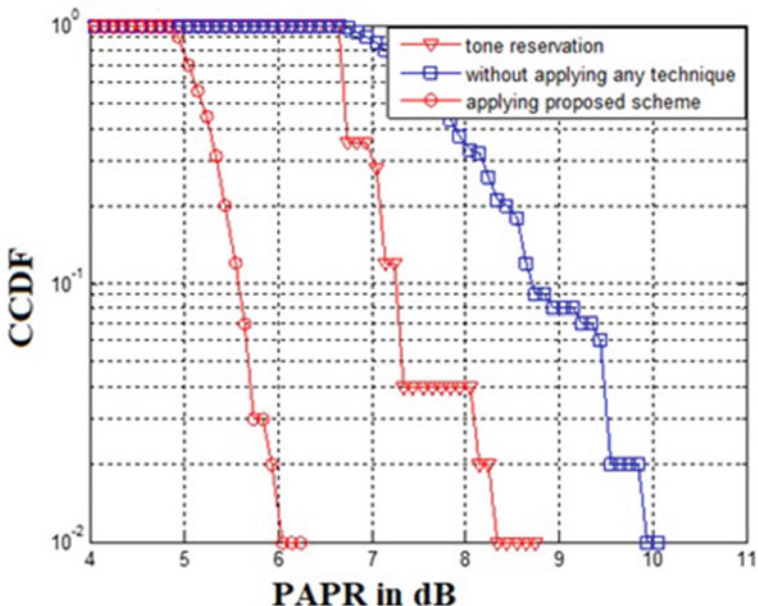


Fig. 6 CCDF versus PAPR for proposed scheme and TR

4 Conclusion

Our proposed Tone Reservation scheme gives better results as compared to Tone Reservation. The proposed Tone Reservation is explained for QAM in terms of the performance of the PAPR and CCDF. A gain of 4 dB is obtained at the probability of 10^{-2} with no applied PAPR reduction technique. The proposed scheme has 2.3 dB gains compared to the Tone Reservation scheme. The proposed scheme has 57.57% more gain compared to the Tone Reservation scheme. The proposed Tone Reservation scheme efficiently reduces PAPR. The advantage of Tone Reservation is that it is applied after generation OFDM data. There is no effect on internal hardware. This technique has very less side information. The side information will not be greater than the 15% of input data symbol. The complexity of the complete OFDM systems increase but it gives better PAPR reduction results. From the point of view, PAPR reduction proposed technique is more beneficial.

In the future, the proposed scheme may be explored that need to transfer less side information. Any mathematical function may be searched that takes less information to implement this technique. The complexity may be reduced after applying the searched mathematical function. Proposed scheme efficiently reduce PAPR, in future proposed technique may be explored that it reduces more PAPR reduction.

Acknowledgements This work is supported by the Third Phase of Technical Education Quality Improvement Program (TEQIP-III) under the “TEQIP Collaborative Research Scheme”, National Project Implementation Unit (NPIU), a unit of Ministry of Human Resource Development (MHRD), Government of India for implementation of World Bank assisted projects in technical education.

References

1. Saltzberg, B.: Performance of an efficient parallel data transmission system. *IEEE Trans. Commun. Technol.* **15**(6), 805–811 (1967)
2. Hwang, T., Yang, C., Wu, G., Li, S., Li, Ye, G.: OFDM and its wireless applications: a survey. *IEEE Trans. Veh. Technol.* **58** (4), 1673–1694 (2009)
3. Zhang, J.Y., Letaief, B.K.: Multiuser adaptive subcarrier-and-bit allocation with adaptive cell selection for OFDM systems. *IEEE Trans. Wirel. Commun.* **3**(5), 1566–1575 (2004)
4. Shi, C., Wang, F., Sellathurai, M., Zhou, J., Salous, S.: Power minimization-based robust OFDM radar waveform design for radar and communication systems in coexistence. *IEEE Trans. Signal Process.* **66**(5), 1316–1330 (2018)
5. Zhang, L., Ijaz, A., Xiao, P., Molu, M.M., Tafazolli, R.: Filtered OFDM systems, algorithms, and performance analysis for 5G and beyond. *IEEE Trans. Commun.* **66**(3), 1205–1218 (2018)
6. Sari, H., Karam, G., Jeanclaude, I.: Transmission techniques for digital terrestrial TV broadcasting. *IEEE Commun. Mag.* **33**(2), 100–109 (1995)
7. Juwono, H.F., Gunawan, D.: PAPR reduction using Huffman coding combined with clipping and filtering for OFDM transmitter. In: 2009 Innovative Technologies in Intelligent Systems and Industrial Applications, pp. 344–347 (2009)
8. Chen, C.J., Chiu, H.M., Yang, S.Y., Li, P.C.: A suboptimal tone reservation algorithm based on cross-entropy method for PAPR reduction in OFDM systems. *IEEE Trans. Broadcast.* **57**(3), 752–756 (2011)

9. Kim, M., Lee, W., Cho, H.-D.: A novel PAPR reduction scheme for OFDM system based on deep learning. *IEEE Commun. Lett.* **22**(3), 510–513 (2018)
10. Xia, Y., Cui, J., Zhang, J.: Sparse repeated preamble-based direct current offset and frequency offset estimator in OFDM direct conversion receivers. *IEEE Access* **7**, 16043–16050 (2019)
11. Wang, F., Gu, F., Wang, S.: Carrier frequency offset estimation based on ESPRIT for OFDM direct conversion receivers. In: 2016 2nd IEEE International Conference on Computer and Communications (ICCC), pp. 1580–1584 (2016)
12. Yang, G., Liang, C.-Y., Zhang, R., Pei, Y.: Modulation in the air: backscatter communication over ambient OFDM carrier. *IEEE Trans. Commun.* **66**(3), 1219–1233 (2018)
13. Zhao, Y., Haggman, G.-S.: Intercarrier interference self-cancellation scheme for OFDM mobile communication systems. *IEEE Trans. Commun.* **49**(7), 1185–1191 (2001)

A Single-Phase Multi-level Inverter Using a Lesser Number of Switching Devices



Ashutosh Kumar Singh, Ravi Raushan, and Pratyush Gauri

Abstract The multi-level inverters with the reduced components are becoming prevalent because a higher number of output voltage levels can be achieved using a comparatively lesser number of devices. This paper proposes a generalized configuration of single-phase symmetric multi-level inverter (MLI) topology using lesser number of power electronic switches. The comprehensive study of the proposed inverter has been done through a specimen nine-level inverter. Level-shifted pulse width modulation (LS-PWM) technique is applied to produce the corresponding gate pulses. Modeling and simulation of the proposed inverter are done using MATLAB/Simulink. The proposed structure of the nine-level inverter is experimentally executed in the laboratory to validate the simulation outcomes. Moreover, a comparative study of the recommended configuration of the multi-level inverter is done.

Keywords DC–AC converter · Multi-level inverter · THD · Pulse width · Modulation · Converter losses

1 Introduction

Multi-level power conversion was introduced more than thirty-five years prior [1]. The multi-level inverter can produce a higher number of output voltage levels, which infers in reduced harmonic content, reduced switching losses, higher voltage capability, improved power quality and enhanced electromagnetic compatibility. Multi-level inverters have several applications including adjustable speed drives, renewable energy sources, static reactive power compensation, etc. [2–4]. The major utility of the multi-level inverter is to build the desired AC voltage using single or various separate DC sources of similar or else of different values [5]. Therefore, many types of topologies for multi-level inverter have been introduced. In general, three types

A. K. Singh (✉) · R. Raushan · P. Gauri
National Institute of Technology, Patna 800005, India
e-mail: ash170723@gmail.com

of classical multi-level inverter (MLI) became prominent in many industrial applications including neutral point clamped (NPC) multi-level inverter [6], flying capacitor (FC) multi-level inverter [7] and cascaded H-bridge (CHB) multi-level inverter [8]. The main demerit of an NPC type converter is that there is uneven voltage sharing among the series-connected capacitors. Moreover, this configuration needs many clamping diodes to achieve an increase in output levels. Unbalancing of capacitor voltage across the storage capacitors and bulkier circuit is the major demerits of the FC-MLI. Conventional CHB-MLI has used a lesser number of diodes and capacitors in comparison with NPC and FC-MLI topology. The CHB-MLI contains various numbers of H-bridges having individual DC sources of equal or unequal magnitudes for each bridge [9]. The MLIs with a reduced number using bidirectional switches and asymmetrical DC sources have been introduced [10, 11]. The MLI topologies using the half-bridge and T-type converter have been proposed [12–15]. Several MLIs with reduced switches, single DC source with capacitor voltage control techniques are presented [16]. Various modulation techniques including level-shifted PWM, carrier phase-shifted PWM technique [17], synchronous optimal PWM [18], active harmonic elimination [19], selective harmonic elimination [20] space vector modulation techniques [21] and nearest level control [22] methods have been reported for the modulation of MLI.

1.1 Proposed MLI configuration

The proposed inverter topology comprises two sections named as level generating part and polarity generating part is represented in Fig. 1. The level generating part develops positive voltage using several cells named as cell-1, cell-2 ... cell- n .

An H-bridge is attached across the level generating part to achieve alternating voltage at the inverter output terminal. Each of such cells contains two switches ($T_{n,1}$ and $T_{n,2}$) in the company of one DC voltage source. Each DC source engaged in this topology has an equal magnitude (E). Each cell either bypasses the current through $T_{n,2}$ or adds voltage of magnitude E .

The mathematical expressions for the number of output voltage levels (N_1) can be represented as follows:

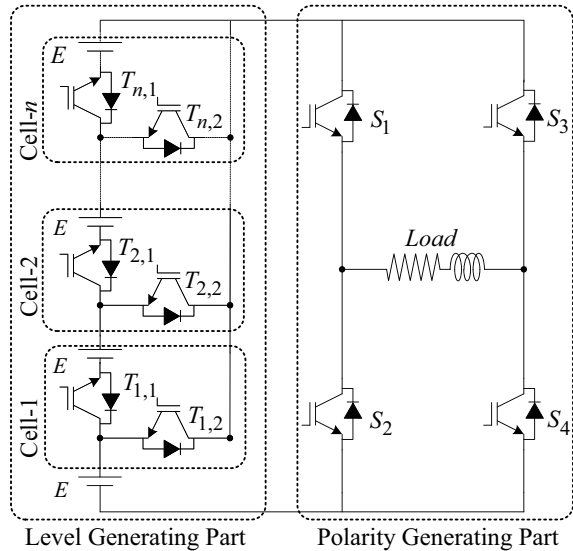
$$N_1 = 2m + 1 \quad (1)$$

The required number of IGBTs (N_{IGBT}) can be expressed as

$$N_{\text{IGBT}} = 2(m + 1) \quad (2)$$

Since no extra diodes are used for the design of the proposed MLI topology, the number of IGBTs will remain equal to the number of diodes (N_{diode}). The magnitude of output voltage depends upon the quantity of cells connected to the level generating

Fig. 1 Generalized structure of the proposed MLI topology



part and the magnitude of each DC source in every cell. Hence, the maximum voltage at the output of the inverter ($E_{o,\max}$) can be represented as follows:

$$E_{o,\max} = mE \quad (3)$$

where m represents the total number of DC voltage source used for the MLI with desired number of levels.

1.2 Proposed Nine-Level Inverter

The proposed inverter for nine voltage levels is considered for further analysis. The schematic circuit diagram of the proposed nine-level inverter is depicted in Fig. 2. Three cells are used in this inverter configuration to synthesize the output voltage of nine levels. The polarity generation part has four switches (S_1 , S_2 , S_3 and S_4), and level generating part employs six switches ($T_{1,1}$, $T_{1,2}$, $T_{2,1}$, $T_{2,2}$, $T_{3,1}$ and $T_{3,2}$). Since the circuit is having four DC voltage sources of equal magnitude (E), this is considered as a symmetrical configuration.

The recommended inverter has nine modes of operation for achieving nine voltage levels at the output. Table 1 expresses the voltage levels generated at the output of nine-level inverter under various combination of switching states.

A stepped waveform of nine-levels ($-4E$, $-3E$, $-2E$, $-E$, 0 , $+E$, $+2E$, $+3E$, $+4E$) under suitable switching states is obtained as the output terminal of the multi-level inverter.

Fig. 2 Recommended structure of the nine-level inverter

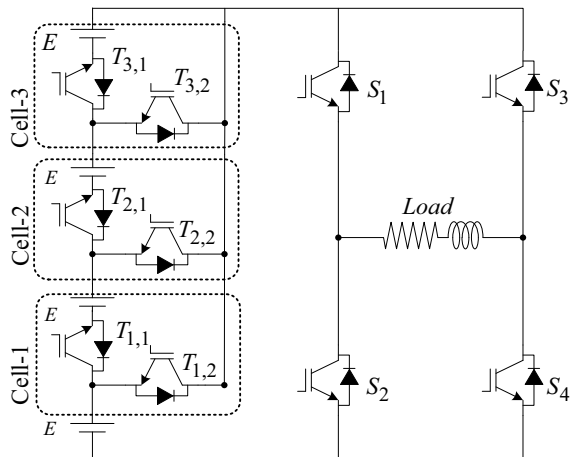


Table 1 Output voltage according to switching states for the proposed nine-level inverter

Status of the proposed MLI switches (0 = OFF, 1 = ON)										Output voltage (V_o)
S_1	S_2	S_3	S_4	$T_{1,1}$	$T_{1,2}$	$T_{2,1}$	$T_{2,2}$	$T_{3,1}$	$T_{3,2}$	
1	0	1	0	0	0	0	0	0	0	0
1	0	0	1	0	1	0	0	0	0	E
1	0	0	1	1	0	0	1	0	0	$2E$
1	0	0	1	1	0	1	0	0	1	$3E$
1	0	0	1	1	0	1	0	1	0	$4E$
0	1	0	1	0	0	0	0	0	0	0
0	1	1	0	0	1	0	0	0	0	$-E$
0	1	1	0	1	0	0	1	0	0	$-2E$
0	1	1	0	1	0	1	0	0	1	$-3E$
0	1	1	0	1	0	1	0	1	0	$-4E$

1.3 Modulation and Control Procedure of the Proposed MLI

Several techniques can be implemented to realize the required gate pulses for the power semiconductor devices such as sinusoidal PWM (SPWM) method, fundamental switching frequency method and space vector PWM method. To generate the gate pulses for the respective semiconductor devices of the recommended inverter, the sinusoidal PWM method is considered for the implementation.

A multi-carrier level-shifted pulse width modulation method is implemented to produce the gate pulses in order to turn-on or turn-off the IGBTs. In this technique, the comparison of eight triangular carrier signals operating at very high frequency (f_c) with the sinusoidal reference signal (V_{ref}) at the fundamental frequency is done to generate the PWM switching signal for the recommended nine-level inverter. These eight carrier signals for positive polarity are termed as V_{cr4+} , V_{cr3+} , V_{cr2+} ,

V_{cr1+} while for the negative polarity is termed as $+V_{cr1-}$, V_{cr2-} , V_{cr3} and V_{cr4-} as represented in Fig. 3. The required waveform of the gate pulses obtained at the carrier frequency (f_c) of 1 kHz through this technique with appropriate digital logic gates is shown in Fig. 4. The amount of switching losses caused by two switches (S_4 and S_1) can be negligible because they are operating at a fundamental frequency as observed from Fig. 4.

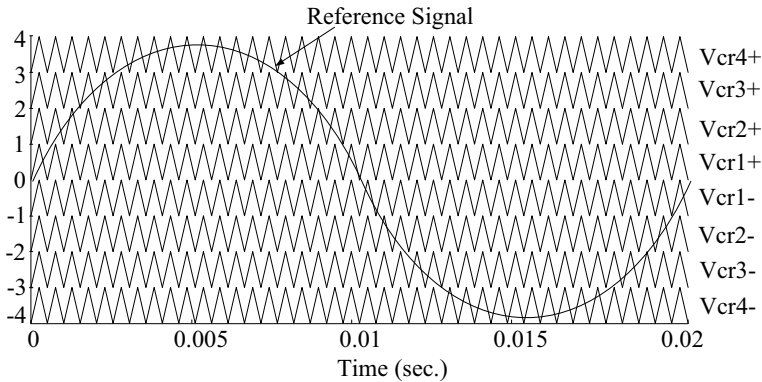


Fig. 3 PWM (level-shifted) implementation technique for the suggested nine-level inverter

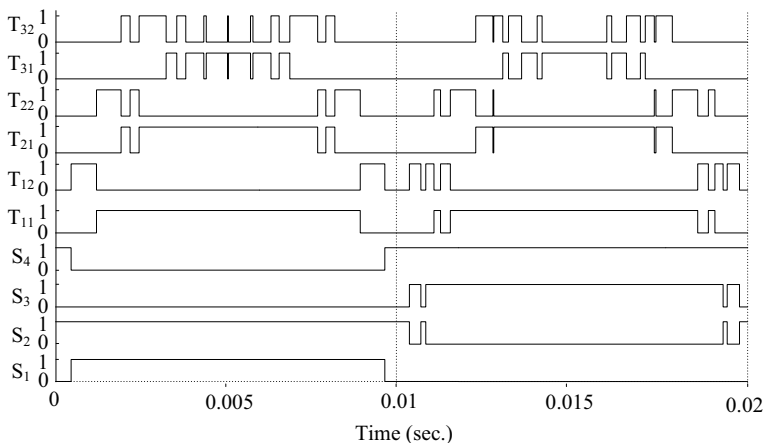


Fig. 4 Gate pulsed obtained for the recommended nine-level inverter topology at the carrier frequency (f_c) of 1000 Hz

2 Simulation and Experimental Results

To approve the performance of the recommended single-level nine-level inverter using level-shifted PWM technique, the modeling and simulation are executed using MATLAB/Simulink, and the corresponding outcomes are discussed. The magnitude of DC voltage sources (E) in each cell of the recommended nine-level inverter is considered as 100 V. The proposed MLI is loaded with a resistive-inductive load ($R = 25 \Omega$ and $L = 10 \text{ mH}$) for the simulation purposes. The carrier frequency (f_c) of the mentioned technique is chosen as 1.5 kHz for improved harmonic content and reduced size of the required low pass filter. The simulation results of output voltage for nine-level inverter and corresponding harmonic spectrum are displayed in Fig. 5. It is witnessed from Fig. 5 that the THD in the output voltage waveform of the recommended nine-level inverter at modulation indices (M_i) 1.0, 0.75 and 0.5 is 8.13%, 13.16% and 19.91%, respectively. It can be evidently noticed that the output voltage (the number of voltage level) decreases by reducing the modulation index. The THD at rated voltage operation is lesser.

The experimental setup is established in the laboratory to validate the corresponding simulation results obtained from the proposed nine-level inverter. The block diagram of the experimental setup is depicted in Fig. 6. The isolated DC voltages for the gate driver circuits are realized using transformer rectifier with capacitor filter.

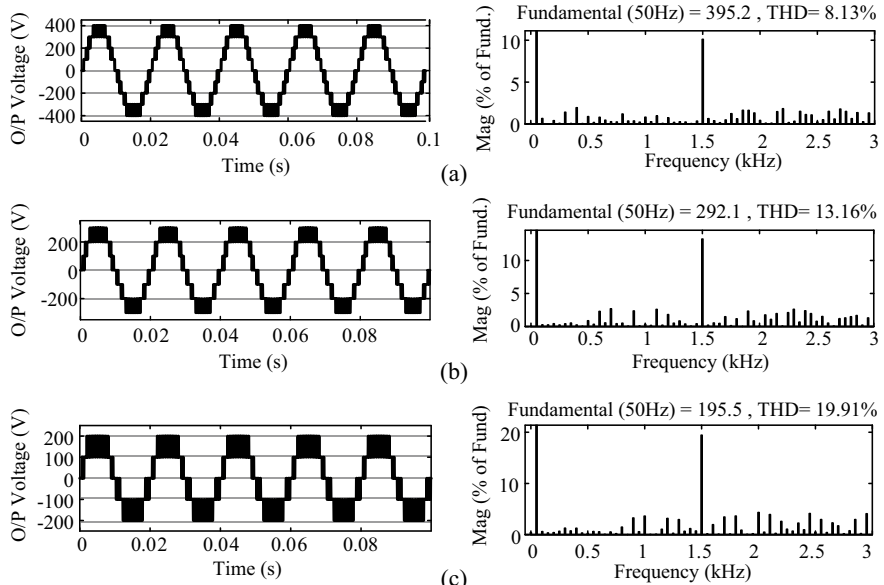


Fig. 5 Output voltage and THD obtained by simulation with $E = 100 \text{ V}$: **a** $M_i = 1$, **b** $M_i = 0.75$ and **c** $M_i = 0.5$

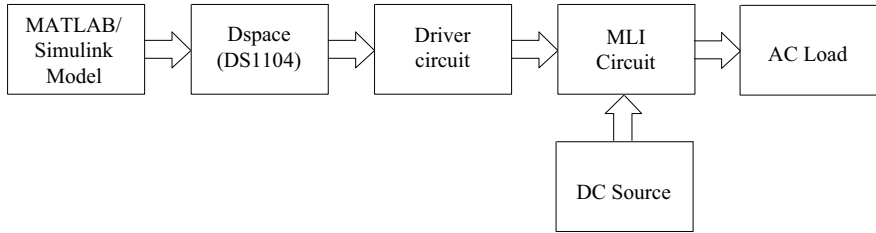


Fig. 6 Basic block diagram of the recommended nine-level inverter system

Moreover, for the proposed inverter, four isolated DC-link voltages of the magnitude of 21 V are achieved from the AC voltage sources using a step down transformer with a bridge rectifier and capacitor arrangements. The gate pulses for the respective switches of the recommended inverter are generated using the level-shifted PWM technique and implemented through a DS1104 real-time controller. The carrier frequency (f_c) of 1.5 kHz is also considered for hardware implementation.

The output voltage waveform of the proposed nine-level inverter is acquired at unity modulation index and presented in Fig. 7.

Few popular MLIs are considered for the comparison in the form of the required number of switches, diodes and capacitors and illustrated in Table 2. Moreover, the component count for nine-level of the referred MLIs and the proposed topology is obtained from Table 2 and represented in Fig. 8. It can be perceived from Fig. 8 that the component count for recommended nine-level inverter topology is lesser than other MLI topology.

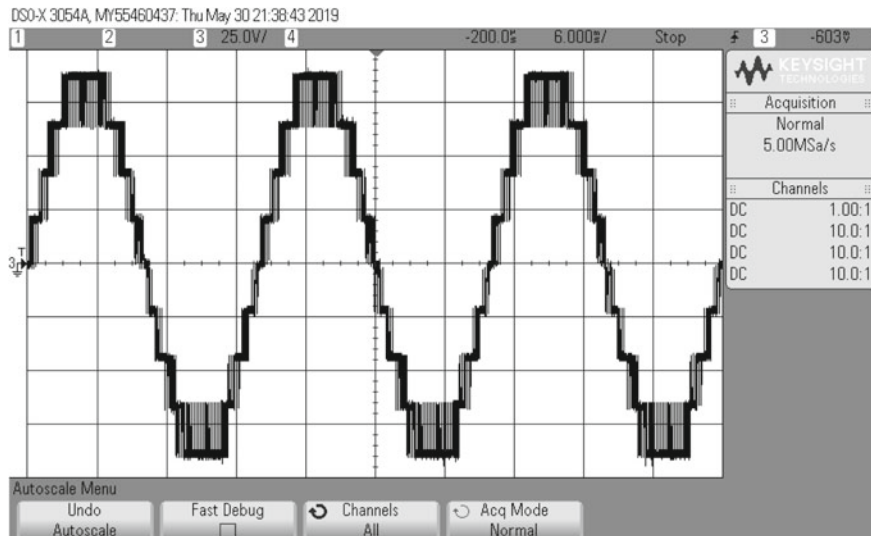
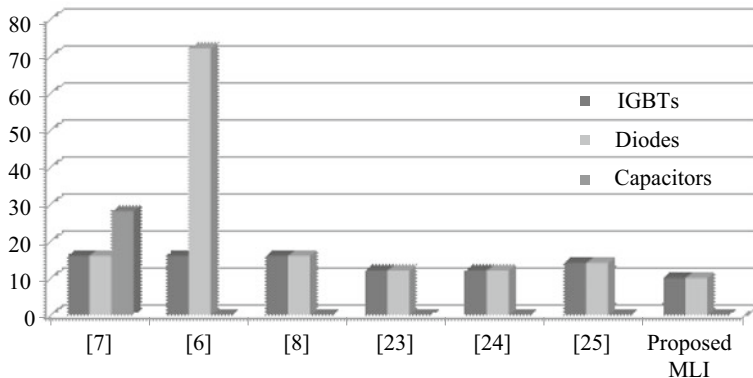


Fig. 7 Experimental result of the output voltage of the recommended inverter at $M_i = 1.0$

Table 2 Component count of different MLIs and the proposed MLI

MLIs	Number of IGBTs (N_{IGBT})	Number of main diodes	Clamping diodes	Balancing capacitor
FC-MLI [7]	$2(N_1 - 1)$	$2(N_1 - 1)$	0	$0.5(N_1 - 1)$ $(N_1 - 2)$
NPC-MLI [6]	$2(N_1 - 1)$	$2(N_1 - 1)$	$(N_1 - 1)(N_1 - 2)$	0
CHB-MLI [8]	$2(N_1 - 1)$	$2(N_1 - 1)$	0	0
[23]	$3(N_1 - 1)/2$	$3(N_1 - 1)/2$	0	0
[24]	$N_1 + 3$	$N_1 + 3$	0	0
[25]	$2(N_1 - 2)$	$2(N_1 - 2)$	0	0
Proposed MLI	$N_1 + 1$	$N_1 + 1$	0	0

**Fig. 8** Comparison of some popular MLI topology for nine-level output voltage

3 Conclusion

A novel topology of symmetrical MLIs has been proposed using a lesser number of switches. The operation of the recommended inverter for nine levels of output voltage has been explained. The mathematical expressions for the device count and output voltage have been established. The proposed MLI structure corresponding to nine-level has been simulated at different modulation indices using MATLAB/Simulink, and corresponding results are presented and justified. The inverter produces rated voltage having 8.13% of THD at unity modulation index. An experimental prototype of the recommended inverter for output voltage of nine levels has been developed, and experiments have been conducted with the resistive-inductive load for the verification of simulation results. The dominance of the recommended inverter above few multi-level inverter topologies in respect of device count has also been reported.

Table 3 Specifications of devices used for designing the laboratory prototype of the recommended nine-level inverter

Component	Specification
IGBTs (CT60AM)	900 V, 60 A
Step down transformer	12–0–12 V, 1 mA
Diode (IN4007)	1 kV, 30 A, 3 W
Capacitor	1000 and 100 μ F, 25 V
Opto-coupler (TLP 250)	10–35 V, ± 1.5 A
Voltage regulator (7912, 7812)	12 V, 1.5 A

The advantage of having reduced component count imposes limitation such as the requirement of separate DC sources.

Appendix 1

The list of components along with their detailed specification used for the experimental setup of the recommended nine-level inverter is presented in Table 3.

References

- Stala, R.: A natural DC-link voltage balancing of diode-clamped inverters in parallel systems. *IEEE Trans. Ind. Electron.* **60**, 5008–5018 (2013). <https://doi.org/10.1109/TIE.2012.2219839>
- Manjrekar, M.D., Steimer, P.K., Lipo, T.A.: Hybrid multilevel power conversion system: a competitive solution for high-power applications. *IEEE Trans. Ind. Appl.* **36**, 834–841 (2000). <https://doi.org/10.1109/28.845059>
- Alonso, R., Román, E., Sanz, A., Martínez Santos, V.E., Ibáñez, P.: Analysis of inverter-voltage influence on distributed MPPT architecture performance. *IEEE Trans. Ind. Electron.* **59**, 3900–3907 (2012). <https://doi.org/10.1109/TIE.2012.2189532>
- Abdul Kadir, M.N., Mekhilef, S., Ping, H.W.: Voltage vector control of a hybrid three-stage 18-level inverter by vector decomposition. *IET Power Electron.* **3**, 601 (2010). <https://doi.org/10.1049/iet-pel.2009.0085>
- Tolbert, L.M., Peng, F.Z.: Multilevel converters as a utility interface for renewable energy systems. *00*, 1271–1274 (2002). <https://doi.org/10.1109/pess.2000.867569>
- Nabae, A., Takahashi, I., Akagi, H.: A new neutral-point-clamped PWM inverter. *IEEE Trans. Ind. Appl.* **IA-17**, 518–523 (1981). <https://doi.org/10.1109/TIA.1981.4503992>
- Meynard, T.A., Foch, H.: Multi-level Conversion: High Voltage Choppers and Voltage-Source Inverters, pp. 397–403 (2003). <https://doi.org/10.1109/pesc.1992.254717>
- McMurray, W.: Fast response stepped-wave switching power converter circuit. United States Pat. (1971)
- Malinowski, M., Gopakumar, K., Rodriguez, J., Perez, M.A.: A survey on cascaded multilevel inverters. *IEEE Trans. Ind. Electron.* **57**, 2197–2206 (2010). <https://doi.org/10.1109/TIE.2009.2030767>
- Babaei, E.: A cascade multilevel converter topology with reduced number of switches. *Power Electron. IEEE Trans.* **23**, 2657–2664 (2008). <https://doi.org/10.1109/TPEL.2008.2005192>
- Babaei, E., Laali, S.: A multilevel inverter with reduced power switches. *Arab. J. Sci. Eng.* **41**, 3605–3617 (2016). <https://doi.org/10.1007/s13369-016-2217-0>

12. Choi, U., Lee, K., Blaabjerg, F.: Diagnosis and tolerant strategy of an open-switch fault for T-type three-level inverter systems. *IEEE Trans. Ind. Appl.* **50**, 495–508 (2014)
13. Raushan, R., Mahato, B., Jana, K.C.: Comprehensive analysis of a novel three-phase multilevel inverter with minimum number of switches. *IET Power Electron.* **9**, 1600–1607 (2016). <https://doi.org/10.1049/iet-pel.2015.0682>
14. Raushan, R., Mahato, B., Jana, K.C.: Optimum structure of a generalized three-phase reduced switch multilevel inverter. *Electr. Power Syst. Res.* **157**, 10–19 (2018). <https://doi.org/10.1016/j.epsr.2017.11.017>
15. Raushan, R., Mahato, B., Jana, K.C.: Operation and control of three-phase multilevel inverter with reduced component. 2016 3rd Int. Conf. Recent Adv. Inf. Technol. RAIT 2016. **2**, 295–299 (2016). <https://doi.org/10.1016/j.epsr.2017.11.017>
16. Vahedi, H., Trabelsi, M.: Single-DC-source multilevel inverters. Springer International Publishing, Switzerland AG (2019). <https://doi.org/10.1007/978-3-030-15253-6>
17. McGrath, B.P., Holmes, D.G.: Multicarrier PWM strategies for multilevel inverters. *IEEE Trans. Ind. Electron.* **49**, 858–867 (2002). <https://doi.org/10.1109/TIE.2002.801073>
18. Rathore, A.K., Holtz, J., Boller, T.: Generalized optimal pulsewidth modulation of multilevel inverters for low-switching-frequency control of medium-voltage high-power industrial AC drives. *IEEE Trans. Ind. Electron.* **60**, 4215–4224 (2013). <https://doi.org/10.1109/TIE.2012.2217717>
19. Hosseini Aghdam, G.: Optimised active harmonic elimination technique for three-level T-type inverters. *IET Power Electron.* **6**, 425–433 (2013). <https://doi.org/10.1049/iet-pel.2012.0492>
20. Lou, H., Mao, C., Wang, D., Lu, J., Wang, L.: Fundamental modulation strategy with selective harmonic elimination for multilevel inverters. *IET Power Electron.* **7**, 2173–2181 (2014). <https://doi.org/10.1049/iet-pel.2013.0347>
21. Jana, K.C., Biswas, S.K.: Generalised switching scheme for a space vector pulse-width modulation-based N-level inverter with reduced switching frequency and harmonics. *IET Power Electron.* **8**, 2377–2385 (2015). <https://doi.org/10.1049/iet-pel.2015.0101>
22. Meshram, P., Borghate, V.: A simplified nearest level control (NLC) voltage balancing method for modular multilevel converter (MMC). *IEEE Trans. Power Electron.* **8993**, 1–1 (2014). <https://doi.org/10.1109/TPEL.2014.2317705>
23. Gui-Jia, S.: Multilevel DC-link inverter. *Ind. Appl. IEEE Trans.* **41**, 848–854 (2005). <https://doi.org/10.1109/TIA.2005.847306>
24. Choi, W.K., Kang, F.S.: H-bridge based multilevel inverter using PWM switching function. INTELEC, Int. Telecommun. Energy Conf. (2009). <https://doi.org/10.1109/INTLEC.2009.5351886>
25. Heidari Yazdi, S.S., Jabbarvaziri, F., Niknam Kumle, A., Jamshidi, M., Fathi, S.H.: Application of memetic algorithm for selective harmonic elimination in multi-level inverters. *IET Power Electron.* **8**, 1733–1739 (2015). <https://doi.org/10.1049/iet-pel.2014.0209>

Symmetric Key Generation and Distribution Using Diffie-Hellman Algorithm



Kaustubh Purohit, Avanish Kumar, Mayank Upadhyay, and Krishan Kumar

Abstract Transfer of data over a network is one of the most endangered things to look for. As the cases of data leaks and theft are increasing exponentially, there is a need of a secure gateway that can prevent the data from getting misused. In group-oriented application such as video conferencing and multi-player gaming, it is necessary that only the trusted member can access the data and that too in a confidential manner in such a way that the prowler is not able to modify or ingress it. The Diffie–Hellman algorithm was one of the first and foremost schemes used for key exchange using a symmetric key encryption technique. The proposed algorithm is an advanced version of the traditional Diffie–Hellman algorithm that can be used efficiently by increasing the time complexity of the current by a fair margin thus making it difficult for the intruder to decrypt the common key.

Keywords Diffie–Hellman · Key sharing · Symmetric key · Public key cryptography

1 Introduction

Data security is the basic need for secure group communication. Data confidentiality means that the data send through the medium is confidential and can only be read by a permitted user. Hence, the confidential data is secured only when it is not tampered or targeted by an unauthorized person or middle man. Data confidentiality is gained using two categories widely known as forwarding secrecy and backward secrecy.

K. Purohit (✉) · A. Kumar · M. Upadhyay · K. Kumar

Department of Computer Science and Engineering, National Institute of Technology
Uttarakhand, Srinagar Garhwal, India

e-mail: purohit.kaustubh998@gmail.com

A. Kumar

e-mail: avanishkr018@gmail.com

M. Upadhyay

e-mail: mayankupadhyay398@gmail.com

K. Kumar

e-mail: kkberwal@nituk.ac.in

© Springer Nature Singapore Pte Ltd. 2020

M. Pant et al. (eds.), *Soft Computing: Theories and Applications*,
Advances in Intelligent Systems and Computing 1154,
https://doi.org/10.1007/978-981-15-4032-5_14

- Forward secrecy: It is a special type of mechanism which makes sure that as soon as a user leaves the communication, he will not be allowed to access the key.
- Backward secrecy: It is a special type of mechanism which makes sure that as soon as a new user enters the communication he will not be allowed to access the previous data [1].

At the early days, data transfer between two independent parties used to rely on a secure medium for the exchange of a private secret key which was initially encrypted then transmitted then further decrypted to get the original message, and this process is done using two cryptography method, viz. symmetric key and asymmetric key, and in the first one, all the communicating entities agree on a common key and then the encryption and decryption of data is done using the common key, whereas in the later, each and every communicating entities have their own unique private and public key and then the encryption and decryption of data is done using their individual keys.

Asymmetric being the later one is much more advanced in terms of security as the private key and public key for each and every entity are different; however, because of this, it increases the time and space complexity of the algorithm than the previous symmetric key encryption as it uses a common shared key for all the entities, however the strength of the cryptosystem totally depends on the complexity of the algorithm. As there were multiple drawbacks in the security of these algorithm, thus to ensure security of the information, it is necessary that the ciphertext must be least greater than the original text and as at every instance it is not possible that a trusted channel is available, hence the need for encryption scheme is a must. In cryptography, if the key protocol agreement is properly executed, it can preserve the secret key from the ill-favored third parties thus keeping the information hidden from the outside world.

Algorithm uses the concept of keys and functions to encrypt the plaintext and decrypt the ciphertext. The way of encryption and decryption totally depends on the design of the algorithm, and the keys or functions are therefore can be private or public depending on the type of cryptosystem used [2]. There are a number of algorithms that can be used to encrypt the plaintext data into a much difficult ciphertext thus securing it from the foreign attackers, some of which are:

1. Symmetric Key: AES, DES, Diffie–Hellman, Mars, IDEA, RC2, RC4, etc.
2. Asymmetric Key: RSA, elliptical curve, etc.

Diffie–Hellman was one of the first ever recorded public key cryptography algorithm that was used to transfer data from one user to the other by keeping the integrity and security of the information. Symmetric key algorithms are generally used because of their efficiency over the public-key algorithm. The critical part of this type of algorithm is that in the end, both the user has the same key, without even sending the common key across the public communication channel [3]. As the existing Diffie–Hellman algorithm can be cracked easily through the means of discrete logarithmic, middle man, and brute force, the proposed technique can be used as it uses many complicated functions to generate the common key for all the users in the network, thus making it much better than the previous and creating a secure and safe channel.

The rest of the paper is organized as follows. Section [4] surveys about the existing Diffie–Hellman algorithm, Section [5] analyzes the methodology for the proposed algorithm, and Section [6] carries the result and discussion for the same.

1.1 Existing Diffie–Hellman Algorithm

In the existing scheme of Diffie–Hellman algorithm we initially select a large prime number 'p' and generator 'g' of the prime number, where 'g' is less than 'p' and the power of 'g' must generate all the number varying from '1' to 'p-1'. In Diffie–Hellman algorithm, the first user should select a random private key k_1 on his own such that its public key is calculated by

$$\text{PublicKey} = g^{(k_1)} \bmod p$$

Similarly, the other user will also select his secret private key ' k_2 '. The public key of the second user will be given in the same way as the first one as

$$\text{PublicKey} = g^{(k_2)} \bmod p$$

Both the users will then share their respective public keys with each other. Each of the users will then use the public key of the other user and its own private key in order to compute the symmetric common key, which will be given as

$$\text{Common Key} = g^{(k_1 * k_2)} \bmod p$$

Using this common key, encryption of the original message will take place and decryption will be done by reversing the above process.

Traditional Diffie–Hellman for Encryption of Key Generation

Select a large prime number 'p'.

Select generator 'g' of prime number.

First User:

Select a random private key K_1

Public key(1)= \$g^(k1) mod p\$

Second User:

Select a random private key K_2

Public key(2)= \$g^(k2) mod p\$

Both the users will now exchange their respective key

First User:

Common Secret Key K= \$public key(2)^K1\$

Common Secret Key K= \$g^(K1*K2) mod p\$

Second User:

Common Secret Key K= \$public key(1)^K2\$

Common Secret Key $K = g^{(K2 \cdot K1)} \bmod p$

Thus, with the help of the existing algorithm, the two users are able to communicate using a secure way as now the plaintext can be sent in an encrypted form. Further, since 'K1' and 'K2' are a private key of the respective user and the other values, 'p', 'g', 'PK(1)', and 'PK(2)' are public, the nemesis must use discrete logarithmic, to determine the secret key. For example, in order to find the value of the key of user A, nemesis must compute the value as

$$'K1' = dlog_{a_q}(publickey(1))$$

and for the private key of user B, nemesis must compute the value as

$$'K2' = dlog_{b_q}(publickey(2))$$

similarly, the secret common key 'K' can be determined in the same way.

1.2 Methodology

The Diffie–Hellman protocol's security lies in the fact that it is easy to calculate the value of the exponential while it is fairly difficult to calculate the value of discrete logarithmic value. For large primes, decryption seems fairly impossible. But since the processor speed has increased exponentially, it has become fairly easier for the intruders to crack the ciphered text.

In the proposed scheme of modified Diffie–Hellman algorithm, we initially select a large prime number 'p' and generator 'g' of the prime number, where 'g' is less than 'p' and the power of 'g' must generate all the number varying from '1' to 'p-1'. In the proposed algorithm, each and every user has to select a random private key 'k' on his own such that its public key is calculated by

$$PublicKey = g^{(k)} \bmod p$$

Considering the case of three users, the proposed algorithm will look like:

Proposed Diffie–Hellman Algorithm for Symmetric Key Generation and Distribution

```
Select a large prime number 'p'.
Select generator 'g' of prime number.
First User:
    Select a random private key K1
    Public key(1)= $g^(k1) mod p
Second User:
    Select a random private key K2
    Public key(2)= $g^(k2) mod p
Third User:
```

```

Select a random private key K3
Public key(3)= $g^(k3) mod p
All the three users will now exchange their respective key
First User:
    Common Key(1)= $public key(3)^K1
    Common Secret(1)= $g^(K1*K3) mod p
Second User:
    Common Key(2)= $public key(1)^K2
    Common Secret(1)= $g^(K2*K1) mod p
Third User:
    Common Key(3)= $public key(2)^K3
    Common Secret(1)= $g^(K3*K2) mod p
All the three users will now again exchange the keys
First User:
    Common Shared Key= $public key(3)^K1
    Common Shared Key= $g^(K1*K3*K2) mod p
Second User:
    Common Shared Key= $public key(1)^K2
    Common Shared Key= $g^(K2*K1*K3) mod p
Third User:
    Common Shared Key= $public key(2)^K3
    Common Shared Key= $g^(K3*K2*K1) mod p

```

Now, to improve the complexity further, we introduce another exponential parameter.

```

First User:
    Select a random key i
    Public key(1)= $Common Shared Key^i
Second User:
    Select a random key j
    Public key(2)= $Common Shared Key^j
Third User:
    Select a random key k
    Public key(3)= $Common Shared Key^k
All the three users will now exchange their respective key
First User:
    Common Key(1)= $public key(3)^i
    Common Secret(1)= $g^(K1*K3*K2*i*k) mod p
Second User:
    Common Key(2)= $public key(1)^j
    Common Secret(1)= $g^(K2*K1*K3*i*j) mod p
Third User:
    Common Key(3)= $public key(2)^k
    Common Secret(1)= $g^(K3*K2*K1*j*k) mod p
All the three users will now again exchange the keys
First User:
    Final Key= $public key(3)^i
    Final Shared Key= $g^(K1*K3*K2*i*j*k) mod p
Second User:
    Final Key= $public key(1)^j
    Final Shared Key= $g^(K2*K1*K3*i*j*k) mod p
Third User:
    Final Key= $public key(2)^k
    Final Shared Key= $g^(K3*K2*K1*j*k) mod p

```

Thus, with the help of the existing algorithm, the users are able to communicate using a secure way as now the plaintext can be sent in an encrypted form. Further, 'i', 'j', and 'k' are other random numbers for users 1, 2, and 3, respectively. Here, 'K1', 'K2', and 'K3' are private keys of the respective users and the other values, 'p', 'g', 'PK(1)', and 'PK(2)' are public; hence, the nemesis must use discrete logarithmic, to determine the secret key. For example, in order to find the value of the key of user

A, nemesis must compute the value as

$$'K1' = dlog_{a_q}(publickey(1))$$

, for the private key of user B, nemesis must compute the value as

$$'K2' = dlog_{b_q}(publickey(2))$$

, similarly for the private key of user 'N', nemesis must compute the value as

$$'Kn' = dlog_{b_q}(publickey(n))$$

similarly, the secret common key 'K' can be determined in the same way. The study for the comparison between the existing Diffie–Hellman key sharing protocol and the proposed modified Diffie–Hellman is done over three parameters: first one being the encryption time, the second one being the decryption, and the last one being the total time.

1.3 Result and Analysis

The performance analysis of the proposed algorithm is done on the encryption, decryption, and the total time taken by the model when run over three different data sets. The time taken by the existing and proposed algorithm is noted and compared which resulted in that the proposed model has a better complexity and efficiency when tested which results in better safety measures. Table 1 (one shown below) gives the clear idea of the time taken by the traditional Diffie–Hellman algorithm when run over three different data sets.

Table 2 (one shown below) gives the clear idea of the time taken by the proposed modified Diffie–Hellman algorithm when run over three different data sets.

1.4 Conclusion

In a known plaintext attack, the ciphertext along with the plaintext is available to the intruder, as it becomes easier for him to find plain data if encrypted data is available.

Table 1 Existing Diffie–Hellman key exchange protocol

	Data set 1	Data set 2	Data set 3
Encrypt (ns)	872,478	483,927	679,874
Decrypt (ns)	51,069,417	40,296,392	46,656,928
Total (ns)	51,941,895	40,780,319	47,336,802

Table 2 Proposed Diffie–Hellman key exchange protocol

	Data set 1	Data set 2	Data set 3
Encrypt (ns)	1,742,468	972,895	1,404,598
Decrypt (ns)	89,321,465	69,128,765	78,539,073
Total (ns)	91,063,933	70,101,660	79,943,671

Further using multiple techniques, the cipheredtext can be easily decrypted This sort of attack is easily possible if the existing traditional Diffie–Hellman key exchange protocol is used.

In the proposed model, we have transformed the existing algorithm for the group communication by making it much more difficult for the middle man to decrypt it. As the number of exponential terms has increased, the time complexity to decrypt the ciphered text from discrete logarithmic also increases. The study for the comparison between the existing Diffie–Hellman key sharing protocol and the proposed modified Diffie–Hellman is done over three parameters: first one being the encryption time, the second one being the decryption, and the last one being the total time.

It is clear from both the table that the proposed model is much better in terms of security than the existing one.

References

1. May, P., Ehrlich, H.C., Steinke, T.: ZIB structure prediction pipeline: composing a complex biological workflow through web services. In: Nagel, W.E., Walter, W.V., Lehner, W. (eds.) Euro-Par 2006. LNCS, vol. 4128, pp. 1148–1158. Springer, Heidelberg (2006)
2. Tahir, R., Hu, H., Gu, D., McDonald-Maier, K., Howells, G: A scheme for the generation of strong ICMetrics based session key pairs for secure embedded system applications. In: 2013 27th International Conference on Advanced Information Networking and Applications Workshops (2013)
3. Taparia, A., Panigrahy, S.K., Jena, S.K.: Secure key exchange using enhanced Diffie–Hellman protocol based on string comparison. In: 2017 International Conference on Wireless Communications, Signal Processing and Networking (WiSPNET) (2017)
4. Arora, S., Hussain, M.: Secure session key sharing using symmetric key cryptography. In: 2018 International Conference on Advances in Computing, Communications and Informatics (ICACCI) (2018)
5. Agarwal, A., Kumar, A.: Encoded IDs symmetric session key exchange. In: 2017 International Conference on Big Data Analytics and Computational Intelligence (ICBDAC) (2017)
6. Deshpande, P., Santhanakshmi, S., Lakshmi, P., Vishwa, A.: Experimental study of Diffie–Hellman key exchange algorithm on embedded devices. In: 2017 International Conference on Energy, Communication, Data Analytics and Soft Computing (ICECDS) (2017)
7. Kumari, S., Chaudhary, P., Chen, C.-M., Khan, M.K.: Questioning key compromise attack on Ostad-Sharif et al.’s authentication and session key generation scheme for healthcare applications 7 (2019) (IEEE Access)

Design of Controllers Using PSO Technique for Second-Order Stable Process with Time Delay



Satyendra Kumar and Moina Ajmeri

Abstract This paper proposes sliding mode control (SMC) and PID control techniques for designing a controller for a second-order stable process. In this paper, the controllers are designed using sliding mode control and Skogestad internal model control (SIMC)-PID control technique and the parameters of these controllers are obtained by the particle swarm optimization (PSO) technique. MATLAB simulation is performed for the second-order plus delay time process (SOPDT) using step input. The results found by the proposed methods are compared with the recently reported methods in the literature. The proposed controller ensures more robustness to parameter variations and fast disturbance rejection capability.

Keywords Sliding mode control · Skogestad internal model control · Particle swarm optimization · First-order plus delay time (FOPDT) · Second-order plus delay time (SOPDT)

1 Introduction

Sliding mode controller design method [1, 2] is very popular approach to control systems with heavy uncertainty, unmodeled dynamics and parameter variation of the system of the system. But the main drawback associated with the SMC is chattering problem [3] which is a undesired vibration in steady state in the system variable. To handle the chattering problem, the main approaches which are developed based on following facts;

- Use of saturation function (continuous approximation of relay).
- In observer dynamics, asymptotic state observer is used.
- By using higher order SMC.

The sliding mode controllers need tuning of various parameters and there is several difficulties in tuning these parameters properly due to nonlinearity and time delay of

S. Kumar (✉) · M. Ajmeri
Electrical Engineering Department, National Institute of Technology, Ashok Rajpath, 800005
Patna, India
e-mail: satyendra.ee17@nitpac.in

the system. It is difficult to find the optimized tuning parameters for the system using conventional methods so in this chapter, a metaheuristic nature-inspired optimization technique so-called particle swarm optimization [4, 5] is proposed for the optimized tuning of the parameters. This technique is random search method which is one of the modern nature-inspired optimization technique initially introduced by Kennedy and Eberhart in 1995. Various works have been recently reported in literature in which different soft-computing theories and optimization techniques were used [11–13].

Proportional-integral-derivative (PID) controllers are very popular and commonly used in industrial control applications due to their high reliability, stability, simple mathematical structure and recovery from control failure. There are many tuning rules for the tuning of PID controller including Ziegler and Nichols [6] and internal model control (IMC) tuning rule [7]. In this paper, PSO optimization technique is used for tuning of parameters of PID controller, and results are compared with recent method available in literature called ‘Skogstad internal model control’ (SIMC) [8].

2 Particle Swarm Optimization Technique

Particle swarm optimization is a popular nature-inspired optimization technique developed by Russian (former USSR) researchers Kennedy and Eberhart in 1995 [4, 9]. The PSO algorithm technique is guided by ‘Pbest’ (i.e., personal experience) and the ‘Gbest’ (i.e., overall experience) of the particle to find the next position in the search space. The ‘Pbest’ and ‘Gbest’ are further multiplied (accelerated) by the factors c_1 and c_2 , also two random numbers r_1 and r_2 between [0,1] is generated. The current moment is multiplied by a factor ‘ w ’ called inertia factor which vary in between $[w_{\min}, w_{\max}]$.

Some notations which are used in the PSO algorithm are as follows:

N = initial swarm (population size)

X = particles

D = dimension of each particle

$X = [X_1, X_2, \dots, X_N]^T$, initial population.

$X_i = [X_{i,1}, X_{i,2}, \dots, X_{i,D}]^T$, individual particle.

$V = [V_1, V_2, \dots, V_N]^T$, initial velocity of particle.

$V_i = [V_{i,1}, V_{i,2}, \dots, V_{i,D}]^T$, velocity of each particle.

The PSO algorithm initiated by positioning the initial particle which are uniformly and randomly distributed in search space and a initial velocity, in the range $[V_{\min}, V_{\max}]$ is assign to each particle. The velocity is updated according to the following equation.

$$V_{i,j}^{k+1} = w \times V_{i,j}^k + c_1 \times r_1 \times (Pbest_{i,j}^k - X_{i,j}^k) + c_2 \times r_2 \times (Gbest_{i,j}^k - X_{i,j}^k) \quad (1)$$

The new position is the sum of previous (old) position and new updated velocity; hence, the new position is updated according to the following equation.

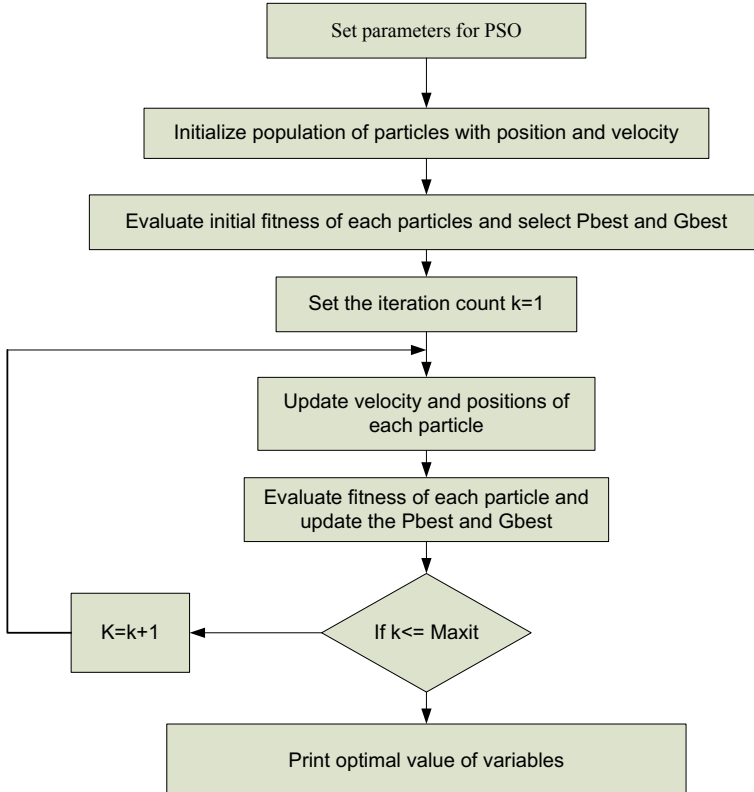


Fig. 1 Flowchart for PSO algorithm

$$X_{i,j}^{k+1} = X_{i,j}^k + V_{i,j}^{k+1}. \quad (2)$$

A number of iterations carried out until the PSO algorithm reaches stopping criteria. The detailed flowchart of PSO considering the above steps is shown in Fig. 1.

3 Problem Formulation and Controller Parameter Setting

An SOPDT system may be written as

$$G(s) = \frac{K}{(1 + \tau_1 s)(1 + \tau_2 s)} e^{-T_d s} \quad (3)$$

where K , T_d , τ_1 and τ_2 are process gain, delay time and time constants, respectively. This mathematical model of the process can be simplified to the following form using Taylor's series approximation.

$$G(s) = \frac{K}{(1 + \tau_1 s)(1 + \tau_2 s)(1 + T_d s)} \quad (4)$$

For the above system, the state space model is found as

$$\begin{bmatrix} \dot{x}_1 \\ \dot{x}_2 \\ \dot{x}_3 \end{bmatrix} = \begin{bmatrix} 0 & 1 & 0 \\ 0 & 0 & 1 \\ -m_1 & -m_2 & -m_3 \end{bmatrix} \begin{bmatrix} x_1 \\ x_2 \\ x_3 \end{bmatrix} + \begin{bmatrix} 0 \\ 0 \\ q \end{bmatrix} u \quad (5)$$

where $m_1 = \frac{1}{\tau_1 \tau_2 \tau_d}$, $m_2 = \frac{(\tau_1 + \tau_2 + \tau_d)}{\tau_1 \tau_2 \tau_d}$, $m_3 = \frac{(\tau_1 \tau_2 + \tau_2 \tau_d + \tau_1 \tau_d)}{\tau_1 \tau_2 \tau_d}$ are process parameters. Here, $x(t)$ is output, $u(t)$ is control input, m_1 , m_2 , m_3 and q are the nominal plant parameters.

Now for the controller design and its parameter estimation, real-time system (3) may be approximated as FOPDT system by half rule approximation technique (as explained in [8]) as

$$G(s) = \frac{X(s)}{U(s)} = \frac{K}{\tau s + 1} e^{-\theta s} \quad (6)$$

where K , $\tau = \tau_1 + \frac{\tau_2}{2}$, $\theta = \tau_d + \frac{\tau_2}{2}$, $X(s)$ and $U(s)$ are the steady-state gain, time constant, deadtime, process output and the control input of the process, respectively.

The deadtime term (6) can be approximated as Eq. (7), by using first-order Taylor's series.

$$\frac{X(s)}{U(s)} = \frac{K}{(\tau s + 1)(\theta +)} \quad (7)$$

Further (5) can be rearranged as,

$$\ddot{x}(t) = -a_1 \dot{x}(t) - a_2 x(t) + b_1 u(t) \quad (8)$$

where $a_1 = \frac{\theta + \tau}{\theta \tau}$, $a_2 = \frac{1}{\theta \tau}$ and $b_1 = \frac{K}{\theta \tau}$.

Furthermore (6) can be generalized as,

$$\ddot{x}(t) = [f(x, t) + \Delta f(x, t)] + [g(x, t) + \Delta g(x, t)]u(t) + d(t) \quad (9)$$

$$\ddot{x}(t) = f(x, t) + g(x, t)u(t) + D(t, u(t)) \quad (10)$$

where $f(x, t) = -a_1 \dot{x}(t) - a_2 x(t)$ and $g(x, t) = b_1$ are the process parameters, $\Delta f(x, t)$ and $\Delta g(x, t)$ are uncertainties in the system dynamics. $x(t)$ and $u(t)$ are the output and input, respectively. $D(t)$ is the lumped uncertainty.

3.1 SMC Controller

For the design of SMC controller, we need to have a sliding surface $\sigma(t)$ for the representation of the system tracking performance. Here, $\sigma(t)$ is selected as Eq. (11).

$$\sigma(t) = \left(\frac{d}{dt} + \lambda \right)^n \int_0^t e(t) dt$$

where $n = 2$,

$$\sigma(t) = \dot{e}(t) + 2\lambda e(t) + \lambda^2 \int_0^t e(t) dt \quad (11)$$

where the $e(t)$ represents tracking error, i.e., $e(t) = r(t) - x(t)$, $r(t)$ is the desired reference input and $x(t)$ is the output of the process. λ and n represent the tuning parameter and the order of the system, respectively. Using second derivative of error $\ddot{e}(t) = \ddot{r}(t) - \ddot{x}(t)$ and substituting 8 in the derivative of Eq. (11), we have

$$\dot{\sigma}(t) = \ddot{r}(t) - f(x, t) - g(x, t)u(t) - D(t, u(t)) + 2\lambda\dot{e}(t) + \lambda^2 e(t) \quad (12)$$

In regulatory control, the set-point values remain constant (or step changes). Therefore, (12) can be written as, (since double derivative of $r(t) = 0$).

$$\dot{\sigma}(t) = -f(x, t) - g(x, t)u(t) - D(t, u(t)) + 2\lambda\dot{e}(t) + \lambda^2 e(t) \quad (13)$$

The continuous (equivalent) control law $u_c(t)\kappa$ is obtained from (13), when $\dot{\sigma}(t) = 0$. Hence, we have,

$$u_c = [g(x, t)]^{-1} [-f(x, t) + 2\lambda\dot{e}(t) + \lambda^2 e(t)] \quad (14)$$

Substituting $f(x, t) = -a_1\dot{x}(t) - a_2x(t)\kappa$ from (10) in above equation, $u_c(t)\kappa$ can be simplified as,

$$u_c = [g(x, t)]^{-1} [a_1\dot{x}(t) + a_2x(t) + 2\lambda(\dot{r}(t) - \dot{x}(t)) + \lambda^2 e(t)] \quad (15)$$

Assuming $\dot{r}(t) = 0$ (set-point input) we have,

$$u_{eq} = [g(x, t)]^{-1} [(a_1 - 2\lambda)\dot{x}(t) + a_2x(t) + \lambda^2 e(t)] \quad (16)$$

For the further simplification of the control action, we assume

$$a_1 - 2\lambda = 0 \quad (17)$$

Now, the continuous control law $u_c(t)\kappa$ may be written as,

$$u_c = [g(x, t)]^{-1} [a_2 x(t) + \lambda^2 e(t)] \quad (18)$$

Discontinuous control law $u_d(t)$ is expressed as,

$$u_d(t) = \frac{K_D}{g(x, t)} \operatorname{sgn}[\sigma(t)] \quad (19)$$

where K_D represents tuning parameter concern with for reaching phase. This control law has a switching element and which shows discontinuity across the sliding surface. To ensure the smooth input, hyperbolic tangent function is used in place of signum function and to reduce the chattering problem, δ is used as tuning parameter.

$$u_d(t) = \frac{K_D}{g(x, t)} \tan h \left[\frac{\sigma(t)}{|\sigma(t)| + \delta} \right] \quad (20)$$

Thus, using the Eqs. (18) and (20), we have complete expression of the control as,

$$u(t) = [g(x, t)]^{-1} [a_2 x(t) + \lambda^2 e(t)] + \frac{K_D}{g(x, t)} \tan h \left[\frac{\sigma(t)}{|\sigma(t)| + \delta} \right] \quad (21)$$

For the analysis of higher order systems, it is common practice to approximate the systems by low-order plus dead time (i.e., FOPDT). The tuning parameters of the SMC controller are calculated by using PSO technique.

3.2 PID Controller

Proportional-integral-derivative (PID) controllers are used in the most of the industries till today. The performance of the control system is greatly affected by the parameters of the PID. The control law for parallel-form PID is given by

$$C(s) = k_c \left(1 + \frac{1}{\tau_I s} + \tau_D s \right) \quad (22)$$

where k_c , τ_D , τ_I , are proportional, derivative and integral tuning parameters, respectively, of the PID controller. Here, the tuning parameters are obtained by the PID controller tuning rule given by Skogestad [8] for second-order plus delay time (SOPDT) system (1) which is given by

$$k_c = \frac{1}{k} \frac{\tau_1}{(\tau_c + \theta)}, \quad \tau_I = \min\{\tau_1, 4(\tau_c + \theta)\}, \quad \tau_D = \tau_2$$

where $\tau_c = \theta$ (SIMC-rule[8]).

4 Simulation Studies and Results

Case study 1: *Comparison of the proposed SMC with PID controller reported in [8].*
Let us consider the following second-order system with delay time (SOPDT) [10].

$$G(s) = \frac{0.5}{s^2 + 11s + 10} e^{-0.5s} \quad (23)$$

Using proposed optimization method (as discussed in Sect. 3), SMC controller settings are obtained as

$$\delta = 1.8, K_D = 13.5, \text{ and } \lambda = 2.1$$

Using SIMC reported in [8], parameters (K_D, K_P, K_I) of PID controller are obtained as

$$K_p = 22, K_I = 20 \text{ and } K_d = 2.2$$

For simulation studies of this system, first of all, the system is converted into state space model and sliding mode controller is applied. A unit step change in the set-point input is introduced at $t = 0$ and an inverse step load disturbance of magnitude 10 is applied at $t = 25$ s to observe the closed loop responses. Figure 2 shows closed loop responses corresponding to the above-said control schemes. It is observed from Fig. 2 that SMC has better load disturbance rejection response as compared to PID controller. Various performance measures for set-point tracking are calculated and summarized in Table 1 which shows the superiority of the proposed work in terms of settling time, rise time and peak time.

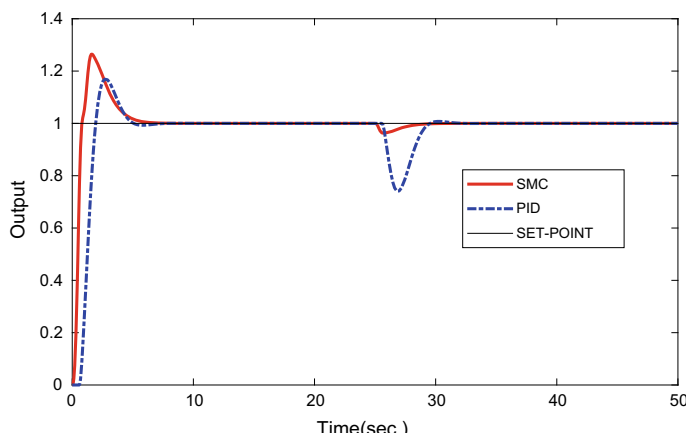


Fig. 2 Step response of the system with the proposed SMC and PID controller [8]

Table 1 Comparative performance values for the PSO-SMC and SIMC-PID

Controller ↓	Rise time	Settling time	Settling min.	Settling max.	Overshoot	Peak	Peak time
PSO-SMC (proposed)	1.3352	7.2001	0.9199	1.3100	31.355	1.3135	1.8
PID [8]	2.2854	7.7102	0.9025	1.1801	18.213	1.1821	2.1

Case study 2: *Comparison of the proposed PID (PSO-based) and PID controller reported in [8].*

The PSO technique is applied to the PID controller for optimizing its parameters and the results are compared with the SIMC tuned PID controller for the process considered in the first case study. The parameters of PID controller are obtained using the PSO technique as follows

$$K_p = 20.5939, K_I = 20.8548 \text{ and } K_d = 0.1$$

Using SIMC reported in [8], parameters (K_D, K_P, K_I) of PID controller are obtained as

$$K_p = 22, K_I = 20 \text{ and } K_d = 2.2$$

A unit step change in the set-point input is introduced at $t = 0$ and an inverse step disturbance of magnitude ‘10’ is given after 15 s to observe system responses. Figure 3 shows closed loop responses for the tuning methods as discussed above. Figure 3 shows that the proposed controller results in improved load disturbance rejection

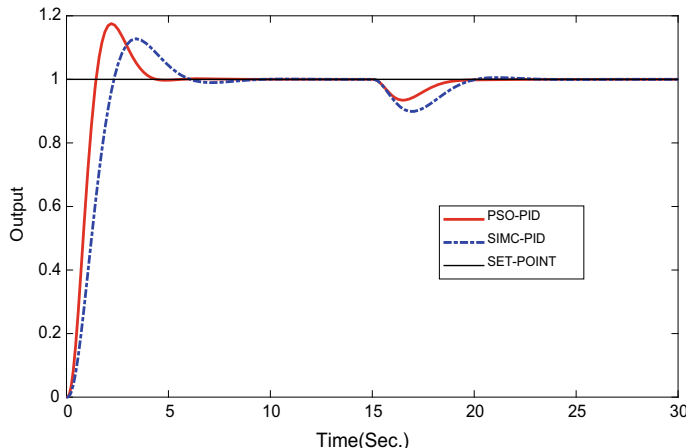


Fig. 3 Step response of the system with PSO-PID and SIMC-PID controller with 20% parameter variation

response as compared to PID reported in [8]. Various performance measures are given in Table 2. This table shows that the proposed approach results in less settling time and rise time.

Case study 3: Comparison of the proposed SMC and proposed PID controller for the process $G(s) = \frac{0.5}{s^2+11s+10} e^{-0.5s}$.

In Fig. 4, closed loop responses for unit step change in the set-point input and the comparative analysis of PSO-based SMC and PSO-based PID is shown. From the figure, it is observed that the overall performance of the PSO-based SMC controller is better than the PSO-based PID controller. The corresponding values of the performance parameters are shown in Table 3.

Table 2 Comparative performance values for the PSO-PID and SIMC-PID

Controller ↓	Rise time	Settling time	Settling min.	Settling max.	Overshoot	Peak	Peak time
PSO-PID	0.8645	3.4582	0.9085	1.1329	13.2923	1.1329	2.306
SIMC-PID	2.2854	7.7102	0.9025	1.1801	18.2132	1.1821	2.1

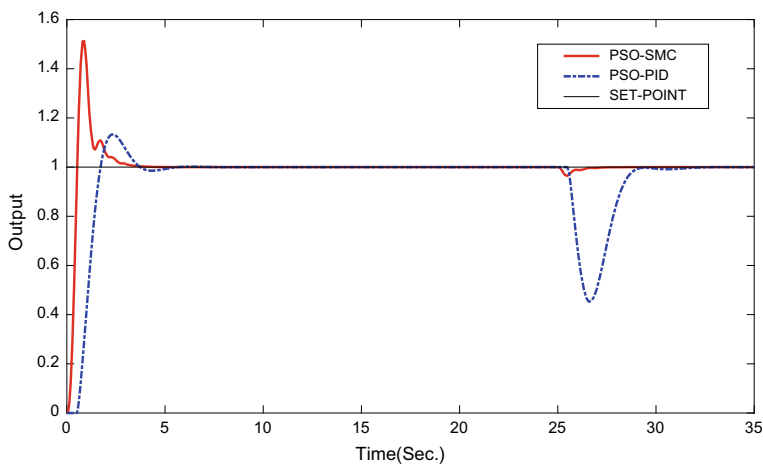


Fig. 4 Step response of the system with PSO tuned SMC and PID controller

Table 3 Comparative performance values for the PSO-based SMC and PID

Controller ↓	Rise time	Settling time	Settling min.	Settling max.	Overshoot	Peak	Peak time
PSO-SMC	0.3194	2.6194	0.9071	1.5127	51.2710	1.5127	0.880
PSO-PID	0.8645	3.4582	0.9085	1.1329	13.2923	1.1329	2.306

5 Conclusion

This paper presents ‘particle swarm optimization (PSO)’ method which is used to select the parameters of the control design, i.e., we optimized the parameters of SMC controller which is applied to second-order plus delay time system and compared the responses with the SIMC tuned PID controller. The SMC controller showed the best performance compared to PID controller in the presence of disturbances and parameter variations. Furthermore, the parameters of the PID controllers are also obtained by the PSO optimization method and results are compared by the SIMC tuned PID controller. The PSO-based PID controller gives better responses compared to the SIMC-based PID controller.

References

1. Utkin, V.I.: Variable structure system with sliding modes. *IEEE Trans. Autom. Control* **22**, 212–222 (1977)
2. Edwards, C.; Spurgeon, S.K. *Sliding mode control theory and applications*; Taylor and Francis; Gunpowder Square, London, (1998)
3. Bartolini, G., Ferrara, A., Usai, E.: Chattering avoidance by second order sliding mode control. *IEEE Trans. Autom. Control* **45**(8), 1711–1717 (2000)
4. Kennedy, J., Eberhart, R.: Particle swarm optimization. *IEEE Int. Conf. Neural Netw.* **4**, 1942–1948 (1995)
5. Coello, C.A.C., Pulido, G.T., Lechuga, M.S.: Handling multiple objectives with particle swarm optimization. *IEEE Trans. Evol. Comput.* **8**(3), 256–279 (2004)
6. Ziegler, J.G., Nichols, N.B.: Optimum settings for automatic controllers (trans. ASME) **64** (11) (1942)
7. Rivera, D.E., Morari, M., Skogestad, S.: Internal Model Control. 4 PID controller design. *Ind. Eng. Chem. Process Des. Dev.* **25**, 252–265 (1986)
8. Skogestad, S.: Simple analytic rule for model reduction and PID controller tuning. *J. Process Control* **13**, 291–309 (2003)
9. Eberhart, R., Kennedy, J.: A new optimizer using particle swarm theory. In: *MHS'95. Proceedings of the Sixth International Symposium on Micro Machine and Human Science* (pp. 39–43). IEEE. (1995)
10. Parvat, B.J., Patre, B.M.: Second order sliding mode controller for second order process with delay time. In: *International conference on Industrial Instrumentation and Control (ICIC)*, College of engineering Pune, India (2015)
11. Yadava, R.D.S., Sonamani Singh, T.: Application of PSO clustering for selection of chemical interface materials for sensor array electronic nose. *Soft Comput. Theories Appl.* **583**(1), 449–456 (2017)
12. Harsh, B., Nandeesh, G.: Critical path problem for scheduling using genetic algorithm. *Soft Comput. Theories Appl.* **583**(1), 15–24 (2017)
13. Pant, M., Ray, K., Sharma, T.K., Rawat, S., Bandyopadhyay, A.: *Soft Computing: Theories and Applications* Proceedings of SoCTA 2 (2016)

A Green Dynamic Internet of Things (IoT)-Battery Powered Things Aspect-Survey



Nitin B. Raut and N. M. Dhanya

Abstract The basic utility of IoT is to convert every physical object into the source of information. Devices linked to the Internet have a tremendous growth for a couple of years; therefore, innovative areas of applications related to IoT have opened, and this moves toward new challenges as green IoT paradigm. Managing the energy by the demanding connected devices in the IoT system and viewing the consumption of energy is a big challenge. The green IoT opens two broader areas. The first one focuses on the designing of energy-efficient devices, communication protocols, and networking architecture for interconnecting the physical objects; the second area speaks about cutting carbon emission, pollution, and enhance energy efficiency. This paper presents the profound view of potential technologies of energy-efficient IoT systems, toxic pollution, and management of E-waste, specifically in battery-powered devices. We investigated the literature and presented the various application of green IoT and barriers in Greener IoT implementation.

Keywords Battery power · Energy efficiency · Efficient IoT · Energy harvesting · Green IoT · Internet of thing (IoT) · IoT applications · M-healthcare

1 Introduction

There is a growing interest in connecting different sensors, appliances, and actuators with the internet, and this is the outcome of the Internet of things [1, 2]. Each sector where humans can be changed by embedded devices in performing activities is covered in IoT applications and services. Examples of applications are smart cities, m-healthcare, remote monitoring, home automation, industrial automation, agriculture,

N. B. Raut · N. M. Dhanya (✉)

Department of Computer Science and Engineering, Amrita School of Engineering, Amrita Vishwa Vidyapeetham, Coimbatore, India
e-mail: nm_dhanya@cb.amrita.edu

N. B. Raut
e-mail: bn_raut@cb.students.amrita.edu

and many more. The setup of linked devices through IoT give synchronized information, which is sharable; also, the life quality can be enhanced, the industrial process can be improved, and the level of quality of services as well as energy efficiency can be increased [3]. Based on the study of IEA-4E (electronic devices and network annex), more than 49 billion devices will be linked to each other by 2020 [4]. The statistical review of World Energy-2017 report suggests that electricity consumption hike over the year 2005–2015 were 2.8% while that in the year 2016 alone was 2.2% [5]. All over the world, awareness of environmental issues is growing. The challenge of sustainability gave birth to data centers optimization technique of distributing architecture, ultimately bring about overall increase efficiency, falling CO₂ emission, and E-waste stuff management [6]. Making information communication technology green enables the use of efficient radio frequency tagging techniques, resourceful sensor networks, efficient computing through clouds, competent data centers, and green machine-to-machine transmission [7], and hence, information communication techniques play a crucial role in effective IoT architecture. IoT applications can be categorized into low data rate applications (<100 kbps), medium data rate application, and high data rate applications. The comprehensive study reveals that low data rate applications will be running on more than 59% of IoT links about 2020 [8]. The major challenge for IoT deployment is constrained resource accessibility for linked devices, i.e., restricted energy, narrow computation, and some degree of processing capability [9], so the concerned subject is extensively studied and implemented by academic researchers and industry professionals. Many techniques are methodically projected in the literature to address this significant topic, for instance, Gorlatova et al. [10] suggested wireless node model kinetic energy harvesting that eases practical IoT node design, Lee and Chang [11] proposed power management unit circuit which gives voltage converterless and storageless harvesting, Ju and Jhang [12] suggested the predictive power management framework investigation in energy harvesting, and Kamalinejad et al. [13] proposed efficient mobile energy harvesting. The technique related to charging the device wirelessly using RF is discussed by Na et al. [8], Costanzo and Masotti [14] optimize wireless link of 5G IoT architecture. Further, Karthikeya et al. [15] proposed power-conscious interconnectivity by using spanning tree algorithm, Takruri et al. [16] proposed wireless charging techniques, and Shafiee et al. [17] designed a circuit for energy harvesting. The contents of this paper in Sect. 2 gives a summary of green IoT, Sects. 3, 4, and 5 confer the concepts and technologies allied with green communication, green cloud computing, and green data center, respectively, various applications of green IoT are listed in 6, and finishing remarks are given in Sec. 7.

2 Summary of Efficient IoT System

Green Internet of things minimizes the technological impact on the ecosystem and health of humans and maintaining natural resources intact and reducing them cost-effectively. Murugesan [18] gave a definition of green IoT like, “the study and practice of designing, using, manufacturing, and disposing of servers, computers, and associated subsystems such as monitors, storage devices, printers, and communication network systems efficiently and effectively with minimal or no impact on the environment.” The effective IoT organizations comprised of practical technologies, namely intend and power technologies. Intend technologies concentrate on the organizing linked device proficiently, network system organization, and connections. Power technologies deal with reducing CO₂ emission and increasing system overall efficiency. Table 3 gives a comprehensive summary of efficient IoT systems.

3 Greener Communication System

The energy budget has a prominent role in deciding the quality of sensor data measurement, analysis time of sensor, and also quantitative data that can spread for radio communication; Rault et al. [19] divided the optimized energy use verticals into sub-categories: these are radio frequency optimization, reduction of data, sleep/wake-up scheme, routing in cost-effective way, and power depletion. Radio frequency optimization technique optimizes the modulation schemes, transmission power, and antenna direction, and reduction in data minimizes transmitted data. The remaining idea is to focus on routing efficiently along with energy scavenging else, getting way to provide power to the system automatically. Table 1 shows various wireless technologies with available battery life extensions.

3.1 Data Reduction

Adaptive sensing is proposed by Perera et al. [20], they projected a policy C-MOSDEN, for selectively acquiring data to reduce energy consumption.

3.2 Sleep/Wake-up Techniques

Khodr et al. [21] proposed the design of radio frequency activation policy for sensors; the policy activates the sensor only after confirmation of IoT device address by the decoder from the received signal; it reduces energy consumption by deleting fake

Table 1 Technologies with battery life [52]

Technology	Zigbee	Wi-Fi	BLE	Z-wave	LoRa	SigFox	INGENU	Weightless-P	LTE-M	ECGSM-IoT	NB-IoT
Battery life	Few year	–	–	10 year	>10 year	10 year	10-20 year	3–8 year	>10 year	~10 year	>10 year

wake-up calls. Perles et al. [22] projected design to advance the years of device power to the extent 20 years with U-LPWAN technologies LoRa & SigFox.

3.3 Radio Techniques

Qureshi et al. [23] studied and proposed radio techniques where a licensed user shares its unused spectrum with unlicensed users. Hence, maximum throughput is achieved, and uninterrupted connection and reliable communication are provided for unlicensed as well as a licensed user. Further Li et al. [24] studied a 5G-based outline in which the intermediate controlling block works as computational service provider and data processing unit and gets data from the physical world, and other authors subdivided the problem of distribution of resources into two more sub-categories of power partition distribution and channel partition distribution. These problems can be solved separately. The effects of 5G technologies on atmosphere and our living are being studied since IoT is growing to make life easier. 5G technology provides maximum coverage connectivity; reduction in latency, higher data rate support, and system ability result in energy saving. 5G technologies enhance further reliability and quality of service of communication between machines to machines and humans. 5G technologies are extensively used in E-health monitoring, robot–human interaction, inter-robotics interaction, transport systems, media houses and logistics services, computer-based learning and governance, the protection of the public, and also in industries. Figure 1 shows the impact of 5G on energy consumption.

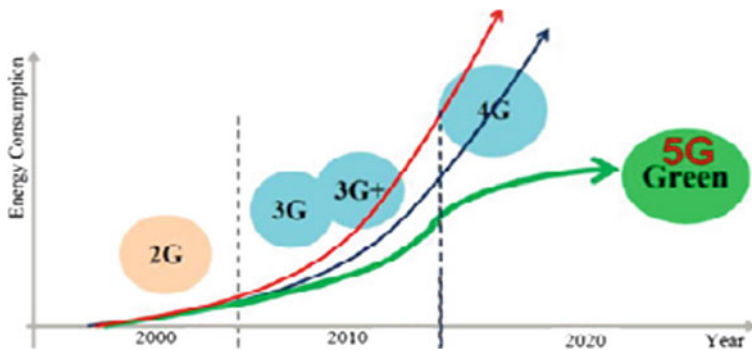


Fig. 1 Impact of 5G on energy consumption [6]

3.4 Routing Approaches

Yi et al. [25] suggested an algorithm in which nodes make the asymmetrical discovery of neighbours. Authors took multiple of two as a reference point for time synchronization and observed that consumption of energy is reduced due to a reduction in wake-up calls needed to search neighbouring nodes. Furthermore, continuous sensing and its effect on the energy consumption of sensors have been studied extensively. Basnayaka et al. [26] projected a modulation scheme that works with low latency and low power mode. Constellation order and random bit are considered to switch between modes. This approach compromised latency for energy efficiency. Shen et al. [27] suggested a protocol for IoT with WSN to achieve higher performance of the network. This clustering-based protocol is used to make power use uniform into a network; the energy of every node is compared with some predefined value. Then, the centroid of a network and nodes in view to energy are evaluated through distances between them. Hence, energy consumption is uniform in a network. The base station avoids long-distance communication by broadcasting the maximum distance to each node. With this, Tian et al. [28] have studied and proposed the concept of network coding and routing, where edge nodes discard the packets those are duplicated along with stores distance in the memory.

3.5 Power Management Techniques

Ahmad et al. [29] enlighten solution for the delivery of power with varying voltage scenario in self-powered IoT. Nan et al. [30] proposed two alternate energy sources with fog computing, where solar will be the main energy and grid as an alternative power source.

4 Greener Cloud Computation

Cloud computation and IoT integration have emerged as one of the prominent solutions for energy efficiency and also has the potential for further research activities. The green cloud computing is an important extension of traditional cloud computation. The main purpose of G-CC is to limit dependency on hazardous materials, enhance the recyclability of previously used products and wastes, and minimize energy consumption. The concept of green computational technologies and information communication technologies are studied and integrated by Shuja et al. [31]. Furthermore, Baccarelli et al. [32] suggested the solution for the green economy in IoT with the fog network. Nandyala and Kim [33] support the idea of green cloud computing, and Zhu et al. [34] implemented data delivery with multiple methods for cloud-sensor integration, where less delivery time and lower cost are maintained.

5 Greener Data Center

The data center is a resource for hosting computing facilities with communication infrastructure for storing data and implementing applications. [35]. Hammadi et al. [36] comprehensively studied and categorized the data center architecture in switch concentric and server concentric topologies along with advantages of virtualization, dynamic management of network, dynamically scaling of frequency and voltage, efficient green routing, dynamic power management, smart cooling, and renewable energy for energy-efficient data center architecture. Baccour et al. [37] proposed parameterizable data center topology (PTNet). Offering gradual scaling in the small interconnecting network to a large network with a different range, furthermore, it chose the smallest path between any two servers. Regardless of size of the data center, authors implemented the routing algorithm, which is power-aware and saves more than 35% energy.

6 Applications of Green IoT

Green IoT is more beneficial than traditional IoT given different power source exploration, such as eco-friendliness and environmental restoration; therefore, the applications of feasible IoT implementation are socially meaningful. The BBC research shows that the growth in green technology is frequently increasing with 9.2% [38]. Table 2 shows various applications of IoT along with the sector.

Table 2 Sectors and applications of green IoT

Sector	Applications	Ref. No.
Home	Smart health applications, security enforcement applications, entertainment boosting applications, appliances controlling applications, personal use	[39]
Transport	Parking management, traffic control applications, emergency services enforcement, highway monitoring, food supply chain	
Society	Surveillance applications, social networking establishment, environment-related applications, smart buildings, smart cities, industrial process applications	
National	Military applications, smart grids, utilities, remote controlling, agriculture	

Table 3 Summary of efficient IoT

Domain	Algorithm/technique	Researcher	Ref. No.
Energy harvesting	Kinetic energy harvesting algorithm	Maria Gorlatova	[10]
	Duty-controlled power management unit	Lee and Chang	[11]
	Energy harvesting in SWIPT network	Vieeralingam G	[53]
	i-Energy	Prakash L	[55]
Wireless charging	RF charging	W. Na	[8]
	5G IoT end-to-end link optimization	Costanzo and Masotti	[14]
	Inductive coupling under resonance conditions	Maen Takruri	[16]
E-waste Management	–	Richard Heeks	[40]
	–	G. Gaidajis	[41]
	–	Sushant B. Wath	[42]
	–	Maksimovic, M	[43]
Green communication	–	Shiraj A. Alvi	[44]
	–	M. M. Alam	[45]
	Adaptive sensing	Perera	[20]
Green cloud computing	Energy consumption model for low intensity and infrequent use.	Jayant Baliga	[46]
	Power requirement minimization	Anubha Jain	[47]
	IoT and cloud integration	Sivakumar	[48]
	PTNet	E. Baccour	[37]
	–	Qiang Liu	[49]
	Port on/off	Zina Chkirkene	[50]
	Energy management in large-scale data center	Sharad S	[54]
	Inductor design	Colin A. Pardue	[51]

7 Conclusion

Green computing is proved to be an important breakthrough. Our contribution can be viewed in the following terms: the detailed review about green communication is enlightened, identifying how it can be effectively used as a green IoT element; lastly, various sectorwise applications are discussed. In the prospect, a useful basic design can be structured by considering the aforesaid literature review.

References

1. Al-Fuqaha, A., Guizani, M., Mohammadi, M., Aledhari, M., Ayyash, M.: Internet of things: a survey on enabling technologies, protocols, and applications. *IEEE Commun. Surveys Tutorials* **17**(4), 2347–2376 (2015)
2. Li, S., Da Xu, L., Zhao, S.: The internet of things: a survey. *Inf. Syst. Front* **17**(2), 243–259 (2015)
3. Shirvanimoghaddam, M., Shirvanimoghaddam, K., Abolhasani, M. M., Farhangi, M., Barsari, V.Z., Liu, H., Naebe, M.: Paving the path to a green and self-powered internet of things using piezoelectric energy harvesting. (2017) arXiv preprint [arXiv:1712.02277](https://arxiv.org/abs/1712.02277)
4. Rogers, E.: Encouraging Intelligent Efficiency Study of Policy Opportunities. Energy-Efficient Ecn, Washington, DC, USA, Tech. Report. IEA-4EDNA (2017)
5. Annual World Energy Economic Statistical Report 2018 <https://www.bp.com/content%20/dam/bp/business-sites/en/global/corporate/pdf/energy-economics/statistical-review/bp-statsreview-2018-full-report.pdf>
6. Alsamhi, S.H., Ma, O., Ansari, M.S., Meng, Q.: Greening internet of things for smart everything with a green-environment life: a survey and future prospects. (2018) arXiv preprint [arXiv:1805.00844](https://arxiv.org/abs/1805.00844)
7. Zhu, C., Leung, V.C., Shu, L., Ngai, E.C.H.: Green internet of things for the smart world. *IEEE Access* **3**, 2151–2162 (2015)
8. Na, W., Park, J., Lee, C., Park, K., Kim, J., Cho, S.: Energy-efficient mobile charging for wireless power transfer in the internet of things networks. *IEEE internet of things J* **5**(1), 79–92 (2017)
9. Musaddiq, A., Zikria, Y.B., Hahm, O., Yu, H., Bashir, A.K., Kim, S.W.: A survey on resource management in IoT operating systems. *IEEE Access* **6**, 8459–8482 (2018)
10. Gorlatova, M., Sarik, J., Grebla, G., Cong, M., Kymmissis, I., Zussman, G.: Kinetic energy harvesting for the internet of things. *IEEE J. Sel. Areas Commun.* **33**, 1624–1639 (2015)
11. Lee, H.G., Chang, N.: Powering the IoT: storage-less and converter-less energy harvesting. In: The 20th Asia and South Pacific Design Automation Conference pp. 124–129
12. Ju, Q., Zhang, Y.: Predictive power management for Internet of battery-less things. *IEEE Trans. Power Electron.* **33**(1), 299–312 (2017)
13. Kamalinejad, P., Mahapatra, C., Sheng, Z., Mirabbasi, S., Leung, V.C., Guan, Y.L.: Wireless energy harvesting for the internet of things. *IEEE Commun. Mag.* **53**(6), 102–108 (2015)
14. Costanzo, A., Masotti, D.: Energizing 5G: near-and far-field wireless energy and data transfer as an enabling technology for the 5G IoT. *IEEE Microw Mag* **18**(3), 125–136 (2017)
15. Karthikeya, S.A., Narayanan, R.: Power-aware gateway connectivity in battery-powered dynamic IoT networks. *Comput. Netw.* **130**, 81–93 (2018)
16. Takruri, M., Attia, H.A., Awad, M.H.: Wireless charging in the context of sensor networks. *Int J Appl Eng Res* **11**(12), 7736–7741 (2016)
17. Shafiee, N., Tewari, S., Calhoun, B., Shrivastava, A.: Infrastructure circuits for lifetime improvement of ultra-low-power IoT devices. *IEEE Trans. Circuits Syst. I Reg Paper* **64**(9), 2598–2610 (2017)
18. San Murugesan, GR.: Harnessing Green IT: Principles and practices. Wiley Publishing (2012)
19. Rault, T., Bouabdallah, A., Challal, Y.: Energy efficiency in wireless sensor networks: a top-down survey. *Comput. Netw.* **67**, 104–122 (2014)
20. Perera, C., Talagala, D.S., Liu, C.H., Estrella, J.C.: Energy-efficient location and activity-aware on-demand mobile distributed sensing platform for sensing as a service in IoT clouds. *IEEE Trans. Comput. Soc. Syst.* **2**(4), 171–181 (2015)
21. Khodr, H., Kouzayha, N., Abdallah, M., Costantine, J., Dawy, Z.: Energy-efficient IoT sensor with RF wake-up and addressing capability. *IEEE Sens. Lett.* **1**(6), 1–4 (2017)
22. Perles, A., Perez-Marin, E., Mercado, R., Segrelles, J.D., Blanquer, I., Zarzo, M., Garcia-Diego, F.J.: An energy-efficient internet of things (IoT) architecture for preventive conservation of cultural heritage. *Future Gener. Comput. Syst.* **81**, 566–581 (2018)

23. Qureshi, F.F., Iqbal, R., Asghar, M.N.: Energy-efficient wireless communication technique based on cognitive radio for the Internet of Things. *J. Netw. Comput. Appl.* **89**, 14–25 (2017)
24. Li, S., Ni, Q., Sun, Y., Min, G., Al-Rubaye, S.: Energy-efficient resource allocation for industrial cyber-physical IoT systems in the 5G era. *IEEE Trans. Ind. Informatics* **14**(6), 2618–2628 (2018)
25. Yi, G., Park, J.H., Choi, S.: Energy-efficient distributed topology control algorithm for low-power IoT communication networks. *IEEE Access* **4**, 9193–9203 (2016)
26. Basnayaka, D.A., Haas, H.: A new degree of freedom for energy efficiency of digital communication systems. *IEEE Trans. Commun.* **65**(7), 3023–3036 (2017)
27. Shen, J., Wang, A., Wang, C., Hung, P.C., Lai, C.F.: An Efficient centroid-based routing protocol for energy management in WSN-assisted IoT. *IEEE Access* **5**, 18469–18479 (2017)
28. Tian, X., Zhu, Y.H., Chi, K., Liu, J., Zhang, D.: Reliable and energy-efficient data forwarding in industrial wireless sensor networks. *IEEE Syst. J.* **11**(3), 1424–1434 (2017)
29. Ahmed, K.Z., Kar, M., Mukhopadhyay, S.: Energy Delivery for Self-Powered IoT Devices. In: 21st Asia and South Pacific Design Automation Conference (ASP-DAC) IEEE, pp. 302–307
30. Nan, Y., Li, W., Bao, W., Delicato, F.C., Pires, P.F., Dou, Y., Zomaya, A.Y.: Adaptive energy-aware computation offloading for the cloud of things systems. *IEEE Access* **5**, 23947–23957 (2017)
31. Shuja, J., Ahmad, R.W., Gani, A., Ahmed, A.I.A., Siddiq, A., Nisar, K., Zomaya, A.Y.: Greening emerging IT technologies: techniques and practices. *J. Internet Serv. Appl.* (2017)
32. Baccarelli, E., Naranjo, P.G.V., Scarpiniti, M., Shojafar, M., Abawajy, J.H.: Fog of everything: energy-efficient networked computing architectures, research challenges, and a case study. *IEEE Access* **5**, 9882–9910 (2017)
33. Nandyala, C.S., Kim, H.K.: Green IoT agriculture and healthcare application (GAHA). *Int. J. Smart Home* **1**(4), 289–300 (2016)
34. Zhu, C., Leung, V.C., Wang, K., Yang, L.T., Zhang, Y.: Multi-method data delivery for green sensor-cloud. *IEEE Commun. Magazine* **55**, 176–182 (2017)
35. Bilal, K., Khan, S. U., Zhang, L., Li, H., Hayat, K., Madani, S.A., Xu, C.Z.: Quantitative comparisons of the state of the art data center architectures. *Concurrency Comput. Pract. Experience* **25**(12) (2013)
36. Hammadi, A., Mhamdi, L.: A survey on architectures and energy efficiency in Data Center Networks. *Comput. Commun.* **40**, 1–21 (2014)
37. Baccour, E., Foufou, S., Hamila, R: PTNet: a parameterizable data center network. In: IEEE Communications and Networking Conference on (WCNC 2016)—Track 4—Service, Application, and Business. IEEE (2016, April)
38. Kaur, N., Aulakh, I.K.: An eagle-eye review on the emerging development trends by application of IOT devices. In IEEE International Conference on Smart Energy Grid Engineering (SEGE) pp. 313–320, IEEE (2018)
39. Talari, S., Shafie-Khah, M., Siano, P., Loia, V., Tommasetti, A., Catalão, J.: A review of smart cities based on the internet of things concept. *Energies* **10**(4), 421 (2017)
40. Heeks, R., Subramanian, L., Jones, C.: Understanding e-waste management in developing countries: strategies, determinants, and policy implications in the Indian ICT Sector. *Inf. Technol. Dev.* **21**(4), 653–667 (2015)
41. Gaidajis, G., Angelakoglou, K., Aktosoglou, D.: E-waste: environmental problems and current management. *J. Eng. Sci. Technol. Rev.* **3**(1), 193–199
42. Wath, S.B., Dutt, P.S., Chakrabarti, T.: E-waste scenario in India, its management, and implications. *Environ. Monit. Assess.* **172**(1–4), 249–262 (2011)
43. Maksimovic, M.: Greening the future: green internet of things (G-IoT) as a key technological enabler of sustainable development. 283–311 (2018)
44. Shiraj A.: Alvi Energy efficient green routing protocol for internet of multimedia things. In: IEEE International Conference on Intelligent Sensor, Sensor Networks and Information Processing (ISSNIP) IEEE (2015)
45. Alam, M.M., Malik, H., Khan, M.I., Pardy, T., Kuusik, A., Le Moullec, Y.: A survey on the roles of communication technologies in IoT-based personalized healthcare applications. *IEEE Access* **6**, 36611–36631 (2018)

46. Baliga, J., Ayre, R. W., Hinton, K., Tucker, R.S.: Green cloud computing: balancing energy in processing, storage, and transport. *Proc. IEEE* **99**(1), 149–167(2010)
47. Jain, A., Mishra, M., Peddoju, S.K., Jain, N.: Energy efficient computing green cloud computing. In: International Conference on Energy-Efficient Technologies for Sustainability pp. 978–982. IEEE. (2013, April)
48. Sivakumar, S., Anuratha, V., Gunasekaran, S.: Survey on integration of cloud computing and internet of things using application perspective. *Int. J. Emerg. Res. Manag. Technol.* **6**(4), 101–108 (2017)
49. Liu, Q., Ma, Y., Alhussein, M., Zhang, Y., Peng, L.: Green data center with IoT sensing and cloud-assisted smart temperature control system. *Comput. Netw.* **101**, 104–112 (2016)
50. Chkirkene, Z., Gouissem, A., Hadjidj, R., Foufou, S., Hamila, R.: Efficient techniques for energy saving in data center networks. *Comput. Commun.* **129**, 111–124 (2018)
51. Pardue, C.A., Bellaredj, M.L.F., Davis, A.K., Swaminathan, M., Kohl, P., Fujii, T., Nakazawa, S.: Design and characterization of inductors for self-powered IoT edge devices. *IEEE Trans. Compon. Packag. Manuf. Technol.* **8**(7), 1263–1271 (2018)
52. Popli, S., Jha, R.K., Jain, S.: A survey on energy efficient narrowband internet of things (NB-IoT): architecture, application, and challenges. *IEEE Access* **7**, 16739–16776 (2018)
53. Vieeralingam, G., Ramanathan, R.: Parametric study of RF energy harvesting in SWIPT enabled wireless networks under downlink scenario. *Procedia Comput. Sci.* **143**, 835–842 (2018)
54. Sharad, S., Sivakumar, P.B., Anantha Narayanan, V.: A novel IoT-based energy management system for large scale data centers. In Proceedings of the 2015 ACM 6th International Conference on Future Energy System pp. 313–318 (2015)
55. Prakash, L., Sugatha Kumari, P.R., Chandran, S., Sachin Kumar, S., Soman, K.P.: Self-sufficient Smart Prosumers of Tomorrow. *Procedia Technol.* **21**, 338–344 (2015)

An Efficient Layout of Single-Layer Full Adder Using QCA



Nilesh Patidar and Namit Gupta

Abstract Quantum cellular automata (QCA) is a new method of computation used in designing of electronic digital circuits at scale of nanometers. QCA has been used to achieve better performance in cell density, high switching speed and low power dissipation. An adder is a very useful component used for designing of arithmetic digital devices. This paper presents a layout of full adder designed on single layer which is efficient in various aspects based on QCA technology proposed. The goal of the research is to minimize the cells used, designed area and delay in designing of full adder based on QCA. The proposed layout of full adder has been efficient in number of cells used, designed area as well as latency in clocks. The proposed layout has been designed using XOR gate and majority voter. The proposed layout of adder consist of 24 cells with an optimized area of $0.016 \mu\text{m}^2$ and 2-clock phases ($\sim 0.125 \text{ ps}$) which shows more efficient from previous work on adders. The layout of full adder has been successfully designed and simulated using QCADesigner-E 2.2.

Keywords Adder · Nano-electronics · QCA

1 Introduction

In 1965, great scientist Gorden Moore predicted that the integration of number of cells or transistors on a single silicon wafer shall be doubled in every 18 months. Nowadays, more reduction in sizing of transistor may not be possible due to some problems in physical integration using CMOS technology. The CMOS has various physical limitations faced in fabrication techniques as we approach the nanometer regime. Due to this, CMOS devices are prone to new realization challenges where device density puts an upper limit in integration due to short channel effect and higher

N. Patidar (✉) · N. Gupta

Department of Electronics Engineering, SVITS, SVVV, Indore, India

e-mail: neel.s.patidar@gmail.com

N. Gupta

e-mail: namitg@hotmail.com

leakage current leading to considerable power dissipation [1]. Thus, semiconductor industry is seeking for new technology and fabrication methods to overcome the issues faced in CMOS era.

The quantum-dot cellular automaton (QCA) proves to be the prominent technology that provides solution at nano-scale and a reliable computational method for digital data [2, 3]. Quantum-dot cellular automata (QCA) represent one of such innovative platforms for designing of digital circuits based on quantum-dots [4]. QCA technology has outstanding features like small size, high switching speed and low energy dissipation [2, 5].

In the previous work, several digital circuits and adders are designed based on QCA, but there were lack of efficiency in terms of cell number, area and delay. The QCA devices are fabricated at size of few nanometers. It is allowing integration of 10^{11} – 10^{12} devices/cm², besides lower power dissipation and tera-hertz frequency operation capability [6]. The QCA does not represent on/off states of transistors as binary 1/0, rather it uses charge configuration of QCA cells to encode it as 1 and 0.

Adder is very useful and important component of many arithmetic and logical circuits. So it is a need for the minimization of different parameters associated with design. In this paper, the design of full adder is proposed which proves efficient in terms of cell complexity, designed area and propagation delay. It is compared with some adders which are previously designed. In Sect. 2, basic concepts and fundamentals of QCA has been described with proposed layout of QCA full adder. The proposed circuit simulation is also discussed in this section. Then, observations and finding has been presented in Sect. 3. Also, show the table of comparison of proposed full adder with previous work. Finally, we concluded in Sect. 4.

2 Experimental Details, Methods and Materials

2.1 QCA Cell

A QCA cell has square architecture having four quantum dots at corners and two electrons residing in quantum dots. All quantum dots are able to localize electric charge; however, electrons localize in two antipodal quantum dots due to columbic repulsive force between them. The basic QCA cell has been depicted in Fig. 1. There are two possible polarizations which are appeared in a QCA cell where the electrons

Fig. 1 Basic QCA cell

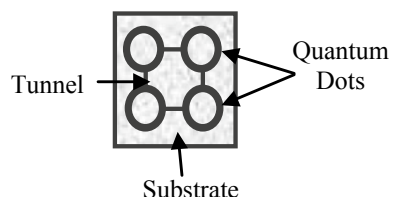


Fig. 2 QCA cell with its polarization

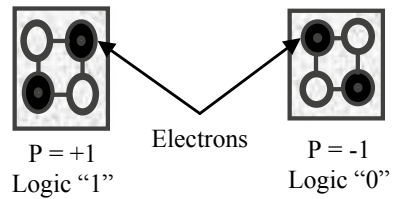
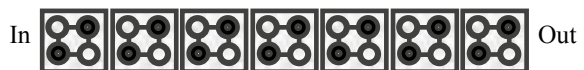


Fig. 3 QCA wire



residue at opposite of its corners. These polarizations of QCA can be represented by binary logic ‘0’ and logic ‘1’ as given in Fig. 2.

2.2 QCA Wire

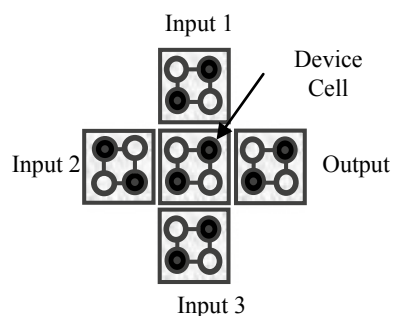
QCA wire can be created by arranging the QCA cells in form of an array. The binary information has been transferred from input cell to output cell by means of columbic interaction between QCA cells. A basic QCA wire has been represented in Fig. 3.

2.3 Basic Logical Devices

2.3.1 Majority Voter Gate

The 3-input majority voter can be designed by utilizing 5 QCA cells as shown in Fig. 4. It produces output 1 when the majority of inputs are 1, otherwise produces 0.

Fig. 4 Majority voter gate



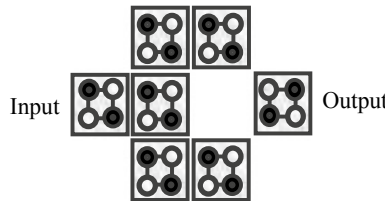


Fig. 5 QCA inverter

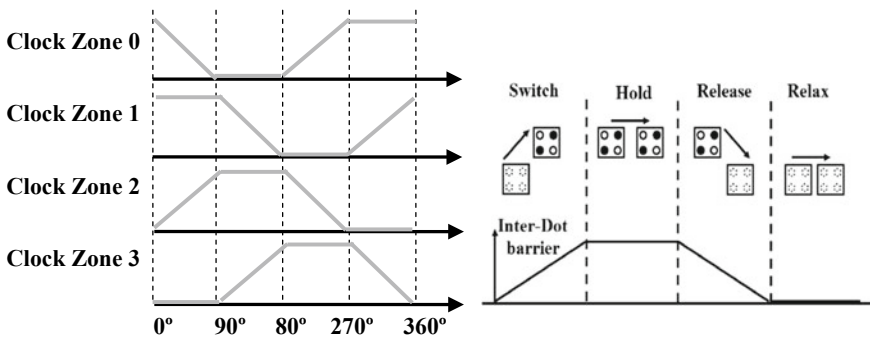


Fig. 6 QCA clocking zones with its four phases

2.3.2 QCA Inverter

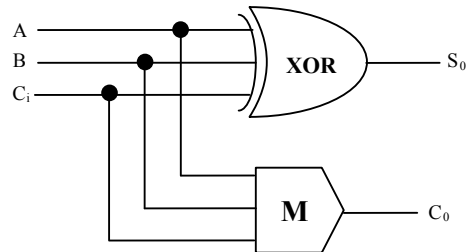
QCA inverter can be designed by placing a cell at offset of its input cell. The design of basic inverter consists of 7 cells which are shown in Fig. 5.

2.4 Clocking in QCA

In QCA technology, clocking is essentially required for digital circuit designs. The purpose of clocking is not only to control the data flow but also to provide power to QCA cells. There are four clocking zones which are clock 0, clock 1, clock 2 and clock 3. These clocks are 90° out of phase. Each clock comprises of four sections: switch, hold, release and relax as shown below in Fig. 6.

2.5 Proposed Layout of Full Adder

In previous works, some of the authors have presented the expression of sum by utilizing more than one MVs and inverters. The proposed layout of full adder is based

Fig. 7 Design of full adder

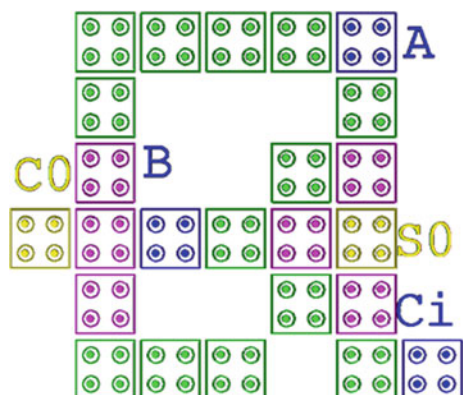
on three-input XOR gate [7] instead of AND and OR realized by MV. Proposed layout of full adder utilizes three-input XOR gate and three-input majority voter presented as M in schematic as shown in Fig. 7. The expressions for sum S_0 and carry C_0 of full adder can be expressed by Eqs. (1) and (2).

$$\text{Sum} - S_0 = \text{XOR}(A, B, C_i) \quad (1)$$

$$\text{Carry} - C_0 = M(A, B, C_i) \quad (2)$$

where A , B and C_i are the inputs.

The layout of full adder has been designed by arranging QCA cells on single layer as shown in Fig. 8. The simulation has been performed using Euler method on coherence vector (w/energy) simulation using QCADesigner-E 2.2 [8]. QCADesigner-E is extension of QCADesigner which can be utilizing to estimate energy dissipation along with simulation of QCA circuits. The simulation result of full adder has been shown in Fig. 9. The rectangular section in the simulation results shows the propagation delay of the full adder.

Fig. 8 Proposed layout of full adder

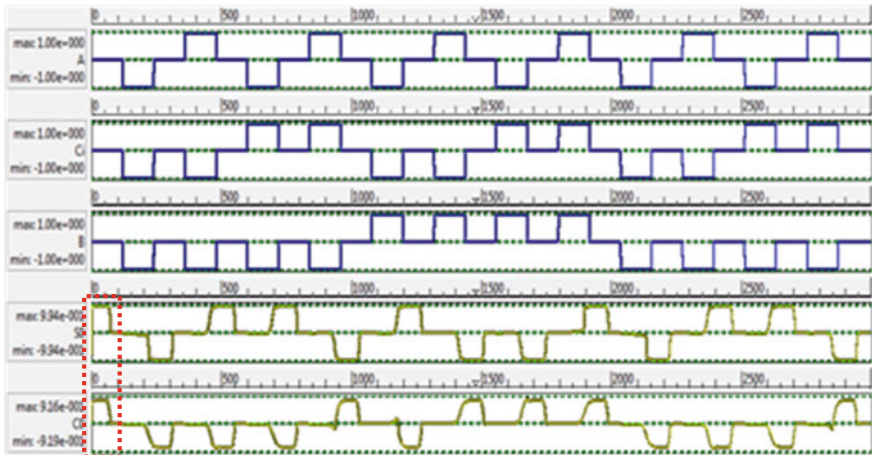


Fig. 9 Simulation results of full adder

3 Observations

In the literature, many designs on full adder have been presented and designed using QCADesigner tool and estimation of energy has been done using QCAPro tool. Previous designs of full adder are both single and multilayer, but single layer designs are preferred over multilayer designs due to the ease of its fabrication.

The comparison table of various designs of full adder in various aspects has been shown in Table 1. Here, it can be seen that the proposed design of adder is efficient in terms of cell complexity. The number of cells reduced by 21 from the design presented in [15]. The designed area is minimized by $0.014 \mu\text{m}^2$ from layout presented in [16]. The latency is also achieved by 0.25 clock compared from layout presented in [9, 10, 12]. Also, energy dissipation is less than the designs of full adder presented in [10–12, 17].

4 Conclusion

The simulation of proposed full adder has been verified and compared with some performance parameters (number of cells, area and delay) and observed that the proposed layout of full adder is area efficient. The proposed design proves to be energy efficient. The layout of full adder composed of 24 cells (reduced by 31% from [15]) with area of $0.016 \mu\text{m}^2$ (optimized by 46% from [16]) and latency of two-clock phases approximately 0.125 ps (improved by 33.3% from [9, 10, 12]) since it has been operated on 4 THz frequency that shows more efficient from previous works on adders. The total energy dissipated by proposed full adder is 24.2 meV estimated using QCADesigner-E. Here, it can be observed that the proposed circuit has lesser

Table 1 Comparison between various parameters of proposed design with existing

Design		Cell complexity (number of cells)	Area (in μm^2)	Latency (number of clocks)	Layers	Total energy dissipation (in meV)
Existing	Navi [14]	55	0.0816	1.25	Multilayer	–
	Roohi [9]	52	0.04	0.75	Multilayer	–
	Abedi [11]	59	0.043	1	Single layer	168.54 ^a
	Labrado [10]	63	0.05	0.75	Single layer	149.4 ^a
	Ramesh [13]	52	0.038	1	Single layer	–
	Mostafa [14]	35	0.0598	1.25	Multilayer	–
	Ramanand [12]	53	0.047	0.75	Single layer	144.62 ^a
	Heikalabad [16]	41	0.03	1	Single layer	–
	Mokhtari [17]	46	0.04	1	Single layer	83.99 ^a
Proposed Design		24	0.016	0.5	Single layer	24.2

^aTotal energy dissipation estimation on $1E_k$ (Kink energy) using QCAPro tool

energy dissipation from others. Proposed efficient layout of full adder can further be used to implement complex arithmetical and logical circuits and is also beneficial for high-performance QCA circuits at nano-scale in future. Our aim is to design digital circuits based on QCA that should have less complexity, optimized area along with faster switching speed. It provides evidence that the QCA technology has more useful and have more advantages over CMOS technology.

References

1. Kim, Y.-B.: Challenges for nanoscale mosfets and emerging nanoelectronics. *Trans. Electr. Electron. Mater.* **11**(3), 93–105 (2010)
2. Orlov, A.O., Amlani, I., Bernstein, G.H., Lent, C.S., Snider, G.L.: Realization of a functional cell for quantum-dot cellular automata. *Science* **277**(9), 28–930 (1997)
3. Tougaw, P.D., Lent, C.S.: Logical devices implemented using quantum cellular automata. *J. Appl. Phys.* **75**(3), 1818–1825 (1994)
4. Lent, C.S., Tougaw, P.D., Porod, W., Bernstein, G.H.: Quantum cellular automata. *Nanotechnology* **4**(1), 49–57 (1993)
5. Tougaw, P.D., Lent, C.S.: Logical devices implemented using quantum cellular automata. *Appl. Phys.* **75**, 1818–1824 (1994)

6. Lent, C.S.: Bypassing the transistor paradigm. *Science* **288**(5471), 1597–1599 (2000)
7. Bahar, A.N., Waheed, S., Hossain, N., Asaduzzaman, M.: A novel 3-input XOR function implementation in quantum dot-cellular automata with energy dissipation analysis. *Alexandria Eng. J* (2017). <http://dx.doi.org/10.1016/j.aej.2017.01.022>
8. Torres, F.S., Wille, R., Niemann, P., Drechsler, R.: An energy-aware model for the logic synthesis of quantum-dot cellular automata. *IEEE Trans. Comput.-Aided Design Integr. Circ. Syst.* **37**(12), 3031–3041 (2018)
9. Roohi, A., Khademolhosseini, H., Sayedsalehi, S., Navi, K.: A symmetric quantum-dot cellular automata design for 5-input majority gate. *J. Comput. Electron.* **13**, 701–708 (2014)
10. Labrado, C., Thapliyal, H.: Design of adder and subtractor circuits in majority-logic based field-coupled QCA nano computing. *Electron. Lett.* **52**(6), 464–466 (2016)
11. Abedi, D., Jaberipur, G., Sangsefidi, M.: Coplanar full adder in quantum-dot cellular automata via clock-zone based crossover. *IEEE Trans. Nanotechnol.* **14**(3), 497–504 (2015)
12. Jaiswal, R., Sasamal, T.N.: Efficient design of full adder and subtractor using 5-input majority gate in QCA. In: Proceedings of Tenth International Conference on Contemporary Computing (IC3), Noida, India (2017)
13. Ramesh, B., Rani, M.A.: Implementation of parallel adders using area efficient quantum dot cellular automata full adder. In: 10th International Conference on Intelligent Systems and Control (ISCO) (2016). <https://doi.org/10.1109/isco.2016.7727057>
14. Navi, K., Farazkish, R., Sayedsalehi, S., Rahimi Azghadi, M.: A new quantum-dot cellular automata full-adder. *Microelectron. J.* **41**, 820–826 (2010)
15. Sadeghi, M., Navi, K., Dolatshahi, M.: A new quantum-dot cellular automata full-adder. In: 5th International Conference on Computer Science and Network Technology (ICCSNT), IEEE, pp. 443–445 (2016)
16. Heikalabad, S.R., Asfestani, M.N., Hosseinzadeh, M.: A full adder structure without cross-wiring in quantum-dot cellular automata with energy dissipation analysis. *J. Supercomput.* **74**(5), 1994–2005 (2018)
17. Mokhtari, D., Rezai, A., Rashidi, H., Rabiei, F., Emadi, S., Karimi, A.: Design of novel efficient full adder circuit for quantum-dot cellular automata. *Electron. Energetics* **31**(2), 279–285 (2018)

A Review of mm-Wave Power Amplifiers for Next-Generation 5G Communication



Pradeep Gorre, R. Vignesh, Rajeev Arya, and Sandeep Kumar

Abstract In this paper, a review study of millimeter wave-based power amplifiers for 5G communication is presented. This literature mainly focuses on major component of the RF transceiver IC, i.e., power amplifier (PA). The upcoming 5G communication envisioned broadband modulation, high speed data rate, and new integration technologies which could overcome key challenges in the design of mobile devices and communication buildings. The power amplifiers in the 5G base station require high output powers (ranging from 2 to 10 W), high efficiency (up to 95%), and high gain (up to 40 dB). The basic building blocks, device technologies, architecture of RF power amplifiers, and parametric performances will be considered in this review. This study reviewed all device technologies (especially IV and III-V semiconductor technologies) for power amplifiers and found that a gallium nitride (GaN)-based PA is the best candidate to provide high output power, high efficiency, and high back-off power. In addition, various architectures of PAs have been reported while doherty power amplifier is one of best candidate for 5G base station.

Keywords 5th generation (5G) · Power amplifier · Device technologies · Communication · Millimeter wave (mm-wave)

1 Introduction

Over the last few decades, the mobile communication witnesses a technological evolution starting from first generation (1G) with only voice calls to fourth generation (4G) which open gates for the real meaning of “mobile broadband” experience. In the early 1890s, Marconi for the first time developed a radio transmitter for telegraphy

P. Gorre · R. Vignesh · S. Kumar (✉)

Department of Electronics and Communication, National Institute of Technology, Surathkal, Karnataka, India

e-mail: sandeep@nitk.edu.in

R. Arya

Department of Electronics and Communication, National Institute of Technology, Patna, Bihar, India

[1]. The budget for mobile communication area had allocated euro 2.7 billion in 2012 and is predicted to touch around euro 4 trillion by 2020. Further, with an increase in demand for media sharing like images and short videos, video chatting and high usage of social network guided to a high-speed mobile data rate (nearly in terms of Gbps). Moreover, current challenges in 4G communications such as no support for heterogeneous wireless network, limited connectivity of devices, high-latency round trip (~10 ms), no channel interference, limited bandwidth in unit area, and poor network coverage in rural areas pave the path for next-generation 5G communication [2]. Hence, to meet the demand for high data rate transfer, it requires a high-bandwidth interconnects for better computational performance and mobile applications. While, 5G spectral band is still ambiguous, recent research work demonstrates that the mm-wave spectral band is an exciting band for 5G mobile regularity [3]. The sub-terahertz (mm-wave) bands offer high possibility to meet high data rate requirement as it has several GHz spectrum availabilities at this frequency band. The future of 5G wireless communication lies in exploiting this high-frequency mm-wave band (3–300 GHz) [4]. Most of the current study in 5G systems are being held at frequencies 15, 28, and 70 GHz bands.

In order to achieve a high speed data rate, heterogeneous networks (Hetnets) is an good approach to deploys a clutch of micro and femto-cells in the 5G cellular communication. Figure 1 shows a RF transceiver IC for HetNets. A HetNet is a wireless network which consists of different nodes with various transmission powers and coverage sectors [5]. The most important block in RF transmitter is power amplifier (PA) whose performance (Gain, linearity, and efficiency) directly affects any transmitter; therefore, the upcoming 5G cellular network requires a novel PA circuit architectures and advanced device technologies to enhance efficiency without degrading linearity of PA [6]. The performance of power amplifier for 5G and vehicular communication exhibited in the work [7–10]. In addition, several validations of dual-band Doherty PAs and dual-band class-AB power amplifiers are presented [11–13]. Hence, while designing RF transmitter for 5G application, the efficiency should be as high as possible. Additionally, in order to obtain a high peak-to-average ratio, power amplifier have need to back-off from the most adequate point where the

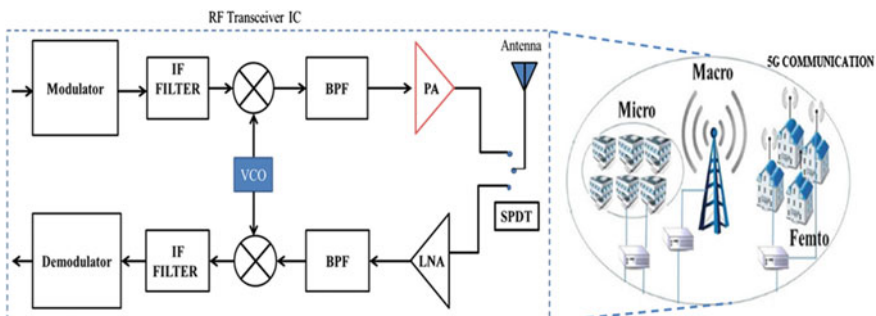


Fig. 1 Typical block diagram of transceiver IC for next-generation 5G communication

efficiency drops slowly [14–16]. Doherty power amplifier (DPA) is the best choice for the power stage in 5G applications [17–19].

The organization of manuscript: Sect. 2 briefs the importance of process technologies followed by various design methodologies for mm-wave PA for 5G at 15 and 28 GHz frequency in Sect. 3 while Sect. 4 briefs the parametric performance of 5G PAs. Section 5 gives conclusion of the survey.

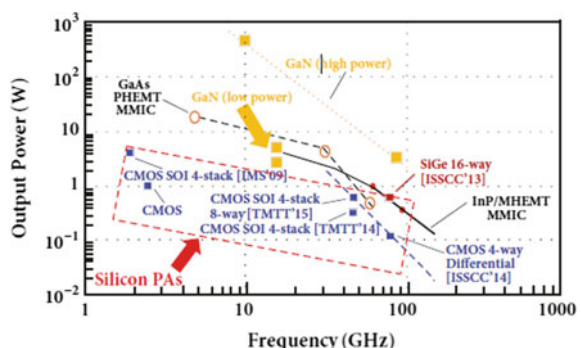
2 Importance of PA Device Technologies

The choice of PA design technology is a hard task due to many factors. The minimum reverse voltage of transistors and their scaling DC supply adversely affect the power amplifier output. Various power combiner techniques are implemented to overcome these issues but counterpart leads to reduction in overall system efficiency. Along with PAs the rest RF transmitter blocks should also be made broadband to use the entire system over the globe to cover the WiGig standard (IEEE802.11ad) [20]. Further, the cost, integration level, and stability are also significant factors to decide the preferred technology for PA implementation. Hence, the design of a high gain, high efficiency, linear, and wideband PA is challenging in device scaling technology.

In addition to the above, RF output power (P_{out}) per PA and number of users are two most critical parameters in choosing PA design technologies. In [21], the estimated output power of each power amplifier is required less than 20 dBm for small cells (i.e. femto and pico cells) while number of users are limited to 20. CMOS/SOI and SiGe PA technologies are preferred for small cells. On the other hand, for macro-cell and microcells whose estimated (P_{out}) per PA is >20 dBm and a number of users are in order of thousands may go with GaN and GaAs PA technologies. GaN intuitively results in high efficiencies, with reduction in power consumption which improves battery life [22].

Figure 2 gives a detailed literature survey of various power amplifier process technologies at mm-wave frequency band. (P_{out}). If stacked CMOS/SOI PAs and cascade SiGe PA are employing power combining techniques so they could exhibit optimum output power for small cell. (P_{out}). However, the output powers are required

Fig. 2 Performances of RF PA adopting fourth and three-five device technologies [23]



of 3 W to 10 W for micro and macro cells which could achieve by using GaN/GaAs PAs.

3 PA Architectures and Considerations

In this section, PA architectures and its considerations would be reviewed through a recent literature survey. The design procedure and implementation of various PAs architectures will be discuss in this section.

3.1 Doherty Power Amplifier (DPA) in $0.15 \mu\text{m}$ GaAs Technology

In 1936, W. H. Doherty for the first time proposed the functioning of the Doherty power amplifier (DPA) [24]. Figure 3 has shown block diagram of a three-stage DPA. In this DPA, a frequency-dependent matching network of conventional DPA is removed and parasitic (C_{ds}) is compensated by shunt inductors through resonance. An $\frac{\lambda}{4}$ inverted transmission line, connected between the main transistor and auxiliary transistor, acts as a load modulator to achieve high efficiency over wideband frequencies.

A three DPA provides a parametric performance where it could achieved an peak PAE of 10% at 15 GHz, drain efficiency of 22% at 8 dB back-off and output power of 22 dBm within range of 14.5 GHz to 15 GHz under the supply voltage of 4 V.

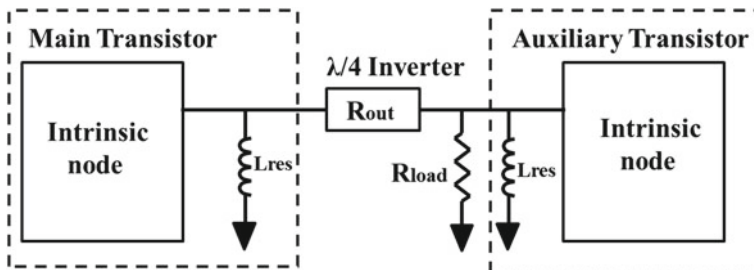


Fig. 3 Block diagram of a three-stage DPA in $0.15 \mu\text{m}$ GaAs technology [25]

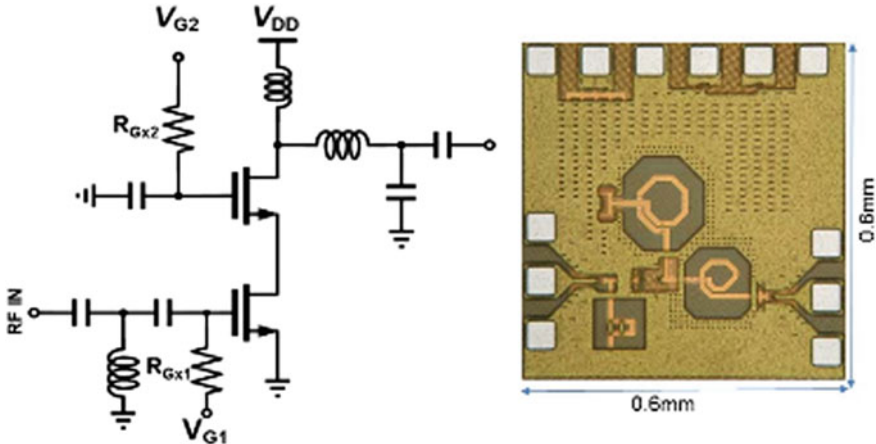


Fig. 4 28 GHz two-stack nMOS SOI and microphotograph [29]

3.2 Two-Stack FET nMOS PAs

In order to achieve maximum efficiency with CMOS, it is lucrative to practice transistor stacking, which models the exact distribution of the voltage between basic transistors [26–28]. In conventional stacking, a capacitor is connected to gate which allows voltage swing proportional to source voltage and holds good at low frequencies but the performance is depraved at high frequencies. The alternative is a two-stack FET nMOS as shown in Fig. 4 [29]. The proposed circuit is designed in 45 nm CMOS-SOI technology, and simulation results a gain of 14 dB at 28 GHz, the output power reaches 20 dBm with respect to bias conditions, and 43% PAE is measured. The two-stack FET nMOS has measured an optimum error vector magnitude (EVM) at an average power of 9.8 dBm for 64 QAM OFDM.

3.3 3-Stage, 4-Stack FET CMOS PA

The work in [30] explains the implementation of PA in 45 nm CMOS/SOI device technology. In this PA design, the output stage as a cascode multi-gate cell achieved optimum output power and high gain at 15 GHz frequency of operation. The complete schematic of 15 GHz PA is shown in Fig. 4. The RF input is applied to a two-stage cascode pre-driver, and RF output is measured at high-power 4-stack multigate-cell stage. The two pre-driver stages along with an output stage realize gain >30 dB. This PA architecture exhibits a peak gain of 31 dB at 13.5 GHz with an attenuation bandwidth from 12.7 to 15.3 GHz, which achieves a limited bandwidth of 20%. The input and the output reflection coefficients are below -10 dB ranging from 13.5 to

15.5 GHz frequency band. The PA achieves (P_{out}) > 25.1 dBm and a maximum PAE of 32.4% at 13.5 GHz.

The attenuation 3 dB bandwidth is 2.6 GHz (nearly 20%). According to the reports, the discussed PA demonstrates the best combination of output power and PAE for 15 GHz CMOS PAs.

3.4 Multistage 0.13 μm GaN HEMT DPA

The basic blocks of GaN HEMT DPA are shown in Fig. 5. It consists of two-stage driver circuit, hybrid coupler, input matching networks, peaking and carrier power amplifier, output matching, and 1:1 filtered balun network. The two-stage driver circuit provides wide amplified signal operation when operated into class-C operation while hybrid coupler splits amplified signal into two RF powers toward the carrier and the power amplifier. The balun-filtered network provides a unified band signal in the desired band of operation [31]. The simulated gain of 32.3 dB while the measured gain of 30.1 dB is achieved. The average output power obtained is 40 dBm when the input power level is taken as 10 dBm. At average output power of 40 dBm, simulated PAE of 85.2% while experimental PAE of 84% is achieved.

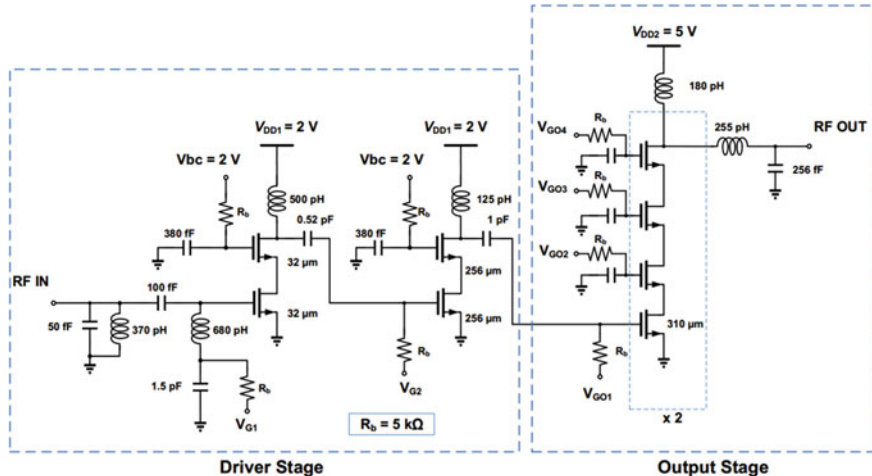


Fig. 5 Schematic of 15 GHz PA with pre-driver and output stage multigate-cell [30]

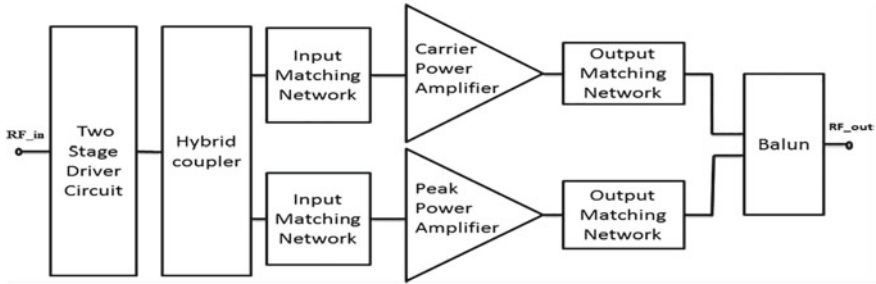


Fig. 6 Block diagram of multistage Doherty PA [31]

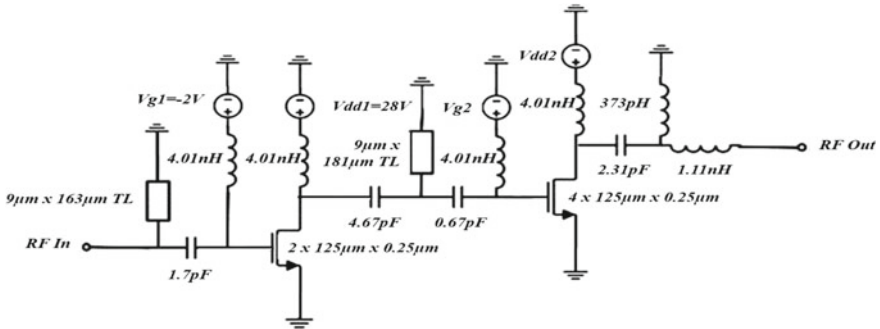


Fig. 7 Circuit diagram of the two-stage 15 GHz fully integrated GaN PA MMIC design [32]

3.5 Two-Stage 15 GHz Fully Integrated GaN-Based Power Amplifier

In [32], a two-stage 15 GHz PA implemented in $0.25\ \mu m$ GaN device technology was discussed and its schematic is shown in Fig. 6. The two-stage fully integrated PA demonstrates a peak PAE and highest linear efficiency. Simulation results in Fig. 7 describes that PA has a peak gain of 24 dB, input reflection coefficient, and output reflection coefficient <10 dB at 15 GHz. Its peak PAE reaches 36.6% at ($P_{out} = 34$ dBm). In addition, the post-layout simulations suggest a drop in supply voltage from 28 to 10 V may moderately enhance the power back-off efficiency.

3.6 28 GHz 5G PA in 28 nm Bulk CMOS

A linear and efficient 28 GHz two-stage PA using 28 nm bulk CMOS technology for 5G phased array radio have been reported in [33, 34]. Figure 8 has shown the design of two-stage transformer-coupled topology. The driver amplifier (DA) current density

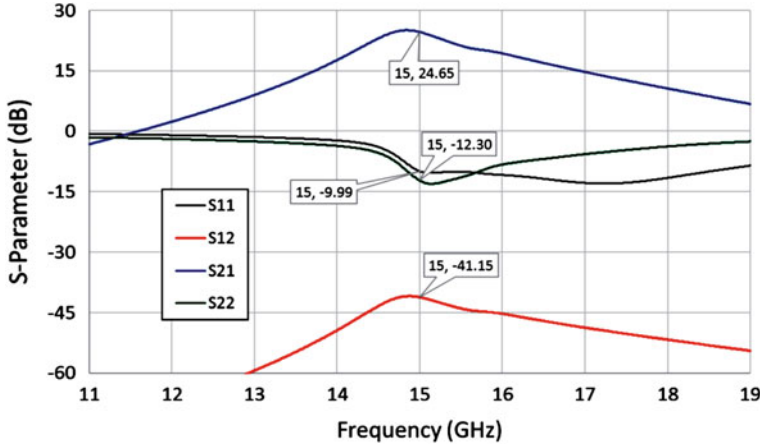


Fig. 8 Post-layout simulations on the GaN PA MMIC small-signal parameters [33]

is made double with respect to a power amplifier (PA) for optimum gain. Capacitors C_n accelerate reverse isolation; transformers provide impedance matching and DC blocking. The measured results demonstrated that a small value of inductor (i.e. = 14pH) lowering the device gain from 10 dB to 8 dB and achieved the output power of 12 dBm with PAE of 48 to 44%.

The unwanted loss resistance in series with the L_{deg} is also contributed to the further PAE reduction. The chosen L_{deg} , however, did not degrade PA's P_{out} significantly.

The 28 nm CMOS PA results ($P_{out} = +4.2$ dBm) with 9% PAE (at EVM = -25 dBc) applying 250 MHz 64 QAM OFDM input. The PA demonstrates 35.5%/10% PAE for continuous wave input at P_{out} , sat/9.6 dB back-off. The values are among the optimum measured PAE values reported for 18–40 GHz band CMOS PAs. The die micrograph of 28 GHz PA is shown in Fig. 9 (Fig. 10).

4 Parametric Performance of 5G PA

This section will be comparing the various PA architectures with its performance parameters in the Table 1. Out of various device technologies-based power amplifiers described in the previous section, it is observed that gallium nitride is shown best performance with the highest output power, highest efficiency, and highest linear gain.

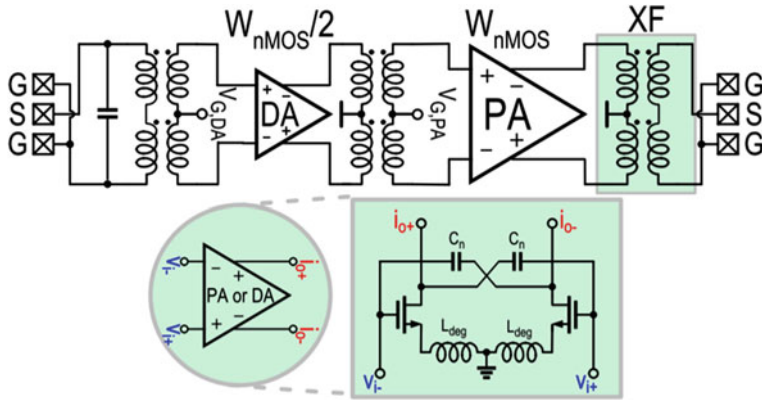


Fig. 9 Schematic of the 28 GHz PA in 28 nm bulk CMOS with two-stage transformer-coupled design [33]

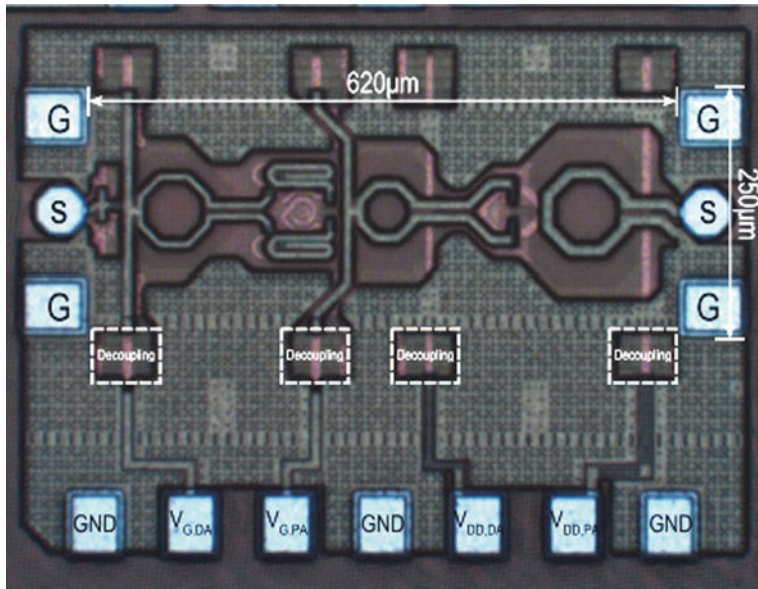


Fig. 10 Die micrograph of 28 GHz PA in 28 nm bulk CMOS [33]

5 Conclusion

This paper concluded a brief review study of mm-wave PAs for fifth-generation wireless communication. A gallium nitride device and technology has found as best

Table 1 Comparison of various PAs for 5G

References	Device technology (μm)	Frequency (GHz)	Output power (dBm)	Overall PAE (%)	Linear gain (dB)	Die area (mm^2)
[11]	0.15 μm GaAs	15	22	10	26	2.8 * 1.6
[5]	CMOS SOI	15	25.1	32.4	30	–
[6]	0.13 μm GaN HEMT	15	40	85.2	32.3	2.8 * 1.2
[7]	0.25 μm GaN	15	34	36.6	24	1.78 * 0.78
[9]	Bulk CMOS	28	4.2	9	–	–
[29]	Stacked nMOS SOI	28	20	43	14	–

– Not available

candidate for contributing high output power among all. The various recent PA architectures with basic building blocks have been reviewed where GaN HEMT-based PA is best among them all.

References

1. Hansen, P.: Developments in high power longwave radio: a brief history. In: Proceedings of the IEEE International Symposium on Antennas and Propagation (APSURSI), pp. 1013–1014, Fajardo, Puerto Rico, 26 June–1 July 2016
2. Vasjanov, A., Barzdenas, V.: A review of advanced CMOS RF power amplifier architecture trends for low power 5G wireless networks. *Electronics* **7**(11), 271 (2018)
3. Hanna, T., Deltimple, N., Frégonèse, S.: A wideband highly efficient class-J integrated power amplifier for 5G applications. In: IEEE International New Circuit and Systems Conference (NEWCAS) (2017)
4. Agiwal, M., Roy, A., Saxena, N.: Next generation 5G wireless networks: a comprehensive survey. *IEEE Commun. Surv. Tutorials* **18**(3) (2018)
5. Hu, R.Q., Qian, Y.: An energy efficient and spectrum efficient wireless heterogeneous network framework for 5G systems. *IEEE Commun. Mag.* (2014)
6. Zhang, N., Cheng, N., Gamage, A.T., Zhang, K., Mark, J.W., Shen, X.: Cloud assisted HetNets toward 5G wireless networks. *IEEE Commun. Mag.* **53**(6), 59–65 (2015)
7. Huang, C.-C., Chen, C.-K.: A CMOS medium power amplifier with built-in power detector for multistandard dedicated short-range communication applications. *IEEE Microwave Wirel. Compon. Lett.* **28**(1), 58–60 (2018)
8. Maroldt, S., Ercoli, M.: 3.5-GHz ultra-compact GaN class-E integrated Doherty MMIC PA for 5G massive-MIMO base station applications. In: Proceedings of European Microwave Integrated Circuits Conference, pp. 196–199, Oct 2017

9. Li, S.-H., Hsu, S.S.H., Zhang, J., Huang, K.-C.: A sub-6 GHz compact GaN MMIC Doherty PA with a 49.5% 6 dB back-off PAE for 5G communications. In: IEEE MTT-S International Microwave Symposium Digest, pp. 805–807, June 2018
10. Choi, P., Goswami, S., Boon, C. C., Peh, L.-S., Lee, H.-S.: A fully integrated 5.9 GHz RF frontend in 0.25 μ m GaN-on-SiC for vehicle-to-vehicle applications. In: IEEE RFIC Symposium Digest, pp. 397–400, June 2014
11. Chen, W., et al.: Design and linearization of concurrent dual-band Doherty power amplifier with frequency-dependent power ranges. *IEEE Trans. Microw. Theory Tech.* **59**(10), 2537–2546 (2011)
12. Quaglia, R., Camarchia, V., Pirola, M.: Dual-band GaN MMIC power amplifier for microwave backhaul applications. *IEEE Microwave Wirel. Compon. Lett.* **24**(6), 409–411 (2014)
13. Ishikawa, R., Takayama, Y., Honjo, K.: Concurrent dual-band access GaN HEMTMMIC amplifier suppressing inter-band interference. In: IEEE MTT-S International Microwave Symposium Digest, pp. 2045–2048, June 2017
14. Cripps, S.C.: *RF Power Amplifiers for Wireless Communications*. Artech House, Norwood, MA, USA (2006)
15. Kerhervé, E., Belot, D.: *Linearization and Efficiency Enhancement Techniques for Silicon Power Amplifiers: From RF to mmW*. Elsevier Science, New York, NY, USA (2015)
16. Colantonio, P., Giannini, F., Limiti, E.: *High Efficiency RF and Microwave Solid State Power Amplifiers*. Wiley, West Sussex, UK (2009)
17. Asbeck, P.M.: Will Doherty continue to rule for 5G? In: 2016 IEEE MTT-S International Microwave Symposium (IMS), pp. 1–4, May 2016
18. Giofre, R., Colantonio, P.: A high efficiency and low distortion 6 W GaN MMIC Doherty amplifier for 7 GHz radio links. *IEEE Microwave Wirel. Compon. Lett.* **27**(1), 70–72 (2017)
19. Colantonio, P., Giannini, F., Giofre, R., Piazzon, L.: The Doherty power amplifier. *Wiley Encyclopedia of Electrical and Electronics Engineering*, pp. 1–31 (2014)
20. Wigig and the Future of Seamless Connectivity. <http://www.wi-fi.org/file/wigig%C2%AE-and-the-future-of-seamless-connectivity-2013>
21. Lie, D.Y.C., Mayeda, J.C., Li, Y., Lopez, J.: A review of 5G power amplifier design at cm-wave and mm-wave frequencies. *Hindawi Wirel. Commun. Mobile Comput.* **2018**, Article ID 6793814, 16 (2018)
22. Nunes, L.C., Cabral, P.M., Pedro, J.C.: AM/PM distortion in GaN Doherty power amplifiers. In: Proceedings of the 2014 IEEE MTT-S International Microwave Symposium, Tampa, FL, USA, 1–6 June 2014
23. Lie, D.Y., Tsay, J., Hall, T., Nukala, T., Lopez, J.: High efficiency silicon RF power amplifier design—current status and future outlook. In: Proceedings of the 2016 IEEE International Symposium on Radio-Frequency Integration Technology (RFIT), pp. 1–4, Taipei, Taiwan, Aug 2016
24. Doherty, W.H.: A new high-efficiency power amplifier for modulated waves. *Bell Syst. Tech. J.* **15**, 469–475 (1936)
25. Nakatani, K., Komatsuzaki, Y., Shinjo, S., et al.: A highly integrated RF frontend module including Doherty PA, LNA and switch for high SHF wide-band massive MIMO in 5G. In: Proceedings of the 2017 IEEE Topical Conference on Power Amplifiers for Wireless and Radio Applications, (PAWR'17), pp. 37–39, Phoenix, AZ, USA, Jan 2017
26. Ezzeddine, K., Huang, H.C.: The high voltage/high power FET (HiVP). In: Proceedings of IEEE Radio Frequency Integrated Circuits Symposium, pp. 215–218, June 2003
27. Chakrabarti, A., Krishnaswamy, H.: High power, high efficiency stacked mmWave class-E-like power amplifiers in 45 nm SOI CMOS. In: Proceedings of IEEE Custom Integrated Circuits Conference, pp. 1–4, Sep 2012
28. Dabag, H., Hanafi, B., Golcuk, F., Agah, A., Buckwalter, J., Asbeck, P.: Analysis and design of stacked-FET mm-wave power amplifiers. *IEEE Trans. Microw. Theory Tech.* **61**(4), 1543–1556 (2013)
29. Rostomyan, N., Özén, M., Asbeck, P.: Comparison of pMOS and nMOS 28 GHz high efficiency linear power amplifiers in 45 nm CMOS SOI. In: Proceedings of IEEE Power Amplifiers Wireless Radio Applications (PAWR), pp. 26–28, Jan 2018

30. Rostomyan, N., Jayamon, J.A., Asbeck, P.: 15 GHz 25 dBm multigate-cell stacked CMOS power amplifier with 32% PAE and ≥ 30 dB gain for 5G applications. In: Proceedings of the 11th European Microwave Integrated Circuits Conference (EuMIC'16), pp. 265–268, London, UK, Oct 2016
31. Kumar, R., Kanuajia, B.K., Dwari, S., Kumar, S.: A high efficiency on-chip reconfigurable Doherty power amplifier for LTE communication cells
32. Mayeda, J.C., Lie, D.Y., Lopez, J.: A highly efficient and linear 15 GHz GaN power amplifier design for 5G communications. In: Proceedings of the 2017 Texas Symposium on Wireless and Microwave Circuits and Systems (WMCS), pp. 1–4, Waco, TX, USA, Mar 2017
33. Shakib, S., Park, H.-C., Dunworth, J., Aparin, V., Entesari, K.: A highly efficient and linear power amplifier for 28-GHz 5G phased array radios in 28-nm CMOS. *IEEE J. Solid-State Circuits* **51**(12), 3020–3036 (2016)
34. Shakib, S., Park, H., Dunworth, J., Aparin, V., Entesari, K.: 28 GHz efficient linear power amplifier for 5G phased arrays in 28 nm bulk CMOS. In: Proceedings of the 2016 IEEE International Solid-State Circuits Conference (ISSCC), pp. 44–45, San Francisco, CA, USA, Jan 2016

Vision-Based Automated Traffic Signaling



H. Mallika, Y. S. Vishruth, T. Venkat Sai Krishna, and Sujay Biradar

Abstract Traffic management has become one of the most complicated issues of recent times in metropolitan cities. Conventional traffic signaling systems are pre-programmed and alternate between red and green lights without any estimation of traffic. This signaling methodology leads to problems during peak hours at the intersections, where traffic ratio in a few lanes are dense when compared to others. Therefore, an efficient model is needed, which can manage the traffic flow at a certain point. The proposed model offers a solution using the CCTV footage from signal cameras to decongest traffic, based on a live estimate of traffic density. A state-of-the-art Deep Neural Network algorithm determines the number of vehicles and their type at a particular signal for object detection called You Only Look Once (YOLO), as it provided speed and accuracy in real-time. Based on vehicle count and road associated parameters, traffic density is computed to provide a dynamic extension of signaling time for a particular lane. Therefore, time saved from empty lanes is used to clear traffic on other busy lanes.

Keywords Density-based · Signal cameras · Adaptive · Real-time · Base Time · Extension Time · Traffic monitoring · GUI

1 Introduction

Recent researches discovered that road traffic incidents are accountable for the loss of billions of dollars in terms of extra fuel and extra travel hours. With the rapid development of the social economy, the problem of traffic congestion has become more and more dangerous. Traffic congestion occurs as the number of vehicles and vehicular usage increases, resulting in a slower speed and longer trip time. The most common form of traffic occurs when there are more vehicles than the roadway can support. The factors causing traffic in urban areas are inadequate infrastructure, vehicles parked at peak traffic locations, and also traffic accumulation at signals due

H. Mallika · Y. S. Vishruth · T. Venkat Sai Krishna (✉) · S. Biradar
Electronics and Communication Department, MSRIT, Bangalore, India
e-mail: sairkrish1477@gmail.com

to pre-historically set timers. Amongst the major causes, traffic accumulation can be solved using technology. Based on the experience of a daily commuter, it was observed that the conventional traffic signal is pre-determined and inefficient. In an intersection, irrespective of traffic density in a lane, the conventional system still provides the same allotted time.

Previously, either hardware extensive technique such as an infrared LED array network [1] or a solely software-based technique such as image processing was used to estimate traffic density. The hardware-oriented approach made use of infrared LED as an infrared emitter and a photodiode as an infrared detector. When infrared radiation of the LEDs reaches the photodiode, output voltages change according to the magnitude of the infrared light. Traffic density was computed by placing an array of infrared LEDs and photodiodes on either side of the road.

Software processing of real-time video input can be done using various techniques. One such approach is image processing [2]. Multiple methods can implement this approach, but the most accurate method is background subtraction [3]. In this method, foreground elements such as vehicles were differentiated from the background by learning empty background frames. The foreground detector detects the vehicles, and a binary computation is done to define rectangular regions [4] around every detected vehicle. Then, the final counting was done by tracking the detected objects and their regions using the Gaussian Mixture model. Images from surveillance cameras are usually complex and contain multiple objects. The inefficiency of image processing techniques in analyzing real-time input obliges the use of much sophisticated artificial intelligence-based techniques to achieve faster and better classification. The conventional traffic signaling model doesn't possess cognitive intelligence and therefore requires timely human intervention to adapt to changing traffic patterns. To overcome this inefficiency of the conventional signaling systems, the proposed model utilizes a dynamic system capable of providing reasonable signaling time based on the real-time density of traffic, estimated using computer vision. The proposed model is designed to act as a closed-loop control system with the density of vehicles at a particular instant serving as feedback. The independency in signaling time and dynamic extension of signaling time characterize the model as automatic.

2 Proposed Methodology

The proposed model takes input from cameras installed at the signals. The frame required for density estimation is sampled, and Region of Interest (RoI) selection is carried out. The YOLO [5–7] detection algorithm provides the count of each class of vehicles. Traffic intersection parameters such as lane width and preset time, i.e., the time allotted to a lane in case of a conventional system, are used to compute density. The green signal time is evaluated based on the density computed and is displayed on the traffic signal counter. The process is repeated in round-robin fashion for each lane of the intersection. Extension in green signal time is provided if density on a

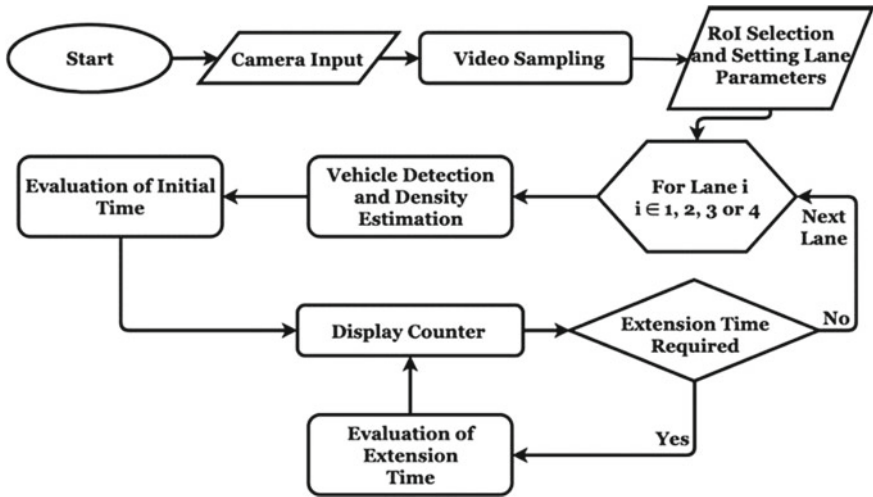


Fig. 1 Flow chart of the proposed method

particular lane is more significant when compared to all other lanes' density. The flowchart and block diagram of the proposed methodology are shown in Figs. 1 and 2, respectively.

2.1 Pre-processing

The live feed from the surveillance cameras placed at the intersections is to be processed to achieve real-time automated signaling. Since processing the whole video is resource exhaustive and not needed for this particular application, pre-processing steps are carried out before the detection and evaluation of signal time.

Video Sampling The model is designed to allocate green signal time in phases and requires only selective time-frames to be processed. This process of selecting frames and processing them improves resource utilization and the speed of response to real-time fluctuation of traffic. The frame to be processed is sampled at the required time using OpenCV.

Region of Interest (RoI) Selection The placement of cameras and road topologies may vary in each case, i.e., the video frame sampled may contain both lanes of a particular road. As the model needs only the on-coming lane traffic for analysis, the user is initially obliged to select the region encompassing the lane to be monitored. This process of selection configures the model with RoI [8] for detection, as shown in Fig. 3, and this process need not be repeated before every detection.

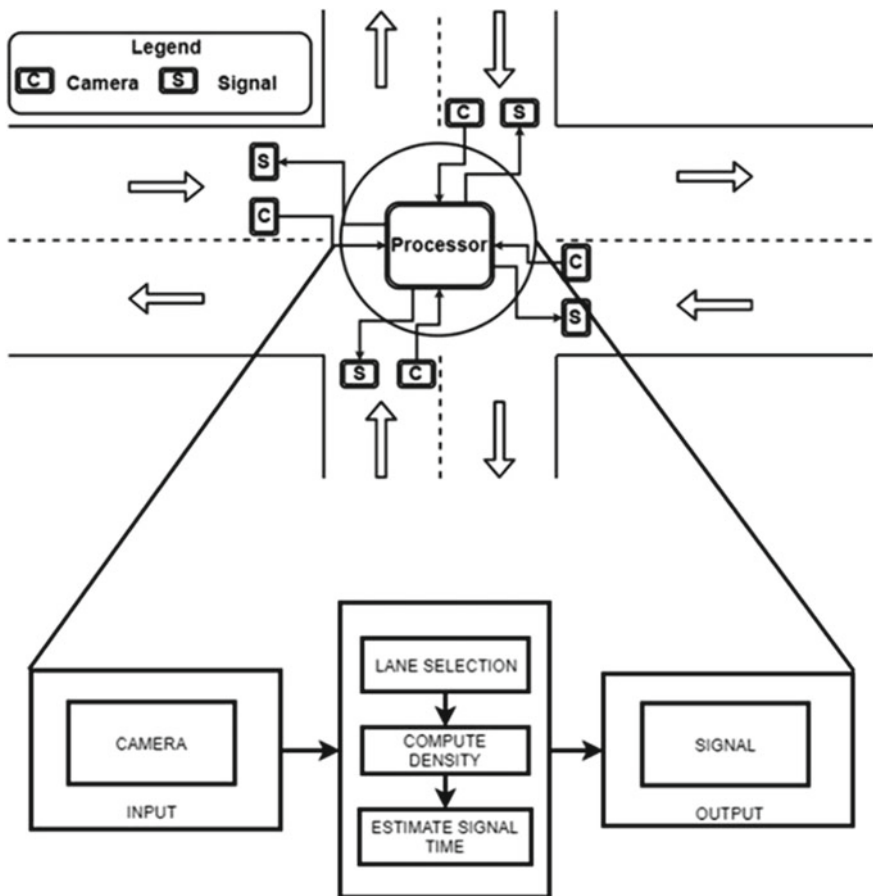


Fig. 2 Block schematic representation of the proposed method



Fig. 3 RoI selection

2.2 Traffic Management Strategy

The automated traffic signaling model is designed to act as a closed-loop control system with the density of vehicles at a particular instant serving as feedback. The green-signaling time allotted to each lane at an intersection is dependent on dynamic and fixed inputs. The dynamic input includes the number of vehicles at an instant of time obtained from the detection model. The fixed inputs initially provided by the user include the preset time and road measurements, which vary for each road at an intersection.

The number of vehicles and their respective class weights plays a crucial role in evaluating road traffic density. Preset time of a lane is the green signal time allotted to the lane by the conventional traffic control system. It serves as an upper threshold in assigning green-signaling times to individual lanes on a round-robin basis and thereby maintains a cyclic gap time. Time evaluated is inversely proportional to the width of a lane, and hence road width is an important parameter for scaling the green signal time accordingly.

Weights are representational values assigned to each class of vehicles based on its properties. Weights, as defined in Table 1, provide the algorithm the characteristic to differentiate the presence of vehicles based on their length and time required to cross an intersection.

Traffic density evaluated in each lane depends on the number of vehicles represented in their weighted form, and on the dimensions of the road.

The scalable feature of this adaptive traffic timer model is achieved by allotting the green-signaling time in phases called as Base Time and Extension Time. Base Time is the green signal time allotted to a particular lane at an intersection based only on the density of vehicles in the lane under consideration. Base Time is always the highest green signal time that could be allotted to a particular lane in that iteration. Extension Time is an additional green signal time allotted if the conditions necessary are satisfied. Extension Time is a fraction of the Base Time and does not exceed the Base Time in any given scenario. The allotment of Extension Time is based on the density of vehicles in the lane currently being considered, as well as the other lanes in that intersection that are queued. Extension numbers are the number of times an Extension Time is allotted to a lane when the required conditions are satisfied. Each subsequent Extension Time is a smaller fraction of the previously allotted time.

Table 1 Vehicle weights

Class	Weight
Bike	0.5
Auto	0.75
Car	1
Bus	4
Truck	5

Table 2 Annotation count of created dataset

Class	Count
Bike	2553
Auto	1301
Car	1882
Bus	403
Truck	646

Traffic density in a particular lane is evaluated by considering the width of the road and the weighted sum of vehicle count. Similarly, in a round-robin fashion density of the other lanes is obtained, and total density is calculated. The initial time ratio is calculated as a ratio of the density of lane under consideration to the total density. Base Time allotted is the product of the initial time ratio and the preset time. The minimum time allotted to a lane is 15 s. An Extension Time is allotted if Extension Time Ratio is above a given threshold. Detection is performed at the final 10 s of the previously allotted time (i.e., Base or Extension Time), providing effective vehicle count and traffic densities at that instant to determine whether an Extension Time needs to be allotted. A maximum of three extension times is allotted to each lane. A similar procedure is repeated for all other lanes in an intersection.

3 Training

The YOLO network is tailored for different datasets like MS COCO, Google Open images, Pascal VOC, among many others. The YOLO MS COCO dataset trained network with 80 classes used for detection contained all the required classes like cars, bus, truck, motorcycle but lacked the autorickshaw class necessary for Indian Roads. A custom trained network for this purpose had to be trained to use the model for Indian Roads.

Dataset was created by annotating the frames selected from the road traffic video captured in Bangalore. LabelIMG tool for manual labeling of different class instances present in each image was used. The annotated data set of 831 images with annotation count for different classes are as shown in Table 2.

Training was performed on Google Cloud Platform with a virtual machine having NVIDIA Tesla V100 GPU for a total of 25,000 iterations with 5000 iterations per class.

4 Traffic Monitoring GUI

The Graphical User Interface (GUI) developed called Traffic Monitoring GUI is a computer interface developed to ease the interaction between humans and the traffic signaling model. It helps in configuring the model with various lane-dependent

parameters such as road width and RoI selection. It also helps to visualize how the backend functions in implementing an automated and adaptive traffic signal. The characteristics of Traffic Monitoring GUI are as follows:

- Live playback of each lane's video is shown with red or green background signifying the respective lane's signal state allotted at that particular instant.
- Timer in the application logger reflects the green-signaling time allotted in phases to the corresponding lane Number specified.
- Overlay counters on the top right corner of each video display countdown for the last 10 s only.

5 Results and Discussion

Results of training performed for five classes on Google Cloud Platform are shown in Fig. 4. Mean average precision (mAP) and F1 score calculated for five classes at a threshold of 0.25 was found to be 70% and 71%, respectively. Following the training, a preprocessed traffic video frame shown in Fig. 5 produced a categorized vehicle count, as shown in Fig. 6. When subjected to frames from different environmental conditions such as low-resolution footage, grayscale footage, and footage with low illumination the detection algorithm produced satisfactory results (Fig. 7).

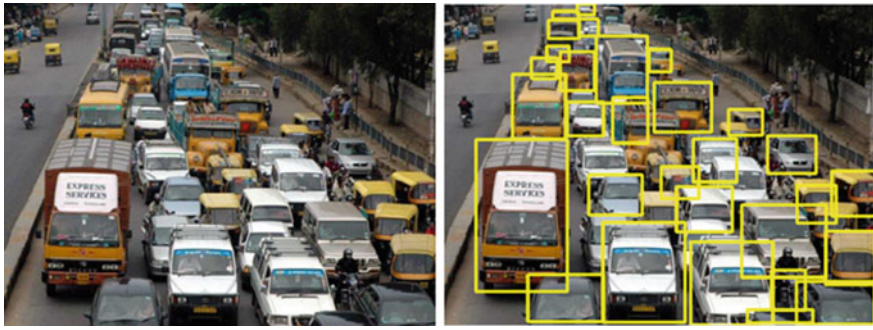
Table 3 summarizes, one cycle of green signal time allotment for the four lanes in the considered intersection. Following the round-robin method, the base green-signaling time was allotted for Lane 1 based on the evaluated traffic density. From Table 3, it is clear that Lane 2 and 3 were granted maximum green-signaling time because of heavy traffic and Lane 4 with the least traffic was allotted minimum

```
Tensor Cores are used. Last accuracy mAP@0.5 .59.61 %
17485: 1.583115, 1.493180 avg loss, 0.001000 rate, 8.270424 seconds
Resizing to initial size: 608 x 608
try to allocate aditonal workspace_size = 108.69 MB
CUDA allocate done!

calculation mAP (mean average precision)...
796
detection count = 23935, unique truth count =3003
class_id = 0, name = Car, ap = 69.95 %
class_id = 1, name = Bus, ap = 66.61 %
class_id = 2, name = Truck, ap = 82.49 %
class_id = 3, name = Motorcycle, ap = 55.79 %
class_id = 4, name = Autorickshaw, ap = 70.69 %
for thresh = 0.25, precision = 0.70, recall = 0.51, F1-score = 0.71
for thresh = 0.25, TP = 1528, FP = 657, FN = 1475, average IoU = 74.95 %

IoU threshold = 50 %
mean average precision (mAP@0.5) = 0.687063, or 68.70 %
```

Fig. 4 Accuracy during training



(a) Original Image

(b) Detection Results

Fig. 5 Detection in dense traffic

```
Please click
clicked [(224.202595467126, 356.273956297056), (769.0764995064551, 211.171
968893), (108.713017980529, 679.052519016006)]
Building User Interface
starting Application
Lane 1
car : 22
bike : 2
bus : 4
truck : 3
auto : 5
Estimated Time = 48 seconds
```

Fig. 6 Vehicle count output from DNN

green-signaling time. The overview of the GUI and the application logger to monitor extension times is shown in Figs. 8 and 9, respectively.

6 Conclusion

The model developed is in true essence automatic, once the lane-dependent constraints are set during the initialization of the system. Since already placed surveillance camera footage is sampled and preprocessed before being fed for detection, it makes the model computationally efficient. The customized trained model provides a more sophisticated DNN with a lesser number of classes, thereby providing faster and satisfactory detection results. The automatic and real-time allotment of Base and Extension Time for each lane based on the instantaneous density of vehicles was tested to be ample and precise. Extension Time allotted in phases reduced the waiting time of motorists and also leads to a decrease in travel time. The development of GUI helps to visualize and monitor this automated and adaptive traffic signaling model.

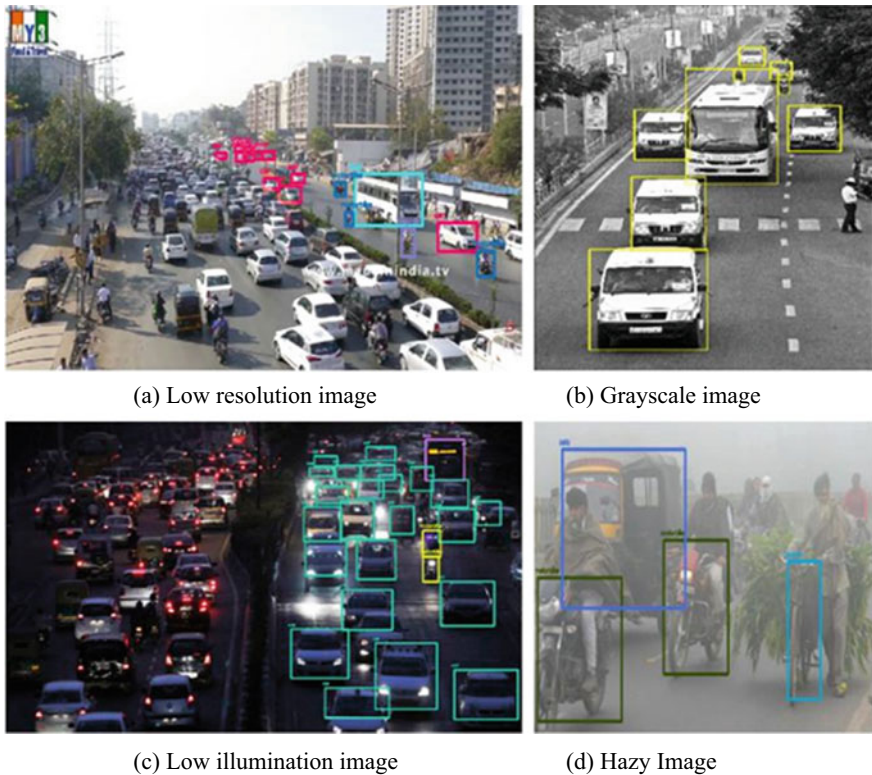


Fig. 7 Detection results in different environments (a) Low resolution image (b) Grayscale image (c) Low illumination image (d) Hazy Image.

Table 3 Evaluated Extension Time with proposed model

Lane	Evaluated Base Time (s)	Evaluated ext time (s)	Total time (s)
1	48	0	48
2	35	21	56
3	40	20	60
4	20	0	20

6.1 Future Scope

- Provide a faster and smooth flow for the passage of Ambulance to its destination by creating a signal-free path.
- Prioritizing lanes with extensive traffic flow at peak hours by deploying an additional Artificial Neural Network.



Fig. 8 GUI for surveillance

```
>>
Lane : 1
Initial Time Calculated : 15
Extenstion Number : 0
Extension Time : 0

>>
Lane : 1
Initial Time Calculated : 15
Extenstion Number : 1
Extension Time : 10

>>
Lane : 1
Initial Time Calculated : 15
Extenstion Number : 2
Extension Time : 0
```

Fig. 9 Application logger to monitor extension times

References

1. Ghazal, B., ElKhatib, K., Chahine, K., Kherfan, M.: Smart traffic light control system. In: 2016 Third International Conference on Electrical, Electronics, Computer Engineering and Their Applications (EECEA), pp. 140–145. IEEE (2016)
2. Choudhari, S.D., Gaikwad, V.T.: Review on traffic density estimation using computer vision, (2018)
3. Chowdhury, M.F., Biplob, M.R.A., Uddin, J.: Real time traffic density measurement using computer vision and dynamic traffic control. In: 2018 Joint 7th International Conference on Informatics, Electronics & Vision (ICIEV) and 2018 2nd International Conference on Imaging, Vision & Pattern Recognition (icIVPR), pp. 353–356. IEEE (2018)
4. Zhu, H., Xu, C., Li, F.: The traffic volume count algorithm based on computer vision. In: 2013 5th International Conference on Intelligent Human-Machine Systems and Cybernetics, vol. 1, pp. 130–133. IEEE (2013)
5. Redmon, J., Divvala, S., Girshick, R., Farhadi, A.: You only look once: unified, real-time object detection. In: Proceedings of the IEEE Conference on Computer Vision and Pattern Recognition, pp. 779–788 (2016)
6. Redmon, J., Farhadi, A.: YOLO9000: better, faster, stronger. In: Proceedings of the IEEE Conference on Computer Vision and Pattern Recognition, pp. 7263–7271 (2017)
7. Redmon, J., Farhadi, A.: Yolov3: an incremental improvement. arXiv preprint [arXiv:1804.02767](https://arxiv.org/abs/1804.02767) (2018)
8. Seenouvong, N., Watchareeruetai, U., Nuthong, C., Khongsomboon, K., Ohnishi, N.: A computer vision-based vehicle detection and counting system. In: 2016 8th International Conference on Knowledge and Smart Technology (KST), pp. 224–227. IEEE (2016)

Performance Comparison of SVM and ANN for Reversible ECG Data Hiding



Siddharth Bhalerao, Irshad Ahmad Ansari, and Anil Kumar

Abstract In the telemedicine industry, data security is a prime aspect because medical data is frequently transferred and stored over networks. In such scenario watermarking emerges as an important technique that ensures data security and integrity. In this work, use of SVM and ANN is investigated for a high capacity ECG data hiding technique. Watermarking is done using prediction error expansion (PEE). SVM and ANN are used to predict the ECG values. Two separate regression SVM models with linear kernel and Gaussian kernel are trained. ANN model used is a feed-forward deep neural network with three hidden layers. The proposed method provides a completely reversible watermarking. The patient's confidential data is used as a watermark. For testing and training of algorithms, signals from MIT-BIH arrhythmia database are used. Performance of both SVM and ANN-based prediction models are evaluated using normalized cross-correlation, signal-to-noise ratio, and percentage residual difference. Linear SVM and deep ANN are comparable in performance and are better than Gaussian SVM.

Keywords Reversible medical data hiding · Deep neural network · Regression SVM

1 Introduction

Engineering and technology is collaborating with medical science to provide better medical facilities and this could be seen in flourishing of telemedicine industry. Technology plays a major role in every aspect of telemedicine. Involvement of technology

S. Bhalerao · I. A. Ansari (✉) · A. Kumar

Electronics and Communication Engineering, PDPM Indian Institute of Information Technology Design and Manufacturing, Jabalpur 482005, India

e-mail: irshad@iitdmj.ac.in

S. Bhalerao

e-mail: siddharthbhalerao@gmail.com

A. Kumar

e-mail: anilkdee@gmail.com

© Springer Nature Singapore Pte Ltd. 2020

M. Pant et al. (eds.), *Soft Computing: Theories and Applications*,

Advances in Intelligent Systems and Computing 1154,

https://doi.org/10.1007/978-981-15-4032-5_20

can be seen starting from a very basic task of making appointments, to complex tasks such as diagnosis and patient data management. With this enhanced participation of technology in the medical domain, there is increased concern of medical data security [1]. This medical data consists of patient's medical records, physiological signals like ECG, EEG, and medical images (X-ray, CT, MRI scans), etc. As medical data is frequently transmitted over networks, stored in hard disks and clouds, there is a chance of medical data contamination with noise. Apart from noise, there could be multiple reasons for knowingly or unknowingly data tampering [2].

In addition to the telemedicine industry, innovation in wearable medical devices has resulted in many fold increase in medical data generation. In this scenario, it is of acute importance to maintain data integrity, because the presence of faulty or tampered medical signals may lead to the wrong diagnosis. One of the most used methods for ensuring data integrity is the watermarking of medical data. Watermarking is the embedding of a signal called as watermark in the host signal. If watermark is clearly discernible then such technique is called visible watermarking. In invisible watermarking techniques, the watermark remains unnoticeable.

Apart from invisibility constraints, an important feature is reversibility. In reversible watermarking schemes, host signal gets perfectly reconstructed from the watermarked signal. When watermarking is irreversible, some artifacts may get added permanently to host signal. For medical signals, even if such artifacts are minute, they could result in wrong diagnosis [2]. This makes reversible watermarking schemes a forerunner in watermarking of medical signals. This paper investigates the use of SVM and ANN for reversible data hiding in ECG signals. Here, the patient's confidential data is used as a watermark. This solves two purposes, first is hiding confidential patient data, and secondly, it establishes the integrity of medical data by acting as the watermark.

Watermarking techniques can be also be classified as a transform domain and spatial domain techniques. Engin et al. [3] developed a non-blind, transform domain technique based on discrete wavelet transform (DWT). Their method was able to identify tampering in ECG signal; this was made possible by adding Gaussian noise to ECG signal. The Gaussian noise was generated using a fixed seed; it was regenerated during extraction using the same seed, and compared with embedded noise. Another wavelet transform based technique was proposed by Ibaida and Khalil in [4]. In this method patient's confidential data was embedded in wavelet decomposition of ECG signal. To enhance data security, the patient's data was encrypted using XOR ciphering and scrambling operation. There was a common key for ciphering and scrambling, which was shared by the sender and receiver. In [5], a low complexity and high capacity technique for wearable sensor devices was introduced. It was a spatial domain, LSB watermarking technique. Prior to watermarking, the signal was pre-processed through a simple linear transform. Chen et al. [6] investigated ECG watermarking using multiple transforms. It was a quantization based watermarking scheme and was tested for DWT, DCT, and DFT separately.

All the techniques discussed till now are nonreversible watermarking techniques. Reversibility is a desirable property for medical signal watermarking. Some of the

schemes used for reversible watermark embedding include data compression, histogram shifting and difference expansion [7]. In compression based techniques, a fixed part of original signal is compressed and embedded in the signal itself. Histogram shifting was basically developed for images; in this technique, grayscale values of pixels are modified to embed watermark in selected histogram bin. It produced good results but was a limited capacity method. In [8], the difference expansion scheme is proposed by Tian. In difference expansion scheme, 1 bit was embedded into a pair of pixels. First image is grouped in pixel pairs and the average value and difference are calculated for each pair. Watermark bit is then embedded into this difference by left shifting its binary representation. An improved form of difference expansion was proposed as prediction error expansion [9]. In PEE, the signal value was predicted by any prediction model and watermark bits are embedded in the difference between original and estimated value.

A transform domain-based reversible ECG watermarking technique is proposed in [10], by Zheng and Qian. Their technique was based on lifting wavelet transform. In this method, QRS segment of ECG signal was identified and the watermark was embedded in non-QRS part only. Arnold's transformation was applied to watermark prior to embedding. As QRS segment was not used for embedding, it was a low capacity method and its performance heavily depends on the correct segmentation of QRS complex. Another lifting based Haar wavelet transform method was proposed in [11], by Wu et al. It was based on PEE and histogram shifting method.

In [7], Dey et al. proposed a tamper detection technique based on Alattar's reversible watermarking scheme. Modified Pan-Tompkins algorithm was used to segment P, QRS, and T waves from ECG signal. The segmented portion is then used to generate a feature matrix, which is combined with a random token matrix. After thresholding of the generated matrix, a binary code called bio-hash code is generated. This bio-hash code is embedded in the ECG signal. It was a low capacity method with high complexity. Wang et al. proposed a high capacity reversible ECG data hiding method in [12]. This method makes use of PEE and histogram shifting for embedding patient's confidential data in ECG signal. This was a progressive recovery method due to which extraction took place in reverse order as compared to embedding. Local linear predictor is used for predicting ECG sample values for PEE.

Shiu et al. have proposed a reversible and robust watermarking scheme in [13]. This was a shared key method based on the hamming code. The knowledge of syndrome, parity check matrix was common for sender and receiver. This scheme was tested for ECG as well as EMG (electromyogram) signals. In [14], a transform domain method was proposed by Yang et al. This method performed FDCT (fast discrete cosine transform) on ECG signal, and watermark bits were embedded in LSB position of DCT coefficients.

In present work, the performance of SVM and ANN is evaluated and compared for ECG data hiding. In Sect. 2, watermark embedding scheme and preliminaries are discussed followed by estimation schemes in Sect. 3. Results and discussions are present in Sect. 4.

2 Watermark Embedding

In this section, watermark embedding and extraction are discussed. Watermark embedding is based on prediction error expansion (PEE) which is described first, and then a description of embedding schemes is provided.

2.1 Prediction Error Expansion

Prediction error expansion was proposed by Thodi and Rodríguez [9]. It was an improved form of difference expansion (DE) method which was proposed by Tian [8]. PEE resulted in superior performance with doubling the embedding capacity as compared to DE. PEE was primarily proposed for images; although, using PEE embedding on any signal can be performed. In [12], PEE is used for hiding patient's confidential data in ECG signals.

In this section, the prediction error expansion (PEE) process is explained for ECG signals. As the name suggests, PEE has two important parts which are signal prediction or estimation, and error expansion or error modification. An estimation mechanism is required to predict the value of signal samples. The estimation schemes utilize neighboring samples for prediction of any particular sample. After sample prediction, the watermark bit is embedded in error between the actual value and predicted value. In case, if x is the actual sample value and \hat{x} is the estimated value of that sample, then the error is calculated using the following equation:

$$e = x - \hat{x} \quad (1)$$

The binary representation of error computed in Eq. (1) is left-shifted once and watermark bit is embedded into LSB of shifted error. This operation is equal to doubling the error and adding watermark bit to it. The modified error is denoted by 'me' and b is the watermark bit. The modified error is obtained by Eq. (2).

$$me = 2e + b \quad (2)$$

As the error is doubled this technique is termed as error expansion method. Watermarked sample value x' is obtained by adding modified error to predicted value (Eq. 3).

$$x' = \hat{x} + me \quad (3)$$

During extraction, the watermarked bit is extracted from modified samples, provided that predicted value is \hat{x} , which is the same as generated during embedding. This is possible when similar process, as followed during embedding is used with same neighboring data. During extraction, the error is calculated again, and the original

value of the sample can be recovered using Eq. (4).

$$x_r = \frac{x' + \hat{x} - b}{2} \quad (4)$$

Watermark bit (b) is obtained from LSB of calculated error during extraction.

2.2 *Embedding and Extraction*

The watermark embedding procedure mentioned in [15] is followed for ECG watermarking. The method proposed in [15] was a high capacity watermarking technique and capacity equal to 0.99 bits per sample (bps) was obtained. To achieve reversibility, data embedding is performed in three phases. In the first phase, one-third of samples are modified with watermark bits and a capacity of 0.33 bps is guaranteed. In the next phase, one-third of samples are modified again from the remaining samples. Thus, the capacity of 0.66 bps is obtained. Following the final phase, the capacity of 0.99 bps is achieved.

Extraction is performed in reverse order, therefore, the watermark embedded in the third phase is retrieved first, and then the second phase, and first phase watermarks are extracted. This is done in order to generate same predicted value as obtained during embedding.

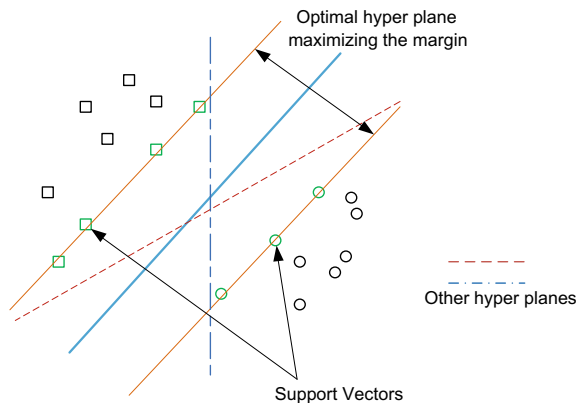
3 Estimation Mechanisms

3.1 SVM

A support vector machine (SVM) is a supervised learning algorithm developed by Vapnik [16]. SVM is primarily used for classification problems. When used in classification, the main goal of SV algorithm is to find the optimal hyperplane, which maximizes the margin between two classes. Figure 1 illustrates the concept of SVM, circles, and squares represent two classes of data. There are three boundaries or hyperplanes which are clearly separating the two classes. It can be deduced intuitively that middle hyperplane is the best solution. SV algorithm tries to find the boundary or hyperplane that maximizes the minimum distance between two classes. In Fig. 1, data is clearly separable and a decision boundary could be reached. When data is non-separable, feasible solution is not possible. In this case, a parameter called as slack is introduced that relaxes the boundaries within permissible error. Such SVM is called as soft margin SVM.

When the input dataset is nonlinearly separable, there is no feasible solution possible. In such case, a function is used which maps input data from input space to

Fig. 1 Hyperplane representation of SVM



a higher dimensional feature space. In feature space, it becomes possible to obtain an optimal hyperplane. This mapping function is called kernel and this approach is called as kernel trick. Examples of some of the kernel functions are the polynomial kernel, Gaussian or radial basis function (RBF), hyperbolic tangent kernel, etc.

The concept of SVM can be extended for data estimation as well. In this case, SVM is called regression SVM, or support vector regression (SVR) [17]. Regression SVM's are used for a wide variety of tasks such as time series prediction, financial forecasting, etc. Data estimation may seem a very complex task, as it can be understood from SVM concept that there are infinite possibilities for value to be estimated. This is achieved by introducing a loss function that keeps error within some permissible value from the actual target. The loss function is insensitive loss function suggested by Vapnik.

3.2 ANN

Artificial neural networks (ANN) are learning algorithms inspired by the human brain. It mimics the biological learning system of humans. A human brain has a dense network of cells called as neurons, the basic unit of an ANN is also called as neuron. ANN is used for wide variety of classification, identification and prediction tasks. ANN is a feed-forward layered network. Figure 2 illustrates a simple neural network with three layers. Apart from the input layer and output layer, the middle layers are called as hidden layers. There could be multiple hidden layers in a network.

A layer consists of multiple neurons. All the inputs to a neuron are added and passed through a function which acts as output for that neuron. This function is called as activation function. The main reason for having activation function is to limit the output within fixed range and introduce nonlinearity. Each neuron may have multiple inputs with weight assigned to each of them. A parameter called bias

Fig. 2 A sample neural network

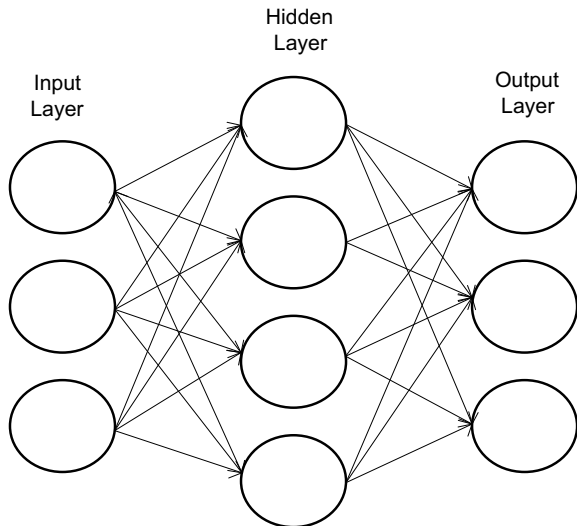
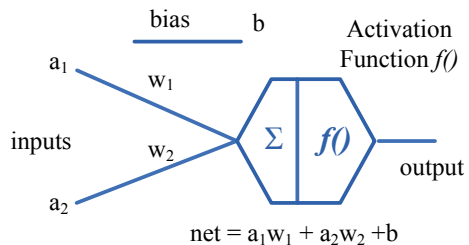


Fig. 3 Structure of a neuron



is also associated with every neuron. A bias is required to add flexibility in data fitting. Figure 3 shows a neuron with two inputs and a bias.

During training, ANN tries to learn the relation between input and output, thereby updating the weights and biases of whole network. When input and target are provided to network before training, it is called as supervised learning. An error function is used at the output that acts as an indicator of performance. Based on this error the output biases and weights are updated through the backpropagation mechanism.

In backpropagation, error from the output layer flows towards input layer, this is called a backward pass. One forward pass and backward pass for complete data constitute an epoch. Training ends when minimum error is achieved or maximum epochs are reached. Optimization algorithms are utilized to achieve error minimization. Few examples of optimization algorithms are gradient descent, stochastic gradient descent (SGD), Adam, etc. A feed-forward network with multiple hidden layers is called as deep neural network. It provides accurate results by learning data features.

4 Results and Discussion

Information on ECG database and metrics used for performance evaluation are discussed in this section along with results for regression SVM and ANN. To test the performance of SVM and ANN-based watermarking algorithm, 46 signals are used from MIT-BIH arrhythmia database [18]. It is a well-known database and is used in multiple ECG watermarking and data hiding algorithms. It contains 48 signals of 30 min duration each, sampled at 360 Hz. Each of these 48 signals consists of ECG signals from two different channels.

Three separate metrics are utilized for performance evaluation of SVM and ANN-based watermarking algorithms. These metrics are PRD (percentage residual difference), SNR (signal-to-noise ratio), and NCC (normalized cross-correlation). These metrics are defined in Eqs. (5), (6), and (7).

$$\text{PRD}(X, Y) = \sqrt{\frac{\sum_{i=1}^N (x_i - y_i)^2}{\sum_{i=1}^N x_i^2}} \times 100\% \quad (5)$$

$$\text{NCC}(X, Y) = \frac{\sum x_i \text{ xor } y_i}{N * N} \quad (6)$$

$$\text{SNR}(X, Y) = 10 \log_{10} \sqrt{\frac{\sum_{i=1}^N x_i^2}{\sum_{i=1}^N (x_i - y_i)^2}} \quad (7)$$

In the above expressions N is the ECG signal length, X and Y are input and output signals respectively and x_i , y_i are corresponding samples of input and output signals, respectively.

4.1 Experiments and Results

Both SVM and ANN were trained and tested on the same set of signals. For both training and testing purposes, 10 s duration of ECG signal was extracted from signals of MIT-BIH arrhythmia database. Training and testing were done on different signals. Dataset for training was prepared in the same manner as proposed in [15]. Two regression SVM models were trained one is linear SVM and the second was SVM with Gaussian kernel. The deep neural network architecture as proposed in [15] was used for ANN. It has three hidden layers with 20:30:20 configuration. SGD was used as an optimization algorithm with sigmoid as activation function and MSE (mean square error) was used as error metrics.

The performance of data hiding algorithm is evaluated for different bps values, ranging from 0.08 to 0.99 bps. The output of different prediction schemes are plotted in Figs. 4, 5, and 6. The output of ANN is shown in green color and linear and

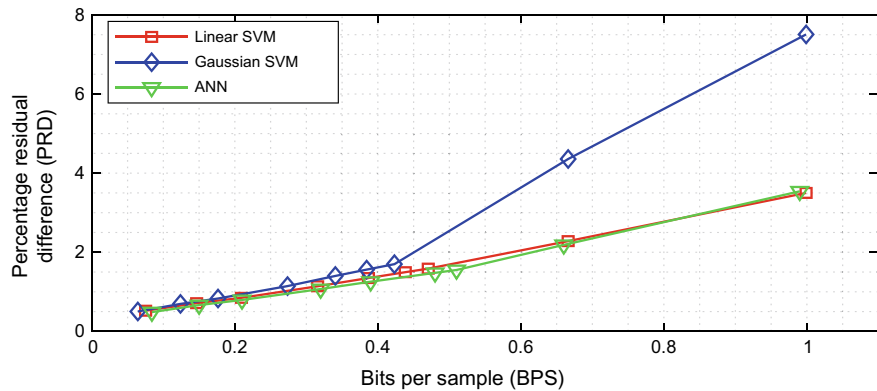


Fig. 4 PRD comparison for linear SVM, Gaussian SVM, and ANN

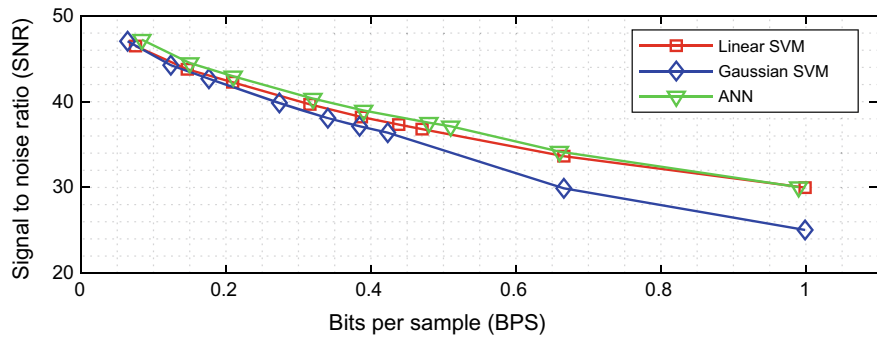


Fig. 5 SNR comparison for linear SVM, Gaussian SVM, and ANN

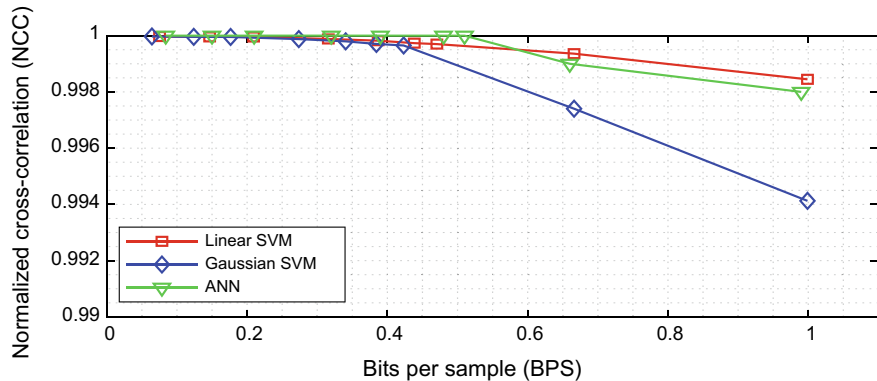


Fig. 6 NCC comparison for linear SVM, Gaussian SVM, and ANN

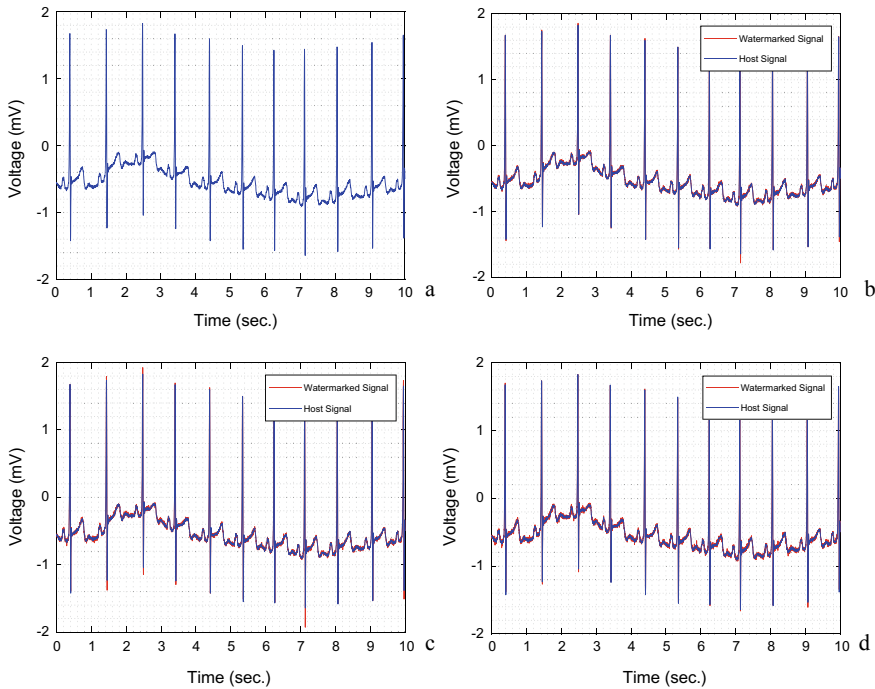


Fig. 7 **a** Host signal, **b** ECG watermarking using linear SVM, **c** ECG watermarking using Gaussian SVM, **d** ECG watermarking using ANN

Gaussian SVMs are shown with red and blue colors, respectively. Figure 4 shows the variation of PRD with respect to bps for both SVM models and ANN. Similarly, Figs. 5 and 6 display variation in SNR and NCC for all the models. It is evident from plots, that the performance of ANN is better than the other two schemes, for almost all bps, except at 0.99 bps where linear SVM catches up to it. Figure 7 shows original and watermarked signals. Figure 7a shows original ECG signal, Fig. 7b-d shows watermarked signal for 0.66 bps. To illustrate the difference clearly between host (blue) and watermarked (red) signal they are plotted overlapping each other in different colors.

5 Conclusion

In this work, a high capacity reversible ECG data hiding method based on PEE was implemented. Performance of linear SVM, Gaussian SVM and ANN-based predictors were compared. ANN-based predictor gave best performance with linear SVM just behind it. Linear SVM turned out to be comparable with ANN for higher bps values.

References

1. Shimizu, K.: Telemedicine by mobile communication. *IEEE Eng. Med. Biol. Mag.* **18**(4), 32–44 (1999)
2. Caldelli, R., Filippini, F., Becarelli, R.: Reversible watermarking techniques: an overview and a classification. *EURASIP J. Inf. Secur.* (2010)
3. Engin, M., Çıdam, O., Engin, E.Z.: Wavelet transformation based watermarking technique for human electrocardiogram (ECG). *J. Med. Syst.* **29**(6), 589–594 (2005)
4. Ibaida, A., Khalil, I.: Wavelet-based ECG steganography for protecting patient confidential information in point-of-care systems. *IEEE Trans. Biomed. Eng.* **60**(12), 3322–3330 (2013)
5. Ibaida, A., Khalil, I., Van Schyndel, R.: A low complexity high capacity ECG signal watermark for wearable sensor-net health monitoring system. In: *Computing in Cardiology*, pp. 393–396. IEEE (2011)
6. Chen, S.T., Guo, Y.J., Huang, H.N., Kung, W.M., Tseng, K.K., Tu, S.Y.: Hiding patients confidential data in the ECG signal via transform-domain quantization scheme. *J. Med. Syst.* **38**(6), 54 (2014)
7. Dey, N., Dey, M., Mahata, S.K., Das, A., Chaudhuri, S.S.: Tamper detection of electrocardiographic signal using watermarked bio-hash code in wireless cardiology. *Int. J. Signal Imaging Syst. Eng.* **8**(1–2), 46–58 (2015)
8. Tian, J.: Reversible data embedding using a difference expansion. *IEEE Trans. Circuits Syst. Video Technol.* **13**(8), 890–896 (2003)
9. Thodi, D.M., Rodríguez, J.J.: Expansion embedding techniques for reversible watermarking. *IEEE Trans. Image Process.* **16**(3), 721–730 (2007)
10. Zheng, K.M., Qian, X.: Reversible data hiding for electrocardiogram signal based on wavelet transforms. In: *International Conference on Computational Intelligence and Security*, CIS'08, vol. 1, pp. 295–299. IEEE (2008)
11. Wu, W., Liu, B., Zhang, W., Chen, C.: Reversible data hiding in ECG signals based on histogram shifting and thresholding. In: *2nd International Symposium on Future Information and Communication Technologies for Ubiquitous HealthCare (Ubi-HealthTech)*, pp. 1–5. IEEE (2015)
12. Wang, H., Zhang, W., Yu, N.: Protecting patient confidential information based on ECG reversible data hiding. *Multimedia Tools Appl.* **75**(21), 13733–13747 (2016)
13. Shiu, H.J., Lin, B.S., Huang, C.H., Chiang, P.Y., Lei, C.L.: Preserving privacy of online digital physiological signals using blind and reversible steganography. *Comput. Methods Programs Biomed.* **151**, 159–170 (2017)
14. Yang, C.Y., Cheng, L.T., Wang, W.F.: Effective reversible data hiding in electrocardiogram based on fast discrete cosine transform. In: *Proceedings of the Future Technologies Conference*, pp. 640–648. Springer, Berlin (2018)
15. Bhalerao, S., Ansari, I.A., Kumar, A., Jain, D.K.: A reversible and multipurpose ECG data hiding technique for telemedicine applications. *Pattern Recogn. Lett.* **125** (2019)
16. Vapnik, V.: *Statistical Learning Theory*. Wiley, New York (1998)
17. Smola, A.J., Schoelkopf, B.: *A Tutorial on Support Vector Regression*, vol. 14 (2004)
18. Moody, G.B., Mark, R.G.: The impact of the MIT-BIH arrhythmia data-base. *IEEE Eng. Med. Biol. Mag.* **20**(3), 45–50 (2001)

Application of Multi-criteria Decision-Making Method for the Evaluation of Tamilnadu Private Bus Companies



S. M. Vadivel , A. H. Sequeira , Sunil Kumar Jauhar , R. Baskaran , and S. Robert Rajkumar

Abstract The rapid growth of Tamilnadu sub-urban population has put enormous efforts on all modes of transportation systems, particularly the bus transportation. The increasing population far exceeds the limited supply of transport infrastructure and services. Mostly, traveling on a public bus and train services are overcrowded, undependable, slow, inconvenient, uncoordinated, and dangerous. Tamilnadu sub-urban desperately needs to improve and expand private transportation services to improve passengers' satisfaction. In this paper, we have presented a multi-criteria decision-making approach for selecting the best private bus operators in Tamilnadu, the southern part of India. The evaluation has been made based on six criteria, twenty-eight sub-criteria, and eight private bus operators as alternatives.

Keywords Analytical hierarchy process (AHP) · Multi-criteria decision-making (MCDM) · Passenger's evaluation · Sub-urban private transportation

S. M. Vadivel · A. H. Sequeira

School of Management, National Institute of Technology Karnataka, Surathkal 575025, India
e-mail: sm16f09.vadivel@nitk.edu.in

A. H. Sequeira

e-mail: ahs@nitk.edu.in

S. K. Jauhar

Indian Institute of Management Jammu, Canal Road, Jammu 180016, India
e-mail: skjauhar@iimj.ac.in

R. Baskaran

Department of Industrial Engineering, College of Engineering, Anna University, Chennai, India
e-mail: baskishree@annauniv.edu

S. Robert Rajkumar

Loyola-ICAM College of Engineering and Technology, Chennai, India
e-mail: robertrajkumar@licet.ac.in

1 Introduction

Multi-criteria decision-making (MCDM) methods classified into two, namely, multiple attribute decision-making (MADM) for a choice problem and multiple objective decision-making (MODM) for a design problem. MADM could be a tool accustomed to solve issues for choice from a limited range of alternatives. Solving a MADM downside involves sorting and ranking [1]. MODM could be a powerful tool to help within the process of finding out selections that best satisfy a multitude of conflicting objectives [2]. The decision table or decision matrix in MADM ways encompasses four entities like alternatives, attributes, weight or relative importance to every attribute, and measures of performance of alternatives with relevance the attributes. Here, the MADM approach has been applied to identify the best private bus companies from the passengers' questionnaire study. One of the MADM tools called Analytical hierarchy process (AHP) discussed step by step approach for finding the best alternative private bus companies in Tamilnadu, the southern part of India. We have considered Chennai is the origin point (Starting point), and other Tamilnadu states or southern Indian states considered as ending spots (Destination). An analytical hierarchy process is one of the powerful multi-criteria decision-making tools for different criteria and degree, which characterize a decision. It was initially developed by Saaty [3]. It can enable decision-makers to represent the interaction of multiple intangible factors, complex and unstructured situations.

This paper organized is as follows: Sect. 2 is the literature review for this research and finding the research gap. Section 3 is the proposed methodology of MCDM. Section 4 is a detailed description of the hierarchy formation structure, and Sect. 5 has the results, conclusions, and future scope of this research work.

2 Literature Support

Specific criteria need to consider judging the best alternative of private bus transportation. For that, a brainstorming session has been conducted and various information was collected about deciding the best travel criteria by carefully studying the literature review. Following that, sub-criteria was also analyzed. The fundamental problem of decision-making is to choose the best option from a set of competing alternatives evaluated under conflicting criteria. The AHP is one of the multi-criteria decision-making tools developed by Saaty in the 1970s [3]. AHP solves a specific class of problems that involve prioritization of potential alternative solutions that considers both qualitative and quantitative criteria. AHP technique consists of a systematic approach based on breaking the decision problem into a hierarchy of interrelated elements. Such a structure clarifies the issue and presents the contribution of each of the items to the final decision. Two features of the AHP differentiate from other decision-making approaches. The first feature provides a general structure that combines intuitive rational and irrational values during the DM process through pair-wise

comparison. The second feature can judge the consistency in the decision-making process. The advantage of the AHP is its flexibility, ease of use, and the ability to provide a measure of the consistency of the decision maker's judgment [4]. Also, this method allows the incorporation of tangible and intangible factors that would otherwise be difficult to take into account. For example, some literature papers [5–7] presented a useful multi-criteria analysis (MA) approach to evaluate the urban public transportation systems. Also, Yeh et al. [5] considered an empirical case study on ten bus companies of an urban public transport system in Taiwan, which is conducted to illustrate the effectiveness of the approach. The AHP used in almost all applications related to decision-making. Vaidya and Kumar [8] critically analyzed a subset of the papers with implementations of the AHP published in international journals of high repute and gave a summary of many of the referred publications. Subramanian and Ramanathan [9] reviewed the literature on the applications of the AHP in operations management and suggested possible gaps from both researchers and practitioners. They found that AHP predominantly used in the engineering, personal, and social sectors. Vadivel et al. (2018) applied various MCDM techniques such as AHP, TOPSIS, Fuzzy TOPSIS, and GRA in India Post Service Industry for the evaluation of operational performance layout [10–12]. There have been a limited number of papers applying AHP in the private bus transport system in the southern part of India. Hence, we have decided to incorporate the AHP methodology for this evaluation.

2.1 MCDM Techniques

The classification of multi-criteria decision-making methods is shown in Fig. 1. For further reference, refer to [13].

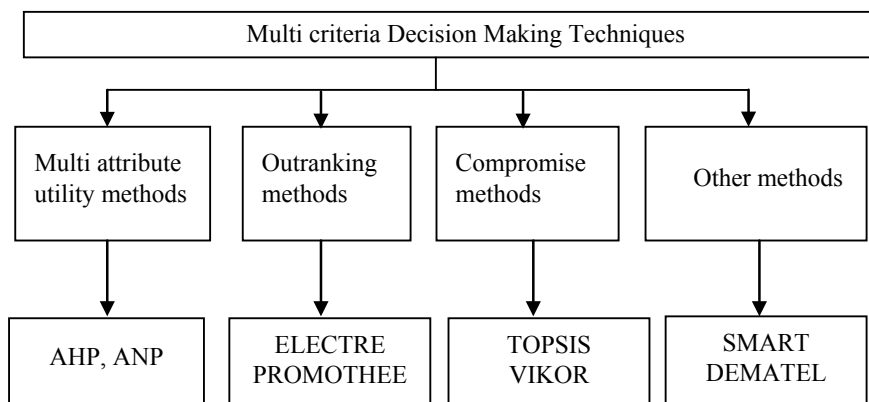


Fig. 1 MCDM classification

3 Research Methods

The analytical hierarchy process is used to derive priorities in multi-criteria decision-making. It is based on the following three principles:

- Decomposition
- Measurement of preferences
- Synthesis.

For further reference, refer to Saaty [3] (Fig. 2).

4 Case Study—Southern India, Tamilnadu, Chennai Passengers

This study aims to bring about the evaluation of private bus transportation. The assessment must be economical to the passengers, and also give customer service. An initial set of alternatives have been discussed, such as A1, A2, A3, A4, A5, A6, A7, and A8 private bus travel companies. Here, there are six criteria defined—Safety, Comfortness, Operation, Service, Social Benefits, and Finance. The criteria are decomposed into sub-criteria so that a detailed analysis is possible. There are six criteria and sub-criteria that consist of—Accidents, Average vehicle age, Medical assistance, Onboard information, Drivers driving skill, Driver appearance, Seat comfort, Driver friendliness, Vehicle cleanliness, Vehicle appearance, Employee utilization, Vehicle utilization, Average km/bus/day, Maximum coverage distance, On-schedule, Service type, Customer service, Other facility services (Physically challenged, children, senior citizens), Entertainment, Service offers, Vehicle air pollution level, Vehicle noise level, Adopt with government policy, Income/statistical period, Average fare/km, Fuel cost/km, and operating expenses.

4.1 Hierarchy Formation

The goal is decomposed into six objectives (criteria)—Safety, Comfort, Operation, Service, Social Benefits, and Finance. The goal should be achieved by considering financial constraints, social benefits to satisfy the passengers. Each criterion is fragmented into sub-criteria. The criteria safety is broken down into three sub-criteria, such as accidents, average vehicle age, and medical assistance. Likewise, the comfortness criteria is fragmented into seven sub-criteria—Onboard information, drivers driving skill, driver appearance, seat comfort, driver friendliness, vehicle cleanliness, and vehicle appearance. The operation criteria is fragmented into four sub-criteria—Employee utilization, vehicle utilization, average km/bus/day, and maximum coverage distance. The service criteria fragmented into seven sub-criteria—On-schedule,

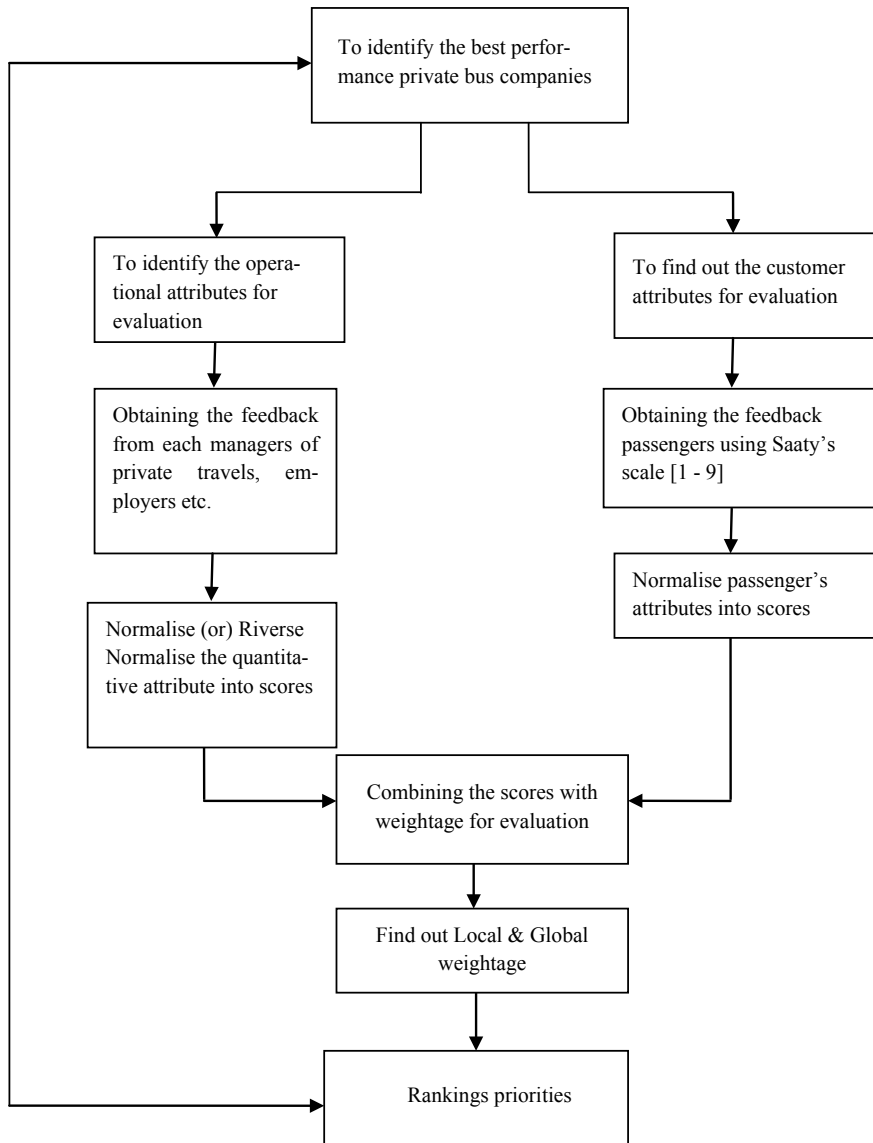


Fig. 2 Methodology for MCDM methods to evaluate private bus companies

service type, customer service, other facilities, services (physically challenged, children, old people), entertainment, and service offers. The social benefits criteria are fragmented into three sub-criteria—Vehicle air pollution level, vehicle noise level, and adopt with government policy. The Finance criteria is fragmented into three

sub-criteria—Income/Statistical period, average fare/mm, fuel cost/km, and operating expenses. Eight alternatives given below are private bus travel companies. These alternatives added at the bottom of the hierarchy, but they stand different from the decision tree. The sub-criteria and criteria connect these alternatives. Thus, a complete hierarchy is formed (Fig. 3).

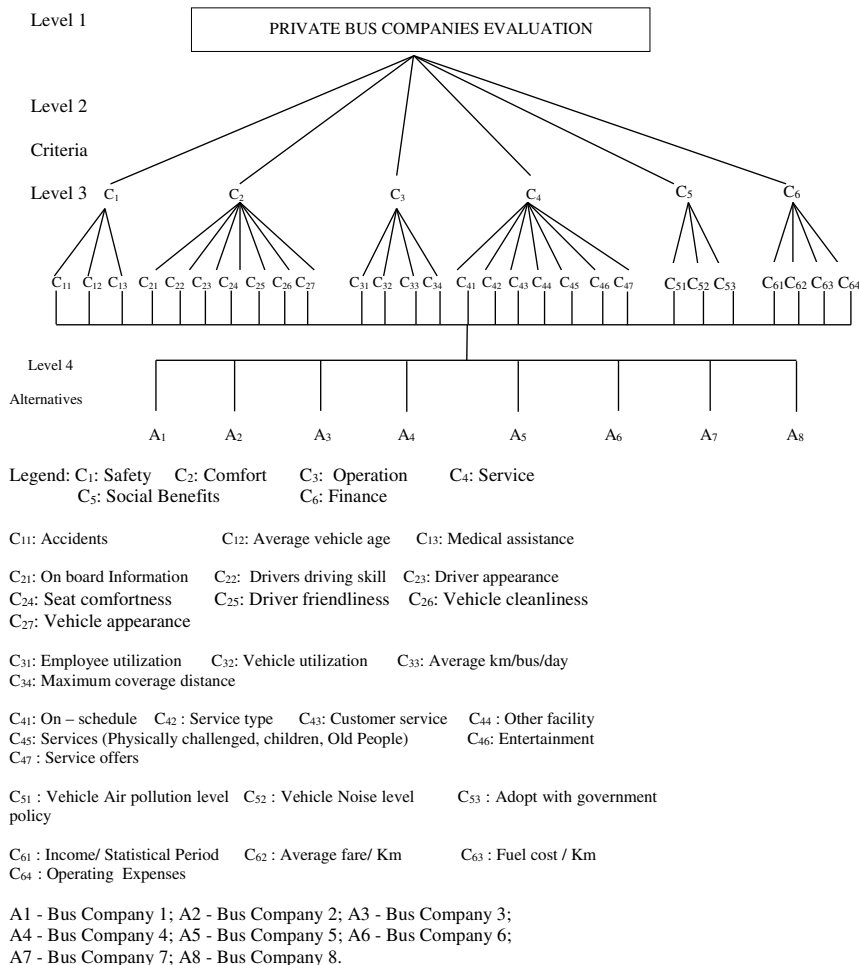


Fig. 3 Hierarchy formations for the selection of private bus companies

Table 1 Pairwise comparison matrix for criteria

Goal	Safety	Comfort	Operation	Service	Social benefits	Finance	Priority
Safety	1	9	6	5	3	1/3	0.2956
Comfort	1/9	1	3	1/2	1/3	1/7	0.0541
Operation	1/6	1/3	1	1/3	1/2	1/5	0.0419
Service	1/5	2	3	1	1	1/4	0.0903
Social benefits	1/3	3	2	1	1	1/5	0.0950
Finance	3	7	5	4	5	1	0.4228
$\lambda_{\text{max}} = 6.4686$		CI = 0.09373			CR = 0.0749		

4.2 Application of AHP Method

In this step, pair-wise comparisons are made, which converted into the framework of a matrix used to derive a local priority vector as an estimate of relative magnitudes associated with the elements compared (Tables 1 and 2).

5 Results of the MCDM–AHP Technique

In this step, synthesized the local priorities that are used to obtain a global measure of preference, which in turn is used in making the final decision (Tables 3 and 4).

6 Conclusion

The transportation system is essential in our day to day life, and it should be safety and security in a city. Commuters in cities are faced with acute road over-crowding, increasing air pollution, and a high level of accident risk. These problems can be solved with a concise and logical urban transport policy. The primary purpose of such a policy should be to provide and promote a private bus transport system for people by improving the efficiency and effectiveness of the city's transport systems. The strategy must be planned in such a way that it has to reduce the need to travel by personalized modes and boost the private transport system. Hence, a practical evaluation approach is essential to improve the quality of decision-making. The proposed AHP methodology is beneficial in terms of efficiency and time-savings. In this method, 28 quantitative and qualitative factors, with eight popular alternatives

Table 2 Pairwise comparison matrix for comfort criteria

Comfort	Onboard information	Driver skill	Driver appearance	Seat comfort	Driver friendliness	Vehicle cleanliness	Vehicle appearance	Priority
Onboard information	1	7	8	9	8	6	9	0.5517
Driver skill	1/7	1	1	1	2	3	2	0.0967
Driver appearance	1/8	1	1	2	4	2	3	0.1203
Seat comfort	1/9	1	1/2	1	2	3	4	0.0960
Driver friendliness	1/8	1/2	1/4	1/2	1	1	2	0.0499
Vehicle cleanliness	1/6	1/3	1/2	1/3	1	1	1	0.0476
Vehicle appearance	1/9	1/2	1/3	1/4	1/2	1	1	0.0384
$\lambda_{\text{max}} = 7.39504$		CI = 0.00584					CR = 0.04874	

Table 3 Calculation of overall global weights

		Local weights								
Criteria	Sub-criteria	Weight	A1	A2	A3	A4	A5	A6	A7	A8
Safety	Accidents	0.74700	0.16000	0.16000	0.05000	0.08000	0.16000	0.08000	0.16000	0.16000
	Avg. vehicle age	0.11930	0.15000	0.10000	0.12000	0.14000	0.15000	0.09000	0.15000	0.10000
Comfort	Medical assistance	0.13355	0.13570	0.18670	0.13360	0.12280	0.12370	0.17140	0.04500	0.08000
	On board information	0.43330	0.14240	0.07610	0.1743	0.10650	0.10660	0.12630	0.14910	0.11820
Service	Drivers driving skill	0.19490	0.06450	0.24170	0.09620	0.13650	0.06610	0.17090	0.08060	0.14330
	Driver app	0.14360	0.14710	0.09210	0.11740	0.13840	0.10390	0.15690	0.11690	0.12700
Operation	Seat comfortness	0.06550	0.14070	0.08550	0.17570	0.13980	0.10420	0.07270	0.13080	0.15050
	Driver friendliness	0.05640	0.16000	0.12380	0.06920	0.20880	0.17420	0.09120	0.04440	0.12800
0.04760	Vehicle cleanliness	0.05060	0.010870	0.20530	0.11710	0.15920	0.13610	0.08990	0.12810	0.05555
	Vehicle cleanliness	0.05540	0.10360	0.12590	0.13920	0.14710	0.11280	0.09110	0.15230	0.12750
0.06340	Employ utilization	0.69270	0.12000	0.13000	0.12000	0.13000	0.13000	0.12000	0.12000	0.12000
	Vehicle utilization	0.16420	0.12000	0.13000	0.013000	0.12000	0.13000	0.12000	0.12000	0.13000
0.54740	Avg. km/bus/day	0.07110	0.08000	0.11000	0.09000	0.17000	0.13000	0.08000	0.19000	0.16000
	Max. coverage distance	0.07170	0.12000	0.12000	0.13000	0.24000	0.09000	0.11000	0.11000	0.07000
0.18030	On-schedule	0.38790	0.11850	0.10400	0.11420	0.14690	0.21000	0.11780	0.12680	0.06150
	Service type	0.23110	0.17000	0.17000	0.17000	0.09000	0.04000	0.13000	0.04000	0.04460
0.11160	Customer service	0.11160	0.17240	0.16230	0.15290	0.18380	0.10070	0.13780	0.04520	0.04460

(continued)

Table 3 (continued)

Criteria	Sub-criteria	Local weights								
		Weight	A1	A2	A3	A4	A5	A6	A7	A8
0.0593	Other facilities	0.07540	0.1098	0.11510	0.13860	0.07100	0.15110	0.13720	0.16180	0.11500
	Services	0.07330	0.15010	0.12090	0.14950	0.13040	0.09420	0.17390	0.06720	0.11360
0.10120	Entertainment	0.05390	0.15970	0.08800	0.11260	0.15530	0.07520	0.16900	0.08730	0.15240
	Service offers	0.06650	0.11040	0.12230	0.13210	0.11650	0.09040	0.20710	0.74700	0.14630
0.18030	Vehicle air pollution	0.36680	0.15000	0.15000	0.15000	0.10000	0.10000	0.15000	0.10000	0.10000
	Vehicle noise level	0.13510	0.10000	0.10000	0.10000	0.10000	0.21000	0.07000	0.21000	0.10000
0.54740	Adopt with govt policy	0.49790	0.13150	0.15440	0.13490	0.11100	0.1598	0.07340	0.10000	0.13460
	Income/statistical period	0.63560	0.11000	0.23000	0.13000	0.21000	0.05000	0.02000	0.15000	0.0600
0.09490	Avg. fare/km	0.17380	0.12000	0.10000	0.11000	0.17000	0.14000	0.12000	0.10000	0.13000
	Fuel cost/km	0.09550	0.09000	0.11000	0.13000	0.13000	0.14000	0.13000	0.13000	0.14000
0.00980	Operating expenses	0.09490	0.13000	0.21000	0.14000	0.27000	0.02000	0.11000	0.06000	0.00125
	Global weights									
Criteria	Sub-criteria	A1	A2	A3	A4	A5	A6	A7	A8	
Safety	Accidents	0.06543	0.06543	0.06543	0.02045	0.03271	0.06543	0.03271	0.06543	
	Avg. vehicle age	0.00980	0.00653	0.00724	0.00914	0.00980	0.00588	0.00980	0.00653	
Comfort	Medical assistance	0.00992	0.01365	0.00977	0.00898	0.00904	0.01253	0.00329	0.00585	
	On board information	0.08514	0.08560	0.08303	0.03857	0.05155	0.08383	0.04580	0.07780	
0.00227	Drivers driving skill	0.00227	0.00849	0.00338	0.00480	0.00232	0.00601	0.00283	0.00504	

(continued)

Table 3 (continued)

Criteria	Sub-criteria	Global weights						
		A1	A2	A3	A4	A5	A6	A7
	Driver app	0.00381	0.00238	0.00304	0.00358	0.00269	0.00406	0.00303
	Seat comfortness	0.00166	0.00101	0.00207	0.00165	0.00123	0.00086	0.00154
	Driver friendliness	0.00163	0.00126	0.00070	0.00212	0.00177	0.00093	0.00045
	Vehicle cleanliness	0.00099	0.00187	0.00107	0.00145	0.00124	0.00082	0.00117
	Vehicle cleanliness	0.00103	0.00121	0.00139	0.00147	0.00113	0.00091	0.00152
	0.02252	0.02096	0.02527	0.02340	0.01871	0.02345	0.02219	0.02242
Operation	Employ utilization	0.00527	0.00571	0.00527	0.00571	0.00571	0.00571	0.00527
	Vehicle utilization	0.00125	0.00135	0.00135	0.00125	0.00135	0.00125	0.00135
	Avg. km/bus/day	0.00036	0.00050	0.00041	0.00077	0.00059	0.00036	0.00086
	Max. coverage distance	0.00055	0.00055	0.00059	0.00109	0.00041	0.00050	0.00072
		0.00743	0.00810	0.00762	0.00882	0.00806	0.00782	0.00788
Service	On-schedule	0.00219	0.00192	0.00211	0.00271	0.00388	0.00218	0.00234
	Service type	0.00187	0.00187	0.00187	0.00099	0.00044	0.00143	0.00044
	Customer service	0.00092	0.00086	0.00081	0.00098	0.00053	0.00073	0.00024
	Other facilities	0.00039	0.00041	0.00050	0.00025	0.00054	0.00049	0.00058
	Services	0.00052	0.00042	0.00052	0.00045	0.00033	0.00061	0.00023
Entertainment		0.00041	0.00023	0.00029	0.00040	0.00019	0.00043	0.00022
	Service offers	0.06550	0.00039	0.00042	0.00037	0.00029	0.00066	0.00036

(continued)

Table 3 (continued)

Criteria	Sub-criteria	Global weights						
		A1	A2	A3	A4	A5	A6	A7
Social benefits	Vehicle air pollution	0.07180	0.00610	0.00652	0.00704	0.00675	0.00554	0.00742
0.0593	Vehicle noise level	0.00330	0.00300	0.00330	0.00220	0.00330	0.00220	0.00081
	Adopt with govt policy	0.00081	0.00081	0.00081	0.00170	0.00057	0.00170	0.00401
	0.00803	0.00871	0.00813	0.00632	0.00866	0.00605	0.00688	0.00386
Finance	Income/statistical period	0.01479	0.00836	0.01351	0.00322	0.00129	0.00965	0.00229
0.10120	Avg fare/km	0.00211	0.00176	0.00193	0.00299	0.00246	0.00211	0.00176
	Fuel cost/km	0.00087	0.00106	0.00126	0.00126	0.00135	0.00126	0.00135
	Operating expenses	0.00202	0.00134	0.00259	0.00048	0.00019	0.00106	0.00058
	0.01130	0.01963	0.01290	0.02035	0.00751	0.00485	0.01372	0.00808
	0.20621	0.14911	0.14347	0.10448	0.10125	0.13154	0.10388	0.12146

Table 4 Ranking of private bus operator agencies using overall global weights

Global wts.	0.17321	0.16311	0.13734	0.13731	0.10467	0.10461	0.09996	0.09391
Rank	1	2	3	4	5	6	7	8
Private bus companies	A7	A1	A4	A5	A2	A3	A6	A8

for each private bus operators (inclusion of feedback from passengers and travel agencies) are considered. The limitation of this study is concerned with bus route in the southern part of India. In the future, researchers can apply other MCDM techniques such as TOPSIS, SAW, PROMETHEE, DEA, GRA, ELECTRE, etc. for this study in an effective manner.

References

1. Devi, K., Yadav, S.P., Kumar, S.: Extension of fuzzy TOPSIS method based on vague sets. *Int. J. Comput. Cogn.* **7**(4) (2009)
2. Kahraman, C.: *Fuzzy Multi-criteria Decision Making: Theory and Applications with Recent Developments*, vol. 16. Springer Science & Business Media (2008)
3. Saaty, T.L.: *The Analytic Hierarchy Process*. McGraw-Hill, New York (1980)
4. Park, K.S., Lim, C.H.: A structured methodology for comparative evaluation of user interface designs using usability criteria and measures. *Int. J. Ind. Ergon.* **23**(5–6), 379–389 (1999)
5. Yeh, C.H., Deng, H., Chang, Y.H.: Fuzzy multi criteria analysis for performance evaluation of bus companies. *Eur. J. Oper. Res.* **126**, 459–473 (2000)
6. Fielding, G.J., Babitsky, T.T., Brenner, M.E.: Performance evaluation for bus transit. *Transp. Res. Part A Gen.* **19**(1), 73–82 (1985)
7. Gomes, L.F.: Multi criteria ranking of urban transportation system alternatives. *J. Adv. Transp.* **23**(1), 43–52 (1989)
8. Vaidya, O.S., Kumar, S.: Analytical hierarchy process: an overview of applications. *Eur. J. Oper. Res.* **169**(1), 1–29 (2006)
9. Subramanian, N., Ramanathan, R.: A review of applications of AHP in operations management. *Int. J. Prod. Econ.* **138**(2), 215–241 (2012)
10. Vadivel, S.M., Sequeira, A.H.: Enhancing the operational performance of mail processing facility layout selection using MCDM. *Int. J. Serv. Oper. Manage.* (2018). Accepted 28 July 2018. <https://doi.org/10.1504/IJSOM.2020.10018620>
11. Murugesan, V.S., Sequeira, A.H., Shetty, D.S., Jauhar, S.K.: Enhancement of mail operational performance of India post facility layout using AHP. *Int. J. Syst. Assur. Eng. Manage.* 1–13 (2019)
12. Vadivel, S.M., Sequeira, A.H.: A novel approach for operational performance based mail sorting FLD selection using GRA: a case on India speed post service industry. In: *International Conference on Intelligent Systems Design and Applications*, pp. 1123–1132. Springer, Berlin (2018)
13. Vadivel S.M.: Implementing lean ergonomics in Indian postal service industries—a case study. Unpublished MS thesis, Indian Institute of Technology Madras, pp. 01–83 (2015)

CNC Machine Shop Floor Facility Layout Design Using Genetic Algorithm



S. M. Vadivel , A. H. Sequeira , Sunil Kumar Jauhar ,
K. S. Amirthagadeswarn , and T. Aravind Krishna

Abstract The facility layout is a well-planned process to assimilate equipment, human resources, and materials for processing a product most effectively. The facility layout problem (FLP) is an optimization problem that involves determining the shape and location of various departments within a facility, based on the inter-department distance and volume measures. CRAFT algorithm is one of the primary methods currently used for the optimization of facility layouts. The aim of this is analyzing and assessing various proposed layouts through this algorithm. The objective is to minimize the total layout cost. It depends on the material flow and distance between the departments. An attempt has also been made to optimize the layout through GA.

Keywords Facility layout planning · Facility layout design · Genetic algorithm · CNC machine cell layout · Material handling · Layout cost

S. M. Vadivel · A. H. Sequeira

School of Management, National Institute of Technology Karnataka, Surathkal 575025, India
e-mail: sm16f09.vadivel@nitk.edu.in

A. H. Sequeira

e-mail: ahs@nitk.edu.in

S. K. Jauhar

Department of Operations and Decision Sciences, Indian Institute of Management, Kashipur, India
e-mail: skjauhar@iimkahipur.ac.in

K. S. Amirthagadeswarn

United Institute of Technology, Coimbatore, India
e-mail: ksag.eswar@gmail.com

T. Aravind Krishna

Chainalytics—Supply Chain Design, Bangalore, India
e-mail: aravindkrishna@gmail.com

1 Introduction

The FLP is multiple optimization problems that create a diversity of production facilities. It is concerned with defining the most effective physical arrangement of different departments with an unequal area of the facility layout. A facility layout is an arrangement of equipment needed for goods production or service delivery. A facility is an entity that enables the performance of any job. It may consider as a work center, a machine tool, a machine shop, a manufacturing cell, a warehouse, a department, etc. It means location planning of all machines, utilities, employee workstations, material storage area, customer service area, aisles, lunchroom, restroom, internal wall, office, and computer room. Usually, the flow will be around materials and people within the shop floor buildings. The facility layout design often depends on the product's variety and production volumes. In general, any organization follows any one type of layout or mixed as follows: fixed product layout, process layout, product layout, and cellular layout. Here, we have considered the product-type layout as a case study with the application of a genetic algorithm to minimize the layout cost for plant relocation nearby areas. GA is a novel approach, which works based on the principle of natural genetics and natural selection to constitute search and optimization procedures. Goldberg [1] described the usual form of genetic algorithm. GA technique starts with an initial set of random solutions called "initial population," which is made by a group of chromosomes. These chromosomes are evolved through the number of successive iteration (generations) to obtain the optimized solution.

This paper is arranged as follows: Sect. 1 covers the introduction. Section 2 briefly describes facility layout design (FLD), GA, and other heuristic algorithms. Section 3 describes the research methodology adoption, and Sect. 4 explores the case study in a CNC machine shop facility layout, while Sect. 5 discusses the results of GA to find the optimal total layout cost (TLC). Finally, Sect. 6 provides a conclusion and future scope.

2 Literature Support

Many authors suggested the methods and algorithms for solving facility layout problems in GA. For example, Michel et al. [2] developed a rule-based approach using GAs to address the unequal area department layout problem. The multiple objective functions of the proposed method involved material flow factor cost, shape ratio factor, and area utilization factor in finding minimal TLC. Paul et al. [3] described that the layout of facilities was modeled using the particle swarm optimization algorithm. A new method is proposed for calculating distances between the facilities. A comparison with existing algorithms (GA and improved GA) was performed to evaluate the proposed algorithm's efficiency. Smutkupt and Wimonkasame [4] explained that the most popular was the Computerized Relative Allocation Facilities Technique (CRAFT). However, they mentioned that the result from CRAFT was limited. The

result of the design showed only the minimum total transfer cost between departments. As a result, the simulation technique is added to plant layout design to display more information about the design, such as full time in the system, waiting time, and utilization. Arikaram et al. [5] concluded that uniting genetic algorithm with simulated annealing or genetic algorithm and simulation techniques may help to get better solutions. Chutima [6] described a genetic algorithm-based model for facility layout problems with unequal departmental areas with different geometric shape constraints. Multi-criteria decision-making (MCDM) methods also applied for solving the FLP in various manufacturing and service industries [7, 8]. Vadivel et al. [9] applied GA and DEA methods in India post FLD for finding the optimal layout and minimum total layout cost, for the operational performance enhancement. Since GA is parameter sensitive, the experiment shows that crossover type, mutation type, mutation probability, and population size are the main parameters.

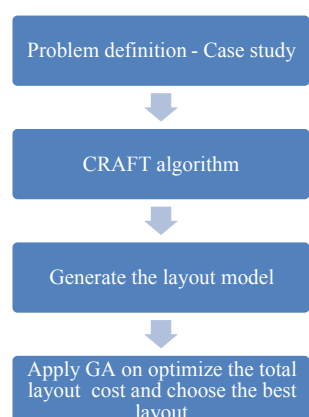
3 Research Methodology

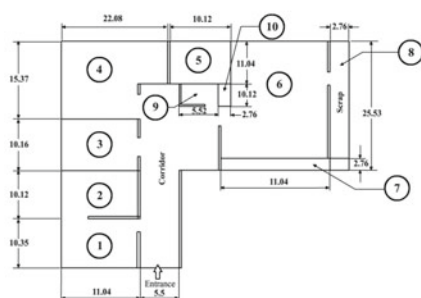
See Fig. 1.

4 Case Study: CNC Machine Shop Floor

XYZ company independently owned ISO 9001-2000 certified, Precision Machine and Manufacturing shop in Coimbatore, Tamil Nadu, the southern part of India: The industry is providing precision products to automobile, textile machinery, jewelry manufacturers, electronics, and domestic appliances industries since 1989. It is fully equipped with machinery of regular varieties and specialized CNC milling, CNC

Fig. 1 Methodological flow of FLP





SL.No	DEPARTMENT	AREA (SQ.FT)
1	SURFACE GRINDING MACHINE CELL 1	114
2	OFFICE	112
3	CNC TURNING CELL 2	112
4	CONVENTIONAL MACHINE CELL 3	350
5	RAW MATERIAL STORAGE	112
6	CNC MILLING CELL 4	350
7	TOOL STORAGE	43
8	SCRAP	70
9	TOILET	56
10	INSPECTION (QUALITY)	28

Fig. 2 Existing layout and active areas—CNC shop floor

turning products, and related services to cater to the needs of industries. Now XYZ company wants to move the pieces of equipment into a new location to minimize the total layout cost through minimum material handling damage and transportation cost. Hence, the managerial implications were justified (Fig. 2).

4.1 Parameters to Be Considered

The objective is minimizing the total layout cost. The following parameters are involved to find the TLC.

Total layout cost (TLC) = MFFC × (SRFwhole/AUFwhole)—Adopted from [2].

1. Material flow factor cost (MFFC) = $\sum \sum F_{ij} \times D_{ij} \times C_{ij}$
where

F_{ij} Material flow between the facility i and j

D_{ij} Distance between centroids of the facility i and j

C_{ij} Transportation costs per unit time from Dept i to j

n Number of departments.

2. Shape ratio factor whole = $\{\pi \text{ pi}/4\sqrt{A_i}\}1/n$
where

P_i Perimeter of the department i

A_i Area of the department i .

3. Area utilization factor whole = $\sum A_i / (\sum A_i + TBA)$
where

TBA Total blank area of whole layout

A_i Area of the department i (Tables 1 and 2).

Table 1 Material flow between departments 1–7

From/To	1	2	3	4	5	6	7
1	—	4	2	4	14	0	0
2	0	—	0	7	0	0	0
3	0	0	—	0	1	2	0
4	0	0	0	—	3	9	0
5	0	3	0	4	—	11	0
6	0	0	0	0	0	—	20
7	0	0	0	0	0	2	—

Table 2 Cost matrix between departments 1–7

From/To	1	2	3	4	5	6	7
1	—	0.93	0.12	0.52	0.31	0	0
2	0.93	—	0	0.93	0.31	0	0
3	0.12	0	—	0.5	0.1	0.4	0
4	0.52	0.93	0.5	—	0.15	0.68	0
5	0.31	0.31	0.1	0.15	—	0.12	0
6	0	0	0.4	0.68	0	—	0.8
7	0	0	0	0	0	0.8	—

4.2 MFFC—Existing Layout

Rectilinear distance and centroid:

To find the centroid of department: $x = a_n X_n / a_n$; $y = a_n Y_n / a_n$.

The distance between any two departments is represented by rectilinear distance between the centroids of the two departments: $D_{ij} = |X_i - X_j| + |Y_i - Y_j|$.

Total number of departments: 7; total number of interchangeable departments: 3.

Centroids of all the departments in the existing layout are calculated and presented below. Here, the left side of the layout is assumed as Y -axis, and the bottom side of the layout is assumed as the X -axis.

- Surface grinding area: $(X_1, Y_1) = 5.52, 5.175$
- CNC turning area: $(X_2, Y_2) = 5.52, 25.55$
- Conventional machining area: $(X_3, Y_3) = 10.04, 39.55$
- Raw material storage: $(X_4, Y_4) = 27.14, 40.98$
- CNC milling area: $(X_5, Y_5) = 39.29, 33.91$
- Inspection area: $(X_6, Y_6) = 23.44, 33.96$
- Dispatch area: $(X_7, Y_7) = 19.3, 25.37$ (Tables 3 and 4).

Material flow factor cost—existing layout = Rs. 1096/-.

Table 3 Distance between departments 1 to 7—existing layout

From/To	1	2	3	4	5	6	7
1	—	20.38	38.9	57.43	62.51	46.71	33.98
2	20.38	—	18.52	37.05	42.13	26.33	13.96
3	38.9	18.52	—	31.53	34.89	17	21.45
4	57.43	37.05	31.53	—	19.11	11.02	23.75
5	62.51	42.13	34.89	19.11	—	8.13	20.86
6	46.71	26.33	17	11.02	8.13	—	12.73
7	33.98	13.96	21.45	23.75	20.86	12.73	—

Table 4 Material flow factor cost—existing layout

From/To	1	2	3	4	5	6	7
1	—	75.81	9.33	119.45	271.3	0	0
2	0	—	0	241.2	0	0	0
3	0	0	—	0	3.48	13.6	0
4	0	0	0	—	8.6	67.44	0
5	0	39.18	0	11.46	—	10.73	0
6	0	0	0	0	0	—	203.68
7	0	0	0	0	0	20.36	—

4.3 MFFC—Proposed Layout Design—1

Total number of departments: 7; total number of interchangeable departments: 3

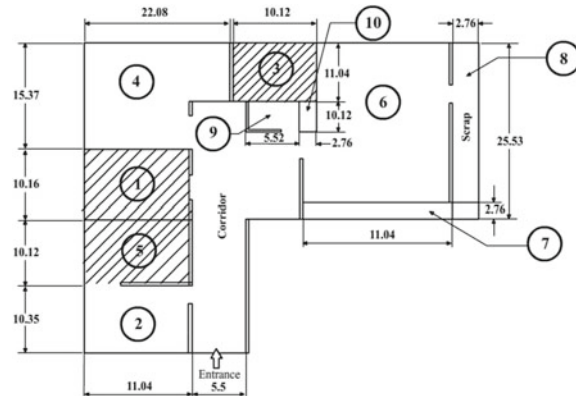
- Raw material storage area: $(X_1, Y_1) = 5.52, 15.41$
- Surface grinding area: $(X_2, Y_2) = 5.52, 25.55$
- Conventional machining area: $(X_3, Y_3) = 10.04, 39.55$
- CNC turning area: $(X_4, Y_4) = 27.14, 40.98$
- CNC milling area: $(X_5, Y_5) = 39.29, 33.91$
- Inspection area: $(X_6, Y_6) = 23.44, 33.96$
- Dispatch area: $(X_7, Y_7) = 19.3, 25.37$ (Fig. 3; Tables 5 and 6).

Material flow factor cost—proposed layout 1 = Rs. 999/-.

4.4 MFFC—Proposed Layout Design—2

Total number of departments: 7; total number of interchangeable departments: 3

- Raw material storage area: $(X_1, Y_1) = 5.52, 5.175$
- Surface grinding area: $(X_2, Y_2) = 5.52, 25.55$

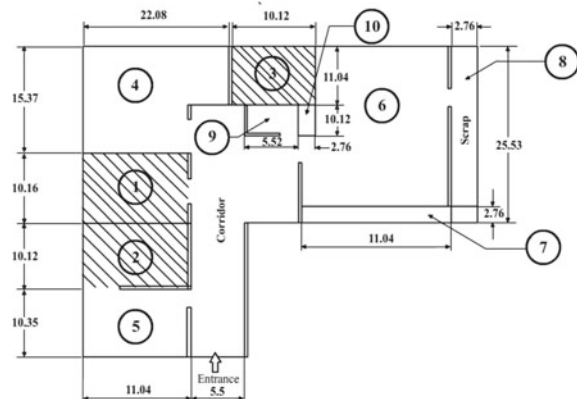
**Fig. 3** Proposed layout 1**Table 5** Distance between departments 1 to 7—proposed layout 1

From/To	1	2	3	4	5	6	7
1	—	10.14	28.66	47.19	52.27	36.47	23.74
2	10.14	—	18.52	37.05	42.13	26.33	13.96
3	28.66	18.52	—	18.53	34.89	18.89	23.44
4	47.19	37.05	18.53	—	19.22	10.72	23.45
5	52.27	42.13	34.89	19.22	—	15.9	28.53
6	36.47	26.33	18.89	10.72	15.9	—	12.73
7	23.74	13.96	23.44	23.75	28.53	12.73	—

Table 6 Material flow factor cost—proposed layout 1

From/To	1	2	3	4	5	6	7
1	—	37.72	6.87	98.15	226.85	0	0
2	0	—	0	241.2	0	0	0
3	0	0	—	0	3.48	15.11	0
4	0	0	0	—	8.65	65.6	0
5	0	39.18	0	11.53	—	20.98	0
6	0	0	0	0	0	—	203.68
7	0	0	0	0	0	20.36	—

- Conventional machining area: $(X_3, Y_3) = 10.04, 39.55$
- CNC turning area: $(X_4, Y_4) = 27.14, 40.98$
- CNC milling area: $(X_5, Y_5) = 39.29, 33.91$
- Inspection area: $(X_6, Y_6) = 23.44, 33.96$
- Dispatch area: $(X_7, Y_7) = 19.3, 25.37$ (Fig. 4; Tables 7 and 8).

**Fig. 4** Proposed layout 2**Table 7** Distance between departments 1 to 7—proposed layout 2

From/To	1	2	3	4	5	6	7
1	—	20.38	38.9	57.43	62.51	46.70	33.98
2	20.38	—	18.52	37.05	42.13	26.33	13.96
3	38.9	18.52	—	31.53	34.89	17	21.45
4	57.43	37.05	31.53	—	19.22	11.02	23.75
5	62.51	42.13	34.89	19.22	—	18.13	20.86
6	46.70	26.33	17	11.02	18.13	—	12.73
7	33.98	13.96	21.45	23.75	20.86	12.73	—

Table 8 Material flow factor cost—proposed layout 2

From/To	1	2	3	4	5	6	7
1	—	75.81	9.33	119.45	271.3	0	0
2	0	—	0	241.2	0	0	0
3	0	0	—	0	3.48	13.6	0
4	0	0	0	—	8.65	67.44	0
5	0	39.18	0	11.53	—	23.93	0
6	0	0	0	0	0	—	203.68
7	0	0	0	0	0	20.36	—

Material flow factor cost—proposed layout 2 = Rs. 1108/-.

4.5 MFFC—Proposed Layout Design—3

Total number of departments: 7; total number of interchangeable departments: 3

- Raw material storage area: $(X_1, Y_1) = 5.52, 5.175$
- Surface grinding area: $(X_2, Y_2) = 5.52, 25.55$
- Conventional machining area: $(X_3, Y_3) = 10.04, 39.55$
- CNC turning area: $(X_4, Y_4) = 27.25, 40.98$
- CNC milling area: $(X_5, Y_5) = 39.29, 33.91$
- Inspection area: $(X_6, Y_6) = 23.44, 33.96$
- Dispatch area: $(X_7, Y_7) = 19.3, 25.37$ (Fig. 5; Tables 9 and 10).

Material flow factor cost—proposed layout 3 = Rs. 1094/-.

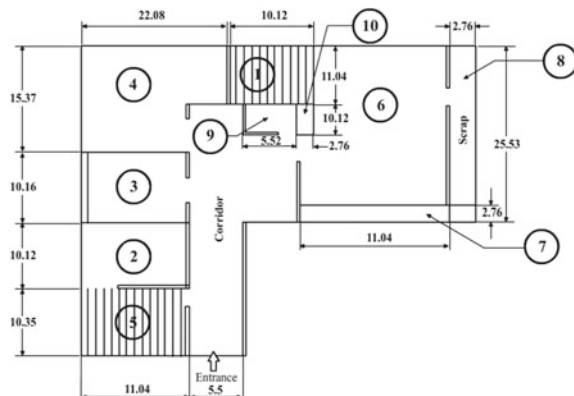


Fig. 5 Proposed layout 3

Table 9 Distance between departments 1 to 7—proposed layout 3

From/To	1	2	3	4	5	6	7
1	—	20.38	38.9	57.43	62.51	46.71	33.98
2	20.38	—	18.52	37.05	42.13	26.33	13.96
3	38.9	18.52	—	31.53	34.89	17	21.45
4	57.43	37.05	31.53	—	19.11	10.83	23.56
5	62.51	42.13	34.89	19.11	—	8.13	20.86
6	46.71	26.33	17	10.83	8.13	—	12.73
7	33.98	13.96	21.45	23.56	20.86	12.73	—

Table 10 Material flow factor cost—proposed layout 3

From/To	1	2	3	4	5	6	7
1	—	75.81	9.33	119.45	271.3	0	0
2	0	—	0	241.2	0	0	0
3	0	0	—	0	3.48	13.6	0
4	0	0	0	—	8.6	66.28	0
5	0	39.18	0	11.46	—	10.73	0
6	0	0	0	0	0	—	203.68
7	0	0	0	0	0	20.36	—

Table 11 GA—parameters

Fitness function	Parameters
No. of variables	3
Lower bound	[999 0.96 0.85]
Upper bound	[1108 1.625 1]
Population type	Double vector
Population size	20
Fitness scaling	Rank
Selection function	Roulette
Cross function	Scattered
Reproduction	Elite count

5 Results of Genetic Algorithm

Objective: Minimum total layout cost (TLC)

Min.TLC = Min.MFFC × (SRFwhole/AUFwhole) (Table 11).

A set of 20 runs have been made, and the observations are calculated in Tables 12 and 13.

6 Conclusion

The FLD is an optimization problem that involves defining the shape and location of various departments within a facility. It was constructed based on the inter-department distance and volume measures. The existing FLD was analyzed and evaluated based on the inter-department distance and volume measures. For that, various measures such as material flow, distance, and material handling cost are considered. Various FLDs have designed with a traditional algorithm known as Computerized Relative

Table 12 GA—results

S. No.	Objective value (TLC)	Min MFFC	SRF	AUF
1	971.06	1010.76	0.9600	0.99
2	959.04	999.00	0.9607	1.0
3	985.59	1025.77	0.9608	0.99
4	974.79	1014.82	0.9605	0.99
5	968.89	1007.10	0.9614	0.9993
6	970.04	1008.87	0.9614	0.9999
7	959.75	999.09	0.9606	0.9999
8	960.44	999.00	0.9612	0.9998
9	971.03	1011.00	0.9602	0.9998
10	973.59	1013.51	0.9604	0.9998
11	1001.62	1039.98	0.9630	0.9999
12	965.41	1004.940	0.9601	0.9994
13	974.59	1014.954	0.9602	0.9999
14	966.14	1006.21	0.9601	0.9999
15	959.04	1018.942	0.9614	0.9999
16	979.62	1007.05	0.9613	0.9999
17	968.14	1001.53	0.9600	0.9999
18	961.50	999.02	0.9600	0.9999
19	959.12	1034.92	0.9618	0.9999
20	972.32	1012.37	0.9604	0.9999

Table 13 Optimized parameters for GA

Optimized parameters for GA	
Minimum material flow factor cost (MFFC)	Rs. 999
Shape ratio factor (SRF)	0.96
Area utilization factor (AUF)	1.00
Minimum total layout cost (TLC)	Rs. 959

Allocation of Facilities Technique (CRAFT). The minimum total layout cost parameters have been estimated using a genetic algorithm. In the future, the proposed layout can be examined using a simulation technique for better layout design.

References

1. Goldberg, D.E.: Genetic Algorithms. Pearson Education India (2006)
2. Hu, M.H., Wang, M.J.: Using genetic algorithms on facilities layout problems. Int. J. Adv. Manuf. Technol. **23**(3–4), 301–310 (2004)

3. Paul, R.C., Asokan, P., Prabhakar, V.I.: A solution to the facility layout problem having passages and inner structure walls using particle swarm optimization. *Int. J. Adv. Manuf. Technol.* **29**(7–8), 766–771 (2006)
4. Smutkupt, U., Wimonkasame, S.: Plant layout design with simulation. In: Proceedings of the International Multi Conference of Engineers and Computer Scientists, vol. 2, 18–20 (2009)
5. Arikaran, P., Jayabalan, V., Senthilkumar, R.: Analysis of unequal areas facility layout problems. *Int. J. Eng.* **4**(1), 44–51 (2010)
6. Chutima, P.: Genetic algorithm for facility layout design with unequal departmental areas and different geometric shape constraints. *Thammasat Int. J. Sci. Tech.* **6**(2), 33–43 (2001)
7. Yang, T., Hung, C.C.: Multiple-attribute decision making methods for plant layout design problem. *Robot. Comput.-Integr. Manuf.* **23**(1), 126–137 (2007)
8. Vadivel, S.M., Sequeira, A.H.: Enhancing the operational performance of mail processing facility layout selection using multi—criteria decision making methods. *Int. J. Serv. Oper. Manag.* Accepted 28 July 2018 (2018). <https://doi.org/10.1504/IISOM.2020.10018620>
9. Vadivel, S.M., Sequeira, A.H., Jauhar, S.K.: Metaheuristic for optimize the India speed post FLD and operational performance based sorting layout selection using DEA method. *Intelligent Systems Design and Applications*, vol. 941, pp. 1035–1044. Springer (2018)

Source of Treatment Selection for Different States of India and Performance Analysis Using Machine Learning Algorithms for Classification



Nitima Malsa, Pooja Singh, Jyoti Gautam, Arpita Srivastava, and Santar Pal Singh

Abstract Pregnancy or gestation is a critical stage of women's life. Pregnancy outcome depends on various factors including selection of source of treatment (child birth place), complication of pregnancy, expenditure of delivery, etc. The paper mainly focuses on selection of source of treatment as well as analyzes the performance of various machine learning algorithms Naïve Bayes, Decision Tree, Random Forest, and Support Vector Machine with respect to the accuracy, standard deviation, and runtime. The dataset has been collected from Kaggle website of India's different states mainly Chhattisgarh, Assam, Bihar, Madhya Pradesh, Jharkhand, and Rajasthan. Implementation of the work has been done using Rapid Miner Tool 9.0 version.

Keywords India · Government versus private hospitals · Machine learning · Classifiers · Source of treatment

1 Introduction

Pregnancy is a very delicate stage for any women. When a woman plans for a pregnancy, there might be issue of her health and care. In India, the situation is very critical due to unawareness of the health issues which may arise during pregnancy. One of the major challenges is to choose place of child birth. Generally expecting mothers and couples still have no knowledge about the family planning, and they do not have correct information about the place of child birth (source of treatment). The source of treatment means where the delivery, operation, or treatment is to be

N. Malsa (✉) · J. Gautam · A. Srivastava
JSS Academy of Technical Education, Noida, India
e-mail: nitima.malsa@gmail.com

P. Singh
Amity School of Engineering & Technology, Delhi, India

S. P. Singh
Galgotia's University, Greater Noida, India

done. In India, mainly two types of source of treatment are available: government and private hospitals [1].

According to the survey of NSSO, the average medical expenditure on hospitals is Rs. 25,850 in private facilities compared to Rs. 6,120 in public facilities. As per the information, it is found that the private hospitals are four times costlier as compared to the government hospitals. As per the report of NSSO, the average total medical expenditure per child birth in public treatment was just Rs. 1,587 as against in private treatment was just Rs. 20,328 [2].

In the research, the data mining techniques have been used to analyze and predict the results of source of treatment which will be helpful in selection of place of child birth.

2 Literature Review

Pregnancy a 40 weeks span during which one or more offspring develops inside a woman. It is enjoyable if it is trouble free. But in some cases, women experience complications. Globally, about 800 women die every day due to these complications out of which 20% are from India [3]. In India, a woman dies every 5 min. The major pregnancy complications are: miscarriage, ectopic pregnancy, hypertension and diabetes in pregnancy, preterm labor, poor fetal growth, preterm rupture of membranes, obstetric cholestasis, and low placenta. [4].

A report in August says that 386 children died at a government hospital in Gorakhpur, Uttar Pradesh, which shows the corruption within government healthcare system. Hence, people in India prefer private hospitals for child birth. As per the NSSO survey report, average medical expenditure in private hospitals is more than government hospitals. Apart from this, rural areas have only government hospitals. This clarifies the strong need of a system which will be helpful in selecting the source of treatment (child birth place) [5]. As per the qualitative study on individuals' preferences [6], the women's decision of selecting hospitals depends on their personal preferences or experience and their peers' experience.

The study [7] presents the various risks or complications during pregnancy. Various machine learning algorithms have been used and compared for the purpose. A comparative study of classification algorithms for classifying gestational risks in pregnant women [8] presents that the Decision Tree algorithm and Naïve Bayes algorithm are effectively used for classifying medical data. The study of a machine learning approach for prediction of pregnancy outcome following IVF treatment [9, 10] aims to analyze and predict IVF pregnancy. Various machine learning algorithms for classification Random Forest, Decision Tree, and Support Vector Machine have been used and compared.

3 Methodology

The research work employed the methodology through the following steps.

3.1 Design Model

The research work has been designed by the following model (Fig. 1).

3.1.1 Data Collection

A large amount of medical data needs to be analyzed as the extract knowledge that can be useful for people around the world. The dataset for the work is taken from Kaggle site [11] which contains data of multiple states of India as—Assam, Bihar, Madhya Pradesh, Jharkhand, Chhattisgarh, and Rajasthan. It has many different attributes as—age, delivered any baby, outcomes of baby, source of treatment for family planning (fp), fp method used, pregnant month, willing to get pregnant, any fp method used, etc.

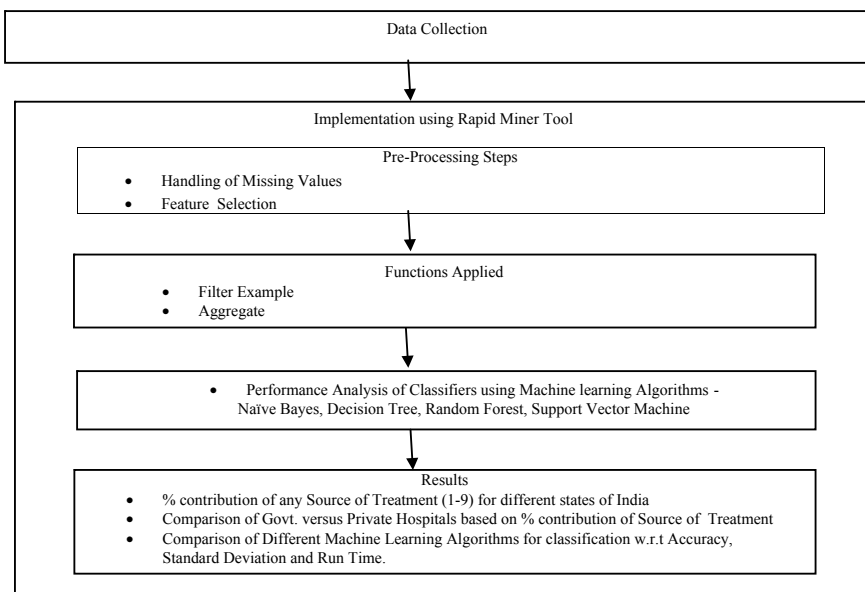


Fig. 1 Design model for the proposed work

3.1.2 Implementation Using Rapid Miner Tool

Implementation has been done using Rapid Miner tool version 9.0. The whole process of implementation can be understood through the snapshot shown in Fig. 2.

Implementation is carried out in the following steps:

Import Data

The data is imported using repository function in Rapid Miner.

Pre-processing Steps

Pre-processing consists of handling missing value followed by attribute selection step.

Handling of Missing Values

Missing values have been replaced using the average value formula.

Feature Selection

Using attribute selection function, mainly delivered any baby, age of expecting mothers, and source of treatment, features have been selected for the work. Delivered any baby feature has value 1 (if delivered alive baby), not delivered any baby feature has value 2 (if not delivered alive baby). Age feature includes ages from 15 to 50, and the source of treatment feature includes different sources of treatment (government/private Hospitals) as described in Table 1. Feature selection has been done by using select attribute operator.

Functions Applied

Mainly two functions filter example and aggregate have been applied.

Filter Example

Filter example function is used to select the value of delivered any baby as 1, which means that the baby is born alive and the results are shown in Fig. 3.

Aggregate

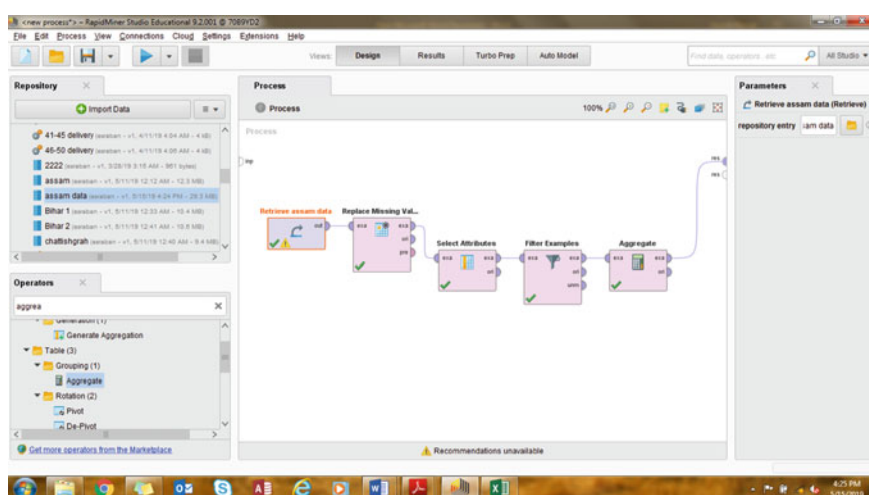
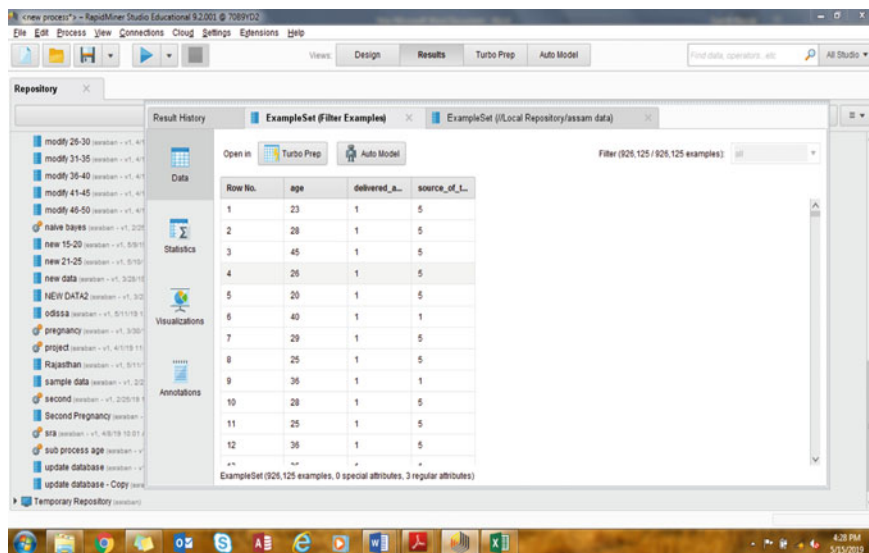


Fig. 2 A design model of whole process system in Rapid Miner Tool

Table 1 Description of all sources of treatment

Name of sources of treatment	Label used
Government-govt./municipal hospital	1
Government-govt. dispensary	2
Government-UHC/UHP/UFWC	3
Government-CHC	4
Government-PHC	5
Government-camp	6
Private-hospital	7
Private-dispensary/clinic	8
Others	9

**Fig. 3** Select delivered any baby feature against all source of treatment

Finally, the aggregate function has been used to find the total count of each source of treatment for all ages of expecting mothers for delivered any baby (Fig. 4).

The % contribution of different states for SOT1–9 has been calculated as given in Table 2.

The comparison of government versus private hospitals based on contribution of source of treatment is given in Table 3.

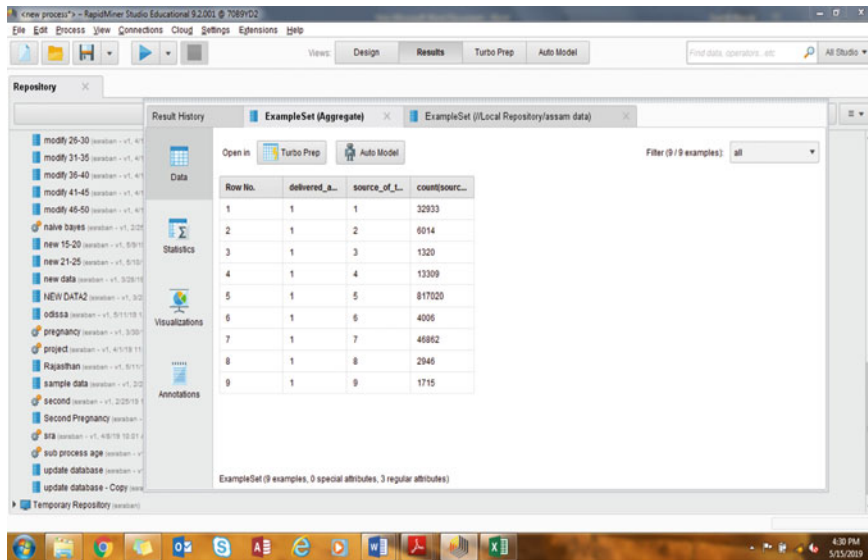


Fig. 4 Total count against each source of treatment for delivered any baby case for Assam state

3.1.3 Performance Analysis of Different Classifiers Using Machine Learning Algorithms

Various machine learning algorithms Naïve Bayes, Decision Tree, Random Forest, and Support Vector Machine have been applied for classifying the source of treatment.

The above-mentioned algorithms have been compared in terms of accuracy, standard deviation, and runtime as given in Table 4.

3.1.4 Results

Table 2 depicts % contribution for any source of treatment (1–9) according to state-wise for delivered baby. The results have been explained through Table 2, and Fig. 5 represents the total count for delivered any baby individually for every SOT (1–9) method.

The following cases have been observed through Table 2 and Fig. 5.

Case 1: For Chhattisgarh state, SOT3 method (Government-Govt. Dispensary) gives the highest result for the case delivered any baby, and it means that this method is the maximum effective treatment for expecting mothers of any age. Percentage contribution using SOT3 (56.36%) is highest for expecting mothers, whereas SOT9 method is the minimum effective treatment for expecting mothers. Case 2: For Rajasthan state, SOT5 is the maximum effective treatment method, whereas SOT9 is the minimum effective method.

Table 2 % Contribution of different states for SOT1-9 methods for delivered baby

State	Total count source of delivered any baby for different methods of source of treatment								Total
	1	2	3	4	5	6	7	8	
Count for SOT1-9 for Chhattisgarh	198220	1851	414390	53886	24081	31908	6866	3952	116
% Contribution of Chhattisgarh for SOT1-9	26.96	0.25	56.36	7.33	3.28	4.34	0.93	0.54	0.02
Count for SOT1-9 for Rajasthan	75857	25992	3044	65137	576204	188890	39072	945	549
% Contribution of Rajasthan for SOT1-9	7.77	2.66	0.31	6.68	59.06	19.36	4.00	0.10	0.06
Count for SOT1-9 for Assam	32933	6014	1320	13309	817020	4006	46862	2946	1715
% Contribution of Assam for SOT1-9	3.56	0.65	0.14	1.44	88.22	0.43	5.06	0.32	0.19
Count for SOT1-9 for Jharkhand	100765	8884	5152	739934	25572	21514	70728	6489	1455
% Contribution of Jharkhand for SOT1-9	10.28	0.91	0.53	75.47	2.61	2.19	7.21	0.66	015
Count for SOT1-9 for Bihar	65972	11021	2235	16870	1342894	48850	97945	35459	1912
% Contribution of Bihar for SOT1-9	4.06	0.68	0.14	1.04	82.73	3.01	6.03	2.18	0.12

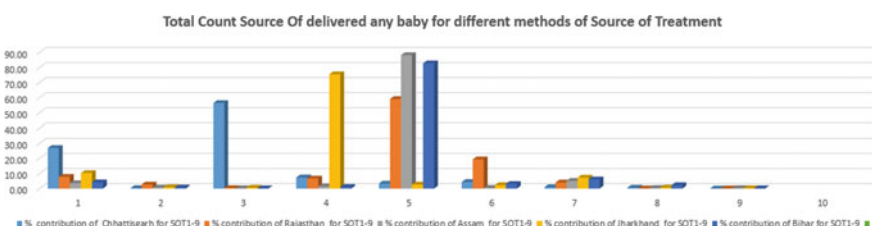
Table 3 Comparison of government versus private hospitals based on contribution of source of treatment for delivered baby

Data of different states in India showing the comparative status for government versus private hospitals (for delivered any baby)

State	Government	Private	Others	Total
Chhattisgarh	724336	10818	116	735270
% Comparative status for gov., private, and others for Chhattisgarh	98.51	1.47	0.02	
Rajasthan	935124	40017	549	975690
% Comparative status for gov., private, and others for Rajasthan	95.84	4.10	0.06	
Assam	874602	49808	1715	926125
% Comparative status for gov., private, &and others for Assam	94.44	5.38	0.19	
Jharkhand	901821	77217	1455	980493
% Comparative status for gov., private, and others for Jharkhand	91.98	7.88	0.15	
Bihar	1487842	133404	1912	1623158
% Comparative status for gov., private, and others for Bihar	91.66	8.22	0.12	

Table 4 Comparison of different classifiers machine learning algorithms

Model	Accuracy (%)	Standard deviation (%)	Runtime (s)
Naïve Bayes	94.2	±0.1	7
Decision tree	94.2	±0.1	5
Random forest	94.2	±0.1	34
Support vector machine	94.3	±0.3	21

**Fig. 5** Bar graph depicting % contribution of states for SOT1-9 methods (for delivered baby) of all age groups

Data of Different States in India showing the comparative status for Government versus Private hospitals (For delivered any baby)

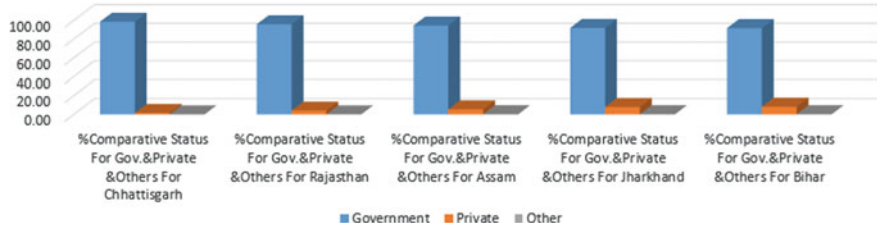


Fig. 6 Bar graph depicting comparison between government versus private hospitals of different states (for delivered baby)

Table 5 Contribution of source of treatment (in percentage) for delivered baby

Source of treatment	Government	Private	Others
Overall % of delivered baby from all sources (govt./private/others)	93.95	5.94	0.11

Case 3: For Assam state, SOT5 is the maximum effective treatment method, whereas SOT3 is the minimum effective method.

Case 4: For Jharkhand state, SOT4 is the maximum effective treatment method, whereas SOT9 is the minimum effective method.

Case 5: For Bihar state, SOT5 is the maximum effective treatment method, whereas SOT9 is the minimum effective method.

Table 3 and Fig. 6 represent the total count for delivered any baby case and compare the government and private hospitals. The graph represents that in Chhattisgarh, government hospitals give the maximum alive baby, whereas in Bihar private hospitals give the maximum alive baby.

3.1.5 Overall Comparison

The table depicts that the contribution of government hospital are maximum, i.e., 93.95%. It means government hospitals are chosen mostly (Table 5).

3.1.6 Performance Analysis of Different Classifying Machine Learning Algorithms

The different machine learning algorithms Naïve Bayes, Decision Tree, Random Forest, and Support Vector Machine have been compared based on various parameters such as accuracy, standard deviation and runtime. The comparison concluded that the Support Vector Machine has given highest accuracy, i.e., 94.3%. The standard

Overview

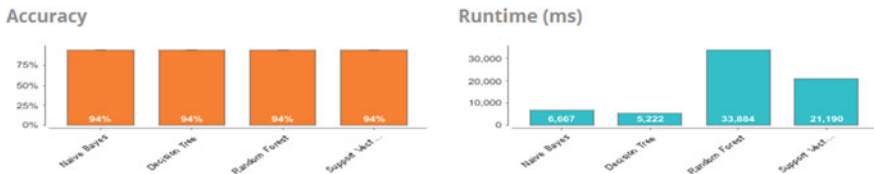


Fig. 7 Accuracy, standard deviation, and runtime for different classifiers

deviation is maximum in Support Vector Machine. The Decision Tree algorithm has taken minimum execution time, i.e., 5 s, and the Random Forest has taken maximum execution time, i.e., 34 s (Fig. 7).

4 Conclusion and Future Scope

As per the research work done, mostly government hospitals are chosen as a source of treatment. The comparison concluded that the Support Vector Machine [12] has given highest accuracy, whereas standard deviation is maximum in Support Vector Machine. The Decision Tree algorithm has taken minimum execution time, and the Random Forest has taken maximum execution time.

The same work can be extended for the other parts of India as well as beyond the country.

References

- Paul, V. K., et al.: Reproductive health, and child health and nutrition in India: meeting the challenge. *The Lancet* **377**, 332–349 (2011) (Elsevier)
- <https://economictimes.indiatimes.com/industry/healthcare/biotech/healthcare/economic-survey-2016-treatment-cost-at-private-hospitals-4-times-than-government-ones>
- Gülmезoglu, A. M., Crowther, C. A., Middleton, P., Heatley, E.: Induction of labour for improving birth outcomes for women at or beyond term. *Cochrane Database Syst. Rev.* (2012)
- <https://timesofindia.indiatimes.com/life-style/health-fitness/health-news/A-pregnant-woman-is-dying-every-5-minutes-in-India-Heres-why/articleshow/52866404.cms>
- Trasi, N.: Childbirth in India. *Encyclopaedia of the History of Science, Technology, and Medicine in Non-western Cultures*, pp. 538–540. Springer (2008)
- Dehbarez, N. T., Lou, S., Uldbjerg, N., Møller, A., Gyrd-Hansen, D., Søgaard, R.: Pregnant women's choice of birthing hospital: a qualitative study on individuals' preferences. *Women and Birth* **31**(6), 389–394 (2018)
- Sharmilan, S., Chaminda, H. T.: Pregnancy complications diagnosis using predictive data mining. In: Proceedings of the International Conference on Innovations in Info-business and Technology (2016)

8. Lakshmi, B. N., Indumathi, T. S., Ravi, N.: A comparative study of classification algorithms for predicting gestational risks in pregnant women. In: 2015 International Conference on Computers, Communications, and Systems (ICCCS), pp. 42–46. IEEE (2015)
9. Khosravi, P., Kazemi, E., Zhan, Q., Malmsten, J.E., Toschi, M., Zisimopoulos, P., Sigaras, A., et al.: Deep learning enables robust assessment and selection of human blastocysts after in vitro fertilization. *Nat. Partner J. Digital Med.* **2** (2019)
10. Hafiz, P., Nematollahi, M., Boostani, R., Jahromi, B.N.: Predicting implantation outcome of in vitro fertilization and intracytoplasmic sperm injection using data mining techniques. *Int. J. Fertil. Steril.* **11**(3), 184–190 (2017)
11. <https://www.kaggle.com>
12. Shao, Y., Lunetta, R.S.: Comparison of support vector machine, neural network, and CART algorithms for the land-cover classification using limited training data points. *ISPRS J. Photogrammetry. Remote Sens.* **70**, 78–87 (2012)

Ant Lion Optimization Technique for Minimization of Voltage Deviation Through Optimal Placement of Static VAR Compensator



Stita Pragnya Dash, K. R. Subhashini, and J. K. Satapathy

Abstract This paper deals with the use of flexible alternating current transmission system (FACTS) devices for the voltage improvement of the network. It is well established that FACTS devices can improve the system operation and management largely. However, the optimal location of such devices in the power systems is a crucial aspect and should be dealt with properly. In this work, the optimal location of static VAR compensator (SVC) is found out through a nature-inspired algorithm called ant lion optimization (ALO) for minimization of voltage deviation (V.D) at the buses. The simulations are done for standard IEEE 30 bus systems.

Keywords Voltage deviation · FACTS · ALO · SVC · Load factor

1 Introduction

The continuous process of hike in the demand for power which is an outcome of development and modernization has led to numerous challenges in front of power engineers. Moreover, the electricity market which used to be a monopoly-based service has become a highly competitive service with new technologies coming up in the area. Therefore, to overcome all the challenges and flaws, either the old system should be completely scrapped, a new installation incorporated or the existing systems should be reformed and revived to meet the current demand besides maintaining the quality. It is obvious that the second option is preferable since it would incur some extra investments which can be paid back instead of the loss that would be caused in case an entire new installation of the system is set up. This has been made easier by the incorporation of power electronic concepts in the area of power system which

S. P. Dash (✉) · J. K. Satapathy
National Institute of Technology Rourkela, Rourkela 769008, India
e-mail: titapragnya87@gmail.com

K. R. Subhashini · J. K. Satapathy
Department of Electrical Engineering, National Institute of Technology Rourkela, Rourkela, Odisha 769008, India

has led to the introduction of FACTS devices [1]. The use of FACTS devices in the power system has proved to be beneficial in more than one way. They help in loss minimization [2], voltage stability improvement [3], system loadability enhancement [4], voltage deviation reduction [5], system security maximization [6], congestion management [7] and the like. However, these devices will operate efficiently only if they are placed at appropriate locations and of proper ratings. The choice of location and the rating of the device to be placed should therefore be estimated with precision since in a network there are numerous possible locations and the ratings of FACTS devices are also many to choose from. This can be done through the application of optimization algorithms which are developed to choose the best possible solution in a n-dimensional search space.

Genetic algorithm (GA) was proposed for the optimal location of FACTS in IEEE networks in order to improve the loadability of the system [8] and to enhance the system security [6]. Similarly, differential evolution (DE) was preferred to find the optimal location of FACTS devices for the loss minimization [9], enhancement of the security of the system [10] and to increase the system load factor [11]. Swarm-based algorithm known as particle swarm optimization (PSO) has been dealt with in detail for this study by many researchers. PSO has been implemented in its natural as well as in modified or enhanced methods for placement of FACTS devices optimally with different objectives framed as functions [3, 12, 13]. Apart from these, other algorithms like touring ant colony optimization (TACO) [14] and cat swarm optimization (CSO) [15] have also been explored in the area of optimal location of FACTS devices. The importance of finding the best location is such that many algorithms have been hybridized with an aim of achieving a better solution in terms of the objective functions [16]. As discussed earlier, FACTS devices can be advantageous in many ways. Therefore, the objective of implementing such devices has been framed as multi-objective functions to achieve more than one benefit [17].

Ant lion optimization (ALO) has been a strong optimizing tool since 2015 [18]. ALO takes its inspiration from a species of insects called antlions who prey on ants. The mechanism of hunting the ants by the antlions into traps is mimicked as an algorithm for optimization. This algorithm has been tested for standard CEC benchmarks function as a validation test and for solving various engineering problems [19] including some specifically in the power sector [20, 21] as well as in other fields like antennae synthesis [22]. In this paper, ALO has been used to find the optimal location and size of shunt-connected FACTS device called static VAR compensator (SVC) in an IEEE 30 bus system to minimize the voltage deviation at buses. It is seen in [23] that VAR support is helpful in maintaining voltage stability which leads to lesser voltage deviation. Therefore, with proper VAR compensation at the buses, the voltage deviation can be reduced.

2 FACTS Allocation in the System

2.1 FACTS Description

The FACTS device considered here is static VAR compensator (SVC). It is a shunt-connected device which can exchange reactive power at the connected bus, thereby enabling both inductive as well as capacitive compensation. The schematic diagram of a SVC is given in Fig. 1. SVC is therefore modeled mathematically through the reactive power it compensates which is given by

$$Q_{\text{SVC},n} = -V_n^2 \times B_{\text{SVC}} \quad (1)$$

where V_n refers to the voltage of the n th bus and B_{SVC} stands for the equivalent susceptance of the SVC given as follows:

$$B_{\text{SVC}} = \frac{X_L - \frac{X_C}{\pi}(2(\pi - \alpha) + \sin(2\alpha))}{X_C * X_L} \quad (2)$$

where X_L and X_C are the inductive and capacitive reactance of the SVC and α is the firing angle of the thyristor. The range for the rating of SVC is chosen as follows:

$$-100 \text{ MVA} \leq Q_{\text{SVC},n} \leq 100 \text{ MVA}. \quad (3)$$

2.2 Problem Formulation

Objective Function In this paper, SVC is used for the improvement in voltage at the buses by minimizing the voltage deviation. In order to achieve this, an optimization problem is formulated with the following objective function

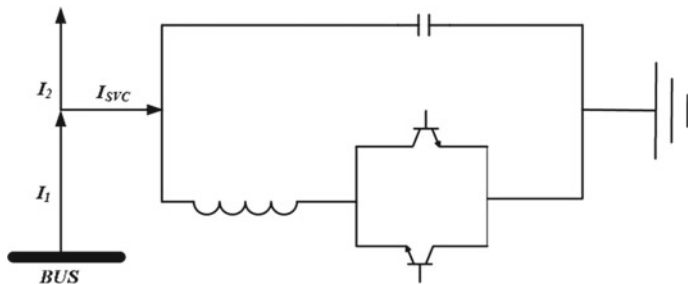


Fig. 1 Circuit diagram of SVC

$$\text{Minimize } J_V = \sqrt{\sum_{n=1}^{\text{NB}} (V_n - 1)^2} \quad (4)$$

where n is the bus number, $\text{NB} = 30$, and V_n is the magnitude of the voltage of n th bus.

Constraints The charm of optimization lies in searching the best possible solution satisfying the objective functions subject to equality and inequality constraints. The constraint for this problem is obtained from the standard operating condition of voltage within which the system must operate. Mathematically,

$$0.95 \leq V_n (\text{in p.u}) \leq 1.05 \quad (5)$$

3 Ant Lion Optimization—An Overview

Ant lion optimization technique is a nature-inspired, meta-heuristic optimization algorithm developed by Mirjalili. ALO imitates the hunting behavior of antlions in trapping ants in nature.

3.1 Basic Concept of Ant Lions

The creatures take their name from their behavior and food which are mostly ants. These predators in their larvae stage of life digs a cone-shaped burrow in the sand by moving in a circular path inward and pushing out the sand. It hides itself inside the pit and waits for insects to be caught inside. The shape of the conical pit and sharp edges force the prey to fall to the inner tip of the cone where the antlion pulls it inside with its jaw for consumption depicted in Fig. 2.

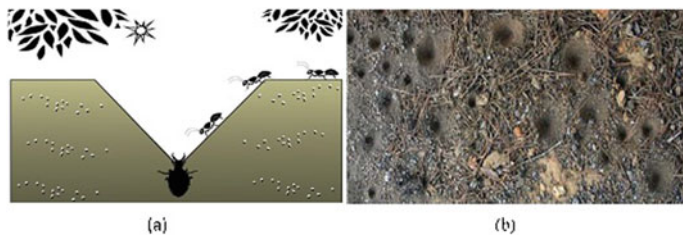


Fig. 2 Cone-shaped traps and hunting behavior of antlions [18]

3.2 Mathematical Modeling of the ALO

The algorithm replicates the mechanism used by antlions for capturing their prey. Therefore, the study is done where the antlions trap the ants and become fitter than the ants which are freely moving in the search space.

Variables in the Algorithm The position of the ants referring to the variables that are optimized in the algorithm (equivalent to the location and rating of SVC in this problem) is stored in the form of a matrix shown below:

$$P_{\text{ant}} = \begin{bmatrix} a_1 \\ \vdots \\ a_n \end{bmatrix} = \begin{bmatrix} a_{11} & a_{12} & a_{13} & \dots & a_{1d} \\ a_{21} & a_{22} & a_{23} & \dots & a_{2d} \\ \vdots & \vdots & \vdots & \ddots & \vdots \\ a_{n1} & a_{n2} & a_{n3} & \dots & a_{nd} \end{bmatrix} \quad (6)$$

where a_{ij} refers to the $i = (1, n)$ position of the ant in a $j = (1, d)$ dimension search space where n is the population number of ants and d is the dimension of search space. These variables when substituted in the objective function (referring to the voltage deviation as in Eq. 4) yield a matrix called the fitness of ants given by

$$\text{Fit}_{\text{ant}} = [\text{Fit}(a_1) \dots \text{Fit}(a_n)]^T \quad (7)$$

Similarly, the antlions which are also present in the search space and hiding in pits have a position in the search space (equivalent to the location and rating os SVC in this problem) given by

$$P_{\text{antlion}} = \begin{bmatrix} al_1 \\ \vdots \\ al_n \end{bmatrix} = \begin{bmatrix} al_{11} & al_{12} & al_{13} & \dots & al_{1d} \\ al_{21} & al_{22} & al_{23} & \dots & al_{2d} \\ \vdots & \vdots & \vdots & \ddots & \vdots \\ al_{n1} & al_{n2} & al_{n3} & \dots & al_{nd} \end{bmatrix} \quad (8)$$

Therefore, these antlions with positions similar to ants correspond to a fitness function (referring to the voltage deviation as in Eq. 4) given as follows:

$$\text{Fit}_{\text{antlion}} = [\text{Fit}(al_1) \dots \text{Fit}(al_n)]^T \quad (9)$$

Random Walk of Ants The ants move about in a probable area in search of food; therefore, their movement is analyzed as a random walk given by the expression as follows:

$$W(k) = [0, \text{csum}(2w(k_1) - 1), \text{csum}(2w(k_2) - 1), \dots, \text{csum}(2w(k_{\text{kmax}}) - 1)] \quad (10)$$

where csum calculates the cumulative sum, k refers to the iteration number, kmax denotes the maximum number of iterations and $w(k)$ is given by

$$w(k) = \begin{cases} 1 & \text{if rand} > 0.5 \\ 0 & \text{if rand} \leq 0.5 \end{cases} \quad (11)$$

where rand is a random number generated between (0, 1). The ants move around the search space randomly to change their positions as given in Eq. 10. However, the position of ants inside the search space and in order to prevent them from going out of the search space normalization is done as per the equation:

$$W_i(k) = \frac{(W_i(k) - a_i(k)) \times (d_i(k) - c_i(k))}{(b_i(k) - a_i(k))} + c_i(k) \quad (12)$$

where $a_i(k)$ is the minimum of random walk of i_{th} variable, $b_i(k)$ is the maximum of random walk in i_{th} variable, $c_i(k)$ is the minimum of i_{th} variable at k_{th} iteration, and $d_i(k)$ indicates the maximum of i_{th} variable at k_{th} iteration.

Trapping in Pits The random walk of ants is affected by the pits created by the antlions. This natural phenomenon can be mathematically represented as Eqs. 13 and 14 where $c_i(k)$ and $d_i(k)$ are already defined.

$$c_i(k) = al_j(k) + c_i(k) \quad (13)$$

$$d_i(k) = al_j(k) + d_i(k) \quad (14)$$

These equations define the space in hyperplane where ants move about, around the traps made by the hidden antlions.

Building of Trap In order to select the fittest, antlion which is solely governed by their ability to catch ants is represented as a roulette wheel model.

Movement of Ants Toward Ant Lions The fitness of the antlion is established by its ability to trap ants when compared to its peers. The antlion accomplishes this task by throwing sand toward the upper periphery of the conical burrow once the ant has started entering it. This makes it difficult for the ant to crawl back as it slips inward toward the decreasing diameter of the cone. This is represented by the following equations:

$$c_i(k) = \frac{c_i(k)}{I_a} \quad (15)$$

$$d_i(k) = \frac{d_i(k)}{I_a} \quad (16)$$

where $c_i(k)$ and $d_i(k)$ are described above, and I_a is an adaption factor given by:

$$I_a = \frac{10^t * k}{k_{\max}}. \quad (17)$$

where k is the current iteration number of the maximum number of iterations given by k_{\max} and t is an integer whose values vary as given in [18].

Catching Ant and Re-Building of Trap This step involves the evaluation of the fitness function given by Eqs. 7 and 9 based on the positions of ants and antlions. The position of the antlion is then updated to the latest hunted ant with a motive of further exploration of the search space and possibility of better results. The update process is then done as the following equation:

$$al_j(k) = a_i(k) \text{ if } \text{Fit}_{\text{ant}_i}(k) > \text{Fit}_{\text{antlion}_j}(k) \quad (18)$$

The Elite This is an important step in the algorithm where retention of the best results from all the solutions obtained is done. Since the elite represents the fittest antlion, it influences the movement of all the ants around it. Therefore, it is presumed that each ant walks randomly around a definite antlion through the roulette wheel selection and elite retention processes simultaneously. The mathematical formulation of this step is done as follows:

$$a_i(k) = \frac{r_{al}(k) + r_e(k)}{2} \quad (19)$$

where $r_a(k)$ represents the random walk around antlion in k th iteration, $r_e(k)$ gives the random walk around elite in k th iteration, and $a_i(k)$ is the position of i th ant in k th iteration.

4 Application and Results

The ALO algorithm is applied to optimally locate three SVCs in a standard IEEE 30 bus system [24] for different cases. The simulations were carried using a MATLAB 2016 software in a 2.60 GHz i5 PC with 8 GB RAM. The experiment is carried out for five independent runs with a population size of 50 and the dimension of search space being 6.

4.1 Case 1: Load Factor Multiplied with Real and Reactive Power of Load

The real and reactive power demand of the load are incremented by 1.6 times in this case. The appropriate location and rating of SVC are found out using ALO for the study mentioned in Table 1. The voltage profile of the weak buses is shown in Fig. 3.

Table 1 Optimal location of SVC

Location (bus number)	8	15	27
Ratings (MVAR)	18	20	25

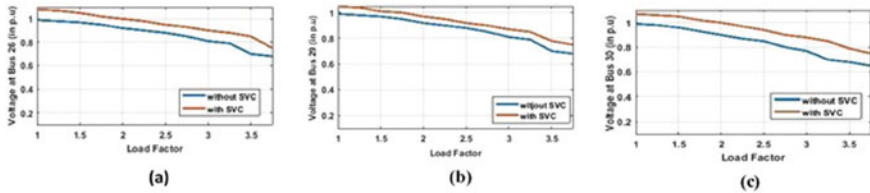


Fig. 3 Voltage at weak buses with and without SVC

Table 2 Optimal location of SVC

Location (bus number)	10	18	22
Ratings (MVAR)	14	27	36

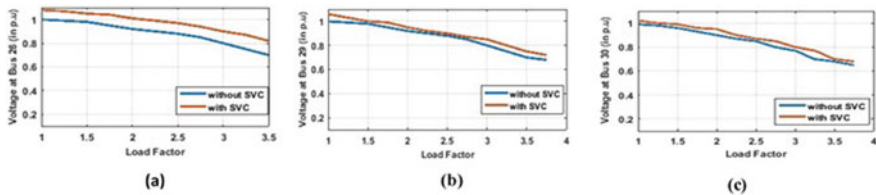


Fig. 4 Voltage at weak buses with and without SVC

It is clearly visible that the degree of voltage deviation is reduced for increased load factor when SVC is incorporated. The voltage at bus 26, bus 29 and bus 30 is seen to lie within a limit of 0.95 p.u to 1.05 p.u for a load factor of 2.25, 2.5 and 2.25, respectively, with SVC in comparison with a load factor of 1.75, 1.75 and 1.5 when SVC is not added to the 30 bus system.

4.2 Case 2: Load Factor Multiplied with Real and Reactive Power of Generator and Load

In this case, the active and reactive power of both load and generator are increased by a factor of 1.6. The increase in generator reactive power is done with an intention of increment in the demand in future. The optimal location and rating of SVC obtained through ALO for the decided objective are given in Table 2. The effect of adding SVC is visible in the reduction in voltage deviation at the weak buses for increased loading on the system (generator and load) as in Fig. 4. Likely to the previous case, in this case also the buses under consideration seem to have their voltages within permissible limits for a loading of 2.25, 2.0 and 2.0 with SVC-aided system in comparison with a load factor of 1.75, 1.75 and 1.5 when SVC is not added to the 30 bus system.

5 Conclusion

In this paper, ALO algorithm is studied through application to a IEEE 30 bus system for the minimization of voltage deviation using SVC. The work amplifies the role of a shunt compensation device in the improvement of voltage at the buses. The study has been conducted for two different cases considering the pattern in change of load factor at the generating and receiving ends. The algorithm is seen to give faster convergence which is shown in the figures as well. It is also seen that the incorporation of SVC in the system results in maintaining the voltage within prescribed limits for a greater load factor in comparison with system without any such compensation.

References

1. Hingorani, N.G., Gyugyi, L., El-Hawary, M.: Understanding FACTS: Concepts and Technology of Flexible AC Transmission Systems, vol. 1. IEEE Press, New York (2000)
2. Rashed, G.I., Sun, Y., Shaheen, H.: Optimal location and parameter setting of TCSC for loss minimization based on differential evolution and genetic algorithm. *Phys. Proc.* **33**, 1864–1878 (2012)
3. Kumarasamy, K., Raghavan, R.: Particle swarm optimization algorithm for voltage stability improvement using multiple statcom. In: 2012 International Conference on Emerging Trends in Electrical Engineering and Energy Management (ICETEEEM), pp. 235–242. IEEE, New York (2012)
4. Ongsakul, W., Jirapong, P.: Optimal allocation of facts devices to enhance total transfer capability using evolutionary programming. In: IEEE International Symposium on Circuits and Systems, 2005. ISCAS 2005, pp. 4175–4178. IEEE, New York (2005)
5. Sundareswaran, K., Nayak, P.S., Venkatesh, C.D., Hariharan, B.: Optimal placement of facts devices using probabilistic particle swarm optimization. In: ISGT2011-India, pp. 53–58. IEEE, New York (2011)
6. Gerbex, S., Cherkaoui, R., Germond, A.: Optimal location of facts devices to enhance power system security. In: 2003 IEEE Bologna Power Tech Conference Proceedings, vol. 3, pp. 7–pp. IEEE, New York (2003)
7. Bhattacharyya, B., Kumar, S.: Approach for the solution of transmission congestion with multi-type facts devices. *IET Gener. Trans. Distrib.* **10**(11), 2802–2809 (2016)
8. Gerbex, S., Cherkaoui, R., Germond, A.J.: Optimal location of multi-type facts devices in a power system by means of genetic algorithms. *IEEE Trans. Power Syst.* **16**(3), 537–544 (2001)
9. Rashed, G.I., Sun, Y., Shaheen, H.: Optimal TCSC placement in a power system by means of differential evolution algorithm considering loss minimization. In: 2011 6th IEEE Conference on Industrial Electronics and Applications, pp. 2209–2215. IEEE, New York (2011)
10. Baghaee, H., Vahidi, B., Jazebi, S., Gharehpetian, G., Kashefi, A.: Power system security improvement by using differential evolution algorithm based facts allocation. In: Joint International Conference on Power System Technology and IEEE Power India Conference, 2008. POWERCON 2008, pp. 1–6. IEEE, New York (2008)
11. Bhattacharyya, B., Goswami, S.: Optimal planning for the placement of facts devices by differential evolution technique for the increased loadability of a power system. In: 2012 Asia-Pacific Power and Energy Engineering Conference, pp. 1–4. IEEE, New York (2012)
12. Jumaat, S.A., Musirin, I., Othman, M.M., Mokhlis, H.: Placement and sizing of thyristor controlled series compensator using PSO based technique for loss minimization. In: 2012 IEEE

- International Power Engineering and Optimization Conference Melaka, Malaysia, pp. 285–290. IEEE, New York (2012)
- 13. Ravi, K., Rajaram, M.: Optimal location of facts devices using improved particle swarm optimization. *Int. J. Electr. Power Energy Syst.* **49**, 333–338 (2013)
 - 14. Sreejith, S., Chandrasekaran, K., Simon, S.P.: Touring ant colony optimization technique for optimal power flow incorporating thyristor controlled series compensator. In: World Congress on Nature & Biologically Inspired Computing, 2009. NaBIC 2009, pp. 1127–1132. IEEE, New York (2009)
 - 15. Nireekshana, T., Rao, G.K., Raju, S.S.: Available transfer capability enhancement with FACTS using Cat swarm optimization. *Ain Shams Eng. J.* **7**(1), 159–167 (2016)
 - 16. Sundareswaran, K., Bharathram, P., Siddharth, M., Vaishnavi, G., Shrivastava, N.A., Sarma, H.: Voltage profile enhancement through optimal placement of facts devices using queen-bee-assisted GA. In: International Conference on Power Systems, 2009. ICPS'09, pp. 1–5. IEEE, New York (2009)
 - 17. Ara, A.L., Kazemi, A., Niaki, S.N.: Multiobjective optimal location of facts shunt-series controllers for power system operation planning. *IEEE Trans. Power Delivery* **27**(2), 481–490 (2012)
 - 18. Mirjalili, S.: The ant lion optimizer. *Adv. Eng. Softw.* **83**, 80–98 (2015)
 - 19. Mirjalili, S., Jangir, P., Saremi, S.: Multi-objective ant lion optimizer: a multi-objective optimization algorithm for solving engineering problems. *Appl. Intell.* **46**(1), 79–95 (2017)
 - 20. Trivedi, I.N., Jangir, P., Parmar, S.A.: Optimal power flow with enhancement of voltage stability and reduction of power loss using ant-lion optimizer. *Cogent Eng.* **3**(1), 1208942 (2016)
 - 21. Ali, E., Elazim, S.A., Abdelaziz, A.: Optimal allocation and sizing of renewable distributed generation using ant lion optimization algorithm. *Electr. Eng.* **100**(1), 99–109 (2018)
 - 22. Subhashini, K.R., Satapathy, J.K.: Development of an enhanced ant lion optimization algorithm and its application in antenna array synthesis. *Appl. Soft Comput.* **59**, 153–173 (2017)
 - 23. Balamurugan, G., Aravindhbabu, P.: Online var support estimation for voltage stability enhancement. *Int. J. Electr. Power Energy Syst.* **49**, 408–413 (2013)
 - 24. Wood, A.J., Wollenberg, B.: Power Generation, Operation, and Control. Wiley, New York, NY (1996)

On Vector Variational Inequalities and Vector Optimization Problems



B. B. Upadhyay and Priyanka Mishra

Abstract This article deals with the relations among Minty and Stampacchia vector variational inequalities and vector optimization problems involving strongly convex functions of higher order. A numerical example has been given to justify the significance of these results. Moreover, we employ KKM–Fan theorem to establish the existence of the solutions for the considered Minty and Stampacchia vector variational inequalities.

Keywords Efficient minimizers · KKM-Fan theorem · Strongly convex functions

1 Introduction

Convexity and generalized convexity have wider applications in optimization theory, engineering, economics, probability theory, and the calculus of variations, see [12, 27, 29] and the references therein. In many real-life problems, the condition of convexity is not always met, therefore in order to generalize the notion of convexity, Mangasarian [22] introduced the notion of pseudoconvex functions. Karamardian and Schaible [16] introduced the notion of strong convexity. Later, Lin and Fukushima [20] defined the class of strongly convex functions of order κ , $\kappa \geq 1$.

In the study of multiobjective optimization problems, the concept of efficient optimal solutions has been studied extensively by several authors [5, 6, 8, 13, 15]. However, in several real-world problems, approximate efficient solutions appear frequently as the algorithms for multiobjective optimization problems terminate finitely and produce efficient solutions with error, for more exposition, see [17, 28, 32]. Cromme [4] studied the notion of strict local minimizers while studying convergence of iterative numerical techniques.

B. B. Upadhyay · P. Mishra (✉)

Department of Mathematics, Indian Institute of Technology Patna, Patna, Bihar 801106, India
e-mail: priyanka.iitp14@gmail.com

B. B. Upadhyay
e-mail: bhooshan@iitp.ac.in

Hartman and Stampacchia [14] introduced the notion of variational inequality while studying some specific classes of partial differential equations. In finite dimension, Giannessi [10] introduced the concept of vector variational inequality (for short, (VVI)). Vector Variational inequalities are either known as Stampacchia vector variational inequalities (for short, (SVVI)) [30] or in the form of Minty vector variational inequalities (for short, (MVVI)) [23]. In literature, most of the scholars discussed applications of (MVVI) and (SVVI) for the vector optimization problem (for short, (VOP)), for more expositions, see [2, 3, 9, 11, 18, 24, 25, 31, 32] and the references cited therein. Lee [18] has studied the relations among (VOP), (MVVI), and (SVVI) for smooth as well as nonsmooth cases involving convex functions. Mishra and Upadhyay [25] studied the equivalence between the quasi-efficient solution for (VOP) and the solution of (VVI) under nonsmooth generalized approximate convexity hypotheses. Al-Homidan and Ansari [1] studied the weak formulation of (MVVI) and (SVVI) and established the relations among the solution of (MVVI), (SVVI), and weak Pareto solution of the (VOP) for the nonsmooth case. Recently, Oveissha and Zafarani [21] established the relationship between (VOP) and (MVVI) using α -invex function in Asplund spaces.

Motivated by the works of Al-Homidan and Ansari [1], Upadhyay et al. [31], Li and Yu [19], and Mishra and Wang [26], we consider a class of (VOP) and two types of (VVI) namely: (MVVI) and (SVVI). We study the relations among the solutions of considered (MVVI) and (SVVI) and efficient minimizer of order (κ) of (VOP) under the hypotheses of strong convexity of order (κ) . To justify the significance of these results, a numerical example is also given. Furthermore, KKM–Fan theorem is employed to establish the existence of the solutions of (MVVI) and (SVVI).

We organize this paper as follows. In Sect. 2 of this paper, we recall some basic definitions and preliminaries. In Sect. 3, we establish the relationship among the solutions of (MVVI), (SVVI), and efficient minimizer of order (κ) of (VOP) for strongly convex functions of order (κ) . In Sect. 4, employing KKM–Fan theorem we establish some conditions under which the solution of (MVVI) and (SVVI) exist.

2 Definitions and Preliminaries

Let $-\mathbb{R}_+^n$ denote nonpositive orthant of \mathbb{R}^n . $\mathbf{0}$ denotes the zero vector in \mathbb{R}^n . Let $\text{int } \mathbb{R}^n$ denote the interior of \mathbb{R}^n and $\Gamma \neq \emptyset$ be a subset of \mathbb{R}^n equipped with Euclidean norm $\|\cdot\|$. Convex hull of $\{z_1, z_2, \dots, z_n\} \subseteq \Gamma$ will be denoted by $\text{co } \{z_1, z_2, \dots, z_n\}$.

For $y, z \in \mathbb{R}^n$, the following notions for inequalities will be used in this paper.

1. $y - z \in -\mathbb{R}_+^n \iff y_j \leq z_j, \quad j = 1, 2, \dots, n;$
2. $y - z \in -\mathbb{R}_+^n \setminus \{\mathbf{0}\} \iff y_j \leq z_j, \quad j = 1, 2, \dots, n, \quad j \neq j_0 \text{ with } y_{j_0} < z_{j_0},$
for some j_0 ;
3. $y - z \in -\text{int } \mathbb{R}_+^n \iff y_j < z_j, \quad j = 1, 2, \dots, n.$

The following definitions are from [31].

Definition 1 The set Γ is said to be a convex set, if for any $z_1, z_2 \in \Gamma$ and for all $\mu \in [0, 1]$, one has

$$z_2 + \mu(z_1 - z_2) \in \Gamma.$$

Throughout the paper, Γ will be a convex set, and $g : \Gamma \rightarrow \mathbb{R}$ be a differentiable real-valued function defined on Γ , unless otherwise specified.

Definition 2 $g : \Gamma \rightarrow \mathbb{R}$ is a strongly convex function of order κ ($\kappa \geq 1$) on Γ , if for any $z_1, z_2 \in \Gamma$ and for all $\mu \in [0, 1]$, there exists $\alpha > 0$, such that

$$g(\mu z_2 + (1 - \mu)z_1) \leq \mu g(z_2) + (1 - \mu)g(z_1) - \alpha\mu(1 - \mu) \|z_2 - z_1\|^\kappa.$$

Definition 3 [20] A function $g : \Gamma \rightarrow \mathbb{R}$ is strongly convex of order κ ($\kappa \geq 1$) on Γ , if for all $z_1, z_2 \in \Gamma$, there exists $\alpha > 0$, such that

$$g(z_2) - g(z_1) \geq \langle \nabla g(z_1), z_2 - z_1 \rangle + \alpha \|z_2 - z_1\|^\kappa.$$

Definition 4 [20] A mapping $G : \mathbb{R}^n \rightarrow \mathbb{R}^n$ is called strongly monotone of order κ ($\kappa \geq 1$) on Γ , if for all $z_1, z_2 \in \Gamma$, there exists $\alpha > 0$, such that

$$\langle G(z_2) - G(z_1), z_2 - z_1 \rangle \geq \alpha \|z_2 - z_1\|^\kappa.$$

Now, we state the following lemma from [7] which relates strong monotonicity and strong convexity of order κ , $\kappa \geq 1$.

Lemma 1 Let $g : \Gamma \rightarrow \mathbb{R}$ is strongly convex function of order κ , then its gradient is strongly monotone of order κ , that is, for all $z_1, z_2 \in \Gamma$, one has

$$\langle \nabla g(z_2) - \nabla g(z_1), z_2 - z_1 \rangle \geq \alpha \|z_2 - z_1\|^\kappa.$$

Now, we state the mean value theorem from [22] that will be used in the sequel.

Theorem 1 Let $g : \Gamma \rightarrow \mathbb{R}$ and let $z_1, z_2 \in \Gamma$. Then, there exist some $\mu \in (0, 1)$, such that

$$g(z_2) = g(z_1) + \langle \nabla g[z_1 + \mu(z_2 - z_1)], z_2 - z_1 \rangle$$

□

We study vector optimization problem in the following form.

$$\begin{aligned} (\text{VOP}) \quad & \text{Minimize } g(z) = (g_1(z), \dots, g_p(z)) \\ & \text{subject to } z \in \Gamma, \end{aligned}$$

where $g_j : \Gamma \rightarrow \mathbb{R}$, $j \in \mathcal{J} := \{1, 2, \dots, p\}$.

Definition 5 [31] A point $z_o \in \Gamma$ is called an efficient minimizer of order κ of (VOP), if there exists a constant $\alpha \in \text{int}\mathbb{R}_+^p$, such that

$$(g_1(z) - g_1(z_o) - \alpha_1 \|z - z_o\|^\kappa, \dots, g_p(z) - g_p(z_o) - \alpha_p \|z - z_o\|^\kappa) \notin -\mathbb{R}_+^p \setminus \{\mathbf{0}\}, \quad \forall z \in \Gamma.$$

Now, we formulate the Minty- and Stampacchia-type vector variational inequalities in terms of gradients given in [18]:

(MVVI): find $z_o \in \Gamma$, such that, for all $z \in \Gamma$, one has

$$(\langle \nabla g_1(z), z - z_o \rangle, \dots, \langle \nabla g_p(z), z - z_o \rangle) \notin -\mathbb{R}_+^p \setminus \{\mathbf{0}\}.$$

(SVVI): find $z_o \in \Gamma$, such that, for all $z \in \Gamma$, one has

$$(\langle \nabla g_1(z_o), z - z_o \rangle, \dots, \langle \nabla g_p(z_o), z - z_o \rangle) \notin -\mathbb{R}_+^p \setminus \{\mathbf{0}\}.$$

3 Relationship Between (MVVI), (SVVI), and (VOP)

In this section, using the concept of strong convexity of order κ , we establish certain relations between the efficient minimizer of order κ of (VOP) and the solutions of (MVVI) and (SVVI).

Theorem 2 Let each g_j , $j \in \mathcal{J}$ be strongly convex function of order κ on Γ . A point $z_o \in \Gamma$ is an efficient minimizer of order κ of (VOP) iff z_o solves (MVVI).

Proof Let $z_o \in \Gamma$ be an efficient minimizer of order κ of (VOP). Then, for all $z \in \Gamma$, there exists $\alpha \in \text{int}\mathbb{R}_+^p$, such that

$$(g_1(z) - g_1(z_o) - \alpha_1 \|z - z_o\|^\kappa, \dots, g_p(z) - g_p(z_o) - \alpha_p \|z - z_o\|^\kappa) \notin -\mathbb{R}_+^p \setminus \{\mathbf{0}\}. \quad (1)$$

Since, each g_j , $j \in \mathcal{J}$ is strongly convex of order κ , hence for all $z \in \Gamma$, we have

$$g_j(z_o) - g_j(z) \geq \langle \nabla g_j(z), z_o - z \rangle + \alpha_j \|z_o - z\|^\kappa, \quad \forall j \in \mathcal{J}. \quad (2)$$

From (2), we get

$$g_j(z) - g_j(z_o) \leq \langle \nabla g_j(z), z - z_o \rangle - \alpha_j \|z - z_o\|^\kappa, \quad \forall j \in \mathcal{J}. \quad (3)$$

Since $\alpha_j > 0$, from (3), we get

$$g_j(z) - g_j(z_o) - \alpha_j \|z - z_o\|^\kappa \leq \langle \nabla g_j(z), z - z_o \rangle - 2\alpha_j \|z - z_o\|^\kappa, \quad \forall j \in \mathcal{J}. \quad (4)$$

From (1) and (4), for all $z \in \Gamma$, we get

$$(\langle \nabla g_1(z), z - z_o \rangle, \dots, \langle \nabla g_p(z), z - z_o \rangle) \notin -\mathbb{R}_+^p \setminus \{\mathbf{0}\}.$$

Hence, z_o is a solution of (MVVI).

Conversely, Let $z_o \in \Gamma$ solves (MVVI), but not an efficient minimizer of order κ of (VOP). Then, there exist $z \in \Gamma$, such that for any $\alpha \in \text{int } \mathbb{R}_+^p$, we get

$$(g_1(z) - g_1(z_o) - \alpha_1 \|z - z_o\|^\kappa, \dots, g_p(z) - g_p(z_o) - \alpha_p \|z - z_o\|^\kappa) \in -\mathbb{R}_+^p \setminus \{\mathbf{0}\}. \quad (5)$$

Let $q(\mu) := z + \mu(z_o - z)$, $\mu \in [0, 1]$. From the convexity of Γ , $q(\mu) \in \Gamma$.

Since each g_j , $j \in \mathcal{J}$ is strongly convex of order κ . Hence, for any $\mu \in [0, 1]$, there exists $\alpha \in \text{int } \mathbb{R}_+^p$, such that, for all $j \in \mathcal{J}$, we have

$$g_j(q(\mu)) = g_j(z + \mu(z_o - z)) \leq \mu g_j(z_o) + (1 - \mu)g_j(z) - \mu(1 - \mu)\alpha_j \|z - z_o\|^\kappa. \quad (6)$$

From (6), for each $\mu \in [0, 1]$, we get

$$g_j(z + \mu(z_o - z)) - g_j(z_o) \leq (\mu - 1)[g_j(z_o) - g_j(z) + \mu\alpha_j \|z - z_o\|^\kappa], \quad \forall j \in \mathcal{J}. \quad (7)$$

From (7), for all $\mu \in (0, 1)$, we get

$$\frac{g_j(q(\mu)) - g_j(q(1))}{(\mu - 1)} \geq g_j(z_o) - g_j(z) + \hat{\alpha}_j \|z - z_o\|^\kappa, \quad \text{where } \hat{\alpha}_j = \mu\alpha_j. \quad (8)$$

From Theorem 1, we can get $\mu_j \in (0, 1)$ and $q(\mu_j) = z + \mu_j(z_o - z)$, such that

$$\langle \nabla g_j(q(\mu_j)), z_o - z \rangle \geq g_j(z_o) - g_j(z) + \hat{\alpha}_j \|z - z_o\|^\kappa, \quad \forall j \in \mathcal{J}. \quad (9)$$

Suppose that $\mu_1, \mu_2, \dots, \mu_p$ are all equal to μ . From (5) and (9), we have

$$(\langle \nabla g_1(q(\mu)), z - z_o \rangle, \dots, \langle \nabla g_p(q(\mu)), z - z_o \rangle) \in -\mathbb{R}_+^p \setminus \{\mathbf{0}\}. \quad (10)$$

Multiplying (10) by $(1 - \mu)$, we get

$$(\langle \nabla g_1(q(\mu)), q(\mu) - z_o \rangle, \dots, \langle \nabla g_p(q(\mu)), q(\mu) - z_o \rangle) \in -\mathbb{R}_+^p \setminus \{\mathbf{0}\}.$$

This implies that z_o does not solve (MVVI). This contradicts our assumption.

Now, suppose that $\mu_1, \mu_2, \dots, \mu_p$ are not all equal. Let us assume, $\mu_k \neq \mu_l$, $k, l \in J$, $k \neq l$, then from (9), we get

$$\langle \nabla g_k(q(\mu_k)), z - z_o \rangle \leq g_k(z) - g_k(z_o). \quad (11)$$

$$\langle \nabla g_l(q(\mu_l)), z - z_o \rangle \leq g_l(z) - g_l(z_o). \quad (12)$$

Since g_k and g_l are strongly convex of order κ , hence, from Lemma 1, ∇g_k and ∇g_l are strongly monotone of order κ .

$$\langle \nabla g_k(q(\mu_k)) - \nabla g_k(q(\mu_l)), q(\mu_k) - q(\mu_l) \rangle \geq \alpha_k \|q(\mu_k) - q(\mu_l)\|^\kappa. \quad (13)$$

Similarly,

$$\langle \nabla g_l(q(\mu_k)) - \nabla g_l(q(\mu_l)), q(\mu_k) - q(\mu_l) \rangle \geq \alpha_l \|q(\mu_k) - q(\mu_l)\|^\kappa. \quad (14)$$

If $\mu_l > \mu_k$, then from (13), there exists $\bar{\alpha}_k > 0$, such that

$$\bar{\alpha}_k \|z - z_o\|^\kappa \leq \langle \nabla g_k(q(\mu_k)) - \nabla g_k(q(\mu_l)), z - z_o \rangle. \text{ where } \bar{\alpha}_k = (\mu_l - \mu_k)^\kappa - 1 \quad (15)$$

From (15), we get

$$\langle \nabla g_k(q(\mu_k)), z - z_o \rangle \geq \langle \nabla g_k(q(\mu_l)), z - z_o \rangle + \bar{\alpha}_k \|z - z_o\|^\kappa, \text{ where } \bar{\alpha}_k = (\mu_l - \mu_k)^{\kappa-1}.$$

From (11), we get

$$g_k(z) - g_k(z_o) \geq \langle \nabla g_k(q(\mu_l)), z - z_o \rangle + \bar{\alpha}_k \|z - z_o\|^\kappa.$$

If $\mu_k > \mu_l$, then from (14),

$$\bar{\alpha}_l \|z - z_o\|^\kappa \leq \langle \nabla g_l(q(\mu_l)) - \nabla g_l(q(\mu_k)), z - z_o \rangle. \text{ where } \bar{\alpha}_l = (\mu_k - \mu_l)^\kappa - 1 \quad (16)$$

From (16), we get

$$\langle \nabla g_l(q(\mu_k)), z - z_o \rangle + \bar{\alpha}_l \|z - z_o\|^\kappa \leq \langle \nabla g_l(q(\mu_l)), z - z_o \rangle, \text{ where } \bar{\alpha}_l = (\mu_k - \mu_l)^{\kappa-1}.$$

From (12), it follows that

$$\langle \nabla g_l(q(\mu_k)), z - z_o \rangle + \bar{\alpha}_l \|z - z_o\|^\kappa \leq g_l(z) - g_l(z_o).$$

Let, $\bar{\mu} \in (0, 1)$, such that $\bar{\mu} = \min \{\mu_k, \mu_l\}$, and sufficiently small, then we get

$$g_j(z) - g_j(z_o) - \bar{\alpha}_j \|z - z_o\|^\kappa \geq \langle \nabla g_j(q(\bar{\mu})), z - z_o \rangle, \text{ for any } j = k, l.$$

Continuing in this way, let $\mu^* = \min \{\mu_1, \mu_2, \dots, \mu_p\}$, such that

$$g_j(z) - g_j(z_o) - \bar{\alpha}_j \|z - z_o\|^\kappa \geq \langle \nabla g_j(q(\mu^*)), z - z_o \rangle, \forall j \in \mathcal{J}. \quad (17)$$

From (5) and (17), we get

$$\langle \nabla g_1(q(\mu^*)), z - z_o \rangle, \dots, \langle \nabla g_p(q(\mu^*)), z - z_o \rangle \in -\mathbb{R}_+^p \setminus \{\mathbf{0}\}. \quad (18)$$

Multiplying (18) by $1 - \mu^*$, we get

$$(\langle \nabla g_1(q(\mu^*)), q(\mu^*) - z_o \rangle, \dots, \langle \nabla g_p(q(\mu^*)), q(\mu^*) - z_o \rangle) \in -\mathbb{R}_+^p \setminus \{\mathbf{0}\},$$

which is a contradiction. \square

Theorem 3 Let each g_j , $j \in \mathcal{J}$ be strongly convex function of order κ on Γ . If $z_o \in \Gamma$ solves (SVVI), then z_o is an efficient minimizer of order κ of (VOP).

Proof Assume that $z_o \in \Gamma$ solves (SVVI), then for any $z \in \Gamma$, we get

$$(\langle \nabla g_1(z_o), z - z_o \rangle, \dots, \langle \nabla g_p(z_o), z - z_o \rangle) \notin -\mathbb{R}_+^p \setminus \{\mathbf{0}\}. \quad (19)$$

Since each g_j , $j \in \mathcal{J}$ is strongly convex function of order κ , then for all $z \in \Gamma$, there exists $\alpha \in \text{int } \mathbb{R}_+^p$, such that

$$\langle \nabla g_j(z_o), z - z_o \rangle + \alpha_j \|z - z_o\|^\kappa \leq g_j(z) - g_j(z_o). \quad (20)$$

From (19) and (20), we get

$$(g_1(z) - g_1(z_o) - \alpha_1 \|z - z_o\|^\kappa, \dots, g_p(z) - g_p(z_o) - \alpha_p \|z - z_o\|^\kappa) \notin -\mathbb{R}_+^p \setminus \{\mathbf{0}\}.$$

Hence, $z_o \in \Gamma$ is an efficient minimizer of order κ of (VOP). \square

From Theorems 2 and 3, we conclude the following result.

Corollary 1 Let each g_j , $j \in \mathcal{J}$ be strongly convex of order κ . If $z_o \in \Gamma$ solves (SVVI), then z_o is a solution of (MVVI).

Now, we exemplify the significance of Theorems 2, 3 and Corollary 1.

Example 1 Consider the following problem:

$$(P) \quad \begin{aligned} & \text{Minimize } g(z) = (g_1(z), g_2(z)) \\ & \text{subject to } z \in \Gamma, \end{aligned}$$

where $\Gamma = \{z = (z_1, z_2) \in \mathbb{R}^2 : z_1 \geq 0, z_2 \in \mathbb{R}\}$ and $g_1, g_2 : \Gamma \rightarrow \mathbb{R}$ be defined as

$$g_1(z) = z_1^2 + 2z_2^2 \quad \text{and} \quad g_2(z) = z_1^2 + z_2^2 + e^{z_1+z_2}.$$

Evidently, g_1, g_2 are differentiable and strongly convex functions of order $\kappa = 2$ with $\alpha_j = 1$, $j = 1, 2$ on Γ . It can be evaluated that

$$\nabla g_1(z) = (2z_1, 4z_2) \quad \text{and} \quad \nabla g_2(z) = (2z_1 + e^{z_1+z_2}, 2z_2 + e^{z_1+z_2}).$$

Let $z_o = (0, 0)$, then it can be verify that z_o is an efficient minimizer of order 2 with $\alpha = (1, 1)$, as for any $z \in \Gamma$, one has

$$(g_1(z) - g_1(z_o) - \alpha_1 \|z - z_o\|^2, g_2(z) - g_2(z_o) - \alpha_2 \|z - z_o\|^2) \notin -\mathbb{R}_+^2 \setminus \{\mathbf{0}\}.$$

Clearly, z_o is a solution of (SVVI), as for any $z \in \Gamma$, we get

$$(\langle \nabla g_1(z_o), z - z_o \rangle, \langle \nabla g_2(z_o), z - z_o \rangle) \notin -\mathbb{R}_+^2 \setminus \{\mathbf{0}\}.$$

Furthermore, z_o also solves (MVVI), as for all $z \in \Gamma$, we get

$$(\langle \nabla g_1(z), z - z_o \rangle, \langle \nabla g_2(z), z - z_o \rangle) \notin -\mathbb{R}_+^2 \setminus \{\mathbf{0}\}.$$

4 Existence of Solutions for (MVVI) and (SVVI)

In this section, by employing KKM–Fan theorem, we establish the conditions under which the solution of (MVVI) and (SVVI) exists.

Let V be a vector space and $\emptyset \neq Z \subseteq V$, be a convex set.

The following definition and lemma are from [19].

Definition 6 A function $\Phi : Z \rightarrow 2^V$ is a KKM map if for any finite subset $\{v_1, v_2, \dots, v_{\bar{m}}\}$ of Z , it satisfies

$$co \{v_1, v_2, \dots, v_{\bar{m}}\} \subseteq \bigcup_{i=1}^{\bar{m}} \Phi(v_i).$$

Lemma 2 (KKM–Fan theorem) *Let $\Phi : Z \rightarrow 2^V$ be a KKM map with closed values. If there exists $\bar{z} \in Z$, such that, $\Phi(\bar{z})$ is compact, then*

$$\bigcap_{z \in Z} \Phi(z) \neq \emptyset.$$

Theorem 4 *Let each $g_j : \Gamma \rightarrow \mathbb{R}$, $j \in \mathcal{J}$ be differentiable function and ∇g_j , $j \in \mathcal{J}$ be strongly monotone of order κ . If $G(v) = \{z \in \Gamma : (\langle \nabla g_1(v), v - z \rangle, \dots, \langle \nabla g_p(v), v - z \rangle) \notin -\mathbb{R}_+^p \setminus \{\mathbf{0}\}\}$, is closed valued for all $v \in \Gamma$ and there exist nonempty compact sets $P, Q \subset \Gamma$ such that Q is convex and for any $z \in \Gamma \setminus P$, we can find a point $v \in Q$, such that $z \notin G(v)$. Then, (MVVI) is solvable on Γ .*

Proof We define a map

$$H(v) := \{z \in \Gamma : (\langle \nabla g_1(z), z - v \rangle, \dots, \langle \nabla g_p(z), z - v \rangle) \notin \mathbb{R}_+^p \setminus \{\mathbf{0}\}\}, \quad \forall v \in \Gamma.$$

Clearly, H is nonempty, since $v \in H(v)$.

Now we claim that $H(v)$ is a KKM map defined on Γ . We proceed by contradiction, let $\{v_1, v_2, \dots, v_{\bar{m}}\} \subset \Gamma$, $\mu_k \geq 0$, $k = 1, 2, \dots, \bar{m}$, and $\sum_{k=1}^{\bar{m}} \mu_k = 1$, such that

$$z_\circ := \sum_{k=1}^{\bar{m}} \mu_k v_k \notin \bigcup_{k=1}^{\bar{m}} H(v_k). \quad (21)$$

Hence, for all v_k , $k = 1, 2, \dots, \bar{m}$, we deduce that

$$(\langle \nabla g_1(z_\circ), z_\circ - v_k \rangle, \dots, \langle \nabla g_p(z_\circ), z_\circ - v_k \rangle) \in \mathbb{R}_+^p \setminus \{\mathbf{0}\}, \quad (22)$$

that is, for each v_k , $k = 1, 2, \dots, \bar{m}$, we have

$$\langle \nabla g_j(z_\circ), z_\circ - v_k \rangle \geq 0, \quad \forall j \in \mathcal{J}, \quad j \neq j_\circ, \quad (23)$$

$$\langle \nabla g_{j_\circ}(z_\circ), z_\circ - v_k \rangle > 0, \quad \text{for some } j_\circ. \quad (24)$$

For all $j \in \mathcal{J}$, we deduce that

$$\begin{aligned} 0 &= \langle \nabla g_j(z_\circ), z_\circ - z_\circ \rangle, \\ &= \left\langle \nabla g_j(z_\circ), z_\circ - \sum_{k=1}^{\bar{m}} \mu_k v_k \right\rangle, \\ &= \sum_{k=1}^{\bar{m}} \mu_k \langle \nabla g_j(z_\circ), z_\circ - v_k \rangle. \end{aligned} \quad (25)$$

From (25), we get

$$\langle \nabla g_j(z_\circ), z_\circ - v_k \rangle = 0, \quad \forall j \in \mathcal{J}, \quad (26)$$

This is in contradiction to inequalities (23) and (24). Now, we will show that $H(v) \subset G(v)$, $\forall v \in \Gamma$. Let $z \in H(v)$, then we get

$$(\langle \nabla g_1(z), z - v \rangle, \dots, \langle \nabla g_p(z), z - v \rangle) \notin \mathbb{R}_+^p \setminus \{\mathbf{0}\}. \quad (27)$$

Since, ∇g_j , $j \in \mathcal{J}$ be strongly monotone of order κ , we get

$$\langle \nabla g_j(v) - \nabla g_j(z), v - z \rangle \geq \alpha_j \|v - z\|^\kappa, \quad \forall j \in \mathcal{J}. \quad (28)$$

From (28), we have

$$\langle \nabla g_j(v), v - z \rangle \geq \alpha_j \|v - z\|^\kappa - \langle \nabla g_j(z), z - v \rangle. \quad (29)$$

From (27) and (29), we get

$$(\langle \nabla g_1(v), v - z \rangle, \dots, \langle \nabla g_p(v), v - z \rangle) \notin -\mathbb{R}_+^p \setminus \{\mathbf{0}\}.$$

Therefore, $z \in G(v)$. Since, we obtain that $H(v) \subset G(v)$ for any $v \in \Gamma$ and thus, G is also a KKM map. From hypotheses, $G(v)$ is a compact set. Thus, $H(v)$ is also a compact set. From the KKM–Fan Theorem

$$\bigcap_{v \in \Gamma} G(v) \neq \emptyset,$$

which means that for all $v \in \Gamma$, we get a $z_o \in \Gamma$, such that

$$(\langle \nabla g_1(v), v - z_o \rangle, \dots, \langle \nabla g_p(v), v - z_o \rangle) \notin -\mathbb{R}_+^p \setminus \{\mathbf{0}\}.$$

Hence, (MVVI) is solvable on Γ . \square

In a similar way of Theorem 4, we have the following result.

Theorem 5 *Let each $g_j : \Gamma \rightarrow \mathbb{R}$, $j \in \mathcal{J}$ be differentiable function and $\nabla(-g_j)$, $j \in \mathcal{J}$ be strongly monotone of order κ . If $G(v) = \{z \in \Gamma : (\langle \nabla g_1(z), v - z \rangle, \dots, \langle \nabla g_p(z), v - z \rangle) \notin -\mathbb{R}_+^p \setminus \{\mathbf{0}\}\}$, is closed valued for all $v \in \Gamma$ and there exist nonempty compact sets $P, Q \subset \Gamma$ such that Q is convex and for any $z \in \Gamma \setminus P$, we can find a point $v \in Q$, such that $z \notin G(v)$. Then, (SVVI) is solvable on Γ .* \square

References

1. Al-Homidan, S., Ansari, Q.H.: Generalized Minty vector variational-like inequalities and vector optimization problems. *J. Optim. Theory Appl.* **144**(1), 1–11 (2010)
2. Ansari, Q.H., Yao, J.C.: On nondifferentiable and nonconvex vector optimization problems. *J. Optim. Theory Appl.* **106**(3), 475–488 (2000)
3. Bhatia, G.: Optimality and mixed saddle point criteria in multiobjective optimization. *J. Math. Anal. Appl.* **342**, 135–145 (2008)
4. Cromme, L.: Strong uniqueness : A far-reaching criterion for the convergence of iterative numerical procedures. *Numer. Math.* **29**, 179–193 (1978)
5. Deng, S.: On approximate solutions in convex vector optimization. *SIAM J. Control Optim.* **35**, 2128–2136 (1997)
6. Gao, Y., Hou, S.H., Yang, X.M.: Existence and optimality conditions for approximate solutions to vector optimization problems. *J. Optim. Theory Appl.* **152**(1), 97–120 (2012)
7. Fan, L., Liu, S., Gao, S.: Generalized monotonicity and convexity of non-differentiable functions. *J. Math. Anal. Appl.* **279**(1), 276–289 (2003)
8. Gao, Y., Yang, X., Teo, K.L.: Optimality conditions for approximate solutions of vector optimization problems. *J. Ind. Manage. Optim.* **7**(2), 483–496 (2011)
9. Giannessi, F.: On Minty variational principle. In: Giannessi, F., Komlósi, S., Rapsack, T. (eds.) *New Trends in Mathematical Programming*, pp. 93–99 (1998)
10. Giannessi, F.: Theorems on the alternative quadratic programs and complementarity problems. In: Cottle, R.W., Giannessi, F., Lions, J.L. (eds.) *Variational Inequalities and Complementarity Problems*, pp. 151–186 (1980)
11. Giannessi, F.: *Vector Variational Inequalities and Vector Equilibria. Mathematical Theories*, Kluwer Academic, Dordrecht (2000)
12. Green, J., Heller, W.P.: Mathematical analysis and convexity with applications to economics. *Handbook Math. Econ.* **1**, 15–52 (1981)

13. Gutiérrez, C., Jiménez, B., Novo, V.: On approximate efficiency in multiobjective programming. *Math. Meth. OR* **64**, 165–185 (2006)
14. Hartman, P., Stampacchia, G.: On some nonlinear elliptic differential functional equations. *Acta Math.* **115**, 153–188 (1980)
15. Jiménez, B.: Strict efficiency in vector optimization. *J. Math. Anal. Appl.* **265**(2), 264–284 (2002)
16. Karamardian, S., Schaible, S.: Seven kinds of monotone maps. *J. Optim. Theory Appl.* **66**(1), 37–46 (1990)
17. Kumar, P., Pant, M., Singh, H.P.: Solving nonlinear optimization problems using IUMDE algorithm. In: *Soft Computing: Theories and Applications*, vol. 584, pp. 245–254. Springer, Singapore (2017)
18. Lee, G.M.: On relations between vector variational inequality and vector optimization problem. In: Yang, X.Q., Mees, A.I., Fisher, M.E., Jennings, L.S. (eds.) *Progress in Optimization, II: Contributions from Australia*, pp. 167–179 (2000)
19. Li, R., Yu, G.: A class of generalized invex functions and vector variational-like inequalities. *J. Inequal. Appl.* **2–14**, (2017)
20. Lin, G.H., Fukushima, M.: Some exact penalty results for nonlinear programs and mathematical programs with equilibrium constraints. *J. Optim. Theory Appl.* **118**(1), 67–80 (2003)
21. Long, X.J., Peng, J.W., Wu, S.Y.: Generalized vector variational-like inequalities and nonsmooth vector optimization problems. *Optimization* **61**(9), 1075–1086 (2012)
22. Mangasarian, O.L.: *Nonlinear Programming*. McGraw-Hill, New York (1969)
23. Minty, G.J.: On the generalization of a direct method of the calculus of variations. *Bull. Amer. Math. Soc.* **73**, 314–321 (1967)
24. Mishra, S.K., Upadhyay, B.B.: *Pseudolinear Functions and Optimization*. Chapman and Hall, CRC Press (2015)
25. Mishra, S.K., Upadhyay, B.B.: Some relations between vector variational inequality problems and nonsmooth vector optimization problems using quasi efficiency. *Positivity* **17**, 1071–1083 (2013)
26. Mishra, S.K., Wang, S.Y.: Vector variational-like inequalities and nonsmooth vector optimization problems. *Nonlinear Anal.* 1939–1945 (2006)
27. Rahtu, E., Salo, M., Heikkilä, J.: A new convexity measure based on a probabilistic interpretation of images. *IEEE Trans. Pattern Anal. Mach. Intell.* **28**, 1501–1512 (2006)
28. Singh, T.P., Yadava, R.D.S.: Application of PSO clustering for selection of chemical interface materials for sensor array electronic nose. In: *Soft Computing: Theories and Applications*, vol. 583(1), pp. 449–456. Springer, Singapore (2017)
29. Smith, P.: *Convexity Methods in Variational Calculus*, vol. 1. Research Studies Press, Letchworth (1985)
30. Stampacchia, G.: Formes bilinéaires coercitives sur les ensembles convexes. *C.R. Acad. Sci. 9*, 4413–4416 (1960)
31. Upadhyay, B.B., Mishra, P., Mohapatra, R.N., Mishra, S.K.: On the applications of nonsmooth vector optimization problems to solve generalized vector variational inequalities using convexificators. *Adv. Intell. Syst. Comput.* (2019). https://doi.org/10.1007/978-3-030-21803-4_66
32. Upadhyay, B.B., Mishra, P.: On generalized Minty and Stampacchia vector variational-like inequalities and nonsmooth vector optimization problem involving higher order strong invexity. *J. Sci. Res.* 182–191 (2020)

Characterizations of the Solution Sets for Constrained Pseudolinear Semi-infinite Programming Problems



B. B. Upadhyay and Akriti Srivastava

Abstract This paper deals with a class of pseudolinear semi-infinite programming problems and derives that the Lagrangian function corresponding to a known solution and associated with a fixed Lagrange multiplier is constant on the solution set. We obtain some characterizations of the solution set for the considered problem. Furthermore, we consider a multiobjective pseudolinear semi-infinite programming problem and establish that an efficient solution under certain conditions becomes a properly efficient solution. The work of this paper extends and unifies several known results of Chew and Choo (Math Program 28(2):226–239, 1984 [3]) and Dinh et al. (Optimization 55(3):241–250, 2006 [6]) to the semi-infinite programming problems.

Keywords Pseudolinear functions · Properly efficient solutions · Efficient solutions · Solution sets · Semi-infinite programming

1 Introduction

In the field of optimization, the notion of convexity plays an important role as for a convex function local minimizer becomes a global minimizer. The generalizations of convex and concave functions were initially presented by Mangasarian [21] as pseudoconvex and pseudoconcave functions, respectively. Kortanek and Evans [15] provided regularity conditions for the maximization problem with pseudoconcave constraints and characterized pseudoconvex as well as pseudoconcave functions. Chew and Choo [3] have called those functions as pseudolinear which are pseudoconvex as well as pseudoconcave.

An optimization problem is called nonlinear in which the objective function or some of the constraints are nonlinear. For the applications of nonlinear optimiza-

B. B. Upadhyay · A. Srivastava (✉)

Department of Mathematics, Indian Institute of Technology Patna, Patna, Bihar 801106, India
e-mail: akriti.iitp@gmail.com

B. B. Upadhyay
e-mail: bhooshan@iitp.ac.in

tion problems, see [16, 30, 34]. To characterize the solution set of optimization problems having more than one optimal solutions is very important to know the behavior of solution methods. Mangasarian [22] characterized the solution set of convex programs. Burke and Ferris [2] amplified the work of Mangasarian [22] to the convex program in which the objective functions were nondifferentiable extended real-valued functions. Jeyakumar and Yang [13] considered the differentiable pseudolinear program and characterized its solution set. Penot [28] and Jeyakumar et al. [11, 12] considered several types of the optimization problem and characterize its solution set. Dinh et al. [6] considered pseudolinear minimization problem and derived some characterizations of its solution set. For more comprehension about pseudolinear optimization problems, we refer to [17, 18, 23–27, 29].

In the semi-infinite programming problems, the finite number of decision variables and infinitely many constraints appear [9, 10, 20]. Recently, many authors have studied about semi-infinite programming problems, see [1, 4, 7, 32, 33]. Kim and Son [14] dealt with a nonconvex semi-infinite programming problem where appearing functions were Clarke regular and characterized the solution set for the considered problem. Later, Son and Kim [31] considered a pseudoconvex semi-infinite programming problem to establish several characterizations of the solution set. Recently, Long et al. [19] considered a nonconvex semi-infinite programming problem and characterized its solution set by using lower Dini subdifferential.

Motivated by the works in [6, 13], we consider a pseudolinear optimization problem with semi-infinite constraints and derive that the Lagrangian function corresponding to a known solution is constant on the solution set. Further, we obtain some characterizations of the solution set for the considered problem. For justifying the significance of these results, we provide a numerical example. Moreover, we obtain the conditions for an efficient solution of pseudolinear multiobjective semi-infinite programming problem to be a properly efficient solution.

2 Definitions and Preliminaries

Throughout this paper, we assume that $\emptyset \neq U \subseteq \mathbb{R}^n$ is an open convex set.

Definition 1 [6] A differentiable function $\phi : \mathbb{R}^n \rightarrow \mathbb{R}$ is called pseudolinear on U , if ϕ is pseudoconvex as well as pseudoconcave on U , that is,

$$y, z_0 \in U, \phi(y) < \phi(z_0) \Rightarrow \nabla\phi(z_0)^T(y - z_0) < 0,$$

$$y, z_0 \in U, \phi(y) > \phi(z_0) \Rightarrow \nabla\phi(z_0)^T(y - z_0) > 0.$$

The following lemma is from Chew and Choo [3].

Lemma 1 *The function ϕ is pseudolinear on U , if and only if there exists a positive real-valued function r defined on $U \times U$ such that, for each $y, z_0 \in U$, one has*

$$\phi(y) = \phi(z_0) + r(z_0, y) \nabla \phi(z_0)^T (y - z_0). \quad (1)$$

□

The following proposition is from Dinh et al. [6].

Proposition 1 *Let $\phi : \mathbb{R}^n \rightarrow \mathbb{R}$ be a pseudolinear function on U and $y, z_0 \in U$. For $\alpha \in [0, 1]$, denote $y\alpha z_0 := y + \alpha(z_0 - y)$. Then, the following statements are equivalent:*

- (i) $\nabla \phi(z_0)^T (y - z_0) = 0$,
- (ii) $\phi(z_0) = \phi(y)$,
- (iii) $\nabla \phi(y)^T (y - z_0) = 0$,
- (iv) $\phi(y\alpha z_0) = \phi(z_0)$,
- (v) $\phi(y\alpha z_0) = \phi(y)$,
- (vi) $\nabla \phi(y\alpha z_0)^T (y - z_0) = 0$.

□

3 Pseudolinear Semi-infinite Programming Problem

In this section, we consider a class of pseudolinear semi-infinite programming problem and obtain the characterization of its solution set.

We consider the following pseudolinear semi-infinite programming problem (PSIP):

$$\begin{aligned} (\text{PSIP}) \quad & \text{minimize } \phi(y) \\ & \text{subject to } y \in \Gamma := \{y \in A \mid \psi_j(y) \leq 0, \forall j \in J\}, \end{aligned}$$

where $\phi, \psi_j : U \rightarrow \mathbb{R}$, $j \in J$ are pseudolinear functions on U containing Γ and A is a convex and closed subset of U . The index set J is an arbitrary, not necessarily finite (but nonempty).

Let the solution set of the problem (PSIP) is denoted by $C := \{y \in \Gamma \mid \phi(x) \geq \phi(y), \forall x \in \Gamma\}$ and $C \neq \phi$. For a given $z_0 \in \Gamma$, let $J(z_0) := \{j \in J \mid \psi_j(z_0) = 0\}$. Let us denote the sets $R^{(T)}$ and $R_+^{(T)}$, respectively, by

$$R^{(T)} := \{\mu = (\mu_j)_{j \in J} : \mu_j = 0, \text{ for all } j \in J, \text{ except for finitely many } \mu_j \neq 0\},$$

and

$$R_+^{(T)} := \{\mu = (\mu_j)_{j \in J} \in R^{(T)} : \mu_j \geq 0, j \in J\}.$$

On the lines of Corollary 3.4 of Long et al. [19], we state the following necessary and sufficient optimality conditions for (PSIP).

Theorem 1 Let z_0 be an element of convex set Γ . Suppose that,

$$(CQ) \quad N_{\Gamma}(z_0) \subseteq \bigcup_{\mu \in D(z_0)} \left(\sum_{j \in J} \mu_j \nabla \psi_j(z_0) \right) + N_A(z_0),$$

where $D(z_0) := \left\{ \mu \in R_+^{(T)} : \mu_j \psi_j(z_0) = 0, \forall j \in J \right\}$. Then, $z_0 \in C$ if and only if there exists a Lagrange multiplier $\mu \in R_+^{(T)}$, such that

$$0 \in \nabla \phi(z_0) + \sum_{j \in J} \mu_j \nabla \psi_j(z_0) + N_A(z_0), \quad \mu_j \psi_j(z_0) = 0, \quad \forall j \in J. \quad (2)$$

□

Theorem 2 For the problem (PSIP), let $z_0 \in C$ and (2) holds with a Lagrange multiplier $\mu \in R_+^{(T)}$. Then, $\sum_{j \in J(z_0)} \mu_j \psi_j(y) = 0$, for every $y \in C$ and $\phi(\cdot) + \sum_{j \in J(z_0)} \mu_j \psi_j(\cdot)$ is constant on C .

Proof From (2), we have

$$\nabla \phi(z_0)^T (y - z_0) + \sum_{j \in J(z_0)} \mu_j \nabla \psi_j(z_0)^T (y - z_0) \geq 0, \quad \forall y \in A. \quad (3)$$

Since the function ϕ is pseudolinear on U , therefore by Lemma 1, there exists a function $r > 0$ such that, for every $y, z_0 \in U$, we get

$$\phi(y) = \phi(z_0) + r(z_0, y) \nabla \phi(z_0)^T (y - z_0). \quad (4)$$

Using (3) and (4), we get

$$\phi(y) - \phi(z_0) + r(z_0, y) \sum_{j \in J(z_0)} \mu_j \nabla \psi_j(z_0)^T (y - z_0) \geq 0, \quad \forall y \in A.$$

Since, for every $y \in C$, $\phi(y) = \phi(z_0)$, we get

$$r(z_0, y) \sum_{j \in J(z_0)} \mu_j \nabla \psi_j(z_0)^T (y - z_0) \geq 0.$$

Since $r(z_0, y) > 0$, therefore, we get

$$\sum_{j \in J(z_0)} \mu_j \nabla \psi_j(z_0)^T (y - z_0) \geq 0. \quad (5)$$

As, each ψ_j , $j \in J(z_0)$ is pseudolinear on U , therefore, by Lemma 1, there exists a function $q > 0$ such that, for every $y, z_0 \in U$, we get

$$\psi_j(y) = \psi_j(z_0) + q(z_0, y) \nabla \psi_j(z_0)^T (y - z_0). \quad (6)$$

Since $q(z_0, y) > 0$, therefore from (5) and (6), we get

$$\sum_{j \in J(z_0)} \mu_j \psi_j(y) \geq \sum_{j \in J(z_0)} \mu_j \psi_j(z_0), \quad \forall y \in C.$$

Since, $\mu_j \psi_j(z_0) = 0$, $j \in J$, therefore, we have

$$\sum_{j \in J(z_0)} \mu_j \psi_j(y) \geq 0, \quad \forall y \in C. \quad (7)$$

Since y is feasible, therefore we have

$$\sum_{j \in J(z_0)} \mu_j \psi_j(y) \leq 0, \quad \forall y \in C. \quad (8)$$

From (7) and (8), we have

$$\sum_{j \in J(z_0)} \mu_j \psi_j(y) = 0, \quad \forall y \in C.$$

From the last equality, we observe that $\phi(.) + \sum_{j \in J(z_0)} \mu_j \psi_j(.)$ is constant on C . \square

Now, in Theorem 3 and Corollary 1, we assume that for each $z_0 \in C$, there exists a $\mu \in R_+^{(T)}$ such that (2) holds. Let $\hat{J}(z_0) := \{j \in J(z_0) \mid \mu_j > 0\}$. Moreover, we define

$$\kappa(z_0) := \left\{ y \in A \mid \psi_j(y) = 0, \quad \forall j \in \hat{J}(z_0) \text{ and } \psi_j(y) \leq 0, \quad \forall j \in J \setminus \hat{J}(z_0) \right\}.$$

Now, we derive the following theorem to characterize the solution set of the (PSIP).

Theorem 3 *For the problem (PSIP), let $z_0 \in C$ and*

$$C_1 := \left\{ y \in A \mid \nabla \phi(y)^T (y - z_0) = 0 \text{ and } y \in \kappa(z_0) \right\},$$

$$C_2 := \left\{ y \in A \mid \nabla \phi(z_0)^T (y - z_0) = 0 \text{ and } y \in \kappa(z_0) \right\},$$

$$C_3 := \left\{ y \in A \mid \nabla \phi(y \alpha z_0)^T (y - z_0) = 0, \quad \forall \alpha \in (0, 1] \text{ and } y \in \kappa(z_0) \right\}.$$

Then, $C = C_1 = C_2 = C_3$.

Proof We only prove that $C = C_2$ and similarly the other equalities can be proved. Assume that $y \in C_2$, and hence $y \in A$, $\psi_j(y) \leq 0$, $j \in J$ and $\nabla \phi(z_0)^T (y - z_0) = 0$. Therefore, from Proposition 1, we have $y \in \Gamma$ and $\phi(z_0) = \phi(y)$, which gives

that $y \in C$. Thus, $C_2 \subseteq C$.

Conversely, let us suppose that $y \in C$, then $\phi(y) = \phi(z_0)$. Applying Theorem 2, we obtain $\sum_{j \in J(z_0)} \mu_j \psi_j(y) = 0$. Hence, $\psi_j(y) = 0$, $j \in \hat{J}(z_0)$ and $\psi_j(y) \leq 0$, $j \in J \setminus \hat{J}(z_0)$, that is, $y \in \kappa(z_0)$. Again, $\phi(y) = \phi(z_0)$, then using Proposition 1, we get $\nabla\phi(z_0)^T(y - z_0) = 0$, which implies $y \in C_2$. Thus, $C \subseteq C_2$. Therefore, $C = C_2$. \square

Corollary 1 For the problem (PSIP), let $z_0 \in C$ and

$$C'_1 := \{y \in A \mid \nabla\phi(y)^T(y - z_0) \leq 0 \text{ and } y \in \kappa(z_0)\},$$

$$C'_2 := \{y \in A \mid \nabla\phi(z_0)^T(y - z_0) \leq 0 \text{ and } y \in \kappa(z_0)\},$$

$$C'_3 := \{y \in A \mid \nabla\phi(y\alpha z_0)^T(y - z_0) \leq 0, \forall \alpha \in (0, 1] \text{ and } y \in \kappa(z_0)\}.$$

Then, $C = C'_1 = C'_2 = C'_3$.

Proof Clearly, $C = C_1 \subseteq C'_1$, $C_2 \subseteq C'_2$ and $C_3 \subseteq C'_3$. Let $y \in C'_1$. Then, $\psi_j(y) = 0$, $j \in \hat{J}(z_0)$ and $\psi_j(y) \leq 0$, $j \in J \setminus \hat{J}(z_0)$, that is, $y \in \kappa(z_0)$.

Now, using Lemma 1, there exists a function $r > 0$ such that,

$$\phi(z_0) - \phi(y) = r(y, z_0) \nabla\phi(y)^T(z_0 - y). \quad (9)$$

Since, $\nabla\phi(y)^T(y - z_0) \leq 0$, therefore from (9), we have $\phi(z_0) \geq \phi(y)$.

As $z_0 \in C$, we get $\phi(y) = \phi(z_0)$, which implies that $y \in C$. Hence, $C'_1 \subseteq C$. Similarly,

$$\phi(y) - \phi(z_0) = r(z_0, y) \nabla\phi(z_0)^T(y - z_0),$$

and

$$\phi(y\alpha z_0) - \phi(z_0) = (\alpha - 1)r(y\alpha z_0, z_0) \nabla\phi(y\alpha z_0)^T(z_0 - y), \forall \alpha \in (0, 1].$$

We can show that $C'_2 \subseteq C_2$ and $C'_3 \subseteq C_3$, respectively, by using the above equalities. \square

The following example justifies the implication of Theorem 1, 2, 3 and Corollary 1.

Example 1 Consider the following example

$$(P) \text{ minimize } \phi(z_1, z_2)$$

$$\text{subject to } \Gamma := \{(z_1, z_2) \in A \mid \psi_j(z_1, z_2) \leq 0, j \in \mathbb{N}\},$$

where $\phi, \psi_j : U = (-2, 2) \times (-2, 2) \rightarrow \mathbb{R}$, $j \in \mathbb{N}$ are functions defined as:

$$\phi(z_1, z_2) = \sin(z_1 + z_2) + z_1 + z_2,$$

$$\psi_1(z_1, z_2) = z_1 - z_2 + 1/2, \psi_2(z_1, z_2) = z_1 + z_2 - 1,$$

and

$$\psi_j(z_1, z_2) = -e^{-j(z_1+z_2)}, j = 3, 4, \dots$$

It is evident that ϕ and ψ_j , $j \in \mathbb{N}$ are locally Lipschitz functions on U and where $A = [-1/2, 0] \times [0, 1/2]$. The gradient of the functions at any point is given by

$$\nabla\phi(z_1, z_2) = (\cos(z_1 + z_2) + 1, \cos(z_1 + z_2) + 1)^T,$$

$\nabla\psi_1(z_1, z_2) = (1, -1)^T$, $\nabla\psi_2(z_1, z_2) = (1, 1)^T$, and $\nabla\psi_j(z_1, z_2) = (je^{-j(z_1+z_2)}, je^{-j(z_1+z_2)})^T$, $j = 3, 4, \dots$. Then, we can verify that the functions ϕ and ψ_j , $j \in \mathbb{N}$ are pseudolinear on U and the feasible set of (P) is $\Gamma = \{(z_1, z_2) \in A \mid z_2 \geq z_1 + 1/2\}$. Now, it is obvious that the optimal solution of the (P) is $z_0 = (-1/2, 0)$, $N_\Gamma(z_0) = \{(z_1, z_2) \in \mathbb{R}^2 \mid -z_1 \geq z_2 \text{ and } z_2 \leq 0\}$, $N_A(z_0) = \{(z_1, z_2) \in \mathbb{R}^2 \mid z_1 \leq 0, z_2 \leq 0\}$, and (2) holds at $z_0 = (-1/2, 0)$ as there exist $\mu_1 = 1$ and $\mu_j = 0$, $j = 2, 3, \dots$ such that

$$0 \in \nabla\phi(z_0) + \sum_{j \in \mathbb{N}} \mu_j \nabla\psi_j(z_0) + N_A(z_0), \quad \mu_j \psi_j(z_0) = 0, \quad \forall j \in \mathbb{N}.$$

We can evaluate that

$C_1 = \{(z_1, z_2) \in A \mid z_1 - z_2 + 1/2 = 0, z_1 + z_2 - 1 \leq 0, -e^{-j(z_1+z_2)} \leq 0, j = 3, 4, \dots\}$, and $\langle \nabla\phi(z_1, z_2), (z_1 + 1/2, z_2) \rangle = 0$.

Hence, $C_1 = \{(-1/2, 0)\}$.

Similarly, $C_2 = C_3 = \{(-1/2, 0)\}$.

Therefore, $C_1 = C_2 = C_3 = C = \{(-1/2, 0)\}$.

Clearly, $J(z_0) = \hat{J}(z_0) = \{1\}$ and $z_0 = (-1/2, 0) \in C$. Further, $\phi(.) + \sum_{j \in J(z_0)} \mu_j \psi_j(.)$ is constant on C .

Now, by similar way, we can find $C'_1 = \{(-1/2, 0)\}$, and $C'_2 = C'_3 = \{(-1/2, 0)\}$. Therefore, $C'_1 = C'_2 = C'_3 = C = \{(-1/2, 0)\}$.

4 Pseudolinear Multiobjective Semi-infinite Programming Problem

In this section, we consider a class of pseudolinear multiobjective semi-infinite programming problems and established that an efficient solution under certain conditions becomes a properly efficient solution.

Consider the following pseudolinear multiobjective semi-infinite programming problem (MOSIP):

$$\begin{aligned}
 (\text{MOSIP}) \quad & \text{minimize } \phi(y) := (\phi_1(y), \phi_2(y), \dots, \phi_r(y)) \\
 & \text{subject to } y \in \tilde{K} := \{y \in \mathbb{R}^n \mid \psi_j(y) \leq 0, \forall j \in J\},
 \end{aligned}$$

where $\phi_i, \psi_j : \mathbb{R}^n \rightarrow \mathbb{R}$, $i \in I := \{1, 2, \dots, r\}$, $j \in J$ are pseudolinear functions. The index set J is an arbitrary, not necessarily finite (but nonempty). For a given $z_0 \in \tilde{K}$, let $\tilde{J}(z_0) := \{j \in J \mid \psi_j(z_0) = 0\}$. For some $1 \leq s \leq r$, we define

$$Z_s(y) := \{\nabla \phi_i(y), i = 1, \dots, s-1, s+1, \dots, r\} \cup \{\nabla \psi_j(y), j \in \tilde{J}(z_0)\}.$$

We recall the following definitions given by Geoffrion [8].

Definition 2 A solution $z_0 \in \tilde{K}$ is said to be an efficient solution of the (MOSIP), if there exists no $y \in \tilde{K}$, such that

$$\phi_i(y) \leq \phi_i(z_0), \forall i \in I, i \neq l$$

$$\phi_l(y) < \phi_l(z_0), \text{ for some } l.$$

Definition 3 A solution $z_0 \in \tilde{K}$ is said to be properly efficient solution of the (MOSIP), if it is efficient and there exists a positive scalar \tilde{M} such that, for each $i \in I$, the inequality

$$\frac{\phi_i(y) - \phi_i(z_0)}{\phi_l(z_0) - \phi_l(y)} \leq \tilde{M}$$

holds for some $l \in I$, such that $\phi_l(y) > \phi_l(z_0)$ whenever $x \in \tilde{K}$ and $\phi_i(y) < \phi_i(z_0)$.

We recall the following theorem of optimality for (MOSIP) provided by Mishra and Upadhyay [26].

Theorem 4 For (MOSIP), let $z_0 \in \tilde{K}$ and let the functions $\phi_i, \psi_j, i \in I, j \in \tilde{J}(z_0)$ are pseudolinear with respect to proportional functions \tilde{p}_i, \tilde{q}_j . Then, z_0 be an efficient solution of (MOSIP), if and only if for each s , $1 \leq s \leq r$, $\text{cone}(Z_s(z_0))$ is closed and there exist $\beta_i \in \mathbb{R}$, $i \in I$ and $\lambda_j \in \mathbb{R}$, $j \in \tilde{J}(z_0)$, finitely many of them are nonzero, such that

$$\begin{aligned}
 & \sum_{i=1}^r \beta_i \nabla \phi_i(z_0) + \sum_{j \in \tilde{J}(z_0)} \lambda_j \nabla \psi_j(z_0) = 0, \\
 & \beta_i > 0, i \in I, \\
 & \lambda_j \geq 0, j \in \tilde{J}(z_0).
 \end{aligned} \tag{10}$$

□

Theorem 5 Let $z_0 \in \tilde{K}$. Then, the following are equivalent statements for the problem (MOSIP):

- (i) z_0 is an efficient solution of the (MOSIP),
- (ii) z_0 is a properly efficient solution of the (MOSIP),
- (iii) there exists $\beta_i > 0$, $i \in I$ such that

$$\sum_{i=1}^r \beta_i \phi_i(y) \geq \sum_{i=1}^r \beta_i \phi_i(z_0), \quad \forall y \in \tilde{K},$$

Proof Obviously (ii) \Rightarrow (i). The proof of (iii) \Rightarrow (ii) is given by Geoffrion [8].

We only need to show that (i) \Rightarrow (iii).

For the problem (MOSIP), let $z_0 \in \tilde{K}$ be an efficient solution. Then by (10), we have

$$\sum_{i=1}^r \beta_i \nabla \phi_i(z_0) + \sum_{j \in \tilde{J}(z_0)} \lambda_j \nabla \psi_j(z_0) = 0, \quad (11)$$

which is equivalent to

$$\sum_{i=1}^r \beta_i \langle \nabla \phi_i(z_0), (y - z_0) \rangle + \sum_{j \in \tilde{J}(z_0)} \lambda_j \langle \nabla \psi_j(z_0), (y - z_0) \rangle = 0, \quad \forall y \in \tilde{K}. \quad (12)$$

Again, we have

$$\psi_j(y) \leq \psi_j(z_0), \quad \forall j \in \tilde{J}(z_0). \quad (13)$$

Since, each ψ_j , $j \in \tilde{J}(z_0)$ is pseudolinear function, therefore, by Lemma 1, there exists a function $\tilde{q}_j > 0$, such that

$$\psi_j(y) = \psi_j(z_0) + \tilde{q}_j(z_0, y) \nabla \psi_j(z_0)^T (y - z_0). \quad (14)$$

Using (13) and (14), we get

$$\tilde{q}_j(z_0, y) \langle \nabla \psi_j(z_0), y - z_0 \rangle \leq 0, \quad \forall j \in \tilde{J}(z_0).$$

Since $\tilde{q}_j(z_0, y) > 0$, $j \in \tilde{J}(z_0)$, therefore, we get

$$\langle \nabla \psi_j(z_0), y - z_0 \rangle \leq 0, \quad \forall j \in \tilde{J}(z_0).$$

Therefore, $\lambda_j \geq 0$, $j \in \tilde{J}(z_0)$, it follows that

$$\left\langle \sum_{j \in \tilde{J}(z_0)} \lambda_j \nabla \psi_j(z_0), y - z_0 \right\rangle \leq 0. \quad (15)$$

Using (15) in (12), we have

$$\sum_{i=1}^r \beta_i \langle \nabla \phi_i(z_0), y - z_0 \rangle \geq 0, \quad y \in \tilde{K}. \quad (16)$$

Since, each ϕ_i , $i \in I$ is pseudolinear function, therefore, by Lemma 1, there exist a function $\tilde{p}_i > 0$, such that

$$\phi_i(y) = \phi_i(z_0) + \tilde{p}_i(z_0, y) \nabla \phi_i(z_0)^T (y - z_0). \quad (17)$$

Since $\tilde{p}_i(z_0, y) > 0$ therefore, from (16) and (17), we get

$$\sum_{i=1}^r \beta_i \phi_i(y) \geq \sum_{i=1}^r \beta_i \phi_i(z_0), \quad \forall y \in \tilde{K}.$$

□

Remark 1 In particular, if we consider finite number of linear inequality constraints, then the results of this paper coincides with the existing results of Dinh et al. [6].

5 Conclusions

In this paper, we consider a class of pseudolinear semi-infinite programming problems (PSIP) and employed a suitable constraint qualification to obtain necessary and sufficient optimality conditions for (PSIP). Using optimality conditions, we derive that the Lagrange function is constant on the solution set corresponding to a known solution. We obtain several characterizations of the solution set for the problem (PSIP). We provide a numerical example for justifying the significance of these results. Moreover, we derived that an efficient solution under certain conditions becomes a properly efficient solution for a multiobjective pseudolinear semi-infinite programming problem.

References

1. Antczak, T., Mishra, S.K., Upadhyay, B.B.: First order duality results for a new class of non-convex semi-infinite minimax fractional programming problems. *J. Adv. Math. Stud.* **9**(1), 132–162 (2016)
2. Burke, J.V., Ferris, M.C.: Characterization of solution sets of convex programs. *Oper. Res. Lett.* **10**(1), 57–60 (1991)
3. Chew, K.L., Choo, E.U.: Pseudolinearity and efficiency. *Math. Program.* **28**(2), 226–239 (1984)
4. Chuong, T.D., Huy, N.Q., Yao, J.C.: Subdifferentials of marginal functions in semi-infinite programming. *SIAM J. Optim.* **3**, 1462–1477 (2009)
5. Clarke, F.H.: Optimization and Nonsmooth Analysis. Wiley, New York (1983)
6. Dinh, N., Jeyakumar, V., Lee, G.M.: Lagrange multiplier characterizations of solution sets of constrained pseudolinear optimizations problems. *Optimization* **55**(3), 241–250 (2006)

7. Dinh, N., Mordukhovich, B.S., Nghia, T.T.A.: Subdifferentials of value functions and optimality conditions for DC and bilevel infinite and semi-infinite programs. *Math. Program.* **123**(1), 101–138 (2010)
8. Geoffrion, A.M.: Proper efficiency and the theory of vector maximization. *J. Math. Anal. Appl.* **22**(3), 618–630 (1968)
9. Goberna, M.A., Lopez, M.A.: Linear Semi-Infinite Optimization. Wiley, Chichester (1998)
10. Hettich, R., Kortanek, O.: Semi-infinite programming: theory, methods, and applications. *SIAM Rev.* **35**(3), 380–429 (1993)
11. Jeyakumar, V., Lee, G.M., Dinh, N.: Lagrange multiplier conditions characterizing optimal solution sets of cone-constrained convex programs. *J. Optim. Theory Appl.* **123**(1), 83–103 (2004)
12. Jeyakumar, V., Lee, G.M., Dinh, N.: Characterization of solution sets of convex vector minimization problems. *Eur. J. Oper. Res.* **174**(3), 1380–1395 (2006)
13. Jeyakumar, V., Yang, X.Q.: On characterizing the solution sets of pseudolinear programs. *J. Optim. Theory Appl.* **87**(3), 747–755 (1995)
14. Kim, D.S., Son, T.Q.: Characterizations of solution sets of a class of nonconvex semi-infinite programming problems. *J. Nonlinear Convex Anal.* **12**(3), 429–440 (2011)
15. Kortanek, K.O., Evans, J.P.: Pseudoconcave programming and Lagrange regularity. *Oper. Res.* **15**(5), 882–891 (1967)
16. Kumar, P., Pant, M., Singh, H.P.: Solving nonlinear optimization problems using IUMDE algorithm. In: Soft Computing: Theories and Applications, vol. 584, pp. 245–254. Springer, Singapore (2017)
17. Lalitha, C.S., Mehta, M.: A note on pseudolinearity in terms of bifunctions. *Asia-Pac. J. Oper. Res.* **24**(1), 83–91 (2007)
18. Lalitha, C.S., Mehta, M.: Characterizations of solution sets of mathematical programs in terms of Lagrange multipliers. *Optimization* **58**(8), 995–1007 (2009)
19. Long, X.J., Peng, Z.Y., Wang, X.F.: Characterizations of the solution sets for nonconvex semi-infinite programming problems. *J. Nonlinear Convex Anal.* **17**(2), 251–265 (2016)
20. Lopez, M.A., Still, G.: Semi-infinite programming. *Eur. J. Oper. Res.* **180**, 491–518 (2007)
21. Mangasarian, O.L.: Nonlinear Programming. McGraw-Hill, New York (1969)
22. Mangasarian, O.L.: A simple characterization of solution sets of convex programs. *Oper. Res. Lett.* **7**(1), 21–26 (1988)
23. Mishra, S.K., Upadhyay, B.B.: Duality in nonsmooth multiobjective programming involving η - pseudolinear functions. *Indian J. Indust. Appl. Math.* **3**, 152–161 (2012)
24. Mishra, S.K., Upadhyay, B.B.: Efficiency and duality in nonsmooth multiobjective fractional programming involving η -pseudolinear functions. *Yugosl. J. Oper. Res.* **22**(1), 3–18 (2012)
25. Mishra, S.K., Upadhyay, B.B.: Nonsmooth minimax fractional programming involving η -pseudolinear functions. *Optimization* **63**(5), 775–788 (2014)
26. Mishra, S.K., Upadhyay, B.B.: Pseudolinear Functions and Optimization, pp. 267–281. CRC Press, New York (2014)
27. Mishra, S.K., Upadhyay, B.B., Hoai An, L.T.: Lagrange multiplier characterizations of solution sets of constrained nonsmooth pseudolinear optimization problems. *J. Optim. Theory Appl.* **160**(3), 763–777 (2014)
28. Penot, J.P.: Characterization of solution sets of quasiconvex programs. *J. Optim. Theory Appl.* **117**(3), 627–636 (2003)
29. Rapcsak, T.: On pseudolinear functions. *Eur. J. Oper. Res.* **50**, 353–360 (1991)
30. Singh, T.P., Yadava, R.D.S.: Application of PSO clustering for selection of chemical interface materials for sensor array electronic nose. In: Soft Computing: Theories and Applications, vol. 583(1), pp. 449–456. Springer, Singapore (2017)
31. Son, T.Q., Kim, D.S.: A new approach to characterize the solution set of a pseudoconvex programming problem. *J. Comput. Appl. Math.* **261**, 333–340 (2014)
32. Son, T.Q., Strodiot, J.J., Nguyen, V.H.: ϵ -optimality and ϵ -Lagrangian duality for a nonconvex problem with an infinite number of constraints. *J. Optim. Theory Appl.* **141**(2), 389–409 (2009)

33. Upadhyay, B.B., Mishra, S.K.: Nonsmooth semi-infinite minmax programming involving generalized (ϕ, ρ) -invexity. *J. Syst. Sci. Complex.* **28**(4), 857–875 (2015)
34. Zaheer, H., Pant, M.: Solution of multiobjective portfolio optimization problem using multiobjective synergetic differential evolution (MO-SDE). In: *Soft Computing: Theories and Applications*, vol. 584, pp. 191–199. Springer, Singapore (2017)

Novel Chaotic Elephant Herding Optimization for Multilevel Thresholding of Color Image



Falguni Chakraborty, Provas Kumar Roy, and Debasish Nandi

Abstract Elephant herding optimization (EHO) is a newly developed metaheuristic algorithm which is inspired from the herding behavior of elephant in nature. However, slow convergence is the main disadvantage of the basic EHO algorithm. To improve the global convergence speed as well as the performance of the basic EHO, we propose a new variant of elephant herding optimization by introducing the chaos theory into it. This new variant of EHO algorithm is called chaotic elephant herding optimization algorithm (CEHO). The CEHO algorithm uses a set of chaotic maps that generate chaotic numbers for tuning the control parameters of the basic EHO. The chaotic maps generate different sets of non-repetitive random numbers in a specified range, which are suitable for increasing the searching domain of the algorithm. The performance of the proposed CEHO is applied to a set of images collected from “Berkeley segmentation dataset” to find the optimal threshold values for multilevel image thresholding. The performance of the proposed algorithm is compared with the basic EHO, cuckoo search (CS), and artificial bee colony (ABC) quantitatively and qualitatively. The simulation outputs show that the proposed algorithm supersedes the others.

Keywords Chaos theory · Elephant herding optimization · Multilevel image thresholding · Image segmentation

1 Introduction

Image segmentation plays an important role in computer vision and image pattern analysis. It is a method of dividing the different parts of an image into non-overlapping region based on a set of features. Among the various segmentation techniques in the

F. Chakraborty (✉) · D. Nandi

National Institute of Technology Durgapur, Durgapur, West Bengal, India
e-mail: falguni.durgapur@gmail.com

P. K. Roy
Kalyani Government Engineering College, Kalyani, West Bengal, India

literature, threshold-based segmentation has been considered as a popular method because of its simplicity, accuracy, and robustness and so, throughout the year, various thresholding methods have been reported in the literature. Searching a set of optimal thresholds for an objective function is the prime goal in any threshold-based image segmentation technique. The classical methods of optimization are not suitable to provide global or near global optimal solutions for non-differentiable objective functions. For those cases, the metaheuristic algorithms, such as particle swarm optimization (PSO) [1], whale optimization algorithm (WOA), moth flame optimization (MFO) [2], teaching–learning-based optimization (TLBO) [3], shuffled frog leaping algorithm (SFLA) [4], and spider monkey optimization (SMO) [5] are considered to be more effective. Every metaheuristic algorithm is associated with two key features: Intensification and diversification. Intensification focuses on searching for the local optima by using the local best candidate information, while the diversification means exploring the searching region globally. Proper balancing of these two aspects leads to achieve the global optima. Most of the metaheuristic algorithms use randomization to explore the searching region and may get stuck into the local optima. This can be overcome by developing chaotic-based techniques [6] to enhance the performance of the basic algorithms. The non-repetitive nature of chaotic sequences increases the searching domain of the problem. This reduces the chances of getting trapped into local optima and increases the chance of getting a better quality solution.

Elephant herding optimization algorithm is a newly developed metaheuristic algorithm proposed by Wang et al. [7] in 2016. Wang has developed a mathematical formulation of the natural herding behavior of the elephants. The algorithm has been successfully used to solve some real-time optimization problems. Meena et al. [8] have used improved EHO for multiobjective DER accommodation in distribution systems. Tuba et al. [9] optimized the support vector machine (SVM) parameters to determine the exact erythematous-squamous diseases. Besides this, there are many problems where EHO has provided good solutions with respect to some contemporary methods. However, the slow convergence of this algorithm has made it unsuitable for some applications.

According to chaos theory, chaotic sequences may be generated by using different nonlinear discrete maps under certain criteria. The nonlinear maps which are able to generate chaotic sequences are called chaotic maps. Several chaotic maps are reported in the literature on chaos theory [6]. A good property of chaotic sequence is non-repetitive property. This property may be used to enhance the searching domain in exploration. Some authors have used it to improve the performance of different metaheuristic algorithms. Alatas [10] introduced chaotic with the bee colony algorithms for solving global numerical optimization and Uniform big bang chaotic big crunch optimization [11]. Coelho et al. [12] solved the economic load dispatch problem by chaotic PSO. Being inspired by the success of the previous works, we have utilized the non-repetitive property of chaos to the basic EHO for improving the convergence rate of the EHO and to improve the quality of the solution. We have also successfully applied the proposed CEHO for solving multilevel thresholding problem in image segmentation.

The paper is presented as follows: problem formulation is discussed in Sect. 2; Section 3 described the EHO algorithm and chaos theory; the proposed chaotic EHO-based multilevel thresholding technique is discussed in Sect. 4; experiments and simulation results are presented in Sect. 5; the conclusions are drawn in Sect. 6.

2 Problem Formulation

Multilevel thresholding for image segmentation is mathematically formulated as:

$$\begin{aligned} R_1 &\leftarrow S \text{ if } 0 \leq S < T_1 \\ R_2 &\leftarrow S \text{ if } T_1 \leq S < T_2 \\ R_{n-1} &\leftarrow S \text{ if } T_{n-1} \leq S < T_n \\ R_n &\leftarrow S \text{ if } T_n \leq S < L - 1 \end{aligned} \quad (1)$$

where $T_1 < T_2 < \dots < T_{n-1} < T_n$ are the threshold values. The optimal threshold values of an objective function (F) are computed as

$$(T_1^*, T_2^*, \dots, T_n^*) = \operatorname{argmax}(F(T_1, T_2, \dots, T_n)) \quad (2)$$

We consider Otsu's [13] between-class variance and Kapur's entropy [14] as objective functions for segmentation.

3 Optimization

3.1 EHO Algorithm

EHO considers the natural herding behavior of elephants. In elephant herding, the group of elephants is divided into numbers of clans. Each clan is composed of females with their calves under the leadership of matriarch. Female elephants like to live with the other family members, whereas the male elephants wish to lead a lonely life. Therefore, they leave their families to either stay alone or find a small male elephant's group. Based on this natural behavior of the elephant, two mathematical expressions are formed to solve an optimization problem.

To fit the elephant herding behavior into the mathematical form, we consider the following points:

- The group of elephants is divided into a number of clans with an equal number of elephants under the leadership of matriarch.

- As the male elephants prefer to leave solitary life, a fixed number of the male elephant (minimum fitness value in case of maximization problem) live away from their family in each generation.
- The head of each clan is considered to be the maximum fitness value.

Clan Updating Operator In each iteration, the updated position of the j th elephant of the clan c_i is given by

$$x_{\text{new},c_{i,j}} = x_{c_{i,j}} + \alpha \times (x_{\text{best},c_i} - x_{c_{i,j}}) \times r \quad (3)$$

where $x_{\text{new},c_{i,j}}$, and x_{best,c_i} represent the new updated position of j th elephant of clan c_i and best elephant in the clan c_i respectively. Matriarch influence factor $\alpha \in [0, 1]$ and $r \in [0, 1]$ are used for updating the position of other members of the clans.

The following equation is used to update the position of the best elephant of the clan c_i .

$$x_{\text{new},c_{i,j}} = \beta \times x_{\text{center},c_i} \quad (4)$$

where $\beta \in [0, 1]$ is the influence factor of x_{center,c_i} on $x_{\text{new},c_{i,j}}$. The x_{center,c_i} of the clan c_i can be defined as follows.

$$x_{\text{center},c_i,d} = \frac{1}{n_{c_i}} \times \sum_{j=1}^{n_{c_i}} x_{c_{i,j},d} \quad (5)$$

where n_{c_i} represents total number of elephant in each clan; d ($1 \leq d \leq D$) is the dimension of an elephant of a clan and D represents the total dimension.

Separating Operator Since the male elephants prefer to live a solitary life, we can mathematically implement this behavior by introducing separating operator in this optimization problem. The worst elephants (having a minimum fitness value) update their positions by the following equation:

$$x_{\text{worst},c_i} = x_{\min} + (x_{\max} - x_{\min}) \times \text{rand} \quad (6)$$

where x_{worst,c_i} represents the worst elephant(minimum objective function value) of the clan c_i of elephant group. x_{\max} , x_{\min} are the maximum and minimum boundary of the search space and $\text{rand} \in [0, 1]$.

3.2 Chaos Theory

It is observed that the traditional EHO algorithm suffers from poor convergence rate in finding the global or near global optima, which makes the optimization algorithm slower. This may be due to repeated generation of the same number by the conventional random number generator which is based on the stochastic ergodic process. We can overcome this limitation by using chaotic maps as a random num-

ber generator with the conventional EHO in place of traditional stochastic ergodic process-based random number generator. Chaotic maps are able to generate the non-repetitive sequence of numbers in a specified range. This property of chaotic maps can be efficiently utilized to improve the searching of global optimal points in the whole searching domain with less searching trials. Hence, it is possible to achieve an improved convergence rate in the optimization process. With this prediction, we have proposed Chaotic EHO by introducing chaotic maps in the conventional EHO to improve the performance in terms of the convergence speed and solution quality.

4 CEHO in Multilevel Image Thresholding

A set of chaotic map as shown in [6] is considered for chaotic sequence generator. Depending upon the performance in terms of mean, standard deviation, and convergence speed property of the selected images, the tent map likely to logistic map is considered as the chaotic sequence generator with the traditional EHO and is applied in multilevel color image segmentation for optimizing thresholds. The details of CEHO and its application to multilevel image thresholding are discussed here.

- Step 1** Initial population (elephant) of size E is generated randomly. Each of the elephants is represented by a vector of size D (i.e., D number of thresholds values).
- Step 2** Evaluate the fitness function of each elephant by the taking Kapur's entropy or Otsu's between-class variance as an objective function.
- Step 3** The total population is divided into a fixed number of clans. The matriarch is the head of each clan. An elephant with the highest fitness value elephant in a clan c_i is treated as the matriarch.
- Step 4 Clan updating operator in CEHO:** j th elephant of clan c_i is updated as,

$$x_{\text{new},c_{i,j}} = x_{c_{i,j}} + u \times (x_{\text{best},c_i} - x_{c_{i,j}}) \times v \quad (7)$$

$$x_{\text{new},c_{i,j}} = w \times x_{\text{center},c_i} \quad (8)$$

where u , v , and w are the chaotic sequences and are generated by the following well-known tent map, respectively.

$$x_{n+1} = \begin{cases} \mu x_n & x_n < 0.5 \\ \mu(1 - x_n) & x_n \geq 0.5 \end{cases} \quad \text{for } \mu = 2 \quad (9)$$

- Step 5 Separating operator in CEHO:** In CEHO, the separating operation is done by using the following equation

$$x_{\text{wrost},c_i} = x_{\min} + (x_{\max} - x_{\min}) \times z \quad (10)$$

where the chaotic sequence z is generated by the tent map with different initial value. After each iteration, select the fittest elephant as the optimum thresholds value.

Step 6 Repeat the Step-2 to Step-5 till the maximum iteration.

5 Experimental Result and Discussion

The performance of the CEHO is evaluated by considering 5-level, 6-level, and 7-level thresholding of different color images. We compare the proposed CEHO with the conventional (basic) EHO [7], CS [15], and ABC [1]. The parameters used for other algorithms are collected from the literature. The number of iterations taken for each algorithm is 100.

We quantify the performance of the algorithms by applying them to a large set of color images for optimizing the thresholds using Kapur's and Otsu's objective functions. More than 50 color images taken from Berkeley segmentation dataset are thresholded for multilevel segmentation using different algorithms. The results of five images (boat, bridge, fishing, lizard, and starfish of Fig. 1) are shown here. Peak signal-to-noise ratio (PSNR), structural similarity index metric (SSIM) [16], and feature similarity index metric (FSIM) [17] are used to quantify the performance of the algorithms. The definitions of these quality metrics are discussed elsewhere [15].

Figure 2 shows the 6-level and 7-level of thresholded outputs of four metaheuristic optimization techniques. The boat image is thresholded by taking the Kapur's entropy as the objective function, whereas for fishing image, Otsu's between-class variance is taken as an objective function. The highest values of the objective functions of the red and green band and the corresponding thresholds for 5–7 level thresholding of different images using different optimization techniques are shown in Table 1 and Table 2. We see from the table that, the proposed CEHO gives better values in most of the cases for each image and for all objective functions.

We know that a metaheuristic optimization algorithm may not give the same result in each execution of the algorithm. Therefore, to verify the performance of

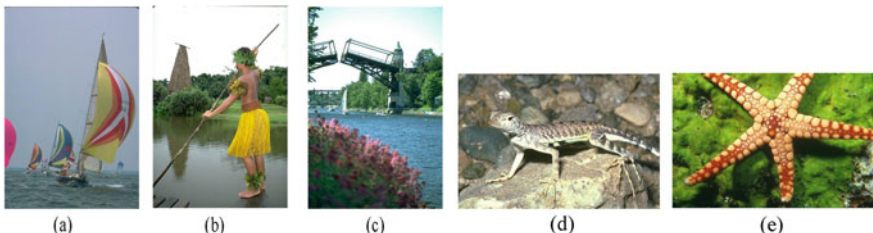


Fig. 1 (a) boat, (b) fishing, (c) bridge, (d) lizard, and (e) starfish are the original images used for experiments

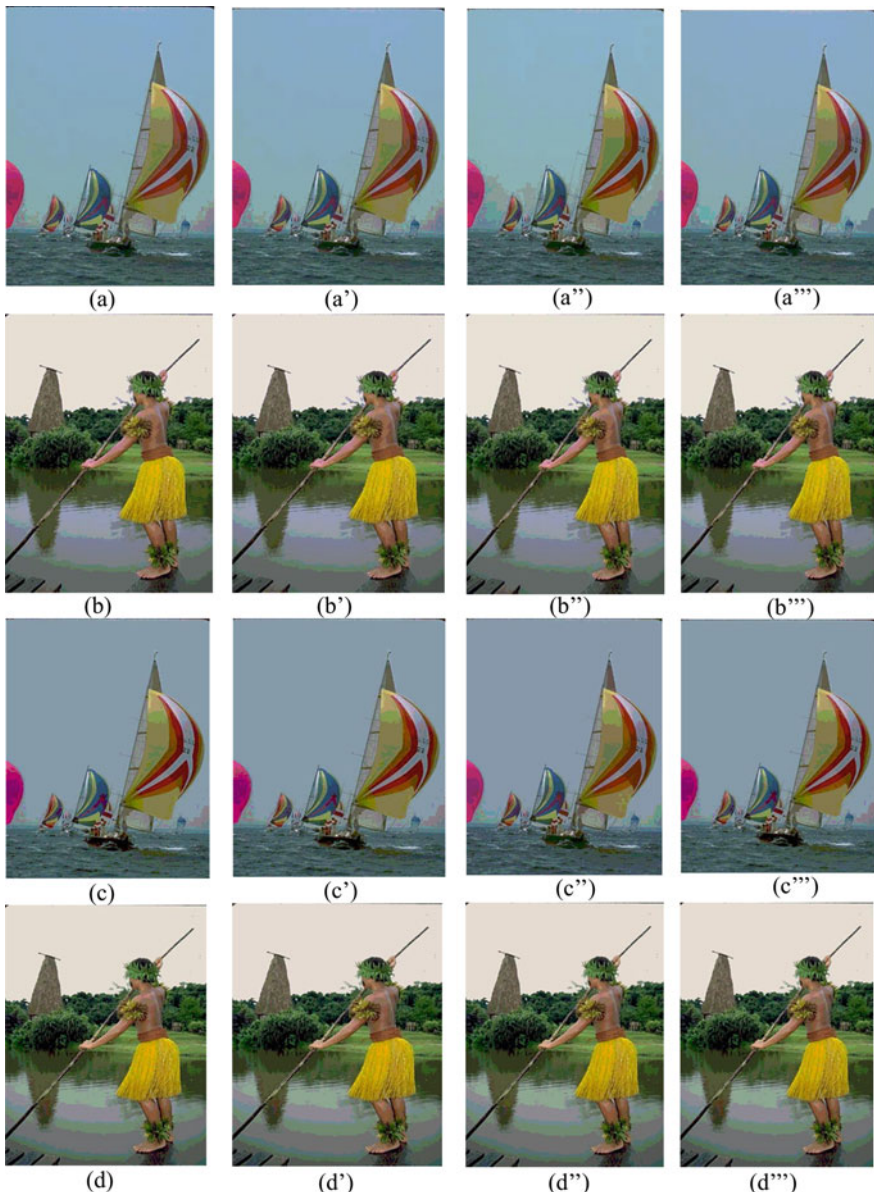


Fig. 2 (a–a'') 7-level thresholded images of boat image Kapur's method. (b–b'') 7-level thresholded images of fishing image using Otsu's method. (c–c'') 6-level thresholded images of boat image using Kapur's method. (d–d'') 6-level thresholded images of fishing image using Otsu's method

Table 1 The Optimum thresholds and objective function values of red color in RGB system of test images taking Kapur's entropy as fitness function

Image	Values of Objective function						Thresholds						
	K	CEHO	EHO	CS	ABC	CEHO	EHO	CS	CEHO	EHO	CS	ABC	
BOAT	5	21.1731	21.1714	21.1527	21.1705	46.92	133	178	212	46.91	133	178	212
	6	23.7947	23.7924	23.7627	23.7551	38.67	101	134	178	38.67	108	133	178
	7	26.1865	26.1558	26.0677	26.1283	37	64	97	133	174	98	132	175
BRIDGE	5	21.6836	21.6824	21.6824	21.6824	44.86	128	171	214	44.85	128	170	214
	6	23.3463	23.451	23.3224	24.3169	38.73	110	144	182	220	36	74	109
	7	26.9110	26.9095	26.8694	26.9087	32	65	96	128	161	194	223	223
LIZARD	5	21.6351	21.6348	21.6295	21.6299	64	103	141	177	214	64	102	141
	6	24.1519	24.1489	24.1403	24.1419	62	94	125	156	188	219	62	92
	7	26.5343	26.5322	26.4847	26.5273	60	87	114	142	169	195	223	58
FISHING	5	20.0875	20.0855	20.0856	20.0830	46.94	140	183	233	48.95	140	183	234
	6	22.6722	22.8687	22.8670	22.8609	42	82	125	166	201	237	41	81
	7	23.5246	25.5174	25.4919	25.4875	35	68	104	137	170	203	36	66
STARFISH	5	21.5733	21.5708	21.5661	21.5620	46	86	127	168	208	51	89	129
	6	24.1833	24.1804	24.1799	24.1786	41	75	109	144	180	214	39	72
	7	26.6596	26.6508	26.6333	26.6491	38	68	98	128	158	218	36	66

Table 2 Optimum thresholds and objective function values of green color in RGB system of test images taking Otsu's method as fitness function

Image	Values of Objective function						Thresholds	
	KCEHO	EHO	ABC	C EHO	EHO	CS		
BOAT	5 1289.5049 1288.9874 1286.1973 1286.1960 1286.0155 1300.7233	75 101.124.149 168 170 150 170 150 170	78 103.126.150 170 150 170 150 170	73 103.126.151 170 172 159 172 159	68 98 123 150 169 174	118 123 142 152 152 174		
BRIDGE	6 6168.7085 6168.7323 6168.7439 6168.7139 58 89 122 156 214 58 89 122 155 213 53 78 105 132 163 216	53 78 106 135 165 218 53 78 106 135 165 218 53 78 105 132 163 216	53 78 106 135 165 218 53 78 105 132 163 216	53 78 105 132 163 216	54 78 106 135 166 219	118 123 142 152 152 174		
LIZARD	5 2777.3368 2727.2902 2727.1640 2727.0551 77 110.141.170 218 74 108.139.175 217 222 49 71 94 119 145 214 222	70 101.126.150 186 223 71 102.127.156 188 224 76 110.139.175 217 224	70 101.126.150 186 223 71 102.127.156 188 224 76 110.139.175 217 224	70 101.126.150 187 224 71 102.127.155 187 223	76 110.141.177 216 223	67 98 117 141 168 197 229	117 141 168 197 229	
FISHING	5 5032.6366 5032.6188 5032.5739 5032.5147 69 102.130.162 218 69 102.130.163 218 68 102.130.163 218	69 102.130.162 218 69 102.130.163 218 68 102.130.163 218	69 102.130.162 218 69 102.130.163 218 68 102.130.163 218	68 102.130.163 218	70 103.132.163 216	117 141 168 197 221		
STARFISH	7 5007.4650 5067.3987 5067.3403 5067.3923 51 80 103 126 149 177 223 51 79 103 125 149 177 225 50 79 103 125 149 177 225	57 93 128 162 201 56 92 128 162 201 52 84 114 142 171 207	57 93 128 162 201 56 92 128 162 201 52 84 114 142 171 207	58 95 130 163 201	54 86 116 144 173 209	117 141 168 197 227		
	7 3073.7541 3073.4174 3073.3361 3073.2986 49 76 102 128 153 179 211 50 77 101 128 154 180 213 49 76 102 128 154 180 214	53 84 113 142 171 206 53 84 113 142 171 207 52 84 114 142 171 207	53 84 113 142 171 206 53 84 113 142 171 207 52 84 114 142 171 207	54 86 116 144 173 209	50 77 102 129 156 182 213			

Table 3 Mean and standard deviation of red color in RGB system of test images taking Kapur's method as fitness function

Image	K	Mean			Standard Deviation		
		CEHO	EHO	CS	CEHO	EHO	CS
BOAT	5	21.1702	21.1543	21.0979	21.1473	0.002425378	0.011484946
	6	23.7803	23.7702	23.6763	23.7300	0.015941808	0.02160815
	7	26.1520	26.0992	25.9869	26.0716	0.036413823	0.040387273
BRIDGE	5	21.6836	21.6798	21.6792	21.6736	0.000129684	0.002646951
	6	24.3415	24.3407	24.3130	24.3379	0.000536726	0.003228666
	7	26.9059	26.9053	26.8072	26.8773	0.000380511	0.003906926
LIZARD	5	21.6327	21.6325	21.6145	21.6178	0.000193868	0.002164535
	6	24.1485	24.1057	24.0877	24.1349	0.002004261	0.004682702
	7	26.5308	26.5219	26.4253	26.4969	0.015076867	0.009126246
FISHING	5	20.0870	20.0847	20.0789	20.0742	0.001846261	0.003313046
	6	22.8631	22.8504	22.8450	22.8496	0.009345622	0.019780133
	7	25.5198	25.5025	25.4418	25.4204	0.004550121	0.007046046
STARFISH	5	21.5671	21.5647	21.5599	21.5611	8.30765E-05	0.00120344
	6	24.1752	24.1720	24.1464	24.1671	0.000159509	0.002482667
	7	26.5396	26.4510	26.3201	26.3771	0.00050117	0.006378341

Table 4 PSNR, SSIM, and FSIM value of images after thresholding taking Otsu's as the objective fitness function

Image	K	PSNR	SSIM			FSIM					
			CEHO	EHO	CS	CEHO	EHO	CS	CEHO	EHO	CS
BOAT	5	28.7871	28.5759	28.5527	28.3431	0.9966	0.9964	0.9963	0.9128	0.9119	0.9107
	6	29.6311	29.5238	29.3173	28.9738	0.9972	0.9970	0.9966	0.9232	0.9230	0.9207
BRIDGE	5	25.3581	25.3511	25.2466	25.3118	0.9907	0.9905	0.9900	0.9145	0.9141	0.9140
	6	26.5072	26.4581	26.4145	26.3956	0.9923	0.9921	0.9918	0.9917	0.9327	0.9314
LIZARD	7	27.3560	27.3159	27.2901	27.2996	0.9928	0.9927	0.9926	0.9399	0.9395	0.9392
	5	23.3255	23.3123	23.3098	23.3012	0.9889	0.9887	0.9886	0.8664	0.8662	0.8663
FISHING	6	24.3780	24.3651	24.3616	24.2917	0.9908	0.9907	0.9907	0.8872	0.8872	0.8854
	7	25.4337	25.4103	25.3735	25.3572	0.9928	0.9925	0.9925	0.9072	0.9071	0.9062
STARFISH	5	24.8644	24.8521	24.8510	24.8432	0.9903	0.9902	0.9901	0.8818	0.8814	0.8816
	6	25.9710	25.9483	25.8923	25.8608	0.9920	0.9920	0.9916	0.8948	0.8928	0.8937
STARFISH	7	26.9518	26.8111	26.7430	26.7691	0.9931	0.9925	0.9925	0.9076	0.9055	0.9052
	5	23.4499	23.4342	23.4163	23.4123	0.9862	0.9861	0.9860	0.8492	0.8491	0.8490
	6	24.7440	24.7136	24.6513	24.6501	0.9891	0.9887	0.9884	0.8778	0.8769	0.8758
	7	25.7709	25.7027	25.6580	25.6320	0.9908	0.9907	0.9905	0.8999	0.8991	0.8965

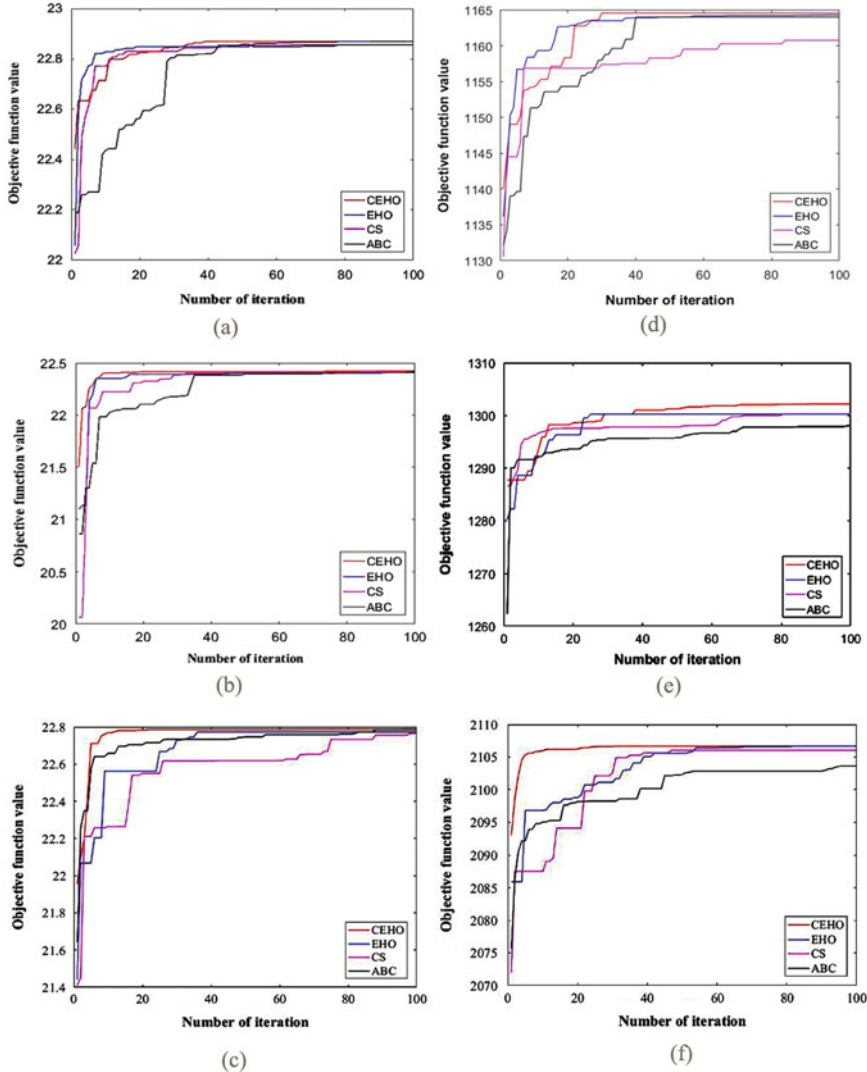


Fig. 3 Convergence graph of fishing and boat image by Kapur's and Otsu's objective function for RGB color space

the algorithms, we execute each algorithm a number of times and then we estimate the mean and the standard deviation (SD) of the objective function values. Table 3 shows the mean and SD of the Kapur's objective function's value for the red color by executing the algorithms 30 times (i.e. 30 runs). We see from the tables that the proposed CEHO algorithm provides better mean values and lesser standard deviations with respect to the other algorithms in 5–7 level thresholding. Table 4 shows the

PSNR, SSIM, and FSIM values of different algorithms for the segmented images by using Otsu's function. The results declare that the proposed CEHO has superior performance over the others in terms of the quality metrics.

To investigate the convergence rate of the different algorithms, we have drawn the convergence graph. Figure 3 shows the convergence graphs for thresholding red, green, and blue color of the boat and fishing images by applying the CEHO, EHO, CS, and ABC using two objective functions of boat and fishing images. We see from the Fig. 3 that the proposed CEHO algorithm has better convergence rate.

6 Conclusion

In this paper, we have proposed an improved elephant herding optimization by embedding chaotic maps within it. Incorporation of chaotic maps has removed the chance of a repetition of a random number in the generated chaotic random sequences due to their capability of generating non-repetitive chaotic numbers. This property has improved the speed of convergence of the EHO. Moreover, it has also improved the quality of solution of the basic (conventional) EHO. The algorithm is successfully applied to solve the problem of multilevel thresholding in color image segmentation. The performance of the algorithm is verified on the RGB color images and compared with other recent algorithms. The results obtained from the simulation explore that the proposed CEHO algorithm gives better performance with respect to traditional EHO, CS, and ABC both in terms of convergence rate and the quality of solution.

References

1. Akay, B.: A study on particle swarm optimization and artificial bee colony algorithms for multilevel thresholding. *Appl. Soft Comput.* **13**, 3066–3091 (2013)
2. Aziz Md, A.E., Ewees, A.A., Hassanien, A.E.: Whale optimization algorithm and moth flame optimization for multilevel thresholding image segmentation. *Exp. Syst. Appl.* **83**, 242–256 (2017)
3. Sheth, P.D., Jagdeo, S.M., Umbarkar, A.J.: Teaching learning-based optimization on Hadoop. *Int. Conf. Soft Comput.: Theor. Appl.* **583**(1), 251–263 (2017)
4. Sharma, T.K., Pant, M.: Opposition-based learning embedded shuffled Frog-Leaping algorithm. *Int. Conf. Soft Comput.: Theor. Appl.* **583**(1), 853–861 (2017)
5. Jain, S., Swami, V., Kumar, S.: An improved spider monkey optimization algorithm. *Int. Conf. Soft Comput.: Theor. Appl.* **583**(1), 73–81 (2017)
6. Saleh Tavazoei, M., Haeri, M.: Comparison of different one-dimensional maps as chaotic search pattern in chaos optimization algorithms. *Appl. Math. Comput.* **187**, 1076–1085 (2007)
7. Wang, G.G., Deb, S., Geo, X.-Z., Coelho, L.D.S.: A new metaheuristic optimization algorithm motivated by elephant herding behavior. *Int. J. Bio-Inspired Comput.* **8**(6), 394–409 (2016)
8. Meena, N.K., Parashar, S., Swarnkar, A., Gupta, N., Niazi, K.R.: Improved elephant herding optimization for multiobjective DER accommodation in distribution systems. *IEEE Trans. Industr. Inform.* (2017)

9. Tuba, E., Ribic, I., Hrosik, R.C., Tuba, M.: Support vector machine optimized by elephant herding algorithm for erythemato squamous diseases detection. *Inform. Technol. Quant. Manage. (ITQM) Proc. Comput. Sci.* **122**, 916–923 (2017)
10. Alatas, B.: Chaotic bee colony algorithms for global numerical optimization. *Exp. Syst. Appl.* **37**, 5682–5687 (2010)
11. Alatas, B.: Uniform Big Bang—Chaotic Big Crunch optimization. *Commun. Nonlinear Sci. Numer. Simulat.* **16**, 3696–3703 (2011)
12. dos Santos Coelho, L., Cocco Mariani, V.: A novel chaotic particle swarm optimization approach using Henon map and implicit filtering local search for economic load dispatch. *Chaos, Solitons Fractals* **39**, 510–518 (2009)
13. Otsu, N.: A threshold selection method from gray-level histograms. *IEEE Trans. SMC* **9**(1), 62–66 (1979)
14. Kapur, J.N., Sahoo, P.K., Wong, A.K.C.: A new method for gray-level picture thresholding using the entropy of the histogram. *Comput. Vis. Graphics Image Process.* **29**, 273–285 (1985)
15. Agrawal, S., Panda, R., Bhuyan, S., Panigrahi, B.K.: Tsallis entropy based optimal multilevel thresholding using cuckoo search algorithm. *Swarm Evol. Comput.* **11**, 16–30 (2013)
16. Zhou, W., Alan, C.B., Hamid, S.R., Eero, S.P.: Image quality assessment: from error visibility to structural similarity. *IEEE Trans. Image Process.* **13**(4), 600–612 (2004)
17. Lin, Z., Lei, Z., Xuanqin, M., Zhang, D.: FSIM: A feature similarity index for image quality assessment. *IEEE Trans. Image Process.* **20**(8), 2378–2386 (2011)

Forecasting Groundwater Fluctuation from GRACE Data Using GRNN



Dilip Kumar and Rajib Kumar Bhattacharjya

Abstract The unplanned exploitation of groundwater has depleted the groundwater table in many parts of the world. As such, groundwater fluctuation study is an essential study for the proper management of water in a region. The fluctuation can be determined from the in situ measurement of groundwater level. However, the temporal and spatial resolution of the data is generally very coarse, specifically in developing countries. As such, in this study, a Generalized Regression Neural Network (GRNN) based model is developed for estimating the groundwater fluctuation of a region. The Gravity Recovery and Climate Experiment (GRACE) satellite data along with the hydro-meteorological data of the region are used in developing the model and the model is calibrated and validated using the observed groundwater level data. The field applicability of the model is demonstrated by applying the model in the state of Uttarakhand of India.

Keywords Artificial neural network · GRNN · GRACE · Groundwater · Pattern recognition

1 Introduction

Groundwater is a vital resource for agriculture, Industries as well as for municipal uses and has been extensively used in the northern part of India [1]. The unplanned exploitation of groundwater has depleted this vital resource in many parts of India as well as in various parts of the world also. As such, there is a need to take up proper management policies for optimal sustainable utilization of groundwater. For developing management policies, groundwater level fluctuation data is required. Further,

D. Kumar (✉)

Department of Civil Engineering, GB Pant Institute of Engineering and Technology, Pauri Garhwal, Uttarakhand, India

e-mail: jhadilip27@gmail.com

R. K. Bhattacharjya

Department of Civil Engineering, Indian Institute of Technology Guwahati, Guwahati, India
e-mail: rkbc@iitg.ac.in

the groundwater fluctuation study also helps in understanding the effect of climate change. The in situ measurement of groundwater level data is very expensive and not available in many parts of India. However, much progress has been made with the estimation of groundwater storage using remotely sensed data [2]. The satellite-based data like GLDAS, NLDAS which consist of the different components of total water storage, and GRACE which measures the anomalies gravity variation across the Earth [3, 4] can be used to estimate the groundwater fluctuation of an area. Considering the advantages of these remotely sensed data, this study proposes a model for predicting the groundwater fluctuation of an area using GRACE data. GRACE data provides the TWSA (Total Water Storage Anomaly) of an area which represents the total change in water mass consisting of SWE (Snow Water Equivalent), GW (Ground Water), SM (Soil Moisture), T (Transpiration), E (Evaporation), and RS (Reservoir Storage). For obtaining the groundwater fluctuation from the TWSA, a Generalized Regression Neural Network (GRNN) based downscaling model is developed. The field applicability of the proposed method is evaluated by applying the model in the state of Uttarakhand, India.

1.1 *GRACE Data*

Since March 2002, the Gravity Recovery and Climate Experiment (GRACE) has provided first estimates of land water storage variations by monitoring the time-variable component of Earth's gravity field. This has proven to be an excellent complement to ground-based hydrologic measurements to monitor water mass storage variation within the Earth's fluid envelopes [5–7]. While comparing GRACE signal from other satellite data, we can see that other satellite can capture soil moisture only up to limited depth, i.e., near the land surface only, while the GRACE signal tells us vertical variation in the total water storage from soil moisture, groundwater at all depths, snowpack, and surface water [4, 8, 9]. However, it is to be noted that GRACE-derived TWSA does not have vertical resolution, i.e., cannot distinguish between water stored as snow, soil moisture, and groundwater [10, 11]. The GRACE data has been widely used to monitor changes in water mass redistribution for various basins globally. The gridded TWSA data is used in this study for predicting groundwater fluctuation. The gridded TWSA data with a spatial resolution of 1×1 and temporal resolution of one month was downloaded from <https://grace.jpl.nasa.gov/data/get-data/monthly-mass-grids-land/> [12, 13]. Each monthly GRACE grid represents the surface mass deviation for that month relative to the baseline average over Jan 2004 to Dec 2009 [14, 15]. Figure 1 shows the schematic diagram of GRACE satellite covering an arbitrary watershed.

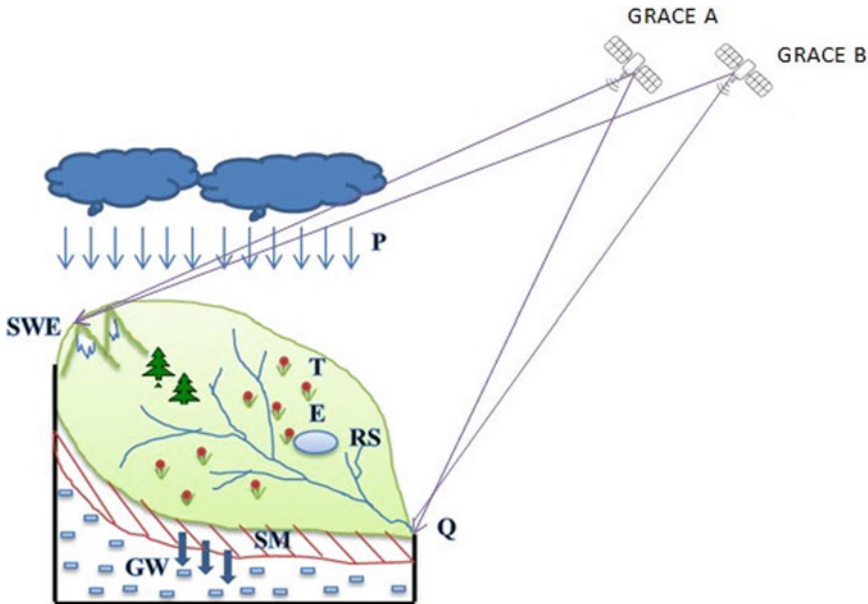


Fig. 1 A schematic diagram indicating GRACE satellite for covering a basin for measuring total water storage which is sum of SWE, GW, SM, T, E and RS

1.2 General Regression Neural Network (GRNN)

The General Regression Neural Networks as explained by Specht is basically a neural network based function predicting algorithm [16, 17]. It predicts the output of a given input data. It requires no data for the iterative training which makes GRNN more suitable than other neural network models [18, 19]. GRNN is capable to approximate any arbitrary continuous function and works on the nonlinear regression concept [20, 21]. The regression of a dependent variable y on an independent variable x estimates the most probable value for y , given x and a training set. The training set consists of pairs of matches (x,y) . The regression method will determine the value of the desired output that contains the minimum value of mean squared error.

1.2.1 Working of GRNN

The fundamental principle of a neural network is that it needs training data to train itself. The training data should contain input-output datasets [22, 23]. In case of a neural network, first we have to train the network with the desired dataset and we test a new set of data, the network gives the result accordingly, i.e., based on the training code. Whereas in the case of GRNN, the new output is determined using a weighted average of the outputs of the training dataset. In GRNN, the weight is

estimated using the Euclidean distance between the training data and test data. If the distance is large then the weight will be less and if the distance is small, it will put more weight to the output.

1.2.2 Network Configuration of a GRNN Model

In general, a GRNN model consists of four basic layers: (i). Input layer, (ii). Pattern layer, (iii). Summation layer, and (iv). Output layer [24]. The basic network design is shown in Fig. 2.

The input layer consists of all input data required for the simulation. The pattern layer computes the Euclidean distance and decides the relevant weight. The summation layer consists of two parts. The first one is the numerator part and the second one is the denominator part. The numerator part contains the summation of the multiplication of training output data, i.e., the product of weight and output. The denominator is the summation of all the weights. The output layer contains one neuron which estimates the output by dividing the numerator part of the summation layer by the denominator part.

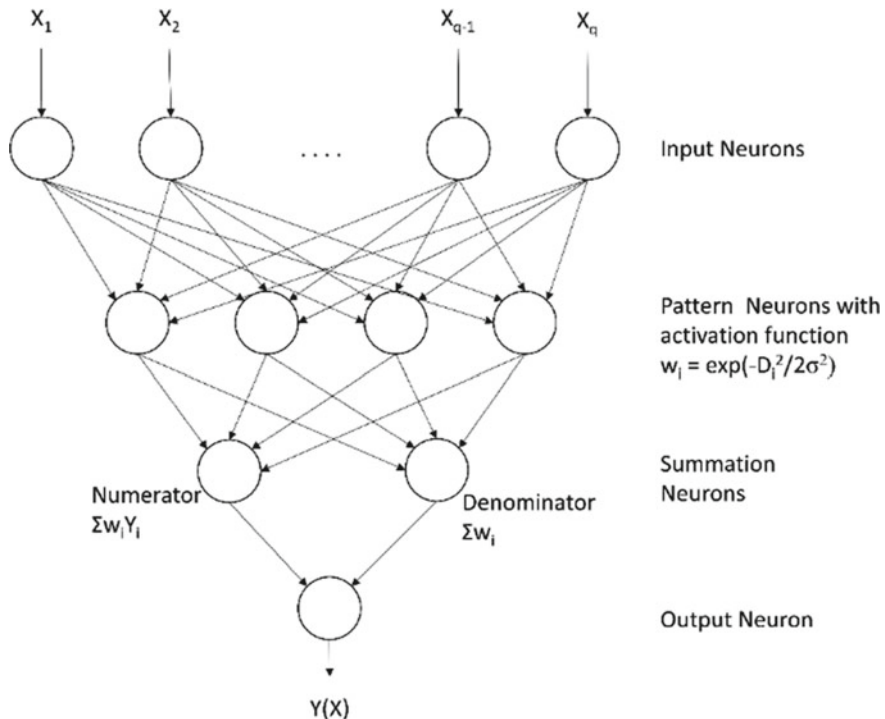


Fig. 2 The basic network diagram of a GRNN model

1.2.3 Calculation of Output

As mentioned in the previous section (working of GRNN), the Euclidean distance of the inputs is the basis for the output of the model and it requires no training. The equation for the calculation of the new output according to the new input as based on training datasets is given in Eq. 1.

$$Y(X) = \frac{\sum Y_i e^{-\left(\frac{d_i^2}{2\sigma^2}\right)}}{\sum e^{-\left(\frac{d_i^2}{2\sigma^2}\right)}} \quad (1)$$

where d_i is the Euclidean distance between new input (X) and the training input (X_i), σ is the spread which enhances the distance factor such that the increase in the value of σ decreases the chance of output near to the extreme values of the inputs and vice versa. Hence, σ is called the spread of the network.

1.2.4 Choosing the Spread (σ) for the Network

The training procedure is to find out the optimum value of σ . The best practice is which finds the value at which the MSE (Mean Squared Error) is minimum. The first step is to divide the whole training sample into two parts, training sample and test sample. Then GRNN is applied to the test data based on training data and finds out the MSE for different values of spread. Now find the minimum MSE and the corresponding value of spread gives the optimum value for the spread σ .

2 Methodology

2.1 Study Area

The one of the hilly State of India, Uttarakhand lies between 28°04' and 31°02' N latitude and 77°03' and 81°02' E longitude (Fig. 3). The state spread over an area of about 53,483 km². Uttarakhand has a diverse hydrogeological structure. The whole region of the state is divided into two distinguished hydrogeological regimes as the Gangetic alluvial plain and the Himalayan mountain belt. The Gangetic alluvial plain is covered with a wide range of alluvium and unconsolidated sedimentary material of different size fractions (ranging from boulder to clay) and is a likely zone for groundwater development [25]. The Himalayan mountain belt, being largely

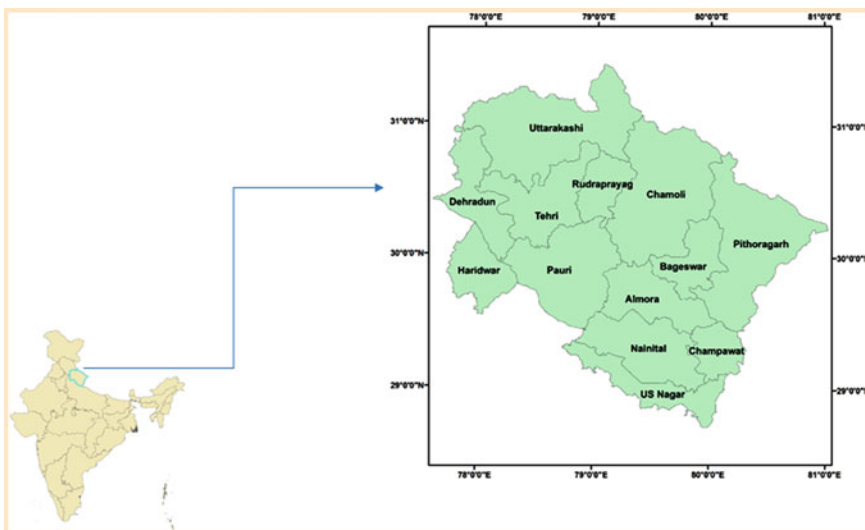


Fig. 3 The study area

hilly, have less capacity for large-scale development of groundwater. Groundwater in the hilly region occurs mostly in fractures and rises as springs. The springs are manageable for the development of groundwater resources in the state but at small-scale.

2.2 *Groundwater Data of Uttarakhand*

As per the central groundwater board data, the annual replenishable groundwater resource in Uttarakhand is 2.27 billion cubic meter (BCM), the net annual groundwater availability is 2.10 BCM and the annual groundwater drift in the state is 1.39 BCM [26, 27]. The state consists of a total of 13 districts, among these 13 districts, the wells are located only in five districts of Uttarakhand namely, Dehradun, Haridwar, Udhampur, Nainital, and Champawat. As per the report of the Ministry of water resource, the Government of India, a total of 167 wells are located in the Uttarakhand, which is confined in the five districts as defined above [28]. The total number of wells located in these five districts of Uttarakhand are shown in Fig. 4.

The data related to the fluctuation water level in these wells are downloaded from India—WRIS (Water Resource Information System). The groundwater data is available on seasonal wise and classified into four seasons as shown in Table 1.

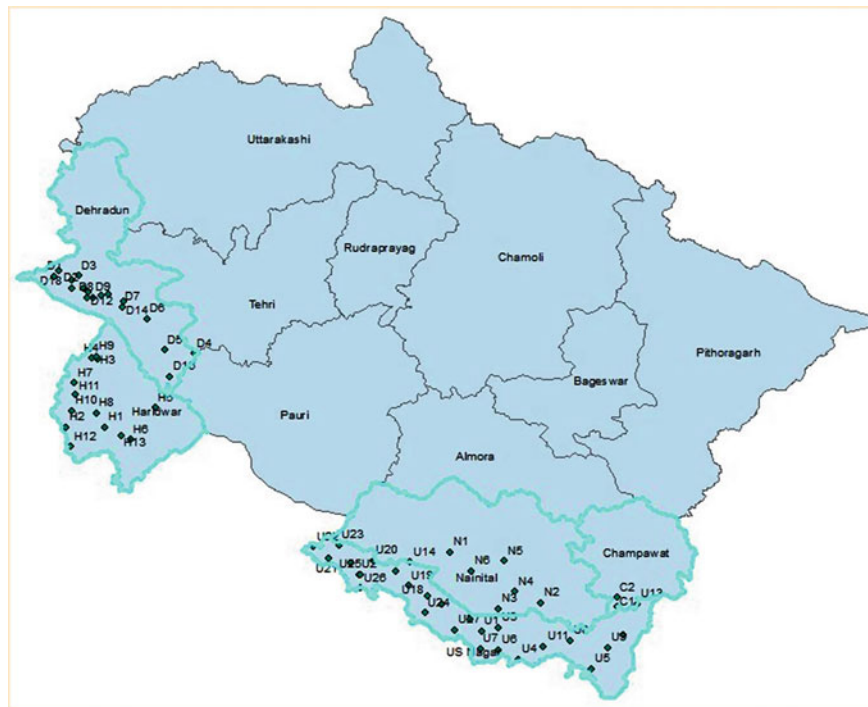


Fig. 4 Showing location of wells in Uttarakhand

Table 1 Groundwater recording season and their corresponding months

S.No.	Season name	Months
1	Post monsoon Kharif	Oct
2	Post monsoon Rabi	Jan
3	Pre monsoon	April
4	Monsoon	July

2.3 *Different Input Used in Formation of GRNN Model*

We used the monthly rainfall data, after processing from IMD rainfall data, GRACE monthly data and average temperature data obtained from IMD as the inputs to the proposed model (Fig. 5). The output from the model is the groundwater fluctuation level.

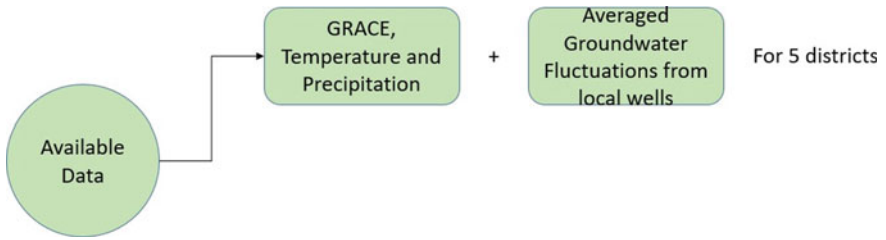


Fig. 5 Summary of the different inputs

2.3.1 Working of GRNN Model

As the main objective of the study is the estimation of groundwater fluctuation for the districts having seasonal variation of groundwater data, so the concept of GRNN model as described above applies to five districts of Uttarakhand namely Dehradun, Haridwar, Nainital, Champawat, and US Nagar to predict the groundwater fluctuation, taking GRACE TWS, average temperature, and precipitation as the inputs. The groundwater level data is available for these five districts. The working model for these five districts is shown in Fig. 6 and explained by the flowchart in Fig. 7.

G^t , T^t , and P^t in Fig. 6 represent the GRACE, temperature and precipitation datasets as inputs for time step “ t ”. GW^k represents the outputs as per the GW observations. The inputs for the corresponding output months are given in Table 2. The input data available is monthly whereas the output data is available for every three months. Therefore, the input data has to be given for the past three months, i.e., for each k , t runs as $k - 1, k - 2, k - 3$. The model is evaluated from April 2005 to January 2016.

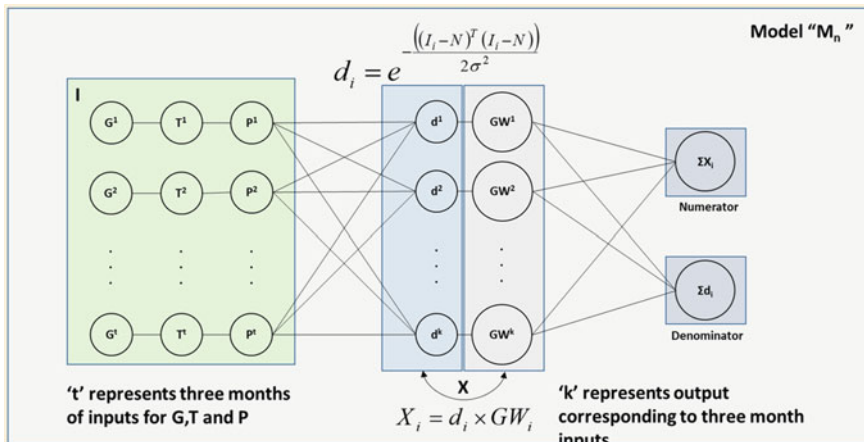


Fig. 6 GRNN modes

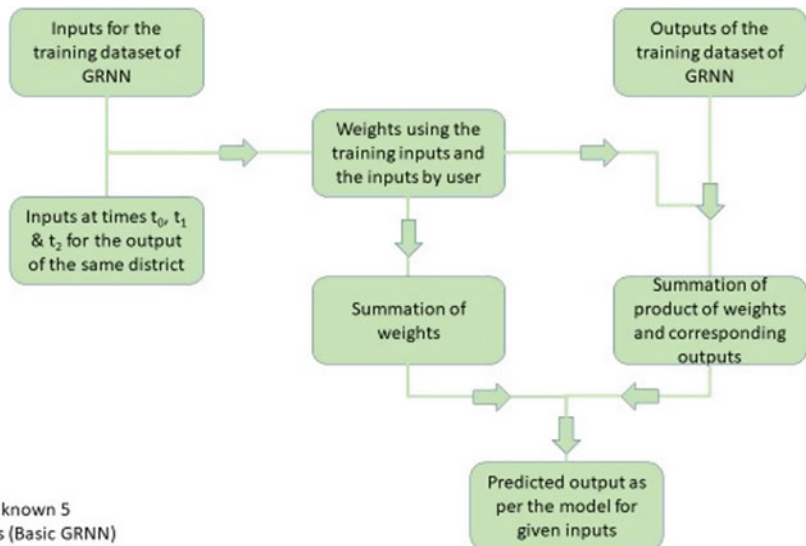


Fig. 7 The flow chart for the five districts where groundwater data is available

Table 2 Input months and corresponding output months for GRNN model

Input months	Output months
January, February, and March	April
April, May, and June	July
July, August, and September	October
October, November, and December	January

3 Results And Discussion

The proposed GRNN model is used in the study to predict the groundwater fluctuation in the five districts of Uttarakhand, where the data related to groundwater is available. The statistical parameter, Coefficient of determination, R^2 is used to evaluate the efficiency of the model. The R^2 values as shown in Fig. 8 verify that the proposed GRNN model is capable to predict the groundwater fluctuation in Dehradun, Haridwar, and Nainital very well. In the case of Champawat and US Nagar, the model prediction is satisfactory in nature with R^2 value of 0.47 and 0.657 respectively.

Since the number of wells is more in Dehradun, Haridwar, and US Nagar as shown in Fig. 4, so the predicted data for fluctuation are satisfactorily obtained by the model (Fig. 9). In the case of Champawat, we have only two observations well. As such, the GRNN model could not predict the fluctuation very well. The graph between spread (σ) and error is shown in Fig. 10. The Fig. 11 presented the scatter plot between observed and GRNN predicted groundwater fluctuation, along with corresponding R^2 value.

Corelation_coeff (R^2) between observed and GRNN predicted groundwater fluctuations.

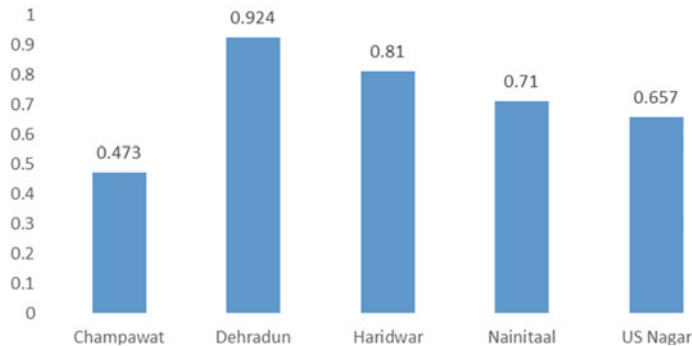


Fig. 8 R^2 between observed and GRNN predicted Groundwater fluctuation in five districts of Uttarakhand

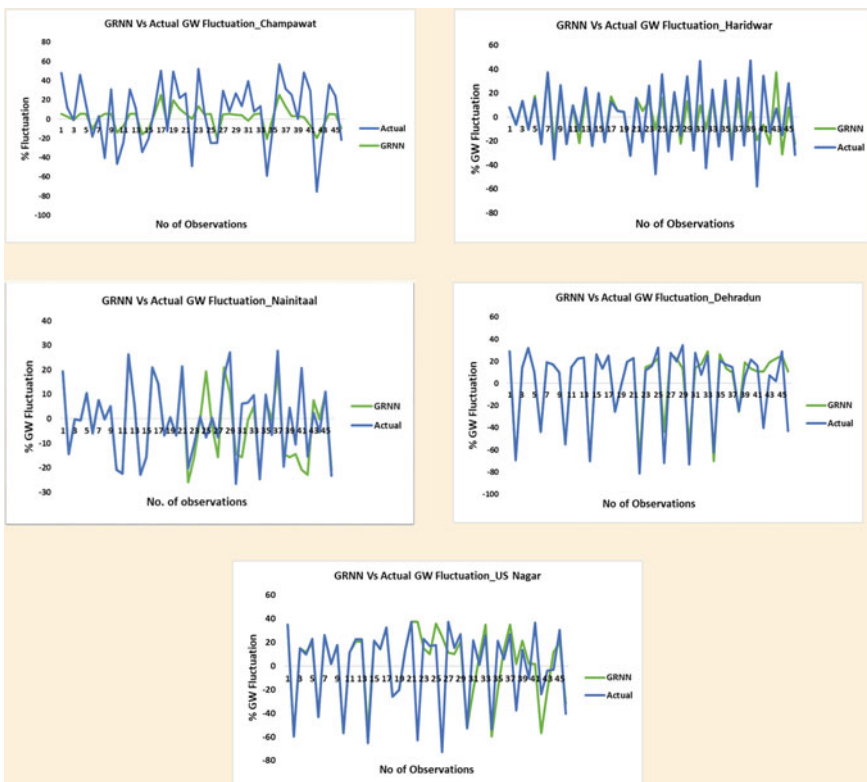


Fig. 9 The comparison of groundwater fluctuation between observed data and GRNN model output:
(i) Dehradun (ii) Haridwar (iii) Nainital (iv) US Nagar, (v) Champawat

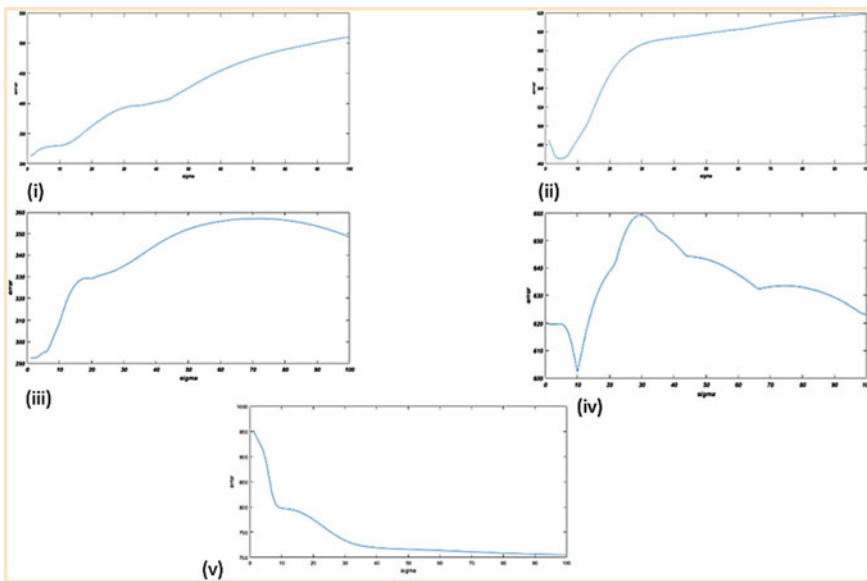


Fig. 10 The graph between sigma and error for (i) Dehradun (ii) Haridwar (iii) Nainital (iv) US Nagar (v) Champawat

4 Conclusion

The GRACE TWSA can be used for monitoring the water resources at a local scale. In the present study, we utilized the GRACE TWS to predict the change in groundwater fluctuation in the different seasons in Uttarakhand. The GRNN model provides us the change in water level instead of actual water level since we are using GRACE data and the available groundwater data is also in terms of fluctuation. The GRNN models used the monthly precipitation data obtained from IMD, the average temperatures, and GRACE TWS as inputs. The main objective is the estimation of groundwater level change. The well data used for validation of the GRNN model is located in the different districts of Uttarakhand. The evaluation of the results shows that the performance of the model is satisfactory at all the districts where groundwater fluctuation data is available.

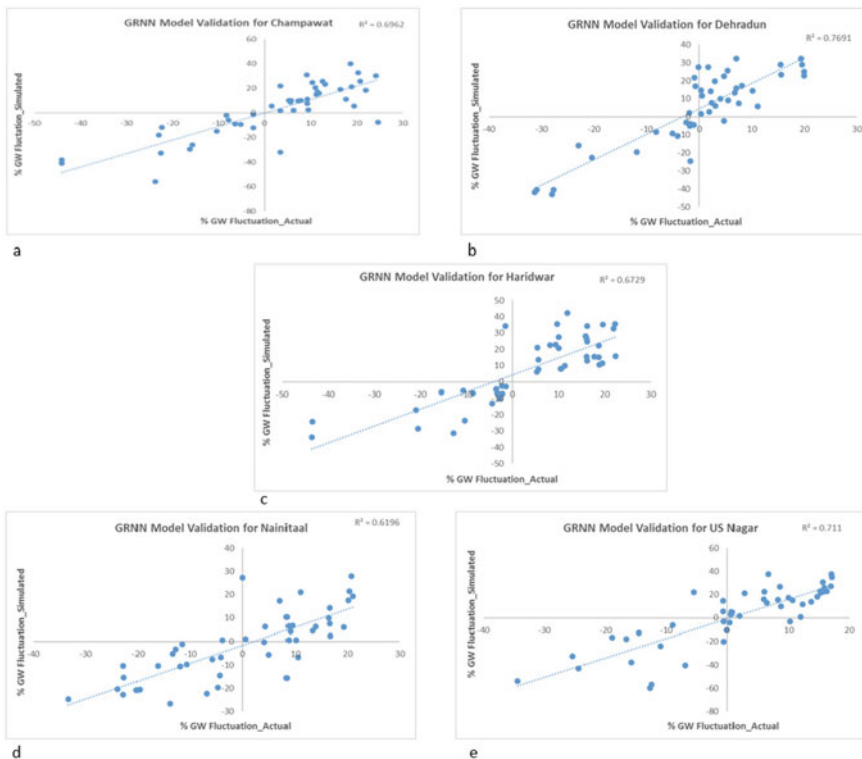


Fig. 11 The scatterplot between actual gw fluctuation and predicted one by GRNN model for five districts where gw fluctuation data is known

References

1. Iqbal, N., Hossain, F., Lee, H., Akhter, G.: Integrated groundwater resource management in Indus Basin using satellite gravimetry and physical modeling tools. *Environ. Monit. Assess.* **189**(3), 1–16 (2017)
2. Tiwari, V.M., Wahr, J., Swenson, S.: Dwindling groundwater resources in northern India, from satellite gravity observations **36**, 1–5 (2009)
3. Hassan, A., Jin, S.: Water storage changes and balances in Africa observed by GRACE and hydrologic models. *Geod. Geodyn.* **7**(1), 39–49 (2016)
4. Li, Q., Luo, Z., Zhong, B., Zhou, H.: An improved approach for evapotranspiration estimation using water balance equation: case study of Yangtze River Basin. *Water* **10**(6), 812 (2018)
5. Houborg, R., Rodell, M., Li, B., Reichle, R., Zaitchik, B.F.: Drought indicators based on model-assimilated gravity recovery and climate experiment (GRACE) terrestrial water storage observations. *Water Resour. Res.* **48**(7) (2012)
6. Chen, J.: Challenges of GRACE data processing the earth's gravity field the geo potential field is determined by mass distribution (2014)
7. Tian, S., Renzullo, L.J., Van Dijk, A.I.J.M., Tregoning, P., Walker, J.P.: Global joint assimilation of GRACE and SMOS for improved estimation of root-zones oil moisture and vegetation response (2018)

8. Gonzalez, R., Ouarda, T.B.M.J., Marpu, P.R., Allam, M.M., Eltahir, E.A.B., Pearson, S.: Water budget analysis in arid regions, application to the United Arab Emirates (2016)
9. Xiao, R., He, X., Zhang, Y., Ferreira, V.G., Chang, L.: Monitoring groundwater variations from satellite gravimetry and hydrological models: a comparison with in-situ measurements in the mid-atlantic region of the United States. *Remote Sens.* **7**(1), 686–703 (2015)
10. Chinnasamy, P., Maheshwari, B., Prathapar, S.: Understanding groundwater storage changes and recharge in Rajasthan, India through remote sensing. *Water (Switzerland)* **7**(10), 5547–5565 (2015)
11. Singh, A., Seitz, F., Eicker, A., Güntner, A.: Water budget analysis within the surrounding of prominent lakes and reservoirs from multi-sensor earth observation data and hydrological models: case studies of the Aral Sea and Lake Mead. *Remote Sens.* **8**(11) (2016)
12. Sun, A.Y.: Predicting groundwater level changes using GRACE data. *Water Resour. Res.* **49**(9), 5900–5912 (2013)
13. Longetal, D.: Global analysis of spatio temporal variability in merged total water storage changes using multiple GRACE products and global hydrological models. *Remote Sens. Environ.* **192**, 198–216 (2017)
14. Forootan, E., Khaki, M., Schumacher, M., Wulfmeyer, V., Mehrnegar, N., Van Dijk, A.I.J.M.: Science of the total environment understanding the global hydrological droughts of 2003–2016 and the irrelationships with teleconnections. *Sci. Total Environ.* **650**(2018), 2587–2604 (2019)
15. Khaki, M., Hoteit, I., Kuhn, M., Forootan, E., Awange, J.: Science of the total environment assessing data as simulation frameworks for using multi-mission satellite products in a hydrological context. *Sci. Total Environ.* **647**, 1031–1043 (2019)
16. Joshi, R.: Artificial neural network (ANN) based empirical interpolation of precipitation. *1*(3), 93–106 (2016)
17. Meena, R.A.Y.S.: Simulation of run off and flood inundation in Kosi River basin using hydrological models, ANN, remote sensing and GIS. M. Tech thesis submitted to Department of Civil Engineering, NIT Rourkela, p. 91 (2012)
18. Mohanty, S., Jha, M.K., Kumar, A., Sudheer, K.P.: Artificial neural network modeling for groundwater level forecasting in a river is land of eastern India. *Water Resour. Manag.* **24**(9), 1845–1865 (2010)
19. Akhterand, M., Ahmad, A.M.: Environment pollution and climate change climate modeling of Jhelum River Basin-a comparative study **1**(2), 1–14 (2017)
20. Nyatume, M., Owusu-Gyimah, V., Ampiah, F.: Statistical analysis of rainfall trend for Volta region in Ghana. *Int. J. Atmos. Sci.* **2014**, 1–11 (2014)
21. Yang, P., Xia, J., Zhan, C., Qiao, Y., Wang, Y.: Monitoring the spatio-temporal changes of terrestrial water storage using GRACE data in the Tarim River basin between 2002 and 2015. *Sci. Total Environ.* **595**, 218–228 (2017)
22. Andrew, R., Guan, H., Batelaan, O.: Estimation of GRACE water storage components by temporal decomposition. *J. Hydrol.* **552**, 341–350 (2017)
23. Kannan, S., Ghosh, S.: Prediction of daily rainfall state in a river basin using statistical down scaling from GCM output. *Stoch. Environ. Res. Risk Assess.* **25**(4), 457–474 (2011)
24. Hannan, S.A., Manza, R.R., Ramteke, R.J.: Generalized regression neural network and radial basis function for heart disease diagnosis. *Int. J. Comput. Appl.* **7**(13), 7–13 (2010)
25. Ground, C., Board, W.: dsUæh; Hkwfe ty cksMZ (2016)
26. Ministry, T., Government, F.: Assessment of environmental degradation and impact of hydroelectric projects during the June 2013 disaster in Uttarakhan. Part I-Main Report (2014)
27. Agricultural Economics Research Centre.: Agriculture Profile of Uttarakhand. Univ. Delhi (2015)
28. Studies, E., Tsakiris, G.P.: Water resources management study of integrated social vulnerability index (SoVI int) of Uttarakhand. India Indian Institute of Technology Guwahati Study of Integrated Social Vulnerability Index (SoVI int) of Uttarakhand, India

Android Application for Recognition of Indian Origin Agricultural Products



Snehal P. Tarale and Veena Desai

Abstract Farmers in India do not get a fair price for their yield. The deal is via middle agents which doesn't help farmers in making a good profit. Moreover, farmers are opting farming practices that incur high input costs to them by using chemical pesticides. The aim of this paper is to build an android application for recognition of agriculture produce using Deep Learning to provide a platform for farmers to sell and give them a fair share for their produce. At the consumer end, the consumers are guaranteed 100% fresh produce that is chemical-free by adopting Zero Budget Natural Farming (ZBNF). This project will be implemented in the buying–selling platform for agricultural products. The application will be enhanced to display the price of the product when the farmer projects his phone camera onto his produce. He can accept the deal if he is getting a fair share for the produce and thus totally eliminate the involvement of middle agents. In supermarkets, the cashier manually enters the code or scans the barcode attached to the product to print the bill. Sometimes the fruits and vegetables may not have barcodes. By using this application, items can be identified based on their appearance alone. Instead of entering the code or scanning the barcode manually, the phone camera is projected onto the product, the app then recognizes the product. It works even if they are in front for a short duration and are not absolutely still.

Keywords Deep Learning · Transfer learning · CNN · MobileNets · TensorFlow · TensorFlowLite · Tfmobile · AWS

S. P. Tarale (✉)

KLS Gogte Institute of Technology, Belgaum, Karnataka, India

e-mail: starale83@gmail.com

V. Desai (✉)

Research Centre Department of E&C, KLS Gogte Institute of Technology, Belgaum, Karnataka, India

e-mail: veenadesai@git.edu

1 Introduction

Deep Learning has a major contribution to the advancement of Artificial intelligence (AI) in today's world. It is changing the world we live in today which makes it necessary for us to understand the basics of Deep Learning. It is a subset of machine learning. The whole idea of machine learning is built-up on the basis of functioning of the human brain. The structure of the human nervous system is such that every neuron is connected to its next consecutive neuron to pass its information. Algorithms in Deep Learning are based exactly on this.

Deep Learning models have multiple layers, each of which accepts information from the previous layer and passes it to the next layer. Typically, there are at least three layers. The performance of these models improves as the amount of data increases. But machine learning models reach a saturation point after a certain level. One of the major differences in Deep Learning and machine learning lies in feature extraction. In machine learning, the features are extracted manually whereas in Deep Learning the model takes care of it. Neural Network architecture is used to implement Deep Learning. The term deep refers to the number of layers in the network that are quite a lot in number. Typical neural networks have around three layers whereas deep networks can have hundreds of layers.

This paper is organized as follows: Sect. 2 presents the literature review. Section 3 describes the tools and softwares required to implement this idea. Section 4 explains the methodology adopted and Sect. 5 lists the results of the proposed method.

2 Literature Review

Rahul et al. [1] have proposed a technique for facial recognition using a multistage hidden Markov model. In this paper, feature extraction is done using partition-based technique to recognize basic expressions like fear, sadness, anger, surprise, disgust, and joy. It is implemented using JAFFE database with an accuracy of 85%.

Singh et al. [2] have presented a new method for the reduction of false alarm of vehicle targets. Two new parameters namely decision parameter and average confidence have been introduced. The efficiency of the technique totally depends on the number of data samples. More the number of data samples, greater is the accuracy. The Bag of Features (BOF) technique is used for feature extraction. It uses keypoint detection, matching, and descriptor extraction to detect objects.

Kumari et al. [3] have proposed a model to extract annotated text from videos to provide extra information to the viewers. It becomes useful for people having hearing impairments and while watching videos in sound-insensitive environment. SVM is used here to extract text more accurately. The multi-resolution processing algorithm is used with the help of which texts of different sizes from the same video can be extracted. SVM is a supervised machine learning algorithm and one of the most powerful families. It is useful to build a strong and powerful model. A clear margin

of separation and number of dimensions greater than number of samples makes a reliable model.

Bonello et al. [4] have demonstrated a seizure detection system using multi-channel EEG sensor data. It is implemented using a small dataset using machine learning. The testing and validation are done using CHB-MIT dataset containing 24 clinically verified records of EEG. Artificial Neural Networks along with other techniques like SVM, ELM, and genetic algorithm are made use of. The main aim of this paper is to use minimum data and achieve desirable results.

Gavai et al. [5] have proposed a flower classifier using MobileNets and TensorFlow. Flower classification becomes an important topic in botany. They experimented on how MobileNets can be used for building faster and smaller applications by using width multiplier and resolution multiplier. They validated the efficiency of MobileNets when applied to a variety of dataset that is huge. They concluded that MobileNets can be optimized by trading off correctness to shrink size and latency.

3 Tools and Software's

This section deals with requirements such as TensorFlow, MobileNets, Android studio, etc. used for the implementation of the proposed idea.

3.1 Deep Learning for Image Classification

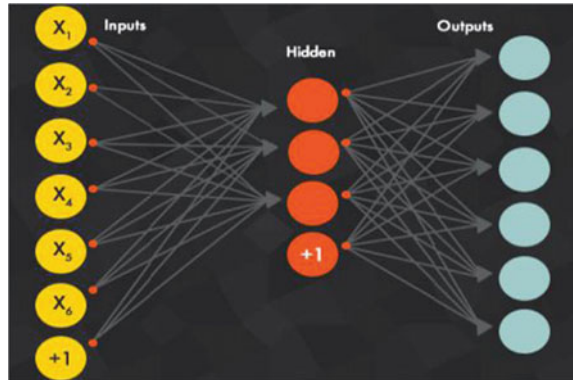
One of the most popular neural network architecture used for image classification is Convolutional Neural Network (CNN). It uses the features of visual cortex of human brain. Facebook uses this architecture for automatic tagging, Amazon generates product recommendation using this, and Google uses it to search through Google photos (Fig. 1).

The network is given the images of the object that it is supposed to recognize with its label. The size of the image is of the form $H \times W \times 3$, where H is the height, W is the width, and 3 is the RGB channel values. Further, concepts that are abstract are constructed through a group of layers of convolution by the computer. To generate the output, the image is passed through a series of convolutional, nonlinear, pooling, and fully connected layers.

3.2 Tensorflow

It is a software library that is open source and used to carry out high-performance numerical computation in machine learning. It was developed by Google, used for both research and production. Its architecture is flexible which makes it easy to

Fig. 1 Convolutional neural networks



deploy computations across various platforms like CPU's, GPU's, and TPU's. It can be deployed across desktops to a cluster of servers.

Tensor Processing Unit (TPU). It is an Integrated Chip (IC) specifically built for the purpose of machine learning and is application-specific. It is designed for TensorFlow. It is programmable and is an accelerator for providing high throughput for low precision mathematical computations (8 bit). It is inclined towards running the model rather than training the model [10]. Google had been using TPU's for a year in their data centers and found out that its performance was better and optimized per watt for machine learning.

TensorFlow Lite/tfmobile. It is used for mobile and embedded devices. It is a lightweight software stack specifically designed to be used for devices having power constraints and low computational power. It provides a binary size, that is small and low latency, enables on-device inference for machine learning. With the use of Android Neural Networks API, it also supports acceleration of hardware. It makes use of various techniques to achieve low latency. Some of those techniques are optimizing mobile app kernels, quantized kernels, and pre-fused activations that allow faster and smaller models.

TensorFlow Lite introduces a new model file format based on FlatBuffers. FlatBuffers is a cross-platform serialization library. It is an efficient and open source. It is similar to protocol buffers. But the difference lies here, in FlatBuffers there is no step of parsing to a secondary representation when you want to use the data. It is combined with per-object memory allocation very often. In addition, protocol buffers have a huge code footprint in contrast to FlatBuffers which have smaller ones.

Android Studio. It is an Integrated Development Environment for the development of android applications. It has support for various platforms like C++, Python, Google Cloud Platform, etc. Apps can be written in languages like android, python, java, etc. It has testing tools, frameworks, and integration with Github.

3.3 *MobileNets*

MobileNets are computer vision models designed for embedded and android devices. They maximize efficiency and accuracy while taking into account the restricted resources of on-device and embedded applications. They are specifically designed to meet the constraints of resources of a variety of use classes. They are low-power models being small providing low latency. They can be used for detection, segmentation, classification, and embeddings. With the help of TensorFlow Mobile, MobileNets can be run efficiently on mobile devices. Considering popular models from literature, these give trade-off between accuracy, size, and latency.

Features of MobileNets

- It is fully compatible with mobile devices and browsers.
- Can be integrated with social networks and media networks, e.g., Twitter, Facebook, etc.
- We can integrate them with different datasource companies.
- Used in Custom Application Development.

We need to choose the appropriate MobileNet model which tailors to our application requirements such as latency and size budget.

3.4 *Amazon Web Services (AWS)*

Since we are dealing with a huge amount of data the local machine that we are using might have memory and processor constraints. In such a scenario, we can opt for carrying out our work on any cloud platform like Google Cloud Platform (GCP), Microsoft Azure, Amazon Web Services, etc. Going for a cloud platform becomes beneficial since it is pay-as-you-go, i.e., you pay when you only use the resources. It becomes useful when we do not have the budget to purchase high-end machines. Also in case of deploying only a single project, it would be a waste buying a high-end machine. Cloud services become beneficial in such situations. Here, we opt to go with Amazon Web Services (AWS).

4 Methodology

This section deals with the methodology adopted for implementation.

4.1 Data Acquisition

To form a dataset, we need to acquire data. Data can be of any form such as audio, video, text, images, etc. For any machine learning application, the performance depends on the quality of dataset that is being used to train the model. Thus, acquiring a good amount of data becomes a need.

For the application being deployed here, the dataset is of images. There are various ways to form this dataset. There are online platforms like Kaggle, ImageNet, etc. where researchers have conducted experiments and have uploaded their datasets, which we can use directly by downloading. This is one way to gather data but it's not the best way since your application might need more/different data than what is available. For the application being deployed here, the dataset required is images of Indian origin agricultural products. So there was a need to acquire a completely new dataset. The images used here are downloaded from the web by adding some add-ons to the Firefox browser which enable downloading of all the images on the web page at once. Care must be taken to retain only relevant images since a lot of irrelevant images might appear while doing so. The data is gathered for 85 classes following this procedure.

4.2 Data Augmentation

The data acquired in the previous step might not be sufficient. For more common classes, the images are available in plenty and for less common they are not. So there comes a need to multiply the dataset. Also the lighting conditions, noise additions should all be considered since we never know how the image is going to be in real-time scenario. All of this can be done using data augmentation technique. Data augmentation means increasing the number of images by adding value to the base information. A small code snippet using python and skimage processing library is used to achieve this. Skimage supports a number of different kinds of image transformations like image rotation at random angles, adding noise, filters to the images to take into account various lighting conditions, etc. The base dataset that was obtained was maintained at 29 images per class. After augmentation, 1073 images we obtained per class resulting in a massive dataset containing 1073×85 images (Figs. 2, 3 and 4).

Hosting an EC2 instance on AWS. The very first step is making the environment ready, in which we would be working. An EC2 ubuntu instance is hosted. It is a t2. micro instance of 8 GB [16]. It is a free tier instance. The detailed procedure of hosting an instance is available in the AWS documentation. After following the documentation, the instance becomes ready to use.

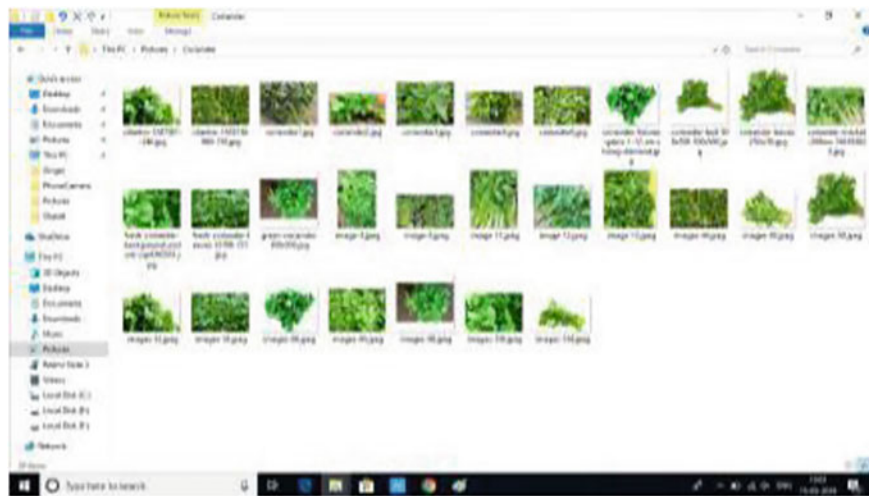


Fig. 2 Coriander dataset

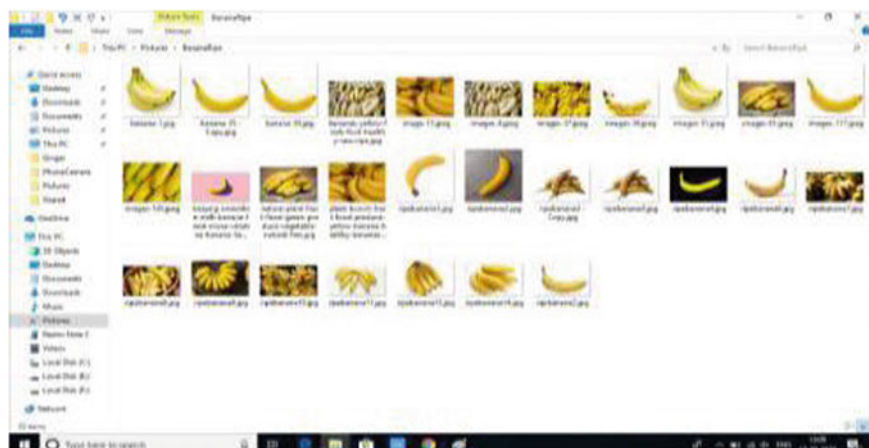


Fig. 3 Banana dataset

The next step is to download all the necessary packages like TensorFlow, Scikit, python, Numpy, Scipy, etc. Once the environment is ready, we can go ahead with the training of the model.

Creating snapshots and volumes. It was found that the 8 GB space that the instance had was not sufficient to train the network. So the volume had to be increased [17]. To do so, first a snapshot has to be created to retrieve our previous data so that

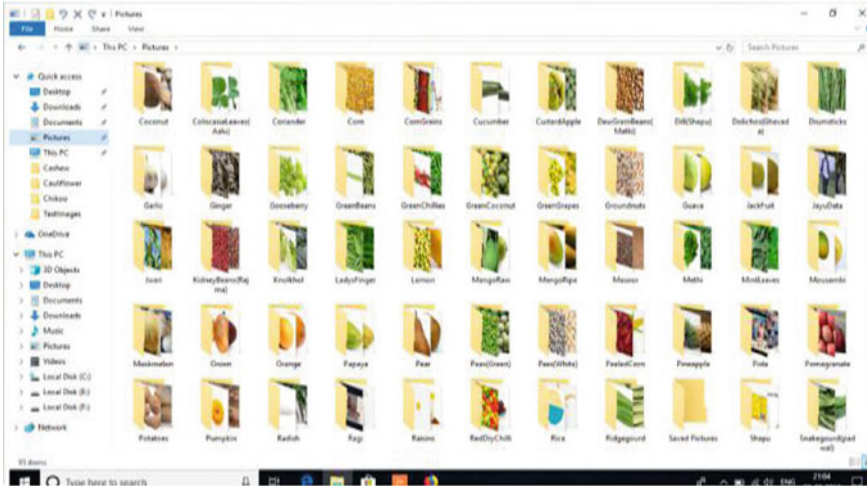


Fig. 4 Dataset of 85 classes

we don't lose it. We then create a new volume by using the snapshot created. Post this, a filesystem has to be created on this volume [18]. The procedure for this is again mentioned in the AWS documentation.

Pseudo Code

- Collect images to form the dataset
- Multiply the dataset by data augmentation
- For augmentation,
 1. Import modules
 2. Give Image Folder Path
 3. Iterate over all the folders using for loop and perform the following actions
 - (a) Resize the image
 - (b) Rotate it in steps of 10 degree.
 - (c) Specify a string with which the image must be stored in the parent folder
 - (d) If image is RGBA, convert it to RGB
 4. Save the converted image back to parent folder
- Clone tensorflow-for-poets-2
- cd into tensorflow-for-poets-2/tf_files
- Configure MobileNet architecture
- Place the dataset in tf_files directory
- Run the retraining script to generate retrained_graph.pb and retrained_labels.txt
- Optimize retrained_graph.pb to generate a file named optimized_graph.pb
- Compress the model using gzip, outputs a file named rounded_graph.pb.gz

- Copy rounded_graph.pb.gz and retrained_labels.txt from cloud onto your local machine
- Launch android studio and move to tensorflow-for-poets-2/android/tfmobile
- Enable developer options on your android phone
- Connect the phone to your local machine using USB
- Run and test the app.

5 Results

An android application that could recognize 85 classes of Indian origin agricultural products was successfully built. The number of iterations used was 2000. The following results were obtained:

Train accuracy = 97.0%

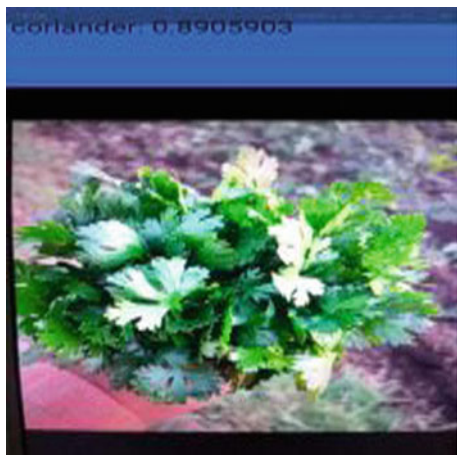
Cross entropy = 0.268414

Validation accuracy = 91.0%.

The snapshots of the results showing the class name and its probability of matching for some of the classes are listed below (Figs. 5, 6, 7, 8, 9, 10, 11, 12, 13, 14, 15, 16, 17, 18, and 19).

Fig. 5 Methi



Fig. 6 Coriande**Fig. 7** Jackfruit

6 Scope of Future Work

The performance of the application is excellent for maximum number of classes. In the case of classes having a similar appearance like Potato–Chikoo, lemon–orange–sweetlime, the output fluctuates within similar classes. This application can be further improved by considering images that provide a clear distinction between these classes and by also considering other algorithms that take this into account.

Fig. 8 Green beans**Fig. 9** Green chillies**Fig. 10** Cauliflower

Fig. 11 Soyabean**Fig. 12** Adzuki beans**Fig. 13** Apple

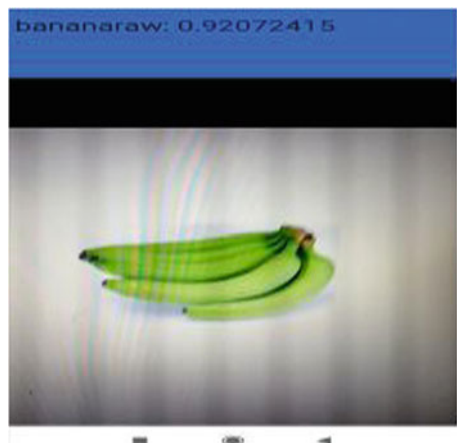
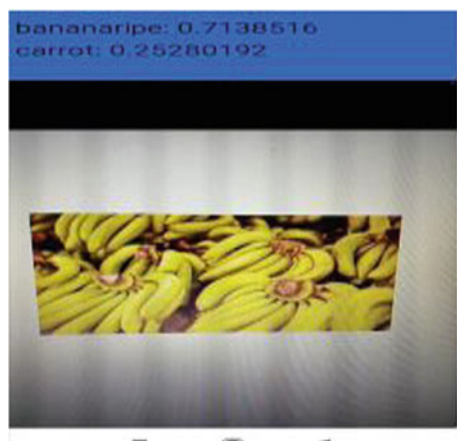
Fig. 14 Banana raw**Fig. 15** Banana ripe**Fig. 16** Beetroot

Fig. 17 Cashew**Fig. 18** Black eyed pea**Fig. 19** Carrot

Acknowledgements We sincerely thank the founder and advisors of Krishiyog Naturals, India for the idea, technical support, and the validation of the results of this work.

References

1. Rahul, M., Mamoria, P., Kohli, N., Agrawal, R.: An efficient technique for facial expression recognition using multistage hidden Markov model. In: 2nd International Conference on Soft Computing Theories and Applications (2017)
2. Singh, A., Kumar, R., Tripathi, R.P.: Study and analysis of different kinds of data samples of vehicles for classification by bag of feature technique. In: 2nd International Conference on Soft Computing Theories and Applications (2017)
3. Kumari, L., Dey, V., Raheja, J.L.: A three layer approach for overlay text extraction in video stream. In: 1st International Conference on Soft Computing Theories and Applications (2016)
4. Bonello, J., Garg, L., Garg, G., Audu, E.E.: Effective data acquisition for machine learning algorithm in EEG signal processing. In: 1st International Conference on Soft Computing Theories and Applications (2016)
5. Gavai, N.R., Jakhade, Y.A., Tribhuvan, S.A., Bhattad, R.: MobileNets For Flower Classification Using TensorFlow. In: International Conference on Big Data, IoT and Data Science (BID) (2017)
6. Riri, H., Elmoutaouakkil, A., Beni-Hssane, A., Bourezgui, F.: Classification and recognition of dental images using a decision tree. In: 13th International Conference Computer Graphics, Imaging and Visualization (2016)
7. Sornam, M., Muthusubash, K., Vanitha, V.: A survey on image classification and activity recognition using deep convolutional neural network architecture. In: Ninth International Conference on Advanced Computing (ICoAC) (2017)
8. Introduction to AI, <https://medium.com/intro-to-artificial-intelligence/deep-learning-series-1-intro-to-deep-learning-abb1780ee20>
9. Convolutional Neural Networks, <https://medium.com/@ksusorokina/image-classification-with-convolutional-neural-networks-496815db12a8>
10. Tensorflow, <https://www.tensorflow.org/>
11. Image classification using deep learning, https://www.nvidia.com/contents/events/geoInt2015/LBrown_DL_Image_ClassificationGEOINT.pdf
12. MobileNets, <https://www.quora.com/What-is-MobileNet>
13. MobileNet_v1, https://github.com/tensorflow/models/blob/master/research/slim/netsmobile_net_v1.md
14. Google Codelabs part 1, <https://codelabs.developers.google.com/codelabs/tensorflow-for-poet-s/#0>
15. Google Codelabs part 2, <https://codelabs.developers.google.com/codelabs/tensorflow-for-poet-s-2/#0>
16. Hosting EC2 instance on AWS, <https://docs.aws.amazon.com/efs/latest/ug/gs-step-one-create-ec2-resources.html>
17. Extending EC2 instance volume, <https://docs.aws.amazon.com/AWSEC2/latest/UserGuide/ebs-creating-volume.html>
18. Creating snapshot, <https://docs.aws.amazon.com/AWSEC2/latest/UserGuide/ec2-ug.pdf#ebs-creating-snapshot>
19. Creating snapshot, <https://docs.aws.amazon.com/AWSEC2/latest/UserGuide/ebs-creating-snapshot.html>

A Fuzzy Logic Based Approach for Prediction of Squamous Cell Carcinoma



Saurabh Jha, Ashok Kumar Mehta, and Chandrashekhar Azad

Abstract Squamous cell carcinoma (SCC) is a type of skin malignancy. It is a fast growing skin disease which rapidly ravel to other parts of the body, if occurs in any particular body part. SCC is a genuinely moderate developing skin disease. Expert system tools such as fuzzy systems, neural networks and genetic algorithms are very useful in prediction of these diseases. In this paper we accordingly developed an approach by applying fuzzy logic technique on various parameters on the input dataset in order to predict the existence of squamous cell carcinoma among the patients. The fuzzy system accepts five information parameters for the data source and generates one yield parameter as an output. The output produced by this fuzzy logic system is analyzed to find the existence of squamous cell carcinoma and its stage. It is worth to mention that the simulation outcomes of the proposed system are better in terms of prediction accuracy of SCC as compared with other prediction techniques.

Keywords SCC · Membership function · Fuzzy logic system · Participation element

1 Introduction

Squamous cell carcinoma (SCC) is a type of skin malignancy. It is a fast growing skin disease which rapidly raves to other parts of the body; it is an uncontrolled advancement of sporadic cells. Sores of SCC may develop and make nearby harm and distortion encompassing skin and contiguous tissue and it may spread all through the body which may even cause in the death of human being [1]. Considering the

S. Jha (✉) · A. K. Mehta · C. Azad
National Institute of Technology, Jamshedpur, Jharkhand, India
e-mail: saurabhsoni.sj@gmail.com

A. K. Mehta
e-mail: akmehta.ca@nitjsr.ac.in

C. Azad
e-mail: csazad.ca@nitjsr.ac.in

expanding occurrence in SCC and the danger of metastasis and repeat, even in patients with negative dirty edges and lymph nodes, it is important to distinguish flowing particles that can help foresee the forecast/development of this infection [2].

In certain patients with anomalous safe frameworks or patients taking certain medications (counting safe suppressive medications, for example, cyclosporine and perhaps some anti-infection drugs), SCC may occur more frequently and develop more quickly [3]. Squamous cell carcinoma of the skin happens when the level, meager squamous cells in the external layer of your skin create errors in their DNA. Commonly, new cells push more seasoned cells toward your skin's surface, and the more established cells bite the dust and are sloughed off. Squamous cell carcinoma becomes very dangerous when it occurs in a particular body part because it has the ability to propagate to another body parts very rapidly, causing the entire body to be affected by it. There are certain stages of squamous cell carcinoma based on the gross area it covered at any particular area of the body. The stages are "stage 1" if gross area lies between 0.5 and 2.5 cm, "stage 2" if gross area lies between 3 and 5 cm and "stage 3" if gross area occupies more than 5 cm area [4, 5].

Fuzzy set and tools are very important in describing the basic data element of the external world by the use of linguistic variables and linguistic values [6]. Several soft computing techniques have been created for directed AI systems [7, 8]. The determination of the fitting system is significant and has been a test among the scientists in creating and actualizing the sicknesses conclusion frameworks [9]. Additionally, these soft computing strategies can be utilized to arrange the ailments through a lot of certifiable informational indexes. Therefore, in order to increase the prediction accuracy we used fuzzy logic approach. The fuzzy system is applied on the cancer patient's data which is collected from "111 Save Life Hospital", Jamshedpur, Jharkhand, India. The membership function for the entire input set is created and fuzzy rules are generated from it. The fuzzy rule base is created by the help of domain experts (i.e. doctors) of 111 Save Life Hospital. The predicted output of the system with related accuracy and error rate is obtained from the system and compared with the prediction accuracy of the existing systems.

Our research work now proceeds in the following order: In Sect. 2, various work on cancer prediction using AI techniques are presented. In Sect. 3, the proposed system architecture and the detailed workflow operations is presented. In Sect. 4, the simulation results are shown. Finally, in Sect. 5, conclusion and future work are presented.

2 Related Work

Various works on cancer prediction using AI utilities are in existence. Some of the most important calculations, in light of past work in this space, are examined beneath.

Min (2019) [3] developed a procedure for skin disease affirmation using a therapeutic AI framework subject to data width improvement and self-learning. They used educational accumulation channel estimation subject to information entropy

to reduce the weight of edge center and meanwhile improve the learning limit of remote cloud examination model. It is found that the high-and low-objectives photos of some skin ailments have little impact on the portrayal precision.

Kale (2018) [9] used an ordinary information based procedure for lung ailment examination and finding. Minute lung pictures are taken for examination and examination by using automated picture dealing with and MATLAB. The data parameters like entropy, standard deviation and MSE for ordinary information technique are completed over a tremendous little lung picture database. The individual quantifiable and numerical parameter examination with its impact on lung danger pictures is adequately done in conclusion the accuracy, selectivity, and affectability of the proposed method is dictated by completing the standard expressive. This method in like manner adequately rejects invalid theory by realizing one of the standard truthful techniques.

Melin (2018) [10] built up a cross breed model using estimated neural frameworks and fluffy framework to give the hypertension danger assurance of a person. This model contemplates age, chance segments and lead of the beat in a period of 24 h. A deliberate neural framework was organized, with three modules, of which the first and second modules contrast with the systolic and diastolic loads and the last one to the beat. The learning accuracy in the central module is 98%, in the subsequent module is 97.62% and the third module is 97.83% independently.

Yilmaz (2016) [11] utilized the neuro-fuzzy model for lung malignancy forecast. In their work, the danger of getting the lung cancer was determined and afterward status of the patient's powerlessness and protection from stress is utilized in deciding the impacts of worry to sickness. The precision of their framework in hazard forecast of lung cancer growth was 94.64% as compared with Einstein product (93.18%) and ANFIS (92.04%).

Banerjee (2016) [12] developed a fluffy understanding in oral prosperity and affinity survey data for a picked Indian people concerning assessing vulnerability to oral pre-sickness and dangerous development. The way of thinking additionally proposed the frailty to oral pre malignancies and squamous cell carcinoma in patients considering a fluffy rule base through If-Then measures with explicit conditions. Joining of closeness assessments was used during change into the phonetic yield of fluffy set to predict the disease result in a dynamically exact manner and related condition of the relevant features.

Buyukavcu (2016) [1] built a strong model that advanced the circumstances and logical results connections among the components that are critical to general well-being. They used a Rule-Based Fuzzy Cognitive Map (RBFCM) approach that effectively speak to learning and human experience, acquainting ideas with speak to the fundamental components and the circumstances and logical results connections among the ideas to display the conduct of any framework. In their methodology, a rule based framework was developed to assess hazard components of breast cancer growth dependent on the data from oncologists. A delicate processing strategy is utilized to mimic the progressions of a framework after some time and address the inquiries to think about between various contextual analyses.

Wang (2015) [2] developed a peril demonstrating and survival figure structure reliant on versatile neuro-fuzzy induction system to help clinicians in prognostic assessment of patients with esophageal sickness and in anticipating the survival of individual patients. Genuine characteristics for serum C-responsive protein, albumins, and time intervals were commitment to the model for use in predicting the survival of individual patients for different time between times. The curves gotten by the ANFIS approach were fitted to those gained using the authentic characteristics.

3 The System Architecture

The proposed framework depends on the Mamdani inference model [13] for recognition of Squamous cell carcinoma. Based on the biopsy report of the patients, collected from the data source, a total of five parameters are taken as input of the fuzzy logic system with one output value. Five base rules are defined based on the type of input supplied to the fuzzy logic system. The detailed system architecture and the fuzzy rule base are shown in Fig. 1.

The fuzzy logic system composed of inputs and output is shown in Fig. 2.

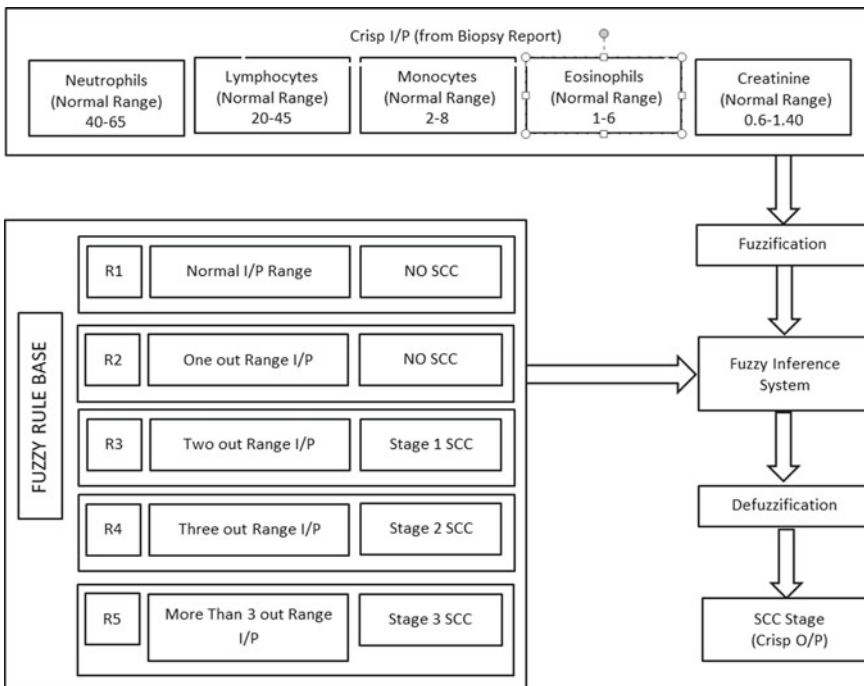


Fig. 1 The fuzzy logic system architecture

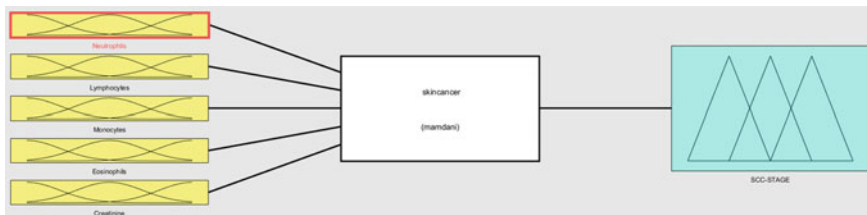


Fig. 2 The fuzzy logic system's inputs and output

Table 1 Membership functions and ranges for Neutrophils

Input-1: Neutrophils: [0–100]		
Membership function	Type	Range
Low	Trimf	[0, 21, 42]
Medium	Trimf	[40, 52.5, 65]
High	Trimf	[64, 82, 100]

Table 2 Membership functions and ranges for Lymphocytes

Input-1: Lymphocytes: [0–100]		
Membership function	Type	Range
Low	Trimf	[0, 14.7, 22]
Medium	Trimf	[20, 32.5, 45]
High	Trimf	[44, 72, 100]

3.1 Inputs

3.1.1 Neutrophils

The scope of three participation elements of Neutrophils is appeared in Table 1.

3.1.2 Lymphocytes

The scope of three participation elements of Lymphocytes is appeared in Table 2.

3.1.3 Monocytes

The scope of three participation elements of Monocytes is appeared in Table 3.

Table 3 Membership functions and ranges for Monocytes

Input-1: Monocytes: [0–15]		
Membership function	Type	Range
Low	Trimf	[−3, 0, 3]
Medium	Trimf	[2, 5, 8]
High	Trimf	[7, 11, 15]

Table 4 Membership functions and ranges for Eosinophils

Input-1: Monocytes: [0–10]		
Membership function	Type	Range
Low	Trimf	[−1.5, 0, 1.5]
Medium	Trimf	[1, 3.5, 6]
High	Trimf	[5, 7.5, 10]

Table 5 Membership functions and ranges for Creatinine

Input-1: Monocytes: [0–4]		
Membership function	Type	Range
Low	Trimf	[−0.7, 0, 0.7]
Medium	Trimf	[0.6, 1, 1.4]
High	Trimf	[1.2, 2.6, 4]

3.1.4 Eosinophils

The scope of three participation elements of Eosinophils is appeared in Table 4.

3.1.5 Creatinine

The scope of three participation elements of Creatinine is appeared in Table 5.

3.2 Output

3.2.1 Scc-Stage

The proposed framework classifies 4 phases of squamous cell carcinoma (SCC) for example “No-SCC”, “SCC- Stage 1”, “SCC- Stage 2” and “SCC- Stage 3” as appeared in Fig. 3.

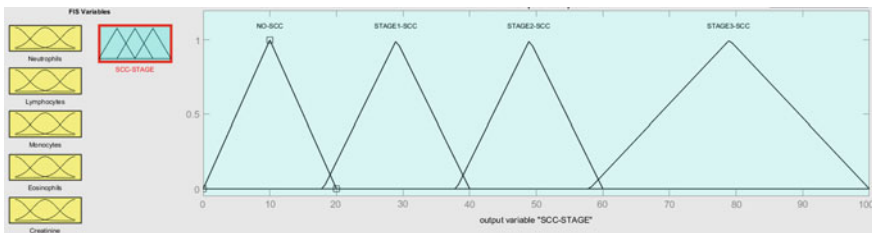


Fig. 3 Membership function plot for output SCC-STAGE

4 Simulation Results

This Intelligent Diagnostic framework is actualized in MATLAB programming utilizing Fuzzy Designer tool kit. Based on the biopsy report of the patients, five inputs namely—Neutrophils, Lymphocytes, Monocytes, Eosinophils and Creatinine are applied to the fuzzy logic system which has one output—“SCC-STAGE”. Each input has its own normal range which is shown in Fig. 1. Any value lying within this range is considered as normal input range. Value below or above the normal input range is considered as out range input. The fuzzy rule base of the fuzzy logic system is constructed on the basis of five “base rules”, which are further distributed into multiple sub rules. A total of 243 sub rules are generated for fuzzy rule base. The details of the five base rules are presented as follows:

1. Base Rule-1: If all the input has normal input range then there is no chance of squamous cell carcinoma and the system generates the output “NO-SCC”.
2. Base Rule-2: If there is one out range input and the remaining four are normal range input then also there is no chance of squamous cell carcinoma because such condition can occur due to some other malady. In this case the system generates the output “NO-SCC”.
3. Base Rule-3: If there are two out range input then, this is the case of stage 1 squamous cell carcinoma. In this case the system generates the output “Stage1-SCC”.
4. Base Rule-4: If there are three out range input then, this is the case of stage 2 squamous cell carcinoma. In this case the system generates the output “Stage2-SCC”.
5. Base Rule-5: If there are three out range input then, this is the case of stage 3 squamous cell carcinoma. In this case the system generates the output “Stage3-SCC”.

Figure 4 shows the stage of squamous cell carcinoma based on certain input parameters.

The output value of “SCC-STAGE” = 37.6 represents “Stag-1 SCC” as Stage 1 lies between the range 18-40 of the output “SCC-STAGE”.

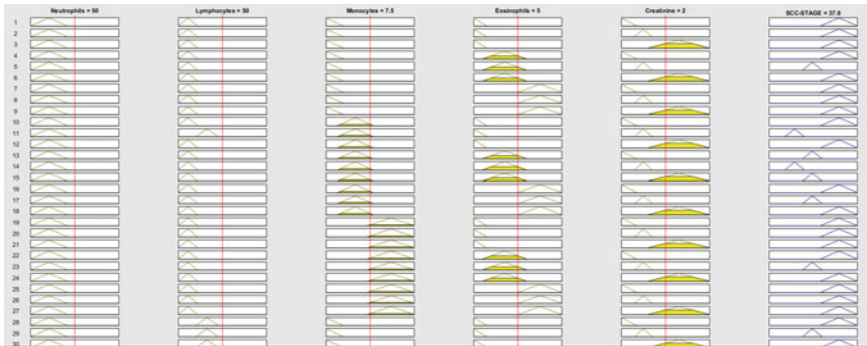


Fig. 4 Representation of “Stag-1 SCC”

The patient’s data collected from the data source is applied on the proposed fuzzy model. The predicted output from the fuzzy model is saved in an excel sheet named “sldata.xlsx”. The comparison of actual output and predicted out is shown in Fig. 5.

Total of 54 patient’s data from the source dataset is applied over the proposed fuzzy model. From Fig. 5, it is clear that our proposed system predicts 50 correct results and 4 incorrect results, which gives an accuracy of 0.92 equals 92%, which is good for small dataset. On increasing the size of the dataset, the accuracy of the proposed system would definitely increase.

5 Conclusion and Future Work

In this paper, an information based framework for squamous cell carcinoma utilizing AI systems has been presented. Input data set is applied as an input to the fuzzy logic system and based on the five base rules, a total of 243 sub rules were generated and stored in the rule base of the fuzzy system. Comparison between actual output and system generated output is done and finally the accuracy value is calculated. The consequences of the analysis on source dataset show that the proposed technique accomplished great expectation precision for characterization of squamous cell carcinoma stages. There is still a lot of work to be done in creating strategies for squamous cell carcinoma infection determination utilizing AI methods in order to use all focal points of these procedures. In the future examination, we intend to assess the proposed strategy with gradual learning on extra restorative informational indexes and specifically on enormous informational collections [14].

F	G	H	I	J	K	L	M	N	O	P	Q	R
SCC-STAGE (Actual Output)	SCC Stage (Predicted output)				Predicted Result							
2	49	←	Stage 2	✓								
0	10	←	NO SCC	✓								
0	10	←	NO SCC	✓								
0	10	←	NO SCC	✓								
2	50	←	Stage 2	✓								
3	79	←	Stage 3	✓								
0	10	←	NO SCC	✓								
2	49	←	Stage 2	✓								
0	10	←	NO SCC	✓								
2	49	←	Stage 2	✓								
0	10	←	NO SCC	✓								
0	10	←	NO SCC	✓								
1	36.34826884	←	Stage 1	✓								
1	50	←	Stage 1	✓								
0	10	←	NO SCC	✓								
2	49	←	Stage 2	✓								
0	10	←	NO SCC	✓								
0	10	←	NO SCC	✓								
3	79	←	Stage 3	✓								
0	10	←	NO SCC	✓								
0	10	←	NO SCC	✓								
1	29	←	Stage 1	✓								
1	29	←	Stage 1	✓								
2	79	←	Stage 3	✗								
2	49	←	Stage 2	✓								
0	10	←	NO SCC	✓								
2	59.01430259	←	Stage 2	✓								
0	10	←	NO SCC	✓								
0	10	←	NO SCC	✓								
2	50	←	Stage 2	✓								
3	73.46266724	←	Stage 3	✓								
2	79	←	Stage 3	✗								
0	10	←	NO SCC	✓								
0	10	←	NO SCC	✓								
1	29	←	Stage 1	✓								
1	67.76117396	←	Stage 3	✗								
0	10	←	NO SCC	✓								
0	10	←	NO SCC	✓								
2	49	←	Stage 2	✓								
1	29	←	Stage 1	✓								
0	10	←	NO SCC	✓								
3	79	←	Stage 3	✓								
3	79	←	Stage 3	✓								
0	10	←	NO SCC	✓								
0	10	←	NO SCC	✓								
2	50	←	Stage 2	✓								
0	10	←	NO SCC	✓								
2	49	←	Stage 2	✓								
0	10	←	NO SCC	✓								
0	10	←	NO SCC	✓								

SCC STAGE RANGE

NO SCC	0-20
SCC STAGE 1	18-40
SCC STAGE 2	38-60
SCC STAGE 3	58-100

Fig. 5 Comparison of actual versus Predicted output

References

1. Büyükkavcu, A., Albayrak, Y.E., Göker, N.: A fuzzy information-based approach for breast cancer risk factors assessment. *Appl. Soft Comput.* **38**, 437–452 (2016)
2. Wang, C.-Y., Tsai, J.-T., et al.: A knowledge-based system for breast cancer classification using fuzzy logic method. *Appl. Soft Comput.* **35**, 583–590 (2015)

3. Chen, M., Zhou, P., Wu, D., Hu, L., Hassan, M. M., Alamri, A.: AI-Skin: Skin disease recognition based on self-learning and wide data collection through a closed-loop framework. *Inf. Fus.* (2019) ISSN 1566-2535
4. Davis, J., Bordeaux, J.: Squamous cell carcinoma. *JAMA Dermatol* **149**(12), 14–48 (2013)
5. Alam, M., Ratner, D.: Cutaneous squamous-cell carcinoma. *New England J. Med.* **344**(13), 975–983 (2001)
6. Zimmermann, H.J.: *Fuzzy Set Theory—and Its Applications*, 4th edn. Kluwer Academic Publication, London (2001)
7. Zadeh, L.A.: *Fuzzy Sets, Fuzzy Logic, and Fuzzy Systems*, 1st edn. World Scientific Publication, New York (1996)
8. Sabharwal, M.: The use of soft computing technique of decision tree in selection of appropriate statistical test for hypothesis testing. *Soft Comput. Theories Appl.* **583**(1), 161–169 (2017)
9. Vaishnav, G.K., Vandana, B.M.: An innovative approach for investigation and diagnosis of lung cancer by utilizing average information parameters. *Procedia Comput. Sci.* **132**, 525–533 (2018)
10. Melin, P., Miramontes, I., et al.: A hybrid model based on modular neural networks and fuzzy systems for classification of blood pressure and hypertension risk diagnosis. *Expert Syst. Appl.* **107**, 146–164 (2018)
11. Yilmaz, Atmç, Ari, Seçkin, et al.: Predicting survival of individual patients with esophageal cancer by adaptive neuro-fuzzy inference system approach. *Comput. Methods Programs Biomed.* **137**, 35–46 (2016)
12. Banerjee, S., Aishwaryaprajna, et al.: Application of fuzzy consensus for oral pre-cancer and cancer susceptibility assessment. *Egypt. Inform. J.* **17**(3), 251–263 (2016)
13. Hilletooth, P., Sequeira, M., et al.: Three novel fuzzy logic concepts applied to reshoring decision-making. *Expert Syst. Appl.* **126**, 133–143 (2019)
14. Harsh, B., Nandeesh, G.: Critical path problem for scheduling using genetic algorithm. *Soft Comput. Theories Appl.* **583**(1), 15–24 (2017)
15. Prabakaran, G., Vaithianathan, D., et al.: Fuzzy decision support system for improving the crop productivity and efficient use of fertilizers. *Comput. Electron. Agricu.* **150**, 88–97 (2018)
16. Melin, P., Miramontes, I., Prado-Arechiga, G., et al.: A hybrid model based on modular neural networks and fuzzy systems for classification of blood pressure and hypertension risk diagnosis. *Expert Syst. Appl.* **107**, 146–164 (2018)
17. Ahmed, U., Rasool, G., Zafar, S., Maqbool, H.F.: SFuzzy Rule Based Diagnostic System to Detect the Lung Cancer. 2018 International Conference on Computing, Electronic and Electrical Engineering (ICE Cube), pp. 1–6. IEEE, Quetta (2018)
18. Azad, C., Mehta, A.K., Jha, V.K.: Improved data classification using fuzzy euclidean hyperbox classifier In: 2018 International Conference on Smart Computing and Electronic Enterprise (ICSCEE), pp. 1–6. IEEE, Malaysia (2018)
19. Azad, C., Jha, V.K.: Fuzzy min–max neural network and particle swarm optimization based intrusion detection system. *Microsyst. Technol.* **23**(4), 907–918 (2017)
20. Melin, P., Miramontes, I., et al.: A knowledge-based system for breast cancer classification using fuzzy logic method. *Telematics Inform.* **34**(4), 133–144 (2017)

Investigating Multilevel Hesitated Patterns Using Vague Set Theory



Abhishek Dixit , Akhilesh Tiwari , and Rajendra Kumar Gupta

Abstract Discovering hesitated frequent itemset is an important task in the online shopping scenario. Hesitated information is composed of those items that are hesitated during online purchasing by the customer and such items are termed as a hesitated itemset. Finding such type of information is crucial for business decision makers as through this knowledge, the state of the hesitated items can be converted to sold items by applying various promotions to the hesitated items. So, for finding frequently hesitated itemset an efficient algorithm is required. In this paper, the author aims in proposing an architecture of a hesitation mining system and a new algorithm for mining hesitated frequent itemset from the transactional database by using vague set theory and multilevel pattern mining.

Keywords Data mining · Vague set · Hesitation information · Hesitation mining · Multilevel frequent pattern mining

1 Introduction

As per very initial practice, data was stored and maintained in traditional file system. Due to the technological revolution, it has become easy to store and maintain the data in the database system and further in the data warehousing system. The primary phase of database and data warehousing has faced some limitation in the data storage capacity [1].

In the current scenario, there is no restriction on the amount of data being stored and managed in different repositories. At the same time, Data Analysis has emerged

A. Dixit () · A. Tiwari · R. K. Gupta

Department of CSE & IT, Madhav Institute of Technology & Science, Gwalior, Madhya Pradesh 474005, India

e-mail: abhishekdxit.cse@gmail.com

A. Tiwari

e-mail: atiwari.mits@gmail.com

R. K. Gupta

e-mail: iitmrgk@gmail.com

as an important dimension for analysis of huge amount of data and creation of Knowledge Base (KB) for referencing to decision makers. A large quantity of data is stored per hour in many organizations. Some typical examples are in the business domain (like e-marketing, stock market etc.) in which a huge amount of information is collected in the database, also in the scientific domain a large amount of data related to satellite streaming, remote-sensing, etc. is collected. This smooth storing and discovering information from data became possible by the evolution of Data Mining.

Data Mining [1, 2] is a very important step in the process of discovering knowledge from databases. Through data mining meaningful patterns and rules are mined which are very useful for the decision makers for making business strategies, as in this business competitive world, business strategies are very important to gain profit by which an organization can survive comfortably.

In this paper, mainly the business domain is considered. E-Marketing application such as Snapdeal, Flipkart, Amazon, etc. comes under the business domain. A customer uses these applications for purchasing items. Business initiatives recognize that customer's information and their buying patterns are very important for their enterprises, that's why at the time of purchasing, a new unique transaction ID is given to the customer and these overall transactions are recorded in the database of individual applications. This recorded data is then further used by the decision maker to make a selling strategy to increase the profit. This is done with the help of data mining technique which uses these recorded data and finds patterns from them and then develop association rules which helps in improving the overall business.

Data mining techniques deal with the items which are sold during the purchase, but not consider the items that are almost sold, which are also responsible for improving the overall profit. In order to consider such items that are almost sold, a new field of mining has been evolved commonly known as Hesitation Mining [7]. These almost sold items are referred as Hesitated Items [7].

In this paper, author proposes an algorithm which deals with the Hesitation Mining. Figure 1, shows the flowchart of occurring hesitation situation in the e-marketing scenario. In the given flowchart, red boxes show the almost sold items i.e. hesitated items and green boxes show the sold items.

Hesitation Mining is the technique which considers sold items and almost sold items. This mining technique identifies the hesitation information, which contains information regarding hesitated items and converts these hesitated items i.e. almost sold items to sold items which is very useful for boosting up the sales of the items.

1.1 Architectural Design

The Architecture of a hesitation information mining system which is referenced from the typical data mining system [2] is shown in Fig. 2.

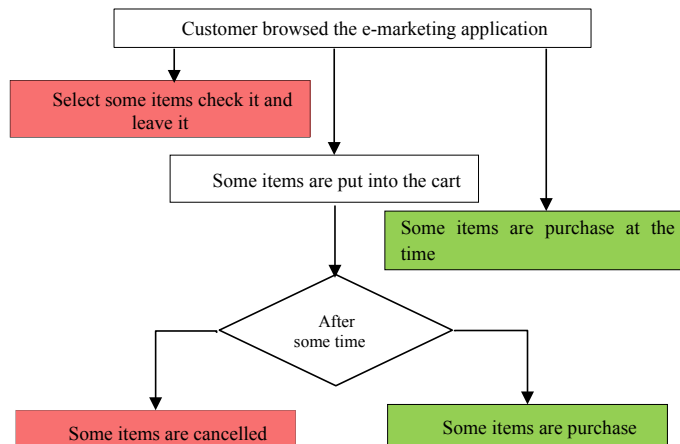


Fig. 1 Flowchart of occurring the hesitation situation in e-marketing scenario

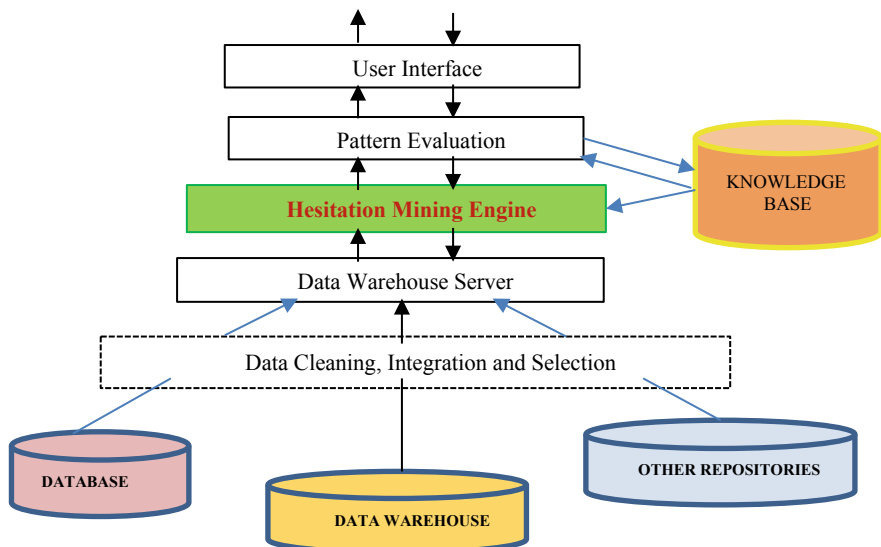


Fig. 2 Architecture of a typical Hesitation Mining System

1.2 Architectural Components

- **Data Cleaning, Integration and Selection:** In this module, the data from different sources is combined, the irrelevant or useless and noisy data is removed from the gathered data and finally transform the data according to the need.

- **Knowledge Base:** It is simply a domain knowledge and for finding the interestingness of subsequent patterns and to guide the searching of patterns a domain knowledge is used.
- **Hesitation Mining Engine:** Hesitation Mining Engine usually consists of a set of functional modules and is very important for mining hesitation information.
- **Pattern Evaluation Module:** This module interacts with the hesitation mining modules and emphasis on searching interesting patterns.
- **User interface:** This is responsible for providing communication between user and the hesitation mining system.

The rest of this paper is organized as follows. Section 2 briefly discusses the background. Section 3 discusses the basic terminologies used. In Sect. 4, the proposed algorithm. Section 5 presents illustration. Section 6 discusses the results interpretation. Finally, Sect. 7 draws a conclusion.

2 Background

Several contributions have been made related to this concept after the introduction of the term hesitation information. Here, all those contributions are discussed below:

In direction to handle uncertainties and imprecise information a number of theories came into existence such as Probability theory, Fuzzy Set theory which was introduced by Zadeh [3], in 1965, Rough Set theory was discovered by mathematician Pawlak [4], in 1980s, a new mathematical tool known as Soft Set theory was introduced by Molodtsov [5], in 1999. But these theories suffer from some limitation such as fuzzy have only one membership degree, rough set has a redundancy problem, etc. [6]. So, to handle vagueness and uncertainty Vague Set theory was proposed by Gau and Buehrer [6], in 1993. Vague theory helps in eliminating the cost of decision table which is present in rough set theory.

In a market basket analysis, hesitation stages are analysed of buying an item. These hesitation states carry hesitation information which is important for decision making strategy. Based on the vague theory, some algorithms have been proposed to deal with vague and uncertain data.

Firstly in 2007, Lu et al. [7] proposed an algorithm to mine the vague data. To achieve this vague data author applied Vague Set theory and generates rules by applying newly proposed Vague Association Rule Mining algorithm.

In 2012, Pandey et al. [8] worked upon mining the course information to identify hesitated courses. Different courses containing topics and their attendance are taken as a database and the vague association rule is applied to generate rules. This helps in making the hesitated course as an interesting course. Later on in 2013, the author extends this concept in the temporal database [9].

In 2015, Badhe et al. [10] pointed out to generate rules of certain profit. To achieve the desired aim author proposed an algorithm for mining profit patterns on vague and uncertain data. Here, new parameter true support and true confidence are calculated

in place of support and confidence. Later on in 2016, Badhe et al. [11] extend this concept along with optimizing the resulted rule by applying the genetic algorithm. To achieve this author calculates fitness function to improve the profit and allowed to survive the rules with maximum profit after optimization.

In 2016, Singh et al. [12], proposed an algorithm that discovers the hesitated information of items using the concept of a vague set by generating all frequent itemset whose support and weighted support is greater than the threshold support.

In 2017, Sowkarthika et al. [13], uses a transaction database and proposed an algorithm for generating optimal profitable seasonal rules and optimize it by using Elephant Herding Optimization. These rules are beneficial for any organization in the current scenario for valuable decision making.

In 2010, Gautam et al. [14] proposed a model that satisfies various support (minimum) at each level of mining multilevel association rules, for mining these rules author use set concepts such as Fuzzy Set, multi-level taxonomy and for item set pruning the Apriori property is used.

3 Preliminaries

This section presents the basic definitions and framework.

3.1 Terminologies

- **Hesitation Information:** During the transaction it is a piece of information which exists in between the purchasing (buying) or not purchasing an item. This information is very useful for enhancing the sales of hesitated items [7].
- **Hesitation Status (Hs/H):** During the process of purchasing, these statuses are the states between buying and not buying the items, which means a customer may drop the selected item at any one of the states for some reason.

Let us consider an example of placing an order with “Snapdeal.com”. The hesitation statuses are considered as:

H_1 : customer browsed an item and check its specification.

H_2 : add the items to the shopping cart.

H_3 : choose the shipping method, provide payment information and submit order.

- **Support:** This defines how frequently item X and Y are bought together in the set of transactions in D .

$$\text{Support } (X, Y) = \frac{|X \cup Y|}{|D|}$$

- **Minimum Support Threshold (MST):** A threshold value for support is defined in advance commonly termed as a minimum support threshold. This value is used

to identify which pattern is considered as a frequent pattern and which pattern is not considered as a non-frequent pattern. Any pattern having support greater than or equal to the minimum support threshold is considered as frequent whereas pattern having support less than minimum support threshold is considered as non-frequent.

- **Frequent Itemsets:** The itemsets having support greater than the minimum support threshold is known as frequent itemsets.

3.2 Vague Set Theory

Crisp Set theory only deals with full membership and it does not handle vague situations [3]. In order to handle a vague situation, a number of theories has been discovered like Fuzzy Set theory, Soft Set theory, Rough Set theory, and Vague Set theory.

Fuzzy Set theory, there is a single grade of membership is defined by which it can handle uncertainty up to a certain limit [4]. To handle this problem Rough Set theory came into existence but this theory also phases some problem of database inconsistent because of eliminating redundant attributes in a rule. These problems may lead to the evolution of alternate set theory called a Vague Set theory [6, 7].

Vague set theory is a very important mathematical tool for handling and studying the vagueness and uncertainty in information system [7, 8, 10, 12, 13]. In comparison to other mathematical tools of set theory this vague set theory expressed the grade of membership in the interval form.

- Vague set theory has a two grade of membership, the first one is true membership and the second one is false membership.
- These memberships represent that an object belongs to or not belongs to object space.
- If membership represents the necessary degree of evidence for object fit for vague set then it is commonly known as true membership. It is represented as $\alpha(x)$, where x is an item or object.
- If membership represents the necessary degree of against evidence for object fit for vague set then it is commonly known as false membership. It is represented as $\beta(x)$, where x is an item or object.
- In this $\alpha(x), \beta(x)$ lies between 0 and 1, the sum of these two should be less than or equal to 1 i.e. $\alpha(x) + \beta(x) \leq 1$.
- Simply true and false membership gives the customer interest in the item.
- For finding vague value another parameter is also calculated as $1 - \beta(x)$ and it is known as possible degree of evidence.

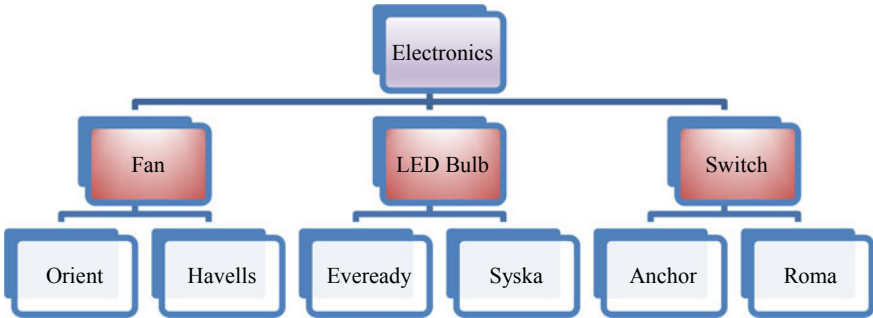


Fig. 3 Multilevel Transactional Hierarchy

3.3 Multilevel Frequent Pattern Mining

Extracting knowledge from data by mining frequent patterns at multiple levels can be possible through only Multilevel Frequent Pattern Mining [14]. By using multilevel frequent pattern mining approach, organization finds the relationship between itemset at various levels.

In multilevel frequent pattern mining, items present in the transaction are represented as a terminal node in the tree or hierarchy. While classes are represented as an internal node.

Consider an example, in the hierarchy, root node “Electronics” is at level 0, internal nodes (such as “Fan”, “LED Bulb”, “Switch”) are at level 1 and the terminal nodes representing brands (such as “Orient”, “Havells”, etc.) are at level 2. Only terminal or leaf nodes present in transactions.

Now, nodes of the tree are first encoded by using sequences of numbers and “*” symbol, the number and “*” are placed according to their places in the tree. For example, the internal node “Fan” (see Fig. 3) is represented as 1*, and the terminal or leaf node Orient as 11.

Multiple level association rule mining can work on Uniform and Reduced type of support.

- Uniform Support: In this type of approach similar minimum support threshold is set at each level of the tree.
- Reduced Support: In this type of approach minimum support is reduced as moving down in the hierarchy.

4 Proposed Algorithm

This algorithm is designed considering only one hesitation status. However, the number of hesitation status can be increased and formulated as per the requirement or on the basis of survey of realistic application domain.

Steps of proposed algorithm is as follows:

- Step 1: Firstly, encode the list of items of each transaction in multilevel taxonomy i.e. encode the item which was purchased in a transaction by a sequence of number (depend on level) followed by “*”.
- Step 2: Consider a variable L , which is used to identify the level number.
- Step 3: Take an index variable I , which is used to identify the itemset.
- Step 4: For each L , we consider the minimum threshold support $\mu = (\text{true support, hesitated support})$. This minimum threshold support can be unique or different for every I in L .
- Step 5: Identify all those items in transaction T_i having similar first L digits and count the occurrence of such items which are completely sold (η). Similarly, count the occurrence of such items which are hesitated (t).
- Step 6: Now, construct I-itemset in each level L , along with their support value = (true support, hesitated support) i.e. support value is in the form of vague set.
- Step 7: Evaluate the support value of itemset i as follows:

$$N_i = \left(\sum \frac{\eta}{\sum_{T_i} \eta + t}, \sum \frac{t}{\sum_{T_i} \eta + t} \right)$$
- Step 8: Put item i in frequent itemset if $N_i \geq \mu$ at particular L . Now, Set $I = I + 1$, for the same level L .
- Step 9: Now, construct $I + 1$ -itemset in each level L . Support value of itemset in this as follows:

$$N(i,j) = (\sum_{min} N_i \wedge N_j) \quad (\text{where, } i \text{ and } j \text{ are frequent itemset from the previous set of frequent itemsets})$$
- Step 10: Do the same till all the level are traversed.

5 Illustration

For the illustration consider multilevel transactional hierarchy as shown in Fig. 3.

Dataset Description: The transactional dataset for the experiment are in the form as shown below in Table 1. Where items are represented as $\{L^{\text{th}} \text{ level item number, } L^{\text{th}} + 1 \text{ level item number, membership}\}$

Now firstly, encode the list of items of each transaction (Table 2).

After encoding, find the frequent itemset at different level as follows:

For Level L = 1, consider Support $\mu = (0.25, 0.50)$

1—Itemset

Table 1 Transactional dataset

Transaction id	Items
T1	{1,1,1}{1,2,h}{3,2,h}
T2	{1,2,1}{2,1,1}{2,1,h}{3,1,h}
T3	{1,1,1}{2,1,1}{3,1,1}{3,2,h}
T4	{1,2,1}{2,1,h}{2,2,1}{3,1,h}

Table 2 Encoded transactional dataset

Transaction id	Items
T1	{1*,1,1}{3*,0,1}
T2	{1*,1,0}{2*,1,1}{3*,0,1}
T3	{1*,1,0}{2*,1,0}{3*,1,1}
T4	{1*,1,0}{2*,1,1}{3*,0,1}

$\{1^*\} = \{(0.33, 0.33)/T1, (0.25, 0)/T2, (0.25, 0)/T3, (0.25, 0)/T4\} = \{1.08, 0.33\}$
 $\{2^*\} = \{(0, 0)/T1, (0.25, 0.25)/T2, (0.25, 0)/T3, (0.25, 0.25)/T4\} = \{0.75, 0.5\}$
 $\{3^*\} = \{(0, 0.33)/T1, (0, 0.25)/T2, (0.25, 0.25)/T3, (0, 0.25)/T4\} = \{0.25, 1.08\}$. Now, the candidate itemsets with their support are mentioned in Table 3 and candidate items which are turned into frequent items are mentioned in Table 4.

2—Itemset

$\{2^*, 3^*\} = \{(0, 0)/T1, (0, 0.25)/T2, (0.25, 0)/T3, (0, 0.25)/T4\} = \{0.25, 0.50\}$. Now, the candidate itemsets with their support are mentioned in Table 5 and the candidate items which are turned into frequent items is mentioned in Table 6.

For Level L = 2, consider Support $\mu = (0.20, 0.45)$

1—Itemset

Table 3 Candidate itemset with support and their status

Candidate items	Support	Status
$\{1^*\}$	{1.08, 0.33}	No frequent item
$\{2^*\}$	{0.75, 0.50}	Frequent item
$\{3^*\}$	{0.25, 1.08}	Frequent item

Table 4 Frequent 1—itemset

Candidate items	Support
$\{2^*\}$	{0.75, 0.50}
$\{3^*\}$	{0.25, 1.08}

Table 5 Candidate itemset with support and their status

Candidate items	Support	Status
$\{2^*, 3^*\}$	{0.25, 0.50}	Frequent item

Table 6 Frequent 2—Itemset

Candidate items	Support
{2*, 3*}	{0.25, 0.50}

Table 7 Candidate itemset with support and their status

Candidate items	Support	Status
{21}	{0.50, 0.50}	Frequent item
{22}	{0.25, 0}	No frequent item
{31}	{0.25, 0.50}	Frequent item
{32}	{0, 0.66}	No frequent item

Table 8 Frequent 1—Itemset

Candidate items	Support
{21}	{0.50, 0.50}
{31}	{0.25, 0.50}

Table 9 Frequent 2—Itemset

Candidate items	Support
{21, 31}	{0.25, 0.50}

$\{21\} = \{(0, 0)/T1, (0.25, 0.25)/T2, (0.25, 0)/T3, (0, 0.25)/T4\} = \{0.50, 0.50\}$
 $\{22\} = \{(0, 0)/T1, (0, 0)/T2, (0, 0)/T3, (0.25, 0)/T4\} = \{0.25, 0\}$
 $\{31\} = \{(0, 0)/T1, (0, 0.25)/T2, (0.25, 0)/T3, (0, 0.25)/T4\} = \{0.25, 0.50\}$
 $\{32\} = \{(0, 0.33)/T1, (0, 0)/T2, (0, 0.33)/T3, (0, 0)/T4\} = \{0, 0.66\}$. Now, the 1-candidate itemsets with their support are mentioned in Table 7 and the 1-candidate items which are turned into frequent items is mentioned in Table 8.

2—Itemset

$\{21, 31\} = \{(0, 0)/T1, (0, 0.25)/T2, (0.25, 0)/T3, (0, 0.25)/T4\} = \{0.25, 0.50\}$. Now, 2-candidate item which is turned into frequent items is shown in Table 9.

6 Results Interpretation

The obtained result in Table 6 provides the information about the frequently hesitated items of size 1 i.e. LED bulb and Switch. But, this information is quite superficial and decision maker need more specific and precise information regarding the hesitation items. So, as described in the approach, after digging into further levels of the hierarchy and applying the proposed algorithm more accurate information is mined as shown in Table 9 i.e. Eveready LED Bulb and Anchor Switch. In this way, through this approach the decision maker will be able to extract more accurate information of

the frequently hesitated items. Furthermore, decision makers may promote the sale of these hesitated items by combining them with sole or combo offers.

7 Conclusion

The proposed algorithm termed as Multilevel Hesitation Pattern Mining, which uses vague set theory along with multilevel taxonomy in order to address the uncertain situations at different levels over the transactional database. Moreover, by using different minimum support for each level author finds a multilevel hesitated frequent pattern. The proposed algorithm is capable of generating a more relevant pattern set. These sets are beneficial for mining rules in vague situations. Due to this proposed algorithm, it is possible to analyze and evaluate the vague/imprecise information. Furthermore, the generated rules help in eliminating the product hesitation status and transform the ‘almost sold’ item to ‘sold’ item. This removal of the hesitation of a product will be beneficial for any enterprise in the current and future scenario for effective decision making.

References

1. Pujari, A.K.: Data Mining Techniques, 3rd edn. Universities Press, India (2013)
2. Han, J., Kamber, M., Pei, J.: Data Mining: Concepts and Techniques. 2nd edn. Morgan Kaufmann, Elsevier (2006)
3. Zadeh, L.A.: Fuzzy sets, *Information and Control*. pp. 338–353 (1965)
4. Pawlak, Z.: Rough sets. *Int. J. Inf. Comput Sci.* 341–356 (1982)
5. Molodtsov, D.: Soft set theory-First results, *Computers and Mathematics with Applications*. pp. 19–31 (1999)
6. Gau, W.L., Buehrer, D.J.: Vague sets. *IEEE Trans. Syst. Man Cybern.* 610–614 (1993)
7. Lu, A., Ng, W.: Mining hesitation information by Vague Association rules. In: Parent Conference 2007, LNCS, vol. 4801, pp. 39–55. Springer, Berlin, Heidelberg (2007)
8. Pandey, A., Pardasni, K.R.: A model for mining course information by using Vague association rule. *Int. J. Comput. Appl.* **58**(20), 1–5 (2012)
9. Pandey, A., Pardasni, K.R.: A model for Vague association rule mining in temporal database. *J. Inf. Comput. Sci.* **8**(1), 063–074 (2013)
10. Badhe, V., Thakur, R.S., Thakur, G.S.: Vague set theory for profit pattern and decision making in uncertain data. *Int. J. Adv. Comput. Sci. Appl.* **6**(6), 182–186 (2015)
11. Badhe, V., Thakur, R. S., Thakur, G. S.: A model for profit pattern mining based on genetic algorithm. *IJRET: Int. J. Res. Eng. Technol.* **5**(8), 43–49 (2016)
12. Singh, A.K., Tiwari, A.: Vague set based association rule mining for profitable patterns. *Int. J. Sci. Adv. Res. Technol.* **2**(2), 1–6 (2016)
13. Sowkarthika, B., Tiwari, A., Singh, U.P.: Elephant herding optimization based Vague association rule mining algorithm. *Int. J. Comput. Appl.* 15–23 (2017)
14. Gautam, P., Pardasani, K.R.: A novel approach for discovery multilevel fuzzy association rule mining. *J. Comput.* **2**(3), 56–64 (2010)

Six Switch Three Phase Five-Level Inverter with Sinusoidal Pulse Width Modulation



Rajesh Kumar Mahto and Ambarisha Mishra

Abstract This chapter presents a new switching strategy using sinusoidal pulse width modulation technique to produce three phase five-level output voltage. The switching gate pulse is developed at over modulation index. The inverter operating devices are in the sequence of either two switches (one positive and one negative) or three switches (two positive and one negative and vice versa) ON at a time. The circuit topology and number of switching devices are same as that of basic three phase two-level voltage source inverter. The circuit configuration and switching pulse are developed in MATLAB/SIMULINK environments and the performance is investigated with different modulation index and switching frequency. The new switching strategy presented in the chapter is capable to produce three phase balanced five-level output line voltages ($0, \pm V_{dc}/2, \pm V_{dc}$) with lesser total harmonics distortion and higher fundamental content in output voltage and current. Based upon simulation result performance the proposed technique is recommended for overall improvement of inverter output without increase in cost.

Keywords Sinusoidal pulse width modulation · Modulation index · Total harmonics distortion

1 Introduction

The basic principle of VSI is to convert fixed DC voltage into variable AC output voltage and frequency. This property of inverter had been used in variable AC drive systems. The conventional VSI is a two-level inverter which is generally used. Multi-level inverter has some attractive feature when it compare with conventional two-level inverter. Now-a-days multi-level inverter (MLI) is used in place of two level inverter. Due to improved quality of AC output voltage. Since last three decade not only most of the research has been done but also work is going on the multi-level inverter to overcome the demerits of conventional two-level inverter [1, 2]. Most

R. K. Mahto (✉) · A. Mishra

Electrical Engineering Department, National Institute of Technology Patna, Patna, India
e-mail: kushwaharajesh431@gmail.com

widely used 3-Φ VSI using six switches with the help of SPWM technique is either two or three-level inverter. The conventional two level inverters are replaced with multilevel inverter to improve the output power quality [3, 4]. These voltage source inverters produce high quality output which is a demand for ac drives. There has been a lot of research done and also going on to improve the quality of output power of the inverter [5, 6]. It has been seen that there is no inverter available which is capable to produce pure sinusoidal waveform. These inverters are having many disadvantage like large number of power electronic components and consequently the more size and weight, very high cost as compared to traditional three-phase VSIs. Each IGBT has its own snubber circuit to avoid electromagnetic interferences (EMI) on driver circuit [7, 8]. In this work with the help of new switching logic the conventional 3-Φ VSI is upgraded and the same inverter circuit is able to produce 5-level output voltage by using six switches only. This technique reduces a huge amount of ripple content in the output waveform without increasing any additional cost. This paper describes the performance analysis by selecting the appropriate conduction period of switches by changing the modulation index. It ensures better power quality of output voltage and current. Here the load is a wye connected load for which inverter produces a 12 step output phase voltage waveform it is closer to sinusoidal waveform than the traditional VSI which produces six steps. For wye connected load it produces seven levels ($0, \pm V_{dc}/3, \pm V_{dc}/2, \pm 2 V_{dc}/3$) in output instead of four levels generated by traditional VSI. This paper presents a modified firing scheme for three-phase VSI which intentionally opens one of three inverter legs per time in a pre-planned sequence. Simulated results using MATLAB SIMULINK software show the validity of proposed scheme for different types of load. Here analysis of frequency spectrum of output is done using FFT and THD is calculated. This paper presents the evaluation of performance for three phase voltage source inverter for different modulation index and switching frequency with various types of load.

2 Mathematical Modeling and Operation of Proposed Technique

2.1 Inverter Model

The circuit shown in Fig. 1 contain six IGBT switches having connected anti-parallel diodes from S1 to S6 out of these, three positive group switches and three negative group switches. The positive group switches are S1, S3, S5 and negative group switches are S4, S6 and S2. The gate pulse of these six switches are provided by sinusoidal pulse width modulation technique. In the sinusoidal pulse width modulation technique when the modulation index is less than 1, it has been seen that lower order harmonics greatly reduced and increases higher order harmonics. The higher order harmonics can be easily suppressed by filter but when the modulation index is greater then one it increases lower order harmonics along with provided higher

Fig. 1 Circuit diagram of basic 3-phase VSI connected with Y load

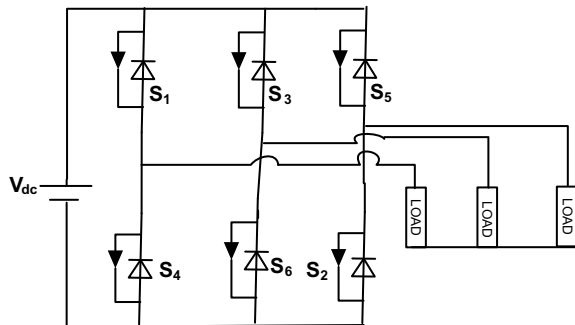
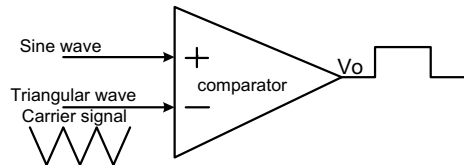


Fig. 2 Sinusoidal pulse width modulation technique



fundamental RMS voltage compare to previous one. In SPWM technique a sinwave signal having frequency (50 Hz) modulated with high frequency carrier wave and the modulated signal is passing through logical comparator. The comparator compare these modulated signal according to set logic and provide rectangular pulse which is given to the gate of the six switches of the IGBT to turn on.

2.2 Pulse Width Modulation Technique

The pulse width modulation technique is used to generate a constant amplitude pulse. In PWM technique a base signal is modulating with carrier signal and the modulated signal is fed to the comparator and based on the logical output the final output pulse is generated. The base signal is desired output signal like sinusoidal signal or square wave signal where as in other hand carrier wave is may be triangular wave or saw tooth wave having frequency greater than the base frequency as shown in Fig. 2.

2.3 Generation of Switching Pulses Using SPWM Technique

In this case phase-A sinewave is considered start with zero amplitude compare with peak amplitude triangular wave at modulation index (1.2). When amplitude of sine wave is greater than triangular wave it will generate output pulse. This pulse as shown in Fig. 3 is used to trigger the switch s_1 .

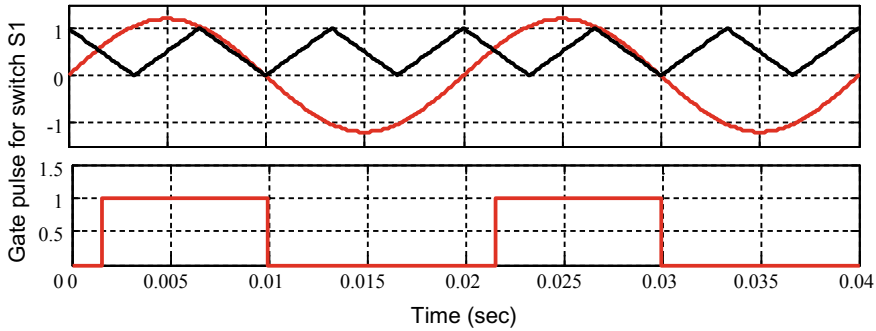


Fig. 3 Modulation of sinewave and triangular wave with generated gate pulse

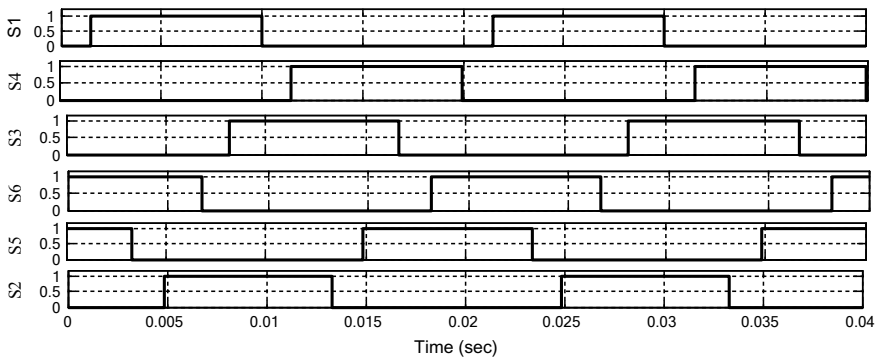


Fig. 4 Generated gate pulse for all the six switches

Similarly all the six switching pulses are generated for 50 Hz frequency up-to two cycles using the same SPWM technique which are shown in Fig. 4. It should be noted here that to generate this gate pulse the modulation index should be greater than 1.2.

2.4 Proposed Switching Strategy with Output Voltage

In the proposed work the basic six-switch inverter as shown in Fig. 1 is used in different operating modes. The output is obtained at different cases as follows.

Case 1: The resultant of the circuit as given in Fig. 1 is shown below when switch s_5 and s_6 are in ON state and all other switches are in OFF state. The output phase voltage is, ($V_a = 0$), $V_b = -(V/2)$, $V_c = (V/2)$ as shown in Fig. 5.

Fig. 5 Circuit configuration when switch S_5 and S_6 are ON

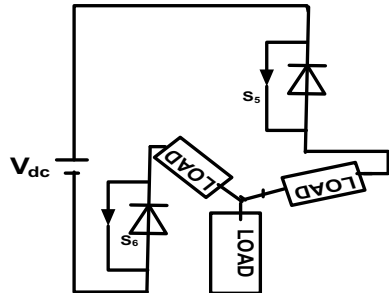
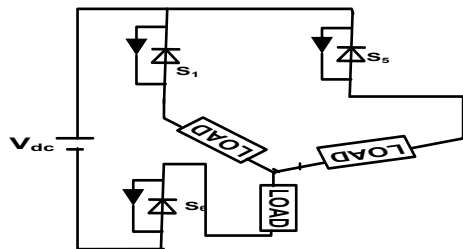


Fig. 6 Circuit configuration when switch S_5 and S_6 are ON



Case 2: In this case two positive group switches s_1 , s_5 and one negative group switch s_6 are in ON state. The output voltage is $V_a = V/3$, $V_b = -(2V/3)$, $V_c = V/3$ from Fig. 6.

Case 3: In the circuit given below one positive group switch S_1 , S_5 and one negative group switch S_6 are in ON and all other switches are off so the output voltage $V_a = V/2$, $V_b = -(V/2)$, $V_c = 0$ as given in Fig. 7.

Case 4: In this case one positive group switch S_1 and two negative group switch S_2 and S_6 are in ON state. The circuit condition and direction of current flow are

Fig. 7 Circuit configuration when switch S_1 and S_6 are ON

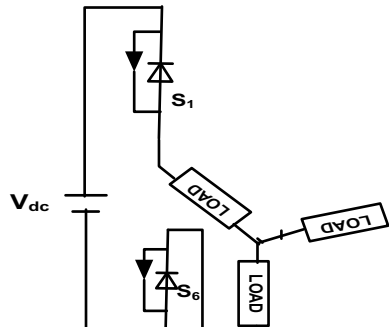


Fig. 8 Circuit configuration when switch S_1 , S_2 and S_6 are ON

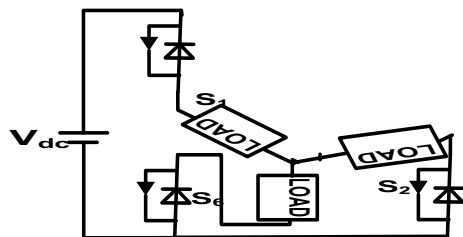
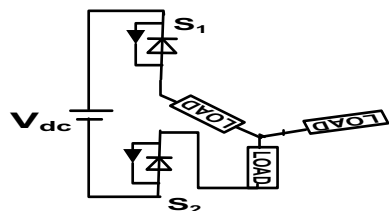


Fig. 9 Circuit configuration when switch S_1 and S_2 are ON



shown in given below circuit. The three phase output voltage $V_a = 2V/3$, $V_b = -(V/3)$, $V_c = -(V/3)$ shown in Fig. 8.

Case 5: In the given circuit shown below two switches are in ON state S_1 and S_2 and it will give the output voltage $V_a = V/2$, $V_b = -(V/2)$, $V_c = 0$ shown in Fig. 9.

Case 6: The given circuit diagram as given below three switches are in on state out these two positive group switch s_1 , s_3 and one negative group switch s_2 . The direction of current is also shown in the circuit given below. The output voltage $V_a = V/3$, $V_b = -(2V/3)$, $V_c = V/3$ as shown in Fig. 10.

Similarly all the twelve state for one cycle has been obtained as given in Table 1. These twelve level phase voltage when compare with basic six switches three phase VSI. It has been seen that voltage stress on each switch reduced for twelve-level hence lower rating switches can utilize for same output power so that cost of the switch reduces and overall inverter cost decreased. It can be noted that these output only obtained when modulation had done at over modulation index. Although at over modulation lower order harmonics increases but content of fundamental component has been increased. It has been advantageous in electric drive as fundamental component is responsible for electromagnetic torque as the fundamental component increase electromagnetic torque will also increases. It has been seen that for the same

Fig. 10 Circuit configuration when switch S_1 , S_2 and S_3 are ON

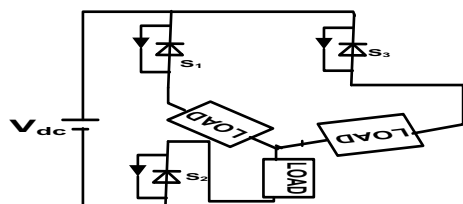


Table 1 Switching table and generated output phase and line voltage

On	Off	Phase voltage \mathbf{V}_{an}	Phase voltage \mathbf{V}_{bn}	Phase voltage \mathbf{V}_{cn}	Line voltage \mathbf{V}_{ab}	Line voltage \mathbf{V}_{bc}	Line voltage \mathbf{V}_{ca}
S_5, S_6	S_1, S_2, S_3, S_4	0	$-\frac{V_{dc}}{2}$	$\frac{V_{dc}}{2}$	$\frac{V_{dc}}{2}$	$-\mathbf{V}_{dc}$	$\frac{V_{dc}}{2}$
S_1, S_5, S_6	S_2, S_3, S_4	$\frac{V_{dc}}{3}$	$-\frac{2}{3}V_{dc}$	$\frac{V_{dc}}{3}$	\mathbf{V}_{dc}	$-\mathbf{V}_{dc}$	$\mathbf{0}$
S_1, S_6	S_2, S_3, S_4, S_5	$\frac{V_{dc}}{2}$	$-\frac{V_{dc}}{2}$	$\mathbf{0}$	\mathbf{V}_{dc}	$-\frac{V_{dc}}{2}$	$-\frac{V_{dc}}{2}$
S_1, S_2, S_6	S_3, S_4, S_5	$\frac{2}{3}V_{dc}$	$-\frac{V_{dc}}{3}$	$-\frac{V_{dc}}{3}$	\mathbf{V}_{dc}	$\mathbf{0}$	$-\mathbf{V}_{dc}$
S_1, S_2	S_3, S_4, S_5, S_6	$\frac{V_{dc}}{2}$	$\mathbf{0}$	$-\frac{V_{dc}}{2}$	$\frac{V_{dc}}{2}$	$\frac{V_{dc}}{2}$	$-\mathbf{V}_{dc}$
S_1, S_2, S_3	S_4, S_5, S_6	$\frac{V_{dc}}{3}$	$\frac{V_{dc}}{3}$	$-\frac{2}{3}V_{dc}$	$\mathbf{0}$	\mathbf{V}_{dc}	$-\mathbf{V}_{dc}$
S_2, S_3	S_4, S_5, S_6, S_1	$\mathbf{0}$	$\frac{V_{dc}}{2}$	$-\frac{V_{dc}}{2}$	$-\frac{V_{dc}}{2}$	\mathbf{V}_{dc}	$-\frac{V_{dc}}{2}$
S_2, S_3, S_4	S_5, S_6, S_1	$-\frac{V_{dc}}{3}$	$\frac{2}{3}V_{dc}$	$-\frac{V_{dc}}{3}$	$-\mathbf{V}_{dc}$	\mathbf{V}_{dc}	$\mathbf{0}$
S_3, S_4, S_5	S_1, S_2, S_6	$-\frac{2}{3}V_{dc}$	$\frac{V_{dc}}{3}$	$\frac{V_{dc}}{3}$	$-\mathbf{V}_{dc}$	$\mathbf{0}$	\mathbf{V}_{dc}
S_4, S_5	S_6, S_1, S_2, S_3	$-\frac{V_{dc}}{2}$	$\mathbf{0}$	$\frac{V_{dc}}{2}$	$-\frac{V_{dc}}{2}$	$-\frac{V_{dc}}{2}$	\mathbf{V}_{dc}
S_4, S_5, S_6	S_1, S_2, S_3	$-\frac{V_{dc}}{3}$	$-\frac{V_{dc}}{3}$	$\frac{2}{3}V_{dc}$	$\mathbf{0}$	$-\mathbf{V}_{dc}$	\mathbf{V}_{dc}

input voltage if fundamental component of output voltage increases, the efficiency of the inverter will improve. Table 1 given below represent complete explanation of switching strategy with generated output phase and line voltages for all the three phase for a complete cycle.

2.5 Simulation Results and Discussion

The proposed modulation scheme for improved performance of inverter is developed in MATLAB. The input voltage V_{dc} 100 V.

Figure 11 Represent the output phase voltage of proposed technique at switching frequency 150 Hz and modulation index ($m_a = 1.2$). Figure 12 Represent the output line voltage of proposed technique at switching frequency 150 Hz and modulation index ($m_a = 1.2$).

Figure 13 Represent the output phase voltage of proposed technique at switching frequency 2500 Hz and modulation index ($m_a = 2$) with 100 V DC source. It can be noted that the output voltages are 0, $\pm V_{dc}/3$, $\pm V_{dc}/2$, $\pm 2V_{dc}/3$.

Figure 14 Represent the output line voltage of proposed technique at switching frequency 2500 Hz and modulation index ($m_a = 2$) with 100 V DC source. It can be

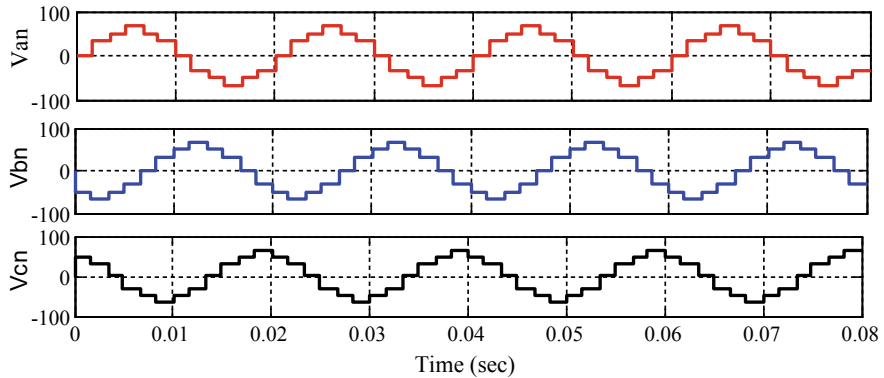


Fig. 11 Simulation result of output phase voltage

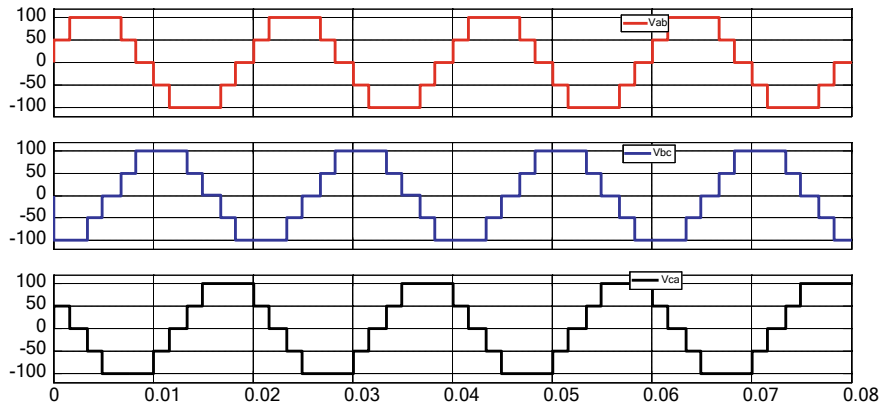


Fig. 12 Simulation result of three phase five-level output line voltage

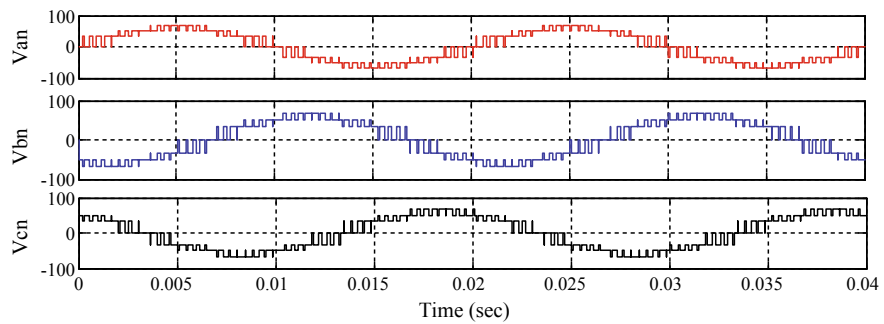


Fig. 13 Simulation result of output phase voltage with high switching frequency

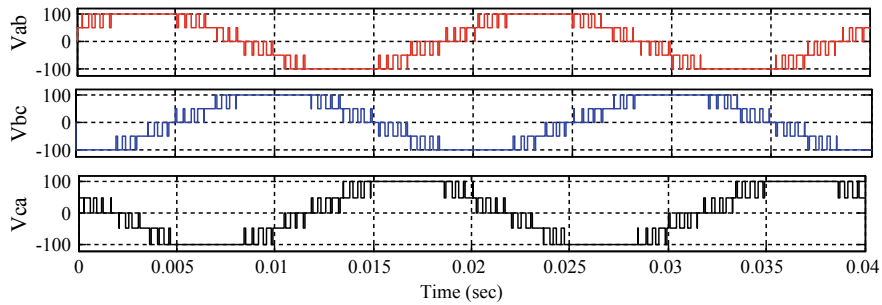


Fig. 14 Simulation result of output line voltage at high switching frequency

Table 2 THD analysis at various modulation index and switching frequency

Modulation index(m_a)	Sinewave frequency (Hz)	Carrier wave frequency (Hz)	THD in line voltage (%)	THD in phase voltage (%)
$m_a = 1.2$	50	150	17.04	16.87
$m_a = 2$	50	2500	23.57	23.35

noted that the output voltages are $0, \pm V_{dc}/2, \pm V_{dc}$. The THD analysis with different carrier frequency and modulation index is given in Table 2.

3 Conclusion

This chapter present three phase five-level output line voltage using six switches with sinusoidal pulse width modulation technique. The simulation result for different conduction mode produce 12-step output phase voltage which is closer to sine-wave which reduces the THD without any additional cost, size and weight. The performance of this topology is investigated with different modulation index and switching frequency and it has been seen that fundamental content in the output voltage increases with modulation index as conduction time of switches is proportional to modulation index. It can be conclude that the proposed technique is recommended for superior performance with lesser total harmonics distortion and higher fundamental content in output voltage and current.

References

1. Rodriguez, J., et al.: Multilevel inverters: a survey of topologies, controls, and applications. *IEEE Trans. Ind. Electron.* **49**(4), 724–738 (2002)
2. Franquelo, L.G., et al.: The age of multilevel converters arrives. *IEEE Ind. Electron. Mag.* **2**(2), 28–39 (2008)

3. Colak, I., et al.: Review of multilevel voltage source inverter topologies and control schemes. *Energy Convers. Manage.* **52**, 1114–1128 (2011)
4. Rodriguez, J., et al.: Multilevel converters: an enabling technology for high-power applications. *Proc. IEEE* **97**(11), 1786–1817 (2009)
5. Ilves, K., et al.: A new modulation method for the modular multilevel converter allowing fundamental switching frequency. *IEEE Trans. Power Electron.* **27**(8), 3482–3494 (2012)
6. Mahrous, E.A., et al.: Three-phase three-level voltage source inverter with low switching frequency based on the two-level inverter topology. *Electr. Power Appl.* **1**, 637–641 (2007)
7. Fei, W.: Novel three-phase three-level-stacked neutral point clamped grid-tied solar inverter with a split phase controller. *IEEE Trans. Power Electron.* **28**(6), 2856–2866 (2013)
8. Yuanmao, Y., Cheng, K.W.E.: A family of single-stage switched capacitor-inductor PWM converters. *IEEE Trans. Power Electron.* **28**(11), 5196–5205 (2013)

AI-Enabled Real-Time Sign Language Translator



Yash Patil, Sahil Krishnadas, Adya Kastwar, and Sujata Kulkarni

Abstract Even in recent times with the advancement in technology, there exists a hindrance in seamless communication with the hearing and speech-impaired section of the society. Inclusive communication is instrumental for a society to function as a whole. It is not only essential for exchanging ideas, but also for progress and innovation. A lack of means for spontaneous communication should not stand in the way of socializing, employment or productivity. We propose an android application that interprets American Sign Language into English language using convolutional neural network with an aim to provide real-time translation to facilitate seamless communication. Although there is a presence of computer-based translation application for sign language recognition, the availability of such applications over an android platform is relatively few in number. The proposed sign language translator finds its applicability in gesture-controlled applications like human–computer interaction, providing control action for various home appliances and electronic gadgets that are triggered by gestures when given as an input. The proposed work is aimed to transform hearing and speech abnormality to normality, thus eliminating their dependencies.

Keywords Convolutional neural network · Real time · Translation · Sign language · Feature extraction

Y. Patil (✉) · S. Krishnadas · A. Kastwar · S. Kulkarni

Department of Electronics & Telecommunication, Sardar Patel Institute of Technology, Mumbai 400058, India

e-mail: yash.patil@spit.ac.in

S. Krishnadas

e-mail: sahil.krishnadas@spit.ac.in

A. Kastwar

e-mail: adya.kastwar@spit.ac.in

S. Kulkarni

e-mail: sujata_kulkarni@spit.ac.in

1 Introduction

Sign language which is predominantly the means of communication with the hearing and speech-impaired community consists of various hand gestures depicting the desired message to be communicated. It is occasionally, however, used by normal hearing people which creates a barrier in communication between the impaired section of the society with the rest of the community and remains as a problem that is yet to be completely solved. Today, about 5 per cent of the world's population, i.e. about 466 million people in the world are speech impaired. However, their impairment obstructs and stands as a barrier to fluent and spontaneous communication, leading to feelings of social exclusion and consequently isolation and loneliness. This also deprives them of employment opportunities, in favour of candidates who do not face problems in communicating, even though they might be equally (or more) capable. If we shift perspectives to that of the employer, we find that they have a cause to hesitate since companies suffer a cumulative annual loss of about USD 750 billion due to loss in productive hours. We wish to create a solution to this basic problem—where the hands talk and the eyes see, to create a conducive environment for this communication to take place and normalize the situation on both sides of the communication barrier. The aim is to design an effective and efficient modelling technique that can characterize the data of class for future decision making [1]. Our solution to this problem is creating a system which translates the ASL being gestured by a speech-impaired person in real time into text, to provide seamless spontaneous communication without the need of expensive hardware or any recording time delays.

2 Literature Survey

There has been intensive work in this area in the past few years, broadly classified into hardware systems and software systems, i.e. glove-based gesture sensing systems and systems image processing and computer vision, respectively. Neuron is the basic building block of an artificial neural network (ANN) which comprehends information like a human brain [2]. In our review of literature for the proposed system, we came across certain key observations, shortcomings and trade-offs.

In 2015, *Purva Badhe and Vaishali Kulkarni* implemented a sign language translation system which first implements data acquisition, followed by pre-processing of gestures to track hand movement which uses a combinational algorithm, and recognition is carried out using template matching [3]. While it provides higher flexibility and functionality by implementing frame processing for gestures, hand extraction and using a vast database of 130,000 videos, it does not give a real-time translation of sign language.

A few papers implemented systems that were specific to the person gesturing or the background against which the gesture was being performed. Starner and Pentland in 1995 [4] and Vogler and Metaxas in the same year [5] used hidden Markov

models and implemented highly accurate person-dependent systems. In 2007, Shamblehet al. extracted features using EOH method and used support vector machine for classification [6], giving a system that was swift but background-dependent. These dependencies limit the scope of use. Al-Jarrah et al. in 2001 [7] used self-organizing feature maps (SOFM) that enhanced HMM-based recognition systems to make system independent of signer. This model was 1.9% more accurate than systems implemented using HMM, but much slower, since it was focused more on feature extraction.

In 2007, Youssif et al. [8] used Fourier transform to remove background noise from captured images and KNN for classification. However, speed was less because it involved image scraping.

Some systems emphasized on feature extraction and extensive amounts of pre-processing. While this reduces the complexity of the system required and increases the speed of the system, it led to trade-offs between other performance parameters, reduced accuracy and need for storage leading to delays in outputs.

3 Objectives

Even with technological and cultural innovations that are now in place (Apps, software, electronic correspondence), basic natural face-to-face communication is still unfeasible. It is also important to facilitate efficient communication among all employees of an organization to overcome various disabilities to enable them to share their opinions, viewpoints and ideas for the benefit of the organization. Such a system will act as a personal, portable interpreter.

Keeping with the observations from our survey of literature, our aim is to design a system:

1. To translate ASL into text in real time.
2. Detecting ASL exhaustively, i.e. not just fingerspelling, but all the gestures that make up ASL.
3. Independent of the person gesturing and the background against which the language is being gestured.
4. That accurate system which learns with every gesture and improves its performance and reduces its delays.
5. That is simple and efficient yet inexpensive moreover portable that eliminates the need for complex hardware.

4 Proposed Methodology

Figure 1 illustrates the basic block diagram of the proposed AI-enabled real-time sign language translator.

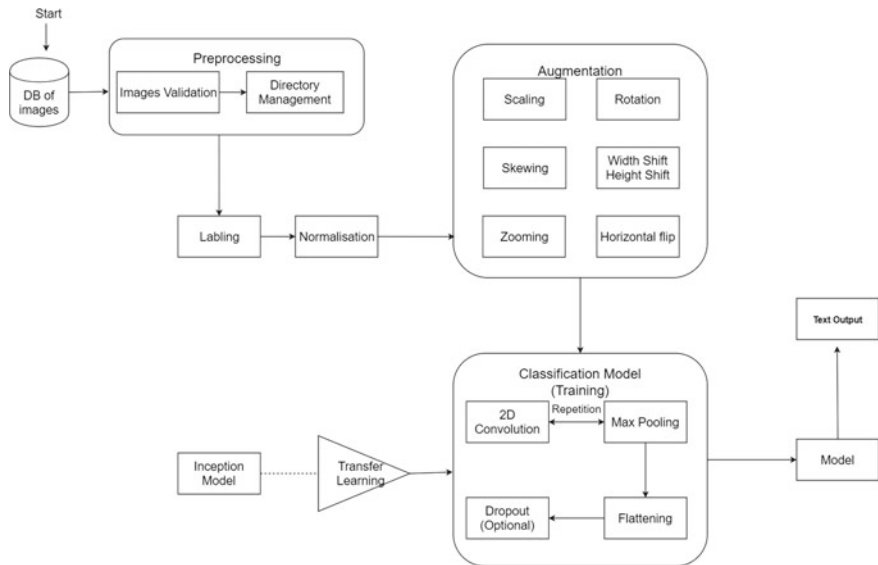


Fig. 1 Block diagram of AI-enabled real-time sign language translator

Our end goal is to create a system that is portable and easy to use, in the form of an android app that can be used on phones to record the gestures being performed by the signer and translate them into text in real time. Our first step towards this is creating a desktop application that will perform the said translation on feed captured through the Web cam. At this stage, our model will recognize fingerspelling in real time. The data set contains about 87,000 images which are each 200×200 pixels in resolution [9]. The images are segregated into 29 classes, which are the fingerspellings for the 26 letters of the alphabet, space, null and delete. Each class has 3000 images.

4.1 Image Pre-processing

We have resized images to create a base size since the images that we capture through cameras and feed to our model may vary in size. Segmentation has been done to separate image foreground from background, remove noise and to separate different objects with different markers. Normalization is used to normalize the intensity values of pixels and to improve the speed of convergence when training the model. Labelling has been performed, since this is a supervised learning model where we need the inputs to be clearly classified into distinct outputs. Thresholding is performed to separate the pixels into background and foreground pixels. Augmentation has been applied by implementing skewing, flipping, zooming and shifting of images to diversify the training set to match actual operating conditions and improve the accuracy of results.

4.2 Convolutional Neural Network Classifier

Convolutional neural network (CNN) is the method we are applying to train our data set to increase the speed of predictions, thus leading to real-time translation. The pooling layers that are being used to downsample the images post convolutional layers are applying max pooling rather than average pooling, as it extracts the most necessary and important features like edges unlike average pooling. Average pooling extracts features smoothly hence is of not much use to our model. The epoch for the training model was set as 15. The classifier had four hidden layers and 512 hidden neurons, with the least number of neurons in every layer that tended to overfit. Increasing the number of hidden units and/or layers may lead to overfitting because it will make it easier for the neural network to learn a function that perfectly separates the training set but that does not generalize to unseen data. On the other hand, neurons could not be lesser for chance of underfitting, i.e. the training set could not fit the network and lead to poor predictive performance. To prevent dips in graph and to reduce overfitting and avoid generalization error, we perform dropout.

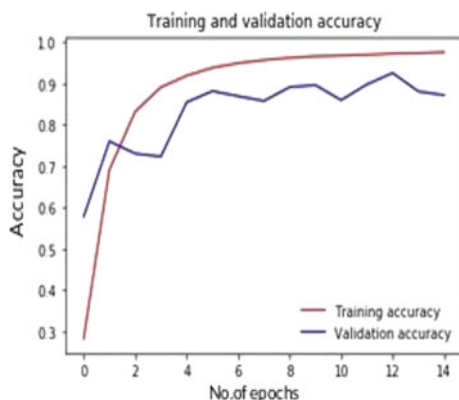
5 Results and Discussion

For epoch value of 15, a graph of training and validation accuracy was plotted against epoch value. A final accuracy of 96.52% was obtained. The model was tested on real-time signed fingerspelling, and it accurately recognized the signed alphabet. The red line shows the accuracy of the model under ideal conditions. The blue line shows the accuracy of the model under practical scenarios.

Figure 2 is the plot of training and validation accuracy against the number of epochs passed.

Figures 3 a and 4a show the video feed being captured. Figures 3b and 4b show the thresholded image obtained after pre-processing F and C, respectively.

Fig. 2 Training and validation accuracy versus epoch value



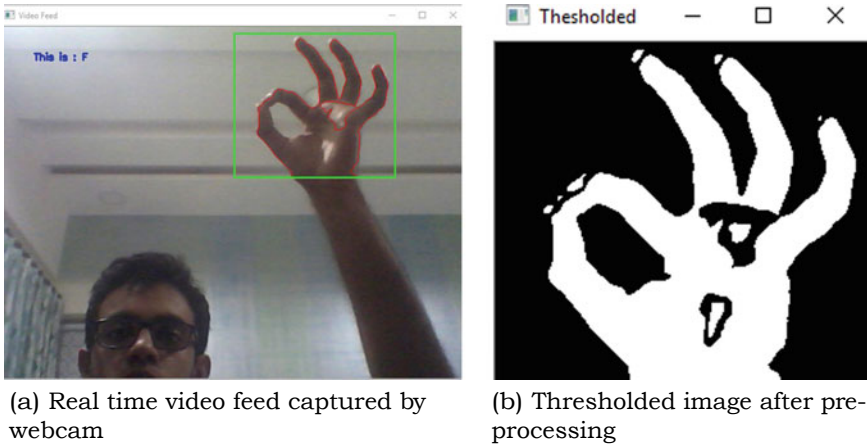


Fig. 3 Real-time translation of fingerspelling for alphabet F

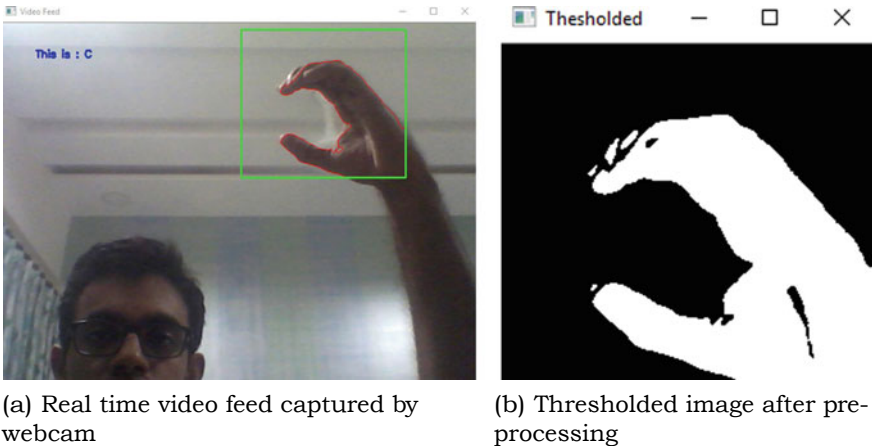


Fig. 4 Real-time translation of fingerspelling for alphabet C

Table 1 illustrates the details of the built model before training, and Table 2 shows the details of the model after it was trained. The number of parameters in a given layer is the number of trainable elements for a filter. The dense layers employed after convolutional layers extract features obtained by these layers. Convolutional layers are used to reduce parameter count and extract patterns. Initially, all the parameters were trainable parameters with 0 non-trainable parameters. In post-training, all parameters were non-trainable.

Table 1 Model summary before training

Model: “sequential”		
Layer (type)	Output shape	Param #
conv2d (Conv2D)	(None, 198, 198, 64)	1792
max_pooling2d (MaxPooling2D)	(None, 99, 99, 64)	0
conv2d_1 (Conv2D)	(None, 97, 97, 64)	36,928
max_pooling2d_1 (MaxPooling2)	(None, 48, 48, 64)	0
conv2d_2 (Conv2D)	(None, 46, 46, 128)	73,856
max_pooling2d_2 (MaxPooling2)	(None, 23, 23, 128)	0
conv2d_3 (Conv2D)	(None, 21, 21, 128)	147,584
max_pooling2d_3 (MaxPooling2)	(None, 10, 10, 128)	0
flatten (Flatten)	(None, 512)	6,554,112
dense (Dense)	(None, 26)	13,338

*Total params 6,827,610**Trainable params 6,827,610**Non-trainable params 0***Table 2** Model summary after training

Model: “sequential”		
Layer (type)	Output shape	Param #
conv2d (Conv2D)	(None, 198, 198, 64)	1792
max_pooling2d (MaxPooling2D)	(None, 99, 99, 64)	0
conv2d_1 (Conv2D)	(None, 97, 97, 64)	36,928
max_pooling2d_1 (MaxPooling2)	(None, 48, 48, 64)	0
conv2d_2 (Conv2D)	(None, 46, 46, 128)	73,856
max_pooling2d_2 (MaxPooling2)	(None, 23, 23, 128)	0
conv2d_3 (Conv2D)	(None, 21, 21, 128)	147,584
max_pooling2d_3 (MaxPooling2)	(None, 10, 10, 128)	0
flatten (Flatten)	(None, 12,800)	0
dense (Dense)	(None, 512)	6,554,112
dense_1 (Dense)	(None, 26)	13,338

*Total params 6,827,610**Trainable params 0**Non-trainable params 6,827,610*

6 Conclusion

The proposed work demonstrates a system that was able to identify the fingerspelling being gestured in real time by means of a CNN classifier, giving a performance precision of 96.52%. The obtained value is much higher than the values obtained on using hidden Markov models for classifying, because CNN takes pre-processing of images into consideration. However, the performance is lesser than that of edge-oriented histogram (EOH) model, because EOH considers plain backgrounds. To combine precision of EOH and the pre-processing capabilities of a CNN, pure hand actions were segmented from continuous real-time frames of images, resulting in background subtraction. Segmentation gave the model an image for prediction which is independent of unwanted background.

7 Future Enhancement

The current system is made to translate fingerspelling of ASL. In the future, this will be extrapolated to attain our objective of detecting ASL exhaustively, i.e. detecting all gestures and motions that are included in ASL over dynamic video feed to translate it into text in real time.

Acknowledgements The authors are grateful to the Sardar Patel Institute of Technology, India, for providing with the necessary facilities to carry out this piece of work.

References

1. Chauhan, R., Jangade, R., Rekapally, R.: Classification model for prediction of heart disease. Proc. SoCTA Adv. Intell. Syst. Comput. **2**, 707–714 (2016)
2. Arora, S., Mishra, N.: software cost estimation using artificial neural network. Proc. SoCTA Adv. Intell. Syst. Comput. **2**, 51–58 (2016)
3. Badhe, P.C., Kulkarni, V.: Indian sign language translator using gesture recognition algorithm. In: 2015 IEEE International Conference on Computer Graphics, Vision and Information Security (CGVIS). Bhubaneswar, pp 195–200. <https://doi.org/10.1109/cgis.2015.7449921> (2015)
4. Starner, T., Pentland, A.: Real-time American sign language recognition from video using hidden markov models. In: Proceedings of International Symposium on Computer Vision. Coral Gables, USA. <https://doi.org/10.1109/iscv.1995.477012>, 23 Nov 1995
5. Vogler, C., Metaxas, D.: Adapting hidden Markov models for ASL recognition by using three-dimensional computer vision methods. In: IEEE International Conference on Computational Cybernetics and Simulation. Orlando, FL (1995)
6. Shaballeh, T., Assaleh, K., Al-Rousan, M.: Spatio-temporal feature-extraction techniques for isolated gesture recognition in arabic sign language. IEEE Trans. Syst. Man Cybern. Part B Cybern. **37**, 641–650 (2007). <https://doi.org/10.1109/TSMCB.2006.889630>
7. Al-Jarraah, O., Halawani, A.: Recognition of gestures in Arabic sign language using neuro-fuzzy systems. Artif. Intell. **133**, 117–138 (2001). [https://doi.org/10.1016/S0004-3702\(01\)00141-2](https://doi.org/10.1016/S0004-3702(01)00141-2)

8. Youssif, A.A., Aboutabl, A.E., Ali, H.: Arabic sign language (ArSL) recognition system using HMM. *Int. J. Adv. Comput. Sci. Appl.* **2**. <https://doi.org/10.14569/ijacsa.2011.021108> (2011)
9. Akash: “ASL Alphabet”, Kaggle. 22 Apr 2018 [Online]. Available <https://www.kaggle.com/grassknotted/asl-alphabet>. Accessed 25 Jun 2019
10. Nanivadekar, P., Kulkarni, V.: Indian sign language recognition: database creation, hand tracking and segmentation. In: Proceedings of CSCITA 2014, IEEE Xplore, pp 358–363

A Comparative Performance of Sorting Algorithms: Statistical Investigation



Priyadarshini and Anchala Kumari

Abstract This paper is aimed at a comparative study of several sorting algorithms with the purpose of evaluating their relative performance when the input array is randomly generated from zero-truncated binomial and poisson distributions. The sorting algorithms to be investigated are quick sort, k-sort, heap sort and merge sort, all having the same average case complexity of $O(N\log N)$. In practical statistical cases, sometimes it is not possible to record or know about the occurrences as they are limited to values which exist above or below a given limit or within a particular range. Such situations result in truncated distributions. The relative performance of the above-mentioned sorting methods was compared on the basis of ‘execution time’ and the ‘number of swapping’ for both the average and worst cases of different algorithms.

Keywords Sorting algorithms · Zero-truncated binomial distribution · Zero-truncated Poisson distribution · Statistical bound

1 Introduction

A truncated distribution is usually obtained by confining the domain of some other probability distribution. The truncation of the domain can be from one side or both sides giving rise to singly truncated or doubly truncated distributions, respectively.

Let X be a random variable with pdf (or pmf) $f(x)$. The distribution of X is said to be truncated at the point $X = a$ if all the values of $X \leq a$ are discarded. Hence, the pdf(or pmf) $g(\cdot)$ of the distribution, truncated at $X = a$, is given by

$$g(x) = \frac{f(x)}{P(X > a)}; x > a$$

Priyadarshini (✉) · A. Kumari
Department of Statistics, Patna University, Patna, India
e-mail: priyadarshini.bca.mmc@gmail.com

$$g(x) = \frac{f(x)}{\sum_{x>a} f(x)}; x > a, \text{ for discrete distribution}$$

$$g(x) = \frac{f(x)}{\int_a^{\infty} f(x)}; x > a \text{ for continuous distribution}$$

In practical statistical cases, sometimes it is not possible to record or know about the occurrences as they are limited to values which exist above or below a given limit or within a particular range. Such situations result in truncated distributions.

For example, the investigation of dates of births of children in a school for admission would naturally be a subject to truncation with respect to all the children in the area with the condition that the school acknowledges only those children within a given age group or on a specific date.

In this paper, two truncated discrete distributions, namely zero-truncated binomial distribution and zero-truncated Poisson distribution have been considered. The objective of this paper is to compare the relative performance of some of the sorting algorithms, namely quick k-sort, heap sort and merge sort, (all exhibiting the same average complexity $O(N\log N)$), while exposing them on the input array generated from the above-mentioned truncated distributions.

The performance of the various sorting algorithms was compared on the basis of the statistical bounds and the number of swapping required by them to sort the given dataset while focusing on the average case and worst case analysis of the sorting algorithms.

A laptop computer (with configuration Intel (R) Core™ i3-4005U Processor @ 1.70 GHz, 8 GB RAM, Windows 7 operating system) was used to perform a serial experiments. The codes were written in Dev C++ using C to compute the execution time and the number of swapping of the algorithms, and various comparative graphs were prepared using Minitab Statistical Package. A considerable large array size was used for the experiments that vary from 10 thousand to 1 lakh.

Zero-Truncated Binomial Distribution

A binomial distribution with zero occurrences omitted gives rise to zero-truncated binomial distribution. For example, ten electronic items are put under test and a number of failures are noted before a certain time t ; either the item fails before time t or does not. Number of failure r before time t follows binomial distribution ($r = 0, 1, 2, \dots, 10$), whereas no item survived (zero failure) before time t will follow zero-truncated binomial distribution.

The inverse transformation method is used for the generation of an array of size N from zero-truncated binomial distribution.

Inverse transformation method:

- Step 1 Compute CDF $F(x)$ for $x = 1, 2, 3, 4, 5, 6 \dots n$ where n is the number of trials (parameter of binomial distribution) and store in an array.
- Step 2 For each binomial variate, generate a $U(0, 1)$ variate u and search the array to find x so that

$$F(x) \leq u < F(x + 1).$$

- Step 3 Return x as the zero-truncated binomial variate.

Zero-Truncated Poisson Distribution

The Poisson distribution is a distribution of rare events. These rare events occur randomly and occur at a constant average rate. There are many real-life situations that involve counting of events and possess the characteristics of this distribution such as number of blinds, number of deaths per day and number of mistakes. It is thus of interest to biologists, agronomists, quality control practitioners as well as many research workers, agricultural scientists, biologists, quality control practitioners, etc., who have deep interest in this distribution.

Zero-truncated Poisson variate is a truncated variate where the form of truncation is the omission of the zero class. This distribution is usually called positive Poisson distribution.

For example, let us consider a random variable Y of the number of objects in a customer's bin at a supermarket pay point. Probably, a customer does not stay in the pay line not having anything to buy, i.e. $Y = 0$ is not possible. Another example, consider Y be the random variable of the number of words in a book. It is impossible to have zero frequency corresponding to $Y = 0$.

The array of size N from zero-truncated Poisson distribution is generated using inverse transformation method.

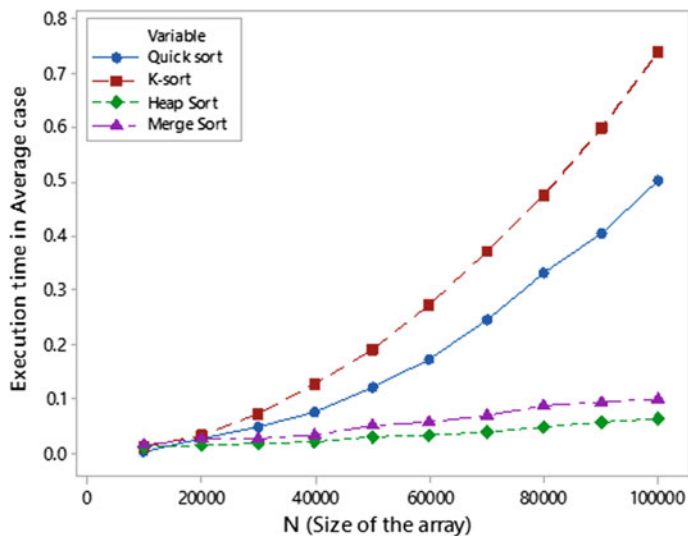
2 Relative Performance of Sorting Algorithms for Zero-Truncated Binomial Input

Complexity as Function of Execution Time

Table 1 and corresponding Fig. 1 show the average execution time for various algorithms for the data simulated from zero-truncated binomial distribution with probability of success $p = 0.5$ and fixed number of trials $n = 1000$. It can be revealed from Table 1 and the corresponding Fig. 1 that for an array of size N , the heap sort gives the best performance, whereas the k-sort gives the worst performance as far as the execution times of various sorting algorithms are considered. As far as the merge sort is considered, it takes almost the same time for sorting an array (size $\leq 40,000$) as heap sort, but after that the complexity gap ($Me - He > 0$) does not change

Table 1 Average case runtime of several sorting algorithms with different sizes of the array

N	Quick sort	K-sort	Heap sort	Merge sort
10,000	0	0.012	0.0092	0.0128
20,000	0.0248	0.0314	0.0124	0.0248
30,000	0.047	0.0718	0.0158	0.0256
40,000	0.0748	0.125	0.0188	0.0308
50,000	0.119	0.191	0.0282	0.05
60,000	0.172	0.2716	0.0312	0.0564
70,000	0.2438	0.3686	0.0374	0.0688
80,000	0.3310	0.475	0.047	0.0876
90,000	0.403	0.597	0.0564	0.0936
100,000	0.5	0.7376	0.0626	0.1004

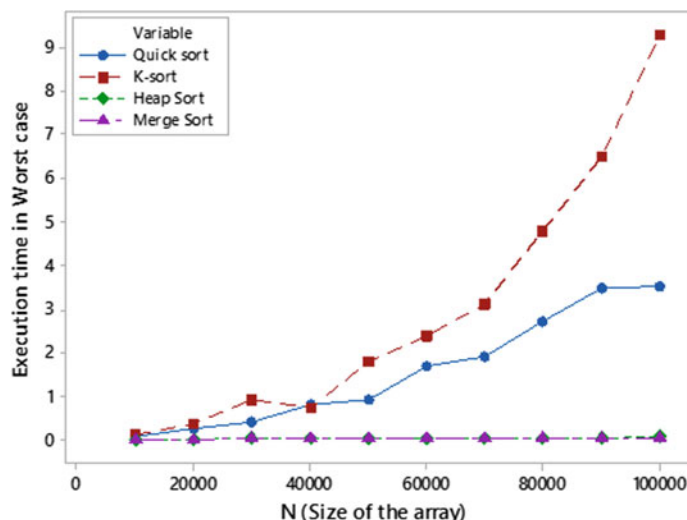
**Fig. 1** Runtime of several sorting algorithms

much with increase in array size. Ke, Qe, Me and He are being the k-sort, quick sort, merge sort and heap sort execution time, respectively. Complexity level of quick sort, though lying between heap sort and merge sort ($Me < Qe < He$), shows a proportional relationship with array size.

Table 2 and the graph in Fig. 2 show the execution time of various sorting algorithms for the worst case. The merge sort and heap sort confirm to same worst case performance. As far as quick sort and k-sort are considered, both consume the same

Table 2 Worst case runtime of several sorting algorithms with different sizes of the array

N	Quick sort	K-sort	Heap sort	Merge sort
10,000	0.0562	0.0968	0	0.0062
20,000	0.2376	0.3532	0.0094	0.0092
30,000	0.3998	0.9184	0.0156	0.0126
40,000	0.8064	0.7372	0.022	0.0154
50,000	0.9060	1.7964	0.0248	0.0252
60,000	1.6934	2.3812	0.0344	0.028
70,000	1.903	3.105	0.0342	0.0312
80,000	2.7096	4.759	0.0408	0.0408
90,000	3.4812	6.4938	0.0468	0.0404
100,000	3.5026	9.2778	0.0496	0.0466

**Fig. 2** Runtime of several sorting algorithms

time for sorting an array of size less than or equal to 20,000, and the difference between the complexity level of the k-sort and quick sort increases with increase in the array size.

Complexity as Function of Number of Swapping

In average case, maximum number of swapping for k-sort as depicted in Table 3 and the plot in Fig. 3 confirm to the highest complexity level of k-sort as indicated for execution time analysis. In worst case also, k-sort has exchanged the values

Table 3 Comparison of the number of swapping related to several sorting algorithms in average case

<i>N</i>	Quick sort	K-sort	Heap sort	Merge sort
10,000	14,254	927,315	138,986	241,022
20,000	28,005	3,624,215	297,801	521,856
30,000	42,747	8,150,619	463,955	817,181
40,000	56,913	14,427,384	635,555	1,123,836
50,000	70,787	22,507,021	811,051	1,436,864
60,000	85,098	32,308,328	988,188	1,754,424
70,000	98,667	44,019,285	1,167,689	2,078,092
80,000	112,911	57,470,292	1,351,069	2,408,002
90,000	128,625	72,506,381	1,536,103	2,739,247
100,000	141,057	89,678,420	1,721,986	3,073,222

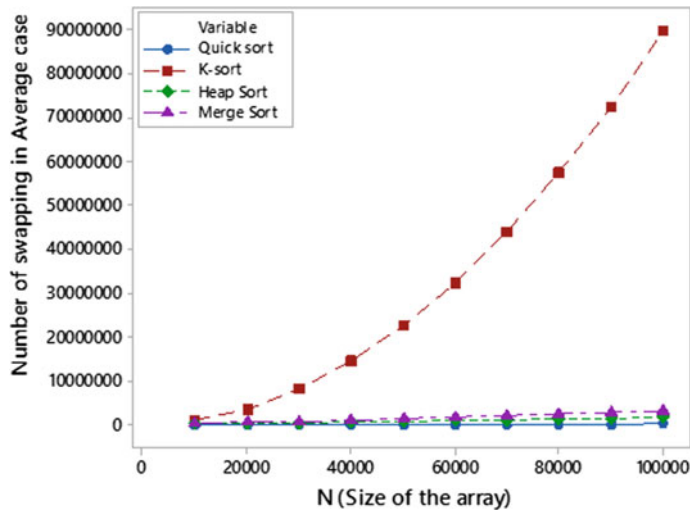
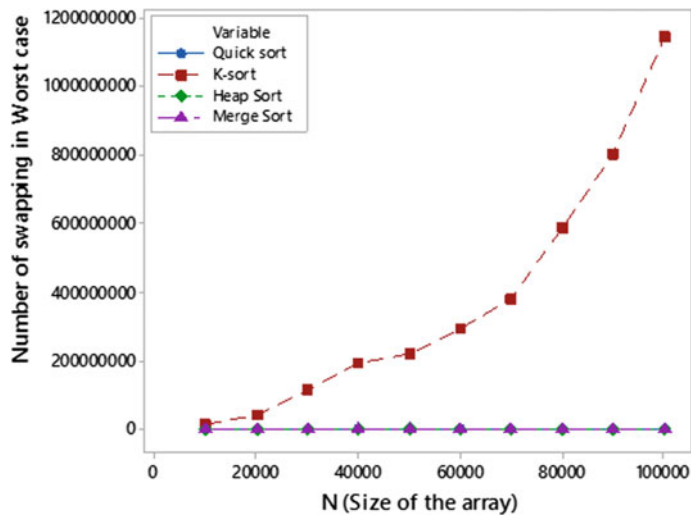


Fig. 3 Number of swapping in average case

maximum number of times for sorting the input dataset of different sizes as shown in Table 4 and Fig. 4. However, interestingly the no. of swapping or exchange of values in case of quick sort is least in both average case and worst case study which shows a contradiction to the fact that average complexity of heap sort is least as indicated in case of execution time analysis. This may be due to increase in the number of ties resulting in increase in average complexity but decrease in number of swapping or the randomly generated data may be partially sorted.

Table 4 Comparison of the number of swapping related to several sorting algorithms in worst case

N	Quick sort	K-sort	Heap sort	Merge sort
10,000	4894	12,020,301	130,332	81,719
20,000	9776	42,767,851	280,888	176,389
30,000	14,659	112,860,909	438,028	267,993
40,000	19,546	190,637,743	599,722	370,412
50,000	24,463	220,850,873	764,512	476,556
60,000	29,322	292,677,189	933,143	587,671
70,000	34,249	381,727,414	1,105,452	682,327
80,000	39,120	587,132,863	1,277,753	796,541
90,000	44,042	800,005,069	1,452,939	894,603
100,000	48,834	1,142,756,905	1,627,166	997,607

**Fig. 4** Number of swapping in worst case

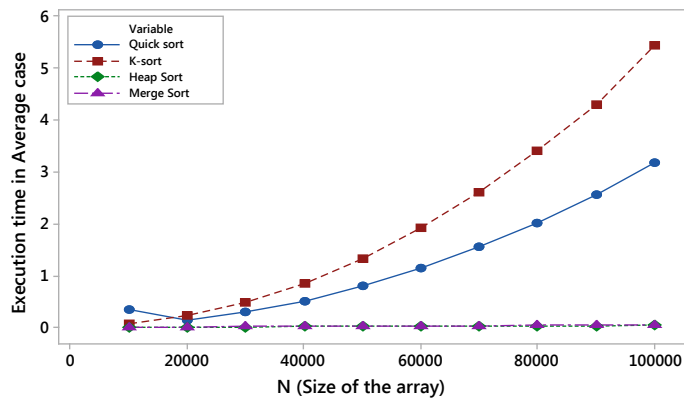
3 Relative Performance of Sorting Algorithms for Zero-Truncated Poisson Input

Complexity as a Function of Execution Time

Execution times for various algorithms for sorting an array generated from zero-truncated Poisson distribution with parameter ($\lambda = 5$) are displayed in Table 5 and corresponding Fig. 5 for average case situation and in Table 6 and corresponding Fig. 6 for worst case analysis.

Table 5 Average runtime of several sorting algorithms with different sizes of the array

<i>N</i>	Quick sort	K-sort	Heap sort	Merge sort
10,000	0.334	0.0572	0.0062	0.009
20,000	0.128	0.2182	0.007	0.009
30,000	0.2862	0.478	0.0098	0.0136
40,000	0.5068	0.8466	0.0132	0.0176
50,000	0.7906	1.3288	0.0172	0.0224
60,000	1.1346	1.911	0.021	0.027
70,000	1.5434	2.6	0.0278	0.0314
80,000	2.0138	3.392	0.0284	0.0356
90,000	2.5592	4.2912	0.0314	0.047
100,000	3.157	5.425	0.035	0.0448

**Fig. 5** Execution time in average case**Table 6** Worst case runtime of several sorting algorithms with different sizes of the array

<i>N</i>	Quick sort	K-sort	Heap sort	Merge sort
10,000	0.0656	0.0844	0.0032	0.0032
20,000	0.2344	0.406	0.0032	0.0032
30,000	0.5214	0.7504	0.0064	0.019
40,000	0.914	1.2366	0.0156	0.016
50,000	1.4344	2.0718	0.0156	0.0218
60,000	2.0532	3.2036	0.0188	0.0342
70,000	2.791	4.8358	0.0248	0.0282
80,000	3.6438	5.938	0.0218	0.031
90,000	4.5892	7.2062	0.028	0.0438
100,000	5.6812	8.549	0.0314	0.0374

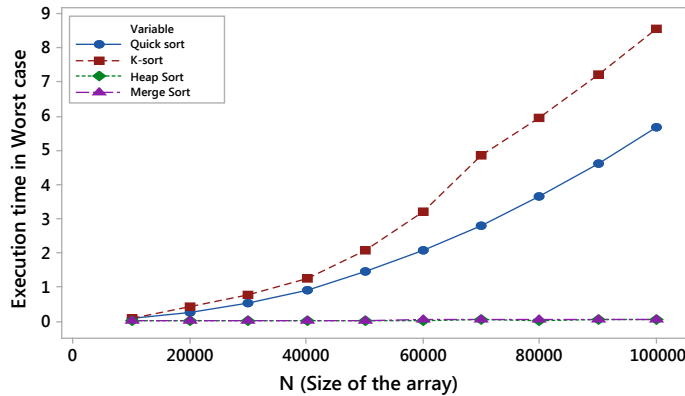


Fig. 6 Execution time in worst case

Here, it can be seen that the performance of heap sort and merge sort is almost identical in both the average and worst cases. In case of quick sort and k-sort, for an array of size $N \geq 20,000$, the execution time K_e is almost double of that of Q_e , and for $N < 20,000$, $Q_e > K_e$ for average case, whereas for worst case the different scenario is observed. The difference ($K_e - Q_e$) increases with increase in array size for $N \geq 30,000$ and for N below 30,000, the complexity levels of quick and k-sort are being almost the same.

Complexity as a Function of Number of Swapping

The number of swapping or exchange of values that took place during sorting by various algorithms in average case has been summarized in Table 7 and shown graphically in Fig. 7. The corresponding worst case results are depicted in Table 8 and the graph in Fig. 8.

Table 7 Comparison of the number of swapping related to several sorting algorithms in average case

N	Quick sort	K-sort	Heap sort	Merge sort
10,000	7457	6,483,734	113,623	120,509
20,000	14,878	25,893,440	245,440	261,028
30,000	22,484	58,215,751	385,067	408,372
40,000	29,637	103,598,340	527,244	562,167
50,000	37,406	162,323,799	675,142	718,276
60,000	44,663	233,153,929	825,010	876,724
70,000	51,671	317,489,299	976,647	1,038,468
80,000	59,814	414,777,897	1,127,270	1,204,162
90,000	66,529	525,503,901	1,282,905	1,370,157
100,000	74,709	646,970,675	1,441,106	1,536,495

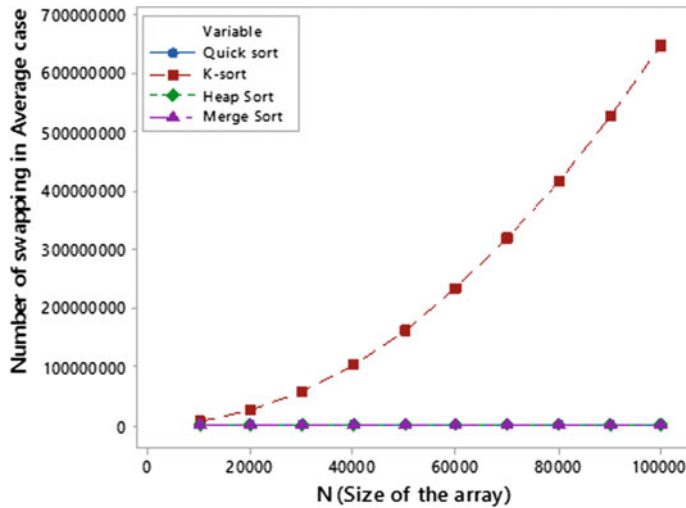


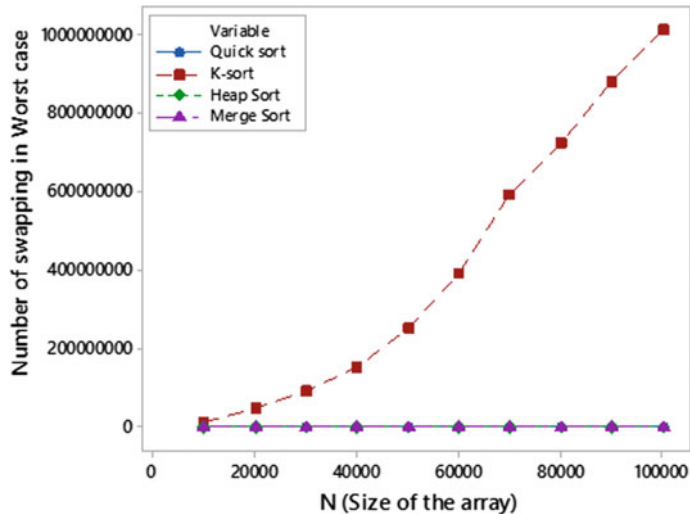
Fig. 7 Number of swapping in average case

Table 8 Comparison of the number of swapping related to several sorting algorithms in worst case

N	Quick sort	K-sort	Heap sort	Merge sort
10,000	6061	9,949,470	87,321	78,914
20,000	12,209	48,930,419	189,294	167,883
30,000	18,251	92,442,722	286,046	257,609
40,000	24,386	150,616,298	406,247	355,417
50,000	30,554	253,199,110	514,866	450,795
60,000	36,804	392,487,482	614,498	546,594
70,000	42,836	593,163,061	711,156	644,594
80,000	48,802	725,257,101	873,598	752,342
90,000	55,119	882,493,236	989,294	856,418
100,000	61,324	1,012,235,852	1,102,890	955,421

We can see that there is almost no change in the number of swapping results of sorting algorithms heap sort, merge sort and quick sort as far as the average case and the worst case are concerned. But the number of swapping in case of k-sort is of very high order as compared to the other algorithms. It has approximately doubled in the worst case than in the average case.

The regression plots have been given both for the average case and worst case to have an idea of relationship between the two variables ‘number of swapping’ and the array size.

**Fig. 8** Number of swapping in worst case

4 Empirical Complexity of Sorting Algorithms

Empirical complexity of ‘execution time’ as a function of ‘size of array’ for various sorting algorithms in average and worst cases for zero-truncated binomial input and zero-truncated Poisson input is summarized in Tables 9 and 10.

Empirical complexity of ‘execution time’ as a function of ‘number of swapping’ for various sorting algorithms in average and worst cases for zero-truncated binomial input and zero-truncated Poisson input is summarized in Tables 11 and 12.

Table 9 Empirical complexity

Sorting algorithm	Truncated binomial distribution			
	Execution time		Number of swapping	
	Average case	Worst case	Average case	Worst case
Heap sort	$O(N^2)$	$O(N^3)$	$O(N^2)$	$O(N^2)$
K-sort	$O(N^2)$	$O(N^3)$	$O(N^2)$	$O(N^3)$
Quick sort	$O(N^2)$	$O(N^3)$	$O(N)$	$O(N)$
Merge sort	$O(N^3)$	$O(N^3)$	$O(N^2)$	$O(N^2)$

Table 10 Empirical complexity

Sorting algorithm	Truncated poisson distribution			
	Execution time		Number of swapping	
	Average case	Worst case	Average case	Worst case
Heap sort	$O(N)$	$O(N)$	$O(N^2)$	$O(N^2)$
K-sort	$O(N^2)$	$O(N^2)$	$O(N^2)$	$O(N^2)$
Quick sort	$O(N^2)$	$O(N^2)$	$O(N)$	$O(N)$
Merge sort	$O(N^3)$	$O(N^2)$	$O(N^2)$	$O(N^2)$

Table 11 Empirical complexity

Sorting algorithms	Truncated binomial distribution	
	Execution time versus number of swapping	
	Average case	Worst case
Heap sort	$O(N^2)$	$O(N^2)$
K-sort	$O(N)$	$O(N)$
Quick sort	$O(N^2)$	$O(N^3)$
Merge sort	$O(N^3)$	$O(N^3)$

Table 12 Empirical complexity

Sorting algorithms	Truncated poisson distribution	
	Execution time versus number of swapping	
	Average case	Worst case
Heap sort	$O(N^3)$	$O(N^3)$
K-sort	$O(N)$	$O(N^2)$
Quick sort	$O(N^3)$	$O(N^2)$
Merge sort	$O(N^3)$	$O(N^3)$

5 Conclusion

On the basis of the results obtained, it can be concluded that heap sort is faster in majority of cases. It is further revealed that for binomial input irrespective of tail probabilities for successes ($p = 0.2$, or $p = 0.8$), [1, 2] it gives the best performance as compared to other algorithms, whether the distribution is truncated or not. Also the exchange of values during sorting is almost uniform for different situations. Merge sort has behaved almost similar to heap sort. Quick sort has performed differently in average and worst cases of truncated binomial input as far as execution time is concerned, but in case of truncated Poisson input it has taken the similar CPU time for both average and worst cases. As far as the exchange of values during sorting is concerned, quick sort has more number of swapping in average case than in worst

case for truncated binomial input. Whereas for truncated Poisson, the exchange of values taken place is almost same for average and worst cases. The performance of k-sort is worst as compared to other sorting algorithms considered here. In case of truncated binomial input, it has taken more time, and more exchange of values has taken place in both the average and worst case analysis, whereas it has performed in a similar manner in average and worst cases for truncated Poisson input.

References

1. Priyadarshini, Kumari, A.: Parameterized complexity analysis of heap sort, K-sort and quick sort for binomial input with varying probability of success. *Int. J. Emerg. Technol. Innov. Res.* **5**(7), 491–495. www.jetir.org, UGC and ISSN Approved, ISSN:2349-5162, July 2018, Available at <http://www.jetir.org/papers/JETIR1807424.pdf>
2. Priyadarshini, Chakraborty, S., Kumari, A.: Parameterised complexity of quick sort, heap sort and k-sort algorithms with quasi binomial input. *Int. J. Future Revolution Comput. Sci. Commun. Eng. IJFRSCE* **4**(1), 117–123
3. Sabharwal, M.: The use of soft computing technique of decision tree in selection of appropriate statistical test for hypothesis testing. In: Pant, M., Ray, K., Sharma, T., Rawat, S., Bandyopadhyay, A. (eds.) *Soft computing: theories and applications. Advances in intelligent systems and computing*, vol. 583. Springer, Singapore (2018)
4. Geyer, C.J.: Lower-truncated poisson and negative binomial distributions, 5 July 2018
5. Kamnethania, D., Kumar, J., Taterh, S.: Study and comparative analysis of various image spamming techniques. *Soft Comput. Theor. Appl.* **583**(1), 351–365 (2017)
6. Grover, P.S., Kakkar, M., Jain, S., Bansal, A.: Is open-source software valuable for software defect prediction of proprietary software and vice versa? *Soft Comput. Theor. Appl.* **583**(1), 227–236 (2017)
7. Kumari, A., Singh, N.K., Chakraborty, S.: A statistical comparative study of some sorting algorithms. *Int. J. Found. Comput. Sci. Technol.* **5**, 21–29 (2015). <https://doi.org/10.5121/ijfcst.2015.5403>
8. Singh, N.K., Chakraborty, S., Malick, D.K.: A statistical peek into average case complexity. *IJEDPO* **4**(2); *Int. J. Recent Trends Eng. Technol.* **8**(1), 64–67
9. Kumari, A., Chakraborty, S.: Parameterized complexity, a statistical approach combining factorial experiments with principal component analysis. *Int. J. Comput. Sci. Eng.* (2013)
10. Kumari, A., Chakraborty, S.: The middle pivot element algorithm. *Int. Sch. Res. Netw. ISRN Comput. Math.* **5** (2012)
11. Prashant, Anchala and Soubhik (2009) parameterised complexity on a new sorting algorithm, a study in simulation. *Annals. Comput. Sci. Ser. VII*
12. Kumari, A., Chakraborty, S.: A simulation study on quick sort parameterized complexity using response surface design. *Int. J. Math. Model. Simul. Appl.* **1**(4) (2009)
13. Kumari, A., Chakraborty, S.: Software complexity: a statistical case study through insertion sort. *Appl. Math. Comput.* **190**(1) (2007)
14. Geyer, C.J.: The K-truncated poisson distribution, 18 June 2006
15. Mahmoud, H.: *Sorting: a distribution theory*. Wiley (2000)
16. Clifford, C.A.: *Truncated and censored samples: theory and applications*. CRC Press
17. Sacks, J., Welch, W.J., Mitchell, T.J., Wynn, H.P.: Design and analysis of computer experiments. *Stat. Sci.* **4** (1989)
18. Rider, P.R.: Truncated binomial and negative binomial distributions. *J. Am. Stat. Assoc.* **50**(271), 877–883 (1955)

Evolutionary Computing for Designing Cryptographic Primitives for Block Cipher: Challenges and Opportunities



Pratap Kumar Behera and Sugata Gangopadhyay

Abstract The cryptographic primitives such as S-Box and permutation layer are primary building blocks for designing block cipher. Since S-Box is the only nonlinear component in a block cipher, it is essential to select secure S-Boxes. The security of any block cipher depends upon the cryptographic properties of an S-Box and the lower bound of the number of active S-Boxes. Apart from S-Boxes, there are several other cryptographic primitives such as permutation layer plays a significant role in increasing the security of block cipher. Since the search space is huge for constructing $n \times m$ S-Box, it is very difficult to find a good S-Box. The problem of finding and evolving an S-Box is an optimization problem. The purpose of our research work is to give a systematic review of how evolutionary techniques can be applied for constructing such cryptographic primitives, challenges of achieving optimal results, and opportunities for applying new techniques or fine-tuning several control parameters to improve the performance of an existing algorithm. In this paper, we discuss the genetic algorithm and memetic algorithm for constructing an $n \times m$ bijective S-Box with important cryptographic properties. We address the challenges and future direction of the currently ongoing research.

Keywords S-Box · Block cipher · Genetic algorithm (GA) · Memetic algorithm (MA)

1 Introduction

The cryptographic primitives of the block cipher are designed based upon confusion and diffusion principle [1]. The two most important cryptanalytic attacks of block cipher are linear approximation attack and differential attack. These two attacks can

P. K. Behera (✉) · S. Gangopadhyay
Indian Institute of Technology Roorkee, Roorkee, India
e-mail: pbehera@cs.iitr.ac.in

S. Gangopadhyay
e-mail: sugatfma@iitr.ac.in

Fig. 1 Tools for automatic design of cryptographic primitives



be mounted by exploiting the weakness of the S-Box properties such as nonlinearity and differential uniformity. The S-Box with high nonlinearity and low differential uniformity is used to resist this attack. However, the search space of an $n \times m$ S-Box is huge, and it is computationally hard to find a cryptographically strong S-Box. Finding an S-Box with strong cryptographic properties can be formulated as an optimization problem. The techniques and the algorithm which solve this optimization problem are called *tools for automatic design* [2] as shown in Fig. 1.

We use the evolutionary computing technique as an automatic tool for S-Box design with required cryptographic criteria. However, due to the conflicting criteria of the cryptographic properties of an S-Box, it is a challenging task to achieve an optimal trade-off. Based on the number of cryptographic properties to be considered or optimized, the problem can be divided into single objective and multi-objective optimization problem. Recently, there are several heuristic and evolutionary techniques used to design the S-Box with an optimal trade-off. However, it fails to achieve the optimal results, and researcher is not able to address the real issues behind not getting the optimal results. In this paper, we will address the challenges and future directions of how evolutionary techniques can be effectively applied for designing secure cryptographic primitives.

2 Cryptographic Primitives and Problem Formulation

The design and optimization of cryptographic primitives can be solved by evolutionary techniques [3] only when the fitness function and input parameters are clearly defined. If the search space of an optimization problem is less and can be solved by the brute force approach or random search, then applying the evolutionary computing (EC) technique is not feasible. We proposed a model of designing cryptographic primitives for symmetric cryptography using evolutionary computing, as shown in Fig. 2.

We formulate the design of S-Boxes as an optimization problem. Since the search space is huge and the objective is clearly defined, the evolutionary technique will be feasible for finding the optimal solution. The S-Box is a mapping of n -bit input to m -bit output vector, i.e., $F: \mathbb{F}_2^n \rightarrow \mathbb{F}_2^m$, and it is represented as a lookup table which is a sequence of m Boolean function [4]. For constructing an $n \times m$ S-Box, the total search space is 2^{m^2} as shown in Table 1. For SPN-based block cipher, the S-Box must be invertible, and the total search space of $n \times m$ invertible S-Box is 2^m !

From the above observation, evolutionary technique can be applied to design and improve the security (cryptographic strength) level of an S-Box due to the following reasons:

Fig. 2 Cryptographic primitive design using evolutionary computing (EC)

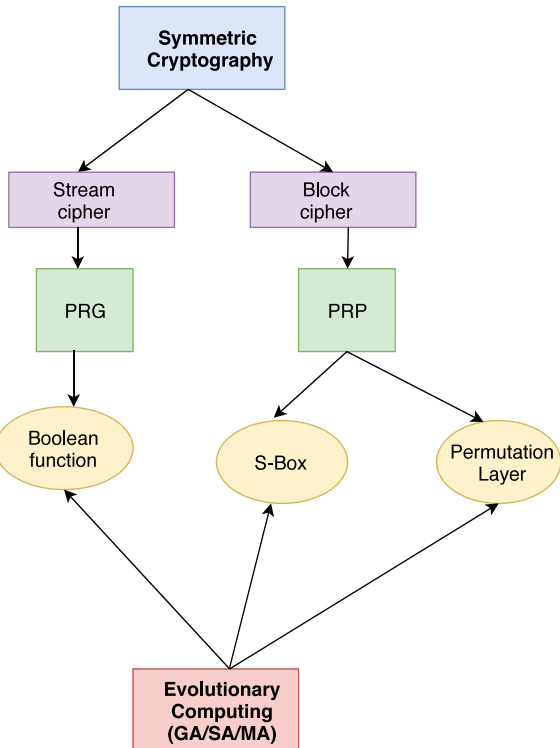


Table 1 Search space of $n \times m$ S-Boxes

$n \times m$	4×4	5×5	6×6	7×7
# S-Boxes	2^{64}	2^{160}	2^{384}	2^{896}
# Bijective S-Boxes	$(16)! \approx 2^{44}$	$(32)! \approx 2^{117}$	$(64)! \approx 2^{296}$	$(128)! \approx 2^{715}$

- The search space is very huge $O(2^m)!$ and cannot be solved by exhaustive search.
- The objective function is clearly defined and quantified (nonlinearity for linear approximation attack).
- The optimal bound of the design criteria is known.
- Cryptographic primitive which has practical significance for the security of block cipher.
- The cryptographic problem whose solution can be further optimized and can be compared with the existing solution.

In this paper, we considered number of cryptographic criteria, problem size, and different representation which is used as an initial parameters for evolving the initial solution.

3 Background

The block cipher is considered as an encryption function which maps n -bit plaintext to n -bit ciphertext. When a block cipher is designed, it must be evaluated to measure the security strength against various cryptanalytic attacks. The two most important cryptanalytic attacks are linear approximation and differential attack. To resist this attack, the S-Box with high nonlinearity and low differential uniformity is a preferred choice. We will describe the different properties of S-Box resistance to linear attack, differential attack, and algebraic attack.

A function which is a mapping of $F:\mathbb{F}_2^n \rightarrow \mathbb{F}_2^m$ is called vectorial Boolean function or (n, m) -function or simply called $n \times m$ S-Box.

3.1 S-Box Representation

An S-Box can be represented either as a lookup table with 2^n words, and each word is of m -bit. The lookup table can be bit string or integer representation ranging from 0 to $2^n - 1$ for $n \times m$ S-Box as shown in Table 2. The lookup table is a matrix of dimension $2^n \times m$, where m is the number of coordinate function or single output Boolean function.

Bit-string Representation: An $n \times m$ S-Box is a sequence of m single output n -variable Boolean function (m coordinate function). The single output n -variable Boolean function is represented as a truth table (0/1) of length 2^n .

Integer Representation: In integer representation, an $n \times m$ S-Box is encoded as an integer form of permutation between 0 to $2^n - 1$. In other words, it is a lookup table of 2^n words, and each word is represented with m -bits. For constructing 8×8 S-Box, the lookup table is a permutation between 0 to 255. If $n = m$, the S-Box is called bijective (invertible) S-Box.

Walsh–Hadamard Transform: For $n \times m$ S-Box F , the Walsh transform is represented as a matrix of $2^m \times 2^n$ dimension. The Walsh transform is a real-valued function, i.e., $f:W_F(u, v) \mapsto \mathbb{R}$, where $u \in \mathbb{F}_2^n$ and $v \in \mathbb{F}_2^m$ and it is defined as follows:

$$W_F(u, v) = \sum_{x \in \mathbb{F}_2^n} (-1)^{u \cdot x + v \cdot F(x)} \quad (1)$$

The value in the Walsh–Hadamard table lies in the range $[-2^n, 2^n]$.

Table 2 Example of 4×4 S-Box and its representation

Input	0	1	2	3	4	5	6	7	8	9	A	B	C	D	E	F
Bit string	1010	1111	0001	1001	0011	1100	0110	0101	0111	0100	1011	0010	1101	1000	1110	0000
Integer	10	15	1	9	3	12	6	5	7	4	11	2	13	8	14	0

3.2 Cryptographic Properties and Bounds

The nonlinearity and differential uniformity are two cryptographic properties to measure the cryptographic strength against linear approximation attack and differential attack respectively [5].

Balancedness: If all the component functions are balanced, then the S-Box is called bijective. Mathematically, $\forall v \in \mathbb{F}_2^{m*}$

$$wt(v \cdot F(x)) = 2^{n-1}$$

Or we can check the balancedness by using the Walsh transform. For all $v \in \mathbb{F}_2^{m*}$, if $W_F(0, v) = 0$, then the S-Box F is called balanced/bijective.

Nonlinearity: The nonlinearity of an S-Box F is the minimum nonlinearity of all component function of F . Mathematically,

$$NL_F = \min_{v \in \mathbb{F}_2^{m*}, g \in \mathcal{A}_n} d_H(v \cdot F, g)$$

where

$$d_H(v \cdot F, g) = \#\{x \in \mathbb{F}_2^n | b \cdot F(x) \neq g(x)\}$$

Differential Uniformity: The maximum value of the differential distribution table of an $n \times m$ S-Box is called as differential uniformity.

$$\delta_F = \max_{a \in \mathbb{F}_2^{n*}, b \in \mathbb{F}_2^m} \delta_F(a, b)$$

where a , and b are called input and output difference, respectively, and $\delta_F(a, b)$ is defined as

$$\delta_F(a, b) = \#\{x \in \mathbb{F}_2^n | F(x) + F(x + a) = b\}$$

Algebraic Degree: The algebraic degree of an S-Box is defined as the minimum degree of its component function. Mathematically,

$$Deg_F = \min_{b \in \mathbb{F}_2^{m*}} deg(b \cdot F)$$

The cryptographic properties, bounds, and the objective of each design criteria are shown in Table 3.

Table 3 Properties and optimal bounds of $n \times m$ S-Box

Cryptographic properties	Bounds	Objective
Balancedness	[Yes/No]	Constraint
Nonlinearity	$[0, 2^{n-1} - 2^{\frac{n}{2}-1}]$	Maximization
Differential uniformity	$[2, 2^n]$	Minimization
Algebraic degree	$[0, n - 1]$	Maximization

4 Evolutionary Computing

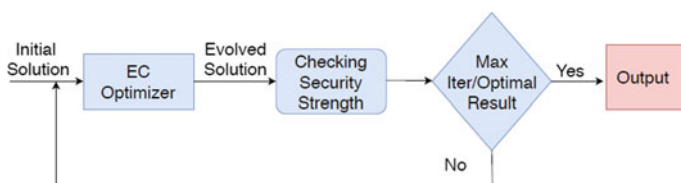
Evolutionary computing (EC) is a meta-heuristic, population-based searching, and optimization techniques [6, 7] which is inspired by nature and biological evolution [8]. The initial candidate solution is evolved in an iterative way till the maximum iteration or optimal solution is found. The flowchart of the EC optimizer for designing cryptographic primitives is shown in Fig. 3.

4.1 Genetic Algorithm

Genetic algorithm is an combinatorial optimization technique [17] designed based on the concept of the “survival of fittest.” The initial solution is evolved through three different genetic operators (selection, crossover, mutation). Our initial solution is a bijective $n \times m$ S-Box, which is a permutation of the length 2^n . We have considered the problem of finding cryptographically strong S-Box as a permutation optimization problem. An initial solution is a fixed-length vector $X = (x_1, x_2, \dots, x_t)$, which is a permutation of length 2^n . An important step of adopting GA for permutation optimization problem is to design all the functionalities of GA with good exploration and exploitation capabilities to make it efficient for finding a better solution in a less computational time.

The permutation optimization problem can be expressed as

$$\max Z = f(X)$$

**Fig. 3** Evolutionary computing optimizer

where, $X \in \prod = \{p_1, p_2, \dots, p_n : \text{set of all permutations}\}$.

Each $p_i = X = (x_1, x_2, \dots, x_t)$, $1 \leq i \leq n$, and f is an objective function, i.e., $f: X \mapsto R$.

Parameters

Selection: The selection mechanism determines which solution will be selected for the breeding process to produce the new solution/child. The selection of individuals is based on the fitness of the candidate solution and specific selection mechanism. There are four different kinds of selection mechanism such as roulette wheel, k -tournament, rank-based selection, and elitism approach.

Crossover: The crossover operator is used for convergence of the solution. The convergence mechanism is based on exploitation to find the locally optimal value. For the permutation encoding problem, the crossover is to be designed in such a way that it must produce the solution with permutation property. The crossover operator, such as single-point crossover and two-point crossover, is not efficient for the permutation optimization problem, since it does not preserve the permutation property. So, it needs a repair operation to satisfy permutation property, which requires extra computational effort. The crossover operation is an important step for evolving invertible S-Box.

Mutation: The mutation operation is used to introduce diversity in the solution. When a solution suffers from local optima, it is essential to explore the search space in a divergent manner to find global optima. So, mutation operator is applied in this scenario. The search space is huge for designing S-Box, so designing effective mutation operator is an important task to maintain the diversity of the solution.

Fitness function: The fitness function plays a major role for selecting quality of solution to achieve the optimal values. The fitness function must be designed in such a way that it can trade-off the multiple cryptographic criteria.

4.2 Memetic Algorithm

The memetic algorithm is an extension of genetic algorithm with integration of local search technique [9, 18]. Sometimes due to the low convergence capacity of genetic algorithm, it is necessary to integrate local search procedure effectively to reduce the likelihood of the premature convergence. The performance may be reduced slightly, but the likelihood of getting optimal solution increases in memetic algorithm. The pseudocode is explained in Algorithm 1.

Algorithm 1: Pseudocode of Memetic algorithm

```

1 Generate random initial population(InitPop) of size  $N$ ;
2 while  $i \leq maxiter$  do
3    $Ch \leftarrow GA(InitPop)$  ;
4    $Ch' \leftarrow LS(Ch)$  ;
5 end

```

Table 4 Cryptographic properties of 8×8 S-Box

Techniques	NL	DU	Deg
Hill climbing [10]	100	NA	NA
Gradient descent [11]	100	8	7
Simulated annealing [12]	102	NA	NA
Genetic algorithm [13]	104	6	NA
Genetic with Tree [14]	104	NA	NA
Modified immune [15]	104	6	7
AES [16]	112	4	7

5 Practical Results and Discussion

We present the results of the previous published 8×8 S-Box designed by the evolutionary and heuristic techniques as shown in Table 4. The highest nonlinearity achieved is 104 by genetic algorithm and modified immune algorithm which is better than the local search techniques. But the result achieved by the genetic algorithm is still far behind than the S-Box generated by the algebraic construction of finite field-based inversion function used in AES block cipher.

6 Challenges and Future Direction

One can investigate different problem sizes and different cryptographic primitives to improve the security of the block cipher. The application of evolutionary technique for finding S-Box with optimal solution which can match with the theoretical upper bound is still an open research issues. But very few researchers try to address these issues and challenges. The understanding about the problem type, choice of fitness function, and conflicting nature of cryptographic properties must be taken into consideration for designing and customizing effective evolutionary technique. The most important part is that both EC and crypto community collaborate together to fill this gap by understanding the inherent problem and customizing the existing techniques to get the optimal solution.

7 Conclusion

In this paper, we explain how evolutionary technique can be effectively applied and become a tool for automatic design of cryptographic primitives for block cipher. There are several other heuristic and evolutionary techniques which can be explored for constructing such cryptographic primitives. We discuss the construction of bijective S-Box resistance to linear and differential attacks. The results achieved by the existing heuristic and EC technique are still far from the optimal solution. This can motivate EC community to solve this problem and can be explored into different problems in cryptographic domain. The use of evolutionary technique can be considered as a tool for automatic design of cryptographic primitives which can create confidence among the crypto community. In this paper, we only discuss the construction of S-Box.

References

1. Shannon, C.E.: Communication theory of secrecy systems. *Bell Syst. Tech. J.* **28**(4), 656–715 (1949)
2. Nikolić, I.: How to use metaheuristics for design of symmetric-key primitives. In: International Conference on the Theory and Application of Cryptology and Information Security, pp. 369–391. Springer, Cham (2017)
3. Behera, P.K., Gangopadhyay, S.: Analysis of cost function using genetic algorithm to construct balanced Boolean function. In: TENCON IEEE Region 10 Conference, pp. 1445–1450. IEEE, New York (2018)
4. Stinson, D.R.: Cryptography: Theory and Practice. Chapman and Hall/CRC (2005)
5. Heys, H.M.: A tutorial on linear and differential cryptanalysis. *Cryptologia* **26**(3), 189–221 (2002)
6. Swami, V., Kumar, S., Jain, S.: An improved spider monkey optimization algorithm. In: Soft Computing: Theories and Applications, pp. 73–81. Springer, Singapore (2018)
7. Bhasin, H., Gupta, N.: Critical path problem for scheduling using genetic algorithm. In: Soft Computing: Theories and Applications, pp. 15–24. Springer, Singapore (2018)
8. Abraham, A., Jain, L.: Evolutionary multiobjective optimization. In: Evolutionary Multiobjective Optimization, pp. 1–6. Springer, London (2005)
9. Ibrahim, A.O., Shamsuddin, S.M., Abraham, A., Qasem, S.N.: Adaptive memetic method of multi-objective genetic evolutionary algorithm for backpropagation neural network. *Neural Comput. Appl.* (2019)
10. Millan, W.: How to improve the nonlinearity of bijective S-boxes. In: Australasian Conference on Information Security and Privacy, pp. 181–192. Springer, Berlin (1998)
11. Kazymyrov, O., Kazymyrova, V., Oliynykov, R.: A Method for Generation of High-Nonlinear S-Boxes Based on Gradient Descent. *IACR Cryptology ePrint Archive* (2013)
12. Clark, J.A., Jacob, J.L., Stepney, S.: The design of S-boxes by simulated annealing. *New Gener. Comput.* **23**(3), 219–31 (2005)
13. Picek, S., Cupic, M., Rotim, L.: A new cost function for evolution of S-boxes. *Evol. Comput.* **24**(4), 695–718 (2016)
14. Tesa, P.: A new method for generating high non-linearity S-boxes. *Radioengineering* **19**(1), 23–6 (2010)
15. Ivanov, G., Nikolov, N., Nikova, S.: Cryptographically strong S-boxes generated by modified immune algorithm. In: International Conference on Cryptography and Information Security in the Balkans, pp. 31–42. Springer, Cham (2015)

16. Daemen, J., Rijmen, V.: The Design of Rijndael: AES-the Advanced Encryption Standard. Springer Science & Business Media (2013)
17. Whitley, D.: A genetic algorithm tutorial. *Statist. Comput.* **4**(2), 65–85 (1994)
18. McLaughlin, J., Clark, J.A.: Using evolutionary computation to create vectorial Boolean functions with low differential uniformity and high nonlinearity. arXiv preprint [arXiv:1301.6972](https://arxiv.org/abs/1301.6972) (2013)

A True Event-Based Metaheuristic Algorithm Optimized AGC Mechanism for a Multi-area Power System



Sariki Murali and Ravi Shankar

Abstract Metaheuristic optimization techniques provide an optimistic solution for various complex problems in several disciplines. In this scenario, this work promotes the application of metaheuristic optimization techniques in the research area of power system dynamics and control. Here, the automatic generation control (AGC) mechanism has been developed to maintain a nominal frequency and tie-line power of a realistic deregulated hybrid power system against a small perturb in load demand. Proportional-integral-derivative controller with derivative filter (PIDN) is deployed for AGC mechanism. A recently developed volleyball premium league (VPL) optimization technique has been successfully implemented to optimize the controller used in the AGC mechanism. The performance analysis of the proposed scheme has been carried out as, compared with particle swarm optimization (PSO)-based AGC scheme, robustness check against various performance indices, and finally compared with previously published work. The overall investigation has been done using MATLAB/Simulink® toolbox.

Keywords AGC · FOD · PIDN · PSO · VPL

1 Introduction

Nowadays, the metaheuristic optimization techniques gaining the attention of researchers to solve the wide range of complex problems in various disciplines owing to advantages of applicability, flexibility, and avoidance of local optima. Many articles providing data regarding the development of metaheuristic optimizations techniques inspired by nature, biological behavior, and procedure followed in games. Particle swarm optimization (PSO) [1], bat-inspired optimization technique [2], firefly technique [3], cuckoo search optimization technique [4], lion optimization techniques

S. Murali (✉) · R. Shankar
National Institute of Technology Patna, Bihar, India
e-mail: Sariki.ee17@nitp.ac.in

R. Shankar
e-mail: ravi@nitp.ac.in

[5], ant colony algorithm [6], etc., are some famous optimization techniques. New gaming-based volleyball premier league (VPL) optimization technique has been developed recently and supremacy over several optimization techniques has been detailed in [7]. In this work, VPL optimization technique is opted to accomplish the solution for power system dynamics problem. In the research area of power system dynamics and control, AGC mechanism is an epoch-making method to retain the frequency and power in tie-line to their nominal values against the small perturb in load demand [8]. Researchers proposed the AGC mechanism by considering several complications like deregulation of power system [9], integration of distributed generation (DG) systems [10], and nonlinearities of generating systems [11].

On another hand, the controller design and optimizing gains play an important role to accomplish the AGC mechanism. Traditional controllers like integral controller, proportional-integral controller, and proportional-integral-derivative controller have a demerit of noise generation. Proportional-integral-derivative controller with derivative filter (PIDN) shows effectiveness over demerits of the conventional controller. Selection of proper gains for the controller which improves the AGC mechanism can be accomplished by optimization techniques. A.K. Barisal et al. proposed an AGC mechanism for a realistic multi-area power system using particle swarm optimization (PSO) technique [12]. AGC mechanism with gray wolf optimization (GWO) technique optimized controller for a multi-area power system is detailed in [13]. Similarly, optimization techniques such as bat-inspired algorithm, fruit fly algorithm [14], and firefly algorithm [15], etc., are adopted optimizing different controllers used for AGC mechanism. This article promotes the application of a recently developed VPL optimization technique to develop an AGC mechanism for a realistic deregulated hybrid power system. The efficacy of VPL optimizing technique is examined by comparing with PSO and the robustness has been checked against various performance indices.

2 System Description

A multi-area realistic deregulated hybrid power system having thermal (GENCOs-1 and 3), DG (GENCOs-2), and gas (GENCOs-4) systems as generating sources is considered for this work as depicted in Fig. 1. The participation factors apf_{11} , apf_{12} , apf_{21} , and apf_{22} for the generation systems are considered as 0.6, 0.4, 0.6, and 0.4, respectively. Nonlinear constraints like generation rate constraints (GRC) of 10% upper and lower generation rates for thermal system as well as 20% upper and lower generation rates for the gas system are considered. The governor dead band (GDB) of ± 10 MHz has been considered for thermal and gas power systems. The proposed system is restructured in bilateral deregulated environment where all the four DISCOs are made contract with all GENCOs in both areas. DG system present in the area-1 consists of wind energy, solar energy, diesel generator, battery energy storage, and fuel cell systems as shown in Fig. 2c. PIDN controller optimized by recently developed VPL optimization technique is employed as a secondary level control of AGC mechanism for the described system. The efficacy of the VPL optimization

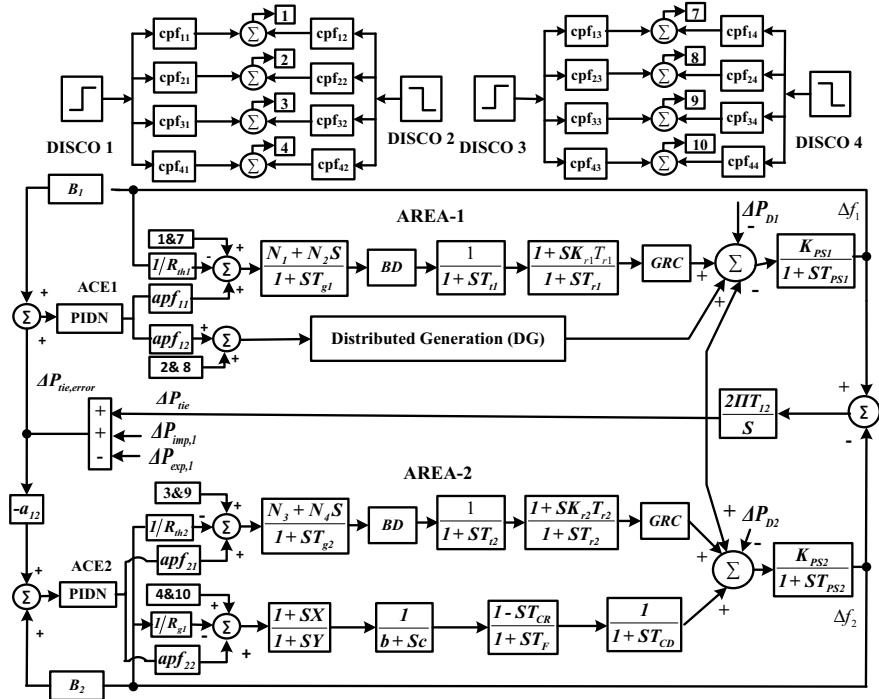


Fig. 1 Schematic diagram representation of the overall investigated system

techniques is examined by subjecting to different performance indices as expressed in Eqs. 1–4.

$$\text{IAE} = \int_0^{t_s} (|\Delta f_1| + |\Delta f_2| + |\Delta P_{12}|) dt \quad (1)$$

$$\text{ISE} = \int_0^{t_s} (\Delta f_1^2 + \Delta f_2^2 + \Delta P_{12}^2) dt \quad (2)$$

$$\text{ITAE} = \int_0^{t_s} t(|\Delta f_1| + |\Delta f_2| + |\Delta P_{12}|) dt \quad (3)$$

$$\text{ITSE} = \int_0^{t_s} t(\Delta f_1^2 + \Delta f_2^2 + \Delta P_{12}^2) dt \quad (4)$$

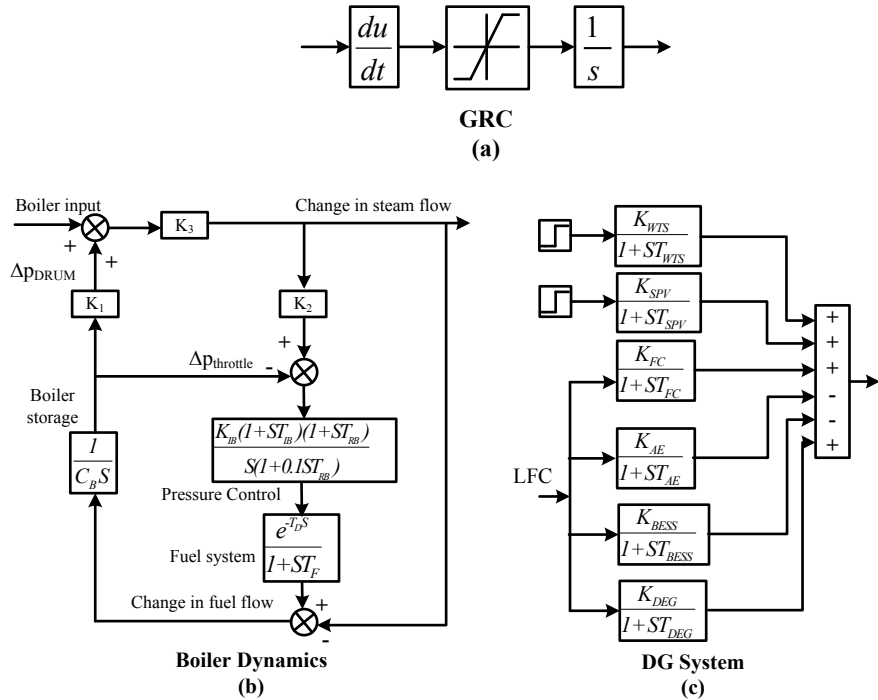


Fig. 2 Transfer function representation of **a** boiler dynamics of thermal power system, **b** generation constraints, and **c** distributed generation system

3 Controller Design and Optimization Technique

3.1 PIDN Controller

The controller design is one of the important tasks for the AGC mechanism. The traditional controllers like integral controller and proportional-integral controller are improved in the senses of overshoot, time response, and undershoot with PID controller. But, the PID controller is suffering from noise due to the derivative controller. The demerit of PID controller can be mitigated using derivative noise filter which can be named as PIDN controller. The gains of the PIDN controller are represented by K_P , K_I , K_D and the coefficient of derivative filter represented by N . The mathematical representation of the described controller is as in 5.

$$\frac{X_i(S)}{Y_i(S)} = \left\{ K_{Pi} + K_{Ii} + K_{Di} \left(\frac{SN}{S+N} \right) \right\} \quad (5)$$

The PIDN controller consists of four tunable parameters. VPL optimization technique is employed here for tuning control parameters based on the objective function given in Eq. 1 subjecting to constraints given in Eq. 6.

$$\begin{aligned} K_{Pi,\min} < K_{Pi} < K_{Pi,\max}, \quad K_{Ii,\min} < K_{Ii} < K_{Ii,\max}, \\ K_{Di,\min} < K_{Di} < K_{Di,\max}, \quad N_{i,\min} < N_i < N_{i,\max} \end{aligned} \quad (6)$$

3.2 Optimization Technique

The volleyball premier league optimization technique is one of the recent gaming-based metaheuristic algorithms. The flowchart for the steps to be followed for VPL algorithm is as depicted in Fig. 3.

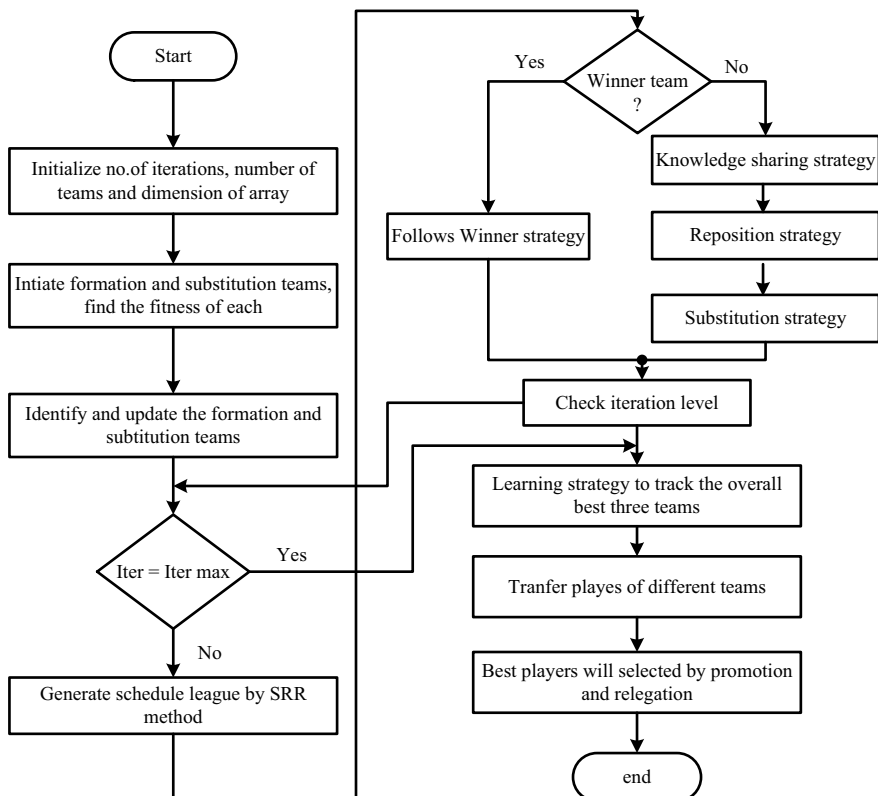


Fig. 3 Flowchart of volleyball premier league (VPL) optimization technique

This algorithm follows the steps followed by the participating teams in the volleyball tournament to win the match. Every team has three important segments, they are formation team, substitution team, and coach. For simplicity, the tournament has been assumed as conducted in single robin round method, where every team faces others once in the whole show. After completion of every season, there will be winners and losers. The winner team will follow the winning strategy, i.e., it updates the position of team members and plans, by competing with best three teams in the league. The looser team follows three strategies named as knowledge sharing strategy, reposition strategy, and substitution strategy. Coach and team players share the information among themselves in the knowledge strategy to compete with winning teams. The positions of players will be shuffle in that team according to information shared by the coach in the repositioning strategy. In substitution strategy formation, team players can be substituted by the players in the substitution team as per the coach decision. After each season, the best three teams will be ranked as first, second, and third. The team stood in the first place will be promoted as best team and last team will be replaced by a new team. Mathematical representation of all the steps explained above is presented in [7] and same followed in this work. The explained VPL optimization technique is deployed to optimize the controller gain value in order to minimize the performance indices given in Eqs. 1–4.

4 Results and Discussion

The AGC mechanism for the described system using VPL optimized PIDN controller has been examined in this work. The incorporation of nonlinearities and DG system to the power system is contaminated for a realistic approach. The thermal system with 10% GRC and gas with 20% GRC are considered in this work. Wind and solar energy systems are assumed that supplying constant power of 0.0015 pu and 0.002 pu, respectively. The tie-line coefficient is considered as 0.0866 for AC tie-line loaded 50%. PIDN controller is deployed to a secondary level of AGC mechanism for the investigated system. The controller gains are optimized by recently developed VPL optimization techniques. The efficiency of the proposed scheme of AGC mechanism has been carried out by comparing with PSO-based scheme, subjecting to several performance indices and comparing with previously published work.

4.1 PSO Versus VPL Algorithm

The described system is subjected to the 1% change in load demand, and PIDN is employed for the AGC mechanism. PSO and VPL optimization techniques are employed to optimize the gains of the controller. The obtained values for the controller gains with PSO as well as VPL is as presented in Table 1. The comparative numerical analysis has been done to examine the effectiveness of VPL technique

Table 1 Optimal gains of controller obtained by PSO and VPL

Controller gains	PSO technique		VPL technique	
	Area-1	Area-2	Area-1	Area-2
K_P	0.3213	0.6045	0.0919	0.9677
K_I	0.5594	0.8258	0.6090	0.8950
K_D	0.8071	0.0925	0.1941	0.9881
N	16.3310	10.6324	24.1355	22.3421

Table 2 Comparative analysis of the AGC mechanism with PSO and VPL-based controller

Optimization technique	Maximum deviation in		% improvement
	Δf_1	Δf_2	
PSO	-3.6	-4.5	10.7692
VPL	-3.25	-3.65	23.2876

upon PSO technique in senses of maximum deviation in dynamic response as tabulated in Table 2. The comparative numerical analysis reveals that an improvement of 10.76 and 23.28% has been achieved in terms of undershoot in deviation frequencies of both areas with the VPL technique over PSO technique. The dynamic response of the described system using the VPL optimization technique and PSO technique is as depicted in Fig. 4.

4.2 Robustness of the Proposed Scheme

The proposed AGC scheme is examined for robustness by subjecting the different performances indices like IAE, ISE, ITAE, and ITSE which are represented in Eqs. 1–4. The controller gain values obtained for different performance indices are as detailed in Table 3. The dynamic response depicted in Fig. 5 shows the investigation done with various performance indices for the described system. The dynamic response ensures the robustness of the proposed system against the variation of performance indices.

4.3 Supremacy of the Proposed Scheme

The supremacy of the proposed AGC scheme for the described system has been checked by comparing it with previously published work on the same platform. The dynamic response of the proposed system comparing with Parmar et al. [9] is as depicted in Fig. 6. The comparative numerical analysis detailed in Table 4 reveals

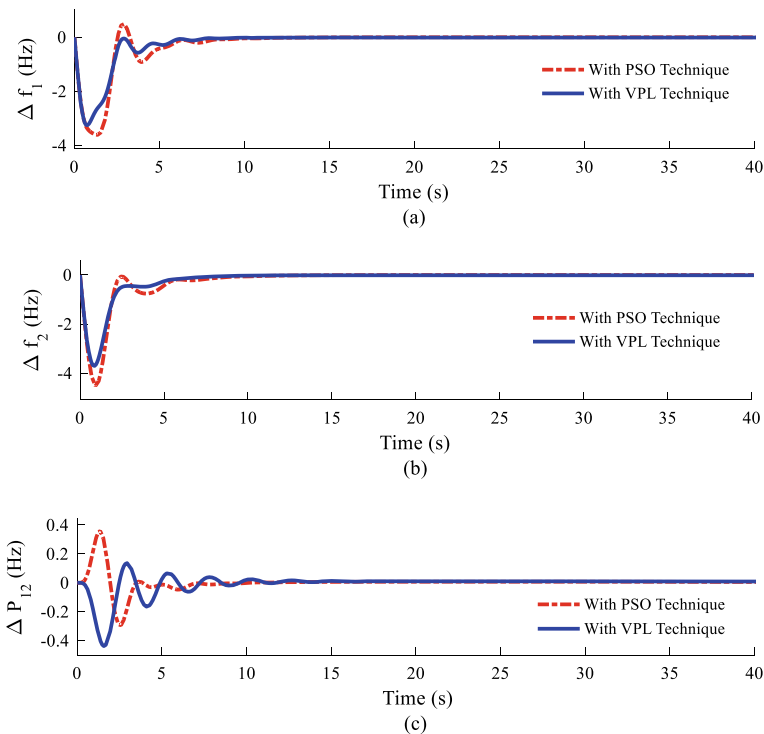


Fig. 4 Dynamic response of the described system **a** area-1 frequency response, **b** area-2 frequency response, and **c** tie-line power

Table 3 Optimal gain values obtained for different performance indices

Gains	IAE		ISE		ITAE		ITSE	
	Area-1	Area-2	Area-1	Area-2	Area-1	Area-2	Area-1	Area-2
K_P	0.8967	0.8622	0.2149	0.6838	0.0919	0.9677	4.3×10^{-3}	0.7179
K_I	0.3604	0.5465	0.5421	0.7887	0.6090	0.8950	0.4608	0.7032
K_D	0.5369	0.1777	0.7084	0.5740	0.1941	0.9881	0.7888	0.0087
N	19.5239	24.436	15.9730	11.9353	24.1355	22.3421	25.0544	9.3206

that the improvement of 73.60, 38.88, and 60% have been obtained in terms of maximum deviation in frequency of areas and tie-line power by using the proposed scheme. The efficacy of the proposed scheme has been proved upon the previously published work.

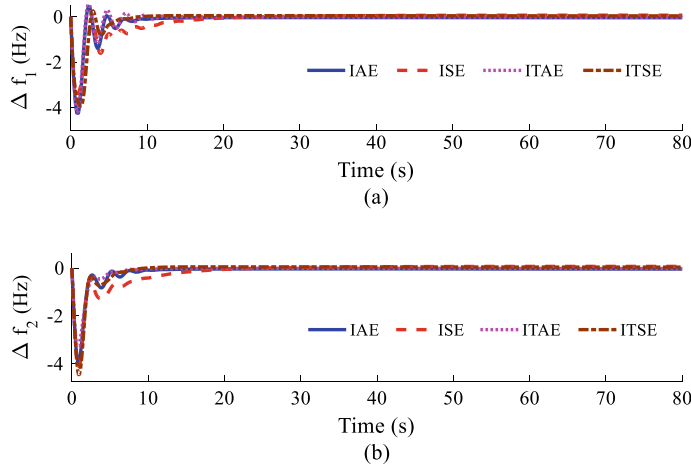


Fig. 5 Dynamic response of the system for different FOD in terms of maximum deviation in **a** area-1 frequency response, **b** area-2 frequency response, and **c** tie-line power

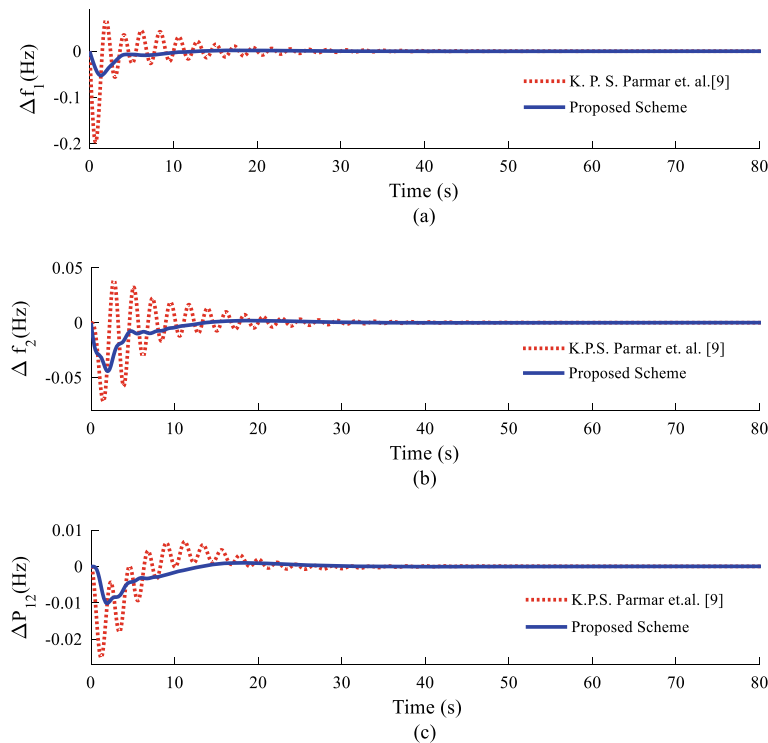


Fig. 6 Comparison of the proposed scheme with previously published work

Table 4 Comparative numerical analysis with previously published work

Maximum deviation in	Parmar et al. [9]	Proposed scheme	% improvement
Δf_1	-0.197	-0.052	73.60
Δf_2	-0.072	-0.044	38.88
ΔP_{12}	-0.025	-0.010	60.00

5 Conclusion

An AGC mechanism for a bilateral deregulated realistic hybrid multi-area power system has been developed. The integration of DG system and generation nonlinearities are contaminated for a realistic approach. Successful implementation of VPL optimization technique to accomplish the optimal gain values of the controller used. The accuracy of the VPL optimization technique has been proved over the PSO technique to accomplish minimum deviation in frequency and power exchange through tie-line. The robustness of considered AGC scheme has been examined for different performance indices and proved. Finally to check the predominance of the proposed scheme over the previously published work has been checked and accomplished.

Appendix

Thermal power plant: $T_{g1} = T_{g2} = 0.08$ s, $K_{r1} = K_{r2} = 0.5$, $T_{r1} = T_{r2} = 10$ s, $T_{t1} = T_{t2} = 0.3$ s, $N_1 = N_3 = 0.8$, $N_2 = N_4 = 0.2/\pi$. Boiler dynamics: $K_1 = 0.85$, $K_2 = 0.095$, $K_3 = 0.92$, $C_B = 200$, $T_D = 0$ s, $T_F = 10$ s, $K_{IB} = 0.030$, $T_{IB} = 26$ s, $T_{RB} = 69$ s. Gas power plant: $X = 0.6$ s, $Y = 1.0$ s, $b = 0.05$ s, $c = 1$, $T_F = 0.23$ s, $T_{CR} = 0.01$ s, $T_{CD} = 0.2$ s, $R_G = 2.4$ Hz/p.u. MW, Power system parameters: $K_{ps1} = K_{ps2} = 120$, $T_{ps1} = T_{ps2} = 20$, $R = 2.4$ Hz/p.u, $B = 0.425$ pu/Hz, DG system: $K_{WTS} = 1$, $T_{WTS} = 1.5$ s, $K_{SPV} = 1$, $T_{SPV} = 1.8$ s, $K_{DEG} = 0.003$, $DEG = 2$ s, $K_{FC} = 0.01$, $T_{FC} = 4$ s, $K_{AE} = 0.002$, $T_{AE} = 0.5$ s. Tie-line: $a_{12} = -1$, $T = 0.0866$.

References

1. Clerc, M., Kennedy, J.: The particle swarm-explosion, stability, and convergence in a multidimensional complex space. *IEEE Trans. Evol. Comput.* (2002). <https://doi.org/10.1109/4235.985692>
2. Yang, X.S.: A new metaheuristic bat-inspired algorithm. In: *Nature Inspired Cooperative Strategies for Optimization*. Springer, Berlin (2010)
3. Yang, X.-S.: Firefly algorithm, Lévy flights and global optimization. In: *Research and Development in Intelligent Systems XXVI* (2010)

4. Fister, I., Yang, X.S., Fister, D., Fister, I.: Cuckoo search: brief literature review. In: Studies in Computational Intelligence (2014)
5. Mirjalili, S.: The ant lion optimizer. *Adv. Eng. Softw.* (2015). <https://doi.org/10.1016/j.advengsoft.2015.01.010>
6. Mirjalili, S.: The ant lion optimizer. *Adv. Eng. Softw.* **83**, 80–98 (2015). <https://doi.org/10.1016/j.advengsoft.2015.01.010>
7. Moghdani, R., Salimifard, K.: Volleyball Premier League algorithm. *Appl. Soft Comput. J.* **64**, 161–185 (2018). <https://doi.org/10.1016/j.asoc.2017.11.043>
8. Kundur, P.S.: Power system dynamics and stability. In: Power System Stability and Control, 3 edn (2017)
9. Parmar, K.P.S., Majhi, S., Kothari, D.P.: LFC of an interconnected power system with multi-source power generation in deregulated power environment. *Int. J. Electr. Power Energy Syst.* **57**, 277–286 (2014). <https://doi.org/10.1016/j.ijepes.2013.11.058>
10. Hajiakbari Fini, M., Hamedani Golshan, M.E.: Frequency control using loads and generators capacity in power systems with a high penetration of renewables. *Electr. Power Syst. Res.* **166**, 43–51 (2019). <https://doi.org/10.1016/j.epsr.2018.09.010>
11. Tan, W., Chang, S., Zhou, R.: Load frequency control of power systems with non-linearities. *IET Gener. Transm. Distrib.* **11**, 4307–4313 (2017). <https://doi.org/10.1049/iet-gtd.2017.0599>
12. Barisal, A.K., Mishra, S.: Improved PSO based automatic generation control of multi-source nonlinear power systems interconnected by AC/DC links. *Cogent Eng.* **5**, 1–20 (2018). <https://doi.org/10.1080/23311916.2017.1422228>
13. Gupta, E., Saxena, A.: Grey wolf optimizer based regulator design for automatic generation control of interconnected power system. *Cogent Eng.* (2016). <https://doi.org/10.1080/23311916.2016.1151612>
14. Shankar, R., Kumar, A., Raj, U., Chatterjee, K.: Fruit fly algorithm-based automatic generation control of multiarea interconnected power system with FACTS and AC/DC links in deregulated power environment. *Int. Trans. Electr. Energy Syst.* **29**, 1–25 (2019). <https://doi.org/10.1002/etep.2690>
15. Pradhan, P.C., Sahu, R.K., Panda, S.: Firefly algorithm optimized fuzzy PID controller for AGC of multi-area multi-source power systems with UPFC and SMES. *Eng. Sci. Technol. Int. J.* (2016). <https://doi.org/10.1016/j.jestch.2015.08.007>

Wireless Emanation of Braille to Text/Voice and Vice Versa



Aishwarya Korde, Omkar Gaikar, Sonam Nikam, and Smita Rukhande

Abstract India currently has around 12 million blind people against 39 million blind people globally, which makes India home to one-third of the world's blind population. Telecommunication technology plays an important role in our day to day life. Despite all these advances in the field of telecommunication, the visually impaired people have no access to these technologies, i.e., due to their disability, visually impaired people face trouble in gaining full advantage of mobile devices and computers. So there is a major step that is needed to be taken to bridge the gap between the blind users and the end-users due to technological advancement in the telecommunication field a system was designed for them by interfacing Braille pad with the mobile devices or desktop computers so that dual impaired person can have the access. This system will help the visually impaired people to communicate with end-users using their Braille language. Even the end-users can communicate with visually impaired people by using their preferred language (English language). The system can be used by visually impaired people to hear the received messages as well by using text to speech translator. The project's main objective is to design and develop a Braille System for the visually impaired individuals that enable them to interact and communicate. By using this system, the impaired people will interact using a Braille pad whereas the visually abled people can interact using their mobile devices or desktop computer via this developed system. The Braille to text translation and vice versa will be done using machine learning technology. The transmission of this converted text will take place using wireless technology that leads to an increase in mobility and efficiency.

A. Korde (✉) · O. Gaikar · S. Nikam · S. Rukhande

Information Technology, Fr. Conceicao Rodrigues Institute of Technology, Vashi, Navi Mumbai, Maharashtra 400703, India

e-mail: aishyk24@gmail.com

O. Gaikar

e-mail: omkargaikar8991@gmail.com

S. Nikam

e-mail: sonamnikam7@gmail.com

S. Rukhande

e-mail: smitarukhande@gmail.com

Keywords Braille · Visually impaired · Text to speech · Wireless technology

1 Introduction

The WHO estimates that in 2012 there were 285 million visually impaired people in the world, of which 246 million have low vision and 39 million are blind from which there are 90% blind who live in the developing world. There is a chronic shortage of teachers who are qualified to teach Braille. It was reported in 2003 that there were approximately 6700 full-time teachers of blind students serving approximately 93,600 students. Experts estimate that 1.3 million blind people live in the United States, and approximately 75,000 people lose all or part of their vision each year. Nowadays, the majority of people in this world use computers and mobile phones for communication. These technologies help people in day to day life with different types of applications that can simplify their work. But blind people cannot communicate using the English language. They don't know how an alphabet is written. They know only the alphabet's pronunciation but don't know how that alphabet is written and hence they can't send any emails or letters to any person as Braille codes are not known by the visually abled people. Significant social challenges are caused due to blindness because there are certain activities in which blind people can't easily take part. Frequent, blindness affects a person's ability to perform various job tasks, which can limit their career opportunities. This may adversely affect their finances and self-esteem. This can limit the blind person's ability to socialize and communicate with new people using technologies. Braille is a system of raised dots that can be used by the blind and visually impaired people. Blind and visually impaired people can be read with the fingers by using this system. Also, this system has Braille codes which are small rectangular blocks called cells which include tiny palpable bumps called raised dots. A full Braille cell includes six raised dots arranged in two columns, each column having three dots and the position of them are identified by numbers from one to six. A cell can be used to represent a letter, digit or even a word. To solve this problem, a system Wireless Emanation of Braille to Text/voice and vice versa is designed which will convert the Braille codes into text and vice versa. The Braille codes will also be converted into voice so that it can be easily understandable by the visually impaired people. Even the visually abled people can give voice inputs. The system will bridge the gap between the person who can see and the visually impaired ones. This system will make both the users to communicate in their language that they understand. Due to this the technological connection gap between the blind person and the visually abled person will reduce.

2 Literature Survey

In FPGA-Based Braille to Text and Speech for Blind Persons, authors presented the implementation of Braille to Text/Speech Converter on FPGA Spartan 3 kit. A text to Braille converter is intended to aid the blind to interact with others at workplaces and homes. Facilities for the sightless have been organized in various places for providing reading facilities to the blind in the form of Braille coded texts. Braille consists of a system of six or eight possible dot combinations that are arranged in a fixed matrix, called a cell. Every dot can be set or cleared, giving 61 combinations in six-dot and 256 combinations in eight-dot Braille. At the intersections of an orthogonal grid, all dots of a Braille page should fall on. The grid of the verso text is shifted when texts are printed double-sided (recto-verso) so that its dots fall in between the recto dots. Braille has a low information density. An average page of size 25 cm × 29 cm, can have 32 characters on a line and 27 lines on a page. Every dot has a diameter value of 1.8 mm. This project presents a solution to such a problem, making the learning process for an unsighted person easy. Since all textbooks are not being available as Braille script or as Audio recordings, developing this system will address this problem. An image of the content in the textbook will be taken and converted into a Braille script. The system is implemented using FPGA. In this, the crux of this Design Implementation is the conversion from the basic “Braille” language to English using FPGA. To meet the needs of high volume, cost-sensitive consumer electronics applications Spartan-3 family of Field-Programmable Gate Arrays are specifically designed. Braille Keyboard (I/P device), LCD (O/P device) and speaker (O/P device) are all interfaced with the FPGA. The software will take the combination of all the six cells from I/P hardware, decode it and give the appropriate O/P on hardware. Whenever the user provides Braille input, the same will be accepted and displayed on the screen and accordingly speech output of the character will be output. After accepting a few characters, the user will press the play button. The device must search for that word from the lookup table and accordingly output it to the speech device. The system consists of a Braille Keyboard (I/P device), an LCD (O/P device) and a speaker (O/P device) all of which are interfaced with the FPGA. The software will take a combination of all the six cells from the I/P hardware, decode it and give the appropriate O/P to the hardware [1]. Moise et al. [2] proposed an “Automatic System for Text to Braille Conversion”. The system uses a microcontroller connected to a special device that can be read by blind persons. For this system, a software-based concept to implementing Finite State Machines (FSM) has been developed. The concept described above has been used to implement the automatic system for text to Braille conversion, with the physical reproduction of Braille characters. The system that performs the conversion is conversion is an implementation of FSM in a software program. It reads a character or a string from a computer and generates sequences of 3×2 arrays of dots and blanks to an output device. Lakshmi Prabha et al. [3] presented a “Low-cost real-time Braille keypad for communication system.” This system suggests an innovative assistive device, a Braille keypad, for the visually impaired that would help them use computers just

like a visually abled person. The Braille keypad implements the Braille cells as six switches that can be pressed simultaneously based on the actual Braille combination to type a particular letter and words. The corresponding letters/words are displayed as well as can be heard by the user. A text to speech algorithm is implemented using putty software which would help the user confirm what he/she has typed is right. Numbers can also be displayed by pressing hash before pressing the combinations. On pressing the right sequence of switches according to the Braille combination the desired outputs can be displayed and the output can also be heard on the computer which would enable the user to confirm that he/she has typed the right characters. In this way it enables them to interact and communicate as well as use computers and mobile phones much like a visually abled person. Dharme et al. [4] proposed a paper on “Designing of English text to Braille conversion system.” This paper is concatenated the problem of blind people regarding their reading of e-book and e-text and the paper gives us information about how it will be beneficial for the blind person to read the digital books in their English Braille language. In this paper, the initiative has been taken to reduce the complications of the visually handicapped person about the reading of the English electronic text with the ease of cost-effectively. In this, a microcontroller is used instead of FPGA. The system will implement English text to Braille conversion with very less complication and fewer efforts.

3 Proposed System

Reading is an easy task for visually able people who can read and write in a common language. However, it is very hard for blind people to face their life like other people. It is very difficult for visually impaired people to read and write any language. Blind people only understand Braille codes. The proposed system is designed for reducing a mechanism having the error rate value low with a faster conversion rate. Since there is no such text to Braille conversion system built previously for the visually handicapped person. So using such mechanisms, proposed designs will help the blind person to read the English text into the Braille codes by using Braille pad hardware. With the help of this proposed work, the blind person can communicate with visually abled people and make jobs available to these people and make their life easy. Considering today’s scenario, where there are thousands of sightless people who have desirable skills and potential in them but their work stops because they have difficulty in finding their work that is to be done. This situation can be dealt with and in turn, productivity can be increased if we use this system. This system will help to grab the various opportunities and provide the following benefits:

- With the help of this system, the communication gap will be decreased between visually abled people and visually impaired people.
- The system will increase the mobility and efficiency using wireless technology.
- The system will work as an interpreter between visually abled people and visually impaired people.

- This system will help visually impaired people to get job opportunities.

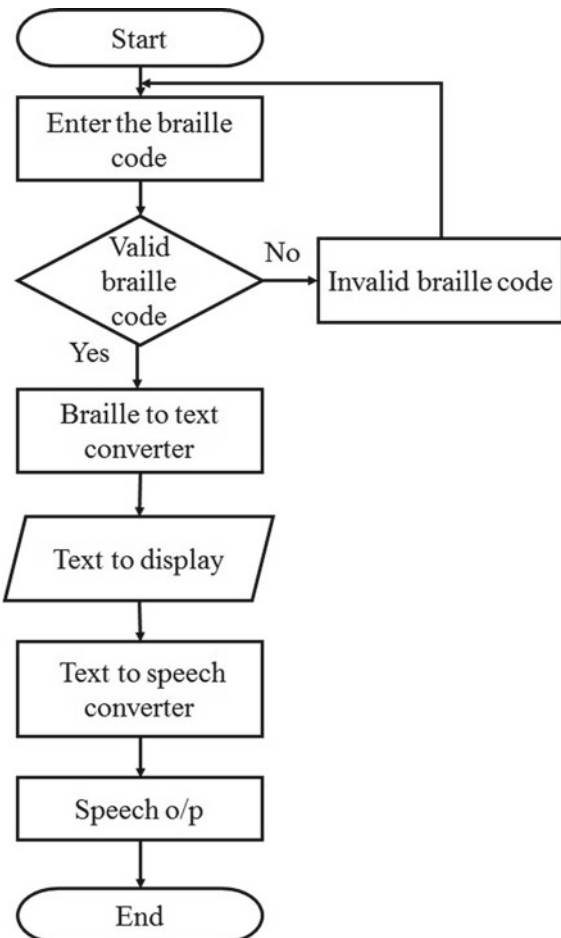
3.1 Working of System

The first step the user needs to do is use this Braille machine which is wireless as he can carry it anywhere now if a visually abled person wants to convey their message to this deaf and blind person he will first give the voice command which will be converted to the text and then this text will be wirelessly passed to the microcontroller. After successfully passing this to the microcontroller will have a connected switch and those switches will have some buzzers which will help to create some vibration so every time the message is conveyed to the blind person the vibration will make the system come to know what text was passed and this way they can communicate. If the blind user wants to communicate or if he wants to send a message or at any workplace, he wants to do any writing work the simple method will be the needs to just press the Braille pad which will have switches and which will create text and this way they can communicate or complete their work. The last part is that the converted Braille language needs to be conveyed to the end-user so that they will have communication so this text will be in English language and it will be converted back to the voice form so that the visually abled person doesn't need to make any effort for communication. The system requires a Braille pad from which visually impaired persons can interact. Normally, a Braille pad is the hardware that consists of six dots that are arranged in cells. The Braille pad includes six dots on a small rectangular box. The system gives 63 combinations (including numbers, special characters, and alphabets) and one blank space. Every six-dot Braille pad hardware consists of a 3×2 matrix of raised dots. Each dot combination is made up using six raised dots that relate to a number, letter or character. This Braille pad hardware is designed using a PCB board, buzzers, vibration motors, and switches. Dip Trace is an EDA/CAD software that is used for creating schematic diagrams and Printed Circuit Boards (PCB). Vibration motors are used for generating vibrations on the Braille pad for sensing the data and a better understanding of the visually impaired people. By using switches visually impaired persons can give Braille inputs.

Figure 1 shows the working flow of how the Braille codes are converted into text or voice. First, it will take the Braille input from the visually impaired person and then will convert into the English language.

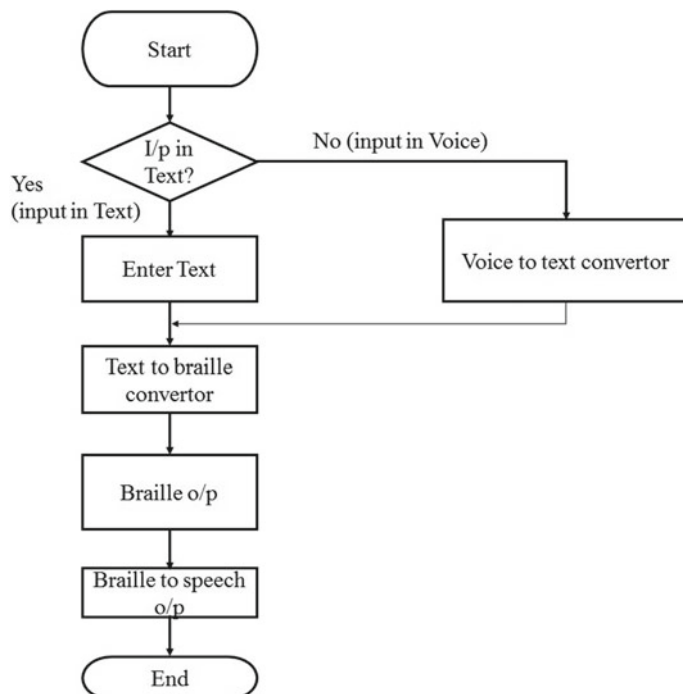
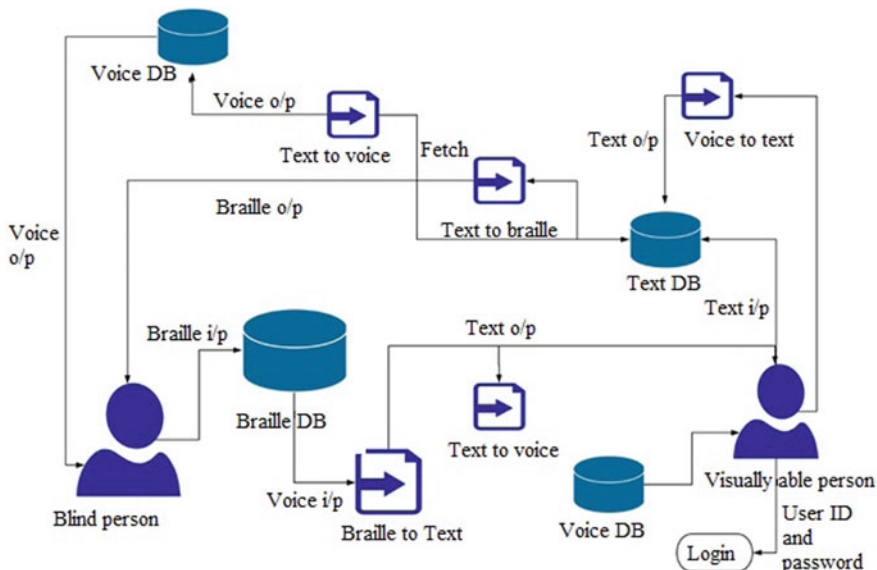
Figure 2 shows the working flow of how the text or voice is converted into Braille codes. First, it will take the text or voice input and then will convert it into Braille output. This Braille output will be converted into speech for better understanding.

Fig. 1 Braille to text/voice conversion



3.2 Implementation

The system will convert the Braille codes into text and vice versa. The text will also be converted into a voice so that it can be easily understandable by the visually impaired people. The system will bridge the communication gap between the people who can see and the visually impaired ones. This system will make both the users to communicate in their language that they understand. Due to this visually impaired people can easily convey their messages to others and can also understand the messages given by people and thus will reduce the communication gap between the blind person and the visually able person. The system block diagram is further explained through Fig. 3 which represents the modules of the system that is how the blind and a visually abled person can communicate through our system.

**Fig. 2** Text/voice to Braille conversion**Fig. 3** Architectural diagram of a system

The system includes modules like Braille to text conversion, text to Braille conversion, Voice to text conversion and text to voice conversion.

3.2.1 Braille to Text Conversion

In this Braille to text is implemented by using Braille keypad hardware. The inputs are taken through Braille keypad and the Braille code id displayed at the sender side and the specified alphabet is displayed at the receiver side [5].

The steps to implement Braille to text conversion are as follows:

- The Braille to text conversion is done by a JavaScript code.
- The sender inputs the Braille code using the Braille keypad (only 2 * 3 keys of the num pad are used).
- After that its Braille code interpretation is displayed on the website.
- The converted Braille code, i.e., its specified alphabet is stored in the database using PHP code.
- At the receiver side, the alphabet is retrieved from the database using PHP code and displayed on the website [6].

3.2.2 Text to Braille Conversion

- The sender inputs text in the English language through their mobile phones.
- The text to Braille conversion is done by a JavaScript code.
- The converted text will be sent to the Braille keypad hardware through the Bluetooth module.
- The generated output will be vibrated on the Braille pad through this visually impaired person can easily sense and understand the output [7].

3.2.3 Voice to Text Conversion

The visually abled person can give the voice input and that voice input will be converted into text using Google speech to text API and that text input will be fed to text to Braille module for further process.

3.2.4 Text to Voice Conversion

The received text will be converted into a voice using Google text to Speech API [8].

4 Conclusion

The system will provide the conversion of Braille to the text as well as voice and vice versa. The system will help both users, i.e., the visually impaired as well as the visually abled people to communicate in their language that they understand. Due to this visually impaired people can easily convey their messages to others and can also understand the messages given by people and thus will reduce the communication gap between the blind person and the visually able person. The transmission of data will be done using wireless technology, i.e., Bluetooth module and will increase mobility and efficiency. In the future, the designed system can be used to update about the date, temperature, time, battery power of the mobile device, etc. to the visually impaired user. This system can be integrated with various sensors to monitor several health parameters of the visually impaired individual to update them about their current health condition or status.

References

1. Rajarapollu, P., Kodolikar, S., Laghate, D., Khavale, A.: FPGA based Braille to text & speech for blind persons. *Int. J. Sci. Eng. Res.* **4**(4) (2013)
2. Moise, A., Bucur, G., Popescu, C.: Automatic system for text to Braille conversion. In: *ECAI 2017—International Conference, Electronics, Computers and Artificial Intelligence*, Targoviste, România, 29 June–01 July 2017
3. Lakshmi Prabha, P., SanjanaMenon, E.J., Samuel, C., Ramesh, G.: Low cost real time Braille keypad for communication. *Int. J. Eng. Technol.* (2018)
4. Dharme, V.S., Karmore, S.P.: Designing of English text to Braille conversion system. In: *International Conference on Innovations in Information Embedded and Communication Systems* (2015)
5. Padmavathi, S., Manojna, K.S., Sphoorthy Reddy, S., Meenakshy, D.: Conversion of Braille to text in English, Hindi and Tamil languages. *Int. J. Comput. Sci. Eng. Appl. (IJCSEA)* **3**(3) (2013)
6. Raghunandan, A., Anuradha, M.R.: The methods used in text to Braille conversion and vice versa. *Int. J. Innov. Res. Comput. Commun. Eng.* (2017)
7. Singh, M., Bhatia, P.: Automated conversion of English and Hindi text to Braille representation. *Int. J. Comput. Appl.* (0975–8887), **4** (2010)
8. Subash, N.S., Nambiar, S., Kumar, V.: Braille key: an alternative Braille text input system. In: *IEEE Proceedings of 4th International Conference on Intelligent Human Computer Interaction*, Kharagpur, India (2012)

An Exploratory Analysis Pertaining to Stress Detection in Adolescents



Mrinal Pandey, Bharti Jha, and Rahul Thakur

Abstract With the rise of social networking era, there is a sudden and great increase in user-generated content. Millions of people share their daily life and status by blogging on social media like Twitter. Therefore, it is a great source to analyze sentiments by simply using the text of social media and simple manner of expression. This paper addresses the issues of mental health such as psychological stress and depression, particularly in adolescents. However, adolescents' emotions are mostly reflected in their posts such as tweets and Facebook posts, which may include some words usually, not spoken freely in an open environment. This paper took the advantages of extracting the data from Twitter and performed an exploratory analysis to identify the stress in adolescents. Four popular machine learning algorithms, namely Naïve Bayes, random forest, support vector machine, and logistic regression, were employed.

Keywords Social media · Mental health · Adolescents · Machine learning · Algorithms · Sentiments

1 Introduction

Psychological stress has always been a major health issue. Nowadays, it is the common health concern among the adolescents. The stress arises when the combination of internal and external pressures exceeds the individual's resources to cope with the situation. Stress if not released on time hurts adolescents physically and mentally which leads to depression, insomnia, suicide, trapping into addiction like smoking, drugs, getting into fights, etc. Thus, there is significant importance to detect stress before it turns into severe problems.

Most of the time adolescents express their emotions on social media in the form of text, images, pictures, different music genres, etc. With the advancement in technology, various machine learning techniques are incorporated with sentiment analysis

M. Pandey (✉) · B. Jha · R. Thakur

Department of Computer Science & Technology, Manav Rachna University, Faridabad, India
e-mail: mrinal@mru.edu.in

of various types of emotions from social media. This paper presented an exploratory analysis of machine learning algorithms pertaining to stress detection in adolescents.

1.1 *Sentiment Analysis*

Sentiment analysis is an application of natural language processing that deals with text analysis and uses artificial intelligence to study human behavior and perception using machine learning with information extraction task and computational algorithm. Sentiments are feelings, opinions, emotions, likes or dislikes, good or bad. The text in an analysis is given the polarity to the given text, document, and sentence, and after that, the language is processed to figure out the sentiment related to that sentence.

Sentiment analysis is an emerging research field that helps the industry in decision making by analyzing and scoring the opinions as negative, positive, or neutral [1]. The opinions, sentiments, and the subjectivity of text when computationally treated are called sentiment analysis or opinion mining. Sentiment analysis has applications in almost every business and social domain and helps in decision making. There are three levels of sentiment analysis: document level, sentence level, and aspect level.

Sentiment analysis can be classified into two categories [1]: lexicon-based sentiment analysis and machine learning-based sentiment analysis. Lexicon-based approach is the part of natural language processing which can be used for creating the bag of words related to entities, product, social problems, etc. The ML-based approach is used to classify the data and for further predictions. Most of the research for sentiment analysis has used supervised ML technique to identify patterns in systems, with the past work, of frequency maps and classifiers. A number of machine learning algorithms for sentiment classification have been employed in [2–6] the literature.

2 Related Work

Psychological stress in adolescents is the major concern as they are the future of the country. A number of research works are being done to resolve this issue and to save the new generation from stress and depression.

In [7], pictures in microblog were used as additional information and sparse deep neural network was used to classify whether the users convey their stress by single tweet on microblog; however, some users do not post anything, or therefore, recurrence of tweeting was too low.

The authors of [8, 9] proposed an adolescent's pressure detection strategy on microblog based on their tweet posting behavior. The features were tested on many classifiers. A microblog platform tHelper was developed based on Gaussian process classifier to ease adolescent's stress by providing assistance depending on the level of stress based on a single tweet. The number of characters in a tweet is limited so it was difficult to analyze the exact reason for stress and duration of stress.

The concept of candlestick charts was used for the teens' stress level prediction on microblog data [10], and stress pattern matching was conducted to identify whether a reversal signal changes the trend of stress on the candlestick chart.

A prediction framework was proposed for predicting future stress level in teenagers from microblog [11]. Machine learning techniques and prediction techniques like SVR and GPR algorithms on multi-variant time series are compared and found that GPR algorithm accurately determined the uncertain value which was missing during the tweet intervals to address the challenge of incompleteness in data and multi-faceted prediction.

Stress in teenagers was detected on the basis of time-sensitive tweets comment and response(C/R) actions with friends and followers [12]. This paper focused on four main categories of adolescent's stress and compared the *F*-measure of a single tweet without C/R action and tweet with C/R action. They analyzed that the performance of stress detection with time sensitivity of C/R action improves the *F*-measure to 23.5%.

The authors of [13] developed a system called tPredictor for predicting future stress in teenagers on social media based on GPR.

A framework to discover the stress which is chronic in teens on microblog was proposed by Xue et al. [14]. The system also identified five chronic change patterns from single tweet aggregation and planning to implant personalization model to teen stress detection.

A recurrent neural network-based model was developed to predict future stress in teenagers based on finding stressor event and stress series correlation. This model worked on improving the stress prediction accuracy [15, 16].

Further [17], Poisson-based probability technique was employed to identify the relationship between the events responsible for stress in teens and their stressful posting behavior. Most of the work needs to be addressed in suggesting coping mechanism to handle stress during a maximum stressful period and to integrate multiple sources to fill the gap of missing data that is not found in microblog to find the stressful period and stressor events.

A stress random walk process prediction algorithm was proposed in [18], and the model was based on Markov chain to detect chronic stress transition pattern which can lead to depression.

In a recent research [19], deep learning techniques were employed for the teenager's sentiment analysis. The authors of Kim et al. [20] proposed sentiment analysis for Korean teenagers based on Korean sentiment dictionary.

3 Proposed Method

The methodology for sentiment analysis starts with the extraction of data using Twitter APIs, followed by preprocessing and classification using machine learning algorithm. Figure 1 shows the methodology adopted for this study. The entire work was carried out in python environment. Table 1 depicts the python libraries used at different stages of the research.

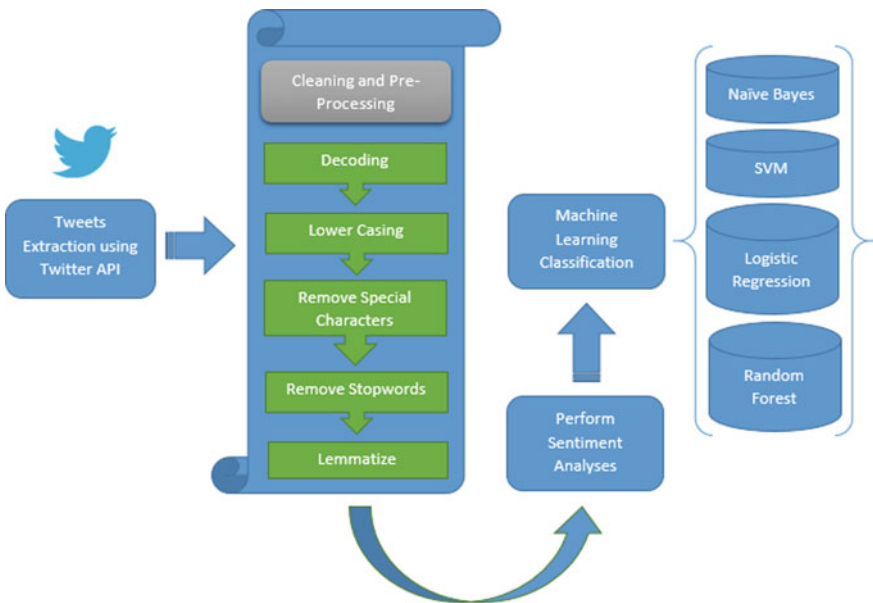


Fig. 1 Methodology

Table 1 Python libraries

S. No.	Process	Python library
1	Data extraction	Tweepy
2	Cleaning and preprocessing	Pandas, Unicode, NLTK, Codecs
3	Sentiment analysis	TextBlob
4	Machine learning	sklearn
5	Graphs	Matplotlib

3.1 Data Collection

In this step, the stress-related tweets were extracted for the month of April 2019 from the Twitter API with the help of relevant keywords. As in Twitter data, the demographic information is mostly missing; therefore, it was a challenge to get the data of adolescents. This issue was addressed by observing the language used by youth and adolescents in their communication. In this research, keywords and # tag were chosen according to language being used by adolescents in the present environment.

Few relevant keywords are as follows:

Table 2 Extracted dataset description

S. No.	Tweets	Numbers
1	Total tweets	10,983
2	Duplicate tweets	838
3	Unique tweets	10,145
4	Neutral tweets	3979
5	Positive tweets	3528
6	Negative tweets	2638

Fig. 2 Word cloud of most relevant keywords for adolescents' sentiments



```
{ "#stress", "#exampressure", "#exams", "#addiction", "#anxiety", "#parents", "#coaching", "#depression", "#depressed", "#sad", "#relationship", "#breakup", "#hollow", "#fastfood", "#students", "#love", "#lonely", "#hostellife", "#collegelife" }
```

However, the total extracted tweets were 10,983 in which 838 tweets were identified as duplicates and removed from the dataset. Table 2 shows the extracted dataset description. Figure 2 shows the word cloud of sentiments.

3.2 Preprocessing

After extraction of tweets, the cleaning and preprocessing tasks need to be performed. Tweets were preprocessed in the following order: decoding, lower casing, removal of special characters, removal of stop words and lemmatization, feature normalization, and dimensionality reduction for normalization of tweets.

3.3 Sentiment Analysis of Tweets

Sentiments can be classified into three categories, namely positive, neutral, and negative. The focus of the research is to identify the negative segments and see if they actually present threats, of any real-life incidents, likely to happen in the future.

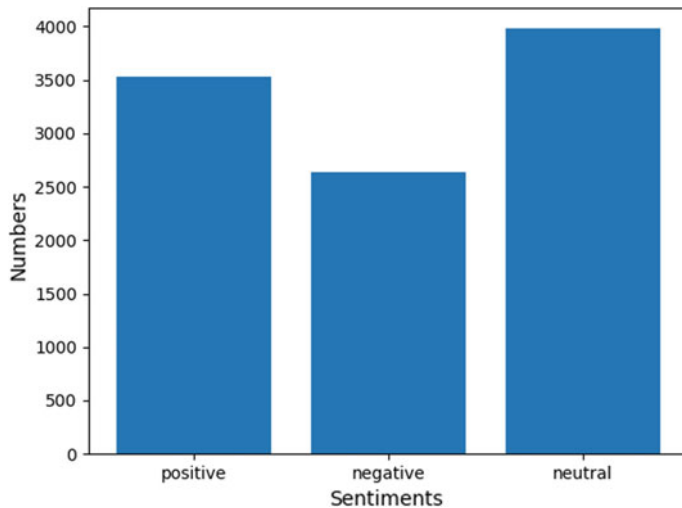


Fig. 3 Sentiment distribution

In this research, initially, sentiments were classified into three categories, namely positive, negative, and neutral. Since the objective of this research is to focus on identification of the patients being suffered from stress or not (positive and negative tweets), the neutral tweets were removed from the datasets. Figure 3 shows the sentiment distribution.

3.4 Sentiment Classification Using Machine Learning

In this step, four machine learning algorithms, namely Naïve Bayes, support vector machine, random forest, and logistic regression, were applied for the sentiment analysis and classification of tweets. These algorithms were compared on a standard set of performance parameters such as precision, recall, and F -measure.

4 Experiments and Results

The experiments were carried out in python programming environment. Various libraries of python programming were used for the experiments.

Figure 4 shows the accuracy graph pertaining to the aforementioned algorithms. It can be noticed from the graph that SVM is the leading classifier with 92% accuracy, while Naïve Bayes is securing least accuracy with 86%. However, only the accuracy parameter is not sufficient enough for accurate classification. Therefore, in this

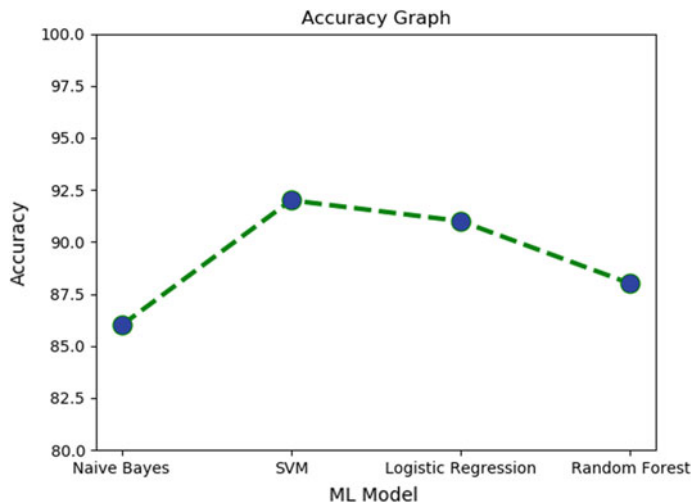


Fig. 4 Accuracy comparison graph

research, three other performance measures, namely precision, recall and *F*-measure, have been considered for the classification of sentiments.

Table 3 illustrates the experimental results in terms of precision, recall, and *F*-measure. Four classifiers, namely Naïve Bayes, support vector machine, logistic regression, and random forest, were employed for the classification of the sentiments. The class 0 represents the negative sentiments, i.e., stress-related sentiments, whereas class 1 represents the positive sentiments, i.e., non-stressed sentiments. In this research, negative sentiments are crucial for the study and required more attention for the action.

Table 3 clearly states that the SVM algorithm is leading as compared to other four algorithms in terms of *F*-measure and precision for positive classes (positive sentiments), while logistic regression is the best suitable algorithm among the aforementioned algorithms for the identification of the negative sentiments in terms of

Table 3 Performance measure for classifiers

Classifier	Classes	Precision	Recall	<i>F</i> -measure
Naïve Bayes	0	0.85	0.82	0.83
	1	0.87	0.9	0.88
SVM	0	0.91	0.89	0.9
	1	0.92	0.93	0.93
Logistic regression	0	0.92	0.86	0.89
	1	0.91	0.95	0.93
Random forest	0	0.91	0.81	0.86
	1	0.87	0.94	0.9

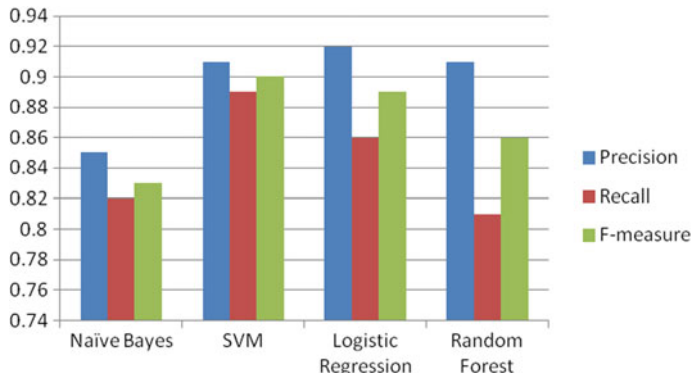


Fig. 5 Performance analysis for negative sentiments

precision. However, the overall performance of the classifier can be determined by F -measure. Therefore, SVM classifier is proposed in this research for the identification of stress in adolescents. F -measure can be calculated as given in Eq. (1).

$$F\text{-Measure} = \frac{2 \times \text{Precision} \times \text{Recall}}{\text{Precision} + \text{Recall}} \quad (1)$$

Figure 5 shows the performance of the aforementioned classifiers, particularly for negative statements; there is a clear observation from the graph that logistic regression is outperformed in terms of precision, while SVM is scoring highest value in F -measure.

5 Conclusion and Future Work

This paper presented an application of sentiment analysis in the area of mental health for detecting stress in adolescents. The results are based on applying four popular machine learning algorithms, namely Naïve Bayes, SVM, random forest, and logistic regression. This paper concludes that the results of SVM and logistics regression were very close for detecting stress in adolescents. However, as per the value of F -measure, SVM is slightly better than logistic regression with the value of 90%. Additionally, due to the high values of accuracy, it can be concluded that data preprocessing was done adequately.

Twitter does not provide the demographic information of the users. In this research, few keywords and # tag were used to extract the data pertaining to stress in youth and adolescents. This approach was language-dependent. Therefore, this issue will be addressed in future work of the current research. Moreover, users of the negative statements will be followed on Twitter for the identification of the stress level, so that proper action can be taken in time to prevent adolescents.

References

1. Medhat, W., Hassan, A., Korashy, H.: Sentiment analysis algorithms and applications: a survey. *Ain Shams Eng. J.* **5**(4), 1093–1113 (2014)
2. Pang, B., Lee, L.: Opinion mining and sentiment analysis. *Found. Trends Inf. Retrieval* **2**(1–2), 1–135 (2008)
3. Pang, B., Lee, L., Vaithyanathan, S.: Thumbs up? Sentiment classification using machine learning techniques. In: Proceedings of the Conference on Empirical Methods in Natural Language Processing (EMNLP), pp. 79–86 (2002)
4. Liu, B.: Sentiment analysis and subjectivity. In: Indurkhya, N., Damerau, F.J. (eds.) *Handbook of Natural Language Processing*, 2nd edn., pp. 627–666. Chapman & Hall (2010)
5. Witten, I.H., Frank, E.: *Data Mining: Practical Machine Learning Tools and techniques*. Morgan Kaufmann, San Francisco (2005)
6. Manning, C.D., Raghavan, P., Schütze, H.: *Introduction to Information Retrieval*. Cambridge University Press, Cambridge (2008)
7. Lin, H., Jia, J., Guo, Q., Xue, Y., Huang, J., Cai, L., Feng, L.: Psychological stress detection from cross-media micro blog data using deep sparse neural network. In: 2014 IEEE International Conference on Multimedia and Expo (ICME), pp. 1–6. IEEE (2014)
8. Xue, Y., Li, Q., Jin, L., Feng, L., Clifton, D., Clifford, G.: Detecting adolescent psychological pressures from micro-blog. In: Proceedings of International Conference on Health Information Science, pp. 83–94 (2014)
9. Li, Q., Xue, Y., Jia, J., Feng, L.: Helping teenagers relieve psychological pressures: a micro-blog based system. In: Proceedings of the 17th International Conference on Extending Database Technology, pp. 660–663 (2014)
10. Li, Y., Feng, Z., Feng, L.: Using candlestick charts to predict adolescent stress trend on micro-blog. *Proc. Comput. Sci.* **63**, 221–228 (2015). <https://doi.org/10.1016/j.procs.2015.08.337>
11. Li, Y., Huang, J., Wang, H., Feng, L.: Predicting teenager's future stress level from micro-blog. In: 2015 IEEE 28th International Symposium on Computer-Based Medical Systems (2015). <https://doi.org/10.1109/cbms.2015.25>
12. Zhao, L., Jia, J., Feng, L.: Teenagers' stress detection based on time-sensitive micro-blog comment/response actions. In: IFIP International Conference on Artificial Intelligence in Theory and Practice, pp. 26–36. Springer, Cham (2015)
13. Huang, J., Li, Q., Feng, Z., Li, Y., Feng, L.: tPredictor: a micro-blog based system for teenagers' stress prediction. In: EDBT, pp. 612–615 (2016)
14. Xue, Y., Li, Q., Zhao, L., Jia, J., Feng, L., Yu, F., Clifton, D.A.: Analysis of teens' chronic stress on micro-blog. In: International Conference on Web Information Systems Engineering, pp. 121–136. Springer, Cham (2016)
15. Li, Q., Zhao, L., Xue, Y., Jin, L., Alli, M., Feng, L.: Correlating stressor events for social network based adolescent stress prediction. In: International Conference on Database Systems for Advanced Applications, pp. 642–658. Springer, Cham (2017)
16. Li, Q., Xue, Y., Zhao, L., Jia, J., Feng, L.: Analyzing and identifying teens' stressful periods and stressor events from a microblog. *IEEE J. Biomed. Health Informat.* **21**(5), 1434–1448 (2017)
17. Li, Q., Zhao, L., Xue, Y., Jin, L., Feng, L.: Exploring the impact of co-experiencing stressor events for teens stress forecasting. In: International Conference on Web Information Systems Engineering, pp. 313–328. Springer, Cham (2017)
18. Xue, Y.: 21. Predicting teens' chronic stress transition patterns from microblog. *J. Faculty Eng.* **32**(12) (2017)
19. Rahman, L., Sarowar, G., Kamal, S.: Teenagers sentiment analysis from social network data. In: Dey, N., Babo, R., Ashour, A., Bhatnagar, V., Bouhlal, M. (eds.) *Social Networks Science: Design, Implementation, Security, and Challenges*. Springer, Cham (2018)
20. Kim, J., et al.: (2019) Sentiment analysis of Korean teenagers' language based on sentiment dictionary construction. In: Hung, J., Yen, N., Hui, L. (eds.) *Frontier Computing. FC 2018. Lecture Notes in Electrical Engineering*, vol. 542. Springer, Singapore (2019)

Load Frequency Control of an Interconnected Multi-source Power System Using Quasi-oppositional Harmony Search Algorithm



Abhishek Saxena and Ravi Shankar

Abstract An effort has been revealed in this paper to develop a novel quasi-oppositional harmony search (QOHS) algorithm-based PID controller for frequency stability in a two-area power system including multiple sources. Both regions with multi-source scheme comprised of a reheat thermal unit and a hydro unit. To make the system effective, physical constraints such as time lag, governor dead band (GDB), boiler dynamics (BD), and generation rate constraints (GRC) are taken into account for thermal and hydro units in frequency stability analysis. For improvement in the ever-changing response of the two-area power system network, a promising attempt has been implied to present an effective and practical approach. With a perspective to minimize the frequency deviation during load perturbation, a peculiar controller is designed. The prominent features of the work are designing a model, simulation, and the optimization employing QOHS algorithm. It is observed that, in the event of load alteration, the nominative frequency regains promptly and productively in contrast with the conventional perspective. The simulation results with applied control technique manifest that the designed two-area power system replica is feasible and the evaluated QOHS optimization technique may be efficacious.

Keywords Load frequency control · Frequency deviation · Interconnected power system

Nomenclature

<i>ACE</i>	Area control error
<i>B</i>	Frequency bias setting (p.u.MW/Hz)
<i>D</i>	Damping coefficient (p.u.MW/Hz)

A. Saxena (✉) · R. Shankar
National Institute of Technology Patna, Patna 800005, India
e-mail: abhishek.ee18@nitp.ac.in

R. Shankar
e-mail: ravi@nitp.ac.in

f	Nominative frequency (Hz)
H	Equivalent inertia constant (sec)
i	Subscript, denotes i th area
K_r	Reheat plant gain
P_{rt}	Rated capacity of the region (MW)
PF_{th}	Participation factors of thermal and hydro units
R_{th}, R_{hyd}	Speed adjustment setting for thermal and hydro plants (Hz/p.u.MW)
T_{12}	Synchronizing coefficient
t_{sim}	Time during simulation (sec)
K_P, K_i & K_d	PID controller gain
T_{gh}	Hydro turbine speed governor time constant (sec)
T_r	Reheat time constant (sec)
T_{rh}	Transient fall time constant of hydro turbine governor (sec)
T_{rs}	Restart time of hydro turbine speed governor (sec)
T_{sg}	Governor time constant of thermal turbine (sec)
T_t	Thermal turbine time constant (sec)
T_w	Starting instant of water in penstock (s)
Δf	Alteration in frequency (Hz)
ΔP_{tie}	Alteration in tie-line power (p.u.MW)

1 Introduction

In the power system network, load frequency control performs a significant contribution. Normally, power inequality between the generation and the power requirement leads to alteration in the frequency, as the requirement of power is continuously varying. Any fluctuation in the power demand may result in frequency deviation. For this reason, perfectly drafted controllers are essential for the settlement of frequency and system stability. Basically, automatic load frequency control supervises the readjustment of the true power generated and its frequency. The foremost intention of load frequency control (LFC) in a power system network is to retain the system frequency and the tie-line power flow not beyond the assigned limit [1, 2]. In case the system frequency is not preserved as per the limit, then it might cause some serious problems such as system collapse, blackouts, and unexpected line tripping. Many researchers so far have suggested numerous control strategies for LFC [3–6]. Research work proposed till now in the area of AGC is thus devoted to persist the system stability. Prior, numerous control action plans were enumerated to resolve the load frequency control issues in the power system network. Application of numerous classical algorithms like genetic algorithm (GA), particle swarm optimization (PSO), and bacterial foraging optimization (BFO) technique so as to optimize the controller gains is thus presented in [7, 8]. Various control actions are thus implied in the literature in view of controller designing. The elegant PI and PID controllers [9, 10] are commonly employed as a result of their simple design. Various controllers

are attaining preference in the frequency control applications. The supremacy of control action in modeling and control design has been motivated for various control applications. Solution to load frequency control problems using distinct controller has been expressed in [11–14].

Recently, the foremost objective of researchers in the field of LFC is to develop a novel approach to retain the system frequency constant, irrespective of varying load demand. From [15–18], it has been found that the research work with multi-source system is in progress. Reference [19] illustrated an adaptive fuzzy logic control mechanism for frequency stabilization. Load frequency control in the interlinked power network using grey wolf optimization is reported in [20]. Multi-area system with multiple sources employing teaching learning-based optimization (TLBO) for sustaining system frequency is conferred in [21]. Frequency settlement employing hybrid bacterial foraging optimization is appropriately discussed in the article [22]. However, harmony search algorithm [23] belongs to the population following optimization methodology that might be employed to deal with frequency monitoring affairs. Shiva and Mukherjee [24] imparted quasi-opposition-based harmony search algorithm in consequence of automatic generation control. All these studies encourage further meticulous research in LFC.

2 System Investigated

The dynamic modeling of a frequency settlement in an intended power network is investigated in this section. Both Area I and Area II of analyzed framework comprise of thermal and hydro units. A simplified transfer function replica of devised interlinked power network is revealed in Fig. 1.

Important distinct constraints namely GDB, BD, and GRC are taken into account in the thermal unit, whereas hydro unit is equipped with GRC for more realistic analysis. In each region, a step loading of 10% change is imposed so as to figure out the dynamic performances of the arrangement. PID controller based on QOHS is employed for the examination of the proposed model.

3 QOHS Optimization Technique

Harmony search algorithm (HSA) is a novel, authentic framework, optimization algorithm. It is influenced by the spontaneity action in hunt of a suitable harmony position. HSA imitate the contrive action related to the artist seek, so as to acquire an excellent level of harmony in music. Firstly, the original population of harmony vectors is arbitrarily constructed and saved in the memory. The optimization stratagem of HSA can be characterized in the following levels:

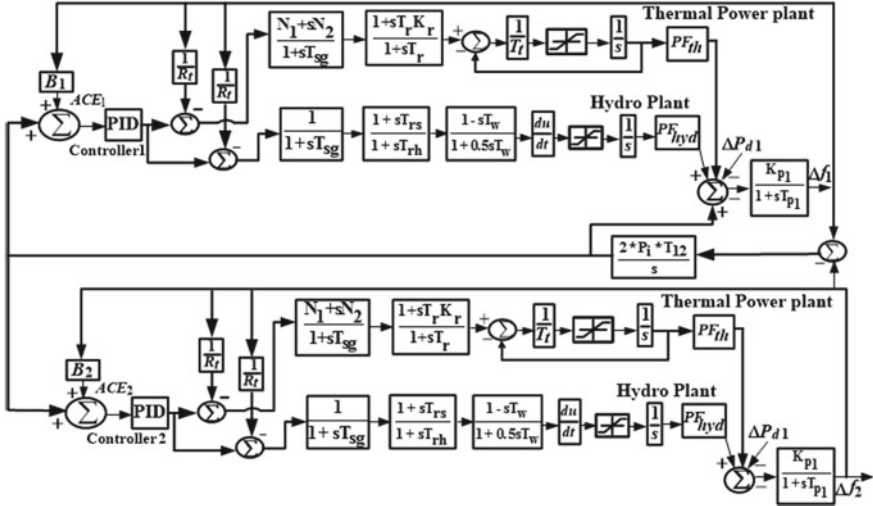


Fig. 1 Simplified transfer function replica of devised interlinked power network framework

Level (i)—Begin: The parameters of the program are assigned, and HM is initialized favoring as many arbitrary induced result vectors in view of the size of harmony.

Level (ii)—Harmony contrive: A unique result vector is formed on memory, tone arrangement, and arbitrary choice.

Level (iii)—Choice: As the stated case is fulfilled, the perfect harmony among the rest is modified. Else, Level (i) and Level (ii) are sequentially replicated.

3.1 QOHS Algorithm

HSA is contrived by applying the quasi-opposition-based idea so as to achieve better accuracy and improve the response. The performance of QOHS is quite elementary, is comfortably realizable, and needs less parameter for the operation.

Quasi-oppositional generation

On the framework concerning jumping probability, after developing latest populace from the operation attributed to algorithm, quasi-opposition-based populace is computed and the suitable HM is preferred from the blend of ongoing populace and the quasi-opposition-based populace. Just as a disparity to quasi-oppositional initiation, it ought to be perceived thereby determine the quasi-opposite populace for generating jumping, the converse of each variant and intermediate terms are vigorously determined. Particularly, the maximal and minimal values of respective variables in

the existing populace have been utilized which enable the calculation of the mid-to-converse extent rather than employing variants. The flowchart of the intended QOHS algorithm is revealed in Fig. 2.

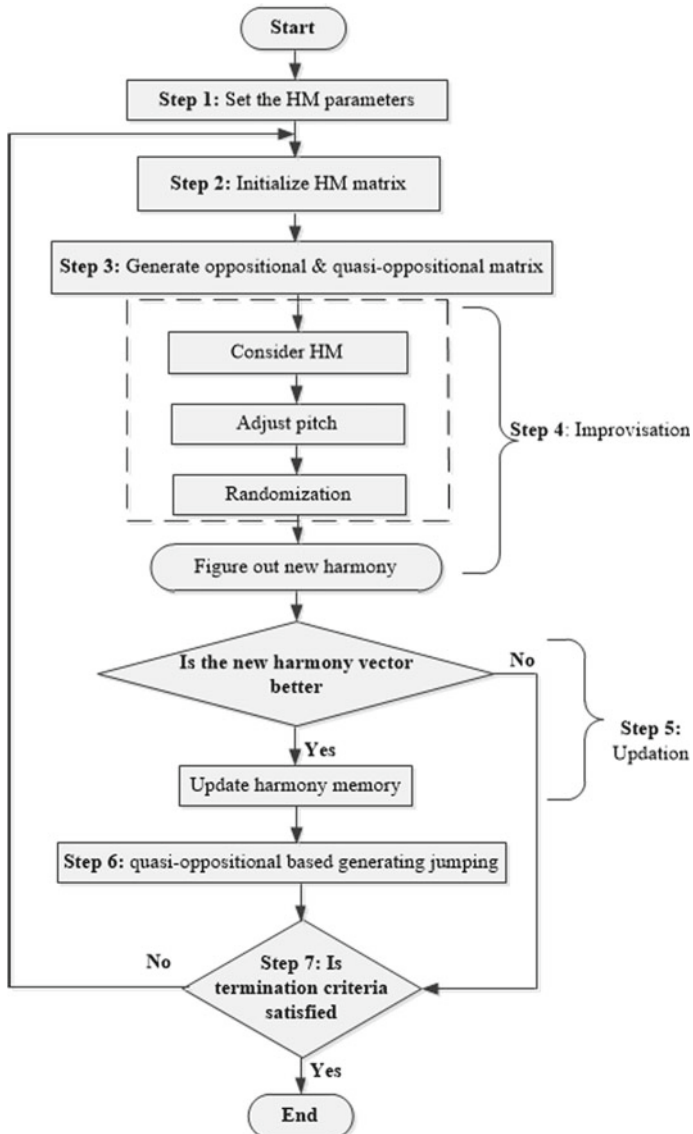


Fig. 2 Flowchart of quasi-oppositional harmony search (QOHS) algorithm

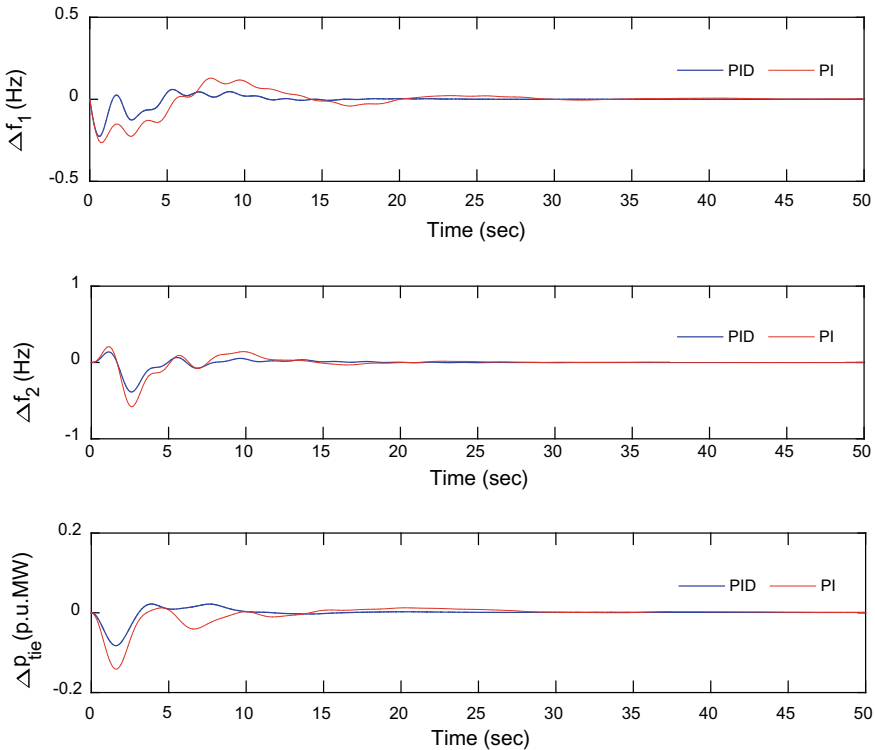


Fig. 3 Dynamic responses acquired from the intended controller compared with the PID controller for the examined two-area system subjected to 10% disturbance

3.2 Simulation Results and Discussion

The simulation results acquired on two-area thermal and hydro systems using QOHS-based PID controller with 10% disruption in each region are revealed in Fig. 3. The analysis of the present work is demonstrated in Table 1.

4 Conclusion

A robust PID controller is designed using quasi-oppositional harmony search (QOHS) algorithm-based optimization mechanism in favor of the intended system. The outcome of the drafted controller for sustaining frequency deviation due to dynamic fluctuation in the load was analyzed for the two-area power network incorporating hydro and thermal units in the respective region. System constraints such as GDB, BD, GRC, and time defer are appended in the framework to improvise it more effectively for authentic approach. A productive effort has been created to produce

Table 1 Optimized controller gains using the proposed technique with 10% disturbances in both areas on studied test system model

Controller	K_{P1}	K_{I1}	K_{d1}	N_1	K_{P2}	K_{i2}	K_{d2}	N_2
QOHS-PID	0.5827	0.0789	0.4875	231.04088	1.9119	.0013	0.02393	321.9476

beneficial and novel course of action to intensify the dynamic performance of the implied two-area network. Thus, the designed controller for the proposed system furnished a favorable damping control for the load perturbation. It is examined that this combination of damping controller can be applied to realistic power network model. The simulation result reveals efficient outcomes for the LFC problem utilizing adapted controller. This work may be further enhanced by considering the deregulated framework under multi-area mechanism.

References

1. Kundur, P.: Power System Stability and Control. Mc Graw Hill, New Delhi (1994)
2. Bevrani, H., Hiyama, T.: Robust decentralised PI based LFC design for time delay power systems. *Energy Convers. Manag.* **49**, 193–204 (2008)
3. Nanda, J., Mangla, A., Suri, S.: Some new findings on automatic generation control of an interconnected hydrothermal system with conventional controllers. *IEEE Trans. Energy Convers.* **21**, 187–194 (2006)
4. Abraham, R.J., Das, D., Patra, A.: Automatic generation control of an interconnected power system with capacitive energy storage. *World Acad. Sci. Eng. Technol.* **39**, 711–716 (2009)
5. Nanda, J., Kothari, M.L., Satsangi, P.S.: Automatic generation control of an interconnected power system considering generation rate constraint and governor deadband. *IFAC Proc.* **12**, 239–240 (1979)
6. Ibraheem, A., Kumar, P., Kothari, D.P.: Recent philosophies of automatic generation control strategies in power systems. *IEEE Trans. Power Syst.* **20**, 346–357 (2005)
7. Bhatt, P., Roy, R., Ghoshal, S.P.: GA/particle swarm intelligence based optimization of two specific varieties of controller devices applied to two-area multi-units automatic generation control. *Int. J. Electr. Power Energy Syst.* **32**, 299–310 (2010)
8. Nanda, J., Mishra, S., Saikia, L.C.: Maiden application of bacterial foraging-based optimization technique in multiarea automatic generation control. *IEEE Trans. Power Syst.* **24**, 602–609 (2009)
9. Rout, U.K., Sahu, R.K., Panda, S.: Design and analysis of differential evolution algorithm based automatic generation control for interconnected power system. *Ain Shams Eng. J.* **4**, 409–421 (2013)
10. Sekhar, G.T.C., Sahu, R.K., Panda, S.: Load frequency control with fuzzy-PID controller under restructured environment. In: 2014 International Conference on Control, Instrumentation, Communication and Computational Technologies, ICCICCT 2014, pp. 112–117 (2014)
11. Ismayil, C., Kumar, R.S., Sindhu, T.K.: Automatic generation control of single area thermal power system with fractional order PID ($P^{\alpha}I^{\beta}D^{\mu}$) controllers. In: IFAC (2014)
12. Debbarma, S., Saikia, L.C.: Effect of fractional-order controller on automatic generation control of a multi-area thermal system. *IET Conf. Publ.* **2011**, 223–228 (2011)
13. Delassi, A., Arif, S., Mokrani, L.: Load frequency control problem in interconnected power systems using robust fractional $P^{\alpha}I^{\beta}D^{\mu}$ controller. *Ain Shams Eng. J.* **9**, 77–88 (2018)
14. Debbarma, S., Chandra, L., Sinha, N.: Solution to automatic generation control problem using firefly algorithm optimized $I^{\alpha}D^{\beta}m$ controller. *ISA Trans.* **53**, 358–366 (2014)
15. Mohanty, B., Hota, P.K.: Comparative performance analysis of fruit fly optimisation algorithm for multi-area multisource automatic generation control under deregulated environment. *IET Gener. Transm. Distrib.* **9**, 1845–1855 (2015)
16. Tavakoli, M., Pouresmaeil, E., Adabi, J., Godina, R., Catalão, J.P.S.: Load-frequency control in a multi-source power system connected to wind farms through multi terminal HVDC systems. *Comput. Oper. Res.* **96**, 305–315 (2018)

17. Pradeepthi, P.A., Abhilash, T.: Multi-area load frequency control of power system involving renewable and non-renewable energy sources. 2017 Innov. Power Adv. Comput. Technol. i-PACT 2017. 2017-Janua, 1–5 (2018)
18. Prajapati, P., Parmar, A.: Multi-area load frequency control by various conventional controller using battery energy storage system. 2016 Int. Conf. Energy Effic. Technol. Sustain. ICEETS 2016. 467–472 (2016)
19. Yousef, H.A., Al-Kharusi, K., Albadi, M.H., Hosseinzadeh, N.: Load frequency control of a multi-area power system: an adaptive fuzzy logic approach. IEEE Trans. Power Syst. **29**, 1822–1830 (2014)
20. Guha, D., Roy, P.K., Banerjee, S.: Load frequency control of interconnected power system using grey wolf optimization. Swarm Evol. Comput. **27**, 97–115 (2016)
21. Sahu, B.K., Pati, T.K., Nayak, J.R., Panda, S., Kar, S.K.: A novel hybrid LUS-TLBO optimized fuzzy-PID controller for load frequency control of multi-source power system. Int. J. Electr. Power Energy Syst. **74**, 58–69 (2016)
22. Panwar, A., Sharma, G., Bansal, R.C.: Optimal AGC design for a hybrid power system using hybrid bacteria foraging optimization algorithm. Electr. Power Components Syst. **0**, 1–11 (2019)
23. Geem, Z.W., Kim, J.H., Loganathan, G.V.: A new heuristic optimization algorithm: harmony search. Simulations **76**(2), 60–68 (2001)
24. Shiva, C.K., Mukherjee, V.: Automatic generation control of hydropower systems using a novel quasi-oppositional harmony search algorithm. Electr. Power Components Syst. **44**, 1478–1491 (2016)

An Extensive Investigation of Wavelet-based Denoising Techniques for Various ECG Signals Utilizing Thresholding Function



V. Supraba, P. Nageswara Rao, and M. N. Giriprasad

Abstract Electrocardiogram (ECG) is a graphical interface to evaluate various cardiovascular problems when enabling cardiovascular electrical activity over time. More than 75% of patients in Pakistan were affected with heart problems, but 30–40% of cases of Sudden Cardiac Deaths (SCD) were reported globally of total death. Several investigations have been convoyed to improve ECG denoising confiscation practices, but do not have a deep research on its performance evaluation. In this paper, we provide an extensive investigation of wavelet-based denoising techniques for various ECG signals utilizing thresholding function. The simulation is carried out using a Matlab by checking SNR and MSE. In this process, the noisy ECG signal taken before the denoising process is performed. This process studies four types of denoising techniques and proposed a hybrid function thresholding technique as a better technique with an SNR value of 29.62 dB and a value of 37.51 MSE.

Keywords Denoising wavelet transform · Thresholding technique · Mixed function · ECG signal

1 Introduction

Sudden Cardiovascular Death (SCD) is a sudden fire of heart function, which has cardiac electro physical abnormalities [1] with severe consequences. About 17 million deaths worldwide have contributed to the disease, with 30% deaths every year. The survival rate in the United States is less than 1% [2]. Although it is less than 5% worldwide for cardiac arrest victims, ECF problem intensity is a research goal for risk stagnation using qualitative electrocardiographically indicators. Alternative

V. Supraba (✉)

Ravidra College of Engineering for Women, Kurnool, India

e-mail: vsupraba@recw.ac.in

P. Nageswara Rao

Vardhaman College of Enginnering, Hyderabad, India

M. N. Giriprasad

JNTU College of Engineering, Anantapur, India

© Springer Nature Singapore Pte Ltd. 2020

433

M. Pant et al. (eds.), *Soft Computing: Theories and Applications*,

Advances in Intelligent Systems and Computing 1154,

https://doi.org/10.1007/978-981-15-4032-5_40

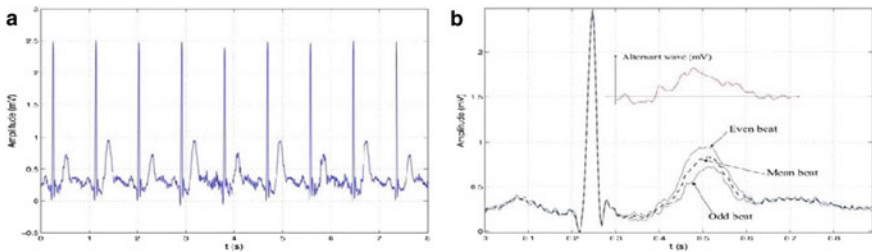


Fig. 1 ECG TWA depiction: **a** ECG signal with TWA, **b** two consecutive ECG beats superimposed to show variation amplitude (adopted from [5])

Resistance T-Wave (TWA) is considered a risk of stratification indicators found in the surface ECG for heart muscle contraction at MSC. Every single alternating ECG examined by the children in TWA is a phenomenon related to the duration and frequency of the waveform in the observable beat ST-T section. ECG is required for the specification. In addition, the alternate size depends on the heart rate and 105 ± 15 beats per minute [3] is expressed by a higher heart rate compared to what the patient has to do (Fig. 1).

Since 2000, many noise-resistant systems have been introduced but improved to improve noise reduction performance.

In 2001, the author investigated in [4] contrasted with different wavelet-based denoising systems for ECG signals. The examination comprises of four noise removal techniques, which precisely evaluate several methods called Visure, soft thresholding and Vanpic-Chervonenkis (VC). Among the given methods, VC performs optimized results.

In 2012, the author explored on wavelet-based thresholding strategies with various wavelet bases. Therefore, the assortment of coif5 and the ringsure methods offer an effective result in removing noise in ECG signals.

In another investigation, a few soft thresholding procedures were considered with ringing, universal routes and minimax. From the abovementioned methods, it proves that the ring method is better than all other techniques [5].

From the above literature, we distinguish the several noise removal techniques, i.e., soft and hard thresholding techniques, and similarly Smoothly Clipped Absolute Deviation thresholding technique (SCAD), proposed mixed function thresholding technique with metrics include Signal-to-Noise Ratio (SNR) and Mean Square Error (MSE) values.

2 Related Works

2.1 ECG Signal, Noise and Wavelet Transform

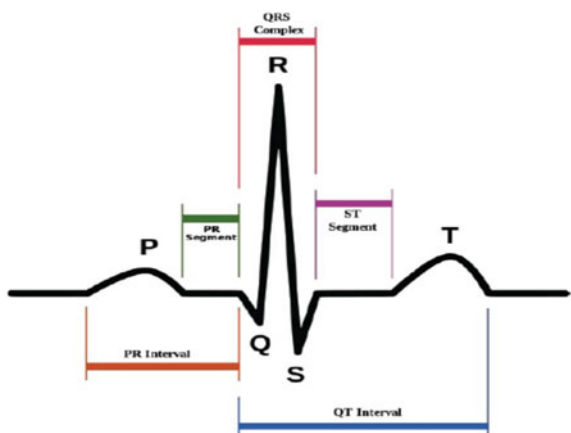
Electrocardiogram (ECG) signals are used to identify cardiovascular diseases. This is not an easy issue for the patient's analysis of the patient's body or analysis due to the lack of ECG signals and the incomplete coincidence of transport noise measurement electrodes. The characteristic of this noise is that a random noise or white noise is uniformly distributed.

Here, we should consider the representations of ECG signals tape, which is shown in Fig. 2, where the signal is arranged into four sections [6], which are depicted here, i.e. Muscle contractions of the atrium generate P waves as an outcome. These waves are small in comparison with thin artinal muscle and also replicates artinal depolarized conditions. An ECG signal is usually labelled with the letters P, Q, R, S and T which implies its critical points as shown in Fig. 1. Waves of QRS, that are affected by thick ventricular muscle shrinkage, consist of three different waves, i.e. Q wave, the R wave and S wave. Usually, T waves arise when the ventricular muscle arrives in the repolarized state.

Most of the ECG signals are affected alike in biomedical signals. Moreover, these noises are not represented by the signal heart reality. The process to reduce or remove the noise from the ECG signal uses the discreet wavelet transformation. This technique acts as a noisy bank that separates the QRS region part which consists of sharp amplitude change, which are found in the QRS waves, which are tainted with the noises that are positioned in P and T waves.

In the ECG signal, the wavelet transform produces an internal noise that crafts a numerical coefficient. You can reduce or remove the noise by eliminating unsolicited coefficients. The omission process can be managed by the wavelet thresholding method [7].

Fig. 2 An instance of ECG wave



2.2 Thresholding

The major process in the greeting of electromagnetic signals is to make noticeable to the human observer certain features of the incoming signals which are noise affected or not that exploit the characteristics of the denoising signal [8]. These technique assistances in decreasing the effected noise by adjusting the coefficient value which is less than the threshold value. Essentially, wavelet thresholding is considered into two methods called hard and soft thresholding method.

Donoho's universal threshold was proposed in 1994; to describe the limit value in the soft Threshold method, the Threshold value (T_h) is defined according to the soft threshold. These thresholds are most often used by professionals for noise reduction signals. Here, we confirm the comparative results of the noisy signal with the hard and soft thresholding shown in Fig. 3 [9].

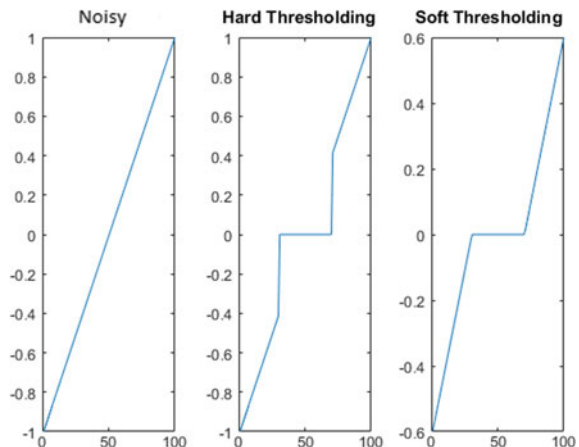
Hard Thresholding. Generally, coefficients that are lower than the threshold for a Hard Threshold value are set to zero, and the value that exceeds the threshold is set to one. This method is expressed as [8]:

$$h(x) = \begin{cases} x, & \text{if } |x| \geq T_h \\ 0, & \text{otherwise} \end{cases} \quad (1)$$

Soft Thresholding. The soft threshold value is also called a wavelet reduction, as the values of positive and negative coefficients are “reduced” to zero. Let n be the vector x in the algorithm of the threshold method. This method is performed according to the following formula [8]:

$$s(x) = \begin{cases} [\text{sign}(x)](|x| - t), & \text{if } |x| \geq T_h \\ 0, & \text{otherwise} \end{cases} \quad (2)$$

Fig. 3 Comparison between noisy signal and its hard thresholding and soft thresholding results



SCAD Thresholding. Smoothly Clipped Absolute Deviation (SCAD) which is represented by $\text{SCAD}(q, T_h)$ and mathematically represent as

$$\text{SCAD}(q, T_h) = \begin{cases} \text{sign}(q)\max(0, |q| - T_h) & \text{if } |q| \leq 2T_h \\ (\alpha - 1)q - \alpha T_h \text{ sign}(q) & \text{if } 2T_h \leq |q| < \alpha T_h \\ q \text{ if } |q| > \alpha T_h \end{cases} \quad (3)$$

2.3 Metrics

Smoothly C. In this section, we need to consider the performance of the several wavelet thresholding techniques for which denoising will be evaluated using Signal-to-Noise Ratio (SNR) and Mean Square Error (MSE). ECG signals denoising performance will be evaluated by the abovementioned metrics.

Signal-to-Noise Ratio (SNR). Signal-to-Noise Ratio (SNR) [8] is the quality indicator for noise signals. The SNR is calculated according to the following formula

$$\text{SNR} = 10 \log_{10} \frac{\sum_{n=0}^{N-1} X(n)^2}{\left(X(n) - \overline{X(n)}\right)^2} \quad (4)$$

The value $X(n)$ represents the clean signal and $\overline{X(n)}$ indicates the signal after the denoising process. The SNR directs the ratio of signal power to noise power. Higher value of SNR shows that denoising signal performing well.

Mean Square Error (MSE). Mean Square Error (MSE) is an additional method to assess the transformation among actual and predicted data. MSE is computed using the following formula [8]:

$$\text{MSE} = \frac{1}{N} \sum_{n=0}^{N-1} \left(X(n) - \overline{X(n)}\right)^2 \quad (5)$$

3 Thresholding Rules

Among several thresholding rules, here we have deliberated the Visu rule for assessing the threshold value.

3.1 Visu Rule

Donoho and Johnston have developed Visu rule; it provides Universal thresholding rule. It doesn't depend on any selected thresholding functions, which is represented mathematically as

$$T_h = \sigma \sqrt{2 \log(n)} \quad (6)$$

where n is length of the signal, σ is the standard deviation and T_h is the threshold value [10].

4 Proposed New Mixed Function

A new hybrid function has been proposed to reduce the received signal noise, taking into account it is a hybrid function that includes Hard and Garrote functions.

Taking into account the above thresholding rule, a new hybrid function is proposed to reduce the noise signal received. This is a club of Hard and Garrote functions. Finally, the entire calculation process was performed by calculating the average function of the Hard function and Garrote function for lower levels, with the result obtained, which represents the value of 20% of the input coefficient. The proposed hybrid function is called mathematically, as shown in Eq. (7) (Fig. 4).

$$\begin{aligned} S(x, T_h) &= \left(x - \frac{T_h^2}{x} \right) + x \quad \text{For all } |x| > T_h \\ &= (0.2)^* x \quad \text{otherwise} \end{aligned} \quad (7)$$

Fig. 4 Waveform of mixed function

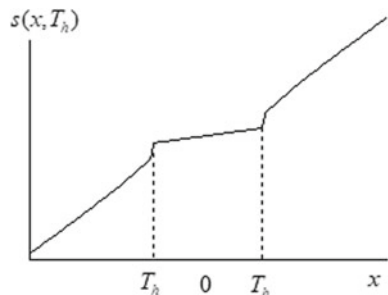


Table 1 Practical results on four wavelet techniques

ECG signals	Hard thresholding		Soft thresholding		SCAD thresholding		Proposed hybrid function	
	SNR	MSE	SNR	MSE	SNR	MSE	SNR	MSE
1	24.55	37.13	19.4	121.45	20.83	140.41	25.82	34.38
2	26.28	35.75	20.34	124.92	21.35	138.92	26.9	35.49
3	30.03	33.26	24.05	126.44	26.26	144.63	29.78	39.52
4	31.4	53.19	27.22	150.63	28.97	153.81	32.15	40.75
5	32.7	44.05	28.09	128.17	30.76	130.89	33.47	37.43
Average	28.99	40.68	23.82	130.32	25.63	141.73	29.62	37.51

5 Methodology

5.1 Practical Design

We have been presented our practical design performance deploying by four denoising techniques, i.e. soft thresholding, hard thresholding, SCAD thresholding and hybrid function thresholding as follows:

Noisy ECG signal. Computation process starts, the signals are captured from the ECG-ID database having noisy and contain both high- and low-frequency noise signals, which are defined in Table 1.

Simulating denoising techniques in Matlab. Following steps are mentioned in denoising techniques in Matlab simulation

1. Signal decomposition: here each and every signal has been separated into parts that are deploying by wavelet basis Daubechies in level 4 of decomposition.
2. Setting thresholding value: while in setting our proposed research, we have been concentrated on four major pillars of threshold techniques: such as hard thresholding, soft thresholding, SCAD thresholding and hybrid function thresholding. For every technique, came up with particular parameter with many times.
3. Signal reconstruction: at this stage, the denoised signal will be performed. Later comparing the resultant signals with the effectiveness of the denoising techniques.

5.2 Simulation Parameters

In this simulation, we used the input as noisy signals and wavelet bases used in the noise reduction process, decay levels and threshold values. These signals come from an authentic source, namely the ECG-ID databases.

The wavelet bases are used to execute the threshold trigger for each signal. In our experiment, we used a four-level distribution for each signal to apply a noise

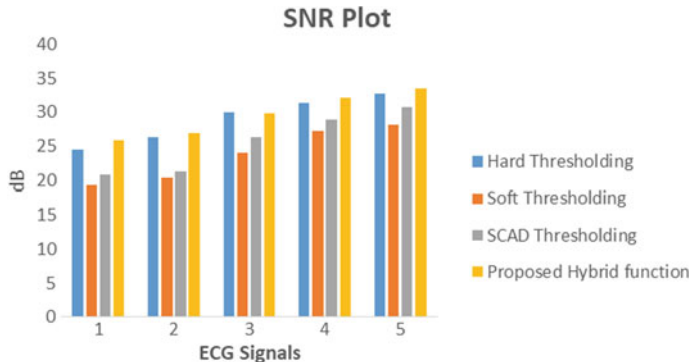


Fig. 5 SNR plot for varied thresholding techniques

reduction technique. To get the optimal threshold for the hard and soft threshold method, we experimented with nine values ranging from 0.1 to 0.9 (degrees 0.1). Our experience shows the value of 0.1 as the optimal value.

6 Practical Results

From the above simulation results, continuous experiments are calculated to measure SNR and MSE values using the simulation as shown in Sect. 3.1. The parameters are mentioned in the paragraph. The results of our study are summarized in Table 1.

From Table 1, it is concluded that our proposed threshold method provides useful results. The SNR of the method has the highest value and the MSE is the lowest average in comparison with other methods, i.e. 29.62 dB and 37.51 MSE, respectively. At the same time, the worst-case threshold for the soft threshold method is SNR of 23.82 dB and MSE is 130.32. The table also shows that the signal-to-noise ratio increases from signal 101 to 123. At this point, the MSE value is usually continuous from signal 101 to 123. Figures 5 and 6 illustrate situations.

Figures 7 and 8 indicate two settings of ECG signals, i.e. noisy signal and denoised ECG signal. From the above section, our proposed hybrid function thresholding performs better in denoising the ECG signal likened with the other three wavelet techniques. The result of the proposed work has been presented in Fig. 8.

7 Conclusion and Future Works

In this article, we looked at the performance of various wavelet-based denoising techniques. A new hybrid function is proposed to reduce the noise signal received, taking into account the threshold value, this is a combination of Hard and Garrote's

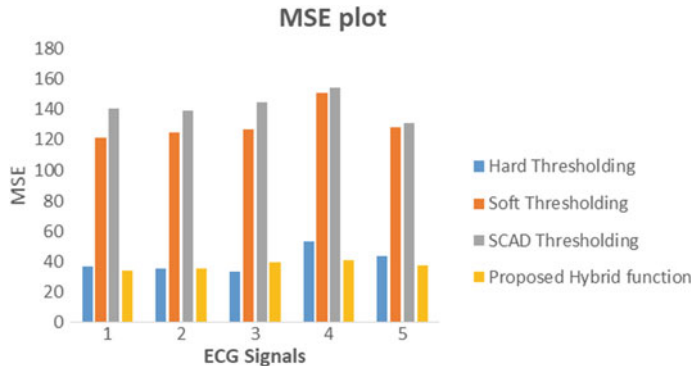


Fig. 6 MSE plot for dissimilar thresholding techniques

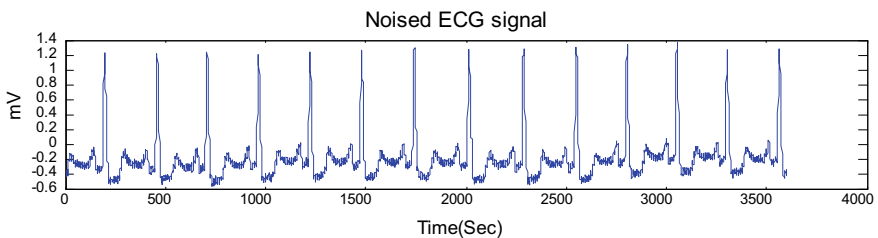


Fig. 7 Noisy ECG signal

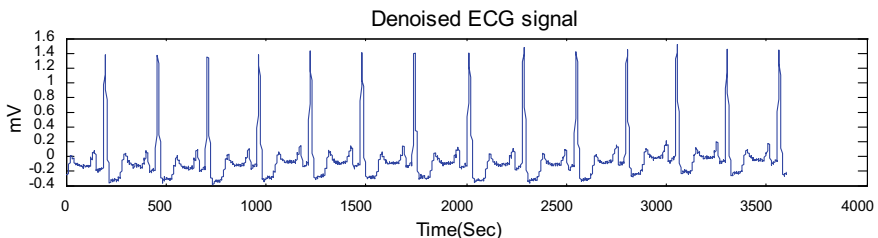


Fig. 8 Denoised signal using hybrid function thresholding

features. This is done by calculating the Mean of Hard and the Garrote function at lower levels. As a result, the optimal performance is obtained with the proposed hybrid function threshold.

References

1. Adabag, A.S., Luepker, R.V., Roger, V.L., Gersh, B.J.: Sudden cardiac death: epidemiology and risk factors. *Nat. Rev. Cardiol.* **7**(4), 216–225 (2010)
2. Mehra, R.: Global public health problem of sudden cardiac death. *J. Electrocardiol.* **40**(6 Suppl), 118–122 (2007)
3. Laguna, P., Cortés, J.P.M., Pueyo, E.: Techniques for ventricular repolarization instability assessment from the ECG. *Proc. IEEE* **104**(2), 392–415 (2016)
4. Cherkassky, V., Kilts, S.: Myopotential denoising of ECG signals using wavelet thresholding methods. *Neural Netw.* **14**(8), 1129–1137 (2001)
5. Joy, J., Peter, S., John, N.: Denoising using soft thresholding. *Int. J. Adv. Res. Electr. Electron. Instr. Eng.* **2**(3), 1027–1032 (2013)
6. Jaenal Arifn, S.T.: Mempelajari Eletrokardigrafi [Online] 2014. [Cited: February 19, 2016]. <http://jaenal.dosen.st3telkom.ac.id/category/elektro-medis/>
7. Karthikeyan, P., Murugappan, M., Yaacob, S.: ECG signal denoising using wavelet thresholding techniques in human stress assessment. *Int. J. Electr. Eng. Inf.* **4**(2), 306 (2012)
8. Awal, M.A.,et al.: An adaptive level dependent wavelet thresholding for ECG denoising. *Biocybern. Biomed. Eng.* **34**(4), 238–249 (2014)
9. Math Works. Denoising Signals and Images [Online]. [Cited: January 1, 2007]. <https://www.mathworks.com/help/wavelet/examples/denoising-signals-and-images.html>
10. Om, H., Biswas, M.: An improved image denoising method based on wavelet thresholding. *J. Signal Inf. Process.* **3**, 109–116 (2012)

Effect of Noise on Segmentation Evaluation Parameters



V. Vijaya Kishore and V. Kalpana

Abstract Lung cancer is the killing disease that maximum vertexes due to drugs, smoking chewing of tobacco. The affliction of this disease is 14% than any other neoplasm, curtailing the functioning and existence of the diseased by 14 years. The overall relative survival rate is less than 18%. Early diagnosis of lung abnormality is a key challenge to improve the survival rates. Identification of malignant nodules from the medical image is a critical task as the image may contain noise during the processing that can be unseen and also having similar intensities of unwanted tissue thickening. This may debase the image standard and lead to wrong predictions. To process and reconstruct a medical image noise is to be eliminated. To exactly diagnose the disease, image is to be properly segmented from the other regions as to identify the lesions. Accuracy of ROI identification depends on the selection of segmentation operators. In this paper the performance of reconstruction is evaluated by using morphological operations and segmentation filters in noisy environment. The analysis is done between the original extracted ROI and noise image based on the evaluation parameters, Global Consistency Error (GCE) and Variation of Information (VOI). The best suitable operator can be used to obtain the ROI which can help for early diagnosis of the disease so as to control the cancer incidence and mortality rates.

Keywords Lung cancer · Nodules · Reconstruction · Morphology · Noise · GCE · VOI

V. Vijaya Kishore ()

Department of ECE, G. Pullaiah College of Engineering & Technology, Kurnool, India
e-mail: kishiee@rediffmail.com

V. Kalpana

Department of ECE, Sree Vidyanikethan Engineering College, Tirupathi, India
e-mail: ksh.v1227@gmail.com

1 Introduction

Lung cancer is cited as a genus of metastasis detailed in lungs. From critical examinations these diseases are characterized into several types based on their disposition and the patterns disparities. Preferable knowledge of the disease is possible with keen identification of abnormalities originated from the organism or cell [1]. Wide range of health survey reports and statistical samples revealed lung cancer to be Non-small cell carcinomas and small cell carcinoma. Aggregately, lung tumors are discerned and ranked as adenocarcinoma leading to maximum malignancy succeeded by transitional and squamous cell carcinomas and rearmost with large cell carcinoma [2]. Paramount genesis of the disorder is due to drug or tobacco consumption attributing to annual mortality of 84% in men and 76% in women. For examining the abnormalities several medical modalities like MRI, CT, US and DICOM exists among which DICOM (Digital Imaging and Communication in Medicine) standard is the bachelor of visualization of contemporary images. Corroboration and prognosis of the tumor pivots on the identification of malignant lumps. Distinguishing the mass or nodule is highly complicated due to their unpredictable size and structure [3]. Image segmentation algorithms have the capability to discern the emanated cell or tissue growth based on the mensuration of magnitude, expansion, structure and appearance of mass. Any form of medical renderings and renditions assimilates structural frontiers with tenebrosity of other organs or muscles that is contemplated as untoward commotion. For this reason, it is recalcitrant to notify the intractable patterns throughout the reconstruction of image from obscured environment [4]. As a result it is imperative to treatise the renditions of varied pre-processing filtrate techniques using morphology for the available medical information getting prone to different noises.

2 Literature Survey

Segmentation and processing of medical images is done by improvising the dissimilarities and obtaining the attributes of the image. Accomplishing fusion segmentation procedures which simultaneously senses the abnormalities on a database of 150 scans from different sources with high ability and less evaluation was presented by Bram van Ginneken and van Rikxort [5, 6]. Medical image segmentation and 3d reconstruction uses conventional edge detection algorithms like gradient based and template based. These conventional techniques fail when concerned to recognize the verges of the image with noise. Li dong zhang and Du yan bi, V. Kalpana and V. Vijaya kishore presented mathematical based morphological algorithms acquire more efficiency for medical image denoising [6]. The detailing of original image and coherence image has the effect of noise during processing. Preference of morphological structuring element in medical image edge detection obtains accurate consistency and quality of the image. Generally the round shaped structuring element is used with a size

of 3×3 . Morphological edge detection algorithms are complex for computation of noise smoothing and edge orientations. V. V. Kishore and Satyanarayana proposed mathematical morphological algorithms that detects lung CT medical image with improved edge reconstruction and by suppressing noise by significantly preserving the edges of the desired image [7]. Extraction of homogenous region contours in a digital image requires lot of attention. Operators that are long-established work with HF elements while smoothing removes the constituents of these frequencies affecting the contour traits that degrade the estimation of dissimilar extremities. Evaluation of edge detection performance is done by subjective and objective methods. This performance helps to achieve high quality images as defined by visual perception [7, 8]. Morphological explorations situate abnormal aggregate cells of minuscule orb in the lung area. This perusal of nodules is the regions of maximum concentration. Extrication of texture features is done by morphological reconstruction operators like opening and closing followed by opening of closing. The conclusions of morphological based reconstruction depend on the spherical, non-spherical and non-flat shaped probes over the image. The appearance of the image after reconstruction is relinquished by the associated features of the image having the noticeable characteristics of another image representation involving the two images [7, 9].

3 Lung Cancer

Lung cancer causes more deaths than any other cancer. Cancers are caused by life style or diet conditions. According to five year cancer survival rates, 99% for prostate cancer, 89% for breast cancer but only 16% for lung cancer. Lung cancer is taking away lives as 18% that never smoked, 21% that currently smoke and 61% of former smokers [9]. Lung cancer initiates internally as anomalous cells thrive and frequently spread to other body parts. Cancer that erupted in lungs is denominated as primary lung cancer or carcinomas derived from epithelial cells. Early diagnosis of the tumor or the abnormality can stop the metastasis not to affect the surrounding organs like brain, bones, lymph nodes, adrenal glands and liver. The metastasis process is affecting the other organs is shown in Fig. 1.

Lung cancer may be due to many causes like external environmental factors, cumulative combination of exposures to tobacco smoke, asbestos, random gas or other air pollutions. Lung cancer may develop from more than 20 different types of tumors or mixed tumors with more than one epitome of carcinoma [10]. Concomitant to the facts, 1.59 million deaths i.e. 87% of lung cancer caused because of tobacco consumption and 3.2 million deaths are due to air pollution. The ingestion of tobacco is the highest menace aspect of lung cancer as tobacco smoke has 7000 toxic chemicals out of which 70 are poisonous. Early deaths are seemed in smokers than non-smokers with a comparative rate of 24%. Lung cancer is differentiated with four stages; stage 1 denotes cancerous cells are only in lungs. If the uncontrolled malignant cells have possibly spread to lymph nodes it may be considered as stage 2 or 3 and if cancerous cells have spread to other organs then it is stage 4 [11]. Two predominant types of

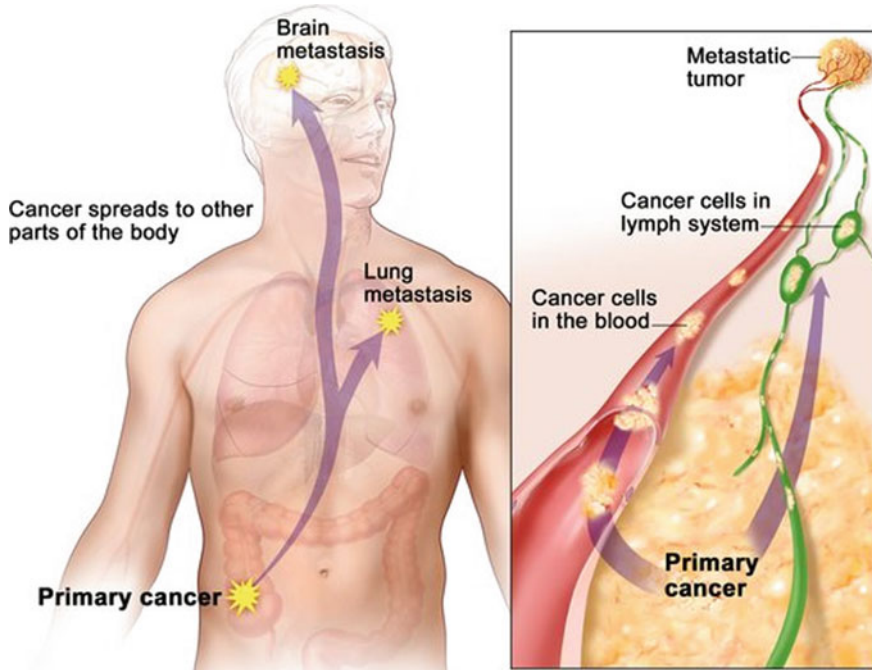


Fig. 1 Metastasis process

lung cancers are non-small cell lung cancers and small cell lung cancer. Cancers due to diminutive cells are only 15% but generous cell lung cancers are over the range as squamous cell carcinoma (30%), adenocarcinoma (40%) and large cell carcinoma (15%). Adenocarcinoma is often found in non smokers and appears at the edge of the lung. There is a chance of adenocarcinoma entering the chest lining forming fluids in the chest cavity and may spread early to other body parts. Squamous carcinoma is associated to those who imbibe cigarette. These inflammations are found in mucous membrane, body cavities and respiratory passages that channel the bronchi. Eventually these tumors can spread beyond bronchi signing coughing up blood. Large cell carcinoma is sporadic category of lung abnormality due to generous cells that grows quickly spreads early. Tumors are less than 1-1/2 inches. The development of tumor in a normal cell is shown in Fig. 2.

Improved sensitivity and specificity across the diagnosis depends on scans. Early detection of these tumors can help the survival rates. These tumors can form as mass which is termed as malignant nodules [12]. Swelling of cells in lungs is agnized in it with a thickness and depth not much greater than 3 cm and when it is greater considered as mass likely to be cancerous. The complexity lies in recognizing pulmonary aberrations from definite patterns because of their commensurate properties and has heterogeneous demeanours like orbicular, horizontal or may be featureless. Nodules endure at the intramural membrane precisely at the boundaries. Revelation of these

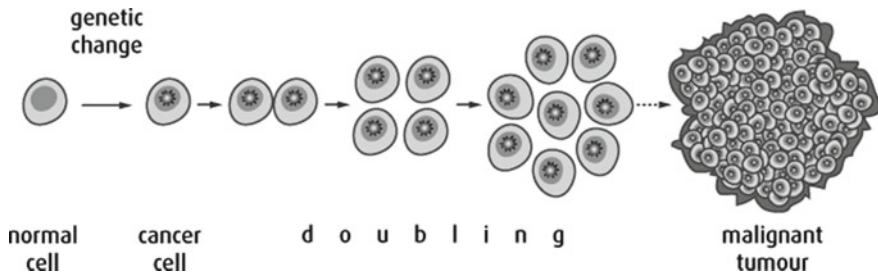


Fig. 2 Normal cell developing into tumour

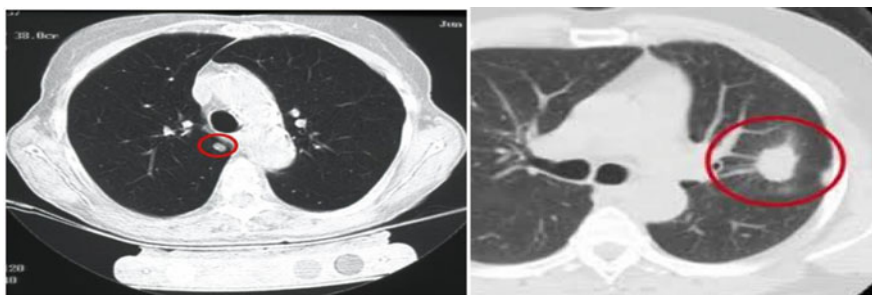


Fig. 3 Representation of CT Lung nodules

nodules has a sizeable impact to mitigate extermination of lung [6, 7]. Figure 3 shows the lung nodule from a CT scan image. Initial evaluation of lung cancer is possible by chest X-rays, CT scan and PET scans but some metastases are visible by CT scan only. Early detection of lung cancer can avoid the disproportionate high prevalence and mortality of advanced abnormalities.

4 Reconstruction of Nodules

For the reconstruction of nodules, the medical image DICOM is to be extracted with ROI of the lung. DICOM yields the counterpart of medical formats, accumulates and stockpiles, apportions and transfers to any kind of contraption regardless of accession, processor or modal quality [13]. DICOM ascends the appearance excellently and emancipates 2D tomographic images for post processing and to describe the original specifications. Noise is contemplated as unfavorable gen that falsifies and declines the image standard. It is a disagreeable quantity which is difficult to remove. Noise in a digital image eventuates in the course of image acquisition, collection, coding, conveyance and it's processing. Files or delineation (images) pretentious to variant noise codifications will always produce erratic unaccustomed information [6].

Image noise, which is termed as electronic noise sometimes is unplanned imbalance of image in its brightness or shade. It is created from scanners, digital equipments and electronic circuits and conceals the actual signal [8]. Image processing strategies involve techniques of imposing noise on image by means of refined methods. The duplication of original image with noise will identify the defiance of the image while getting processed through different noise filters. This corruption and identification helps in the medical image processing for diagnosis [12]. **Gaussian noise** is alluded as additive noise that unfurls unduly in frequency domain and impacts appearance of the image rapidly. **Poisson Noise** known as photon noise is because of undetermined light variations produced from equipments while recovering the image during their reproduction. Divulging and maintaining the data concerns electron emission with the effect of average poison distribution [13]. **Detector Noise** arises from unconnected actuality of energy conveyance. This is a zero mean normal distribution that reports difference of value from its mean. **Speckle Noise** is specified as data ceased due to transmission inexactitudes. It is unspecified, unknown and ascertain [14]. The repeated occurrence of pixels changes the illumination of the image making it appear as white flakes on image. It is also known as texture. **Salt & Pepper Noise** is considered as error when two or more images are transmitted at same rate and time. Image intensities that are least and high are grouped so that they appear in the pattern of salt and pepper. The magnitude of pepper noise is proximate to 0 and for salt is 225 [15, 16].

To extract the clear ROI even during processing, the image is artificially subjected to noise not to misinterpret the analysis [17]. Image is superimposed with unlike noises to determine the aptness of desperate filters during reconstruction. In this paper the DICOM image is added with Speckle noise, Poisson noise, Gaussian noise and salt & pepper noise to extract the lung ROI. Image can be perused once it is cleaved from the other parts of the body. Segmenting is broached as severance of digital image into multifarious portions. The principal involvement of this process is to elucidate the renditions of image in an uncomplicated comprehend fashion in terms of image shade, mien, extremity and magnitude [14]. By using the segmentation method extraction of image in noise environment may detect the contours and also noise. So morphological methods and watershed transform are used to eliminate the noise and extract the exact ROI intended for the reconstruction of nodules. Morphological interpretations are non-sequential transfigurations to revamp the shape, quality and attributes of the representation obliterating the extraneousness [18]. The processes and operations used in this work refine the computations than the conventional techniques and also evade the hindrances. Discovering the extremities using morphology methods prefer systemic component and rudimentary principles of structural relations that incorporates connection, inception, abrasion and distending of image. Unaccepted lineation's that arise during the detection of outlines are exhibited as ridges. Sectioning of image using watershed procedure expects ridge lines and exerts productively for both indistinct and bright specifications [19, 20].

5 Methodology

- Step 1: Take the true lung CT DICOM image.
- Step 2: Prepend four different Noises to the actual image.
- Step 3: undergo the image with Pre-processing filters.
- Step 4: Procure gradients for the image.
- Step 5: perform reconstruction using Morphology
- Image is applied with structuring element with a defined size and shape.
 - Morphological interpretations like opening, closing followed by compliment are implemented.
 - Reconstruction process is completed to extricate the real data.
- Step 6: Evaluate the implementation procedure by using Global consistency error and Variation of information between the image taken in Step 1 and Step 5.

6 Results and Evaluation

Edge detecting filters like Sobel, Gaussian, Average, Laplacian, LoG, unsharp and Prewitt are guesstimated for DICOM lung image followed with and without noise in the reconstruction of nodules. DICOM lung image is corrupted with Speckle noise, Poisson noise, Gaussian noise and Salt & pepper noise at the earliest and the ROI is detected using the preprocessing filters.

The performance of reconstruction process for different filters with Speckle noise, Poisson noise, Gaussian noise and salt & pepper noise is validated using the parameter Global Consistency Error (GCE) and Variation of Information (VOI). GCE brings the refinement of image ROI between the original ROI and noise extracted ROI. VOI characterizes the distance between the original ROI and noise extracted ROI and quantifies the changes. ROI extracted original image is taken as ground truth image. A sample figure for extraction of nodules with Speckle noise, Poisson noise, Gaussian noise and salt & pepper noise is considered with the methods Sobel, Gaussian, Average, Laplacian, LoG, Unsharp and Prewitt is illustrated in the Figs. 4a–g, 5a–g, 6a–g, and 7a–g. The evaluation of GCE and VOI for nodules extraction in noise environment using different filters is shown in Tables 1 and 2.

7 Conclusion and Future Scope

Early detection of tumors can be possible by significant screening using ameliorate modalities and suggestible approaches. This paper considers DICOM image influenced with Speckle noise, Poisson noise, Gaussian noise and Salt & pepper noise. For diagnosing the abnormality in noise environment and to analyze the best suitable

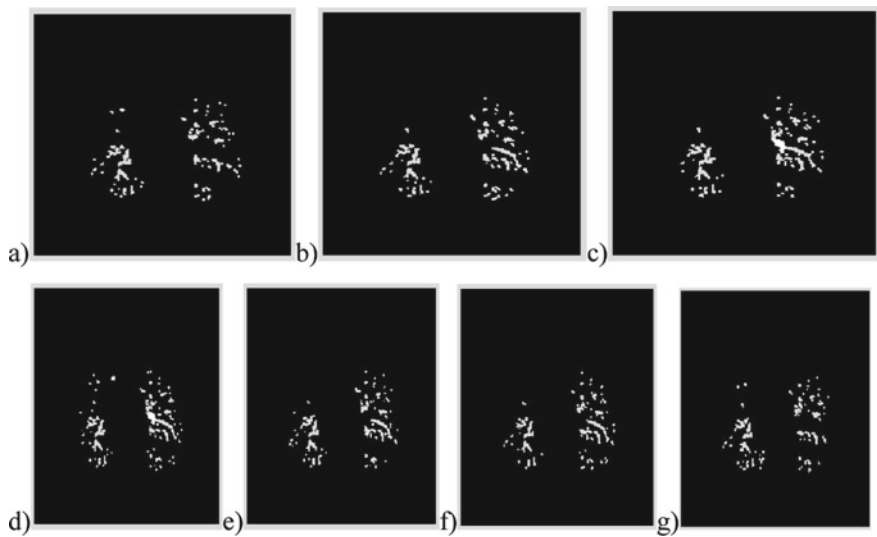


Fig. 4 Nodule reconstruction with overlap of ROI with Gaussian noise extracted ROI using filters
a Sobel b Gaussian c Average d Laplacian e LoG f Prewitt and g Unsharp

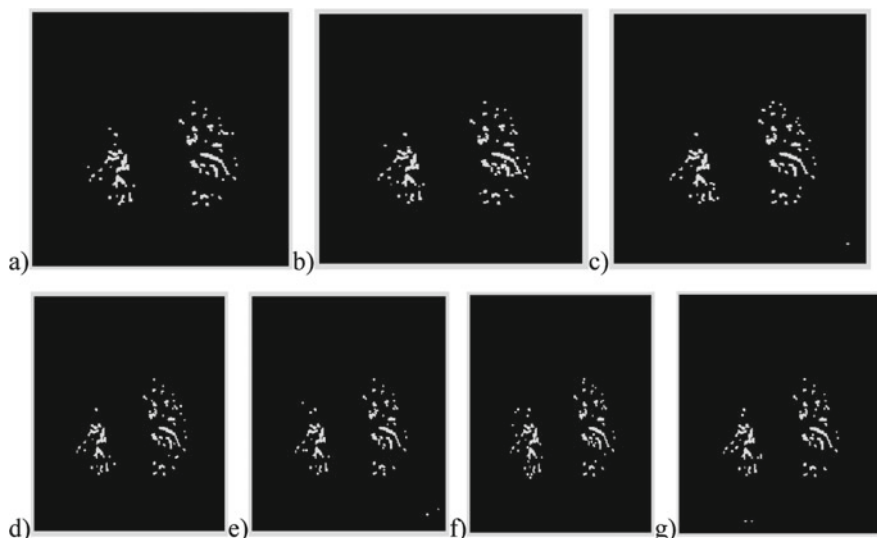


Fig. 5 Nodule reconstruction with overlap of ROI with Salt and pepper noise extracted ROI using filters
a Sobel b Gaussian c Average d Laplacian e LoG f Prewitt and g Unsharp

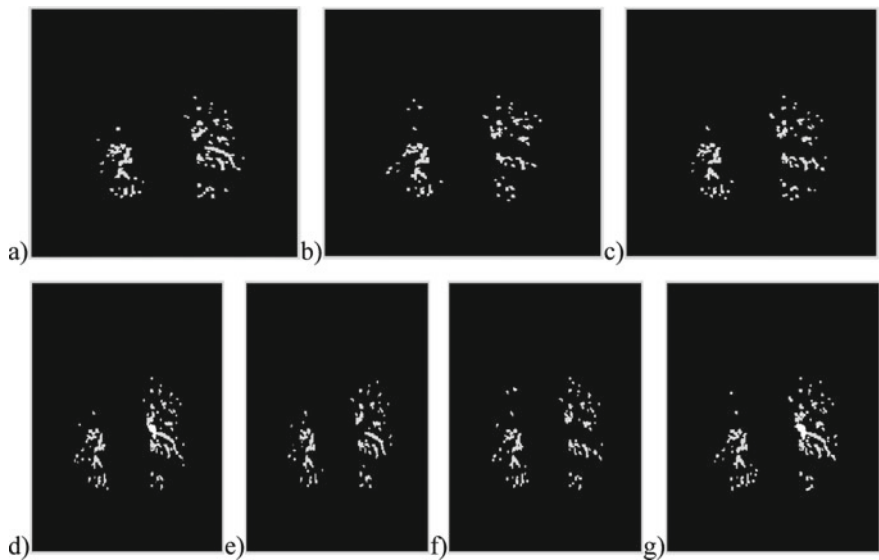


Fig. 6 Nodule reconstruction with overlap of ROI with Speckle noise extracted ROI using filters
a Sobel **b** Gaussian **c** Average **d** Laplacian **e** LoG **f** Prewitt and **g** Unsharp

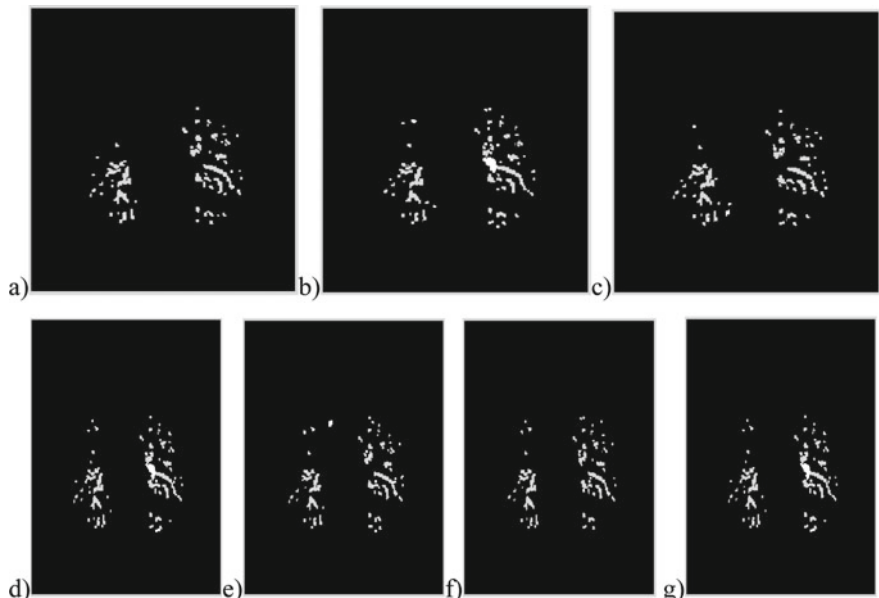


Fig. 7 Nodule reconstruction with overlap of ROI with Poisson noise extracted ROI using filters
a Sobel **b** Gaussian **c** Average **d** Laplacian **e** LoG **f** Prewitt and **g** Unsharp

Table 1 GCE for ROI of lung image with noises and segmentation operators

	GCE			
	Poisson noise	Gaussian noise	Speckle noise	Salt and pepper noise
Average	0.0025	0.0068	0.0051	0.00016
Gaussian	0.0049	0.0032	0.0052	0.0004
Laplacian	0.0050	0.0055	0.0057	0.00006
LOG	0.0033	0.0033	0.0039	0.0005
Prewitt	0.0027	0.0031	0.0054	0.00038
Sobel	0.0025	0.0052	0.0055	0.00002
Unsharp	0.0050	0.0062	0.0061	0.00002

Table 2 VOI for ROI of lung image with noises and segmentation operators

	VOI			
	Poisson noise	Gaussian noise	Speckle noise	Salt and pepper noise
Average	0.0357	0.0645	0.062	0.0120
Gaussian	0.0574	0.0460	0.066	0.0138
Laplacian	0.0569	0.0789	0.067	0.0077
LOG	0.0466	0.0473	0.047	0.0103
Prewitt	0.0354	0.0453	0.061	0.0162
Sobel	0.0330	0.0590	0.058	0.0075
Unsharp	0.0569	0.070	0.074	0.0080

segmentation operator, GCE and VOI are assessed. Prewitt operator attains desirable value with Gaussian noise and Sobel operator exhibits better performance than all other operators in Salt & Pepper and Poisson noise. LoG operator shows the best extraction of nodules with Speckle noise.

The explorations of sequences reinforce the recognition and treatment at the early stage to improve the survival rates. The performance of reconstruction process can be further done on different filters can evaluated by using parameters such as probabilistic rand index, structural similarity index, Local consistency error and PSNR to examine the influence of noise and the selection of preprocessing filters to minimize the consequences of noise for the assistance of better prognosis.

References

1. Daffner, F.: Clinical Radiology, the Essentials, 2nd edn. Williams & Wilkins, Baltimore, MD (1999)
2. Van Ginneken, B., Romeny, B.T.H., Viergever, M.A.: Computer-aided diagnosis in chest radiography: a survey. IEEE Trans. Med. Imaging **20**(12), 1228–1241 (2001)

3. Quekel, L., Kessels, A., et al.: Use of diagnostic imaging procedures: a nationwide hospital study in radiology. *Radiology* **163**(2), 569–573 (1987)
4. Becker, H., Nettleton, W., et al.: Digital computer determination of a medical diagnostic index directly from chest X-ray images. *IEEE Trans. Biomed. Eng. BME* **11**, 67–72 (1964)
5. van Rikxoort, E.M., de Hoop, B., Viergever, M.A., Prokop, M., van Ginneken, B.: Automatic lung segmentation from thoracic computed tomography scans using a hybrid approach with error detection. *Med. Phys.* **36**(7), 2934–2947 (2009)
6. Kalpana, V., Vijaya Kishore, V.: Performance study of different medical images based on morphology in noisy environment. *Int. J. Adv. Res. Eng. Technol.* **2**(1), 158–168 (2013)
7. Vijaya Kishore, V., Satyanaryana, R.V.S.: Performance assesment of morphological based medical image reconstruction by varying SEs and edge filters. Organized by NARL, Department of Space, International Union of Radio Science URSI-RCRS (2017)
8. Kalpana, V., Rajini, G.K.: Segmentation of lung lesion nodules using DICOM with structuring elements and noise-A comparative study. IEEE Digital Xplore Library. <https://doi.org/10.1109/upcon.2016.7894661>
9. Serra, J.: *Image Analysis and Mathematical Morphology*. Academic Press, New York (1982)
10. Speeuwerts, Heijden, L.J., Van der, F.: In: Forstner, W., Ruwiedel, S (eds) *Evaluation of Edge Detectors using Average Risk*. Robust Computer Vision. Wichmann, Karlsruhe (1992)
11. Sharifi, M., Fathy, M., Mahmoudi, M.T.: A classified and comparative study of edge detection algorithms. In: *Proceedings of International Conference on Information Technology: Coding and Computing (ITCC'02)* IEEE (2002)
12. Maini, R., Sohal, J.S.: Performance evaluation of Prewitt edge detector for noisy images. *GVIP J.* **6**(3) (2006)
13. Roushdy, M.: Comparative study of edge detection algorithms applying on the grayscale noisy image using morphological filter. *GVIP J.* **6**(4) (2006)
14. Vijaya Kishore, V., Satyanaryana, R.V.S.: Performance evaluation of edge detectors—morphology based ROI segmentation and nodule detection from DICOM lung images in the noisy environment. In: *2013 3rd IEEE International Advance Computing Conference (IACC)*, pp. 1131–1137 (2013)
15. Vincent, L.: Morphological grayscale reconstruction in image analysis: applications and efficient algorithms. *IEEE Trans. Image Process.* **2**(2), 176–201 (1993)
16. Kalpana, V., Vijaya Kishore, V.: Preliminary quantitative analysis of lung nodule extraction from noise image. *Int. J. Sci. Res.* **17**(2), 193–197 (2018)
17. Haralick, R.M., Sternberg, S.R., Zhuang, X.: Image analysis using mathematical morphology. *IEEE Trans. Pattern Anal. Mach. Intell. PAMI* **9**(4), 532–550, (1987)
18. Zhang, L.D., Bi, D.Y.: An improved morphological gradient edge detection algorithm. In: *IEEE International Symposium on Conference: Communications and Information Technology, ISCIT 2005*, vol. 2, pp. 1280–1283 (2005)
19. Robertson, I.D., Saveraid, T.: Hospital, radiology, and picture archiving and communication systems. *Vet. Radiol. Ultrasound* **49**(1, 1), S19–S28 (2008)
20. Sourabh Yadav, A.S.: Patient specific modeling for pattern identification in clinical events using data mining models and evolutionary computing. *Soft Comput. Theor. Appl.* **583**(1), 209–216 (2017)

A Review Paper on Feature Selection Techniques and Artificial Neural Networks Architectures Used in Thermography for Early Stage Detection of Breast Cancer



Kumod Kumar Gupta, Ritu Vijay, and Pallavi Pahadiya

Abstract For primary stage breast cancer detection, mammography techniques are being used for a long time. The disadvantage associated with the technology is taking a long time required by the radiologist to diagnose each image pattern. Moreover, this technique is not suitable for the detection of cancer in younger women. At present, the technique has been upgraded by using the technology-based classifiers, which adds the accuracy, specificity, sensitivity, and time requirement by differentiating malignant and benign. Only limited reviews are available, that focuses on features reduction algorithm and artificial neural networks architecture to enhance the detection techniques. The purpose of this paper is to collect the recently used techniques, algorithms, and future scope related to thermography. The author further suggests the technique to divide the features according to different age groups and to find a unique feature for all.

Keywords Infrared radiation thermograms (IRT) · Mammography images · Feature extraction · Malignant · Benign · Region of interest (ROI) · Artificial neural network (ANN)

1 Introduction

According to the report of the World Health Organization (WHO), twenty-seven million new cases of cancer will occur till 2030. Breast cancer is one of the most commonly diagnosed forms of cancer in the female population. The American Cancer Society's journal published a "Cancer Statistics, 2019," a total of 609,640 patients deaths from cancer and 1,735,350 new cancer cases come in the USA in 2019 [1].

K. K. Gupta (✉) · R. Vijay · P. Pahadiya
Department of Electronics, Banasthali Vidyapith, Tonk, Rajasthan, India
e-mail: kumodkumargupta@gmail.com

R. Vijay
e-mail: rituvijay1975@yahoo.co.in

P. Pahadiya
e-mail: pallavi_19_2000@yahoo.com

The death rate due to cancer was found to increase in both developing and developed countries. Moreover, the death rate can be controlled, if a disease can be diagnosed and treated early, which can lead to a better survival chance; though mammography is considered a good imaging technique, this technique fails to detect breast cancer in dense breasts of younger women. The failure of mammography in detecting small tumors of size less than 1.66 cm has been noticed by Keyserlingk et al. [2].

In order to overcome the disadvantage of harmful X-ray radiation, new technology to detect breast cancer in the early stage is developed. For the measurement of abnormal temperature pattern, infrared thermal imaging has become more accurate as an alternate medical diagnostic tool.

The abnormal body temperature is generally defined as illness. The authors proposed a non-invasive technique for measuring body temperature. This technique is passive, fast-acting, non-contact technology named infrared thermography technology (IRT). IRT is a harmless imaging methodology with better temperature sensitivity, and spatial resolution of various software packages is used for storing and post-processing of thermal image to get the insight of thermal pattern [3].

The physicians are using artificial neural network as an analytical tool to diagnose a patient. ANN is preferred compared to other classifiers because of its accurate result and fast assessment. The applications of ANN are mammograms, ultrasound, thermal imaging, and infrared imaging for early diagnosis of breast cancer [4, 42]. Figure 1 shows the process for detection of breast abnormality.

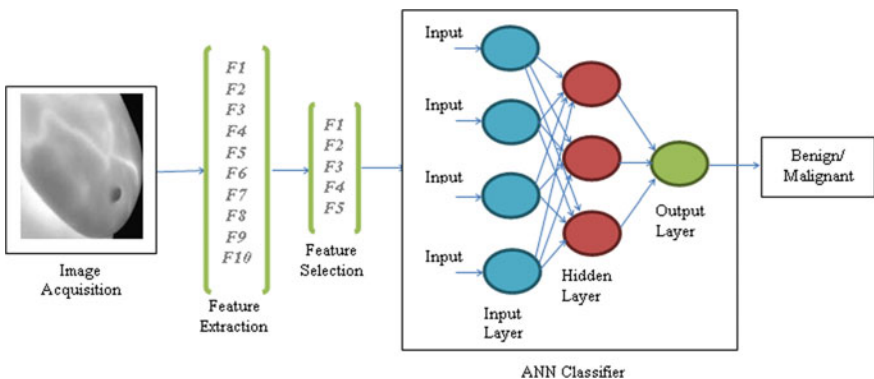


Fig. 1 Process for the detection of breast abnormality

2 Feature Selection and ANN Architecture Used in Breast Cancer Detection

The rapid growth of the dataset selection of features is an important issue for classifiers. To load the big dataset in the memory for the single data scan is the biggest problem. To solve this problem, select the features which contain the relevant information that also assists to decrease the computation time. In other words, this can be achieved by removing redundant, irrelevant, and noisy data; it selects the actual features to acquire the desired output.

The feature selection methods are

- (a) Filter method
- (b) Wrapper method
- (c) Hybrid method/embedded method.

Filter method: This method is fast to compute efficient and low-computational cost but reliability is poor. It is suitable for high-dimensional datasets. The learning algorithm is not used in this method.

Wrapper method: In this method, the learning algorithm is used that selects an optimal feature subset that is best suitable. In this method, every feature set should be examined with the trained classifier. Due to this, the feature selection process is slow and increases the computational cost. However, this method's performance is better because the feature selection process is optimized for the classifier and at the same time it is highly reliable.

Hybrid/Embedded method: The hybrid method is developed so that utilizes the benefit of both the above-mentioned methods. In this method, the learning algorithm is used. It is related to input and output features as well as searches locally for features that allow good local discrimination.

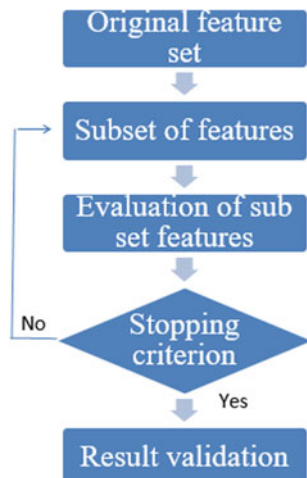
There are four basic steps for feature selection: (a) subset of features, (b) evaluation of subset features, (c) stopping criterion, and (d) result validation (Fig. 2).

Artificial neural network (ANN) is extensively used in several areas such as medical diagnosis, pattern recognition, and machine learning. ANN is made of layers. ANN classifier shown in Fig. 1 consists of three layers namely the input layer, hidden layer, and output layer. The output value decides the patient's cancer is benign or malignant. The number of hidden layers may depend on input vector sizes, output vector sizes, test data size, and training data size.

Dheeba et al. have introduced mammography which is the best method used in hospitals for early stage detection of breast cancer. The mortality rate is reduced by approximately 30% by using mammography. The main purpose of mammography is to detect the tumor in early stage and remove it [5].

Marques et al. have suggested that thermal imaging has the ability to show regions where there is any potential cancer by indicating areas of the body where there is an abnormality temperature variation. By using thermography, the suspicious region can be detected in patients of any age group as well as in dense breasts which cannot be detected by mammography [6].

Fig. 2 Steps for the feature selection process



de Vasconcelos et al. have analyzed several methods of classification of digital images. Infrared images were acquired and processed. On the bases of appropriate temperature ranges from the thermograms, the extraction of the characteristics was performed. the extracted data were used for the classification process [7]. Marcus et al. have aimed to detect breast cancer by using the morphological process. In the morphological process, the abnormality is detected in the form of a spot [8].

Qi et al. have proposed a technique, which can detect breast cancer and breast thermogram in the symmetric analysis of the left & right breast. The texture feature helps in detecting the minute difference in two breasts, through quantitative assessments of breast thermograms. Several experimental studies have also been made, with different statistical parameters, toward the asymmetric analysis of breast thermogram [9, 10].

Mamta and Hanmandlu have introduced the concept of inner product classifier (IPC). The process of this classifier is quite simple and easily implemented. This technique is implemented in a robust ear-based authentication system [11]. Acharya et al. have evaluated statistical data for each breast image. The calculated data is given to the artificial neural network as input features. Two backpropagation training algorithms, i.e., The Levenberg–Marquardt and Resilient backpropagation are compared and shown results are equal [12, 13].

Pagariya et al. have suggested the ANN model which is used in mammography analysis and biopsy decision making [14, 15]. Singh et al. have suggested a fully automated segmentation approach for better accuracy, higher reproducibility, and less time consumption to detect breast cancer [16].

Summary of methods with feature reduction and ANN in breast cancer is shown in Table 1.

Table 1 Summary of feature reduction and ANN techniques

S. No.	Author and Year	Input	Segmentation technique	Feature extraction	Feature reduction	Classifier ANN	Result and finding	Remark
1	Mrinal Kanti Bhowmik, 2016 [17]	IR Thermography image	Canny edge	Gray-level co-occurrence matrix (GLCM)	—	—	Sensitivity 90%, specificity 90%, accuracy 90%	standard deviation, not the efficient parameter
2	Sheeja V. Francis, 2013 [18]	IR Thermography image	—	GLCM, Gray level run length matrix(GLRLM)	—	Feed-forward Backpropagation network	Sensitivity 83.33%, specificity 33.33%, accuracy 66.67%	—
3	Sheeja V. Francis, 2014 [19]	IR Thermography image	Sobel edge	Curvelet transform	—	Support vector machine (SVM)	Texture features, sensitivity 81.82%, specificity 100% accuracy 90.91%	

(continued)

Table 1 (continued)

S. No.	Author and Year	Input	Segmentation technique	Feature extraction	Feature reduction	Classifier ANN	Result and finding	Remark
4	Sheeja V. Francis, 2014 [20]	IR Thermography image	No need	GLCM	Principal component analysis (PCA)	Support vector machine (SVM) using a kernel function	Texture feature, pre cool condition, sensitivity 83.3%, specificity 83.3%, accuracy 83.3%	ANN is the best classifier for pattern recognition
5	Usha Rani Gogoi, 2017 [21]	IR Thermography image	Convolve the mask to the RGB	Statistical and texture features	Statistical test	SVM, <i>K</i> -nearest neighborhood, ANN, Decision Tree	–	–
6	Satish Saini, 2014 [22]	Mammogram images	Manually	GLCM	–	Feedforward backpropagation ANN architecture	Accuracy 92.8% for 7 neurons and accuracy 87.5% for 8 layers	Levenberg–Marquardt backpropagation (LMBP) algorithm to train the network
7	J. Dheeba, 2014 [5]	Mammogram images	Global threshold technique	Texture features	–	Gradient descent algorithm backpropagation	Sensitivity 94.167%, specificity 92.05%	The feed-forward ANN is a widely used statistical tool design

(continued)

Table 1 (continued)

S. No.	Author and Year	Input	Segmentation technique	Feature extraction	Feature reduction	Classifier ANN	Result and finding	Remark
8	H. Liu, 2009 [23]	–	Big data	Filter method, wrapper method	Machine Learning	Wrapper method provides better accuracy than the filter method	Wrapper methods provide better results and performance than the filter method	
9	Gautam, A, 2018 [15]	Mammogram images	GLCM	–	Backpropagation ANN (BP-ANN)	Accuracy 96.4%	Better accuracy using BP-ANN	
10	Mohanty, F, 2018 [24]	Mammogram images	Feature extracted Contourlet transformation	Forest optimization feature selection algorithm	SVM, KNN	Accuracy 100%	Wrapper method based feature reduction technique	
11	Vijaya Madhavi, 2019 [25]	Thermography Image	–	Texture feature, GLCM, Gray-level run length matrix	T-test Least square support vector machine	Sensitivity 100%, specificity 92%, accuracy 96%	Feature find from frontal & lateral thermograms	

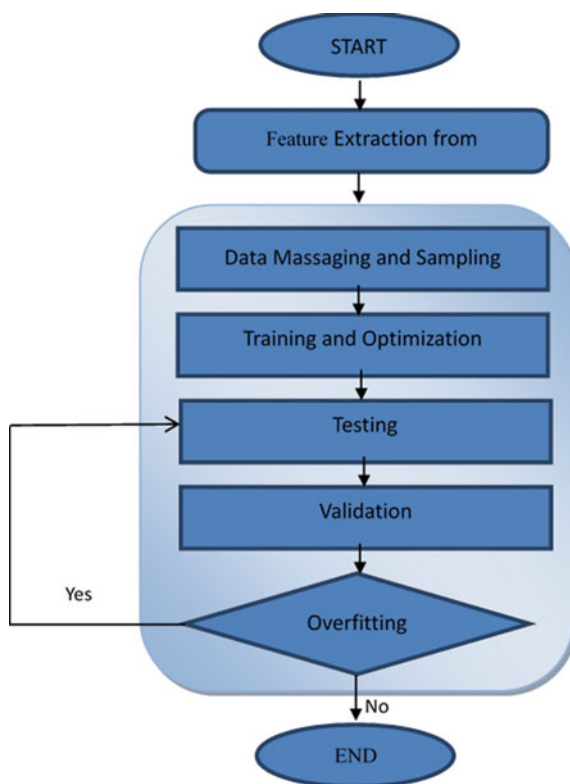
3 Features Reduction Technique and ANN for Breast Cancer Detection in Early Stage

From literature, it is observed that the wrapper method approach can be used for feature reduction in the future with the genetic algorithm. It is a random approach. This algorithm consists of a particular class of evolutionary algorithms, which are based on biological techniques such as inheritance, mutation, selection, and crossover. Applications of genetic algorithm are pattern recognition, neural networks, machine learning, combinational optimization, and hyperspectral data (Fig. 3).

For the thermography images, it has been proven that the exposure of breast cancer depends on the statistical parameters based on the temperature behavior of the tissues and the asymmetry difference of the contralateral breasts. Hence, image classification ways and resources based on ANN are somewhat successful in thermography. Due to astonishing computational influence, the ANN plays a vital role in the detection and analysis of breast cancer. Still, several studies in the works share several collective limitations, so used in limited applications.

The utmost common limitations comprise: (a) deficient in ample assessment of the perception accuracy, (b) overfitting, and (c) complexity problems. Due to the

Fig. 3 Data flowchart of ANN



data limitations, the testing of the model is not possible on an independent dataset. The cross-validation must be done to decrease potential bias. Still, several studies lacked such estimations and as a consequence, in utmost cases, the fault rates were dramatically miscalculated. Furthermore, the utmost literature did not pay attention to overfitting. The general natural networks extensively depend on the number of hidden layers. When they are too much, the network is likely to have the use of very huge number of hidden layers as compared to the size of the training data, and however, it did not consider whether overfitting has happened. Finally, in numerous studies, the computational difficulty of the artificial neural network was not appropriately described. Several measured the difficulty only by using the number of input nodes which would take too lightly the computational difficulty. Accurately reporting the difficulty of an ANN model is essential as the computational power and several potential difficulties such as overfitting are carefully associated with the difficulty of the model. The forthcoming studies in this field should sensibly study and remove these restrictions for effective uses of ANNs in thermography analysis.

4 Discussion

In the literature, this had been certified that feature reduction technique makes a system highly reliable, fast, needs low memory, and also provides reliable dataset to train the ANN. ANN is having the potential to help to understand the thermography as well as a breast cancer diagnosis. In the nutshell, ANN construction is simple and the complex nonlinearities can be easily found out between interpreters and outcomes.

ANN is having several disadvantages. In the medical system, it has been noticed that the clinical observations made by the forecast model play an important role. Till now, ANN is suffering from the poor capability to obviously explain the causal relations between predictive issues and outcomes, which one is the main drawback. Another disadvantage, to share a well-trained ANN model with other researchers is a challenging task. The reason is that the information extracted from the data is completely encoded into a big weight matrix, which one is a typical task to share and understand. However, the complexity of the ANN model building makes this additional likely to overfitting, the instance where the system mimics and over learns the training dataset but performs unwell when existing to an outside dataset. From the literature survey, it has been observed that the data may be divided according to the age groups and then trained to the ANN networks.

5 Conclusion

Breast cancer is the most prominent disease found in female, and if breast cancer is detected in the preliminary stage, it is curable. To detect breast cancer, medical practitioner is using mammography from the decades. It has many problems mainly

Table 2 Gives a summary of the number of features according to age group

Patients age group	20–30 years	30–40 years	40–50 years	50–60 years	60–70 years
Number of features	V	W	X	Y	Z

not suitable for younger women and time taking process. This paper enlists different feature selection techniques to reduce the time, and in most cases, the wrapper method is better due to enormous advantages. It has been minutely observed from the literature that by using BP-ANN architecture as a classifier, the results accuracy, sensitivity, and specificity are as desirable.

Proposed technique: From the literature survey, it has been observed that researchers are calculating the same feature for all age groups of females and also doing the same in existing technique, i.e., mammography. However, the physiology of breasts is different in different age groups and a single approach cannot be fruitful to analyze them. So, to overcome the limitation of the existing approach, we are proposing the technique which will consider the feature of different age groups at the time of feature selection and also try to find out unique feature for all age groups. In Table 2, V , W , X , Y , and Z show the features number.

It is further suggested to eliminate the insignificant features by applying the feature reduction techniques, i.e., sequential forward selection, sequential backward selection, and backtracking algorithm to find the best one. The reduced feature by the feature reduction technique is treated as the input to the artificial neural network (ANN). The ANN will decide the patient is having malignant or benign cells behavior. ANN is preferred compared to other classifiers as it gives a more accurate result and fast assessment.

References

1. American Cancer Society: Breast cancer facts & figures. <https://www.cancer.org/research/cancer-facts-statistics/all-cancer-facts-figures/cancer-facts-figures-2019.html>
2. Keyserlingk, J.R., Ahlgren, P.D., Yu, E., Belliveau, N.: Infrared imaging of the breast: initial reappraisal using high-resolution digital technology in 100 successive cases of stage I and II breast cancer. *Breast J.* **4**(4), 245–251 (1998)
3. Lahiri, B.B., Bagavathiappan, S., Jayakumar, T., Philip, J.: Medical applications of infrared thermography: a review. *Infrared Phys. Technol.* **55**(4), 221–235 (2012)
4. Mehdy, M.M., Ng, P.Y., Shair, E.F., Saleh, N.I., Gomes, C.: Artificial neural networks in image processing for early detection of breast cancer. *Comput. Math. Methods Med.* 1–15 (2017)
5. Dheeba, J., Singh, N.A., Selvi, S.T.: Computer-aided detection of breast cancer on mammograms: a swarm intelligence optimized wavelet neural network approach. *J. Biomed. Inform.* **49**, 45–52 (2014)
6. Marques, R.S., Conci, A., Perez, M.G., Andaluz, V.H., Mejia, T.M.: An approach for automatic segmentation of thermal imaging in computer-aided diagnosis. *IEEE Latin Am. Trans.* **14**(4), 1856–1865 (2016)
7. de Vasconcelos, J.H., dos Santos, W.P., de Lima, R.C.F.: Analysis of methods of classification of breast thermographic images to determine their viability in the early breast cancer detection. *IEEE Latin Am. Trans.* **16**(6), 1631 (2018)

8. Araújo, M.C., Lima, R.C.F., de Souza, R.M.C.R.: Interval symbolic feature extraction for thermography breast cancer detection. *Exp. Syst. Appl.* **41**(15), 6728–6737 (2014)
9. Qi, H., Kuruganti, P.T., Snyder, W.E.: Detecting breast cancer from thermal infrared images by asymmetry analysis. *Med. Med. Res.* **38** (2012)
10. Giri, P.J., Gajbhiye, A.R.: ANN-based modeling for flood routing through gated spillways. In: Pant, M., Ray, K., Sharma, T., Bandyopadhyay, A. (eds.) *Soft Computing: Theories and Applications. Advances in Intelligent Systems and Computing*, vol. 583. Springer, Singapore (2018)
11. Mamta, Hanmandlu, M.: Robust ear based authentication using local principal independent components. *Exp. Syst. Appl.* **40**(16), 6478–6490 (2013)
12. Acharya, U.R., Ng, E.Y.K., Tan, J.H., Sree, S.V.: Thermography based breast cancer detection using texture features and support vector machine. *J. Med. Syst.* **36**(3), 1503–1510 (2012)
13. Gupta, V., Sunita, Singh, J.P.: Study and analysis of back-propagation approach in artificial neural network using HOG descriptor for real-time object classification. In: Ray, K., Sharma, T., Rawat, S., Saini, R., Bandyopadhyay, A. (eds.) *Soft Computing: Theories and Applications. Advances in Intelligent Systems and Computing*, vol 742. Springer, Singapore (2019)
14. Pagariya, R., Bartere, M.: Review paper on artificial neural networks. *Int. J. Adv. Res. Comput. Sc.* **4**(6) (2013)
15. Gautam, A., Bhateja, V., Tiwari, A., Satapathy, S.C.: An improved mammogram classification approach using back propagation neural network. In: *Data Engineering and Intelligent Computing*, pp. 369–376. Springer, Singapore (2018)
16. Singh, J., Arora, A. S.: Automated approaches for ROIs extraction in medical thermography: a review and future directions. *Multimedia Tools Appl.* 1–24 (2019)
17. Gogoi, U.R., Majumdar, G., Bhowmik, M.K., Ghosh, A.K., Bhattacharjee, D.: Breast abnormality detection through statistical feature analysis using infrared thermograms. In *2015 International Symposium on Advanced Computing and Communication*, pp. 258–265. IEEE (2015)
18. Francis, S.V., Sasikala, M.: Automatic detection of abnormal breast thermograms using asymmetry analysis of texture features. *J. Med. Technol.* **37**(1), 17–21 (2013)
19. Francis, S.V., Sasikala, M., Saranya, S.: Detection of breast abnormality from thermograms using curvelet transform based feature extraction. *J. Med. Syst.* **38**(4), 23 (2014)
20. Francis, S.V., Sasikala, M.: Breast cancer detection in rotational thermography images using texture features. *Infrared Phys. Technol.* **67**, 490–496 (2014)
21. Gogoi, U.R., Bhowmik, M.K., Ghosh, A.K., Bhattacharjee, D., Majumdar, G.: Discriminative feature selection for breast abnormality detection and accurate classification of thermograms. In: *International Conference on Innovations in Electronics, Signal Processing, and Communication (IESC)*, pp. 39–44. IEEE (2017)
22. Saini, S., Vijay, R.: Optimization of artificial neural network breast cancer detection system based on image registration techniques. *Int. J. Comput. Appl.* **105**(14), 26–29 (2014)
23. Liu, H., Zhao, Z.: Manipulating data and dimension reduction methods: feature selection. *Encycl. Complex. Syst.* 5348–5359 (2009)
24. Mohanty, F., Rup, S., Dash, B., Majhi, B., Swamy, M. N. S.: Mammogram classification using contourlet features with forest optimization-based feature selection approach. *Multimedia Tools Appl.* 1–30 (2018)
25. Madhavi, V., Thomas, C.B.: Multi-view breast thermogram analysis by fusing texture features. *Quant. Infrared Thermogr. J.* **16**(1), 111–128 (2019)

An Artificial Neural Network Model for Estimating the Flood in Tehri Region of Uttarakhand Using Rainfall Data



B. G. Rajeev Gandhi, Dilip Kumar, and Hira Lal Yadav

Abstract The region of Tehri is vulnerable to heavy rainfall and floods and other natural disasters. There is a need for an efficient flood forecasting system in the state of Uttarakhand so that preventive measures can be taken before the event occurs in any area. Artificial Neural Networks are a great tool to analyse complex systems in terms of simple weights and biases. The ANN once used efficiently to train, validate and test different datasets on a large scale can be an effective tool for flood forecast. In this paper, we have used monthly data of rainfall and discharge from the year 1964 to 2012 to train and test an ANN model with three hidden layers. Later the climate change data is used to estimate the rainfall for the future century and that rainfall is used as an input for the trained model to estimate the flood for the coming century (up to 2099). The results have been proven to be satisfactory in the training stage and more than 10 instances of high floods are forecasted for the future using climate change inputs.

Keywords Artificial neural networks · Flood forecast · Tehri · Climate change

1 Introduction

The state of Uttarakhand in India is the most vulnerable state to heavy rainfall, floods, and other natural disasters. Thousands of people get affected due to such events and there is a ton of property loss. The flash flood in the year 2013 alone has proven to be fatal for 5748 people and more than 70,000 people have been stranded in this event [1, 2]. Although this event has occurred due to the cloud burst, most of the floods occur due to normal but heavy rains. The average rainfall in the state of Uttarakhand is 1896 mm [2, 3]. Eight of the thirteen districts of the state are hilly terrains and are vulnerable to floods and rainfall. Tehri is the district that has the highest dam and also the most amount of discharge in the natural channels is the most affected area in the

B. G. Rajeev Gandhi (✉) · D. Kumar · H. L. Yadav
Department of Civil Engineering, G.B. Pant Institute of Engineering and Technology, Pauri,
Garhwal 246194, Uttarakhand, India
e-mail: rajeevgandhi17@gmail.com

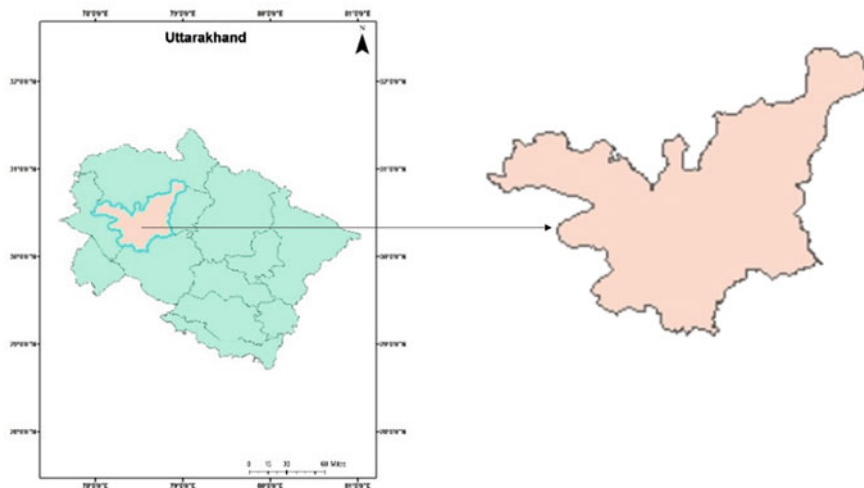


Fig. 1 Showing the study area

state of Uttarakhand [2]. But, to estimate the discharge in a natural channel is a very difficult thing as the deterministic relation between the rainfall and the floods are very complex and difficult to achieve [4]. Therefore, we have attempted to estimate the discharge by using rainfall as input in the artificial neural network. The neural network is trained and tested with data from 1964 to 2012 and the results obtained were more than satisfactory.

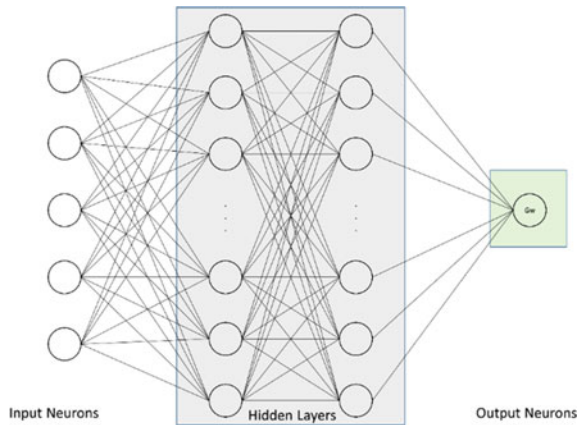
1.1 Study Area

One of the hilly State of India, Uttarakhand lies between 28°04' and 31°02'N latitude and 77°03' and 81°00'E longitude (Fig. 1). The whole region of the state is divided into two distinguished hydrogeological regimes as the Gangetic alluvial plain and the Himalayan mountain belt. The Tehri district of Uttarakhand is famous of Tehri dam and flash flood event [2–5].

1.2 Working of Artificial Neural Network (ANN)

The artificial neural network is a representation of the neurons in a human brain. The neurons and the synapses work together by carrying weights and taking decisions based on their weights to simplify a complex process [6–9]. ANN is an emerging technology that would prove to be most effective in the near future [10, 11]. The process is very simple and easy to understand. Every dataset given to ANN is divided

Fig. 2 Typical example of an artificial neural network



into inputs and targets [7]. The goal is to achieve the targets with the given inputs and corresponding weights designed by the model. The input and target dataset are divided into a training dataset, validation dataset and testing dataset. The training dataset is where the model is trained to fit the parameters so that the expected targets are achieved. The validation dataset is where parameters are fine-tuned to achieve better results at the targets. The testing dataset is used to check the accuracy of the model. We have used a training dataset of 70%, validation of 15% and testing dataset of 15%. In addition to these, the passage from input to output is done through hidden layers. We have used three hidden layers while analysing this discharge through rainfall. The basic structure of the neural network is given in Fig. 2. This particular figure represents five inputs to one output with two hidden layers. In our model, we have used one input layer and one output layer with three hidden layers.

1.3 Climate Change and Its Impact on Discharge

Climate change also plays a major role in effecting the floods as well as the rainfall in all the regions [5, 12, 13]. The impact of such climate change is being studied in many parts of the world through various climatic experiments. The impacts of different scenarios of climate change are estimated and the projected datasets are made available all over the world so that one can use them in the local regional-scale models [14]. The globally available models are called Global Climatic Models (GCM) and the regionally developed models are called Regional Climatic Models (RCM) [15, 16]. The RCMs are to be developed by the modeller regionally so that it represents the regional observations accurately. The transfer of data from the GCM level to RCM level is called downscaling. The ANN can be used to downscale GCMs called statistical downscaling [10, 17, 18]. The GCMs are many and any one of them can be used to estimate the impacts of climate change on global levels. One such GCM datasets is Can ESM 2. This GCM is focused mainly in Canada but is available for the

whole world; however the resolution other than Canada is $2.8^\circ \times 2.8^\circ$. This model is used to predict the rainfall for the next century (up to 2099) [19]. The process used in the projection of rainfall data is out of the scope of this paper. However, there are three major climatic conditions named RCP 26, RCP 45 and RCP 85 (RCP meaning Representative Concentration Pathway) [20–22]. The rainfall is forecasted by using this and the discharge is predicted based on these three scenarios of climate change.

2 Methodology

The datasets of daily discharges and daily rainfall are obtained from Indian Meteorological Department (IMD) and the local authorities concerned. The discharges and the rainfall are initially averaged to the monthly scale, as it would make the model less complex and easy to analyse. The datasets are taken as per the availability of the discharge datasets from 1964 to 2012. This comprising on the monthly scale contributes to 588 datasets for inputs and for outputs. The training samples are 412 (70%), and 88 (15%) each for validation and testing. The methodology of the ANN model is given in the following flowchart in Fig. 3.

The model input is a rainfall dataset and the output is discharge dataset. There are three hidden layers between the input and output. The model is trained, validated and tested by using the methodology as described in Fig. 2 and then the climate change data is used as an input to predict the discharge for the next century. The ANN model trained, tested and validated is a tool to predict the effect of the most complex changes in climate on the discharge and can be seen clearly in the results.

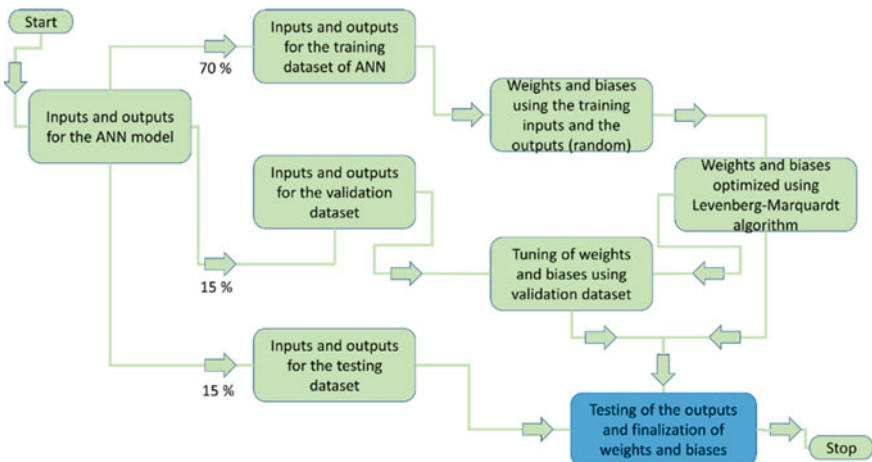


Fig. 3 Working of ANN model and methodology

3 Results and Discussion

The impact of the climate changes on the rainfall can be seen in Fig. 4. There is a common period of rainfall from 2006 to 2012 in the climatic models and the actual datasets. This period can be used to see the monthly variations in the rainfall between these periods. As can be seen, there is a lot of variation in the rainfall trends from actual and climate change datasets.

The blue line represents the actual data and the red, purple and green lines represent the RCP 26, RCP 45 and RCP 85 datasets. The maximum rainfall is just 225 cm in RCP 85 and the rest of the trends are almost the same with slight variation in maximum and minimum monthly. These datasets are used for the prediction of the discharge for the future and the same diagram can be seen in the prediction models of discharge in Fig. 5 from 2006 to 2012.

As it can be observed in this figure, the ANN model predicts the most complex behaviour of the Discharge and Rainfall mostly well. There is not much correlation between the rainfall and discharge and is a complex non-linear relation between these two datasets. Still, it can be seen in Fig. 4 that the climate experiments discharge are almost in unison with the rainfall trends in the years 2009 and 2010. However, this didn't prove to be much threatening as the maximum discharge is shown in the actual dataset itself. But, the average discharge in the actual data is 225 m³/s whereas the average in RCP 26, RCP 45 and RCP 85 are 307, 275 and 315 m³/s, respectively.

3.1 Performance of the ANN Model

The ANN model has performed significantly well and has obtained a correlation of 0.701 between the observed and predicted discharges overall. Figure 6 is based on

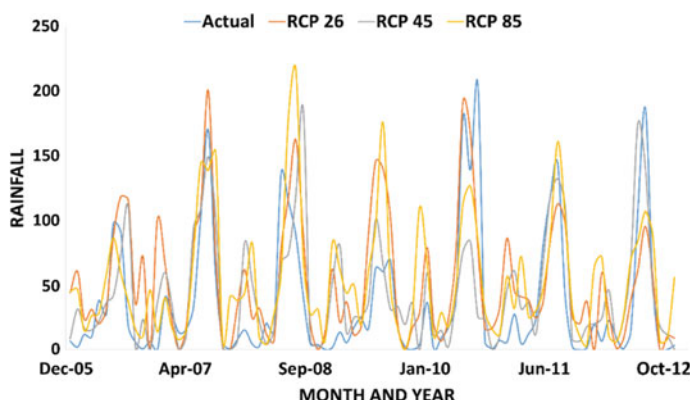


Fig. 4 Rainfall variation for different climate change datasets for the common period of 2006–2012

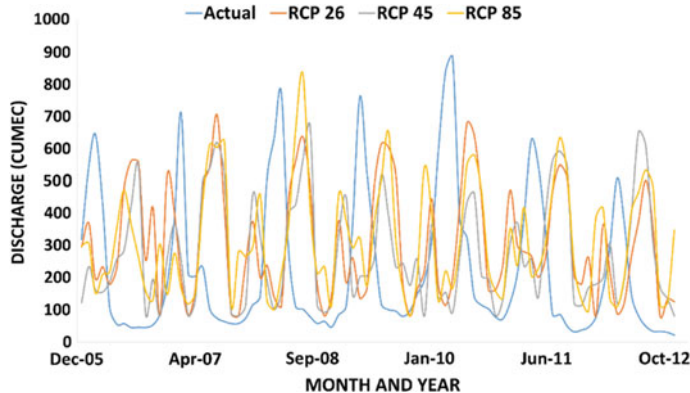


Fig. 5 Discharge variation for different climate change datasets for the common period of 2006–2012

the result of the ANN model. The performance of the ANN model is given in detail in Fig. 6, which explains the correlation coefficients for the monthly average datasets at different stages of training, validation and testing and the overall model. At the training stage, the weights and biases are selected randomly at first and then they are optimized based on the Levenberg–Marquardt algorithm until they best represent the outputs with weights and biases and inputs. Then the validation dataset fine-tunes the weights and biases to get a best correlation and Mean Square Error (MSE). Finally, the testing datasets tests with the weights and biases which gives a correlation of 0.76 which is highly satisfactory.

As can be seen in Fig. 6, the correlations for the training of the dataset is 0.71, for validation is 0.61 and for testing, it is 0.76 giving an overall correlation of 0.701 which is in the acceptable range of correlation. The Nash Sutcliffe Efficiency coefficient (NSE) is also calculated for this predicted and observed datasets and found to be 0.4926. The closer NSE to 1, the better the model is. Also, a value of 0.5–0.65 represents a good fit for a hydrological model. Here the value of NSE is almost equal to 0.5 which means a reasonable prediction for the model. This means that the relation between the rainfall and the discharge which is almost having a correlation of 0.68 is very complex and difficult to achieve with one input and output. If the rainfall and other weather parameters would have to be used for model prediction, the results would improve much more.

3.2 Pseudo Codes and Program Codes

Pseudocode for this task is given so that the problem can be coded in any language with ease. The program code is also given along with this paper so that anyone can

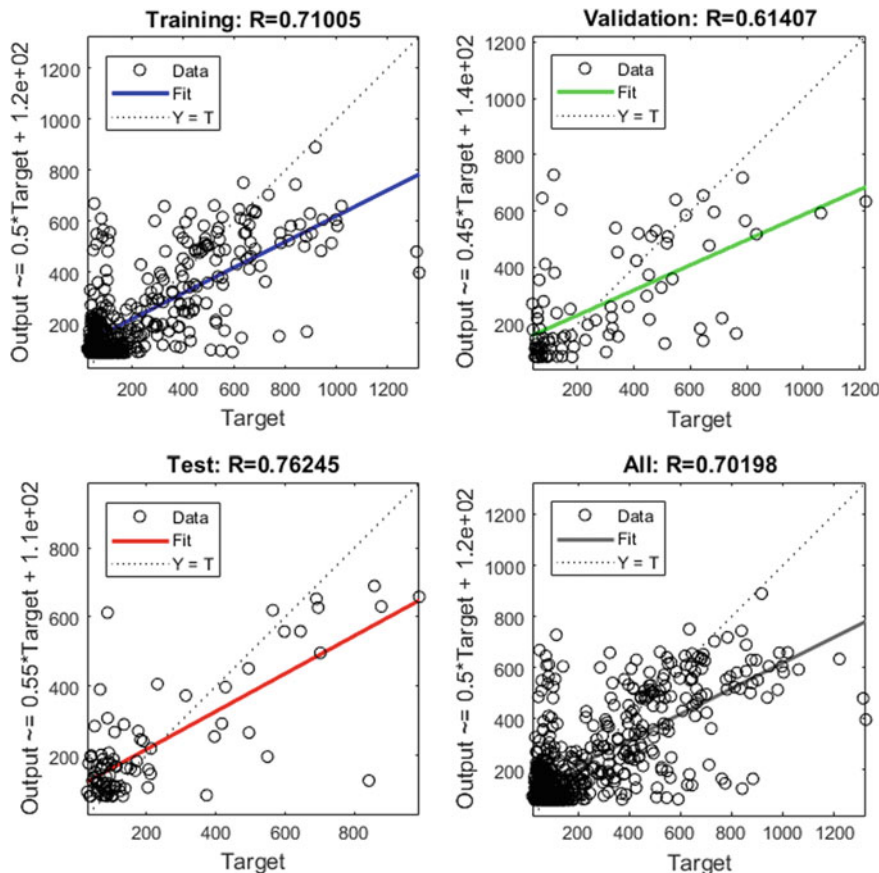


Fig. 6 Correlations from training validation and testing of ANN model

attempt this problem without much difficulty. This program is developed in MATLAB version 2017 b. This code consists of some inbuilt functions and the ANN toolbox that is available only for MATLAB users. Therefore, care should be taken while transforming the same code into different languages.

Averaging Monthly Discharge and Rainfall

1. Read the datasets of date and discharge/rainfall from the tables in.xlsx format
2. Convert the date into vector format to read the number of days for each month
3. Calculate the mean of datasets for each month
4. Record the mean values as per month and year and export to.xlsx format.

```

function Dataset = Average_monthly(filename)
[~,SheetNames] = xlsfinfo(filename);
nSheets = length(SheetNames);
for iSheet = 1:nSheets
    Name = SheetNames{iSheet};
    Data = readtable(filename, 'Sheet', Name) ;
    S(iSheet).Name = Name;
    S(iSheet).Data = Data;
end
% clear Name Data iSheet nSheets SheetNames;
for j = 1:nSheets
    for i = 1:size(S(j).Data,1)
        D(j).Data(i,1:6) = datevec(S(j).Data{i,1});
    end
    D(j).Data(:,7) = table2array(S(j).Data(:,2));
end
for j = 1:nSheets
    n = 1;
    for i = 1:size(D(j).Data,1)-1
        if D(j).Data(i,3)+1 ~= D(j).Data(i+1,3)
            n1(i,1) = 1;
            A(j).Data(sum(n1(1:i,1)),1) =
mean(D(j).Data(n:i,7));
            n = i+1;
        end
    end
end
Dataset = A.Data;
End

```

Main Program

1. Calculate the monthly average discharge and rainfall using previous code
2. Prepare the inputs as rainfall and outputs as discharge for training of neural network
3. Separate the datasets at random with 70% for training, 15% for validation and 15% for testing
4. Train the neural network, validate and test with the separated datasets
5. Calculate the monthly average for GCM datasets of rainfall
6. Using the weights and biases for the tested neural network calculate the discharges for the GCM inputs of the three RCPs.

```

clc; clear variables;
Dis = Average_monthly('Tehri_Discharge_2.xlsx');
Rain = Average_monthly('Tehri_Rainfall_2.xlsx');
A = load('Data_For_NN.mat');
RainRCP = A.Rainfall_RCP;
n2 = [31 28 31 30 31 30 31 31 30 31 30 31];
for j = 1:3
E(j).Data = reshape(RainRCP(:,j),sum(n2),[]);
n3 = 1;
for i = 1:size(n2,2)
    E1(j).Data(i,:) =
mean(E(j).Data(n3:sum(n2(1,1:i))),:));
    n3 = sum(n2(1,1:i))+1;
end
RCPmean(:,j) = E1(j).Data(:);
end
n = 3; %Hidden Layers
net = feedforwardnet(n);
net.trainParam.max_fail = 100;
[net,TR] = train(net,Rain',Dis');
O1 = net(RCPmean(:,1)'); O2 = net(RCPmean(:,2)'); O3 =
net(RCPmean(:,3)');

```

This whole program runs in the default options in ANN model, one can change the different algorithms and other parameters to achieve better results. We have tried different number of hidden layers and other changes, but this model runs well under the conditions of three hidden layers as described above.

3.3 Flood Forecast

The forecast for the floods can be seen for the future using the ANN model and the floods for the coming century (up to 2099) can be seen in Fig. 7 as shown below. It can be seen that the figure below doesn't include the 2013 flash flood event, as the Climate models doesn't forecast such flash floods. Also, it can be observed that there are major events of floods in the coming century in all the three climatic models. The maximum discharge is nearly $1700 \text{ m}^3/\text{s}$ which is very much higher as per the capacity of the natural channels. There are at least 10 occurrences of such events in the coming century. Therefore care should be taken against such changes and preventive measures and preparation against such events must be taken so as to face such disasters.

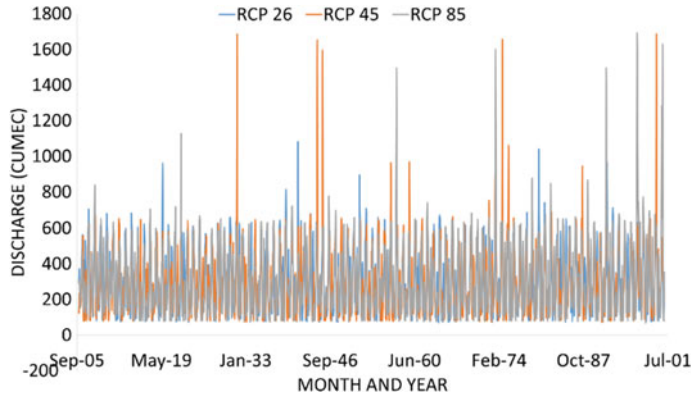


Fig. 7 Flood forecast up to 2099 showing monthly variation in discharge as per ANN model

4 Conclusions and Limitations

The conclusion of this study is that the relation between rainfall and discharge is not as straight forward as it seems. The results indicate that rainfall alone is not responsible for the floods in any stream. The correlation between the rainfall and discharge alone is 0.68 and then when they are used as an input and output of an ANN model the results just improved to be 0.71 between the predicted and the actual discharge. This means that there are some other factors that play a major role in the determination of discharge. The model can be much improved when one considers other weather parameters such as temperature, relative humidity, runoff rate, and other such parameters that convert the rainfall into the actual discharge. However, the data is not so easy to be obtained in such areas and thus this work is limited to use only rainfall as an input. The climate change datasets can be used more effectively by initially using more input layers rather than one input layer. The rainfall alone is taken to affect the discharge of the stream. But, the temperature, surface pressure, pressure at different heights, wind velocity, and many more inputs are available in the climate change data which can be used as inputs for the ANN model. This gives a much higher correlation for flood forecasting. The model output gives high flood instances in at least 10 instances, these instances have to be verified accordingly with different climatic models and the common areas of strikes are to be taken to exactly predict the future events. The preventive measures can be taken then about the events [23]. Overall these results have proven to be satisfactory but there is a scope for further improvement in this model as a tool for forecasting floods.

References

1. Agricultural Economics Research Centre.: Agriculture profile of Uttarakhand, University of Delhi (2015)
2. Government of Uttarakhand, G.: Uttarakhand action plan on climate change: transforming crisis into opportunity (2014)
3. Ministry, T., Government, F.: Assessment of environmental degradation and impact of hydroelectric projects during the June 2013 disaster in Uttarakhand part I-Main report (2014)
4. Meena, R.A.Y.S.: Simulation of Runoff and Flood Inundation in Kosi River Basin Using Hydrological Models, ANN, Remote Sensing and Gis Rourkela Department, p. 91 (2012)
5. Mishra, A.: Changing temperature and rainfall patterns of Uttarakhand. 7(4), 1–6 (2017)
6. Haykin, S.: Neural Networks: A Comprehensive Foundation, 2nd edn. Prentice Hall, New Jersey (1999)
7. Schalkoff, R.J.: Artificial Neural Networks. McGraw-Hill, New York (1997)
8. Kumar, D., Bhishm, S.K., Khati, S.: Black box model for flood forecasting. J. Civ. Eng. **40**, 47–59 (2012)
9. Supharatid, S.: Skill of precipitation projection in the Chao Phraya river basin by multi-model ensemble CMIP3-CMIP5. Weather Clim. Extrem. **12**, 1–14 (2015)
10. Akhter, M., Ahmad, A.M.: Environment pollution and climate change climate modeling of Jhelum river basin—A comparative study. **1**(2), 1–14 (2017)
11. Li, Q., Luo, Z., Zhong, B., Zhou, H.: An improved approach for evapotranspiration estimation using water balance equation: case study of Yangtze river basin. Water **10**(6), 812 (2018)
12. Joshi, R.: Artificial neural network (ANN) based empirical interpolation of precipitation. Int. J. Math. Eng. Manag. Syst. **1**(3), 93–106 (2016)
13. Long, D., et al.: Global analysis of spatiotemporal variability in merged total water storage changes using multiple GRACE products and global hydrological models. Remote Sens. Environ. **192**, 198–216 (2017)
14. Nyatuame, M., Owusu-Gyimah, V., Ampiah, F.: Statistical analysis of rainfall trend for volta region in Ghana. Int. J. Atmos. Sci. **2014**, 1–11 (2014)
15. Fang, G.H., Yang, J., Chen, Y.N., Zammit, C.: Comparing bias correction methods in downscaling meteorological variables for a hydrologic impact study in an arid area in China. Hydrol. Earth Syst. Sci. **19**(6), 2547–2559 (2015)
16. Mathison, C., Wiltshire, A.J., Falloon, P., Challinor, A.J.: South Asia river flow projections and their implications for water resources. Hydrol. Earth Syst. Sci. Discuss. **12**(6), 5789–5840 (2015)
17. Pichuka, S., Prasad, R., Maity, R.R., Kunstmann, H.: Development of a method to identify change in the pattern of extreme stream flow events in future climate: Application on the Bhadra reservoir inflow in India. J. Hydrol. Reg. Stud. **9**, 236–246 (2017)
18. Pervez, M.S., Henebry, G.M.: Projections of the Ganges-Brahmaputra precipitation-downscaled from GCM predictors. J. Hydrol. **517**, 120–134 (2014)
19. Joshi, R.: Artificial neural network (ANN) based empirical interpolation of precipitation. Int. J. Math. Eng. Manag. Sci. **1**(3), 93–106 (2016)
20. Onyutha, C., Tabari, H., Rutkowska, A., Nyeko-Ogiramo, P., Willems, P.: Comparison of different statistical downscaling methods for climate change rainfall projections over the Lake Victoria basin considering CMIP3 and CMIP5. J. Hydro-Environ. Res. **12**, 31–45 (2016)
21. Wang, L., Guo, S., Hong, X., Liu, D., Xiong, L.: Projected hydrologic regime changes in the Poyang Lake basin due to climate change. Front. Earth Sci. **11**(1), 95–113 (2017)
22. Parth Sarthi, P., Ghosh, S., Kumar, P.: Possible future projection of Indian Summer Monsoon Rainfall (ISMR) with the evaluation of model performance in coupled model inter-comparison project phase 5 (CMIP5). Glob. Planet. Change **129**, 92–106 (2015)
23. Joseph, S., et al.: Extended Range Prediction of Uttarakhand Heavy Rainfall Event by an Ensemble Prediction System based on CFSv2, vol. 03 (2013)

Advanced Virtual Apparel Try Using Augmented Reality (AVATAR)



Sourav Shaw, Swapnali Kadam, Shreya Joshi, and Dhanashree Hadsul

Abstract The new trends in fashion and newly designed outfits motivate customers for shopping. Constraints of place and time have been suppressed by rapid growth in online stores. Predicting the appropriate size and quality remains an unsolved problem. Offline shopping is another option that is preferred by a majority of customers. The trial of the same apparel by multiple customers may lead to various skin diseases and degrades the quality of apparel. The privacy of customers can be violated due to spy cameras in trial rooms. Advanced Virtual Apparel Try using Augmented Reality (AVATAR) proposes a multi-sensor body scanner combined with social media technologies. This revolutionizes the classic desktop paradigm into the direction of intuitive, “natural interaction” where people interface with the technological world through hand gestures, speech, and body language. AVATAR consists of an IoT mirror acting as a virtual trial room. The system is benefited by the web camera and TensorFlow which gathers real-time coordinates of the customer’s body. The OpenCV library scales the 3D model of the apparel following the coordinates. Hand gestures are used to interact with the system. Face color recognition using machine learning drives the recommendation system to suggest suitable apparel colors to customers. Besides, a web interface facilitates sharing the real-time experience of the customers trying the 3D apparel model for quick feedback.

Keywords IoT mirror · OpenCV · Tensorflow · Face color recognition · Recommendation system

1 Introduction

Apparel shopping is the most fascinating form of shopping. Apparel are of different styles, fashions, and are more often wore according to occasions. Shopping for opportune and redress sized apparel is an art. The act of browsing apparels present at online stores and buying the indispensable ones is a tiresome task.

S. Shaw (✉) · S. Kadam · S. Joshi · D. Hadsul
Fr. C. Rodrigues Institute of Technology (FCRIT), Navi Mumbai, Maharashtra 400703, India
e-mail: fypvirtualfit@gmail.com

Traditionally, the shopping hubs have to be physically visited to buy desired garments. This includes authentically culling of the garments you relished. Additionally, the unflattering angles and the fluorescent lighting of the trial rooms make it arduous to judge the look of apparel you are endeavoring. The trail of the same cloth by multiple users may lead to sundry skin diseases to the customer and additionally degrade the quality of cloth. The chances of having a camera in the trial room and contravening the privacy of customers are a major issue in India. On the other hand, the seller's job additionally becomes tedious to again repack the messed apparel. All these factors degrade the experience of shopping for customers and adversely affect the sales of shopkeepers.

Optically canvassing the apparel online in the form of a 2D image and analyzing its look and culling opportune size is authentically a challenging task. The chances of receiving the precisely same product you viewed online may vary. Variations in a distributed product than that of selected ones lead to a deplorable review of customers resulting in the fall of sales for the shopkeeper. Analyzing such quandaries, and to find a solution that can increment shopping experience is essential. This solution has to be utilize cordial, efficient and embedded with advanced technology.

AVATAR endeavors to eliminate all the quandaries that are generally faced while apparel shopping. It provides virtual trial rooms, to visualize a genuine view of the culled garment without physically wearing them. The recommending system helps customers for appropriate culling. Besides, a web interface facilitates sharing the real-time experience of the customers trying the 3D apparel model for quick feedback. Such technological involvement in shopping attracts customers. AVATAR may surely prove the most efficient way for shopping garments in the coming era, by superseding the traditional way and overcoming all the prevailing issues.

2 Literature Survey

The following are the IEEE papers referred for the literature survey.

- **Paper title:** A Mixed Reality Virtual Clothes Try-on System [1].

The authors of this paper are Miaolong Yuan (Institute for Infocomm Research), Ishtiaq Rasool Khan (University of Jeddah), Farzam Farbiz (Institute for Infocomm Research), S.s. Yao (Agency for Science, Technology, and Research (A*STAR)).

This paper has a brief description of a mixed reality system for 3D virtual clothes try-on. Based on the user's body size and skin color, it automatically customizes an invisible (or partially visible) avatar and uses it for proper clothes fitting, alignment, and clothes simulation. The system can enable users to enjoy a private virtual try-on experience at their own homes. It requires offline manual interventions to generate a 3D model of a user.

- **Paper title:** Virtual Try-On Through Image-based Rendering [2].

This paper is proposed by Stefan Hauswiesner, Student Member, IEEE, Matthias Straka, and Gerhard Reitmayr, Member, IEEE. The paper describes a method that transfers the appearance of a garment recorded from one user to another by matching input and recorded frames, image-based visual hull rendering, and online registration methods. By using images of the real garment instead of virtual models, a realistic rendering quality can be achieved. Required number of cameras to capture the real-time view of garments, which is costlier.

- **Paper title:** Implementation of Virtual Fitting Room Using Image Processing [3].

This paper is proposed by Srinivasan K. (Department of Electronics and Instrumentation Engineering, Sri Ramakrishna Engineering College, Coimbatore, India), Vivek S. (Department of Electronics and Instrumentation Engineering, Sri Ramakrishna Engineering College, Coimbatore, India).

The paper proposes an algorithm that would enable people to check out themselves with different dresses with fewer restrictions and regardless of background light. Also morphological structuring element for applying the Laplacian filter to separate background.

The algorithm works well on varying light intensities provided that the background has got rid of the presence of highly projecting bodies.

At present, the algorithm is unable to find the human silhouette with a variable background and noisier environment.

3 Proposed System

AVATAR is proposed as a two-phase system involving both hardware and software implementation.

Phase 1. IOT SMART MIRROR.

Phase 2. AUGMENTED REALITY DRESSING ROOM.

Figure 1 shows an overall view of the AVATAR system with all its detailed components and control flow. There are mainly six modules in this system as listed below:

- IoT Smart Mirror
- Hand Gesture Mouse Control
- Adding virtual clothes on the video
- AVATAR Web Interface
- Skin Segmentation and Dominant Tone/Color Extraction
- Recommendation Module.

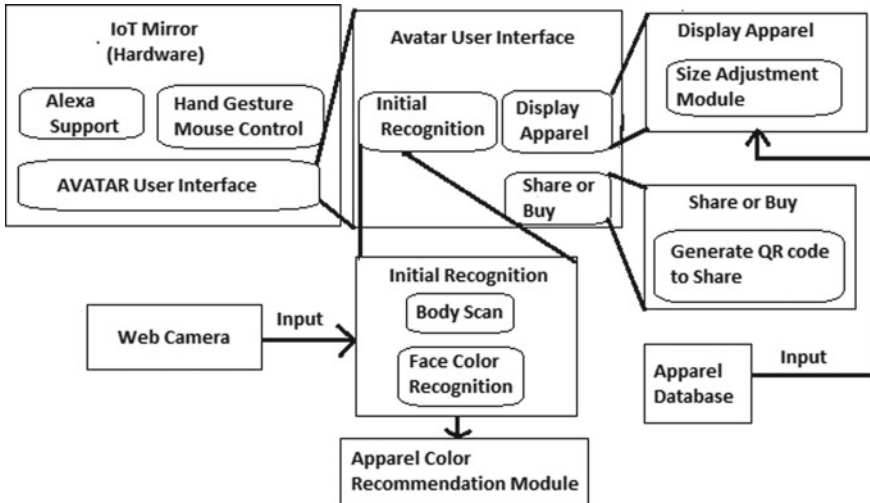


Fig. 1 Architectural diagram of AVATAR

3.1 IoT Smart Mirror

The system uses a raspberry pi based processor board along with display and IoT-based circuitry and the recognition sensor interfaced together. The outer frame is constructed by a precisely modeled panel. A specialized glass consisting of a back frame to encase the system is used. The frame cavity is fitted with precisely positioned mounts for the display housing to be fitted in the mirror. This is necessary to achieve the desired effect. Then raspberry pi is used to connect with the internet using IoT circuits through the use of a Wi-Fi module. This allows receiving data through the IoT platform. IoTGecko used to connect the system to the internet and get 3D models from the database.

IoT Smart Mirror acts as a User Interface (UI). The customers can select from varied apparel categories. The 3D model of those apparel will be overlapped on their body reflection in the mirror [4]. The customers can choose to capture their look option and do social media sharing (Fig. 2).

3.2 Hand Gesture Mouse Control

It is a mouse simulation system that performs all the functions performed by the mouse corresponding to the hand movements and gestures. Simply speaking, the video is captured by the camera and depending on the hand gestures, you can move the cursor and perform select, a left-click, right-click, drag, and scroll up and down. The hand gestures and tasks to be performed are predefined. This enables the customer

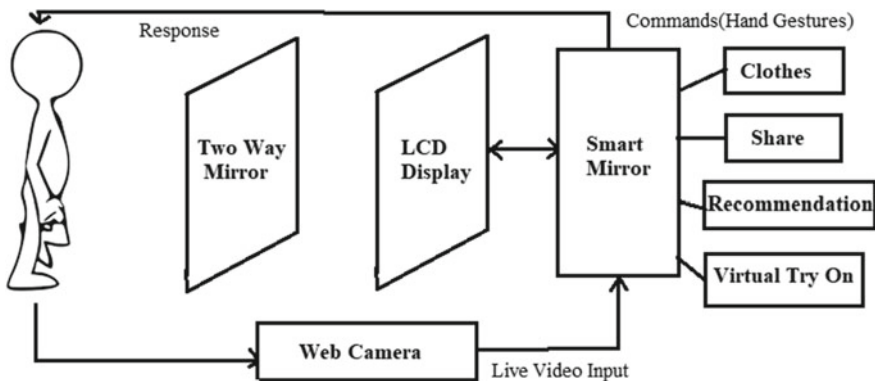
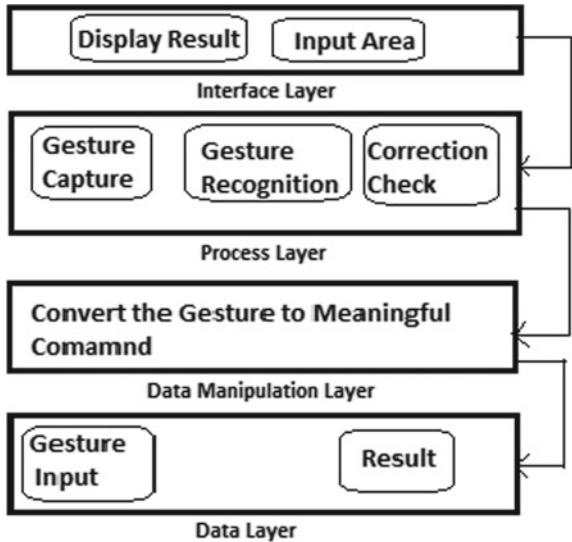


Fig. 2 Architecture diagram for IoT mirror

to select the clothes, scroll through the list of clothes and other activities by their hand gestures. Mouse events in OpenCV used the following functions which proved to be beneficial (Fig. 3):

- cv2.VideoCapture()
- np.array()
- calibrateColor()
- cv2.contourArea()

Fig. 3 Architecture for hand gesture mouse control [5]



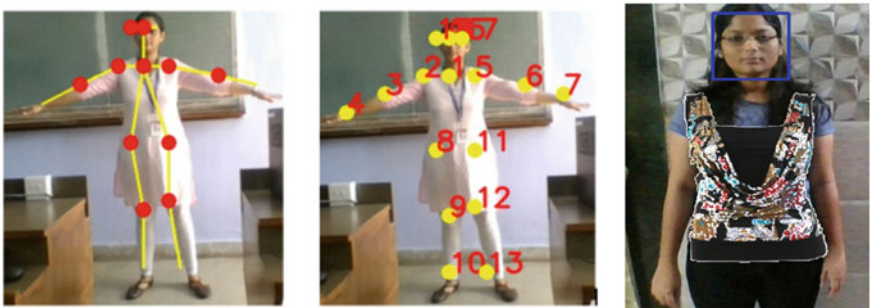


Fig. 4 The skeleton joints found by web camera and the overlapped cloth

3.3 Adding Virtual Clothes on the Video

The customer stands in front of the mirror and selects through the list of clothes displayed using hand gestures. To create skeleton tracking a webcam and TensorFlow along with AI technology is used. The Kinect sensor used in the existing system makes the product expensive. The original Kinect algorithm was based on a machine learning technique called a forest of trees. The original algorithm worked with much cleaner data in the form of the RGB plus depth signal from the camera. However, a neural network can do the job much better and only using RGB. This makes it possible to more or less turn any low-cost webcam in the equivalent of the Kinect in the skeleton tracking model [6].

To place the cloth on the customer, the cloth is resized following with the skeleton points obtained [7]. Upon his/her body movements, the skeleton's related joints change, resulting in the change of position of the related clothing pieces (Fig. 4) [8].

3.4 AVATAR Web Interface

The website facilitates, the customers to easily and rapidly share their images with friends and family. After trying the clothes, the customer can click a photo of their look by giving commands to the system using hand gestures. After the photo is clicked, the customers can select the share option in the mirror. A QR code will be generated. Using the website, the customers can scan the QR code and then select the social media sharing option to share their look and get suggestions. HTML5, CSS3, bootstrap, and jQuery used to create the website [9].

3.5 Skin Segmentation and Dominant Tone/Color Extraction

There is a variance in the skin color of customers. Most of the time they are confused about which color suits them. AVATAR encompasses a recommendation system wherein the customers will be recommended on which color suits them based on their skin tone. For skin tone recognition, following steps are implemented [10].

- Read Image—this is done using OpenCV. OpenCV reads color images in “BGR Color Space”
- Segment out the skin from the image—this is done using OpenCV. Skin Segmentation is done in the HSV Color space using thresholding. `cv2.inRange()` method used to do the thresholding and `cv2.bitwise_and()` to get the final subtracted image from the binary image.
- Find the Dominant Colors—this is the main goal. The K-Mean Clustering Algorithm with the help of the Scikit-learn python package is used (Fig. 5).



Fig. 5 Skin segmentation and dominant tone/color extraction

```
(tensorflow_env) C:\Users\hp\Desktop\AVATAR>python final.py
Color Information
{'cluster_index': 4,
 'color': [141.7131242741013, 113.34378629500529, 96.87340301974407],
 'color_percentage': 0.3061877667140825}

{'cluster_index': 1,
 'color': [105.85929648241134, 81.42378559464017, 73.07202680066956],
 'color_percentage': 0.21230440967283074}

{'cluster_index': 0,
 'color': [172.9273648648658, 147.7550675675675, 131.44594594594582],
 'color_percentage': 0.21052631578947367}

{'cluster_index': 2,
 'color': [67.08092485549172, 49.31599229287089, 38.28709055876688],
 'color_percentage': 0.1845661450924609}

{'cluster_index': 3,
 'color': [201.9629629629626, 189.18106995884804, 184.9506172839504],
 'color_percentage': 0.0864153627311522}
```

Fig. 6 Recommendation system

3.6 *Recommendation Module*

The Skin Segmentation and Dominant Tone/Color Extraction Module provide the input to this module. A predefined set of skin colors and their corresponding cloth color is present. The algorithm searches for the input color in the set and finds out its corresponding cloth color and gives it as a recommendation to the customer on the UI (Fig. 6).

4 Conclusion

AVATAR presents an efficient and affordable method for the real-time virtual dress-up system. The method consists of two major steps, capture image using a web camera and dresses up using unity. It uses an automatic scaling function to resize the input dress images following the skeleton points of the body. The system has made it easier for customers to choose apparel within a short time with social media sharing and cloth color recommendation features. With the use of TensorFlow the web camera performs the function of the Kinect sensor and thus makes the system affordable.

The system works with intermediate accuracy. Our future project improvements involve increasing the accuracy and response time. We plan to make software for shopkeepers to convert 2d cloth images into 3d and directly store it into a database. The integration of this system with the online shopping portals to ease the shopping will be implemented.

References

1. https://www.researchgate.net/publication/259444143_A_Mixed_Reality_Virtual_Clothes_Try-on_System
2. <https://ieeexplore.ieee.org/document/6487501/>
3. <https://ieeexplore.ieee.org/abstract/document/7944092>
4. Onishi, K., Takiguchi, T., Ariki, Y.: 3D human posture estimation using the HOG features from monocular image. In: 19th International Conference on Pattern Recognition
5. <https://www.slideshare.net/VivekKhutale/virtual-mouse-14918971>
6. <https://www.i-programmer.info/news/194-kinect/11522-turn-any-webcam-into-a-microsoft-kinect.html>
7. Shotton, J., Fitzgibbon, A., Cook, M., Sharp, T., Finocchio, M., Moore, R., Kipman, A., Blake, A.: Real-time human pose recognition in parts from single depth images. In: Proceedings of IEEE Conference on Computer Vision and Pattern Recognition, pp. 1297–1304 (2011)
8. Li, H., Liu, Z.: A more practical automation dressing method for clothes animation. In: 8th International Conference on Intelligent Human-Machine Systems and Cybernetics (2016)
9. <http://avatarshare.000webhostapp.com/>
10. <https://medium.com/datadriveninvestor/skin-segmentation-and-dominant-tone-color-extraction-fe158d24badf>

A Novel Fault-Detection Scheme for Nearest-Neighbor-Based Reversible Circuits



Anirban Bhattacharjee, Chandan Bandyopadhyay, Bappaditya Mondal,
and Hafizur Rahaman

Abstract Since last couple of years, the field of reversible logic synthesis has progressed significantly. Starting from improved design methodologies to efficient testing algorithms, this field has witnessed several prominent research findings, and still research is going for developing more reliable design techniques. Inspired from existing testing works, here, we are proposing an efficient testing scheme that finds the missing of SWAP gates from nearest neighbor (NN) circuits using only single test pattern. Unlike conventional testing algorithms that highly rely on a set of test vectors, here, we test the circuit by finding a design for testability (DFT) model. This testing scheme is very capable to find not only single missing SWAP gates but also can detect multiple missing of SWAP gates in design using the single test pattern. In order to find the correctness of our approach, we have tested our algorithm over a large spectrum of benchmarks and have compared our obtained results with some peer-reviewed works.

Keywords Quantum circuit · Quantum gate · Nearest neighbor (NN) · SWAP gate

1 Introduction

Quantum computing is an alternative computing model based on the rules of quantum physics using quantum circuits for solving certain computational problems more efficiently than existing classical algorithms [1]. Quantum circuits are exploited for

A. Bhattacharjee · C. Bandyopadhyay (✉) · B. Mondal · H. Rahaman

Department of Information Technology, Indian Institute of Engineering Science and Technology, Howrah, West Bengal 711103, India

e-mail: chandanb.iiest@gmail.com

A. Bhattacharjee

e-mail: anirbanbhattacharjee330@gmail.com

B. Mondal

e-mail: bappa.arya@gmail.com

H. Rahaman

e-mail: rahaman.h@gmail.com

© Springer Nature Singapore Pte Ltd. 2020

M. Pant et al. (eds.), *Soft Computing: Theories and Applications*,
Advances in Intelligent Systems and Computing 1154,
https://doi.org/10.1007/978-981-15-4032-5_45

processing quantum bits (qubit) represented as quantum information units. These quantum data units are considered equivalent to Boolean values of 0 and 1 used in classical circuit. Such quantum bits can be realized either as states of electronic spins (up and down) or polarization states (horizontal and vertical) of photon, and these correspond to computational basis states of $|0\rangle$ and $|1\rangle$.

Furthermore, a massive challenge toward efficient realization of quantum computer is to accomplish quantum error correction [2]. To address this, error correcting codes like surface codes [3] is needed. Implementation of these codes demands nearest-neighbor architecture where the qubits are allowed to interact with only adjacent neighbors, and the simplest NN architecture is referred to as linear nearest neighbor (LNN). To realize such architectural design, we need to incorporate additional gates so-called SWAP in a given quantum circuit. Application of such gates increases the depth of the resultant circuit which in turn becomes a challenge for an efficient final representation. Therefore, synthesis of efficient LNN realization has been extensively studied for some essential application like Clifford + T [4] and error correction [2].

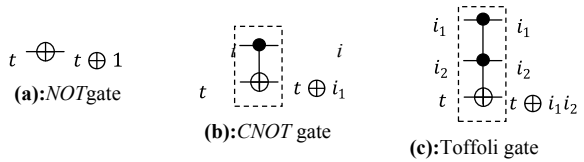
Basically, LNN-based optimization has been undertaken on quantum circuit specifications, but recently, such optimization problem is also being considered essential for reversible functions as discussed in the articles [5, 6], respectively. Conventionally, reversible function specifications need to be represented using Toffoli gate network [7]. Before realizing LNN-based reversible representation, such networks need to be developed using various synthesis approaches like ESOP-based methods [8–11], transformation-based method [12], group theory-based methods [13–15], and BDD-based approach [16], respectively. In NN realization process, SWAP gates play a significant role, and here in this article, we have studied the effect generated considering missing of any SWAP gates in the resultant LNN architecture. To uncover such SWAP missing fault, a DFT structure has been designed, and experimentally, it is verified by running over a set of reversible benchmark specifications.

In the next section (Sect. 2), we have discussed on the fundamentals of quantum circuit and nearest-neighbor representation. Problem formulation and motivation of the work are summarized in Sect. 3. The proposed methodology with examples is stated in Sect. 4. Section 5 contains the experimental results and an analysis of our design methodology. Finally, the concluding remarks appear in Sect. 6.

2 Background

Any Boolean function $f: B^n \times B^m$ acting over a variable set $X = \{x_1, x_2, x_3, \dots, x_n\}$ is said to be reversible if it satisfies the bijective mapping condition between the inputs (n) and outputs (m) (each input vector uniquely maps to an output vector). In addition to this, the number of input lines n must be equal to the number of output lines m ($n = m$). Reversible circuits can be realized by combining a set of reversible logic gates. Schematic representations of some of the well-known reversible gates like NOT, CNOT, Toffoli (NCT) are depicted in Fig. 1.

Fig. 1 Basic reversible gates



These MCT gates are used to form an MCT circuit, and such a circuit having gate with multi-control input is shown in Fig. 2a. This MCT circuit does not attend LNN architecture as it contains a three-control MCT gate which needs to be represented into a set of Toffoli gate network. For this purpose, initially, the circuit shown in Fig. 2 has been decomposed into an equivalent NCT circuit (see Fig. 2b) by decomposing this three-control gate using standard decomposition rules discussed in [20]. Decomposition of this MCT gate into its corresponding NCT representation requires a garbage line g shown in Fig. 2b. Now, this circuit can be transformed into its corresponding LNN structure (see Fig. 2c) by placing SWAP gates as stated in [6].

SWAP gate is a kind of reversible gate with only two target inputs interchanging the values fed to the circuit as shown in Fig. 3a. This swapping functionality is realized using a cascade of three CNOT gates acting on two lines such that the control and target inputs of each gate are placed on alternating lines as represented in Fig. 3b, c, respectively. The symbolic notation of SWAP gate along with its functional composition is depicted in Fig. 3.

Basically, SWAP gates are inserted before gates whose control and target nodes are not located at adjacent positions and thereby make the corresponding gate NN-compliant. The logic values provided at the input of these gates are interchanged

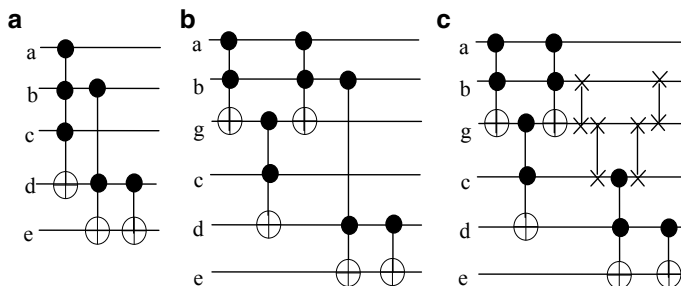
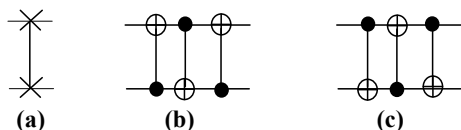


Fig. 2 **a** MCT circuit, **b** NCT equivalent of Fig. 2a, **c** LNN design of Fig. 2a using [10]

Fig. 3 Structural representation of SWAP gate



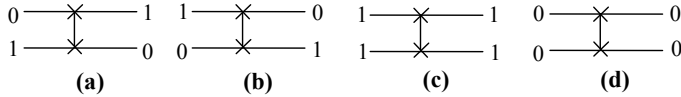


Fig. 4 SWAP gate functionality over different logic values

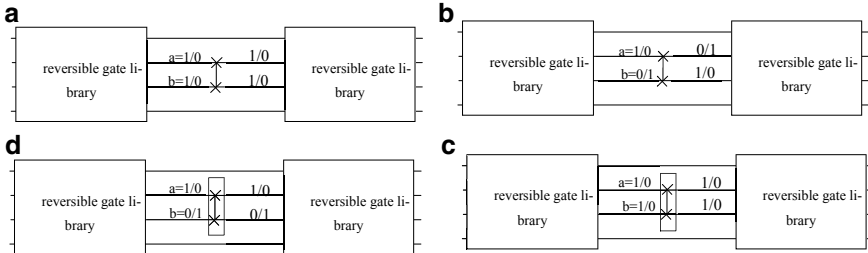


Fig. 5 **a** Effect of SWAP gate for inputs 11, 00 in a reversible circuit. **b** Effect of SWAP gate for inputs 10, 01 in a reversible circuit. **c** Effect of removal of SWAP gate for inputs 11, 00 in a reversible circuit. **d** Effect of removal of SWAP gate for inputs 10, 01 in a reversible circuit

to become its corresponding output values. However, if any of the inserted SWAP gates disappears from the resultant NN circuit, then such a missing gate fault can be identified by providing only distinct logic values of 0 and 1 at its inputs, otherwise application of similar logic values of either 1 or 0 fails to detect this SWAP gate fault. Presence or absence of SWAP gate produces identical values at the output for similar input logic values. For better understanding, behavior of SWAP gate for four different input logic value combinations has been depicted in Fig. 4.

This phenomenon has been more clearly described considering a reversible netlist as illustrated in example 1.

Example 1

Consider a reversible circuit shown in Fig. 5a–d with SWAP gate (G_s) having inputs (a, b) and a reversible gate library containing the basic reversible gates.

The effect of removal of SWAP gate (G_s) in a reversible circuit has been described here. For the given circuit, presence of a SWAP gate produces the outputs (1, 1), (0, 0), (0, 1), (1, 0) for the corresponding input patterns (1, 1), (0, 0), (1, 0), (0, 1) generated at inputs a and b of G_s , whereas complete removal of G_s (represented within a box) produces the pattern (1, 1), (0, 0), (1, 0), (0, 1) at the outputs as depicted in Fig. 5a–d.

3 Motivation and Problem Formulation

From the previous discussions, it is evident that NN property is an important phenomenon in the physical implementation of quantum circuit. Additionally, if such NN-based circuit suffers fault due to missing of SWAP gates, then it is very important

to detect and correct the occurred fault. Though existing testing algorithms are sufficient to detect such fault, it takes a large number of test vectors to find the error, which eventually increases the time requirement in finding the fault. Aiming to improve the fault finding rate, here, we are proposing a DFT-based fault model for efficient detection of missing SWAP gates from NN-based designs.

4 Proposed Method

In this article, a design methodology has been described that facilitates in determining missing of SWAP gates in a given reversible LNN circuit. For this purpose, a design for testability (DFT) has been developed. The DFT structure along with the testing scheme is discussed next.

Lemma 1 *In any reversible circuit C_R with n input lines, missing of any SWAP gate (G_s) in C_R with inputs a and b can be detected if the input logic values (a, b) of G_s are complement to each other. For instance, if $a = 0$ and $b = 1$ or $a = 1$ and $b = 0$, then the fault can be identified, otherwise it remains undetected.*

Proof

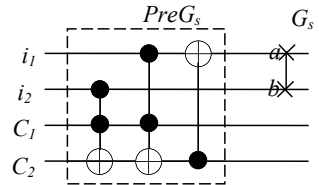
In reversible circuit C_R , if any of the patterns (0, 1) or (1, 0) or (1, 1) or (0, 0) are fed at the inputs (a, b) of any SWAP gate G_s , then these input values get exchanged and become the outputs of the corresponding gate G_s as shown in Fig. 5.

By referring Fig. 5a–c, it can be seen that the input pattern (00) and (11) does not have any effect on the missing of SWAP gate in reversible circuit. So, the pattern 00 and 11 fails to identify this fault. But from Fig. 5b, d, it can be verified that the patterns 01 and 10 can generate different input/output combinations for the presence and removal of SWAP gates in a circuit. Therefore, 01 and 10 can be used to identify any SWAP gate missing fault in the given circuit.

4.1 Testable Design for Detecting SWAP Gate Missing Fault

To construct the DFT structure, a pre-block ($\text{Pre}G_s$) structure containing a network of Toffoli and CNOT gates are appended before a SWAP gate (G_s). In pre-block, two extra garbage lines ($C1$ and $C2$) in addition to the input lines ($i1, i2$) containing SWAP gate G_s are used. For testing purpose, these lines are set at logic value 1, otherwise they can be set anything at normal condition. In pre-block, two Toffoli gates (PreToff1 , PreToff2) are placed in such a way that their target nodes are positioned at line $C2$ and one of their control nodes are located at line $C1$ while the other control nodes are placed at the input lines of SWAP gate as depicted in Fig. 6. After the application of two consecutive Toffoli gates, a CNOT gate (PreCNOT) is applied whose control

Fig. 6 Pre-block structure of SWAP gate (G_s)



node is placed on the same line as that of the one containing the target nodes of the Toffoli gates (PreToff1, PreToff2), and its target node is placed at the input line i_1 . The purpose of applying pre-block is to make the inputs a and b complementary to each other so as to generate the input pattern 10 and 01 at the output of PreGs irrespective to the logic values applied at the inputs i_1, i_2 of a reversible circuit CR and thereby making it possible to detect missing of SWAP gates. More precisely, for any reversible circuit with a sequence of n CkNOT gates ($K \geq 0$), our intention is to design a DFT structure by supplementing some redundant gates along with a couple of additional input lines (C_1 and C_2) such that application of any test pattern at the input end uncovers the fault in the given circuit. The pre-block design structure for any gate SWAP gate (G_s) in a circuit CR has been represented in Fig. 6.

Example 2

Consider again the reversible circuit shown in Fig. 6 containing the pre-block design structure of SWAP gate G_s generating the input pattern $a = 1, b = 0$ or $a = 0, b = 1$ for G_s regardless of any input combination (i_1, i_2) applied to the circuit. The two garbage lines C_1 and C_2 are initially set at logic value 1 and used in PreGS to produce the desired binary pattern at the inputs a, b . For the binary pattern $i_1 = 1, i_2 = 1, C_1 = 1, C_2 = 1$ applied to the given circuit generates the combination 0111 at the output of PreGS or the inputs a , bare assigned the logic pattern 01 as shown in Fig. 7a. Similarly, for other circuit input patterns such as 0011, 0111, and 1011

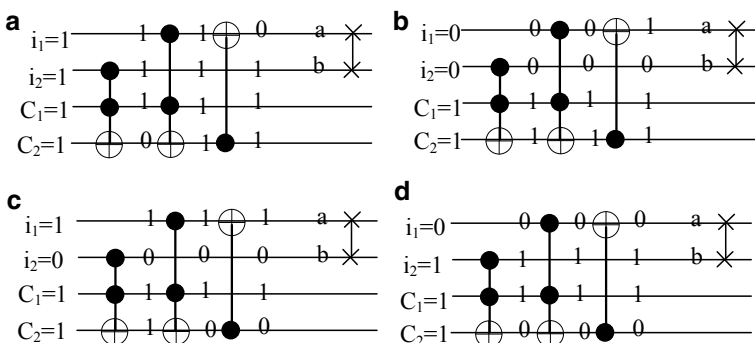


Fig. 7 **a** Pre-block output for input 1111. **b** Pre-block output for input 0011. **c** Pre-block output for input 1011. **d** Pre-block output for input 0111

produce the values 1011, 1010, 0110 at the outputs of PreGs, and accordingly, the inputs (a, b) of G_S are set as 10, 10, and 01 (see in Fig. 7b–d).

Lemma 2 *In an n input reversible circuit CR for any binary string supplied at the input of pre-block (PreGS) of a two-input SWAP gate, G_S (a, b) produces either of the vectors ab or ab at the inputs of G_S .*

Proof

Consider the pre-block design structure of SWAP gate G_S shown in Fig. 6 and assume that the inputs $i_1 i_2 C_1 C_2$ are applied at Pre_{GS}. This pattern $i_1 i_2 C_1 C_2$ will be processed as follows

$$\text{Pre}_{T\text{off}1}(i_2, C_1; C_2) : C_2 = C_2 \oplus C_1 i_2 = 1 \oplus 1. i_2 = 1 \oplus i_2 = \bar{i}_2 [C_1 = C_2 = 1]$$

$$\text{Pre}_{T\text{off}2}(i_1, C_1; C_2) : C_2 = C_2 \oplus C_1 i_1 = \bar{i}_2 \oplus 1. i_2 = 1 \oplus i_2 [C_2 = i_2, C_1 = 1]$$

$$\text{Pre}_{\text{CNOT}}(i_1, C_2) : i_1 = i_1 \oplus C_2 = i_1 \oplus i_1 \oplus \bar{i}_2 = \bar{i}_2$$

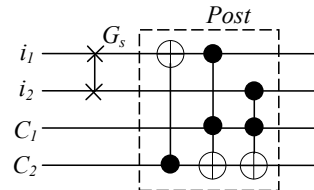
Furthermore, it can be observed from Fig. 6 that $a = i_1 = i_2$ and $b = i_2$, so a, b are complementary to each other and thereby making the detection of removal of G_S from C_R becomes possible.

Moreover, by examining Fig. 7a–d, it can be observed that the inputs a, b of SWAP gate G_S are at different logic states viz when $a = 1$ then $b = 0$ and vice versa.

It can be observed from Fig. 7c, d that for the input combinations 1011, 0111 the logic value of line C_2 inverted from 1 to 0 as the corresponding output pattern obtained after pre-block are 1010 and 0110, respectively.

However, the logic value of C_2 remains at state 1 for the other two input combinations 1111 and 0011 as depicted in Fig. 7a, b. The logic value at line C_2 needs to be restored to its original for further identifying the missing SWAP gates from the selected circuit. In order to restore the logic state of C_2 back to 1, a post-block (Post _{G_S}) design template has been appended after a SWAP gate. To construct Post _{G_S} , a design structure equivalent to that of Pre _{G_S} has been implemented but applied in the reverse order. In other words, the same set of gates used in Pre _{G_S} is also implemented in Post _{G_S} , but the position of the gates are being changed like the first and last gate viz Pre_{Toff1} and Pre_{CNOT} exchanges their respective positions while the position of the second gate (Pre_{Toff2}) remains unchanged. For better apprehension, the pictorial representation of post-block Post _{G_S} for a SWAP gate in a reversible circuit has been depicted in Fig. 8.

Fig. 8 Post-block structure of SWAP gate (G_S)



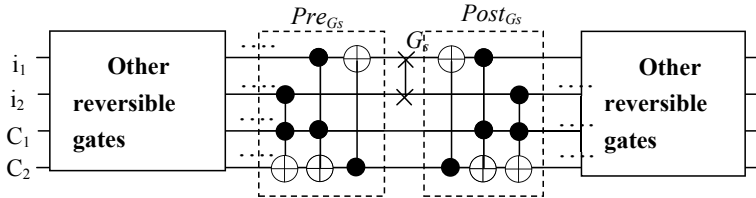


Fig. 9 Testable design structure for SWAP gate in reversible circuit

The purpose of Pre_{G_s} and Post_{G_s} in our DFT structure has already been explained earlier along with their corresponding gate composition as depicted in Figs. 6 and 8, respectively. For compact representation, now, both the Pre_{G_s} and Post_{G_s} of a SWAP gate G_s are combined together to form the complete testable design template for any SWAP gate in a reversible netlist as shown in Fig. 9.

Detection of such SWAP gate missing in a reversible circuit can be made possible by comparing only the inputs and outputs of pre-block and post-block, respectively. To ease the understanding, it has been explained in the following two cases.

Case 1 $G_s \neq \text{NULL}$ (SWAP gate is not missing)

In this case, investigation of any such non-removal of SWAP gate G_s from a given circuit can be ensured provided the input combination of Pre_{G_s} is distinct from the output combination of Post_{G_s} . In other words, if the input and output patterns of Pre_{G_s} and Post_{G_s} completely mismatch, then non-removal of the corresponding gate G_s can be ensured.

Case 2 $G_s = \text{NULL}$ (SWAP gate is missing)

This case indicates that a SWAP gate G_s is missing from a reversible circuit, and it can only be verified if the input pattern of Pre_{G_s} is identical to the output pattern of Post_{G_s} .

Algorithm 1 DFT structure

Input: reversible circuit C_R with $n(i_1, i_2, i_3, \dots, i_n)$ lines, N gates and s SWAP gates.

Output: Testable Design (TD) for each of the s SWAP gates in reversible circuit C_R .

Begin

1. Add two lines C_1, C_2 and set $C_1 = C_2 = 1$.

2. **for** $i = 1$ to N

 2.1 **if** ($i \neq s$) **then**

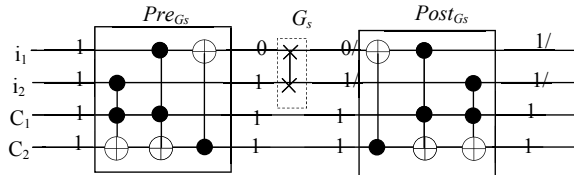
 2.1.1 **continue**

 2.2 **else**

 2.2.1 pos = COMP_POS_SG(i);

 2.2.2 ARR [2] = FIND_INPS _SG(i);

Fig. 10 Missing of SWAP gate detection from the input/output combination of Pre_{G_s} and $Post_{G_s}$



```

2.2.3 Set temp = pos;
2.2.4 ADD PRECNOT(ARR[0],C2) at temp-1;
2.2.5 ADD PreTOFF2(ARR[0],C1,C2) at temp-2;
2.2.6 ADD PreTOFF1(ARR [1],C1,C2) at temp-3;
2.2.7 Duplicate PRECNOT(ARR[0],C2) at pos+1;
2.2.8 Duplicate PreTOFF2(ARR[0],C1,C2) at pos+2;
2.2.9 Duplicate PRECNOT(ARR[0],C2) at pos+3;

3 end if
4 end for
5 return TD
6 end

```

Example 3 For the reversible circuit shown in Fig. 10 with only SWAP gate G_s together with its Pre_{G_s} , $Post_{G_s}$ are represented to identify the missing of G_s . For the vector 1111 applied at the input, Pre_{G_s} generates 0111 at its output and 01 at input of G_s . Removal of the corresponding gate G_s (indicated with dotted box) passes the pattern 0111 unchanged and becomes the input of $Post_{G_s}$. For the vector 0111, $Post_{G_s}$ produces the corresponding output vector 1111 which is identical to the input of Pre_{G_s} and thereby confirming the removal of gate G_s from the given circuit. On the other hand, in presence of G_s , the combination 1011 would have been generated at the input of $Post_{G_s}$ as the input 01 of G_s gets swapped (10) and produces the combination 1011 at the input of $Post_{G_s}$. Applying the vector 1011 at $Post_{G_s}$ generates 0011 at its output, which is not identical to that input vector 1111 of Pre_{G_s} and ensures the existence of the corresponding SWAP gate G_s .

In Algorithm 1, the details about the construction of DFT structure have been described that generates a testable design (TD) in order to detect missing of any SWAP gate from a given reversible circuit.

5 Experimental Results

In way to verify the correctness of our algorithm, we have tested the design flow over a wide range of benchmarks [17] and the obtained results are summarized in Table 1. Comparison with two relevant state-of-the-arts design works [18, 19] is also given in the result table. From the results, it is very pertinent that our testing model improves the testing overhead considerably as it takes only single test vector to find

Table 1 Comparison with other testing approaches

Benchmarks specifications		Required test vectors from work [18] to detect SWAP missing	Test vectors needed to detect SWAP missing using work [19]	Test vectors needed to detect SWAP missing using our proposed approach	% improvement over	
Circuit name	No. of lines				Work [18]	Work [19]
<i>ham3</i>	3	3	2	1	66	50
<i>nth prime</i>	3	4	3	1	75	66
<i>317_tc</i>	3	5	3	1	80	66
<i>decode_v1_39</i>	4	4	4	1	75	75
<i>mod10_176</i>	4	4	2	1	75	50
<i>mod5d270</i>	5	2	2	1	50	50
<i>rd32_v0_67</i>	4	3	3	1	66	66
<i>4gt_11_84</i>	5	6	5	1	84	80
<i>4gt_v1_93</i>	6	11	8	1	90	88
<i>xor5_254</i>	6	10	4	1	90	75
<i>alu_v4_37</i>	5	6	4	1	84	75
<i>123_v3_101</i>	5	3	3	1	66	66
<i>ex1_226</i>	6	5	4	1	80	75
<i>decode24_enable_125</i>	6	8	8	1	88	88
<i>4mod5_v1_22</i>	5	3	3	1	66	66
<i>aj_e11_168</i>	4	4	3	1	75	75
<i>BAC_v1_06</i>	6	21	14	1	95	93
<i>ABC_v1_05</i>	5	9	7	1	89	81
<i>BAC_v1_07</i>	7	8	7	1	86	81
<i>BAC_v1_08</i>	8	21	15	1	94	92
<i>rd53_139</i>	8	14	11	1	93	90
<i>ABC_v1_07</i>	10	31	23	1	96	95
<i>ABC_v1_06</i>	14	43	34	1	98	97

missing SWAP gates from the designs, where other two test model takes huge test vector to find the fault.

6 Conclusion

Here, we have shown a DFT-based model for efficient detection of SWAP gates from NN designs. We have also demonstrated that our proposed testing scheme can detect all type of SWAP missing faults from NN designs using a single test vector. A variety of benchmarks are executed to test our fault-detection model, and the obtained results are recorded in result table. Comparisons with relevant test works also have been made in our work.

References

- Shor, P.W.: Quantum computing. In: Documenta Mathematica-Extra Volume. ICM, pp. 1–1000 (1998)
- Fowler, A.G., Hill, C.D., Hollenberg, L.C.: Quantum-error correction on linear-nearest-neighbor qubit arrays. *Phys. Rev. A* **69**(4), 042314 (2004)
- Fowler, A.G., Mariantoni, M., Martinis, J.M., Cleland, A.N.: Surface codes: towards practical large-scale quantum computation. *Phys. Rev. A* **86**(3), 032324 (2012)
- Biswal, L., Bandyopadhyay, C., Chattopadhyay, A., Wille, R., Drechsler, R., Rahaman, H.: Nearest neighbor and fault-tolerant quantum circuit implementation. In: IEEE International Symposium on Multiple-Valued Logic (ISMVL), pp. 156–161 (2016)
- Wille, R., Lye, A., Drechsler, R.: Considering nearest neighbor constraints of quantum circuits at the reversible circuit level. *Quant. Inf. Process.* **13**(2), 185–199 (2014)
- Chakrabarti, A., Sur-Kolay, S., Chaudhury, A.: Linear nearest neighbor synthesis of reversible circuits by graph partitioning. arXiv preprint: 1112.0564 (2011)
- Toffoli, T.: Reversible computing. In: International Colloquium on Automata, Languages and Programming. Springer, Technical Memo-MIT/LCS/TM-151, MIT Laboratory for Computer Science (1980)
- Rice, J.E., Suen, V.: Using autocorrelation coefficient-based cost functions in ESOP-based Toffoli gate cascade generation. In: Canadian Conference on Electrical and Computer Engineering. Calgary, Canada, pp. 1–6 (2010)
- Rice, J.E., Nayem, N.: Ordering techniques for ESOP-based Toffoli cascade generation. In: Pacific Rim Conference on Communications, Computers and Signal Processing (PacRim), Victoria, Canada, pp. 274–279, (2011)
- Nayem, N.M., Rice, J.E.: A shared-cube approach to ESOP-based synthesis of reversible logic. *Facta Universitatis Niš E, Elec. Energ.* **24**(3), 385–402 (2011)
- Fazel, K., Thornton, M.A., Rice, J.E.: ESOP-based Toffoli gate cascade generation. In: Pacific Rim Conference on Communications, Computers and Signal Processing (PacRim), Victoria, Canada, pp. 206–209 (2007)
- Miller, D.M., Maslov, D., Dueck, G.W.: A transformation based algorithm for reversible logic synthesis. In: Design Automation Conference (DAC), Anaheim, USA, pp. 318–323 (2003)
- Saeedi, M., Sedighi, M., Zamani, M.S., Cayirci, E.: A library-based synthesis methodology for reversible logic. *Elsevier Microelectron. J.* **41**(4), 185–194 (2010)
- Saeedi, M., Zamani, M.S., Sedighi, M., Sasanian, Z.: Reversible circuit synthesis using a cycle-based approach. *ACM J. Emerg. Technol. Comput. Syst.* **6**(4), 13:1–13:26 (2010)
- Sasanian, Z., Saeedi, M., Sedighi, M., Zamani, M.S.: A cycle-based synthesis algorithm for reversible logic. In: Design Automation Conference (DAC), San Francisco, USA, pp. 745–750 (2009)
- Wille, R., Drechsler, R.: BDD-based synthesis of reversible logic for large functions. In: Design Automation Conference (DAC), San Francisco, USA, pp. 270–275 (2009)

17. Wille, R., Große, D., Teuber, L., Dueck, G.W., Drechsler, R.: RevLib: an online resource for reversible functions and reversible circuits. In: International Symposium on Multi-Valued Logic (ISMVL), pp. 220–225. RevLib is available at <http://www.revlib.org>. (2008)
18. Mondal, B., Kole, D.K., Das, D.K., Rahaman, H.: Generator for test set construction of SMGF in reversible circuit by Boolean difference method. In: Proceedings of IEEE Asian Test Symposium, pp. 68–73 (2014)
19. Kole, D.K., Rahaman, H., Das, D.K., Bhattacharya, B.B.: Derivation of automatic test set for the detection of missing gate faults in reversible circuits. In Proceedings of IEEE Symposium on Electronic System Design, pp. 200–205 (2011)
20. Perkowski, M., Lukac, M., Shah, D., Kameyama, M.: Synthesis of quantum circuits in linear nearest neighbor model using positive Davio Lattices. Facta Universitatis, Series: Electron. Energetics **24**(1), 71–87 (2011)

Automated Railway Gate Control Using Internet of Things



B. Arunjyothi and B. Harikrishna

Abstract The extensive development on the internet of things (IoT) like radio blaze, multiple local connections and software, and hardware-related marketing shows product demands but managing the connections of IoT machines create a barrier to services. In order to increase capability and suitable conditions the Innovative railway enterprise (smart railways) like a gateway, multiple local connections of IoT, and platform server makes an easy grip on wide railway field conditions. To analyse the efficiency of RATs which is Radio Access Technologies on system-level field testing, we introduce Network architecture on power usage perspective.

Keywords Internet of things · Smart railway · Condition-based maintenance · Power consumption · Coverage

1 Introduction

Automatic railway gate system may be a terribly helpful project, that assistance is mechanically gap and shutting the railway gate upon police investigation arrival or departure of the train. The train accidents are in the main as a result of collisions of trains at railway crossings. Railway crossing is associate degree intersection of the road and railway line it wants human coordination to open or shut the gates, lack of this ends up in an accident. Therefore, to avoid human mistakes, throughout the operation of gates, a replacement automatic railway gates system practice IoT is developed. In general, Railway gates unit opened or closed manually by a gatekeeper. The information concerning the arrival of train for gap or closing of the door is received from close to station. But some railway crossings are completely unmanned and lots of railway accidents occur at these unmanned level crossings. To avoid human intervention at level crossings utterly, we want to modify the method of

B. Arunjyothi (✉) · B. Harikrishna

Professor, ECE Department, St.Martin's Engineering College, Secunderabad, Telangana, India
e-mail: bojjaarunjyothi@gmail.com

B. Harikrishna

e-mail: harikrishna07@gmail.com

© Springer Nature Singapore Pte Ltd. 2020

501

M. Pant et al. (eds.), *Soft Computing: Theories and Applications*,
Advances in Intelligent Systems and Computing 1154,
https://doi.org/10.1007/978-981-15-4032-5_46

railway gate management. Automatic railway gate management systems have evidenced to be best-suited resolution to such instances. Track circuiting technique is employed to search out the cracks in the railway track at a awfully early stage that is electrical wiring on tracks is simply determined by station master from the room and repaired. However some isolated places tracks cannot be determined by gang men negligence to date that areas automatic automaton is assigned to sleuthing these areas and causing that data through GPS to require immediate actions. To prove this technique, on wood plank equal metal tracks are factory-made and separated into sections. wherever all sections are marked as numbers and tracks are organized beside tiny metal plates. If any tracks get broken it doesn't pass voltage across rails [1]. This technique doesn't want any human involvement. Infrared radiations are accustomed to build invisible detection employed in railway systems, within which IR sensors are accustomed to notice the locomotion and temperature of the thing. IR light-emitting diode that could be a lightweight Emitting Diode emits rays and detects mistreatment science photodiode. Once the same wavelength of IR Rays emits and received by the photodiode [2]. The amendment in magnitude is analogous to the output voltage and resistance.

2 Literature Survey

Wang et al. [3] explained regarding the advanced train safety system. In this paper, authors defines that within the method of developing ATSS, a fault tolerance methodology was applied for each the hardware and therefore the code elements. The railway gate automation system was in turn enforced in Choosen. The implementation of the system in Choosen effectively reduced the accident rate at the extent cross and therefore the magnetic sensors were utilized in rail-approach gate automation system. Magnetic sensors were placed in underground to sight the movement of trains. However, this method isn't price effective and does not providing destination notification facilities to passengers. Kottalil et al. [4], in this paper, deals with the subject of abundant modern relevancy. In this paper, the authors projected a singular and economical methodology for up the protection at railway level crossings. The projected methodology works on microcontroller. The system uses AT mega 16A microcontroller, IR sensors for watching the arrival and departure of the train and therefore the gate is operated consequently. However, this method isn't providing destination notification facility to passengers. Chellaswamy et al. [5] explained regarding management ling railway gates mistreatment detectors, GPS and GSM. The authors mentioned regarding carrefour controller utilizing GPS and GSM. During this work, the authors combined the employment of GPS (Global Positioning System) trailing system and GSM (Global System for Mobile communication) electronic equipment to accomplish an economical gate closing at the extent crossings. Detectors area unit accustomed sense the arrival and departure of the train and additionally forward this data to the following crossings. The system has been enforced and therefore the results of this projected system showed that it's high speed, accurate, strong and

versatile. Krishnamurthi et al. [6] gave the system that tries to manage the gap and shutting of gates mechanically at railway level crossings. In most of the countries, wherever the gates area unit operated by the gatekeeper at carrefour, the gates stay closed for long durations which can cause dense traffic at close to the gates because of the late arrival of train. The authors were used IR obstacle sight ion sensors to detect the arrival and going away of trains at the railway carrefour. Here authors were used Arduino board to manage the gap or closing of gates. In [7], the journalist addresses the net of Things and its sanctioning agency that is that the affiliation of many technologies and recommendation solutions. In [8, 9], the authors gift an assay of technologies, applications and assay challenges for IOT, its immense inactive and therefore the higher than problems that charge to be tackled to plot avant-garde deep solutions.

3 Proposed System

Figure 1 shows the diagram of the proposed system. In this, the power supply, IR sensors, GPS, Track line are the inputs of the system these are connected to raspberry pi and the outputs are gate(which indicates open and close of railway gate), indicator lights indicate the signal to rail, thing speak is the output.

The power supply 5v is given to the raspberry pi. IR sensors are used to detect the motion of the train on the track. Three sensors are used to represent the status of trains at different distances. Red, Yellow and Green IR sensors indicate the status of gate. If the train is near to the first IR sensor detects the train and given indication as

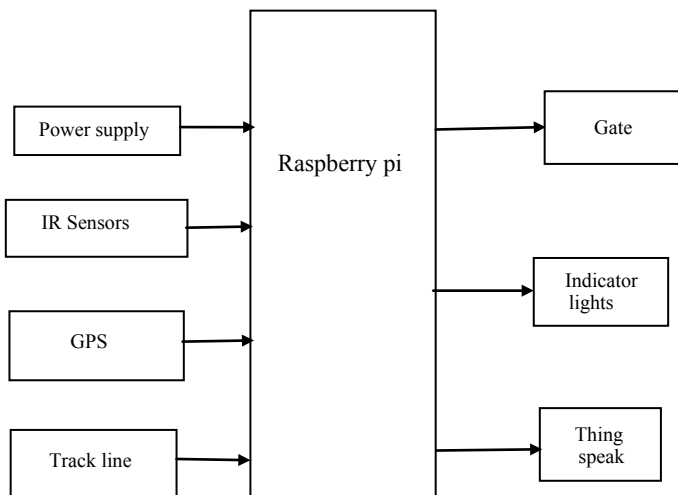


Fig. 1 Implementation of method

yellow light then the gate is opened and when the train is at the gate the second IR sensor detects the train and given indication as red light that time the gate is closed, if the train is crossed the gate the third IR sensor detects the motion of the train and given indication as green light then the gate is opened. The track line is also given to the raspberry pi, The track line is used to find out the track damage. If the track line is disconnected or opened it indicates the track damage and if it is closed there is no damage on the track. The GPS (global positioning system) is to track the location which is shown in thing speak. The thing speak available in cloud, by using the thing speak longitude and latitude values we can see the location by entering these values in Google. The advantage of this system is no need for any manual gate control. It can be done automatically. By using IOT the location of the train can be obtained from anywhere. The prototype consists of raspberry pi, IR sensors, LED, GPS, servomotor.

The raspberry pi runs Linux for an operating system. In this, the raspberry pi is used as a controller. This proposed system can be developed by using raspberry pi. The closing and opening of a gate, all the logic was implemented in python and dumped into the raspberry pi. The raspberry pi controls all the actions opening and closing of a gate, The arrival and departure of train sensing using sensors and tracking of location. An IR sensor is used in this proposed system to sense the arrival and departure of the train. An IR sensor generally comprises of two components: an IR Transmitter and an IR Receiver. An IR Transmitter is a device that emits IR Rays. Similarly, an IR Receiver is a device that detects the IR Rays. This system consists of three LED's (yellow, red, green) when the train arrives or at the gate the red LED will glow and the train departures (near or left at the gate) the yellow, green LED will glow. The servo motor used as railway gate in this proposed system. The opening and closing of gate work on the status of LED. When the train is detected by the IR sensor if it is near to the gate the motor opens the gate and yellow LED will glow. If the train is at the gate, train is detected by the IR sensor and gate motor closes the gate and red LED will glow, if the train is left the gate, it is detected by the IR sensor the gate motor opens the gate and green LED will glow. The global positioning system (GPS) is used to track the location of a train. A GPS receiver is a device that captures signals and provides accurate location. In this, GPS tracks the location and given information to the server. we can see the location of a train in thing speak.

4 Results and Discussion

In this section detailed discussion on the result is done. Figures 2, 3, 4, 5, 6, 7, 8 and 9 show the different results obtained at different condition. Figure 4 shows the hardware kit of the implementation of raspberry pi, IR sensors, servo motor, GPS, LED.

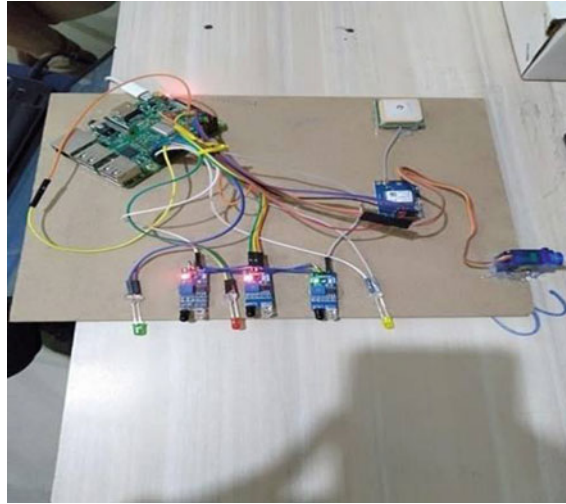


Fig. 2 Hardware kit

Figure 2 shows the hardware of the smart railway feasibility project, which contains raspberry pi, GPS, IR sensors and their connections. As shown in Figs. 3 and 4 If the IR sensor values get high, the GPS location values (long and lat) will send to thing speak, which is freely available in cloud. By using the thing speak longitude and latitude values, we can see the location by entering these values in Google Maps.

Figure 5 explains that the status of the gate (servo motor) and indication light (LED). In this, the train is near to the gate and it is detected by the IR sensor and given indication as yellow light, gate is in open condition. Figure 6 shows that the train is at the gate and it is detected by the IR sensor and the gate is in closed condition, given indication as red light. Figure 7 shows that the train departure or left the gate and it is detected by the IR sensor and the gate in open condition, given indication as green light.

Figures 8 and 9 explain about track damage detection. In Fig. 8 the track line is closed it shows that there is no damage on the railway track. Figure 9 shows that the track line is opened it shows that damage on the track. If it is open it does not pass voltage across the rails and get repaired.

Figure 10 shows the python code of the automatic railway gate control system and it shows all the connections happen through raspberry pi. In this, the gate opening and closing are done automatically according to the train arrival and departure. It gives indication light (yellow, red, green) based on the status of gate (servo motor). The location of a train can be obtained in the thing speak. Figure 11 shows the workflow of the proposed system. In this, if the track line is open then there is damage on the railway track and if it is closed there is no damage. Indicating lights (yellow, red, green) status with respect to the gate status (open, close) can be shown in the above figure. If the indication light or signal is yellow then the gate will be opened and it

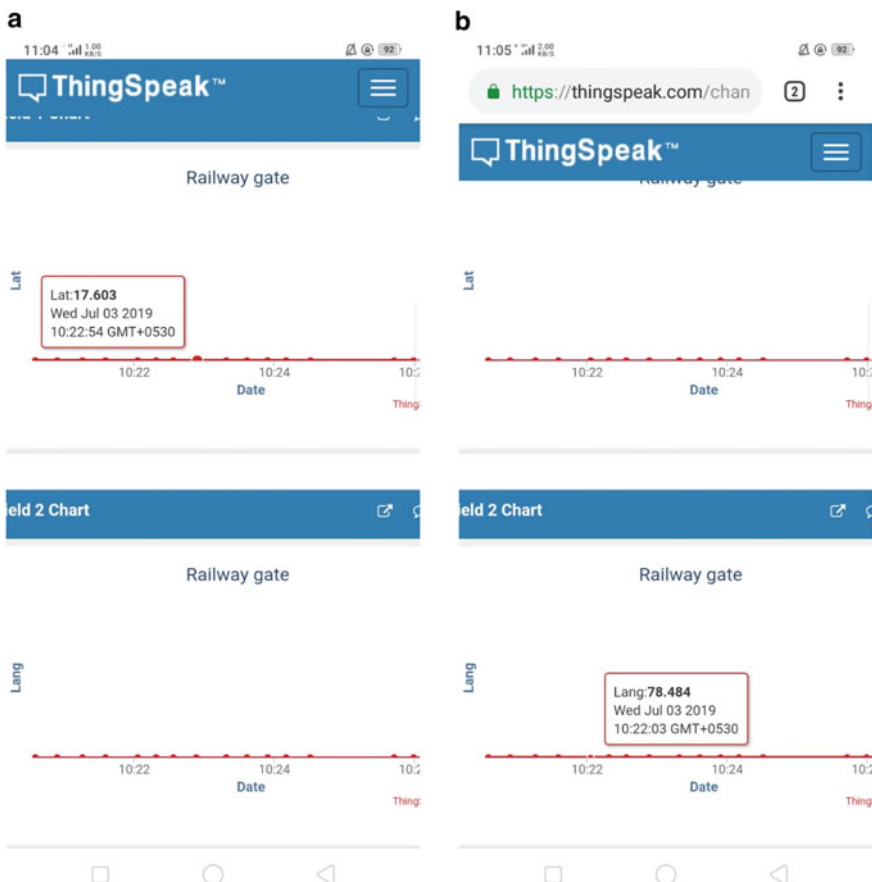


Fig. 3 Thing speak values **a** latitude value, **b** longitude value

indicates that train is near to the gate. If the signal is red then the gate will be closed and it indicates that train is at the gate, If the signal is green then the gate will be opened and it indicates that the train is left the gate.

5 Conclusion

Different IoT methods are used and verified in these railways systems. These IoT systems are the first and widely used traditional methods which are similar connections of the CBM to reduce maintenance burden cost and increase efficiency. So finally conclude that following the given instructions using this IoT-based application in various developed cities make more efficiency in production and reduce time cost and financial burden.

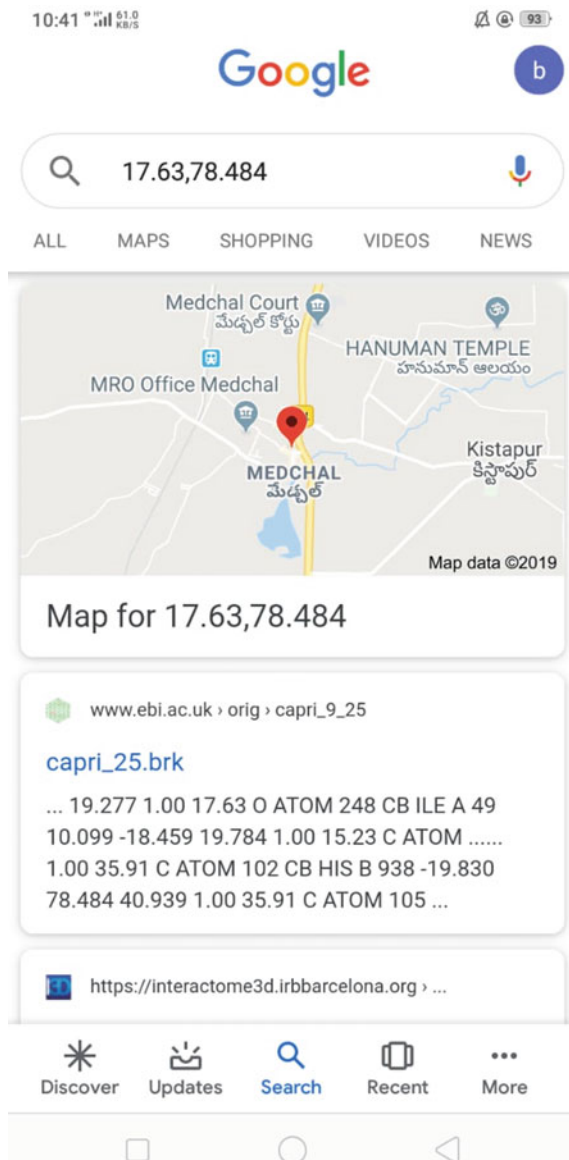


Fig. 4 Location given by the lag and lat values

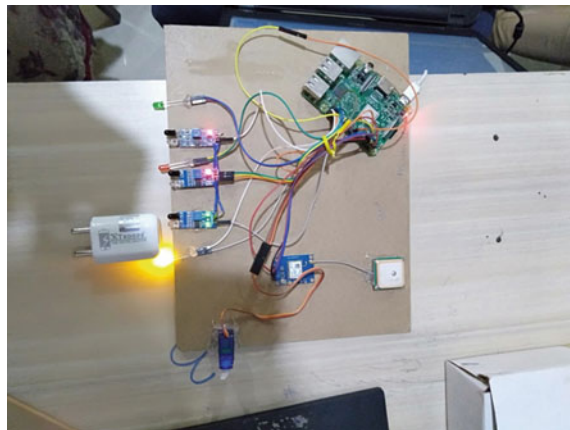


Fig. 5 Yellow LED indicates that gate is open

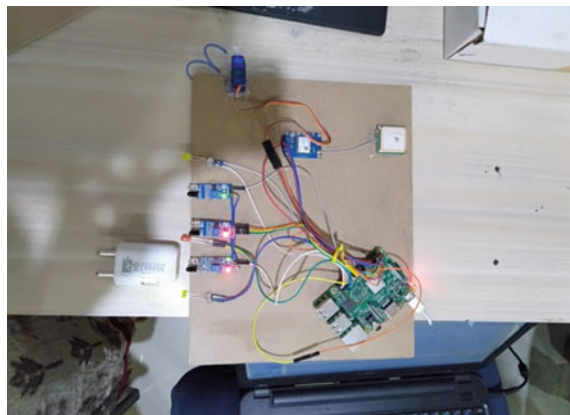


Fig. 6 Green LED indicates that gate is open

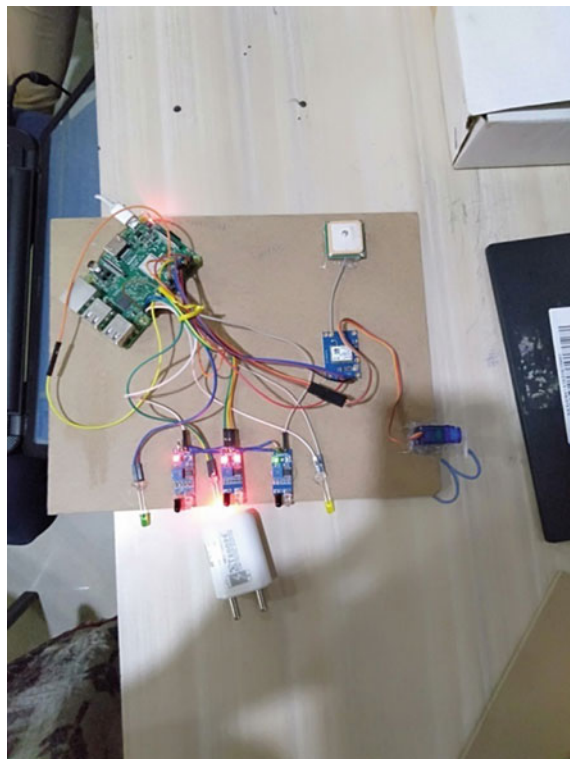


Fig. 7 Red LED indicates that gate is closed

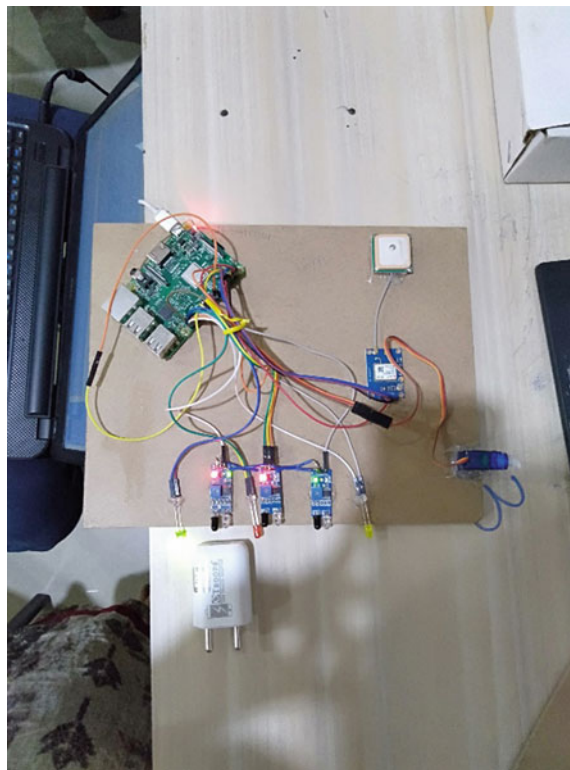


Fig. 8 The track line is closed in the above it indicates there is no damage on the track

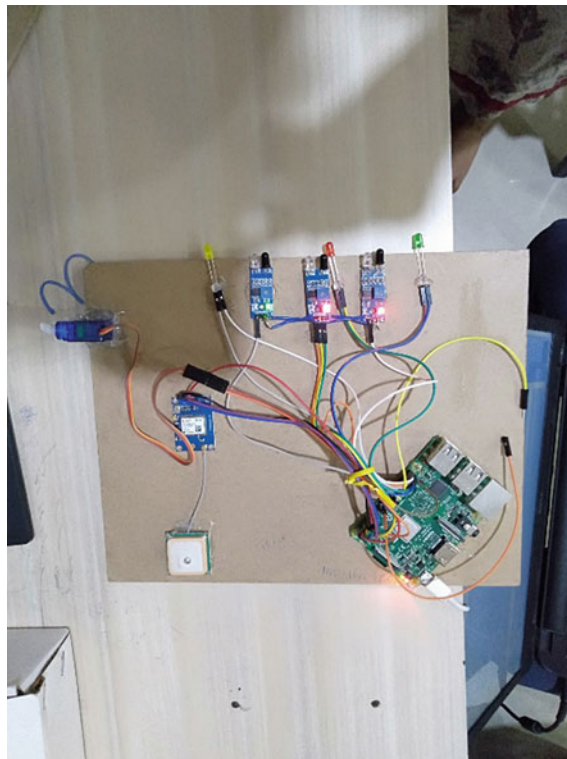


Fig. 9 The track line is open in the above it indicates the damage

```
if useUnsecuredTCP:  
    tTransport = "tcp"  
    tPort = 1883  
    tTLS = None  
  
if useUnsecuredWebsockets:  
    tTransport = "websockets"  
    tPort = 80  
    tTLS = None  
  
if useSSLWebsockets:  
    import ssl  
    tTransport = "websockets"  
    tTLS = {'ca_certs':"/etc/ssl/certs/ca-certificates.crt",'tls_version':ssl.PROTOCOL_TLSv1}  
    tPort = 443  
topic = "channels/" + channelID + "/publish/" + apiKey
```

Fig. 10 Python code of the connections

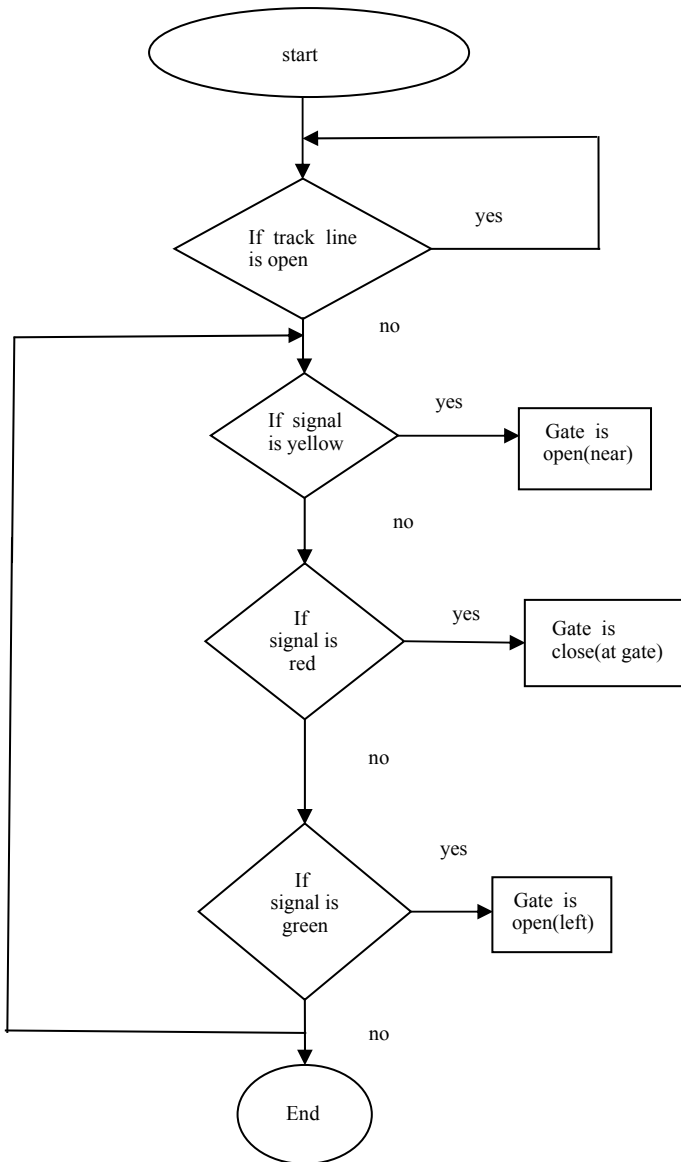


Fig. 11 Flow chart of the proposed system

References

1. Cheng, C.-T., Ganganath, N., Fok, K.-Y.: Concurrent data collection trees for IoT applications. *IEEE Trans. Ind. Informat.* **13**(2), 793–799 (2017)
2. Jo, O., Kim, Y.-K., Kim, J.: Internet of things for smart railway: feasibility and applications. *IEEE Internet Things J.* **5**(2), 482–490 (2017)
3. Wang, X., Bin, N., Yinhang, C.: A new microprocessor based approach to an automatic control system. In: International Symposium on Industrial Electronics, pp. 842–843 (1992)
4. Kottalil, A.M., Abhijith, S., Ajmal, M.M., Abhilash, L.J., Babu, A.: Automatic railway gate control system. *Int. J. Adv. Res. Electr. Electron. Instrum. Eng.* **3**(2) (2014)
5. Chellaswamy, C., Srinivasan, S., Ramesh, R., Babu, A.: Humanitarian intelligent level crossing controller utilizing GPS and GSM. In: 2014 IEEE Global Humanitarian Technology Conference-South Asia Satellite (GHTC-SAS), Trivandrum, Sept 26–27 (2014)
6. Krishnamurthi, K., Bobby, M., Vidya, V., Baby, E.: Sensor based automatic control of railway gates. *Int. J. Adv. Res. Comput. Eng. Technol. (IJAR CET)* **4**(2) (2015)
7. Atzori, L., Iera, A., Morabito, G.: The internet of things: a survey. *Comput. Netw.* **54**(15), 2787–2805 (2010)
8. Miorandi, D., Sicari, S., De Pellegrini, F., Chlamtac, I.: Internet of things: vision, applications and research challenges. *Ad Hoc Netw.* **10**(7), 1497–1516 (2012)
9. Li, S., Da Xu, L., Zhao, S.: The internet of things: a survey. *Inf. Syst. Front.* **17**(2), 243–259 (2015)

Simulated Annealing Based Algorithm for Tuning LDA Hyper Parameters



Nikhlesh Pathik and Pragya Shukla

Abstract LDA is a very popular unsupervised model used to find thematic information about the documents. The performance of the LDA greatly depends on its hyper parameter values. If its parameters are tuned properly then LDA may produce much better results. This paper mainly focused on finding good LDA configurations for finding improved LDA output as compare to the traditional LDA model. We have proposed and implemented SA-LDA algorithm that uses Simulated Annealing (SA) to find optimal values of LDA parameters. An empirical evaluation using customer review datasets from three different domains namely Mobile, Hotel and Movie is conducted. The experiment results show that SA-LDA gives better performance when it is evaluated by the coherence score.

Keywords Hyper parameters · LDA · Simulated annealing · Reviews

1 Introduction

Topic modeling is an unsupervised natural language processing approach that is used to get various topics from a text document for interpretation. Topic modeling is a method to understand, organize, and summarize huge collections of textual information and documents. Topic model works in unsupervised manner to learn topics on unlabeled documents. Basically, a document holds multiple topics in different proportions. The topics are a set of similar words that are produced by topic modeling techniques. Widely used topic modeling algorithms are Latent Dirichlet Allocation (LDA), Latent Semantic Analysis (LSA) or Latent Semantic Indexing (LSI), and Hierarchical Dirichlet Process (HDP). The most frequently adopted topic modeling technique is LDA to extract topics from the textual data. LDA [1, 2] generates a

N. Pathik · P. Shukla

Institute of Engineering & Technology, Devi Ahilya University, Indore, India
e-mail: pathiknikhlesh@gmail.com

P. Shukla
e-mail: pragyashukla_iet@yahoo.co.in

probability distribution of a topic for each document. Corpus of documents is pre-processed and transformed into $d \times w$ document-word co-occurrence matrix $M1$, where w is number of unique terms in all the documents and d represents number of documents.

This $M1$ is input for LDA, which in turn will generate two matrices $M2$ and $M3$. $M2$ is $d \times t$ document-topic matrix, where d represents number of documents and t representing the number of topics. $M3$ represents $t \times w$ topic-word matrix where t represents number of topics and w representing the number of words.

In the last decade, LDA is extensively used for finding hidden topics from the text. The Dirichlet priors α, β has a great impact on the performance of LDA. If α, β are set to appropriate value, LDA output will significantly improve. This paper proposed and implemented SA-LDA for tuning hyper parameters for finding the best LDA configurations.

Rest of the paper is organized as follows: In Sect. 2, related research works are mentioned. Section 3 discussed the proposed algorithm. Section 4 describes the experimental setup and results. Section 5 concludes the paper.

2 Related Work

Recently different optimization approaches are used to tuned LDA parameters like Ant Colony Optimization (ACO), Genetic Algorithm (GA), Hill climbing, Simulated Annealing (SA), etc. We have summarized recent optimization research here.

Yarguy and Kanarkard [3] proposed ACO-LDA method for tuning Latent Dirichlet Allocation (LDA) parameters to improve its performance. They have opted Ant Colony Optimization (ACO) to solve the computational problem by adding parameter tuning. Experiments have conducted on various datasets fetched from the UCI and evaluated on perplexity score. Dit et al. [4] have proposed the concept of LDA-GA and represent an experiment on TraceLab. They extend their approach for software engineering tasks towards a new IR method. A multiobjective optimization algorithm based on simulated annealing approach is suggested by Bandyopadhyay et al. [5]. Gultekin et al. [6] proposed an asymptotic version of simulated annealing for variational inference. Foulds and Smyth [7] introduced new Annealed importance sampling annealing paths a Monte Carlo integration technique. This estimates the relative performance of the models. This strategy can exhibit much lower empirical variance than earlier approaches. The described strategy computes the ratio of the possibility of two models rather than computing the possibility of each model separately. Elhaddad [8] has proposed a hybrid optimization technique by combining GA and SA. This algorithm has been tested on instances of symmetric Traveling Salesman Problem (TSP) from known TSPLIB.

A heuristic approach is proposed by Zhao et al. [9] to estimate the most appropriate number of topics for LDA. The rate of perplexity change (RPC) is calculated and determined by the change point of RPC to the appropriate number of topics. George and Doss [10] combined the Markov Chain Monte Carlo and sampling, for estimating

the hyper parameters. The choice of hyper parameters is completely on the Bayes approach, by putting a prior on the hyper parameter vector, which adds one layer to the hierarchical model. Gultekin et al. [11] have evaluated a stochastic annealing strategy for Bayesian posterior optimization with variational inference. Kuzmenko [12] presented a collapsed Gibbs sampling formula for the LDA model. The results they have shown allow the topics to have asymmetric Dirichlet priors on words and topics in LDA. Wallach et al. [13] explored various classes of structured priors for topic models and shown that an asymmetric Dirichlet prior has significant advantages over a symmetric prior. This prior structure approximate efficient hyper parameter optimization steps. Pathik and Shukla [14] explained various extended LDA models and hyper parameter values statistics along with justification for optimizing hyper parameter values.

From the above study, it can be concluded that Dirichlet priors α, β has a great impact on the performance of LDA. If they are set to appropriate values, LDA output will significantly improve. We are proposing SA-based approach for finding the best LDA configuration for producing high-quality output. SA-LDA optimizes the coherence of the topic produced by LDA for the considered input dataset.

3 Proposed Algorithm

SA is a random search approach which is developed in 1983. One of the reasons for popularity of SA is its simplicity. SA allows the transition to weaker solutions or we can say downward steps which make it more feasible for global optimal. Unlike hill-climbing type search which may stick in local optimal solution. SA can be considered as advanced hill climbing which allows downhill as well.

We have used Gensim implementation of LDA and optimized it using our developed SA algorithm. Hyper parameters α and β are tuned using SA and find out the optimal values so that LDA output will improve. Once the best values for α and β are obtained we optimize number of topic T corresponding to it. The reason for tackling T separately is that range of T is very different from α and β . Also dataset size affects T very much whereas α and β are not affected much.

3.1 SA-LDA Algorithm

1. Initialize and define hyper parameter ranges, number of iterations and control parameter. Hyper parameters are α and β , iterations i and Control Parameter is CP.
2. Generate a random population and its corresponding solution S (coherence value) based on the initial parameters value.
3. Generate a random neighboring population and calculate its corresponding solution.

4. Apply acceptance criteria on step 3
 - (a) If $S_{\text{new}} > S_{\text{old}}$: move to new solution.
 - (b) If $S_{\text{new}} < S_{\text{old}}$: move with acceptance probability if more than random no otherwise go to step 3.
5. Repeat 3–5 for a large number of iterations so that max search space is explored.
6. Once we got the best parameter value for α and β we again apply SA-LDA with α_{best} and β_{best} for optimizing number of topics also. After this step, we will get best LDA configuration in terms of parameters α , β , and T .

Figure 1 demonstrates the flow of the proposed algorithm.

Using Metropolis Criterion acceptance probability is defined as follows:

$$P(X_n) = e^{(dS/(i*S_{\max,i}))}$$

where:

$P(X_n)$: Probability of acceptance of n th point X_n

dS : $S_{\text{new}} > S_{\text{old}}$, i.e. change in coherence value

$S_{\max,i}$: Max value of coherence for up to i th iteration

i : number of iterations

CP: Control parameter $CP = i * S_{\max}$.

S_{new} and S_{old} are Coherence values for LDA configuration. Performance of LDA will be evaluated based on this value. Coherence is our objective function.

Acceptance Criteria is a function of both the control parameter and objective function. As the value of the control parameter increases, the probability of acceptance decreases. The same is desired initially that the probability of acceptance should be higher so that majority of points should be accepted. It will initially explore solution space to maximum. As control parameter increases after every iteration and reduces the probability which helps to converge on some global optimal values.

4 Experimental Setup and Results

We have used the Gensim implementation of LDA and optimized it using our developed SA algorithm. Gensim provides various text processing libraries implemented in Python and customized it by implementing SA-LDA in Python. The experiment was conducted on Desktop Workstation with Intel Xeon CPU X5675 3.07 GHz with 16.0 GB RAM and 64 bit Operating System. Anaconda platform is used for Python programming.

We have considered three datasets from three different domains namely Hotel reviews, Product review, and Movie review. As our approach is unsupervised so we have only considered review text from datasets, i.e. we haven't used labeled dataset (Table 1).

Fig. 1 Flow chart for SA-LDA algorithm

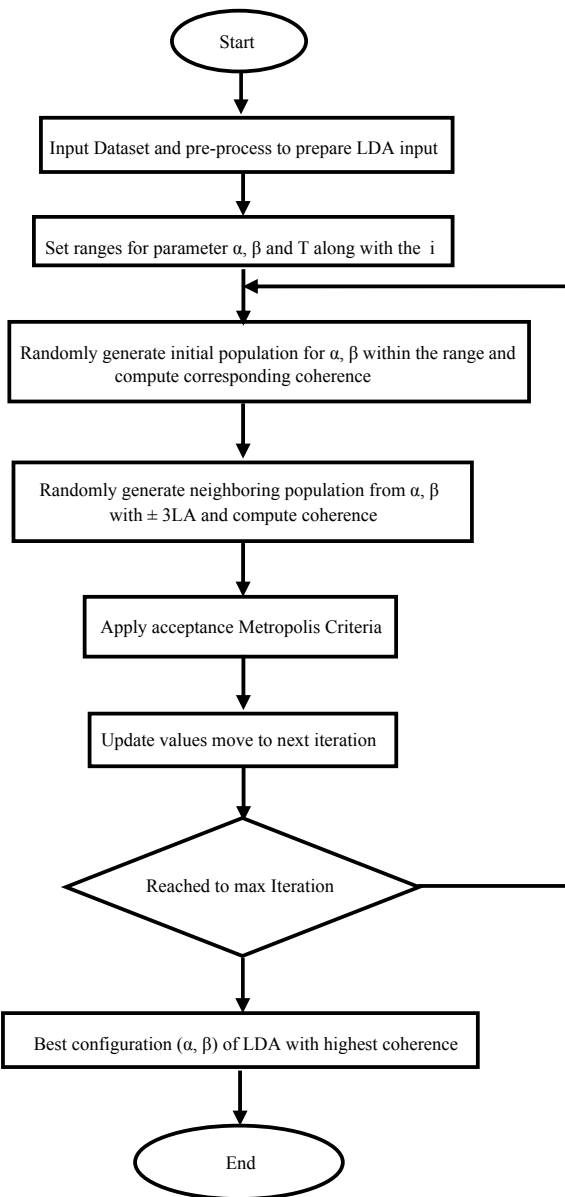


Table 1 Dataset statistics

Domain	Source of data	No of documents	No of sentences	No of words
Mobile reviews	Amazon	310	807	52,565
Hotel reviews	Yelp	3000	29,053	527,271
Movie reviews	IMDB	1000	10,872	272,803

Table 2 Pre-processing statics in term of number of words

Dataset	No of words	After removing punctuations	After removing stop words
Mobile	52,565	45,832	22,411
Hotel	527,271	460,297	200,127
Movie review	272,803	231,882	103,074

Text prepossessing reduces text input by half of its size. Or in text mining if free text is considered as input like text document then after pre-processing it will remain half in size. From Table 2 it is clear that pre-processing has a great impact on the aspect extraction step.

In most of the papers, number of topics are taken between 10 and 20 that is why we have used $T = 15$ for our SA-LDA for tuning α and β . After getting best values of α and β we have tried to find out optimal value of topics also by applying simple iterative process.

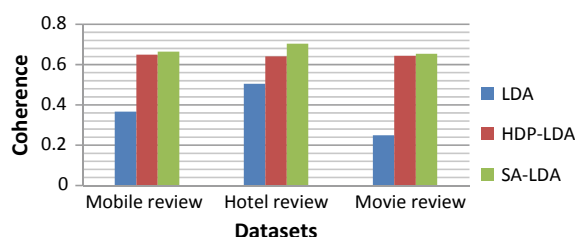
For the Hotel review dataset the value of hyper parameter was $\{\alpha, \beta, T\} = \{0.9, 0.69, 20\}$ and optimal value of coherence was 0.704. Same experiment is repeated with Mobile review dataset and we got values of hyper parameter $\{\alpha, \beta, T\} = \{0.79, 0.89, 22\}$ and optimal value of coherence was 0.665. For Movie review dataset $\{\alpha, \beta, T\} = \{0.60, 0.62\}$ and optimal value of coherence was 0.645.

We have compared with Gensim LDA implementation with autoconfiguration of α , β and found significant improvement in the value of coherence. We have also compared it with HDP-LDA and found our SA-LDA better in terms of coherence value. Table 3 shows comparative analysis and Fig. 2 shows a comparative graph for it.

It is clear from Fig. 2 SA-LDA is having better performance in comparison to LDA and HDP-LDA, when it is evaluated by coherence score.

Table 3 Comparison based on coherence value

Datasets	LDA	HDP-LDA	SA-LDA	α	β	T
Mobile review	0.367	0.649	0.665	0.79	0.89	22
Hotel review	0.505	0.641	0.704	0.90	0.69	20
Movie review	0.249	0.644	0.654	0.60	0.62	22

Fig. 2 Comparative Graphs for LDA, HDP-LDA, and SA-LDA

5 Conclusion

This paper proposed SA-LDA algorithm for finding hidden topics from the review datasets. The different datasets (Hotel, Mobile, and Movie) were taken. The performance of LDA is improved by tuning hyper α and β . Simulated Annealing based optimization gives best LDA configuration that produces most coherent topics. For evaluation of our SA-LDA algorithm, we have compared coherence of LDA, HDP-LDA with it for all three datasets. The comparison results show that SA-LDA gives better performance as compared to LDA and HDP-LDA in terms of coherence score.

References

1. Blei, D., Carin, L., Dunson, D.: Probabilistic topic models. *IEEE Signal Process. Mag.* **27**(6), 55–65 (2010)
2. Blei, D.M., Ng, A.Y., Jordan, M.I.: Latent Dirichlet allocation. *J. Mach. Learn. Res.* **3**(1), 993–1022 (2003)
3. Yarguy, T., Kanarkard, W.: Tuning latent Dirichlet allocation parameters using ant colony optimization. *J. Telecommun. Electron. Comput. Eng. (JTEC)* **10**(1–9), 21–4 (2018)
4. Dit, B., Panichella, A., Moritz, E., Oliveto, R., Di Penta, M., Poshyvanyk, D., De Lucia, A.: Configuring topic models for software engineering tasks in Tracelab. In: 2013 7th International Workshop on Traceability in Emerging Forms of Software Engineering (TEFSE), IEEE, pp. 105–109 (2013)
5. Bandyopadhyay, S., Saha, S., Maulik, U., Deb, K.: A simulated annealing-based multiobjective optimization algorithm: AMOSA. *IEEE Trans. Evol. Comput.* **12**(3), 269–283 (2008)
6. Gultekin, S., Zhang, A., Paisley, J.: Asymptotic simulated annealing for variational inference. In: IEEE Global Communications Conference (GLOBECOM), IEEE, pp. 1–7 (2018)
7. Foulds, J.R., Smyth, P.: Annealing Paths for the Evaluation of Topic Models. *UAI*, pp. 220–229 (2014)
8. Elhaddad, Y.R.: Combined simulated annealing and genetic algorithm to solve optimization problems. *World Acad. Sci. Eng. Technol.* **68**, 1508–1510 (2012)
9. Zhao, W., Chen, J.J., Perkins, R., Liu, Z., Ge, W., Ding, Y., Zou, W.: A Heuristic approach to determine an appropriate number of topics in topic modeling. In: *BMC Bioinformatics*, vol. 16, no. 13, p. S8. BioMed Central (2015)
10. George, C.P., Doss, H.: Principled selection of hyper-parameters in the latent Dirichlet allocation model. *J. Mach. Learn. Res.* **18**, 162 (2017)
11. Gultekin, S., Zhang, A., Paisley, J.: Stochastic annealing for variational inference. [arXiv:1505.06723](https://arxiv.org/abs/1505.06723) (2015)
12. Kuzmenko, A.: Gibbs sampling for LDA with asymmetric Dirichlet priors. akuz.me/wp-content/uploads/2014/01/akuz_lda_asym.pdf (2011)
13. Wallach, H.M., Mimno, D.M., McCallum, A.: Rethinking LDA: Why priors matter. In: *Advances in Neural Information Processing Systems*, pp. 1973–1981 (2009)
14. Pathik, N., Shukla, P.: An Ample analysis on extended LDA models for aspect based review analysis. *Int. J. Comput. Sci. Appl.* **14**(2), 97–106 (2017)

A Better Group Consensus Ranking via a Min-transitive Fuzzy Linear Ordering



Sukhamay Kundu

Abstract The current fuzzy methods for determining a group consensus ranking (GCR) or, equivalently, a linear order of items of a finite set S from a given set of weighted linear orders $\mathcal{L} = \{L_1, L_2, \dots, L_M\}$ on S are ad hoc in nature. This is because the underlying key fuzzy relations used in determining the GCR are not min-transitive. We present here a better method for GCR based on a min-transitive fuzzy linear order on S obtained from \mathcal{L} . We define a collection of probability distributions $P_x(j)$, $x \in S$, on the rank set $\{1, 2, \dots, |S|\}$ based on the linear orders \mathcal{L} . The distributions $P_x(j)$ give a min-transitive fuzzy partial order $\mu_{\mathcal{L}}(\cdot, \cdot)$ on S , where $\mu_{\mathcal{L}}(x, y)$ says how “left” the distribution $P_x(\cdot)$ is to $P_y(\cdot)$. We then extend $\mu_{\mathcal{L}}(\cdot, \cdot)$ to a best possible min-transitive fuzzy linear order $\mu_{\mathcal{L}}^*(\cdot, \cdot)$ on S , which gives the desired ranking of items in S .

Keywords Group ranking · Weighted linear orders · Fuzzy partial order · Fuzzy linear order · Min-transitivity

1 The Group Consensus Ranking Problem

A ranking of the items of a set $S = \{x_1, x_2, \dots, x_n\}$, $n \geq 2$, is simply an assignment of distinct ranks 1 to n to the items in S . Because assigning ranks j to x_{i_j} , $1 \leq j \leq n$, is equivalent to choosing the linear order $L = \langle x_{i_1}, x_{i_2}, \dots, x_{i_n} \rangle$ on S , and finding a group consensus ranking (GCR) of items of S is the same as finding a group consensus linear ordering (GCO) on S . We use the terms GCO and GCR henceforth interchangeably. Given a set of linear orders $\mathcal{L} = \{L_1, L_2, \dots, L_M\}$, $M \geq 2$, on S with weight or probability $w_k > 0$ for L_k and $\sum_k w_k = 1$, we can form a group consensus Boolean partial order $\Pi_{\mathcal{L}}$ (in short, Π) on S such that $x <_{\Pi} y$ if and only

S. Kundu (✉)

Computer Science and Engineering, Louisiana State University,
Baton Rouge, LA 70803, USA
e-mail: kundu@csc.lsu.edu

if $x <_{L_k} y$ for each $L_k \in \mathcal{L}$.¹ Any linear order on S which is consistent with Π can be taken now as a solution GCO.

Example 1 Let $\mathcal{L}_0 = \{L_1, L_2\}$, where L_1 is an arbitrary linear order on S , L_2 is the reverse order of L_1 , and $0 < w_1, w_2 < 1$ arbitrary with $w_1 + w_2 = 1$. This gives $\Pi =$ the empty partial order, and hence, every linear order on S is an equally good GCO. However, for $w_2 > w_1$, one would like L_2 to be the unique GCO. This happens when we use fuzzy techniques. A fuzzy approach gives, in general, a better GCO than the Boolean approach. A key problem in the above Boolean approach is not accounting for the weights w_k . \square

2 Existing Fuzzy Methods

Given an \mathcal{L} , we can define the memberships $\mu(x, y)$ of a fuzzy relation on S by Eq. (1), which gives the probability of $x < y$ in the linear orders in \mathcal{L} . If each $w_k = 1/M$, Eq. (1) gives the definition of $\mu(x, y)$ in [2].

$$\mu(x, y) = \sum w_k, \text{ summed over } L_k \in \mathcal{L} \text{ such that } x <_{L_k} y. \quad (1)$$

Clearly, $\mu(x, x) = 0$ for all $x \in S$, $\mu(x, y) + \mu(y, x) = 1$ for all $x \neq y$ in S , and hence, $\sum_{x,y} \mu(x, y) = n(n - 1)/2$. See Fig. 1a, b. The alternate linear orders $L'_1 : \langle b, a, c, d \rangle$, $L'_2 : \langle b, c, d, a \rangle$, $L'_3 : \langle a, d, b, c \rangle$, $L'_4 : \langle d, b, a, c \rangle$, and $L'_5 : \langle a, d, c, b \rangle$, with the weights w_i as in Fig. 1a give the same $\mu(\cdot, \cdot)$ as in Fig. 1b. In both cases, Π is empty, as indicated by $\mu(x, y) < 1$ for all x and y .

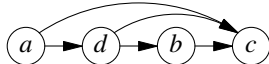
We now find the largest α -cut of $\mu(\cdot, \cdot)$ which is an anti-symmetric (Boolean) relation on S such that it can be extended, if necessary, to a linear order. That means $\alpha = \min\{\mu(x, y) : \mu(x, y) > 1/2\} > 1/2$; this assures that the α -cut is anti-symmetric. Figure 1b gives $\alpha = 5/8$, and Fig. 1c shows this α -cut of $\mu(\cdot, \cdot)$. Note that the α -cut is not transitive as a Boolean relation (and hence not a partial order). It would be transitive if $\mu(\cdot, \cdot)$ in Fig. 1b were min-transitive, i.e., $\mu(x, z) \geq \min\{\mu(x, y), \mu(y, z)\}$ for all x, y , and z . Unfortunately, that is not the case because $\mu(a, b) = 4/8 < 5/8 = \min\{\mu(a, d), \mu(d, b)\}$. This makes the definition of $\mu(\cdot, \cdot)$ in Eq. (1) and its use in [2] to create a GCO an ad hoc method and naive. In [2], any linear order extending the largest α -cut of $\mu(\cdot, \cdot)$ is taken as a possible GCO for \mathcal{L} . In general, such a GCO is not unique although the linear order $\langle a, d, b, c \rangle$ in Fig. 1d which extends the α -cut in Fig. 1c gives the unique GCO for Fig. 1a.

We remark that the strict form $\mu^s(x, y) = \max\{0, \mu(x, y) - \mu(y, x)\}$ of $\mu(x, y)$ in Fig. 1a, based on Orlovsky's construction [5], is not min-transitive either. From Fig. 1b, we get $\mu^s(a, d) = \mu^s(d, b) = 2/8 = \min\{\mu^s(a, d), \mu^s(d, b)\} > 0 = \mu^s(a, b)$. This means defining $\alpha = \min\{\mu^s(x, y) : \mu^s(x, y) > 1/2\}$ and extending that α -cut of

¹We consider throughout only the strict part $(x, y), x < y$, of a partial or linear order “ $<$ ” on S ; thus, the empty partial order has no (x, y) pair in it.

Weights w_k	Linear Orders L_k
$w_1 = 1/8$	$L_1: \langle a, b, c, d \rangle$
$w_2 = 2/8$	$L_2: \langle a, d, b, c \rangle$
$w_3 = 2/8$	$L_3: \langle b, a, c, d \rangle$
$w_4 = 1/8$	$L_4: \langle d, a, b, c \rangle$
$w_5 = 2/8$	$L_5: \langle d, c, b, a \rangle$

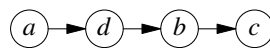
(a) Five linear orders L_k on $S = \{a, b, c, d\}$ and their weights w_k



(c) The largest anti-symmetric α -cut of (b), obtained for $\alpha = 5/8$

	a	b	c	d
a	0	4/8	6/8	5/8
b	4/8	0	6/8	3/8
c	2/8	2/8	0	3/8
d	3/8	5/8	5/8	0

(b) The memberships $\mu(x, y) =$ the probability of $x < y$ for the linear orders in (a)



(d) The Hasse-diagram of the linear order which extends (c) and gives the GCO for (a)

Fig. 1 Illustration of fuzzy memberships $\mu(x, y)$ and the GCO based on its α -cuts

$\mu^s(\cdot, \cdot)$ to form a GCO would be equally ad hoc as using $\mu(\cdot, \cdot)$. Orlovsky [5] showed that $\mu^s(\cdot, \cdot)$ is min-transitive if $\mu(\cdot, \cdot)$ is any min-transitive fuzzy relation. However, many useful probability-based definitions of $\mu(x, y)$ are known [3, 4] for which $\mu^s(\cdot, \cdot)$ is min-transitive although $\mu(\cdot, \cdot)$ is not. The membership function $\mu(\cdot, \cdot)$ in Eq. (1) is not in that category.

2.1 An Unsuccessful Variant of Eq. (1)

For a linear order $L = \langle x_{i_1}, x_{i_2}, \dots, x_{i_n} \rangle$, we say the pairs $(x_{i_k}, x_{i_{k+1}})$ of consecutive items in L , which correspond to the links of its Hasse-diagram, are the “core” links of L . The other pairs $(x_{i_j}, x_{i_{k+1}})$, $j < k$, are obtained from the core links by the transitivity property of L . One may think that focusing on the core links and defining the modified form $\underline{\mu}(x, y)$ of $\mu(x, y)$ as in Eq. (2) might help. However, neither of $\underline{\mu}(\cdot, \cdot)$ and $\mu^s(\cdot, \cdot)$ is min-transitive, in general. For L in Fig. 1a, $\underline{\mu}^s(d, c) = 0 < 2/8 = \min\{\underline{\mu}^s(d, b), \underline{\mu}^s(b, c)\}$ violates min-transitivity. Here, we get $\underline{\alpha} = \min\{\underline{\mu}(x, y) : \underline{\mu}(x, y) > 1/2\} = 3/8$, and this $\underline{\alpha}$ -cut of $\underline{\mu}(\cdot, \cdot)$ equals the (Boolean) partial order $\underline{L} = \{(b, a), (b, c), (c, d)\}$, which has three linear order extensions, and they are different from the one in Fig. 1d.

$$\underline{\mu}(x, y) = \sum w_k, \text{ summed over } L_k \in \mathcal{L} \text{ in which } (x, y) \text{ is a core link.} \quad (2)$$

2.2 Another Naive Approach

Let $\bar{r}(x) = \sum_{L_k \in \mathcal{L}} w_k \text{rank}_{L_k}(x)$, the average rank of x , and let $x < y$ if $\bar{r}(x) < \bar{r}(y)$. For \mathcal{L} in Fig. 1a, we get $\bar{r}(a) = \frac{17}{8} < \bar{r}(b) = \frac{19}{8} = \bar{r}(d) < \bar{r}(c) = \frac{25}{8}$, which give $a < b < c$, $a < d < c$, and $\{b, d\}$ are incomparable. The linear orders consistent with this partial order “ $<$ ” are $L = \langle a, b, d, c \rangle$ and $L' = \langle a, d, b, c \rangle$, with L' same as the one in Fig. 1d. We take either of them as the GCO for \mathcal{L} . This approach is similar in spirit to [1, 6], where an aggregate of pointwise values for each $x \in S$ based on some given facts is used to define a partial order on S and extend to a linear order if needed. We feel this pointwise aggregate approach is too naive.

3 Our New Fuzzy Approach

We represent a linear order $L = \langle x_{i_1}, x_{i_2}, \dots, x_{i_n} \rangle$ by the $n \times n$ permutation matrix P_L , where $P_L(i_j, j) = 1$ and $P_L(i, j) = 0$ for $i \neq i_j$. Each row and column of P_L has exactly one 1, and all other entries are 0.

Definition 1 For a given \mathcal{L} , let $P_{\mathcal{L}} = \sum_k w_k P_{L_k}$, i.e., $P_{\mathcal{L}}(i, j) = \sum_k \{w_k : L_k \in \mathcal{L} \text{ and } \text{rank}_{L_k}(x_i) = j\}$, the probability of $\text{rank}(x_i) = j$, for $1 \leq i, j \leq n$. $P_{\mathcal{L}}$ is an $n \times n$ doubly stochastic matrix, with each row (column) sum equal to 1.

The i th row of $P_{\mathcal{L}}$, denoted by $P_{x_i}(j)$, gives the probability distribution on $\{1, 2, \dots, n\}$ for $\text{rank}(x_i)$. Figure 2a shows the rank probabilities $P_{x_i}(j)$ for \mathcal{L} in Fig. 1a. Figure 2b shows an alternate set of linear orders and their associated weights which give the same $P_{x_i}(j)$ as in Fig. 2a. We remark that each doubly stochastic $n \times n$ matrix equals $P_{\mathcal{L}}$ for some (weighted) \mathcal{L} for a set S of size n because each doubly stochastic matrix is a convex sum of permutation matrices.

x	$j=1$	$j=2$	$j=3$	$j=4$	Weights w_m	Linear Orders L_m
a	3/8	3/8	0	2/8	$w_1 = 1/8$	$L_1: \langle a, b, c, d \rangle$
b	2/8	1/8	5/8	0	$w_2 = 2/8$	$L_2: \langle a, c, b, d \rangle$
c	0	2/8	3/8	3/8	$w_3 = 2/8$	$L_3: \langle b, d, c, a \rangle$
d	3/8	2/8	0/8	3/8	$w_4 = 3/8$	$L_4: \langle d, a, b, c \rangle$

- (a) Probabilities $P_{x_i}(j)$ of $\text{rank}(x) = j$ for $1 \leq j \leq 4$ and $x \in S = \{a, b, c, d\}$ based on the linear orders in Fig. 1(a)
- (b) An alternate set of 4 linear orders and their associated weights that give the same rank-probabilities as in (a)

Fig. 2 Illustration of the probability distributions $P_x(j)$ on $\{1, 2, \dots, |S|\}$ for $x \in S$

3.1 A Min-transitive Fuzzy Partial Order on S from P_x 's

We now define a (min-transitive) fuzzy partial order $\Lambda_d(\cdot, \cdot)$ on S based on the rank probability distributions $P_x(\cdot)$, $x \in S$.

Definition 2 A min-transitive fuzzy relation $\mu(\cdot, \cdot)$ on S is a fuzzy partial order (in short, FPO) if it is anti-symmetric, i.e., for all $x, y \in S$, if $\mu(x, y) > 0$, then $\mu(y, x) = 0$ (in particular, $\mu(x, x) = 0$ for all $x \in S$). We say $\mu(\cdot, \cdot)$ is a fuzzy linear order (in short, FLO) if, in addition, exactly one of $\mu(x, y)$ and $\mu(y, x)$ is > 0 for $x \neq y$. Here, $\mu(x, y) > 0$ is the support for $x < y$ in the FPO or FLO.

Suppose X and Y are two probability distributions on $N_n = \{1, 2, \dots, n\}$. For $i, j \in N_n$, let $L(i, j) = \max\{0, j - i\}$, which shows how much “left” i is to j , and let $R(i, j) = L(j, i)$. In [3], we defined $L(X, Y)$ by Eq. (3), which shows how much left X is to Y ; likewise, we defined $R(X, Y) = L(Y, X)$ by Eq. (4), which shows how much right X is to Y . Note that $L(X, X) = R(X, X) \neq 0$ unless X is concentrated at one point with probability 1. Finally, we defined the min-transitive fuzzy relation $\Lambda_d(X, Y)$ by Eq. (5), where the numerator $\max(0, L(X, Y) - R(X, Y))$ is based on Orlovsky's construction [5] and the denominator $L(X, Y) + R(X, Y)$ assures us that $0 \leq \Lambda_d(X, Y) \leq 1$. It is shown in [3] that $L(X, Y) - R(X, Y) = \bar{Y} - \bar{X}$, where \bar{X} and \bar{Y} are the averages of X and Y ; in particular, $\Lambda_d(X, Y) > 0$ if and only if $\bar{X} < \bar{Y}$.

$$L(X, Y) = \sum_{i,j} P_X(i)P_Y(j)L(i, j) = \sum_i P_X(i) \left(\sum_{i \leq j} P_Y(j)(j - i) \right) \geq 0 \quad (3)$$

$$R(X, Y) = \sum_{i,j} P_X(i)P_Y(j)R(i, j) = \sum_i P_X(i) \left(\sum_{i \geq j} P_Y(j)(i - j) \right) \geq 0 \quad (4)$$

$$\Lambda_d(X, Y) = \begin{cases} \frac{\max(0, L(X, Y) - R(X, Y))}{L(X, Y) + R(X, Y)}, & \text{if } L(X, Y) + R(X, Y) > 0 \\ 0, & \text{otherwise.} \end{cases} \quad (5)$$

Definition 3 We write $L(P_x, P_y)$ for $L(X, Y)$ when X and Y are the rank probability distributions $P_x(\cdot)$ and $P_y(\cdot)$ for $x, y \in S$. Also, we write $\Lambda_d(x, y) = \Lambda_d(P_x, P_y)$. It is shown in [3] that $\Lambda_d(x, y)$ is a fuzzy partial order on S .

Figure 3 shows the matrix of $L(P_x, P_y)$, $x, y \in S$ and the resulting (min-transitive) fuzzy partial order $\Lambda_d(x, y)$ on S based on Fig. 2a. Note that $\Lambda_d(b, d) = 0 = \Lambda_d(d, b)$. The following theorem is immediate from Definitions 2 and 3.

Theorem 1 *The fuzzy relation $\Lambda_d(\cdot, \cdot)$ on S based on the rank probability distributions $P_x(\cdot)$, $x \in S$, is a fuzzy partial order.*

	a	b	c	d
a	0.61	0.75	1.22	0.80
b	0.50	0.42	0.91	0.67
c	0.22	0.16	0.42	0.33
d	0.55	0.67	1.08	0.70

(a) The matrix of $L(P_x, P_y)$ for $x, y \in S = \{a, b, c, d\}$ based on Fig. 2(a)

	a	b	c	d
a	0.00	0.20	0.70	0.19
b	0.00	0.00	0.71	0.00
c	0.00	0.00	0.00	0.00
d	0.00	0.00	0.53	0.00

(b) The fuzzy memberships $\Lambda_D(x, y) = \Lambda_D(P_x, P_y)$ for $x, y \in S$ based on (a)

Fig. 3 Illustration of $\Lambda_D(\cdot, \cdot)$ on probability distributions $P_{x_i}(j)$'s in Fig. 2

x	$j=1$	$j=2$	$j=3$	$j=4$
a	w_1	0	0	w_2
b	0	w_1	w_2	0
c	0	w_2	w_1	0
d	w_2	0	0	w_1

(a) Probabilities $P_x(j)$ of rank(x) = j for $1 \leq j \leq 4$ and $x \in S = \{a, b, c, d\}$

	a	b	c	d
a	$3w_1w_2$	c_1	c'_1	$3w_1^2$
b	c_2	w_1w_2	w_1^2	c'_1
c	c'_2	w_2^2	w_1w_2	c_1
d	$3w_2^2$	c'_2	c_2	$3w_1w_2$

(b) The matrix $L(P_x, P_y)$, where $c_i = w_i^2 + 2w_1w_2$ and $c'_i = 2w_i^2 + w_1w_2$

Fig. 4 Probability distributions P_x 's and $L(P_x, P_y)$ for \mathcal{L}_0

Example 2 Consider the linear orders $\mathcal{L}_0 = \{L_1, L_2\}$, with $L_1 = \langle a, b, c, d \rangle$, $L_2 = \langle d, c, b, a \rangle$ = the reverse of L_1 , $0 < w_1, w_2 < 1$, and $w_1 + w_2 = 1$ (cf. Example 1). It is clear from Fig. 4, which shows the matrix of $L(P_x, P_y)$'s, that for $w_1 < w_2$ the fuzzy partial order $\Lambda_D(\cdot, \cdot)$ is a linear order, where $d <_{\Lambda_D} c <_{\Lambda_D} b <_{\Lambda_D} a$, i.e., the same as L_2 having larger weight. \square

3.2 Extending an FPO to an FLO

Assume now that $\mu(\cdot, \cdot)$ is an arbitrary FPO on S , unless stated otherwise.

Definition 4 Let $\mu(\cdot, \cdot)$ be an FPO on S and $x \neq y$ are two items in S . We say x and y are (or, equivalently, the node pair $\{x, y\}$ is) incomparable if $\mu(x, y) = 0 = \mu(y, x)$; otherwise, we say x and y are comparable.

If x and y are incomparable, then we have to increase exactly one of $\mu(x, y)$ or $\mu(y, x)$ to extend $\mu(\cdot, \cdot)$ to an FLO (which has no incomparable node pairs). However, increasing $\mu(x, y)$ from 0 to $\mu_{xy} > 0$, say, can cause $\mu(\cdot, \cdot)$ to loose the min-transitivity when one of (a)-(b) below holds.

- (a) For some y' , $\mu(x, y') < \min\{\mu_{xy}, \mu(y, y')\}$.
- (b) For some x' , $\mu(x', y) < \min\{\mu(x', x), \mu_{xy}\}$.

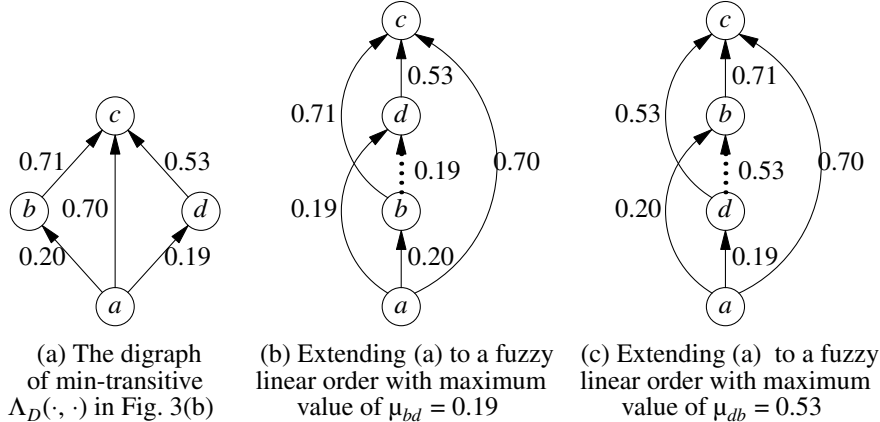


Fig. 5 Extending the fuzzy partial order $A_D(\cdot, \cdot)$ in Fig. 3b to fuzzy linear orders

Note that (a) implies $\mu(y, y') > 0$ and $\mu(x, y') < \mu(y, y')$, and (b) implies $\mu(x', x) > 0$ and $\mu(x', y) < \mu(x', x)$. These lead us to the following definitions.

Definition 5 Let $y_x^+ = \{y' : \mu(y, y') > 0 \text{ and } \mu(x, y') < \mu(y, y')\}$, and $\epsilon(y_x^+) = \min\{\mu(x, y') : y' \in y_x^+\}$, where we let $\epsilon(y_x^+) = 1$ if $y_x^+ = \emptyset$. Likewise, let $x_y^- = \{x' : \mu(x', x) > 0 \text{ and } \mu(x', y) < \mu(x', x)\}$, and $\epsilon(x_y^-) = \min\{\mu(x', y) : x' \in x_y^-\}$, where we let $\epsilon(x_y^-) = 1$ if $x_y^- = \emptyset$. Finally, we let $\epsilon(x, y) = \min\{\epsilon(y_x^+), \epsilon(x_y^-)\}$.

Example 3 Consider the FPO $\mu(x, y) = A_D(x, y)$ on S in Fig. 3b. Figure 5a shows a digraph representation of it, where we show only the links (x, y) and its $\mu(x, y)$ if $\mu(x, y) > 0$. For $(x, y) = (b, d)$, we have $d_b^+ = \emptyset$, $\epsilon(d_b^+) = 1$, $b_d^- = \{a\}$, $\epsilon(b_d^-) = 0.19$, and $\epsilon(b, d) = 0.19$. Figure 5b shows the FLO obtained by increasing $\mu(b, d)$ from 0 to $\epsilon(b, d)$. On the other hand, for $(x, y) = (d, b)$, we have $b_d^+ = \{c\}$, $\epsilon(b_d^+) = 0.53$, $d_b^- = \emptyset$, $\epsilon(d_b^-) = 1$, and $\epsilon(d, b) = 0.53$. Figure 5c shows the FLO obtained by increasing $\mu(d, b)$ from 0 to $\epsilon(d, b)$. Because $\epsilon(d, b) > \epsilon(b, d)$, we take the fuzzy linear order in Fig. 5c as the group consensus for the linear orders \mathcal{L} in Fig. 1a. Note that the Boolean linear $\langle a, d, b, c \rangle$ corresponding to Fig. 5c is the same as that in Fig. 1d. Also, the Boolean linear orders $\langle a, b, d, c \rangle$ and $\langle a, d, b, c \rangle$ associated with Fig. 5b, c are the ones obtained from the Boolean partial order associated with Fig. 5a. \square

Lemma 1 If x and y are incomparable, we can increase $\mu(x, y)$ to a positive value preserving the min-transitivity of $\mu(\cdot, \cdot)$ if and only if $\epsilon(x, y) > 0$; the maximum possible increased value of $\mu(x, y)$ is $\epsilon(x, y)$.

Proof Assume that $\epsilon = \epsilon(x, y) = \min\{\epsilon(x_y^-), \epsilon(y_x^+)\} > 0$, and we increase $\mu(x, y)$ from 0 to $\mu'(x, y) = \epsilon$. Then, for any $y' \in y_x^+$, we have $\mu(x, y') \geq \epsilon = \mu'(x, y) \geq \min\{\mu'(x, y), \mu(y, y')\}$ and thus (a) above does not hold for $\mu(\cdot, \cdot)$. Likewise, for

any $x' \in x_y^-$, we have $\mu(x', y) \geq \epsilon = \mu'(x, y) \geq \min\{\mu(x', x), \mu'(x, y)\}$ and thus (b) above does not hold for $\mu(\cdot, \cdot)$. This proves the “if” part of the lemma. The proof of the “only if” part is trivial. (Fig. 5a–c illustrate the proof.) \square

3.3 Applying Lemma 1

To apply Lemma 1 to an incomparable node pair $\{x, y\}$, we first compute $m_{xy} = m_{yx} = \max\{\epsilon(x, y), \epsilon(y, x)\}$, and then if $m_{xy} > 0$, we increase one of $\mu(x, y)$ and $\mu(y, x)$ to m_{xy} (but not both even if they are equal) depending on whether $\epsilon(x, y) = m_{xy}$ or $\epsilon(y, x) = m_{xy}$. Indeed, some incomparable node pairs $\{x, y\}$ can have $m_{xy} = 0$. We show next that each FPO which is not an FLO has at least one incomparable node pair $\{x, y\}$ with $m_{xy} > 0$.

Definition 6 If $\{x, y\}$ is an incomparable node pair, we say y is maximal for x if $\mu(y, z) > 0$ implies $\mu(x, z) > 0$ (or, equivalently, $\{x, z\}$ are comparable because $\mu(z, x) > 0$ would imply $\mu(y, x) > 0$ by min-transitivity of $\mu(\cdot, \cdot)$ and hence $\{x, y\}$ are not incomparable). The notion of x being minimal for y is defined similarly.

Definition 7 If $\{x, y\}$ is an incomparable node pair such that x is minimal for y and y is maximal for x or the role of x and y are reversed, then we say $\{x, y\}$ is a min–max incomparable node pair.

Lemma 2 *If $\mu(\cdot, \cdot)$ is an FPO which is not an FLO, then there is at least one min–max incomparable node pair $\{x, y\}$ such that $\epsilon(x, y) > 0$.*

Proof Let $\{u, v\}$ be any incomparable node pair. If v is not maximal for u , then there is some v_1 such that $\mu(v, v_1) > 0$ and $\{u, v_1\}$ are incomparable. We can apply the same argument repeatedly until we get a chain of nodes v_1, v_2, \dots, v_m such that each of $\mu(v, v_1), \mu(v_1, v_2), \dots, \mu(v_{m-1}, v_m)$ is > 0 (and hence $\mu(v, v_m) > 0$) and each node pair $\{u, v_j\}$, $1 \leq j \leq m$ is incomparable and, moreover, v_m is maximal for u . Likewise, if u is not minimal for v_m , then we can find u_k such that $\{u_k, v_m\}$ is an incomparable node pair and u_k is minimal for v_m . If v_m is maximal for u_k , we are done because it is easy now to see that $\epsilon(u_k, v_m) > 0$. If v_m is not maximal, continue the above process, and S being finite it will come to a stop at some point. \square

Definition 8 A fuzzy linear extension $\mu^*(\cdot, \cdot)$ of an FPO $\mu(\cdot, \cdot)$ on S is called optimal if the total sum of its membership values $\sum_{x,y} \mu^*(x, y)$ is maximum.

Example 4 For the FPO in Fig. 6a and the incomparable node pair $\{a, b\}$, a is minimal for b but b is not maximal for a . However, $\{a, d\}$ is a min–max incomparable node pair and so is $\{b, c\}$. Here, $m_{ab} = 0$ and we cannot increase either of $\mu(a, b)$ and $\mu(b, a)$ to a positive value; likewise, $m_{cd} = 0$ and we cannot increase either of $\mu(c, d)$ and $\mu(d, c)$. Nevertheless, we can successively apply Lemma 1 to the node pairs $\{a, d\}$, $\{a, b\}$, $\{c, d\}$, and $\{b, c\}$ in that order to get the fuzzy linear extension of Fig. 6a as shown in Fig. 6b. Applying Lemma 1 to those node pairs in a different order gives the

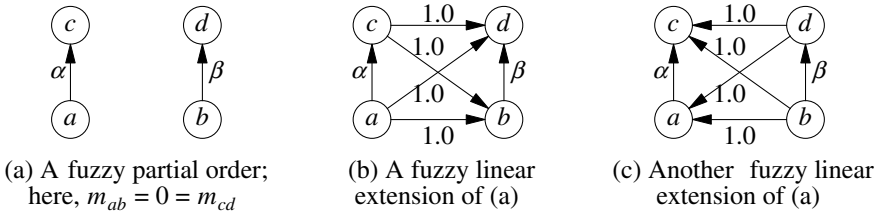


Fig. 6 FPO with incomparable node pairs $\{x, y\}$ such that $m_{xy} = 0$ and its optimal linear extensions

fuzzy linear extension as shown in Fig. 6c. These are the only optimal fuzzy linear extensions of Fig. 6a. \square

Lemma 3 Let $\mu(\cdot, \cdot)$ be a fuzzy partial order on S , $m_\mu = \min\{\mu(x, y) > 0 : x, y \in S\}$, and $\bar{\mu}(\cdot, \cdot)$ is a fuzzy linear extension of $\mu(\cdot, \cdot)$, then $m_{\bar{\mu}} = m_\mu$.

Proof Let $\{x, y\}$ be an incomparable node pair. If $\epsilon(x, y) > 0$, then clearly $\epsilon(x, y) \geq m_\mu$; likewise, if $\epsilon(y, x) > 0$, then $\epsilon(y, x) \geq m_\mu$. This immediately implies the lemma. (See Fig. 7 for an illustration of the lemma.) \square

3.4 Simultaneous Use of Lemma 1 for Multiple Node Pairs

The FPO in Fig. 7a has the non-disjoint incomparable node pairs $\{a, b\}$ and $\{a, c\}$, with the common node a and both $m_{ab}, m_{ac} > 0$. The individual applications of Lemma 1 to $\{a, b\}$ and $\{a, c\}$ give the min-transitive extensions in Fig. 7b, c. However, the simultaneous application of Lemma 1 to these node pairs gives the non-min-transitive relation in Fig. 7d. On the other hand, there are two optimal linear extensions of Fig. 7a as shown in Fig. 7e, f, and they are obtained by applications of Lemma 1 to Fig. 7b, c.

We give below a sufficient condition for a simultaneous application Lemma 1 to multiple incomparable node pairs $\{x_i, y_i\}$, $1 \leq i \leq k (\geq 2)$, to be min-transitive.

Lemma 4 If the incomparable node pairs $\{x_i, y_i\}$, $1 \leq i \leq k (\geq 2)$ are disjoint, i.e., the node x_i s and y_i s form $2k$ distinct nodes such that each $\epsilon(x_i, y_i) > 0$, then the extension obtained by simultaneous application of Lemma 1 to $\mu(\cdot, \cdot)$ by increasing $\mu(x_i, y_i)$ from 0 to $\epsilon(x_i, y_i)$ is min-transitive.

Proof We give here the argument for $k = 2$; the same argument applies for $k > 2$ as well. The disjointness of $\{x_1, y_1\}$ and $\{x_2, y_2\}$ implies $\epsilon(x_2, y_2)$ and $\epsilon(y_2, x_2)$ do not change when $\mu(\cdot, \cdot)$ is extended by applying Lemma 1 to the node pair $\{x_1, y_1\}$. Thus, a second application of Lemma 1 to the extension of $\mu(\cdot, \cdot)$ with respect to $\{x_1, y_1\}$, now applied to the node pair $\{x_2, y_2\}$, gives the same result as applying Lemma 1 simultaneously to $\{x_1, y_1\}$ and $\{x_2, y_2\}$. \square

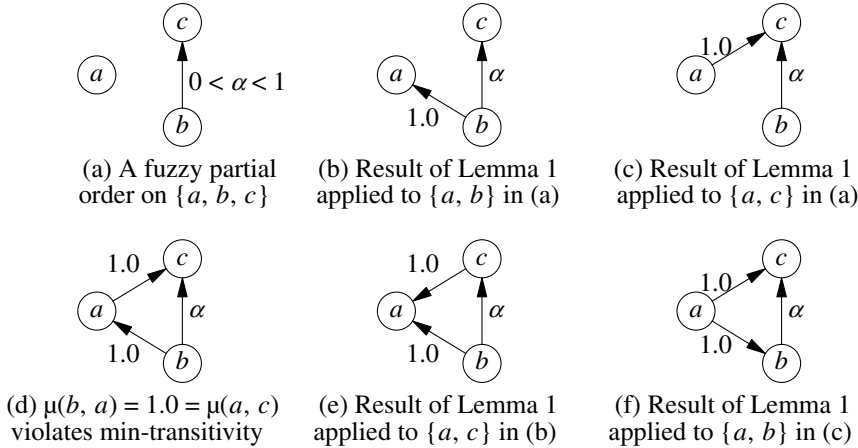


Fig. 7 Violation of min-transitivity due to simultaneous application of Lemma 1 to two incomparable node pairs $\{a, b\}$ and $\{a, c\}$ as shown in part (d)

Example 5 In Fig. 6a, the incomparable node pairs $\{a, d\}$ and $\{b, c\}$ are disjoint, and the application of Lemma 4 to these node pairs gives a min-transitive partial order extension of Fig. 6a with $\mu(a, d) = 1.0 = \mu(b, c)$. If we assume $\alpha \leq \beta$, then now $\epsilon(a, b) = \alpha$, $\epsilon(b, a) = \beta$, $\epsilon(c, d) = \beta$, and $\epsilon(d, c) = \alpha$. So, another application of Lemma 4 to the node pairs $\{a, b\}$ and $\{c, d\}$ gives now $\mu(b, a) = \beta = \mu(c, d)$, resulting in a min-transitive linear extension of Fig. 6a. However, this is not optimal, showing that Lemma 4 may not be always useful in obtaining an optimal linear extension. \square

Figure 7 shows that for two non-disjoint incomparable node pairs $\{x, y\}$ and $\{y, z\}$ increasing $\mu(x, y)$ from 0 to m_{xy} may cause the new $\epsilon(z, y)$ to the common mode y to increase (to even 1.0) and $\epsilon(y, z)$ to decrease (from even 1.0) to an arbitrary small value. The opposite may happen if $\mu(y, x)$ were increased.

4 A Greedy Heuristic for Optimal Extension

We give next a simple greedy algorithm to extend an FPO to a semi-optimal FLO. Finding an efficient algorithm to determine an optimal fuzzy linear ordering remains an open research problem. Step 3(b) below avoids recomputation of $\epsilon(x', y')$ and $\epsilon(y', x')$ for an incomparable node pair $\{x', y'\}$ as much as possible following an increase of some $\mu(x, y)$. It also uses only a limited case of Lemma 4.

Algorithm FPO-to-FLO:

Input: An FPO $\mu(\cdot, \cdot)$ on a finite set S , which is not an FLO.
Output: An extension of $\mu(\cdot, \cdot)$ to a (semi-)optimal FLO on S .

1. Let I = set of all incomparable node-pairs in $\mu(\cdot, \cdot)$.
2. Determine $\epsilon(x, y)$, $\epsilon(y, x)$, and $m_{xy} = \max\{\epsilon(x, y), \epsilon(y, x)\}$ for all $\{x, y\} \in I$.
3. Do the following until (I is empty):
 - (a) Compute $\bar{m} = \max\{m_{xy} : \{x, y\} \in I\}$. // $\bar{m} > 0$
 - (b) If ($\bar{m} = 1.0$) then let I' = a maximal subset of mutually disjoint $\{x, y\}$'s in I with $m_{xy} = 1.0$.
Otherwise, let I' = the set of one node-pair $\{x, y\} \in I$ with $m_{xy} = \bar{m}$.
 - (c) For all $\{x, y\} \in I'$ do the following:
 - i. Increase $\mu(x, y)$ or $\mu(y, x)$ from 0 to m_{xy} depending on whether $\epsilon(x, y) = m_{xy}$ or $\epsilon(y, x) = m_{xy}$ (but not both if $\epsilon(x, y) = \epsilon(y, x)$).
 - ii. Remove $\{x, y\}$ from I .
 - (d) Let $I'' = \{\{x', y'\} \in I : \{x', y'\} \text{ intersects some } \{x, y\} \in I'\}$.
 - (e) Recompute $\epsilon(x', y')$, $\epsilon(y', x')$, and $m_{x'y'}$ for each $\{x', y'\} \in I''$ based on new $\mu(\cdot, \cdot)$ as modified in step 3(c.i).

5 Conclusion

We give here an intuitively appealing and mathematically sound method for defining a group consensus ranking, i.e., an optimal fuzzy linear ordering $\mu_{\mathcal{L}}^*(\cdot, \cdot)$ on a finite set S for a set of weighted Boolean linear orderings $\mathcal{L} = \{L_i ; 1 \leq i \leq M\}$ ($M \geq 2$) on S . There have been many attempts [1, 2, 6] in defining a group consensus ranking. However, they are either naive (depend on pointwise aggregation) or ad hoc (depend on non-min-transitive fuzzy relations).

References

1. Herrera, F., Herrera-Viedma, E.: Linguistic decision analysis: steps for solving decision problems under linguistic information. *Fuzzy Sets Syst.* **115**, 67–82 (2000)
2. Klir, G.J., St. Clair, U., Yuan, B.: *Fuzzy Set Theory: Foundations and Applications*, 1st ed. Prentice Hall (1997)
3. Kundu, S.: A min-transitive fuzzy left-relationship on finite sets based on distance to left. In: Proceedings of the International Conference on Soft Computing: Theory and Applications (SoCTA-2017), India, Dec. 22–24 (2017)
4. Kundu, S.: The min-transitive fuzzy left-relationship $\lambda_d(A, B)$ on intervals: a generalization of $\lambda(A, B)$. In: Proceedings of the International Conference on Soft Computing: Theory and Applications (SoCTA-2018), India, Dec. 21–23 (2018)
5. Orlovsky, S.A.: Decision making with a fuzzy preference relation. *Fuzzy Sets Syst.* **1**, 155–167 (1978)
6. Xu, Z.: A note on linguistic hybrid arithmetic averaging operator in multiple attribute group decision making with linguistic information. *Group Decis. Negot.* **15**, 593–604 (2006)

A Novel Metaheuristic Approach for Resource Constrained Project Scheduling Problem



Bidisha Roy and Asim Kumar Sen

Abstract The Resource Constrained Project Scheduling Problem (RCPSP) is a prominent and a noteworthy NP-hard Combinatorial Optimization problem in the field of Operations Research and Management. It is a proven complex problem which involves constrained availability of resources, within which activities in a project should be optimally organized, keeping in mind the activity precedences, so that the project schedule is minimized. To efficiently solve the problem, many Evolutionary and Swarm Intelligence metaheuristics have been proposed, which have attempted to solve the problem optimally. This paper presents a novel Swarm Intelligence algorithm based on the Firefly Algorithm (FA). Applying the FA to solve the RCPSP problem, however, involved discretizing the FA as RCPSP is a discrete problem and FA by nature is continuous. The presented algorithm has been checked on standard benchmark test problems available in the literature and also compared with existing contemporary Swarm Intelligence and Evolutionary Algorithms available. The results of the experiments also justify the effectiveness of the proposed algorithm.

Keywords RCPSP · Metaheuristics · Discrete Firefly Algorithm · Swarm Intelligence

1 Introduction

Scheduling activities in a project, also known as project scheduling, has always been an important matter of concern in project management since the inception of the field of operations research. It is recurrently encountered in a broad range of applications in many industries like process and production engineering, operations and

B. Roy (✉)

St. Francis Institute of Technology, University of Mumbai, Mumbai, India

e-mail: bidisha.bhaumik.roy@gmail.com

A. K. Sen

Faculty, OERC Academy, Turbhe, Navi Mumbai, India

e-mail: asim_sen@linuxmail.org

maintenance, construction, software industry, etc. [1]. A classic project scheduling problem deals only with the precedence constraints of activities, i.e., it involves trying to find the minimum makespan (C_{\max}) keeping in mind that an activity or job can only be carried out if all its preceding activities have been completed. A more relevant version is to keep in mind the fact that the activities require resources (renewable or non-renewable) for their completion. Also, the availability and capacity of these resources are limited over the time frame of the project. Hence, in such a case, the completion of the project would involve not only addressing the constraints of precedences along with the resource constraints. This type of scheduling is typically called the Resource Constrained Project Scheduling Problem (RCPSP), which is a frequently occurring problem in large-scale project management in many spheres.

As a crucial concept in the field of operations management, RCPSP is characteristically intricate and nonlinear in its behavior. Also, as the problem is so very complex, that, in the most popularly used sets of benchmark test problems; PSPLIB [2], the optimal makespan has been found only for the project containing 30 activities. For higher projects, it still remains unfound and unknown. As a complex problem with high practical relevance, finding solution for RCPSP, which is nearly optimal, has always been an inquisitive field of research for scientists and engineers.

Many early solutions based on exact methods of problem-solving were proposed to solve the RCPSP problem [3, 4]. However, like the job-shop, flow-shop, and other prominent scheduling variants, it is a Combinatorial Optimization problem proven to be NP-hard in the strongest sense [5]. Hence, the exact methods can only solve problems at a smaller-scale commensurately. As the problem size increased, the solutions became harder to converge. This led to research in the direction of heuristics such as priority rule-based methods [6] to try and attain a near-optimal solution to the problem. Metaheuristics do not come with a guarantee of providing optimal solutions. They are however suited to find solutions for problems of larger size. Thus, many metaheuristics based on Simulated Annealing, Tabu Search, Genetic Algorithms [6], Ant systems [3, 7], and other Evolutionary and Swarm Intelligence methods were proposed to solve the problem.

All metaheuristic techniques have their own typical set of features and process; they also possess a lot of common similarities and traits. The main similarity consists of the fact that they evaluate the entire solution space and in major cases are successful in detecting the global optima, hence steering from falling into the local optima. In this paper, the use of a version of another swarm intelligence algorithm, namely the Firefly Algorithm [8], to find a solution for RCPSP, is put forward. The algorithm is implemented on one of the benchmark test problems from PSPLIB [2], and the results have been presented.

Paper structure. In Sect. 2, the RCPSP is described. After that, Sect. 3 describes the previous related work in this field. In Sect. 4, the basic Firefly Algorithm and its discretization have been described. Section 5 mentions the benchmark problems used to check the algorithm. In Sect. 6, we analyze the experimental results. Section 7 offers the concluding remarks.

2 The Resource-Constrained Project Scheduling Problem

To mathematically depict the RCPSP [9], we would need an activity set which consists of $j = 1$ to n activities which have their own processing durations, say p_j . In every time interval of p_j , the activity j consumes a certain amount of resource k , i.e., $k = 1, 2, 3, \dots, r$ are the amount of resources available for the project. Also, a set of precedence constraints need to be specified between activities i and j , indicating that an activity j can begin only after activity i has completed. Thus, the objective of RCPSP problem is to decide the set of start times S for all activities such that:

- At any time, the availability of a resource does not exceed its demand, i.e., Resource Constraints are fulfilled
- Precedence Constraints are satisfied, i.e., no activity begins unless its predecessor activity is finished
- We define an objective function $f(C_1, \dots, C_n)$, which needs to be minimized where $C_j = S_j + p_j$ is the completion time of activity j .

Thus, we can formally define RCPSP mathematically as a tuple (V, p, E, R, B, b) , where

- Activity set, i.e., set of project activities is given by $V \rightarrow \{A_0, \dots, A_{n+1}\}$
- $p \rightarrow$ Processing time of activities, $p_0, p_{n+1} = 0$
- $E \rightarrow$ Activity precedences, represented by a set of ordered pairs (A_i, A_j) indicating that activity A_j is successor of activity A_i .
- $R = \{R_1, \dots, R_r\} \rightarrow$ Available **Resources** for the project timeline (renewable).
- $B \rightarrow$ Resources availability of every resource for each activity with every B_k denoting availability of resource R_k .
- $b \rightarrow$ **Resource demand**, which is the amount of resource utilized by every activity per unit time, with b_{ik} representing the amount of resource R_k used per time period during the execution of A_i .

For this tuple, we try to find an optimal minimal makespan schedule S . S is a set of S_i representing starting times of A_i . The set C consists of all C_i denoting the completion times of A_i , i.e., $C_i = S_i + p_i$. A feasible schedule is which adheres to

- Precedence constraints

$$S_j - S_i \geq p_i \quad \forall (A_i, A_j) \in E \quad (1)$$

- Resource constraints

$$\sum_{A_i \in A_t} b_{ik} \leq B_k, \quad \forall R_k \in R, \forall t \geq 0 \quad (2)$$

Hence, RCPSP as a mathematical formulation would be:

Min C_{\max} subject to (1) and (2) above.

Solving RCPSP is thus trying to find a schedule for a set of project activities satisfying both the resource and precedence constraints (only non-pre-emptive schedules).

3 Related Work

The mathematical model for RCPSP presented in the previous section can be solved using exact methods like Linear Programming, Branch and Bound, Dynamic Programming, etc., but they are not feasible for instances of projects with a large number of activities. Hence, studies to apply different approximate techniques to be able to near optimally solve large problem instances remains an active area of research. Over the years, heuristic and metaheuristic methods have emerged as the better applicable strategies to solve practical RCPSP problems. Though unlike exact methods, heuristic and metaheuristic methods do not every time guarantee an optimal solution, they have always been proven to provide a solution nearing an optimal solution for very large problem instances as well, which make them useful.

3.1 Heuristic Methods

Heuristics are techniques that begin with an initial null set of schedule wherein none of the activities have yet been scheduled. The empty schedule is subsequently filled up in each step with activities based on certain priority rules and scheduling schemes. Activities are scheduled based on their ranks, and ranks are provided to activities using priority rules. Researches in [6, 10–12] have put forward different heuristic techniques to solve the RCPSP problem. These included different Schedule Generation Schemes (both serial and parallel), X-pass methods, Forward–Backward improvement and also priority rule-based heuristics. Kolisch et al. in [6, 10] also compared these heuristics over metaheuristics like genetic algorithms (GA), simulated annealing (SA), and tabu search (TS). The tests were carried out on benchmark test problems from the PSPLIB [2]. It was experimentally observed that the average standard deviation from optimal solutions was better in case of metaheuristics over heuristic techniques. Research put forward in these papers also started the idea of first generating feasible solutions using heuristic methods and applying metaheuristic methods over them to generate optimal schedules.

3.2 Metaheuristic Methods

Metaheuristic methods generally start with an initial solution set, which constitute the initial generations. They then constantly evolve and improve the solutions by

applying a set of operations to transform one or many solutions into others. Solutions based on TS and SA as proposed in [6, 10] maintained one solution in each cycle of the algorithm, which they try to better up iteratively.

Other metaheuristics like the ones based on Ant Colony Optimization [3, 7], Particle Swarm Optimization [13, 14], and Bee Algorithms [15] worked on the approach maintaining a set of feasible solutions in each cycle of the algorithm. The initial population is hereafter evolved by repeatedly applying a set of operators on old solutions, hence transforming them into new solutions. Recently, some solutions based on discrete cuckoo search [16] were also presented.

These studies have shown that metaheuristic methods have been successful in solving the RCPSP problem efficiently as the problem size increases. Metaheuristics inspired the intelligent social behavior of fireflies [8] is an upcoming strategy which has been applied to various engineering applications [17, 18]. This investigation tries to present a new approach by discretizing the otherwise continuous Firefly Algorithm (FA) to efficiently solve the RCPSP problem.

4 Discrete Firefly Algorithm

4.1 Basic Firefly Algorithm

FA is a swarm-based metaheuristic belonging to the category of nature-inspired optimization algorithms. It is designed by observing intelligent social conduct of fireflies. Fireflies generate fleeting rhythmic flashes which they use for communication or attracting potential prey or partner. FA, as developed by Yang [8], is based on three generic rules: (1) Fireflies, being unisexual would be attracted to the other firefly. (2) The attractiveness of a firefly is in proportion to their brightness, i.e., the firefly with lesser brightness would be attracted to one with higher brightness. (3) The objective function governs the firefly's brightness.

For a problem with a maximization objective, brightness is in proportion to the objective function. However, RCPSP is a minimization optimization problem. Hence, the brightness is taken as the reciprocal of the objective function, in this case, the reciprocal of makespan. Each firefly typically represents a feasible solution for the given problem. Here, for a project instance with n activities, each firefly will represent a feasible solution in n dimensions, i.e., a feasible schedule of a sequence on n activities. The pseudocode for the FA is given in Algorithm 1.

Algorithm 1 Pseudocode of FA

Input:

n: Number of Fireflies in a swarm

max_Gen: maximum number of generations

Initialization:

Objective function: $f(x)$, $x = (x_1, x_2, \dots, x_d)$

Generate initial population of fireflies, x_i ($i=1, 2, \dots, n$)

Light Intensity I_i at x_i determined by $f(x_i)$

Define light absorption coefficient γ

Update:

While ($t < \text{max_Gen}$)

for $i=1:n$ all n fireflies

for $j=1:i$ all n fireflies

if ($I_j > I_i$), Move firefly i towards j in d -dimension

Attractiveness varies with distance r via $\exp(-\gamma r)$

Evaluate new solutions and update light intensity

End for j

End for I

End while

Termination:

Select the best-so-far and return it as the final solution

1. Attractiveness

The light intensity determines the attractiveness of a firefly and is computed using the equation

$$\beta(r) = \beta_0 e^{(-\gamma r^2)} \quad (3)$$

where β_0 is the initial attractiveness coefficient and r is the distance between fireflies.

2. Distance

Originally, the distance between two fireflies **k** and **l** at X_k and X_l in d -dimension is the Cartesian distance calculated as follows:

$$r_{kl} = \|X_k - X_l\| = \sqrt{\sum_{o=1}^d (X_{k,o} - X_{l,o})^2} \quad (4)$$

3. Movement

A lower intensity firefly k attracted to a higher intensity firefly l moves toward it using the following equation:

$$X_k = X_k + \beta_0 e^{-\gamma r_{kl}^2} (X_l - X_k) + \alpha \left(\text{rand} - \frac{1}{2} \right) \quad (5)$$

where α denotes the randomization parameter controlling light intensity decrease.

4.2 Discrete Firefly Algorithm (DFA)

The FA was initially designed as an algorithm to solve problems that were continuous in nature. However, the classic RCPSP is a deterministic discrete optimization problem. Hence, the FA cannot be directly applied to the RCPSP problem in its original form. Hence, in this study, we made some modifications to the algorithm to be able to solve the discrete problem.

The significance of each firefly and initial intensity remains the same as mentioned in the previous section. However, the distance and attractiveness have been modified to make it suited to discrete problems.

1. Distance

In a discrete problem, the distance between two population entities could be measured in two ways: (1) Hamming distance, calculated as the difference between non-corresponding elements in the schedule sequence, i.e., the number of activities which are out of sequence between two fireflies. (2) The number of swaps required to convert the first firefly order into the second one. In this investigation, we have used Hamming distance as a distance measure.

2. Movement

The firefly movement in this case is a slight modification of Eq. (5) as follows:

$$X_k = X_k + \beta (X_l - X_k) + \alpha (\text{rand}_{int}) \quad (6)$$

where the attractiveness β is given by:

$$\beta = \beta_0 / (1 + \gamma r^2) \quad (7)$$

rand_{int} is a random positive integer between the minimum and maximum number of activity in a firefly (representing a feasible schedule).

This is done to remove the exponential function in a discrete problem and has been inspired by research done in [18] where DFA was used to solve another NP-hard scheduling problem.

Table 1 Values of parameters

J	NC	RF	RS
120	2.1, 1.8, 1.5	1, 0.75, 0.5, 0.25	0.5, 0.4, 0.3, 0.2, 0.1

5 Benchmark Test Problem and Parameters

To check the DFA, we used a set of test problem instances from the PSPLIB [2]. PSPLIB is the most popularly used set of test instances for the RCPSP problem. It not only has the test instances, but also their optimal solutions in case of smaller benchmark instances and their lower bound solutions in case of larger instances. For this experiment, we have tested on the set j120.sm, which represents projects' instances containing 120 activities; the largest instance set in PSPLIB.

These instances have been generated using three parameters: Network Complexity (NC), Resource Factor (RF), and Resource Strength (RS). The various parameter values taken by these three are as shown in Table 1:

Thus, we see that these three parameters make up 60 combinations. After every 10 instances, the combinations of parameter values are changed, thus generating 600 instances. To save time, we take one kind from each instance for 10 scenarios, thus testing all the instances.

The results are calculated in terms of average standard deviation (σ) of all the tested instances against the critical path solution available in PSPLIB for the corresponding instances.

$$\sigma = \frac{\sum_{i \in BI} \text{make_span}_i - \sum_{i \in BI} \text{best_so_far}_i}{\sum_{i \in BI} \text{best_so_far}_i} \quad (8)$$

where BI stands for Benchmark Instances.

6 Experimental Results

Implementation was done in MATLAB programming language in Windows 7 64-bit environment and all experiments were carried out on a Intel Core i3 1.8 GHz machine with 8 GB RAM.

The heuristic method over which the DFA metaheuristic was applied was the serial schedule generation scheme (SSGS) [9]. SSGS was used to generate an initial population of fireflies which were updated based on the DFA algorithm operators. The solutions were tested over 5000 schedules.

The other parameters were fixed as follows: Number of fireflies (n) = 10. The main parameters β_0 , α , and γ were set after experiments to 1, 0.2, and 0.8, respectively.

Table 2 Comparison of algorithms

Algorithm	Deviation for 5000 schedules (%)
AS—RCPSP [3]	36.7
MMAS [7]	31.55
LST-2opt [7]	26.99
GA [10]	36.74
ABC [15]	36.82
BSO [15]	36.51
BA [15]	36.76
DFA—this study	16.22

The results obtained by this experiment are compared against the other algorithms. Some of the results are tabulated in Table 2.

The results tabulated clearly demonstrate that the DFA is highly efficient in solving the RCPSP problem with a very competitive value for the average standard deviation against other seminal works mentioned in the literature. The nonlinear attraction mechanism of DFA creates a stronger short-distance attraction as compared to long-distance attractions in other SI techniques. This results in the formation of subswarms within swarms which can search locally to generate diverse and better global solutions. As the different algorithms were tested in different settings and environments, we have not tested the algorithms for their computation times. As far as deviation from optimal solutions is concerned, the result of this experiment is by far the best.

7 Conclusion

In this paper, a prominent nature-inspired metaheuristic the FA was presented and adapted to be able to solve the discrete RCPSP problem. The continuous algorithm was converted into a discrete form, DFA, by altering some of the operators, namely the distance parameter and the attractiveness operator. The performance of DFA has been tested on the j120 instance from the PSPLIB. The comparisons of results show that DFA is an efficient and superior algorithm to solve this problem (an improvement of almost 10% compared to the earlier algorithm with the best smallest deviation).

Future work may involve testing the DFA on other benchmark instances from the PSPLIB. Also, only the SSGS heuristic has been used to generate initial schedules. The DFA can also be tested over other heuristics like the priority rule-based heuristics or permutation-based serial scheduling. Each nature-inspired algorithm comes with its own set of traits and features. Hence, a hybrid metaheuristic model may be a way to improve the efficiency further.

References

1. Artigues, C.: The Resource-Constrained Project Scheduling Problem. http://www.iste.co.uk/data/doc_dtalmanhopmh.pdf
2. Sprecher, A., Kolisch, R.: PSPLIB-a project scheduling problem library: OR software-ORSEP operations research software exchange program. *Eur. J. Oper. Res.* **96**(1), 205–216 (1997)
3. Merkle, D., Schmeck, H., Middendorf, M.: Ant colony ofor resource-constrained project scheduling. *IEEE Trans. Evol. Comp.* **6**(4), (2002)
4. Brucker, P., Knust S., Schoo A., Thiele, O.: A branch and bound algorithm for the resource-constrained project scheduling problem, *Eur. J. Oper. Res.* **107**, 272–288 (1998)
5. Blazewicz, J., Lenstra, J.K., Rinnooy, K.A.H.G.: Scheduling subject to resource constraints: classification and complexity. *Discret. Appl. Math.* **5**(1), 11–24 (1983)
6. Hartmann, S., Kolisch, R.: Experimental evaluation of state-of-the-art heuristics for the resource-constrained project scheduling problem. *Eur. J. Oper. Res.* **127**(2), 394–407 (2000)
7. Zhou, Y., Guo, Q., Gan, R.: Improved ACO algorithm for Resource-Constrained Project Scheduling Problem. In: International Conference on Artificial Intelligence and Computational Intelligence, AICI '09, IEEE, vol. 3, pp. 358–365 (2009)
8. Yang, X.S.: Nature-inspired Metaheuristic Algorithm. Luniver Press (2008)
9. Vanhoucke, M.: Project management with dynamic scheduling. Springer, Berlin (2012). <https://doi.org/10.1007/978-3-642-40438-2>
10. Kolisch, R., Hartmann, S.: Experimental investigation of heuristics for resource-constrained project scheduling: an update. *Eur. J. Oper. Res.* **174**, 23–37 (2006)
11. Kolisch, R., Hartmann, S.: Heuristic algorithms for solving the resource-constrained project scheduling problem: classification and computational analysis. In: Weglarz, J. (ed.) *Project Scheduling: Recent Models Algorithms and Applications*, pp. 147–178. Kluwer Academic Publishers, Berlin (1999)
12. Kolisch, R., Padman, R.: An integrated survey of deterministic project scheduling. *Omega* **29**, 249–272 (2001)
13. Koulinas, G., Kotsikas, L., Anagnostopoulos, K.: A particle swarm optimization based hyper-heuristic algorithm for the classic resource constrained project scheduling problem. *Inf. Sci.* **277**, 680–693 (2014)
14. Kumar, N., Vidyarthi, D.P.: A model for resource-constrained project scheduling using adaptive PSO. *Soft. Comput.* **20**(4), 1565–1580 (2016)
15. Ziarati, K., Akbari, R., Zeighami, V.: On the performance of bee algorithms for resource-constrained project scheduling problem. *Appl. Soft Comput.* **11**(4), 3720–3733 (2011)
16. Bibiks K., Hu F., Li J., Smith, A.: Discrete Cuckoo Search for Resource Constrained Project Scheduling Problem. In: International Conference on Computational Science and Engineering, IEEE, pp. 240–245 (2015)
17. Marichelvam, M.K., Prabhakaran, T., Yang, X.S.: A discrete firefly algorithm for the multi-objective hybrid flowshop scheduling problems. *IEEE Trans. Evol. Comput.* **18**(2), 301–305 (2014)
18. Karthikeyan, S., Asokan, P., Nickolas, S., Page, T.: A hybrid discrete firefly algorithm for solving multi-objective flexible job shop scheduling problems. *Int. J. Bio-Inspired Comput.* **7**(6), 386–401 (2015)

A Novel Approach to Handle Huge Data for Refreshment Anomalies in Near Real-Time ETL Applications



N. Mohammed Muddasir and K. Raghubeer

Abstract Real-time analysis of data is the new trend to get useful insights in very less time spend on data preprocessing. Analysis of data requires the movement of data from various heterogeneous/homogenous sources to a common place known as the data warehouse. Data source for data warehouse is the transaction processing systems. Movement of data from the transactional database to the data warehouse is done using the process of extract, transform, and load (ETL). ETL previously was done during of peak hours like a night load or on weekends. The requirement of real-time analysis demands the ETL to be fast and not wait for off-peak hours. This leads to the concept of near real-time ETL, and here techniques are employed to identify the potential changed data at the transaction database and move it to the analysis database with a very minimal delay. This movement of data in real time from multiple sources in an incremental form could lead to anomalies in the data warehouse. This work discusses the various causes of anomalies and solutions to overcome them. Our main contribution is the application of loading data into temporary tables for reducing query execution time in case of overcoming refreshment anomalies.

Keywords Near real-time ETL · Refreshment anomalies · TPC-DS

1 Introduction

Anomalies could possibly occur in case of parallel execution of data warehouse loads and analysis queries. Data warehouse loads by near real-time ETL and real-time analysis of refreshed data are two contemplating tasks. Near real-time ETL process expects the analysis task to wait until the complete load, and on the other hand, analysis task is always expecting real-time refreshed data with minimal delay.

N. Mohammed Muddasir (✉)
Department of IS&E, VVCE, NIE, Mysuru, India
e-mail: ndmsir@gmail.com

K. Raghubeer
Department of IS&E, NIE, Mysuru, India
e-mail: raghunie@yahoo.com

Trying to accomplish both at the same time could result in loss of some information. In this paper, the information talked about is in relational database format hence it could be loss of certain rows. Also, it could be that some of the rows are already stale and deleted at source but are not refreshed, and hence they appear in the analysis results. Anomalies could be those missing rows that are present in the source and not refreshed at the data warehouse or it could be those rows that are removed at the source but are present in the analysis results. Further, any rows that are updated also could lead to erroneous analysis results if not reflected at the data warehouse. The problem of refreshment anomalies is caused not only because of parallel execution of ETL and analysis query but also because of various heterogeneous sources that have to be referred. The different types of formats of data storage at these heterogeneous sources, the various transformations that have to be applied to normalize the data from these sources before loading add further to the anomalies. There are two ways data could be loaded into the data warehouse during ETL, one is full load and other is incremental load. Full load is moving all the data from source to destination. This is required during the initial setup of the data warehouse. But once the initial data warehouse is loaded, subsequent loads need not be full load they could be incremental loads. Triggering the ETL process on arrival of analysis query could possibly reduce the anomalies was proposed in [1]. The idea is to put the query on hold until the ETL task is accomplished so that the query result is without any anomalies. The disadvantage of the above approach is query execution time is increased because it has to wait until the ETL task is finished. What we propose is to perform the ETL task from the temporary tables [2] instead of original tables so that the waiting time of the query is reduced. This work focuses on identifying the reasons for anomalies and provides solutions to overcome the anomalies. This work covers a literature review of the existing work on anomaly identification and resolution. and also proposes a mechanism to reduce query execution time while handling anomalies in incremental loading scenario.

2 Reasons for Refreshment Anomalies

At first refreshment anomalies were identified by the authors of view maintenance [3]. Their work was focused on legacy systems where the source would not be aware of the concept of views in a relational database (DW). The source needs to inform the data warehouse about the update, and the warehouse would query the source to receive the update. The idea is illustrated in Fig. 1: Update processing. Anomalies in this setup could occur if the first update info from the source while been propagated to the data warehouse is being interleaved by another update there would be duplicates at the data warehouse. The anomaly is illustrated using sample data in Table1: EMP and Table2: DEPT as shown below. Initial state of Table1 is empty and later if one row is updated in blue color, the update is sent to the warehouse and the warehouse sends back the join query projecting the DNAME as shown in Table3: EMP_DEPT. While the query for the first update is being executed, if there is a second update at

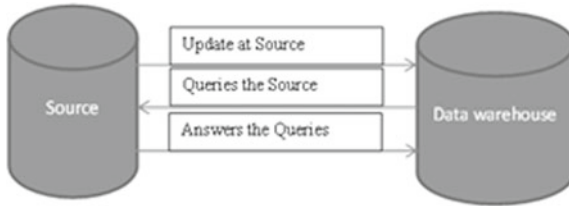
**Fig. 1** Update processing

TABLE1: EMP		TABLE2: DEPT		TABLE3: EMP_DEPT	
SSN	DEPNO	DNO	DNAME	DNAME	
100	10	10	IT	IT	
200	10			IT	

Fig. 2 Scenario demonstration interleaving queries

source and the warehouse receives the second update, it sends the second query. This is a scenario of duplicates being propagated to the warehouse. The scenario is shown in Fig. 2 where the second update is shown in red color. They proposed algorithm to overcome the anomalies known as eager compensation algorithm.

Another work on multiple source integration to update the warehouse the authors of [4] has identified anomalies due to interleaving of queries. They illustrate the scenario by taking three relation tables each placed in three different sources. The data warehouse update requires joining all the three tables. The scenario for the anomaly is if the second table at the source two is initially empty and if it is updated the incremental load requires it to join with table of source one and source three. The first join is with source one and next with source three. After the join with source one, if the source one row is deleted then the join with source three is not aware and leads to inconsistent data warehouse update. The above explanation is illustrated in Fig. 3, where the three tables from three sources are EMP, WORKSON, and PROJECT. Initially, WORKON is empty and updated with one row shown in blue color. This update requires moving to the data warehouse, and hence, first join is with EMP. Next join is with PROJECT. But while the second join is taking place if the row in EMP is deleted as shown in red, then this is not aware while join WORKON and PROJECT and leads to inserting the row of EMP in the ware house.

The authors discussed two ways to overcome the anomalies; one is to have copies of all relations on all sources. This would lead to any new update before the changes

Table1:EMP		Table2: WORKSON		Table3:PROJECT	
Name	SSN	SSN	PNO	PNO	PNAME
RAJU	100	100	999	999	IT

Fig. 3 Anomalies due to multiple sources

moved to the data warehouse to be captured and avoiding the anomaly. This solution would require additional storage requirement and would not be an option in huge data warehouses. The other solution is to run the queries across all sources in a distributed fashion so that no new updates are missed. But this would require huge processing capacities. Hence, they developed strobe family of algorithm that intelligently process queries as atomic units. In the above scenario of anomaly, the second update of EMP table is captured at the warehouse and applied to the final data before moving to the data warehouse, i.e., if the row in EMP is deleted, warehouse table has nothing to be loaded, and this is taken care in their work.

Using outer joins to capture missed rows, in turn, leads to additional deletions. This also generates null values that are to be identified and deleted when the actual data are updated [5]. To illustrate, consider the two relations Table3: EMPLOYEE and Table4: DEPARTMENT shown below, respectively. The column deptno in employee is referencing column dept in department table. If there is a warehouse that joins $\text{EMP} \bowtie \text{DEPT}$, then result would be as shown in Table5: EMP_DEPT. As seen in Table5, one row each from EMPLOYEE and DEPARTMENT has been missed in the warehouse. To get the complete data, outer join is required as it captures the mismatched rows. There are three variants of outer joins left, right, and full. Based on the context and importance of data appropriate, outer join operations would be applied. Assuming data from both the tables is required, and important full outer is applied. The result is shown in Table6: EMP_DEPT_FULL. The problem with outer joins is that they generate NULL values. Null values could lead to inconsistent database states and incorrect query results. Also, they require additional maintenance task if in case during the incremental load rows that were having null values now have actual values. For example, if SSS 222 is now assigned to deptno 20, as shown in Table7: NEW_EMPLOYEE, then result of outer join would be as shown in Table8: EMP_DEPT_INCR. Row 4 in Table8 shown in red is part of the incremental load. The scenario is shown in Fig. 4 that row 2 and row 3 have to be deleted, and they are no longer valid and leading to anomalies. To address the removal of null values after incremental load in [5], they have developed two algorithms. According to the algorithms, row 2 and row 3 from Table8 need to be removed to make the database in a consistent state without refreshment anomalies.

Delay in capturing the changes in deltas leads to deletion and update anomalies as discussed in [6]. The deltas of the new insert and new delete are captured in the tables ΔEMP , ΔDEPT and ∇EMP , ∇DEPT , respectively. Later, incremental load is calculated using the following join queries. $\Delta\text{EMP_DEPT} = (\text{EMP}_{\text{new}} \bowtie \Delta\text{DEPT}) \cup (\Delta\text{EMP} \bowtie \text{DEPT}_{\text{new}})$ for inserted values and $\nabla\text{EMP_DEPT} = (\text{EMP}_{\text{new}} \bowtie \nabla\text{DEPT}) \cup (\nabla\text{EMP} \bowtie \text{DEPT}_{\text{new}}) \cup (\nabla\text{EMP} \bowtie \nabla\text{DEPT}_{\text{new}})$ for deleted values. The warehouse table EMP_DEPT is incrementally loaded by inserting of all rows of $\Delta\text{EMP_DEPT}$ and deleting in EMPT_DEPT all rows of $\nabla\text{EMP_DEPT}$. The deletion anomaly is shown here where the initial state of EMP, DEPT, and EMP_DEPT as in Table9, Table10, and Table11. Respectively, contains one row. If the row is deleted (shown as strike text with red color font) from EMP and DEPT, it had to be captured in ∇EMP and ∇DEPT but if there is delay in capturing then those tables are empty as shown in Table12 and

Table3: EMPLOYEE

SSN	ENAME	SAL	DEPTNO
111	Ravi	200000	10
222	Ramesh	300000	

Table4: DEPARTMENT

DEPTNO	DNAME	DLOC
10	IT	INDIA
20	ACCOUNTS	US

Table5: EMP_DEPT

SSN	ENAME	SAL	DEPTNO	DEPTNO	DNAME	DLOC
111	Ravi	200000	10	10	IT	INDIA

Table6: EMP_DEPT_FULL

SSN	ENAME	SAL	DEPTNO	DEPTNO	DNAME	DLOC
111	Ravi	200000	10	10	IT	INDIA
222	Ramesh	300000	NULL	NULL	NULL	NULL
NULL	NULL	NULL	NULL	20	ACCOUNTS	US

Table7: NEW_EMPLOYEE

SSN	ENAME	SAL	DEPTNO
111	Ravi	200000	10
222	Ramesh	300000	20

Table8 EMP_DEPT_INCR

SSN	ENAME	SAL	DEPTNO	DEPTNO	DNAME	DLOC
111	Ravi	200000	10	10	IT	INDIA
222	Ramesh	300000	NULL	NULL	NULL	NULL
NULL	NULL	NULL	NULL	20	ACCOUNTS	US
222	Ramesh	300000	20	20	ACCOUNTS	US

Fig. 4 Scenario anomalies of outer join

Table13. This would lead to an empty table ∇ EMP_DEPT for deletion related join queries as shown in Table14. Now, because ∇ EMP_DEPT is empty there are no rows to be deleted from EMP_DEPT (the main table) so the row is not deleted leading to deletion anomaly as shown in Fig. 5. The authors have also discussed the scenario of insertion anomalies. They have mentioned the reasons for delay in capturing the deltas and various ways to reduce the delay like using a snapshot etc.

The latest work on identification of anomalies and solution to them is done by Qu et al. [7], and in their work, they overcome the anomalies due to delay in capturing the deltas. The idea is while a business query hits the data warehouse, and the data warehouse before answering the query pause it until all the tables related to the query have been checked for any new updates. This way the query execution time is increased but the business user is sure of getting the updated information always. They addressed the real-time maintenance of view (snapshot) in the data warehouse. Snapshot is always consistent but missed some of the updates that are done just before the query is fired. Hence put the query on hold and retrieve the latest updates and then answer the query. They extended their work to carry of multiple maintenance jobs in parallel in the work [1].

Table9: EMP

SSN	ENAME	SAL	DEPTNO
222	Ramesh	300000	10

Table11: EMP_DEPT

SSN	ENAME	SAL	DEPTNO	DEPTNO	DNAME	DLOC
222	Ramesh	300000	10	10	IT	INDIA

Table12: ▼EMP

SSN	ENAME	SAL	DEPTNO

Table13: ▼DEPT

DEPTNO	DNAME	DLOC

Table14: ▼EMP_DEPT

SSN	ENAME	SAL	DEPTNO	DEPTNO	DNAME	DLOC

Fig. 5 Scenario of deletion anomaly

To summarize the above discussion, the various causes of refreshment anomalies during incremental loads are interleaving of queries, outer joins, and delay is capturing the deltas.

3 Reduce Query Execution Time with Updated Records

This work focuses on the refreshment anomalies and the mechanism to reduce the query execution time. As discussed in the literature, the authors of [7] have put the query on hold until the deltas are captured. This gives rise to a scenario of concurrent execution of query while the data warehouse is being loaded. Query put on hold takes more time as compared to a query that is allowed to execute with the data warehouse update. But query on hold gives updated information with no anomalies, while the query executed immediately runs faster but could have any possible anomalies as discussed in the previous section. This work focuses on how we could reduce the execution time of query while it is waiting for the data warehouse to be updated. So, we got this idea of reduction in query execution time from the work by authors in [2] continuous data integration by replication of data warehouse schema. During incremental load, instead of capturing the deltas into the original warehouse, tables capture them into temporary replica tables. These replica tables are small in size and without any constraints hence loading is fast. Because the loading is fast the query execution time with updated record is less. The query execution time is reduced if the incremental deltas are loaded into temporary tables as shown in [2]. The work in this paper combines the idea to accomplish updated information with less time and without refreshment anomalies. The query is put on hold as described in [7], but the updates are retrieved from temporary table as described in [2], and this way query

execution time is reduced at the same time also giving updated records. The proposed idea is demonstrated by using TPC-DI [8] data source. We simulate a concurrent execution of standard queries from TPC-DI and loading the data warehouse. The results show that we get better query execution time with data loaded into temporary replica tables. How this work differs from [2] is they have not used concurrent execution and load. Also, this work is different from [7] because they have not used temporary replica tables for loading the deltas changes.

4 Implementation and Results

The implementation of loading incremental data into temporary tables to reduce the query execution time was done using postgres DBMS and Pentaho Kettle data integration tool using the TPC-DI data source. The simulation of query waiting for update was done by parallel run of query and update. Initially, the update is done and query is executed serially. The updates on the main table and temporary table have been done serially. The time taken for query to execute in case of temporary table is less. This ascertains the results shown in [2]. Next, to simulate the query hold until updates, parallel run of update and query was done. This also was done on both the main table and temporary table. Again the results show the query execution time in case of temporary table is less. The queries were from TPC-DI specification [8] working on STORE_SALES data mart this work executed query27 and query82 by generating test data of 1 GB. The hardware used is intel core i5 with 4 GB RAM. The work simulated parallel load and query by using repeated job run in pentaho kettle and\watch utility in postgres DBMS. The results for serial load and query execution are shown in Fig. 6 for query27. The initial load was 10 k rows and each incremental load was again 10 k rows. The Y-axis is the execution time for the query in milliseconds, and the X-axis is the number of rows returned for initial and incremental load up to 10 incremental loads. Next Fig. 7 shows the results for query27 in case of parallel load. As seen, the temporary table solution for incremental load works with reduced query execution time in case of parallel query execution and

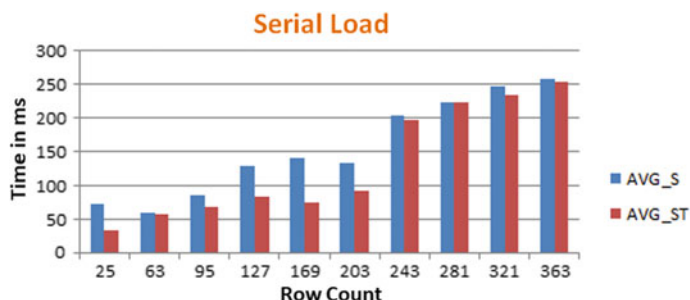


Fig. 6 Serial load and execution Q27

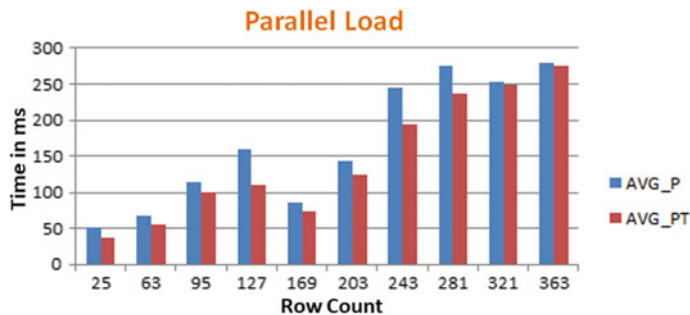


Fig. 7 Parallel load and execution Q27

updates. The query was executed several times on the data size like for 10 k about 10 times and for 80 k about 12 times recording various times of execution and took the average as a measure to plot the final result. The work shows similar results for query82 in Figs. 8 and 9. In this case, the initial load was 80 k rows and incremental load was 50 k rows to 1 lac rows. The query return rows from 1 to 10 for the said amount of data, final load was 7 lac rows. The graph shows in most of the cases parallel execution takes more time than serial, that is because the query is but on

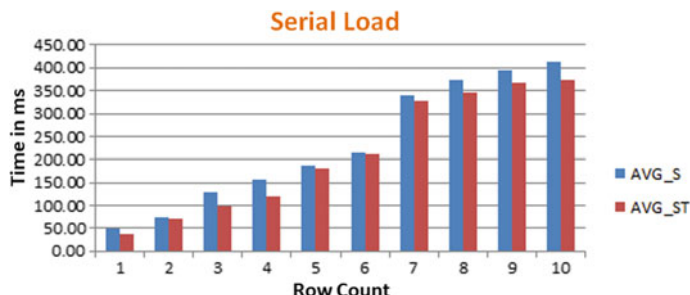


Fig. 8 Serial load and execution Q82

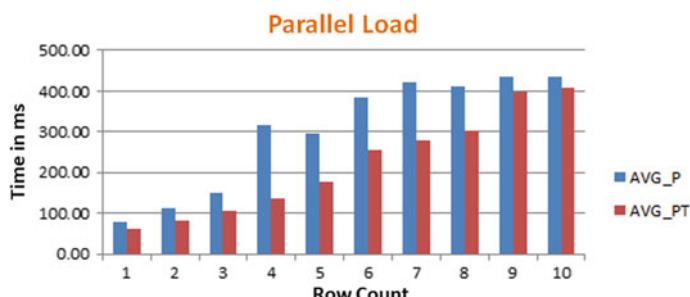


Fig. 9 Parallel load and execution Q82

hold until all the updates are received. Even then loading into temporary tables have reduced the execution time of the query.

5 Conclusion and Future Work

This work focuses on upon three main causes of anomalies, and they are due to interleaving of queries, delayed updates, and outer joins. Many other anomalies like levels of consistency between source and views, order of processing of updates, and the validity of the view are discussed in [9–12]. Reducing the query execution time and maintaining consistency is the main contribution of this work. With the results shown, it could be concluded that if analysis query is put on hold while there is a concurrent update on the data warehouse, the waiting time of the query could be reduced if loads are performed on temporary replica tables. Applying this idea to overcome refreshment anomalies in near real-time ETL has benefited in maintaining consistency and remove anomalies due to refreshment. This work was part of our research on optimization techniques in near real-time ETL. Refreshment anomalies handled effectively would optimize near real-time ETL. Major work in optimization of ETL is done in [13]. The actual simulation of anomalies was carried out in this work, which would be the future enhancement. Also, in future, we plan to work on in big data and how ETL techniques are used to handle big data as discussed in [14, 15].

References

1. Qu, W., Deßloch, S.: Incremental ETL Pipeline Scheduling for Near Real-Time Data Warehouses. Gesellschaft für Informatik, Bonn (2017). 978-3-88579-659-6
2. Ricardo.: Real-time data warehouse loading methodology. In: IDEAS '08 Proceedings of the 2008 International Symposium on Database Engineering and Applications, ACM, Coimbra (2008)
3. Yue, Z., Hector G.-M., Hammer, J., Widom, J.: View Maintenance in a Warehousing Environment. ACM, San Jose, California (1995)
4. Yue, Z., Hector, G.-M., Wiener, J.L.: Consistency Algorithms For Multi-Source Warehouse View Maintenance. Kluwer Academic Publisher, Boston (1997)
5. Gupta, A., Jagadish, H.V., Mumick, I.S.: Data integration using self maintaince views. ACM, Cambridge (1999)
6. Jörg, T., Dessloch, S.: Near Real-Time Data Warehousing Using State-of-the-Art ETL Tools. Springer, Berlin (2010)
7. Qu, W., Basavaraj, V., Shankar, S., Dessloch, S.: Real-Time Snapshot Maintenance With Incremental ETL Pipelines in Data Warehouses. Springer, Dawak, pp. 1611–3349 (2015)
8. TPC.: TPC BENCHMARK™ DS. s.l., TPC (2019)
9. Agrawal, D., El Abbadi, A., Singh, A., Yurek, T.: Efficient View Maintenance at Data Warehouses. s.l., ACM (1997)
10. Mumick, I.S., Gupta, A., Jagadish, H.V.: Data Integration Using Self-Maintainable Views (1996)
11. Zhou, R., Hull, G.: A Framework for Supporting Data Integration Using the Materialized and Virtual Approaches. s.l., ACM (1996)

12. Zhou, R., Hull, G.: Towards the Study of Performance Trade-offs Between Materialized and Virtual Integrated Views. s.l., VIEWS (1996)
13. Sellis, A., Simitsis, P., Vassiliadis, T.: Optimizing ETL Processes In Data Warehouses. IEEE, Tokyo (2005)
14. Liu X., Thomsen C., Pedersen T.B.: A highly scalable dimensional ETL framework based on map reduce. In: Hameurlain, A., Küng, J., Wagner, R., Cuzzocrea, A., Dayal, U. (eds.) Transactions on Large-Scale Data- and Knowledge-Centered Systems, VIII. Springer, Berlin (2013)
15. Bala, M., Boussaid, O., Alimazighi Z.: Big-ETL: Extracting—Transforming—Loading Approach for Big Data. CSREA Press, Las Vegas (2015)

Comparison of Photodetection Capability of Spin Coated TiO₂ Thin Film and In₂O₃ Thin Film Devices



Rahul Raman, Amitabha Nath, and Mitra Barun Sarkar

Abstract The fabrication of TiO₂ thin film (TF) and In₂O₃ thin film (TF) separately using Spin Coating deposition technique and the analysis of their different characteristics like structural and optical properties has been reported in this paper and based upon the comparisons of these properties the superiority as a photodetector device of both the devices has been decided. The structural properties of both the prepared samples have been discussed and the FESEM characterization result confirms the Thin Film depositions. The UV-visible absorption characterization has been performed to reveal the optical properties of the fabricated samples in which the main band absorption was found at ~370 nm for TiO₂ TF and ~274 nm for In₂O₃ TF structure. The Bandgap obtained for TiO₂ TF was ~3.1 eV and that obtained for In₂O₃ TF was ~3.3 eV. This characterization result ensures the better performance of TiO₂ TF as a photodetector as compared to In₂O₃ TF.

Keywords Photodetection · Spin Coating deposition technique · Structural and optical property · Thin film · Bandgap

1 Introduction

A photodetector works on the principle of conversion of light energy to electrical energy where we need to make a junction between two materials possessing anti-reflection properties so that an efficient number of photons can be trapped at the junction. TiO₂ is a wide Bandgap n-type semiconductor whose Bandgap is in the range of 3.1–3.3 eV for rutile and anatase phase [1]. TiO₂ films based devices have a number of applications such as dye-sensitized photovoltaic cells [2], gas sensors [3], electrochromic displays [4], and planar waveguides [5], as a heterogeneous catalysis [6], as a photocatalyst in solar cells [7], as a pigment [8], coating for corrosion-protection [9], anti-fogging [10], in optical applications [11], in porcelains [12], and in many

R. Raman · A. Nath · M. B. Sarkar (✉)

Department of Electronics and Communication Engineering, National Institute of Technology Agartala, Agartala, India
e-mail: mbarun.ece@nita.ac.in

electrical and electronic appliances like memory registers [13], photochromic [14] etc. Titanium dioxide is highly demanding among various photocatalytic materials because it is easily available, inexpensive, environment-friendly and chemically stable [15]. Indium oxide (In_2O_3) semiconducting material has been used extensively because of its very wide Bandgap (nearby 3.5 eV) [16], highly transparent [17], better chemical stability [18], greater mobility [19] and large electrical conductivity [20]. It is commonly used in many applications of the various fields of electronics, in photovoltaic and optoelectronic devices such as gas sensors [21], in solar energy conversion [22], in biocatalytic redox transformation [23], in light emitting diodes (LED) [24] and anti-reflecting coatings [25].

A thin film-based device preparation has been reported by various techniques such as physical vapor deposition (PVD) [26], chemical vapor deposition (CVD) [27], Atomic layer deposition (ALD) [28], Plasma enhanced CVD (PECVD) [29], Molecular Beam Epitaxy (MBE) [30], pulsed laser deposition (PLD) [31], DC magnetron sputtering [32], spray pyrolysis [33], spray ultrasonic [34], sol-gel process [35], dip coating method [36], spin coating method [37] etc., but among these methods the Spin Coating Deposition method can be considered as the best one for the deposition of a thin film because of its processing simplicity, easy control of chemical components, uniformity, low cost of equipments etc. In this paper, two samples p-Si/ TiO_2 TF and p-Si/ In_2O_3 TF have been prepared using the Spin Coating method and the Gold metallization over the samples are done using thermal evaporator method. The thickness and uniformity of the films prepared by spin coating depends upon the angular velocity of the spin coater, the viscosity of the solution, the acceleration of the spin coater and the duration of the thin film deposition.

Figure 1a, b shows the proposed schematic diagram for the fabricated TiO_2 TF and In_2O_3 TF devices respectively. Both the samples are comprised of p-type Si <100> substrate with resistivity $35 \Omega\text{-cm}$ upon which a thin film of thickness approximately 150 nm was deposited. The thickness for both the samples were kept almost the same. After the deposition of thin-film, a gold metallization were done for both the samples.

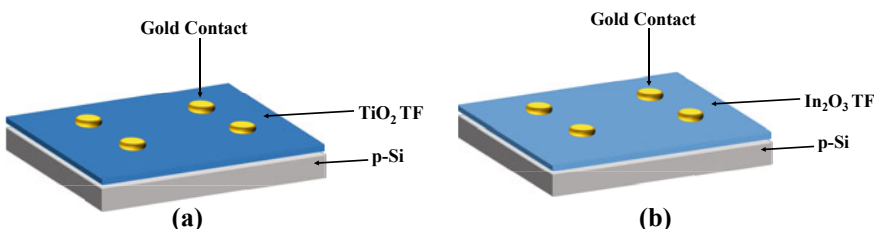


Fig. 1 **a** Proposed structure of TiO_2 TF device. **b** Proposed structure of In_2O_3 TF device

2 Experiments

Both TiO₂ TF and In₂O₃ TF devices were prepared separately using Spin Coating deposition technique. A 1 cm × 1 cm p-type Si(100) was cut down from a Si wafer as a substrate. The Si material was processed through RCA cleaning using methanol, ethanol, acetone and DI water. Now the TF depositions over the substrate were done using Spin Coating deposition technique. The different precursor solutions of the depositing material for both the samples were prepared with a proper concentration. For making the precursor solution of TiO₂ TF, a solution of Titanium Tetra Isopropoxide, Acetic Acid and Ethanol were prepared and followed by magnetic stirring at room temperature for 4–5 h. The precursor solution preparation for In₂O₃ TF involved several steps, a solution of In(NO₃)₃ and distilled water of 0.05 M strength was prepared followed by magnetic stirring at room temperature for 30 min. A 5 M Ammonium Hydroxide was added to the solution under stirring which resulted in the white precipitate of the solution. The precipitate was washed by Ethanol 3 times and a solution of precipitate, acetic acid and water was prepared. Thereafter another solution of CMC and water of 1 wt% was prepared which was used as a thickener solution and finally, the two prepared solution were mixed such that CMC solution was 10% by volume. Thereafter the prepared solutions were deposited over the Si substrate using Spin Coating deposition technique followed by drying at 80 °C. The deposition and drying processes were repeated 5 times to obtain the required thickness of TF and finally, calcination was performed at 600 °C for 2 h using Tube Furnace. After making the precursor solution the same processes were followed for both the samples.

After the preparation of both the samples, different characterizations such as FESEM (Field Emission Scanning Electron Microscopy) and Optical Absorption were performed over it. Optical Absorption measurement was done by a UV-visible spectrophotometer (Lambda 950, Perkin Elmer) to determine the Bandgap and the Absorption capabilities of the devices. Figure 2 shows the various steps used for the fabrication of the devices. All the fabrication steps were the same for making the final product of both the devices accept the making of precursor solution which was different for the two prepared devices.

3 Results and Discussion

3.1 Field Emission Scanning Electron Microscopy (FESEM)

The Field Emission Scanning Electron Microscopy (FESEM) has been performed for both the fabricated samples using the SIGMA ZESIS instrument. The Top view of the fabricated samples was scanned with a very high resolution and the result of the FESEM characterization confirms that the deposited structure is thin film.

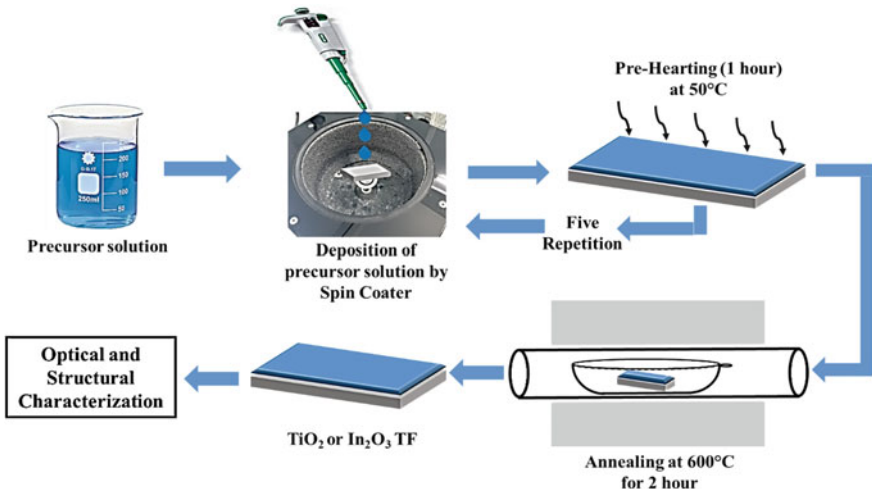


Fig. 2 Steps involved in the preparation of the device using the spin coating method

Figure 3a, b shows the top view of fabricated TiO_2 TF and In_2O_3 TF respectively deposited by Spin Coating deposition technique. Rough thin film surfaces have been observed for both the samples. From the FESEM top view of the deposited samples, it can be seen that there are some cracks present over the deposited thin film and these cracks appeared because of the annealing process done at $600\text{ }^\circ\text{C}$ over the samples [38]. The appeared cracks in the deposited thin film helps in more trapping in electrons which results in better photodetection and absorption by the fabricated samples. The uniformity and thickness of the deposited thin film layer depends upon the speed of spinning, acceleration of the spinning and the time for which the deposition is carried out. In the present work, the speed of the Spin Coater was kept at 2000 rpm,

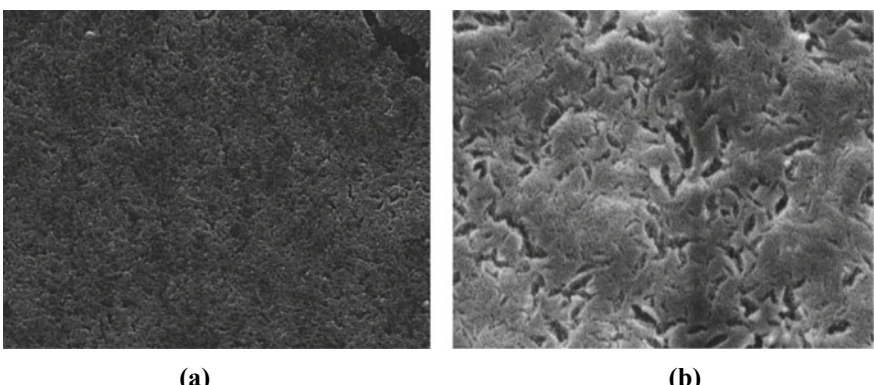


Fig. 3 **a** Top view FESEM images of TiO_2 TF sample. **b** Top view FESEM images of In_2O_3 TF sample

the acceleration was kept as 30 m/s² and the deposition was carried out for 30 s. A thin film of thickness of around 30 nm was achieved in one time deposition, so the deposition process was repeated for 5 times to get the thin film of thickness order of 150 nm.

3.2 Optical Property

The Optical absorption characterization for both the as-deposited samples were done using UV-Visible Spectrophotometer (Lamda950, Perkin Elmer) for the wavelength range of 200–800 nm at room temperature. This characterization reveals the optical properties and also gives information about the various bandgaps of the fabricated samples. In this paper, this characterization showed the absorption capability of both the samples and gave the various Bandgap values like main Bandgap and sub Bandgap values. Figure 4a, b shows the Optical Absorption of the samples In₂O₃ TF and TiO₂ TF respectively.

The main band absorption was located at 370 nm for TiO₂ TF based device and at 275 nm for In₂O₃ TF device. The main band absorption takes place due to the transition of free electrons from the valance band to the conduction band [39]. The optical Bandgap has been calculated for the obtained peak using Tauc's formula $(\alpha h\nu)^{1/n} = A(h\nu - E_g)$, here $n = 2$ for indirect Bandgap transition and $n = 2$ for direct Bandgap transition [40]. In this case value of n is taken as 1/2, because a direct Bandgap transition is considered here due to the sudden change in the absorption of light in the range of 200–400 nm which can be seen from the above figure. Figure 5a, b shows the graph of $(\alpha h\nu)^2$ versus $h\nu$ for TiO₂ TF and In₂O₃ TF samples respectively, where α represents the optical absorption coefficient and $h\nu$ represents the photon energy. The absorption coefficient can be determined with the help of measured transmission coefficient (T) by using Eq. (1).

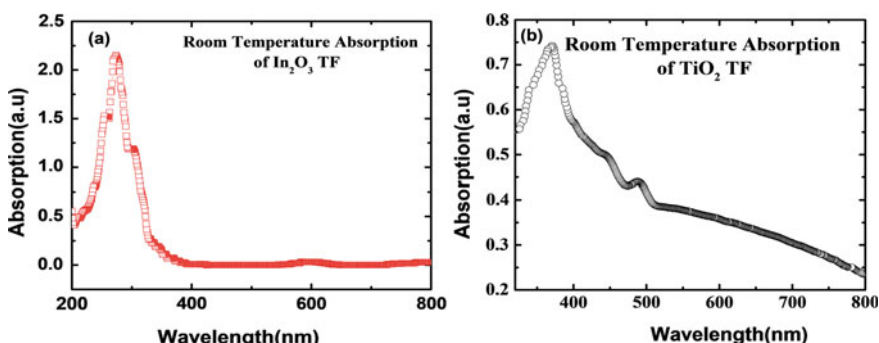


Fig. 4 **a** Optical absorption of In₂O₃ TF. **b** Optical absorption of TiO₂ TF

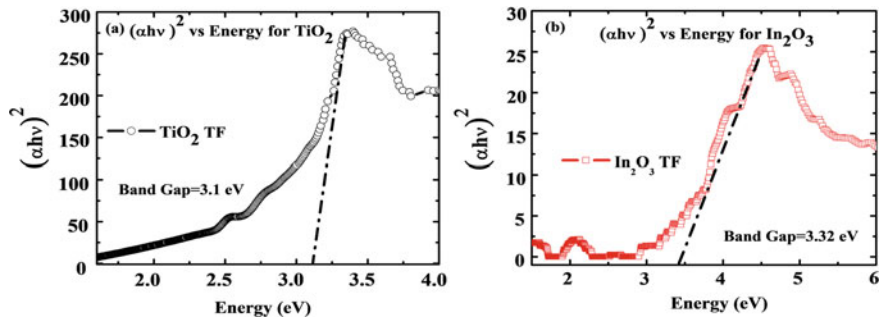


Fig. 5 **a** $(\alpha h\nu)^2$ versus Energy plot for TiO_2 TF. **b** $(\alpha h\nu)^2$ versus energy plot for In_2O_3 TF

$$\alpha = 2.303 \log(T/d) \quad (1)$$

where d is the thickness of the sample.

The Bandgap for both the samples were calculated by doing the extrapolation of the linear part of the $(\alpha h\nu)^2$ versus $h\nu$ plot. For TiO_2 TF device Bandgap was calculated as $Eg = 3.1$ eV while for In_2O_3 TF device it was found to be $Eg = 3.3$ eV which are approximate to the standard value depicted in Table 1. As the Bandgap of TiO_2 TF is less as compared to the In_2O_3 TF, so TiO_2 TF device can be considered as a better photodetector due to the ease of transition of carriers from valance band to the conduction band.

Their photodetection capability has been compared by comparing their various parameters obtained from the morphological and optical characterization, which are enlisted in the table given below:

Table 1 A comparison of the obtained best tradeoff performance between both the fabricated devices

SI. No.	Devices structure	Oxide used	Fabrication method	Precursor solution constituents	Phase	Main band absorption wavelength (nm)	Bandgap (eV)
1	p-Si/ TiO_2 TF	TiO_2	Spin coating	Titanium tetra isopropoxide, acetic acid and ethanol	Anatase	370	3.1
2	p-Si/ In_2O_3 TF	In_2O_3	Spin coating	$\text{In}(\text{NO}_3)_3$, distilled water, ammonium hydroxide, ethanol, CMC	Bixbyite	275	3.3

4 Conclusion

Two separate samples p-Si/In₂O₃ TF and p-Si/TiO₂ TF were fabricated using Spin Coating Fabrication method and their Optical Absorption and FESEM characterization were done. The FESEM characteristics describe the morphological behaviour of the fabricated samples and the top view shows the fabrication of thin-film over the substrate for both the samples. From the Optical Absorption result graph, it can be observed that the Absorption peak widening is greater in case of TiO₂ TF device and it is noticed that the In₂O₃ TF device can absorb the light in UV region only whereas the TiO₂ TF device can absorb the light in UV as well as in visible region. Since TiO₂ TF device shows better optical absorption capability, so it can be considered as a better photodetector device. The Bandgap obtained for TiO₂ TF device was 3.1 eV at 370 nm wavelength and the Bandgap obtained for In₂O₃ TF device was 3.3 eV at 275 nm wavelength which also confirms the superiority of TiO₂ TF device as a photodetector.

Acknowledgements Authors are grateful to Dr. Ardhendu Saha for providing Optical Absorption Spectroscopy facility, Centre of Excellence of Advanced Material, NIT Durgapur for providing FESEM characterization and NIT Agartala for all kind of supports.

References

1. Sarkar, M.B., Mondal, A., Choudhuri, B., Mahajan, B., Chakrabartty, S., Ngangbam, C.: Enlarged broadband photodetection using indium doped TiO₂ alloy thin film. *J. Alloys Compd.* **615**, 440–445 (2014). <https://doi.org/10.1016/j.jallcom.2014.06.184>
2. Roy, P., Kim, D., Lee, K., Spieckerb, E., Schmuki, P.: TiO₂ nanotubes and their application in dye-sensitized solar cells. *Nanoscale* **2**, 45–59 (2010). <https://doi.org/10.1039/b9nr00131j>
3. Garzella, C., Comini, E., Tempesti, E., Frigeri, C., Sberveglieri, G.: TiO₂ thin films by a novel sol-gel processing for gas sensor applications. *Sens. Actuators B. Chem.* **68**(1–3), 189–196 (2000). [https://doi.org/10.1016/s0925-4005\(00\)00428-7](https://doi.org/10.1016/s0925-4005(00)00428-7)
4. Toma, S.H., Toma, H.E.: Versatile electro chromic displays based on TiO₂ nano porous films modified with triruthenium clusters. *Electrochim. Commun.* **8**(10), 1628–1632 (2006). <https://doi.org/10.1016/j.elecom.2006.07.043>
5. Bradley, J.D.B., Evans, C.C., Parsy, F., Phillips, K.C., Senaratne, R., Marti, E., Mazur, E.: Low-loss TiO₂ planar waveguides for nano photonic applications. In: 2010 IEEE Photonic Society's 23rd Annual Meeting (2010). <https://doi.org/10.1109/photonics.2010.5698885>
6. Ibadon, A., Fitzpatrick, P.: Heterogeneous Photocatalysis: recent advances and applications. *Catalysts* **3**(1), 189–218 (2013). <https://doi.org/10.3390/catal3010189>
7. Nakata, K., Fujishima, A.: TiO₂ photocatalysis: design and applications. *J. Photochem. Photobiol. C* **13**(3), 169–189 (2012). <https://doi.org/10.1016/j.jphotochemrev.2012.06.001>
8. Braun, J.H., Baidins, A., Marganski, R.E.: TiO₂ pigment technology: a review. *Prog. Org. Coat.* **20**(2), 105–138 (1992). [https://doi.org/10.1016/0033-0655\(92\)80001-d](https://doi.org/10.1016/0033-0655(92)80001-d)
9. Shen, G.X., Chen, Y.C., Lin, C.J.: Corrosion protection of 316 L stainless steel by a TiO₂ nanoparticle coating prepared by sol-gel method. *Thin Solid Films* **489**(1–2), 130–136 (2005). <https://doi.org/10.1016/j.tsf.2005.05.016>

10. Lai, Y., Tang, Y., Gong, J., Gong, D., Chi, L., Lin, C., Chen, Z.: Transparent super hydrophobic/super hydrophilic TiO₂-based coatings for self-cleaning and anti-fogging. *J. Mater. Chem.* **22**(15), 7420 (2012). <https://doi.org/10.1039/c2jm16298a>
11. Welte, A., Waldauf, C., Brabec, C., Wellmann, P.J.: Application of optical absorbance for the investigation of electronic and structural properties of sol–gel processed TiO₂ films. *Thin Solid Films* **516**(20), 7256–7259 (2008). <https://doi.org/10.1016/j.tsf.2007.12.025>
12. Zhang, Z., Li, X.: Effect of TiO₂-SiO₂-SnO_x sol-gel coating on the bonding strength of titanium-porcelain. *Mater. Lett.* **180**, 288–290 (2016). <https://doi.org/10.1016/j.matlet.2016.05.155>
13. Lin, C.-C., Liao, J.-W., Li, W.-Y.: Resistive switching properties of TiO₂ film for flexible non-volatile memory applications. *Ceram. Int.* **39**, S733–S737 (2013). <https://doi.org/10.1016/j.ceramint.2012.10.171>
14. Naoi, K., Ohko, Y., Tatsuma, T.: TiO₂ films loaded with silver nanoparticles: control of multi-color photochromic behavior. *J. Am. Chem. Soc.* **126**(11), 3664–3668 (2004). <https://doi.org/10.1021/ja039474z>
15. Singh, S., Mahalingam, H., Singh, P.K.: Polymer-supported titanium dioxide photocatalysts for environmental remediation: a review. *Appl. Catal. A* **462–463**, 178–195 (2013). <https://doi.org/10.1016/j.apcata.2013.04.039>
16. Sarkar, M.B., Choudhuri, B., Bhattacharya, P., Barrman, R.N., Ghosh, A., diwedi, S., Dhar, M.M., chakrbartty, S., Mondal, A.: Improved UV photodetection by indium doped TiO₂ thin film based photodetector. *J. Nanosci. Nanotechnol.* **18**, 4898–4903 (2018). <https://doi.org/10.116/j.jnn.2018.15295>
17. Minami, T., Kumagai, H., Kakumu, T., Takata, S., Ishii, M.: Highly transparent and conductive ZnO-In₂O₃ thin films prepared by atmospheric pressure chemical vapor deposition. *J. Vac. Sci. Technol. Vac. Surf. Films* **15**(3), 1069–1073 (1997). <https://doi.org/10.1116/1.580431>
18. Hong, J.-S., Rhee, B.-R., Kim, H.-M., Je, K.-C., Kang, Y.-J., Ahn, J.S.: Enhanced properties of In₂O₃–ZnO thin films deposited on soda lime glass due to barrier layers of SiO₂ and TiO₂. *Thin Solid Films* **467**(1–2), 158–161 (2004). <https://doi.org/10.1016/j.tsf.2004.03.014>
19. Warmsingh, C., Yoshida, Y., Readey, D.W., Teplin, C.W., Perkins, J.D., Parilla, P.A., Gingley, D.S.: High-mobility transparent conducting Mo-doped In₂O₃ thin films by pulsed laser deposition. *J. Appl. Phys.* **95**(7), 3831–3833 (2004). <https://doi.org/10.1063/1.1646468>
20. Girtan, M.: The influence of post-annealing treatment on the electrical properties of In₂O₃ thin films prepared by an ultrasonic spray CVD process. *Surf. Coat. Technol.* **184**(2–3), 219–224 (2004). <https://doi.org/10.1016/j.surfcoat.2003.10.136>
21. Gurlo, A., Ivanovskaya, M., Bärsan, N., Schweizer-Berberich, M., Weimar, U., Göpel, W., Diéguez, A.: Grain size control in nanocrystalline In₂O₃ semiconductor gas sensors. *Sens. Actuators B. Chem.* **44**(1–3), 327–333 (1997). [https://doi.org/10.1016/s0925-4005\(97\)00199-8](https://doi.org/10.1016/s0925-4005(97)00199-8)
22. Manifacier, J.-C., Szepessy, L., Bresse, J.F., Perotin, M., Stuck, R.: In₂O₃: (Sn) and SnO₂: (F) films—application to solar energy conversion part II—electrical and optical properties. *Mater. Res. Bull.* **14**(2), 163–175 (1979). [https://doi.org/10.1016/0025-5408\(79\)90115-6](https://doi.org/10.1016/0025-5408(79)90115-6)
23. Willner, I., Katz, E.: Integration of layered redox proteins and conductive supports for bioelectronic applications. *Angew. Chem. Int. Ed.* **39**(7), 1180–1218 (2000). [https://doi.org/10.1002/\(sici\)1521-3773\(20000403\)39:7%3c1180::aid-anie1180%3e3.0.co;2-e](https://doi.org/10.1002/(sici)1521-3773(20000403)39:7%3c1180::aid-anie1180%3e3.0.co;2-e)
24. Kim, H., Horwitz, J.S., Kushto, G.P., Qadri, S.B., Kafafi, Z.H., Chrisey, D.B.: Transparent conducting Zr-doped In₂O₃ thin films for organic light-emitting diodes. *Appl. Phys. Lett.* **78**(8), 1050–1052 (2001). <https://doi.org/10.1063/1.1350595>
25. Attaf, A., Bouhdjari, A., Saidi, H., Benkhetta, Y., Bendjedidi, H., Nouadji, M., Lehraki, N.: Influence of growth time on crystalline structure, morphologic and optical properties of In₂O₃ thin films (2015). <https://doi.org/10.1063/1.4914207>
26. Yi, J., He, X., Sun, Y., Li, Y.: Electron beam-physical vapor deposition of SiC/SiO₂ high emissivity thin film. *Appl. Surf. Sci.* **253**(9), 4361–4366 (2007). <https://doi.org/10.1016/j.apsusc.2006.09.063>
27. Purica, M.: Optical and structural investigation of ZnO thin films prepared by chemical vapor deposition (CVD). *Thin Solid Films* **403–404**, 485–488 (2002). [https://doi.org/10.1016/s0040-6090\(01\)01544-9](https://doi.org/10.1016/s0040-6090(01)01544-9)

28. Rosental, A., Tarre, A., Gerst, A., Sundqvist, J., Härsta, A., Aidla, A., Uustare, T.: Gas sensing properties of epitaxial SnO₂ thin films prepared by atomic layer deposition. *Sens. Actuators B. Chem.* **93**(1–3), 552–555 (2003). [https://doi.org/10.1016/s0925-4005\(03\)00236-3](https://doi.org/10.1016/s0925-4005(03)00236-3)
29. Lee, W.G., Woo, S.I., Kim, J.C., Choi, S.H., Oh, K.H.: Preparation and properties of amorphous TiO₂ thin films by plasma enhanced chemical vapor deposition. *Thin Solid Films* **237**(1–2), 105–111 (1994). [https://doi.org/10.1016/0040-6090\(94\)90245-3](https://doi.org/10.1016/0040-6090(94)90245-3)
30. Mahan, J.E., Vantomme, A., Langouche, G., Becker, J.P.: Semiconducting Mg₂Si thin films prepared by molecular-beam epitaxy. *Phys. Rev. B* **54**(23), 16965–16971 (1996). <https://doi.org/10.1103/physrevb.54.16965>
31. Suda, Y., Kawasaki, H., Ueda, T., Ohshima, T.: Preparation of high quality nitrogen doped TiO₂ thin film as a photocatalyst using a pulsed laser deposition method. *Thin Solid Films* **453–454**, 162–166 (2004). <https://doi.org/10.1016/j.tsf.2003.11.185>
32. Takeda, S., Suzuki, S., Odaka, H., Hosono, H.: Photocatalytic TiO₂ thin film deposited onto glass by DC magnetron sputtering. *Thin Solid Films* **392**(2), 338–344 (2001). [https://doi.org/10.1016/s0040-6090\(01\)01054-9](https://doi.org/10.1016/s0040-6090(01)01054-9)
33. Perednis, D., Gauckler, L.J.: Thin film deposition using spray pyrolysis. *J. Electroceram.* **14**(2), 103–111 (2005). <https://doi.org/10.1007/s10832-005-0870-x>
34. Singh, P., Kaushal, A., Kaur, D.: Mn-doped ZnO nanocrystalline thin films prepared by ultrasonic spray pyrolysis. *J. Alloy. Compd.* **471**(1–2), 11–15 (2009). <https://doi.org/10.1016/j.jallcom.2008.03.123>
35. Pal, B., Sharon, M.: Enhanced photocatalytic activity of highly porous ZnO thin films prepared by sol-gel process. *Mater. Chem. Phys.* **76**(1), 82–87 (2002). [https://doi.org/10.1016/s0254-0584\(01\)00514-4](https://doi.org/10.1016/s0254-0584(01)00514-4)
36. Ge, C., Xie, C., Cai, S.: Preparation and gas-sensing properties of Ce-doped ZnO thin-film sensors by dip-coating. *Mater. Sci. Eng., B* **137**(1–3), 53–58 (2007). <https://doi.org/10.1016/j.mseb.2006.10.006>
37. Chung, W.-Y., Sakai, G., Shimano, K., Miura, N., Lee, D.-D., Yamazoe, N.: Preparation of indium oxide thin film by spin-coating method and its gas-sensing properties. *Sens. Actuators B. Chem.* **46**(2), 139–145 (1998). [https://doi.org/10.1016/s0925-4005\(98\)00100-2](https://doi.org/10.1016/s0925-4005(98)00100-2)
38. Chinnamuthu, P., Mondal, A., Singh, N.K., Dhar, J.C., Das, S.K., Chattopadhyay, K.K.: Structural and optical properties of glancing angle deposited TiO₂ nanowires array. *J. Nanosci. Nanotechnol.* **12**, 1–4 (2012). <https://doi.org/10.1166/jnn.2012.6455>
39. Eagles, D.M.: Optical absorption and recombination radiation in semiconductors due to transitions between hydrogen-like acceptor impurity levels and the conduction band. *J. Phys. Chem. Solids* **16**(1–2), 76–83 (1960). [https://doi.org/10.1016/0022-3697\(60\)90075-5](https://doi.org/10.1016/0022-3697(60)90075-5)
40. Mondal, A., Shougajam, B., Goswami, T., Dhar, J.C., Singh, N.K., Choudhury, S., Chattopadhyay, K.K.: Structural and optical properties of glancing angle deposited In₂O₃ columnar arrays and Si/In₂O₃ photodetector. *Appl. Phys. A.* **115**(1) (2014). <https://doi.org/10.1007/s00339-013-7835-8>

Development of IDS Using Supervised Machine Learning



Indrajeet Kumar, Noor Mohd, Chandradeep Bhatt,
and Shashi Kumar Sharma

Abstract In the era of modern lifestyle, the internet and networking are essential things for everyone. With the help of these facilities everyone can exchange information between intranet and internet-connected people. During the information exchange, so many intermediate devices are involved, so that the security of information or data is a primary concern for each and every involved system. Attackers or intruders belong to inside the network or outside of the network. To detect an intruder or attacker an intrusion detection system (IDS) has been proposed for the detection of normal and attack data packets for a network. In this work, KDD-99 dataset is used for the development of IDS. A total set of 32,640 samples are considered, in which 12,440 samples of normal and 20,200 samples of attack class are used. These samples are further bifurcated into training and testing set in balanced manner. Thus, 16,320 samples (normal: 6220 and attack: 10,100) are used for training set and same number of set is used for the testing set. For the supervised learning, SVM and kNN classifiers are used to differentiate between normal data packets and attack data packets with PCA as dimensionality reduction. After the successful completion of experiments, it has been found that PCA-kNN yields maximum accuracy of 90.07% at pc value of 5 using cosine distance.

Keywords Intrusion detection system · Supervised learning · SVM classifier · kNN classifier · Principal component analysis

I. Kumar (✉) · C. Bhatt · S. K. Sharma
Graphic Era Hill University, Dehradun, Uttarakhand, India
e-mail: erindrajeet@gmail.com

C. Bhatt
e-mail: bhattchandradeep@gmail.com

S. K. Sharma
e-mail: 12sksharma@gmail.com

N. Mohd
Graphic Era Deemed to be University, Dehradun, Uttarakhand, India
e-mail: noormohdcs@gmail.com

Research scholar, GBPIET, Pauri Garhwal, Uttarakhand, India

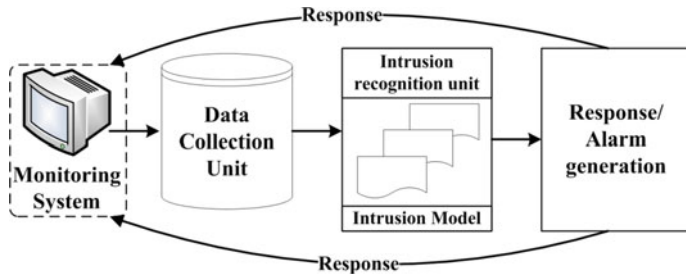


Fig. 1 IDS architecture

1 Introduction

The security and unauthorized accessed of data is still an open research area for the researchers. There are so many research communities working on this problem and so many systems had been already developed. Among them, Intrusion Detection System (IDS) is an authentic outcome of research development. It is a system used for monitoring traffic in the network and protecting the network from suspicious activity. It refers to as a tool, method, and software application used to find out the unauthorized network activities. It is typically a type of software installed around a system or network device that protects the overall network.

Intrusion Detection was initially introduced in the early 1980s succeeding the evolution of the internet with surveillance and monitoring. IDS was put in place as formal research when a technical report wrote by James Anderson for the U.S. Air force [1, 2]. Later on, Denning [3] focused on the implementation part of IDS and observed as major research recognition in 1987. Until the present day, it has been followed by many researchers. The basic building block and architecture of the IDS system is shown in Fig. 1.

2 Related Work

After the study of past research, it had been observed that IDS involve two broad categories on which researchers have worked named as signature-based and anomaly-based detection [4]. Signature-based IDS are also called as rule-based IDS, in which a set of predefined rules are used for differentiation between various attacks. If the behavior of the network activity is matched to any deviation from predefined rules, then it will be predicted as an attack. However, rule-based system is unable to detect new security attack or those attacks which have no predefined rules [5]. Therefore, the development of signature-based IDS is also suitable for the machine learning concept. In this research era, so many studies were performed and reported few major contributions.

Initially, an intrusion detection system is proposed by the author [6] that is capable of detecting known packet. This IDS model was based on the concept of genetic programming. It was effective against a variety of attacks such as a denial of services (DOS) and the unauthorized access. IDS used the variant of GP such as linear GP, multi-expression programming (MEP), and genetic expression (GEP). The proposed IDS model based on neural network is addressing the detection of anomaly-based attacks. A similar type of attack has been also explored in the study [7] and optimized results are reported. Further, a distributed intrusion detection system consists of multiple IDS over a big network with a centralized server that facilitates advanced network monitoring. The concept of fuzzy rule based IDS system was developed [8]. The fuzzy rule set IDS showed outstanding performance with respect to the existing IDS. Another important approach decentralized rule-based is used for the development of IDS is found in the study [9]. The proposed system is limited to detecting only routing-based attacks.

After the study of literature, it has been observed that the prediction of data packets or network traffic activity is a kind of problem that can be significantly solved by the concept of machine learning techniques. Therefore, authors attempt to design an IDS using k -means technique to detect if the network traffic is a type of attack or not. The proposed model used KDD Cup 1999 dataset for training and testing purposes. The author didn't use feature selection technique in the proposed work to select the prime attributes [10]. It has been also observed that PCA is used for selecting the prime attributes [11]. In this study, k -mean is used for the clustering to design IDS. The concept of machine learning for IDS development has been also explored in the studies [7, 12–16]. In these studies, SVM, Naive Bayesian, Decision Tree, Random Forest ANN, and neuro-fuzzy classifiers are used. The study reported in [7] shows the performance evaluation of IDS designed by classification techniques like ANN and SVM.

The study reported in [17] attempts to design an IDS using unsupervised learning which is capable of detecting unknown attacks. In this, Markov model is used, which learns the time-related changes. The proposed model was able to detect the changes and events with respect to time, so that any malicious activity can be recognized. It has been also found that the IDS had been designed for Big Data Environment [18]. In this work, the authors performed data preprocessing and normalization to figure out the improved IDS. Decision tree classifier is used and compared the performance of Naive Bayesian and kNN classifier based IDS. A similar type of work has been also done in the study [19], in which SVM multi-class classifier is used. For gaining higher accuracy, optimizations techniques like artificial bee colony, GA, and PCA are used [20].

It has been also found that the open-source software suite called "Weka" has been used to design IDS and evaluate the system [21]. In this work, artificial neural network classifier is used and observed the role of number of hidden layers. After the experiments, it has been concluded that the prediction rate varies with the number of hidden layers.

It has been also observed that the concept of deep learning is used for the development of IDS. In the study [22], authors have been developed an IDS using the

concept of deep learning. The proposed work applied LSTM architecture and RNN using the KDD Cup 1999 dataset. In this work, the size of hidden layers is varied and the outcome for accuracy and learning rate, author changing the size of the hidden layer. A similar type of concept has been also used in the study [23]. In this study, PCA-SVM is used and gives better results. This work is further extended with the help of deep learning model autoencoder. The work explained in the study [24] designed an IDS using RNN deep learning model noted as RNN-IDS.

In the present work, an IDS model is designed with the help of SVM and kNN classifier. Initially, a feature set of length 41 is used and passed to the SVM and kNN classifier. For SVM different kernel functions are used and optimum results are reported. Similarly, kNN classifier is used for the same feature vector length for different distance metrics. PCA-kNN classifier is used for different principal component and obtained results are reported.

3 Materials and Methods

The proposed model comprises of three sections such as (a) Network data packet collections, (b) intrusion detection engine, and (c) alert generation. The description of each section is given here.

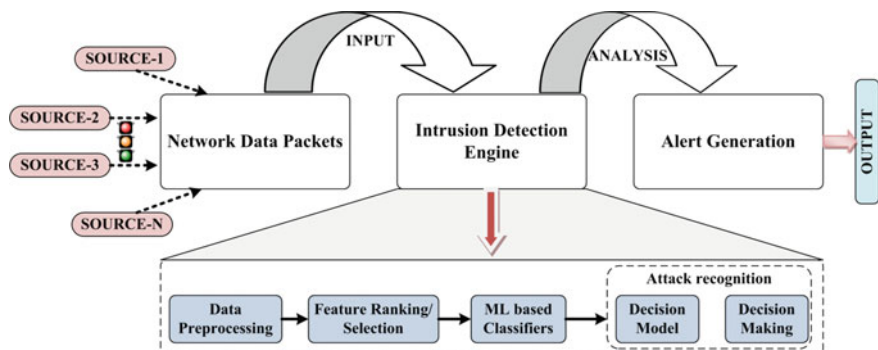
3.1 Network Data Packet Collection

This section is used for the dataset collection on which tedious experiments have been conducted. The used dataset for the proposed IDS model is taken from the KDD-99 dataset [25], which is comprised of 4 GB archived raw samples. The network traffic of DARPA net is monitored through *tcpdump* tool for seven weeks. The complete KDD dataset consist of seven million of samples [26]. Each sample is represented in the form of 41 attributes also called features. The brief summary of KDD dataset is given in Table 1.

From Table 1, it has been observed that KDD-99 dataset is consisting of 4,898,431 samples having 972,781 samples of normal class and 3,925,650 samples of attack class. It is also mentioned that the attack class is a combination of four types of attacks like DOS, R2L, U2R, and probing. In this experiment, a total set of 32,640 samples are considered, in which 12,440 samples of normal and 20,200 samples of attack class are used. These samples are further bifurcated into training and testing set in a balanced manner. Thus, 16,320 samples (normal: 6220 and attack: 10,100) are used for training set and the same number of the set is used for the testing set.

Table 1 Description of dataset

Type	No. of samples	Used samples	Dataset bifurcation	
			Training	Testing
Normal	972,781	12,440	6220	6220
Attack	3,925,650	20,200	10,100	10,100
Total	4,898,431	32,640	16,320	16,320

**Fig. 2** Development of ML-based IDS

3.2 *Intrusion Detection Engine*

Intrusion detection engine is the heart of any IDS, which is used to generate an alarm signal for input samples on the basis of their decision rules. This section is consisting of a set of rules or machine learning algorithms that are widely used for the development of any decision-making system. In this work, machine learning based classification techniques are used to design IDS. The structure of machine learning based IDS is shown in Fig. 2.

3.3 *Alert Generation*

This section is used for the alert signal generation. After the analysis of activities at the detection engine, an alarm signal is generated for the particular activity. According to the generated alarm signal required action has been taken. Thus, the activity is detected as normal activity or an attack. If the activity is detected as normal, then

their request has been further processed otherwise their request has been blocked. So that the designed system shall provide the required system security and attain the desired goal.

4 Experiments and Result Analysis

4.1 Experimental Work Flow

The working and experimental workflow diagram is given in Fig. 3.

From the experimental workflow diagram, it has been observed that the input samples for IDS development are taken from KDD-99 dataset. The input samples are raw data, so there is a need for normalization. In this work, *minmax* approach is used for normalization. Then normalized input feature set is bifurcated into training set and testing set. Training set is used to train the classifiers and trained model is tested by the testing set. The performance parameters overall classification accuracy, individual class accuracy, and misclassification accuracy are used for the evaluation of the proposed system.

The extracted attributes are passed to classifiers. In this work, two classifiers support vector machine (SVM) and *k*-nearest neighbor (kNN) classifiers are used [27–29]. For SVM, different kernel functions are explored with the help of same

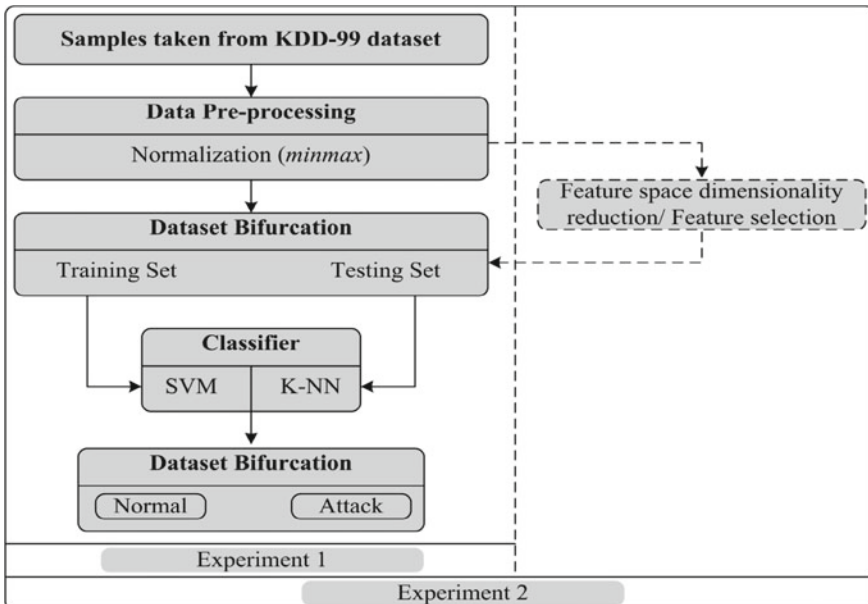


Fig. 3 Experimental workflow

Table 2 Brief description of experiments

Experiment No.	Description
<i>Experiment No. 1</i>	Development of an IDS using SVM classifier
	Development of an IDS using kNN classifier
<i>Experiment No. 2</i>	Development of an IDS using PCA-SVM classifier
	Development of an IDS using PCA-kNN classifier

training and testing dataset. Similarly, kNN classifiers have been explored with different distance measuring parameters. The performances of each case are reported in the results section.

It has been also noticed that some of the features are redundant and not relevant to the detection task. Therefore, principal component analysis (PCA) is used for dimensionality reduction [30]. In this work, the value of principal component (pc) is varied from 1 to 15 and the outcomes of each experiment are reported in the results section.

In this work, two exhaustive experiments have been performed. The brief description of the experiments is given in Table 2.

Experiment No. 1.1: In this experiment, a feature set of length 41 is used for development of an IDS using SVM classifier. For SVM classifier, different kernel functions are used in the experiments and obtained results are given in Table 3.

Experiment No. 1.2: In this experiment, a feature set of length 41 is used for the development of an IDS using kNN classifier. For kNN classifier, different distance measuring methods are evolved for the value of $k = 1, \dots, 10$ in the experiment and obtained results are given in Table 4.

Table 3 Results of different kernel function for SVM classifier

Sr. no.	Kernel function	CM			Indiv. Acc. (%)	Accuracy (%)	Miss. Acc. (%)
			Attack	Normal			
1.	mlp	Attack	7512	2588	74.37	81.01	18.99
		Normal	510	5710	91.80		
2.	rbf	Attack	8049	2051	79.69	86.88	13.12
		Normal	90	6130	98.55		
3.	Linear	Attack	7742	2358	76.65	83.77	16.23
		Normal	290	5930	95.33		
4.	Quadratic	Attack	2598	7502	25.72	19.05	80.95
		Normal	5708	512	08.23		

Note mlp: multilayer perceptron, rbf: Gaussian Radial Basis Function, CM: confusion matrix, Indiv. Acc.: individual class classification accuracy, Miss. Acc.: misclassification accuracy

Table 4 Results of different distance methods using kNN classifier

Sr. No.	Value of k	Distance	CM			Indiv. Acc. (%)	Accuracy (%)	Miss. Acc. (%)
				Attack	Normal			
1.	$k = 1$	Cosine	Attack	8149	1951	80.68	87.24	12.76
			Normal	130	6090	97.90		
2.	$k = 1$	Euclidean	Attack	8049	2051	79.69	86.17	13.83
			Normal	115	6105	98.15		
3.	$k = 5$	Cityblock	Attack	7149	2951	70.78	79.89	20.11
			Normal	330	5890	94.69		
4.	$k = 1$	Correlation	Attack	7760	2340	76.80	83.75	16.25
			Normal	312	5908	95.33		

Experiment No. 2: In this experiment, PCA is used for dimensionality reduction. The reduced feature set is further bifurcated into training set and testing set. To get the optimum number of principle components, extensive work has been performed by varying the value of $p = '1, 2, \dots, 15'$. Then the selected feature set is used for training the model. In this experiment, SVM with PCA (PCA-SVM) and kNN with PCA (PCA-kNN) are used to develop an IDS system.

Experiment No. 2.1: In this experiment, an IDS is designed using PCA-SVM classifier. The results of each experiment are given in Table 5.

Experiment No. 2.2: In this experiment, an IDS is designed using PCA-kNN classifier. The results of each experiment are given in Table 6.

Table 5 Results of different kernel function for PCA-SVM classifier

Sr. no.	Kernel function	p	CM			Indiv. Acc. (%)	Accuracy (%)	Miss. Acc. (%)
				Attack	Normal			
1.	mlp	15	Attack	8349	1751	82.66	88.71	11.29
			Normal	90	6130	98.55		
2.	rbf	5	Attack	8452	1648	83.68	89.46	10.54
			Normal	72	6148	98.84		
3.	Linear	9	Attack	8049	2051	79.69	85.41	14.59
			Normal	330	5890	94.69		
4.	Quadratic	5	Attack	8149	1951	80.68	87.24	12.76
			Normal	130	6090	97.90		

Bold indicates highest accuracy

Table 6 Results of different distance methods using kNN classifier

Sr. No.	Value of k	Distance	p	CM	Attack	Normal	Indiv. Acc. (%)	Accuracy (%)	Miss. Acc. (%)
1.	$k = 6$	Cosine	5	Attack	8540	1560	84.55	90.07	9.93
				Normal	60	6160	99.03		
2.	$k = 7$	Euclidean	15	Attack	8149	1951	80.68	87.24	12.76
				Normal	130	6090	97.90		
3.	$k = 3$	Cityblock	5	Attack	8100	2000	80.19	85.72	14.28
				Normal	330	5890	94.69		
4.	$k = 3$	Correlation	5	Attack	7149	2951	70.78	81.30	18.70
				Normal	100	6120	98.39		

4.2 Result Analysis

After the extensive experimentations, the following major observations have been pointed as:

1. There are two experiments that have been performed with the help of SVM and kNN classifiers. One experiment has been performed on the entire feature vector of length 41, and second experiment has been performed using PCA as feature vector dimensionality reduction and SVM, kNN as classifier so PCA-SVM and PCA-kNN are used.
2. From Table 3, it has been found that the maximum prediction rate or classification accuracy is 86.88% using SVM classifier with *rbf* function. The individual class classification accuracy for normal and attack is 98.55% and 79.69%, respectively. The same dataset has been tested on kNN classifier (results are reported in Table 4) and observed that the maximum prediction accuracy is 87.24% for the value of ' $k = 1$ '. In this exercise, the feature vector length is 41. Among these features, some features are redundant and not relevant for the classification task, so PCA is applied to reduce the dimensionality of feature vector. And the results are put in Tables 5 and 6.
3. From Table 5, it has been found that the highest prediction rate between normal and attacks is 89.46% for *rbf* kernel function using PCA-SVM classifier at the value of ' $p = 5$ '. The prediction rate for normal and attacks is 98.84% and 83.68%, respectively.
4. The same set of testing samples is passed through PCA-kNN classifier and obtained results are reported in Table 6. It has been observed that the maximum classification rate is 90.07% for ' $p = 5$ ' and ' $k = 6$ '. The individual class classification accuracy is 84.55 and 99.03% for normal and attack detection, respectively.

4.3 Comparative Analysis

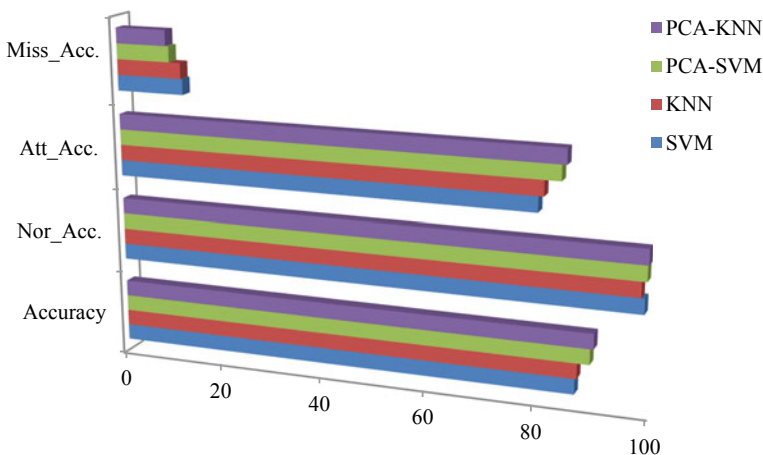
The developed IDS is compared with the study performed in [24]. It has been found that the accuracy reported for normal and attack discriminations is 83.28% but in the proposed system the achieved accuracy is 90.07%. The summary of results is given in Table 7.

The graphical representation of the obtained results is shown in Fig. 4.

Table 7 Comparative analysis of results obtained from different experiments

Sr. No.	Classifier	Accuracy	Nor_Acc.	Att_Acc.	Miss_Acc.
1	SVM	86.88	98.55	79.69	13.12
2	kNN	87.24	97.9	80.68	12.76
3	PCA-SVM	89.46	98.84	83.68	10.54
4	PCA-kNN	90.07	99.03	84.55	9.93

Note Nor_Acc.: individual class classification accuracy for normal, Att_Acc.: individual class classification accuracy for attack
Bold indicates highest accuracy

**Fig. 4** Comparative analysis for outcome of tedious experiments

5 Conclusion

Intrusion detection system is a tool that monitors the network traffic and generates an alarm if any malicious activity occurred. The development of IDS is either signature-based or anomaly-based. The development of signature-based IDS is rule-based techniques, so this kind of tool can be also developed with the help of supervised machine learning based techniques. Thus, the authors have made an attempt to develop an IDS system using SVM and kNN classifiers. For this task, a benchmark dataset KDD-99 is used which comprised of 4,898,431 raw samples. Among the huge set of samples, a total set of 32,640 samples is considered. The used set is further bifurcated as training and testing set in balanced manner so that the training set consists of 16,320 samples and testing set consist of 16,320 samples.

After the experiments carried out for the development of IDS using supervised learning the obtained maximum accuracy for feature vector length of 41 is 87.24% with the help of kNN classifier. The PCA is used for the feature vector dimensionality

reduction and the obtained best-case accuracy is 90.07% using PCA-kNN classifier. Thus, it has been concluded that the PCA-kNN classifier performs better for IDS development. It is also worth mentioning that this work has been further extended to design IDS for a complete KDD-99 dataset using some advance machine learning techniques.

References

1. Endorf, C., Schultz, E., Mellander, J.: *Intrusion Detection & Prevention*. McGraw-Hill, Osborne Media (2004). ISBN: 0072229543
2. Anderson, J.P.: Computer security threat monitoring and surveillance. In: James, P. (eds) Technical Report. Anderson Company (1980)
3. Denning, D.E.: An intrusion-detection model. *IEEE Trans. Softw. Eng.* **2**, 222–232 (1987)
4. Verwoerd, T., Hunt, R.: Intrusion detection techniques and approaches. *Comput. Commun.* **25**(15), 1356–1365 (2002)
5. Khan, S., Loo, J., Din, U.Z.: Framework for intrusion detection in IEEE 802.11 wireless mesh networks. *Int. Arab J. Inf. Technol.* **7**(4), 435–440 (2017)
6. Abraham, A., Grosan, C., Martin-Vide, C.: Evolutionary design of intrusion detection programs. *IJ Netw. Secur.* **4**(3), 328–339 (2007)
7. Tiwari, A., Ojha, S.K.: Design and analysis of intrusion detection system via neural Network, SVM, and neuro-fuzzy. In: *Emerging Technologies in Data Mining and Information Security*, pp. 49–63. Springer, Singapore (2019)
8. Abraham, A., Jain, R., Thomas, J., Han, S.Y.: D-SCIDS: distributed soft computing intrusion detection system. *J. Netw. Comput. Appl.* **30**(1), 81–98 (2007)
9. Roman, R., Zhou, J., Lopez, J.: Applying intrusion detection systems to wireless sensor networks. In: *IEEE Consumer Communications & Networking Conference (CCNC 2006)* (2006)
10. Karataş, F., Korkmaz, S.A.: Big data: controlling fraud by using machine learning libraries on spark. *Int. J. Appl. Math. Electron. Comput.* **6**(1), 1–5 (2018)
11. Peng, K., Leung, V.C., Huang, Q.: Clustering approach based on mini batch K-means for intrusion detection system over big data. *IEEE Access* (2018)
12. Anuar, N.B., Sallehudin, H., Gani, A., Zakaria, O.: Identifying false alarm for network intrusion detection system using hybrid data mining and decision tree. *Malaysian J. Comput. Sci.* **21**(2), 101–115 (2008)
13. Golovko, V., Kochurko, P.: Intrusion recognition using neural networks. In: *2005 IEEE Intelligent Data Acquisition and Advanced Computing Systems: Technology and Applications*, pp. 108–111. IEEE (2005)
14. Tian, S., Yu, J., Yin, C.: Anomaly detection using support vector machines. In: *International Symposium on Neural Networks*, pp. 592–597. Springer, Berlin (2004)
15. Chen, W.H., Hsu, S.H., Shen, H.P.: Application of SVM and ANN for intrusion detection. *Comput. Oper. Res.* **32**(10), 2617–2634 (2005)
16. Belouch, M., El Hadaj, S., Idhammad, M.: Performance evaluation of intrusion detection based on machine learning using Apache Spark. *Proc. Comput. Sci.* **1**(127), 1–6 (2018)
17. Li, Y., Parker, L.E.: Intruder detection using a wireless sensor network with an intelligent mobile robot response. In: *IEEE Southeast Con 2008*, pp. 37–42. IEEE
18. Peng, K., Leung, V., Zheng, L., Wang, S., Huang, C., Lin, T.: Intrusion detection system based on decision tree over big data in fog environment. *Wirel. Commun. Mobile Comput* (2018)
19. Ye, K.: Key feature recognition algorithm of network intrusion signal based on neural network and support vector machine. *Symmetry* **11**(3), 380 (2019)

20. Kalaivani, S., Vikram, A., Gopinath, G.: An effective swarm optimization based intrusion detection classifier system for cloud computing. In: 2019 5th International Conference on Advanced Computing & Communication Systems (ICACCS), pp. 185–188. IEEE (2019)
21. Taher, K.A., Jisan, B.M., Rahman, M.M.: Network intrusion detection using supervised machine learning technique with feature selection. In: 2019 International Conference on Robotics, Electrical and Signal Processing Techniques (ICREST), pp. 643–646. IEEE (2019)
22. Kim, J., Kim, J., Thu, H.L., Kim, H.: Long short term memory recurrent neural network classifier for intrusion detection. In: 2016 International Conference on Platform Technology and Service (PlatCon), pp. 1–5. IEEE (2016)
23. Al-Qatf, M., Lasheng, Y., Al-Habib, M., Al-Sabahi, K.: Deep learning approach combining sparse autoencoder with SVM for network intrusion detection. *IEEE Access* **12**(6), 52843–52856 (2018)
24. Yin, C., Zhu, Y., Fei, J., He, X.: A deep learning approach for intrusion detection using recurrent neural networks. *IEEE Access* **12**(5), 21954–21961 (2017)
25. Bay, S.D., Kibler, D.F., Pazzani, M.J., Smyth, P.: The UCI KDD archive of large data sets for data mining research and experimentation. *SIGKDD Explor.* **2**(2), 81–85 (2000)
26. Cup, K.D.: Dataset, p. 72. Available at the following website <http://kdd.ics.uci.edu/databases/kddcup99/kddcup99.html> (1999)
27. Kumar, I., Virmani, J., Bhaduria, H.S., Panda, M.K.: Classification of breast density patterns using PNN, NFC, and SVM classifiers. In: Soft Computing Based Medical Image Analysis, pp. 223–243. Academic Press (2018)
28. Kumar, I., Bhaduria, H.S., Virmani, J.: Wavelet packet texture descriptors based four-class BIRADS breast tissue density classification. *Proc. Comput. Sci.* **1**(70), 76–84 (2015)
29. Kumar, I., Bhaduria, H.S., Virmani, J., Thakur, S.: A hybrid hierarchical framework for classification of breast density using digitized film screen mammograms. *Multimedia Tools Appl.* **76**(18), 18789–18813 (2017)
30. Kumar, I., Virmani, J., Bhaduria, H.S., Thakur, S.: A breast tissue characterization framework using PCA and weighted score fusion of neural network classifiers. *Classification Tech. Med. Image Anal. Comput. Aided Diag.* **12**, 129 (2019)

Automated Traffic Light Signal Violation Detection System Using Convolutional Neural Network



Bhavya Bordia, N. Nishanth, Shaswat Patel, M. Anand Kumar, and Bhawana Rudra

Abstract Automated traffic light violation detection system relies on the detection of traffic light color from the video captured with the CCTV camera, detection of the white safety line before the traffic signal and vehicles. Detection of the vehicles crossing traffic signals is generally done with the help of sensors which get triggered when the traffic signal turns red or yellow. Sometimes, these sensors get triggered even when the person crosses the line or some animal crossover or because of some bad weather that gives false results. In this paper, we present a software which will work on image processing and convolutional neural network to detect the traffic signals, vehicles and the white safety line present in front of the traffic signals. We present an efficient way to detect the white safety line in this paper combined with the detection of traffic lights trained on the Bosch dataset and vehicle detection using the TensorFlow object detection SSD model.

Keywords Convolutional neural networks · Object detection · TensorFlow · Traffic light detection

1 Introduction

The increase in number of vehicles and the ignorant driving of the drivers in big cities are a severe concern. Due to this, the number of accidents has increased. The aim of the development of this system is to reduce the violation of the traffic rules and reduce the road accidents that occur, and mostly the pedestrians are victimized.

B. Bordia (✉) · N. Nishanth · S. Patel · M. Anand Kumar · B. Rudra

Department of Information Technology, National Institute of Technology Surathkal, Surathkal, Karnataka 575025, India

e-mail: bhavyabordia@gmail.com

M. Anand Kumar

e-mail: m_anandkumar@nitk.edu.in

B. Rudra

e-mail: bhawanarudra@nitk.edu.in

This application will minimize the effort of traffic police and keep the roads traffic-free and accident-free. The system will automatically detect the safety line crossing violation by the vehicles on the traffic signal and will store the frames vehicles crossing lines when the traffic light is yellow or red. As most of the people today are in hurry and violate the rules at the signal and cross the safety line even when the signal is changing from yellow to green or changing from yellow to red, this leads to many road accidents. There have been approaches to track the violation of the traffic rules like installation of the CCTV cameras at the traffic signal or in front of some shop near signal, but even after installation this requires manual working to detect the vehicles which are violating the rules. Most of the metro cities in India are using CCTV cameras for surveillance and are monitored manually by persons. In Bengaluru, the traffic police had installed around 170 CCTVs [1]. The command center at the Bruhat Bengaluru Mahanagara Palike, the city municipality, has another 731 cameras, while other public and corporate bodies have set up 400 cameras across the city, said by the law enforcement authorities [1]. The state cabinet of Mumbai approved installing 5625 more CCTV cameras to cover slums, arterial roads, bylanes and the Mumbai coast [2]. In October 2016, the Mumbai police had installed 4717 CCTV cameras on 2293 poles at 1510 locations on main roads and traffic junctions. With the installation of additional CCTV cameras, the city will be covered by 10,342 high-tech cameras [2].

In Delhi, 96 cameras will be installed at 24 intra-sections for monitoring red light violations under the 3D radar-based red light violation detection camera (RLVD) project [3]. The surveillance requires human interaction to find the law breaker. We propose an automated system which will detect the rule breakers on the traffic signal when the traffic light is red or yellow. The remaining part of the paper is as follows: In Sect. 2, work done so far is in the field of traffic rules violation. In Sect. 3, we propose our methodology along with the testing results. In Sect. 4, we proposed a combined system for the working of the prototype with the results followed by a conclusion.

2 Literature Survey

As per the statistics of the year 2017, 464,910 road accidents were reported, in which 147,913 lives losses were claimed and 470,975 persons were injured [4]. The highest number of road accidents was reported in Tamil Nadu, whereas the highest number of people who were killed in road accidents was reported in Uttar Pradesh [4]. Also there were some states like Maharashtra, Gujarat and West Bengal which achieved reduction in road accidents and injuries [4]. In some states like Bihar and Uttar Pradesh, there was a significant increase in the number of road accidents compared to 2016 [4]. These road accidents were mainly caused due to the traffic rules violations. In order to minimize the road accidents rate, government has come up with the interesting ideas on how the violations can be detected.

Previously, there were many different approaches proposed for the detection of the traffic lights, the vehicle detection and to detect traffic rules violation. The method of detection of the color of traffic light may have less accuracy since there can be factors like fading red light or dim red light as proposed by Pasit Wonghabut, Jetsada Kumphong, Rujchai Ung-arunyawee, Watis Leelapatra and Thaned Satiennam [5]. HSV (Hue, Saturation, Value) software technique was used to detect the red color light [5]. The color was stable in light condition in HSV system. The reason behind that was when the images are bright, only the brightness value changes not the color intensity and the color value. The system would trigger to check for violation if the color is red [5]. A video-based traffic light violation detection system was proposed which used background difference method to determine approximate speed of the vehicle and the speeding violation [6]. First, the background from the image is saved, and then each frame was being checked with respect to the background. Using dynamic tracking, the violations are detected. To detect the red light runners, a radar trajectory data approach was proposed [7, 8]. The aim of the approach was to maximize the green light period and to minimize the number of red light runners and to reduce the number of vehicles caught in the dilemma zone. Dilemma zone is the time at which the traffic light changes from green to yellow. The driver has to make a decision of either stopping or moving ahead. To detect the red light, a direct connection of traffic signals from the traffic signal box was proposed to use. The accuracy of detecting the signals increased significantly as the signals were taken from the signal box [8]. To detect the violation, other hardware devices like laser-based motion detection devices, traffic light queue control system and inductive loop were proposed [8].

Most of the accidents on roads happened because of driving in the wrong lane, illegal overtaking and dangerous lane changing. Police eyes was implemented in Thailand to deal with the above problems. The system with the use of image processing and computer vision detected the illegal crossing of lanes [9]. The obtained images will have background subtracted, followed by shadow detection and blob detection. The intersection between the detected blobs and the marker solid lines will trigger a violation alarm [9]. A complete system comprising tracker, classifier and traffic light detector was implemented in order to bring down violations at the traffic signals. The whole system was based on the technique of deep learning, vehicle odometry and stereo vision which perceives traffic lights in real time. They used the YOLO architecture for the detection of the lights and contributed the making of the largest dataset Bosch small traffic light dataset [10]. Vehicular ad hoc networks (VANET) is a new technology which allows an ad hoc network to be formed by the vehicles on the road enabling them in easy exchange of safety-related information [11]. Vehicle-to-vehicle (V2V) or vehicular ad hoc networks (VANETs) are the name given to the direct communication between vehicles using an ad hoc network. Thus, in this network, vehicles are equipped with wireless transceiver and controller allowing them to connect with the surrounding one [11]. Another method was implemented by R. Shreyas, B.b. Pradeep Kumar and their colleagues, which assists the traffic violation detection systems. When the violation is detected, the system detects the vehicle number and sends a SMS to the owner of the vehicle [12]. They used the

automated number plate detection (ANPR) algorithm for the detection of the number on plate. Using the proposed method to extract the vehicle number, the number is then given to GSM modem for further SMS feedback [13].

Our contribution toward the cause of traffic light violation detection is to detect the vehicles violating the rules at the traffic signals as most of the people ignore the traffic signals and move forward on their way, and this had led to many accidents in past. We will capture the image of the vehicle violating the rule, and this image would be used by the officials to take the action. Our work will help the traffic police to decrease the number of incidents of breaking of traffic signals and would help them to track for further process.

3 Proposed Methodology

The development of the system is divided into four phases: first the traffic light detection, second is the white traffic line detection on the traffic signals, third is the vehicle detection, and the fourth phase is the integration of all the modules and detecting the crossover.

Traffic Light Detection: For detection of traffic light, we have two main tasks: find the position of traffic light in the extracted image, identify the color of the signal detected. The detection of the traffic light is done using the Tensor Flow Object Detection and the color of the traffic light is being detected using faster R-CNN, as explained in the next section.

Traffic Line Detection: To detect the traffic line, frames from the video extracted from camera will be converted into a grayscale image, and apply algorithm based on Canny edge detector and Hough transform, as explained in the next section.

Vehicle Detection and checking for the intersection of the vehicle with traffic line: For the vehicle detection, we use the TensorFlow object detection API to detect the vehicles. Then, the coordinates of the traffic line are analyzed with that of the coordinates of the car, and if there is an intersection of these coordinates, then there is a violation of traffic rule, as explained in the next section.

The system requires the use of two cameras—one facing the traffic signal to detect traffic light and the other facing the traffic in order to detect vehicles and the line. First, the color of traffic light is being detected, and in parallel the system fetches the video from the other CCTV cameras and then it detects the traffic line along with vehicles. Based on the output, it will classify which vehicles are crossing the traffic line. An image of the instance is saved at the moment when someone violating the rules is detected, and the signal would be sent to the authority about the violation.

3.1 Traffic Line Detection

Traffic line refers to the white safety line behind the zebra crossing. This module will be used to detect that line. The detection of the line will have following steps: extract frames from the video recorded from the camera which is placed facing the traffic, convert the image to a grayscale image, check for all the occurrences of line in the image, consider the longest line detected and extend the particular line as a reference.

Grayscale Conversion Conversion from RGB to grayscale is done to remove the color from the image as our main target is to detect the white line. So, the grayscale image will be free from the color noise containing white and black pixels only. This will make the computation easier and will decrease the complexity of the code. Another reason to use grayscale image is that it is faster to process and easy to visualize.

Canny Edge Detection It is an edge detection algorithm proposed by John F. Canny. It involves the following steps: noise reduction, gradient, non-maximum suppression and thresholding.

Noise reduction: To detect the edges, noise should be removed. In order to remove the noise, Gaussian filter is used. The size of filter used is 5×5 .

Intensity gradient: To get the first derivative in horizontal and vertical direction, the smoothed image is filtered with a kernel in both horizontal and vertical directions. Sobel kernel was used as the filter. From the images obtained, edge gradient and direction for each pixel could be found out as follows:

$$D = \sqrt{D_x^2 + D_y^2} \quad (1)$$

$$\text{Angle}(\theta) = \tan^{-1}(D_y/D_x) \quad (2)$$

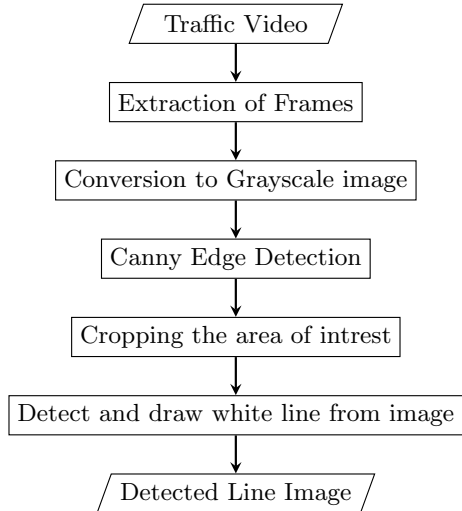
The direction of the gradient is always perpendicular to the edges. The direction is then rounded to one of four angles, i.e., horizontal, vertical or the two diagonals one.

Non-maximum suppression: To remove the unwanted pixels from the image, a full scan of the image is done after getting gradient magnitude and direction. For that, each pixel is checked whether it is a local maximum in its neighborhood direction or the gradient or not (Fig. 1).

Hysteresis thresholding: After the non-maximum suppression, real edges have to be differentiated with all the edges point that we got. For differentiating, two threshold values are used: minimum value and maximum value. The edges with intensity gradient lesser than the minimum value are discarded, whereas greater than the maximum value are considered as edges. Those intensity gradients which lies in between minimum value and maximum value are classified edges or non-edges based on connectivity. If those pixels are connected to the real edges, then those pixels are also part of real edges.

Region of Interest We know that image from the camera will contain different objects like vehicles, people and other things, we can term them to be noise as they

Fig. 1 Flow diagram for white safety line detection



are not helpful in detecting white line, and it would be very large to process these at a time. So, it is better to crop the image to our region of interest. In our case, the traffic camera position will be at the traffic light directly facing the line so the half containing the line in the image is our region of interest, i.e., the half closed to viewing in the image, and it is best to use that part only. Thus, for our model, we have done the cropping of image with the dimension of $(0, \text{height}/2)$ and $(0, \text{width}/2)$.

Detection and Drawing of White Line For the detection of lines in the cropped image, we first applied Hough transformation and then used the result with our algorithm to get the white line. If the shape could be presented in the mathematical form, Hough transformation is used to detect any arbitrary shape. Even if the shape is broken or distorted a little, it could be detected [14]. To detect the straight lines, we have used Hough transformation. To use Hough transform, edge detection should be done in the image. Here, we had used the Canny edge detector to do the preprocessing as explained above. As we know, line in the image space can be represented in both the Cartesian form and the polar form. In the Cartesian form, the general equation is

$$y = mx + c \quad (3)$$

where (m, c) are the parameters, whereas in the polar form

$$r = x\cos(\theta) + y\sin(\theta) \quad (4)$$

where r and θ are the parameters in the image space. Any line in the image space of Hough transformation can be represented by r and θ . Hough transform creates 2D array for the value of r and θ and sets the values in the array to 0 initially. Let r denote the number of rows and θ denote the number of columns. The size of the array is

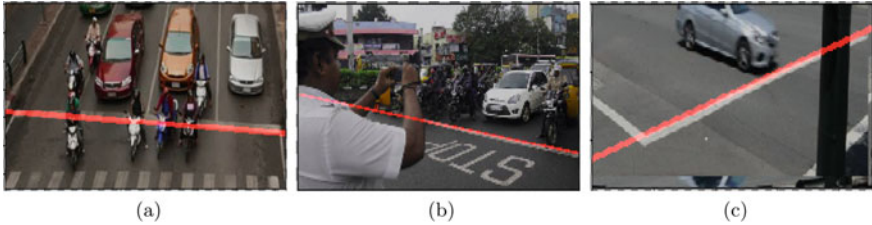


Fig. 2 White safety line detection

dependent on the accuracy you need. Hough transform uses the voting principle to select the value of r and θ , i.e., for each and every value of x and y known on line, it calculates the value of r and θ and the one value which has maximum number of votes is chosen as the correct value of r and θ .

After all the preprocessing of the image with grayscale conversion, Canny edge, region of interest and Hough transformation, the final step consists of the detection of the white line. So from all the lines which we have obtained from the Hough lines transform, select the line with the maximum Euclidean distance. The reason for selecting the line with maximum Euclidean distance is whenever you see the image of the traffic signal standing behind the line, the line is the longest line among all in the picture detected by the Hough lines. After the detection of the longest line, the next step comes is to extra plot the lines this is because most of the times the lines which are drawn on roads the longest line detected in the image will also not cover the whole lane because of the noise present in the image. So using the line equation, we detect the line:

$$y - y_1 = m(x - x_1) \quad (5)$$

$$m = (y_2 - y_1)/(x_2 - x_1) \quad (6)$$

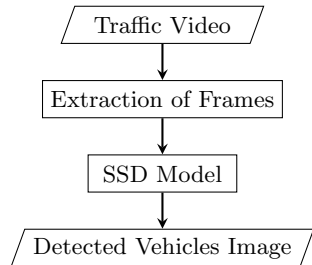
After seeing the coordinates of the end points of the longest line obtained, we check the orientation of the line whether it is a horizontal line or the vertical line or the line with positive slope or the line with the negative slope. After identifying the orientation of the line, we use the specific coordinates of the line 0, width, height in place of x_1, y_1, x_2, y_2 according to the specific condition satisfying the above cases. This gives the end coordinates of the line which crosses the image thoroughly in order to draw the line.

Figure 2 shows some examples of the line detection.

3.2 Vehicle Detection

This module detects the vehicles present in the image. This is being done with the help of Single Shot Multi-box Detector model with MobileNet as the base network

Fig. 3 Flow diagram for vehicle detection



layer to detect and classify vehicles. The reason of using SSD is that multiple objects within the image will get detected in just one single shot. Whereas regional proposal network (RPN)-based approaches such as R-CNN series require two shots: one for generating region proposals and one for detecting the object of each proposal [15].

In the SSD approach, the final detections are produced after the non-maximum suppression of the fixed-size collection of bounding boxes and scores for the presence of object class instances are obtained from the feedforward convolutional network.

The idea is to use single network (for speed), and there is no need of region proposals instead it uses different bounding boxes and then adjusts the bounding box as part of the prediction. Different bounding box predictions are achieved by each of the last few layers of the network responsible for predictions for progressively smaller bounding box, and final prediction is the union of all these predictions.

The image after going through the convolutions of feature extraction, a feature layer of $m \times n$ number of locations with p channels is obtained, and then a 3×3 convolution is applied on $m \times n \times p$ feature layer. For each location, k bounding boxes are obtained which are of different sizes and different aspect ratios are obtained and saved to be used later for the detection of vehicles crossing. For each box, c classes scores are calculated and later used for classification as shown in Fig. 3.

We detected the vehicles with the use of SSD MobileNet which is trained on the COCO dataset. We use the model to detect the vehicles like car, motorcycles, buses and trucks. The output would be in the form of boxes depicting the vehicles in the images, and the coordinates of the object detected are saved from the result. Outputs of the module for some static images have been shown in Fig. 4.

3.3 Traffic Light Detection

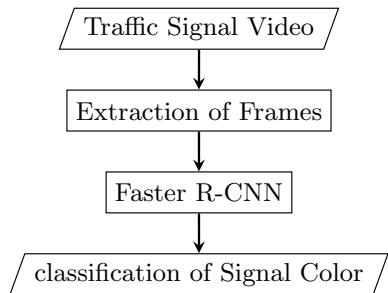
This module is used for detecting the traffic light and the color (i.e., red, yellow or green). The work is divided into two parts: detection of the traffic signal and the other one is the identification of the color of the signal. We are using faster R-CNN model for the detection and classification of traffic lights (Fig. 5).

For the purpose of object detection, faster R-CNN is used which is a computer vision toolkit based on TensorFlow. It is different from fast R-CNN and CNN model



Fig. 4 Results of vehicle detection

Fig. 5 Flow diagram for traffic light detection



in the way that it has a separate network which is used to predict the proposed regions, whereas in them selective search algorithm is used for the region proposals.

It starts with an image to extract the following information

- A list of bounding boxes of traffic signals present.
- Assign label to bounding box.
- Getting probability of each label and box

To find up to a predefined number of regions(bounding boxes) which may contain objects, region proposal network is used over the features extracted from CNN.

Using the extracted features and the bounding boxes with the relevant objects, we can extract new features by applying region of interest pooling and store them in new tensor. Finally, the new tensors obtained are used to classify the content in the bounding box using the label or discarding it if it has no label and thus adjusting the bounding box coordinates such that it fits the object.

Faster R-CNN model is used to identify traffic signals boundary using the COCO dataset [16]. We trained the model to identify the color of traffic light using the Bosch small traffic train RGB dataset [10, 17]. The dataset comprises the following:

- No. of images = 5093 and No. of annotated traffic lights = 10,756
- 15 different labels
- Median traffic lights width: 8.6 pixels
- Lights which are partially occluded = 170

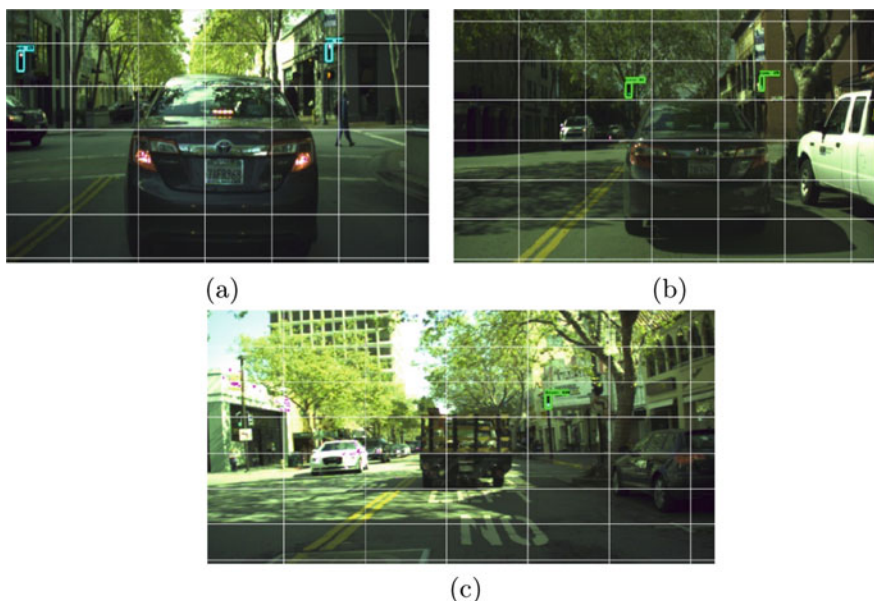


Fig. 6 Traffic light detection

The model is tested on Bosch small traffic test RGB dataset which comprises as follows:

- No. of consecutive images = 8334 and No. of annotated traffic light = 13,486
 - Median traffic lights width: 8.5 pixels
 - Lights which are partially occluded = 2088

Results of some static images have been shown below (Fig. 6).

The model was trained and tested for different number of epochs like 10 K, 20 K, 40 K and 60 K. The training was done on the Google Colab GPU server. The results of each testing phase are summarized in Table 1.

We stopped training the model at 60,000 epochs and got an accuracy of 74.14 %.

Table 1 Results of traffic signal light detection

Number of epochs	Accuracy (%)
10,000	0.024
20,000	5.48
40,000	70.36
60,000	74.14

3.4 Detection of Vehicle Crossing

The working of the proposed model requires two camera—one for the detection and classification of the traffic light which will be facing the traffic signal, and other will be facing the traffic and the work of it would be classify the vehicles and the white safety line present on the signal. The white safety line detection and the vehicle detection modules are combined together in such a way that they can detect the vehicles crossing the lines when the signal turns yellow or red and then captures the frame from the video which will be used later by the security agency to take the necessary action as demonstrated in Fig. 7.

The line detection module and the vehicle detection module could be combined together to process the frame at the same time. We first take the frame and apply the line detection algorithm explained above and store the coordinates of the line obtained from the module, and then we take the same frame to apply the vehicle detection model and store the coordinates of the vehicles detected from the frame.

From the line detection module, we are getting the end points of the line as (x_1, y_1) as p and (x_2, y_2) as q, whereas from the vehicle detection module we will be getting the coordinates of the diagonal of the rectangular box, let them be d_1 and d_2 . If the vehicles are crossing the line, this means that the orientation of the point d_1 and d_2

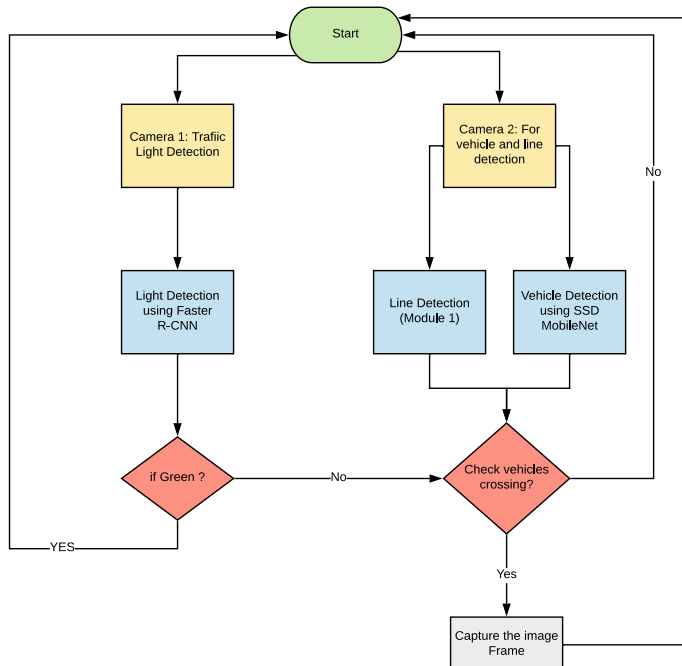


Fig. 7 Structure and flow of application

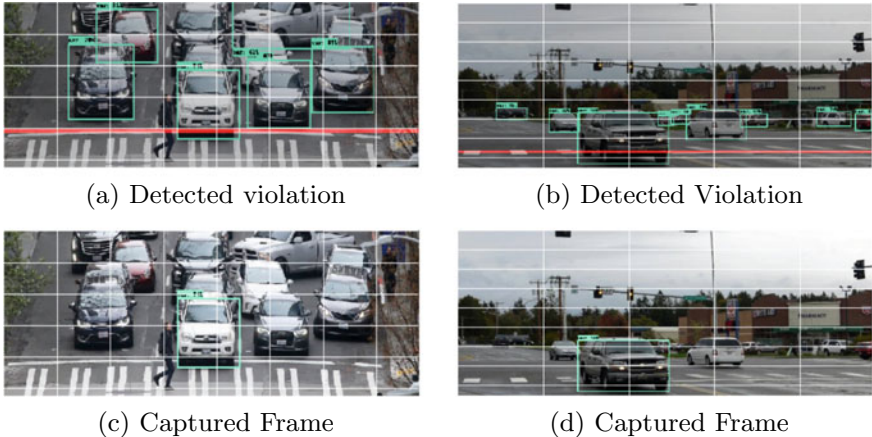


Fig. 8 Violation detection

with respect to the points p and q would be different. The orientation of an ordered triplet in a plane could be clockwise, counterclockwise or collinear. If the points (p, q, d_1) and the points (p, q, d_2) have different orientations as shown in Fig. 8, d_1 has counterclockwise orientation, whereas d_2 has clockwise orientation with respect to p and q , then the vehicle is crossing the line and the image of it is saved.

Mathematically, put the coordinates of the points d_1 and d_2 in the equation of the line formed by the point p and q . Consider the equation of the line formed by the points p and q

$$ax + by + c = 0 \quad (7)$$

Let us take the coordinates of the points d_1 be (x_1, y_1) and the coordinates of the points d_2 be (x_2, y_2) . Now put the coordinates in the Eq. 7, you will get

$$m_1 = ax_1 + by_1 + c \quad (8)$$

$$m_2 = ax_2 + by_2 + c \quad (9)$$

$$\text{If, } m_1 \cdot m_2 < 0 \quad (10)$$

means that the vehicle is crossing the white safety line on the traffic signal. Some examples of the combined result of vehicle and line detection are given below. The traffic signal detection and the vehicle detection along with line detection will run parallel in a synchronous way. As when the traffic light turns red or yellow, the vehicle crossing safety line module will run and store the image in case of violation.

4 Conclusion and Future Work

The model we proposed has been quite effective to classify the vehicles crossing the white safety line, detecting the violation of the traffic rules and capturing the frame at the moment. The model currently deals with the detection of the white safety line on the signals along with the detection of the vehicles restricted to car, motorcycles, trucks, buses and the detection of the traffic in a separate module which will run simultaneously. Results from detection of white safety line give positive outcomes in different scenarios given that the camera is positioned in front of the line and the line lies in the lower part of the image. The use of the single shot detector for the vehicle detection trained on COCO dataset gives the results which are to the mark as shown in the results of the vehicle detection. The use of faster R-CNN for the detection of the traffic light also gave the accuracy 74.14 % which can be improved with more training. The accuracy and range of the models for classifying different vehicles could be increased in the future by training the model over the variety in dataset. Also creating our own dataset using the CCTV images will be targeted. Moreover, the module could be further extended to detect the number plate on the vehicles and capture the number from it and store it in the records so that directly the fine report could be sent to the corresponding person stating the incident with the image. The number plate will be detected only for those vehicles which will violate the rule. This will make the work of the security/traffic police department more effective and efficient.

References

1. Poovanna, S.: How CCTVs are monitoring Bengaluru, India's IT capital. <https://www.livemint.com/Politics/45mFAB2D952ybCUY2dDYYO/How-CCTVs-are-monitoring-Bengaluru-Indias-IT-capital.html> (2018)
2. Hindustan Times. 5625 more CCTV cameras to keep watch on Mumbai. <https://www.hindustantimes.com/mumbai-news/5-625-more-cctv-cameras-to-keep-watch-on-mumbai/story-y0LaH1azFHAtpMm9pG9QO.html> (2019)
3. The New Indian Express. Speed detection cameras to come up at 100 more locations in Delhi. <http://www.newindianexpress.com/cities/delhi/2019/feb/25/speed-detection-cameras-to-come-up-at-100-more-locations-in-delhi-1943459.html> (2019)
4. Autocarindia. Road accidents in India—2017. <https://www.autocarindia.com/industry/road-accidents-in-india-claim-more-than-14-lakh-lives-in-2017-410111> (2018)
5. Wonghabut, P., et al.: Traffic light color identification for automatic traffic light violation detection system. In: 2018 International Conference on Engineering, Applied Sciences, and Technology (ICEAST). July 2018, pp. 1–4. <https://doi.org/10.1109/ICEAST.2018.8434400>
6. Wang, X., et al.: A video-based traffic violation detection system. In: Proceedings 2013 International Conference on Mechatronic Sciences, Electric Engineering and Computer (MEC). December 2013, pp. 1191–1194. <https://doi.org/10.1109/MEC.2013.6885246>
7. Zaheri, D., Abbas, M.: An algorithm for identifying red light runners from radar trajectory data. In: 2015 IEEE 18th International Conference on Intelligent Transportation Systems, September 2015, pp. 2683–2687. <https://doi.org/10.1109/ITSC.2015.431>

8. Klubsuwan, K., Koodtalang, W., Mungsing, S.: Traffic violation detection using multiple trajectories evaluation of vehicles. In: 2013 4th International Conference on Intelligent Systems, Modelling and Simulation, January 2013, pp. 220–224. <https://doi.org/10.1109/ISMS.2013.143>
9. Marikhu, R., et al.: Police eyes: real world automated detection of traffic violations. In: 2013 10th International Conference on Electrical Engineering/Electronics, Computer, Telecommunications and Information Technology, May 2013, pp. 1–6. <https://doi.org/10.1109/ECTICon.2013.6559635>
10. Behrendt, K., Novak, L., Botros, R.: A deep learning approach to traffic lights: detection, tracking, and classification. In: 2017 IEEE International Conference on Robotics and Automation (ICRA), May 2017, pp. 1370–1377. <https://doi.org/10.1109/ICRA.2017.7989163>
11. Elsagheer Mohamed, S.A.: Automatic traffic violation recording and reporting system to limit traffic accidents : based on vehicular Ad-hoc Networks (VANET). In: 2019 International Conference on Innovative Trends in Computer Engineering (ITCE), February 2019, pp. 254–259. <https://doi.org/10.1109/ITCE.2019.8646449>
12. Shreyas, R., et al.: Dynamic traffic rule violation monitoring system using automatic number plate recognition with SMS feedback. In: 2017 2nd International Conference on Telecommunication and Networks (TEL-NET), August 2017, pp. 1–5. <https://doi.org/10.1109/TEL-NET.2017.8343528>
13. Zhai, X., Bensaali, F., Sotudeh, R.: OCR-based neural network for ANPR. In: 2012 IEEE International Conference on Imaging Systems and Techniques Proceedings, July 2012, pp. 393–397. <https://doi.org/10.1109/IST.2012.6295581>
14. Yenginer, H., Korkmaz, H.: Lane line detection by using Hough Transform. In: 2018 26th Signal Processing and Communications Applications Conference (SIU), May 2018, pp. 1–4. <https://doi.org/10.1109/SIU.2018.8404650>
15. Gazzah, S., Mhalla, A., Essoukri Ben Amara, N.: Vehicle detection on a video traffic scene: review and new perspectives. In: 2016 7th International Conference on Sciences of Electronics, Technologies of Information and Telecommunications (SETIT), December 2016, pp. 448–454. <https://doi.org/10.1109/SETIT.2016.7939912>
16. Coco Dataset Dataset. <http://cocodataset.org>
17. Heidelberg Collaboratory. Bosch Small Traffic Dataset. <https://hci.iwr.uni-heidelberg.de> (2017)

An Enhanced Butterfly Optimization Algorithm for Function Optimization



Sushmita Sharma, Apu Kumar Saha, and Sukanta Nama

Abstract Butterfly optimization algorithm (BOA), a newly developed optimization algorithm, has captured the researcher's interest in solving real-life and engineering optimization problems due to its simplicity, efficiency and robustness. On the other hand, symbiosis organisms search algorithm has proved its efficiency in solving complex real-life optimization problem. In this paper, a new combinatorial optimization approach has been introduced combining the explorative advantages of BOA with the exploitative advantage of SOS to eliminate weak exploitation ability of BOA and weak exploration ability of SOS. Efficiency and robustness of the algorithm have been evaluated using twenty-five classical benchmark problems and compared with some state-of-the-art optimization algorithms. The compared results show that the proposed method to be superior and reliable than the other algorithms.

Keywords Metaheuristics · Hybrid algorithms · Butterfly optimization algorithm · Symbiosis organisms search · SymBOA · Benchmark functions

1 Introduction

Nature is full of different social, physical and chemical phenomena relating to the natural activities, individual or collective behaviour of different species. Amongst these phenomenon, the ultimate goal of the species behaviour is to survive, inter-communicate in herds, groups, schools, flocks and colonies for various reasons like foraging, hunting and searching. Nature has developed all these activities in such a way to get the optimal solution for various fields. So, in recent decades, scientists and

S. Sharma (✉) · A. K. Saha · S. Nama

Department of Mathematics, National Institute of Technology Agartala, Agartala, India

e-mail: snsush01@gmail.com

A. K. Saha

e-mail: apusaha_nita@yahoo.co.in

S. Nama

e-mail: sukanta1122@gmail.com

researchers are adopting these natural phenomena and utilizing those in optimization problems to get a (near) optimal solution. Such models fall into the metaheuristic optimization algorithms group. These methods are reliable, efficient, flexible and derivation-free. A huge number of optimization methodologies are developed till now and the count continuously increasing; the purpose of such a method is to obtain the set of values for parameters of a system for the optimum result. These methods start with randomly generated probable solutions, named population. These populations are updating themselves with the raise of generation until find the optimal values of the parameters that also abide by the constraints and more accurate than the initial randomized values. Global exploration and local exploitation are salient and conflicting feature of optimization system where exploration is searching the whole domain and exploitation is searching for the better solution in the neighbourhood. Some of the nature's inspired metaheuristics found in literature are differential evaluation (DE) [1], artificial bee colony (ABC) [2], particle swarm optimization (PSO) [3], symbiosis organisms search (SOS) [4], butterfly optimization algorithm (BOA) [5], backtracking search algorithm (BSA) [6], ant colony optimization (ACO) [7], etc.

BOA and SOS are swarm intelligent-based optimization algorithm found in literature with increasing popularity. SOS has been developed based on the interactive relation amongst the different species in the ecosystem. A numbers of works have been found in literature with SOS: A hybrid symbiosis organisms search algorithm [8], improved symbiotic organisms search algorithm [9], modified symbiosis organisms search algorithm [10] and hybrid symbiotic organisms search algorithm [11].

BOA also developed with the food searching strategy of butterflies. Some of works done with BOA are as follows: Modified butterfly optimization algorithm [12], improved butterfly optimization algorithm [13] and novel butterfly enhanced with mutualism scheme [14].

It has been observed that combinatorial or hybrid metaheuristic algorithms are more efficient than single optimization algorithms to optimize complex optimization problems. Some of the hybrid methods may found in literature, for example, [15–17]. On this perspective, the present theory has introduced an enhanced combinatorial optimization algorithm, viz. SymBOA, assembling the merits of BOA and SOS. To justify the efficiency and reliability of the proposed technique, it has evaluated with 25 classical benchmark functions and the obtained results are compared with some of other metaheuristics found in literature. The aim of the envisage is given below:

- Introduce a new efficient BOA algorithm, namely SymBOA, enhanced with the mutualism and parasitism phase of SOS, to enhance the exploitation characteristics of the original BOA.
- In SymBOA, the modification of the switch probability of the original BOA to stabilize the exploration and exploitation strategy.
- Also, to enhance the searching strategy, the mutation and parasitism phase of SOS have been merged with the original BOA. Comparison between SymBOA,

conventional BOA, conventional SOS and some of the metaheuristic is found in literature to check the efficiency of the introduced SymBOA.

- Twenty-five classical benchmark functions have been involved to evaluate and demonstrate the productivity of the introduced SymBOA.

2 Butterfly Optimization Algorithm

It is a nature-influenced optimization technique which copies the food searching strategy of butterflies. This method was proposed by Arora & Singh in 2018. Here, butterflies are used as searching agents. It is assumed that each butterfly is capable of generating and capturing of fragrance with some intensity, denoted by function evaluation value and with the change of location this function evaluation value will also change. This fragrance use to promulgate in the search region and thus sharing of knowledge is done through this fragrance. Thus, a network based on collaborative communicative awareness is formed. At the time the best aroma smelled by other butterflies, they use to go towards that region which is termed as the exploration stage. On the other hand, at the time when butterflies are not able to sense any fragrance, they use to take a random walk for searching which is denoted as exploitation stage.

The major source of the searching strategy of BOA lies in the modulation of fragrance. The fragrance is captured and involved in sensation by the chemoreceptors of butterflies. The fundamental theory of sensation of these butterflies depends on three most important parameters: stimulus intensity (I), sensory modality (c) and power exponent (a).

In BOA sensory modality (c) describes the way to measure the fragrance and how it is processed. The differentiation of individual fragrance is done by sensory modality. Stimulus intensity (I) represents the magnitude of aroma relating the functional evaluation of the butterflies. With greater intensity, the attraction power of butterfly will be greater.

The parameter power exponent (a) denotes the response compression here, which means if the stimulus gets stronger, species will be less sensitive to the change of stimulus [18, 19].

The food searching strategy of butterflies mainly depend on two issues: formulation of f and variation of I where I is related to the functional evaluation and f is relative, i.e. it will use to sense by other butterflies. So, with concept in BOA, the formulation of fragrance is as follows:

$$f_i = c * I^a \quad (1)$$

Here, f_i is the value of fragrance recognized by the i th butterfly. In BOA, there are mainly two important steps (i) global exploration and (ii) local exploitation. In global exploration, butterfly takes step towards the most strong butterfly represent by g^b with the following equation

$$x_i^{t+1} = x_i^t + (r^2 * g^b - x_i^t) * f_i \quad (2)$$

Where x_i^t is i th candidate solution at t th iteration and g^b is the strongest solution of recent ongoing iteration. A random number is represented as r in the range $[0, 1]$.

The exploitation strategy is formulated as the following equation

$$x_i^{t+1} = x_i^t + (r^2 * x_j^t - x_k^t) * f_i \quad (3)$$

Where x_j^t and x_k^t represents k th and j th butterfly in t th iteration chosen randomly. The food searching may occur in both exploration and exploitation phase. In this regard, a switch probability factor ‘ p ’ is used to switch any of these two phases.

3 Symbiosis Organisms Search

Symbiosis organisms search (SOS) is swarm intelligent optimization algorithm developed by Cheng and Prayogo [4]. SOS has been implemented by mimicking the interactive relation of different organisms in the environment. Mainly, three types of interactive relation are found in the ecosystem: Mutualism where both the species of interaction benefitted from each other. When one species gets benefit and other is neither harmed nor benefited then commensalism occurs. Parasitism occurs when an organism gets benefit but another organism gets harm, but may not be destroyed always. The execution of SOS needs only common controlling parameters like number of candidate solution and number of iterations. Different execution steps of SOS are discussed below.

3.1 Mutualism Phase

In this stage, a random population x_j is taken from the set of solutions to make interaction with the population x_i , the i th member in the ecosystem. Both of the solution interact with a mutual beneficial tendency to be benefited from each other. After interaction, the new updated population x^{t+1} and $x_{j\text{new}}^{t+1}$ in the ecosystem is calculated as following equation:

$$x_{\text{new}}^{t+1} = x_i^t + r * (x_{\text{best}}^t - M_{\text{Vec}} * BF_1) \quad (4)$$

$$x_{j\text{new}}^{t+1} = x_i^t + r * (x_{\text{best}}^t - M_{\text{Vec}} * BF_2) \quad (5)$$

Here, r represents a randomly generated value in $[0, 1]$ and BF_1, BF_2 is the benefit factor, level of benefit, is a randomly determined value either 1 or 2. M_{Vec} is the

mutual vector, which represents the relationship characteristic between x_i^t and x_j^t , can be calculated as the Eq. 5.

$$M_{\text{Vec}} = (x_i^t + x_j^t)/2 \quad (6)$$

3.2 Commensalism Phase

Here, a population x_i^t gets benefited from population x_j^t to a higher degree of benefit factor during interaction. In this interactive relation, the population updated as follows:

$$x_{\text{inew}}^{t+1} = x_i^t + r * (x_{\text{best}}^t - x_j^t) \quad (7)$$

3.3 Parasitism Phase

“Parasite_{Vector}” is an artificial parasite generated by duplicating population x_i^t and then modifying the randomly selected dimensions by using random quantity of the population x_i^t . Another organism x_j^t is taken randomly from the environment which acts as a host to the parasite vector (Parasite_{Vector}). If the Parasite_{Vector} is superior, it will replace x_j^t and gather its place in the environment. If the function evaluation value of x_j^t is superior, i.e. x_j^t will have dominant over the parasite and the Parasite_{Vector} will not survive in that environment.

4 Proposed Methodology

When the intensification strategy is stronger than diversification, the candidate solution loses its diversity causing premature convergence, and on the other hand, when diversification is stronger than intensification, the algorithm waste huge time in searching useless region of the search space leading to slow convergence rate and also has the chance to lose the optimal solution.

In the current scenario, hybridization of the butterfly optimization algorithm and the two phases of SOS namely mutation and parasitism have been done. The basic BOA performs in an effective way that results the exploration and exploitation, selected by the switch probability parameter. According to basic BOA, the diversity of population is preserved with the global exploration phase, whereas intensification of the butterflies is encounter when the butterflies take a random levy flight search. But with literature survey, it has found in the basic BOA that the populations are not exploited much; as a result, the BOA is prone to show premature convergence.

Moreover, due to the random selection of exploration and exploitation depending on the value of p sometimes causes the BOA to lose way and move away from the global best solution, as the value of the switching probability is taken as very high ($p = 0.8$ in original BOA).

So, in the present scenario, an enhanced BOA is introduced where the work ability of the basic BOA has been enhanced with the mutualism and parasitism strategies of SOS. In the basic BOA, the evaluation of the switch probability is taken as $p = 0.8$, due to which the maximum number of population moves through the exploration state which results the exploitation to be neglected up to a certain extent. To address the problem, the enhanced BOA assembled the mutualism and parasitism phases of SOS algorithm with the exploration and exploitation phases, respectively, of the BOA. This modification effectively exploits the search space to find near optimal solution. Here, value of power of exponent (a) is taken in between [0.1, 0.3]; initially 'a' starts with the value 0.1 and increased in each iteration uniformly up to 0.3. Here, the algorithm executes by following the same strategy as BOA does. We have examined the evaluation of the enhanced method with different values of p , e.g. $p = 0.5, 0.6, 0.7$ and 0.8 . It has been observed that at $p = 0.5$, the proposed method works better. So, in this paper, the value of switch probability (p) is considered to be 0.5. Also, the magnitude of sensory modality (c) is taken to be 0.01 as taken in original BOA. At the same time, the benefit factor BF 1 and BF 2 has taken as either 1 or 2.

The mechanism of the proposed method is briefly described below:

Every initialized population use to generate fragrance using equation

$$f_i = c * I^a \quad (8)$$

After that, we introduce a random number and check whether r is less or greater than p ; In this method, there is two ways of search, which includes exploitation and exploration both in each way. In the random number rp , one way executes the global exploration phase of BOA and mutualism phase of SOS. Another way executes with the local exploitation phase of BOA and parasitism phase of SOS. In this way, for any population in any iteration, it will explore as well as exploit the search space. The first way is executed with the strategy given below:

At the time of global exploration, the selected population move towards the strongest butterfly/population g^* by using the following equation

$$x_i^{t+1} = x_i^t + (r^2 * g^b - x_i^t) * f_i \quad (9)$$

After this step, a local exploitation phase named as mutualism phase is introduced, which is represented as follows:

$$x_{\text{inew}}^{t+1} = x_i^t + r * (x_{\text{best}}^t - M_{\text{Vec}} * BF_1) \quad (10)$$

$$x_{\text{jnew}}^{t+1} = x_i^t + r * (x_{\text{best}}^t - M_{\text{Vec}} * BF_2) \quad (11)$$

$$M_{\text{Vec}} = (x_i^t + x_j^t)/2 \quad (12)$$

where X_j is randomly selected another population and X_{inew} , X_{jnew} is the updated new population.

On the other search phase, the other population selected for $r > p$ exploit the search phase using Eq. (13) and then explore the search phase using the parasitism phase of SOS.

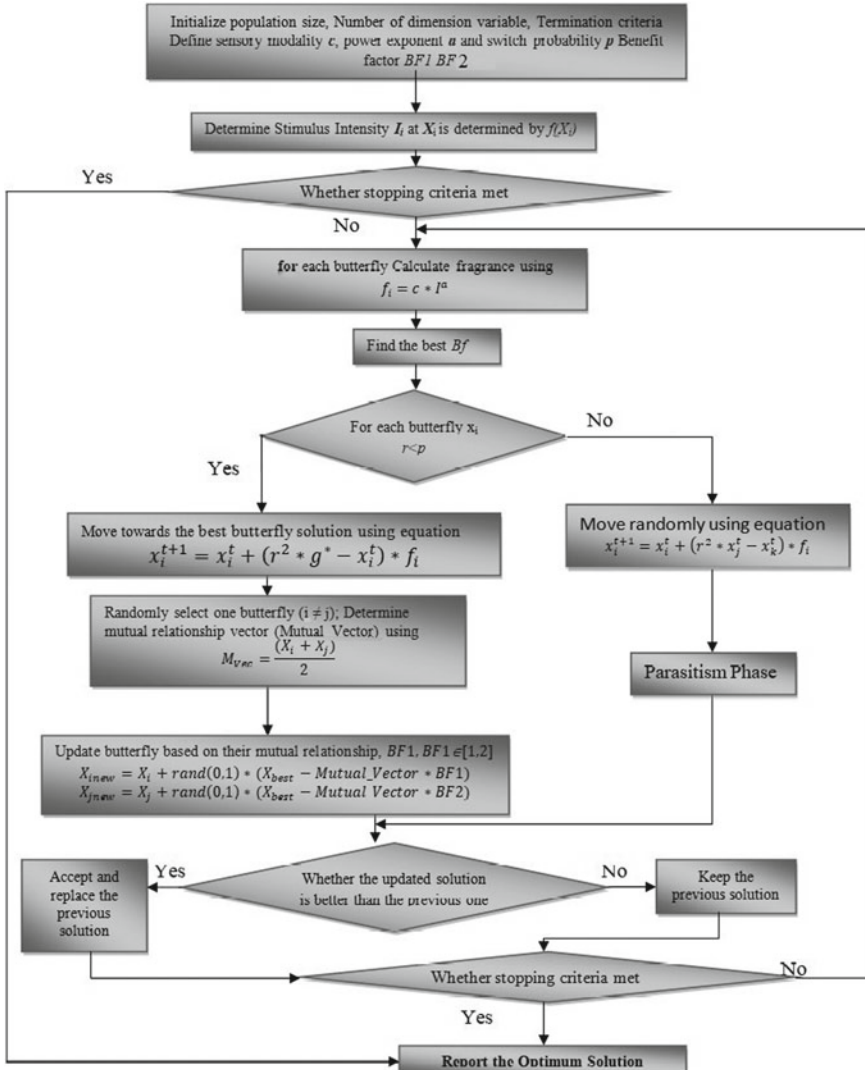


Fig. 1 Flowchart of the proposed SymBOA method

$$x_i^{t+1} = x_i^t + (r^2 * x_j^t - x_k^t) * f_i \quad (13)$$

where x_j^t and x_k^t are j th and k th population from the search domain. If x_j^t and x_k^t are of the same species and r is a random number in $[0, 1]$, then Eq. (13) shows a local random walk. The flow chart of the newly introduced method are given in Fig. 1.

5 Experimental Set-up and Results

5.1 Numerical Benchmarks and Experimental Criteria

For enquiry of the robustness of the newly introduced algorithm, the hybrid SymBOA algorithm is examined on twenty-five classical benchmark problems. We do not make any modification of these functions. These functions are: f_1 Foxholes (MS), f_2 Goldstein and price (MN), f_3 Beale (UN), f_4 Bohachevsky1 (MS), f_5 Bohachevsky2 (MN), f_6 Bohachevsky3 (MN), f_7 Booth (MS), f_8 Branin (MS), f_9 Griewank (MN), f_{10} Matyas (UN), f_{11} Restigin (MS), f_{12} Schafer (MN), f_{13} Schwefel 1.2 (UN), f_{14} Shekel5 (MN), f_{15} Shekel7 (MN), f_{16} Shekel10 (MN), f_{17} Shubert (MN), f_{28} Sphere (US), f_{19} Step (US), f_{20} Sumsquare (US), f_{21} Zakharov (UN), f_{22} Leon (UN), f_{23} Cigar(UN), f_{24} Levy (MN) and f_{25} Alpine (MN). The functions are classical and standard benchmark functions (said above) that may separate into four criteria: unimodal functions, simple multimodal functions, separable and non-separable. To judge the effectiveness, the proposed hybrid algorithm has executer for 30 times with population size 50 (candidate solution) and compared to some of the other metaheuristics. For every algorithm, the stopping criteria have been set to 10,000 iterations per execution.

5.2 Compared Algorithms and Parametric Setup

The results of the suggested hybrid scheme is equate with other state-of-the-art algorithms like SCA [20], PSO [3], DE [1], JAYA [21], SOS [4] and BOA [5]. All these algorithms need to initialize the algorithm specific parameter value before execution of the program. The values of the specific parameters have been taken as in the original paper given [5]. The optimal values for these parameters depend on the algorithm. So, in maximum cases, the optimal values are decided using trial and error method. The proposed hybrid algorithm has been simulated with specific switch probability $p = 0.5, 0.6, 0.7$ and 0.8 . Amongst these at $p = 0.5$ and 0.6 , the results are better. And hence, in this proposed algorithm, we have balanced the exploration and exploitation properties with of $p = 0.5$. Other parameters have been taken same as the original paper [5] like sensory modality ‘ c ’ is 0.01 and power exponent ‘ a ’ is increased from 0.1 to 0.3 in the entire execution.

Table 1 Performance results of SymBOA, BOA, SOS, JAYA, SCA, PSO, DE

$f(x)$		SymBOA	BOA	SOS	JAYA	SCA	PSO	DE
1	MEAN	9.98e-01	2.66e+00	9.98e-01	9.98e-01	1.54e+00	9.16e+00	9.98e-01
	STD	0.00e+00	1.56e+00	0.00e+00	4.65e-04	1.09e+00	5.75e+00	0.00e+00
2	MEAN	3.00e+00	3.24e+00	3.00e+00	3.00e+00	3.00e+00	1.95e+01	3.00e+00
	STD	2.01e-15	5.64e-01	1.24e-15	1.52e-03	4.43e-05	2.07e+01	1.88e-15
3	MEAN	0.00e+00	2.87e-01	0.00e+00	7.55e-05	3.04e-05	1.79e-01	0.00e+00
	STD	0.00e+00	3.49e-01	0.00e+00	1.83e-04	1.64e-04	3.13e-01	0.00e+00
4	MEAN	0.00e+00	0.00e+00	0.00e+00	0.00e+00	1.09e-03	4.35e+01	0.00e+00
	STD	0.00e+00	0.00e+00	0.00e+00	0.00e+00	3.79e-03	1.00e+02	0.00e+00
5	MEAN	0.00e+00	0.00e+00	0.00e+00	0.00e+00	1.61e-03	1.87e+01	0.00e+00
	STD	0.00e+00	0.00e+00	0.00e+00	0.00e+00	5.65e-03	5.27e+01	0.00e+00
6	MEAN	0.00e+00	0.00e+00	0.00e+00	2.04e-17	1.50e-03	3.27e+01	0.00e+00
	STD	0.00e+00	0.00e+00	0.00e+00	4.94e-17	4.12e-03	6.11e+01	0.00e+00
7	MEAN	0.00e+00	1.11e-01	0.00e+00	0.00e+00	1.66e-03	8.56e-01	0.00e+00
	STD	0.00e+00	2.16e-01	0.00e+00	0.00e+00	3.91e-03	1.43e+00	0.00e+00
8	MEAN	3.98e-01	6.10e-01	3.98e-01	3.98e-01	3.98e-01	5.04e-01	3.98e-01
	STD	0.00e+00	5.39e-01	0.00e+00	0.00e+00	2.03e-06	1.96e-01	0.00e+00
9	MEAN	0.00e+00	0.00e+00	0.00e+00	2.14e-02	1.92e-01	1.70e+00	0.00e+00
	STD	0.00e+00	0.00e+00	0.00e+00	2.93e-02	2.73e-01	4.55e-01	0.00e+00
10	MEAN	0.00e+00	0.00e+00	0.00e+00	2.82e-21	0.00e+00	2.16e-02	1.72e-189
	STD	0.00e+00	0.00e+00	0.00e+00	6.96e-21	0.00e+00	3.78e-02	0.00e+00
11	MEAN	0.00e+00	0.00e+00	0.00e+00	1.67e+02	1.61e-02	1.14e+02	0.00e+00
	STD	0.00e+00	0.00e+00	0.00e+00	2.52e+01	3.38e-02	2.93e+01	0.00e+00
12	MEAN	0.00e+00	0.00e+00	0.00e+00	5.25e-11	1.21e+00	6.91e+01	0.00e+00
	STD	0.00e+00	0.00e+00	0.00e+00	4.30e-11	2.26e+00	9.99e+01	0.00e+00
13	MEAN	0.00e+00	0.00e+00	0.00e+00	3.69e-33	1.78e+00	1.14e+04	2.34e-218
	STD	0.00e+00	0.00e+00	0.00e+00	3.59e-33	3.13e+00	3.84e+03	0.00e+00
14	MEAN	-4.05e+03	-1.81e+02	-9.64e+00	-7.43e+00	-5.43e+00	-2.00e+00	-1.02e+01
	STD	5.40e+03	3.50e+02	1.56e+00	2.62e+00	1.04e+00	1.86e+00	7.23e-15
15	MEAN	-5.81e+03	-1.47e+02	-1.04e+01	-8.40e+00	-5.47e+00	-1.83e+00	-1.04e+01
	STD	1.73e+04	2.83e+02	1.81e-15	2.92e+00	1.21e+00	1.30e+00	1.81e-15
16	MEAN	-3.74e+03	-1.03e+02	-1.05e+01	-9.79e+00	-5.21e+00	-2.31e+00	-1.05e+01
	STD	6.06e+03	1.59e+02	1.48e-15	1.67e+00	4.00e-01	1.98e+00	1.71e-15
17	MEAN	8.84e+01	8.95e+01	8.84e+01	8.84e+01	8.84e+0	8.92e+01	8.84e+01
	STD	2.46e-06	2.04e+00	5.33e-12	1.75e-02	1.89e-05	1.84e+00	1.45e-14
18	MEAN	0.00e+00	0.00e+00	0.00e+00	3.30e-34	1.01e-01	1.32e+03	2.11e-219
	STD	0.00e+00	0.00e+00	0.00e+00	4.45e-34	2.14e-01	4.72e+02	0.00e+00
19	MEAN	0.00e+00	0.00e+00	0.00e+00	0.00e+00	0.00e+00	7.70e+02	0.00e+00
	STD	0.00e+00	0.00e+00	0.00e+00	0.00e+00	0.00e+00	3.79e+02	0.00e+00
20	MEAN	0.00e+00	0.00e+00	0.00e+00	0.00e+00	0.00e+00	9.09e-23	0.00e+0
	STD	0.00e+00	0.00e+00	0.00e+00	0.00e+00	0.00e+00	4.98e-22	0.00e+00
21	MEAN	0.00e+00	0.00e+00	0.00e+00	3.6492e-10	4.37e+00	7.09e+01	1.97e-37
	STD	0.00e+00	0.00e+00	0.00e+00	3.00e-10	5.59e+00	3.43e+01	4.33e-37
22	MEAN	0.00e+00	2.21e-02	0.00e+00	1.41e-07	1.11e-03	1.54e-01	0.00e+00
	STD	0.00e+00	3.22e-02	0.00e+00	2.01e-07	2.52e-03	3.46e-01	0.00e+00

(continued)

Table 1 (continued)

$f(x)$		SymBOA	BOA	SOS	JAYA	SCA	PSO	DE
23	MEAN	0.00e+00	0.00e+00	0.00e+00	2.74e-26	5.43e+06	2.84e+09	2.80e-144
	STD	0.00e+00	0.00e+00	0.00e+00	3.12e-26	1.18e+07	2.28e+09	4.18e-144
24	MEAN	1.35e-31	1.42e+00	1.35e-31	1.35e-31	1.47e-03	1.26e+00	1.35e-31
	STD	6.68e-47	6.49e-01	6.68e-47	6.68e-47	5.17e-03	1.31e+00	6.68e-47
25	MEAN	0.00e+00	0.00e+00	0.00e+00	6.76e-08	1.35e-11	2.94e-06	0.00e+00
	STD	0.00e+00	0.00e+00	0.00e+00	2.63e-07	7.38e-11	8.21e-06	0.00e+00

5.3 Results Discussion

On evaluating the mean results and standard deviation results acquired by SymBOA and other algorithms with different benchmark function, the evaluation is as follows: The proposed method is superior from BOA, SOS, JAYA, SCA, PSO and DE in resp. 10, 4, 20, 21, 25, 9 functions; similar to 15, 20, 5, 3, 0, 14 occasions and inferior in 0, 1, 0, 1, 0, 2 cases. Multimodal functions of high dimension have many local minima, and the result of the functions shows that the ability of algorithm is strong to escape from poor local minima and obtain the global optimum. As the result of mean and standard deviation is best in comparison to other algorithm, it can be seen that hybrid SymBOA is successful to finding the global optimum.

Also, a statistical rank, viz. Friedman rank test has been done by taking the mean performance of all the functions and compared to that of other state-of-the-art algorithm. Here, the rank for SymBOA is 1 (mean rank 2.24), for BOA is 4 (mean rank 4), for SOS is 2 (mean rank 3.70), for JAYA is 5 (mean rank 5), for SCA is 6 (mean rank 6), for PSO is 7 (mean rank 6.80) and for DE is 3 (mean rank 3).

6 Conclusion

This paper presents an enhanced hybrid SymBOA with balanced exploration and exploitation ability to enrich the efficiency and rate of convergence of the BOA. To examine the efficiency of newly proposed SymBOA, a number of popular benchmark functions are collected from the literature and conducted the numerical experiments. In this study, the proposed SymBOA is compared with BOA, SOS and also four other popular algorithms such as DE, PSO, JAYA and SCA. From simulation results, it can be concluded that SymBOA is efficient than the compared algorithms (Table 1).

References

1. Storn, R., Price, K.: Differential evolution—a simple and efficient heuristic for global optimization over continuous spaces. *J. Global Optim.* **11**(4), 341–359 (1997)
2. Xu, Y., Fan, P., Yuan, L.: A simple and efficient artificial bee colony algorithm. *Math. Prob. Eng.* **14**, (2013). <https://doi.org/10.1155/2013/526315>
3. Kennedy, J., Eberhart, R.: Particle swarm optimization. In: Proceedings of ICNN'95 - International Conference on Neural Networks, vol. 4, pp. 1942–1948 (1995)
4. Cheng, M.Y., Prayogo, D.: Symbiotic organisms search: a new metaheuristic optimization algorithm. *Comput. Struct.* **139**, 98–112 (2014)
5. Arora, S., Singh, S.: Butterfly optimization algorithm: a novel approach for global optimization. *Soft Comput.* **23**, 715–734 (2019)
6. Civicioglu, P.: Backtracking search optimization algorithm for numerical optimization problems. *Appl. Math. Comput.* **219**, 8121–8144 (2013)
7. Marco, D., Mauro, B., Thomas, S.: Ant colony optimization. *Comput. Intell. Mag.* **1**, 28–39 (2006)
8. Nama, S., Saha, A.K., Ghosh, S.: A hybrid symbiosis organisms search algorithm and its application to real world problems. *Memetic Comput.* **9**. <https://doi.org/10.1007/s12293-016-0194-1>
9. Nama, S., Saha, A.K., Ghosh, S.: Improved symbiotic organisms search algorithm for solving unconstrained function optimization. *Decis. Sci. Lett.* **5**, 361–380 (2016). <https://doi.org/10.5267/j.dsl.2016.2.004>
10. Do, D., Lee, J.: A modified symbiotic organisms search (MSOS) algorithm for optimization of pin-jointed structures. *Appl. Soft Comput.* **61**, 683–699 (2017)
11. Wu, H., Zhou, Y.-Q., Luo, Q.: Hybrid symbiotic organisms search algorithm for solving 0–1 knapsack problem. *Int. J. Bio-Inspired Comput.* **12** (2018). <https://doi.org/10.1504/IJIBC.2018.093334>
12. Arora, S., Singh, S., Yetilmezsoy, K.: A modified butterfly optimization algorithm for mechanical design optimization problems. *J. Brazilian Soc. Mech. Sci. Eng.* **40**(1), 21 (2018)
13. Arora, S., Singh, S.: An improved butterfly optimization algorithm for global optimization **8**, 711–717 (2016)
14. Sharma, S., Saha, A.K.: m-MBOA: a novel butterfly optimization algorithm enhanced with mutualism scheme. *Soft Comput.* (2019). <https://doi.org/10.1007/s00500-019-04234-6>
15. Sharma, T.K., Pant, M.: Opposition-based learning embedded shuffled Frog-Leaping Algorithm. *Soft Comput.Theor. Appl.* **583**, 853–861 (2017)
16. Jain, S., Swami, V., Kumar, S.: An improved Spider Monkey optimization algorithm. *Soft Comput.Theor. Appl.* **583**(1), 73–81 (2017)
17. Sheth, P.D., Jagdeo, S.M., Umbarkar, A.J.: Teaching-learning-based optimization on Hadoop. *Soft Comput.Theor. Appl.* **583**(1), 251–263 (2017)
18. Zwislocki, J.J.: Sensory Neuroscience: Four Laws of Psychophysics. Springer Science & Business Media, Berlin (2009)
19. Stevens, S.S.: Psychophysics. Transaction Publishers, Piscataway (1975)
20. Mirjalili, S.: SCA: a sine cosine algorithm for solving optimization problems. *Knowl. Based Syst.* **96**, 120–133 (2016)
21. Rao, V., Jaya, R.: A simple and new optimization algorithm for solving constrained and unconstrained optimization problems. *Int. J. Ind. Eng. Computat.* **7**, 19–34 (2016)

Dynamic Analysis of Wind Turbine Drivetrain Under Constant Torque



Rishi Kumar and Sankar Kumar Roy

Abstract Frequency spectra of torsional vibration and contact force are very important to understand the dynamic behavior of a horizontal axis wind turbine drivetrain system (WTDS). The drivetrain has three gear stages, namely one planetary and two parallel gear stages. Hence, a mathematical model is developed to understand the dynamic behavior of the system using a lumped parameter model. Governing equations of motion are derived using Lagrange's formulation by taking the kinetic and potential energy of the system into Lagrange's function. The equations of motion include time varying parameters like time varying gear mesh stiffness and damping coefficient, which are estimated by analytical approach. The concept of mesh phasing is incorporated in the first stage of drivetrain. Steady-state dynamic responses are computationally obtained using Houbolt method and responses are analyzed in time and frequency domain. Thus, effect of damping on WTDS has been studied.

Keywords Wind turbine drivetrain · Time varying mesh stiffness · Damping · Fast Fourier transform

1 Introduction

Demand of electricity is omnipresent. With this, its production and supply is one of the important domains inevitable in recent times. We have ever grown our dependence to some sort of energy resources, but most of them are reserved as well as scarce in availability. The abundance of renewable energy is promising alternative to bet on. This has attracted some serious attention from academic and industrial people to harness the opportunity coming in the form of wind energy. Wind turbine (WT) is a mechanical device to harness energy and convert it into electricity. Gearbox is a critical component in wind turbine drivetrain system (WTDS).

R. Kumar (✉) · S. K. Roy

Department of Mechanical Engineering, National Institute of Technology Patna, Patna 800005, India

e-mail: rishi.me15@nitp.ac.in

In the last decade, good number of research works is published which analyzes the dynamic behavior of WTDS. Peeters et al. [1] presented a gear transmission system in three different models. They calculated Eigen frequencies and Eigen modes for different stages separately but neglected the damping effects and nonlinearity in gear mesh stiffness. Peeters et al. [2] have put more stress on second and third model this time and indicated the significance of Eigen modes in a wider frequency window. They also worked for transient loads in their subsequent gear pairs. Todorov et al. [3] investigated a horizontal axis wind turbine system having three stages of gear trains. Linear spring is used to represent the gear meshing. With Lagrange's equations, they calculated natural frequencies and mode shapes. Todorov and Vukov [4] analyzed the parametric torsional vibration for the previous model using time varying mesh stiffness. Time domain and frequency domain characteristics of torsional vibrations are studied. Helsen et al. [5] presented a flexible multibody model and computed Eigen frequencies and mode shapes of wind turbine gearbox considering time varying mesh stiffness, damping and backlash effects. Wang and Wu [6] included time varying mesh stiffness, nonlinear backlash and meshing error excitation in their model and derived the governing equations of motion using Lagrange's equation to study the natural frequencies, mode shapes of the WTDS. Although, effects of damping ratio in pure rotational model are investigated but they have not incorporated the concept of mesh phasing for multiple gear meshing in the planetary gear stage. Shi et al. [7] investigated a horizontal axis wind turbine drivetrain for torsional vibration in one direction. Mesh stiffness obtained from Fourier series is used to observe the transient responses of the WTDS in time and frequency domain. Shi et al. [8] reused the model in three dimensions incorporating flexibilities in shafts, gear mesh, support bearings and gravity forces. The upgradation of model gave more satisfying results in understanding the dynamic responses of drivetrain. Srikant and Sekhar [9] proposed a model with a nonstationary wind load excitation with stochastic torque loadings. Eigen frequencies and Eigen vectors are computed at mean gear mesh stiffness. They made remarks about the torsional vibration at lower modes. The duo [10] investigated the same model for varying external aerodynamic torque and internal resistive torque. Hence, aerodynamic torque is assumed to be a function of ramp, gust, mean and turbulence components of wind. Fast Fourier transform (FFT) is an important tool in signal processing to extract the characteristics features hidden in the system [15]. Hence, vibrational responses of WTDS are studied in time and frequency domain.

The underlying remarks with this literature survey state that a very crude and elementary drivetrain model has been developed by the researchers by incorporating parameters like mesh stiffness of rectangular waveform, constant damping, etc. Recently, researchers have estimated time varying mesh stiffness calculated from analytical approach since rectangular waveform of mesh stiffness has some shortcomings which have been explored for the planetary gear set [11]. Based on the literature review, no one has incorporated the time varying mesh stiffness estimated by analytical approach, time varying damping and concept of mesh phasing during gear meshing into the WTDS. So, aim of this paper is to deal with dynamic analysis of WTDS using earlier mentioned time varying mesh stiffness, damping and mesh phasing.

2 Mathematical Model of the Drivetrain

The schematic diagram of wind turbine drivetrain is shown in Fig. 1. The three stages in the gear drive are assembled to get the required gear ratio at the generator end. Planetary gear stage (spur gear) is connected with the rotor through planet carrier. Annular ring gear is assumed to be fixed with the gearbox housing. Three planets are assembled between the fixed ring gear and centrally positioned sun gear supported by the planet carrier. Planet carrier takes the constant rotational torque from the rotor and put the subsequent planet meshed between the ring gear and sun gear into rotational tendency. Output shaft from the planetary gear stage is connected to the second stage and pinion from the second stage is connected to the third stage. Finally, output shaft from the third stage connected to the generator with constant velocity joint to produce electricity. Each lumped member in the entire transmission system possesses three rotational as well as three translational degrees of freedom. To refrain from complexity of the model dynamics, only rotational motion along shaft axis is assumed in the present work. Thus, the proposed drivetrain model has 11 degrees of freedom. Power transmission is routed from rotor (rot) via planet carrier (c), planet 1 (cp1), 2 (cp2), and 3 (cp3), sun gear (s), second stage gear 1 ($g1$) and gear 2 ($g2$), third stage gear 3 ($g3$) and gear 4 ($g4$), to generator (gen), respectively. Rotational displacements of three planets (y_{cpi} , $i = 1, 2, 3$) are taken in relative coordinate frame with respect to planet carrier and remaining rotational displacements (y_{rot} , y_c , y_s , y_{g1} , y_{g2} , y_{g3} , y_{g4} , y_{gen}) are taken in absolute frame of reference.

$$y_{cpi} = y_{pi} - y_c \quad (1)$$

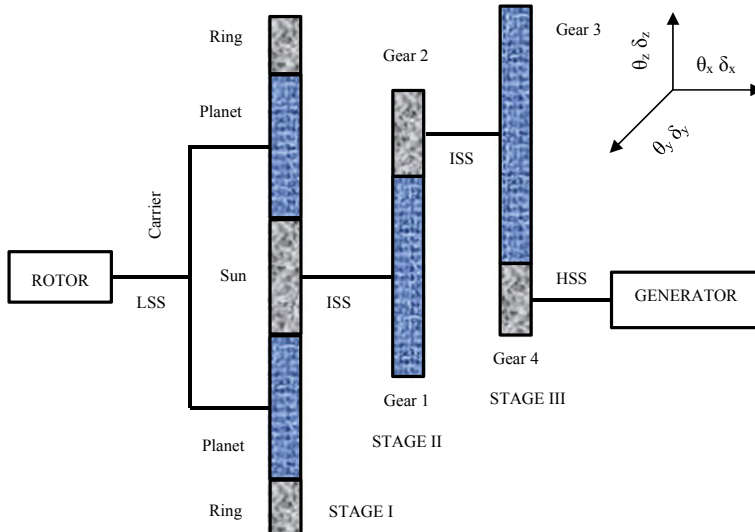


Fig. 1 Schematic diagram of wind turbine drivetrain system

$$\delta_{\text{spi}} = r_s y_s - r_c y_c + r_p y_{\text{pi}} \quad (2)$$

$$\delta_{\text{rpi}} = -r_c y_c - r_p y_{\text{pi}} \quad (3)$$

$$\delta_{ij} = r_i y_i + r_j y_j \quad (4)$$

Here, r is the base circle radius of gears of the drivetrain and r_c is the position of planet center with respect to center of the sun gear. Equation (4) is representing the relative displacement for parallel gear stages in which i and j are two gear pairs. The ' n ' planets are positioned at some circumferential angle, ψ_i , with respect to the sun gear. For this model, ' n ' is 3.

$$\psi_i = \frac{2\pi(i-1)}{n} \quad (5)$$

The tooth meshing (either external or internal) between two gears can be represented by only spring or by spring and damper taken together. Energy is stored in different forms in the meshing gears and some fraction of this stored energy is dissipated due to material damping. Spring stiffness or gear mesh stiffness is calculated using potential energy method [11]. Resultant time varying mesh stiffness (k) for one pair of gear meshing (either external or internal) is calculated as follows:

$$k = \sum_{i=1}^2 \frac{1}{\frac{1}{k_{b1,i}} + \frac{1}{k_{s1,i}} + \frac{1}{k_{a1,i}} + \frac{1}{k_{h,i}} + \frac{1}{k_{b2,i}} + \frac{1}{k_{s2,i}} + \frac{1}{k_{a2,i}}} \quad (6)$$

$$c_{ij} = 2\xi \sqrt{\frac{k_{ij} J_i J_j}{J_i r_j^2 + J_j r_i^2}} \quad (7)$$

Gear mesh damping coefficient, c_{ij} , is taken from [13]. Damping ratio ξ is taken to be 1.5% for the present computation [10]. The second and third planets are having some phase shift when first planet is at zero reference point with respect to centrally positioned sun gear. This mesh phase shift is seen in the time varying mesh stiffness for sun-planet (k_{spi} , $i = 1, 2, 3$) and for ring-planet (k_{rpi} , $i = 1, 2, 3$) gear meshing. Sign convention for phase angle is taken to be positive for clockwise rotation of planet in case of sun-planet (γ_{spi}) gear meshing and vice versa in case of ring-planet (γ_{rpi}). The formulation for mesh phasing is given by [12]:

$$\gamma_{\text{spi}} = \pm \psi_i \frac{Z_s}{2\pi} \quad (8)$$

$$\gamma_{\text{rpi}} = \mp \psi_i \frac{Z_r}{2\pi} \quad (9)$$

The mesh stiffness is shifted by the amount equal to fractional part of phase angle obtained. The mesh phasing between sun-planet (i th) and ring-planet (i th) gear meshing is given by γ_{rs} . The value of γ_{rs} is estimated using theoretical formulation given in [12] and is equal to 0.6518. The time varying mesh stiffness is written as:

$$k_{\text{spi}} = k(t - \gamma_{\text{spi}} T) \quad (10)$$

$$k_{\text{rpi}} = k(t - \gamma_{\text{rpi}} T - \gamma_{rs} T) \quad (11)$$

Mesh cycle time period (T) between sun-planet (i th) and ring-planet (i th) gear meshing in gear drive is given by:

$$T = \frac{2\pi}{\Omega Z_p} \quad (12)$$

Ω is the gear mesh frequency of meshing gear and Z_p , Z_s and Z_r are number of teeth for planet gear, sun gear and ring gear, respectively. ω_s (in Hz) is rotational frequency of sun gear. For planetary gear drive, gear mesh frequency (GMF) is given by:

$$\Omega = \omega_s \frac{Z_r Z_s}{Z_r + Z_s} \quad (13)$$

For parallel gear drive, GMF is the product of rotational frequency (ω , in Hz) of a gear and its number of teeth (Z).

$$\Omega = \omega Z \quad (14)$$

For the damped dynamic drivetrain model, Lagrange's equation is used to derive the discrete equations of motion which is given as follows:

$$\frac{d}{dt} \left(\frac{\partial L}{\partial \dot{y}_l} \right) - \frac{\partial L}{\partial y_l} + \frac{\partial R}{\partial \dot{y}_l} = \Gamma_l \quad (15)$$

The ' l ' may be substituted with rot, c , cp1, cp2, cp3, s , $g1$, $g2$, $g3$, $g4$, gen in Eq. 14. The Lagrange's function ' L ' and Rayleigh dissipation function ' R ' for the system are written as follows:

$$L = T - V \quad (16)$$

$$L = \frac{1}{2} \left\{ J_{\text{rot}} \dot{y}_{\text{rot}}^2 + (J_c + 3mR_c^2) \dot{y}_c^2 + J_p (\dot{y}_{\text{cp1}} + \dot{y}_c)^2 + J_p (\dot{y}_{\text{cp2}} + \dot{y}_c)^2 + J_p (\dot{y}_{\text{cp3}} + \dot{y}_c)^2 + J_s \dot{y}_s^2 + J_{g1} \dot{y}_{g1}^2 + J_{g2} \dot{y}_{g2}^2 + J_{g3} \dot{y}_{g3}^2 + J_{g4} \dot{y}_{g4}^2 + J_{\text{gen}} \dot{y}_{\text{gen}}^2 \right\}$$

$$\begin{aligned}
& -\frac{1}{2} [k_{sp1}(r_s y_s - r_s y_c + r_p y_{cp1})^2 + k_{sp2}(r_s y_s - r_s y_c + r_p y_{cp2})^2 \\
& + k_{sp3}(r_s y_s - r_c y_c + r_p y_{cp3})^2 + k_{rp1}(r_r y_c + r_p y_{cp1})^2 \\
& + k_{rp2}(r_r y_c + r_p y_{cp2})^2 + k_{rp3}(r_r y_c + r_p y_{cp3})^2 \\
& + k_3(r_{g1} y_{g1} + r_{g2} y_{g2})^2 + k_4(r_{g3} y_{g2} + r_{g4} y_{g3})^2 \\
& + k_{t1}(y_c - y_{rot})^2 + k_{t2}(y_{g1} - y_s)^2 + k_{t2}(y_{g3} - y_{g2})^2 \\
& + k_{t3}(y_{g4} - y_{gen})^2 + k_{bc} y_c^2 + k_{bs} y_s^2]
\end{aligned} \tag{17}$$

$$\begin{aligned}
R = & \frac{1}{2} \{ c_{sp1}(r_s \dot{y}_s - r_s \dot{y}_c - r_p \dot{y}_{cp1})^2 + c_{sp2}(r_s \dot{y}_s - r_s \dot{y}_c - r_p \dot{y}_{cp2})^2 \\
& + c_{sp3}(r_s \dot{y}_s - r_s \dot{y}_c - r_p \dot{y}_{cp3})^2 + c_{rp1}(r_r \dot{y}_c + r_p \dot{y}_{cp1})^2 \} \\
& + c_{rp2}(r_r \dot{y}_c + r_p \dot{y}_{cp2})^2 + c_{rp3}(r_r \dot{y}_c + r_p \dot{y}_{cp3})^2 \\
& + c_{g12}(r_{g1} \dot{y}_{g1} + r_{g2} \dot{y}_{g2})^2 + c_{g34}(r_{g3} \dot{y}_{g3} + r_{g4} \dot{y}_{g4})^2
\end{aligned} \tag{18}$$

Eleven coupled ordinary differential equations are obtained with the help of Lagrange's formulation. These equations will govern the motion of the drivetrain system. The governing equations in matrix form are represented as:

$$M\ddot{e} + C\dot{e} + Ke = \Gamma \tag{19}$$

displacement vector, e ,

$$e = [y_{rot} \ y_c \ y_{cp1} \ y_{cp2} \ y_{cp3} \ y_s \ y_{g1} \ y_{g2} \ y_{g3} \ y_{g4} \ y_{gen}]^T \tag{20}$$

force vector, Γ ,

$$\Gamma = [\Gamma_{rot} \ 0 \ 0 \ 0 \ 0 \ 0 \ 0 \ 0 \ 0 \ 0 \ \Gamma_{gen}]^T \tag{21}$$

Mass matrix [M], damping matrix, [C], and stiffness matrix, [K], are defined as below in Eqs. 22–24.

3 Numerical Analysis

The equations of motion for the drive train model are numerically integrated by Houbolt method to obtain the dynamic response. In this method, the current state of any assumed variable is a function of previous state as well as the current state itself. Based on Taylor's series approximation, the equations that correlate the displacement (e), velocity (\dot{e}) and acceleration (\ddot{e}) terms can be given below in Eqs. 25 and 26.

Houbolt method falls into the category of implicit integration method which is initiated with the help of the central difference method. This method is conditionally stable for the step size which is equal to or less than the critical time period [14]. The equations of motion of the model are discretized to eliminate the velocity and acceleration terms by displacement term using Houbolt method [substituted by Eqs. (25) and (26) into Eq. (19)].

$$M = \begin{bmatrix} J_{\text{rot}} & 0 & 0 & 0 & 0 & 0 & 0 & 0 & 0 & 0 \\ 0 & J_c = 3J_p + mr_c^2 & J_p & J_p & J_p & 0 & 0 & 0 & 0 & 0 \\ 0 & J_p & J_p & 0 & 0 & 0 & 0 & 0 & 0 & 0 \\ 0 & J_p & 0 & J_p & 0 & 0 & 0 & 0 & 0 & 0 \\ 0 & J_p & 0 & 0 & J_p & 0 & 0 & 0 & 0 & 0 \\ 0 & 0 & 0 & 0 & 0 & J_s & 0 & 0 & 0 & 0 \\ 0 & 0 & 0 & 0 & 0 & 0 & J_{g1} & 0 & 0 & 0 \\ 0 & 0 & 0 & 0 & 0 & 0 & 0 & J_{g2} & 0 & 0 \\ 0 & 0 & 0 & 0 & 0 & 0 & 0 & 0 & J_{g3} & 0 \\ 0 & 0 & 0 & 0 & 0 & 0 & 0 & 0 & 0 & J_{g4} \\ 0 & 0 & 0 & 0 & 0 & 0 & 0 & 0 & 0 & J_{\text{gen}} \end{bmatrix} \quad (22)$$

$$C = \begin{bmatrix} 0 & 0 & 0 & 0 & 0 & 0 & 0 & 0 & 0 & 0 \\ 0 & C_{2,2} & C_{2,3} & C_{2,4} & C_{2,5} & C_{2,6} & 0 & 0 & 0 & 0 \\ 0 & C_{3,2} & C_{3,3} & 0 & 0 & C_{3,6} & 0 & 0 & 0 & 0 \\ 0 & C_{4,2} & 0 & C_{4,4} & 0 & C_{4,6} & 0 & 0 & 0 & 0 \\ 0 & C_{5,2} & 0 & 0 & C_{5,4} & C_{5,6} & 0 & 0 & 0 & 0 \\ 0 & C_{6,2} & C_{6,3} & C_{6,4} & C_{6,5} & C_{6,6} & 0 & 0 & 0 & 0 \\ 0 & 0 & 0 & 0 & 0 & C_{7,7} & C_{7,8} & 0 & 0 & 0 \\ 0 & 0 & 0 & 0 & 0 & 0 & C_{8,7} & C_{8,8} & 0 & 0 \\ 0 & 0 & 0 & 0 & 0 & 0 & 0 & C_{9,9} & C_{9,10} & 0 \\ 0 & 0 & 0 & 0 & 0 & 0 & 0 & 0 & C_{10,9} & C_{10,10} \\ 0 & 0 & 0 & 0 & 0 & 0 & 0 & 0 & 0 & 0 \end{bmatrix} \quad (23)$$

$$K = \begin{bmatrix} K_{1,1} & K_{1,2} & 0 & 0 & 0 & 0 & 0 & 0 & 0 & 0 \\ K_{2,1} & K_{2,2} & K_{2,3} & K_{2,4} & K_{2,5} & K_{2,6} & 0 & 0 & 0 & 0 \\ 0 & K_{3,2} & K_{3,3} & 0 & 0 & K_{3,6} & 0 & 0 & 0 & 0 \\ 0 & K_{4,2} & 0 & K_{4,4} & 0 & K_{4,6} & 0 & 0 & 0 & 0 \\ 0 & K_{5,2} & 0 & 0 & K_{5,4} & K_{5,6} & 0 & 0 & 0 & 0 \\ 0 & K_{6,2} & K_{6,3} & K_{6,4} & K_{6,5} & K_{6,6} & 0 & 0 & 0 & 0 \\ 0 & 0 & 0 & 0 & 0 & -k_{t2} & K_{7,7} & K_{7,8} & 0 & 0 \\ 0 & 0 & 0 & 0 & 0 & 0 & K_{8,7} & K_{8,8} & 0 & 0 \\ 0 & 0 & 0 & 0 & 0 & 0 & 0 & K_{9,9} & K_{9,10} & 0 \\ 0 & 0 & 0 & 0 & 0 & 0 & 0 & K_{10,9} & K_{10,10} & -k_{t3} \\ 0 & 0 & 0 & 0 & 0 & 0 & 0 & 0 & -k_{t3} & -k_{t3} \end{bmatrix} \quad (24)$$

$$\dot{e}_{i+1} = \frac{1}{6\Delta t}(11e_{i+1} - 18e_i + 9e_{i-1} - 2e_{i-2}) \quad (25)$$

$$\ddot{e}_{i+1} = \frac{1}{(\Delta t)^2}(2e_{i+1} - 5e_i + 4e_{i-1} - e_{i-2}) \quad (26)$$

The expressions obtained after the substitution of respective terms and rearranging them in sequence are as follows:

$$\begin{aligned} e_{i+1} &= \left[\frac{2}{(\Delta t)^2}M + \frac{11}{6\Delta t}C + K \right]^{-1} \\ &\quad * \left\{ \Gamma_{i+1} + \left(\frac{5}{(\Delta t)^2}M + \frac{3}{\Delta t}C \right)e_i - \left(\frac{4}{(\Delta t)^2}M + \frac{3}{2\Delta t}C \right)e_{i-1} \right. \\ &\quad \left. + \left(\frac{1}{(\Delta t)^2}M + \frac{1}{3\Delta t}C \right)e_{i-2} \right\} \end{aligned} \quad (27)$$

Initially, at $t = 0$, displacement and velocity are assumed to be zero. Then, acceleration at the simultaneous time is calculated using Eq. (19) as given as:

$$\ddot{e}_{i+1} = M^{-1}(\Gamma_{i+1} - C\dot{e}_{i+1} - Ke_{i+1}) \quad (28)$$

For the first two iterations, central difference method has been executed with the help of initial conditions obtained whose results become the initial conditions for the next iteration. The third iteration of the drivetrain system became the first iteration for the Houbolt method which is continued henceforth.

4 Results and Discussion

Table 1 and Table 2 summarize the specifications of meshing gears and their material properties. MATLAB software is used for the entire computation. Dynamic analysis is done assuming constant input rotor torque, $\Gamma_{\text{rot}} = 15000 \text{ Nm}$, and constant output generator torque, $\Gamma_{\text{gen}} = -\frac{\Gamma_{\text{rot}}}{\text{Gear Ratio}}$. There are no external loadings put onto any of the drivetrain components. Rotor is supposed to be excited with rotational frequency of 0.3 Hz. Rotational frequency of drivetrain gears is estimated empirically, input being taken from planet carrier rotational speed. Eigen values and natural frequencies of the system are calculated from QR-decomposition technique and results obtained are verified by power method and MATLAB default program. Mean gear mesh stiffness is used [9] in QR-decomposition technique. Potential energy method is used to estimate the varying gear mesh stiffness analytically. Material damping is used based on time varying mesh stiffness and geometrical configurations of gear pair. Concept of mesh phasing and phase shifting are incorporated in the planetary gear stage. Linear spring and damper are assembled in parallel to connect the gears pair. Steady-state responses

Table 1 Parametric specifications of drivetrain components for the model

Parameters components	Base circle radius, r (mm)	Moment of inertia, (kg-m ²)	Gear mesh frequency, (Hz)
rotor, rot	—	4.18e06	—
carrier, c	270	57.72	—
ring, r	430	—	25.2
planet, p	160	1.12	25.2
sun gear, s	110	0.86	25.2
gear 1, g_1	290	14.32	83.8
gear 2, g_2	95	1.515	83.8
gear 3, g_3	185	0.105	326.5
gear 4, g_4	80	0.2	326.5
generator, gen	—	93.22	—

Table 2 Parametric specifications of drivetrain components for the model

Parameters components	Torsional stiffness, N-m/rad	Mean stiffness, N-m	Bearing stiffness, N-m
LSS (rotor and carrier)	7.19e7	—	—
ISS (sun and gear 1)	1.4e7	—	—
ISS (gear 2 and gear 3)	1.4e7	—	—
HSS (gear 4 and generator)	0.15e7	—	—
carrier	—	—	7.19e7
sun gear	—	—	1.4e7
ring-planet mesh	—	6.3477e9	—
sun-planet mesh	—	4.6971e9	—
gear 1-gear 2 mesh	—	4.9349e9	—
gear 3-gear 4 mesh	—	6.3851e9	—
Pressure angle, $A = \pi/9\text{rad}$			
Young's modulus, $E = 206 \times 10^9 \text{ N/m}^2$			
Poisson's ratio, $\nu = 0.3$			
Face width of gear tooth, $L = 11 \times \text{module}$			

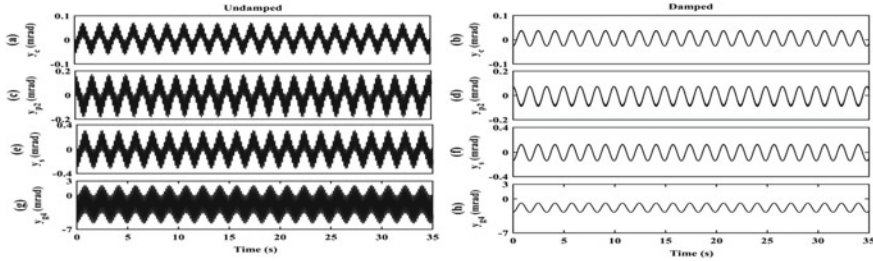


Fig. 2 Torsional deflection of un-damped and damped system for **(a, b)** carrier, **(c, d)** planet 2, **(e, f)** sun gear, and **(g, h)** gear 4 in time domain spectrum

are obtained for the drivetrain components and analysis is done to understand the dynamic behavior.

Torsional deflections of carrier, planet 2, sun gear and last stage pinion are plotted in Fig. 2. It is observed that deflections are quite significant for the system when there is no damper being used. With the damped system, the magnitude of deflection is reduced. Different gears of the drivetrain are rotating differently. Last stage pinion gear is running at maximum frequency.

In the frequency spectrum, f_n^i and f_l^m are natural frequencies and GMFs, respectively. Value of i is ranging from 1 to 11 and l is varying between 1 and 3 for three stages of the drivetrain. In the damped system, higher natural frequencies are not observed or observed with negligibly small amplitude as compared to un-damped system. GMFs and its harmonics with side bands are excited in un-damped and damped system. Frequency of sidebands is natural frequencies. It means that the GMFs are amplitude modulated by natural frequencies. For the damped system, only the smallest natural frequency modulates the GMFs. Contact forces are also plotted and same comments are applicable for them in time and frequency domain spectra. F_{sp2} , F_{rp2} , F_{g12} and F_{g34} are contact forces between sun-planet 2, ring-planet 2, second stage meshing gear pair and third stage gear pair, respectively.

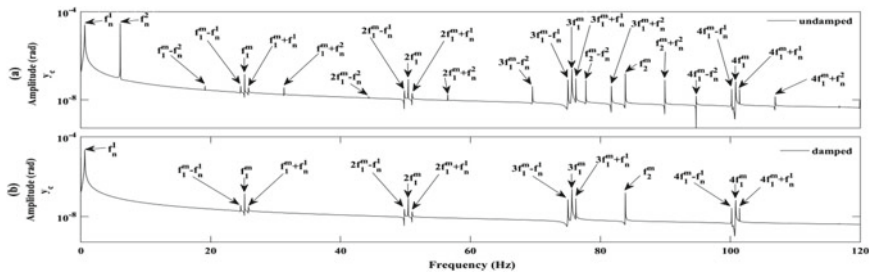


Fig. 3 Torsional deflection of carrier in frequency domain spectrum of **a** un-damped system and of **b** damped system

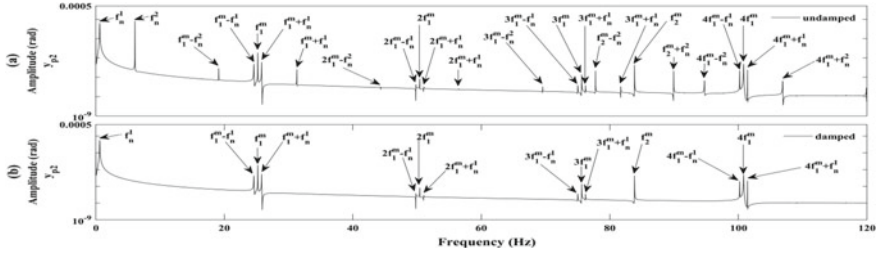


Fig. 4 Torsional deflection of planet 2 in frequency domain spectrum of **a** un-damped system and of **b** damped system

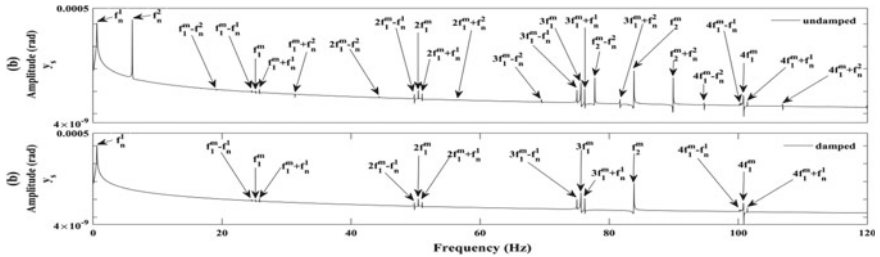


Fig. 5 Torsional deflection of sun in frequency domain spectrum of **a** un-damped system and of **b** damped system

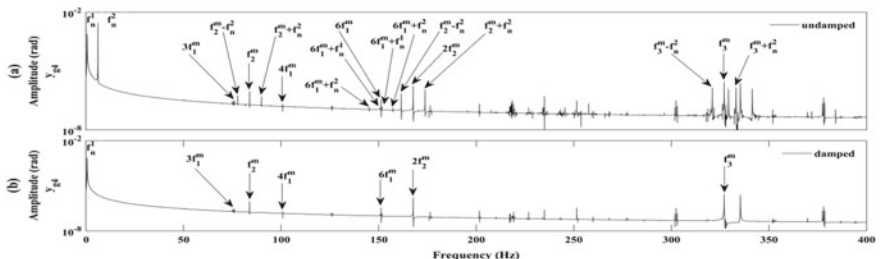


Fig. 6 Torsional deflection of gear 4 in frequency domain spectrum of **a** un-damped system and of **b** damped system

5 Conclusions

A mathematical model is proposed for a horizontal axis WTDS to study the torsional response under constant input and output torque. Therefore, time varying mesh stiffness, damping, mesh phasing, bearing and shaft stiffness are incorporated into the model. The equations of motion are solved by Houbolt method. Rotational deflections and gear tooth contact forces are compared between un-damped and damped system by analyzing in time and frequency domain. In un-damped system, frequency

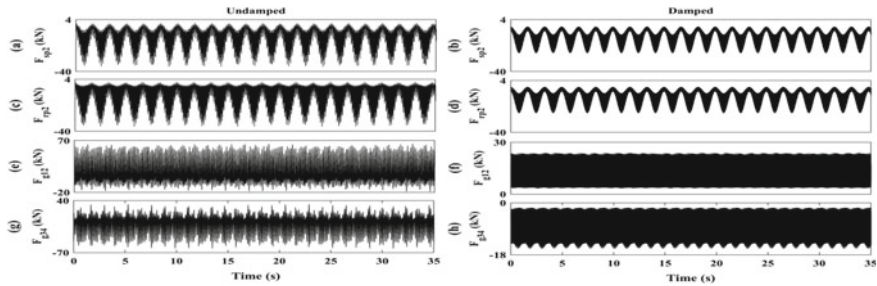


Fig. 7 Contact forces (kN) of un-damped system for **(a)** carrier, **(c)** planet 1, **(e)** sun, **(g)** gear 4 and of damped system for **(b)** carrier, **(d)** planet 1, **(f)** sun, **(h)** gear 4 in time domain spectrum

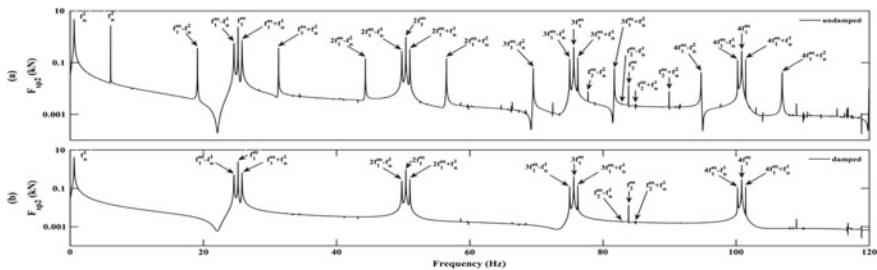


Fig. 8 Contact forces (kN) of **a** un-damped system and of **b** damped system for sun-planet 2 in frequency domain spectra

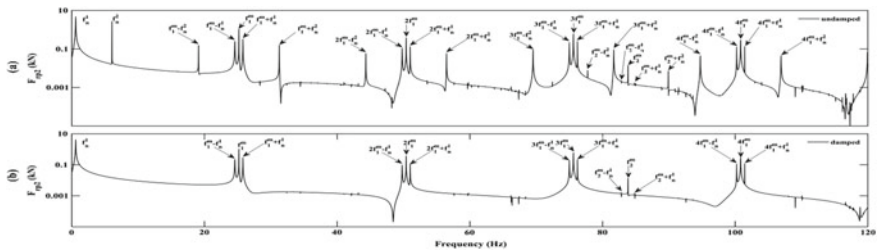


Fig. 9 Contact forces (kN) of **a** un-damped system and of **b** damped system for ring-planet 2 in frequency domain spectra

spectra of rotational deflections and gear tooth contact forces show GMFs and its harmonics with sidebands. The frequency of sidebands is natural frequencies. Thus, the GMFs are amplitude modulated by the natural frequencies. In damped system, higher natural frequencies are not excited. Hence, only lowest frequency modulates the GMFs. This work may be improved for better approximation to dynamic behavior by increasing the model's DOF's. This will add to the process of refinement of the model from crude one.

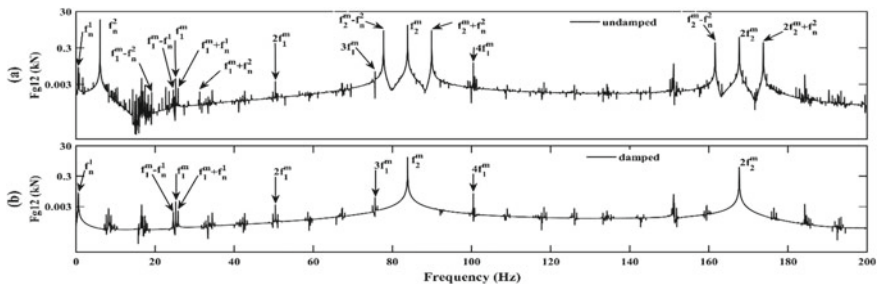


Fig. 10 Contact forces (kN) of **a** un-damped system and of **b** damped system for gear 1 and gear 2 in frequency domain spectra

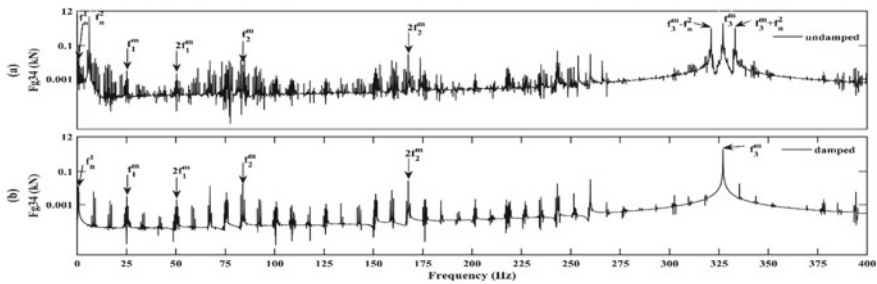


Fig. 11 Contact forces (kN) of **a** un-damped system and of **b** damped system for gear 3 and gear 4 in frequency domain spectra

References

1. Peeters, J.L.M., Vandepitte, D., Sas, P.: Analysis of internal drive train dynamics in a wind turbine. *Wind Energy* **9**(1–2), 141–161 (2006)
2. Peeters, J., Vandepitte, D., Sas, P.: Structural analysis of a wind turbine and its drive train using the flexible multibody simulation technique. *Proc. Int. Conf. Noise Vib. Eng.* **6**, 3665–3679 (2006)
3. Todorov, M., Dobrev, I., Massouh, F.: Analysis of torsional oscillation of the drive train in horizontal-axis wind turbine. In: 2009 8th International Symposium on Advanced Electromechanical Motion Systems & Electric Drives Joint Symposium, pp. 1–7. Lille (2009)
4. Todorov, M., Vukov, G.: Parametric torsional vibrations of a drive train in horizontal axis wind turbine. In: Proceedings of CFSER-2010, pp. 1–17. Damas (2010)
5. Helsen, J., Vanhollebeke, F., Coninck, F.D., Vandepitte, D., Desmet, W.: Insights in wind turbine drive train dynamics gathered by validating advanced models on a newly developed 13.2 MW dynamically controlled test-rig. *Mechatronics* **21**(4), 737–752 (2011). ISSN: 0957-4158
6. Wang, X., Wu, S.: Nonlinear dynamic modelling and numerical simulation of the wind turbine's gear train: national nature science foundation of China (51005170, 50875189), pp. 2385–2389 (2011)
7. Shi, W., Kim, C.W., Chung, C.W., et al.: *Int. J. Precis. Eng. Manuf.* **14**, 153 (2013). <https://doi.org/10.1007/s12541-013-0021-2>
8. Shi, W., Park, H.C., Na, S., et al.: *Int. J. Precis. Eng. Manuf.* **15**, 1351 (2014). <https://doi.org/10.1007/s12541-014-0476-9>

9. Srikanth, P., Sekhar, A.S.: Dynamic analysis of wind turbine drive train subjected to nonstationary wind load excitation. *J. Mech. Eng. Sci.* **229**(2), 429–446 (2015)
10. Srikanth, P., Sekhar, A.S.: Wind turbine drive train dynamic characterization using vibration and torque signals. *Mech. Mach. Theory* **98**, 2–20 (2016)
11. Liang, X., Zuo, J., Patel, T.H.: Evaluating time varying mesh stiffness of a planetary gear set using potential energy method. *Proc. Inst. Mech. Eng. Part C: J. Mech. Eng. Sci.* **228**(3), 535–547 (2014)
12. Parker, R.G., Lin, J.: Mesh phasing relationships in planetary and epicyclic gears. *J. Mech. Des.* **126**, 365–370 (2004)
13. Inman, D.J.: *Engineering Vibration*, 4th edn. Pearson Prentice Hall, Upper Saddle River, NJ 07458 (2014)
14. Rao, S.S.: *Mechanical Vibrations*, 5th edn. Pearson Prentice Hall, Upper Saddle River, NJ 07458 (2011)
15. Himanshu, S., Millie, P., Sudhir, K., Yogita, S.: Application of unnormalized and phase correlation techniques on infrared images. *Adv. Intell. Syst. Comput.* **584**, 461–471 (2018)

To Build Scalable and Portable Blockchain Application Using Docker



Priyanka Kumar and Maharshi Shah

Abstract In modern digital era, digitalization has improved not only security but reduced time and effort to maintain all records. Nowadays, birth certificate is the only proof of age and basis of all the important document identities like Birth Certificate, Aadhar card, Pan Card, Passport, etc. So, identifying the correct birth certificate of any person is a major challenge. In this paper, we have proposed and implemented an efficient and more secure way of storing birth certificates by using Inter Planetary File System (IPFS) and most demanded “BLOCKCHAIN” technology. Further, the rising of Docker technology and Containerization as a Service (CaaS), we deployed this application inside a container using docker-compose which is used to create Multi-Container Docker application.

Keywords Blockchain technology · Secure · Scalable · Portable · Birth record · Docker

1 Introduction

Blockchain technology is consensus-based computing which registers all transactions without the involvement of any third party. With the advent of blockchain technology, we see a shift towards the use of it in systems where transactions frequently occur. It is decentralized, distributed, and immutable in nature. Because of these properties, blockchain technology has become more and more popular over a series of time. In recent years, digitalization is on extreme demand where vital documents such as passports, birth records, medical records, land records, and even

P. Kumar (✉)

Department of Computer Science and Engineering, Amrita School of Engineering, Amrita Vishwa Vidyapeetham, Coimbatore, India
e-mail: k_priyanka@cb.amrita.edu

M. Shah

Department of Computer Science and Engineering, Amrita Vishwa Vidyapeetham, Amrita Vishwa Vidyapeetham, Coimbatore, India
e-mail: cb.en.p2cse17015@cb.students.amrita.edu

transactions are being digitized. It has a great impact on every aspect of life. For example, in the banking and finance department, governmental parties, Chambers of Commerce and Land Registry, and in healthcare department.

Despite being secure, several fraud incidents occur such as fake birth certificate rackets which were identified in Delhi, India on August 2018 [1]. We require an efficient technology to store birth records which cannot be tampered as well as easy to maintain, well secured, and easily shareable. Recently, new technology is emerging coined as “BLOCKCHAIN TECHNOLOGY” which has proved it worth in many of the top-notch applications like Virtual Currencies such as Bitcoin, Ethereum, Ripple, etc. Blockchain will completely rule over today’s conventional technology in the near future. May it be banking, medical records, government records, and identity records all will be shortly using blockchain technology [2, 3]. In this work, we mainly focus on enhancing birth certificates by using recent developments in blockchain technology. Another way of securing data is by using Biometric techniques which are the most preferred techniques to establish the identity of an individual [4]. These techniques are used mainly for authentication purposes. These techniques are mainly used to replace passwords, pins, smartcards, keys, and tokens which are the means of authentication previously. The disadvantages of using the pins or passwords might be that they are difficult to remember and also there is a good chance that they might be hacked. Smart cards, keys, tokens may be stolen by someone or we might misplace or forget them in an undesired place which can lead to many security issues. Magnetic cards have a good chance of getting corrupted and make them unreadable. Biometrics are nothing but using our biological traits for authentication purposes which we know that they cannot be replaced by anyone as they are unique [5]. But using biometrics to secure birth certificate is neither conventional nor feasible as fingerprints change slightly over time [6].

In this work, we will show how to use blockchain technology to secure birth records and easily verify and authenticate a birth record. The recent rise in Docker technology which provides Container as a Service (CaaS), gave us the initiative to deploy our application using Docker. Docker is a tool that allows developers, sys-admins, etc. to easily deploy their applications in a sandbox (called *containers*). Key benefit of Docker is that it allows users to package an application with all of its dependencies into a standardized unit for software development. Unlike virtual machines, containers do not have high overhead and hence enable more efficient usage of the underlying system and resources.

2 Background

Blockchain technology was first introduced by Satoshi Nakamoto in 2008 where the world saw its first virtual currency “BITCOIN” [7]. Blockchain technology is immutable as well as distributed technology where all the data is been replicated to all the participating clients in a blockchain [8]. So, if we want to tamper a record, we need to tamper data on each client to whom data has been distributed which is nearly

impossible because of the availability of computing power. Hence, the blockchain is seen as one of the most secure technology ever the world has witnessed [9]. Integrating blockchain to secure birth records will not just only save paperwork but it will be more secure, and all the fake birth certificate rackets would shut down, no more duplicate birth certificate would be valid. Also, we can easily share certificates on blockchain which can be used for verification purposes such as Passport verification, Aadhar card verification, Pan Card verification, etc. [8].

Docker is a software that uses OS-level virtualization to deliver software in packages called containers. The Docker engine hosts the container. It was founded in 2013. Containers are isolated from each other and bundle their own software, configuration files, libraries, and can communicate with each other. All containers are lightweight compared to the virtual machine. We need to specify a dockerfile to create a Docker image which in turn creates a container. Docker is capable of creating single container application. To create multi-container Docker application we use docker-compose. Compose is a tool for defining and running multi-container Docker application. With compose, you use a YAML file to configure your application services.

To stop fraud birth records and convert each individual birth record into digital format using Inter Planetary File System (IPFS) and Blockchain technology which is more secure and easily accessible from anywhere across the network.

If we want to deploy this application in another machine, we require few configurations and software such as Linux OS, Python 3.6, several python libraries, IPFS servers. This is very cumbersome, so there should be a way to directly run the application without these requirements to be fulfilled. Here Docker comes in the picture, which creates container with all tools, software, configuration prebuilt which is easy to run anywhere in any OS without installing all the requirements (Fig. 1).

In India, digitalization of birth records is available in few states such as Andhra Pradesh, Karnataka, Chhattisgarh, Delhi, Bihar, Himachal Pradesh, Kerala, Madhya

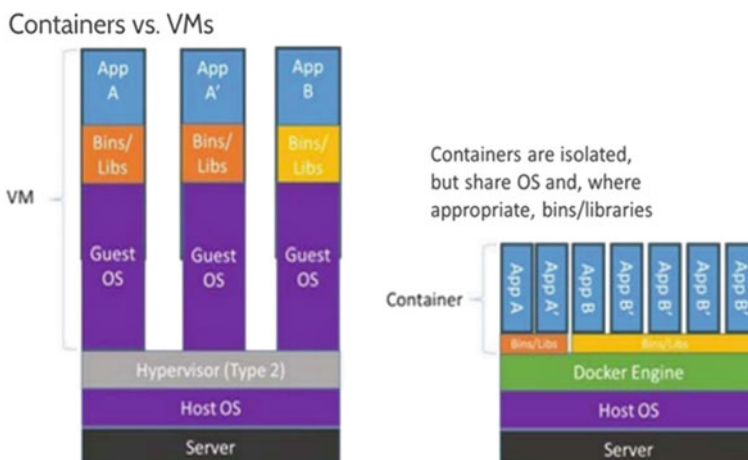


Fig. 1 Container versus VM

Pradesh, Rajasthan, Uttrakhand, and Uttar Pradesh [10]. Still, the system is not fully functional and secure. There is no mechanism of sharing birth records with other authorities such as the passport office, government office, etc. Each time we need to manually provide a birth certificate for verification. This gave an initial motivation for this work. Further, Enhancing Breeder Document Long term Security using Blockchain Technology [11] proposed a model on how to use blockchain technology with biometrics to secure birth records, but it was only proposed model they have not implemented it. Evaluating Suitability of Applying blockchain [12] helped to understand what the parameters are, use cases, advantages and disadvantages of blockchain over conventional methods. Tamper-proof Data Distribution in the Electoral process [13] gave a direction for security perspective which gave an idea to include cryptography to make it more secure and reliable. An improved P2P file system scheme based on IPFS and blockchain [14] guided Blockchain and IPFS can be merged together to form a secure platform for implementing this project. Further studied show how IPFS is different from HTTP which helped to understand the strength of IPFS over HTTP.

3 Proposed Model

In this section, the proposed model is depicted in Fig. 2.

4 Design and Implementation

This proposed application consists of the following modules. We have successfully implemented and containerized it using Docker as well.

User Registration: User will register on an application using Name and Phone Number. While registration, RSA key pair as well as bigchainDB key pair will be generated which will be stored in JSON format? For future perspective, it can be embedded in RFID chip for quick access.

User Login: This module will help the user to access his account. While login data would be taken from JSON file which was stored in the computer during login.

User registration on blockchain: This module will help user to register with blockchain, all the information such as RSA public key, BigchainDB public key, Name, Phone Number would be registered on blockchain, so it will be easier to find any user on blockchain.

Adding file to blockchain: Whenever a birth certificate governing body wants to add certificate, it will find user's phone number from blockchain. When the client's phone number is used, it will generate one AES key which will encrypt the content of file and on top of this, AES key will be encrypted using client's RSA public key,

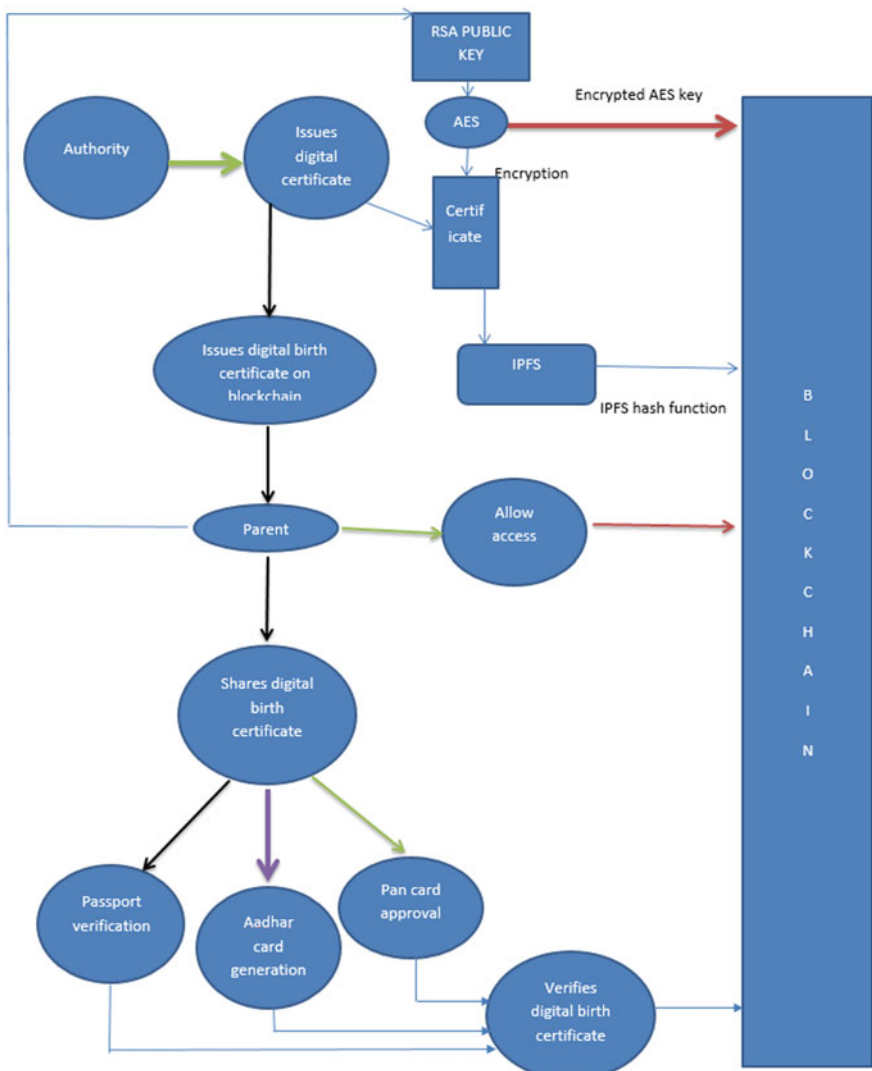


Fig. 2 Proposed model [15]

so that only dedicated user with RSA private key can decrypt. In the meantime, transaction will be sent to IPFS and one hash function will be generated, which will be stored inside a block of blockchain (Figs. 3 and 4).

Retrieve file from blockchain: When the user wants to retrieve the file, the RSA private key will decrypt the AES key, only the user whose RSA public key was used for encryption can decrypt it using its RSA private key. After obtaining AES key, key will be applied on the file to decrypt data. On successful decryption user will

```
missu@Lenovo-PC:/mnt/d/New Folder/hospital$ blocks add child_cert.txt --phone 3456734567
/usr/lib/python3/dist-packages/requests/_init_.py:80: RequestsDependencyWarning: urllib3 (1.23)
  RequestsDependencyWarning)
[+] Fetching user data from the blockchain
[+] Found user with mobile number!
[+] Got Public RSA key
-----BEGIN PUBLIC KEY-----
MIIGMA0GCSqGSIb3DQEBAQUAA4GNADCBiQKBgQckPydU1R377imSyXP21XBREs1G
/gxtt2WIKAuRNW5jX4aRwSeL6agV6VUn6HPSD9NbFLetXxj1imzguoUTba9Hm3I
nSggYVLFUMEFBiuwAYcmEPW0Z6UwxLNyPSk25FyQ57DbkTXvuxf4BbqpuymESwk
Rty290GsgnvFilolQOIDAQAB
-----END PUBLIC KEY-----
[+] Generating random AES key
[+] Encrypting data...
[+] Writing encrypted data to IPFS
[+] Connected to local IPFS node
[+] Data written to IPFS: QmljewokES45wtLmFamq2mZshAosjB1sLbrTYrwnUwozBZY
[+] Encrypting AES key with RSA public key
[+] Preparing CREATE transaction with {'schema':...
[+] Signing with private key
[+] Creating Block on the Blockchain
[+] Created: bb12dc94fb43a157f7499e67c2c973fa7d5a58117aab386ed14ba35551a4fdf
[+] Transferring Block to patient: Hkvz1lC2BHpMRws7FLlh7K3MbaRdu8m8NUTiw7sQhHu
[+] Preparing TRANSFER transaction with encrypted key
[+] Signing transaction
[+] Asset block confirmed on the blockchain: 20207
[+] Sending on the blockchain
[+] Transaction sent: 6e52194f942a97c60971aa60a66248cf0ca60a17e64bdd7b154e68823792f49a
```

Fig. 3 Hospital issuing birth certificate for a user [15]

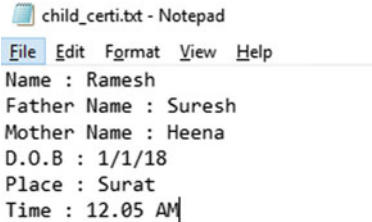


Fig. 4 Birth certificate

able to see actual content of file. During this process, the IPFS hash function stored inside the block will be mapped to IPFS server and according to it, the file will be downloaded in the system. On successful download of file from IPFS, system will automatically apply RSA private key from the JSON file to decrypt the AES key. Once we obtain AES key, we need to apply this AES key on the file which was used to encrypt data. And on successful decryption, we will get the content of file (Figs. 5 and 6).

Permit other user to view file: If user wants to share file with another user such as passport authority for birth certificate verification he can simply add file with permit flag and phone number of the user whom we can easily find on blockchain. In this module, all the above steps will be repeated but instead of users RSA key, the third party whom we want to give access will be used to encrypt AES key [15] (Fig. 7).

YAML FILE

Docker-Compose uses a YAML file to configure our services. In this YAML file, we define two services, IPFS and Server. The ipfs service uses a public ipfs image pulled from Docker Hub Registry. The Server service uses an image that is built from the

```
missu@Lenovo-PC:/mnt/d/New_folder/parent$ blocks login user.json
/usr/lib/python3/dist-packages/requests/_init_.py:80: RequestsDependencyWarning:
  RequestsDependencyWarning)
This will overwrite all previous user data. Are you sure? [y/N]: y
[+] Writing to .blocks
[+] Serializing to JSON
[+] Loading user from .blocks
Name: Parent1
Phone: 3456734567
RSA public key:
-----BEGIN PUBLIC KEY-----
MIIFMA0GCSqGSIb3DQEBAQUAA4GNADCBiQKBgQCkPydU1R377im5yXP21XBREsJG
7gxtt2WIKaRNW5jX4aRwvSeL6agV6Vn6HPSD9nbFLetXxj1imZqcuoUTba9Hm3I
nSggYVLfUWEfHbuwASytmEPwOZ6UwxLNyP5k25FyQ57DbK1Xvuxf4BbqpuymESwk
Rty290GsgnvF1ol0QIDAQAB
-----END PUBLIC KEY-----
Blockchain public key: HkvZ1JC2BhlpMRws7FL1h7K3MbaRdu8m8NUTiw7sqHu
[+] Loading all records of user on the blockchain
Registered on the Blockchain!
Blocks: 1
```

Fig. 5 Updated increment of block pointer on user login [15]

```
missu@Lenovo-PC:/mnt/d/New_folder/parent$ blocks get bb12dc94f1b43a157f7499e67c2c973fa7d5a58117aab386ed14ba35551a4fdf
/usr/lib/python3/dist-packages/requests/_init_.py:80: RequestsDependencyWarning: urllib3 (1.23) or chardet (3.0.4) does
  RequestsDependencyWarning)
[+] Decrypted AES key
[+] Retrieving file from IPFS
[+] Connected to local IPFS node
[+] Decrypting file
[+] File decrypted
Length: 105
...Head display...
Name : Ramesh
Father Name : Suresh
Mother Name : Heena
D.O.B : 1/1/18
Place : Surat
Time : 12.05 AM
[+] Writing to bb12dc94f1b43a157f7499e67c2c973fa7d5a58117aab386ed14ba35551a4fdf.txt
[+] Done:
```

Fig. 6 User retrieving birth certificate [15]

```
missu@Lenovo-PC:/mnt/d/New_folder/Passport$ blocks list --phone 3456734567
/usr/lib/python3/dist-packages/requests/_init_.py:80: RequestsDependencyWarning:
  RequestsDependencyWarning)
[+] Found user with mobile number!
-----block 1-----
ID: bb12dc94f1b43a157f7499e67c2c973fa7d5a58117aab386ed14ba35551a4fdf
IPFS hash: QmUeWokES45wLmFamq2mXZshAosjB1sLbrTYrnwzBZY
File Format: txt
Permitted addresses: 1
Current user cannot decrypt
missu@Lenovo-PC:/mnt/d/New_folder/Passport$
```

Fig. 7 Permission required for decrypting file [15]

dockerfile present in current working directory. Dockerfile is used to build a Docker image that contains all the dependencies of the python application required and the python itself (Fig. 8).

One command to run docker-compose: We can start our application by running **docker-compose up**. Compose pulls an ipfs image, builds an image of our code, and starts the service we mentioned in YAML file. By running **docker-compose run server** service, it creates two containers, one containing python code and other

```

version: '3'
services:
  ipfs:
    image: "jbenet/go-ipfs:latest"
  server:
    build: .
    volumes:
      - .:/code
  depends_on:
    - ipfs

```

Fig. 8 YAML file to create multi-container application

```

$ docker-compose run server
Starting blocks_ipfs_1 ... done
/tmp #
/tmp #

```

Fig. 9 Run Docker-compose

Name	Command	State	Ports
blocks_ipfs_1	/sbin/tini -- /usr/local/b ...	Up	4001/tcp, 5001/tcp, 8080/tcp, 8081/tcp
blocks_server_1	sh	Exit 0	
blocks_server_run_9	sh	Up	

Fig. 10 Output of Docker-compose

containing IPFS server. By running this service we enter inside a container that consists of our python code (Fig. 9).

Output of docker-compose: We can view the list of active containers using **docker-compose ps** (Figs. 10 and 11).

This is the detailed background of how services are created using docker-compose, it also shows how IP addresses are assigned inside Docker container, and how multi-containers are created.

5 Conclusion and Future Work

There are many methods for securing birth records by using biometrics, cryptography, cryptography plus biometrics, etc. But we are using Blockchain technology along with Cryptography and Inter Planetary File System (IPFS) protocol to secure birth records, as well as access records from anywhere in the network, also share records anywhere with user permission and to validate or authenticate records within a few

```
$ docker-compose up
blocks_ipfs_1 is up-to-date
Recreating blocks_server_1 ... done
Attaching to blocks_ipfs_1, blocks_server_1
ipfs_1    Changing user to ipfs
ipfs_1    ipfs version 0.4.20
ipfs_1    initializing IPFS node at /data/ipfs
ipfs_1    generating 2048-bit RSA keypair...done
ipfs_1    peer identity: QmVBLdsq1DNkCK4tfifhRi4oGjpSavu48h7RozQ2ZQCBeo
ipfs_1    to get started, enter:
ipfs_1
ipfs_1    ipfs cat /ipfs/QmS4ustL54uo8FzR9455qaxZwuMiUhyvMcX9Ba8nUH4uVv/readme
ipfs_1
ipfs_1    Initializing daemon...
ipfs_1    go-ipfs version: 0.4.20-
ipfs_1    Repo version: 7
ipfs_1    System version: amd64/linux
ipfs_1    GoLang version: go1.12.5
ipfs_1    Swarm listening on /ip4/127.0.0.1/tcp/4001
ipfs_1    Swarm listening on /ip4/172.22.0.3/tcp/4001
ipfs_1    Swarm listening on /p2p-circuit
ipfs_1    Swarm announcing /ip4/127.0.0.1/tcp/4001
ipfs_1    Swarm announcing /ip4/172.22.0.3/tcp/4001
ipfs_1    API server listening on /ip4/0.0.0.0/tcp/5001
ipfs_1    WebUI: http://0.0.0.0:5001/webui
ipfs_1    Gateway (readonly) server listening on /ip4/0.0.0.0/tcp/8080
ipfs_1    Daemon is ready
ipfs_1
```

Fig. 11 Service creation using docker-compose

moments. This is just a prototype, we can embed JSON file in RFID chip to easily access birth records, also we can create JAVA version to integrate with Android applications. The application is deployed using docker-compose, in future we can scale application using Kubernetes. Also, we can containerize BigchainDB, thus creating a three container application in which one container will be hosting python application, another container would be running IPFS server in background, and last container would be storing BigchainDB.

References

1. Buchmann, N., Rathgeb, C., Baier, H., Busch, C., Margraf, M.: Enhancing breeder document long-term security using blockchain technology. In: IEEE 41st Annual Computer Software and Applications Conference (2017)
2. Nomura Research Institute: Survey on blockchain technologies and related services (2016)
3. Bond, C.F., Amati, F., Blousson, G.: Blockchain, academic verification use case (2015)
4. Blanchette, J.F.: The digital signature dilemma Le dilemme de la signature numérique. Ann. Des Télécommunications **61**(7), 908–923 (2006)
5. Thompson, S.: The preservation of digital signatures on the blockchain—Thompson—See Also. Univ. Br. Columbia iSchool Student J. **3**, (2017). Spring
6. Smolenski, N., Hughes, D.: Academic credentials in an era of digital decentralization academic credentials in an era of digital decentralization learning machine cultural anthropologist contents preface (2016)
7. Nakamoto, S.: Bitcoin: a peer-to-peer electronic cash system. [Www.Bitcoin.Org](http://www.Bitcoin.Org) (2008). p. 9

8. Kumar, P., Dhanush, G. A., Srivatsa, D., Nithin, A., Sahisnu, S.: A buyer and seller's protocol via utilization of smart contracts using blockchain technology. Presented at ICAICR—2019, vol. CCIS, vol. 1075, pp 464–474 (2019)
9. MIT Media Lab: what we learned from designing an academic certificates system on the blockchain. Medium (2016)
10. Lo, S.K., Xu, X., Chiam, Y. K., Lu, Q.: Evaluating Suitability of Applying Blockchain. In: International Conference on Engineering of Complex Computer Systems (2017)
11. Shaheen, S.H., Yousaf, M., Jalil, M.: Temper proof data distribution for universal verifiability and accuracy in electoral process using blockchain. In: IEEE Conference (2017)
12. Smith, T.D.: The blockchain litmus test. In: IEEE International Conference on Big Data (BIGDATA) (2017)
13. Chen, Y., Li, H., Li, K., Zhang, J.: An improved P2P file system scheme based on IPFS and blockchain. In: IEEE International Conference on Big Data (BIGDATA) (2017)
14. Sidhu, J.: Syscoin: a peer-to-peer electronic cash system with blockchain-based services for e-business (2008)
15. Shah, M., Kumar, P.: Tamper proof birth certificate suing blockchain technology. Int. J. Recent Technol. Eng. (IJRTE) 7(5S3) (2019). E-ISSN:2277-3878

Text Summarization: An Extractive Approach



Vishal Soni, Lokesh Kumar, Aman Kumar Singh, and Mukesh Kumar

Abstract Text summarization method produces the shorter or abstract version of text after giving the large source text. It provides the meaningful information of the source text, i.e. the text's meaning is intact and accurate. Text summarization tools have a powerful impact on today's world due to the increasing information with a massive rate on the Internet. It is very difficult for a person to describe and ingest the whole content. The manual conversion or summarization is very difficult task, hence automation is need. The automation can be achieve using artificial intelligence techniques. Text summarization methods are classified into two categories: Extractive and abstractive. The extractive method, as its name suggests, consists of extracting important sentences or paragraph from some source of text and rejoining them to get the summarized form of the source content. The criteria for evaluating an importance of a sentence or paragraph is based on the statistical features parameter of the sentences, and the abstractive method is all about knowing the source text and re-writing the text in a few words that describes the whole source text. In addition, this method uses a linguistic approach to check and interpret the source text. In this article, extractive text summarization methods are applied to the job. The validation of the model is performed using the bench-marked source text. From the obtained result, it is evident that the summarization model performs well and do the summarization which is very precise and meaningful.

Keywords Text summarization · Extractive · Abstractive · TF-IDF

1 Introduction

There is a massive information content present on the Internet today, It is increasing exponentially with the high rate everyday, so it is a difficult task to handle that much amount of information manually. There is a need of accessing the information and

V. Soni · L. Kumar · A. K. Singh · M. Kumar (✉)
Department of CSE, NIT Patna, Patna, Bihar 800005, India
e-mail: mukesh.kumar@nitp.ac.in

processing it for the companies and organizations. For containing the information, text documents are the most commonly used in today's digital world [1]. Humans cannot consume that much amount of information because of the limited memory capacities. Usually, when we do a search for some information on Internet, Internet displays more information than is needed, so we unconsciously want to retrieve the most important information that is relevant to our problem and describes the most of the content, this is called "summarization." Automatic text summarizer tools are used for extracting the main points of the original source text without the need to read the complete document. Text summarization methods are basically specified in two categories: (i) Extractive and (ii) Abstractive [2]. Extractive method is all about selecting the most relevant sentences and paragraphs and concatenating them in a shorter form. In abstractive approach, it develops an understanding of given text and expresses it in fewer words in natural language. Automatic text summarization process may be done in three steps:

Identification: This is the first step of the process. In this step, the most important and relevant topics are identified. In simple words, summary of given document is generated by concatenating the important bit of the text.

Interpretation: In this step, sentences that are identified in the previous step are combined in more meaningful ways. During this step, some modification can be done to the original sentences.

Generation: In this step, the result of the previous step can create some confusion to the reader. Generation step gives exact summary of the original document by doing some modification in the result of the second step to produce an understandable summary to the reader.

In this article, extractive summarization method of text has been discussed.

The rest of the article is organized as follows: The literature survey of the natural language processing and its sub-fields (text summarization) is studied in Sect. 2. The implementation details for the proposed approach are described in Sect. 3. Section 4 highlights the results obtained and the interpretation derived from them. Section 5 finally concludes this article.

2 Related Work

In the field of text summarization, there are many proposals for automatically summarizing the page information into shorter form. Researchers and practitioners have done a tremendous research work in machine learning and natural language processing (NLP) [3–5]. Text summarization is one of the research fields of NLP, where summarization of long text can be done in shorter form. The meaning of the text should not be changed. In other words, it is the abstract or summary of the given text [6].

Nazari et al. [2] describe different kinds of methods like abstractive, extractive, single-documents and multi-documents. This article also consists of various sum-

marization techniques like statistical, machine learning, semantic-based, and swarm intelligence-based method. Villa-Monte et al. [7] carried out a research based on capacity of the metrics of selected sentences, even in different languages. Emphasis of the article is on identifying the most representative metrics for extracting sentences coherently. Qazvinian et al. [8] proposed a method where they use the citation summaries to understand the main contribution of documents. They showed that how their clustering method outperforms one of the current state-of-the-art multi-documents summarizing algorithms. Saggion et al. [9] proposed a method of text summarization which produces indicative informative abstracts. Experiments reported here addressed the evaluation of the indicative abstracts using a categorization task.

Mehdi et al. [10] surveyed on different approach of text summarization. They described different extractive summarization approaches as well as three tasks which all summarizers need to perform:

- Build an intermediate representation for the input text, which is the main aspect of the text.
- Assign the weight or score of sentences on the basis of the intermediate representation.
- Generate the summary constituting the number of sentences.

They also addressed some popular approaches like topic representation approach, frequency-driven approach, graph-based or machine learning techniques, etc.

Since Hinton proposed Deep in Belief Network (DBN) in 2006, people began to use neural networks for abstracting text. Wu et al. [11] described a method based on knowledge of graph technology to make automatically text summarizer by extracting abstract texts. They also described that this method can not only perform higher-level text extraction but can also help making answer generating model to any given question. They have also done same related work by studying old research papers of different researchers. They experimented on the CNN-based dataset named CNN DAILYMAIL. They used knowledge of graph query language named SPARQL to create summaries from texts by choosing important templates. In order to obtain a high quality abstract text summary, they propose the use of neural networks for entity recognition. This approach uses human-based perception to extract the entities and generate the relationship between words. So, their method uses full concept of human thinking more, so the proposed model can achieve very good results.

Atmadja et al. [12] proposed a text summarizer model “Automated text summarization for Indonesian Article Using Vector Space Model.” Obviously, writing an abstract requires an in-depth analysis, as the content would affect both the reader’s interest and the lack of interest in a particular subject. The aim of this research article is to construct a automation summarizer for summarizing a Indonesian article. In this article, they are using two methods to summarize an article that is, A Term Frequency-Inverse document frequency (TFIDF) is to get keywords and weights of the words and secondly, Vector Space Model has been used to generate abstract text into a vector. They have also done literature survey on different useful topics which are vector space model, text mining, text preprocessing, and TF/IDF. The result of

this research shows that automatic text summarizer produces a summary consisting of more than three same sentences compared to the manual summary generated.

Ramachandran et al. [13] proposed a model that uses graph-based summarization to generate related texts for short answer scoring. By matching the student response with one or more sample texts, it is possible to generate an automated scoring of short answers. Each provided text may contain very specific and different correct responses, and finding and hand-creating short answer may be very time consuming and expensive by these responses. In this proposed model, they used the top scoring responses. They use a graph-based cohesion technique that extracts the content from the top score responses. They used a tool called MEAD which is a state-of-the-art extractive technique. They described the graph-# based cohesion technique and about the MEAD tool also. The corpus was used as data containing short answers from two different sources: Beetle and SciEntsBank. In result, graph-based cohesion technique generated summary that contains 62 words for Beetle and average of 39 for SciEntsBank . The results show that the approach can be successfully applied to improve the score of short answers responses.

Khan et al. [14] proposed a text summarization model. They used extractive summarization based on k-means clustering with TF-IDF. This research article also reflects on the idea of true K and using that value of K divides the sentences of the input document to present the summary as result. In this, they merge the k-means and TF-IDF with the provided k -value and predict the resulting summary, which is best result. In this article, they described the clustering, k-means clustering, and TF-IDF in very detail. They have also done some literature work and described the literature work in detail also. They showed the experimental elbow method diagrammatically.

3 Methodology Used

In this section, a general purpose graph-based summarization technique called text rank algorithm is applied for summarization of the text document. The text rank algorithm is a type of graph-based algorithm. The graph-based extractive cohesion technique are applied to group the sentences that represents the relationship between sentences. The text rank algorithm are used for ranking the sentences for our text summarization model. Before applying the text rank algorithm, Pre-processing has to be done, that generates a structured representation of the given text input. The pre-processing of the text includes the following steps:

- Sentences boundary identification: In English, the boundary of the sentence is identified with the presence of a dot or question mark at the end of the sentence.
- Stop-word elimination: In the words which have no contribution for selecting the important sentences as prepositions, articles, pronouns means common word with no semantics has been removed.
- Stemming: Stemming is nothing but obtaining of the radix of each words, which indicates its semantics.

After preprocessing, the text summarization model is applied. In this step, features emphasizing the importance of sentences are determined and calculated. The weights are assigned to these features after identification of the important sentences using the weight learning method. By using feature-weight equation, final score of each tokenized sentences is determined. Top-ranked sentences will get the chance to be in final summary. It is evident that the summary of the paragraphs should be coherent. This should be precise and meaningful in nature so that reader can understand the actual meaning of the text as given in the input set. The steps are as follows:

1. Convert the paragraph in sentences.
2. Text processing.
3. Tokenization.
4. Evaluate the weighted occurrence frequency of the words.
5. Substitute words with their weighted frequencies.

3.1 Term Frequency-Inverse Document Frequency

TF-IDF searches important data in the corpus, and figure out most relevant data for generating the summary in the document. Term frequency measures the occurrence of a word in the document, so the word that occurs frequently in the document is probably important data for the summary. Inverse document frequency measures the occurrence of a word in an entire set of document or corpus.

Steps to compute TF-IDF:

1. Compute term frequency (TF):

$$\text{TF}(t, d) = N(t, d) \quad (1)$$

Term frequency for a term t in document d ,

2. Compute Inverse Document frequency (IDF):

$$\text{IDF}(t, d) = N(t, d) \quad (2)$$

Inverse Document frequency for term t in document d ,

3. Compute Term Frequency-Inverse Document frequency

$$\text{TF-IDF}(t, d) = \text{TF}(t, d) * \text{IDF}(t, d) \quad (3)$$

Term Frequency-Inverse Document frequency of term t in document d .

3.2 Graph Method for Summarization

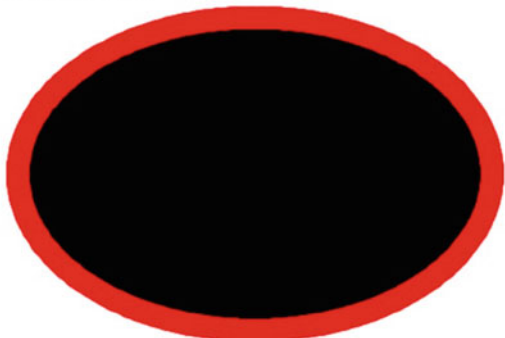
Graph-based approach is used for summarizing the text. This method is extractive method. In this, the generated graph represents the documents as a connected graph and in the graph, vertices represent sentences of the graph and edges represent the relationship between the sentences. This relationship measures the similarity between the two sentences. A common technique on a graph-based approach is to connect two vertices to measure the similarity of two sentences and if it is greater than a certain threshold, the sentences are connected. The most commonly used method for measuring similarity is TF-IDF, which returns weights for words. It results in two outcomes. The first is the creation of discrete important topics covered in the documents, and the second is the identification of important sentences in the document. Vertices that are connected to many other vertices in the graph are possibly the very important sentence in the graph and that is more likely to be included in the summary. Graph-based approach can be used for both single and multi-document summarization. Similarity evaluation of sentences using TF-IDF weighting scheme has some limitations as it only requires the frequency of words as an input and does not take syntactic and semantic information to measure similarity. Thus, the syntactic and semantic information-based similarity measures improve the performance of the summarization system but still TF-IDF provides us with enough details to summarize the document. Figure 1 represents the network of the entities of the text with their association.

3.3 Text Rank Algorithm

Text rank algorithm is used for ranking the sentences in the document. The text rank algorithm is completely based on the page rank algorithm [15]. The page rank algorithm is used by Google since this algorithm rank the websites for showing the

Fig. 1 Network of all entities in the text sample

Number of edges 95586
Number of vertices 540



The memory used by the graph in Bytes is: 56

search result of Web pages. The working procedure of text rank algorithm is similar to the page rank algorithm where sentences are used in place of pages. Text rank algorithm used same formula of the page rank algorithm which is as follows:

$$TR(s) = (1 - d) + d(TR(T1)/C(T1) + \dots + TR(Tn)/C(Tn)) \quad (4)$$

$TR(s)$ is the text rank of the sentence s and d is the damping factor that can be put between 0 and 1. The graph is symmetrical in case of text rank algorithm, and does not require any training as it is a unsupervised method. After this algorithm, we have picked up top-ranked sentences and generated the summary from those sentences.

4 Result and Discussion

In this section, the verification and validation of the summarizer model is discussed. The summarization model used the text document as a input. This text document contains five hundred forty (540) sentences of a story. Our proposed model produced the result of ninety eight (98) sentences by picking important sentences using TF-IDF. Figures 2 and 3 show the content of input document and the summarized output, respectively, which are shown as follows:

Venu had spent the day with his mother at the busy bazaar in Kodaikanal town selling their crops of fresh cauliflower, cabbage, garlic and onions. As they wearily made their way back to their village, Venu played his flute. He carried this flute everywhere and played exquisite music which always made his mother happy. On entering their farmhouse in Vilpatti, Venu sat on a stool next to the bed where his father was resting. 'Tantai,' said the boy, 'please eat some more rice. It does not look like you have eaten at all today and the doctor said you need to try and keep eating regularly so that you might keep up your strength.' The old man looked lovingly at his son. 'Venu, my sweet boy, the doctor says all sorts of things, but the truth is my health is getting no better. If only I had not worked in that mining factory for all those years I am sure my health would not be so bad. Poor Adhir's wife has received no compensation from the company after losing her husband and he worked so hard. What does the company do? They just brush it aside under the carpet as if nothing happened. They are getting away with murder!'

Venu was always upset whenever his father spoke of his illness. 'Tantai, please don't talk like that, it makes me sad. I love you, Tantai!'

'I love you too, my boy, but there is no future for you here.' It was then that the old man's face took on a very serious expression. 'That is why you must leave this place. I do not want you ever working in the mining factory. Not ever!'

'But I don't want to leave, Tantai. I love the forest and have many friends here. I don't want to leave.'

The boy was very upset at his father's words and he began to cry, but the old

Fig. 2 Sample of input text

After the merchant had left from the city Dick was on his own again with the mice and rats crawling over him by night and the cook being even nastier in the day because there was no-one to stop her. The other thing that made Dick sad was that he had to sleep in a tiny room at the very top of the house and it was full of rats and mice that crawled all over his face and tried to bite his nose. 'And one day soon,' he thought, 'I will return home to my family and to Laila and the kurinji flowers, and all of the beautiful gifts of the forest.' 'And one day soon,' he thought, 'I will return home to my family and to Laila and the kurinji flowers, and all of the beautiful gifts of the forest.'

In Banaras District there is a village called Bira in which an old, childless widow used to live. 'Yes, Tantai,' he said in a quiet voice, 'I understand that you love me and want what is best for me so I will go to London.'

Venu held his father as tightly as he could because he did not know when he would see him again. 'Yes, Tantai,' he said in a quiet voice, 'I understand that you love me and want what is best for me so I will go to London.'

Venu held his father as tightly as he could because he did not know when he would see him again. The man explained how many of the people who worked for the charity had listened to the song on the internet and how they were all very impressed. The man explained how many of the people who worked for the charity had listened to the song on the internet and how they were all very impressed. But he carried a glimmer of hope in his heart; He hoped that one day he would return to the forest, that he would come back and see the tall trees and the monkeys. But he carried a glimmer of hope in his heart; He hoped that one day he would return to the forest, that he would come back and see the tall trees and the monkeys. People went to Panditji and asked him to

Fig. 3 Extracted output sample of the input text

5 Conclusion

In this article, a text summarization model using text rank algorithm is proposed and implemented. It is a general purpose graph-based approach. The model is very helpful for summarizing the large amount of data. In extractive approach, graph-based method for establishing relationship between sentences and text rank algorithm for assigning the rank to the sentences has been applied. The rank assigned to the sentence denotes the significance of the sentence and summarizes the sentence on the basis of the rank. The produced result shows the significant summarization of the given input text, i.e., meaningful and abstract. Further, various deep learning models such as encoder, LSTM, and its variants can be studied to obtain better summarization of the input text. These models may help in reducing the complexity and automation of the summarization process.

References

1. Gupta, V., Lehal, G.S.: A survey of text summarization extractive techniques. *J. Emerg. Technol. Web Intell.* **2**(3), 258–268 (2010)
2. Das, D., Martins, A.F.T.: A survey on automatic text summarization. *Liter. Surv. Lang. Stat. II Course at CMU* **4**(192–195), 57 (2007)
3. Sabharwal, M.: The use of soft computing technique of decision tree in selection of appropriate statistical test for hypothesis testing. In: *Soft Computing: Theories and Applications*, pp. 161–169. Springer (2018)

4. Motwani, K.R., Jitkar, B.D.: A model framework for enhancing document clustering through side information. In: Soft Computing: Theories and Applications, pp. 195–207. Springer (2018)
5. Mohd, M., Hashmy, R.: Question classification using a knowledge-based semantic kernel. In: Soft Computing: Theories and Applications, pp. 599–606. Springer (2018)
6. Mahajan, R.: Emotion recognition via EEG using neural network classifier. In: Soft Computing: Theories and Applications, pp. 429–438. Springer (2018)
7. Villa-Monte, A., Lanzarini, L., Bariviera, A.F., Olivas, J.A.: User-oriented summaries using a PSO based scoring optimization method. *Entropy* **21**(6), 617 (2019)
8. Qazvinian, V., Radev, D.R.: Scientific paper summarization using citation summary networks. In: Proceedings of the 22nd International Conference on Computational Linguistics, vol. 1, pp. 689–696. Association for Computational Linguistics (2008)
9. Saggion, H., Lapalme, G.: Concept identification and presentation in the context of technical text summarization. In: NAACL-ANLP 2000 Workshop: Automatic Summarization (2000)
10. Allahyari, M., Pouriyeh, S., Assefi, M., Safaei, S., Trippe, E.D., Gutierrez, J.B., Kochut, K.: Text summarization techniques: a brief survey. [arXiv:1707.02268](https://arxiv.org/abs/1707.02268) (2017)
11. Wu, P., Zhou, Q., Lei, Z., Qiu, W., Li, X.: Template oriented text summarization via knowledge graph. In: 2018 International Conference on Audio, Language and Image Processing (ICALIP), pp. 79–83. IEEE (2018)
12. Cepi Slamet, A.R., Atmadja, D.S., Maylawati, R.S., Lestari, W.D., Ali Ramdhani, M.: Automated text summarization for Indonesian article using vector space model. In: IOP Conference Series: Materials Science and Engineering, vol. 288, p. 012037. IOP Publishing (2018)
13. Ramachandran, L., Cheng, J., Foltz, P.: Identifying patterns for short answer scoring using graph-based lexico-semantic text matching. In: Proceedings of the Tenth Workshop on Innovative Use of NLP for Building Educational Applications, pp. 97–106 (2015)
14. Khan, R., Qian, Y., Naeem, S.: Extractive based text summarization using k-means and tf-idf (2019)
15. Langville, A.N., Meyer, C.D., Fernández, P.: Google’s pagerank and beyond: the science of search engine rankings. *Math. Intell.* **30**(1), 68–69 (2008)

Clifford+T-based Fault-Tolerant Quantum Implementation of Code Converter Circuit



Laxmidhar Biswal, Chandan Bandyopadhyay, and Hafizur Rahaman

Abstract Design of high-scalable quantum information processor (QIP) towards achieving quantum supremacy is still now in infancy due to catastrophic obstacles from decoherence. In way to address this problem, the use of quantum error correction code (QECC) and fault-tolerant circuit is highly enticiable, which further promises not only to protect extreme fragile quantum state from decoherence but also from other noises. It is seen that the fault-tolerant property can be achieved by the use of transversal primitive unitary operators. Here, we show the design of fault-tolerant implementation of BCD-to-Excess-3 and 2's complement code converter which is pivotal in the design of high-scalable QIP. In this transformation process, first we transform the input circuit to an intermediate form where we obtain its NCV-based representation. In the second phase, this design is extensively used to form the fault-tolerant design. We also have compared our design with some of the existing works and have registered 39% improvement in design cost. In terms of *T-count* and *T-depth* metrics, our proposed designs also provide near-optimal solution.

Keywords Clifford+T · QECC · Excess-3 · 2's complement · *T-depth* · *T-count*

1 Introduction and Motivation

In recent years, quantum computer has emerged as a new computational machine in alternation to classical computer that promises to solve some certain problems with exponential faster which could not be solved by so-called classical computer

L. Biswal (✉) · H. Rahaman
School of VLSI Technology, IEST Shibpur, Howrah, India
e-mail: laxmidhar.cvrce@gmail.com

H. Rahaman
e-mail: hafizur@vlsi.iests.ac.in

C. Bandyopadhyay
Department of Information Technology, IEST Shibpur, Howrah, India
e-mail: chandanb.iest@gmail.com

[1, 2]. On the other side, due to the power loss [3] and atomic limit [4]; the current CMOS technology is facing great embarrassment while designing hardware to encode that powerful quantum algorithm. To address this issue, the concept of quantum information processor (QIP) is evolved as new information processor based on reversible logic [5], and quantum mechanics [6] which operates on quantum bit known as qubit. Apart from the field of circuit design, quantum computing has many more promising applications in various disciplines, *viz.* searching, optimization, secure computing, machine learning, material science, cryptography, quantum chemistry, sampling, condensed matter physics and quantum dynamics [7]. However, it is hard to realize an efficient quantum circuit due to opposition of no-cloning theorem [8] in logical level and decoherence in physical level [9]. Thus, robust QIP, fault-tolerant quantum circuit is mostly desirable [10] which can be achieved by continuous encoding-decoding into quantum error correction code (QECC).

In this regard, the popular 2-D NN compliance surface code has been used [11] for highest threshold limit (approximately 0.75%), low size of stabilizer operators, i.e. 4, which enable to initialize all ancillary qubits simultaneously [12]. However, to protect error rate per gate of the quantum circuit within threshold limit of QECC on account of decoherence is an important matter of concern.

In this conjecture, a set of primitive transversal operators are the only solution to address all these concerns. In this regard, the Clifford+T-group has been used as universal gate set that contains quantum gate, namely H -gate, S -gates, T -gate and two qubit $CNOT$ gate [13]. Consequently, the surface code implemented over Clifford+T has turned to be the default technology for performing design of fault-tolerant quantum computation [14].

Moreover, achieving quantum supremacy in theory as well as in practice is considered as prime objective which needs high potential QIP. The code converter circuit is an important block of every processor, especially binary-to-BCD and BCD-to-Excess-3 code in arithmetic logic unit (ALU) [15]. Now, here, we are reviewing some the related works in Sect. 1.1 and then presenting our problem statement in Sect. 1.1.1.

1.1 Previous Work and Problem Definition

The close Hamiltonian of any quantum circuit is reversible in nature for which reversible circuit is considered as an integral part of the quantum circuit. BCD-to-Excess-3 code converter circuit based on reversible logic using universal reversible gate (URG) and Feynman gate (FG) is reported in [16]. On the other hand, incorporation of large number of garbage outputs turns a design costly due to the loss of energy, so it is necessary to achieve reversibility. In [17], zero garbage output-based code converter circuit is reported where TSG gate is used to design the circuit. Though in the design, no garbage outputs are used, but the overall quantum cost of the design has gone up. Like as [17], a similar work is reported in [18] where, inspite of TSG

gate, HNG gate is used in the design and this approach has successfully reduced the cost of the converter circuit.

Maity et al. has proposed a low quantum cost-based code converter circuit using NG and PG gate [19], but the decomposition of NG gate into primitive quantum operator is erroneous. Recently, an optimized code converter circuit based on PG, CNOT and NOT gate is reported [20] where the cost of the design has reduced considerably. In fact, none of the approaches amount to property of fault tolerance which is mostly desirable for efficient quantum computation.

1.1.1 Contribution

In this paper, we propose a new approach where we shown the design of BCD-to-Excess 3 code converter in quantum domain. Our design policy not only attributed towards the fault-tolerant design but aimed to make the design efficient by lowering the phase depth which is necessary to limit the decoherence. At the end, we also have also proposed fault-tolerant quantum Excess-3 code-based binary adder and 4-bit BCD-to-2's complement code converter. Our designed circuits will not only help towards the realization of efficient ALU but also will contribute to improve the QIP model.

The rest of the paper is organized as follows: In Sect. 2, the principle of reversibility, reversible gate, quantum circuit and performance parameter is discussed. In Sect. 3, our approach is presented. In Sect. 4, experimental result and comparative analysis are described. Finally, the work is concluded in Sect. 5.

2 Preliminaries

This section provides essential preliminaries on quantum logic and its associated cost functions.

2.1 Reversible Circuit and Reversible Gate

Definition 1 (*Reversible gate*) Any gate that maps from each input assignment into unique output vector is called a reversible gate.

Basically, reversible gate has equal number of inputs and outputs. Toffoli, Fredkin gates are examples of well-known reversible gates.

Definition 2 (*Reversible circuit*) A circuit formed with reversible gates only is known as reversible circuit.

2.2 Quantum Circuit and Performance Parameters

Definition 3 (*Quantum circuit*) Entanglement of primitive unitary operators operating over qubits is known as quantum circuit and that set of primitive elementary operators are called quantum gates.

For better apprehension, a list of elementary quantum gates with their properties is presented in Table 1.

Definition 4 (*Quantum cost*) It can be defined as the minimum number of primitive unitary operators used in the quantum circuit to represent any Boolean function.

Definition 5 (*T-count*) It can be defined as the minimum number of primitive unitary operators exist in Clifford+T-based representation of input function.

Definition 6 (*T-depth*) The minimum number of *T*-cycle required to execute all the *T*-gate in a Clifford+T circuit is termed as *T-depth*.

Table 1 Elementary quantum gates and properties

Name of elementary quantum gate	Block diagram	Transformation matrix	Properties
NOT (X)		$\begin{bmatrix} 0 & 1 \\ 1 & 0 \end{bmatrix}$	$X 0\rangle = 1\rangle$ $X 1\rangle = 0\rangle$
CNOT(CN)		$\begin{bmatrix} 1 & 0 & 0 & 0 \\ 0 & 1 & 0 & 0 \\ 0 & 0 & 0 & 1 \\ 0 & 0 & 1 & 0 \end{bmatrix}$	$ 00\rangle \rightarrow 00\rangle$ $ 01\rangle \rightarrow 01\rangle$ $ 10\rangle \rightarrow 11\rangle$ $ 11\rangle \rightarrow 10\rangle$
Z gate		$\begin{bmatrix} 0 & 0 \\ 0 & -1 \end{bmatrix}$	$X 0\rangle = 0\rangle$ $X 1\rangle = - 1\rangle$
S gate		$\begin{bmatrix} 1 & 0 \\ 0 & i \end{bmatrix}$	$S 0\rangle = 0\rangle$ $S 1\rangle = e^{\frac{i\pi}{2}} 1\rangle$
S^\dagger gate		$\begin{bmatrix} 1 & 0 \\ 0 & e^{\frac{-i\pi}{2}} \end{bmatrix}$	$S^\dagger 0\rangle = 0\rangle$ $S^\dagger 1\rangle = e^{\frac{-i\pi}{2}} 1\rangle$
<i>T</i> gate		$\begin{bmatrix} 1 & 0 \\ 0 & e^{\frac{i\pi}{4}} \end{bmatrix}$	$T 0\rangle = 0\rangle$ $T 1\rangle = e^{\frac{i\pi}{4}} 1\rangle$
T^\dagger gate		$\begin{bmatrix} 1 & 0 \\ 0 & e^{\frac{-i\pi}{4}} \end{bmatrix}$	$T^\dagger 0\rangle = 0\rangle$ $T^\dagger 1\rangle = e^{\frac{-i\pi}{4}} 1\rangle$
Hadamard (H)		$\frac{1}{\sqrt{2}} \begin{bmatrix} 1 & 1 \\ 1 & -1 \end{bmatrix}$	$H 0\rangle = \frac{1}{\sqrt{2}}(0\rangle + 1\rangle)$ $H 1\rangle = \frac{1}{\sqrt{2}}(0\rangle - 1\rangle)$

2.3 BCD Code, Excess-3 Code and 2's Complement Code

Definition 7 (BCD) Binary-coded-decimal (BCD) code is also known as 8421 code, where each digit of decimal number is represented through fixed number of binary digits, usually 4-bits.

Definition 8 (Excess-3 code) Excess-3 binary code is a unweighted self-complementary BCD code generated by adding (0011) into BCD (8-4-2-1)-code.

The most significant property of this code is that the 1's complement of an Excess-3 number is the Excess-3 code of the 9's complement of the corresponding decimal number and this is the reason for which it is known as self-complementary code. This code has wide range of applications in arithmetic operation, viz. addition and subtraction.

Definition 9 (2's complement code) 2's complement is a method to represent values of both positive and negative integer in binary. The novelty of 2's complement is auto inclusion of sign bit and same method is followed while performing arithmetic operation over both signed and unsigned integer.

The 2's complement code can be found by adding 1 into 1's complement code. The 1's complement code for any given BCD can be derived by flipping each bit, i.e. '0' to '1' and vice-versa.

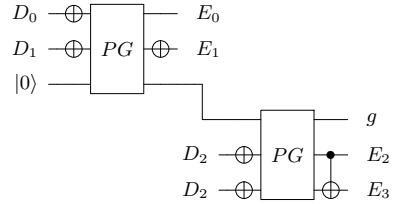
3 Proposed Technique

In this section, we have shown an efficient implementation of converter circuits. In the first design, we have shown the Clifford+T-based design of BCD-to-Excess 3 code converter, and BCD-to-2's complement code converter circuit is proposed in the second design. Both the designs are made on top of Clifford+T library where NCV quantum gate library has been used for intermediate representation.

3.1 4-Bit BCD-to-Excess-3 Code Converter Quantum Circuit

From any BCD code to its equivalent Excess-3 code can be generated by simply adding (0011) into given (8-4-2-1)-weighted based BCD code. Here, input 4-bit BCD code is represented by D_0, D_1, D_2, D_3 , whereas E_0, E_1, E_2, E_3 represent corresponding Excess-3 code. As the reversible circuit is basic building block of quantum circuit, overall circuit could resume quantum property on account of replacement of each small unit of reversible circuit with its equivalent quantum operators. Usually, this code conversion is achieved in reversible domain by using four-bit reversible carry look ahead adder circuit as stated in literature. However, same task can be performed directly by using two Peres gate (PG) that eventually will leads to lower

Fig. 1 BCD-to-Excess-3 code converter using PG, FG and NOT as presented in [20]



design overheads. To make the proposed designs efficient, here a template matching scheme is used over an intermediate design which further is pre-optimized.

As we have stated previously, the reversible code converter circuit of [20, Fig. 2] is used here as an intermediate reversible circuit. The intermediate design is shown in Fig. 1.

By examining the design of Fig. 1 is composed of PG gate, CNOT and NOT gate only. Here, each unit of reversible operator(s) within Fig. 1 is considered as template(s) which now is to be mapped into most promising Clifford+T-group that consists traversal primitive quantum operator(s). In fact, unlike PG gate, both NOT, and CNOT gates are part of Clifford+T-group which remain unaltered during mapping. On other hand, equivalent Clifford+T-based circuit of reversible PG gate can be derived from Fig. 2b and through Fig. 2c.

The NCV-based realization of PG gate into Clifford+T-group can be transformed through another intermediate architecture using Jacobian by the help of two H -gate. Here, the mathematical model of [21] is used extensively in mapping of PG gate into low phase depth-based quantum circuit. The PG gate consists of one Toffoli gate and one CNOT gate each. So without exercising the mathematical model in details; the

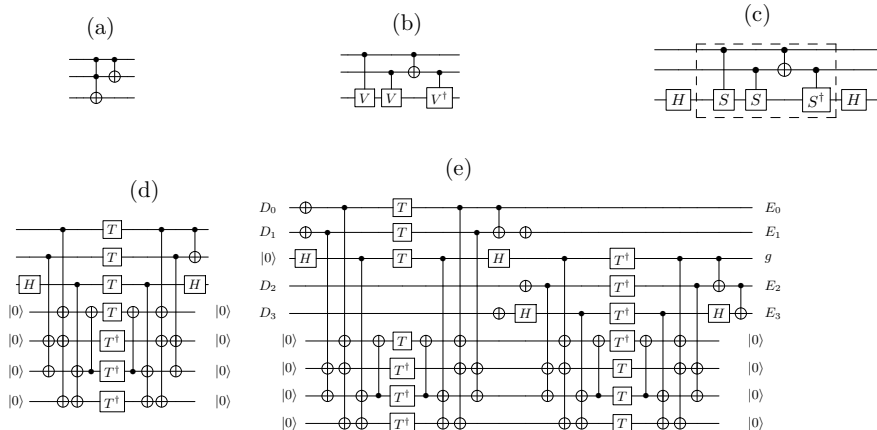


Fig. 2 **a** PG gate. **b** NCV realization of PG gate. **c** NCV realization of PG gate. **d** Clifford+T-based PG gate. **e** Clifford+T-based Excess-3 code converter circuit

Toffoli gate is replaced by its equivalent Clifford+T representation as presented in [21] and resulting Clifford+T-based PG gate is given in Fig. 2d.

Now, all the templates of Fig. 1 are replaced by its equivalent Clifford+T-based equivalent templates and the resulting quantum circuit is presented in Fig. 2e.

3.2 4-Bit BCD-to-2's Complement Code Converter Quantum Circuit

Here, Clifford+T-based BCD-to-2's complement code converter circuit is proposed. The input 4-bit BCD code is represented by D_0, D_1, D_2, D_3 , whereas C_0, C_1, C_2, C_3 represent corresponding 2's complement code. An efficient Clifford+T-based quantum circuit can be derived from any reversible BCD-to-2's complement code converter circuit by means of template matching scheme as stated in earlier section. The reversible circuit that presented in [19, Fig. 5] is used here as intermediate reversible structure that contains reversible NG gate and FG gate. However, the decomposition of that reversible NG gate is problematic but the comparison table in [19, Table 3] is erroneous too.

Our proposed mapping scheme for reversible circuit to Clifford+T-group is splitted into two phases. In phase-1, we have proposed a new reversible gate which is termed as MNG gate. In phase-2, quantum domain design of BCD-to-2's complement code converter circuit is proposed.

3.2.1 Proposed Reversible MNG gate

The proposed MNG gate maps from input $I_v(A, B, C, D)$ to $O_v(P, Q, R, S)$ with a functional relationship $P = \bar{A}$, $Q = A \odot B$, $R = \bar{A} \cdot \bar{B} \oplus C$. Figure 3a depicts the block diagram of reversible MNG gate. Subsequently, Fig. 3b presents equivalent

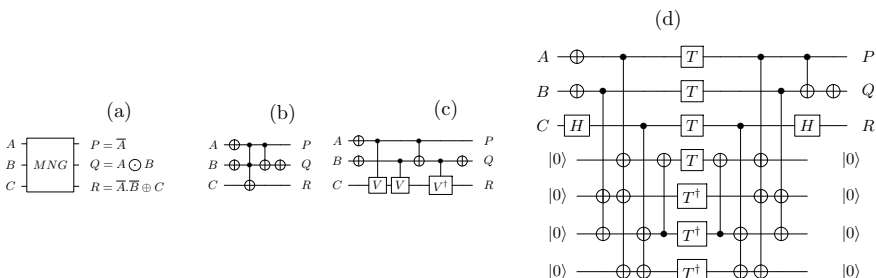


Fig. 3 **a** Block diagram representation of purpose MNG gate. **b** Toffoli-based realization of reversible MNG gate. **c** Decomposition of reversible MNG gate into elementary quantum operator. **d** Clifford+T-based implementation reversible MNG gate

Toffoli-based realization of MNG gate and its equivalent quantum decomposition is presented in Fig. 3c. The decomposition of MNG gate incurs 7 quantum cost (QC). Finally, Fig. 3c maps into Clifford+T-group using methodology stated in [21] and resulting circuit is presented in Fig. 3d. The mapping of newly proposed MNG gate into BCD-to-2's complement code converter quantum circuit is described in the next subsection.

3.2.2 Proposed BCD-to-2's Complement Code Converter

The proposed 2's complement code converter quantum circuit is designed by using two MNG gate and one CNOT gate formed design is presented in Fig. 4b. The proposed Clifford+T-based 2's code converter can be derived from Fig. 4b by using replacement approach based on template matching scheme.

Figure 4b is scanned from left and in top-down fashion where the MNG gate is replaced by its equivalent Clifford+T structure, i.e. Fig. 3d. Final representation is presented in Fig. 5 after due procedure of mapping and cancellation of redundant gates.

On view of the performance, the proposed design structure of code converter circuit has 14 T-count and 2 T-depth.

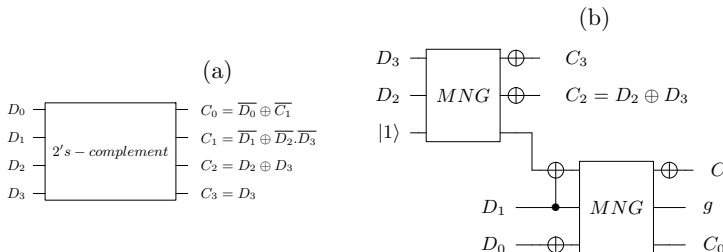


Fig. 4 **a** Block diagram representation of proposed code converter. **b** Proposed reversible BCD-to-2's complement code converter circuit using reversible MNG gate

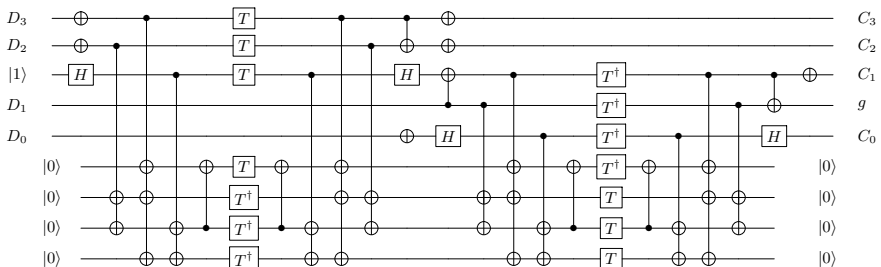


Fig. 5 Clifford+T-based proposed BCD-to-2's complement code converter circuit with optimized in T-depth

4 Comparison with Previous Work and Analysis

In this paper, we have designed two code converter circuit in quantum domain which is essential part of the ALU towards the realization of high-scalable QIP. Prior to this work, multiple works on code converter circuit are already being reported which is discussed in Sect. 1.1. Here, both the code converter circuits are analysed separately as follows: the Clifford+T-based representation of BCD-to-Excess 3 code converter circuit is depicted in Fig. 2e. This design is optimal in terms of cost overhead. To ensure the optimality in *T-depth*, four ancilla input has been added; otherwise, the phase depth would become 6 in lieu of 2. On finding the performance of the proposed designs, it is seen that the circuit has 14 in *T-count* and 2 in *T-depth*. As, the none of the works from the present state of the art is in this domain; thus, we are unable to compare the above design.

In Sect. 3.2, a low *T-depth* and QC-based quantum circuit have been proposed for BCD-to-2's complement code converter. The design of Fig. 4b contains two MNG gates along with four CNOT gates and one NOT gate. A pair of NOT gate that presented in upper MNG gate is cancelled while decomposing of Fig. 4b into NCV quantum gate library. So, the proposed circuit has incurred 17 QC which is 39.28% lower w.r.t. design-1 of [22] and 52.77% w.r.t. design-2 of [22].

On other hand, the proposed quantum circuit as presented in Fig. 5 is also design efficient due to low *T-depth*, i.e. 2 which is most desirable for fault-tolerant quantum computation. There is hardly exist any fault-tolerant quantum circuit for this code converter circuit for which proposed design could not be compared with any other works.

5 Conclusion and Future Work

The authors have proposed Clifford+T-based quantum circuit for two code converter models, *viz.* 4-bit BCD-to-Excess 3 and BCD-to-2's complement. The function of both the code converters circuit has high significance in the operation of ALU. Our proposed design approach is not only efficient in the view of fault tolerance but also addresses decoherence due to low execution time. The proposed design approach will be very useful towards designing high-scalable QIP which is most desirable to achieve quantum supremacy.

References

1. Shor, P.W.: Polynomial-time algorithms for prime factorization and discrete logarithms on a quantum computer. *SIAM J. Sci. Statist. Comput.* **26**, 1484–1509 (1997)
2. Grover, L.K.: Quantum mechanics helps in searching for a needle in a haystack. *Phys. Rev. Lett.* **79**, 325–328 (1997)

3. Landauer, R.: Irreversibility and heat generation in the computing process. *IBM J. Res. Develop.* **5**(3), 183–191 (1961)
4. Moore, G.E.: Cramming more components onto integrated circuits. *Electronics* **38**(8) (1965)
5. Bennett, C.H.: Logical reversibility of computation. *IBM J. Res. Develop.* **17**(6), 525–532 (1973).<https://doi.org/10.1147/rd.176.0525>
6. Feynman, R.P.: Quantum mechanical computers. *Found. Phys.* **16**, 507–531 (1986)
7. <https://blog.usejournal.com/quantum-computings-promise-for-the-brave-&-new-world-fa15b651cced>
8. Wootters, W.K., Zurek, W.H.: A single quantum cannot be cloned. *Nature* **299**, 802–803 (1982)
9. DiVincenzo, D.P.: The physical implementation of quantum computation. *Fortschr. Phys.* **48**, 771
10. Preskill, J.: Fault tolerant quantum computation. In: Lo, H.K., Popescu, S., Spiller, T. (eds.), *Introduction to Quantum Computation and Information*, Chap. 8, p. 213. World Scientific, River Edge, NJ (1998). <https://arxiv.org/abs/quant-ph/9712048>
11. Fowler, A.G., Mariantoni, M., Martinis, J.M., Cleland, A.N.: Surface codes: towards practical large-scale quantum computation. *Phys. Rev. A* **86**, 032324 (2012)
12. Fowler, A.G., Stephens, A.M., Groszkowski, P.: High threshold universal quantum computation on the surface code. *Phys. Rev. A* **80**, 052312 (2009)
13. Paetznick, A., Reichard, B.W.: Universal fault-tolerant quantum computation with only transversal gates and error correction. *Phys. Rev. Lett.* **111**(9), 090505 (2013)
14. Jones, N.C., Whitfield, J.D., McMahon, P.L., Yung, M.H., Meter, R.V., Aspuru-Guzik, A., Yamamoto, Y.: Faster quantum chemistry simulation on fault-tolerant quantum computers. *New. J. Phys.* **14**, 115023 (2012)
15. <https://bitshifters0.files.wordpress.com/2015/03/digital-logic-and-computer-design-by-morris-mano-2nd-edition.pdf>
16. Saravanan, M., Manic, K.S.: Energy efficient code converters using reversible logic gates. In: *IEEE International Conference Green High Performance Computing (ICGHPC)*, pp. 1–6 (2013)
17. Thapliyal, H., Arabnia, H.R., Bajpai, R., Sharma, K.K.: Design of testable reversible sequential circuits. *IEEE Trans. Very Large Scale Integr. (VLSI) Syst.* **21**(7), 1201–1209 (2013)
18. Haghparast, M., Hajizadeh, M., Hajizadeh, R., Bashiri, R.: On the synthesis of different nanometric reversible converters. *Middle-East J. Sci. Res.* **7**, 715–720 (2011)
19. Maity, H., Barik, A.K., Biswas, A., Bhattacharjee, A.K., Pal, A.: *J. Circuit. Syst. Comput.* **27**, 1850184 (2018)
20. Maity, H., Biswas, A., Pal, A., Bhattacharjee, A.K.: Design of BCD to Excess-3 code converter circuit with optimized quantum cost, garbage output and constant input using reversible gate. *Int. J. Quant. Inf.* **16**(07), 1850061 (2018)
21. Biswal, L., Das, R., Bandyopadhyay, C., Chattopadhyay, A., Rahaman, H.: A template-based technique for efficient Clifford+T-based quantum circuit implementation. *Microelectron. J.* **81**, 58–68 (2018)
22. Shukla, V., Singh, O.P., Mishra, G.R., Tiwari, R.K.: Design of a 4-bit 2's complement reversible circuit for arithmetic logic unit applications. In: *Proceedings of International Conference in Communication Computing and Information Technology (ICCCMIT) Special Issue of International Journal of Computer Applications*, pp. 1–5. Chennai, India (2012)
23. Gandhi, M., Devishree, J., Venkatesh, J., Sathish Mohan, S.: Design of reversible circuits for code converter and binary incrementer. *J. Inf. Technol. Mech. Eng. (IJITME)* **1**, 24–33 (2014)

Applying Deep Learning for Discovery and Analysis of Software Vulnerabilities: A Brief Survey



Shashank Kumar Singh and Amrita Chaturvedi

Abstract Machine learning has been proved very successful in analyzing and detecting software vulnerabilities. One of the limitations of machine learning is that it heavily depends on human expertise for feature selection. Deep learning can be used to reduce this burden of manual feature selection. The objective of this paper is to survey the feasibility and advantages of applying deep learning techniques for the analysis and detection of software vulnerability. However, deep learning has been developed for a very different class of problems so it needs to be tailored in such a way that it can easily fit in the application of software vulnerability. This paper emphasizes on all such modifications required for deep learning approaches to efficiently accommodate the problem of detection of software vulnerabilities. We have also discussed the various vulnerability databases/resources and some of the recent successful applications of deep learning in predicting vulnerabilities present in the software.

Keywords Machine learning · Deep learning · Software security practices · Software vulnerabilities

1 Introduction

Although there have been various advances in the field of programming languages, still software can be easily subjected to bugs, errors, and vulnerabilities. The common vulnerability and exposure (CVE) have around 12% more vulnerabilities registered from the year 2017 to 2018 [1]. In 2018, there were 16,412 vulnerabilities published, as compared to 14,595 published in 2017. Moreover, it is observed that in [2] that there is a rise of 20% more vulnerabilities in browser-based products. It declares

S. K. Singh (✉) · A. Chaturvedi
Computer Science and Engineering, IIT (BHU), Varanasi, India
e-mail: mail.shashank67@gmail.com

A. Chaturvedi
e-mail: amrita.cse@iitbhu.ac.in

that the company which is most exploited for vulnerabilities is Microsoft and the most vulnerable software product is Google Android. These facts show that even the most recent programming paradigm and the companies practicing modern software engineering methods are not free from bugs, errors, and vulnerabilities. However, the presence of the vulnerabilities in the software itself is not a severe problem but can cause other serious security concerns once got exploited. It may lead a hacker or an intruder to get unauthorized access of the host system or to manipulate host database. Due to the exploitation of vulnerabilities, there have been many security breaches in the past, such as Equifax breach [3], ShellShock [4], Apache Commons [5], WannaCry [6] which have affected millions of people worldwide.

So, proper methodologies and techniques are needed to analyze and detect the vulnerabilities present in the software. However, scientists, academicians, and cyber-security personnel are working on vulnerabilities from the very beginning. Various data mining-based approaches and machine learning methods have been successfully applied in analyzing and detecting vulnerabilities present in a system. A comprehensive survey of such methods was published by Shahriar and Zulkernine [7]. They have described several approaches such as dynamic analysis, static analysis, and various other testing methods which were applied from 1994 to 2010 to mitigate vulnerabilities. Another organized review has been given by Ghaffarian et al. [8] where mostly they have highlighted application of machine learning models (supervised/unsupervised) and pattern matching techniques to tackle the problem of software vulnerabilities. They further suggested that the software vulnerability analysis can also be considered as a computational problem “to find whether, in a given program, any of the known security vulnerabilities exist.” Whereas, another paper [9] advocates that developing a system based on detection of software vulnerabilities cannot be sound and complete simultaneously. Considering its computational nature and completeness, we have to apply some approximation techniques while dealing with this problem. Generally, these conventional approximation approaches are divided into classes such as static, dynamic, and hybrid. A basic comparison between them is provided in Table 1.

Software vulnerability analysis mainly consists of activities such as identifying, prioritizing, giving a definition to the vulnerabilities present in the software [10]. The major concern of these analyses is to make software secure against the violation of vulnerabilities present in them. In the current software industry, several security practices are being followed to mitigate the effect of vulnerabilities. Williams et al. [11] describe 113 such software security practices which are used by 109 different firms. These software security practices are monitored for over more than 4 years. The authors further classified these practices as prevention, detection, and response. Moreover, detecting and analyzing vulnerabilities require trained cybersecurity experts, and according to studies, there would be a lack of approx. 1.8 million experts by 2020 [2]. So, currently, there is a need for methods that can reduce human effort and can easily mitigate the effect of damages done due to presence of a software vulnerability. In present scenario, machine learning has been very effective

Table 1 Comparison of different software vulnerability analysis approaches

S. No.	Metrics	Static analysis	Dynamic analysis	Hybrid analysis
1	Code execution	No	Yes, with specific input	Program is analyzed using mixture of static and dynamic approaches
2	Target code coverage	High	Less	Moderate
3	Soundness/Completeness	At-best be sound	At-best be complete	Cannot be complete and sound simultaneously
4	Application	Information flow	Fuzzing	Mixed approach

in dealing software vulnerabilities. Most of the development in this field is being dominated by machine learning techniques. Table 2 summarizes some of the significant work done in this area. Ghaffarian et al. [8] have given a detailed survey of machine learning approaches applied in this domain. Mainly, the authors have organized these approaches as software metrics-based vulnerability prediction model, pattern recognition based on vulnerable code, anomaly detection-based approaches, and miscellaneous approaches.

Although machine learning has performed nicely while dealing with software vulnerabilities, there are several limitations to it. One of the concerns with machine learning is that it requires manual effort in feature selection. Manual feature selection heavily depends on human expertise, which directly affects the accuracy of the system. Moreover, using machine learning to solve a problem involves dividing it into several sub-processes such as data prepossessing, feature selection (extracting relevant features from data), and model training. This decomposition acts as an overhead in finding a solution to a problem. So, to deal with this overhead, the modern trend is shifting toward a deep learning paradigm. Deep learning approach creates a single end to end system instead of decomposing it into many more sub-processes. So, deep learning approach can be collectively understood as a universal function approximation technique [12] which could reduce human intervention in solving problems by extracting most of the features automatically. Considering these advantages, deep learning has found its applications in many modern problem-solving domains including software vulnerability detection. The rest of this paper summarizes the recent research work done with deep learning in the field of software vulnerability. Various advancements, challenges, and other issues related to the application of deep learning techniques for software vulnerability are also discussed.

Table 2 Different machine learning approaches for predicting software vulnerabilities

Paper	Learning methods	Characteristics
Yamaguchi et al. [13]	Applied principle component analysis	Uses FFmpeg (0.6.0) API usage pattern to find vulnerabilities
Yamaguchi et al. [14]	Applied syntax tree analysis	Uses source code of LibTIFF, FFmpeg, Pidgin and Asterisk to construct a syntactic representation of vulnerable source code
Shar et al. [15]	Uses multilayer perceptron for supervised learning	Applied static analysis to predict vulnerability in PHP web-based application
Shar et al. [16]	Uses classification as well as clustering.	Applied supervised and unsupervised approach to find SQL based vulnerabilities
Hung Nguyen et al. [17]	Applied Naive Bayes, random forest, decision tree, K-nearest neighbor, SVM for classification	Predicts which component contains software vulnerability
Neuhaus et al. [18]	Support vector machines	Suggests that component having import and functions call from same source are likely to be vulnerable
Gegick et al. [19]	CART	Proposed vulnerability model for CISCO software based on collected reports
Chowdhury et al. [20]	Bayesian network, SVM and random forests	Uses coupling, cohesion and complexity of the programs as a metrics to predict vulnerabilities
Grieco et al. [21]	Supervised learning	Applied static analysis as well as dynamic analysis on binary to find vulnerability based on function call sequences
Smith and Williams [22]	Logistic regression	Achieved average precision of 28%, utilize Trac issue reports for predictions
Yamaguchi et al. [23]	Clustering	Uses API function calls to predict vulnerability by applying static approach
Shin et al. [24]	Logistic regression	Uses red hat Bugzilla, Mozilla foundation security advisories (MFSA) as a vulnerability resource and code churn as a metrics to predict the vulnerabilities

2 Deep Learning for Software Vulnerability

Detecting software vulnerability automatically is an important research problem for security experts. However, most of the existing common approaches require human expertise and also these approaches are subjected to a high false-negative rate [25].

Deep learning-based approaches can be used to save from the labor of manual feature selection. But these approaches are mainly developed for a very different class of problems such as computer vision, automatic machine translation, natural language processing, object classification, and character text generation they cannot be directly applied in analyzing software vulnerabilities. So, some basic guiding principles are required for tailoring deep learning methods to deal with software vulnerability.

Li et al. [25] describe such a guiding principle for choosing the granularity of input data while predicting software vulnerabilities using deep learning. However, there are some other important issues too that needs to be explored in detail, such as “what should be the proper representation of software program to act as an input for deep learning architecture?” and even more the choice of deep neural architecture.

2.1 *Choosing Proper Input Data Representation for Deep Neural Network*

Deep learning can be used to build a model, which can learn known vulnerable patterns and can further predict its presence while testing. Such a model must be trained with vulnerable test cases. These test cases are generally in the form of a corpus of text/source code. One of the issues with deep neural networks is that they are incapable of processing text as a direct input; it mainly takes vector or numeric representation as an input. So, in order to use source codes as an input to the deep neural network, source codes need to be converted into vectors. Also, for better efficiency, it is advisable that the source codes must be represented in such a form that the context information is not lost. The context here represents information such as data and control flow dependencies. One of the solutions for abovementioned issues is the use of Word Embeddings [26]. It is a popular approach used in natural language processing for converting programs/text into numeric or vector representation [12].

If the input dataset is having a group based distribution One Hot Encoding [27] can be used as an encoding mechanism. This mechanism simply converts the words into numeric or vector notation. The encoded vector contains the numeric value “1” at the place where that specific word is present in the sentence and the vector has a length equivalent to the total number of words in the sentence.

For further better accuracy, Li et al. [25] suggest the initial conversion of input source code into an intermediate representation, before converting it into fixed-length vectors. The author uses Code Gadget [28] for this purpose. However, one of the most

efficient and popular methods for conversion of text or input into vectors is Word2vec model [29].

2.1.1 Word2vec Model

This algorithm transforms the words as a continuous vector in which the words with the same meaning are mapped nearer or proximity in the n-dimensional vector space. The advantage of this approach is that it produces vectors [30] from unlabeled data or raw corpus of text. There are unique representations for each word as a different vector. In word2vec, user can specify the word embedding vector size, while the total size of the vector space depends upon the total number of the word in the vocabulary. It uses mainly two techniques for the vector representation: (a) Continuous bag-of-words, (b) Continuous skip-gram. In continuous bag-of-words, the missing or context word can be predicted using a neural network with one hidden layer architecture, while in skip-gram model on given a context, the related words can be predicted. However, there are some other modifications of base models such as Fasttext [31], Adagram [32] and Wang2vec [33]. These variant models of word2vec can also be applied in converting the source code to vectors for training deep learning models for vulnerability detection

2.2 Vulnerability Databases/Resources

The software vulnerabilities are mainly the loopholes in the computational logic in the source code which if exploited can produce an adverse effect in confidentiality, integrity, or even data availability, as per the CVE [34]. However, all vulnerabilities are not equally dangerous. There must be classification or standardization so that priority can be made while providing the patches for them. The more dangerous vulnerability must be dealt initially, while a delay can be made while dealing with less vulnerable code. The CVSS provides such an open framework for defining the behavior and impact of these software vulnerabilities. Generally, NVD [34] provides a CVSS score for all the known vulnerabilities. There are two standards for Common Vulnerability Scoring System CVSS v2.0 and CVSS v3.0. These scoring systems are based on FIPS 199 [35] system rating. This system also provides the qualitative ranking of the software vulnerabilities in low, medium, and high based on the score generated. This score can be generated by the online calculator provided by the NVD [36, 37].

There are some of the other groups maintaining the database and other-related information of software vulnerabilities [34, 38–44].

Training deep learning models initially require large amount of dataset to train the architecture for predicting software vulnerabilities. The abovementioned database can be used to obtain such a training dataset.

2.3 Choosing Deep Neural Network Model/Architecture

Neural networks have proved them in solving a variety of difficult tasks in computer vision, natural language processing, signal processing, and speech recognition. These problem domains differ widely from the detecting software vulnerability in their methodologies as well as approach. So, the vulnerability detection problem has to be framed in such a way that hidden vulnerability patterns can be learned by the neural network architectures. These patterns can further be applied to detect vulnerabilities while testing source code or software applications. Some of the software vulnerability patterns depend upon the context information (data dependency and control dependency) [25]. So, the deep learning architecture used must be capable of processing contextual information while applying learning algorithms. In natural language processing, the context plays an important role in text classification, text parsing, question answering. These applications mainly use neural networks such as recurrent neural networks (RNN) and its variants such as GRU and LSTM [45, 46].

The use of RNN is limited as it suffers from vanishing gradient problem while dealing with a large dataset. However to deal with issues its different variants called GRU [47], LSTM [48] was proposed. These architectures have different behavior, and depending upon the nature of the problem, they are applied to solve them. Some of the specific properties of these neural networks are that it can efficiently deal with sequential data and some of the papers utilize this property for program analysis [32, 49, 50]. However, the use of GRU and LSTM is also preferred over RNN as both of them can easily deal with long term dependencies. LSTM has proved better over GRU in many of the applications of language modeling [51]. Even LSTM performance is also limited due to its unidirectional nature. While Li et al. [25] suggest that the arguments of the function call are also very much affected by earlier and later statement in the flow diagram. To accommodate the contextual information, architecture capable of bidirectional information processing must be applied. Bidirectional LSTM [52] is generally applied for this vulnerability detection. This bidirectional architecture is beneficial just because it can easily accommodate the contextual information from both sides, which can lead to better vulnerability predictions.

3 Conclusion

The paper summarizes practical issues and their solution while applying deep learning for the detection and analysis of software vulnerabilities. In this paper, we have tried to provide a detailed overview of current progress and key challenges in the field of applying deep learning for software vulnerability. However, recent papers claim that deep learning is highly successful in detecting software vulnerabilities with high precision but still less work has been done in this area. There is a need for more research to be done to explore deep learning potential in this field. More-

over, there is a possibility that deep learning may learn some of the new complex vulnerable patterns which human cannot easily identify, which in fact could lead us to build a more robust technique to mitigate software vulnerability. Currently, there are many automated and sophisticated methods being deployed to exploit software vulnerabilities so an appropriate shift in mitigation techniques must also be done. Deep learning can be proved very helpful in finding such a mitigation technique. There is also a need for exploring the new advanced deep neural architectures so as to improve the accuracy in predicting software vulnerabilities.

References

1. CVE Details the ultimate security vulnerability datasource. <https://www.cvedetails.com/index.php>. Accessed 30 May 2019
2. Vulnerability and threat trends report. <https://lp.skyboxsecurity.com/WICD2018-02ReportVulnerabilityThreat18Asset.html>. Accessed 30 May 2019
3. Federal trade commission protecting America's consumers. <https://www.ftc.gov/equifax-data-breach>. Accessed 30 May 2019
4. Perlroth, N.: Security experts expect ‘shellshock’ software bug in bash to be significant. <https://www.nytimes.com/2014/09/26/technology/security-experts-expect-shellshock-software-bug-to-be-significant.html>. Accessed 30 May 2019
5. Breen, S.: What do weblogic, websphere, jboss, jenkins, opennms, and your application have in common? this vulnerability. <http://foxglovesecurity.com/2015/11/06/what-do-weblogic-webspherejboss-jenkinsopennms-and-your-application-have-in-common-this-vulnerability/>. Accessed 30 May 2019
6. Belot, H.: Ransomware attack still looms in Australia as government warns wannacry threat not over. <https://www.abc.net.au/news/2017-05-15/ransomware-attack-to-hit-victims-in-australia-government-says/8526346>. Accessed 30 May 2019
7. Shahriar, H., Zulkernine, M.: Mitigating program security vulnerabilities: approaches and challenges. ACM Comput. Surv. (CSUR) **44**(3), 11 (2012)
8. Mohammad Ghaffarian, S., Reza Shahriar, H.: Software vulnerability analysis and discovery using machine-learning and data-mining techniques: a survey. ACM Comput. Surv. (CSUR) **50**(4), 56, r5445
9. Xie, Y., Naik, M., Hackett, B., Aiken, A.: Soundness and its role in bug detection systems. In: Proceedings of the Workshop on the Evaluation of Software Defect Detection Tools, pp. 22–37 (2005)
10. Jimenez Freitez, W.R., Mammar, A., Rosa Cavalli, A.: Software vulnerabilities, prevention and detection methods: a review. In: SEC-MDA 2009: Security in Model Driven Architecture, pp. 1–11 (2009)
11. Williams, L., McGraw, G., Migues, S.: Engineering security vulnerability prevention, detection, and response. IEEE Softw. **35**(5), 76–80 (2018)
12. Bengio, Y., Courville, A., Vincent, P.: Representation learning: a review and new perspectives. IEEE Trans. Pattern Anal. Mach. Intell. **35**(8), 1798–1828 (2013)
13. Yamaguchi, F., Lindner, F., Rieck, K.: Vulnerability extrapolation: assisted discovery of vulnerabilities using machine learning. In: *Proceedings of the 5th USENIX Conference on Offensive Technologies*, pp. 13–13. USENIX Association (2011)
14. Yamaguchi, F., Lottmann, M., Rieck, K.: Generalized vulnerability extrapolation using abstract syntax trees. In: Proceedings of the 28th Annual Computer Security Applications Conference, pp. 359–368. ACM (2012)

15. Khin Shar, L., Kuan Tan, H.B., Briand, L.C.: Mining sql injection and cross site scripting vulnerabilities using hybrid program analysis. In: Proceedings of the 2013 International Conference on Software Engineering, pp. 642–651. IEEE Press (2013)
16. Khin Shar, L., Kuan Tan, H.B.: Predicting common web application vulnerabilities from input validation and sanitization code patterns. In: 2012 Proceedings of the 27th IEEE/ACM International Conference on Automated Software Engineering, pp. 310–313. IEEE (2012)
17. Hung Nguyen, V., Sang Tran, L.M.: Predicting vulnerable software components with dependency graphs. In: Proceedings of the 6th International Workshop on Security Measurements and Metrics, p. 3. ACM (2010)
18. Neuhaus, S., Zimmermann, T., Holler, C., Zeller, A.: Predicting vulnerable software components. In: ACM Conference on Computer and Communications Security, pp. 529–540. Citeseer (2007)
19. Gegick, M., Rotella, P., Williams, L.: Toward non-security failures as a predictor of security faults and failures. In: International Symposium on Engineering Secure Software and Systems, pp. 135–149. Springer (2009)
20. Chowdhury, I., Zulkernine, M.: Using complexity, coupling, and cohesion metrics as early indicators of vulnerabilities. *J. Syst. Arch.* **57**(3), 294–313 (2011)
21. Grieco, G., Luis Grinblat, G., Uzal, L., Rawat, S., Feist, J., Mounier, L.: Toward large-scale vulnerability discovery using machine learning. In: Proceedings of the Sixth ACM Conference on Data and Application Security and Privacy, pp. 85–96. ACM (2016)
22. Smith, B., Williams, L.: Using sql hotspots in a prioritization heuristic for detecting all types of web application vulnerabilities. In: 2011 Fourth IEEE International Conference on Software Testing, Verification and Validation, pp. 220–229. IEEE (2011)
23. Yamaguchi, F., Golde, N., Arp, D., Rieck, K.: Modeling and discovering vulnerabilities with code property graphs. In: 2014 IEEE Symposium on Security and Privacy, pp. 590–604. IEEE (2014)
24. Shin, Y., Meneely, A., Williams, L., Osborne, J.A.: Evaluating complexity, code churn, and developer activity metrics as indicators of software vulnerabilities. *IEEE Trans. Softw. Eng.*, **37**(6), 772–787 (2010)
25. Li, Z., Zou, D., Xu, S., Ou, X., Jin, H., Wang, S., Deng, Z., Zhong, Y.: Vuldeepecker: a deep learning-based system for vulnerability detection (2018). [arXiv:1801.01681](https://arxiv.org/abs/1801.01681)
26. Mikolov, T., Sutskever, I., Chen, K., Corrado, G.S., Dean, J.: Distributed representations of words and phrases and their compositionality. In: Advances in Neural Information Processing Systems, pp. 3111–3119 (2013)
27. Potdar, K., Pardawala, T.S., Pai, C.D.: A comparative study of categorical variable encoding techniques for neural network classifiers. *Int. J. Comput. Appl.* **175**(4), 7–9 (2017)
28. Vincenzo Davi, L.: Code-reuse attacks and defenses. Ph.D. Thesis, Technische Universität (2015)
29. Mikolov, T., Sutskever, I., Chen, K., Corrado, G.S., Dean, J.: Distributed representations of words and phrases and their compositionality. In: Burges, C.J.C., Bottou, L., Welling, M., Ghahramani, Z., Weinberger, K.Q. (eds.), *Advances in Neural Information Processing Systems*, vol. 26, pp. 3111–3119. Curran Associates, Inc. (2013)
30. Mikolov, T., Chen, K., Corrado, G., Dean, J.: Efficient estimation of word representations in vector space (2013). [arXiv:1301.3781](https://arxiv.org/abs/1301.3781)
31. FastText. <https://research.fb.com/downloads/fasttext/>. Accessed 30 May 2019
32. Santoro, A., Bartunov, S., Botvinick, M., Wierstra, D., Lillicrap, T.: Meta-learning with memory-augmented neural networks. In: International Conference on Machine Learning, pp. 1842–1850 (2016)
33. wlin12/wang2vec the ultimate security vulnerability datasource. <https://github.com/wlin12/wang2vec/blob/master/README.md>. Accessed 30 May 2019
34. National vulnerability database. <https://nvd.nist.gov/vuln-metrics/cvss>. Accessed 30 May 2019
35. Fips 199 standards for security categorization of federal information and information systems. <https://nvd.nist.gov/vuln-metrics/cvss/v3-calculator?name=CVE-2016-005>. Accessed 30 May 2019

36. Common vulnerability scoring system calculator version 2—cve-2007-1001. <https://nvd.nist.gov/vuln-metrics/cvss/v2-calculator?name=CVE-2007-1001>. Accessed 30 May 2019
37. Common vulnerability scoring system calculator version 3. <https://nvd.nist.gov/vuln-metrics/cvss/v3-calculator?name=CVE-2016-005>. Accessed 30 May 2019
38. OsVDB everything is vulnerable. <https://blog.osvdb.org/>. Accessed 30 May 2019
39. Standards for security categorization of federal information and information systems. <https://www.0day.today/>. Accessed 30 May 2019
40. Published advisories. <https://www.zerodayinitiative.com/advisories/>. Accessed 30 May 2019
41. Securiteam. <https://securiteam.com/>. Accessed 30 May 2019
42. Mozilla foundation security advisories. <https://www.mozilla.org/en-US/security/advisories/>. Accessed 30 May 2019
43. Database for vulnerability analysis. <https://hpi-vdb.de/vulndb/>. Accessed 30 May 2019
44. Software engineering institute cert coordination center: vulnerability notes database. <https://www.kb.cert.org/vuls/>. Accessed 30 May 2019
45. Montemagni, S., Pirrelli, V.: Augmenting wordnet-like lexical resources with distributional evidence. An application-oriented perspective. In: Usage of WordNet in Natural Language Processing Systems (1998)
46. Su, J., Tan, Z., Xiong, D., Ji, R., Shi, X., Liu, Y.: Lattice-based recurrent neural network encoders for neural machine translation. In: Thirty-First AAAI Conference on Artificial Intelligence (2017)
47. Bengio, Y., Simard, P., Frasconi, P., et al.: Learning long-term dependencies with gradient descent is difficult. *IEEE Trans. Neural Netw.* **5**(2), 157–166 (1994)
48. Hochreiter, S., Schmidhuber, J.: Long short-term memory. *Neural Comput.* **9**(8), 1735–1780 (1997)
49. Zhang, J., Zheng, Y., Qi, D., Li, R., Yi, X.: Dnn-based prediction model for spatio-temporal data. In: Proceedings of the 24th ACM SIGSPATIAL International Conference on Advances in Geographic Information Systems, p. 92. ACM (2016)
50. White, M., Tufano, M., Vendome, C., Poshyvanyk, D.: Deep learning code fragments for code clone detection. In: Proceedings of the 31st IEEE/ACM International Conference on Automated Software Engineering, pp. 87–98. ACM (2016)
51. Jozefowicz, R., Zaremba, W., Sutskever, I.: An empirical exploration of recurrent network architectures. In: International Conference on Machine Learning, pp. 2342–2350 (2015)
52. Schuster, M., Paliwal, K.K.: Bidirectional recurrent neural networks. *IEEE Trans. Signal Process.* **45**(11), 2673–2681 (1997)

Fuzzy Decision Making System for Better Staff Performance Appraisal in Institutional Organization



Soni Sweta and Ajit Kumar Pandey

Abstract Performance of an educational institution primarily depends upon the performance of teachers. Methodical and continuous assessment enhanced overall teaching capabilities and further development. The sixth pay commission specified certain criteria to evaluate the performance of teachers in terms of Teaching, Learning, Evaluation, Research, and Publication and so on. Human thoughts and thinking can only be defined by fuzzily because these are uncertain and vague, we cannot measure it in terms of crisp value. In the proposed model, the aim is to build up a fuzzy inference system (FIS) for measuring the performance of university teaching staff using Matlab software. In this way, we explore various influencing factors to measure performance matrix.

Keywords Fuzzy inference system · Performance · MATLAB · Membership function · Performance appraisal

1 Introduction

Quality teaching focuses on enhancing student results and reducing loop hole in the education system. The Teacher Performance Appraisal System gives educators important input that energizes skillful learning and development. The procedure intends to inculcate improvement and distinctly open doors for additional support where required [1]. By enabling educators to achieve their maximum capacity, performance appraisal procedure enables component of accomplishing elevated student's performance.

Traditional assessment models utilize quantifiable parameters that could not measure qualitative aspects of assessments. It becomes invariably difficult to measure the overall teacher's performance. It also helps teachers to make their appraisal precisely

S. Sweta (✉) · A. K. Pandey
Amity University Jharkhand, Ranchi, India
e-mail: ssweta@rnc.amity.edu

A. K. Pandey
e-mail: akpandey@rnc.amity.edu

on the basis of what is expected and what they have achieved. Fuzzy methodology can be applied successfully for handling imprecision and uncertainty in these areas [2]. This is way to deal with performance appraisal which enables the institution to practice and make a proficient judgment in assessing its teaching faculties.

Our research aims to build a Fuzzy Inference System (FIS) for teaching staff performance appraisal utilizing Matlab [3]. This model may be seen as an option to consider the fuzzification of crisp values in contrast to the traditional method which is used to taking the sum of individual scores from different quantifiable parameters. The fuzzified variables used for assessing the performance as its input parameters. The research uses FIS to manage the issue related to rule generation [4]. The proposed FIS is actually utilizing Mamdani-type inference. To defuzzify, the subsequent fuzzy set, the centroid defuzzification method is chosen.

2 Fuzzy Logic—An Overview

Fuzzy logic depends on the hypothesis of fuzzy sets [5], where an item's membership of a set is progressive instead of being a part or not being a part. Fuzzy logic utilizes the entire interval of real numbers among False and True to create logic as a reason for standards of inference. It intends to change the linguistic experience into scientific data. It consists of three stages as Fig. 1 [6] depicts.

- A. Fuzzification is defined as a method for mapping estimated input into fuzzy membership functions [7]. A membership function is a way that characterizes how each point in the input space is mapped to membership value somewhere in the range of 0 and 1 [8]. The various types of membership functions are triangular, trapezoidal, Gaussian, bell-shaped, etc.
- B. Inference should be possible by if then rule that standards which relates different input and output factors [9]. So, fuzzy logic can depict even nonlinear systems.
- C. Defuzzification is a transformation of inner fuzzy output factors into crisp qualities that can really be utilized [10]. This step is carried out after the assessment of inputs and applies them to the standard base. Defuzzification generally uses the centroid technique.



Fig. 1 Fuzzy logic system

3 Academic Performance Factors—An Overview

According to U.G.C. guideline endorsed by Government of Maharashtra, the Academic Performance Indicators include [11]:

Classification I: Teaching, Learning, and Assessment-Related Exercises:

- Lectures, instructional exercises, seminar, tutorial, contact hours embraced taken as the level of addresses designated.
- Lectures and other teaching load as per UGC standards.
- Preparation and Imparting of information/guidance according to educational plan; prospectus improvement by giving the extra assets to understudies.
- Use of contributory and creative teaching-learning philosophies; update of subject matter, course refinement, and so forth.
- Examination obligations according to distribution.

Classification II: Co-curricular, Extension, and Professional Development Related Activities:

- Institutional Co-curricular exercises, Positions held in the association, Socio-Cultural and Sports Program, Community work.
- Contribution to Corporate life, Governance duties, Participation in panels, Responsibility for Students Welfare, Counseling and Discipline Organization of Conference/Training.
- Membership in advisory groups related to profession, participation in subject affiliations, participation in National International seminar, membership in training committees, articles published in journals newspaper and magazines.

Classification III: Research, Publications, and Academic Contributions:

- Papers publication in Referred Journals, Non-refereed but recognize, indexed and reputed Journals, Papers distributed in Conference Proceedings.
- Other Research Publications, Research Monographs, Text Books, Reference Books, Chapters added to altered information, Editing the procedures of the Seminar.
- Research Projects—Ongoing and Completed, Consultancy Projects.
- Research Guidance.

4 Structural Design of Proposed System

The primary goal of this exploration is to propose another procedure to complete performance appraisal of faculties. So as to examine and sort out the appraisal data a FIS with explicit attributes is proposed. The proposed engineering depends on Fuzzy Inference System contains the following modules:

1. Fuzzy module for Teaching, learning, and assessment-related exercises
2. Fuzzy module for Co-curricular, Extension, Professional Development Activities
3. Fuzzy module for Research, Publications and Academic Contributions.

Figure 2 shows the parts of the proposed FIS with its modules, input and output parameters. It speaks to the development of a multi-input, non-straight model.

5 Implementation of FIS

Since the exploration is in progress here we are giving clarification of FIS for Teaching, learning, and assessment fuzzy module. Fuzzification contains the way toward changing crisp an grade into the evaluation of membership for linguistic terms of fuzzy sets. The MF is utilized to relate an evaluation to each membership term. The initial phase in utilizing FL inside is to recognize the parameters that will be fuzzified and to decide their separate scope of qualities. The last aftereffect of this collaboration is the grade for every performance parameter.

5.1 Factors affecting on Responsibility and Punctuality

The input and output factors are made in FIS editor as shown in the Fig. 3. We have thought about five input parameters and two outputs of the classification 1 and connected to the FIS.

Estimating the educator's performance includes relegating a number to reflect an instructor's performance in the distinguished measurements. In fact, numbers are not mandatory. Names, for example, "Excellent", "Good", "Average", "Fair", and "poor" are utilized. The rating size of input and output parameters is characterized into various classes as given in Tables 1 and 2.

5.2 Membership Functions

Fuzzification contains the way toward changing crisp value into the evaluation of membership [12]. The MF is utilized to relate an evaluation to each linguistic term.

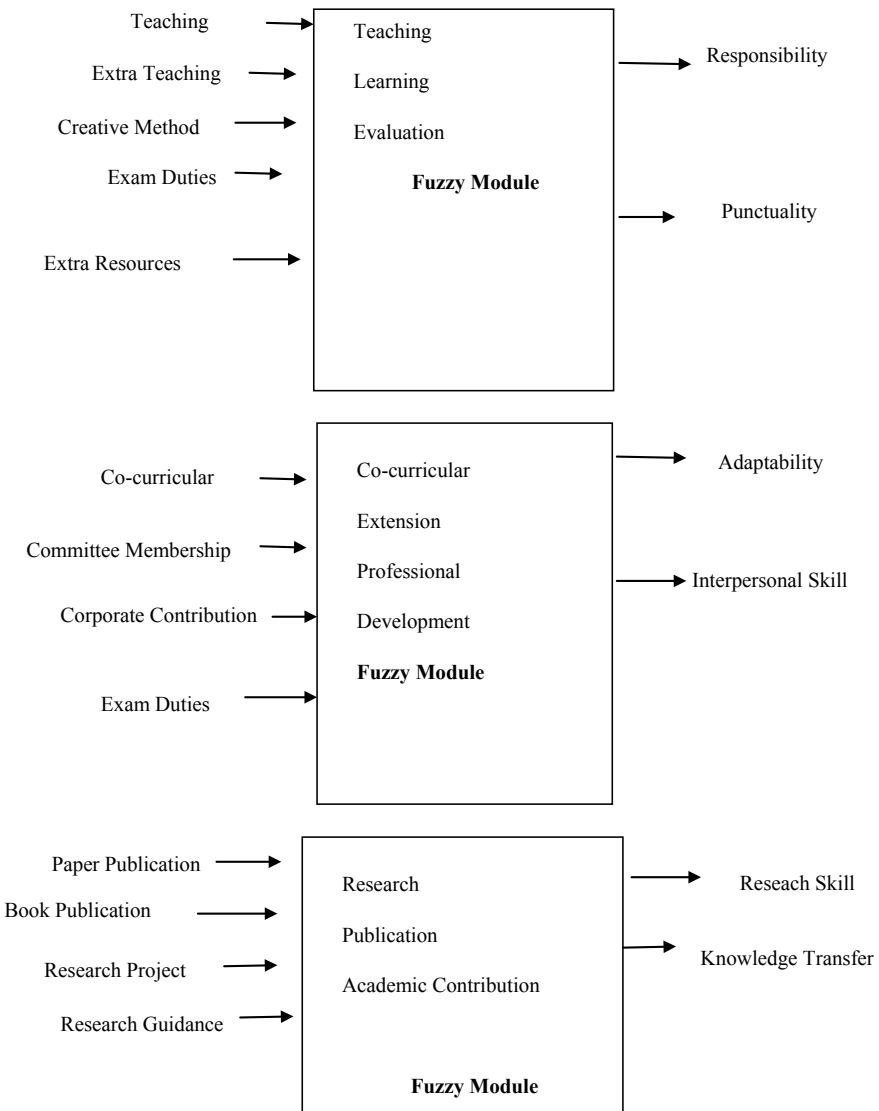


Fig. 2 Proposed fuzzy inference system architecture

The MF editorial manager is utilized to characterize the properties of the MF for the systems factors. Figure 4 demonstrates the fuzzification of the first fuzzy module with membership function as clarified in Table 1, the MF is covering with one another for accomplishing the best outcomes.

Figure 5 demonstrates fuzzification with MF as clarified in Table 2, the MF is contacting with one another for accomplishing better outcomes.

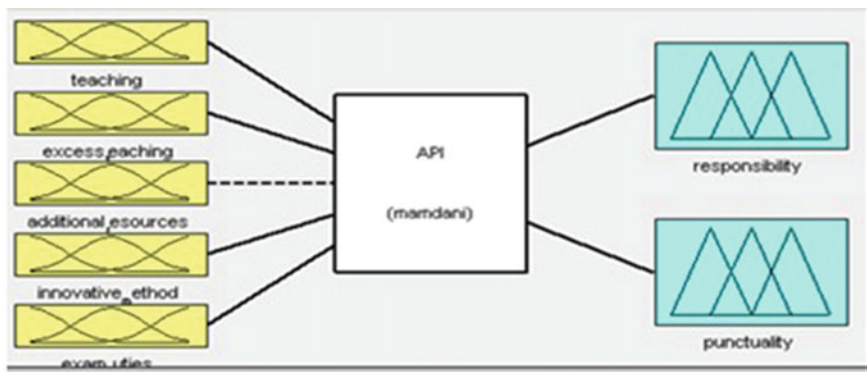


Fig. 3 Input and output factors

Table 1 Rating scales of input parameters

Input name	Linguistic
Teaching (T)	Poor
	Fair
	Average
	Good
	Excellent
Excess teaching (E_T)	Poor
	Average
	Good
Additional resources (A_R)	Low
	Medium
	High
Innovative method (IM)	Abstract
	Better
	Relevant
Exam duties (E_D)	Poor
	Fair
	Average
	Good
	Excellent

5.3 Fuzzy Rule

A fuzzy rule base is a combination of information in the If-Then configuration from specialists. It frame the connection between fuzzy input-output parameters. It is utilized to show how output is reliant on any a couple of the inputs. According to

Table 2 Score scales output parameters

Output	Linguistic term
Responsibility	Poor
	Fair
	Average
	Good
	Excellent
Punctuality	Good
	Fair
	Average
	Excellent
	Poor

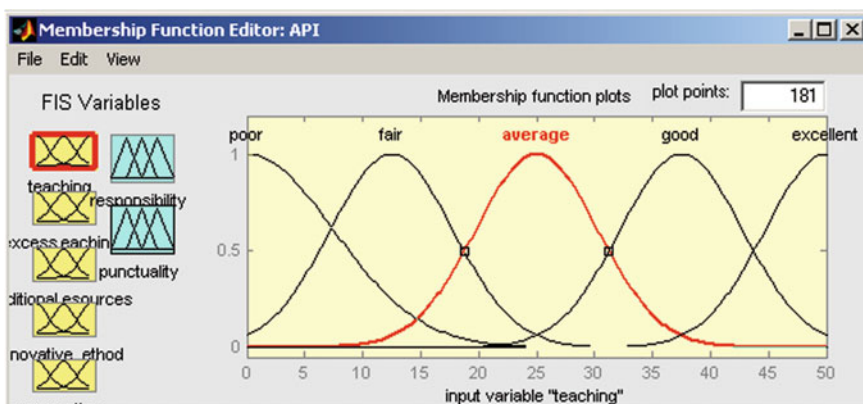


Fig. 4 Membership function “teaching activities” (TA)

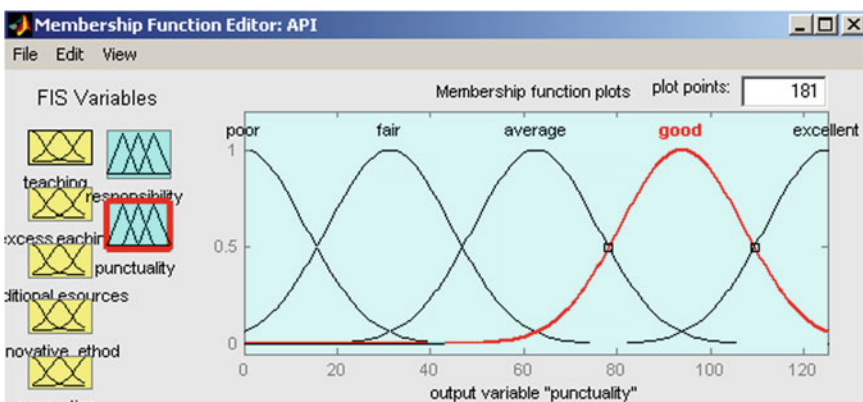


Fig. 5 Membership functions “punctuality”

the input–output fuzzified, the rule base is produced by applying thinking to assess the performance of an educator. There are 34 quantities of principles created. The following are the example guidelines gathered from the standard base, which are the influencing factors of the appraisal:

1. IF (T is excellent) and (E_T is good) and (A_R is high) and (I_method is relevant) then (responsibility is excellent) (punctuality is excellent).
2. IF (T is fair) and (A_R is high) and (I_method is relevant) then (responsibility is average).
3. IF (T is average) and (A_R is low) and (I_method is abstract) then (Responsibility is fair).
4. IF (T is excellent) and (E_T is good) and (A_R is high) and (I_method is relevant) and (Test_duties is excellent) then (responsibility is excellent) (punctuality is excellent).

If then rule that (T is poor) and (ET is poor) and (AR is low) and (I_method is abstract) and (exam_duties is excellent) then (responsibility is poor)(punctuality is fair).

5.4 Results Analysis

According to the above scenario, the proposed strategy is connected to assess the performance appraisal of teaching staff. Test information was inspected and randomly chooses for the present investigation. This is a case of the activation of rule of standards with respect to a part of the staff performance appraisal for the underlying FIS. Figures 6 and 7 demonstrate previews of consequences of work done in MATLAB. The rule viewer is a read only tool that shows the entire fuzzy inference chart. The surface viewer is additionally a read only instrument. Table 3 shows input and output parameters for the given cases.

6 Conclusion

Apart from academic infrastructure and student's receptivity, the performance of teachers lead the institutions in the right direction and instill effectiveness in overall teaching. A model to measure teacher's performance linguistically helps them to fine-tune their teaching methodology, skills and attitude toward educational excellence. It also motivates them to do relevant research work. Real-time data collected from institutes in which fuzzy inference system give qualitative evaluation in terms of imparting better decisions.

This FIS goes about as an answer for subjective appraisal. Countless components influencing the teacher's performance were distinguished and infused in the educational system. The membership functions and fuzzy rules bases were created on

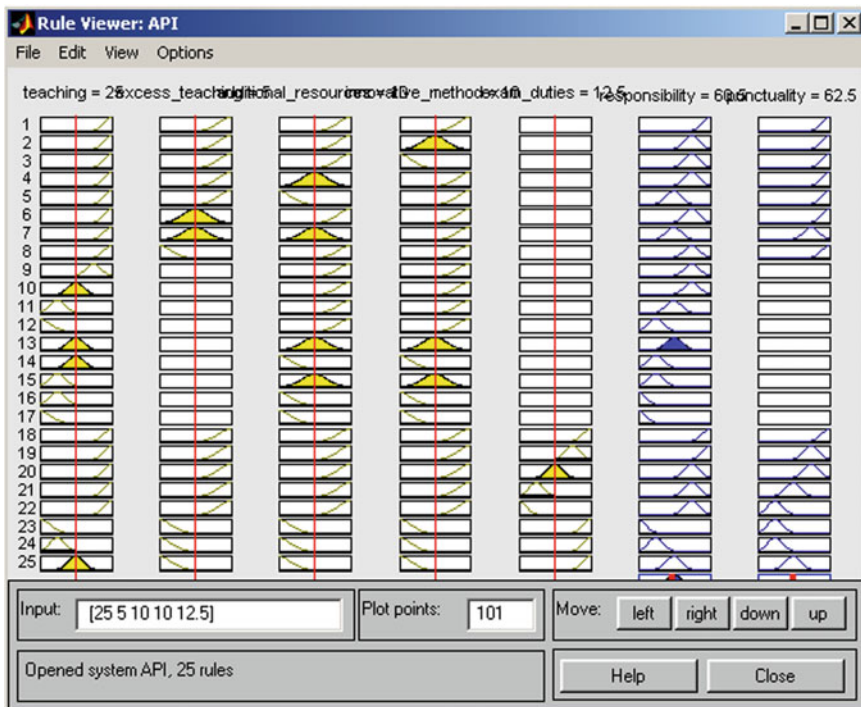


Fig. 6 Rule viewer of input, output parameters

logical thinking. The outcomes obtained from the proposed system can be utilized to improve the proficiency in teaching performance which was unrealistic in past system of quantitative Academic Performance Indicator (API). By proposed research work the factors of good teaching like value, amleness, fulfillment, productivity and overall development in teaching. This research work can be extended for future study by selective other assessment variables for teacher's performance for formative purposes that may be further utilized in the advance educational field.

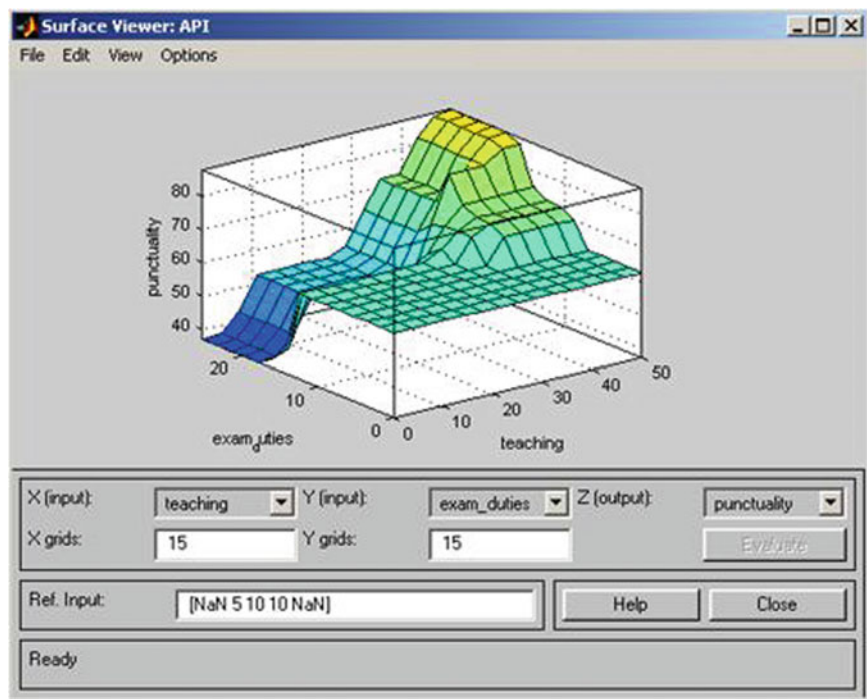


Fig. 7 Surface viewer

Table 3 Selected case inputs and outputs

S. No.	Input variables					Output	
	Teaching (0–50)	Excess teaching (0–10)	Additional resources (0–20)	Innovative method (0–20)	Exam_Duties (0–25)	Responsibilities (0–125)	Punctuality (0–125)
1	24	5	10	10	13	61	31.9
2	19.5	3.25	7.5	6.07	8.77	50.2	32.6
3	16	2.70	5.55	4.44	6.54	45	28.5
4	5.78	1.54	3.28	3.5	3.20	18.5	18.5
5	36.5	1.08	19.7	19.5	1	91.5	88.6
6	48.2	1.17	11.5	13.5	7.5	70.4	90.5
7	43.7	1.65	7.2	10.5	16.2	60.3	75.2
8	45.2	4.2	14.5	15	22	75.4	95.5
9	48.8	2.2	18.23	17.9	23	91	105
10	38.5	9.45	5.8	3.56	23	50	35.2

References

1. Neogi, A., Mondal, A.C., Mandal, S.K.: A cascaded fuzzy inference system for university non-teaching staff performance appraisal. *J. Inf. Process. Syst.* **7**, 595–612 (2011)
2. Burhan I.: Chaos Theory in Politics, pp. 17–28 (2014). <https://doi.org/10.1007/978-94-017-8691-1>
3. Bhosale, G.A.: Role of fuzzy techniques in performance appraisal of teaching staff. *Int. J. Latest Trends Eng. Technol. (IJLTET)* **0**, 139–141 (2013)
4. Bhosale, G.A.: Fuzzy inference system for teaching staff performance appraisal. *Int. J. Comput. Inf. Technol.* **2**, 381–385 (2012)
5. Zadeh, L.A.: Fuzzy logic.. *Comput. Complex. Theory, Tech. Appl.* 9781461418, pp. 1177–1200 (2013). https://doi.org/10.1007/978-1-4614-1800-9_73
6. Sweta, S., Lal, K.: Learner model for automatic detection of learning style using FCM in adaptive E-learning. *System* **18**, 18–24 (2016). <https://doi.org/10.9790/0661-1802041824>
7. Ray, K., Sharma, T.K.: Soft Computing : Theories and Application, AISC SoCTA2 2
8. Mago, V., Fellow, P.: Fuzzy Logic and Fuzzy Cognitive Map (2011)
9. Sweta, S., Lal, K.: In: Ravi, V., Panigrahi, K.B., Das, S., Suganthan, N.P. (eds.) *Proceedings of the Fifth International Conference on Fuzzy and Neuro Computing (FANCCO—2015)*, Springer, Cham, pp. 353–363 (2015). https://doi.org/10.1007/978-3-319-27212-2_27
10. Bourgani, E., Stylios, C.D., Manis, G., Georgopoulos, V.C.: Fuzzy Cognitive Maps Modeling and Simulation, pp. 561–570 (2013)
11. UGC Guidelines for University Grants Commission, pp. 1–57 (2017)
12. Sweta, S., Lal, K.: Personalized adaptive learner model in e-Learning system using FCM and fuzzy inference system. *Int. J. Fuzzy Syst.* **19**, 1249–1260 (2017). <https://doi.org/10.1007/s40815-017-0309-y>

A Graph-Theoretic Approach for Sustainable New Product Development (SNPD) in Supply Chain Environment



Amit Kumar Sinha and Ankush Anand

Abstract The growing competition worldwide in the engineering sector calls for the development of products in a shorter possible product development process. This is possible only with a holistic involvement of all stakeholders in the decision-making process, in particular, the designer at the early design stages. Decision-making in product design often involves a lot of conflicting situations, which makes the decision-making process cumbersome and complex. To address this issue, an effort has been made in this research article to suggest a framework using the concept of graph theory in solving sustainable new product development problems in the supply chain network environment. The sequential use of this technique will help decision-makers in effective decision-making. Graph theory has indeed proved as a versatile tool in various areas of science and technology. The parametric analysis has been used for new product development in conjunction with combinatorial mathematics. A case study has been included in this article to illustrate the framework.

Keywords Product design · Graph theory · Modelling · Multi-criteria decision-making

1 Introduction

To address various issues of real-life world where complex engineering systems are used one way or the other, the process of research in various fields of engineering and science is augmented by effective implementation and analysis of various physical systems/components [1]. As far as a physical system is concerned, we may consider it as something composed of a large number of sub-systems/components. These sub-systems/components may significantly affect the performance characteristics of a larger system [2]. The purpose of this article is to highlight the role and the potential

A. K. Sinha (✉) · A. Anand

Department of Mechanical Engineering, Shri Mata Vaishno Devi University, Katra, Jammu & Kashmir 182320, India

e-mail: amitsinha5050@gmail.com

of a modelling technique called graph theory, which can be used for analysis and may pave way for suggesting a feasible solution to new product development (NPD).

The term sustainability is originated from silviculture, and later on, sustainability has been adopted by United Nation Environment Programme (UNEP) in his Vision 2030. Now, sustainability becomes the ultimate goal of PD [3].

NPD is a complete step-by-step processor which leads towards launching a new product to market. Product design is a major important step of NPD, which conforms the sustainability of the product. New product should be sustainable in the market from the aspect of economic, environmentally as well as socially acceptable, and then only new product will be able to grasp the market opportunity, otherwise it is hard to launch a new product in a global sustainable environment. In general, cost, time and quality are the three main attributes which always provide a platform for sustaining in the global market. The uncertainty of the market is also a challenging task for NPD. In nutshell, it can be concluded that a holistic framework of sustainable NPD is necessary for the domain of supply chain environment. In this regard, we need multi-criteria decision-making tools which help decision-makers during the early stage of NPD.

Faisal et al. [4] proposed a risk mitigation index using the concept of graph theory in a supply chain environment. Anand and Wani [5] used the concept of modified graph theory for product lifecycle modelling and evaluation at the conceptual design stage. Developing and maintaining NPD is a challenging task for both practitioners and researchers [6]. Gmeli and Stefan [6] developed a conceptual framework for sustainable NPD with emphasizing the importance of lifecycle product development. Although the sustainability of NPD is widely accepted in the global market scenario, it is hardly implemented in real-life situations [7]. The reason is unavailability of the integrated model of sustainability and NPD in supply chain environment. Therefore, the integral model of sustainable NPD in a supply chain environment is necessary for any manufacturing industry.

In view of the developments in the field of sustainability over the past few decades, companies have been continuously striving for efforts not only to meet environmental regulations but also to systematically minimize the consumption of resource (natural and artificial) and also the environmental impact by incorporating the sustainability aspects in product design. Some advanced companies have recently implemented various product lifecycle design methodologies from a sustainability perspective [8–12].

Based on the above-cited literature, it can be observed that graph theory has been extensively used in the field of mechanical engineering for mechanism and machine theory, computer-aided design and manufacturing. The applications include representation and identification of kinematic structure and for enumeration of kinematic chains and mechanisms in a relatively simple and systematic manner. It has proved to be useful in the identification of known, as well as unknown chains. Representation and analysis of design variants are more efficient using graph and digraph models and in particular, during the conceptual design stage of a system. In the field of computer engineering, graph theory has been used to develop various research studies—depth,

breadth, heuristic, etc—for the development of efficient algorithms. Extensive use of graph theory has been carried out in the development of expert systems.

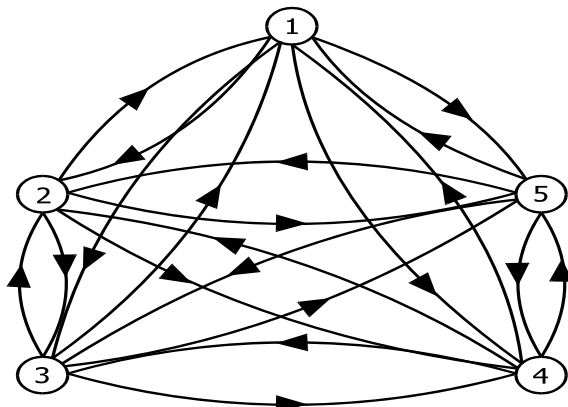
The data structures have also been generalized in terms of graphs/digraphs. Fuzzy hypergraphs have been used to reduce the requirement of data in clustering problems. These are used to represent a fuzzy partition visually. The dual hypergraphs can represent the elements, which can be grouped into a class at level 0. The strength of an edge is useful to discriminate strong classes (subsets) from other parts.

2 Structural Analysis of a Sustainable New Product Development Using Graph Theory

To address any sustainable new product development problem, where graph theory is to be applied as a tool, it becomes quite necessary to understand the concept of graph theory and its structural analysis [13].

A digraph is basically a graph with directed edges. The digraph has nodes $N = \{ni\}$, with $i = 1, 2, \dots, M$ and associated directed edges $E = \{eij\}$. A node ni represents i th material selection factor, and the edges represent the relative importance among these factors. There are equal number of nodes as that of material selection factors. If a node ‘ i ’ is having relative importance over another ‘ j ’ in the material selection, then a directed edge is drawn from node ‘ i ’ to node ‘ j ’ (i.e. eij). If ‘ j ’ is having relative importance over ‘ i ’, then a directed edge is drawn from node ‘ j ’ to node ‘ i ’ (i.e. eji). The concept is well understood when we take some problem for analysis. The following graphs may be used for structural analysis for supplier selection during the early stage of sustainable new product development problem (see Fig. 1).

Fig. 1 A five-node supplier selection problem for sustainable NPD



3 Case Study

Let us consider a case where an engineering component is to be manufactured using processes like casting, machining, etc., if the choice of suppliers for materials listed below is to be made such that only one best supplier is to be recommended. Now how to decide, which is the best supplier out of 5 listed suppliers (S1, S2, S3, S4 and S5) for sustainable NPD?. The hierarchy of selection of best suppliers for sustainable NPD in a supply chain environment is illustrated in Fig. 2.

Therefore, using the concept of graph theory, the analysis for each supplier can be done. Due to space constraints, we are not showing here the procedure. However, we have only shown the ranking of various suppliers and a numeric value is written against every supplier. Such that supplier can be recommended. Supplier with the maximum value is the best supplier of the material for sustainable NPD (The detailed procedure, however, will be presented during the conference) (Table 1).

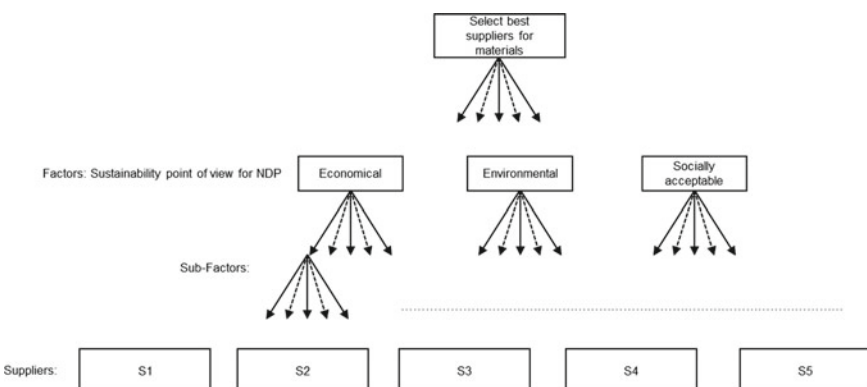


Fig. 2 Hierarchy for selection of best supplier in sustainable NPD

Table 1 Detailed information about suppliers

S. No.	Suppliers	Index value
1	S1	496.8
2	S2	253.4
3	S3	292.7
4	S4	508.3
5	S5	206.3

Bold indicates the best supplier because it shows largest value of index value

4 Conclusions

Graph theory owing to its great potential is instrumental in solving a large number of supplier problems for sustainable NPD in a supply chain environment. It is indeed a novel approach while addressing several issues where structural analysis and modelling are carried out. It will pave way for future research in various areas of engineering, science and technology. A methodology called graph theory is used for supplier selection for sustainable NPD-based case study in the present work. The methodology is quite logical and has proved as a powerful technique in other areas of modelling and analysis.

References

1. Haimes, Y.Y.: Models for risk management of systems. *Int. J. Syst. Syst. Eng.* **1**(1–2), 222–236 (2008)
2. Tseng, M.M., Kyellberg, T., Lu, S.C.Y.: Designing the new e-Manufacturing era. *Ann. CIRP* **52**, 1 (2003)
3. Klöpffer, W.: Life-Cycle Based Methods for Sustainable Product Development (2003)
4. Faisal, M.N., Banwet, D.K., Shankar, R.: Quantification of risk mitigation environment of supply chains using graph theory and matrix methods. *Eur. J. Ind. Eng.* **1**(1), 22–39 (2007)
5. Anand, A.: Wani MF (2010) Product life-cycle modeling and evaluation at the conceptual design stage a digraph and matrix approach. *J. Mech. Des.* **132**(9), 1–9 (2010)
6. Gmeling, H., Stefan, S.: Determinants of a sustainable new product development. *J. Clean. Prod.* **69**, 1–9 (2014)
7. Kaebernick, H., Kara, S., Sun, M.: Sustainable product development and manufacturing by considering environmental requirements. *Robot. Comput. Integrat. Manuf.* **19**(6), 461–468 (2003)
8. Khan, R.A., Anand, A., Wani, M.F.: A holistic framework for environment conscious based product risk modeling and assessment using multi criteria decision making. *J. Clean. Prod.* **174**, 954–965 (2018)
9. Sinha, A.K., Anand, A.: Towards fuzzy preference relationship based on decision making approach to access the performance of suppliers in environmental conscious manufacturing domain. *Comput. Ind. Eng.* **105**, 39–54 (2017)
10. Sinha, A.K., Anand, A.: Development of sustainable supplier selection index for new product development using multi criteria decision making. *J. Clean. Prod.* **2018**(197), 1587–1596 (2016)
11. Anand, A., Khan, R.A., Wani, M.F.: Development of a sustainability risk assessment index of a mechanical system at conceptual design stage. *J. Clean. Prod.* **139**, 258–266 (2016)
12. Anand, A., Wani, M.F.: Product life-cycle modeling and evaluation at the conceptual design stage: a digraph and matrix approach. *J. Mech. Des.* **132**, 091010 (2010)
13. Bondy, J.A., Murty, U.S.R.: Graph theory with applications, vol. 290. Macmillan, London (1976)

Generalization Performance Comparison of Machine Learners for the Detection of Computer Worms Using Behavioral Features



Nelson Ochieng, Waweru Mwangi, and Ismail Ateya

Abstract This study addresses the problem of detecting computer worms in enterprise networks. The study analyzes, empirically, various classifiers and feature selection algorithms on a darknet dataset. The output of the study is a performance comparison of various classifiers especially in terms of generalization to unseen datasets. Feature selection experiments yield the best feature set for the detection of computer worms as time to live (TTL), Internet protocol (IP) packet length, value or number of packets in the packet capture interval whose header fields match the FlowTuple key, well-known destination ports or destination ports within the range 0–1024 and IP packet source country. The study finds outs that various classifiers perform almost as well as each other. Each of them is therefore a candidate for the final model. The algorithms also perform just as well as similar studies reported in the literature and therefore imply that the most value in machine learning should be obtained by feature engineering and feature selection. However, decision trees, nearest neighbors classifier and support vector machines did not generalize well.

Keywords Generalization error · Computer worm detection · Auto-encoders

1 Introduction

Computer and network resources are important for the operational excellence of organizations. In addition, they can be leveraged for competitive advantage. A number of critical threats exist that could hamper these benefits. The most prevalent threats and attacks reported by preeminent security organizations include worms, botnets, Trojans, ransomware, spam, phishing, Web attackers and crypto-miners.

The study’s scope is computer worm detection in an organization’s network. Reference [1] defines a computer worm as “a process that can cause a (possibly evolved)

N. Ochieng (✉)
Strathmore University, 59857, Nairobi 00200, Kenya
e-mail: nochieng@strathmore.edu

W. Mwangi · I. Ateya
JKUAT, Nairobi, Kenya

copy of it to execute on a remote computational machine.” Worms self-propagate across computer networks by exploiting security or policy flaws in widely used network services. Unlike computer viruses, worms do not require user intervention to propagate nor do they piggyback on the existing files. Their spread is very rapid [2, 3] with the ability to infect as many as 359,000 computers in under 14 h, or even faster. Computer worms therefore present unique challenges to security researchers.

Different measures may be taken to counter computer worms including prevention and detection. Prevention may not always be wholly possible due to inherent vulnerability in all systems. The approach this study takes is to profile and detect attacks. Once detection has happened, other mitigation measures may be taken.

A number of approaches for computer worm detection have been reviewed in the literature. These include content-based signature schemes, anomaly detection schemes and behavioral signature-based detection. Approaches that utilized machine learning have particularly yielded good results. Machine learning has been defined as a field of study that gives computers the ability to learn without being explicitly programmed [4]. The use of machine learning can help correlate events, identify patterns and detect anomalous behavior to improve the security posture of any defense program [5]. Some of the studies are here summarized in terms of the datasets used for the training and testing of the learners, the unique approaches used and the features used.

The features used to profile computer worms and other related malware in reviewed studies include malware images [6, 7], Windows API system calls and opcodes [8–13], control flow graph features [14], PE import table functions [15], network flow features [16–18]. It is evident that the most popular feature type is the Windows API system calls and opcodes. There are some studies that use network flow features, but these are fewer. Computer worms, being just network packets, especially during their propagation phase, can be profiled by using feature obtainable from network packets. This is the approach adopted in this study.

Some of the off-line datasets used in studies reviewed in the literature include KDD dataset [19], the Malicia dataset [9, 10], unpacked windows console applications [14], Malimg dataset [7, 20], UNB ISCX [17], Comodo cloud security dataset [21], Malia dataset [21], Microsoft challenge dataset [22], Malheur dataset [11].

Most of the datasets are fairly old, for example, KDD dataset (1999), Malicia dataset (2013) and Malimg data (2011). They are also quite general and not specific to computer worm research. Even though the dataset used in this study is of a similar age, it is more specific to computer worm research.

This study will have as its major contribution an investigation of the performance of various learners on the particular dataset used. To place it in context, the study here reviews the approaches that have been used in the existing studies and their performance evaluation results.

Reference [19] eliminates bias by introducing multistage feature selection and attempts to understand feature contribution. Reference [23] proposes using two deep neural networks with the first being limited to only determining if the traffic is normal or suspicious and the second classifying the traffic as a multiclass problem. Reference [6] uses convolutional neural networks for detection based on image similarity and claims an accuracy of 98%. Reference [8] uses system calls and trains convolutional neural networks and recurrent neural networks. Reference [9] investigates the class imbalance problem with methods like random sampling and cluster-based sampling. They use auto-encoders for dimensionality reduction. In their work, random forest outperforms deep neural networks with a claimed accuracy of 99.78%. Reference [11] trains a convolutional neural network using the execution run time behavioral features of PE files. The work achieves a claimed accuracy of 97.97%. Reference [20] uses convolutional neural networks and achieves an accuracy of 98%. Reference [12] proposes a deep learning architecture using stacked auto-encoders with input being Windows API calls extracted from the PE files. It uses unsupervised feature learning and then supervised fine-tuning. The model outperforms artificial neural networks (ANNs), support vector machines (SVMs), naïve Bayes (NB) and decision trees (DTs). Reference [24] uses deep belief networks implemented with a deep stack of denoising auto-encoders generating an invariant compact representation of the malware behavior. The study claims 98.6% accuracy in classifying new malware variants. Reference [21] computes clusters using K-means and expectation–maximization algorithm with the underlying scores based on hidden Markov models. The results from the algorithms are compared and the interplay between the dimensions (i.e., number of models used for clustering and the number of clusters with respect to the accuracy of the clustering). EM outperforms K-means. Further, EM improves as the number of clusters increases. Accuracy in excess of 90% is claimed. In [10], auto-encoders are used for dimensionality reduction or feature extraction while [14] estimate the similarity between malicious instances by calculating the string edit distance between the string representatives of the control flow graphs of malware instances. They then use the quality threshold clustering algorithm. In [15], support vector machines (SVMs) achieve the best result, while naïve Bayes (NB) achieves the worst result. Reference [7] trains convolutional neural networks (CNNs) translating the malware classification problem into an image classification. An accuracy of 99.97% is claimed. Reference [11] trains a CNN on dynamic behavioral features of the PE files (n-grams used to create images) to detect and classify obscure malware. An accuracy of 97.97% is claimed. In [16], J48 and PART learners are the best performing learners. Reference [17] uses SVM to perform clustering as well as dimensionality reduction. Reference [18] uses independent component analysis (ICA) to separate features extracted from network traces into two estimated distributions of malware and benign traffic while [13] uses K-means clustering algorithm and thereafter performs boosting using genetic algorithm.

These studies, and many others, rely on accuracy alone as the metric to measure performance for the algorithms. This may not be enough. Other metrics may need to

be used such as Receiver Operating Characteristics (ROCs) curves. More importantly, [25] explains that the fundamental goal of machine learning is to generalize beyond the examples in the training set. It would be useful to investigate the generalization capability of the learners. This study will use the bias-variance decomposition to attempt to understand the generalization capability of the evaluated learners.

2 Methodology

2.1 Datasets

The datasets used for the experiments were requested and obtained from the University San Diego California Center for Applied Data Analysis. The center operates a network telescope that consists of a globally rooted/8 network that monitors large segments of lightly used address space. There is little legitimate traffic in this address space; hence, it provides a monitoring point for anomalous traffic that represents almost 1/256th of all IPv4 destination addresses on the Internet.

Two sets of datasets were requested and obtained from this telescope. The first is the Three Days of Conficker dataset [26] containing data for three days between November 2008 and January 2009 during which Conficker worm attack [27] was active. This dataset contains 68 compressed packet capture (pcap) files, each containing one hour of traces. The pcap files only contain packet headers with the payload having been removed to preserve privacy. The destination IP addresses have also been masked for the same reason. The other dataset is the Two Days in November 2008 dataset with traces for November 12–19, 2008, containing two typical days of background radiation just prior to the detection of Conficker.

The datasets were processed using the CAIDA Corsaro software suite, a software suite for performing large-scale analysis of trace data. The raw pcap datasets were aggregated into the FlowTuple format. This format retains only selected fields from captured packets instead of the whole packet, enabling a more efficient data storage, processing and analysis. The eight fields are source IP address, destination IP address, source port, destination port, protocol, time to Live, TCP flags and IP packet length. An additional field, value, indicates the number of packets in the interval whose header fields match this FlowTuple key.

The instances in the Three Days of Conficker dataset have been further filtered to retain only instances that have a high likelihood of being attributable to Conficker worm attack. Reference [27] discusses Conficker's TCP scanning behavior (searching for victims to exploit) and indicates that it engages in three types of observable network scanning via TCP port 445 or 139 (where the vulnerable Microsoft software Windows Server service runs) for additional victims. The vulnerability allowed attackers to execute arbitrary code via a crafted RPC request that triggers a buffer

overflow. These include local network scanning where Conficker determines the broadcast domain from network interface settings, scans hosts nearby other infected hosts and random scanning. Other distinguishing characteristics include TTL within reasonable distance from Windows default TTL of 128, incremental source port in the Windows default range of 1024–5000, 2 or 1 TCP SYN packets per connection attempt instead of the usual 3 TCP SYN packets per connection attempt due to TCP’s retransmit behavior.

This dataset solves the privacy challenge by removing the payload and also masking out the first octet of the destination IP address.

2.2 Feature Engineering Experiments

1000 instances of the Conficker dataset FlowTuples were chosen randomly. These were then filtered out into 294 FlowTuples using the distinguishing characteristics of Conficker worm attacks. The rest of the FlowTuples (i.e., 706) were discarded as there was the possibility that they could be traffic not attributable to Conficker worm. The features were as obtained from the obtained dataset from CAIDA.

The datasets were then marked malicious by adding another column to the data frame. Similarly, random instances were chosen from the Two Days in November 2008 dataset. These represented background traffic before the onset of the Conficker worm. An equal number of instances were picked at random, hence 294 instances. These were then marked benign.

The two datasets were then mixed together and randomized. The datasets as retrieved from CAIDA have the destination IP address masked to preserve anonymity. This field therefore contributes no value for the purposes of the research. It was therefore dropped. The source IP address column was encoded into the corresponding country using the GeoIP database and tool. An additional column to hold a value 1 if the source port was similar to the destination port and a value 0 otherwise was added. Same source and destination ports may be indicative of worm activity since worms attack similar services in machines that are vulnerable. Worms attack most commonly used services. Ports in the range 0–1024, otherwise known as well-known ports, are more likely to be candidates for worm traffic. A column was further added to take care of this. This was done for both source port and destination ports. In addition, worm attacks are likely to originate from hosts that rarely initiate traffic in usual communications. A column was added to capture this situation. Categorical columns were then encoded using dummy variables. The total number of columns (features) after the transformations was 91, while the number of instances (rows) was 588. These are what were then used for the subsequent feature selection experiments.

The variance threshold was set to 0.8, and features selected using variance threshold baseline method. The variance threshold is a simple baseline approach to feature selection. It removes all features whose variance does not meet some threshold. By

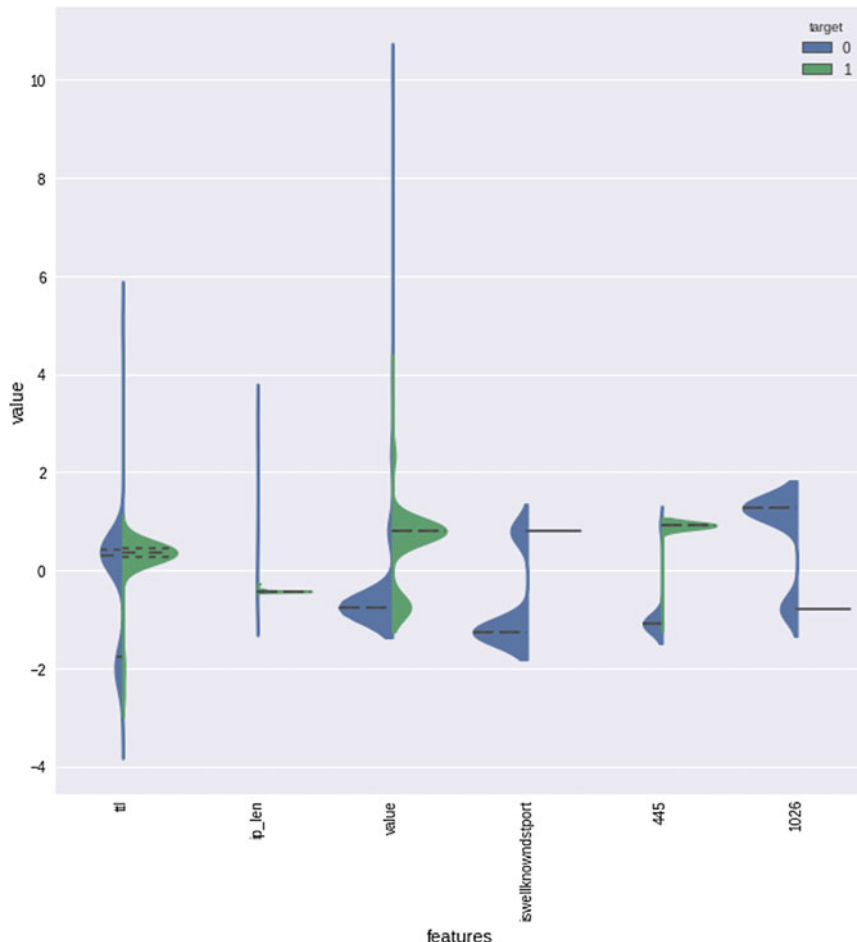


Fig. 1 Violin and swarm plot

default, it removes all zero-variance features, that is, features that have the same value in all samples. The premise is that a feature which does not vary much within itself has very little predictive power. The features that met this threshold included time to live, IP packet length, value, port range 0–1024 (iswellknowndstport), destination port 445, destination port 1026, TCP and UDP protocol numbers 6 and 17, TCP null and SYN flags and source country China.

Data analysis was thereafter performed. Figure 1 shows the violin and swarm plot for the dataset.

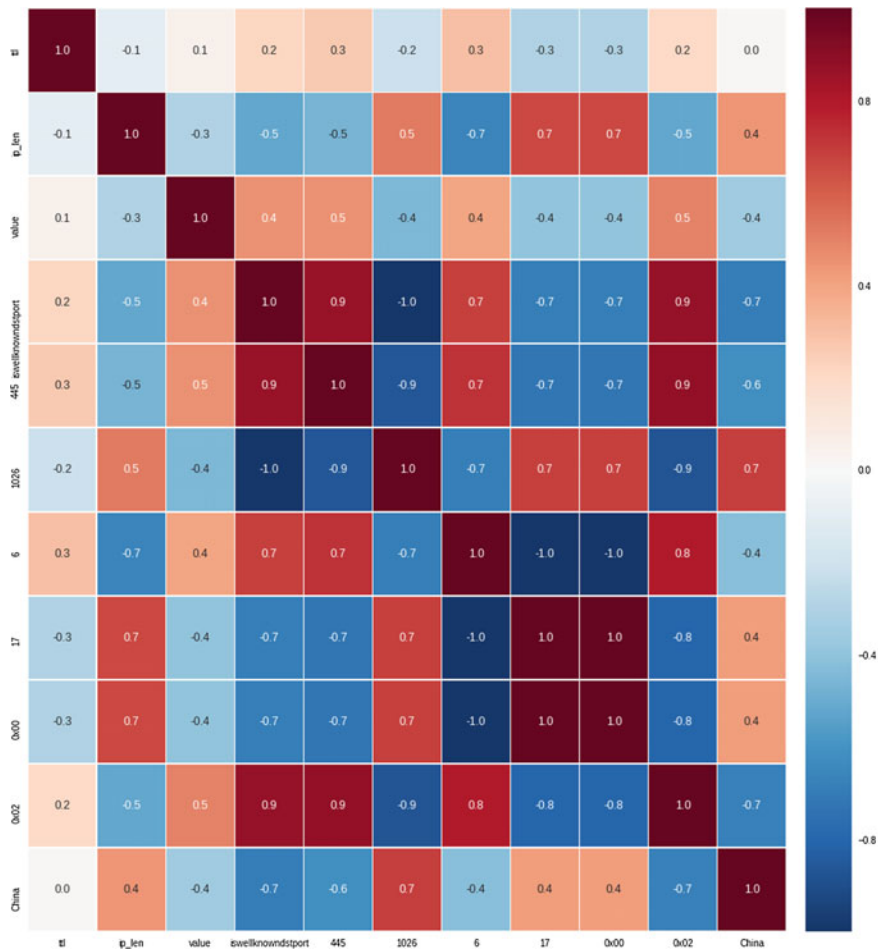


Fig. 2 Correlation map

A correlation map of all the features was plotted as can be seen in Fig. 2.

As is evident, many features were correlated. The useful features for classification were isolated as ttl, value, China, ip len and iswellknowndstport.

Feature selection with correlation and LinearSVC yielded an accuracy of 0.9096. Performing univariate feature selection using SelectKBest technique picked the four best features as ip len, ttl, iswellknowndstport and China. Recursive feature elimination (RFE) with LinearSVC picked the four best features as iplen, value, iswellknowndstport and China.

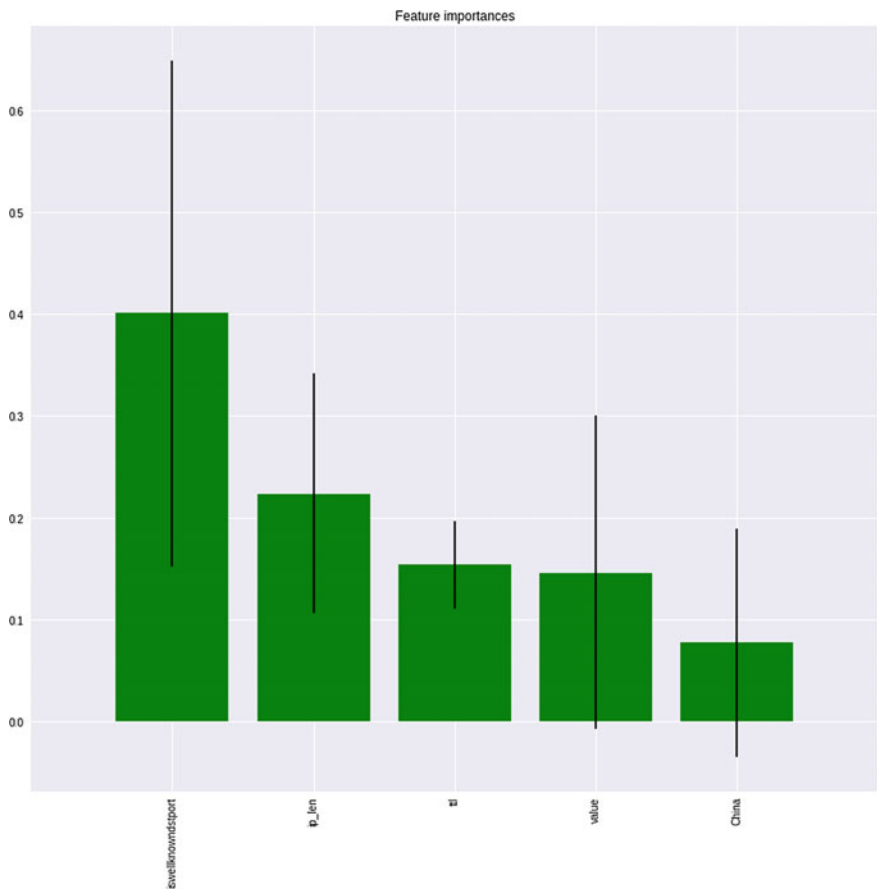


Fig. 3 Tree-based feature selection

Tree-based feature selection and random forest classifier ranked the features as illustrated (Fig. 3).

2.3 Machine Learning Algorithms

Various machine learners were explored, and their performance was evaluated. These included k-nearest neighbors (kNNs), naïve Bayes (NB), support vector machines (SVMs), decision trees (DTs) and logistic regression. Python programming language was used for the classification experiments and more specifically the Scikit-learn library as seen in Sect. 2.4.

2.4 Machine Learning Experiments

In order to perform sanity checks on classifier accuracies, a dummy classifier was trained. The strategy adopted was uniform, and the reported accuracy was 0.5508.

A spot check of popular algorithms was then performed. A sample of the results obtained is reported. Logistic regression with the best parameter set found to be $C = 0.1$ and $\text{penalty} = 11$ achieved the results as shown in Table 1.

ROC curve for logistic regression for this case is as shown in Fig. 5, while the learning curve is shown in Fig. 4. Logistic regression achieved a Cohen kappa score of 0.83.

Table 1 Logistic regression performance

Class	Precision	Recall	F1
0	1.00	0.85	0.92
1	0.84	1.0	0.91
Average	0.93	0.92	0.92

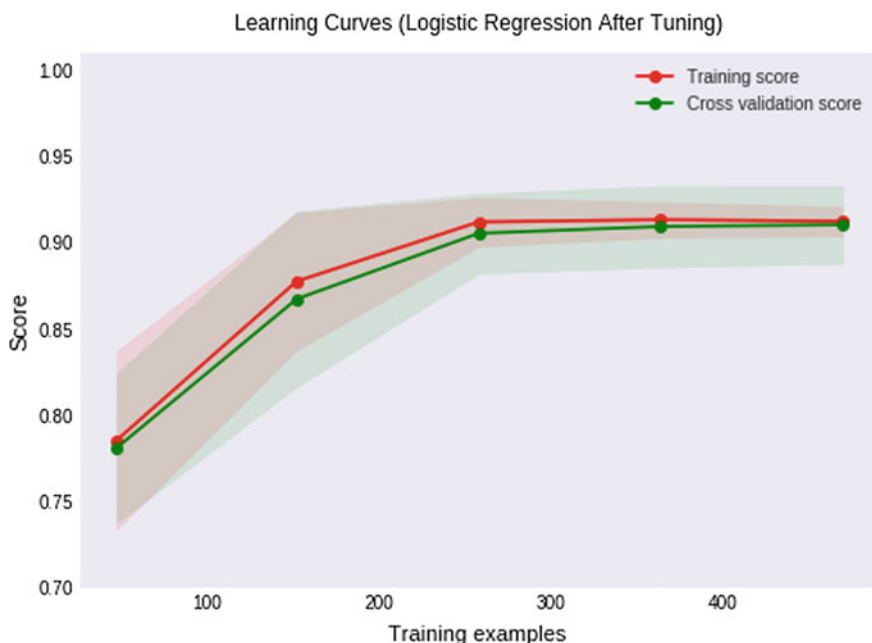


Fig. 4 Learning curve logistic regression

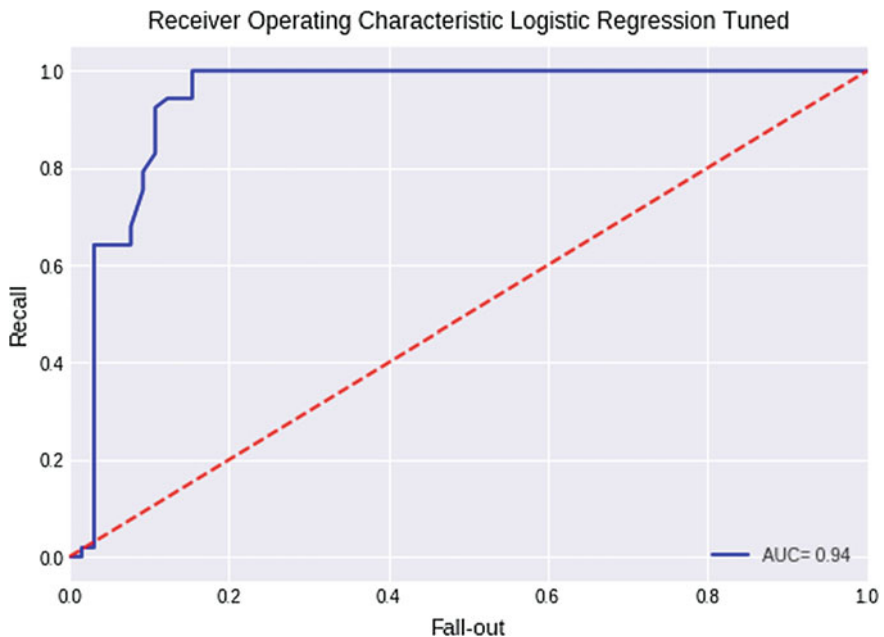


Fig. 5 ROC logistic regression

Table 2 Decision tree performance

Class	Precision	Recall	F1
0	0.97	0.91	0.94
1	0.89	0.96	0.93
Average	0.93	0.93	0.93

Results for Decision Tree are as shown in Table 2 and Figs. 6 and 7, while those for support vector machine, Naive Bayes and k Nearest Neighbors' performance are shown Table 3 and Figs. 8 and 9, 10, 11, 12.

3 Discussion of Results

Logistic regression reported an accuracy of 0.917, obtained by setting the penalty to 11 and a C of 0.1. In logistic regression, C is the regularization parameter and controls the trade-off between allowing the model to increase its complexity while remaining simple. L1 regularization is a type of regularization that shrinks the less important feature's coefficient to zero, thus removing it altogether. These results compare well

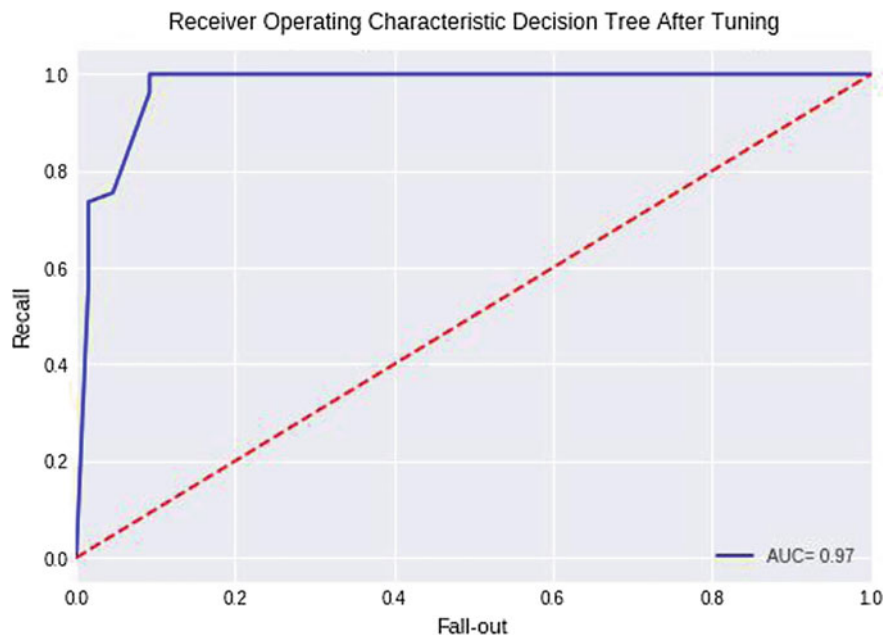


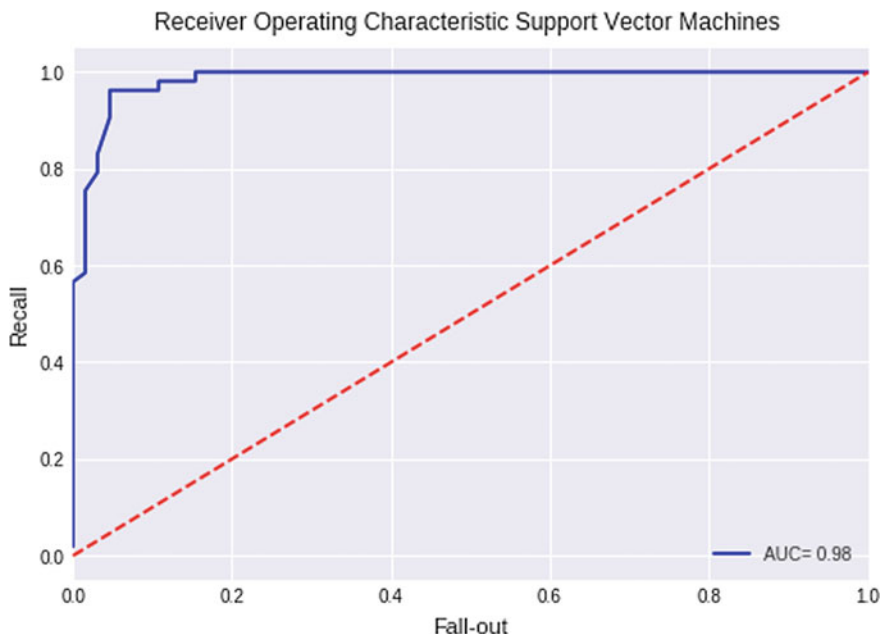
Fig. 6 ROC decision tree



Fig. 7 Learning curve decision tree

Table 3 SVM performance

Accuracy	Precision	Recall	F1
0.91	0.88	0.96	0.92
1	0.84	1.0	0.91
Average	0.93	0.92	0.92

**Fig. 8** ROC decision tree

with what is reported in the literature. A Cohen kappa score of 0.832 was obtained, which can be interpreted as very good agreement between the model's predictions and the true values. This is, however, slightly lower than the figures reported for raw accuracy implying that accuracy metric is more optimistic for this case. Precision obtained was 0.867 implying that logistic regression predicts worm packets as such about 87% of the times. Recall was 0.996, almost a perfect recall score. This means that the model does well in predicting worms from the traffic packets. The F1 score obtained was 0.926. This high harmonic mean indicates that the model does very well at both precision and recall. The ROC curve obtained for logistic regression approaches the left top corner with an AUC score of 0.94 which can be interpreted as outstanding. The model is thus outstanding at identifying worm traffic packets. The learning curve for logistic regression revealed very high train and test scores. The gap between the train and test scores was also very narrow implying that logistic

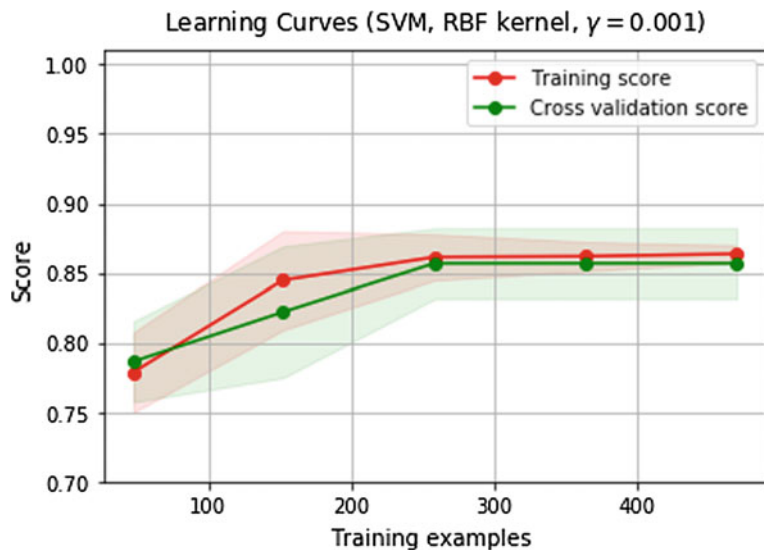


Fig. 9 Learning curve SVM

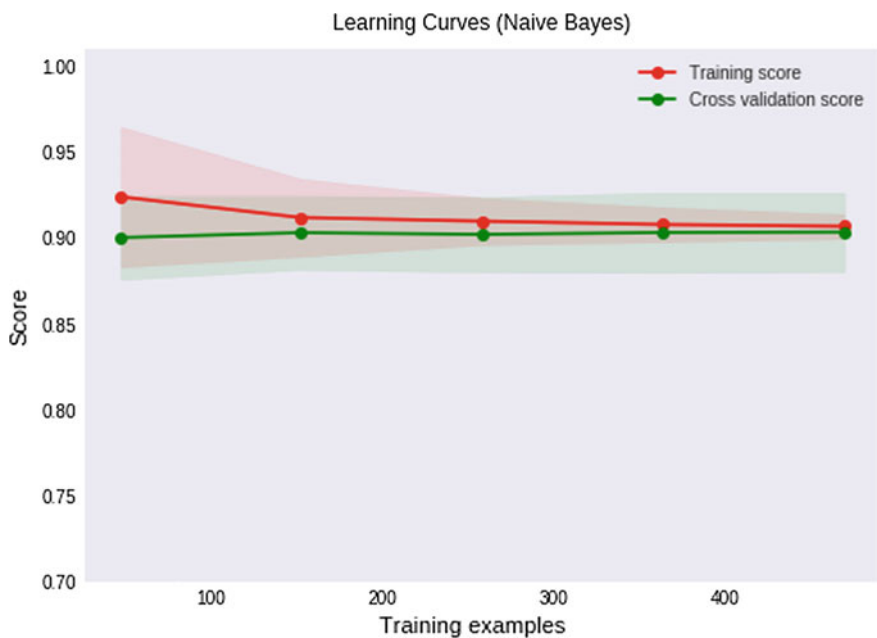


Fig. 10 Learning curve NB

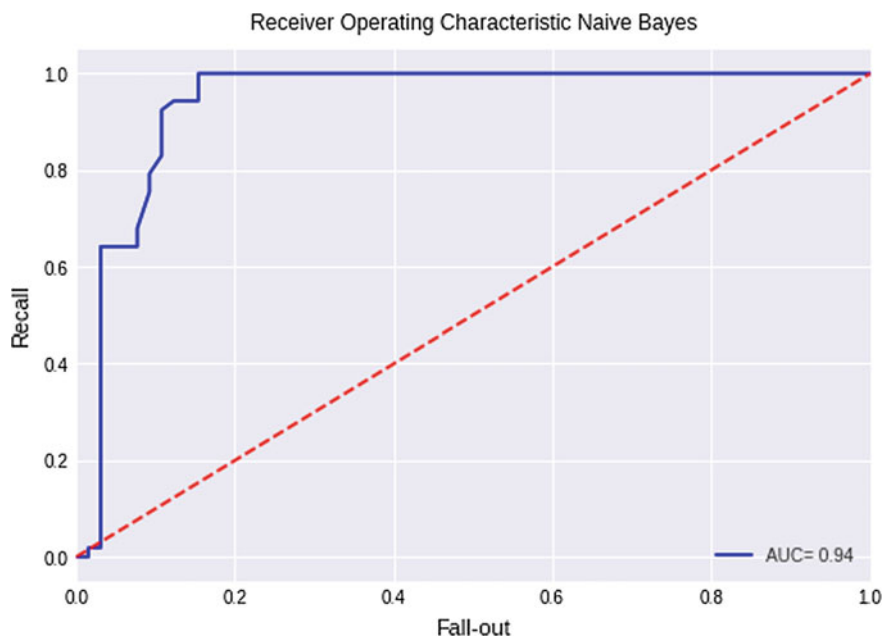


Fig. 11 ROC NB

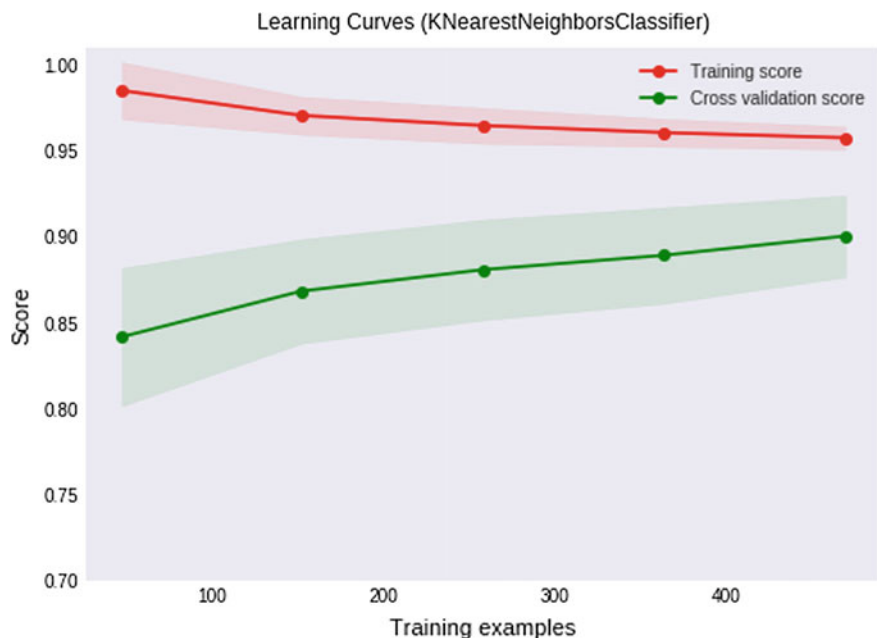


Fig. 12 Learning curve kNN

regression did not over-fit for the dataset. The model is thus useful at classifying previously unseen traffic packets as worms and not worms.

Decision tree obtained a raw accuracy of 0.924 slightly better than the result obtained for logistic regression. A Cohen kappa score of 0.864 was obtained for decision tree indicating a slightly higher optimism for raw accuracy but still interpreted as very good agreement between the model's predictions and the true values. The best parameters were returned as decision tree criterion entropy, a maximum depth of 5 and a minimum samples per leaf of 3. Criterion is the function used to measure the quality of a split. Entropy uses information gain for this. Maximum depth refers to the depth beyond which the tree is not allowed to grow, while minimum samples per leaf refers to the minimum number of samples required for a node to be a leaf node.

Decision tree f1 score was 0.930, slightly higher than that obtained by logistic regression. An AUC score of 0.97 was achieved for decision tree again interpreted as outstanding. Decision tree however did not generalize as well as logistic regression.

Support vector machine achieved accuracy of 0.911, less than that of decision tree with a Cohen kappa score of 0.881 interpreted as very good agreement between the model's predictions and the true values. The f1 score for SVM was 0.918. The best parameters were $C = 10$, gamma = 0.03 and kernel = rbf. C, the soft-margin constant, is the penalty assigned to margin errors, while the kernel is the kernel function. Here, rbf is the radial basis function kernel. Since the dataset is not highly dimensional, the results obtained for SVM are not particularly better than those obtained for the other classifiers as would be the case for high-dimensional datasets (BenHur and Weston 2010). An almost perfect AUC score of 0.99 is obtained, and the ROC curve approaches the left uppermost corner. Both the training and test scores are high at about 0.95 and 0.90, respectively, for most sizes of training examples. The figures stay constant mostly. The classifier does not generalize very well as the gap between the training and test curves remains constant and wide even with increased size of examples. This remains so even after classifier tuning.

Naive Bayes achieved an accuracy of 0.906 which was comparable to logistic regression, decision tree and support vector machines. A Cohen kappa score of 0.831 was obtained showing a slightly over-optimistic accuracy figure. Precision and recall scores were also high at 0.871 and 0.963, respectively. The GaussianNB classifier used achieves a very high AUC score of 0.99, and the ROC curve approaches the left uppermost corner. The training and test scores are high at 0.93 for most sizes of examples. The classifier generalizes very well as the two curves, training curve and test curve, almost merge, for example, sizes greater than 100.

Nearest neighbor classifier, kNN, achieved an accuracy of 0.885, and a Cohen kappa score of 0.864 was obtained, validating the accuracy score. Precision was 0.874, while recall was 0.909. The best parameters were found to be a leaf size of 3, a metric of Euclidian, number of neighbors of 3 and weights of distance. The model does not generalize well.

4 Conclusion

The study addressed the problem of detecting computer worms in networks. The datasets used for the experiments were obtained from the University San Diego California Center for Applied Data Analysis (USCD CAIDA).

Logistic regression, naive Bayes and support vector machines performed the best in terms of accuracy and generalization. However, there were no marked differences between the classifiers.

It is apparent that the particular classifier used may not be the determinant in classification in machine learning experiments but rather the choice of features. While this is largely consistent with other similar studies, it should be further confirmed by future research.

It is true that not all computer worms can be detected by a single method. In the future, it is recommended that a combination of different detection approaches be combined to be able to detect as many types of computer worms as possible. Also, the span of features used for detection should be expanded to include even more features for the detection. The contribution of each feature to the detection ability should be documented.

Unsupervised learning has not been investigated in this research. Unlabeled traffic datasets are available to security researchers and practitioners. The cost of labeling them is high. This makes unsupervised learning useful for threat detection. The manual effort of labeling new network traffic can make use of clustering and decrease the number of labeled objects needed for the usage of supervised learning.

References

1. Ellis, D.: Worm anatomy and model. In: Proceedings of the 2003 ACM Workshop on Rapid Malcode. ACM (2003)
2. Moore, D., Shannon, C., et al.: Code-red: a case study on the spread and victims of an internet worm. In: Proceedings of the 2nd ACM SIGCOMM Workshop on Internet measurement, pp. 273–284. ACM (2002)
3. Moore, D., Paxson, V., Savage, S., Shannon, C., Stanford, S., Weaver, N.: Inside the slammer worm. *IEEE Secur. Priv.* **99**(4), 33–39 (2003)
4. Samuel, A.L.: Some studies in machine learning using the game of checkers. *IBM J. Res. Dev.* **3**, 210–229 (1959)
5. Buczak, A.L., Guven, E.: A survey of data mining and machine learning methods for cyber security intrusion detection. *IEEE Commun. Surv. Tutorials* **18**(2), 1153–1176 (2015)
6. Kumar, R., Xiaosong, Z., Khan, R.U., Ahad, I., Kumar, J.: Malicious code detection based on image processing using deep learning. In: Proceedings of the 2018 International Conference on Computing and Artificial Intelligence, pp. 81–85. ACM (2018)
7. Kalash, M., Rochan, M., Mohammed, N., Bruce, N.D., Wang, Y., Iqbal, F.: Malware classification with deep convolutional neural networks. In: 2018 9th IFIP International Conference on New Technologies, Mobility and Security (NTMS), pp. 1–5. IEEE (2018)
8. Kolosnjaji, B., Zarras, A., Webster, G., Eckert, C.: Deep learning for classification of malware system call sequences. In: Australasian Joint Conference on Artificial Intelligence, pp. 137–149. Springer, Cham (2016)

9. Rathore, H., Agarwal, S., Sahay, S.K., Sewak, M.: Malware detection using machine learning and deep learning. In: International Conference on Big Data Analytics, pp. 402–411. Springer, Cham (2018)
10. Sewak, M., Sahay, S.K., Rathore, H.: An investigation of a deep learning based malware detection system. In Proceedings of the 13th International Conference on Availability, Reliability and Security, p. 26. ACM (2018)
11. Shiva Dharshan, S.L., Jaidhar, C.D.: Windows malware detector using convolutional neural network based on visualization images. *IEEE Trans. Emerg. Topics Comput.* (2019)
12. Hardy, W., Chen, L., Hou, S., Ye, Y., Li, X.: DL4MD: a deep learning frame-work for intelligent malware detection. In: Proceedings of the International Conference on Data Mining (DMIN), p. 61. The Steering Committee of the World Congress in Computer Science, Computer Engineering and Applied Computing (WorldComp) (2016)
13. Martin, A., Menéndez, H.D., Camacho, D.: Genetic boosting classification for malware detection. In: 2016 IEEE Congress on Evolutionary Computation (CEC), pp. 1030–1037. IEEE (2016)
14. Awad, R.A., Sayre, K.D.: Automatic clustering of malware variants. In: 2016 IEEE Conference on Intelligence and Security Informatics (ISI), pp. 298–303. IEEE (2016)
15. Ma, X., Biao, Q., Yang, W., Jiang, J.: Using multi-features to reduce false positive in malware classification. In: 2016 IEEE Information Technology, Networking, Electronic and Automation Control Conference, pp. 361–365. IEEE (2016)
16. Jiménez, J.M.H., Goseva-Popstojanova, K.: The effect on network flows-based features and training set size on malware detection. In: 2018 IEEE 17th International Symposium on Network Computing and Applications (NCA), pp. 1–9. IEEE (2018)
17. López-Vizcaíno, M., Dafonte, C., Nóvoa, F., Garabato, D., Álvarez, M.: Network data unsupervised clustering to anomaly detection. *Multi. Digital Publishing Instit. Proc.* **2**(18), 1173 (2018)
18. Mekky, H., Mohaisen, A., Zhang, Z.L.: Separation of benign and malicious network events for accurate malware family classification. In: 2015 IEEE Conference on Communications and Network Security (CNS), pp. 125–133. IEEE (2015)
19. Iglesias, F., Zseby, T.: Analysis of network traffic features for anomaly detection. *Mach. Learn.* **101**(1–3), 59–84 (2015)
20. Kabanga, E.K., Kim, C.H.: Malware images classification using convolutional neural network. *J. Comput. Commun.* **6**(01), 153 (2017)
21. Pai, S., Di Troia, F., Visaggio, C.A., Austin, T.H., Stamp, M.: Clustering for malware classification. *J. Comput. Virol. Hacking Tech* **13**(2), 95–107 (2017)
22. Yousefi-Azar, M., Varadarajan, V., Hamey, L., Tupakula, U.: Autoencoder-based feature learning for cyber security applications. In: 2017 International joint conference on neural networks (IJCNN), pp. 3854–3861. IEEE (2017)
23. I-Maksousy, H.H., Weigle, M.C., Wang, C.: NIDS: neural network based intrusion detection system. In: 2018 IEEE International Symposium on Technologies for Homeland Security (HST), pp. 1–6. IEEE (2018)
24. David, O.E., Netanyahu, N.S.: Deepsign: deep learning for automatic malware signature generation and classification. In: 2015 International Joint Conference on Neural Networks (IJCNN), pp. 1–8. IEEE (2015)
25. Domingos, P.M.: A few useful things to know about machine learning. *Commun. ACM* **55**(10), 78–87 (2012)
26. CAIDA UCSD Network Telescope “Three Days of Conficker”. http://www.caida.org/data/passive/telescope-3days-conficker_dataset.xml
27. Emile Aben. Conficker/Conflicker/Downadup as seen from the UCSD Network Telescope. Technical report, CAIDA, February 2009. <https://www.caida.org/research/security/ms08-067/conficker.xml>

Fully Annotated Indian Traffic Signs Database for Recognition



Banhi Sanyal, R. K. Mohapatra, and Ratnakar Dash

Abstract We present a fully annotated database of Indian traffic signs for classification with nearly 1700 images. The images have been taken in varied weather conditions in daylight. The images are of varied parameters and reflect strong variations in terms of occlusion, illumination, skew, distance and other conditions. Semi-automated annotation makes the ground truth reliable. This is the first such attempt to make an Indian database to the best of our knowledge.

Keywords Traffic signs · Indian database · Fully annotated · Semi-automated · Classification · Varied weather conditions

1 Introduction

Traffic signs are indicators at the side of the roads to inform the drivers about the conditions of the road ahead. Traffic sign recognition (TSR) aims at recognizing these signs and inform the driver. TSR is a relatively emerging topic due to its huge importance in the field of traffic safety and automatic driving.

Traffic signs vary widely from each other in terms of size, shape, color, texts, digits, etc., and as such traffic signs vary from state to state depending on the traffic rules established in the states. As such to attain higher efficiency of traffic sign recognition in a particular country, the training set should also be of that same country.

B. Sanyal (✉) · R. K. Mohapatra · R. Dash
Department of CSE, NIT Rourkela, Rourkela, Odisha, India
e-mail: banhisanyal9@gmail.com

R. K. Mohapatra
e-mail: mohapatrark@nitrkl.ac.in

R. Dash
e-mail: ratnakar@nitrkl.ac.in



Fig. 1 Examples of Chinese traffic signs



Fig. 2 Examples of German traffic signs

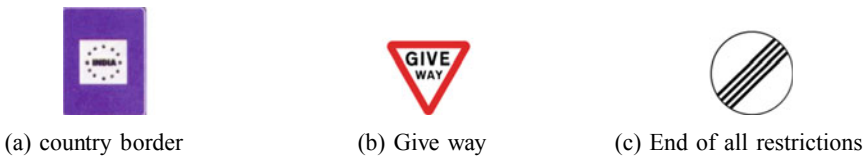


Fig. 3 Examples of Indian traffic signs

A few databases are available publicly but any Indian database for traffic sign recognition is not available to the best of our knowledge. Figures 1, 2 and 3 show the huge variation in traffic signs which are specific to the countries and not available in other databases. This proves the necessity of an exclusive Indian traffic sign database. This research work aims at designing a database with all possible Indian traffic signs considering the challenges of low illumination, occlusion, blur and other real-time challenges and also to make it publicly available.

The rest of the paper is organized as follows. Section 2 gives related work. Section 3 gives details about the database and Sect. 4 gives discussion. Concluding remarks are given in Sect. 5.

2 Related Work

The efficiency of any TSR system increases with the robustness of its training images. As such over the period many such recognition databases have been developed in many countries. The most prominent among them is the German traffic sign recognition benchmark (GTSRB) [1] database which was developed as a part of a competition. GTSRB has 39,252 and 12,631 images for training and testing classes,

Table 1 Details of standard databases

Name	Country	Training images	Testing images	Classes
GTSRB	Germany	39,252	12,631	43 training 43 testing
BTSC	Belgium	4575	2520	62 training 53 testing
rMASTIF	Croatia	4044	1784	31 training 31 testing
DITS	Italy	8650	1159	59 training 57 testing
ChineseTSD	China	4170	1994	58 training 58 testing

respectively. This is one of the largest databases of traffic signs. It also provides the features of HAAR, HOG and hue in HSV format as it was constructed to be a part of a competition for image recognition. The leading teams of the competition used support vector machine (SVM) and convolutional neural network (CNN) as classifiers. CNN has also been widely used as efficient classifiers in other fields such as emotion analysis [2], mobile communication [3], productivity improvement in manufacturing systems [4], etc. Timofte et al. [5] created the Belgium traffic sign for classification (BTSC) using multiple cameras has 4575 training images and 2520 images in 62 training and 53 testing classes. Laboratory for Intelligent and Safe Automobiles (LISA) traffic sign database by Mogelmose et al. [6] gives US images and videos for traffic sign recognition which has 49 classes and 6610 images. It has not been divided into predefined training and testing classes, but code in python language has been provided to divide the database randomly into training and testing images. Mapping and Assessing the State of Traffic Infrastructure (MASTIF) [7] and revised MASTIF (rMASTIF) [8] give Croatian signs for classification. MASTIF dataset has all its images annotated in three parts which have 6000, 3000, 1000 images, respectively. The database rMASTIF has 4044 training images and 1784 testing images in 31 classes. Dataset of Italian traffic signs (DITS) [9], Chinese traffic sign database [10] and traffic signs of Swedish roads [11] is also available. DITS has 8650 training and 1159 testing images sorted into 59 training and 57 testing classes. The Chinese dataset has 4170 training images, 1994 testing images and 58 classes. Sweden database has more than 20,000 images with 20% of them labeled. None of these databases are practical for Indian roads. Only LISA database provides video tracks. Annotations of databases other than GTSRB, BTSC, MASTIF and rMASTIF do not follow any convention. Automated or semi-automated annotation has been claimed only by a few (GTSRB, BTSC, LISA). The details of the databases are given in Table 1.

3 Database Design

The dataset was collected in the city of India in daylight in January and February. The data collection was done over 12 h of time. To maintain variety in the database, the database was collected using two devices. A total of 333 images of 3.35 MB with resolution 3264×1836 pixels each were taken using a mobile camera of handset Samsung SM-J320F, exposure time 1/611 s, 3 m focal length, 2.3 max aperture, Metering mode: Center weighted average without flash. Other 1361 images were taken by Canon EOS 80D camera with a focal length of 30 mm, exposure time 1/400 s in sunny daylight conditions. The images have a dimension of 6000×4000 pixels and a size of 27.9 MB each and is of .CR2 format. The .CR2 images were converted to .JPEG using Lightroom CC app [12]. The images were taken in daylight in clear and partially clouded weather.

Let each physical traffic sign be called as a traffic sign instance. Each instance has been photographed multiple times and a track in training images consists of the same physical traffic sign. There are 1692 traffic sign images taken in total which is divided into training and testing images. The training set has 1397 images and the test set has 294 images in total. The number of images in each class may vary widely depending on the occurrence of the sign on the roads. The training set is divided into 49 classes numbered from 0000 to 0048. Each class may have multiple tracks, indexing starting from 0, each track refers to images of the same traffic sign instance. Each track has multiple images. The first part of the image refers to the track number, whereas the second part refers to the image number. For example, image 0_12 will refer to the thirteenth image in the 0th track. The number of images per track may vary. The test set is also divided into 49 classes. The images in a test class are named such that the first part refers to the class number and the second part refers to the image number. For example, image 0000_09 will refer to the tenth image in the class 0000. The dataset is in .JPEG format. The distribution of images in the database is given in Table 2 and represented in Fig. 4. It is evident from the given table that the database is unbalanced to reflect the true distribution of different symbols on the Indian roads.

The images vary between 3264×1836 pixels or 6000×4000 pixels. The region of interest (traffic sign) of the image may be placed anywhere in the image and not necessarily in the middle. This makes the model using the database more robust.

Annotations are done manually using the VGG image annotator tool [13] in offline mode. The ground truth is reliable due to the semi-automated annotation. The annotation done is in .CSV format. Each class of the training set has an annotation file consisting of the annotations of all the images of that class. The test set also has annotations in each of its classes.

Table 2 Database table

Class	Testing	Training, Tracks	Indications
0000	11	40.2	Bumps
0001	3	15.1	Track crossing
0002	9	36.2	Accident prone
0003	4	16.1	No standing
0004	2	17.1	40 kmph
0005	3	14.1	No overtaking from right
0006	4	17.1	National highway
0007	4	16.1	Side road left
0008	10	50.2	60 kmph
0009	5	20.2	Gap in median
0010	9	32.2	Left hand curve
0011	7	22.4	U turn
0012	3	8.2	Object hazard right
0013	4	16.2	Single chevron
0014	11	58.3	Traffic merging from right
0015	8	32.1	Narrow bridge
0016	8	32.1	Petrol pump
0017	4	27.2	50 kmph
0018	6	24.1	School ahead
0019	10	61.3	Bus stop
0020	9	51.2	Overhead cables
0021	8	40.2	Stop
0022	4	23.1	80 kmph
0023	12	74.4	People on road
0024	4	21.2	Right curve
0025	4	30.2	No standing
0026	4	16.1	Industrial area
0027	10	43.2	Police station
0028	3	10.2	30 kmph
0029	7	23.3	Speed breaker
0030	6	28.1	Weigh bridge ahead
0031	8	32.2	Right reverse band
0032	2	13.2	Compulsory keep left
0033	14	66.2	Hospital
0034	2	11.1	Truck lay by
0035	2	2.1	Truck lay by

(continued)

Table 1 (continued)

Class	Testing	Training, Tracks	Indications
0036	5	25.1	Built up area
0037	4	30.2	Round about
0038	6	33.1	Series of bends
0039	6	29.1	Pass either side
0040	6	29.2	Zonal no parking
0041	4	28.2	20 kmph
0042	5	27.1	Children in vicinity
0043	4	17.1	Vehicles prohibited in both directions
0044	6	33.1	50 kmph for cars and bikes
0045	4	17.1	Bump ahead
0046	9	36.3	40 kmph
0047	6	33.1	Intersection major road ahead
0048	4	24.2	Single chevron

4 Discussion

Any real-time TSR system depends on the database system it was trained with. The more the database system reflects the real-time scenarios the more robust the trained model will be. As such, much effort has been given to include real-life scenarios in the proposed database. During image acquisition it had been noted that the traffic signs on the Indian roads may or may not be in ideal condition. Degradation of the signs with time is very common which will make the recognition procedure more difficult. Few of the common degradation were in the form of broken traffic signs (Fig. 5a, b). Accumulation of dirt over time may cause illegibility 5c. The second type of challenges faced are common to any TSR system. These challenges are of low illumination (Fig. 5d), over illumination Fig. 5e, blur (Fig. 5f), skew (Fig. 5g, h) and occlusion Fig. 5l. The third set of challenges is typical to the traffic sign set being dealt with. For example, Fig. 5i, j both represent the same speed limit sign but are represented in different ways. Figure 5i, j show how a difference does not change the sign while Fig. 5j, k show how a change can represent different signs. All these add to the variety of the database. The fourth criteria of the database are all its images are annotated semi-automatically in the database which makes the training more reliable.

This work is an attempt to create a standard fully annotated image for Indian roads. The variety of the traffic signs and its semi-automatic annotation makes it reliable and robust. This database can be further extended by adding more images and/or annotated images in later stages.



Fig. 4 Samples of all the classes placed sequentially in the proposed database

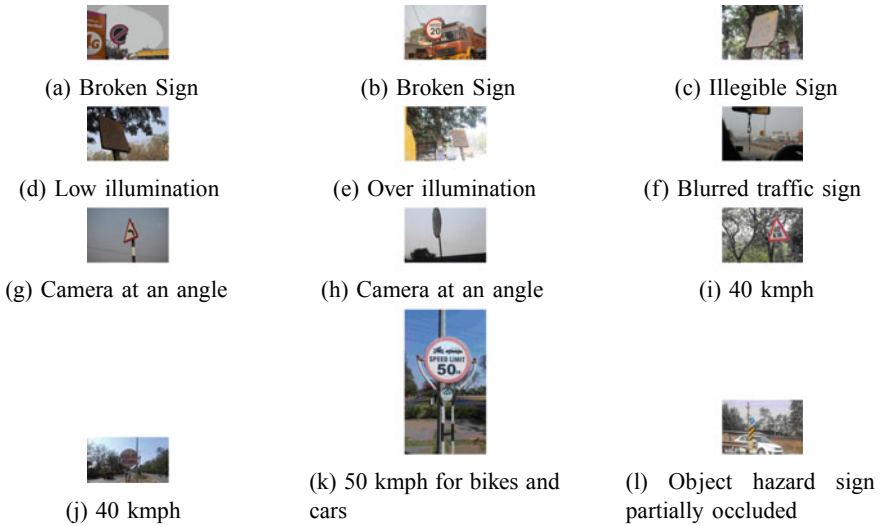


Fig. 5 Challenges included in the databases

5 Conclusion

We present an attempt of creating a publicly available fully annotated Indian traffic signs database for recognition. Section 4 shows the diversity of images that have been included while creating this database. The database is available at https://nitrkl.ac.in/oldwebsite/Academic/Academic_Centers/Centre_For_Computer_Vision.aspx. The semi-automatic annotation and unbalanced nature make it reliable and robust. In the future, annotated videos are to be added to the existing database.

References

1. Stallkamp, J., Schlipsing, M., Salmen, J., Igel, C.: The German traffic sign recognition benchmark: a multi-class classification competition. In: IJCNN, vol. 6, p. 7 (2011)
2. Mahajan, R.: Emotion recognition via EEG using neural network classifier. In: Soft Computing: Theories and Applications, pp. 429–438. Springer, Singapore (2018)
3. Srivastava, M., Saini, S., Thakur, A.: Analysis and parameter estimation of microstrip circular patch antennas using artificial neural networks. In: Soft Computing: Theories and Applications, pp. 285–292. Springer, Singapore (2018)
4. Giri, J.P., Giri, P.J., Chadge, R.: Neural network-based prediction of productivity parameters. In: Soft Computing: Theories and Applications, pp. 83–95. Springer, Singapore (2018)
5. Timofte, R., Gool, L.V.: Sparse representation based projections. In: British Machine Vision Conference (BMVC, UK) (2011)
6. Mogelmose, A., Trivedi, M.M., Moeslund, T.B.: Vision-based traffic sign detection and analysis for intelligent driver assistance systems: perspectives and survey. IEEE Trans. Intell. Transp. Syst. **13**(4), 1484–1497 (2012)

7. University of Zagreb Faculty of Electrical Engineering and Computing. <http://www.zemris.fer.hr/~ssegvic/mastif/datasets.shtml>
8. University of Zagreb Faculty of Electrical Engineering and Computing. <http://www.zemris.fer.hr/~kalfa/Datasets/rMASTIF/>
9. Department of Computer Engineering, Automatic and Management, Sapienza University. <http://users.diag.uniroma1.it/bloisi/ds/dits.html>
10. National Laboratory of Pattern Recognition. <http://www.nlpr.ia.ac.cn/pal/trafficdata/recognition.html>
11. University of California San Diego. <https://www.cvl.isy.liu.se/research/datasets/traffic-signs-dataset/download/>
12. Adobe. <https://www.adobe.com/in/products/photoshop-lightroom.html>
13. Visual Geometry Group Department of Engineering Science, University of Oxford. <http://www.robots.ox.ac.uk/~vgg/software/via/>

Streamlining Choice of CNNs and Structure Framing of Convolution Layer



Sonika Dahiya, Rohit Tyagi, and Nishchal Gaba

Abstract Convolutional neural networks (CNNs) are a kind of deep neural networks which were designed from the biologically driven models. Researchers focused on how humans perceive an image in the brain. As an image is passed through different layers in the human brain, in the same way, CNNs have many layers. In this paper, the structure of CNN is described, guidelines on the design of the convolution layer and decision making on when to use a pre-trained CNN model with transfer learning and when to design our custom architecture CNN model. This will help future researchers in a quick start with CNN modeling. Experimentation is done on two popular image datasets, i.e., CIFAR-100 and Stanford clothing attribute dataset, where CIFAR-100 is a clean dataset of 60,000 images belonging to 100 classes and Stanford clothing attribute dataset is highly noisy and imbalanced data as it has uneven distribution of samples for different attributes and many of the samples do not have a clear distinction between the classes resulting in overlapping training data. Four CNNs were designed, where two models were pre-trained CNN models and two were customized CNN models and compared their performance on image classification task and treatment of the missing data in the dataset. Based on this comparison and related study, we framed the guidelines for designing a convolution layer and making choice between using a pre-trained (transfer learning) or customized CNNs.

Keywords Machine learning · Convolutional neural network · Transfer learning · Image classification

S. Dahiya (✉) · R. Tyagi
Delhi Technological University, New Delhi, India
e-mail: sonika.dahiya11@gmail.com

N. Gaba
Unreal AI Technologies Pvt. Ltd., New Delhi, India

1 Introduction

Convolutional neural network is an extension of artificial neural network which is popularly used for many applications like medical image analysis, recommender systems, natural language processing, image classification, image and video recognition, etc. There are many layers in CNN, which include: convolution layer, activation layer, pooling layer, batch norm layer, dropout layer and fully connected layer. Convolutional neural networks (CNNs) have gained immense popularity since AlexNet won the ImageNet Challenge in 2012 [3].

In numerous fields such as computer vision, they are becoming the state of art achieving near human or better performance. They sound fascinating but designing a CNN is a herculean task in itself. Till now there is no fixed formula for the design of CNN. Many researchers have come up with the general suggestions but they do not always hold and even with small changes at critical places in a CNN, huge improvements have been seen, such as pooling design is studied by [1], smaller convolutional filters for better accuracy in case of Imagenet [5, 8] and study of very deep convolutional networks for large-scale image recognition [6]. But these conditions do not hold always, as the dependency of the classification task on a dataset is as important as its dependency on an algorithm.

CNN exploits the spatial hierarchical features of data, extracts features and helps classify them into different classes. This has led to the development to a stream of data augmentation and pre-processing to increase the data, as more data allows for the chance of better training and avoiding over-fitting. This helps build models that are more robust to new samples as we try to make it more generalized to noise at the training phase.

This paper implements four convolutional neural network models to understand the concept of structuring of the convolutional layer of CNN. This context will help the researchers, what choice to make while working on datasets to achieve good results early, rather than going through a whole range of hit and trial cycles for finalizing the structure of a convolutional layer of their CNNs.

To choose between the pre-trained model and our model (customized CNN) efficiently, there exists a set of factors that helps in better understanding and correct methodology for selecting the model. These factors include number of features, number of classes, noisy and imbalanced dataset, presence of stark features between samples of different classes, etc. This also fits in the concept of transfer learning and using pre-trained models to make predictions on the different datasets rather than the ones they are trained to which is known as fine-tuning the models to a new dataset. In this paper, we have also formulated the structure of the convolutional layer which helps develop the custom models and putting their layers in a finite range rather than an infinite pool of possibilities.

We implemented the image classifiers for two datasets, CIFAR-100 [2] and Stanford clothing attribute dataset [4] and compared the results of a custom network against a pre-trained model VGG16 with Imagenet weights using Keras and Tensorflow python frameworks. This helped in understanding the important aspects of the

transfer learning process. The second dataset taken into consideration was Stanford clothing attribute classifier which demonstrated the problems of not pre-processing the dataset efficiently. It depicted that the pattern variation in pixels was full of noisy pixels. In this case, the background and region of interest (ROI) were to be focussed before training the specified network model using techniques such as cropping of ROI. Also, while discussing the layers, we see the computation feasibility of different types of layer architectures and their effect on the speed of convergence toward achieving minimal error. Using this, the design of CNN which is although a hit and trial can be narrowed to a list of possibilities to be tested and help form hypotheses for results based on patterns identified by previous researchers.

2 Basic Description of CNN Structure

This section discusses the design structure of CNN based on data and the optimization techniques that can help most of the CNNs with low dependency on the structure. We are going to see the techniques in a reverse manner similar to the flow of a back-propagation to demonstrate the learning cycle of a CNN.

2.1 *Output of CNN*

The output of a CNN in tasks such as classification is usually the probability of different outputs. For example, if the final output of a CNN has four units (usually denoted as classes), they are normalized into the probability of occurrence of these classes, and the unit with maximum probability is labeled as the output class. This may vary for task-specific cases such as facial recognition, where the output is an encoded form of the input rather than the representation of output for a particular class. Back-propagation helps to minimize the error by reducing the error/cost function which helps in shaping the values of the weights so that the accuracy is increased. There are different types of optimizers to help train the network by reducing the loss such as Adam optimizer, momentum optimizer and others, these are generally used in classification tasks. For special requirements of loss functions, such as in case of facial recognition requiring embedding rather than classifying to a particular class, triplet loss is used.

2.2 *Fully Connected Layer*

The structure from top to down usually forms a pyramid structure, the number of parameters in these layers keep on converging until they finally reach the number of desired classes. Increasing the number of hidden units in the layer can increase the

learning ability of the network, but there is a saturation of the increase in the accuracy of the network. There is no formulation of the units you choose; it is a hit and trial usually. There are two factors taken into account in terms of fully connected layers, the number of units in each layer and the depth of the mesh of the fully connected layers. Increasing the number of units help increase accuracy initially, but reaches a saturation soon and then the accuracy starts decreasing. Depth is very useful to make a hierarchy of features but too many layers may cause an increase in computational cost and hence decrease in the speed of the network. Most of the networks in research usually perform well with several units in multiples of 64. Two–three layer networks are good if enough patterns are being passed to the network after flattening the outputs of the convolutional layers. Generally, a convolution layer is followed by an activation layer and later by dropout layer to help generalize the network. This is one of the problems with designing CNNs from scratch that you mostly have to settle for acceptable accuracy and trying to achieve always the best solution. As most CNNs already take a long time to train, getting an acceptable range of accuracy is preferred if done within a feasible time frame. Here, transfer learning or using pre-trained proven architectures give a great starting point provided there is enough data to tune the weights to be able to classify a custom dataset. One important point to note while training the CNN is preparing for generalization. CNNs work very well on inference data if its pattern is also similar to the training data using which the CNN was trained with. But giving vastly varying data for classification can lead to abrupt results. Hence, data augmentation for robustness to noise is an important aspect. This will be very crucial to understand when we see transfer learning in the following sections.

2.3 Dropout Layer

The dropout layer is usually applied after the layer containing neurons in the fully connected network. The dropout layer is a regularization layer. It helps to create robustness in the layer by dropping a fraction of units randomly from the previous layer usually kept around 20–50% of the original input. This helps create noisy input for the next layer and makes it more adaptable for such noisy samples.

2.4 Pooling Layer

These are usually used in two settings, max pooling and average pooling. But recently some advanced styles of pooling such as mixed pooling and gated pooling are also used in some networks. Max pooling helps to reduce the dimensionality of the previous layer such as scaling down the width and height of the previous layer by half by keeping only the maximum values in the nearby range, but this may cause some

information loss. The concept behind these is that adjacent or nearby pixels can be approximated by the maximum information-carrying pixel.

2.5 Activation Layer

An activation layer in a convolutional neural system comprises of an activation function that takes the convolved feature map produced by the convolutional layer and makes the activation map as its yield. Activation functions are those functions that map a specific output to a specific set of inputs. So they are used for containing the output in between 0 and 1 or -1 to 1. They are also used to impart a nonlinearity in the machine learning models and are one of the important factors which affect the results and accuracy of the machine learning models. There are some important activation functions used in machine learning such as identity function, sigmoid function, binary step function, Tanh function, ReLU function and leaky ReLU function. This layer mostly uses ReLU as an activation function. ReLU is a function that is used to set all negative values to zero and keeps the positive value as it is. The ReLU activation function definition is:

$$R(z) = \max(0, z) \quad (1)$$

2.6 Convolutional Layer

Convolutional layer introduces the concept of shared weights. The shared weights /filters in these layers usually comprise of three factors kernel size (square matrix) (width of the kernel), stride of the convolution and number of filters. Although the parameters in these layers are less than the ones in the bottom layers, these present a computational bottleneck for the networks. Even small networks can scale up to millions of parameters, for networks such as AlexNet which has 60 million parameters. These require the most data to train and hence enough data has to be provided for them to be optimized. Usually, the standard filter sizes used are 7×7 , 5×5 , 3×3 and most recently 1×1 . The recent inception modules have shown that the computation of smaller kernel sizes has faster computation and perform at par with large kernel sizes usually. The other aspect comes is the depth of the filters or the number of filters. The computation scales highly as the depth increases. [Rethinking the inception architecture for computer vision, Szegedy et al .] shows the factorization of bigger convolutions into smaller convolutions and also gives the example of a comparison of a 5×5 layer into two 3×3 layers and the performance difference. The mathematical details of the increase in speed are presented in [7] (Fig. 1).

So, how CNN actually works is basically a step by step process of corresponding layers operations such as convolution layer operation, activation layer (ReLU) operation, pooling layer operation, flattening, and finally, flattened vector data is fed

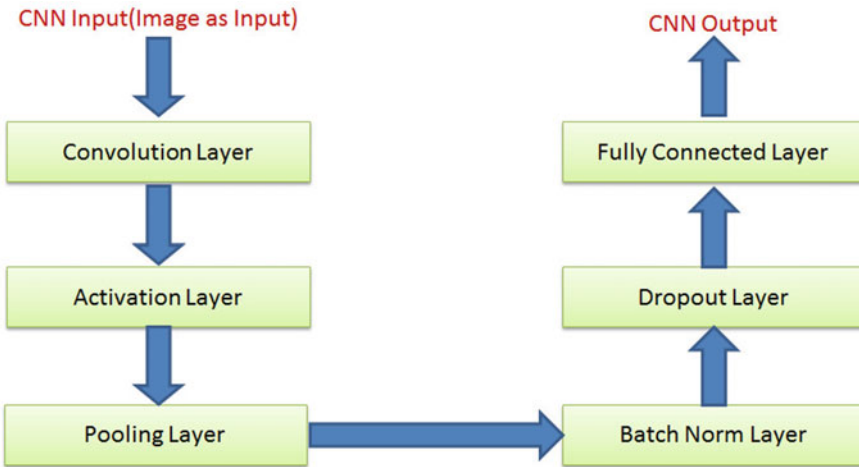


Fig. 1 Basic structure of CNN

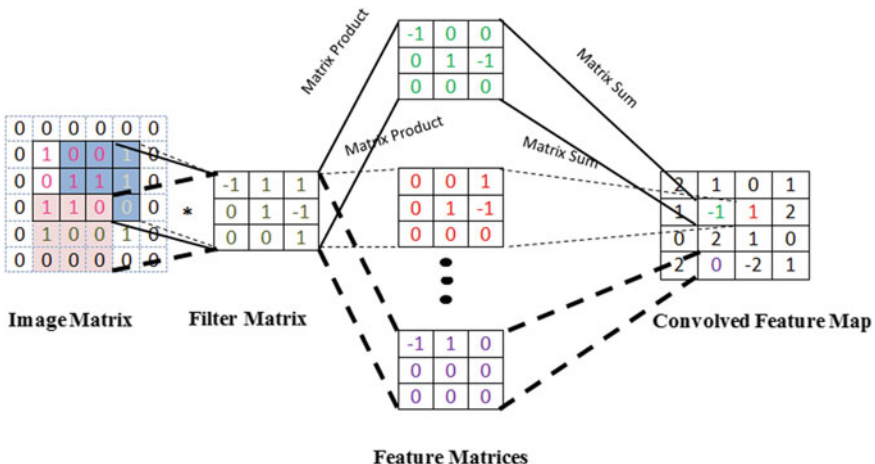
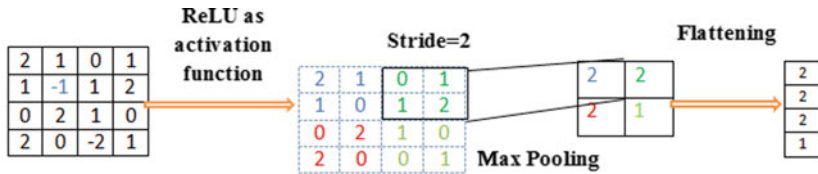


Fig. 2 Matrix map of convolution

to fully connected layer as an input, where one vector value is given to one input node of the network. Taking an example: First of all, CNN uses a filter matrix over an array of images and perform convolution to get a convolved feature map and this operation is called convolution operation (Figs. 2 and 3).

After this operation, the activation layer (ReLU as activation function) operation, max pooling and flattening occurs.

And in the last, this flattened vector data is fed to a fully connected layer/neural network as an input, where one vector value is given to one input node of the network.

**Convolved Feature Map****Fig. 3** Activation, pooling and flatten

3 Transfer Learning

One of the powers of machine learning is learning something from one place and makes use of its prior knowledge in performing similar tasks to get a better initial learning point, hence, helping the loss converge faster. Optimization of very deep convolutional networks and millions of images might take up months, and retraining a new network on such data is not quite feasible in most cases. But what if we can start from the previously learned networks, use the optimization that they have already done and form layers of our own over it? This question gave birth to the field of transfer learning or knowledge transfer, where a previously optimized network can be used as a base model for optimization for the same or different datasets with room for customization.

It comes with its pros and cons. Although it helps the new classifiers get a better initial learning point, these pre-trained networks pack a lot of baggage with them, for example, the VGG16 model trained on Imagenet is quite heavy to be run on normal laptops/desktops and as they are fine-tuned on millions of images, the new data should have a good chunk of samples to make a dent into the previous weights and help the network perform classification on the new data. It is although possible to make custom networks perform better than pre-trained networks with small samples as well which although for the lighter weight of the models and faster inference speed but requires prior knowledge of the functions of each CNN layer and might require a lot of hit and trial. One such example is seen for the Stanford clothing attribute classification dataset [4].

4 Decision Making on Choices of, Pre-trained CNN or Customized CNN

4.1 Pre-trained Versus Custom CNN

The prominent finding of our work is to formulate soft guidelines for the structure of the convolution layer of CNN and to decide when a pre-trained CNN may work better or a custom design may give better results. The structure of CNN does not

have a closed best solution, hence, one cannot say for a dataset that this is the best ever CNN that cannot be improved further. Hence, we do not target the best structure but rather providing a feasible solution with the guidelines. We divide the choice of a CNN based on the availability and pattern of data, as data is a very important part of a model because if there are not good patterns to be found, and it is very difficult that the CNNs will give good and distinct results. There are four categories of data we look into:

- Data with a high number of images (10K+ overall, approximately 1k per class) and good differentiable patterns between different classes. For instance, one class is of a flower and the other class is an automobile, and they have quite different spatial patterns. In such a case, it is quite useful to develop a pre-trained CNN. Although there might be a custom CNN that might give better results, but transfer learning will help you get a substantial solution very quickly as well. The most common choice of pre-trained CNN is VGG16 or ResNet50. VGG has quite a heavy model size and does require a lot of epochs to train, as you are fine-tuning the weights again for your classes.
Custom CNN in this case if developed should have 4–6 convolutional layers and approximately 14 overall layers, similar to what the structure of these pre-trained CNNs to give a good starting point in terms of structure, other hit and trial methods lead to a better structure as well for a particular dataset, because patterns in the data is the key to structuring the CNN, and there is no particular formula to see this degree of pattern.
- Data with a high number of images but somewhat overlapping patterns, such as two classes of very similar shaped flowers and little difference in the color. This is a tricky one, and a custom CNN design is better in this case because pre-trained CNN usually is not good at picking such low differences and get biased toward a particular category. In our observation, in this case, the balance of data for each class also plays a big role, if a number of samples for a class are quite high compared to other classes with an overlapping pattern, the pre-trained CNNs will give biased results for the class with more samples. Hence, although on checking accuracy sometimes, we might be misled with pre-trained giving a higher accuracy in some cases, but many of them just give biased class results and not generalized and distinct results. A custom CNN design with a large number of epochs will be very useful in such cases.
- Data with a low number of images and distinct patterns, both the pre-trained and custom CNN can give good results here. Two–three convolutional layer architectures can give satisfactory results in these cases. Transfer learning seems to have a little edge in the training phase though because they have weights already distributed to different classes compared to initial random weights of a custom design. Hence, although custom CNNs can give good results, here, but if one wants to avoid the hit and trial phase, a pre-trained CNN can give quite significant results still.

- Data with a low number of images and overlapping patterns, a custom CNN design is a better approach in this case, as discussed earlier for the case of the high number of images because pre-trained CNNs mostly give biased results for these cases.

4.2 Designing Guidelines for Convolution Layer

We discuss the convolutional layer in detail in this paper as it is a prominent part of the whole CNN architecture. We are not formulating the rest of the layers currently in this work, which we wish to do in the extension of our current work. The convolutional layer comprises independent filters that are convoluted (dot product in the case of CNN) over the input image or the output of the previous layer and helps to extract spatial hierarchical features using shared weights. The filters usually consist of four dimensions, namely filter height, filter width, input filter dimension (the one coming from the previous layer) and output filter dimension. The choice of filter height and width affect the feature identified and is usually chosen to be an odd dimension between 1 and 7. The filter height and width are kept the same. As seen in the work of [7], the convolutions of 3×3 and 1×1 are computationally more efficient to have as compared to higher filters such as 5×5 and 7×7 . Hence, we recommend keeping the filter sizes between 1 and 3. And size 5 in some cases only, where the

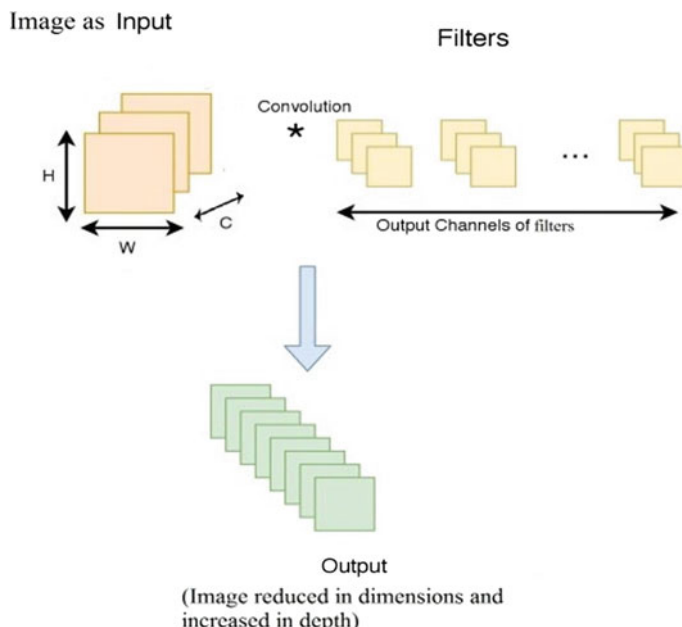


Fig. 4 General structure of convolution

patterns seem quite distinct between different classes. We have used the filters to be 3×3 in our research models. The output dimensions of the filter may vary, usually, for grayscale inputs, it is kept to be 8 or for RGB input images many research models use 16 or 32 as the output channels. This is a choice of the user, but we recommend usually not going beyond a multiple of 8 of the previous channel, as the number of weights will increase and there depth of features identified may not be improved comparably in terms of the increased resources required for higher channels (Fig. 4).

5 Implementation and Results of Choices of Pre-trained VGG16 and Custom Designed CNN

Implementation is done on Ubuntu OS with i7-4th Gen CPU using python frameworks in Jupyter IDE such as Keras and Tensorflow.

5.1 *Datasets*

We have worked on two datasets, CIFAR-100 and Stanford clothing attribute dataset. These two datasets are strategically chosen to analyze the effect of variation in the CNN structure as well as internal aspects of the dataset such as the number of classes, data patterns, pre-processing, etc.

CIFAR-100 consists of 60,000 images belonging to 100 classes which can further be divided into 20 super-classes. This allows the coarse label of training and identifying the accuracy of the network in similar cases, for example, two objects within a class such as vehicles. Each image is of size $32 * 32 * 3$ and in each class, there are 600 images. The training set is of 50,000 images with 500 images from each class and a testing set of 10,000 images with 100 images from each class.

Classifying classes with overlapping features is more difficult than the ones with easily differentiating features. Distinguishing a flower from a truck is easier than separating a truck from a car as spatially, car and truck have more features overlapping as compared to a flower.

Clothing attribute dataset consists of 1856 images and 26 ground truth clothing attributes that are collected using the Amazon Mechanical Turk crowd-sourcing tool. These attributes are labeled as necktie, collar, gender, placket, skin exposure, wear scarf, solid pattern, floral pattern, spotted pattern, graphics pattern, plaid pattern, striped pattern, red color, yellow color, green color, cyan color, blue color, purple color, brown color, white color, gray color, black color, many (>2) colors, sleeve length, neckline and category in the same order. The values of some attribute entries are NaN, indicating no acceptable category reached by all the turks mutually. This will help us tackle the problem of missing data. We tackle these two different ways actually, one is taking any of the random classes for these and the other is dropping

the samples which NaNs in the results category, both produce quite different results and help us prepare better for real-life data scenarios as this.

5.2 Results

Custom CNNs trained on clothing attribute dataset did not provide great results on small networks and also the results varied highly based on categories based on the variation of patterns in each particular category, for example, black color category. We trained a VGG16 pre-trained model of black color attribute from the above dataset and compared it to a custom CNN and the result was highly dissatisfying for pre-trained CNNs. There was a lot of missing or unlabeled data in this category, there were choices to either drop such data or to label it randomly to one of the categories and pass to the system for training. The later harmed the custom CNN designs, as initial learning is very important for such CNNs to be able to differentiate with pixels into different categories. CNNs take huge advantage of hierarchical spatial features, and the black color category corresponds to color attributes and also with corrupt (randomly labeled data which was previously missing) the features are even harder to classify. We cropped the image around the center so that the background color does not contribute to the color classification of the clothing. Custom design of four convolutional layers was able to provide average results for the classification, but many results were biased toward the black color. For pre-trained VGG, the change in output probability was very low for white color and was mostly biased for black color.

This proved our hypothesis of training a custom CNN for fewer images and difficult to identify features. Good results were expected from pre-trained CNN from this as well, but due to missing or corrupt data, the features could not change the network weights significantly as there are millions of weights to be optimized in such a big network.

During training, the pre-trained CNN displayed a training accuracy of 82% after 30 epochs, compared to 80% in a four layer designed CNN (this could be improved further for different architectures, but this was considered a satisfactory network to verify the hypothesis). But the test results were only biased to black for pre-trained CNN; hence, this measure for pre-trained CNN is considered incorrect, whereas the custom CNN did produce different classes for a variety of samples, but it also showed hints of bias due to quantity of data tilted toward black data.

Patki and Suresha [4] provide results of their custom CNN versus pre-trained model (Fig. 5).

For CIFAR 100 custom CNN, we created for overall 14 layers achieved an accuracy of 49%, whereas the VGG 16 transfer learning model for CIFAR 100 achieves accuracy of almost 69% for our model. This proves our hypothesis that for datasets with a high number of images and distinct features can be trained easily using a pre-trained CNN and would require more hit and trial in case of custom CNNs, hence, it is easier to start with pre-trained CNNs in such cases (Table 1).

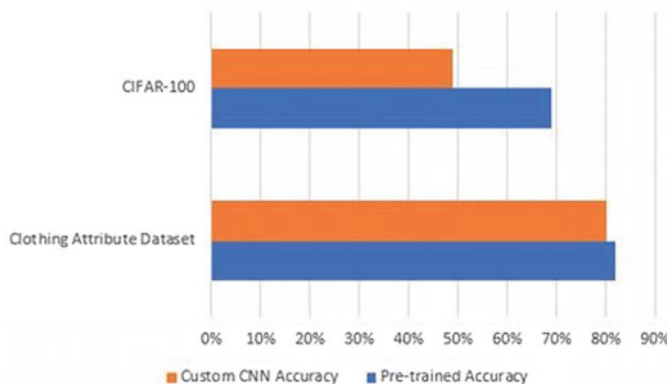


Fig. 5 Accuracy results

Table 1 Classifier accuracies

S. No.	Dataset	Pre-trained CNN (%)	Custom CNN (%)
1	CIFAR 100	69	49
2	Clothing attribute dataset	82	80

6 Conclusions

In this work, we explored the design cycle of convolutional neural network, and especially the formulation of the convolution layer. There is no particular solution design for a CNN for a particular task such as image classification as it may be good for one specific dataset and not the other. Hence, we looked at some determining factors for these such as data volume, data imbalance and overlapping between different classes. We in this work are exploring the structural formation factor of CNN into two categories, existing structure of CNN for retraining on new data (transfer learning) and a custom design CNN for the data that involves heavy hit and trial for the structural formation of different layers and how each of them individually affects the CNN as a whole. Implementing the research on two datasets, namely CIFAR-100 and Stanford clothing attribute dataset, and see the performance of custom CNN vs a pre-trained CNN for the above datasets. Seeing the above results, we found that for large volume datasets, and non-overlapping clean features, both pre-trained and custom model perform well, but using a pre-trained network will save the time to researching the structure of a good CNN. These two datasets are being tested over two models, viz. Custom CNN and Pre-trained CNN model, whose results are depicted in the figure. It shows that CIFAR 100 over the pre-trained CNN model gives an accuracy of 69% compared to 49% for the custom CNN model. Similarly, pre-trained CNN model over Stanford clothing attribute dataset gives 82% accuracy

and custom CNN gives 80% accuracy. Although if the aim is achieving extremely high accuracies, custom CNN can do a good design as well as an alternative to a good solution but this is a herculean task for someone new to the design of CNN theory. For a dataset such as clothing attribute dataset, the images were less for each class as well as noisy samples were observed, which caused a lot of data to be not readily usable. Two strategies can be employed, such as dropping this data altogether and the other is assigned a random class of the possible ones to it and then train it. We have employed the strategy of data drop as although the data is less, but the samples are truly labeled, whereas in the second case, there might be some data samples with wrong labels, causing loss of accuracy in the overall training. In this case, a custom CNN worked extremely well as compared to a pre-trained CNN as usually these pre-trained models have millions of parameters and it is not optimal to retrain them with such a low number of images. We also provided general guidelines for the structure of CNN, such as the number of layers to be implemented for such datasets and also the internal parameters such size of kernel filters, which we feel is a good starting point for someone beginning with the design of CNNs.

7 Future Work

In this work, we studied the design of CNNs and developed some soft guidelines based on the data and the number of images and patterns in the images. Experiments have been performed to decide when to choose custom CNNs of less or more layers and when to choose transfer learning or pre-trained models for better solutions. In our future work, we want to explore more mathematical bounds of different kinds of layers and how their combined architecture might affect the patterns in one of these data as well. Currently, the major focus is on four sections, which include firstly the data with a high number of images (10K+ overall, approximately 1k per class) and also good differentiable patterns between different classes. For instance, one class is of a flower and the other class is an automobile, they have quite different spatial patterns. Secondly, data with a high number of images but somewhat overlapping patterns, such as two classes of very similar shaped flowers, and the little difference in their color. Thirdly, data with a low number of images and distinct patterns too and in the last, data with a low number of images and overlapping patterns as well.

So, we have developed these, later, we first need to expand our work to more datasets. Currently, we are restricting to the image datasets but we will go for much heavier datasets other than the CIFAR-100 dataset and Stanford clothing attribute dataset. And then, we will try to formalize the current theory as well for different frameworks and see the effect on varying image data such as RGB, grayscale and HSV. We have currently employed our work on RGB images mainly in this paper so we wish to do that as well. And also formalized mathematical bounds for these, and the effect, if any identified for different kinds of images for RGB, HSV, grayscale, etc.

References

1. Boureau, Y.-L., Ponce, J., LeCun, Y.: A theoretical analysis of feature pooling in visual recognition. In: Proceedings of the 27th International Conference on Machine Learning (ICML-10) (2010)
2. Krizhevsky, A., Hinton, G.: Learning multiple layers of features from tiny images, vol. 1, No. 4. Technical report, University of Toronto (2009)
3. Krizhevsky, A., Sutskever, I., Hinton, G.E.: Imagenet classification with deep convolutional neural networks. *Adv. Neural Inform. Process. Syst.* (2012)
4. Patki, R., Suresha, S.: Apparel classification using CNNs. Unpublished results (2016)
5. Sermanet, P., et al.: Overfeat: integrated recognition, localization and detection using convolutional networks. arXiv preprint [arXiv:1312.6229](https://arxiv.org/abs/1312.6229) (2013)
6. Simonyan, K., Zisserman, A.: Very deep convolutional networks for large-scale image recognition. arXiv preprint [arXiv:1409.1556](https://arxiv.org/abs/1409.1556) (2014)
7. Szegedy, C., et al.: Rethinking the inception architecture for computer vision. In: Proceedings of the IEEE Conference on Computer Vision and Pattern Recognition (2016)
8. Zeiler, M.D., Fergus, R.: Visualizing and understanding convolutional networks. In: European Conference on Computer Vision. Springer, Cham (2014)

SNAP N' COOK—IoT-Based Recipe Suggestion and Health Care Application



Diksha Mukherjee, Albin Paulson, Shajo Varghese, and Mukta Nivelkar

Abstract Epicure interests in trying a variety of food recipes and explore unknown dishes. People with the circumscribed amount of subject area in the field of cooking may face such difficulty in finding new recipes. Of course, there are ways to find a variety of recipes in books and a lot of websites providing the same, but it is a time-consuming process. One needs to first check out base ingredients present with them and then search manually. Recipes found out may or may not be healthy according to a person's health preferences. Snap N' Cook—IoT-based Recipe suggestion and health care application would help users to explore the variety of new recipes that can be tried with vegetables available with them. The device will identify the vegetables using image processing and object detection methods, at periodic intervals set by the user or could be scanned as per user's need and will suggest recipes from vegetables recognized in real-time from the internet by web scraping. This would be an automated system using a web camera installed at the targeted device and can also be accessed by a user from a remote location. Recipes will be recommended depending on health preferences given by users and will also calculate calorie intake for each day using BMR (Basal Metabolic Rate). Stale vegetable which is uncooked for seven days would also be discovered using a motion sensor. Whenever a motion is detected, the image will be captured and compared. On the discovery of new vegetables, it would be included in the database along with a timestamp. If that vegetable is uncooked for seven days alert notification would be sent to a user regarding the same.

Keywords Vegetable detection · Android application · IoT · Basal metabolic rate (BMR) · Recipe suggestion

D. Mukherjee (✉) · A. Paulson · S. Varghese · M. Nivelkar
Fr. C. Rodrigues Institute of Technology [FCRIT], Maharashtra, Navi Mumbai 400703, India
e-mail: mukherjeediksha30@gmail.com

1 Introduction

Food is the most essential requirement for the growth of any living being. Starting from having healthy eating habits to nutritious food it is important to maintain a good diet. Every day there is food craving to eat something new, something different, but eating fast food is not a healthy alternative for one's health. The second option arises to cook food at home in a variant manner, again then is the barrier of having a restricted knowledge of recipes, thus leading to former recipes and quotidian dishes.

In India, there is a majority of women cooking food in houses being housewives or working women. The same frustrating question encountered each day is 'What's in dinner?'. The book searching method is very tedious while, searching recipes on websites require manually entering a list of vegetables available and then optimize the results best according to choice. Recipes found out may or may not be healthy according to a person's health preferences and background health-related issues. Consumers with diabetes problems should not eat food with sugar nor may person with high blood pressure should consume food with less salt in them. This should be considered as a filter that users should be suggested recipes according to their preferences and health issues.

In a competitive new era and fast new world, people are busy with their lives that they pay the least attention to their eating habits. This causes bad effects and also leads to severe health issues. Consumption of stale food may also result in similar results. People should be aware of dried out vegetables and fruits for the maintenance of good health. The amount of calorie intake by a particular person each day is also a very important factor. Each one should pay special attention to their diet and eating habits to be healthy and wealthy. Having food with high-calorie intake seems delicious and tempting but after its consumption, if any physical activity is not performed it may cause a disastrous effect like stress on your digestive system, uneasiness, overweight, length of life span decreases along with the quality of life. But if calorie intake is low then too it leads to health issues like reduced muscle's mass. The body searches for sources of energy to just keep vital organs functioning and it will turn to the muscle mass for those energy foods. This is called catabolism. The metabolic rate will drop dramatically if consumed too little calories and after three days of low-calorie intake this will compound muscle mass loss.

SNAP N' COOK—IoT-based Recipe suggestion and health care application would help users to get explore a variety of new recipes that can be tried with vegetables available with them. Currently, users have ways to get to know about the recipes they can try but requires manual efforts. This system will provide them various alternatives based on preferences. Finally, Snap N' Cook will help improve the overall experience of an epicure and revolutionize traditional cooking experience.

2 Literature Survey

The Following are the IEEE papers referred to perform literature survey.

- Paper Title: Automatic Vegetable Detection and Recipe Suggestion.
The authors are Swati Kalyanasundar (MCA 2015–18, K. J. Somaiya Institute of Management Studies and Research, India) and Sangeetha Rajesh (Assistant Professor, IT, K. J. Somaiya Institute of Management Studies and Research, India). In this paper, various techniques are used to find out the best matching image based on features such as color, shape, texture, and size. One of the techniques used is by comparing the Histograms of the captured image and the stored image. Another technique is to classify based on the texture of the vegetable in the image. These two methods help in identifying the parent class of the vegetable that is to be identified. If multiple vegetables are belonging to the same parent class then another method called gray level threshold levels [1].
- Paper Title: Classification of Vegetables Using TensorFlow.
The authors are Om Patil, Prof (Dr.) (Department of Electronics Engineering, Vishwakarma Institute of Technology, Pune), Vijay Gaikwad (Department of Electronics Engineering, Vishwakarma Institute of Technology, Pune).
This paper is proposing a glimpse of the recognition of a particular vegetable. This is being implemented on the TensorFlow platform, which is making use of OpenCV as the main library database. First the given frame is converted into an image and differentiated into cubical parts from which the features are extracted, so to converge it into the data set. Such data sets are encapsulated from every cubical unit, emerged as a whole bunch of values after traversing thoroughly through a given frame. A certain frame is categorized into one of the sets of images provided, at the conclusion side percentage-wise isolation of objects is done, and here the vegetables are being identified and the corresponding action should be executed [2].
- Paper Title: High-Performance Vegetable Classification from Images Based on AlexNet Deep Learning Model.
The authors are Ling Zhu^{1,2,3}, Zhenbo Li^{1,2,3}, Chen Li^{1,2,3}, Jing Wu^{1,2,3}, Jun Yue⁴
 1. College of Information and Electrical Engineering, China Agricultural University, Beijing 100083, China.
 2. Key Laboratory of Agricultural Information Acquisition Technology, Ministry of Agriculture, Beijing 100083, China.
 3. Beijing Engineering and Technology Research Center for the Internet of Things in Agriculture, Beijing 100083, China.
 4. College of Information and Electrical Engineering, Ludong University, Yantai 264025, China, 2018.

This paper emphasizes on AlexNet model construction and model training. The vegetable image data sets were rotated at 90°, 180°, and 270° by the method of data expansion. By this method, the image data sets were enlarged by 4 times. Caffe deep learning techniques are used as it has a lot of expansion options. AlexNet model

construction and model training is used as it is quite good for traditional machine learning classification complex algorithms. Convolutional Neural Networks is used as it is effective even in complex models. It had an accuracy of 92.1% which is optimal when compared to BP Neural networks (78%) and SVM classifier methods (80.5%) [3].

3 Proposed System

SNAP N' COOK is proposed as a two-phase system involving both hardware and software implementation.

1. HARDWAE module (IoT) to capture images of vegetables
2. MOBILE APPLICATION on the user device.

The following figure shows an overall view of SNAP N' COOK system with all its detailed components and control flow. There are mainly six modules in this system as listed below:

- Vegetable Recognition Module
- Recipe Suggestion Module
- Health-related preferences and calorie intake module
- Stale vegetable detection
- Mobile application for user
- Online social media platform (Fig. 1).

3.1 Vegetable Recognition Module

This module will capture images using a web camera installed on a targeted device. The captured image would then be preprocessed for vegetable identification using TensorFlow object detection API and image processing techniques with the help of R-CNN (Region Convolution Neural Network) algorithm [4]. Region-CNN (R-CNN) is one of the state-of-the-art CNN-based deep learning object detection approaches. Based on this, there are fast R-CNN and faster R-CNN for faster speed object detection as well as mask R-CNN for object instance segmentation [5] (Table 1).

Following Fig. 2 is a snapshot of the implemented module where vegetables like tomato, potato, and onion are detected with a score greater than 70%.

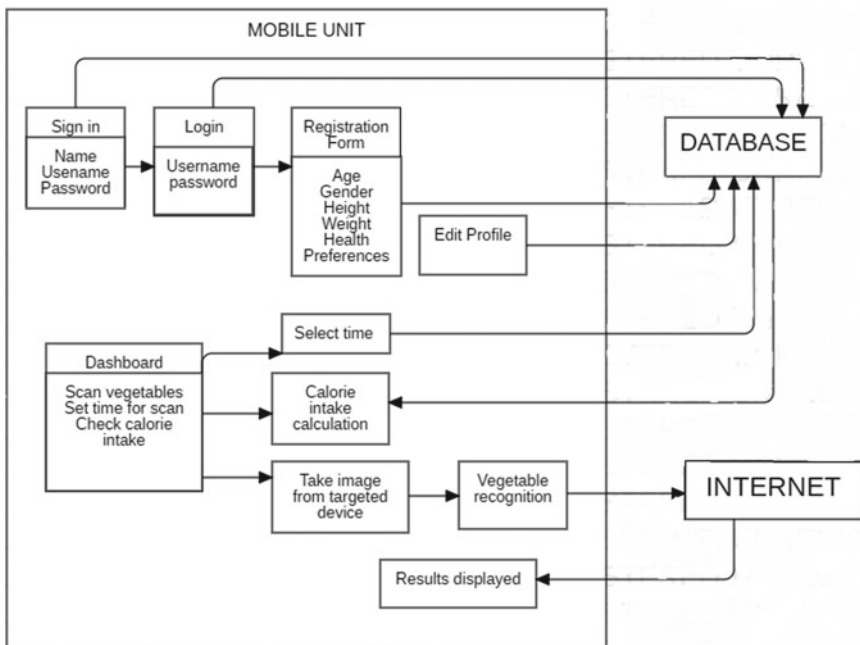


Fig. 1 Architectural diagram of SNAP N' COOK (software implementation)

3.2 *Recipe Suggestion Module*

Vegetables recognized from the vegetable recognition module would now be considered for this module. Recipe suggestion module will suggest recipes from vegetables identified in real-time from the internet by web scraping. Web scraping is a technique employed to extract large amounts of data from websites [6] (Fig. 3).

3.3 *Health Preference and Calorie Intake Module*

This module will suggest recipes according to health preferences given by the user and will also calculate calorie intake for each day using BMR (Basal Metabolic Rate). Basal metabolic rate is the amount of energy per unit time that a person needs to keep the body functioning at rest. BMR is calculated with parameters gender, age, weight, height and also the type of work done like:

- Sedentary (Little or no exercise)
- Lightly Active (Light Exercise 1–3 days/week)
- Moderately Active (Moderate Exercise 3–5 days/week)
- Very Active (heavy exercise/sports 6–7 days/week)

Table 1 Steps involved in vegetable detection [9]

No.	Name	Description
1	Gathering data	To train a classifier, we need a lot of pictures that should differ a lot from each other, having different backgrounds, random objects, different positions, and varying lighting conditions. We have used 50 images of each vegetable to be detected. Images would have high resolution so we want to transform them to a lower scale in order to make the training process faster. So we resize images to 800×600
2	Labeling data	Images have to be divided into two parts training data and testing data. 80% of data in the training folder and 20% of data in the testing folder. In order to label data, we use some kind of image labeling software. LabelImg is a great tool for labeling images. After labeling data, XML files of each image will be created
3	Generating TFRecords for training	XML files to CSV need to be done to maintain a tabular structure of our data along with its features like height, width, classification. A TFRecord file stores data as a sequence of binary strings. With the images labeled, we need to create TFRecords that can be served as input data for the training of the object detector
4	Configuring training	Label Map is a file to label id with the vegetable name to be identified
5	Training model	The model is trained with the above steps as input parameters
6	Testing object detector	The trained model is run and an image is passed to test object detector

- Super Active (Heavy Exercise twice a day, every day).

BMR calculated using Revised Harris-Benedict Equation:
For men:

$$\text{BMR} = 13.397W + 4.799H - 5.677A + 88.362 \quad (1)$$

For women:

$$\text{BMR} = 9.247W + 3.098H - 4.330A + 447.593 \quad (2)$$

where

W is body weight in kg, H is body height in cm, A is age

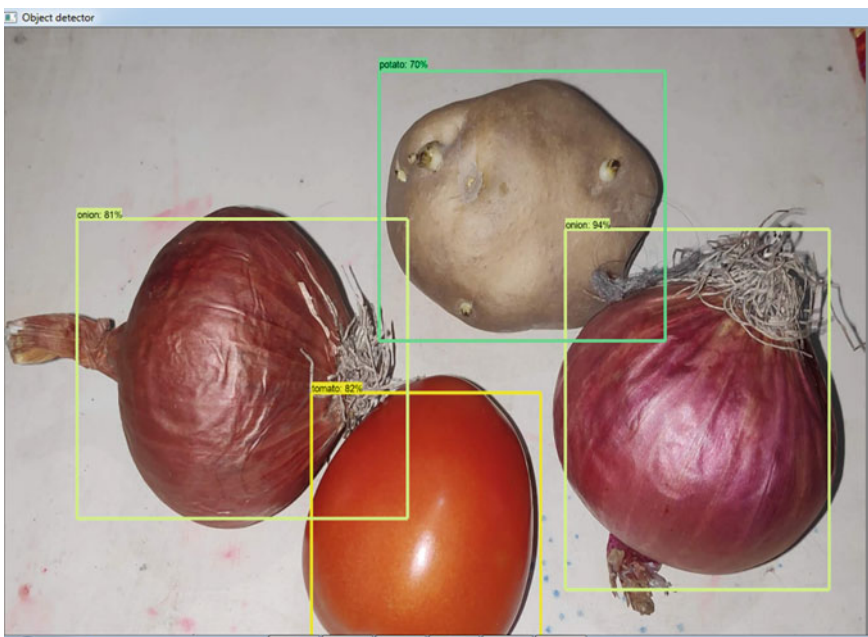


Fig. 2 Vegetable recognition module

This value is multiplied by an activity factor (generally 1.2–1.95), dependent on a person's typical levels of exercise, in order to obtain a more realistic value for maintaining body weight [7].

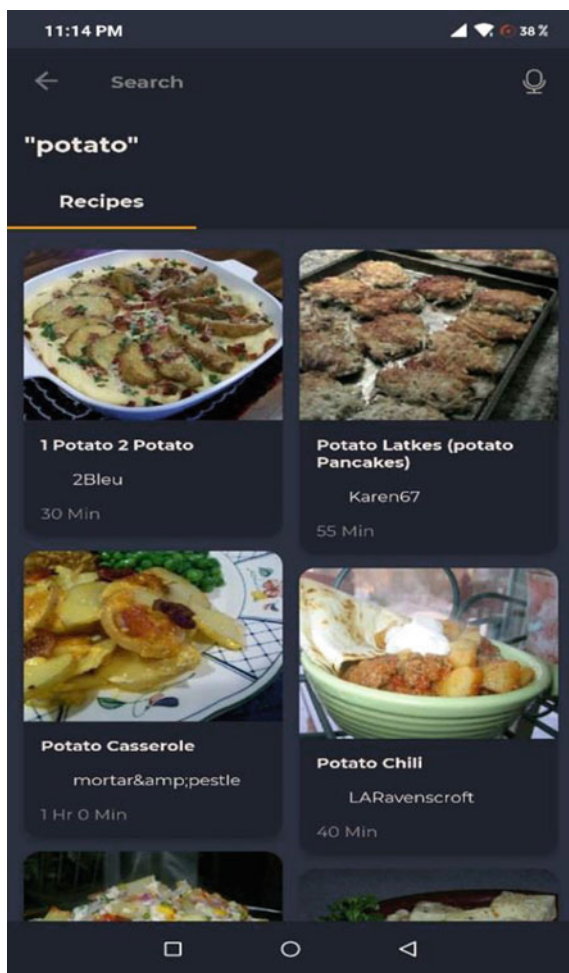
3.4 *Stale Vegetable Detection*

A motion sensor will be installed at a targeted device. Whenever a motion is detected the camera will capture the image and will compare it with the previous image if a new vegetable is detected it would be included in the database along with the timestamp. If that vegetable is uncooked for seven days alert notification would be sent regarding the same. This would be implemented with a hardware module consisting of the Raspberry pi, camera module and IoT sensors (Fig. 4).

3.5 *Mobile Application on the User's Device*

Users will have a mobile application installed at their device. The first step is to register and set up a web camera with the system to use system functions. For

Fig. 3 Recipe suggestion module using web scraping [8]



registration, the user will have to use mail id. Once the user is registered successfully, the user can access the system using the registered account. After the successful registration, the user will be prompted to input height, weight, age, physical activity type. This will help the system in calculating daily calorie intake.

After successful registration, the user can set predefined time for vegetable scanning or can scan anytime as per choice. The camera will capture an image on a predefined time or whenever requested which is connected to Raspberry Pi. The list of identified vegetables will be displayed to the user. Users can select vegetables out of the list for which the recipes should be searched.

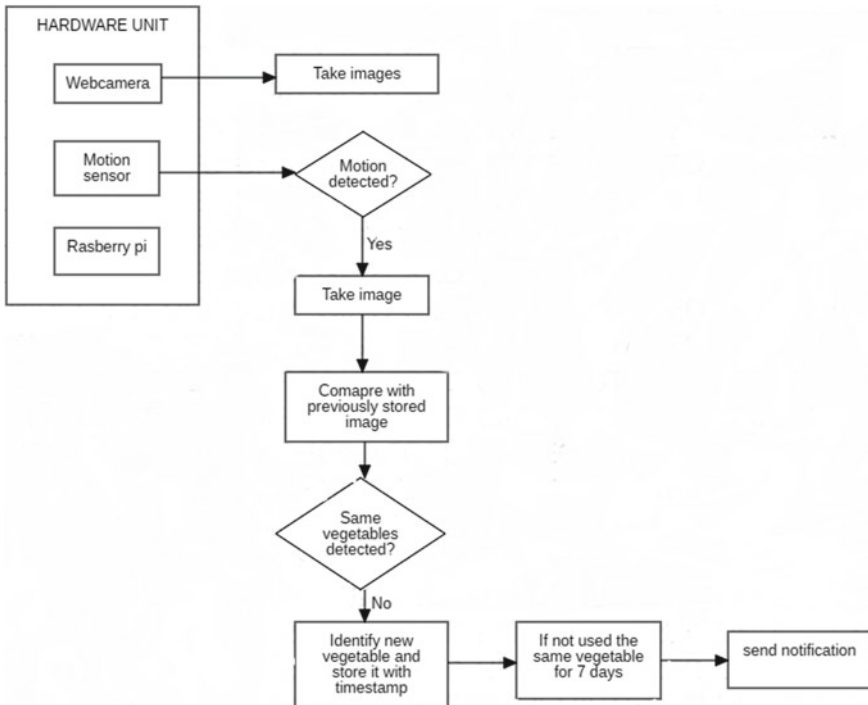


Fig. 4 Stale vegetable detection (hardware implementation)

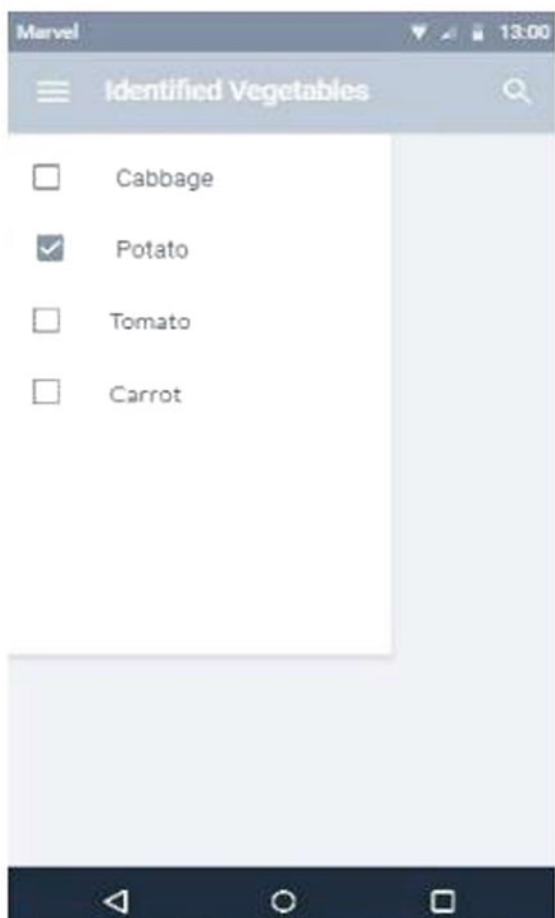
3.6 Online Social Media Platform

SNAP N' COOK will also allow the users to upload their recipes, photos, and experiences. This would help build a community for all people who love to try something new to cook and also help others to learn from this platform. Users can also bookmark their favorite recipes and follow other users of similar interests (Figs. 5 and 6).

4 Conclusion

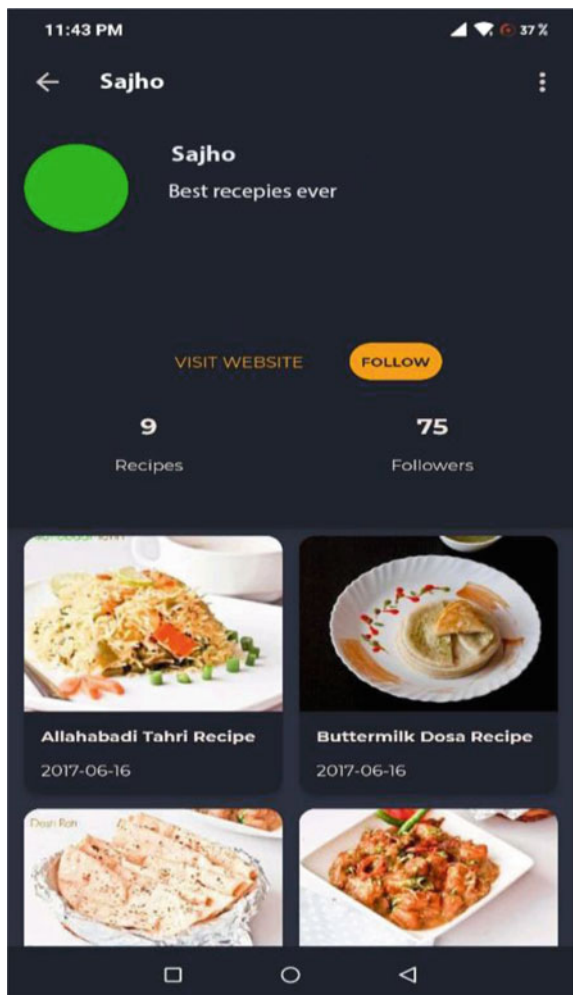
Snap N' Cook-IoT-based Recipe suggestion and healthcare application is a system of the modern cooking system using technologies like IoT and computer vision. The system is capable of combining four modules viz. vegetable recognition, recipe suggestion, health-related preferences, and calorie intake module and stale vegetable detection into one application. Its purpose is to allow housewives to automate the storing process and thereby improving the process of cooking food through a mobile application. The system also has some limitations. Internet Connectivity is required since recipes are online. Also, the quantity of vegetables available is an important

Fig. 5 User interface of mobile application at the user end (Sample) [1]



factor for recipe suggestion which is not included in the system. Thus we would like to conclude that the system achieves its objectives of suggesting new recipes from vegetables available along with health care applications. A user-friendly interface and automated system make it more appealing to end-users. Regarding all these limitations, there is a future scope to work on.

Fig. 6 User interface of online social media platform (Sample) [8]



References

1. Swati, K., Sangeetha, R.: Automatic vegetable recognition and recipe suggestion MCA 2015–18. IOSR J. Comput. Eng. (IOSR-JCE) **2**, 78–85. e-ISSN: 2278-0661, p-ISSN: 2278-8727 (2018)
2. Patil, O., Gaikwad, V.: Classification of vegetables using TensorFlow. Int. J. Res. Appl. Sci. Eng. Technol. **6**(IV) (2018)
3. Zhu, L., Zhenbo, L., Chen, L., Jing, W., Jun, Y.: High performance vegetable classification from images based on AlexNet deep learning model. Int. J. Agric. Biol. Eng. **11**(4) (2018)
4. Mane, S., Mangale, S.: Moving object detection and tracking using convolutional neural networks. In: Second International Conference on Intelligent Computing and Control Systems (ICICCS) (2018)
5. <https://medium.com/coinmonks/review-r-cnn-object-detection-b476aba290d1>

6. Mejd, S., Safran, A.A., Che, D.: Improving relevance prediction for focused web crawlers. In: IEEE/ACIS 11th International Conference on Computer and Information Science (2012)
7. <https://www.active.com/fitness/calculators/bmr>
8. <https://recipebook.io/>
9. <https://towardsdatascience.com/creating-your-own-object-detector-ad69dda69c85>

Accuracy-Based Performance Analysis of Alzheimer's Disease Classification Using Deep Convolution Neural Network



Ketki C. Pathak and Swathi S. Kundaram

Abstract Many researchers have utilized various statistical and machine learning models for detection of Alzheimer's disease. There is been a common practice of analyzing magnetic resonance imaging (MRI) for Alzheimer's disease diagnosis in clinical research. Based on similarity between healthy and demented MRI data of older people has been done for Alzheimer's disease detection. Recently, advanced deep learning techniques have successfully illustrated human-level performance in various fields, including medical image analysis, which is advantageous over hand crafted feature extraction methods. Convolutional neural network (CNN) provided better potential for accuracy in diagnosis the Alzheimer's disease such as to classify the given input as cognitively normal (CN), mild cognitive impairment (MCI) and Alzheimer disease (AD). In this work, we have presented a framework based on DCNN for Alzheimer's disease detection in terms of accuracy. We have achieved 97.98% accuracy on our dataset without using any handcrafted features for training the network. Validation accuracy achieved is 91.75%. Experimental data is obtained from ADNI and total 13,733 images from 266 subjects are used.

Keywords Convolution neural network · Accuracy · Alzheimer's disease · Deep learning · Classification

1 Introduction

Alzheimer's disease (AD) is an irreversible neurological brain disorder that gradually declines memory and other thinking abilities. This is due to progressive damage in functioning of neurons, including death of neurons. A survey showed that more than 5 million Americans are living with Alzheimer's disease. However, distinguishing between different stages of Alzheimer's is not easy. In this study, with the help of deep neural networks, we will classify patient's brain as cognitively normal (CN), mild cognitive impairment (MCI) and Alzheimer disease (AD) brain with MRI modality.

K. C. Pathak (✉) · S. S. Kundaram
Sarvajanik College of Engineering and Technology, Surat, India
e-mail: ketki.joshi@scet.ac.in

Deep learning models consists of more hidden layers compared to artificial neural networks, which extracts high-level feature representation from the dataset for multi-way classification. Deep learning algorithms always tries to simulate human brain to build and analyze the learning process of neural networks similar to artificial intelligence, which imitates the learning technique of the human brain when it attempts to understand unknown concepts. Deep learning methods have two obvious advantages in feature representation, as follows:

- Feature extraction is done automatically using deep learning algorithms compared to other machine learning algorithm from any application database, which indicated no prior knowledge is required.
- These algorithms are most suitable for larger dataset.

Different deep learning methods and its tools used for image classification as well as feature representation are listed out in Table 1.

In this work, a framework-based DCNN is implemented for detection of AD, which uses three layer of CNN model for three classes—AD, MCI and NC. This work does not use any rigid segmentation for gray matter (GM) of the data. Experimental evaluation is performed in terms of accuracy and loss on both training as well as testing dataset. The rest of the papers describes basics of Alzheimer's disease, literature review in Sect. 2, methodology and implementation in Sect. 3, experiments and results discussion in Sect. 4 and conclusion in Sect. 5.

Table 1 Different deep learning classification and techniques [1]

Image classification	Commonly used deep learning tools	Deep learning tools applied to MRI images	MATLAB tools
(a) Convolution Neural Network (CNN)	(a) Caffe (b) Tensor flow (c) Deeplearning4j	(a) BrainNet (b) LiviaNET (c) DIGITS (d) Reet_cnn_mri_adni	(a) Deep learning Tool
(b) Recurrent Neural Network (RNN)	(d) Theano (e) Pylearn2 (f) Keras	(e) Mrbrain (f) DeepMedic	
(c) Deep Convolution Neural Network (DCNN)	(g) Torch (h) CNTK (i) MXNet		
(d) Stacked auto-encoders (SAE)	(j) Chainer (k) Deeplearn Toolbox		
(e) (extraction and reconstruction)	(l) SINGA		
(f) Deep belief networks and restricted Boltzmann machines (DBM-RBM)	(m) maxDNN		
(g) ANN	(n) MatConvNet		
(h) Instructional set architecture (ISA)			

1.1 Alzheimer's Disease

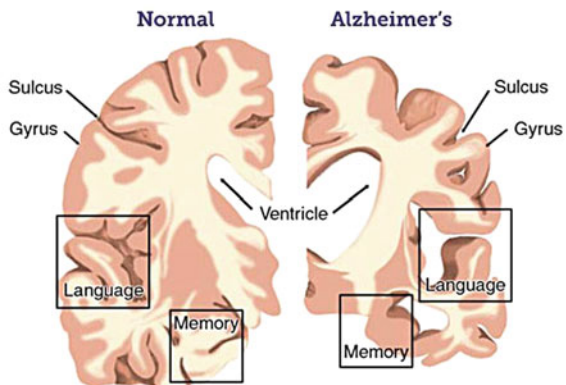
Alzheimer's disease (AD) is the most popular dementia in elderly people worldwide. According to Alzheimer's association, it is the sixth leading cause of death in USA [2]. A survey [3] stated that there will be 131.5 million people living with dementia worldwide and most of them with age greater than 65 has higher rate of risk with this disease. The brain region includes thinking ability, memory, reasoning of the patient wrinkle up and shrinks in the hippocampus area. This is the main cause of suffering from AD. The visualization of AD and healthy brain is shown in Fig. 1, gives the idea that memory and language muscles have diminished. Genetic mutation is another cause for AD; estimated to affect about 1% or less than 1% people [3].

2 Related Work

Much research shows the worldwide growth of age-related neurodegenerative diseases like Alzheimer's disease (AD) [3]. Developments and improvements in research are necessary for prevention, treatment, drug discovery and health-care services. Interdisciplinary efforts in medicine, healthcare, computer science, economics and other disciplines have combined to address this rising crisis.

Traditional approach for classification of AD to assist diagnosis was to generate feature wavelets using discrete wavelet transform (DWT) method. This does not give detection of disease; machine learning algorithms are required to do further processing [5]. Machine learning approaches are best for accurate classification of AD [6]. Most popular among these approaches is support vector machine (SVM). Rathore et al. [7] proposed a framework uses feature-based ranking method with SVM to classify the disease as AD and healthy controls (HC). SVM is used to build predictive classification models, which extracts informative features, high dimensional from

Fig. 1 Brain cross sectional to visualize difference between healthy brain and Alzheimer brain [4]



the MRI [7]. However, this requires handcrafted features of brain structures, which is laborious and time consuming leading to need of experts' advice. In the following sections, we describe previous works and different methods in the neuroimaging field.

Ortiz et al. [8] discussed many deep learning architectures for early diagnosis of AD. Convolutional neural network (CNN) is motivated from human visual cortex and learns the features from simple edges to more complex edges from the dense hierarchical structure. It is building block of convolution and pooling layers. Convolutional layer provides the feature maps by multiplying the input image with the kernel and pooling layer down samples the image keeping the similarity features [5]. This stimulated many neuroscience researchers to find their solution to the problem associated with neuroimaging. Liu et al. [9] described multimodal classification of AD with four class. Staked autoencoders (SAEs) are used for feature learning for both MRI and PET. These features are fused and trained using SVM, which achieved very less accuracy compared to other available multimode classification.

Cui et al. [12] addressed sequential analysis of MRI image along time axis by measuring the longitudinal progression. Multi-layer perceptron (MLP) is used for spatial features and to train these features Recurrent neural network (RNN) is used. However, such algorithm requires rigid segmentation as a pre-processing task. The accuracy achieved is 89.69% in two-way classification as AD and NC. Islam and Zhang [10] proposed a DCNN model for four classes. In this, five DCNN models have trained and output features are fused to get the prediction of disease. The uniqueness of this approach is that every model gives various features differ from one another making the model generalized for unseen data prediction with accuracy 93.18%. There are many works available on CNN method for detection of AD. Gunawardena et al. [13] addressed the problem for pre-detection of AD for three classes with accuracy achieved is 84.4%. Combination of CNN and RNN is a new approach for AD diagnosis proposed by Liu et al. [11]. 3D PET images sliced into 2D images, which trained by CNN and RNN are used to classify the CNN features with accuracy 91.2% for one-versus-all of three classes. Khvostikov et al. [14] uses fusion of structural MRI and mean diffusivity-diffusion tensor imaging (MD-DTI) on hippocampal ROI region for AD diagnosis. Wang et al. [15] proposed an eight layer CCN for with different types of activation functions and pooling operations for two classes, achieved accuracy is 97.65%.

Existing algorithm comparison in the area of machine learning for AD diagnosis gives better idea of research gap. From all these deep learning technique, CNN showed much better performance in diagnosing the disease compared to other. It gave better accuracy, which is indeed requirement in medical image diagnosis. Most of this requires pre-processing task to accomplish the classification. Table 2 shows all techniques used, advantages and disadvantages.

Table 2 Comparison of existing algorithms in the field of Alzheimer's disease

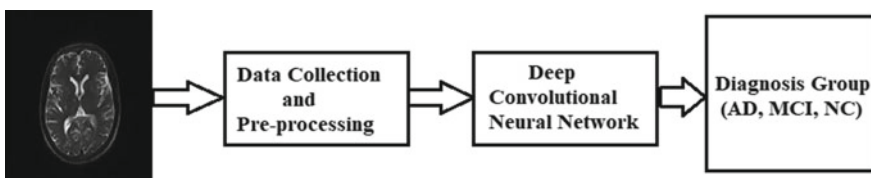
Paper	Technique	Advantage	Disadvantage
Islam and Zhang [10]	DCNN	Better accuracy in AD diagnosis	Sometimes needs to address over fitting problem
Liu et al. [11]	CNN and RNN	Have better performance in classification with 3D image	Lower accuracy in diagnosing disease
Liu et al. [9]	SVM and SAE	High accuracy on the training set and have better potential for multimodal learning architectures for AD diagnosis and better extraction of features with low variance	Have over fitting problem when dealing with multi-class diagnosis and low accuracy on testing data
Cui et al. [12]	RNN and MLP	MLP (spatial features) and BGRU (temporal features) improve the performance of AD classification	Pre-processing task is required such as tissue segmentation and registration and increases computation cost

3 Proposed Methodology

The flow of proposed methodology which consists of two steps; pre-processing and network training are shown in Fig. 2. The detail description is in the following subsections.

3.1 Data Pre-processing

Medical images when acquired from any imaging equipment is in digital imaging and communications in medicine (DICOM) format. After acquisition, they need to

**Fig. 2** Proposed deep learning flow for classification of Alzheimer's into AD, MCI and NC

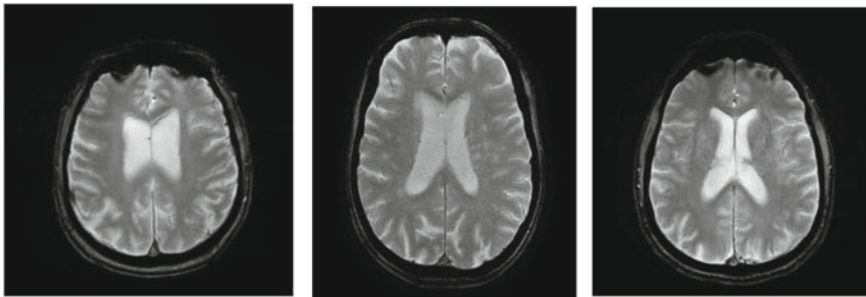


Fig. 3 JPEG slices for each diagnosis class after pre-processing (left: AD, center: MCI, right: NC)

be converted into proper format (JPG, PNG, TIFF, etc.) for further processing. In our work, we have converted MRI samples into JPEG slices in MATLAB tool. Pixel size of each sample is reduced to 8-bit from 14-bit size by rescaling to 255. Processed slices for each class are shown in Fig. 3.

3.2 Network Architecture

Convolutional neural networks (CNN) are inspired from human visual system. The visual system has small number of neuron cells sensitive to a specific field, i.e., some neurons in the brain fired only in the presence of edges in particular orientation. Such operation is depicted in CNNs. The functioning of convolution layer is to automatically extract features maps from the input images by using element wise multiplication with filter along entire image. Pooling layer is generally used to avoid over fitting problem, i.e., when network memorizes the data instead of generalization. Rectified linear unit (ReLU) activation is used to fire the neuron or to determine the output of neural network. Feature maps are extracted with combination of several such Conv-ReLU-Pool operations and reach the final single or multiple fully connected layers. The detail operation of proposed architecture is as follows.

Our proposed model shown in Fig. 4 is an ensemble of three blocks; each of the individual blocks has several layers performing three basic operations, which are:

- Convolution
- ReLU activation
- Max pooling.

The architecture consists of three convolutional layers; each includes a max-pooling layer. Then followed by neurons flattening there are two fully connected

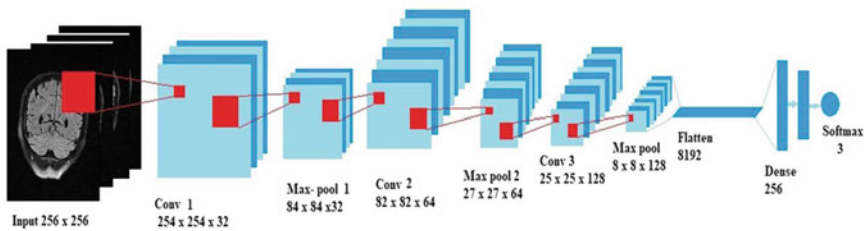


Fig. 4 Architecture of proposed methodology

layers and finally a softmax/sigmoid classifier. Output has three classes, which are normal control (NC), mild cognitive impairment (MCI) and Alzheimer disease (AD). The input for architecture is a 256×256 grayscale image, which passes through the first convolutional layer with 32 feature maps with filters having size 3×3 , a stride of one, and pooling is made zero with ReLU activation function. The image dimensions changes from $256 \times 256 \times 1$ to $254 \times 254 \times 32$, according to the dimension formula given below:

$$n^{[l]} = \frac{(n^{[l-1]} + 2p^{[l-1]} - f^{[l]})}{s^{[l]} + 1} \quad (1)$$

where n is the size of input image or previous layer image, p refers to padding and s refers to stride, l refers to current layer and f refers to the filter size. Then, the network applies max-pooling layer with a filter size 3×3 and a stride of one. The resulting image dimension reduced to $84 \times 84 \times 32$. Finally, there is a fully connected softmax output layer with 10 possible values corresponding to the digits from 0 to 9. Specification of the proposed model is shown in Table 3.

3.3 Database

The dataset used in this work obtained from Alzheimer's disease neuroimaging initiative (ADNI) [16]. Dataset consists of 110 AD, 105 MCI and 51 NC subjects, where each subject contains 44–50 sample of images. Out of which 110 AD subjects are collected from Horizon imaging center [17]. There are total of 9540 images used for training the network and 4193 images for testing. Data augmentation on images is done with rescale operation. Dataset is of axial brain type.

Table 3 Specifications of the proposed CNN model

Layer	Output shape	Parameters
Image	256 × 256 × 3	—
Conv2D_1	254, 254, 32	896
ReLU	254, 254, 32	0
Max pooling_1	84, 84, 32	0
Conv2D_2	82, 82, 64	18,496
ReLU	82, 82, 64	0
Max pooling_2	27, 27, 64	0
Conv2D_3	25, 25, 128	73,856
ReLU	25, 25, 128	0
Max pooling_3	8, 8, 128	0
Flatten_1	8192	0
Dense_1	256	2,097,408
ReLU	256	0
Drop out	256	0
Dense	3	771
Softmax	3	0
Total params	0	2,191,427
Trainable	0	2,191,427
Non trainable	0	0

4 Experimental Setup and Results

Proposed model is implemented with the keras library with tensor flow backend. The experiments are conducted on laptop with 8 GB RAM of Dell Intel Core i7. **Network** trained on NVIDIA Ge Force 540 M GPU with 8 GB memory. **ReLU** activation is applied for each neuron of CNN. Output classified as Alzheimer's disease (AD), mild cognitive impairment (MCI) and normal brain (NC). Database consists of 110 AD, 105 MCI and 51 NC subjects, where each subject contains 44–50 sample of images. There are total of 9540 images are used for training the network and 4193 images for validation. Batch size taken is 10. Loss function is categorical cross-entropy and optimizer Adam.

We have conducted four experiments of our dataset. For two experiments, as shown in Table 4, 70% of the data was used for training and 30% for validation. Remaining two experiments are conducted with our dataset by removing some blank

Table 4 Percentage and size of training and validation dataset 1

	Training	Validation
Percentage (%)	70	30
Images	9540	4193

Table 5 Percentage and size of training and validation dataset 2

	Training	Validation
Percentage (%)	75	25
Images	8657	2908

Table 6 Parameter specification of Model I and II

Parameter	Model I	Model II
Dataset	1	1
Epochs	10	10
Layer activation	ReLU	ReLU
Dense activation	Softmax	Softmax
Rescale	1./255	1./255
Optimizer	Adam	Adam
Dense drop out	0.5	0.5
Conv_2D_1 drop out	—	0.5
Conv_2D_2 drop out	—	0.5

and unwanted images. In this, 75% of the reduced data was used for training and 25% for validation for remaining two experiments are shown in Table 5.

Parameter specification of Model I and II is addressed in Table 6, performance evaluated in terms of accuracy and loss for training as well as validation set. Loss gives the best knowledge of how fit is the model. For our dataset, Adam optimizer gives best accuracy with less loss because it gradients are updated with momentum and works well with little tuning of hyperparameters. The accuracy versus epoch and loss versus epoch graph for both training and validation set for Model I are shown in Fig. 5.

It is seen that, for model I, training set has the accuracy reached 96.98% and loss is dropped down to zero. This gives the measure of progression during training period of the model. While the validation set gives the measure of the quality of the model. Validation accuracy has reached 81.72%, which describes that with 81.72% accuracy model can predict the detection on new data but the validation loss is constantly increasing, i.e., the model is starting to fit on noise and is beginning to overfit. This ultimately loses the model's ability to predict on new data.

To overcome this problem, drop out is added between two intermediate stages of convolution layer in model IV. Parameter specifications for Model III and Model IV is shown in Table 7. Due to this training and validation accuracy are improved and validation loss is maintain as desire level. This still does not giving the better accuracy as this model is prone to over fitting because it is clearly seen that validation accuracy is less than training. Both accuracy should have minimum difference of 4–5% in between to justify the model with better performance.

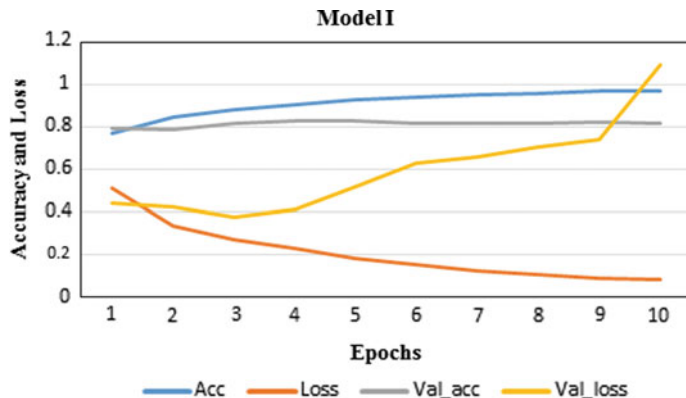


Fig. 5 Accuracy and loss for training and validation—Model I

Table 7 Parameter specification of Model III and IV

Parameter	Model III	Model IV
Dataset	2	2
Epochs	10	10
Layer activation	ReLU	ReLU
Dense activation	Softmax	Softmax
Rescale	1./255	1./255
Optimizer	Adam	Adam
Dense drop out	0.5	0.5
Padding	Same	
Conv_2D_1 filter	–	5 × 5
Conv_2D_2 filter	–	5 × 5

In order to reduce over fitting and to have better accuracy, dataset 2 is used for same proposed model, parameter specification is shown in Table 7. Overall comparison of all four models is shown in Table 8. Model III has achieved accuracy of 98.47% and validation accuracy is 91.44%. Hence, this model has less over fitting problem compared to above two models but the model is still fitting toward noise, as validation loss is 0.6702. To remove noise, filter size in two-convolution layer is increased to

Table 8 Performance of proposed framework

Model	Training accuracy	Training loss	Validation accuracy	Validation loss
I	0.9696	0.0814	0.8176	1.927
II	0.9557	0.1081	0.7858	0.4899
III	0.9847	0.0445	0.9144	0.6702
IV	0.9798	0.0532	0.9175	0.5632

5×5 to ignore some features that containing noise in Model IV and validation loss achieved is 0.5632 along with training and validation accuracy is 97.98 and 91.75%. Thus, Model IV can be considered for giving better performance in detecting the Alzheimer disease. All four model's graphs are shown in Figs. 5, 6, 7 and 8, respectively. Overall comparison with other approaches is shown in Table 9.

Performance comparison of proposed methodology of Model IV with other approaches along with techniques, data modalities and different dataset is addressed in Table 9. Among all the approaches, our proposed model have achieved accuracy as

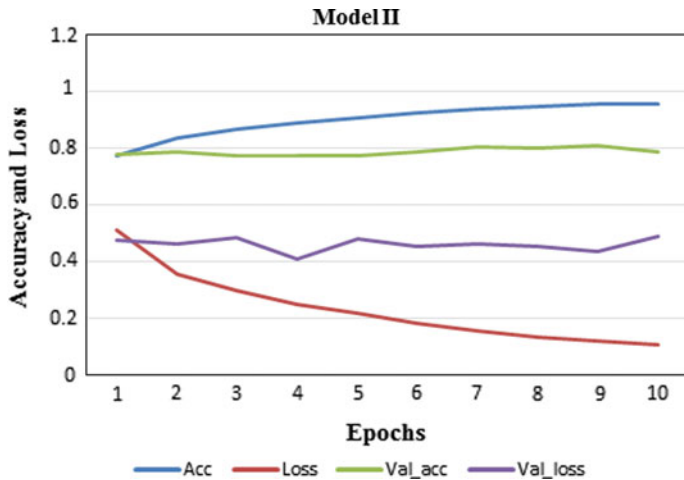


Fig. 6 Accuracy and loss for training and validation—Model II

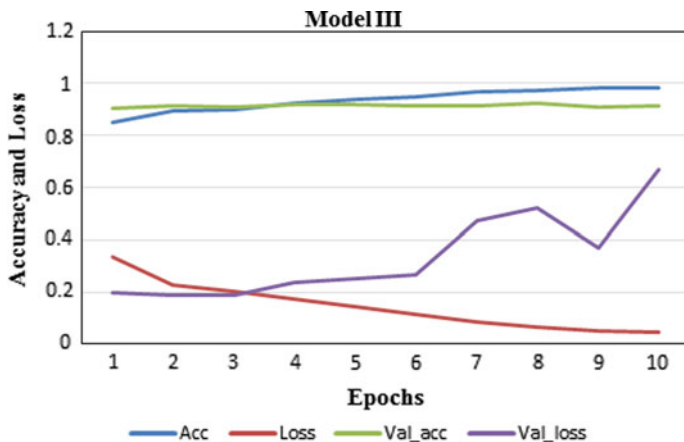


Fig. 7 Accuracy and loss for training and validation—Model III

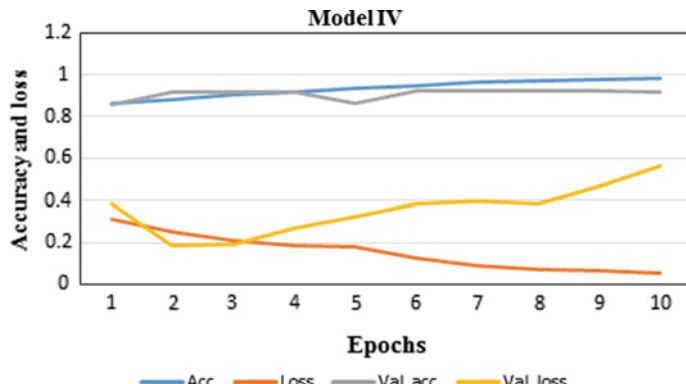


Fig. 8 Accuracy and loss for training and validation—Model IV

high as 97.98% without any pre-learnt features. Evaluation parameter for comparison is considered only accuracy for detection of Alzheimer disease.

5 Summary and Future Scope

Convolutional neural network is widely emphasized for diagnosis of any diseases. Though some problems occur with deep learning techniques such as over fitting; which is successfully handled by doing augmentation on the dataset, described in [10]. Among all deep learning techniques, which are SAE, SVM, RNN, etc. CNN provided better potential for accuracy in diagnosis the Alzheimer's disease such as to classify the given input as AD, MCI and NC. In this work, we have presented a framework based on deep convolutional neural network for Alzheimer's disease detection in terms of accuracy. We have achieved 97.98% accuracy on our dataset without using any handcrafted features for training the network. Validation accuracy achieved is 91.75%. Experimental data is obtained from ADNI and total 13,733 images from 266 subjects are used. Further studies will focus on achieving performance parameters such as specificity, sensitivity, recall and F1-score by improving the DCNN model. Therefore, another experiment can be implemented to test the prediction of disease by tuning hyperactive parameters. As a future enhancement, we will use support vector machine to classify the DCNN features.

Table 9 Performance comparison of proposed framework with other approaches

Approach	Techniques	Classification	Modalities	Accuracy (%)	Dataset
Islam and Zhang [10]	DCNN	4 class (AD/cMCI/MCI/NC)	MRI	93.18	OASIS
Liu et al. [11]	DCNN-RNN	3 class (AD/MCI/NC)	FDG-PET	91.2 with AD versus NC, 89.9 with MCI versus NC	ADNI
Shi et al. [9]	SAE and SVM	4 class (AD/ncMCI/cMCI/NC)	MRI + PET	0.53 ± 0.47 with SAE, 0.47 ± 0.18 with SVM	ADNI
Cui et al. [12]	MLP-RNN	2 class (AD/NC)	MRI	89.69	ADNI
Proposed	CNN	3 class (AD/MCI/NC)	MRI	97.98%	ADNI

References

1. Liu, J., Pan, Y., Li, M., Chen, Z., Tang, L., Lu, C., Wang, J.: Applications of deep learning to MRI images: a survey. *Big Data Min. Anal.* **1**(1), 1–18 (2018)
2. Alzheimer's Association. Alzheimer's disease facts and figures. *Alzheimer's Dementia* **12**(4), 459–509 (2016)
3. Alzheimer's Association.: Alzheimer's disease facts and figures. *Alzheimer's Dementia* **14**(3), 367–429 (2018)
4. Friston, K.J., Holmes, A.P., Worsley, K.J., Poline, J.P., Frith, C.D., Frackowiak, R.S.: Statistical parametric maps in functional imaging: a general linear approach. *Hum. Brain Mapp.* **2**(4), 189–210 (1994)
5. Milletari, F., Navab, N., Ahmadi, S.A.: V-net: fully convolutional neural networks for volumetric medical image segmentation. In: IEEE Fourth International Conference on 3D Vision (3DV), pp. 565–571 (2016)
6. de Bruijne, M.: Machine learning approaches in medical image analysis: from detection to diagnosis. *J. Med. Image Anal.* **33**, 94–97 (2016)
7. Rathore, S., Habes, M., Iftikhar, M.A., Shacklett, A., Davatzikos, C.: A review on neuroimaging-based classification studies and associated feature extraction methods for Alzheimer's disease and its prodromal stages. *NeuroImage* **155**, 530–548 (2017)
8. Ortiz, A., Munilla, J., Gorri, J.M., Ramirez, J.: Ensembles of deep learning architectures for the early diagnosis of the Alzheimer's disease. *Int. J. Neural Syst.* **26**(07), 1650025 (2016)
9. Liu, S., Liu, S., Cai, W., Che, H., Pujol, S., Kikinis, R., Feng, D., Fulham, M.J.: Multimodal neuroimaging feature learning for multiclass diagnosis of Alzheimer's disease. *IEEE Trans. Biomed. Eng.* **62**(4), 1132–1140 (2014)
10. Islam, J., Zhang, Y.: Brain MRI analysis for Alzheimer's disease diagnosis using an ensemble system of deep convolutional neural networks. *Brain Inf.* **5**(2), 2 (2018)
11. Liu, M., Cheng, D., Yan, W., Alzheimer's Disease Neuroimaging Initiative.: Classification of Alzheimer's disease by combination of convolutional and recurrent neural networks using FDG-PET images. *Frontiers Neuroinf.* **12**, 35 (2018)
12. Cui, R., Liu, M., Li, G.: Longitudinal analysis for Alzheimer's disease diagnosis using RNN. In: 2018 IEEE 15th International Symposium on Biomedical Imaging (ISBI 2018), pp. 1398–1401 (2018)
13. Gunawardena, K.A.N.N.P., Rajapakse, R.N., Kodikara, N.D.: Applying convolutional neural networks for pre-detection of Alzheimer's disease from structural MRI data. In: 2017 24th IEEE International Conference on Mechatronics and Machine Vision in Practice (M2VIP), pp. 1–7 (2017)
14. Khvostikov, A., Aderghal, K., Benois-Pineau, J., Krylov, A., Catheline, G.: 3D CNN-based classification using sMRI and MD-DTI images for Alzheimer disease studies. [arXiv:1801.05968](https://arxiv.org/abs/1801.05968) (2018)
15. Wang, S.H., Phillips, P., Sui, Y., Liu, B., Yang, M., Cheng, H.: Classification of Alzheimer's disease based on eight-layer convolutional neural network with leaky rectified linear unit and max pooling. *J. Med. Syst.* **42**(5), 85 (2018)
16. ADNI—Alzheimer's Disease Neuroimaging Initiative. Available <http://adni.loni.usc.edu/>
17. Horizon Radio Imaging Centre. Surat, Gujarat, India

Multiple Information Fusion and Encryption Using DWT and Yang-Gu Mixture Amplitude-Phase Retrieval Algorithm in Fractional Fourier Domain



Muhammad Rafiq Abuturab

Abstract A new multiple information fusion and encryption using a wavelet transform and Yang-Gu mixture amplitude-phase retrieval algorithm in fractional Fourier domain are proposed. In this scheme, four color images are decomposed by using DWT and then the four LL sub-bands are fused to form an input color image. R , G , and B channels of input image are encoded individually by Yang-Gu mixture amplitude-phase retrieval algorithm in fractional Fourier domain together with coupled logistic maps. The individual binary random key and parameters of coupled logistic maps are used as decryption keys. The chaotic phase mask reduces the intricacy of the scheme. The multiple-decryption keys can evade various types of attacks. Numerical simulation results prove the security and feasibility of the strategy.

Keywords Yang-Gu mixture amplitude-phase retrieval algorithm · Coupled logistic maps · Fractional Fourier transform

1 Introduction

With the rapid development of modern communication technology, both information security and intellectual property protection have become one of the most important issues [1]. Refregier and Javidi first proposed optical security scheme using double random phase encoding (DRPE) [2]. A number of DRPE-based encryption methods have been put forwarded to achieve higher security [3–7]. However, most of the DRPE-based encryption techniques are symmetric. Qin and Peng suggested asymmetric encryption techniques [8]. However, this technique has been found susceptible to a specific attack [9]. So, an asymmetric cryptosystem using Yang-Gu mixture amplitude-phase retrieval algorithm (YGAPRA) has been proposed [10]. This

M. R. Abuturab (✉)

Department of Physics, Maulana Azad College of Engineering and Technology,
Patna 801113, India

e-mail: rafiq.abuturab@gmail.com

method has been further extended [11–13]. Recently, DWT-based multiple-image encryption systems have been developed [13–16].

In this paper, multiple-color image encryption based on DWT and YGAPRA in fractional Fourier transform (FRFT) is proposed. The encrypted image is not only protected by decryption keys but also parameters of FRFT. Numerical simulation results show the validity and reliability of the proposed scheme.

2 Theory

2.1 Two-Coupled Logistic Maps

The iterative forms of two-coupled logistic maps are obtained as [17]

$$x_{t+1} = px_t(1 - x_t) + \varepsilon(y_t - x_t) \quad (1)$$

$$y_{t+1} = py_t(1 - y_t) + \varepsilon(x_t - y_t) \quad (2)$$

where ε is coupling constant and satisfies $-2 < \varepsilon < 2$. Suppose that the size of the 2D image is $M \times N$ pixels; so two sequences $X = \{x_1, x_2, \dots, x_{M+K}\}$, $x_i \in (0, 1)$ and $Y = \{y_1, y_2, \dots, y_{N+K}\}$, $y_i \in (0, 1)$ are generated by using Eqs. (1) and (2) with different initial values (x_0 and y_0) and an integer K . The previous values of K are rejected to increase randomness and disorder, so the two new sequences are employed to scramble the input image. The parameters x_0 , y_0 , p , K , and ε are used as decryption keys.

2.2 Fractional Fourier Transform

The FRFT at parameter α of a 2D complex field function $f_{\text{in}}(x_{\text{in}}, y_{\text{in}})$ is [18]

$$\begin{aligned} f_{\text{out}}(x_{\text{out}}, y_{\text{out}}) &= F^\alpha[f_{\text{in}}(x_{\text{in}}, y_{\text{in}})](x_{\text{out}}, y_{\text{out}}) \\ &= \int_{-\infty}^{+\infty} \int_{-\infty}^{+\infty} f_{\text{in}}(x_{\text{in}}, y_{\text{in}}) K_\alpha(x_{\text{in}}, y_{\text{in}}; x_{\text{out}}, y_{\text{out}}) dx_{\text{in}} dy_{\text{in}} \end{aligned} \quad (3)$$

where $(x_{\text{in}}, y_{\text{in}})$ and $(x_{\text{out}}, y_{\text{out}})$ indicate the input and output dimensionless plane coordinates, respectively.

The Kernel of FRFT is defined as

$$K_\alpha(x_{\text{in}}, y_{\text{in}}; x_{\text{out}}, y_{\text{out}}) = A_\phi \exp \left\{ i\pi \left(\frac{x_{\text{in}}^2 + x_{\text{out}}^2 + y_{\text{in}}^2 + y_{\text{out}}^2}{\tan \varphi} - \frac{2(x_{\text{in}}x_{\text{out}} + y_{\text{out}}y_{\text{in}})}{\sin \varphi} \right) \right\} dx_{\text{in}} dy_{\text{in}} \quad (4)$$

where $\phi = \alpha\pi/2$, $0 < |\alpha| < 2$, and A_ϕ is expressed as

$$A_\phi = \frac{\exp\{-i[\pi \operatorname{sgn}(\sin \phi)/4 - \alpha/2]\}}{\sqrt{|\sin \phi|}} \quad (5)$$

A_ϕ is a constant output phase factor which depends on the fractional order.

2.3 Yang-Gu Mixture Amplitude-Phase Retrieval Algorithm

The flowchart of the YGAPRA process is shown in Fig. 1. The secret image $I(x_{\text{in}}, y_{\text{in}})$ and encrypted image $E(x_{\text{out}}, y_{\text{out}})$ are, respectively, the input and output of the FRFT, which are related as [9]

$$E(x_{\text{out}}, y_{\text{out}}) P(x_{\text{out}}, y_{\text{out}}) = F^\alpha \{I(x_{\text{in}}, y_{\text{in}}) \exp[i\varphi(x_{\text{in}}, y_{\text{in}})]\} \quad (6)$$

where $F^\alpha\{\}$ represents FRFT operator. $P(x_{\text{out}}, y_{\text{out}})$ is public random phase key (PRPK). $\varphi(x_{\text{in}}, y_{\text{in}})$ and $E(x_{\text{out}}, y_{\text{out}})$ are, respectively, unknown phase and amplitude which require to be retrieved to satisfy Eq. (6).

First, $E_0(x, y)$ is generated randomly in an interval $[0, 1]$. If, k th iteration, $E_k(x_{\text{out}}, y_{\text{out}})$ is known which is multiplied with $P(x_{\text{out}}, y_{\text{out}})$ and then inverse fractional Fourier transformed. The transformed image is given by

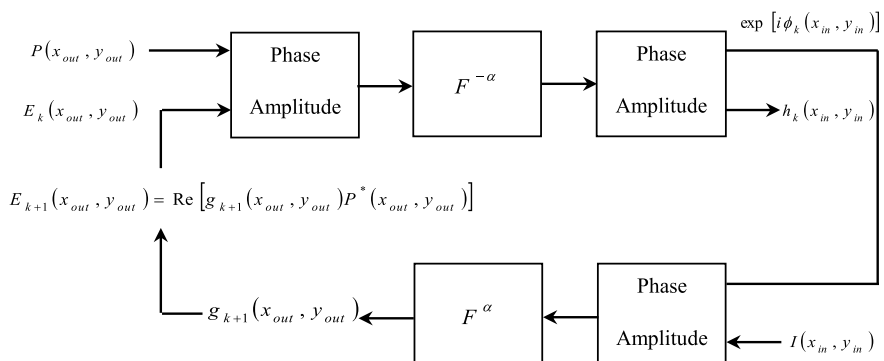


Fig. 1 k th iterative process of YGAPRA

$$H_k(x_{\text{in}}, y_{\text{in}}) = F^{-\alpha} \{E_k(x_{\text{out}}, y_{\text{out}}) P(x_{\text{out}}, y_{\text{out}})\} \quad (7)$$

If the amplitude and phase of transformed image $H_k(x_{\text{in}}, y_{\text{in}})$ are, respectively, $h_k(x_{\text{in}}, y_{\text{in}})$ and $\phi_k(x_{\text{in}}, y_{\text{in}})$, after k th iteration, $E_{k+1}(x_{\text{out}}, y_{\text{out}})$ is updated by

$$g_{k+1}(x_{\text{out}}, y_{\text{out}}) = F^{\alpha} \{I(x_{\text{in}}, y_{\text{in}}) \exp[i\phi_k(x_{\text{in}}, y_{\text{in}})]\} \quad (8)$$

$$E_{k+1}(x_{\text{out}}, y_{\text{out}}) = \text{Re}[g_{k+1}(x_{\text{out}}, y_{\text{out}}) P^*(x_{\text{out}}, y_{\text{out}})] \quad (9)$$

The normalized mean square error (NMSE) is used as convergence criterion and defined as

$$\text{NMSE} = \frac{\sum_{x,y} [I(x_{\text{in}}, y_{\text{in}}) - h_k(x_{\text{in}}, y_{\text{in}})]^2}{\sum_{x,y} I^2(x_{\text{in}}, y_{\text{in}})} \quad (10)$$

When NMSE is lower than a preset threshold value (near to 0), the iteration stops. A one-way binary phase modulation $\exp[i\pi b(x_{\text{out}}, y_{\text{out}})]$ is introduced, and $b(x_{\text{out}}, y_{\text{out}})$ is generated by

$$b(x_{\text{out}}, y_{\text{out}}) = \begin{cases} 1 & E_{k+1}(x_{\text{out}}, y_{\text{out}}) < 0 \\ 0 & E_{k+1}(x_{\text{out}}, y_{\text{out}}) > 0 \end{cases} \quad (11)$$

Thus, the detectable amplitude of encrypted image is obtained as

$$E'_{k+1}(x_{\text{out}}, y_{\text{out}}) = E_{k+1}(x_{\text{out}}, y_{\text{out}}) \exp[i\pi b(x_{\text{out}}, y_{\text{out}})] \quad (12)$$

The decryption key is produced by

$$D'(x_{\text{out}}, y_{\text{out}}) = P(x_{\text{out}}, y_{\text{out}}) \exp[i\pi b(x_{\text{out}}, y_{\text{out}})] \quad (13)$$

3 Proposed Asymmetric Cryptosystem

The steps in the encryption process are the followings.

Step 1: The chaotic permutation process is employed to scramble the fused image $I(x_{\text{in}}, y_{\text{in}})$ into $I'(x_{\text{in}}, y_{\text{in}})$. The two-coupled logistic maps are employed to obtain a sequence of chaotic pairs.

- (a) The values of x_0, y_0, p, ε and K are set; the two random sequences with length $M + K$ and $N + K$ are, respectively, generated by using

- Eqs. (1) and (2). The front K values are rejected, and two sequences $X' = \{c(x)|x = 1, 2, \dots, M\}$ and $Y' = \{r(y)|y = 1, 2, \dots, N\}$ are produced.
- (b) The sequences X' and Y' are sorted in ascending or descending order; the two sequences $X'' = \{c[w(x)]|x = 1, 2, \dots, M\}$ and $Y'' = \{r[w(y)]|y = 1, 2, \dots, N\}$ are obtained, where w denotes address code. For each sequence, the values of the elements are not changed but the positions are varied.
 - (c) Finally, the scrambled secret image $I'(x_{in}, y_{in})$ is obtained by using the sequences X'' and Y'' .

Step 2: The chaotic phase mask (CPM) is produced by using $I'(x_{in}, y_{in})$ as

$$P(x_{in}, y_{in}) = \exp[i2\pi I'(x_{in}, y_{in})] \quad (14)$$

Step 3: $I_1(x_{in}, y_{in})$, $I_2(x_{in}, y_{in})$, $I_3(x_{in}, y_{in})$, and $I_4(x_{in}, y_{in})$ are the four input images allotted to four different authorized users. Each image is decomposed by DWT to obtain W_{LL} , W_{HL} , W_{LH} , and W_{HH} sub-bands.

Step 4: The LL sub-bands W_{LL_1} , W_{LL_2} , W_{LL_3} , and W_{LL_4} of four images are merged as

$$I(x_{in}, y_{in}) = [W_{LL_1}, W_{LL_2}; W_{LL_3} W_{LL_4}] \quad (15)$$

Step 5: $I(x_{in}, y_{in})$ is split into R , G , and B channels which are denoted as $I_R(x_{in}, y_{in})$, $I_G(x_{in}, y_{in})$, and $I_B(x_{in}, y_{in})$, respectively.

Step 6: $I_j(x_{in}, y_{in})$ and $E_j(x_{out}, y_{out})$ are, respectively, used as an input and an output of an optical system. $E_j(x_{out}, y_{out})$ is retrieved by YGAPRA using Eqs. (7)–(9), where $j = R, G, B$. The CRM is used as PRPK.

Step 7: $\exp[i\pi b_j(x_{out}, y_{out})]$ is obtained by employing Eq. (11).

Step 8: The encrypted image $E'_j(x_{out}, y_{out})$ is generated by using Eq. (12).

$$E'_j(x_{out}, y_{out}) = E_j(x_{out}, y_{out}) \exp[i\pi b_j(x_{out}, y_{out})] \quad (16)$$

Finally, the encrypted R , G , and B channels are combined to form encrypted image.

$$E'(x_{out}, y_{out}) = [E'_R(x_{out}, y_{out}), E'_G(x_{out}, y_{out}), E'_B(x_{out}, y_{out})] \quad (17)$$

Step 9: The decryption keys for R , G , and B channels are generated by using Eq. (13).

$$D_R(x_{out}, y_{out}) = P_R(x_{out}, y_{out}) \exp[i\pi b_R(x_{out}, y_{out})] \quad (18)$$

$$D_G(x_{out}, y_{out}) = P_G(x_{out}, y_{out}) \exp[i\pi b_G(x_{out}, y_{out})] \quad (19)$$

$$D_B(x_{\text{out}}, y_{\text{out}}) = P_B(x_{\text{out}}, y_{\text{out}}) \exp[i\pi b_B(x_{\text{out}}, y_{\text{out}})] \quad (20)$$

The steps in the decryption process are followings.

Step 1: The encrypted image $E'(x_{\text{out}}, y_{\text{out}})$ is split into $E'_R(x_{\text{out}}, y_{\text{out}})$, $E'_G(x_{\text{out}}, y_{\text{out}})$, and $E'_B(x_{\text{out}}, y_{\text{out}})$.

Step 2: The encrypted channels $E'_R(x_{\text{out}}, y_{\text{out}})$, $E'_G(x_{\text{out}}, y_{\text{out}})$, and $E'_B(x_{\text{out}}, y_{\text{out}})$ are multiplied by corresponding decryption keys $D_R(x_{\text{out}}, y_{\text{out}})$, $D_G(x_{\text{out}}, y_{\text{out}})$, and $D_B(x_{\text{out}}, y_{\text{out}})$ and then executed inverse FRFT.

$$I_R(x_{\text{in}}, y_{\text{in}}) = |F^{-\alpha_R} [D_R(x_{\text{out}}, y_{\text{out}}) \cdot E'_R(x_{\text{out}}, y_{\text{out}})]| \quad (21)$$

$$f_G(x_{\text{in}}, y_{\text{in}}) = |F^{-\alpha_G} [D_G(x_{\text{out}}, y_{\text{out}}) \cdot E'_G(x_{\text{out}}, y_{\text{out}})]| \quad (22)$$

$$f_B(x_{\text{in}}, y_{\text{in}}) = |F^{-\alpha_B} [D_B(x_{\text{out}}, y_{\text{out}}) \cdot E'_B(x_{\text{out}}, y_{\text{out}})]| \quad (23)$$

Step 3: The decrypted R , G , and B channels are combined.

$$I(x_{\text{in}}, y_{\text{in}}) = [I_R(x_{\text{in}}, y_{\text{in}}), I_G(x_{\text{in}}, y_{\text{in}}), I_B(x_{\text{in}}, y_{\text{in}})] \quad (24)$$

Step 4: Finally, the fused image $I(x_{\text{in}}, y_{\text{in}})$ is decomposed into W_{LL_1} , W_{LL_2} , W_{LL_3} , and W_{LL_4} , which denote corresponding decrypted input images $I_1(x_{\text{in}}, y_{\text{in}})$, $I_2(x_{\text{in}}, y_{\text{in}})$, $I_3(x_{\text{in}}, y_{\text{in}})$, and $I_4(x_{\text{in}}, y_{\text{in}})$.

4 Numerical Results

The MATLAB R2018a (Version 9.4) platform has been used for numerical simulations so as to evaluate the validity and viability of the proposed technique. The parameters of CPM exploited as decryption keys are set to $x_0 = 0.21$, $y_0 = 0.82$, $k = 2000$, $p = 3.52995$, and $\varepsilon = -0.471$ m. The values of fractional order are set to $\alpha_R = 5$, $\alpha_G = 6$, and $\alpha_B = 7$.

Figure 2a–e shows Father, Ali, Mahdi, Barbara, and fused image, respectively. Figure 2f–g displays chaotic phase mask and binary random key, respectively. Figure 2h–l illustrates retrieved fused image, Father, Ali, Mahdi, and Barbara, respectively. Figure 2a–h is all of size $512 \times 512 \times 3$ pixels, and Fig. 2i–l is all of size $256 \times 256 \times 3$ pixels.

The correlation coefficient (CC) is

$$CC = \frac{E\{[I_{\text{in}} - E[I_{\text{in}}]] \cdot [I_{\text{out}} - E[I_{\text{out}}]]\}}{\sqrt{E\{[I_{\text{in}} - E[I_{\text{in}}]]^2\}} \sqrt{E\{[I_{\text{out}} - E[I_{\text{out}}]]^2\}}} \quad (25)$$

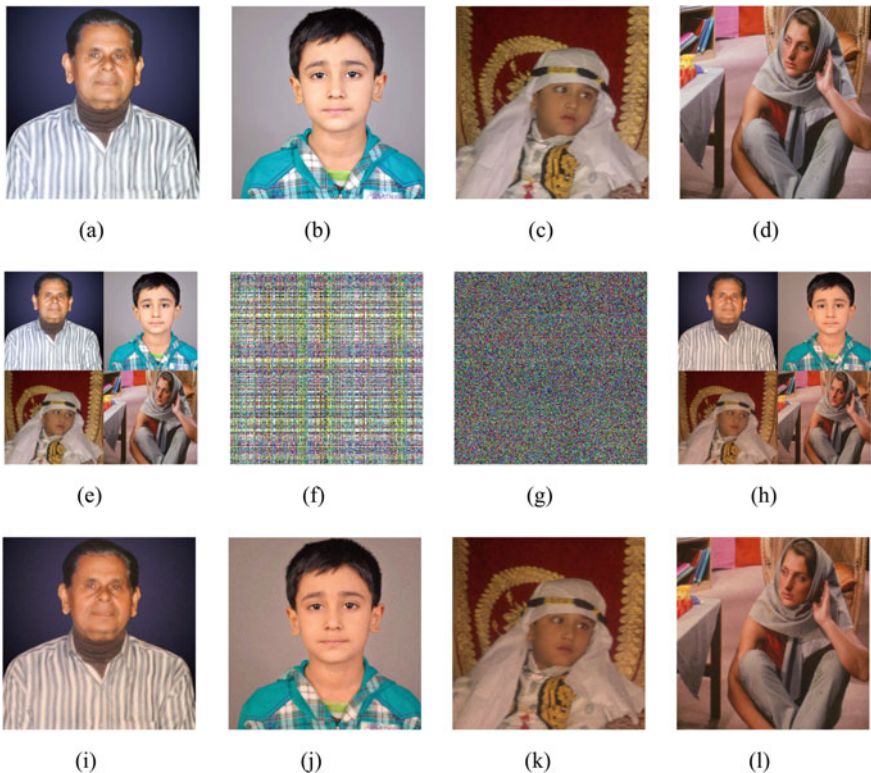


Fig. 2 **a** Father, **b** Ali, **c** Mahdi, **d** Barbara, **e** fused image, **f** chaotic phase mask, **g** binary random key; decrypted images with correct keys **h** fused image, **i** Father, **j** Ali, **k** Mahdi, **l** Barbara, [(a)–(h) are of size $512 \times 512 \times 3$ pixels], and [(i)–(l) are of size $256 \times 256 \times 3$ pixels]

where I_{out} and I_{in} are, respectively, decrypted and image to be encrypted. $E[\cdot]$ is the expected value operator.

Figure 2i–l demonstrates decrypted images of Father, Ali, Mahdi, and Barbara with all correct keys, respectively. After 299 iterations, the corresponding CC values of R , G , and B channels are (0.9997, 0.9995, 0.9992), (0.9995, 0.9983, 0.9975), (0.9987, 0.9991, 0.9988), and (0.9991, 0.9983, 0.9985). These values are approximately one. The secret color images are retrieved successfully.

Figure 3a–e shows encrypted fused image, Father, Ali, Mahdi, and Barbara with all correct keys, respectively. After 299 iterations, the CC values of R , G , and B channels of corresponding secret color-images are ($-0.0357, -0.0274, -0.0229$), ($-0.0229, -0.0051, -0.0143$), ($-0.0646, -0.1021, -0.0703$), and ($0.0081, 0.0030, 0.0032$). These values are very low. The secret color images are encoded into noise-like signals.

For simplicity, Barbara as shown in Fig. 2d has been studied. The robustness of the binary random key has been investigated. The decrypted (Barbara) image without binary random key is displayed in Fig. 4a. The CC values of R , G , and B

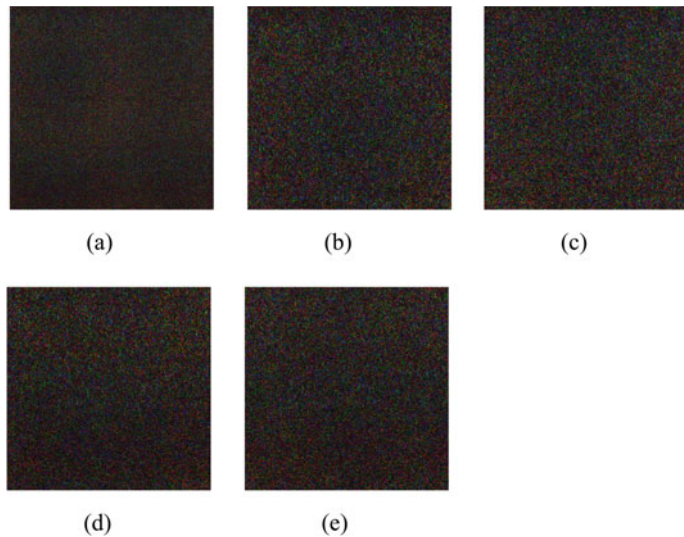


Fig. 3 Encrypted images with all correct keys: **a** fused image **b** Father, **c** Ali, **d** Mahdi, **e** Barbara, [(a) is of size $512 \times 512 \times 3$ pixels], and [(b)–(e) are of size $256 \times 256 \times 3$ pixels]

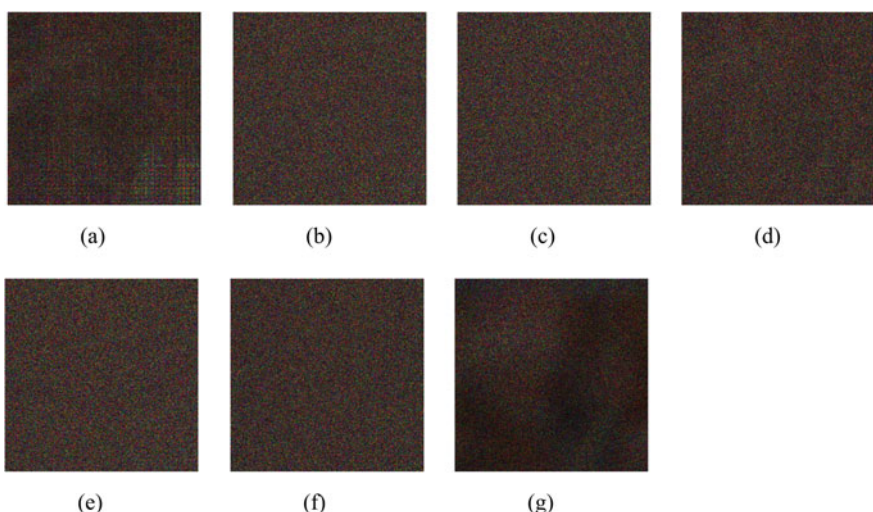


Fig. 4 Sensitivity of decrypted image (Barbara): **a** without binary random key **b** with x_0 changed by 1×10^{-17} , **c** with y_0 changed by 1×10^{-17} , **d** with k changed by 5, **e** with p changed by 1×10^{-15} , **f** with ε changed by 1×10^{-17} , **g** with $\alpha_R = 5$, $\alpha_G = 6$, and $\alpha_B = 7$ changed by 1

channels are, respectively, 0.0945, 0.0922, and 0.0766. The CC values are low. It can be observed that the retrieved images can be recognized.

The sensitivity of the parameters of CPM has been probed. The value of $x_0 = 0.21$ is changed by 1×10^{-17} . The decrypted (Barbara) image is displayed in Fig. 4b. The CC values of R , G , and B channels are, respectively, 0.0104, 0.0011, and 0.0007. The value of $y_0 = 0.82$ is changed by 1×10^{-17} . The retrieved (Barbara) image is demonstrated in Fig. 4c. The CC values of R , G , and B channels are, respectively, -0.0028, 0.0006, and -0.0006. The value of $k = 2000$ is changed by 5. The recovered (Barbara) image is exhibited in Fig. 4d. The CC values of R , G , and B channels are, respectively, 0.0774, 0.0717, and 0.0697. The value of $p = 3.52995$ is changed by 1×10^{-15} . The resulted (Barbara) image is shown in Fig. 4e. The CC values of R , G , and B channels are, respectively, 0.0031, -0.0034, and -0.0035. The value of $\varepsilon = -0.471$ is changed by 1×10^{-17} . The obtained (Barbara) image is shown in Fig. 4f. The CC values of R , G , and B channels are, respectively, 0.0037, -0.0071, and 0.0005. It can be concluded that the CC values of R , G , and B channels are very low. Hence, no information about the input image can be observed.

The sensitivity of the transformation angles of fractional Fourier transform has been tested. The transformation angles α_R , α_G , and α_B of Barbara are changed by 1. The recovered image is depicted in Fig. 4g. It can be observed that only noise-like image is obtained.

The public random phase function is used as public key, and decryption key is produced by performing the binary modulations to the public key. In the proposed scheme, the CPM is used as public key, and decryption key is produced by performing the binary modulations to the public key but the parameters (x_0 , y_0 , p , k , and ε) of CPM are exploited as decryption keys. Thus, the proposed system can avoid various types of attacks.

5 Conclusion

A new multiple information security scheme using DWT and YGAPRA in FRFT domain is introduced. The ciphertext image is real-valued function, which is more convenient for storage and transmission. The decryption key is produced by performing the binary modulation to the CPM. It has multiple storing keys as decryption keys, which are more convenient for management and thus reduces the complexity of the cryptosystem. Moreover, the multiple-decryption keys can circumvent potential attacks. The security is enhanced significantly due to high sensitivity of the decryption keys. Numerical simulation results confirm the efficiency and performance of the method.

References

1. Alfalou, A., Brosseau, C.: Optical image compression and encryption methods. *Adv. Opt. Photon.* **1**, 589–636 (2009)
2. Refregier, P., Javidi, B.: Optical image encryption based on input plane and Fourier plane random encoding. *Opt. Lett.* **20**, 767–769 (1995)
3. Rodrigo, J., Alieva, A.T., Calvo, M.L.: Application of gyrator transform for image processing. *Opt. Commun.* **278**, 279–284 (2007)
4. Alfalou, A., Brosseau, C.: Dual encryption scheme of images using polarized light. *Opt. Lett.* **35**, 2185–2187 (2010)
5. Abuturab, M.R.: Color image security system using double random-structured phase encoding in gyrator transform domain. *Appl. Opt.* **51**, 3006–3016 (2012)
6. Abuturab, M.R.: Color information security system using Arnold transform and double structured phase encoding in gyrator transform domain. *Opt. Laser Technol.* **45**, 525–532 (2013)
7. Liu, Z., Li, S., Liu, Wang, W. Y., Liu, S.: Image encryption algorithm by using fractional Fourier transform and pixel scrambling operation based on double random phase encoding. *Opt. Lasers Eng.* **51**, 8–14 (2013)
8. Qin, W., Peng, X.: Asymmetric cryptosystem based on phase-truncated Fourier transforms. *Opt. Lett.* **35**, 118–120 (2010)
9. Wang, X., Zhao, D.: A special attack on the asymmetric cryptosystem based on phase-truncated Fourier transforms. *Opt. Commun.* **285**, 1078–1081 (2012)
10. Liu, W., Liu, Z., Liu, S.: Asymmetric cryptosystem using random binary phase modulation based on mixture retrieval type of Yang-Gu algorithm. *Opt. Lett.* **38**, 1651–1653 (2013)
11. Sui, L., Liu, B., Wang, Q., Li, Y., Liang, J.: Color image encryption by using Yang-Gu mixture amplitude-phase retrieval algorithm in gyrator transform domain and two-dimensional Sine logistic modulation map. *Opt. Lasers Eng.* **75**, 17–26 (2015)
12. Liu, W., Xie, Z., Liu, Z., Zhang, Y., Liu, S.: Multiple-image encryption based on optical asymmetric key cryptosystem. *Opt. Commun.* **354**, 184–196 (2015)
13. Abuturab, M.R.: Securing multiple information using wavelet transform and Yang-Gu mixture amplitude-phase retrieval algorithm. *Opt. Lasers Eng.* **118**, 42–51 (2019)
14. Kong, D., Shen, X.: Multiple-image encryption based on optical wavelet transform and multichannel fractional Fourier transform. *Opt. Laser Technol.* **57**, 343–349 (2014)
15. Abuturab, M.R.: Group-multiple-image encoding and watermarking using coupled logistic maps and gyrator wavelet transform. *J. Opt. Soc. Am. A* **32**, 1811–1820 (2015)
16. Abuturab, M.R.: Multiple color-image fusion and watermarking based on interference and wavelet transform. *Opt. Lasers Eng.* **89**, 47–58 (2017)
17. Zhusubaliyev, Z.T., Mosekilde, E.: Multilayered tori in a system of two coupled logistic maps. *Phys. Lett. A* **373**, 946–951 (2009)
18. Ozaktas, H.M., Zalevsky, Z., Kutay, M.A.: *The Fractional Fourier Transform with Applications in Optics and Signal Processing*. Wiley (2001)

Development of Intrusion Detection System Using Deep Learning for Classifying Attacks in Power Systems



Ankitdeshpandey and R. Karthi

Abstract Interconnected devices have increased rapidly, and smart power grids have adapted this technology for increased reliability and fault tolerance. Due to exposure of power grid devices to the Internet, it is highly vulnerable to unauthorized access and susceptible to unsettling, inexorable cyberattacks. Power grid is a critical component of infrastructure, whose unimpaired survivability is an irrevocable requirement in recent times. This paper investigates the applicability of machine learning (ML) algorithms, to detect and identify attacks on power grids, as these algorithms can identify subtle variations in data caused by cyberattacks in the power grid networks. A standard power system dataset, from Mississippi State University and Oak Ridge National Laboratories (MSU-ONL dataset) were employed in this study. A deep neural network (DNN) model was built to classify the power system data as attacks, normal, and no-events classes. Conventional ML models such as OneR, K Nearest Neighbour (KNN), Random Forest, Support Vector Machines (SVM) and Naïve Bayes were compared with DNN, to gauge DNN's efficacy in the detection of cyberattack. Principal Component Analysis (PCA) was applied to reduce the dimensionality of the acquired data, and its effects on performance measures were studied. The empirical results show that the Random Forest model, which is an ensemble classifier, identifies attacks with highest accuracy compared to the other ML and deep learning options. SVM and DNN show improved performance when combined with PCA. Test results substantiate that SVM, Random Forest and DNN algorithms are apropos to deployment of Intrusion Detection System (IDS) appliances on power grid systems.

Keywords Power system · Intrusion detection system (IDS) · Machine learning · Classification · Cyberattacks · Deep learning

Ankitdeshpandey · R. Karthi ()

Department of Computer Science and Engineering, Amrita School of Engineering, Amrita Vishwa Vidyapeetham, Coimbatore, India
e-mail: r_karthi@cb.amrita.edu

Ankitdeshpandey
e-mail: CB.EN.P2CSE17006@cb.students.amrita.edu

1 Introduction

Industrial Control Systems (ICS) such as smart electric grid, are becoming more complex in their architecture and design. In recent times, power systems have been rapidly transitioning from proprietary, isolated control systems to standard distributed systems. The downside of usage of open protocols and standards is the heightened exposure of these systems to cyberattacks [1]. Industrial process control systems, such as Supervisory Control And Data Acquisition (SCADA), Distributed Control Systems (DCS), Programmable Logic Controllers (PLC), Remote Terminal Unit (RTU) and Intelligent Electronic Device (IED), facilitate an environment to carry out power management operations efficiently. SCADA, DCS, PLC, RTU and IED are interconnected through physical interfaces, and rely on communication protocols, to interact with each other. ML algorithms are designed to leverage the complex patterns in data and help in building classifiers, deployable in various applications [2, 3].

Attack is any attempt to breach the confidentiality, availability and integrity of a smart electric grid system or network. Smart grids are susceptible to different types of attacks from hackers; common forms of cyberattacks are Denial-of-Service attack, Man-in-Middle attack, spoofing attack, malware and worm attacks. Smart grids should be reinforced with components to identify threats to normal operational disturbances, across the grid network. Power system states have been classified into three categories: normal, natural faults and attack which represent normal functioning of services, an event of power fault, and cyberattack, respectively [1].

Faults in power systems are manifested as natural disruptions, in the services provided by power grids such as short circuit, transformer blow-up, generator failure or non-functioning of individual components such as sensors, relays, snort log. Solution for such events is to manually repair the component or maintenance of physical devices. Cyberattacks are more complex and occur at different levels, which can attack any individual device on the network grid, or on software operations. Defensive postures adopted to control or minimize attacks include access control, authentication, firewalls and intrusion detection system. Design of IDS poses quite a challenge to maintain normal services, and defend property and personnel against numerous types of relentless cyberattacks.

The central point of this paper deals with building ML algorithms, to distinguish between a power fault and cyberattacks, in protection systems of electrical power grids. All operations in power generation, transmission and distribution systems are categorized into normal (no-event), natural event and attacks. Diverse ML models have been built to understand the operational behaviour of power systems, using measured features of power grids. Machine learning algorithms are able to leverage complex patterns [4] that can be used to identify normal, natural and attack events in power grids. Deep learning models are also being explored to understand its effectiveness in identifying cyberattacks on power grid. The paper is organized as follows: Sect. 2 discusses the current machine learning methods to identify attacks on power grids. Section 3 elaborates on the system architecture of test bed used to

simulate power grid, and Sect. 4 discusses the classification algorithm used in the paper. Section 5 summarizes the results and inferences from this research, with final concluding remarks in Sect. 6.

2 Related Work

Due to never-ending, sophisticated attacks by hackers on power grids, several techniques have been reported by researchers to characterize cyberattacks on smart grids. Extant IDSes are based on network [5], signature, specification and anomaly methods [6]. Studies were done on how machine learning methods can be used for discrimination of power system disturbances, and attacks on protection systems of power grids [7]. A test bed was built, and data is simulated for normal, disturbance and attack scenarios and classified using ML algorithms. Margin Setting Algorithm (MSA) was proposed to detect false data injection attacks on smart grids, were playback and time attacks were used to modify the state estimate parameter in the system [8]. Simulink model of a six bus power system in a wide area network is used as test bed and real-time data from Phasor Measurement Unit (PMU) was used for the study. The performance of MSA algorithm was evaluated in comparison with Artificial Neural Network (ANN) and SVM algorithms.

IDS algorithms were developed that use the temporal transition states specifications in power systems to classify normal behaviour, disturbance and cyberattacks [9]. FP-growth (Frequent Pattern) algorithm was used to mine the common transition paths, and temporal patterns were used to classify system in normal or cyberattacks state. A cyber-physical power system test bed is built to aid in IDS development and validate activities such as faults, normal and cyberattacks in power systems [1]. Wide area measurement system based test bed was developed to simulate power system contingencies and cyberattacks. Data sets were generated for different scenarios which were used to classify attacks in power systems using machine learning techniques [10]. Different surveys for studying cyberattacks are presented based on protocols in the system from where the attack is done [11] and from attacker's perspective [12]. Cyberattacks on power grids and countermeasures used to defend against them are elaborated in the study [11, 12]. ML algorithm to classify attacks on smart grid using deep neural networks approach were studied; attacks were performed on the network infrastructure of the system and four malicious attacks were simulated on the substation [13].

From the study, we infer that smart grids are heterogeneous networks that require comprehensive security procedures to safeguards and address the vulnerability of cyberattacks. Development of test bed to understand cyberattacks is a challenge due to cost and expertise needed to build the system. Many classification methods have been developed using machine learning strategies to understand attacks. A standard power system dataset (MSU-ONL), that simulated various attacks, was reported by Borges Hink et al. [7], and this dataset, used in this study. Few attempts have been made to understand the feasibility of deep learning models to identify attacks

in protection systems of power grids. This study intends to build deep learning classifiers, and understand the utility of pre-processing, reduction methods on the performance of classifiers. Comparative analysis was conducted, using conventional classifiers and their performance was evaluated on the parameters of accuracy, error rate, sensitivity (recall), precision, and specificity and F1 measure.

3 System Architecture

The architecture of test bed system is shown in Fig. 1. The test bed [7] has intelligent electronic devices, control system, which is connected using a networking framework. Attacker has access to switches and network and sends attack commands to substations. Figure 1 has 4 relays, R1–R4, and breakers, BR1–BR4, which are controlled by relays that switch them on and off. Generators, G1 and G2, buses, B1, B2 and B3, and line L1, spans between buses B1 and B2; line L2 spans between buses B2 and B3. Phasor Data Concentrator (PDC) consolidates the data of Phasor Measurement Units (PMU), which has synchrophasor measurements from each of the relays. Data logs are created with timestamp that records PMU measurements, relay log, control panel log and snort log information. The attacks are simulated from attacker machine on the network.

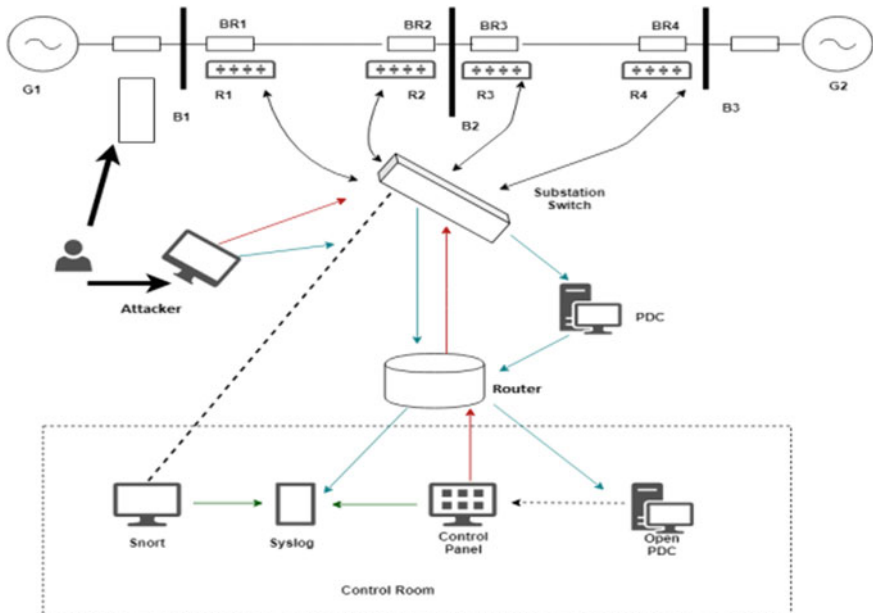


Fig. 1 Architecture of test bed

4 Classification Methodology

There are various popular machine learning classifiers reported for intrusion analysis. Few attempts have been made to assess their viability on smart grids. The most common and important classification algorithms used in this study is given below:

4.1 OneR

OneR [4] uses the property of distribution of data over all the classes and returns the label of class that is most frequent in the processed data. The algorithm is used to establish a lower bound for accuracy of classifiers.

4.2 K Nearest Neighbour

K Nearest Neighbour [4] is a non-parametric lazy learning algorithm. It makes no assumption about the distributed characteristics of data. Lazy algorithm does not require any data for learning and building the model, as it builds the model at runtime, during testing. The model building computations are deferred until classification is done by the KNN algorithm.

4.3 Random Forests

Random forests [14] is a supervised learning algorithm. Random Forest is an ensemble classifier that avoids problem of overfitting. The disadvantage of using Random Forest is that many decision trees are built in the model; it is difficult to interpret the results and generate rules. It can be used for classification and regression analysis.

4.4 Naïve Bayes

Naïve Bayes [4] classifier is a supervised learning algorithm based on Bayes theorem. It is a probabilistic classifier. It assumes conditional independence between its input features. Naïve Bayes algorithm calculates the prior, and likelihood probabilities for the data, and applies Bayes theorem to calculate the posterior probability.

4.5 Support Vector Machines

Support Vector Machines [15] is a supervised learning model, which can be used for classification and regression analysis, and a non-probabilistic classifier. The SVM algorithm finds a best separating hyperplane, with the maximal margin that partitions the data.

4.6 Deep Neural Network

Deep learning algorithms [16] use neural network architectures, where the number of hidden layers is higher compared to traditional neural networks. Deep learning models are trained with large sets of data; these models learn and extract features directly from the data. Each layer in the network learns to transform the input data into a more abstract and composite representation. DNN can model linear and non-linear relationships, and each layer captures primitive features, from the lower layers and build composite features to model complex data.

5 Experimental Results and Discussion

5.1 Mississippi State University and Oak Ridge National Laboratory Dataset (MSU-ONL Dataset)

The MSU-ONL data set used for the study is the open-source power systems dataset provided by Mississippi State University and Oak Ridge National Laboratory and this dataset simulates attacks on protection devices of power grid. The current, voltage and phase angle are measured in the experiment which is drawn from PMU. PMU makes time-synchronized measurements of voltage and current at multiple remote points on the grid. The MSU-ONL data set contains 128 features and one class label feature, which labels the data to a particular class. In the case of three class problems, the dataset contains 78,377 records, which were classified as attack events, natural event and no-event. For this study, sampling of records was performed on the original data set, and 4400 records were randomly sampled, for each of the three classes, and three class problems is considered for the study.

5.2 Experimental Results and Discussion

OneR, KNN, Random Forest, Naïve Bayes, SVM and DNN algorithms, were used to classify the data. Performance metrics (accuracy, error rate, sensitivity (recall),

Table 1 Performance metrics for classifiers

Measure	Formula
Accuracy	$\frac{TP+TN}{P+N}$
Error rate	$\frac{FP+FN}{P+N}$
Precision	$\frac{TP}{TP+FP}$
Sensitivity (recall)	$\frac{TP}{P}$
Specificity	$\frac{TN}{N}$
F-Score ($F1$)	$\frac{2 * (\text{Precision} * \text{Recall})}{(\text{Precision} + \text{Recall})}$

specificity, precision and $F1$) were used to gauge how good a classifier was, in predicting the class label, for untrained tuple. Table 1 shows the evaluation measures of classifiers considered in this study [4].

The confusion matrix was used to calculate the performance metrics of classifiers. Holdout method was used for random sampling of data, and partitioning the data into two independent sets for training and testing the classifiers. The training data set was used to build the classifier model and test data was used for evaluation of the accuracy of the classifier. In this study, ML model was built on 80% of the data, and the residual 20% was used to test the performance of the classifier.

Thirteen thousand two hundred samples were randomly selected from the original MSU-ONL data set, and 80% of samples were used to build the classifier. Equal number of samples was selected from each of the three classes. 20% of samples were used for testing the classifier. Confusion matrix and performance metrics were then computed for each classifier. The data was normalized to the range [0–1] for all numeric attributes, which helps in reducing the effects of large value attributes outweighing smaller range value attributes. Binary valued attributes control panel, snort logs and relay logs that capture the status of device not considered for normalization.

Performance on Normalized data: Table 2 shows the confusion matrix obtained for each of the classifier models on the test data. Table 2a shows the confusion matrix for OneR classifier; from the table, we infer that OneR has predicted attacks and natural events to no-events class. Table 2b shows the confusion matrix for KNN classifier; the results show that KNN algorithm has predicted natural events like attacks and attacks as natural events.

Table 2c shows the results of Random Forest classifier and as this algorithm is an ensemble classifier, it has the highest accuracy among all the classifiers. The few reported errors were due to misclassification between natural and attack events. Table 2d shows the results of Naïve Bayes algorithm, where the misclassifications are high. The attack and natural events were classified as no-events by the classifier, and Naïve Bayes algorithm assumed independence between the attributes, but there is correlation between the variables and leads to many misclassifications. Table 2e shows the results of SVM algorithm, where errors are contributed, due to misclassification of data, to all the three classes. Table 2f shows the results of DNN algorithm; there is equal distribution of data to classes and there is misclassification, among all the classes similar to SVM.

Table 2 Confusion matrix for various classifiers

(a) OneR classifier				(b) KNN classifier			
Actual class	Predicted class			Actual class	Predicted class		
	Att*	Nat*	NoE*		Att	Nat	NoE
Att	293	81	507		771	90	20
Nat	273	124	483		94	764	22
NoE	56	25	799		NoE	23	34
(c) Random Forest classifier				(d) Naïve Bayes classifier			
Actual class	Predicted class			Actual Class	Predicted class		
	Att	Nat	NoE		Att	Nat	NoE
Att	827	46	8		77	44	760
Nat	45	828	7		Nat	67	94
NoE	4	10	866		NoE	11	7
(e) SVM classifier				(f) DNN classifier			
Actual class	Predicted class			Actual class	Predicted class		
	Att	Nat	NoE		Att	Nat	NoE
Att	453	147	281		592	71	157
Nat	215	415	250		Nat	167	747
NoE	117	46	717		NoE	122	62

Note *Att represents Attack class, Nat represents natural class, and NoE represents No-Event class

Table 3 Performance measures of classifiers

	OneR	KNN	Random Forest	Naïve Bayes	SVM	DNN
Accuracy	0.4604	0.8928	0.9546	0.3998	0.6002	0.7274
Error rate	0.5396	0.1072	0.0454	0.6002	0.3998	0.2726
Precision	0.4856	0.8934	0.9546	0.5262	0.6114	0.7274
Sensitivity	0.4605	0.8929	0.9546	0.4000	0.6002	0.7299
Specificity	0.7302	0.9464	0.9773	0.7000	0.8001	0.8662
F-score	0.4727	0.8931	0.9546	0.4545	0.6057	0.7287

Table 3 shows the performance measures of different classifiers considered in this study. It is apparent from the table, that Random Forest has the best accuracy, among all the classifier models.

Performance on Dimensionality Reduced data: Dimensionality reduction is the process of reducing the number of features by the process of selection or transformation. PCA is a process of mapping data to lower dimensional space, such that variance of data in the lower dimensional space is maximized. PCA is applied to MSU-ONL dataset and 116 numeric variables that represent the PMU measurements were subjected for data reduction. These 116 variables were reduced to 31 principal components and were appended with control, snort and relay log binary variables. A total of 43 reduced features were derived to represent MSU-ONL data after PCA transformation.

Table 4 shows the confusion matrix of each for each of the classifier models on the test data. Table 4a shows the confusion matrix for the OneR classifier, where many of the natural events are classified as attack and no-events. Table 4b shows the confusion matrix for KNN classifier; the results show that KNN algorithm predicted natural events like attacks and attacks as natural events, and there is minimal effect of PCA on the performance of classification. Table 4c shows the results of Random Forest classifier; it had the highest accuracy among all the classifiers. Misclassification was high between the natural and attacks classes, after reduction in attributes.

Table 4d shows the results of Naïve Bayes algorithm, where the misclassifications rate was reduced, after reduction of dimensionality. Table 4e shows the results of SVM algorithm; the performance got improved by 28% after reduction of dimensionality in data. Table 4f shows the results of DNN algorithm; the performance got improved after dimensionality reduction in data.

Table 5 shows the performance measures of various classifiers and the experiment demonstrates that Random Forest algorithm performs well and is suitable for power system attack classification. Table 6 shows the percentage difference in accuracy for each of the classifier models considering all attributes and reduced dimensions (when PCA is applied on the data). There is about 28 and 23% increase in performance for SVM and DNN when data is transformed using PCA. Table 6 bears testimony to infer that SVM and DNN show improved performance, when the transformation is applied on the data, to extract the salient features. Simple probabilistic algorithms have fewer improvements in classification rates due to reduced dimensionality.

Table 4 Confusion matrix for various classifiers

(a) OneR classifier				(b) KNN classifier			
Predicted class		Actual class		Predicted class		Actual class	
Actual	Att	Att*	Nat*	NoE*	Att	Att	Nat
class	Att	471	5	405	758	98	25
	Nat	346	10	524	Nat	84	778
	NoE	353	5	522	NoE	24	27
(c) Random Forest classifier							
Predicted class		Actual Class		Predicted class		Actual Class	
Actual	Att	Nat	NoE	Att	Att	Att	NoE
class	Att	779	89	13	108	41	732
	Nat	72	797	11	Nat	77	99
	NoE	20	29	831	NoE	31	0
(d) Naïve Bayes classifier							
Predicted class		Actual Class		Predicted class		Actual Class	
Actual	Att	Nat	NoE	Att	Att	Att	NoE
class	Att	582	171	128	757	26	98
	Nat	203	610	67	Nat	23	835
	NoE	33	8	839	NoE	83	17
(e) SVM classifier							
Predicted class		Actual class		Predicted class		Actual class	
Actual	Att	Nat	NoE	Att	Att	Att	NoE
class	Att	582	171	128	757	26	98
	Nat	203	610	67	Nat	23	835
	NoE	33	8	839	NoE	83	17
(f) DNN classifier							
Predicted class		Actual class		Predicted class		Actual class	
Actual	Att	Nat	NoE	Att	Att	Att	NoE
class	Att	582	171	128	757	26	98
	Nat	203	610	67	Nat	23	835
	NoE	33	8	839	NoE	83	17

Note *Att represents Attack class, Nat represents natural class and NoE represents No-Event class

Table 5 Performance measures of the classifiers

	OneR	KNN	Random Forest	Naïve Bayes	SVM	DNN
Accuracy	0.3798	0.8955	0.9114	0.3998	0.7690	0.8981
Error rate	0.6202	0.1045	0.0886	0.6002	0.2310	0.1019
Precision	0.4208	0.8959	0.9124	0.5262	0.7653	0.8983
Sensitivity	0.3797	0.8955	0.9114	0.4000	0.7691	0.8982
Specificity	0.6899	0.9477	0.9557	0.7000	0.8845	0.9491
F-score	0.3992	0.8957	0.9119	0.4545	0.7672	0.8982

Table 6 Percentage increase in performance of classifiers

OneR	KNN	Random Forest	Naïve Bayes	SVM	DNN
-0.1752	0.0030	-0.0452	0.0000	0.2814	0.2348

6 Conclusion

In this study, Machine learning algorithms are built to identify attacks in power systems. Data using synchrophasor units, syslogs, relays logs and control logs capture the state of power system and these features are used to identify attack, natural and normal (no-events) states. Deep learning network models are applied for monitoring attacks on power protection systems. The effects of reduction techniques in the performance of machine learning models are also studied. Confusion matrix with various performance metrics are analyzed for many machine learning models. From the study, we propose that Random Forest can be used to build an IDS for identifying attacks on protection system of power grid. SVM and Deep Neural Networks can be effectively used for identifying attacks when PCA based reduction techniques are applied on the data. Attacks are efficiently identified using the principal features captured from the data.

References

1. Adhikari, U., Morris, T.H., Pan, S.: A cyber-physical power system test bed for intrusion detection systems. In: 2014 IEEE PES General Meeting Conference & Exposition, pp. 1–5. IEEE (2014)
2. Karthi, R., Rajendran, C., Rameshkumar, K.: Neighborhood search assisted particle swarm optimization (npso) algorithm for partitional data clustering problems In: Abraham, A., Mauri, J.L., Buford, J.F., Suzuki, J., Thampi, S.M. (eds.) Advances in Computing and Communications. ACC 2011. Communications in Computer and Information Science, vol. 192, pp. 552–561. Springer, Berlin (2011)
3. Reddy, K.R.P., Srija, S.S., Karthi, R., Geetha, P.: Evaluation of water body extraction from satellite images using open-source tools. In: Thampi, S., et al. (eds.) Intelligent Systems,

- Technologies and Applications. Advances in Intelligent Systems and Computing, vol. 910, pp. 129–140. Springer, Singapore (2020)
- 4. Han, J., Pei, J., Kamber, M.: Data Mining: Concepts and Techniques. Elsevier (2011)
 - 5. Yang, Y., McLaughlin, K., Sezer, S., Littler, T., Pranggono, B., Brogan, P., Wang, H.F.: Intrusion detection system for network security in synchro phasor systems. In: IET International Conference on Information and Communications Technologies (IETICT 2013), pp. 246–252. Beijing, China (2013)
 - 6. Lee, W., Stolfo, S.J., Mok, K.W.: A data mining framework for building intrusion detection models. In: Proceedings of the 1999 IEEE Symposium on Security and Privacy, pp. 120–132. Oakland, CA, USA (1999)
 - 7. Borges Hink, R.C., Beaver, J.M., Buckner, M.A., Morris, T., Adhikari, U., Pan, S.: Machine learning for power system disturbance and cyber-attack discrimination. In: 2014 7th International Symposium on Resilient Control Systems (ISRCS), pp. 1–8. Denver, CO (2014)
 - 8. Wang, Y., Amin, M.M., Fu, J., Moussa, H.B.: A novel data analytical approach for false data injection cyber-physical attack mitigation in smart grids. *IEEE Access* **5**, 26022–26033 (2017)
 - 9. Pan, S., Morris, T., Adhikari, U.: Developing a hybrid intrusion detection system using data mining for power systems. *IEEE Trans. Smart Grid* **6**(6), 3104–3113 (2015)
 - 10. Adhikari, U., Morris, T., Pan, S.: WAMS cyber-physical test bed for power system, cybersecurity study and data mining. *IEEE Trans. Smart Grid* **2744–2753** (2017)
 - 11. Wang, W., Lu, Z.: Cyber security in the smart grid: survey and challenges. *Comput. Netw.* **57**(5), 1344–1371 (2013)
 - 12. El Mrabet, Z., Kaabouch, N., El Ghazi, H., El Ghazi, H.: Cyber-security in smart grid: survey and challenges. *Comput. Electr. Eng.* **67**, 469–482 (2018)
 - 13. Liang, Z., Ouyang, X., Ying, H., Han, L., Cheng, Y., Zhang, T.: Cyber-attack classification in smart grid via deep neural network, In: Proceedings of the 2nd International Conference on Computer Science and Application Engineering, p. 90. ACM (2018)
 - 14. Ho, T.K.: Random decision forests. In: Proceedings of 3rd International Conference on Document Analysis and Recognition, vol. 1. IEEE (1995)
 - 15. Corinna, C., Vapnik, V.: Support-vector networks. *Mach. Learn.* **20**(3), 273–297 (1995)
 - 16. Ciregan, D., Meier, U., Schmidhuber, J.: Multi-column deep neural networks for image classification. *IEEE Conf. Comput. Vision Pattern Recog. Providence RI* **2012**, 3642–3649 (2012)

An Improved Adaptive Transfer Function for Explosion Spark Generation in Fireworks Algorithm



Tapas Si and Amit Mukhopadhyay

Abstract Fireworks algorithm (FWA) is a swarm intelligence algorithm simulating the explosion process of fireworks in the sky at night. An improved FWA with an adaptive transfer function (ATF) termed as (FWA-ATF) is recently developed. This ATF is used to compute the number of “explosion sparks” and the amplitudes of explosion. This paper devises a modified FWA-ATF algorithm with deterministically controlled ATF and the best selection strategy. The improved ATF controls the exploration and exploitation of the fireworks, whereas the best selection strategy is used to keep diversity in the search space. The devised algorithm is applied on fifteen CEC2015 benchmark optimization problems and a comparative study has been made with state-of-the-art variants of FWA such as FWA-ATF, dynamic FWA with covariance mutation (DynFWA-CM) and cooperative framework in FWA (CoFFWA). The experimental results demonstrate that the devised algorithm statistically outperforms others in function optimization.

Keywords Artificial intelligence · Swarm intelligence · Fireworks algorithm · Adaptive transfer function · Best selection strategy · Function optimization

T. Si (✉)

Department of Computer Science & Engineering,
Bankura Unnayani Institute of Engineering, Bankura, West Bengal, India
e-mail: c2.tapas@gmail.com

A. Mukhopadhyay

Department of Electronics & Communication Engineering,
Bankura Unnayani Institute of Engineering, Bankura, West Bengal, India
e-mail: amit.ece@buie.ac.in

1 Introduction

The FWA is a swarm intelligence algorithm developed by Tan and Zhu [1] in 2010. The FWA is modeling the explosion process of fireworks in the sky at night. Each location of fireworks represents a solution in the search space. There are two types of sparks such as “explosion sparks” and “Gaussian sparks” in FWA. A good *trade-off* between exploration and exploitation is maintained during the search process. Exploration or global search is carried out using the bad fireworks with less number of “explosion sparks” having higher amplitudes. Exploitation or local search is carried out using the good fireworks with a higher number of “explosion sparks” having less amplitudes. Gaussian mutation is used to create “Gaussian sparks” in FWA for more diversification in the search space. Finally, a crowding distance-based roulette wheel selection mechanism is used to select the best locations from fireworks and their all types of sparks for the next generation. But FWA suffers from the following snags: (i) the explosion sparks generated from the best fireworks have a very low amplitude which is closed to zero. This results in bad exploitation of the best fireworks. (ii) A Gaussian distributed random number with zero mean and one standard deviation is multiplied with fireworks selected randomly to create the “Gaussian sparks.” When this random number is closed to zero, the mutated spark moves toward the origin. This type of spark is not effective when the global optima are located far away from the origin. (iii) It takes high computational time cost due to crowding distance-based selection.

During the past few years, different variants of FWA have been developed to overcome these aforesaid drawbacks. An enhanced FWA (EFWA) developed by Pei et al. [2], outperformed FWA in CEC2013 benchmark function optimization. Zheng et al. [3] developed a hybridization of FWA and differential evolution (DE) algorithm. Liu et al. [4] enhanced the FWA using random mutation in place of Gaussian sparks and best selection scheme (IFWABS). Li et al. [5] developed an adaptive FWA (AFWA) which was a modification of EFWA. A dynamic search in FWA (DynFWA) is proposed by Zheng et al. [6]. DynFWA is also a modification of EFWA. DynFWA is further improved by covariance mutation operator [7]. Zheng et al. [8] proposed an FWA with a cooperative framework (CoFFWA) which incorporates the independent selection scheme for each firework and crowdness-avoiding cooperative strategy among the fireworks. A cultural FWA proposed by Gao et al. [9] and it was applied in digital filter design. An improved FWA with differential mutation (FWA-DM) is proposed by Yu et al. [10]. In FWA-DM algorithm, the differential mutation is used in EFWA to improve the interaction mechanism among the fireworks. Li and Tan [11] proposed a bare bones FWA (BBFA). Li et al. [12] proposed a guiding spark using the objective function’s information of explosion spark. Li and Tan [13] proposed an FWA with loser-out tournament selection. Si et al. [14] developed an improved version of IFWABS (FWA-ATF) by employing (i) an adaptive transfer function to compute the number of “explosion sparks” and the amplitude of the explosions and (ii) different perturbation in different dimensions in the position of the fireworks during the generation of explosion sparks. This paper proposes an improvement of

FWA-ATF algorithm by incorporating a deterministically controlled adaptive transfer function and group best selection strategy to make a good *trade-off* between exploration and exploitation in the search space. The developed method is termed as FWA-IATFGS in the remaining of this paper. The developed method statistically outperforms the state-of-the-art variants of FWA such as CoFFWA, DynFWA-CM and FWA-ATF in the minimization of CEC2015 benchmark problems.

The remaining of this paper is organized as follows: FWA-ATF is discussed in Sect. 2. The proposed FWA-IATFGS is described in Sect. 3. The experimental results are given in Sect. 4 and discussed in Sect. 5. Finally, a conclusion with future works is given in Sect. 6.

2 FWA-ATF

In FWA-ATF, an adaptive transfer function is used to generate the numbers of “explosion sparks” and the amplitudes of explosions.

2.1 Adaptive Transfer Function (ATF)

In FWA-ATF, an ATF values are calculated using the score values of the fireworks \mathbf{X}_i in the sorted front. First, objective function values f_i are normalized in the range $(0, 1)$ as follows:

$$\dot{f}_i = \frac{f(\mathbf{X}_i) - y_{\min}}{y_{\max} - y_{\min}} \quad (1)$$

Let \dot{f} values are sorted in ascending order as $\ddot{f}_1, \ddot{f}_2, \ddot{f}_3, \dots, \ddot{f}_i, \dots, \ddot{f}_{\mathcal{N}}$ in the sorted front \ddot{F} .

The distance ($\text{dist}_{\text{Best},i}$) of i th firework from the best firework based on fitness values in \ddot{F} is defined as:

$$\text{dist}_{\text{Best},i} = |\ddot{f}_{\text{Best}} - \ddot{f}_i| \quad (2)$$

The value of $\text{dist}_{\text{Best},i}$ is always in the range $(0, 1)$ as $\ddot{f}_i \in (0, 1)$.

An adaptive score value r_i of the i th firework is defined as follows:

$$r_i = i + \text{dist}_{\text{Best},i} \quad (3)$$

The score value of best firework is always 1 as $\text{dist}_{\text{Best},1} = 0$. The maximum score value of worst firework is closed to $(\mathcal{N} + 1)$ when $\text{dist}_{\text{Best},N} \rightarrow 1$. The value of the adaptive transfer function is calculated as follows:

$$\mathcal{T}_i = \frac{1}{1 + \exp(r_i)} \quad (4)$$

2.2 Generation of “Explosion Sparks”

The number of “explosion sparks” for i th firework is calculated by:

$$\mathcal{S}_i = \mathcal{M} \times \frac{\mathcal{T}_i}{\sum_{i=1}^N \mathcal{T}_i} \quad (5)$$

where \mathcal{M} is the maximum number of “explosion sparks.” The amplitude of the “explosion sparks” for i th firework is calculated by:

$$\mathcal{A}_i = \mathcal{A} \times \frac{\mathcal{T}_{(N-i+1)}}{\sum_{i=1}^N \mathcal{T}_i} \quad (6)$$

where $\mathcal{A} = (X_{\max} - X_{\min})$ is the magnitude of explosion. The “explosion sparks” for i th firework are created using Algorithm 1 given in next.

Algorithm 1: Explosion Spark Generation

```

1 Initialize the spark's location:  $\dot{x}_e \leftarrow \mathbf{X}_i$ 
2 Select the number of positions randomly:  $\mathcal{P} \leftarrow [\mathcal{D} \times \text{rand}(0, 1)]$ 
3 for  $p \leftarrow 1$  to  $\mathcal{P}$  do
4   | Select the position's index  $k \in [1, \mathcal{D}]$  randomly
5   | Calculate the displacement:  $\Delta x \leftarrow \mathcal{A}_i \times \text{rand}(-1, 1)$ 
6   |  $\dot{x}_{ek} \leftarrow \dot{x}_{ek} + \Delta x$ 
7   | if  $\dot{x}_{ek} < X_{\min}$  or  $\dot{x}_{ek} > X_{\max}$  then
8   |   |  $\dot{x}_{ek} \leftarrow X_{\min} + |\dot{x}_{ek}| \% (X_{\max} - X_{\min})$ 
9   | end
10 end
```

2.3 Random Mutation Operator

In FWA-ATF algorithms, the random mutation operator is used to keep diversity in the search space. This mutation operator for j th dimension of randomly selected r th fireworks is defined as:

$$x_{rj} = X_{\min} + (X_{\max} - X_{\min}) \times \text{rand}(0, 1) \quad (7)$$

Details of this operator are given in Algorithm 2.

Algorithm 2: Random Mutation

```

1 Initialize the spark's location:  $\dot{x}_g \leftarrow \mathbf{X}_r$ 
2 Select the number of positions randomly:  $\mathcal{P} \leftarrow [\mathcal{D} \times \text{rand}(0, 1)]$ 
3 for  $p \leftarrow 1$  to  $\mathcal{P}$  do
4   | Select the positions' index  $k \in [1, \mathcal{D}]$  randomly
5   |  $\dot{x}_{gk} \leftarrow X_{min} + (X_{max} - X_{min}) \times \text{rand}(0, 1)$ 
6 end

```

2.4 Best Selection Strategy

First, fireworks and all type of sparks of the current generation are sorted according to their fitness. Then, the best \mathcal{N} locations are selected from the sorted front.

3 Proposed Method

FWA-IATFGS is the modification of FWA-ATF algorithm by incorporating (i) a linearly time-varying ATF to compute the number of “explosion sparks” and the amplitudes of explosions, (ii) a mapping operator for unbounded solution in the search space and (iii) group best selection strategy.

3.1 Improved ATF

For any search algorithm, it is desirable to encourage the exploration at the beginning of the search and exploitation during the end of the search. Therefore, it is required to make a good balance between exploration and exploitation in the search process. The worst firework has always the largest distance from the best firework. An improved ATF is devised in this paper. It is defined as follows:

$$\dot{T}_i = \frac{1}{1 + \exp(w \cdot r_i)} \quad (8)$$

In the proposed transfer function, the score value of fireworks is weighted by a factor $w \in (0, 1)$. The control parameter w is linearly increasing in the range $(w_{\min}, w_{\max}) = (0.1, 0.9)$ by the following equation:

$$w = w_{\min} + (w_{\max} - w_{\min}) \times \left(\frac{\text{fitcount}}{\text{FEs}} \right) \quad (9)$$

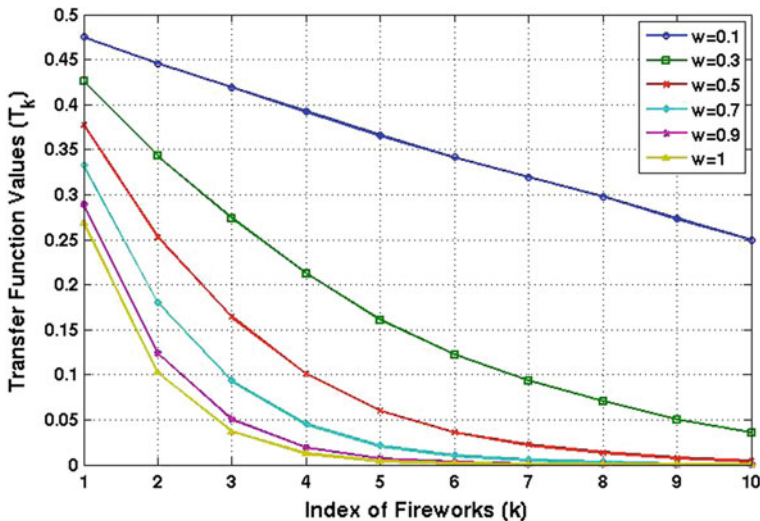


Fig. 1 Transfer function

where fitcount is the number of function evaluations in the current iteration and FEs is the maximum number of function evaluations. The control parameter w is used to reduce the effectiveness of adaptation at the beginning stage of the search and to enhance the adaptation at the later stage of the search. When $w = 1$, the proposed transfer function becomes identical to the ATF used in FWA-ATF.

For the analysis of the proposed transfer function, ten fireworks are initialized in the range $[-100, 100]$ and their objective values are evaluated for the shifted and rotated Ackley's function [16]. The transfer function values of these fireworks for different values of the control parameter w are plotted in a graph against the index (k) of fireworks in Fig. 1. The number of explosion sparks and the amplitudes of the explosions are given in Figs. 2 and 3, respectively. From the graph, in Fig. 1, it is seen that the differences among transfer function values of fireworks are very less for $w = 0.1$, whereas these differences are large for $w = 1$. Therefore, the number of sparks and their amplitudes are almost same for all fireworks for smaller values of w that creates exploration based on all fireworks. In the later stage of the search, the transfer function becomes more adaptive as w increases over time. Therefore, the adaptive score values of fireworks, based on their distances from the best fireworks, have more effect on the transfer function values. Hence, the exploration and exploitation are controlled by the adaptive nature of the transfer function.

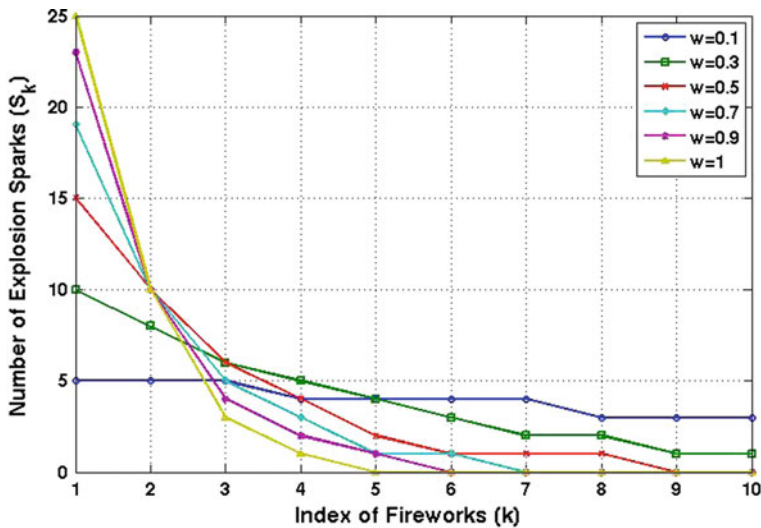


Fig. 2 Number of explosion sparks of fireworks

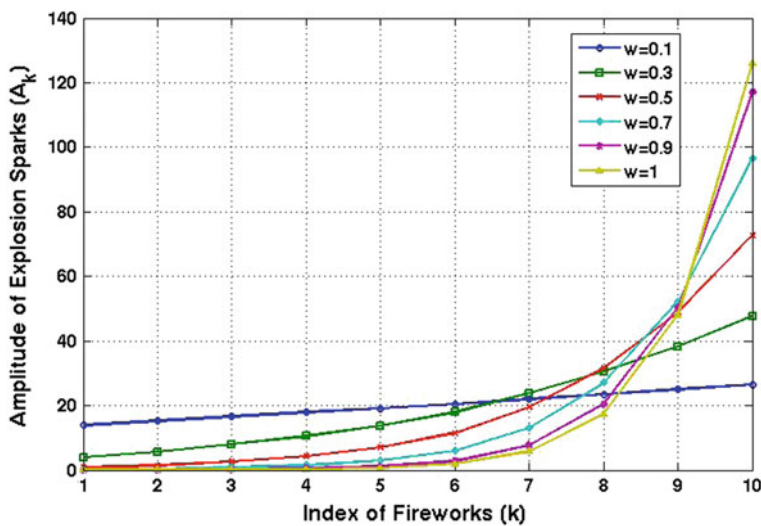


Fig. 3 Amplitude of explosion sparks of fireworks

3.2 Generation of Explosion Sparks and Mutated Sparks

In FWA-IATFGS, the explosion sparks are generated using Algorithm 1 given in Sect. 2.2 with one exception in mapping operator for unbounded sparks in the search space. In FWA-ATF, when a new spark exceeds the search space range in j th, and then it is mapped to a new location using the following mapping operator:

$$\dot{x}_{ej} = X_{\min} + |\dot{x}_{ej}| \% (X_{\max} - X_{\min}) \quad (10)$$

When the search space range is equally distributed (i.e., $X_{\max} = |-X_{\min}|$), the newly mapped position \dot{x}_{ej} will be very closed to the origin. This mapping operator is useful when the global optima of function is closed to the origin. When the global optima is far away from the origin, this operator is not effective. Therefore, this mapping operator is replaced by a uniformly distributed random mapping operator as follows:

$$\dot{x}_{ej} = X_{\min} + (X_{\max} - X_{\min}) \times \text{rand}(0, 1) \quad (11)$$

where $\text{rand}(0, 1)$ is uniformly distributed random number. The mutated sparks in the proposed FWA-IATFGS algorithm are created using Algorithm 2 given in Sect. 2.3. The mutation operator is used in the location of each firework instead of randomly selected fireworks in the aforesaid algorithm.

After the generation of explosion sparks and mutated sparks from each firework, group best selection strategy [7, 8] is used in the selection of the best solutions and it is discussed in the next section.

3.3 Group Best Selection

The group best selection strategy is used in the proposed method. Each firework creates a set of explosion sparks and one random mutated spark in each iteration. Therefore, each firework forms a group which includes its explosion sparks, mutated sparks and itself. Therefore, N number of fireworks form N groups of solutions. In group best selection strategy, the best from each group is selected for the next iteration.

In the best selection strategy, the N best solutions are selected from all the original fireworks and all type of sparks. There is a chance that all the N best solutions are selected from a single region where the solutions are very closed to each other. The exploration and exploitation are took place in this region, while other regions are left uncovered. In this circumstance, the diversity in the search space is lost due to which global search is effected. On the other hand, the group best selection strategy selects the best solution from the region of each firework located in the search space. Therefore, it provides a set of best solutions located in different regions of the search space for the next iteration and ensures the global search in the search space.

The complete algorithm of FWA-IATFGS is described in Algorithm 3.

Algorithm 3: FWA-IATFGS algorithm

```

1 Initialize  $\mathcal{N}$  locations  $\mathbf{X}$  of fireworks in  $[X_{min}, X_{max}]^D$ 
2 Evaluate the objective function values  $f$ 
3 while termination criteria do
4   Calculate the control parameter  $w$  using Eq. (9)
5   Sort the fireworks in ascending order with respect to  $f$ 
6   Calculate the score values  $r_i$  for each firework
7   for  $i \leftarrow 1$  to  $\mathcal{N}$  do
8     Calculate the ATF values  $\dot{T}_i$  using Eq. (8)
9     Calculate the number of “explosion sparks”  $S_i$  using Eq. (5)
10    Calculate the amplitude  $A_i$  of explosion using Eq. (6)
11   end
12   for  $i \leftarrow 1$  to  $\mathcal{N}$  do
13     Generation of explosion sparks and mutated sparks
14     Evaluate the objective function values of sparks
15     Select the group best location from  $i$ th fireworks and its all type of sparks
16   end
17 end

```

4 Experimental Results

4.1 CEC2015 Benchmark Functions

There are 15 different global optimization problems, including unimodal functions ($F_1 - F_2$), simple multimodal functions ($F_3 - F_5$), hybrid functions ($F_6 - F_8$) and composite functions ($F_9 - F_{15}$) in CEC–2015 [16]. All functions are to be minimized. The details of these functions can be obtained from [16].

4.2 Parameter Settings

The common parameters of DynFWA-CM, CoFFWA, FWA-ATF and FWA-IATFGS are set as follows: $\mathcal{N} = 10$, $\mathcal{M} = 40$, boundary constraints on $S_i = [2, 32]$, and termination criteria: $FEs = 300,000$.

In DynFWA-CM, the number of better μ sparks is set to 50% of the number of sparks generated from all fireworks. In both DynFWA-CM and CoFFWA, the amplification factor (C_a) and reduction factor (C_r) are set to 1.2 and 0.9, respectively.

4.3 PC Configuration

CPU: Intel® Core™ i7-4770 @3.4 GHz, RAM: 8 GB, Operating System: Windows 7 64-bit, Software: MATLAB 2016a.

4.4 Results

DynFWA-CM, CoFFWA, FWA-ATF and proposed FWA-IATFGS are applied to optimize 15 benchmark functions with 30 dimensions for 51 independent runs. The same initial locations are used for each run in order to make a fair comparison among the algorithms. The means and standard deviations of run-best-errors over 51 runs are given in Table 1. The run-best-error is the absolute difference between the global optimal solution $f(X^*)$ of the function and best solution $f(X)$ obtained from the run (i.e., $E = |f(X^*) - f(X)|$). The best of results obtained from all algorithms are marked as bold in Table 1.

5 Discussion

5.1 Performance Analysis

The results of the proposed FWA-IATFGS are compared with the results achieved by other algorithms. To check whether there is any statistically significance difference in the performances, t-test is conducted on the results obtained from FWA-IATFGS and the results obtained from other algorithms with confidence interval 95% and degree of freedom $51 + 51 - 2 = 100$. The p -values of the test and significance are given in Table 2. Sig. columns of the same table indicate the significance of the test. ‘ \approx ’ indicates that there is no significant difference between the results of FWA-IATFGS and the results from other algorithms. ‘+’ indicates that the results of FWA-IATFGS have statistically higher significance than its peers. From the t-test results, it is observed that FWA-IATFGS outperforms DynFWA-CM for unimodal function F1, simple multimodal functions F5, hybrid functions F6-F8, composite functions F9-F11, F13 and F14. There are no significant differences in the performances of FWA-IATFGS and DynFWA-CM for functions F2-F4, F12 and F15.

FWA-IATFGS outperforms CoFFWA for unimodal functions F1, F2, simple multimodal functions F4, F5, hybrid functions F6-F8, composite functions F10, F11, F13 and F14. There are no significant differences in the performances of FWA-IATFGS and CoFFWA for functions F3, F9, F12 and F15.

FWA-IATFGS outperforms FWA-ATF for all functions except functions F3 and F15. This indicates that improved transfer function and group best selection strategy significantly improve the performance of FWA-ATF algorithm.

Table 1 Mean and standard deviation (in parentheses) of run-best-errors over 51 independent runs for 30D problems

$\mathcal{F}\#$	DynFWA-CM	CoFFWA	FWA-ATF	FWA-IATFGS
1	1033118.546 (396723.1873)	1182469.08 (563279.9118)	1229782.262 (863634.9936)	572152.5817 (267466.6568)
2	2144.7518 (2486.2766)	4442.2776 (4567.3976)	4028.7612 (4714.5600)	2340.6281 (2414.7558)
3	20.0001 (0.00098)	19.9999 (1.17052E-06)	20.0007 (0.0038)	20.0003 (0.00018)
4	115.4548 (28.9120)	129.1061 (24.5026)	139.3188 (33.5891)	105.9069652 (16.4103)
5	3394.1844 (715.5910)	2585.8397 (354.6906)	2935.7572 (703.0584)	2339.9793 (342.1604)
6	68574.4320 (49092.9099)	89750.5562 (66149.6282)	110353.6342 (86143.3091)	45365.8438 (26640.7398)
7	19.1421 (15.8454)	14.7518 (2.4582)	19.3806 (17.8864)	8.3352 (1.8427)
8	32332.7497 (15861.3934)	56101.5052 (37570.865)	69329.1229 (49571.6061)	21281.2945 (17598.3010)
9	123.0451 (48.4135)	110.3519 (1.2820)	141.0510 (79.4254)	107.3830 (0.5880)
10	30520.5200 (17966.0003)	53509.0549 (40087.3224)	22086.2329 (19105.1685)	9032.3701 (4706.6665)
11	811.2818 (209.7447)	513.5017 (286.3366)	908.9697 (166.2837)	393.7588 (197.5509)
12	121.0023 (23.7572)	112.3338 (1.2515)	121.3197 (23.5714)	112.0472 (0.9682)
13	0.0517 (0.0286)	0.01744 (0.0021)	0.0158 (0.0028)	0.0136 (0.0006)
14	46045.9407 (1621.3059)	40990.5428 (3806.4166)	41634.0770 (4887.6601)	35983.7416 (3445.7801)
15	100 (8.1105E-13)	100 (1.35146E-12)	100.01956 (0.1386)	100.0026 (0.0004)

The Wilcoxon signed ranks test [15] is carried out between the pairs comprised of FWA-IATFGS and each of other algorithms to test the overall performance over 15 functions for 30 dimensions. From the results of this test statistics given in Table 3, it has been observed that FWA-IATFGS statistically outperforms DynFWA-CM, CoFFWA and FWA-ATF with a level of significance $\alpha = 0.01$.

To make a comparison of the convergence behavior of the algorithms, the best objective function values of function F5 are plotted against the number of function evaluations in Fig. 4. The best objective function values are obtained from the runs of the algorithms where the same initial population is used to make a fair comparison. From the aforementioned graph, it is seen that the proposed FWA-IATFGS has a better *trade-off* between exploration and exploitation than that of other algorithms.

Table 2 T-test statistics

$\mathcal{F}\#$	FWA-IATFGS versus DynFWA-CM		FWA-IATFGS versus CoFFWA		FWA-IATFGS versus FWA-ATF	
	$p - value$	Sig.	$p - value$	Sig.	$p - value$	Sig.
1	5.10E-09	+	6.27E-10	+	1.83E-06	+
2	0.923625359	\approx	0.002376333	+	0.022817597	+
3	0.999801928	\approx	0.999621329	\approx	0.999413131	\approx
4	0.066672872	\approx	2.63E-05	+	2.66E-07	+
5	1.48E-11	+	0.017128072	+	3.17E-05	+
6	0.007052583	+	5.48E-05	+	2.02E-06	+
7	2.82E-06	+	4.39E-20	+	3.96E-05	+
8	0.002532565	+	5.96E-08	+	4.62E-09	+
9	0.039457411	+	0.337608639	\approx	0.008990039	+
10	5.28E-12	+	7.51E-12	+	1.14E-05	+
11	4.88E-15	+	0.032352313	+	1.32E-21	+
12	0.058076186	\approx	0.931234622	\approx	0.048783114	+
13	6.88E-15	+	1.63E-12	+	1.40E-05	+
14	5.52E-12	+	0.000286556	+	0.000116256	+
15	0.999270471	\approx	0.999270471	\approx	0.995116991	\approx

Table 3 Wilcoxon signed ranks test statistics for 30D problems

S. No.	Comparison	R^+	R^-	Z	$p(2 - tailed)$
1	FWA-IATFGS versus DynFWA-CM	109	11	-2.783	0.00538567 < 0.01
2	FWA-IATFGS versus CoFFWA	117	3	-3.237	0.00120632 < 0.01
3	FWA-IATFGS versus FWA-ATF	120	0	-3.408	0.00065496 < 0.01

R^+ : sum of positive ranks, R^- : sum of negative ranks

The robustness of the metaheuristic algorithm is measured in terms of the standard deviation of results. The lower standard deviation of run-best-errors over several independent runs indicates the higher robustness of the algorithm. It is observed from Table 1 that the proposed FWA-IATFGS has a lower standard deviation of run-best-errors for most of the functions. Therefore, FWA-IATFGS is more robust than other algorithms.

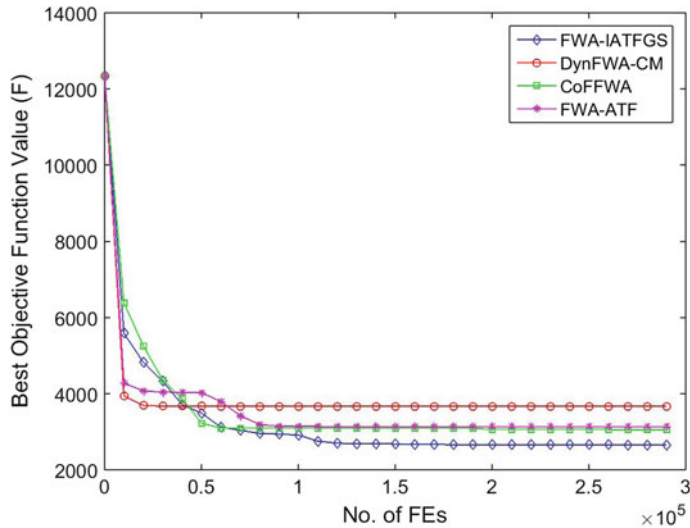


Fig. 4 Convergence graph for function F5

Table 4 Computation complexities (in seconds) of DynFWA-CM, CoFFWA, FWA-ATF and FWA-IATFGS for function F1 with dimension = 30

Algorithm	T_0	T_1	\bar{T}_2	$(\bar{T} - T_1)/T_0$
DynFWA-CM	0.108217	1.270773	22.9428	200.2645
CoFFWA	–	–	16.5344	141.0465
FWA-ATF	–	–	14.2542	119.9759
FWA-IATFGS	–	–	14.8089	124.2908

5.2 Computational Complexities

Computational complexities of all the algorithms are measured according to the procedure given in Ref. [16]. The computational complexities (in seconds) are given in Table 4. FWA-IATFGS has lower computational cost than DynFWA-CM and CoFFWA. Though FWA-IATFGS has higher computational cost than FWA-ATF, FWA-IATFGS significantly outperforms FWA-ATF.

By analyzing the results of all problems, it may be concluded that FWA-IATFGS produces better results than all other algorithms for most of the problems. FWA-IATFGS maintains a good balance between exploration and exploitation in the search space. Group best selection strategy helps to cover the different search regions that leads to the good exploration of the search space. This strategy also helps in good exploitation of better fireworks located in different more promising regions rather than a single region (where all fireworks are located) of the search space.

5.3 Analysis of the Effectiveness of Different Components of FWA-IATFGS

To analyze the effectiveness of the improved transfer function and the group best selection strategy in FWA-IATFGS, FWA-IATFGS is run with different components in the following way:

1. FWA-IATFGS without improved transfer function and group best selection strategy (FWA-ATF with new mapping operator for unbounded solutions).
2. FWA-IATFGS without group best selection strategy named as FWA-IATF.
3. FWA-IATFGS without improved transfer function named as FWA-ATFGS.

The results of FWA-ATF, FWA-IATF and FWA-ATFGS over separate 51 runs for 30 dimensions are given in Table 5. To check whether the difference in the results is significant or not, Wilcoxon signed ranks tests are conducted and results are given in

Table 5 Mean and standard deviation (in parentheses) of run-best-errors obtained from FWA-ATF, FWA-IATF, FWA-ATFGS and FWA-IATFGS over 51 independent runs for 30D problems

$\mathcal{F}\#$	FWA-ATF	FWA-IATF	FWA-ATFGS	FWA-IATFGS
1	1441781.814 (1122428.135)	2618674.117 (1208487.067)	2341367.83 (799065.5664)	572152.5817 (267466.6568)
2	3597.952992 (4490.743625)	3928.597145 (4592.0726)	1196.508085 (1556.93144)	2340.6281 (2414.7558)
3	20.0003 (0.0018)	19.9999 (4.38934E-07)	20.00000013 (1.10808E-06)	20.0003 (0.00018)
4	150.3026 (32.1118)	107.0503 (28.0460)	107.523 (21.0855)	105.9069652 (16.4103)
5	3114.9310 (659.8512)	2847.496832 (463.3176)	2613.7962 (427.1985)	2339.9793 (342.1604)
6	107729.469 (82592.06)	327557.3351 (237626.7673)	161819.0616 (100494.356)	45365.8438 (26640.7398)
7	16.6104 (15.5312)	19.3414 (16.0437)	13.0503 (2.0438)	8.3352 (1.8427)
8	66170.0708 (50121.9899)	137439.4308 (106515.8494)	46176.3094 (23006.4797)	21281.2945 (17598.3010)
9	119.9683 (50.2971)	128.9231 (54.6406)	112.0075 (0.7173)	107.3830 (0.5880)
10	22823.5040 (18233.7773)	49038.0585 (27769.7838)	21036.1790 (10508.5614)	9032.3701 (4706.6665)
11	912.8776 (179.0098)	900.1929 (108.8831)	812.3944 (296.5975)	393.7588 (197.5509)
12	128.7990 (31.4926)	127.2141 (29.7697)	112.1711 (0.9891)	112.0472 (0.9682)
13	0.0170 (0.0028)	0.0159 (0.0025)	0.0163 (0.0015)	0.0136 (0.0006)
14	42224.7135 (4463.6619)	40690.9009 (4939.3086)	41609.0372 (2336.5382)	35983.7416 (3445.7801)
15	100.0002 (3.39226E-05)	100.0502 (0.3583)	100.0004 (0.0002)	100.0026 (0.0004)

Table 6 Wilcoxon signed ranks test statistics to check the effectiveness of improved transfer function and best selection strategy

Sl. No.	Comparison	R^+	R^-	Z	$p(2 - tailed)$
1	FWA-IATF versus FWA-ATF	42	78	-1.022	0.30662412 > 0.05
2	FWA-ATFGS versus FWA-ATF	90	30	-1.704	0.08840248 > 0.05
3	FWA-IATFGS versus FWA-IATF	119	1	-3.351	0.00080528 < 0.01
4	FWA-IATFGS versus FWA-ATFGS	107	13	-2.669	0.00759822 < 0.01

R^+ : sum of positive ranks, R^- : sum of negative ranks

Table 6. From this test, it is found that there is no significant difference in the results of FWA-ATF and FWA-IATF. This indicates that improved transfer function can not improve the performance of FWA-ATF. It is also found that there is no significant difference in the results of FWA-ATF and FWA-ATFGS. This indicates that only the group best selection cannot improve the performance of FWA-ATF. But, it is interesting to notice that FWA-IATFGS statistically performs better than both FWA-IATF and FWA-ATFGS with significance level $\alpha = 0.01$. This analysis establishes that the improved transfer function is effective when group best selection strategy is used. From the results given in Table 6, it is also observed that FWA-IATFGS produces more robust solutions than FWA-ATF, FWA-IATF and FWA-ATFGS for most of the problems. The group best selection strategy is useful to maintain diversity in the search space. When there is diversity in the search space, the distances based on fitness values between the best fireworks and other fireworks are large. Hence, the differences in their transfer function values are large. As the control parameter w is linearly increasing with time, the transfer function becomes more adaptive during the end of the search. At this stage, the exploration and exploitation are taking place according to the adaptive nature of the transfer function.

6 Conclusion

In this paper, a modified FWA with the time-varying adaptive transfer function for the generation of explosion sparks and group best selection strategy is proposed. The adaptivity of the transfer function is deterministically controlled using a control parameter which is increased linearly with time. The improved transfer function is used to maintain a good trade-off between exploration and exploitation during the search. In FWA-IATFGS, the deterministically controlled adaptive transfer function is effective only when there is diversity in the search space and group best selection strategy is used to keep diversity in the search space. The proposed FWA-IATFGS statistically outperforms DynFWA, CoFFWA and FWA-ATF algorithms in solving fif-

teen CEC2015 benchmark optimization problems with 30 dimension. FWA-IATFGS is more robust than DynFWA, CoFFWA and FWA-ATF. FWA-IATFGS is also computationally more cost-effective than DynFWA and CoFFWA. The application of FWA-IATFGS in solving more complex and real-world problems will be the future works of this paper.

References

1. Tan, Y., Zhu, Y.: Firework algorithm for optimization. In: Tan, Y., et al. (eds.) ICSI 2010, Part I, LNCS 6145, pp. 355–364. Springer, Berlin (2010)
2. Pei, Y., Zheng, S., Tan, Y., Hideyuki, T., : An empirical study on influence of approximation approaches on enhancing fireworks algorithm. In: Proceedings of the IEEE Congress on System, Man and Cybernetics, vol. **2012**, pp. 1322–1327. IEEE, New York (2012)
3. Zheng, Y., Xu, X., Ling, H.: A hybrid fireworks optimization method with differential evolution operators. Neurocomputing **148**, 75–82 (2015)
4. Liu, J., Zheng, S., Tan, Y.: The improvement on controlling exploration and exploitation of firework algorithm. In: Tan, Y., et al. (eds.) ICSI 2013, Part I, LNCS 7928, pp. 11–23. Springer, Berlin (2013)
5. Li, J., Zheng, S., Tan, Y.: Adaptive fireworks algorithm. In: Proceedings of 2014 IEEE Congress on Evolutionary Computation (CEC), Beijing, China, pp. 3214–3221, July 6–11 (2014)
6. Zheng, S., Janecek, A., Li, J., Tan, Y.: Dynamic search in fireworks algorithm. In: Proceedings of 2014 IEEE Congress on Evolutionary Computation (CEC), Beijing, China, pp. 3222–3229, July 6–11 (2014)
7. Yu, C., Kelley, L.C., Tan, Y.: Dynamic search fireworks algorithm with covariance mutation for solving the CEC 2015 learning based competition problems, pp. 1106–1112 (2015). <https://doi.org/10.1109/CEC.2015.7257013>
8. Zheng, S., Li, J., Janecek, A., Tan, Y.: A cooperative framework for fireworks algorithm. IEEE/ACM Trans. Comput. Biol. Bioinform. pp. 1–14 (2015). <https://doi.org/10.1109/TCBB.2015.2497227>
9. Gao, H., Diao, M.: Cultural firework algorithm and its application for digital filters design. Int. J. Modell. Identif. Control **14**(4), 324–331 (2011)
10. Yu, C., Li, J., Tan, Y.: Improve enhanced fireworks algorithm with differential mutation. In: IEEE International Conference on Systems, Man, and Cybernetics, pp. 264–269, San Diego, CA, USA October 5–8 (2014)
11. Li, J., Tan, Y.: The bare bones fireworks algorithm: a minimalist global optimizer **62**, 454–462 (2018)
12. Li, J., Zheng, S., Tan, Y.: The effect of information utilization: introducing a novel guiding spark in the fireworks algorithm. IEEE Trans. Evol. Comput. **21**(1), 153–166 (2017)
13. Li, J., Tan, Y.: Loser-out tournament based fireworks algorithm for multi-modal function optimization. IEEE Trans. Evol. Comput. **22**(5), 679–691 (2018)
14. Si, T., Ghose, R.: Explosion sparks generation using adaptive transfer function in fireworks algorithm. In: IEEE Third International Conference on Signal Processing, Communications and Networking (ICSCN 2015), March 26–28, 2015, Chennai, India, pp. 1–9. <https://doi.org/10.1109/ICSCN.2015.7219917>
15. Derrac, J., Garcia, S., Molina, D., Herrera, F.: A practical tutorial on the use of nonparametric statistical tests as a methodology for comparing evolutionary and swarm intelligence algorithms. Swarm Evol. Comput. **1**, 3–18 (2011)
16. Liang, J.J., Qu, B.Y., Suganthan, P.N., Chen, Q.: Problem definitions and evaluation criteria for the CEC 2015 competition on learning-based real-parameter single objective optimization. http://www.ntu.edu.sg/home/EPNSugan/index_files/CEC2015/CEC2015.htm (2014)

NSE Stock Prediction: The Deep Learning Way



Ankit K. Barai, Pooja Jain, and Tapan Kumar

Abstract Stock market forecasting plays a vital role in the decision making of financial firms and investors. This paper focuses and details a comparative study for stock price prediction of Indian industries with stock data from National Stock Exchange (NSE). A lot of research is concentrated for stock forecasting from the last decades which got significance with the emergence of deep learning. The deep learning techniques focused are long short-term memory (LSTM), gated recurrent unit (GRU) and recurrent neural network (RNN). Stock data of automobile and financial industries are taken for analysis. This paper compares the results with ARIMA model, a statistical model for stock prediction as baseline. Mean average percentage error (MAPE) is used as a performance criterion. This work reveals how the investors can make use of deep learning techniques to revise their investment decisions and strategies to hone better returns over time. It helps financial analysts and business communities to make informed decisions.

Keywords LSTM · GRU · RNN · ARIMA · Deep learning · Stock market

1 Introduction

Stock market is a platform where buyers and sellers can exchange their financial assets in the form of shares in companies listed in the stock market. NSE is National Stock Exchange of India, and BSE stands for Bombay Stock Exchange. Stock market characterizes for each trading company with parameters like open price, close price and lowest price of that day and the highest price of the day and volume of stock

A. K. Barai (✉) · P. Jain · T. Kumar
Indian Institute of Information Technology Nagpur, Nagpur, India
e-mail: ankit.barai@cse.iiitn.ac.in

P. Jain
e-mail: poojaalld@yahoo.com

T. Kumar
e-mail: tapankumarjain@gmail.com

exchanges in terms of the number of transactions of that company's stocks on a particular day. Prediction in stock market is very important to make informed decisions which might result in loss or gains of millions of dollars. Traditionally, linear statistical models like autoregressive integrated moving average (ARIMA) [1], ARMA and MA were used. The problem with such statistical models was that they might model a given company stock data well but may not model other companies data. During this decade, there had been a number of researches on how the deep neural network (DNN) for time series prediction like LSTM, RNN and GRU may model the stock data. Stock market prediction is a source of interest for financial companies as well as individuals. Closing price of stock market is one of the major parameters used to make decisions for trading over that stock on the next day. It makes use of DNN for time series modeling like LSTM, RNN and GRU, etc., for stocks from three different sectors, namely SBI, NTPC and Infosys with all three DNNs. It has been observed that a DNN which may fit given company stock in best might not be best for other stock data as visible in results. All the DNN like LSTM, RNN and GRU are related to each other with slight modifications, and each of them has its own pros and cons as discussed in the background work.

2 Related Works

There are a number of research groups working on application of DNN for time series modeling especially stock market. Rather et al. [2] make use of RNN to capture the nonlinearity of stock markets. Dass and Srivastava [3] give insight into how the recurrent fuzzy networks could be used to approximate complex systems. Various studies on the optimization of artificial neural networks with the use of genetic algorithms are carried out as in [4]. Neural networks find application in optimizing the cycle time of manufacturing plants [5]. Traditional neural networks are not able to retain information over time, while RNN simulates human brain's power of inference based on previous findings. RNN contains loops which favor for passing information from one step of network to the next. Selection of activation functions is an important part of neural network architecture as studied in [6]. Deep learning for stock prediction is studied on Chinese stock markets [7]; it also shows how it outperforms the traditional backpropagation neural network and radial basis neural network. Comparative study of support vector machine and DL algorithms for stock prediction [8] shows DL algorithms to be better. Study on efficient approach to forecast Indian stock market price helps naive investors in making informed decisions. Stock market is affected by national and international events which could also be taken into consideration for event-driven stock prediction [9] by extracting information from news text. Sharma et al. [10] give study of sentiment analysis using GloVe and RNN.

3 Background

3.1 Neuron

Neurons in AI are inspired by biological neuron which works like a mathematical function taking number of inputs with weights and corresponding outputs. The local induced field of j th neuron v_j is given by Eq. 1 and effective output y_j is as shown in Eq. 2:

$$v_j = \sum_{i=1}^m (x_i * w_i) + b \quad (1)$$

$$y_j = \phi(v_j) \quad (2)$$

3.2 Neural Network

Neural network can be mathematically defined as a differentiable function that maps one kind of variable to another kind of variable. A classification problem involves vectors to vectors mapping while regression problem involves vector to scalar mapping. NN contains interconnection between neurons, which can be visualized as layers of neurons where info is transferred from one layer to other layers. Three types of layers are input, hidden and output layer. There is no connection in between neurons of same layer. Multilayer perceptron (MLP) is a type of feedforward neural networks with at least three layers and utilizes backpropagation for training. It has nonlinear activations that differentiate it from linear perceptron.

3.3 Recurrent Neural Network

They are used for a variety of applications like speech recognition, language modeling, image captioning and many more applications. The connection between nodes of RNN forms a directed graph exhibiting a temporal sequence. RNN uses their internal states to process onto a sequence of inputs. It takes two inputs as compared to one input in case of MLP, one from past and other from present. RNN represents a general structure for two broad classes of networks, where one is finite impulse and the other is infinite impulse. A finite impulse recurrent network can be unrolled to form a feedforward neural network while infinite impulse neural network cannot be unrolled. Both of them have an additional stored state which is directly controlled by neural network and can be replaced by a network or a graph. Such controlled states form a part of long short-term memory and gated recurrent units.

3.4 Grated Recurrent Unit

GRU is advanced RNN cell with memory unit whose architecture has a update gate which decides if the previous output is to be passed to next cell or not and acts accordingly.

3.5 Long Short-Term Memory

LSTM is a specific RNN with capacity of learning longtime data dependency. Simple RNN has a simple feedback loop in traditional NN but LSTM contains memory blocks. It has two additional gates: forget gate and output gate along with update gate as in GRU. Forget gate adds new set of mathematical operations with new weights. LSTM is more controllable for outputs compared to other two but with increased computational costs.

4 Experiments

The historical dataset is taken from NSE stock data from the year 2000 to till date for three different sectors, namely banking, mining and information technology. The companies from these sectors are SBI, NTPC and Infosys, respectively. The models are trained with training data from over 19 years of stock data. The dataset comprises various attributes, namely date, low, high, open, close and volume. Closing price of stocks is extracted from the dataset to train the model since the decision about a stock is made based upon the closing price for that stock on previous day. The training data range is high, and hence, it is normalized before feeding it to DNN for training using Eq. 3

$$y_{\text{norm}} = \frac{(y - y_{\min})}{(y_{\max} - y_{\min})} \quad (3)$$

The training data are trained over 200 epochs with varying window size (*batch size*) to tune the hyperparameters.

The error criterion used in mean average percentage error (MAPE) is given in Eq. 4 where y is actual output and d is desired output.

$$\text{MAPE} = \sum \left(\frac{(y - d)}{d} * 100 \right) \quad (4)$$

The algorithms used are Algorithms 1 and 2 which does task of selecting the neural network type and predicting stocks, respectively. It is needed to fine-tune the hyperparameters to get better predictions. Dropout layers are used to prevent over fitting of the model. The batch size and the number of epochs for training were

optimized, after doing prediction on one of the industries from each of the sectors; prediction is done for some more industries from those sectors.

Algorithm 1: get_Model

Input: *train_x.shape, n, dropout, modelType, predWindow*

```

/* Where train_x-training data,                                */
/* n-list of no. of Neurons in each layer,                  */
/* drop-Dropout ratio between layers,                      */
/* modelType-lstm,gru,rnn, predWindow- Number of          */
/* days to predict                                         */

```

Output: Neural network is returned

Result: DNN ready for stock prediction

```

// Sequential model
1 model = sequential();
2 input_shape= (train_x.shape[1], train_x.shape[2]);
  // add Layers
3 model.add( modelType(n[0], input_shape, return_sequences=True));
  // add dropout to prevent overfitting
4 model.add( Dropout(drop));
5 model.add( modelType(n[1], input_shape, return_sequences=True));
6 model.add( Dropout(drop));
7 model.add( Dense(predWindow));
8 model.compile( loss='mape',optimiser='adam');
9 return model ;

```

Algorithm 2: Predict Stocks

Input: *ep, bt, ntype, dataset*

```

/* Where ep- Number of epochs, bt-batch size,
   ntype-DNN type, dataset-Dataset of historical
   stock prices                                         */

```

Output: Prediction of stock prices

Result: Predicted stock prices helps in informed decision making and thus reduced loss

```

// get train and test data
1 train_x,train_y,test_x,test_y=splitData(datset);
  // Normalise the data
2 train_x,train_y,test_x,test_y=Normalisation( train_x,train_y,test_x,test_y );
  // get the DNN for prediction
3 dnn=get_model( train_x.shape,n,dropout,modelType,predWindow) ;
  // fit the DNN with training data
4 model_fit_output=dnn.fit(
  train_x,train_y,epochs=ep,batch_size=bt,validation_data=(test_x,test_y));
  // Predict with trained model
5 output=dnn.predict( test_x );
6 return output ;

```

5 Results and Discussions

This work uses ARIMA model as its primary benchmark which is a statistical model used by business analyst extensively for stock prediction. MAPE is used for comparing the performances of deep neural network (DNN) with the statistical ARIMA model. The DNNs were trained for historical stock prices from NSE for past 19 years from 2000 to 2019. It compared the prediction results for 10 future days from June 03, 2019, till June 20, 2019, with the actual data for all three DNNs and the best fitting models for each of the stocks with minimal MAPE which is selected as the results. For SBI, statistical model ARIMA gave MAPE of 3.99% which reduced to 0.89% with DNN, for Wipro error reduced from 6.36 to 0.77% with shift from statistical model to DNN, while as for Infosys it reduced from 7.16% to LSTM was better for NTPC with 2.94% error and with 2.24% error for Infosys. The results of predictions for validation on test data for Infosys are in Fig. 1, for NTPC in Fig. 2 and for SBI in Fig. 3. Tables 1 and 2 compare the performance of statistical ARIMA with other deep learning algorithms. Figures 4 and 5 compare the predictions with actual result for ten future days, and it is evident that predicted prices are very close to actual stock prices and will help businesses to make informed decisions. A study of deep learning algorithms is also validated on various industry sectors as given in Tables 3, 4 and 5.

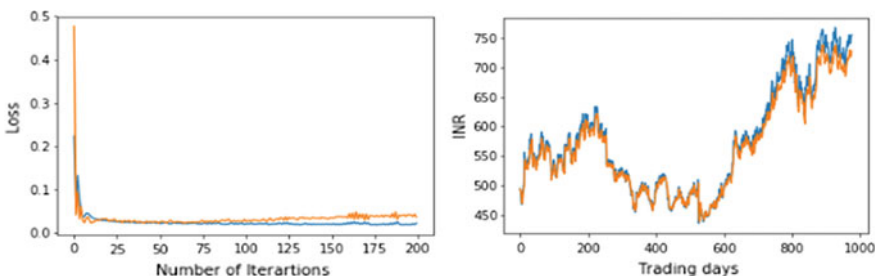


Fig. 1 Training loss curve and prediction (validation data) curve for INFY

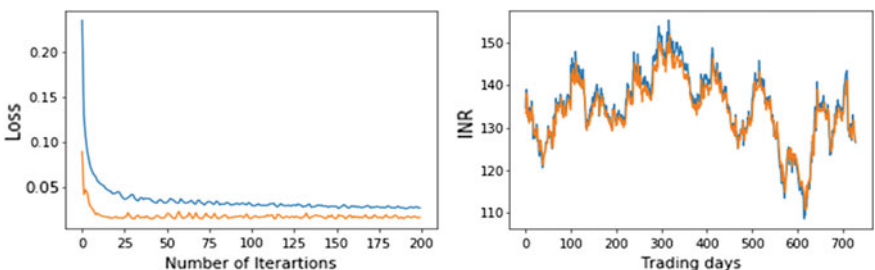


Fig. 2 Training loss curve and prediction (validation data) curve for NTPC

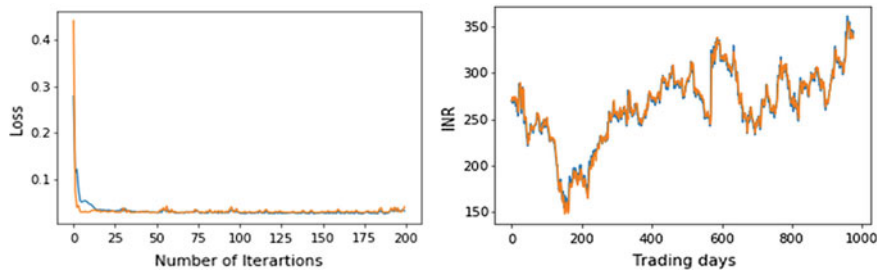


Fig. 3 Training loss curve and prediction (validation data) curve for SBI

Table 1 MAPE for 10days prediction with DNN model

MAPE %			
Industry	GRU	RNN	LSTM
SBI	2.11	3.89	4.82
NTPC	5.41	1.66	2.94
Infosys	2.4	2.78	2.29

Table 2 MAPE for 10days prediction with ARIMA model

MAPE %	
Industry	ARIMA
SBI	3.99
NTPC	12.78
Infosys	7.16

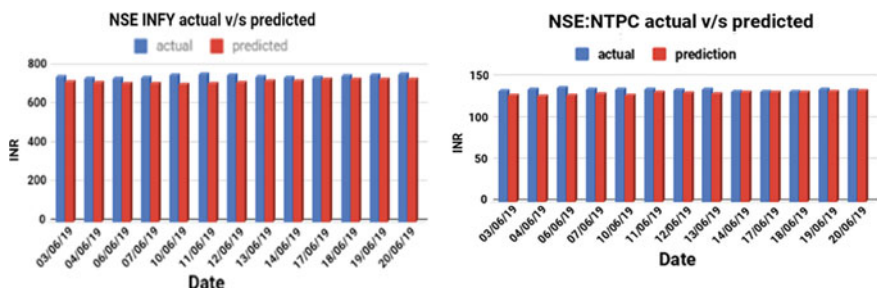


Fig. 4 Actual-predicted graph for INFY and NTPC (left to right)

Table 3 Banking industry stock prediction

MAPE %		
Industry	DNN	ARIMA
BOI	1.37	2.57
SBI	2.11	3.99
UBI	8.08	12.99

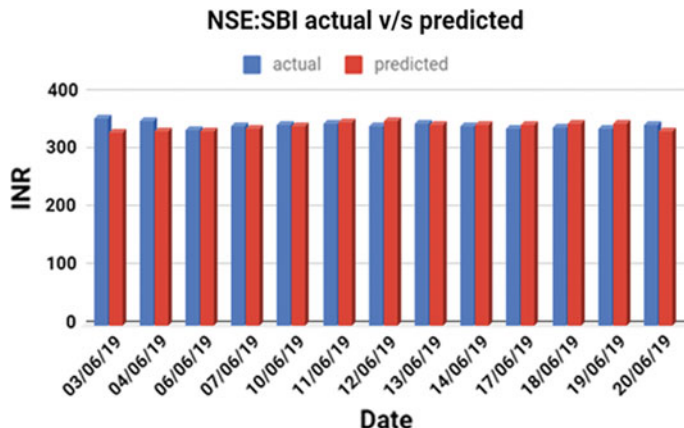


Fig. 5 Actual-predicted graph for SBI

Table 4 Information technology industry prediction

MAPE %		
Industry	DNN	ARIMA
INFY (Infosys)	2.29	7.16
ROLTA	1.47	6.07
WIPRO	0.77	6.36

Table 5 Mining industry prediction

MAPE %		
Industry	DNN	ARIMA
NTPC	1.66	12.78
ONGC	2.11	4.45
RCF	1.9	3.58

6 Conclusions and Future Scope

This paper makes use of three DNNs for time series modeling of stock data from three different sectors, namely banking, mining and information technology. The companies from these sectors were SBI, NTPC and Infosys, respectively. The prediction was made for ten days in the future and was compared with actual results. DNN models were found to be better than statistical models like ARIMA, and they model stock data well. LSTM and GRU are related to each other and either of them may give a better fit for a given stock depending upon the tuning of hyperparameters. It is concluded that DNN better models stock data compared to linear statistical models like ARIMA and outperforms it in performance. This work does not take into account other factors affecting stock markets like political and social media

trends. Sentiment analysis using social media analytics can also be integrated with stock prediction to account for these factors. This work would be further extended by integrating sentiment analysis with stock prediction.

References

1. Ariyo, A.A., Adewumi, A.O., Ayo, C.K.: Stock price prediction using the Arima model. In: 2014 UKSim-AMSS 16th International Conference on Computer Modelling and Simulation, pp. 106–112. IEEE, New York (2014)
2. Rather, A.M., Agarwal, A., Sastry, V.: Recurrent neural network and a hybrid model for prediction of stock returns. *Exp. Syst. Appl.* **42**(6), 3234–3241 (2015)
3. Dass, A., Srivastava, S.: On comparing performance of conventional fuzzy system with recurrent fuzzy system. In: Soft Computing: Theories and Applications, pp. 389–403. Springer, Berlin (2018)
4. Bhasin, H., Gupta, N.: Critical path problem for scheduling using genetic algorithm. In: Soft Computing: Theories and Applications, pp. 15–24. Springer, Berlin (2018)
5. Giri, J.P., Giri, P.J., Chadge, R.: Neural network-based prediction of productivity parameters. In: Soft Computing: Theories and Applications, pp. 83–95. Springer, Berlin (2018)
6. Dhamayanthi, B., Vaiz, J.S., Ramaswami, M.: A study of deep neural networks in stock trend prediction using different activation functions. In: International Conference on Recent Trends in Engineering, Computers, Information Technology and Applications (ICRTECITA-2017)
7. Chen, L., Qiao, Z., Wang, M., Wang, C., Du, R., Stanley, H.E.: Which artificial intelligence algorithm better predicts the chinese stock market? *IEEE Access* **6**, 48625–48633 (2018)
8. Nivetha, R.Y., Dhaya, C.: Developing a prediction model for stock analysis. In: 2017 International Conference on Technical Advancements in Computers and Communications (ICTACC), pp. 1–3. IEEE, New York (2017)
9. Ding, X., Zhang, Y., Liu, T., Duan, J.: Deep learning for event-driven stock prediction. In: Twenty-Fourth International Joint Conference on Artificial Intelligence (2015)
10. Sharma, Y., Agrawal, G., Jain, P., Kumar, T.: Vector representation of words for sentiment analysis using glove. In: 2017 International Conference on Intelligent Communication and Computational Techniques (ICCT), pp. 279–284. IEEE, New York (2017)

Recent Development of AI and IoT in the field of Agriculture Industries: A Review



Amith A. Kulkarni, P. Dhanush, B. S. Chethan, C. S. Thammegowda, and Prashant Kumar Shrivastava

Abstract In this, paper presents the new technology which in turn increases the area of application for the technology, amongst that, one of them is the agricultural application such as the adding artificial intelligence (AI) and Internet of things (IoT) in the machinery is to make it a smart device which will be capable of making decision-making capacity based on the past experiences and learning, it is the system that includes IoT (Internet of things) where automated machine learning of the process can be done, and the AI involves many logics and methods for the problem-solving process. This technology is used for the application of agricultural system, and it overcomes the various problems in the agriculture such as the crop disease infestations, lack of storage management, pesticide control, weed management, and lack of irrigation and drainage facilities, and the technology uses wireless networks for the monitoring and controlling. The main aim of this study is to explore the present and future aspects of the AI and IoT in the agriculture industries that make the agriculture systems easy, effective, and minimize the human efforts.

Keywords Automation · Robotics · Artificial intelligence · Good agricultural practices (GAP) · Radio frequency identification (RFID) · GPS

A. A. Kulkarni · P. Dhanush · B. S. Chethan · C. S. Thammegowda · P. K. Shrivastava (✉)
Department of Mechanical Engineering, Vidyavardhaka College of Engineering, Mysuru,
Karnataka, India
e-mail: er.prashant1986@gmail.com

A. A. Kulkarni
e-mail: Amith.kulkarni.54@gmail.com

P. Dhanush
e-mail: Dhanushp147@gmail.com

B. S. Chethan
e-mail: Chethanbs050@gmail.com

C. S. Thammegowda
e-mail: Thammegowda.cs@vvce.ac.in

1 Introduction

Agricultural system modernization is one of the important factors for the today's economy to develop, because the country is fully dependent on the factor that the today's resource management in agriculture is most complicated, such as the water resource; the agriculture uses 70% of the fresh water; hence, water management is the most critical part in the agriculture to accomplish; hence, to achieve this, there are certain areas in agriculture where it is dependent such as the crop section for the soil, and in this factor, a PH sensor is used to measure the acidity in the solution; an IoT gate way is used to connect the field devices with the wireless Internet networks which could be wide area network (WAN) or a remote controlled device; the device can be an integration of IoT with cloud computing and sensors, and other resource combined will be managed by the cloud computing along with raspberry pi sensor which is a module to which various sensors such as the temperature and humidity are interfaced and also other will be the provision for the GSM-based automatic irrigation system for the efficient use of resources and crop planning; and when it comes to the operation of the system initially, the user registration is compulsory for the verification, and then, the admin checks the data provided by the user and allows to control the system; raspberry pi kit takes the sensor values and sends to Google spread sheet attached to the raspberry pi kit, the Google spread sheets used for maintaining real-time information and a data related to crop saved on these sheets, and then with ANN algorithm, sensor values maintain on Google spread sheets, compare according to threshold values, and check which crop is suitable for soil; this process is distributed in modules, this proposed system is best suitable for the crop selection based on the soil quality, and unwanted water wastage things are completely eliminated [1].

2 Literature Review

Application of AI and IoT in agriculture field reduce the human efforts, minimize the human time, and make the process easy and effective. Suppose if we applied in the field of irrigation we put the moisture sensores and connect with the IoT when the range of moisture increase after threshold value sensors send the information to your mobile then you can swith off the water moter. There are various types of industries like automobile, electronics, food, medical, marine, defense, and most important agriculture which are using these technologies for better results. The use of these technologies helps food safety, environment sustainability, good agricultural practices (GAP), AI in the machinery with decision making, GPS, and better agriculture production, and also helps in crop protection and integrated pest management, and if required, it helps for pest and disease management in the crops; based on these factors, the application equipment is to be selected, and the application equipment

does the microbial safety, and thus, the agricultural equipment can be made much more smarter for real-time fertilizers for the crop treatment [2].

Moreover, new technologies are introduced day by day and its applications also increased gradually. The agriculture field has huge scope for adding new technologies like artificial intelligence (AI) and Internet of things (IoT). By adding this, smart devices will be capable for decision making based on past experience and learning. Smart and automated machines make this process easy.

The AI involves many logics and methods for the problem-solving process such as the fuzzy logic, artificial neural networks (ANN), neuro-fuzzy logic, and expert systems, amongst these, the ANN is most used and prescribed method, and the ANN system uses various algorithms like Silva and Almeidas algorithm, and the dynamic adaption algorithm; hence, ANN is a task-based method which tells the system to operate based on the given inbuilt rather than a conventional computational programmed task, the ANN consists of input layer, hidden (middle) layer, output layer, and moreover, the AI and machine learning are hypothesis and theories for the implementation algorithm and logic-based concepts for the hardware-software interface as this technology is used for the application of agricultural system; it overcomes the various problems in the agriculture such as the crop disease infestations, lack of storage management, pesticide control, weed management, and lack of irrigation and drainage facilities, and the technology uses wireless networks for the monitoring and controlling the systems which in turn helps to control the devices that can be used for agricultural practices; hence, it can be used for the agricultural automation models [3].

However, the radio frequency identification is used in many areas of agriculture as it has many features such as non-contact, high recognition rate, bulk storage memory, securely access, and easily compatible with any system, the seed quality tracking system based on RFID is composed in four subsystems naming (1) seed quality management system in manufacture procedure, in this system, the breeders can use a tag on which the test should be conducted and then taking a portable interrogator to note the messages such as the watering time, fertilizing time, pests controlling time, blossoming time, and setting seeds time in RFID tag as these data are very important for the breeders as they maintain the quality in subsequent procedures; (2) seed quality management system in logistics procedure in which the RFID tag on the seed contains data such as the transport means, transport time, transport batches, started location, and arrived location, store environmental procedures, etc., as these data are the critical foundation data for tracking the problems when the quality incident occurs; (3) seed management and supervision system in this system, the data in RFID tags, and seed packages are highly encrypted and cannot be trespassed by the unauthorized and allow only the authorized supervision personnel to read the data; (4) seed planting service system in this system as the RFID tag contains all the data and application program updated by the supervisor, it allows the farmer to easily identify the quality of the product and also about its storage requirements, planting guidance, etc., which becomes very helpful for the farmers; hence, to store all these data a suitable type of RFID tag, the RFID tag is selected based on the frequency range as it ranges from 125 kHz to 245 GHz based on the end application,

and another factor to be considered is the anti-collision of the tags because there will be multiple tags; hence, care is taken such as using different algorithms for different RFID tag; hence, the tag collision is reduced, and use of RFID is benefitted for the farmers [4].

Amongst various developed technologies for the agriculture, the use of IoT (Internet of things) is also one the emerging technologies which helps in reducing the hard conventional farming method; the technology uses graphic-related touch screens with high resolutions for multitasking along with using the external sensors; the system uses a embedded system to control the overall system; the controller unit consists of Arduino microcontroller which is from 8 to 32 bits, which is used to store the programs for the specific task; and then, for the given program, the Arduino controller controls the output devices connected to the output terminal of the controller, and it can also be controlled with wireless network such as the RFID technology; the IoT is a interconnection of various objects along with wireless network driven by a power source for accomplishing various tasks along using various sensors [5–10].

Moreover, this automated design system helps in getting data such as the soil moisture, and various agricultural parameters using a user-defined system; usually, the system consists of two my RIO boards as one board is static and controls the valves and the other board controls the robot car, and the communication through the boards is achieved by the virtual interface and will usually be through wireless network; hence, the my RIO system controls and monitors the overall system, and further, this system is interfaced with the robot car, in which the my RIO board controls the robot car using batteries by using various integrated circuits and solenoid valves; and based on these a specific software compatible for the work, the user is used for writing the program based on the task to be performed by the system, and the program will be fed into the Arudino microcontroller system, and the system input is given by the various sensors such as the soil sensors; based on the required parameters, various sensors are used, and the data collected by the sensors will be displayed in the GUI. The indication of the data in the display is displayed in the interface [11].

3 Discussion

There are various developments taking in the word for the food safety and traceability, and various initiatives are being taken for the food safety and environment sustainability which can be achieved by good agricultural practices (GAP); it is a standard for primary agricultural production and everyone uses this standard that is being sourcing of food; either it is process farmed or if it is freshly produced, it is the global activity, the GAP works on the principles of basic concepts they are the food safety based on the application of HACCP principles, and then reducing the inappropriate use of chemicals for eliminating the quantity of residues found on the food crops; another principle is for environmental protection which holds the standard for minimizing negative impacts of agricultural production on the environment and then

comes the occupational health and safety welfare as it creates awareness and responsibility regarding socially related issues, and then the animal welfare (where applicable) creates a global level of animal welfare criteria on farmers as the principles are applied the requirement of GAP which can be fulfilled; hence, various measures are used to accomplish it such as the GPS and GAP; the traceability requirement for the precision farming and use of GPS allow it on agricultural machinery to make the system full proof. The artificial intelligence (AI) in the machinery is to make it a smart device which will be capable of making decision-making capacity based on the past experiences and learning, the system includes IoT (Internet of things) where automated machine learning of the process can be done, the AI involves many logics and methods for the problem-solving process such as the fuzzy logic, artificial neural networks (ANN), neuro-fuzzy logic, and expert systems, and amongst these, the ANN is most used and prescribed method; the ANN system uses various algorithms which must be suitable for all types of crops, crop protection, and integrated pest management, and if required, pest and disease management for the crops also; based on these factors, the application equipment is to be selected, and the application equipment does the microbial safety, and thus, the agricultural equipment can be made much more smarter for real-time fertilizers for the crop treatment.

Traditionally, agriculture processes depend on the human efforts and different types of controlled and un-controlled factors that affect the agriculture results. Farmers are facing so many difficulties in the farming due to lack of information like what is the suitable timing for particular crops, moisture, humidity, irrigation, water level, weed selection, seed selections, and also soil testing. Now, un-traditional and smart agriculture processes make it easy and responsible for the better agriculture results. The application of AI and IoT in un-traditional agriculture minimizes the human efforts and time and increases the agriculture results compared to the traditional agriculture processes [12, 13].

4 Conclusions

The objective of this study is to minimize the human efforts and provide the information about the smart and hybrid farming systems that makes the agriculture practices easier and also responsible for the better agriculture results compared to the traditional agriculture practices. In this study, we have discussed about the different types of smart and IoT-based agriculture applications that makes it easy and effective. Further, all these applications are still far for the farmers reach. So, we need to explore the better way to make it reach for every farmer of the INDIA, that is, they can use these smart technologies, improve the agriculture practices as well as agriculture results, and also need to explore the better and effective way to apply the AI and IoT in the field of irrigation, food safety and appropriate selection of chemicals and pesticide, weed selection and control and maintain the quality.

Acknowledgements The manuscript is prepared by taking assistance from Accendere Knowledge Management Services Pvt. Ltd. We are thankful to them. We also express our gratitude to our teachers and mentor for guiding us throughout the work.

References

1. Shingarwade, N.D., Suryavanshi, S.C.: Performance evaluation of cloud based farm automation. In: 2017 International Conference on Computing, Communication, Control and Automation (ICCUBEA), pp. 1–6 (2017)
2. De Baerdemaeker, J.: Precision agriculture technology and robotics for good agricultural practices. *IFAC Proc.* **46**(4), 1–4 (2013)
3. Bashiri, B., Mann, D.D.: Automation and the situation awareness of drivers in agricultural semi-autonomous vehicles. *Biosyst. Eng.* **124**, 8–15 (2014)
4. Li, H., Wang, H., Shang, Z., Li, Q., Xiao, W.: Application of RFID in agricultural seed quality tracking system. In: 2010 8th World Congress on Intelligent Control and Automation, pp. 3073–3077 (2010)
5. Mohanraj, I., Ashokumar, K., Naren, J.: Field monitoring and automation using IOT in agriculture domain. *Procedia Comput. Sci.* **93**, 931–939 (2016)
6. Prathibha, S.R., Hongal, A., Jyothi, M.P.: IOT based monitoring system in smart agriculture. In: 2017 International Conference on Recent Advances in Electronics and Communication Technology (ICRAECT), pp. 81–84 (2017)
7. Baranwal, T., Pateriya, P.K.: Development of IoT based smart security and monitoring devices for agriculture. In: 2016 6th International Conference-Cloud System and Big Data Engineering (Confluence), pp. 597–602 (2016)
8. Suma, N., Samson, S.R., Saranya, S., Shanmugapriya, G., Subhashri, R.: IOT based smart agriculture monitoring system. *Int. J. Recent Innov. Trends Comput. Commun.* **5**(2), 177–181 (2017)
9. Cambra, C., Sendra, S., Lloret, J., Garcia, L.: An IoT service-oriented system for agriculture monitoring. In: 2017 IEEE International Conference on Communications (ICC), pp. 1–6 (2017)
10. Gondchawar, N., Kawitkar, R.S.: IoT based smart agriculture. *Int. J. Adv. Res. Comput. Commun. Eng.* **5**(6), 838–842 (2016)
11. Harane, A., Bhoir, S., Patkar, T., Karia, D.: Design and development of farm automation system using NI myRIO. In: 2017 International Conference on Energy, Communication, Data Analytics and Soft Computing (ICECDSC), pp. 751–754 (2017)
12. Sneha, K., Kamath, R., Balachandra, M., Prabhu, S.: New Gossiping Protocol for Routing Data in Sensor Networks for Precision Agriculture, pp. 139–152. Springer, Singapore (2019)
13. Kamelia, L., Ramdhani, M.A., Faroqi, A., Rifadiapriyana, V.: Implementation of automation system for humidity monitoring and irrigation system. *IOP Conf. Ser. Mater. Sci. Eng.* **288**(1), 012092 (2018)

Optimized Fuzzy Rule-Based System to Measure Uncertainty in Human Decision Making System



Soni Sweta and Kanhaiya Lal

Abstract An evaluation system to measure the performance of the students is uncertain. Normally, analytical techniques could not hold good result and evaluation may be skewed on certain human attributes. Moreover, examinations and periodic evaluation and other assessment techniques could not measure student performance in totality. Therefore, fuzzy rules which measure uncertainty may be applied in such cases to measure student's performance in a range of particular attributes. So, researchers adapted soft computing techniques to measure uncertainty in human knowledge and their overall assessments. The aim of this paper is to use hybrid system by fusion of concepts of fuzzy with genetic algorithm to evaluate the performance module. Such a module can be helpful for evaluation imprecision in the knowledge adopting and decision-making system. The number of rules generated by fuzzy rule-based system increase exponentially. As a result, it increases the time and space complexity. This approach works in three phases' knowledge base, coding and optimization. The analysis of this method with other traditional system showed that the optimized rule-based system is dynamic, adaptive and more responsive than that of only fuzzy rule-based system.

Keywords Optimization · Uncertainty · Human decision · Genetic algorithm · Fuzzy system

S. Sweta (✉)
Amity University Jharkhand, Ranchi, India
e-mail: ssweta@rnc.amity.edu

K. Lal
Birla Institutes of Technology, Mesra, Ranchi, India
e-mail: klal@bit.ac.in

1 Introduction

Traditional education system is based on mathematical and statistical analysis in which we evaluate with the help of measurable variables. It gives us a crisp value by which it can be determined that where the performance lies. Of late, many alternate techniques have been evolved in the domain of soft computing area [1]. There are numerous methods like fuzzy logic, fuzzy cognitive map and genetic algorithm by which we can measure the performance. Each and every soft computing technique has their own advantages and disadvantages [1]. Moreover, the combination with two or more soft computing techniques gives different perspectives of performance evaluation and evaluation of student's holistic performance [2] where interpretability and understandability can be interpreted with manageable and measurable variables.

The main reason of choosing fuzzy mathematics is uncertainty of human-made decision-making system and limitation of complex mathematical algorithm of classical method. Human-made models are also adaptable [3, 4]. In this papers, [5–7] author observed that the fuzzy inference-based evaluation method has many drawbacks. It depends on expert knowledge and generates exponential amount of fuzzy rules with huge amount of input and output variables as a result it decreases the interpretability. Another reason is, there are duplicity and redundancy in rules which are meaningless and cannot convey any useful information. The performance of fuzzy rule-based system (FRBS) may decrease due to exponentially increased fuzzy rules which create problem [8, 9]; and redundant rules, which create conflict between rules. Depending on the tool used to reduce the RB, to enhance accuracy [10].

Selection of optimized fuzzy rule has been very critical issue of the fuzzy controller structure for student's assessment. The mechanized finding of fuzzy rules from information has been formulated by hybrid fuzzy system and fuzzy clustering [11, 12]. Even though this approach is very simple but it also have some disadvantage of interpretability, which associated with the fuzzy decision model to uncover the task in a reasonable manner; and correctness of model, which focuses to the capacity of the fuzzy model to reliably understand the modeling system. Despite the decent variety of learner performance assessment techniques, the scientists believe that there are some alternative ways to be examined in the field of fuzzy logic, genetic algorithms, etc. The investigation of a FIS system can be seen as an optimization issue of high dimensionality. Numerous authors have explored the use of the improved FL hypothesis in instructive optimization, particularly in grading assessment [13–15]. The paper offers a methodology dependent on a genetic algorithm for acceptance and determination of fuzzy rules.

The following sections of the paper are organized as follow. Section 2 depicts a portion of view of literature in terms of related works dependent on fuzzy set hypothesis. The point by point depiction of the methodology of proposed system has been given in Sect. 3. The experimental result and outcomes on the specified dataset are given in Sect. 4. At last, Sect. 5 explains conclusion.

2 Fuzzy-Based Performance Evaluation—A Literature Review

At present, different fuzzy expert system and fuzzy rule-based system strategies have been issued so as to oversee inadequate student performance issue. It can be classify into three main classes [16, 17] (i) methods using fuzzy inference system, (ii) strategies utilizing based on fuzzy number and (iii) procedures actualizing the expert system (FES) based on fuzzy system. The advantage of the principal technique is that the inference rules are unmistakably comprehensible and justifiable. The disadvantage is that they normally require an enormous development work done by human experts. The researchers in [18] exhibited a hybrid (neuro-fuzzy) methodology for segregate students into various categories. The hybrid classifier connected results obtained in prior test and other relevant factors as info factors and ordered students dependent on their evaluated scholarly exhibition [19]. Other related literature work that used FES is introduced by Yadav and Singh [1]. The disadvantage of this strategy is that it includes difficult complex computational procedures and cannot coordinate diverse fuzzy conditions. An FES for student academic performance assessment based on FL techniques is very well explained in [20]. In this work, two membership functions triangular and trapezoidal are used along with fuzzy rules.

Furthermore, Yadav and Ahmed [21] presented a dynamic fuzzy expert framework based on regression technique that is equipped for controlling imprecision and unavailable information. This model naturally changes new sets into fuzzy sets with the utilizing C-mean clustering algorithm. Furthermore, it is totally defenseless to the initialization handling, which ordinarily needs from the earlier information of the group numbers to establish the underlying bunch focuses [22]. Faiyaz and Iqbal [23] detailed about the utilization of a fuzzy semantic summarization methods dependent on found weight on fuzzy on the off chance that standards for student learning action.

All things considered, gathering rules from specialists is not a simple occupation, and then again, it is hard for an information designer to deduce rules from unchangeable databases. Consequently, rule extraction turns into a demerit in the information configuration process [24]. Errand like many-sided rules occur due to human's intuitive and perceptual aptitudes. Unfortunately, it is found that is no general plan for making a FL controller for assessment from first standard, and heuristics are ordinarily required just as enough experimentation to deliver a fuzzy logic controller that fulfills the structure's objectives and limitation. The proposed system expands from the previously expressed techniques as it deals with genetic algorithm having a completely computerized fuzzy rule-based assessment.

3 Proposed Methodology

Fuzzy systems along with GA are mainly used as soft computing techniques in a simple way for the basic decision making of vague and unsure data and for optimization of fuzzy rules in human decision-making system. The precision value of the model

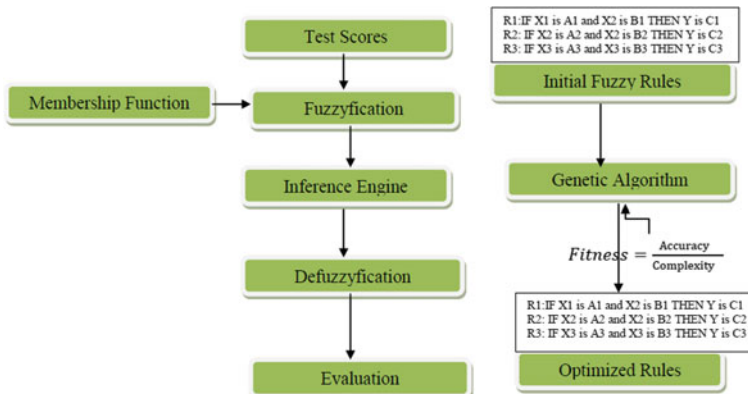


Fig. 1 Block diagram of the proposed system

determines the accuracy of the model of the system. We perceive the relationship between's the reactions of the genuine system and the fuzzy model [25]. Fuzzy logic has the advantage of displaying the subjective points of view of human information, just as decisions given by individual by utilizing the rules of the rule base [26]. In this research paper, general rules are made utilizing genetic algorithm for implementing at a minimal learning base in two phases. The main phase prompted structure the underlying principles begin from a specialist, and the second phase is figured out how to decrease these rules by utilizing GA algorithm. The technique of proposed hybrid genetic fuzzy system FES for learner's assessments and evaluation is explained in Fig. 1. The given subparts examine and elaborate the steps in detail.

3.1 Scores in Test

Students appeared and obtained three scores in semester examination, mark score-1, mark score-2, and mark score-3.

3.2 Fuzzification

Triangular fuzzy membership function is utilized by this framework for effortless-ness to fuzzify information and yield factors (1) [27]. The fuzzy arrangement of information factors is appeared Table 1. For thought processes of reasonableness inside the application, a worth range somewhere in the range of 0 and 1 was picked (see Table 2).

Table 1 Linguistic input variables

Linguistic terms	Symbol	Interval
Extremely low	VL	(0, 0, 25)
Low	L	(0, 25, 50)
Average	A	(25, 50, 75)
High	H	(50, 75, 100)
Extremely high	VH	(75, 100, 100)

Table 2 Linguistic output variables

Linguistic term	Symbol	Interval
Extremely unsuccessful	VU	(0, 0, 0.25)
Unsuccessful	U	(0, 0.25, 0.5)
Moderate	M	(0.25, 0.5, 0.75)
Successful	S	(0.5, 0.75, 1)
Extremely successful	VS	(0.75, 1, 1)

$$\text{triangular}(x, a, b, c) = \max\left(\min\left(\frac{x-a}{b-a}, \frac{c-x}{c-b}\right), 0\right) \quad (1)$$

3.3 Fuzzy Rule Base and Inference

After defuzzification, the corresponding crisp value of linguistic term are generated by Mamdani fuzzy inference engine [16, 28] is shown in Table 3 (125 rules = 53). As per discussion with the experienced members of education system, rules are generated from their experiences [29].

$$\mu_c(y) = \max_k(\min(\mu_{A1}(t1).\mu_{B1}(t2))), \quad k = 1, 2, \dots r \quad (2)$$

Table 3 Fuzzy rule set

Rule no.	Rules
1	IF exam 1 is EL and exam 2 is EL and exam 3. Then, result is EU is EL
2	IF exam 1 is EL and exam 2 is H and exam 3 is EH
3	IF exam 1 is L and exam 2 is A and exam 3 is EH
4	IF exam 1 is A and exam 2 is L and exam 3 is EH
5	IF exam 1 is H and exam 2 is EL and exam 3 is EH
:	:
125	IF exam 1 is H and exam 2 is EH and exam 3 is EH. Then, the result is ES

where r represent the number of rules. Mamdani's max–min composition is used where implication is modeled by means of the minimum operator, and the resulting output MFs are joined using the maximum operator.

3.4 Evaluation of Performance Value by Defuzzification

After carrying out the fuzzy decision process, the collected fuzzy numbers must be changed to a crisp value. This procedure is named defuzzification. In this investigation, a 'centroid' routine was executed, which is a standout among the most famous techniques. The fresh worth is processed by the formula given below [30].

$$\text{Weighted average} = \frac{\sum(\mu(x)) * (z)}{\sum(\mu(x))} \quad (3)$$

where z is the output score, and $\mu(x)$ denote the membership function (MF) of fuzzy output area.

3.5 Enhanced GA-Based Fuzzy Rules

There are two regular approaches used for producing fuzzy rules as stated earlier. The first approach required expert data to manufacture these rules which probably would not be the best things because of limitation of expert data. The second strategy has been actualized to make optimized fuzzy rules from the open info yield results [31]. So, the genetic fuzzy logic (in light of a transformative FS) enhances rule bases utilized by student assessment evaluation system that is embraced [24] for crafted programming.

- **Initial population:** The genetic algorithm requirements of sensible answer of a population are arranged and refreshed all through the evaluation procedure of the proposed methodology; rules the underlying population is shown in Table 3 responsible to derived new FBs.
- **Rules Encoding:** To encode rules inside a population of individual (see Fig. 2) follows Pittsburgh approach. The main reason for using binary coding is that it has advantage of simple coding and decoding for better searching and easily implementation of crossover and mutation [30].
- **Fitness Evaluation:** To understand a reduced RB from an underlying population, the genetic algorithm selects parent FS standards with high fitness esteems for reproduction (mating). An evaluation capacity is a lot of test desires which have the precedents and verifiable facts then utilized to achieve and qualify the inferred rule base. The exhibition of the gathered rule base with their worth of fitness is

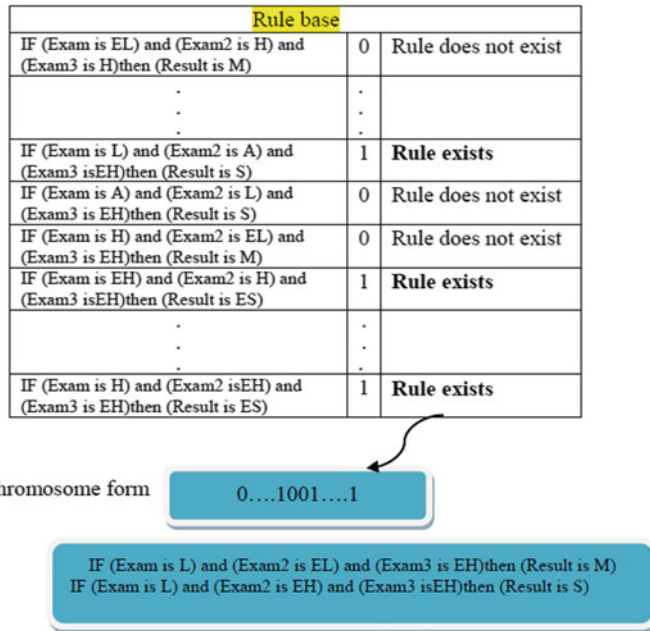


Fig. 2 Encoding scheme

bolstered reverse to the GA to proceed. Two variables are used in surveying the got fuzzy rules, accuracy, and complexity nature which are characterized underneath.

$$\text{Accuracy} = \frac{N_m}{N_t} \quad (4)$$

$$\text{Complexity} = \frac{N_{\text{CPR}}}{N R_{\text{IP}}} \quad (5)$$

$$\text{Fitness} = \frac{\text{Accuracy}}{\text{Complexity}} \quad (6)$$

where N_m refers to student's record number currently matched, N_t is the total students records, N_{CPR} current population rules and total rules in initial population are denoted by $N R_{\text{IP}}$.

- **Selection:** In this proposed system, authors has selected and implement roulette wheel selection [32] for evaluation of fitness function. Best chromosomes having more potential outcomes to be select as antecedents. The working of Roulette wheel calculation is characterized beneath:

(i) [Sumup] Evaluation each individual's fitness value in the population. (ii) [Selection] finding an arbitrary number among sample interval. (iii) [Loop] repeat on the basis of the fitness of whole populations [33].

$$p_n = \left| \frac{\text{fitness}}{\sum_{i=1}^n \text{fitness}_i} \right| \quad (7)$$

Probability of selection is shown by p_n of selection, and fitness of the chromosome n is denoted by fitness_n .

Crossover: In this work, one point crossover is applied as a basic and regularly employed technique for GAs: [34].

- **Mutation:** Crossover activity of GAs cannot create totally changed offspring from their parents in light of the fact that the gathered data is used to join the chromosomes. Mutation can investigate new spaces as opposed to the crossover [32, 35]. Given 125 basic rules, GA yields just 46 rules to decides both precision and complexity nature. This methodology does not require any human impedance during the enhancement stage. The time required is in this way subject to the PC execution speed, yet not on human specialists. The proposed methodology is versatile; at the same time, the expanding number of standard sets may increase the validity of the resulting knowledge base.

4 Experimental Results Generation

In this paper, the proposed hybrid system (GA with fuzzy system) for student assessment has been implemented using MATLAB. Table 4 indicates different GA parameters taken up for the enhancement of fuzzy rule controller. Using the traditional, FL and genetic fuzzy assessment techniques are given in Table 5. For examination, normal scores with old style technique are separated into 100 and the achievement farthest point is acknowledged as 0.5. The mean absolute error (MAE) between the traditional technique and both FL and genetic fuzzy assessment strategies are additionally featured; MAE is determined as [32]

Table 4 GA's factor

Encoding style	Binary coding Pittsburgh approach
Number of generations	20
Crossover size	0.8
Mutation rate	0.2
Population size	50
Crossover type	One-point
Selection type	Roulette wheel

Table 5 Comparisons of rule-based fuzzy system with proposed system (using triangular MF)

S. No.	Mark score-1	Mark score-2	Mark score-3	Classical method	Fuzzy method	Genetic fuzzy method
1	67	20	60	0.490	0.407	0.17
2	100	90	78	0.893	0.909	0.910
3	89	45	89	0.743	0.680	0.740
4	65	89	34	0.626	0.637	0.613
5	78	98	34	0.700	0.719	0.740
6	50	45	87	0.606	0.677	0.658
7	45	87	34	0.553	0.620	0.502
8	99	65	52	0.720	0.751	0.741
9	95	85	79	0.863	0.827	0.830
10	63	73	75	0.703	0.750	0.722
11	80	999	90	0.896	0.886	0.910
12	30	36	40	0.353	0.319	0.334
13	40	35	45	0.400	0.354	0.367

$$\text{MAE} = \frac{1}{m} \sum_{k=1}^m |t_k - y_k| \quad (8)$$

where t_k is the real (desired) value, y_k is the predicted value created by the model, and m is the all out number of perceptions. At the point, when the results are evaluated, a change in results is acknowledged between the traditional strategy and the FL method. This difference is decreased with the proposed genetic fuzzy system. While the classical technique holds fast to a consistent scientific principle, assessment with genetic FL has extraordinary adaptability. At first, the standards of the fuzzy framework have been resolved (125 rules) as indicated by the master sentiment. The exactness of the consequences of this model is 90%. At that point, the fuzzy principles have been improved by GA. The new model, improving the fuzzy standards (46 rules), has created new results having higher accuracy ratio, 93%, compared with the previous model. The optimization method is figured out how to accomplish decrease of fuzzy rules complexity nature as far as number of principles by 60% and precision improvement by 3% with a drop of enhancement execution time by 6%.

4.1 Discussion and Analysis

Over fitting are a big issues and the most evident weakness of fuzzy rule-based student performance evaluation system gathered from named information [36]. The

Table 6 Comparison between student's performance evaluation algorithm

Method	MAE
FL [37]	0.0694
Hybrid subtractive clustering fuzzy C-means (SC-FCM) [38]	0.1030
Genetic fuzzy system	0.0363

Table 7 Membership function evaluation techniques using student's dataset with factors evaluation

MF type	Data size	MAE	Accuracy
Triangular	30 students	0.731	92.7
	50 students	0.0757	92.4
Trapezoidal	30 students	0.0681	93.1
	50 students	0.0684	93.1

utilization of GA may give an incredible potential to FL-based enhancement approach for deciphering vulnerability and similitude seeing someone among system factors. In this paper [11], fuzzy C-mean [36] and data are shown in Table 6 indicate that the optimized FL method reached at higher average predictive accuracy than the other methods. The received outcomes approve that the enhancement strategy to get the fuzzy rule base is attractive with a basic GA. Table 7 represents the impact of various factors, for example, the quantity of tests and participation type to the productivity of the system regarding accuracy. The reaction of the system under trapezoidal MF has a superior execution than the triangular MF on the grounds that the semantic of the fuzzy controller in trapezoidal capacity is progressively proper to depict the dataset and the trapezoidal MF mirrors a decent controller of the imprecision of the system more than triangular MF indicating the worldwide presentation improvement.

To decrease this problem, the proposed system has incorporated a few heuristics in terms of fitness function of the genetic algorithm. After the investigation of results, it very well may be inferred that the fuzzy principle learning with genetic algorithm give models with a marginally expanded accuracy, which is adjusted by a significant decrease in the complexity of the model.

5 Conclusion

Genetic algorithm apply for optimization on post fuzzy rule base which provides better rule for taking better decision for expert knowledge base. Fuzzy rules formulation is generated using expert knowledge and given sample data. This task basically improves in evaluation result and also increases the interpretability of the new optimized model. Experiment analysis shows that this hybrid genetic-fuzzy scheme using for performance evaluation purpose take less time with high precision value in context of training and testing and result is very much close to the desired one. To

conclude, using the proposed system for student performance evaluation produces a substantial significant reduction of fuzzy rules complexity and accuracy.

Final result also shows that this model performs prediction more accurately with 93.56%. The accuracy of this classification model can also be increased further by the changing different genetic algorithmic configurations.

References

1. Yadav, R.S., Singh, V.P.: Modeling academic performance evaluation using soft computing techniques: a fuzzy logic approach. *Int. J. Comput.* **3**, 676–686 (2011). ISSN: 0975-3397
2. Capovilla, D., Hubwieser, P., Shah, P.: DiCS-index: predicting student performance in computer science by analyzing learning behaviors. In: Proceedings—2016 International Conference on Learning and Teaching in Computing Engineering. LaTiCE 2016, pp. 136–140 (2016). <https://doi.org/10.1109/latice.2016.12>
3. Mandelson, P.: HRM in Action : Employee Engagement as a Strategic and Appraisal, pp. 234–261 (n.d.)
4. Nedungadi, P., Remya, M.S.: Predicting students' performance on intelligent tutoring system—Personalized clustered BKT (PC-BKT) model. In: Proceedings of Frontiers in Education Conference FIE. 2015–February (2015). <https://doi.org/10.1109/fie.2014.7044200>
5. Biswas, R.: An application of fuzzy sets in students' evaluation. *Fuzzy Sets Syst.* **74**, 187–194 (1995). [https://doi.org/10.1016/0165-0114\(95\)00063-Q](https://doi.org/10.1016/0165-0114(95)00063-Q)
6. Kapranos, P.: Teaching and learning in engineering education—are we moving with the Times? *Procedia—Soc. Behav. Sci.* **102**, 3–10 (2013). <https://doi.org/10.1016/J.SBSPRO.2013.10.707>
7. Yusoff, Y.M., Zaharim, A.: Evaluation of graduates' performance using fuzzy approach. *Procedia—Soc. Behav. Sci.* **102**, 64–73 (2013). <https://doi.org/10.1016/J.SBSPRO.2013.10.714>
8. Cordón, O., Gomide, F., Herrera, F., Hoffmann, F., Magdalena, L.: Ten years of genetic fuzzy systems: current framework and new trends. *Fuzzy Sets Syst.* **141**, 5–31 (2004). [https://doi.org/10.1016/S0165-0114\(03\)00111-8](https://doi.org/10.1016/S0165-0114(03)00111-8)
9. Cordón, O., Del Jesus, M.J., Herrera, F., Lozano, M.: MOGUL: a methodology to obtain genetic fuzzy rule-based systems under the iterative rule learning approach. *Int. J. Intell. Syst.* **14**, 1123–1153 (1999). [https://doi.org/10.1002/\(SICI\)1098-111X\(199911\)14:11%3c1123:AID-INT4%3e3.3.CO;2-Y](https://doi.org/10.1002/(SICI)1098-111X(199911)14:11%3c1123:AID-INT4%3e3.3.CO;2-Y)
10. Gacto, M.J., Alcalá, R., Herrera, F.: Adaptation and application of multi-objective evolutionary algorithms for rule reduction and parameter tuning of fuzzy rule-based systems. *Soft. Comput.* **13**, 419–436 (2009). <https://doi.org/10.1007/s00500-008-0359-z>
11. Herrera, F.: Genetic fuzzy systems: taxonomy, current research trends and prospects. *Evol. Intell.* **1**, 27–46 (2008). <https://doi.org/10.1007/s12065-007-0001-5>
12. Roubos, H., Setnes, M., Abonyi, J.: Learning fuzzy classification rules from data. *Dev. Soft Comput.* **150**, 108–115 (2012). https://doi.org/10.1007/978-3-7908-1829-1_13
13. Borg, S.: Teacher cognition in language teaching: a review of research on what language teachers think, know, believe, and do. *Lang. Teach.* **36**, 81–109 (2003). <https://doi.org/10.1017/S0261444803001903>
14. Castillo, O., Melin, P., Alanis, A., Montiel, O., Sepulveda, R.: Optimization of interval type-2 fuzzy logic controllers using evolutionary algorithms. *Soft. Comput.* **15**, 1145–1160 (2011). <https://doi.org/10.1007/s00500-010-0588-9>
15. Kharola, A., Kunwar, S., Choudhury, G.B., Kharola, A., Kunwar, S., Choudhury, G.B.: Students performance evaluation: a fuzzy logic reasoning approach. *PM World J.* **IV**, 1–11. [www.pmworldlibrary.net](http://pmworldlibrary.net) (2015)

16. Zadeh, L.A.: Fuzzy logic. *Comput. Complex. Theory, Tech. Appl.* 1177–1200 (2013). https://doi.org/10.1007/978-1-4614-1800-9_73
17. Romero, C., Espejo, P.G., Zafra, A., Romero, J.R., Ventura, S.: Web usage mining for predicting final marks of students that use Moodle courses. *Comput. Appl. Eng. Educ.* **21**, 135–146 (2013). <https://doi.org/10.1002/cae.20456>
18. Jang, J.S.R., Sun, C.T., Mizutani, E.: Neuro-fuzzy and soft computing—a computational approach to learning and machine intelligence [Book Review]. *IEEE Trans. Automat. Contr.* **42**, 1482–1484 (2005). <https://doi.org/10.1109/tac.1997.633847>
19. Casillas, J., Cordón, O., del Jesus, M.J., Herrera, F.: Genetic tuning of fuzzy rule deep structures preserving interpretability for linguistic modeling. *IEEE Trans. Fuzzy Syst.* **13**, 13–29 (2005)
20. Naim, S., Hagras, H.: Granular Computing and Decision-Making (2015). <https://doi.org/10.1007/978-3-319-16829-6>
21. Yadav, R.S., Ahmed, P.: Academic performance evaluation using Fuzzy C-Means. *Int. J. Comput. Sci. Eng. Inf. Technol. Res.* **2**, 55–84 (2012). http://www.tjprc.org/view_archives.php?year=2013&id=14&jtype=2&page=4
22. Fahad, A., Alshatri, N., Tari, Z., Alamri, A., Khalil, I., Zomaya, A.Y., Foufou, S., Bouras, A.: A survey of clustering algorithms for big data: taxonomy and empirical analysis. *IEEE Trans. Emerg. Top. Comput.* **2**, 267–279 (2014). <https://doi.org/10.1109/TETC.2014.2330519>
23. Doctor, F., Iqbal, R.: An intelligent framework for monitoring student performance using fuzzy rule-based Linguistic Summarisation. *IEEE Int. Conf. Fuzzy Syst.* (2012). <https://doi.org/10.1109/FUZZ-IEEE.2012.6251312>
24. Darwish, S.M.: Uncertain measurement for student performance evaluation based on selection of boosted fuzzy rules. *IET Sci. Meas. Technol.* **11**, 213–219 (2016). <https://doi.org/10.1049/iet-smt.2016.0265>
25. Casillas, J., Cordón, O., Herrera, F., Magdalena, L.: Accuracy Improvements to Find the Balance Interpretability-Accuracy in Linguistic Fuzzy Modeling: An Overview, pp. 3–24 (2013) https://doi.org/10.1007/978-3-540-37058-1_1
26. Rusmiari, N.M., Putra, K.G.D., Sasmita, G.M.A.: Fuzzy logic method for evaluation of difficulty level of exam and student graduation. *Int. J. Comput. Sci. Issues* **10**, 223–229 (2013)
27. Kharola, A.: A Hybrid ANFIS Technique for Effective Performance Evaluation, vol. IV, pp. 1–9 (2015)
28. Saleh, I., Kim, S.: A fuzzy system for evaluating students' learning achievement. *Expert Syst. Appl.* **36**, 6236–6243 (2009). <https://doi.org/10.1016/j.eswa.2008.07.088>
29. Jamsandekar, S.S., Mudholkar, R.R.: Performance evaluation by fuzzy inference technique. *Int. J. Soft Comput. Eng.* 2231–2307 (2013). <https://pdfs.semanticscholar.org/3fdf/3fe33aaec8ce33873f6760c37af1c33dd3dc.pdf>
30. Sweta, S., Lal, K.: Personalized adaptive learner model in e-learning system using FCM and fuzzy inference system. *Int. J. Fuzzy Syst.* **19**, 1249–1260 (2017). <https://doi.org/10.1007/s40815-017-0309-y>
31. Harb, H.M.H., Desuky, A.A.S.: Adaboost Ensemble with Genetic Algorithm Post Optimization for Intrusion Detection, Update. *Int. J. Comput. Sci. Issues* **2**, 1 (2011). <https://doi.org/10.1.1.402.9250>
32. Malhotra, R., Singh, N., Singh, Y.: Genetic algorithms: concepts, design for optimization of process controllers. *Comput. Inf. Sci.* **4**, 39–54 (2014). <https://doi.org/10.5539/cis.v4n2p39>
33. Lee, M.A., Takagi, H.: Integrating design stage of fuzzy systems using genetic algorithms, 612–617 (2002). <https://doi.org/10.1109/fuzzy.1993.327418>
34. Sweta, S., Lal, K.: Web usages mining in automatic detection of learning style in personalized e-learning system. In: Ravi, V., Panigrahi, K.B., Das, S., Suganthan, N.P. (eds.) *Proceedings of the Fifth International Conference on Fuzzy and Neuro Computing (FANCCO—2015)*. Springer International Publishing, Cham, pp. 353–363 (2015). https://doi.org/10.1007/978-3-319-27212-2_27
35. Cordón, O.: A historical review of evolutionary learning methods for Mamdani-type fuzzy rule-based systems: designing interpretable genetic fuzzy systems. *Int. J. Approx. Reason.* **52**, 894–913 (2011). <https://doi.org/10.1016/j.ijar.2011.03.004>

36. Kumar, M., Jangra, A., Diwaker, C.: Genetic optimization of fuzzy rule-base system. *Int. J. Inf. Technol.* **2**, 287–293 (2010). <http://www.csjournals.com/IJITKM/PDF3-1/22.pdf>
37. Huapaya, C.R.: Proposal of fuzzy logic-based students' learning assessment model, XVIII Congr. Argentino Cienc. Comput. (2012)
38. Singh Yadav, R., Pratap Singh, V.: Modeling academic performance evaluation using Fuzzy C-Means clustering techniques. *Int. J. Comput. Appl.* **60**, 15–23 (2017). <https://doi.org/10.5120/9711-4174>

A Review on Detection of Breast Cancer Cells by Using Various Techniques



Vanaja Kandubothula, Rajyalakshmi Uppada, and Durgesh Nandan

Abstract This paper discussed a framework for the detection of breast cancer cells by using various techniques. Dangerous cancer is mostly observed in women's breast. The mortality rate can be decreased when breast cancer is detected at an early stage. By using different techniques, breast cancer cells can be detected. From the past decade, to detect and identify the stage of the cancer, computer-aided diagnosis (CAD) system has been initiated. This system consists of different steps like pre-processing, nuclei detection, segmentation, feature extraction, and classification to detect breast cancer cells. The approaches and methodologies in each step of the CAD system are applied to the images for cancer cell detection. Classification is done by using different classifiers. Features and classification results of different techniques for various images for detecting breast cancer cells are reviewed.

Keywords CAD system · Grayscale image · RGB image · SVM · MLP

1 Introduction

Breast cancer is mostly observed in ladies which leads to mortality all over the world. By using proper preoperative tests like physical examination, mammography (which is used for screening purpose to determine the location and the breast tissue), and FNAC (works on samples of breast tissue), breast cancer can be diagnosed easily. Mostly, computer-aided diagnosis is used [11]. MRI and ultrasound are also effective tools for determining cancer cells. Some issues take place like image quality

V. Kandubothula

Department of ECE, Aditya Engineering College, Surampalem, India

e-mail: vanaja.kandubothula@gmail.com

R. Uppada · D. Nandan (✉)

Accendere Knowledge Management Services Pvt. Ltd., CL Educate Ltd., New Delhi, India

e-mail: durgeshnandano51@gmail.com

R. Uppada

e-mail: rajyalakshmiuppada@gmail.com

and human errors which increase the misdiagnosis. The CAD system is most useful in differentiating benign and malignant tumors. Different modalities in CAD systems are used in diagnosing the different diseases [12]. Due to high sensitivity and softness, detecting all the lesions of the breast using these modalities is enough. Digital radiography acts as a useful modality in detecting the lesions of the breast. By using the MATLAB programming techniques, breast cancer can be detected with its characteristics like mass with a specific site, texture, border, and shape that can easily identify under image processing [1, 5]. Low dose X-rays are used to detect breast cancer in mammography. In this, the image is partitioned into different segments to analyze easily, i.e., image segmentation. In image segmentation, double threshold segmentation approach is used to easily detect cancer. Using Hough transform method, nuclei locations are identified and used the modified Marker-controlled watershed approach (MMCWA) for nuclei segmentation. The small secured structuring size element to remove the bright and dark details during the opening and closing morphology and to remove high contours details of the image large size element is used [8, 23]. By using microscoping analysis, the area affected under breast cancer is detected. Pixel intensity cannot be used for segmentation due to homogeneities. Level set (LS) methods are initiated to overcome the homogeneities. LS functions represent a bias field for image intensity inhomogeneities [24].

In this, a lot of research is available on breast cancer identification. CAD system plays a crucial role in detecting breast cancer cells. CAD system contains various steps to detect breast cancer. Several authors discussed various techniques for identification and for detection of breast cancer which are discussed in the literature section. In these techniques and process, some are not accurate, and the performance of some techniques is not effective. Among all the techniques, the best and the important techniques are discussed in methodology (Sect. 3) which gives better accuracy and effective results in the identification of breast cancer. In the results section, we compare the techniques which are discussed in methodology. Finally, we concluded with the best technique which gives a high accuracy rate and its future work.

2 Literature Work

Ghongade et al. proposed that breast cancer is mostly observed in ladies and has become a severe problem that leads to mortality. To overcome this problem, it should be identified in the earlier stage. Here, machine learning based on the RF classifier method is used to diagnose breast cancer. The quality of an image is done by using the preprocessing method. The features which have to improve the accuracy of classification are smoothness, mean, standard deviation, ASM, and correlation. Detecting and diagnosis of breast cancer cells by using this method achieve a good result [12]. Jalalian et al. proposed that the mortality rate in ladies will decline by the detection of breast cancer in the starting stage. Detection and diagnosis of cancer cells are done by a radiologist. Some issues take place like human errors, image quality place which leads to misdiagnosis of breast cancer. To overcome this problem, CAD is used.

It consists of four stages. This method has some advantages and disadvantages. It consists of different modalities like ultrasound, mammography, and MRI based on these modalities, and it also classifies benign and malignant tumors. To overcome the imbalanced dataset issues, sampling techniques are preferred [15]. Bagchi et al. proposed that different CAD systems are used to diagnose breast cancer cells. In signal processing applications, different techniques are used for de-noising the wavelet transform. Curvelet analysis is used for better masses and special characteristics. A semi-automated segmentation method was used to characterize all micro clarifications. The accuracy achieved by the deep learning process is 87.3%. Accuracy of micro classification and masses is calculated by using the SVM classifier [6, 29]. Saha et al. proposed that for the detection of breast cancer, imprint cytology and FNAC play an integral role. By using CAD, various methods for machine and algorithms are developed by the pathologists. To discourse numerous concerns in breast, cytology-based CAD that included preprocessing, segmentation, feature extraction, and diagnostic classification shows an overview of image processing. This paper provides a better understanding of breast cancer detection and diagnosis [25].

Kowal et al. proposed that detecting and diagnosing cancer cell by using CAD play a key role in this field. Benign or malignant cells are classified by using cytological images of needle biopsies. In densely clustered cells in the image nuclei, separation is done by a robust segmentation procedure. The erosion process is used to obtain a nucleus in the cell. This segmentation method is applicable for most sophisticated clustered images [18]. Kaura et al. proposed that the multi support vector machine and deep learning mechanisms were initially proposed for breast cancer mammograms for an automated system. Images are preprocessed for de-noising and resizing. For feature extraction and classification, the obtained images are fed to a trained network using SVM. K-means clustering and MSVM give a better approach [16].

Kaymaka et al. proposed that breast cancer cell detection and diagnosis at an earlier stage are very crucial. For breast cancer diagnosis, different CAD methods are proposed. This paper presents the classification of images for detecting breast cancer cells. To classify the image backpropagation, neural network method is used, and for further improvement, radial basis neural networks (RBNN) are used, whose accuracy is more, i.e., 70.02% [17]. Ragab et al. proposed modified CAD methods for detecting breast cancer. Two segmentation approaches are used in the CAD system. ROI is the first approach physically from the new image using circular contours, and the second approach is threshold and region-based. Alexie is a deep convolution neural network method to classify the classes to two instead of 1,000. By using extreme learning machine (ELM), algorithm classification is done [22, 29].

Win et al. proposed the best method to detect breast cancer cells. Intensity modification and average filtering are used to improve the quality of the image. To identify the cell nuclei, a method called K-means clustering is used. By using shape-based analysis, overlapped nuclei regions are found. From the nucleus, features are extracted. To predict the malignant in the nucleus from selected features, ECBDT classifier is used. Some failures are obtained in detecting the malignant. To detect different malignant tumors and to overcome the failures, combined analysis is done [30]. Uppada et al. discussed that the distinguished non-subsampled counterlet transform

is used to emphasize the edges of the tissue structure. To get better performance for other segmentation, NSC and multi-phase level set approaches are proposed. From partitioned images of 96 trained images, 13 shape morphology, 33 textural, and 2 intensity features are extracted [28].

Jagdalea et al. proposed the mammogram images of breast cancer having the ability to detect the diseases caused by the abnormal growth of cells. A smart sensing device in a CAD system is used in detecting the cancer cells. For low power and fast processing applications in CMOS, active pixel sensors in smart sensing are used. Two separate chips for processing and sensing are integrated to detect breast cancer cells [14]. Araujo et al. proposed that CAD systems contribute to reduce the cost and increase the efficiency in detecting breast cancer cells. For classification convolution, neural network (CNN) method is proposed. The value of sensitivity is high for this method [3, 13].

Biswas et al. proposed that for classification and evaluation of breast cancer cell image, support vector machine and backpropagation algorithm techniques are used. For image reconstruction, SVM with a BPNN technique is used. The classification accuracy of the SVM technique is high [7]. Singh and Gupta et al. proposed that the CAD system is very well known by mammogram images for the detection of breast cancer cells. On averaging and thresholding, the image processing techniques are used to detect the cancer cells. For tumor detection, max-mean and least variance techniques are used. Basic image processing techniques are used in which the process is simple and fast [27].

Durgesh et al. proposed that in the detection of breast cancer cells, classification is the most important task. The SVM classifier is one type of machine learning which is used to classify the breast cancer cells in the classification phase which is developed from statistical learning methods. It is a novel learning method, and it is applied to different datasets for detecting breast cancer cells. The SVM method does not support any limitations of data. Its efficiency is high compared to other classifiers [10]. Maitra et al. proposed that in detecting breast cancer cells, CAD system gives an effective performance. Medical processing and a multi-disciplinary science that involve the development of computational algorithms on medical images are required by the CAD system. It includes some steps for detecting breast cancer cells. This system improves the quality of work and also gives better results for different techniques [20].

Angayarkanni et al. proposed that the detection of cancer in the starting stages plays an important role in the decline of the mortality rate in women. In mammogram images for the detection of breast cancer cells, different algorithms are used. Digital mammography images are considered for improvement in breast imaging. The quality of the image accuracy is 100% [2]. McDonald et al. proposed the breast cancer diagnosis and its management system are undergoing a paradigm shift. This article includes different phases for detecting cancer cells [21]. Dhas et al. proposed that among women, breast cancer is a type of threatening disease. Mammogram images are used for the detection of breast cancer. For de-noising, oriented Rician noise reduction anisotropic diffusion (ORNRAD) filter is used, and for segmentation of K-means clustering and gray tone spatial dependence, matrix techniques are used.

For feature extraction, the Tamura method is used. The SVM classifier is used to obtain the abnormality and its accuracy is 98.1% [9, 26].

This CAD system plays a crucial role in detecting breast cancer cells. For the identification and detection of breast cancer cells, these systems contain various techniques. Several authors discussed different techniques for the detection and identification of breast cancer. In those techniques, some are not accurate, and the performances of some of the techniques are not good. Among all the techniques, the best and the important techniques are discussed in methodology which gives the best accuracy and effective results in the identification of breast cancer.

3 Existing Methodologies

The techniques with better performance and which have a high accuracy rate which are explained by different authors for the identification of breast cancer are discussed below.

George et al. described that the colored images are converted into grayscale images as the colored images do not contain any important information and that information can be removed to reduce time complexity. A grayscale image is obtained from a colored image by removing the colored components. It can also obtain by using the below formula:

$$Y = 0.229R + 0.587G + 0.114B \quad (1)$$

This is the preprocessing step. Cell nuclei detection (removing noisy circles using circular Hough transform technique), segmentation (watershed approach, fuzzy C-means clustering), and features are extracted based on shape, textual, and region. Classification is done by using SVM, LVQ, and MLP techniques [11].

$$h_g(x, y) = \exp(-(x^2 + y^2)/2\sigma^2) \quad (2)$$

Kowal et al. explained that the image contains noise. By increasing contrast later in preprocessing, step noise can be intensified and may cause aircraft in the segmentation process. The Gaussian low-pass filter or Wiener filter is used for noise removal in the image [12]. Segmentation is done by using adaptive thresholding and K-means clustering techniques. These techniques are applied to distinguish the dark image from the bright background. Different features are extracted based on the area and the length of the nuclei. Classification is done by using KNN and SVM [18], which consists of different steps to identify the cancer cells as discussed in Fig. 1. The steps that included in CAD system after the grayscale image obtained are preprocessing (to divide the observation, K-mean clustering is used), region of interest (ROI) method, cell nuclei detection (removing noisy circles using circular Hough transform technique), segmentation (watershed approach, multi-phase level sets approach), features extraction (shape-based, intensity-based, textual-based features), classifications support vector machine (SVM), and MCS (multi-class support)) [24].

Jalalian et al. explained that preprocessing is the step to remove the noise and to modify the defects in the image. This ultrasound is used to remove noise. The segmentation techniques are classified based on discontinuity approaches (edge-based approaches), similarity approaches (threshold-based, region-based, clustering), and other related approaches (artificial neural network and level set methods). Features also extracted based on the color. The last step classification is done based on unsupervised techniques (K-means clustering, self-organize map) and supervised techniques (SVM, MLL) [15].

Kaura et al. discussed that the preprocessing of an image plays a crucial role in the detection of cells. Mammogram images are considered for testing and training. RGB images are separated from the original image to make the process easy. By using the median filter, mean filter, and morphological operation, the noise in the original image is removed, and the quality of the image is enhanced. This process can apply to both colored and the grayscale images shown in Fig. 2. In this for classification, K-means clustering and SVM techniques are used [4, 16].

Win et al. explained by resizing the image to 1024×1024 pixels, the preprocessing step is done which makes it easy to enhance. By using median filter, noise is removed in the RGB image. By using supervised learning approach, segmentation is done. Based on the Haar filter and adaboost classifier, this approach is done. The other

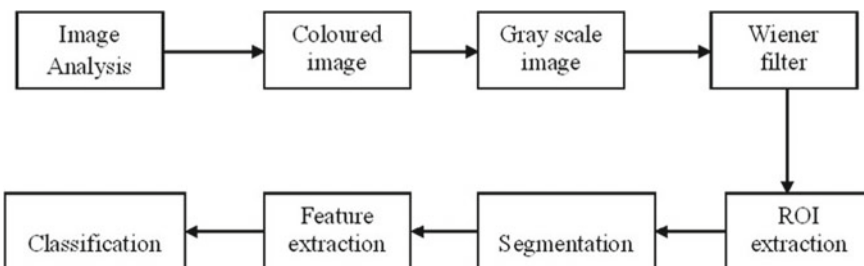


Fig. 1 Steps in CAD system

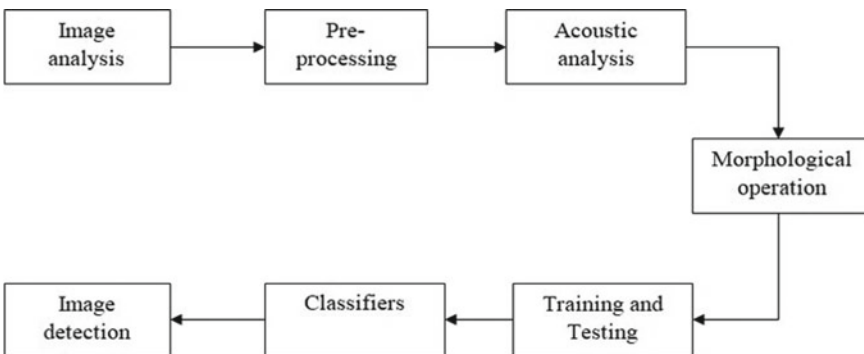


Fig. 2 Image analysis and detection using morphological operation

approaches for segmentation are K-means clustering, Ostu threshold, mean shift clustering, graph cut method, and Chan vessel level set. To distinguish between benign and malignant cells, the extracted features are applied as input to the classifiers like SVM, Naive Bayes (NB), and ANN [30].

Kumar et al. proposed that the preprocessing step makes the process of detecting the cancer cells easy. Microscopy images are considered in this stage and to remove noise contrast limited adaptive histogram equalization (CLAHE) method is used. For segmentation purposes, K-means clustering is the best approach for microscopy images. In this, the features are extracted based on the nucleus area, textually based, color-based, morphology, and shape-based. The final step classification is done by using different methods. In the classification method, K-nearest neighbor, support vector machine (SVM), and random forest (RF) classifiers are used. KNN is used as a classifier for biopsy images [19].

4 Result

In this section, we will compare the results of various techniques, and finally, conclude the best possible approach for the detection of breast cancer cells.

George et al. experiment is done by using FNAC images by using six datasets, out of them two datasets are benchmark Wisconsin datasets. For eliminating all the noisy circles, Ostu's threshold method is used. FNAC images provide a better diagnosis in detecting malignancy cells as discussed in Table 1 [11].

Kowal et al. have calculated accuracy of the image by using the KNN classifier 1. It has 80% accuracy for six features, image accuracy was in the range of 60–80%, and it was below 60% for 42 images [18].

Uppada et al. explained integration of ASEMCWA and NMPLS to extract the nuclei of H and E stained breast cancer histology images. RGMA, MCWA, and NMPLS methods are used, and sensitivity, specificity, and accuracy percentages are calculated. Average segmentation sensitivity and specificity are increased to 99.01 [24]. Jalalian et al. explained by using 12,860 mammogram images that are considered. Clinical image processing and supervised classification techniques are used. For boosting, support vector machine in functional level Kernel transformation and biased penalty approaches are recommended. To overcome the imbalanced dataset issues at the data level, sampling techniques are mostly used, and mainly over-sampling and under-sampling techniques are widely used [15].

Kaura et al. explained that the image database used manual and automated pre-processed datasets, which consists of 322 mammograms breast images. For feature extraction, 77×100 ROI with three channels and seven layers of CNN is used. By using noise handling and resizing operations, the preprocessing phase is well defined. As compared to the decision tree model, K-means clustering and MVSM techniques give a better result. K-means clustering and MSVM give better results as compared to the decision tree model [16]. Yadanar et al. explained to pre-segment the image into a small compact superpixels. SLIC method is firstly used by comparing the ground

Table 1 Comparison of different techniques

Dataset	Features and the techniques	Results	Limitations
FNAC images, six datasets are considered	Performance of sensitivity and specificity using SVM, LVQ, PNN, and MLP classifiers	Classification performance is up to 99.7% for our given datasets. For the evaluated datasets, LVQ and multiperceptron have the less predictive ability than the PNN and SVM [11]	This approach is not suitable for histology images
450 real medical cytology images are considered	84 features were extracted for each image. In this, KNN, DT, and SVM classifiers are used	Accuracy of patients and images is calculated using KNN, DT, and SVM techniques. In this, accuracy of patients results 100% [12]	This approach is not suitable for histology images
96 images for training and 24 images for testing (32 for benign and 64 for malignant)	Sensitivity, specificity, accuracy DS, and J are calculated for different segmentation techniques. In this, novel segmentation technique is used	They discussed the results of only two images. For normal image segmentation, accuracy is improved to 99.12% [24]	Considered less number of images for training and testing
Mammogram images	Region-based segmentation and cluster-based algorithms are used. For classification, artificial intelligence and support vector machine techniques are widely used	For high sensitivity, specificity, and accuracy, unsupervised path followed by a backpropagation algorithm is used in a CAD system [15]	This approach is not suitable for histology images and cytology images
208 normal images, 322 mammogram images	7 × 100 ROI with three channels and seven layers of CNN is used for feature extraction	For Mini-Batch, accuracy is approximately increased by 15% [16]	This approach is not suitable for histology images and cytology images
125 CPE (cytological pleural effusion) images	From each nucleus, 14 morphometric features, six colorimetric features, and 181 texture features are extracted	Sensitivity is 87.97%, specificity is 99.40%, accuracy is 98.70%, and F-score is 87.79%. [30]	This approach is not suitable for histology image
Microscopic images. (RGB image is considered and then converted into grayscale image)	MSE and regression values	For 248 iteration, the accuracy is 94% [19]	This approach is not suitable for cytology image

truth and classification results concerning the four performance matrices discussed in Table 1. The classification performance is evaluated [30]. Kumar et al. considered a microscopic image as the dataset, and for training the network, Levenberg–Marquard backpropagation is used. Mean square error and regression values are calculated or training and testing data [19].

A brief description and comparison of the results from various approaches in the literature were discussed in Table 1.

5 Conclusion

Mammogram images and microscopic images are used to detect breast cancer cells easily in a CAD system. Different datasets are considered to examine different features in each cell. The prepossessing phase is critical and crucial. For enhancement of microscopic biopsy images, contrast limited adaptive histogram equalization-based method was used. Segmentation is done by using the technique K-means clustering. Features are extracted from each nucleus based on region, color, area, and textual. SVM and KNN classifiers are used in the classification phase to classify the cancer cells. Sensitivity, specificity, and accuracy are calculated for different classifiers. The performance of SVM and KNN classifiers is effective, and also they provide good accuracy.

6 Future Scope

The future perspective of this work is to do with larger datasets. This work can also be done by using cytology and also histology images.

References

1. Abdallah, Y.M., Elgak, S., Zain, H., Rafiq, M., Ebaid, E.A., Elnaema, A.A.: Breast cancer detection using image enhancement and segmentation algorithms. *Biomed. Res.* **29**(20), 3732–3736 (2018)
2. Angayarkanni, N., Kumar, D., Arunachalam, G.: The application of image processing techniques for detection and classification of cancerous tissue in digital mammograms. *J. Pharm. Sci. Res.* **8**(10), 1179 (2016)
3. Araújo, T., Aresta, G., Castro, E., Rouco, J., Aguiar, P., Eloy, C., Polónia, A., Campilho, A.: Classification of breast cancer histology images using convolutional neural networks. *PLoS one* **12**(6), e0177, 544 (2017)

4. Arpana, M., Kiran, P.: Feature extraction values for digital mammograms. *Int. J. Soft Comput. Eng. (IJSC)* **4**(2), 183–187 (2014)
5. Badawy, S.M., Hefnawy, A.A., Zidan, H.E., GadAllah, M.T.: Breast cancer detection with mammogram segmentation: a qualitative study. *Int. J. Adv. Comput. Sci. Appl. (IJACSA)* **8**(10) (2017)
6. Bagchi, S., Huong, A.: Signal processing techniques and computer-aided detection systems for diagnosis of breast cancer—a review paper (2017)
7. Biswas, S.K., Mia, M.M.A.: Image reconstruction using multi layer perceptron (mlp) and support vector machine (svm) classifier and study of classification accuracy. *Int. J. Sci. Technol. Res.* **4**(2), 226–231 (2015)
8. Chan, A., Tuszyński, J.A.: Automatic prediction of tumour malignancy in breast cancer with fractal dimension. *R. Soc. Open Sci.* **3**(12), 160,558 (2016)
9. Dhas, A.S., Vijikala, V.: An improved cad system for abnormal mammogram image classification using svm with linear kernel (2017)
10. Durgesh, K.S., Lekha, B.: Data classification using support vector machine. *J. Theor. Appl. Inf. Technol.* **12**(1), 1–7 (2010)
11. George, Y.M., Zayed, H.H., Roushdy, M.I., Elbagoury, B.M.: Remote computer-aided breast cancer detection and diagnosis system based on cytological images. *IEEE Syst. J.* **8**(3), 949–964 (2013)
12. Ghongade, R., Wakde, D.: Computer-aided diagnosis system for breast cancer using rf classifier, pp. 1068–1072 (2017)
13. Jadoon, M.M., Zhang, Q., Haq, I.U., Butt, S., Jadoon, A.: Three-class mammogram classification based on descriptive cnn features. *BioMed Res. Int.* (2017)
14. Jagdale, S., Kolekara, M.H., Khot, U.P.: Smart sensing using bayesian network for computer aided diagnostic systems. *Proc. Comp. Sci.* **45**, 762–769 (2015)
15. Jalalian, A., Mashohor, S., Mahmud, R., Karasfi, B., Saripan, M.I.B., Ramli, A.R.B.: Foundation and methodologies in computer-aided diagnosis systems for breast cancer detection, p. 113. Leibniz Research Centre for Working Environment and Human Factors (2017)
16. Kaur, P., Singh, G., Kaur, P.: Intellectual detection and validation of automated mammogram breast cancer images by multi-class svm using deep learning classification. *Inform. Med. Unlock.* 100151 (2019)
17. Kaymak, S., Helwan, A., Uzun, D.: Breast cancer image classification using artificial neural networks. *Proc. Comput. Sci.* **120**, 126–131 (2017)
18. Kowal, M., Filipczuk, P.: Nuclei segmentation for computer-aided diagnosis of breast cancer. *Int. J. Appl. Math. Comput. Sci.* **24**(1), 19–31 (2014)
19. Kumar, R., Srivastava, R., Srivastava, S.: Detection and classification of cancer from microscopic biopsy images using clinically significant and biologically interpretable features. *J. Med. Eng.* (2015)
20. Maitra, I.K., Bandyopadhyay, S.K.: Cad based method for detection of breast cancer (2018)
21. McDonald, E.S., Clark, A.S., Tchou, J., Zhang, P., Freedman, G.M.: Clinical diagnosis and management of breast cancer. *J Nucl Med* **57**(Suppl 1), 9S–16S (2016)
22. Ragab, D.A., Sharkas, M., Marshall, S., Ren, J.: Breast cancer detection using deep convolutional neural networks and support vector machines. *PeerJ* **7**, e6201 (2019)
23. Rajyalakshmi, U., Rao, S.K., Prasad, K.S.: Supervised classification of breast cancer malignancy using integrated modified marker controlled watershed approach, pp. 584–589 (2017)
24. Rao, S.K.: Integrated novel multi-phase level sets with modified marker controlled watershed for segmentation of breast cancer histopathological images (2017)
25. Saha, M., Mukherjee, R., Chakraborty, C.: Computer-aided diagnosis of breast cancer using cytological images: a systematic review. *Tissue Cell* **48**(5), 461–474 (2016)
26. Saraswathi, D., Srinivasan, E., Ranjitha, P.: Extreme learning machine for cancer classification in mammograms based on fractal and glcm features. *Asian J. Appl. Sci. Technol. (AJAST)* **1**(4), 1–6 (2017)
27. Singh, A.K., Gupta, B.: A novel approach for breast cancer detection and segmentation in a mammogram. *Proc. Comput. Sci.* **54**, 676–682 (2015)

28. Uppada, R., Sanagapallela, K.R., Kodati, S.P.: Image automatic categorisation using selected features attained from integrated non-subsampled contourlet with multiphase level sets, pp. 67–75 (2019)
29. Wang, J., Yang, X., Cai, H., Tan, W., Jin, C., Li, L.: Discrimination of breast cancer with microcalcifications on mammography by deep learning. *Sci. Rep.* **6**, 27,327 (2016)
30. Win, K.Y., Choomchuay, S., Hamamoto, K., Raveesunthornkiat, M., Rangsirattanakul, L., Pongsawat, S.: Computer aided diagnosis system for detection of cancer cells on cytological pleural effusion images. *BioMed Res. Int.* (2018)

Analysis of Security Issues and Possible Solutions in the Internet of Things for Home Automation System



P. Sai Ramya and Durgesh Nandan

Abstract Security and privacy are the two main required factors for home automation. Nowadays, human can operate devices using the Internet of things. These are sensor-based and network-based devices. At the same time, the user wants his information to be secured while he is accessing the devices through the Internet. In the process of transmission of data, the hackers could easily breach the security even if there is a minimum possibility. In this paper, the security challenges that a user faces while monitoring and controlling devices are discussed. The challenges are resource and energy constraints, unauthorized access to data during transmission and physical access. In this paper, we also discuss the techniques which ensure security to the user data. These provide user and device authentications. These systems are formed by using some schemes and algorithms according to the security challenges it deals with. By installing these techniques, the user can easily detect the intruder through the surveillance system, using PIR sensor and triggering circuit, the surveillance system can be operated which reduces the storage space for footage and by information stamping, at the corner of the footage, it can be used for future use. The user can use a smartphone to operate the smart devices by connecting through servers even the user is far away from home. The system sends the message alerts and generates alarms if any intrusion is detected. The data will be encrypted to ensure security while transmitting the report to the user. The techniques and methodologies discussed in this paper help ensure security for home automation.

Keywords Authentication · Internet of things · Surveillance · Communication · Security · Encryption · Decryption · Smart home · Zigbee module · Home area network (HAN)

P. S. Ramya

Department of ECE, Aditya Engineering College, Surampalem, India

e-mail: ramyasai424@gmail.com

D. Nandan (✉)

Accendere Knowledge Management Services Pvt. Ltd., CL Educate Ltd., New Delhi, India

e-mail: durgeshnandano51@gmail.com

1 Introduction

A smart home automation system is making user life easier. Reducing the power consumption and to inform the user if any housebreaking is detected is by using wireless sensor networks like LabVIEW statechart module [11]. Many wireless home automation systems are introduced, but they are useful for single applications. Bluetooth and Wi-Fi could not provide an unlimited range of communication. So, a multi-hop, low power, strong secure standard known as Zigbee [29] is implemented in the home automation system. Cloud services can greatly improve the capabilities of mobile and smart devices. Some of the security threats can be reduced, by using CoT-based group key management scheme for home area networks (HAN). Symmetric key cryptography is used where each smart device has a unique key. When necessary, the keys are exchanged securely which are generated by the scheme. So, the data transfers securely which can withstand the changes in the network [2]. The IoT consists of interconnected devices, and this connectivity of devices can generate a very large amount of data transmissions where it requires authenticity. The security challenges like resource constraints, end to end secure communications and physical access like tampering, and jamming is needed to be authenticated [13, 19].

As technology increases, the size of the devices is decreased, and the use of microprocessors is increased. And the user wants to control the devices through the Internet. Thus, the users can use network-based services, remote control and several services. But connecting smart appliances to the Internet is not safe. An intruder can steal our information such as contact info and credit card information used to pay such services. So, to decrease the cyber-attacks, TOR is used [14]. IoT enhances the quality of our lives. It gives complete secured IoT solutions by biometric and cryptography techniques [15], voiceprint verification method and Internet-based mobile authentication system [28]. As elderly people cannot participate in social activities, advanced Information and Communication Technology (ICT) can make it happen. It uses a human-centric safe and secure framework of ubiquitous living environment (Ubi-Liven) [17]. The user can get all the information about the home condition by using the AMQP as the communication protocol and to make sure that data is secured, RSA or AES algorithm is used [1]. By observing the applications and challenges faced by the smart home network, we can say that this type of heterogeneous connection-based IoT devices cannot provide efficient security. A key management system which uses Internet key management protocols enhances performance, security and energy efficiency. To improve security, we use the Scyther tool and formal validation concerning security [25].

The security challenges and possible techniques which ensure security representation are shown in Fig. 1. In Sect. 2, a brief overview of techniques is discussed. Section 3 explained the existing techniques for efficiency in securing. In Sect. 4, we compared the techniques and given parameters achieved through that method. In Sect. 5, we discussed the application of securing methods in real life. In Sect. 6, we discussed what should be done in future to reduce the challenges and the conclusion.

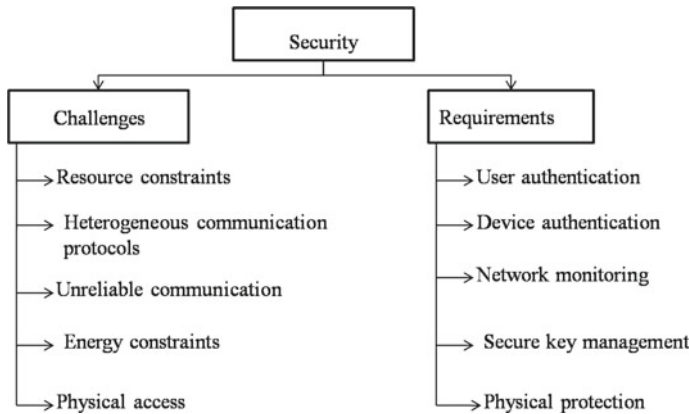


Fig. 1 Security challenges and security requirements in home automation

2 Literature Review

Smart homes give innovative, automated and interactive services for users through distributed and collaborative operations. These are based on sensors and network-enabled. We need to provide an adequate level of protection. For intelligent building surveillance, a smart wireless home security technique called Zigbee, which includes Bluetooth and Wi-Fi, is used. By combining the features of Zigbee and sensors, we can secure data [29, 33]. A secure chip is implemented in a smart card like a credit card which contains high strength encryption algorithms [20] that can secure information in user side. So, it is a user authentication process. Cloud of Things (CoT) is as same as the IoT and provides monitoring and control. The security scheme is implemented on cloud, this virtual layer can drive the home area network (HAN), and it secures the information [2, 3, 22]. By using three levels of Kerberos authentication, security can be increased in the smart home system on the server side [12]. To reduce the cyber-attacks while accessing the appliances through the Internet, TOR is used [14].

Based on passwords, the two-factor authentication cannot be able to give efficient security between different devices and servers connected through IoT. This can be solved with biometrics and cryptography because everyone has unique biometrics and cryptography identity [15]. The smart home system can enhance security through the voiceprint verification method [28]. We need to differentiate the security and privacy issues. Sensors and devices based on IoT should communicate securely with the controller so that he can communicate with legal users. MAC is used by the communication protocol to provide the message morality [31]. By the symmetric encryption scheme, the data is secured while transmission with security keys is being generated by chaotic systems and message authentication codes (MAC).

It performs user authentication. It is unnecessary to monitor all the time in the absence of human at some places like bank vaults. By using the PIR sensor, we can detect humans. In the presence of a human, the Raspberry Pi operates and controls

the video cameras sensing, so that all data gets recorded for future use [16, 18]. Lightweight and secure key management schemes are proposed as security is not provided by the interconnected devices [25].

To overcome the load alteration attacks and price integrity, an intrusion detection system (IDS) is developed [30]. According to the International Data Corporation, every house generated 2 TB data on average by 2014, and it can be increased to 10 TB by 2020. This huge amount of volume cannot be stored by a cloud. So, a fog computing based on Zigbee protocol is used. It is more efficient and leads us to implement house energy management system [7].

The time required to process the data in fog computing is shorter than cloud computing. Several new attacks occur on voice interface which leads to unauthorized access by the intruder. It can be overcome by the novel voice liveliness detection system [23]. Nowadays, big companies are investing a huge amount on devices under IoT for better comfort security and safety. To do betterment in existing protocols, they study and research on them [26]. Some of the security issues of the IoT system are present on the security layer with small devices. To secure this, a hybrid cryptosystem is used, for key exchange, ECDH is used, and for the encryption–decryption process, ATS is used [4]. In case of any intrusion in home, temples, colleges, offices, etc., . . . an alarm is raised so the neighbouring people will know about the intrusion. This can be done by IoT smart security system called Theft Control Unit (IoT-TCU) [6].

Due to the development of new devices under IoT, the user wants to secure and protect its advanced information services. So, a smart hub is proposed which is implemented with evolutionary algorithms whose main focus is to give intelligent protection against attacks or intrusions [9]. A two-security system is designed which is a wireless sensor-based, one for internal security like home and the other for external security like open areas [8]. It is more efficient than CCTV cameras. It ensures the safety of life and wealth. A firewall [27] is used to ensure security from Internet threats. Thus, the intruder cannot reach smart devices. A Vigilia [32] is a new technique to secure smart home, and it restricts the accessing of a network. Access of network is possible only when the user has a clear configured application to a specific device. We can control the devices through Xenia, a secure smart home platform and an intelligent agent who has human traits like voice or text chatting [10]. The accessing of IoT devices in smart home through a smartphone, increases the workload on the phone. So, based on an authentication scheme, physical unclonable function (PUF) is implemented for session key [24]. When users remotely access the devices, then the users should authenticate themselves with many protocols which are inconvenient. Then that (IFTTT) scheme is proposed [21].

3 Existing Techniques

3.1 Security System Using Zigbee

This system is used for an unlimited range of communication securely. The Zigbee modules called XBEE devices [29] are used to implement this system. All these devices are working as end devices using XCTU software. These are placed in different areas like on doors, windows, along with sensors like magnetic contact door sensors and PIR sensors are connected such that the sensors monitor the home all the time. These end devices are configured with routers which are intermediate nodes. The sensor monitors all the time, and in case of any security issues happened it transmits the reports from one node to other safely. Even the coordinator is far, through several hops. If any intrusion is detected, then coordinator gives an alarm to alert the owner and sends a message him using GSM. The user can get the image of the unknown person and alert to user mobile phone by using client server-based home automation [5].

3.2 Symmetric Encrypted Scheme with Secret Keys

Smart house architecture consists of some groups in which agents work on different issues like an appliance status, monitoring, controlling and user interfacing. The current appliances status is sent to controller by appliance group of agents. To ensure security and privacy, we use lightweight securely and privacy-preserving communication protocol that uses encryption and message authentication codes (MAC) [25, 31]. As the computing power of the agent is limited, an asymmetric cryptographic system which is used for encryption of transmitted data is used. The secret keys and MAC calculations are generated by two different disorganized systems. So, they are highly secure and efficient. So, the requirement of memory is reduced, and key management becomes easier.

3.3 Smart Surveillance Monitoring System

Everyone wants their valuables to be safe and secure. So, video surveillance is used. But it is not worth to monitor continuously because it is a waste of power consumption and storage space for the footage [16]. By using the PIR sensor [18], when there is a human detection, then it activates the surveillance as it contains a triggering circuit and records the video. It transmits the video through the Internet to smartphones. A live stream can be done with WAN or different LANs. By using the background subtraction algorithm called visual background extractor (ViBe) [16], we can detect motion in red alert zones, the places where valuables are placed. An alert and video

recorded are sent to the user. So, it is easy to trace the intruder. Video footage can be secured by Blowfish encryption and decryption algorithm.

3.4 Authentication System Using Voiceprint

This system architecture consists of two subsystems. One system is the mobile authentication system which is nothing but a voiceprint app in mobile, and the other is the home device control system. These are linked by the virtual private network (VPN) which provides safety during transmission of data. To control the devices with a legal identity, the user should sign in the app. The user must enrol the app by using his voiceprint. This app combines the Gaussian mixture model (GMM) with universal background model (UBM) [28]. Using GMM, a ratio score is implemented in verification. If the score is more, then it detects as he is the user with a legal identity. If the score is less, then it detects them as an intruder.

In a control system, all the systems at home are connected to the Raspberry Pi which has normal functions of the computer, but it is in small size. It is connected to the authentication system through a VPN. For accessing the devices, the Raspberry Pi links all the devices through general-purpose input/output port (GPIO). Through this port, control signals get transmitted between them. If the output signal is high, then the switch will be ON, and devices act as per the user requirement. If the output signal is low, then the switch is OFF, and the devices are in OFF condition.

3.5 Biometric-Based IoT System

Biometric-based IoT system [15] requires an end to end security as the information passes through different layers.

3.5.1 Device Layer

It consists of smart devices and biometric sensors. These will help us to collect the data related to the user through smart things. The device layer senses the required information through biometric sensors. And this sensed data is given to the server through the communication layer. As the information is not encrypted yet, we should protect it through traditional techniques.

3.5.2 Communication Layer

The sensed data from the device layer is transmitted to data centres present in the cloud layer. Here, the smartphone is used as a key for communication between

the smart things and cloud through communication technologies like Wi-Fi, Bluetooth, Zigbee, satellite and machine to machine communications (M2M). When they are connected to the cloud through the Internet, hackers can attack. So, the data is encrypted here.

3.5.3 Cloud Service Layer

The IoT devices and smart things get connected to the private cloud through short-range communication technologies. The public cloud (e.g. Amazon, Google) has remote-based data centres, and they can connect to both short- and long-range communications. The pairing of smart biometric devices with the cloud-based solution can be the present authentication process. But users are concerned about their sensitive data stored in a public cloud, and there may be unauthorized access to their data. There must be some mechanism to avoid replay attack and ensure security. So, pairing-based cryptography is used for security.

3.5.4 Application or Service Layer

The developers can create different applications or services like health care, home care, social media services and emergency service through different application programming interfaces (APIs). The device layer can connect directly to the service layer. This layer should be protected from feature extractors and replay attack. So, these biometric-based IoT systems ensure more security compared to password-based devices.

3.6 *Three-Level Kerberos Authentication*

It is a three-level process, and it is designed for more security [12].

3.6.1 Level 1

The user has to login to the server, as he wants to monitor and control his smart house. To login, the server requests the user to put his registered username and the correct password. By encrypting, the string that contains user ID, password and time stamp sends it to the key distribution centre for authentication. By using the Secure Hash Algorithm (SHA1), the string is encrypted.

3.6.2 Level 2

By decryption and comparing the entered username and registered username in the database, the authentication finds whether the user is authenticated or not. If the user is authenticated, then the password gets hash using the SHA1 algorithm. The server replies with a key generated and a ticket for service. It also checks the time stamp with login time to secure from viruses. If the time taken is more, the server does not provide any service.

3.6.3 Level 3

As the key is in encrypted form, the AS will collect and apply the SHA1 hash for all the data of profile. The password is the combination of profile and time. By using the secret key which is generated by the server or ticket-granting server (TGT), the user can access the service. The final data also gets encrypted by using the final key. A ticket generated by TGT is also in encrypted form and contains clients IP address, client ID and server IP address. If the user IP address changes, then the user gets logoff automatically, and then the devices get OFF. Households can get monitored and controlled easily and safely.

4 Result

To ensure security for smart home, many techniques are proposed for different security challenges. LabVIEW statechart model provides reliable, low cost, low power consumption for data acquisition. Zigbee gives an unlimited range of communication. Using the cloud, we can host home energy management by the secure scheme for HAN. While using online services, the three-level Kerberos authentication process gives more security. And infrastructure based on biometrics is better than devices based on passwords. For fast home authentication and more security, voice and Internet-based authentications are used. Human-centric safe and framework scheme is for elders to live independently and proactively. WiVo is a two-factor authentication method, and it verifies the voice commands and determines whether that is user voice or spoof voice. Privacy communication protocol for home automation can be provided by symmetric encryption scheme with secret keys generated by jumbled systems. While using cameras for security to record the things, then using PIR motion detection sensor provides low power consumption, decreases the required storage space for recording and reduces the need for manual labour (Table 1).

Table 1 Comparison of references

Technique used	Parameter achieved
LabView statecharts and tag4M device can be used, to realize monitoring and control system [11]	Reliable, low cost, low power consumption generates alarm during an intrusion
A smart and contemporary home security system called Zigbee [29]	Provides an unlimited range of communication in the house, low power, reliable
A secure scheme for home area network (HAN) based on CoT [2, 22]	Home energy management system can be hosted by the cloud, and the data can be transmitted securely
Three-level Kerberos authentication process [12]	More secured while using online services
Infrastructure for biometrics based on end to end secure solutions [15]	Better secure than appliances based on passwords
Authentication system using voiceprint and modified voiceprint verification [28]	Fast smart home authentication and more secure. Modified verification can reduce the false rejection rate
Human-centric safe and secure framework by utilizing cyber technologies [17]	To assist elderly persons to live life independently and proactively
A novel wireless signal-based voice liveness detection framework called WiVo. During the spoofing attacks, it is used [23]	It verifies the liveness of voice commands and determines whether it is the user voice or spoofing voice
Symmetric encryption scheme with secret keys being generated by jumbled systems [25]	Energy-efficient, a secure and privacy-preserving communication protocol for home automation
PIR motion detection sensor to activate the smart camera [16, 18]	Less power consumption and decreases the required storage space for recording reducing the need for manual labour
Like if this then that (IFTTT) and key agreement [21]	Mutual authentication is present between the users and the server. To minimize the threat from the server, an anti-tracking is designed

5 Applications

Smart home automation system ensures security and makes the user life easier. The user wants to monitor and control his smart home. The user can monitor and control the devices at every layer of the communication layer through some authentication processes. If an intruder enters into the smart home, then the smart surveillance system generates an alarm and sends message alert to the owner. While operating the devices through public server, then key management system secures the user data as there is a chance of hacking.

The user can use his voice to operate the devices securely. We can also detect the spoof voice in case any fraud wants to enter into the home. So, the smart home with IoT devices can help the users in many ways like smoke detection, intrusion detection, security cameras, smart door locks which provide security and intimate the user and alert him through sending messages or generating alarms.

6 Conclusion and Future Scope

We discussed some of the techniques used for securing the smart home while controlling and monitoring it. These techniques are making use of some sensors, algorithms according to the security challenge and wireless networks. These techniques help us to achieve some features like low power consumption, less storage space for recording data, reduce the manual work, to detect the intruder and remote accessing. The authentication process is done at every level of communication. So, the information will be transmitted securely.

New security challenges can come through these developed techniques which give a way to the hacker to attack our data. In the future, the methods should be more efficient and user-friendly. When the user was habituated to the smart home, then he wants more smart devices implemented at home. So, the use of IoT devices increases and communication between devices also increases. As a result, security breaches increase. So, future work must be efficient to reduce security breaches. The possibility to record remote settings using a browser has to implement in the future.

References

1. Adiono, T., Manangkalangi, B.A., Muttaqin, R., Harimurti, S., Adjarto, W.: Intelligent and secured software application for iot based smart home. In: 2017 IEEE 6th Global Conference on Consumer Electronics (GCCE), pp. 1–2. IEEE (2017)
2. Alohal, B., Merabti, M., Kifayat, K.: A cloud of things (cot) based security for home area network (han) in the smart grid. In: 2014 Eighth International Conference on Next Generation Mobile Apps, Services and Technologies, pp. 326–330. IEEE (2014)
3. Babu, V.S., Kumar, U.A., Priyadarshini, R., Premkumar, K., Nithin, S.: An intelligent controller for smart home. In: 2016 International Conference on Advances in Computing, Communications and Informatics (ICACCI), pp. 2654–2657. IEEE (2016)
4. Bandung, Y., et al.: Design of secure iot platform for smart home system. In: 2018 5th International Conference on Information Technology, Computer, and Electrical Engineering (ICTACEE), pp. 114–119. IEEE (2018)
5. Brundha, S., Lakshmi, P., Santhanalakshmi, S.: Home automation in client-server approach with user notification along with efficient security alerting system. In: 2017 International Conference On Smart Technologies For Smart Nation (SmartTechCon), pp. 596–601. IEEE (2017)
6. Chandrappa, D., Pavan, H., Sagar, M., Dakshayini, M.: Iot security solution to avoid theft. In: 2018 International Conference on Wireless Communications, Signal Processing and Networking (WiSPNET), pp. 1–3. IEEE (2018)

7. Chen, Y.D., Azhari, M.Z., Leu, J.S.: Design and implementation of a power consumption management system for smart home over fog-cloud computing. In: 2018 3rd International Conference on Intelligent Green Building and Smart Grid (IGBSG), pp. 1–5. IEEE (2018)
8. Chowdhury, F.H., Shuvo, B., Islam, M.R., Ghani, T., Akash, S.A., Ahsan, R., Hassan, N.N.: Design, control & performance analysis of secure you iot based smart security system. In: 2017 8th International Conference on Computing, Communication and Networking Technologies (ICCCNT), pp. 1–6. IEEE (2017)
9. Del Pozo, I., Cangrejo, D.: Creating smart environments: analysis of improving security on smart homes. In: 2018 IEEE 6th International Conference on Future Internet of Things and Cloud (FiCloud), pp. 303–310. IEEE (2018)
10. El Mougy, A., Khalaf, A., El Agaty, H., Mazen, M., Saleh, N., Samir, M.: Xenia: Secure and interoperable smart home system with user pattern recognition. In: 2017 International Conference on Internet of Things, Embedded Systems and Communications (IINTEC), pp. 47–52. IEEE (2017)
11. Folea, S., Bordencea, D., Hotea, C., Valean, H.: Smart home automation system using wi-fi low power devices. In: Proceedings of 2012 IEEE International Conference on Automation, Quality and Testing, Robotics, pp. 569–574. IEEE (2012)
12. Gaikwad, P.P., Gabhane, J.P., Golait, S.S.: 3-level secure kerberos authentication for smart home systems using iot. In: 2015 1st International Conference on Next Generation Computing Technologies (NGCT), pp. 262–268. IEEE (2015)
13. Han, J.H., Jeon, Y., Kim, J.: Security considerations for secure and trustworthy smart home system in the iot environment. In: 2015 International Conference on Information and Communication Technology Convergence (ICTC), pp. 1116–1118. IEEE (2015)
14. Hoang, N.P., Pishva, D.: A tor-based anonymous communication approach to secure smart home appliances. In: 2015 17th International Conference on Advanced Communication Technology (ICACT), pp. 517–525. IEEE (2015)
15. Hossain, M.S., Muhammad, G., Rahman, S.M.M., Abdul, W., Alelaiwi, A., Alamri, A.: Toward end-to-end biomet rics-based security for iot infrastructure. IEEE Wirel. Commun. **23**(5), 44–51 (2016)
16. Jain, A., Basantwani, S., Kazi, O., Bang, Y.: Smart surveillance monitoring system. In: 2017 International Conference on Data Management, Analytics and Innovation (ICDMAI), pp. 269–273. IEEE (2017)
17. Jin, Q., Wu, B., Nishimura, S., Ogihara, A.: Ubi-liven: a human-centric safe and secure framework of ubiquitous living environments for the elderly. In: 2016 International Conference on Advanced Cloud and Big Data (CBD), pp. 304–309. IEEE (2016)
18. Kumar, J., Ramesh, P.R.: Low cost energy efficient smart security system with information stamping for iot networks. In: 2018 3rd International Conference On Internet of Things: Smart Innovation and Usages (IoT-SIU), pp. 1–5. IEEE (2018)
19. Lee, C., Zappaterra, L., Choi, K., Choi, H.A.: Securing smart home: Technologies, security challenges, and security requirements. In: 2014 IEEE Conference on Communications and Network Security, pp. 67–72. IEEE (2014)
20. Lee, Y.S., Kim, E., Kim, Y.S., Jeon, H.Y., Jung, M.S.: A study on secure chip for message authentication between a smart meter and home appliances in smart grid. In: 2013 International Conference on IT Convergence and Security (ICITCS), pp. 1–3. IEEE (2013)
21. Lyu, Q., Zheng, N., Liu, H., Gao, C., Chen, S., Liu, J.: Remotely access “my” smart home in private: an anti-tracking authentication and key agreement scheme. IEEE Access **7**, 41835–41851 (2019)
22. Manimuthu, A., Ramesh, R.: Privacy and data security for grid-connected home area network using internet of things. IET Netw. **7**(6), 445–452 (2018)
23. Meng, Y., Zhang, W., Zhu, H., Shen, X.S.: Securing consumer iot in the smart home: architecture, challenges, and countermeasures. IEEE Wirel. Commun. **25**(6), 53–59 (2018)
24. Muhal, M.A., Luo, X., Mahmood, Z., Ullah, A.: Physical unclonable function based authentication scheme for smart devices in internet of things. In: 2018 IEEE International Conference on Smart Internet of Things (SmartIoT), pp. 160–165. IEEE (2018)

25. Naoui, S., Elhdhili, M.E., Saidane, L.A.: Lightweight enhanced collaborative key management scheme for smart home application. In: 2017 International Conference on High Performance Computing & Simulation (HPCS), pp. 777–784. IEEE (2017)
26. Ray, A.K., Bagwari, A.: Study of smart home communication protocol's and security & privacy aspects. In: 2017 7th International Conference on Communication Systems and Network Technologies (CSNT), pp. 240–245. IEEE (2017)
27. Rehman, S., Gruhn, V.: An approach to secure smart homes in cyber-physical systems/internet-of-things. In: 2018 Fifth International Conference on Software Defined Systems (SDS), pp. 126–129. IEEE (2018)
28. Ren, H., Song, Y., Yang, S., Situ, F.: Secure smart home: a voiceprint and internet based authentication system for remote accessing. In: 2016 11th International Conference on Computer Science & Education (ICCSE), pp. 247–251. IEEE (2016)
29. Sabeel, U., Chandra, N.: A smart and contemporary home security system using 802.15. 4 standard. In: 2013 5th International Conference and Computational Intelligence and Communication Networks, pp. 374–379. IEEE (2013)
30. Saghezchi, F.B., Mantas, G., Ribeiro, J., Al-Rawi, M., Mumtaz, S., Rodriguez, J.: Towards a secure network architecture for smart grids in 5g era. In: 2017 13th International Wireless Communications and Mobile Computing Conference (IWCMC), pp. 121–126. IEEE (2017)
31. Song, T., Li, R., Mei, B., Yu, J., Xing, X., Cheng, X.: A privacy preserving communication protocol for iot applications in smart homes. *IEEE IoT J.* **4**(6), 1844–1852 (2017)
32. Trimananda, R., Younis, A., Wang, B., Xu, B., Demsky, B., Xu, G.: Vigilia: Securing smart home edge computing. In: 2018 IEEE/ACM Symposium on Edge Computing (SEC), pp. 74–89. IEEE (2018)
33. Vivek, G., Sunil, M.: Enabling iot services using wifi-zigbee gateway for a home automation system. In: 2015 IEEE International Conference on Research in Computational Intelligence and Communication Networks (ICRCICN), pp. 77–80. IEEE (2015)

Utilization of the Internet of Things in Agriculture: Possibilities and Challenges



P. Mani Sai Jyothi and Durgesh Nandan

Abstract Agriculture is the backbone of most of nation. A nation's economy mostly depends upon the growth of agriculture. It is a combination of several processes which include a lot of manpower and hard work. Internet of things (IoT) is the process of connecting several devices over a single network. It ensures the connectivity of several devices. Data can be transferred easily from one device to the other. Hence, the integration of IoT with agriculture seems to be an effective way to improve the productivity of agriculture. It reduces the problems faced by the farmers thereby increasing the profits. Agriculture seems to be a risky job as it mainly depends upon the unpredictable environmental conditions. During the production process, IoT devices like sensors could be used to monitor the environmental factors periodically and thereby take the remedial action. Harvesting is another phase in agriculture which involves much labour. But with the application of IoT, robotic arms along with few sensors could be used to harvest the crop. With the use of RFID technology, we could easily collect the data regarding the product from time to time. During the process of packing and grading, a few sensors which detect the ripe crop could be used. While transporting the produce to the required location, IoT plays a major role. The products could be tracked easily by using GPS and the products reach the destination without any wastage. Even after reaching the retail stores, IoT makes the job of the retailer easy by regularly giving the data about the products available to the server so that the order could be placed easily. So, IoT helps to observe and study the complete cycle of agriculture from the process of growing the crop to selling. The existing techniques of IoT in agriculture are briefly explained in this paper.

P. Mani Sai Jyothi

Department of ECE, Aditya Engineering College, Surampalem, India

e-mail: nanaji698@gmail.com

D. Nandan (✉)

Accendere Knowledge Management Services Pvt. Ltd., CL Educate Ltd., New Delhi, India

e-mail: durgeshnandano51@gmail.com

Keywords IoT · Agriculture · Polyhouse · Cloud computing · RFID tags · Robotic arms · Global positioning system (GPS) · Sensors · Cold storage · Digitalization · Supply chain management (SCM)

1 Introduction

Internet of things (IoT) helps to connect humans to electronic devices through the use of a network. This helps to make the life of mankind comfortable and free. The use of IoT in agriculture could yield fruitful results. It helps to overcome the problems of the farmers and other agriculture-related workers by easing their work. The employment of IoT in agriculture in processes like growing the crop, harvesting, storage, transportation, marketing and retailing makes it easy for the farmers and the intermediaries to perform their tasks effectively and in a profitable manner. The digitalization of agriculture [29], i.e monitoring of crop stock, etc., through the use of PDA [28] or some such device proves to be useful.

The different phases of agriculture using the Internet of things are shown in Fig. 1. In the process of cultivation of the crop, there are many factors which determine the yield such as fertility of the soil [32], pH content of the soil, irrigation of the crop [12, 31] and also the leaf size and pattern. These factors can be monitored effectively with the help of IoT. Soil conductivity can be determined with the help of conductivity sensors and some such devices [2]. By taking care of the crop in the initial stage by monitoring the above-mentioned factors helps the farmers to get more crop to hand.

After the process of cultivation, the next task is to harvest the crop. During harvesting, IoT can be used to take care that no crop is wasted. The entire production is obtained effectively without any drawbacks. The role of agents and other intermediate people can be reduced to the maximum level by using IoT. During the transportation of this harvested crop, IoT helps us to ensure that the right temperature and humidity are maintained in the vehicles used for transportation.

The next process is the storage of this production. To monitor the stock in the warehouse, we may make use of RFID tags [33], which can be used to effectively collect the data regarding the available stock in the warehouse [8]. There are many ways and methods to regulate the data acquired by RFID and other IoT devices. The stock from the warehouse is then sent to the retailers. The marketing of the crop more profitably can be done with the help of IoT-based services. Securing these systems also plays a prominent role in this process [15]. The regulation of stock in the stores can be done efficiently by employing the tools of IoT. Periodically the stock can be monitored in the stores with the help of RFID tags. Hence in this way in the field of agriculture, from the initial process of cultivation to the final process of selling, IoT plays an important role. It helps to reduce the number of agents in the chain of agriculture and thus proving to be economical for the farmers as well as the end consumers. In this paper, the applications of IoT in different phases of agriculture are studied. The brief overview of the process of agriculture using IoT-based devices is described in Sect. 2. The existing techniques related to IoT which help to improve

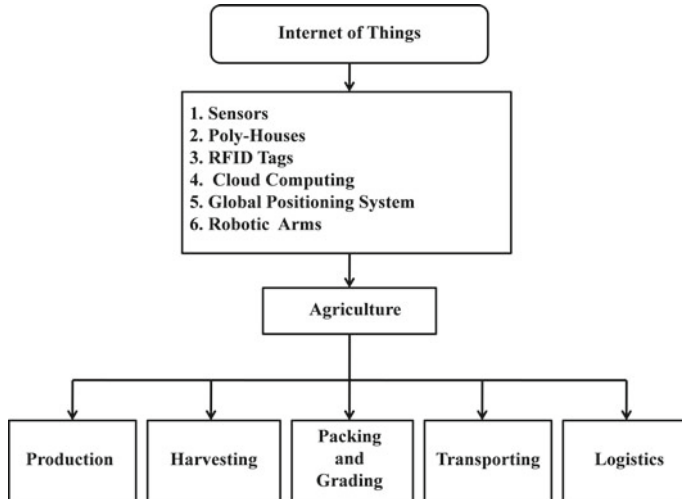


Fig. 1 Different phases of agriculture using the Internet of things

the productivity of the agricultural process are described in Sect. 3. The different experimental set-ups used and the parameters achieved are compared in Sect. 4. The different applications of using IoT in agriculture are listed in Sect. 5. Finally, in Sect. 6, the functionalities of different IoT devices and their importance to farmers are briefly explained. The developments to be achieved in this area are also described.

2 Literature Review

Internet of things (IoT) is a way to connect numerous devices and sensors via a network. It helps in the transfer of data from one device to another. Agriculture is a complex job which includes numerous tasks to be performed such as the cultivation of the crop, harvesting, transporting, marketing, delivering the product to the retail stores. In this process, we can observe that there is a lot of wastage. To reduce this wastage and optimize the agricultural process, IoT must be made a part of the agricultural process [35]. With the growth in the population, the need for adopting smart agriculture [22, 29] is also increased. IoT includes the use of several existing technologies like wireless sensor networks, cloud computing, data analytics, etc [7]. The importance of IoT devices in every stage of the agricultural process can be described as under.

2.1 During Cultivation of the Crop

To get fruitful production, the cultivation must take place in friendly environmental conditions. The soil moisture [15], pH of the soil [2], nutrients content [32], humidity and the temperature must be monitored from time to time [3, 4, 6, 12, 25, 31]. Greenhouses [21] can be used to protect the crop from different adversities such as storms, heavy rains and pest attacks, [14]. Best quality products can be obtained through the use of polyhouses [27]. Polyhouses include different sensors connected through Wifi or Bluetooth to the main server. The data acquired by the sensors is transferred to the server and accordingly, the factors are adjusted. For example, the temperature can be monitored through the use of temperature sensors and the data is sent to the server which changes the temperature accordingly [6, 12]. The central receiver stores the complete data regarding all the actions which can be helpful to analyse the process effectively.

2.2 Harvesting

The process of harvesting is carried out with the help of robotic arms and sensors. These sensors help us to detect the ripe crop by examining the colour and shape of the produce. The crop is then harvested. The harvested crop is stored in baskets and labelled using RFID tags and beacons [33]. Sensors are used to detect if the basket is full and then an empty basket is taken and the procedure is repeated. The produce is then transported using conveyor belts and sent for the process of grading.

2.3 Packaging

The produce sent for grading is unloaded and is manually checked if there is any unripe or damaged produce. After this process of grading, the product is packed according to the demand. The packed produce is then labelled and shipping address is specified on each package and sent in large amounts to the cold storage. Supply chain management (SCM) system [26] plays an important role in deciding which packages should be clubbed in which refer vehicle along with route plan for that vehicle.

2.4 Transporting

The referred vehicles usually carry 10–15 tons of products which supply to different areas [27]. It includes sensors which monitor the temperature inside the vehicle and send the data to the central server. If the temperature is not as desired, then the driver

is notified to correct it, but in case, if it is not possible, then the central server notifies the driver about the nearest possible storage location. When the produce is unloaded, the RFID tags will detect the data about the pallets and send the data to the server. In this way, the server will gather the data about the pallets unloaded and the time at which they are unloaded.

2.5 *At the Retail Stores*

The produce is unloaded at the retail stores [20] and is arranged in the shelves at the store. The RFID tags help to give the details of the product on the shelves. It helps to know when the stock is low with the retailer and supply accordingly [13]. The RFID tags give the data regarding the product to the analytic server which is used to estimate the quantity of the product required in future to supply accordingly.

The above-mentioned procedures include a lot of data which have to be processed and managed efficiently [5]. The data must be carefully analysed using proper methods which will give fruitful results. Hence, IoT helps the farmers to get good products and reduces the burden of costs on end consumers by reducing the number of agents in the supply chain.

3 Existing Techniques

IoT helps to simplify the process of agriculture by reducing manual work and increasing smart work. Some of the technologies which help to increase productivity and simplify the process of agriculture are as given below:

3.1 *Polyhouses*

A polyhouse is a building or structure which can be used to grow plants or crop under suitable environmental conditions [27]. It is usually made of steel and covered with polythene which allows natural light to enter. The interior of the poly house gets heated up due to the radiation from the sun. The warmth of the air inside the building gets retained by the roof and wall. Apart from temperature, humidity, as well as ventilation, can be controlled by using the devices in the polyhouse. In this way, polyhouses can be useful to control the factors affecting production. These also help in reducing the pest attacks on the crop. Nowadays, in agriculture, polyhouses include a lot of IoT-based devices such as sensors, beacons, wifi modules and central receiver. The polyhouse consists of a central receiver to which several sensors like soil conductivity sensor [2], pH sensor, humidity sensor, temperature sensor, etc., are connected via a network [3]. The sensors periodically monitor the environmental

conditions present in the polyhouse and send the data to the central receiver, which uses that data to control the factors affecting the growth of the crop accordingly. In this way, the polyhouses using IoT-based devices help to improve the quality of the produce.

3.2 Robotic Arms

Robotic arms are devices used to replace the hard work of the farmers. These are used to perform the complex and time-taking processes performed by the farmers. Robotic arms perform the manual work much faster and perfect [27]. Some of the functions performed by the robotic arms are:

- Picking and harvesting
- Weed control
- Phenotyping
- Autonomous mowing, pruning, seeding, spraying and thinning
- Sorting and packing
- Utility platforms.

Robotic arms prove to be much useful in the process of harvesting as they increase the accuracy and speed of the process and even reduce the wastage of crop. In the process of harvesting, robotic arms help to get the crop which is ripe enough. The robotic arms take the help of some sensors to identify the colour and size of the crop and accordingly harvest the crop which is ripe enough. The harvested crop or the product obtained is then packed. The robotic arms collect empty baskets and load it with the product; when the basket is filled, then that basket is sent for loading in the vehicle with the help of conveyor belt and again an empty basket is taken. In this way, the robotic arms use IoT to harvest the crop efficiently.

3.3 RFID Tags

RFID refers to radio frequency identification tags which are used to track the items [9, 13, 33]. They use radio frequency technology. The radio waves are used to transmit the data stored in the tags to the readers which are then sent to the computers [34]. An RFID system consists of two main parts—an antenna and a chip. The chip consists of all the information that the reader wants. There are two types of RFID tags: battery-operated and passive. When a reader is used to scan a passive RFID tag, the data from the chip reaches the antenna and the information is then transmitted to the RFID computer for interpretation. These tags prove to be useful in the process of transporting, packing, marketing, etc [20]. The RFID tags are used to get the data of the products loaded in the vehicles during transportation. When the vehicle is unloaded, these tags help in getting the data regarding the produce unloaded. This

data is then sent to the central server. When the product reaches the retail stores and arranged in the shelves, the RFID tags are used to send the data to the server regarding the stock available with the retailer. These tags make the process of supply chain management [17] easier by obtaining the data regarding the product from time to time.

3.4 Sensors

Sensors are devices which are used to measure any parameters or properties such as temperature, moisture [21], humidity, pressure and so on [3, 24, 25, 31]. Apart from moisture and humidity, sensors for measuring wind speed and wind direction are also developed [23]. These are of utmost importance in the IoT technology. In the process of agriculture, these sensors are mostly used in the production phase. The atmospheric conditions near the crop are detected from time to time [12]. For the healthy growth of the crop, the environmental conditions must be favourable. Hence, some sensors are used in the phase of production such as soil conductivity sensor [2] to detect the conductivity of the soil, temperature sensor [12] to detect the atmospheric temperature, moisture sensor [12] to measure the water content in the soil and humidity sensor to measure the humidity in the air around the crop. The data collected by these sensors is then sent to a central receiver using a network. On receiving the data, the receiver takes the required corrective actions, to ensure the healthy growth of the crop. Apart from the production phase, sensors are also used while packing to detect if the baskets are loaded completely or not. Sensors are also used in harvesting to detect the ripe crop by considering the colour and size of the crop. In this way, sensors find many applications in the field of agriculture using the Internet of things.

3.5 Global Positioning System (GPS)

GPS is a satellite-based navigation system which is used to find the position of an object on the earth. In IoT, GPS also plays a key role. In the process of agriculture, GPS is used to send to the central receiver the information regarding the position where the crop is affected by pests or the position where the conductivity of the soil is more, etc. While transporting the produce, GPS is used to detect the position of the vehicle. If the temperature inside the vehicle fluctuates, then the vehicle is to be directed to the nearest cold storage. So to know the nearest cold storage, initially, the location of the vehicle must be known. Hence, in this way, GPS helps in the process of IoT-based agriculture.

3.6 Cloud Computing

Cloud computing [10] is the process of computing that is based on shared computing resources other than local servers or personally handled devices [11, 19, 30]. In the process of digitalization of agriculture, we need to handle a lot of data. This data must be properly disseminated to ensure that there is no problem to be faced in the process of agriculture. Cloud computing is applied in agriculture as follows:

During the growth of the crop—Based on the data retained by using cloud computing, many decisions related to production are taken. Data retained by using cloud computing is shown in Fig. 2.

This database can be used to make the analysis of productivity and thereby make the required plans to overcome the problems in the process of production. Cloud computing enables the automatic analysis of the key problems faced by the plants and the crop.

To analyse the productivity effect of different management measures—Cloud computing helps us to estimate the productivity effects of different management measures using computer simulation techniques and mathematical modelling.

To trace and control the farm produce activity—By using the existing information technology of computers, cloud computing can trace the security of the farm produce from the place of production until it reaches the end consumer. Cloud computing collects the information regarding the produce during the process of selling and logistics like the freezing conditions and delivery, the arrangement of the produce in the shelves of retail stores and sends it to the server. Cloud computing also acts as a ready source of information to the customers regarding where the product is present and to track it easily.

To monitor the growing plant—Cloud computing enables to monitor the growth of the plant by identifying the pattern and it helps to dynamically monitor the growth of a plant using other devices (Table 1).

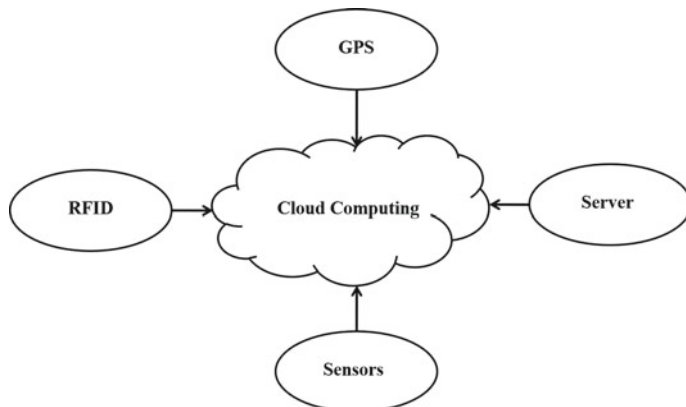


Fig. 2 Data retained by using cloud computing

Table 1 Different experimental set-ups used for agriculture based on IoT

Experiment set-up	Parameter achieved	Improvement required
Image recognition using OpenCV [27]	An efficiency of 60–65% was achieved	Use of IR sensor with location detection could be used
Agricultural production system using IoT technology and implemented as GUI visualization software [16]	Improved quality of agricultural products	IoT data must be processed efficiently for generating various products
Customized sensor node on top of TinyOS 2.x [18]	The requirement in terms of reliability, cost and application-specific features was met	Solar power must be used to the existing sensor nodes to make them operate for a long time
PTC Thing Worx composer [1]	To enable easy access to sensor data and to predict the location of the agro robot by knowing the coordinates obtained by GPS	Addition of real-time interface to the described system
ARM 7 processor along with the sensors (temperature, humidity and water level) [24]	Easy to access and control the agricultural production and saving the input materials, improving efficiency, productivity and profitability in farming production system	The system must be further developed to detect the probability of disease in advance
ESP8266, RFID tags and RFID readers [26]	Information about the products is given to the farmers avoiding intermediaries thus increasing the profits	Instead of RFID tags and readers, EPC technology could be used

4 Result

When IoT is used as a graphical user interface (GUI) visualization software, it helps the farmers to study the entire cycle of agriculture from growing the crop to selling it. It hence helps the farmers to analyse the growth of the crop. This proves to maximize the profits of the farmers. It also helps to improve the quality of the products. When ARM7 processor is used with sensors such as temperature sensor, humidity sensor and soil conductivity sensor, the access of the farmers to the process of production increases. Using these, the environmental conditions near the crop can be predicted and thus accordingly, the parameters affecting the crop growth can be modified. PTC ThingWorx composer is used to enable easy access to the sensor data and it helps to know the coordinates of the agro robot which is used in the process of production of the crop. Use of customized sensor nodes in the process of production increases the reliability, reduces the cost and also increases the efficiency. To recognize the efficiency of identification of ripe crop during harvesting, OpenCV can be used. The efficiency of identification achieved by using this device is 60–65%. RFID technology used along with ESP8266 Wi-Fi module gives the information to the farmers about the products easily by eliminating middlemen.

5 Applications

The process of adopting IoT into an agricultural process is proved to have numerous advantages. It helps to minimize the manual work and thereby increasing efficiency and profits. It has the following applications:

- To monitor the soil fertility regularly.
- To analyse the environmental conditions such as temperature, humidity and pH.
- In some cases, the IoT devices are used to predict the weather conditions thereby helping the farmers to reduce the loss.
- To detect the pests and weeds initially to lessen their effect.
- The data obtained through IoT devices helps the farmers to analyse which crop gives more yield in that area.
- Wastage during the process of harvesting can be reduced.
- Manually cutting the crop is eliminated and hence, the tiresome work is not required to be done by the people.
- Packing the product obtained will be easy.
- During the process of transportation, it will be easy for the customers as well as the retailers to track the order.
- Time frame and cost will be reduced.

6 Conclusion

In this paper, we discussed how IoT technology applied in the field of agriculture proves to be fruitful. The agricultural process can be simplified by using IoT devices. Due to the use of IoT technology, the rate of production increases. The efficiency and profits earned by the farmers also increase. With the use of sensors in the production process, we can ensure healthy growth of crop by monitoring the environmental factors affecting the growth. By using RFID tags, the access to the data related to products increases. Tracking of the products during transportation could be made easy. The digitalisation of agriculture also helps the end consumers to know the information related to products regularly. In this way, IoT in agriculture proves to be advantageous to the farmers as well as end consumers.

Data obtained in this process is very large. The process proves to be advantageous if and only if this data is carefully accessed. Hence, in future, new methods which help in the process of data dissemination have to be proposed. The methods should be such that they are easily understandable by the farmers. The efficiency of sensors used for the identification of crop is usually low. Hence, the design of the sensors must be improved such that the efficiency increases at least up to 90%. The work to improve new methods must be catalysed so that the problems of the farmers can be reduced.

References

1. Akash Raj, N., Srinivasan, B., Deepit Abhishek, D., Sarath Jeyavanth, J., Vinith Kannan, A.: IoT based agro automation system using machine learning algorithms. *Int. J. Innov. Res. Sci. Eng. Technol.* (An ISO 3297: 2007 Certified Organization) **5** (2016)
2. Amin, M., Aimrun, W., Eltaib, S., Chan, C.: Spatial soil variability mapping using electrical conductivity sensor for precision farming of rice. *Int. J. Eng. Technol.* **1**(1), 47–57 (2004)
3. Awati, J., Patil, V., Awati, S.: Application of wireless sensor networks for agriculture parameters. *Int. J. Agric. Sci.* **4**(3), 213 (2012)
4. Cambra, C., Sendra, S., Lloret, J., Garcia, L.: An iot service-oriented system for agriculture monitoring. In: 2017 IEEE International Conference on Communications (ICC), pp. 1–6. IEEE (2017)
5. Chawathe, S.S., Krishnamurthy, V., Ramachandran, S., Sarma, S.: Managing rfid data. In: Proceedings of the Thirtieth International Conference on Very Large Data Bases, vol. 30, pp. 1189–1195. VLDB Endowment (2004)
6. Diedrichs, A.L., Bromberg, F., Dujovne, D., Brun-Laguna, K., Watteyne, T.: Prediction of frost events using machine learning and iot sensing devices. *IEEE IoT J.* **5**(6), 4589–4597 (2018)
7. Elijah, O., Rahman, T.A., Orikumhi, I., Leow, C.Y., Hindia, M.N.: An overview of internet of things (iot) and data analytics in agriculture: benefits and challenges. *IEEE IoT J.* **5**(5), 3758–3773 (2018)
8. Fabian, B., Günther, O., Spiekermann, S.: Security analysis of the object name service (2005)
9. Gan, W., Zhu, Y., Zhang, T.: On rfid application in the tracking and tracing system of agricultural product logistics. In: International Conference on Computer and Computing Technologies in Agriculture, pp. 400–407. Springer (2010)
10. Gayatri, M., Jayasakthi, J., Mala, G.A.: Providing smart agricultural solutions to farmers for better yielding using iot. In: 2015 IEEE Technological Innovation in ICT for Agriculture and Rural Development (TIAR), pp. 40–43. IEEE (2015)
11. Jaiganesh, S., Gunaseelan, K., Ellappan, V.: IoT agriculture to improve food and farming technology. In: 2017 Conference on Emerging Devices and Smart Systems (ICEDSS), pp. 260–266. IEEE (2017)
12. Jha, R.K., Kumar, S., Joshi, K., Pandey, R.: Field monitoring using iot in agriculture. In: 2017 International Conference on Intelligent Computing, Instrumentation and Control Technologies (ICICICT), pp. 1417–1420. IEEE (2017)
13. Jia, X., Feng, Q., Fan, T., Lei, Q.: Rfid technology and its applications in internet of things (iot). In: 2012 2nd International Conference on Consumer Electronics, Communications and Networks (CECNet), pp. 1282–1285. IEEE (2012)
14. Kodali, R.K., Jain, V., Karagwal, S.: IoT based smart greenhouse. In: 2016 IEEE Region 10 Humanitarian Technology Conference (R10-HTC), pp. 1–6. IEEE (2016)
15. Laiolo, P., Gabellani, S., Pulvirenti, L., Boni, G., Rudari, R., Delogu, F., Silvestro, F., Campo, L., Fascati, F., Pierdicca, N., et al.: Validation of remote sensing soil moisture products with a distributed continuous hydrological model. In: 2014 IEEE Geoscience and Remote Sensing Symposium, pp. 3319–3322. IEEE (2014)
16. Lee, M., Hwang, J., Yoe, H.: Agricultural production system based on iot. In: 2013 IEEE 16th International Conference on Computational Science and Engineering, pp. 833–837. IEEE (2013)
17. Li, L.: Application of the internet of thing in green agricultural products supply chain management. In: 2011 Fourth International Conference on Intelligent Computation Technology and Automation, vol. 1, pp. 1022–1025. IEEE (2011)
18. Ma, J., Zhou, X., Li, S., Li, Z.: Connecting agriculture to the internet of things through sensor networks. In: 2011 International Conference on Internet of Things and 4th International Conference on Cyber, Physical and Social Computing, pp. 184–187. IEEE (2011)
19. Mekala, M.S., Viswanathan, P.: A novel technology for smart agriculture based on iot with cloud computing. In: 2017 International Conference on I-SMAC (IoT in Social, Mobile, Analytics and Cloud) (I-SMAC), pp. 75–82. IEEE (2017)

20. Nukala, R., Panduru, K., Shields, A., Riordan, D., Doody, P., Walsh, J.: Internet of things: a review from ‘farm to fork’. In: 2016 27th Irish Signals and Systems Conference (ISSC), pp. 1–6. IEEE (2016)
21. Pallavi, S., Mallapur, J.D., Bendigeri, K.Y.: Remote sensing and controlling of greenhouse agriculture parameters based on iot. In: 2017 International Conference on Big Data, IoT and Data Science (BID), pp. 44–48. IEEE (2017)
22. Patil, K., Kale, N.: A model for smart agriculture using iot. In: 2016 International Conference on Global Trends in Signal Processing, Information Computing and Communication (ICGT-SPICC), pp. 543–545. IEEE (2016)
23. Pusatkar, A.C., Gulhane, V.S.: Implementation of wireless sensor network for real time monitoring of agriculture. IRJET) ISSN, pp. 2395–0072 (2016)
24. Rubala, J.I., Anitha, D., Student, P.: Agriculture field monitoring using wireless sensor networks to improving crop production. Int. J. Eng. Sci. **52****16** (2017)
25. Satyanarayana, G., Mazaruddin, S.: Wireless sensor based remote monitoring system for agriculture using zigbee and gps. In: Proceedings of the Conference on Advances in Communication and Control Systems-2013. Atlantis Press (2013)
26. Shambulingappa, H.S., Pavankumar, D.: Application of iot in supply chain management of agricultural products. Int. J. Eng. Develop. Res. (IJEDR) **5**, 863–867 (2017)
27. Shenoy, J., Pingle, Y.: Iot in agriculture. In: 2016 3rd International Conference on Computing for Sustainable Global Development (INDIACoM), pp. 1456–1458. IEEE (2016)
28. Sorathia, V., Laliwala, Z., Chaudhary, S.: Towards agricultural marketing reforms: web services orchestration approach. In: 2005 IEEE International Conference on Services Computing (SCC '05), vol. 1, pp. 260–267. IEEE (2005)
29. Tang, S., Zhu, Q., Zhou, X., Liu, S., Wu, M.: A conception of digital agriculture. In: IEEE International Geoscience and Remote Sensing Symposium, vol. 5, pp. 3026–3028. IEEE (2002)
30. TongKe, F.: Smart agriculture based on cloud computing and iot. J. Converg. Inf. Technol. **8**(2) (2013)
31. Venkatesan, R., Tamilvanan, A.: A sustainable agricultural system using iot. In: 2017 International Conference on Communication and Signal Processing (ICCPSP), pp. 0763–0767. IEEE (2017)
32. Verma, N.K., Usman, A.: Internet of things (iot): A relief for Indian farmers. In: 2016 IEEE Global Humanitarian Technology Conference (GHTC), pp. 831–835. IEEE (2016)
33. Vogt, H.: Efficient object identification with passive rfid tags. In: International Conference on Pervasive Computing, pp. 98–113. Springer (2002)
34. Wasson, T., Choudhury, T., Sharma, S., Kumar, P.: Integration of rfid and sensor in agriculture using iot. In: 2017 International Conference on Smart Technologies for Smart Nation (SmartTechCon), pp. 217–222. IEEE (2017)
35. Zhao, J.C., Zhang, J.F., Feng, Y., Guo, J.X.: The study and application of the iot technology in agriculture. In: 2010 3rd International Conference on Computer Science and Information Technology, vol. 2, pp. 462–465. IEEE (2010)

Study on Real-Time Face Recognition and Tracking for Criminal Revealing



A. Krishna Chaitanya, C. H. Kartheek, and Durgesh Nandan

Abstract Face recognition describes a surface framework, which is capable of processing image and detection. The proposed paper demonstrates three contributions: the first is to introduce the image representation, known as an integral image, the second application of Ada Boost learning algorithm, and the third is the cascaded framework. This includes observation, bio-metrics and video coding. Here, the primary objective is to implement a real-time system using a field-programmable gate array (FPGA) to track and detect human expression. The expression recognition involves colour-shaped coating separation and image purifying. Moreover, it involves different types of search engines which are based on computer vision. A computer controls Pan Tilt Zoom (PTZ) cameras in CCTV for surveillance systems for the face. The multi-view face tracking on a mobile platform has three methods (local binary patterns) and enhancing procedure. These face detectors are adaptable, extended for multi-opinion face recognition over the revolution ability and face matrix partition scheme is proposed to accelerate the face tracking process.

Keywords CCTV · Criminal detection · Face recognition · Motion analysis · Pattern matching · Skin filter method

A. K. Chaitanya · C. H. Kartheek
Department of ECE, Aditya Engineering College, Surampalem, India
e-mail: chaitanyaammanamanchi@gmail.com

C. H. Kartheek
e-mail: chegodikartheek007@gmail.com

D. Nandan (✉)
Accendere Knowledge Management Services Pvt. Ltd., CL Educate Ltd, New Delhi, India
e-mail: durgeshnandano51@gmail.com

1 Introduction

By criminal detection and tracking, the policemen will be benefited by easy recognition of the criminal's face. In real time, it has a server-clients based on video expression recognition investigation function [1]. It is also applied for detection of the face and tracing by android phone at user sideways and based on video face identification on server-side [1]. First, the police will capture the criminal's photograph using the smartphone camera and send that photocopy to the server which sends the result back to the policemen [2]. To acquire, detect and analyse the face images, many methods are utilized. It is used to identify scenes captured by a camera in a real-world situation; many tracking methods create problems for the exposed research area. The face is traced by different tracking schemes. The distinctive features of the face are implemented by using android studio [1].

To trace the object, optical tributary is used. An algorithm that is based on the previous result of the frame and the optical method of flow extracted by a vital point by their conversion of consequent frames [3]. Android developers develop compatible applications for android users to support bio-metric use as face tracking. Face tracking using handheld cameras must consider blurring effect and also face object android platform has a benefit of open computer vision binary (OpenCV). OpenCV is a collection of software design utilities for concurrent computer visualization. This approach is free for Commercial and academic uses and it has C, C++, Java and soon Python will be introduced to the aAndroid platform [4]. This is the collection of more than 2500 enhanced joint algorithm in image processing for face tracking system [2]. Viola-Jones method is one of the real-time face detectors proposed in 2001. It performs the face detection using a classifier which extracts several windows from the face image [5]. The instantaneous optical flow can be improved by Ada Boost cataract face tracking which objectives are calling the Viola-Jones algorithm for each frame amongst the 20 frames. The likelihood map can also be employed for face detection, which is inserted with optical flow information [6]. The skin shade recognition is an essential topic in computer image research [7].

The situation is reasonable to identify that most relevant method to face detection that is used of colour information, where by calculating area with skin colour is the first step for such type of strategy. Using the skin shade detection technique as a feature for tracking a face has several advantages. Copious of the film colour detection of the face is based on RGB [8]. The camera model is the main part [4]. The high-quality camera model openly effects and be contingent upon the absolute standardization result. That's why, it is most vital to choose the suitable camera prototypical and that makes assured of external and internal limitations. This camera exemplary of regulation procedure in OpenCV is based on pinhole structure [9].

2 Literature Evaluation

In 2004, P. Viola and M. Jones have been described that a face recognition methodology that is accomplished in handling images quickly. Meanwhile, it achieved a high identification rate. Detection of face and tracing is imperative and vigorous subject of research since its efficacy for many claims such that the video observation, video coding and bio-metric [10]. The important objectives of this development are to modify an immediate system on a field-programmable gate array (FPGA) sheet to sense and track the human face. The face recognition methodology complicated colour dependent skin separation and image clarifying and software methods were tested on the stagnant image in MATLAB [1]. Even if the changeover amongst Verilog and MATLAB was not as plane as expected. The investigational result delivers the accurateness and usefulness of immediate system smooth further down other circumstances of hardware could be done in real-time with a smaller amount effort [3]. The recognition-based article delivers powerful and objects recognition rates in the instantaneous projected in 2001 by P. Viola and M. Jones. Even though it could be competent to identify the verity of article modules. There are three main stages.

1. Integral image.
2. Ad boost algorithm.
3. Cascading.

In 2000, the CCTV surveillance system is used for detection of potential criminal activity [9]. The investigation part of the common people openly profitable nearby their usual occupation. It would be apprehension after the experiential movement of specific vehicles as well as the people counterpart somewhat of predefined like apprehensive performance standards automated addicted to the method [2]. Computer Pan Tilt Zoom (PTZ) cameras are used to obtain the video recording (close up) of any vehicles and people and similar sectors at the same time. Automatic surveillance are provided in this system for a different scenario like parking areas commercial areas and housing, etc., and this system is particularly used and suited for the protection of commercial buildings located within the city streets and public areas [11].

In 2016, face detection and tracking suffered from drastic pose variations in the face with limited resources. In this article, a graphic inspection and a real-time face tracking scheme are provided on a portable stage. In this, elementary detector is instructed by confined binary outline as well as improved by the algorithm. This is useful for the multi-view face detection with the help of rotation facility of a local binary pattern. Strong face-mask position elimination procedure and expression medium organization are projected to accelerate the face tracking process [9].

The authors present an interestingly new face tracing method; everywhere visual flow information is integrated obsessed by an adapted form of the Viola and Jones recognition procedure. Detection is static, and information from previous frames is not considered. Additionally, we use CCTV and smartphones to detect and track the face information for security supervision. Tracking capability is provided by generalizing the location of the probability plan to the succeeding frame by the

optical flow figuring. The projected procedure works in real time on the processor at the server sideways and smartphone or tablet on the client-side [5].

The dependency of face-mask changing aspects for the appreciation of face-mask terminologies after the duplicate arrangements is obtainable. The procedures make use of visual flow figuring towards recognizing the path of unbending and non-rigid gestures that is produced by the face-mask expressions. A smooth representative motivated by psychosomatic deliberations is industrialized. Acknowledgement is six face-mask expressions, in addition to eye flashing, established on a great usual of image arrangements [12].

3 Techniques of Criminal Detection Using Video Surveillance

There are few techniques for criminal detection using video surveillance.

3.1 Automatic Detection of Crimes Using Motion Analysis Technique

The proposed method automates the video investigation for criminal cases detection. These type surveillances are known as public security scheme (PSS). If the surveillance camera captures approximately unusual situations such as reward grabbing, kidnapping and aggressive on the way, the public safety system recognizes the circumstances and immediately report to the agency.

There are three different motions; individuals are strong-minded from the video tributary.

- a. The distance amongst the objects

If the camera captures any two objects simultaneously, it will calculate the distance between them.

- b. Moving velocity of the objects

When the camera is capturing a scene, it will also calculate the velocity of the moving objects in that particular scene.

- c. Area of the objects

This will tell about the area covered or occupied by the objects. These characteristics are recycled to regulate human behaviour. Here, crime scene is described using human behaviour [13].

3.2 Real-Time Monitoring Scheme Utilizing the Design Identical Technique

This simple system detects as someone enters the room by associating pattern for each combination of time. Amongst the various design corresponding methods, simple unique is Euclidean distance. If there are some different patterns, the system will blow an alarm [7]. We use a capture application for this purpose. The application can capture the images in a periodic manner and compare the latest image with the previously captured image [14]. This results from the detection of every suspecting objects coming into the scope of the Webcam or closed-circuit television (CCTV). Moreover, the captured videos are not stored to reduce memory preservation [10].

3.3 Tracking People Using Facial Recognition Technique

We use facial recognition very less and we do not have more knowledge about facial recognition system in India. The system employs facial identification for tracking or identifying or searching the target person out of real-time footage, like video footage from the surveillance system [15]. First, the system is captured with the live video footage that has already been scanned in the system will be installed with a set of images like missing image of a person, criminal, etc. Once the system gets installed with these images, a predefined conventional of face-mask appearances is extracted by the contribution video footage by the system, which is provided earlier, then after comparing the images with the video footage, if there is any matching, system will identify and regards the person genuine [6]. This system can also be used for existing surveillance systems. This will reduce the cost and these types of systems are used in an organization like military, police, and a municipal corporation and in large private companies, etc., to track the people [13].



Fig. 1 Example of tracking using facial recognition [16]

Figure 1 explains how facial recognition is done. As we can see a face matching in Fig. 1. The picture is matched with the required image; it will mark the person and report [4].

3.4 Skin Filter Method

In HD videos, low false alarm rate can be obtained by skin filter method and it includes adaptive image resizing founded on previous information of noticeable face dimension is smallest. It avoids the other non-facial (unwanted) regions based on skin filter [17].

Figure 2 explains how the face gets detected and how the skin filter is used in that and how an image gets processed. As we can see two faces in the image, each image has a different structure; based on the structure and pattern the image gets processed [19].

There are three contributes in skin filter technique; first scheme is fast using adaptive down-sizing system (smallest face dimension of texture-based face indicator). Subsequent law to exclude non-facial areas false alarm rate using skin filter. The last type is simple detection using existing face detection scheme [10].

Figure 3 explains how the system works and the process. Here, the first block is a surveillance system then it goes to the detection block where the block contains the process of skin filter, pattern matching and facial recognition [20]. The third block represents the nature of the objects like shape, motion and texture of the object. After all these blocks, finally, the human face gets detected [21].

Figure 4 describes the process of how criminal detection is done using server and database; first, the picture is taken from a mobile phone by the policemen and then



Fig. 2 Example of detection of skin filter [18]

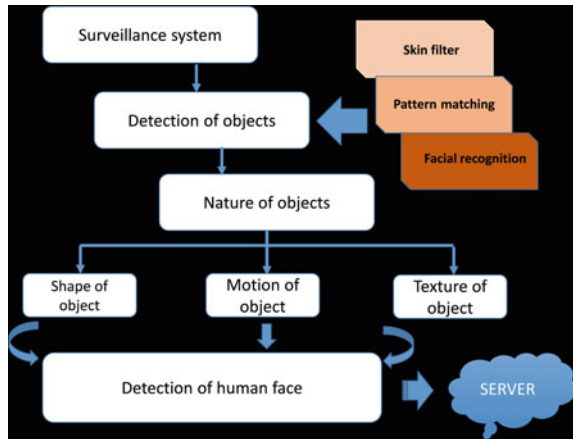


Fig. 3 Block diagram representation

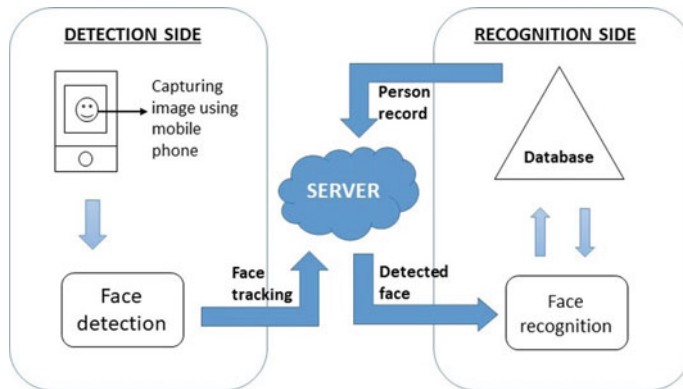


Fig. 4 Framework for detection of criminal

the detection process takes place. The picture is sent to the server and then to the database where all the data is present. Then the picture is compared with different data which is available in the database. If the data is matched or recognized, then record of that person will send back to the policemen.

4 Results and Discussion

Android operating system: Basically, majority of the system is depending upon the android platform. The device (mobile) which we used to capture a picture of a person. And android OS is a user-friendly and very easy to operate such type of works. By using this OS the result will be more accurate.

Pattern matching result: Pattern matching technique is capable of detecting the people by comparing their patterns for every couple of minutes and will trigger an alarm if there is a change in the pattern.

Face detect and tracking result: Face detection and tracking are done by using the android platform and tested on real-time videos. The face detection is used to track or identify a target or identify a target person from real-time video footage with the help of a surveillance system. By this, the complications will be reduced and searching a person will be very easy.

5 Applications

Few most popular applications concluded here.

1. Police surveillance.
2. Military surveillance.
3. Home surveillance.
4. Public sectors.
5. Shopping complexes.
6. Street views.
7. Cost-effective system.

6 Conclusion

In this article, illegal recognition is accessible using CCTV surveillance. This system is detection and in real-time, video-based recognition surveillance. This paper mainly focused on the implementation of the detection side and recognition side face recognition and tracing on android mobile phones. The face implementation provided by OpenCV-library and for tracking stages of detection optical flow has used for detection stage in CCTV surveillance. There are some techniques to follow for a better result like skin filter, pattern matching, and face recognition. By these techniques an accurate results achieved.

References

1. Elrefaei, L.A., Alharthi, A., Alamoudi, H., Almutairi, S., Al-rammah, F.: Real-time face detection and tracking on mobile phones for criminal detection. In: 2017 2nd International Conference on Anti-Cyber Crimes (ICACC), pp. 75–80. IEEE (2017)
2. Jia, X.: Fabric defect detection based on open source computer vision library opencv. In: 2010 2nd International Conference on Signal Processing Systems, vol. 1, pp. V1–342. IEEE (2010)

3. Ranftl, A., Alonso-Fernandez, F., Karlsson, S.: Face tracking using optical flow. In: 2015 International Conference of the Biometrics Special Interest Group (BIOSIG), pp. 1–5. IEEE (2015)
4. Lienhart, R., Kuranov, A., Pisarevsky, V.: Empirical analysis of detection cascades of boosted classifiers for rapid object detection. In: Joint Pattern Recognition Symposium, pp. 297–304. Springer (2003)
5. Ranftl, A., Alonso-Fernandez, F., Karlsson, S., Bigun, J.: Real-time adaboost cascade face tracker based on likelihood map and optical flow. *IET Biometrics* **6**(6), 468–477 (2017)
6. Yang, M.H., Kriegman, D.J., Ahuja, N.: Detecting faces in images: a survey. *IEEE Trans. Pattern Anal. Mach. Intell.* **24**(1), 34–58 (2002)
7. Viola P., Jones, M.: Robust real-time face detection. *Int. J. Comput. Vis.* **57**(2), 747–752 (2001)
8. Dadgostar, F., Sarrafzadeh, A.: An adaptive real-time skin detector based on hue thresholding: a comparison on two motion tracking methods. *Pattern Recogn. Lett.* **27**(12), 1342–1352 (2006)
9. Wang, Y., Li, Y., Zheng, J.: A camera calibration technique based on opencv. In: The 3rd International Conference on Information Sciences and Interaction Sciences, pp. 403–406. IEEE (2010)
10. Reddy, K.B.S., Loke, O., Jani, S., Dabre, K.: Tracking people in real time video footage using facial recognition. In: 2018 International Conference on Smart City and Emerging Technology (ICSCET), pp. 1–6. IEEE (2018)
11. Kurylyak, Y.: A real-time motion direction for video surveillance system, pp. 386–389. IEEE (2009)
12. Kurylyak, Y.: A real-time motion detection for video surveillance system. In: 2009 IEEE International Workshop on Intelligent Data Acquisition and Advanced Computing Systems: Technology and Applications, pp. 386–389. IEEE (2009)
13. Albiol, A., Silla, J., Mossi, J., Sanchis, L.: Automatic video annotation and event detection for video surveillance (2009)
14. Otluman, H., Aboulnasr, T.: Low complexity 2-d hidden markov model for face recognition. In: 2000 IEEE International Symposium on Circuits and Systems. Emerging Technologies for the 21st Century. Proceedings (IEEE Cat No. 00CH36353), vol. 5, pp. 33–36. IEEE (2000)
15. Terrillon, J.C., Shirazi, M.N., Fukamachi, H., Akamatsu, S.: Comparative performance of different skin chrominance models and chrominance spaces for the automatic detection of human faces in color images. In: Proceedings Fourth IEEE International Conference on Automatic Face and Gesture Recognition (Cat. No. PR00580), pp. 54–61. IEEE (2000)
16. Tracking using facial recognition. <https://images.app.goo.gl/iKBGhor3Lcj4DsG7>. Accessed 13 Nov 2019
17. Lienhart, R., Maydt, J.: An extended set of haar-like features for rapid object detection. In: Proceedings. International Conference on Image Processing, vol. 1, pp. I–I. IEEE (2002)
18. Detection of skin filter. <https://images.app.goo.gl/54WSH1EBcfJ1CzrXA>. Accessed 13 Nov 2019
19. Viola, P., Jones, M., et al.: Rapid object detection using a boosted cascade of simple features. *CVPR (1)* **1**(511–518), 3 (2001)
20. Garcia, E., Jimenez, M.A., De Santos, P.G., Armada, M.: The evolution of robotics research. *IEEE Robot. Autom. Mag.* **14**(1), 90–103 (2007)
21. Freund, Y., Schapire, R.E.: Schapire r: Experiments with a new boosting algorithm. In: Thirteenth International Conference on ML. Citeseer (1996)

Analysis of Precision Agriculture Technique by Using Machine Learning and IoT



Y. Sasi Supritha Devi, T. Kesava Durga Prasad, Krishna Saladi, and Durgesh Nandan

Abstract IoT is one of the best among the emerging technologies. Its scope has gone into the field of agriculture in which farmers learn to control his farm using IoT. Due to the lack of continuous human effort and optimal climatic conditions, many crops go waste every year. This paper discusses various methods that prevent manual action and added automatic control of the farm by using machine learning algorithms and IoT sensors. For example, support vector machine (SVR) is the method to check the weather conditions in every interval of time and gives data to the farmer and automatically takes the respective action. To detect the pests, image processing is the best-used technique. For controlling pests, we use pesticides spray by Drones and agricultural robots. This reduces costs, human effort and saves time. Irrigation can also be controlled by using the k-means clustering algorithm. Greenhouses are the best technique, which is being used nowadays in the precision agriculture that takes information about the growth of a particular plant and gives that information to the farmer. It also checks the internal climatic conditions.

Keywords Precision agriculture · IoT · Greenhouses · Smart irrigation · Disease detection · Support vector machine · Arduino Uno

Y. Sasi Supritha Devi · T. Kesava Durga Prasad · K. Saladi
Department of ECE, Aditya Engineering College, Surampalem, India
e-mail: sasisuprithadevi2@gmail.com

T. Kesava Durga Prasad
e-mail: kesavadvp0121@gmail.com

K. Saladi
e-mail: krishna.s@aec.edu.in

D. Nandan (✉)
Accendere Knowledge Management Services Pvt. Ltd., CL Educate Ltd., New Delhi, India
e-mail: durgeshnandano51@gmail.com

1 Introduction

This paper explains techniques that provide best solution to many problems that are stated above. By using the sensors, we can calculate the amount of moisture in the soil, temperature of the surroundings, humidity present in the air, sun intensity, etc. All this information is then given to the farmer through a simple SMS (The suggested method is almost similar to the one proposed by Arvindan et al. [2]), and also the farmer just sitting in the home or from that place itself, he can send another responding message either to ON or OFF the respective switch. In this way, he can control the farm. By using image processing, we can easily detect the pests, and also, it gives a better idea about fertilizers to be used. This method results in high accuracy and less human efforts. For example, in Microsoft's Farm-Beat project [3], IoT techniques are being used to improve the productivity of the farm and to decrease the cost. Intel put forward a slogan: "Feed the world—with IoT", in increasing food production [4]. The technology nowadays is running so fast, and it is bringing drastic changes in all fields. But the field of agriculture is still following the same old culture for cultivating the crops that need a large number of workers and constant efforts of the farmer. Out of 100, 74 farmers blamed that they were not getting any information related to farming from officials of agriculture. Due to the crop damage, every year, there is a loss of 11 billion dollars [1]. This is mainly due to a lack of knowledge of the modern way of agriculture. From the last few years, there were drastic changes in the climatic conditions: unexpected rainfalls in the summer days, very hot weather in the winter season and many more. Farmer should be able to predict what kind of soil is suitable for the respective crop, and also, he should know all the climatic conditions that satisfy the crop.

Greenhouses are one of the best practices for precision agriculture. Sensors, actuators, drones, robots all are IoT devices that are meant to improve the efficiency and precision of greenhouses [5–8]. With the help of IoT and a little AI, reliable, unique, smart methods of farming were developed right from irrigation to harvesting, which includes predicting the life of the crop. Now, the farmer can have complete control over his crop globally with the help of the Internet.

This paper explains about the usage of IoT in agricultural farms. Section 2 of this paper gives the literature work on the above topic. That means the work carried by various persons in IoT and ML in the stream of agriculture. Section 3 gives a brief idea about the methods that are followed by them. Section 4 is the design methodology that explains the concepts using a flowchart. Finally, the paper ended by providing a good conclusion based on the results and applications of IoT in agricultural fields.

2 Literature Work

Crop water stress index (CWSI) [9] is for the effective use of water. Based on the direct soil water measurement system, CWSI proposed automatic irrigation scheduling. Ludenaand et al. [10] have been suggested to use a system called geographical

information system (GIS), and in this, using a software called GIS gives better results regarding soil properties, weed, pest population, the response of the plant growth, requirements of the fertility, weather predictions and market projections. Electric nose techniques [11] are used for detecting the diseases, but it can identify only when the disease had spread to its last stage. The laboratory-based detection system can detect the initial stage of the disease. The minute features of the pests can be easily identified by using high-resolution images [12]. The affected leaf must be separated from the plant. In this type of technique, we must ensure that the images for the plant should be taken from the top with a uniform background. Thermal imaging [13] is the process used in irrigation management. In the process, we check the water content in the plant in continuous time intervals, and the water is supplied according to shade temperature distribution of the crop. Evapotranspiration (ET) is a process in which crop features are influenced by the climatic conditions. We can save water up to 42% by the ET-based approach over a time-based approach [14].

Venkata Lakshmi and Devi [15] have been suggested about a system called decision support system (DSS) for crop cultivation for India, an agricultural-based country, where 56.6% of its population depends on agriculture. His research says that the growth of seasonal crops mainly depends on three factors. The first is the soil type, the second is the season and third is crop type. These parameters are tested by using a technique named "Netica." These are the outputs that can be applied in real-time usage in mobile applications. Rao et al. [16] used cloud computing techniques for IoT for agricultural applications.

Bendre et al. [17] introduced information communication technology (ICT) in precision agriculture. As a result, it increased productivity, decreased unnecessary cost related to harvesting and effective use of pesticides and fertilizers. Srbinovska et al. [18] proposed a wireless sensor network (WSN) architecture for vegetable greenhouses. WSN is helpful in precision agriculture. This method results in low cost and high productivity. Aiello et al. [19] introduced a technique that is meant for the reduction in the usage of pesticides and fertilizers by using fusion methodology. Not only using sensors and actuators, but also IoT and AI also plays a major role in the agricultural field by the introduction of robots and drones. Nissimov et al. [20] thought that obstacle detection is very important for agricultural robots. He used a sensor called Kinect 3D sensor for the construction of the obstacle detecting robot. More reports on IoT-based applications in the field of greenhouses can be found in Azfar et al. [21] and Shamshiri et al. [22]. A motion control system and an eye-in-hand system were reported by Barth et al. [5] for agricultural robots in dense vegetation and tested the result using simulated sweet pepper harvesting. Simon et al. [8] stated that the drones can be used in agricultural fields and proposed a model using hexa-rotor drone to achieve the navigation of drones in greenhouses. Haar Cascade Classifier algorithm is one of the techniques in image processing. It is meant to solve the complexity of pest identification and disease control [23–25]. In the early days, identification of the biological pests were done by using natural enemies of the targeted pest. The above method had replaced these old techniques.

3 Existing Methodologies

A. In India, there are many types of soils, and according to Pudmular et al. [26], for the growth of the particular crop, the two major requirements are the type of soil and the amount of moisture content. The dataset consists of the preferred conditions required for plant growth. By using the logistic regression model with TensorFlow, takes the current inputs such as soil type, temperature, moisture and predicts whether the conditions are suitable or not for plant growth. The sensed data by the sensors is stored as elements of a numpy array. The sensors read the temperature, moisture content, humidity and also the type of the soil. This info was given to the server and then to the farmer. He gets info in the form of SMS statements and should take necessary action. If he fails to do, then the system automatically tries to get back to the optimal conditions. Support vector machine (SVM) [27] is used as a classifier to detect whether the conditions are optimal or not.

B. For the disease detection of a crop, we mainly use two techniques. Image Processing and machine learning.

Image Processing: It has four phases for the easy detection of the disease

1. Image acquisition: The process of acquiring images from different sources.
2. Image preprocessing: To improve quality, unwanted noise is removed from the image. Nowadays, smartphones became the way of life of every human being. With this advancement of technology, farmers are not only using the mobiles for calling but also for controlling his farm. All the above methods are based on the sensors which give the information about the crop, climatic conditions and also about the irrigation methods that are to be followed to save the water, to the server and then to the farmer. He can monitor everything and can take necessary actions. These methods increase urban agriculture also. This reduces the human effort. These methods bring a lot of awareness among the farmers about the technology and how to use them and all. This ultimately develops the country. It can also increase the productivity and efficiency of the farm, with the least investment. Finally, this increases the economy of the country. It saves a lot of time.
3. Image Segmentation: Used to divide the image into segments.
4. Feature Extraction: Removes the unwanted part, and only the required or the disease portion will be present.

Machine Learning: It constructs various algorithms, takes the inputs and finally predicts the output. The sensors take all the input parameters and give to the Arduino UNO board, which is then sent to ThingSpeak server. Then, the decision tree classifier algorithm is the one that predicts the output by comparing the optimal conditions with the input conditions [28].

C. The IoT-based smart irrigation system consists of several components. In small farming fields, environmental conditions are taken using sensors, and the output is read by an Arduino UNO which is connected by a Raspberry Pi. The code is

written using Python language, and the data is stored in the SQLite database. In big farming areas, a wireless sensor network is used in which multiple sensor nodes can be implemented. The output of the sensors is read by an Arduino Uno connected to Zigbee for sending data to the gateway [29–31]. A Web service is developed to collect the weather forecasting data, and this information is provided in these portals HTML, XML format. The Web service read the specified path data using API, and the data is stored in MYSQL database, and this is considered to the prediction algorithm [32]. This algorithm is used to predict the soil moisture and also gives the weather report with the data using the SVR model and also includes a k-means clustering algorithm. Based on the above data, it provides the irrigation suggestions. The system provides water up to a level with a threshold value of the soil moisture and stops after achieving that value [33].

D. Vegetable greenhouses had a major role nowadays that are developed using IoT, and it consists of the following steps. In the early days, farmers used to go and check the plant conditions and manually operate the corresponding adjustment devices in greenhouses. It is a time-consuming process and also needs continuous human effort. But with the help of IoT, many automatically controlling devices are built to check the condition of plants in greenhouses and gives warning signals to the farmers. This reduces the cost and also unnecessary work and increases productivity [34]. In most of the greenhouses, agricultural specialists are not employed due to limitations on the cost of operation. They were called at only when the crop is at its last stage since only specialists can identify the threat. But, the IoT equipped devices can easily identify the defective crops and the pests with the help of enabled sensors in IoT device.

4 Design Methodology

General block diagram of precision agriculture technique by using machine learning and IoT has been shown in Fig. 1. The first block consists of sensors that can read the temperature, moisture content in the soil and humidity present in the surrounding air. The second one consists of a camera for disease detection. This uses image processing techniques. And the third one consists of drones and agricultural robots for spraying of pesticides and fertilizers. All this sensed information is then given to the analog-to-digital converter (ADC) through an Arduino and then to a Raspberry Pi. The data is exchanged between the Raspberry Pi and the server. These sensors regularly update the information of the crop to the farmer. He can take the necessary action by sending a responding message, which was carried to the respective devices and the person who operated device. If not, then the system can automatically take the action to bring the crop to optimal conditions.

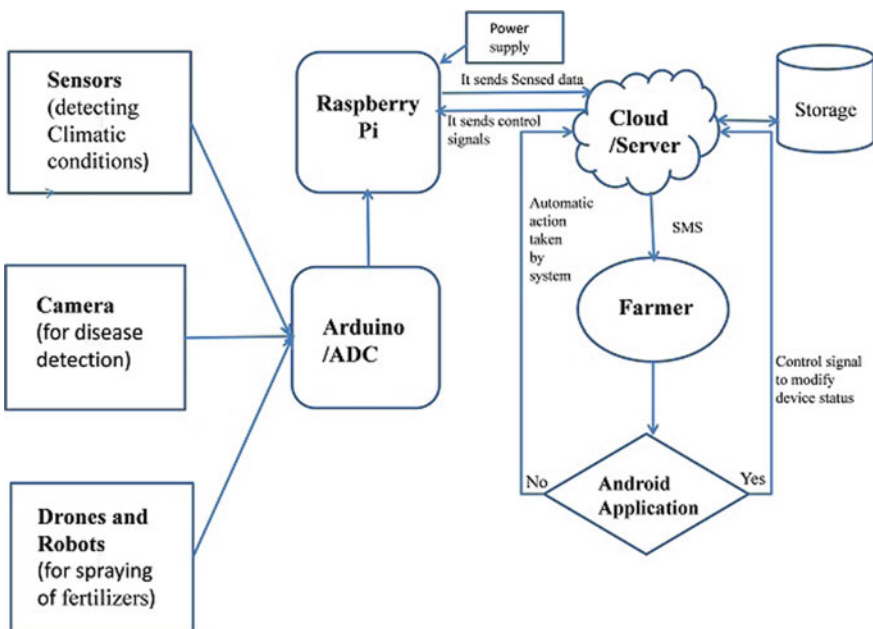


Fig. 1 Block diagram of precision agriculture technique by using machine learning and IoT

5 Result

Using sensors in the stream of agriculture reduces manual work and efforts nearly 50%. The climate nowadays is changing minute to minute, and it is very important to know about the weather conditions on the farm, and to have continuous human effort is a very difficult task because man cannot detect the environmental conditions. This paper gives idea about the sensors that are used to detect the temperature, humidity in the air, moisture levels in the soil and also leads to achieving smart irrigation. This paper also suggests some easy techniques for disease detection and pest prediction. The camera captures the image of the crop. With the help of image processing and machine learning, the automatic actions were taken by the system. Apart From these, a new span in the technology is agricultural robots and drones. These play a major role in the fields. They are used to take the survey of the fields and also give information about the crop by taking pictures. These are also used in spraying the fertilizers and pesticides accurately in the affected region.

6 Applications

Generally, all of us know that IoT is just confined to smart devices like Google Home Voice Controller, August Smart Lock, Amazon Dash Button. There is a huge development of IoT techniques in the field of agriculture also. Precision farming is one of the most famous applications that provide accurate ways of growing crops. Agricultural drones are playing a major role in the current scenario. Mostly, they are used to take the survey that includes soil type, crop growth and also for spraying the fertilizers. Greenhouses are another important application of IoT whose main concept is by using IoT sensors to provide internal climatic conditions. Smart irrigation can be achieved using machine learning techniques. It works when there is an immediate need for water that cannot be predicted by the farmer.

7 Conclusion

Nowadays, Smartphones became the way of life of every human being. With this advancement of technology, farmers are not only using the mobiles for calling but also for controlling his farm. All the above methods are based on the sensors which give the information about the crop, climatic conditions, and also about the irrigation methods that are to be followed to save the water, to the server and then to the farmer. He can monitor everything and can take necessary actions. These methods increase Urban Agriculture also. This reduces the human effort. These methods bring a lot of awareness among the farmers about the technology and how to use them and all. This ultimately develops the country. It can also increase the productivity and efficiency of the farm, with the least investment. Finally, this increases the economy of the country. It saves a lot of time.

References

1. Burney, J., Ramanathan, V.: Recent climate and air pollution impacts on Indian agriculture. *Proc. Natl. Acad. Sci.* **111**(46), 16319–16324 (2014)
2. Arvindan, A., Keerthika, D.: Experimental investigation of remote control via android smart phone of arduino-based automated irrigation system using moisture sensor. In: 2016 3rd International Conference on Electrical Energy Systems (ICEES), pp. 168–175. IEEE (2016)
3. Microsoft, farm beats: Ai & iot for agriculture. <https://www.microsoft.com/en-us/research/project/farmbeats-iot-agriculture/>. Accessed 22 Jan 2019
4. Intel. Feed the world-with iot. <https://www.intel.co.uk/content/en/it-managers/smart-farming-iot.html>. Accessed 22 Jan 2019
5. Barth, R., Hemming, J., van Henten, E.J.: Design of an eye-in-hand sensing and servo control framework for harvesting robotics in dense vegetation. *Biosyst. Eng.* **146**, 71–84 (2016)

6. Kampianakis, E., Kimionis, J., Tountas, K., Konstantopoulos, C., Koutroulis, E., Bletsas, A.: Wireless environmental sensor networking with analog scatter radio and timer principles. *IEEE Sens. J.* **14**(10), 3365–3376 (2014)
7. Malaver, A., Motta, N., Corke, P., Gonzalez, F.: Development and integration of a solar powered unmanned aerial vehicle and a wireless sensor network to monitor greenhouse gases. *Sensors* **15**(2), 4072–4096 (2015)
8. Simon, J., Petkovic, I., Petkovic, D., Petkovics, A.: Navigation and applicability of hexa rotor drones in greenhouse environment. *Tehnički vjesnik* **25**(Supplement 2), 249–255 (2018)
9. Idso, S., Jackson, R., Pinter Jr., P., Reginato, R., Hatfield, J.: Normalizing the stress-degree-day parameter for environmental variability. *Agric. Meteorol.* **24**, 45–55 (1981)
10. Grisso, R.D., Alley, M.M., McClellan, P., Brann, D.E., Donohue, S.J.: Precision farming: a comprehensive approach (2005)
11. Laothawornkitkul, J., Moore, J.P., Taylor, J.E., Possell, M., Gibson, T.D., Hewitt, C.N., Paul, N.D.: Discrimination of plant volatile signatures by an electronic nose: a potential technology for plant pest and disease monitoring. *Environ. Sci. Technol.* **42**(22), 8433–8439 (2008)
12. Prasad, S., Kumar, P., Jain, A.: Detection of disease using block-based unsupervised natural plant leaf color image segmentation. In: International Conference on Swarm, Evolutionary, and Memetic Computing, pp. 399–406. Springer (2011)
13. Wang, X., Yang, W., Wheaton, A., Cooley, N., Moran, B.: Efficient registration of optical and ir images for automatic plant water stress assessment. *Comput. Electron. Agric.* **74**(2), 230–237 (2010)
14. Davis, S., Dukes, M.: Irrigation scheduling performance by evapotranspiration-based controllers. *Agric. Water Manage.* **98**(1), 19–28 (2010)
15. Saravanan, R.: Icts for agriculture extension: Global experiments. In: Innovations and Experiences. New India Publishing (2010)
16. Cukier, K., Mayer-Schoenberger, V.: The rise of big data: how it's changing the way we think about the world. *Foreign Aff.* **92**, 28 (2013)
17. Bendre, M., Thool, R., Thool, V.: Big data in precision agriculture: Weather forecasting for future farming. In: 2015 1st International Conference on Next Generation Computing Technologies (NGCT), pp. 744–750. IEEE (2015)
18. Srbinovska, M., Gavrovski, C., Dimcev, V., Krkoleva, A., Borozan, V.: Environmental parameters monitoring in precision agriculture using wireless sensor networks. *J. Clean. Prod.* **88**, 297–307 (2015)
19. Aiello, G., Giovino, I., Vallone, M., Catania, P., Argento, A.: A decision support system based on multisensor data fusion for sustainable greenhouse management. *J. Clean. Prod.* **172**, 4057–4065 (2018)
20. Nissimov, S., Goldberger, J., Alchanatis, V.: Obstacle detection in a greenhouse environment using the kinect sensor. *Comput. Electron. Agric.* **113**, 104–115 (2015)
21. Azfar, S., Nadeem, A., Basit, A.: Pest detection and control techniques using wireless sensor network: a review. *J. Entomol. Zool. Stud.* **3**(2), 92–99 (2015)
22. Shamshiri, R., Kalantari, F., Ting, K.C., Thorp, K.R., Hameed, I.A., Weltzien, C., Ahmad, D., Shad, Z.M.: Advances in greenhouse automation and controlled environment agriculture: a transition to plant factories and urban agriculture (2018)
23. Anand, R., Veni, S., Aravinth, J.: An application of image processing techniques for detection of diseases on brinjal leaves using k-means clustering method, pp. 1–6. IEEE (2016)
24. Miranda, J.L., Gerardo, B.D., Tanguilig III, B.T.: Pest detection and extraction using image processing techniques. *Int. J. Comput. Commun. Eng.* **3**(3), 189 (2014)
25. Venkataraman, D., Mangayarkarasi, N.: Computer vision based feature extraction of leaves for identification of medicinal values of plants. In: 2016 IEEE International Conference on Computational Intelligence and Computing Research (ICCIC), pp. 1–5. IEEE (2016)
26. Pudumalar, S., Ramanujam, E., Rajashree, R.H., Kavya, C., Kiruthika, T., Nisha, J.: Crop recommendation system for precision agriculture. In: 2016 Eighth International Conference on Advanced Computing (ICoAC), pp. 32–36. IEEE (2017)

27. Krishika, P., Veni, S.: Leaf disease detection on cucumber leaves using multiclass support vector machine. In: 2017 International Conference on Wireless Communications, Signal Processing and Networking (WiSPNET), pp. 1276–1281. IEEE (2017)
28. Chopda, J., Raveshiya, H., Nakum, S., Nakrani, V.: Cotton crop disease detection using decision tree classifier. In: 2018 International Conference on Smart City and Emerging Technology (ICSCET), pp. 1–5. IEEE (2018)
29. Gutiérrez, J., Villa-Medina, J.F., Nieto-Garibay, A., Porta-Gándara, M.Á.: Automated irrigation system using a wireless sensor network and gprs module. *IEEE Trans. Instrum. Meas.* **63**(1), 166–176 (2013)
30. Ojha, T., Misra, S., Raghuvanshi, N.S.: Wireless sensor networks for agriculture: the state-of-the-art in practice and future challenges. *Comput. Electron. Agric.* **118**, 66–84 (2015)
31. Pandey, V., Sharma, D., Shukla, A., Tyagi, S.: A low-cost zigbee based temperature and humidity acquisition system for research and industrial applications. In: 2017 International Conference on Communication Computing and Networking, pp. 379–385 (2017)
32. Weather api: Openweathermap (2012). <https://openweathermap.org/api>. Accessed 8 Mar 2017
33. Goap, A., Sharma, D., Shukla, A., Krishna, C.R.: An iot based smart irrigation management system using machine learning and open source technologies. *Comput. Electron. Agric.* **155**, 41–49 (2018)
34. Ruan, J., Hu, X., Huo, X., Shi, Y., Chan, F.T., Wang, X., Manogaran, G., Mastorakis, G., Mavromoustakis, C.X., Zhao, X.: An iot-based e-business model of intelligent vegetable greenhouses and its key operations management issues. *Neural Comput. Appl.* 1–16 (2019)

Dispersive Nature of the FEL Amplifiers in the Whistler Mode



Ram Gopal, M. Sunder Rajan, Priti Sharma, and Abhinav K. Gautam

Abstract The analytical formalism for whistler-pumped FEL amplifiers in collective Raman regime is developed. Compton regime (CR) has also feasible for the low-current gain; however, in practical, it does not exist for reasonable growth rate due to require of extremely high magnetic fields density (i.e., 10–15 T) to operate up to 200–250 GHz frequencies; hence, Raman regime plays an important role with the finite space charged mode only. The dispersive nature of the whistler-pumped FEL amplifiers is sensitive to frequency of electron cyclotron, plasma frequency, and magnetic fields of the amplifiers. The simultaneously of the pumped frequency with strong magnetic fields and plasma frequency should be synchronized for electron cyclotron frequency, which can rapidly increases the wiggler wave number to the radiation of amplification in the slow-whistler mode for high frequencies from millimeter to the sub-millimeter ranges. It is also clear that the background plasma should be lesser than the beam density for the charge neutralization and guiding of the signal into waveguides; hence, the plasma density can also improve the stability of high frequencies. In Raman regime, the growth rate is larger while it decreases as increases the frequency of operations and vice versa. The tapering of an axial field also plays a typical role to raise the efficiency as well as reduction in the length of interaction with axis.

Keywords FEL amplifiers · Axial field · Wiggler field and whistler

R. Gopal (✉)

Department of Electronics Engineering, CRMT, Indian Institute of Technology (Banaras Hindu University), Varanasi, UP, India
e-mail: ramgopal.rs.eee@itbhu.ac.in

M. S. Rajan

Faculty of Electrical and Computer Engineering, Institute of Technology, Arba Minch University, Arba Minch, Ethiopia

P. Sharma

Department of Electronics and Communication Engineering, UNSIET, Purvanchal University, Jaunpur, UP, India

A. K. Gautam

Department of Electrical Engineering, Kamla Nehru Institute of Technology, Sultanpur, UP, India

1 Introduction

The conventional sources of radiation offer very little in THz range. The microwave sources operate below 60 GHz, while lasers operate above 30 THz and gyrotrons are limited to 30–200 GHz range. Free electron lasers can offer an alternative. The free electron lasers (FELs) are a fast-wave electron-beam device. The distinguishing features of the FELs are determined by a short-pulse laser or the relativistic electron beams (REBs). The FEL amplifiers are extremely adaptable light sources for the production of very wide range of electromagnetic spectrum from microwaves to X-rays. The radiated periods of electron beams in amplifiers λ_1 scale with wiggler wavelength λ_0 and relativistic gamma factor (γ_0) as $\gamma_0 = 1 + E_b/mc^2$ as $\lambda_1 = \lambda_0/2\gamma_0^2$ where E_b is kinetic energy of beams, m is the electrons rest mass, and c is speed of light in vacuum [1–5]. Sharma and Tripathi [6, 7] explored the electromagnetics and electrostatics behavior in wiggler fields as whistler-pumped and examined the feasibilities for the low-current gain; however, in practical, Compton regime (CR) does not exist for reasonable growth rate due to require of extremely high magnetic fields density (i.e., 10–15 T) to operate up to 200–250 GHz frequencies; hence, Raman regime plays an important role with the finite space charged mode only. Pant and Tripathi have studied a nonlocal theory and examined the possibilities in a strong static magnetic wiggler and axial guided magnetic field [8]. In FEL amplifier (FELA), Chung [9] has developed nonlinear theory and simulation techniques to estimate 14 kW signal for 10.6 μm wavelengths and 2 GW power.

In 1984, first time, Gold [10] demonstrated experimentally and examined 35 GHz radiation frequency for 1.2 dB/cm growth rates and >3% experimental efficiency with 50 dB gain while estimated power as >75 MW at 75 GHz with 6% experimental efficiency to the both end tapering for the FEL amplifiers [11, 12]. Orzechowski et al. estimated 35 GHz with peak output power 180 MW with beams energy 3.6 Mev/850 A and increase operating band width 10% to 1.4 m wiggler lengths with 6% extraction efficiency approximately. Freund et al. have observed extraction efficiency of 35% for 8 mm wavelengths while about of 1% at 800 nm wavelengths for tapered wiggler [13, 14]. Freund [15], Freund and Ganguly [16] have also explored the nonlinear theory and simulation techniques and examined an efficiency of 27% at 33.4 GHz frequency, however, experimental efficiency achieved by 35% for same frequency with tapered wiggler using beams energy of 3.5 Mev/850 A to the high-power collective Raman regime operations. Gardelle et al. [17] explored the possibilities of space charge effect and beams quality to improve the efficiency an amplifiers, while Parker et al. have studied the collective effect in FEL amplifiers and estimated an efficiency of 2.5% to 35 MW at 4 mm lengths [18]. Gopal and Jain have studied the Raman regime operation in whistler mode and estimated an extraction efficiency raised by 20% to the generation of $\omega_1 = 6.2 \times 10^{10}$ rad/sec frequency for radiation mode and also explored the Eigen mode simulation in FEL amplifies [19–21].

In this paper, author studied the dispersion relation and their behavior with linear tapered axial magnetic field in collective Raman regime. An axial magnetic fields tapering also plays a typical role to raise the efficiency as well as reduction in the

length of interaction with axis. In Sect. 2, we study an evaluation of Raman regime in FEL amplifiers and their relevant equations including with space charge effects. In Sect. 3, the momentum and efficiency equation in FEL amplifiers has been studied. The results' discussion is summarized in Sects. 4 and 5 explored their conclusions.

2 Evaluation of Raman Regime in FEL Amplifiers

Considering here, the wiggler field $k_o(z)$ is employed into the interaction region $0 < z < L$ which is varying with the function of 'z' and comprises with plasma electron density n_{op}^o immersed in a negative linear taper guided magnetic field $B_s(\hat{z})$, and therefore, we have

$$B_s = B_{os}(1 - z/L) \quad (1)$$

where $\vec{B}_{os} = B_o(\hat{x} + i\hat{y})e^{ik_o dz}$, B_o is wiggler field in whistler mode, and a circularly polarized whistler wave and radiated wave are propagating with the plasma medium along $-\hat{z}$ direction; hence, electric fields [20] are as

$$\vec{E}_o = A_o(\hat{x} + i\hat{y})e^{-i(\omega_o t + \int k_o dz)} \quad (2)$$

and

$$\vec{E}_1 = A_1(\hat{x} + i\hat{y})e^{-i(\omega_1 t - k_1 z)} \quad (3)$$

Here, $k_o = \frac{\omega_o}{c}\varepsilon^{1/2}$, $k_1 = \omega_1/c$, $\varepsilon = [1 - \frac{\omega_p^2}{\omega_o(\omega_o - \omega_c)}]$, and $\omega_c = \omega_{co}(1 - \frac{z}{L})$, $\omega_{co} = \frac{eB_{os}}{mc}$, $\omega_p = (\frac{n_{op}^o e^2}{\varepsilon_{op} m})^{1/2}$. ω_{co} and ω_c are initial electron cyclotron and electron cyclotron frequency, the wiggler wave number is k_o , ω_o is wiggler frequency, plasma frequency is ω_p , the back ground plasma density is n_{op}^o , m is the rest mass, $-e$ is electronic charge, the scale length is L , c is the speed of light, and ε_o and ε are the free space and relative permittivity, respectively.

Simultaneously, the synchronism of the fields and frequencies can rapidly increase the wave number of wiggler to the radiation of amplification in the slow-whistler mode for high frequencies from millimeter to the sub-millimeter ranges. If radiated electrons synchronized with whistler wave, then $\omega = \omega_1 - \omega_o$ and $k = k_o + k_1$; hence, it can be written as

$$\omega_1 = \gamma_{ob}^{o/2} \omega_o (1 + v_{ob}/c) (1 + \varepsilon^{1/2} v_{ob}/c) \quad (4)$$

If the whistler wave and beat-wave exert a ponderomotive force at (ω_1, k_1) and $\vec{\omega}_1 \gg \vec{\omega}_c$, and therefore, the total ponderomotive force is as

$$\vec{F}_{pb} = e\nabla\Phi_{pb} = -\frac{e}{2c}\vec{v}_{ob}^* \times \vec{B}_1 - \frac{e}{2c}\vec{v}_{1b} \times \vec{B}_o^* \quad (5)$$

On solving the above Eq. (5), one obtains

$$\vec{F}_{pb} = -\left(\frac{e^2 A_o^* A_1}{imc\omega_1\omega_o\gamma_{ob}^o}\right) \left[k_o + \frac{k_1(\omega_o + k_o v_{ob}^o)}{(\omega_o + k_o v_{ob}^o - \omega_c/\gamma_{ob}^o)} \right] \hat{z} e^{-i\psi} \quad (6)$$

Therefore, the nonlinear beams current density for electron at (ω_1, k_1) can be written as

$$\vec{J}_{b\perp}^1 = -en_{ob}^o \vec{v}_{1b} - \frac{1}{2} en_{2b} \vec{v}_{ob} - en_{ob}^o \vec{v}_{2zo}, \quad (7)$$

Since in Raman regime, due to high beam current, i.e., $(\chi_b \gg 1)$, the free space charge potential (Φ) is considerable, i.e., $(\Phi \gg \Phi_{pb})$, and therefore, the total current density ($\vec{J}_{T\perp}^1 = \vec{J}_{b\perp}^1 + \vec{J}_{p\perp}^1$) is given as

$$\begin{aligned} \vec{J}_{T\perp}^1 &= -\frac{1}{4\pi} \left[\frac{\omega_{pb}^2}{i\gamma_{ob}^o\omega_1} + \frac{\omega_p^2}{i\omega_1} + \frac{1}{2} \frac{e\omega_p^2\omega_c A_o^*}{m\omega_o\omega_1^2 c(\omega_1 - \omega_c)} \left\{ k_o + \frac{\omega_o k_1}{(\omega_o - \omega_c)} \right\} \right] \vec{E}_{1\perp} \\ &+ \frac{1}{2} \frac{1}{4\pi} \frac{ek^2\omega_{pb}^2(\omega_o + k_o v_{ob}^o)\vec{E}_o}{im\omega_o\gamma_{ob}^{o4}(\omega_1 - kv_{ob}^o)^2(\omega_o + k_o v_{ob}^o - \omega_c/\gamma_{ob}^o)} \Phi \\ &- \frac{1}{2} \frac{1}{4\pi} \frac{k\omega_{pb}^2\omega_c}{\gamma_{ob}^{o4}(\omega_1 - \omega_c/\gamma_{ob}^o)(\omega_1 - kv_{ob}^o)} \Phi \\ &- \frac{1}{2} \frac{1}{4\pi} \frac{k\omega_p^2\omega_c}{\omega_1(\omega_1 - \omega_c)} \Phi. \end{aligned} \quad (8)$$

Now putting the value of $\vec{J}_{T\perp}^1$ into the wave equation $(\omega_1^2 - k_1^2 c^2) \vec{E}_{1\perp} = -4\pi i\omega_1 \vec{J}_{T\perp}^1$, we have

$$R.\varepsilon = B \left[\begin{aligned} &\frac{ek_b A_o^*}{mc\omega_o\omega_1\gamma_{ob}^o(k_o + k_1)} \left\{ k_o + \frac{(\omega_o + k_o v_{ob}^o)k_1}{(\omega_o + k_o v_{ob}^o - \omega_c/\gamma_{ob}^o)} \right\} \\ &+ \frac{ek_p A_o^*}{mc\omega_o\omega_1(k_o + k_1)} \cdot \left\{ k_o + \frac{\omega_o k_1}{(\omega_o - \omega_c)} \right\} \end{aligned} \right],$$

or

$$\Rightarrow R.\varepsilon = Q. \quad (9)$$

where

$$R = \omega_1^2 - k_1^2 c^2 - \frac{\omega_{pb}^2}{\gamma_{ob}^o \omega_1} - \frac{\omega_p^2}{\omega_1} - \frac{1}{2} \frac{i e \omega_p^2 \omega_c A_o^*}{m \omega_o \omega_1 (\omega_1 - \omega_c)} \left[k_o + \frac{\omega_o k_1}{(\omega_o - \omega_c)} \right]$$

$$B = -\frac{k \omega_1}{2} \left[\frac{e k \omega_{pb}^2 (\omega_o + k_o v_{ob}^o) \vec{E}_o}{m \omega_o \gamma_{ob}^{o^4} (\omega_1 - k v_{ob}^o)^2 (\omega_o + k_o v_{ob}^o - \omega_c / \gamma_{ob}^o)} \right.$$

$$\left. - \frac{i \omega_{pb}^2 \omega_c}{\gamma_{ob}^{o^4} (\omega_1 - \omega_c / \gamma_{ob}^o) (\omega_1 - k v_{ob}^o)} - \frac{i \omega_p^2 \omega_c}{\omega_1 (\omega_1 - \omega_c)} \right]$$

and

$$Q = -\frac{k \omega_1}{2} \left[\frac{e k \omega_{pb}^2 (\omega_o + k_o v_{ob}^o) \vec{E}_o}{m \omega_o \gamma_{ob}^{o^4} (\omega_1 - k v_{ob}^o)^2 (\omega_o + k_o v_{ob}^o - \omega_c / \gamma_{ob}^o)} \right.$$

$$\left. - \frac{i \omega_{pb}^2 \omega_c}{\gamma_{ob}^{o^4} (\omega_1 - \omega_c / \gamma_{ob}^o) (\omega_1 - k v_{ob}^o)} - \frac{i \omega_p^2 \omega_c}{\omega_1 (\omega_1 - \omega_c)} \right]$$

$$\cdot \left[\frac{e k_b A_o^*}{m c \omega_o \omega_1 \gamma_{ob}^o (k_o + k_1)} \left\{ k_o + \frac{(\omega_o + k_o v_{ob}^o) k_1}{(\omega_o + k_o v_{ob}^o - \omega_c / \gamma_{ob}^o)} \right\} \right.$$

$$\left. + \frac{e k_p A_o^*}{m c \omega_o \omega_1 (k_o + k_1)} \left\{ k_o + \frac{\omega_o k_1}{(\omega_o - \omega_c)} \right\} \right].$$

In the above Eq. (9), if both factors in LHS is zero, then Eq. (9) is called the dispersion relation equation and plays an important role which gives the operation of the device in Raman regime operations, i.e.,

$$R = 0, \varepsilon = 0 \quad (10)$$

Hence, the amplifiers growth rate [1] can be written as

$$\Gamma = \left[-Q \left| \frac{\partial \varepsilon}{\partial \omega_1} \cdot \frac{\partial R}{\partial \omega_1} \right|_{\omega_1=\omega_{1r}}^{-1} \right]^{1/2} \quad (11)$$

3 Momentum and Efficiency in FEL Amplifiers

In the FEL amplifiers, amplitude of the ponderomotive wave is growing with trapped electrons; therefore, the electric field \vec{E}_{pb} is

$$\vec{E}_{pb} = \left(\frac{e A_o^* A_1}{i m \omega_1 \omega_o \gamma_{ob}^o} \right) \left[k_o + \frac{k_1 (\omega_o + k_o v_{ob}^o)}{(\omega_o + k_o v_{ob}^o - \omega_c / \gamma_{ob}^o)} \right] \hat{z} e^{-i \psi} \quad (12)$$

where $\psi = \omega t - \int (k_o + k_1) dz$, $\omega = \omega_1$, and, $k = |k_o| + k_1$.

Now the momentum equation for the beat-wave from Eq. (6) and taking real part, we have

$$\frac{d\gamma_e}{dz} = -\frac{eA_{pb}}{mc^2} \cos \psi \quad (13)$$

where $\frac{d\gamma_e}{dz} = \frac{1}{mc^2} P_{pbz}$ and γ_e is the electron relativistic energy at any point z , $\vec{A}_{pb} = -i \vec{E}_{pb}$, $E_{pb} = (\frac{a_1 A_o^* c}{\omega_o \gamma_{ob}^o}) [k_o + \frac{k_1 (\omega_o + k_o v_{ob}^o)}{(\omega_o + k_o v_{ob}^o - \omega_1 c / \gamma_{ob}^o)}]$ and $a_1 = \frac{e A_1}{m \omega_1 c}$.

Now defining variables $\Delta\gamma_e = \gamma_e - \gamma_r$ and $\psi = kz - \omega_1 t$, where γ_e is the relativistic energy, and the resonant energy for a uniform wiggler is denoted by γ_r . For the resonance case, the deviation of energy, $\Delta\gamma_e = \gamma_e - \gamma_r$, $\psi = kz - \omega t$ are also effective, and therefore,

$$\frac{d\Delta\gamma_e}{dz} = -\frac{eA_{pb}}{mc^2} \cos \psi \quad (14)$$

Now Eq. (14) is dimensionalizing z by $\xi = z/L$ which could constitute the phase momentum and energy evolution equations and could be written as

$$\begin{aligned} \frac{dP}{d\xi} &= -A \cos \psi \\ \frac{d\psi}{d\xi} &= P \end{aligned} \quad (15)$$

where A is constant, i.e., $P = \frac{d\psi}{d\xi} \frac{d\psi}{d\xi} = \frac{\omega_1 L \Delta\gamma_e}{2c(\gamma_r^2 - 1)^{3/2}} A = \frac{eA_{pb} L^2 \omega_1}{2mc^3(\gamma_r^2 - 1)^{3/2}}$.

Now the trajectories of the trapped electrons with the phase space (P, ψ) at different values of (P_{in}, ψ_{in}) , if $P_{in}^2 + 2A \sin \psi_{in} \leq 2A$ and $P^2 > 0$, all values of ψ are not accessible, i.e., trajectories of electrons are representing localized and trapped. Therefore, the separatrix (see Fig. 6) is given by

$$P^2 = 2A(1 - \sin \psi) \quad (16)$$

Initially, at $z = 0$ and $P = P_{in}$, electron horizontally lies uniform with the (P, ψ) plane, and trapped electrons are in the separatrix. If $z > 0$, electrons are outside the separatrix, i.e., electrons lose energy or some gain energy; hence, the transferred energy to the wave lost by an electron is $\Delta P \equiv P_{in} - P(\xi = 1)$ or $\Delta P \equiv -(P_1 + P_2)_{\xi=1}$. Now, the average values of $\langle \Delta P \rangle$ over the initial phases yields

$$\langle \Delta P \rangle = -\frac{A^2}{8} \frac{d}{dx} \left(\frac{\sin^2 x}{x^2} \right) \quad (17)$$

where $x = \frac{P_{\text{in}}}{2}$; hence, the gain function is given as $G \equiv -\frac{d}{dx} \left(\frac{\sin^2 x}{x^2} \right)$ for P_{in} or $\gamma_o - \gamma_r$ (Fig. 8). If $\gamma_o > \gamma_r$, the net transferred energy from electrons to the waves is between $-\pi/2$ and $\pi/2$, i.e., π at exit point is estimated, and therefore, the total efficiency of FEL amplifiers [1, 2, 20] is

$$\eta = \frac{\gamma_r(\xi = 0) - \gamma_r(\xi = 1)}{\gamma_r(\xi = 0) - 1} \quad (18)$$

4 Results and Discussion

In the whistler-pumped FEL amplifiers, the dispersion curves for the beam mode (curves I and II) and radiation mode (curve III) are shown in Fig. 1 to the Raman regime operation [1, 20]. The dispersive nature of the whistler-pumped FEL amplifiers is sensitive to frequency of electron cyclotron, plasma frequency, and magnetic fields of the amplifiers. The simultaneous of the whistler wave with strong magnetic fields and plasma frequency should be synchronized for electron cyclotron frequency, which can rapidly increase the wave number of the wiggler to the radiation of amplification in the slow-whistler mode for high frequencies from millimeter

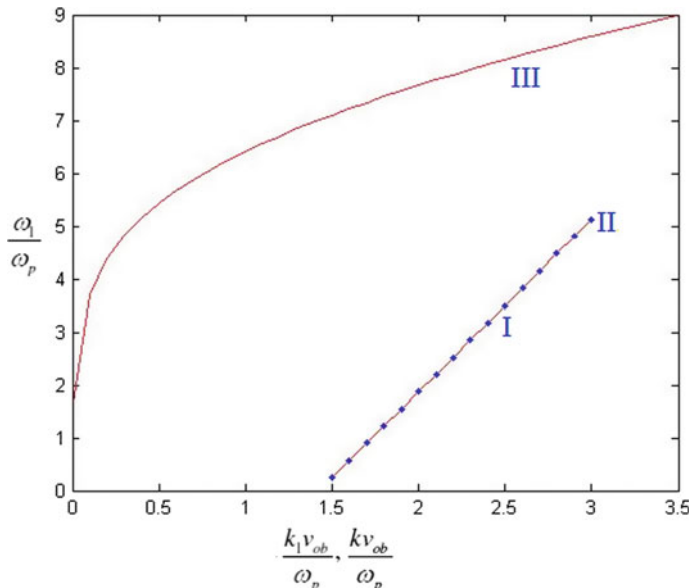


Fig. 1 Dispersion curves for the beam mode (curves I (solid line) and II (dotted line for validation) and radiation mode (curve III). Parameters are as: ($\omega_{pb} = 0.2\omega_p$, $\omega_c = 4\omega_p$, $v_{ob} = 0.4c$, $k_o = 3 \text{ cm}^{-1}$, $\omega_p = 2 \times 10^{10} \text{ r/s}$)

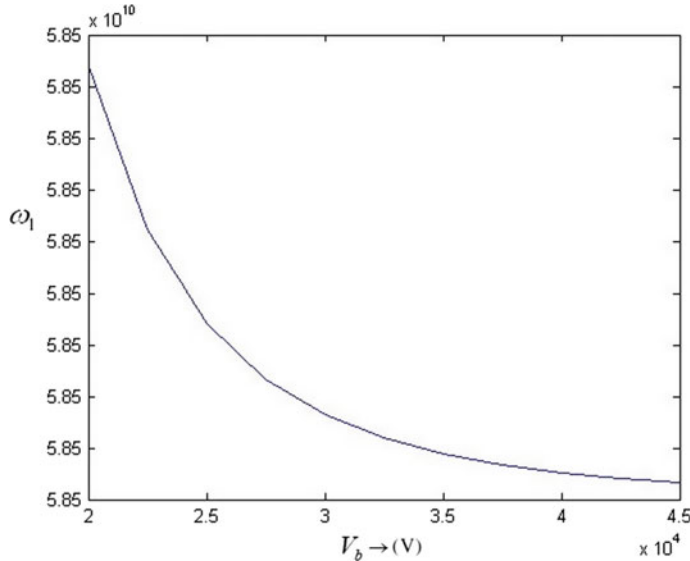


Fig. 2 Frequency of radiation (ω_1) versus beam voltage (V_b), the given parameters are as: ($\omega_{pb} = 0.2\omega_p$, $\omega_c = 4\omega_p$, $v_{ob} = 0.4c$, $k_o = 3 \text{ cm}^{-1}$, $\omega_p = 2 \times 10^{10} \text{ r/s}$)

to the sub-millimeter ranges. Figure 2 showed the radiation frequency (ω_1) versus beam voltage (V_b) curve as quietly considerable as radiation signal slowed down with beam density comparable to higher density of background plasma. It was also noted that the growth rate is increasing as it decreases the radiation frequency and vice versa; however, growth rate is always larger (see Fig. 3) as increase of beam voltage (V_b), it is quite possible at higher frequencies. In Figs. 4 and 5, the frequency of radiation increases as decreases of growth rates while it is unaffected in Compton regime [1]. Since the ponderomotive wave will essentially trap some of the electrons and these some of the electrons when they move from a smaller value of momentum energy, inside the separatrix, then they lose energy and give to radiation and amplify it (see Fig. 6). The variation of gain function ‘ G ’ with phase momentum (P_{in}) is shown in Fig. 8, which is quite considerable at $V_b \geq 40 \text{ KV}$ which is enhanced in the efficiency of the device adiabatically. The tapering of magnetic field also plays an important role to enhance the efficiency (η) of the net transferred energy to the waves (see Fig. 7) which is observed as 20% [19, 20] while an interaction region reduces about 10% [1]; however, the device beams intensity is influenced by tapering which might not be detrimental to the instability.

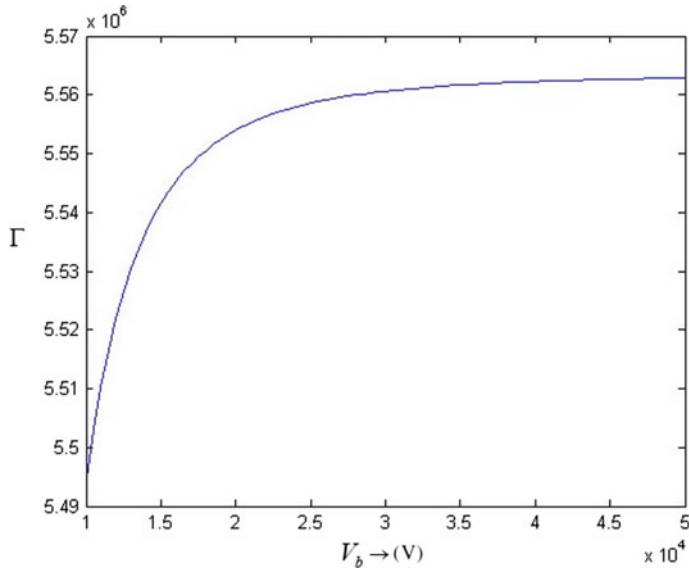


Fig. 3 Growth rate (Γ) versus beam voltage (V_b), the given parameters are as: ($\omega_{pb} = 0.2\omega_p$, $\omega_c = 4\omega_p$, $v_{ob} = 0.4c$, $k_o = 3 \text{ cm}^{-1}$, $\omega_p = 2 \times 10^{10} \text{ r/s}$)

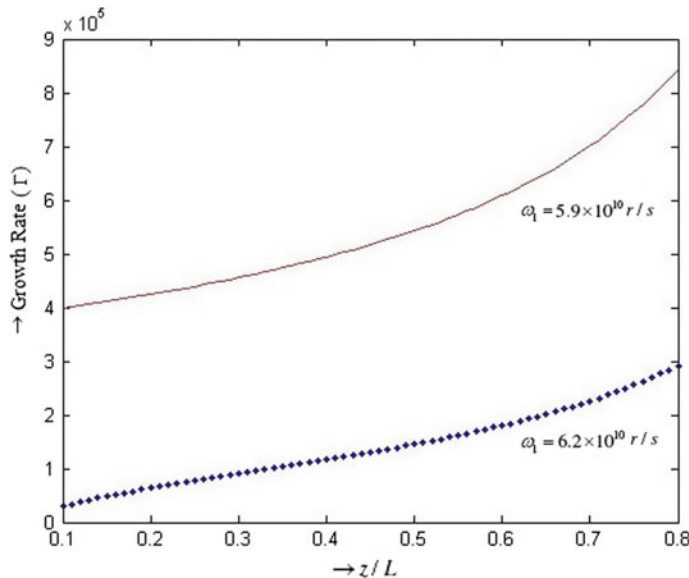


Fig. 4 Growth rate (Γ) versus normalized lengths (z/L), the given parameters are as: $\omega_{pb} = 0.2\omega_p$, $\omega_c = 4\omega_p$, $v_{ob} = 0.4c$, $k_o = 3 \text{ cm}^{-1}$, $\omega_p = 1.9 \times 10^{10} \text{ r/s}$, ($\omega_p = 2 \times 10^{10} \text{ r/s}$, $\omega_1 = 5.9 \times 10^{10} \text{ r/s}$, $\omega_1 = 6.2 \times 10^{10} \text{ r/s}$, $L = 40 \text{ cm}$)

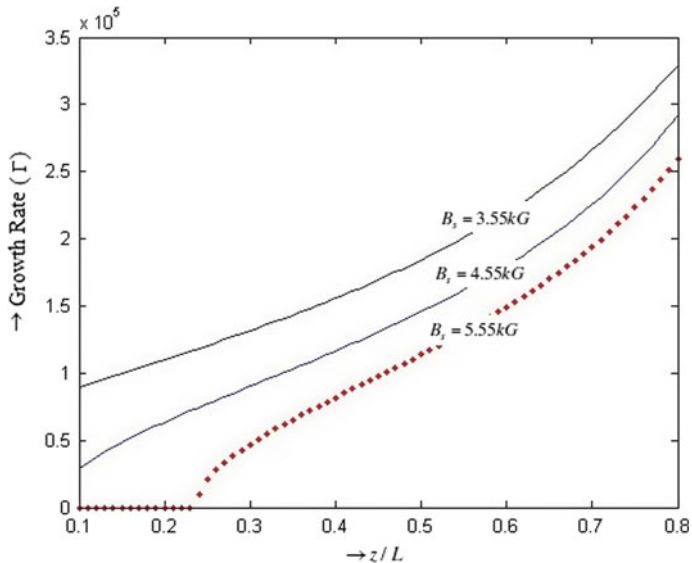


Fig. 5 Growth rate (Γ) versus normalized distance (z/L), the given parameters are as: $\omega_{pb} = 0.2\omega_p$, $\omega_c = 4\omega_p$, $v_{ob} = 0.4c$, $k_o = 3 \text{ cm}^{-1}$, $\omega_p = 1.9 \times 10^{10} \text{ r/s}$, ($\omega_p = 2 \times 10^{10} \text{ r/s}$, $\omega_1 = 5.9 \times 10^{10} \text{ r/s}$, $\omega_1 = 6.2 \times 10^{10} \text{ r/s}$, $L = 40 \text{ cm}$)

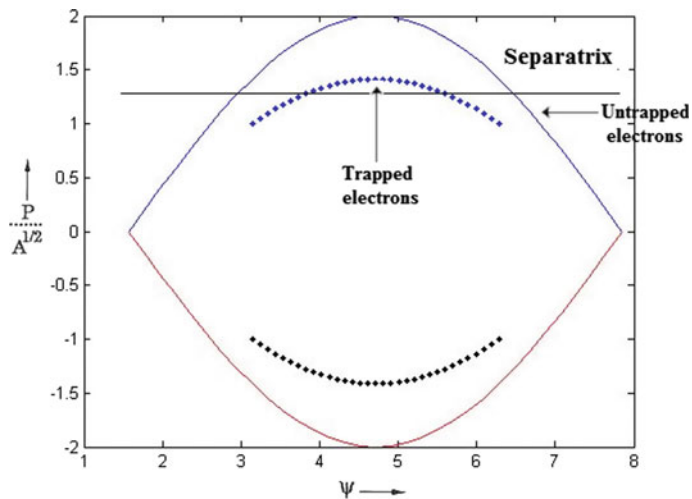


Fig. 6 Trapped electrons phase space (P , ψ) trajectories for $P_{in}^2 + 2A \sin \psi_{in} \leq 2A$ and $P^2 > 0$

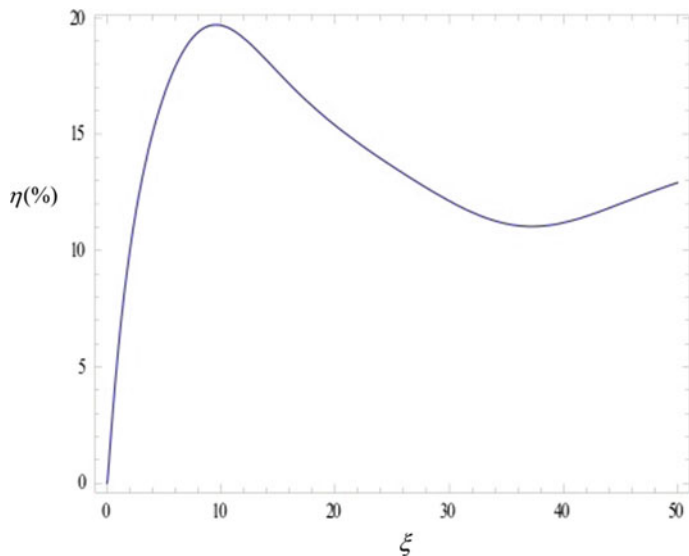


Fig. 7 Efficiency (η) versus normalized distance (z/L), the given parameters are as: ($\gamma_0 = 10$, $a_1 = 0.2$, $a_o = 0.028$, $\omega_0 = 1.5$, $\omega_{co} = 1.6$)

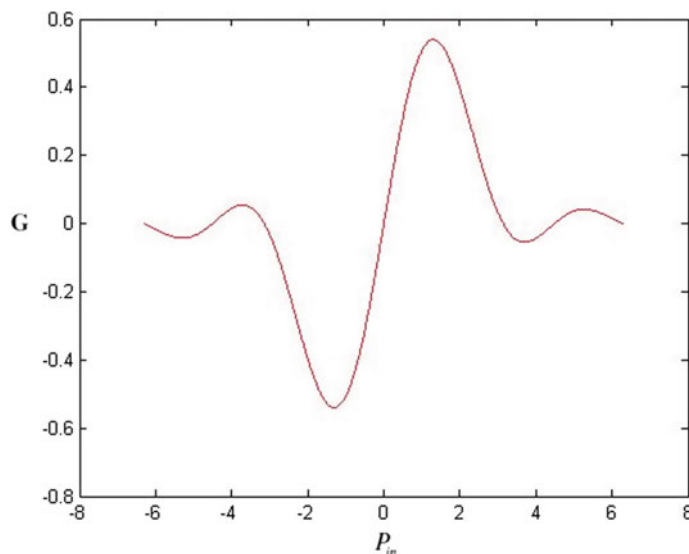


Fig. 8 Gain function (G) versus phase momentums (P_{in}) of electrons, the given parameters are as: $\omega_1 = 6.2 \times 10^{10}$ r/s, $L = 40$ cm

5 Conclusion

This paper studied the dispersive behavior of the whistler-pumped FEL amplifiers in collective Raman regime operation. The dispersive nature of the whistler-pumped FEL amplifiers is sensitive to frequency of electron cyclotron, plasma frequency, and magnetic fields of the amplifiers. The simultaneous of the pumped frequency with strong magnetic fields and plasma frequency should be synchronized for electron cyclotron frequency, which can rapidly increases the wiggler wave number to the radiation of amplification in the slow-whistler mode for high frequencies from millimeter to the sub-millimeter ranges. The tapering of magnetic field also plays an important role to enhance the efficiency (η) of the net transferred energy to the waves (see Fig. 7) which is observed as 20% while an interaction region reduces about 10%. Finally, we studied here the radiation of $\omega_1 = 6.2 \times 10^{10}$ rad/sec frequency using with mildly REBs in the operation of Raman regime. The area of FELs application is typically not all the science but used in engineering physics, classical physics, material science, applied mathematics, life science, medicine, biology, nuclear physics and engineering, electronics engineering, electrical engineering, mechanical engineering, and many other curriculums.

References

- Pant, K.K., Tripathi, V.K.: Free electron laser operation in the whistler mode. *IEEE Trans. Plasma Sci.* **22**(3) (1994)
- Sharma, A., Tripathi, V.K.: A plasma filled gyrotron pumped free electron laser. *Phys. Plasmas* **3**, 3116 (1996). <https://doi.org/10.1063/1.871658>
- Liu, C.S., Tripathi, V.K.: *Interaction of Electromagnetic Waves with Electron Beams and Plasmas*. World Scientific (1994)
- Marshall, T.C.: *Free Electron Lasers*. MacMillan, New York (1985)
- Shea, P.G.O., Freund, H.P.: Free electron lasers: status and applications. *Nature* **292**(5523), 1853–1858 (2001). <http://www.jstor.org/stable/3083925>
- Sharma, A., Tripathi, V.K.: Kinetic theory of a whistler-pumped free electron laser. *Phys. Fluids B* **5**(1) (1993). <https://doi.org/10.1063/1.860850>
- Sharma, A., Tripathi, V.K.: A whistler pumped free electron laser. *Phys. Fluids* **31**, 3375–3378 (1988)
- Pant, K.K., Tripathi, V.K.: Nonlocal theory of a whistler pumped free electron laser. *Phys. Plasmas* **1**, 1025 (1994)
- Chung, T.H., Kim, S.H., Lee, J.K.: Simulation of tapered FEL amplifiers in millimetre and infrared regions. *Nuclear Instrum. Phys. Res. A* **331**, 482–486 (1993)
- Gold, S.H., Hardesty, D.L., Kinkead, A.K., Barnett, L.R.: High gain 35-GHz free electron laser amplifier experiment. *Phys. Rev. Lett.* **52**(14), 1218–1221 (1984)
- Gold, S.H., Black, W.M., Freund, H.P., Granatstein, V.L., Kinkead, A.K.: Radiation growth in a millimeter-wave free electron laser operating in the collective Regime. *Phys. Fluids* **27**(3), 746–754 (1984). <https://doi.org/10.1063/1.864650>
- Gold, S.H., Freund, H.P., Bowie: free electron laser with tapered axial magnetic field. The United States of America as represented by the Secretary of the Navy, Patent Number: 4,644,548, Washington, DC (1987)

13. Orzechowski, T.J., Anderson, B.R., Fawley, W.M., Prosnitz, D., Scharlemann, E.T., Yarema, S.M.: High gain and high extraction efficiency from a free electron laser amplifier operating in the millimeter wave regime. *Nuclear Instrum. A* **250**, 144–149 (1986)
14. Orzechowski, T.J., Anderson, B.R., Clark, J.C., Fawley, W.M., Paul, A.C., Prosnitz, D., Scharlemann, E.T., Yarema, S.M.: *Phys. Rev. Lett.* **57**(17) (1986)
15. Freund, H.P.: Comparison of free-electron laser amplifiers based on a step-tapered optical klystron and a conventional tapered wiggler. *Phys. Rev.* **16**, 060701 (2013)
16. Freund, H.P., Ganguly, A.K.: Nonlinear simulation of a high-power, collective free electron laser. *IEEE Trans. Plasma Sci.* **20**(3) (1992)
17. Gardelle, J., Labrouche, J., Taillandier, P.-L.: Free electron laser simulations: effects of beam quality and space charge. *Phys. Rev.* **50**(6) (1994)
18. Parker, R.K., Jackson, B.H., Gold, S.H., Freund, H.P., Granatstein, V.L., Efthimion, P. C., Kinkead, A.K.: Axial magnetic-field effects in a collective-interaction free electron laser at millimeter wavelengths. *Phys. Rev. Lett.* **48**(4) (1982)
19. Gopal, R., Jain, P.K.: Tapering effect of an axial magnetic field on whistler-pumped amplifier. *Eng. Sci. Technol. Int. J.* **8**(2), 4–10 (2018)
20. Gopal, R., Jain, P.K.: Effect of axial magnetic field tapering on whistler-pumped FEL amplifier in collective Raman regime operation. *Int. J. Eng. Technol.* **7**(4), 2044–2050 (2018). <https://doi.org/10.14419/ijet.v7i4.15298>
21. Gopal, R., Jain, P.K.: Design methodology and simulation study of a free electron laser amplifier. *Int. J. Eng. Technol.* **7**(4), 3175–3181 (2018). <https://doi.org/10.14419/ijet.v7i4.19277>

An Improved Energy-Efficient Faulty Information Extraction Scheme Using PFDIAES and PFDIF Algorithms



P. T. Kalaivaani and Raja Krishnamoorthy

Abstract Wireless Sensor Networks (WSNs) comprises tiny sensor nodes which have been used for various applications such as Health Monitoring, Forest Fire Detection, Data Collection, Temperature Sensing, Military Application, and Security applications. Among the applications, Security in WSNs is the most challenging one because faulty information can be easily injected into the network by the intruder/attacker. Faulty information injection at the sink level may reduce the lifetime of the network and also energy wastage due to the difficulty in updating information with Base Station (BS). Two algorithms are proposed to detect and drop the false data such as Prevention of False Data Injection using Advanced Encryption Standard (PFDIAES) and Prevention of False Data Injection with Fuzzy-based method (PFDIF). The proposed improved energy-efficient faulty information extraction using PFDIF and PFDIAES algorithms is used to filter and prevent false data at the destination node. To analyze the performance of the network in critical condition, the gang attack is also considered. From the simulation results, PFDIAES has an average energy efficiency value of 1.7% and PFDIF has 5.5% of energy efficiency than the existing algorithms such as AES and FUZZY-based method.

Keywords Base station · Energy wastage · Faulty information extraction · Gang attack · PFDIAES · PFDIF · Security · WSNs

P. T. Kalaivaani (✉)

Department of ECE, Vivekanandha College of Technology for Women, Tiruchengode, Namakkal 637205, Tamilnadu, India
e-mail: ptkalaivaani@gmail.com

R. Krishnamoorthy

Department of ECE, CMR Engineering College, Kandlakoya Village, Hyderabad, Telangana 501401, India
e-mail: krajameae@gmail.com

1 Introduction

WSNs are associated without fixed infrastructure. It is the ultimate model for hostile and unattended environments such as sea, hill, deep forests and countryside. When thousand number of sensors are sprinkled, the large coverage area is possible. If anyone sensor is failed to work then other sensors in the network will continue the function accurately [1]. Fault tolerance can be achieved through high levels of redundancy. Through the Internet, sink node can communicate with the other networks to access the rem WSNs can improve remote access to WSNs minimize human intervention and management [2]. They have the self-organizing capability and short-range broadcast communication, and multi-hop.

The proposed work considers PFDIAES, PFDIF algorithms along with the impact of gang attack in WSNs region. The impact of gang attack is possible in the network when multiple nodes from neighborhood region are trying to attack/inject false data to the source node available in another region. The source node transfers the faulty information to the destination node. Energy wastage occurs when multiple nodes are trying to send false data through the source node and thus the battery level of those nodes is drained easily. Therefore gang attack indirectly affects the energy efficiency of the network.

A brief literature survey is presented about false data injection and spatial correlation and security attacks. The authors investigated a cooperative authentication scheme for extracting faulty information. When the faulty information is detected very early, the energy wastage is greatly minimized [3]. Authors proposed a generalized Fuzzy logic approach to energy-aware WSNs [4]. Different types of sensor nodes and different types of energy metrics are taken into account. Cluster-based approach is considered for the analysis. Fuzzy rules are used to determine the link cost between the nodes in WSNs. The drawback of this work is that only PFDIF set is considered as a novel scheme. Energy efficiency algorithms have not been discussed. Authors proposed AES scheme for low power circuits in WSNs [5]. Hardware also developed for the analysis. Drawback of the work is that none of the other security algorithms are tested. Neighbor router-based filtering scheme to filter the false data is adopted. Gang attack is not considered. Authors investigated the injection of faulty information with the help of security protocols on binary pairing [6]. It resists path-based denial of service attack. The proposed protocol requires less storage space to store the data and increases the value of energy savings. Demerits of this work are that only path-based denial of attack and false data injection is considered as attacks. Other types of attacks are not discussed. Security algorithms are not discussed in detail to detect and filter the false data injection.

To maximize the lifetime of the network, the Fuzzy Clustering Algorithm is proposed [7]. In FCA, three parameters are considered which are related to the radius, distance, energy of each sensor node available in the network. FCA algorithm is compared with the LEACH protocol and it yields better results than LEACH. This algorithm has not analyzed the parameters such as degree, density and local distance in detail. Authors proposed the BECAN scheme with a hybrid authentication

method to reduce false data injection [8]. Proposed scheme is analyzed with existing routing protocols. One of the demerits of the work is that security algorithms are not discussed in detail. Authors proposed a lightweight implementation of public key infrastructure entitled as cluster-based public infrastructure (CBPKI) [9]. This method is based on the security and authentication of BS. CBPKI yields low power consumption and gang attack is not discussed in detail. Authors proposed a routing algorithm based on fuzzy logic and it is energy optimized [10]. Balanced value of energy efficiency and network life span are the major strength of the work. Quality of Service (QoS) is not discussed in detail. Symmetric key-based method is approached without any attack for consideration. The authors discussed a novel en-route filtering scheme for Cyber-Physical Networked System with clustering concept [11]. Each node stores two polynomial values such as check polynomial and authentication polynomial. These two polynomials are used for supporting and checking the reports. The drawback of this work is that none of the security-based algorithms are discussed.

2 Proposed Work

To perform the en-route filtering scheme, the proposed method consists of four phases. The network should start with the initialization phase and the session should be set for further processing. To send the information very confidentially to sink, en-route phase is needed. Finally, after the information is received at the sink side then it verifies the transferred data from source side. Nodes are assigned with their own ID in the network. Dijkstra shortest path algorithm is used to establish and adjust the routing table for each sensor node. In the session set-up phase, sink node selects a Cluster Head (CH) node in a specific region and prepares the session key and witness key for CH [12]. Sink node verifies the report received from source node and source side private keys before it accepts the report [3].

3 PFDIAES and PFDIF Algorithms

The PFDIAES uses 64 bits for key generation using chain-based key generation method. Each time the message originates from the source node to the destination node, 64 bits key is generated automatically to encode the message. It is also impossible for the intruder to identify the exact combination of 64-bit key to decode the information. It is impossible to generate false key each time, the intruder hacks the information in the sensor node. Therefore the frequency of injection of false data is reduced and the energy efficiency level is also improved.

PFDIAES is a security algorithm to provide better encryption to the data being transferred from source node to sink node. PFDIAES is designed to secure information from gang attacks. PFDIAES uses 64-bit key levels. The key used in the proposed system has to be refreshed in a frequent interval. The nodes available in

a specific cluster share a common group key to all the group members. Authorized new nodes got group key information through the key server and group re-keying is possible when the key changes. KGN is a Key Generation Node that is available for each group. The hacker hacks the value of KGN by capturing few KGNs of specific groups. Therefore, re-keying operation is performed between the sensor node and BS secretly. Each sensor node is pre-loaded with secret key along with its unique ID. The BS generates a key that is shared among the clusters through the session key. This makes communication more efficient between the clusters.

To filter the injected false data, the prevention of false data with Fuzzy-based algorithm (PFDIF) is proposed. In prevention of false data injection using PFDIF algorithm (PFDIF), malicious nodes are not allowed inside the network and their threshold range is “0”, “0.9”, and “1” based on Dynamic Threshold Algorithm. Three different types of nodes are considered in PFDIF technique. They are low, moderate and high performer nodes. Low performer nodes carry false data and therefore are moved to ideal regions. Low performer nodes carry “0” as the threshold value. Due to low performer nodes, node losses occur in overall network. Low performer nodes are responsible for false data injection inside the network [13]. Moderate performer nodes already participate in the network operation. After a certain period of time, they are moved to ideal state region because of the introduction of false data. Moderate performer nodes have a threshold value from “0.5” to “0.9”. The main cause of the moderate performers is node delay. High performer nodes are active participants of mesh networks. They result in better performance of the network compared to low and medium performers. High performer node gives the best results in the network when compared to good and low performer nodes.

Figure 1 shows the algorithm for PFDIF. According to the Fuzzy rule, PFDIF has three different threshold value: 0, 0.5, and 1. If the false data injection is very high, the threshold value of the node is set to 0. If the false data value of the node is medium then the threshold value of the node is 0.5. If the false data injection is low or zero then the threshold value is set to 1. During the injection of false data into the network, there is a possibility for gang attacks in WSNs [14]. Based on the threshold value of the node, the current node is selected for each round.

Fig. 1 Algorithm for PFDIF

Step 1: Fix the values of total number of nodes, current node, source node, destination node Step2: Check the injected false data in each node available in the network Step 3: Set the threshold value as zero when the false data injection is very high among the nodes Step 4: Set the threshold value as 0.5 when the false data injection is medium among the nodes Step 5: Set the threshold value as 1 when the false data injection is zero or minimum among the nodes Step 6: Find the nodes based on the threshold value & Assign the current node based on its threshold

To perform a filtering scheme, BS has to update the details of hop count, number of normal reports, number of false or redundant reports of the individual nodes in each group. Based on the three values, the prevention of false data injection is performed at BS.

In Average Hop Count (AHC), the report travels through multiple hop to reach BS or destination node. If hop count increases then the energy consumption also increases (Su Man Nam et al. 2011). Average Number of Normal Reports (ANNR) is calculated by average number of normal reports without any false or injected data successfully delivered by BS or destination node. If more number of reports are transmitted by the nodes involved in each cluster then network lifetime and energy efficiency also decrease. In Average Number of False or Redundant report (ANFR), more number of false reports or redundant reports are transmitted from each sensor node through the CH to BS. If BS receives many false reports or redundant report then there is a probability for reduction in its energy. BS needs to improve its energy to detect the false report at the same time, security needs to be improved to save the original data at BS. The condition for AHC and ANNR and ANFR is given. AHC & ANNR = {L (Low), M (Medium), H (High)}, ANFR = {F (Few), M (Many)}.

Figures 2, 3, and 4 indicate AHC, ANNR, and ANFR at three conditions such as low, medium, high. In AHC, low threshold value is in the range between 0 and 0.4, high threshold value is 1 and medium threshold value is 0.5 [2]. In ANNR, low threshold value is between 0 and 0.45, medium threshold value is between 0.45 and

Fig. 2 Average number of hop count

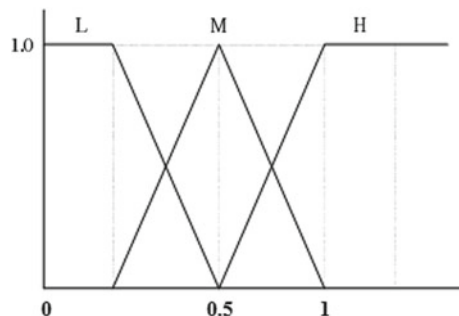


Fig. 3 Average number normal report

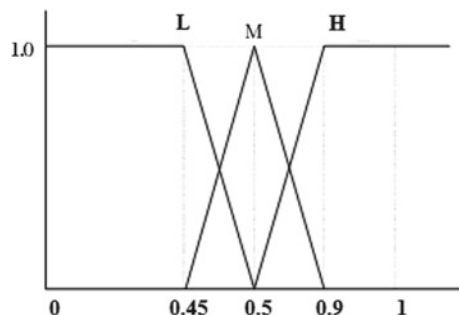
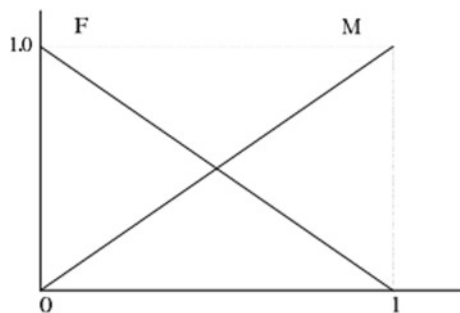


Fig. 4 Average number of false report



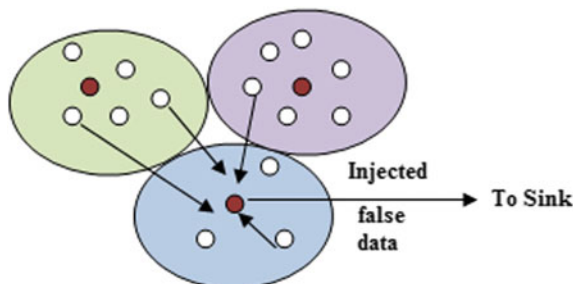
0.9 and high threshold value is 1. In ANFR, few reports are received at the threshold value of 0 and many reports are received at the maximum threshold value of 1.

4 Gang Attack with Injection of False Data

Gang attack occurs when all the clusters inside WSNs feed the same data to update at BS. Single attack affects the WSNs when the data is forwarded from the source node. Then there is a possibility to hack the data by the intruder and to inject the false data. The routine work of the nodes is distressed by the attacker. If it happens in sink level, the information collection process from each region is entirely collapsed. Therefore extracting faulty information at destination level and nodes in the region level are significant. The proposed method concentrates the filtering mechanism at the sink level.

Figure 5 shows the illustration of gang attack from source to sink. In each region, red-colored nodes are identified as the source and other nodes are neighbors. Vector Quantization Method is adapted to update the position of the individual nodes available in codebook. The communication between the nodes in each region is also updated. Due to the accumulation of nodes from neighbor regions around the source node, introduction of faulty information inside each region happens. Therefore, the source nodes are ready to transfer the faulty information to sink [15].

Fig. 5 Illustration of gang attack from source to sink



5 Results and Discussion

Network Simulator (NS2) tool is used for simulation of an improved energy-efficient en-route filtering scheme for WSNs. In the proposed work, PFDIAES and PFDIF algorithms are used. Figures 6, 7, 8, 9 and 10 show the simulations at 20 and 100 ms. Details of simulation parameters are given as follows. Network area of 1500×1500 is used and 100 number of data collected from an application of patient monitoring. Spatial correlation radius of 100 m, 512 bytes of packet length, and 100 Joules of initial energy are considered. Bandwidth of 2.4 GHz and 250 Kbps of data rate and 2 and 1 μW of Transmitting and receiving power of 2 and 1 μW , 0.001 μW is considered with random and mesh topologies.

5.1 End-to-End Delay

Figure 6 shows the plot of end-to-end delay with time for the proposed PFDIAES and PFDIF algorithms and the existing algorithms such as AES- and FUZZY-based algorithms. The analysis is carried out for 100 ms. The proposed PFDIAES has a delay of 1.1 ms which is very low value than the existing AES algorithm. PFDIAES is more secure to protect the data in the network from attacks such as gang attack, Denial of Service attack, and Sybil attack. The proposed PFDIF has a delay of 2.4 ms which is lesser value than the existing algorithm. In PFDIF algorithm, low delay value is produced for non-real-time traffic. Also, a prioritization based mechanism is used for the effective utilization of the network.

Fig. 6 Time versus end-to-end delay

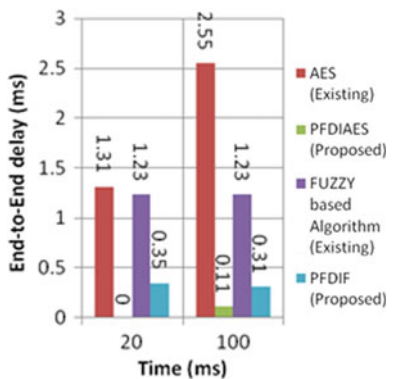
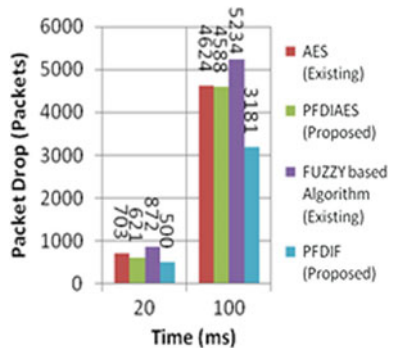


Fig. 7 Time versus packet drop



5.2 Packet Drop

Figure 7 shows the plot of time versus packet drop analysis. In the time period 100 ms, PFDIAES drops 36 packets which is very low value than the existing AES algorithm as PFDIAES uses 64-bit key levels. At the time instant of 100 ms, PFDFIF has 2053 packets drop which is very low value than the existing FUZZY-based algorithm. In PFDFIF the user generates different priority traffic. when the buffer overflow occurs, packets from low priority flow is selectively discarded.

5.3 Packet Delivery Ratio

Figure 8 shows the plot of time versus packet delivery ratio analysis. At the time instant of 100 ms, the proposed PFDIAES has 9 packet delivery ratio which is higher

Fig. 8 Time versus packet delivery ratio

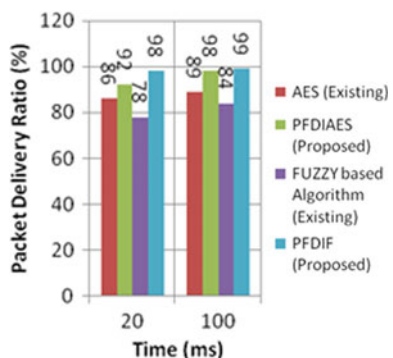
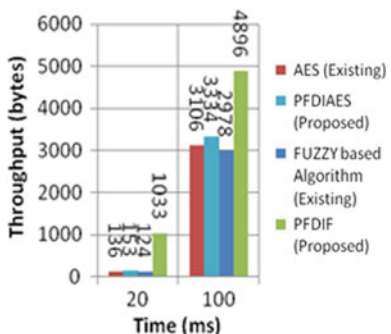


Fig. 9 Time versus throughput



value than the existing AES algorithm. At the time instant of 100 ms, PFDIF has 15% higher packet delivery ratio than the existing algorithm as PFDIF has the option to detect false or redundant reports by calculating average number of false or redundant reports.

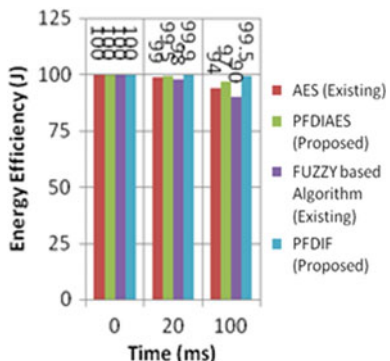
5.4 Throughput

Figure 9 shows the plot of throughput with time for the proposed PFDIAES and PFDIF algorithms and the existing algorithms such as AES- and FUZZY-based algorithms. At the time interval of 100 ms, PFDIAES has 1790 bytes of throughput which is very higher than the existing AES algorithm. At the time instant of 100 ms, PFDIF has 356 bytes of throughput which is higher value than the FUZZY algorithm. Based on the threshold, the malicious node is easily filtered.

5.5 Energy Efficiency

Figure 10 shows the plot of Time versus Energy Efficiency. At the time instant of 100 ms, the proposed PFDIAES has 3 Joules of energy efficiency which is high value than the existing AES algorithm. The frequency of injection of false data is reduced and energy efficiency level is also improved using PFDIAES algorithm. At the time instant of 100 ms, the proposed PFDIF has 9.5 Joules energy efficiency which is higher value than the existing FUZZY-based algorithm.

Fig. 10 Time versus energy efficiency



6 Conclusion

An improved energy-efficient faulty information extraction using PFDIF and PFDF-AES algorithms is proposed to prevent false data injection at node, sink. PFDF algorithm achieves better results towards energy efficiency than the PFDIAES algorithm because based on the threshold value of nodes, the false data injection inside the network is eliminated at node level itself. The results have been tabulated and it shows the evaluation of proposed versus existing schemes. On average, PFDIF has 14.74% end-to-end delay which is very low value and 69% energy efficiency which is higher value than that of PFDIAES algorithm. From the results, PFDIF provides better results in terms of energy efficiency. In the future, en-routing filtering scheme may be analyzed using various security algorithms and the performance of the network will be analyzed using different types of attacks.

References

1. Bhattacharyya, D., Kim, T.-H., Pal, S.: A comparative study of wireless sensor networks and their routing protocols. *Sensors* **10** (2010)
2. Chong, C.-Y., Kumar, S.P.: Sensor networks: evolution, opportunities and challenges. *Proc. IEEE* **91**(8) (2003)
3. Lu, R., Lin, X., Zhu, H., Liang, X.: BECAN: A bandwidth—Efficient cooperative authentication scheme for filtering injected false data in wireless sensor networks. *IEEE Trans. Parallel Distrib. Syst.* **23**(1), 32–43 (2012)
4. Haider, T., Yusuf, M.: A fuzzy approach to energy optimized routing for wireless sensor networks. *Int. Arab J. Inf. Technol.* **6**(2), 179 (2009)
5. Kim, M., Kim, Y., Cho, H.: Design of cryptographic hardware architecture for mobile computing. *J. Inf. Process. Syst.* **5**(4), 187 (2009)
6. Zhang, Z., Jiang, C.: False data injection—Resilient security routing protocols for wireless sensor networks. *J. Netw.* **7**(12), 2025–2030 (2012)
7. Godbole, V.: Performance analysis of clustering protocol using fuzzy logic for wireless sensor network. *IAES Int. J. Artif. Intell. (IJ-AI)* **1**(3), 103–111 (2012)

8. Shahina, K., Pavithran, A.: Filtering scheme for injected false data in WSN. *IOSR J. Comput. Eng.* **13**(6), 29–31 (2013)
9. Benamar, K., Djilalli, M., Mohammed, F., Abdellah, M.: An efficient key management scheme for hierarchical wireless sensor networks. *Wirel. Sens. Netw.* **2012**(4), 155–16 (2012). <http://dx.doi.org/10.4236/wsn.2012.46022>
10. Jiang, H., Sun, Y., Sun, R., Xu, H.: Fuzzy-logic-based energy optimized routing for wireless sensor networks. *Int. J. Distrib. Sens. Netw.* **2013**(216561) (2013)
11. Yang, X., Lin, J., Yu, W., Moulema, P.M., Fu, X., Zhao, W.: A novel en-route filtering scheme against false data injection attacks in cyber-physical networked systems. *IEEE Trans. Comput.* **64**(1), 4–18 (2015)
12. Vuran, M.C., Akyildiz, I.F.: Spatial correlation—Based collaborative medium access control in wireless sensor networks. *IEEE ACM Trans. Netw.* **14**(2), 316–329 (2006)
13. Lee, H.Y., Cho, T.H.: Fuzzy-based adaptive threshold determining method for the interleaved authentication in sensor networks. In: Proceedings of 5th Mexican International Conference on Artificial Intelligence. Lecture Notes in Computer Science, Advances in Artificial Intelligence, vol. 4293, pp. 112–121 (2006)
14. Moon, S.Y., Cho, T.H.: Key index-based routing for filtering false event reports in wireless sensor networks. *IEICE Trans.* **95-B(9)**, 2807–2814 (2012)
15. Gao, Zhipeng, Cheng, Weijing, Qiu, Xuesong, Meng, Luoming: A missing sensor data estimation algorithm based on temporal and spatial correlation. *Int. J. Distrib. Sens. Netw.* **2015**, 1–10 (2015)



P. T. Kalaivaani received her B.E degree in Electronics and Communication Engineering from Periyar University, Salem in 2004. She received her M.E degree from Anna University, Chennai in 2006. She is a Goldmedalist in M.E. She obtained her Ph.D. degree in Information and Communication Engineering from Anna University, Chennai in 2018. She has 13 years of teaching experience. Her areas of research include Wireless Sensor Networks, Network Security, Digital Image Processing, Neural Network, Digital Signal Processing, Cloud Computing, and IoT. She is currently working as an Associate Professor and Head of the department in the Department of Electronics and Communication Engineering, Vivekananda College of Technology for Women, Tiruchengode, Tamilnadu, India.



Raja Krishnamoorthy received his B.Tech Degree from Anna University, Chennai, India in 2007, M.Tech degree from Anna University, Coimbatore, India in 2011 and the Ph.D. degree from Anna University, Chennai, India in 2017. His primary area of research activity is low power VLSI Design, Wireless Sensor Networks with IOT, and Biomedical Engineering. He has published many research articles in refereed journals. He has 12 years of teaching experience. He is currently working as Professor in the Department of Electronics and Communication Engineering at CMR Engineering College, Hyderabad, Telangana.

Cyber Attacks and Security—A Critical Survey



Nithin Kashyap, Hari Raksha K. Malali, and H. L. Gururaj

Abstract We know that all live in the era of the internet where most of everyday task is done over the internet from online transaction to net banking. Since web is a global stage that connects people around the world everyone can access the resources provided by the internet from anywhere. This Internet is sometimes used by few people for criminal purposes like invading person's privacy, scams, cyberbullying, etc. These acts are termed as cybercrime. This paper provides a survey of these cybercrimes which are performed using various attacking mechanisms in India.

Keywords Cybercrime · Internet · Cyber-attacks · Technology · Networks

1 Introduction

Today the internet technology is used by almost everyone across the globe. This is a global network of inter-connected computers where one can be connected to another computerized device. From sharing their knowledge, messages to online banking, internet encompasses everything we deliver in our daily lives almost touching every aspect of life. The nation has become much dependent on this internet that it has almost 295 million users in urban India and 180 plus in Rural India and this has paved us a way to stand second in terms of internet users in the world. The explosion of Internet has brought blast of hacking and hacking society with its very own progression and guidelines.

With the wildly developing utilization of the web by the clients, ensuring their significant data is the need of great importance. A modernized gadget that isn't having suitable security controls can be tainted with noxious logic or by cross-site scripting assault and accordingly any kind of data can be accessed at any particular

N. Kashyap (✉) · H. R. K. Malali · H. L. Gururaj
Department of Computer Science and Engineering, Vidyavardhaka College of Engineering,
Mysuru, Karnataka, India
e-mail: nithin.kashyap98@gmail.com

H. R. K. Malali
e-mail: rakshamalali@gmail.com

time. The number of contaminated Web Pages and noxious sites can be seen each day that taints the computer and enable programmers to increase illicit access to other computer frameworks. A decade ago, cyber-threats were just a 4-digit number and today a decade later it is almost an 8-digit number. The danger of this cyber-crime is even actually looming large on the fields of defense, education, and even the telecom sectors too. According to the census made, dating back to 2015, around 164 government websites were hacked. The risk is bigger because of lack of digital hygiene is critical as well as non-critical sectors. According to the recent survey conducted in India reveals that many organizations have neither a formal information security policy nor training for information security awareness.

2 Related Work

The Internet was first figured in the late 50s under the rules of the Department of Defense's Advanced Research Project Agency (DARPA) which lead into a little system ARPANET which was an early packet-switching system and the main system to execute the convention suite TCP/IP, which structure the firm establishment of the Internet [1]. The following two decades or so went on with lively research, and later it was made available to the overall population and today zillions of individuals over the globe are subject to this. The roots began crawling to India with the dispatch of the Educational Research Network (ERNET) in 1986, with the inception by the Department of Electronics (DOE), with the financing support from the Government of India and United Nations Development Program (UNDP) including eight chief organizations as participating agencies—NCST Bombay, Indian Institute of Science, five Indian Institutes of Technology at Delhi, Bombay, Kanpur, Kharagpur and Madras, and the DoE in New Delhi [2], till then system was just made accessible in research and education communities. Later on August 15, 1995 Videsh Sanchar Nigam Limited (VSNL) propelled open Internet access in India, which changed the elements ever of. Since 1995, in any case, practically all traffic is extended TCP/IP.

2.1 Cyber Crime

In the epoch of technology and advancement in science possibilities of data theft is high. This was later called cyber-crime. Cyber-crime is any crimes include a computer and a system, sometimes computer might be utilized to carry out crime, in different cases computer may have been the objective of crime. Making infections and spreading it is called Cyber-crime. Current society today requests a level of network between the financial establishments, instructive organizations, residents and the administrations which must cross a wide range of political and social boundaries. Today, this is satisfied by the advanced innovation and gives its clients numerous profitable advantages, and at the same time it is giving a refined situation to crimes

that extend from vandalism to the stolen personality to theft of government data. The development and the historical backdrop of information burglary can be effectively followed and it even really correspond with the advancement of the system itself. The main crime was of straightforward hacks to steal data from the neighborhood. With the development in web so did the assaults as well. The primary real blow of cyber-crime accompanied the growth of email during the late '80s. It allowed for a large group of hacks or malware to be conveyed to the inbox. The second blow in the history of cybercrime timeline came in the early '90s with advancement in the web and with this most were vulnerable to viruses whenever the questionable websites were visited it was more prone to viruses, some even caused the computer to lag, some caused the irritating spring up of commercials to swarm the screen or even divert to some awful pornography destinations. Crime truly started to take off in the mid-2000s when online networking sprung up. Flood of individuals putting all their data into a profile database made a pool of individual data and this raised ID burglary. Cheats utilized this database in various ways including getting to ledgers, setting up Visas or other budgetary extortion. It is significant to make reference to that the initial Data robbery occurred in the Bhabha Nuclear Research Center (BARK) in 1998, which was maybe the primarily recorded Internet crime in India [3].

2.2 *Types of Cybercrime*

The various cybercrimes are discussed in this section

1. Web Hijacking

The process of modifying a browser with the help of unwanted software which changes the settings of the user without his/her permission on injecting unwanted advertising into the user's browser. This results in replacing the homepage, error page and search engine on its own. This forceful intervention to control another person's website is termed web hijacking [4].

2. Virus Dissemination

A virus is capable of self-replication on a given machine. This may spread between disks or files but the emphasizing character is that it can recreate itself on its own without traveling to a new host. Currently there are around 30,000 plus computer viruses in existence. The first virus was created to show software loopholes [5].

- (a) Trojan Horses: Unlike viruses' Trojan horses cannot duplicate itself, nor can it propagate without end user's assistance. Usually, the malware programming is hidden in the innocent-looking email attachments or in the free downloads, on clicking these attachments the malware hidden in it is transferred to the user's computing device and this even actually can erase the entire hard disk [6].
- (b) Worms: They are the little bit of software that uses the gadget, web, and security to duplicate its copy of the worm that searches the network for another gadget that has an unambiguous security opening. Consequently, it duplicates itself to new gadget utilizing the security gap and begins to repeat [7].

- (c) Email Viruses: This sort of infection moves around in email messages to imitate itself by automatically mailing itself to many individuals in the victim's email address [8].
- (d) SQL Injection: It is a code injection technique widely used by hackers to exploit software or application that runs a website. This assault can be utilized against an unprotected SQL database. This technique includes entering bits of SQL code into a web structure section field, generally username and passwords to give the programmer access to the backend or to a client's record. The data provided in the sign-in fields is changed over into SQL commands. This order checks the information entered against a pertinent table, in the event that the information matches, at that point access to that table is conceded [9].

SQL injection can have a huge impact on a business. A successful attack may destroy its database and may, in turn, result in a loss or leak of important information [9].
- (e) Denial-of-Service (DOS): DOS assault is an unequivocal endeavor by aggressors to refuse service to the clients of that administration. It includes a way towards sending a resource with a larger number of solicitations than it can deal with. This makes the asset crash or backs off essentially so nobody can get to it with this method, the aggressor renders a site inoperable because of enormous traffic.
- (f) Phishing: It is a social engineering attack that is used to retrieve private data like credit card details and passwords by posing themselves as a legal enterprise. This is done usually by spoofing a mail which contains the link to a website that appears to be a legitimate website but is actually a phishing website [9].
- (g) Vishing (voice phishing): It includes calling a victim by using counterfeit personality and tricking them into believing the call to be from a trusted association. For instance: They may profess to be from a bank and may request the victim's account number [9].
- (h) Cyberstalking: This is a type of cybercrime where a person is followed or pursued by someone online. Cyber Stalker doesn't seek after the victim physically however does as such practically by following their online activity and collect data from it. They then use this information to harass the victim usually through verbal intimidation, emails or chat rooms. This is a direct violation of a person's privacy online [4].
- (i) Email Bombing and Spamming: This kind of assault includes the aggressor sending immense volumes of email to a focused on victim bringing about the crashing of the victim's email account or mail server. Email bombing is typically completed by utilizing botnets. This sort of assault is progressively hard to control or oversee because of many source addresses and these botnets will be modified to send various messages to thrashing spam channels. Spamming is a sort of email besieging where mass messages are sent to enormous number of clients unpredictably. Opening these emails may contain a link to phishing websites hosting malware to get the victim's credentials or more precisely their confidential information [10]. Accessibility evaluation of private and public website in India [11].

3 Analysis Survey

Figure 1 indicates the cybercrime rates in various Indian states. We can observe that the ratio between complaint lodged and people arrested is highest in Madhya Pradesh then followed by Maharashtra then the other states.

Figure 2 gives a brief estimate about the various kinds of cyber-attacks India witnessed between the year 2014–17.

Figure 3 indicates the impact of cyber-attacks in various industries. It is observed that technology and social media industry was affected the most according to the survey conducted between 2014 and 2018. Other industries followed with the least affected being retail and consumer products industry.

Fig. 1 Indicates the cybercrime rates in various Indian states

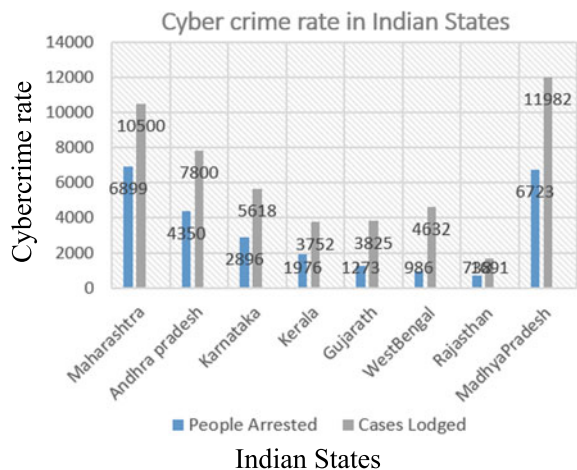
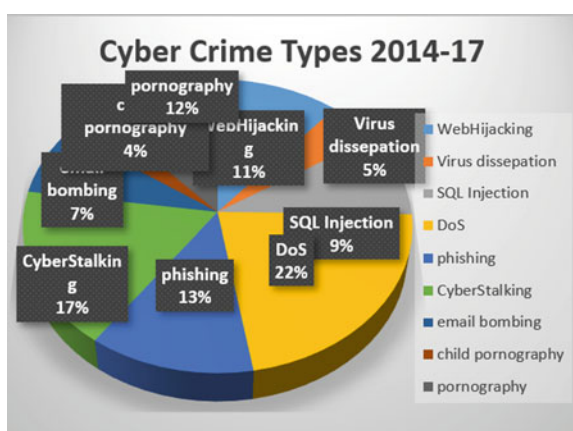


Fig. 2 Different types of cyber-attack and its impact between 2014 and 2017



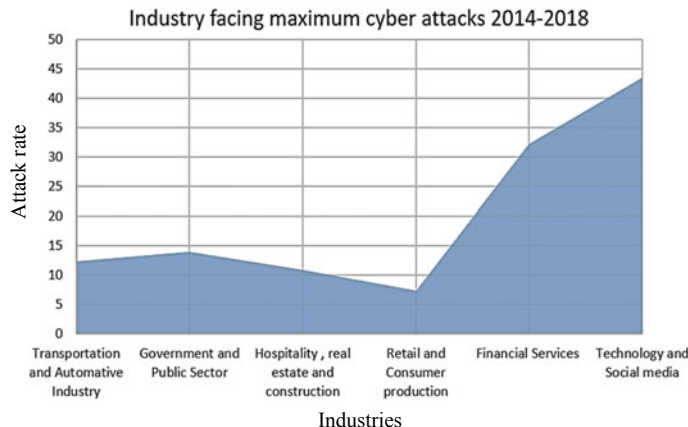
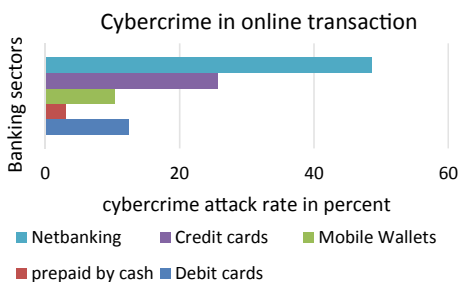


Fig. 3 Cyber-attacks on various industries

Fig. 4 Cybercrime related to online transaction



In reference to Fig. 4, we can say that, Digitalization took India by storm with this cybercrime did increase two folds. Cybercrime related to payment is enough to rattle anyone. In the above graph throws light on the crime rate during online transactions.

4 Case Studies

4.1 Call Fraud in Mphasis Citibank Pune

Many ex-workers of BPO part of Mphasis limited Msouce, misled US clients of Citi Bank by getting practically 1.5 crores accounts were compromised. This created concern in regards to information assurance. This wrongdoing was submitted by unapproved access to the client's electronic record space. Therefore, it falls in the domain of cybercrime.

Information technology act (ITA)-2000 is flexible so as to take into consideration of crimes that are not specified in ITA-2000 but are mentioned in other sections of law. Hence this case was registered under this act [12].

4.2 *The Bank NSP Case*

This case is where a trainee of the bank was going to get married, the couple used to trade messages from organization's Computers because of some reason they separated, not long after from that point forward, the young lady made many phony email id's and sent mail to the boy's international customers, she utilized bank's computer to do this wrongdoing. The boy's organization lost numerous customers and they prosecuted that bank. The bank was considered in charge of the messages sent by their framework [12].

4.3 *SONY.SAMBANDH.COM Case*

India witnessed its first-ever cybercrime conviction. It started when Sony India which ran a site www.sony-sambandh.com. This site targets nonresidential Indians to purchase Sony items and convey them to their companions or family remaining in India; when the installment is done by means of on the web. In May 2002, an individual with the name Barbara Campa requested a shading TV and a cordless earphone. The exchange was made through her Mastercard and requested that the item be conveyed to Arif Azim in India. It was conveyed to the individual after all confirmation procedure by the organization alongside the advanced photos that the customer had gotten and ended the exchange. Anyway one and half months later the Mastercard office informed the organization that it was an unapproved exchange and the genuine proprietor denied making any such buy. The organization stopped a grievance for web based cheating at CBI which at that point enrolled a case under IPC area 418,419,420. The court sentenced Arif after the charged conceded his guilt [13]. This was the first run through where a cybercrime was convicted [12].

4.3.1 *Case Study on Cyber Crime in Bengaluru*

Bengaluru which is a technology hub is also regarded as the IT capital of India. It holds first place re the list of cities with most number of cybercrimes in India. The city registered most number of cases regarding cybercrimes in the year 2018. India's technology capital is said to have registered more than 5000 FIRs at the

cybercrime police station. In comparison Bengaluru has more cybercrime related cases in comparison with other major cities of the country. Based on the report released by the National Crime Records Bureau in the year 2016 Bengaluru stood in second position among the metro cities with 762 cybercrime cases, behind Mumbai which tops the list with 980 cases. Rest of the metros were behind with Hyderabad accounting for 291 cases, Kolkata with 168 cases, Delhi with around 90 and Chennai accounted for 36 cases. The numbers saw a huge increase in Bengaluru from 762 to 5035 while in Mumbai increase was not that sharp. It was stated that most of these cases regarding cybercrimes involved job related frauds like fake promises of job opportunities. Even though popularity of Bitcoin was increasing there were no cases regarding theft of crypto-currencies [14].

5 Is Internet Safe

5.1 *Impact of Social Media*

Social Media platforms like Facebook, Twitter allows users to provide personal details which in turn may turn out to be privacy or personal security risk. For example: users may reveal about them not being in their house which increases the chances of their house being robbed. We see an immense growth in trends towards location services which can be used to inform friends and family about their location which again is a privacy risk [2].

5.2 *Cyber-Terrorism*

In this era of technological revolution, the Internet has helped the world in establishing individual identities for everyone and has connected people from all around the globe. Terrorist organizations have made use of this build themselves independent web nodes Terrorist Organizations like Al-Qaeda and ISIS are utilizing web to engender their belief systems and fear monger exercises [15]. Their systems are firmly settled to work anywhere around the globe. Today every country is combating for the protection and security of its residents. Fear-based oppressors are catching the virtual space subsequently making physical outskirts old. Obviously in this age data and learning are a type of riches in this way in the coming years the internet will be bereft of assets or military [16].

6 Prevention and Measure

6.1 Initiatives by the Government of India

Information Security Awareness: This initiative was to focus on to create awareness in students, special care to home users as they are more inclined towards online buying and non-IT professionals in a methodical way. C-DAC Hyderabad has been consigned to this venture.

Information Security Education and Awareness Project: System Administrators are trained here by offering a Diploma Course in Information Security domain. This helps the government to earn skilled issues and educational exchange programs.

National Initiative for Cybersecurity Education (NICE): The main objective is to establish a functioning, viable and constantly improving the education program in order to boost the national security issues [1].

6.2 Ways to Protect Ourselves

Using Strong Passwords: A strong password consists of a combination of alphabets, numbers and special characters, with minimum 10 characters [17].

Using an Anti-virus Software: To prevent the virus from infecting our system we should make sure that our anti-virus software is up and running with the latest update.

Encrypting the Messages: Sometimes when sending some important messages, we should encrypt the message with the help of certain encryption algorithms. Most eminently used is the RSA algorithm in which encryption can be done with the help of two large prime numbers. Encryption is given with the formula $c = me \bmod n$ where e and n are public keys of receiver. Decryption can be done with the formula $m = cd \bmod n$ where d is the private key of the receiver and m is the message.

Mobile Device Security: Mobile devices are also prone to viruses and malware so it is always advisable to download applications from only trusted sources.

7 Conclusion

The increase in growth of various technology crimes associated with it also increases. Cybercrime is proving to be a major threat to humans of this generation. Though not all folks are prey to cybercrimes we are definitely at risk. Crimes vary by degrees and not always they occur behind the systems at times systems execute it too. Hackers can be anywhere of age 11–70 years. At times hackers can be miles away from targets and wouldn't even know if they are hacked. Protection against these crimes has become need of the hour. The IT act of 2000 and cyber laws enacted by the Government of India plays a major role in taking actions against these cybercrimes. Victims who

have undergone cybercrimes should lodge a complaint to the cyber police even if they are petty crimes. The purpose of this paper is to spread responsiveness among common people about various kinds of cyber-attacks and cybercrimes taking place and to protect themselves as well as to educate the mass from the crimes.

References

1. Deepa, T.: Survey on need for cyber security in India (2014)
2. Dwivedi, D.: Technological challenges to human security in the age of information and cyber wars. *Int. J. Basic Appl. Res.* **8**, 40–48 (2018)
3. Defort, M.: Human security in the digital age: a relocation of power and control over security from state to non-state actors. *Small Wars J.* (2015)
4. The 12 types of cyber crime. <https://www.digit.in/technology-guides/fasttrack-to-cyber-crime/the-12-types-of-cyber-crime.html>. Last accessed 21 Nov 2016
5. Rouse, M.: Trojan Horse (computing). <https://searchsecurity.techtarget.com/definition/Trojan-horse>. Last accessed 29 May 2019
6. O'Hanley, R., Tiller, J.S.: *Information Security Management Handbook*. Auerbach Publications (2013)
7. Cyber Crimes in India—What is, Types, Web Hijacking, Cyber Stalking. <http://www.helplinlaw.com/employment-criminal-and-labour/CCII/cyber-crimes-in-india-what-is-types-web-hijacking-cyber-stalking.html>. Last accessed 17 Feb 2019
8. Rouse, M.: Email virus. <https://searchsecurity.techtarget.com/definition/email-virus>. Last accessed 29 May 2019
9. Sebastian, Z.: Security 1:1—Part 3—Various types of network attacks. <https://www.symantec.com/connect/articles/security-11-part-3-various-types-network-attacks>. Last accessed 06 June 2019
10. Email bomb. https://en.wikipedia.org/wiki/Email_bomb. Last accessed 24 June 2019
11. Rajendra, A.B., Rajkumar, N., Prafulla, Naveenkumar, M.R.: Accessibility evaluation of private and public websites in India. In: Pant, M., et al. (eds.): *Soft Computing: Theories and Applications*, vol. 1053. *Advances in Intelligent System and Computing* (2018)
12. Important Cyber Law Case Studies. <https://www.cyberlegalservices.com/detail-casestudies.php>. Last accessed 21 Mar 2019
13. Zhang, Y., Chen, B., Lu, X.: Intelligent monitoring system on refrigerator trucks based on the internet of things. In: *Lecture Notes of the Institute for Computer Sciences, Social-Informatics and Telecommunications Engineering* (2012)
14. Kaushik, T.: Bengaluru is India's cybercrime capital. <https://economictimes.indiatimes.com/tech/internet/whatsapp-can-trace-message-origin-says-iit-m-professor/articleshow/70580443.cms>. Last accessed 13 Apr 2019
15. Michael, G.: The new media and the rise of exhortatory terrorism. *Strateg. Stud. Q.* 40–68 (2013)
16. Morgan, S.: Cybercrime damages \$6 trillion by 2021. <https://cybersecurityventures.com/hackerpocalypse-cybercrime-report-2016/>. Last accessed 18 May 2019
17. Rubin, A.D., Geer, D., Ranum, M.J.: *Web Security Sourcebook*. Wiley (1997)

A Comparative Study on Different Techniques of Sentimental Analysis



K. S. Peeyusha, G. Pooja, S. Shreyas, and S. P. Pavankumar

Abstract Sentimental Analysis is the technique of understanding the emotions embedded in the user response or text, i.e., part of datasets. There are various methods that can be employed to analyze the emotions. This understanding is helpful in the design and development of various products, opinions about fields like politics, entertainment, trade, etc. The main focus of this paper is to understand various techniques that can be implemented for sentimental analysis. The different methods we have considered for comparative analysis in this paper are machine learning techniques, Stanford NLP libraries, sentimental sentence dictionary based on various parameters.

Keywords Machine learning technique · Twitter · Stanford NLP libraries · Sentimental sentence dictionary

1 Introduction

Sentimental Analysis plays a vital role in most of the social networking sites. Opinions are central to almost all human activities and are key influencers of our behaviors [1]. Opinions are usually subjective expressions that describe the sentiment of people, appraisals or feelings toward entities, events and their properties [2]. Therefore, the analysis of the emotions is widely applicable to the work of customer content such as reviews obtained and responses of the surveys, online and social media, and healthcare content for those applications. And hence carried out by the management which includes sales and marketing to customer care of clinical medicine.

Generally, the purpose of the emotional analysis is to determine the perception of the speaking, author or anyone related to a topic this implies the overall contact polarity or emotional response to the document, conversation or activity taking place. Attitude can be a decision or evaluation (see evaluation theory), an influential state

K. S. Peeyusha (✉) · G. Pooja · S. Shreyas · S. P. Pavankumar
Department of Computer Science and Engineering, Vidyavardhaka College of Engineering,
Mysuru, Karnataka, India
e-mail: peeyusha.kshivayogi@gmail.com

(i.e., the emotional state of the writer or speaker), or the desired emotional communication (meaning, the emotional impact or interlocutor made by the author). Despite the flux involved, a comparative study is necessary for the crystallizing of the results. The various methods considered in this paper for the study are as follows:

1. Machine learning technique
2. Stanford NLP libraries
3. Sentimental sentence dictionary.

2 Related Work

In [3], the author has chosen machine leaning for sentimental analyses of Twitter data. He cites that the process involves the identification and classification of the primary text that is available on social media, a place for a huge amount of data expressing about products, events through tweets, status updates, blog posts and many more. The challenge in the analysis of Twitter data compared to common sense analysis is the presence of glitch words, misspelled words and the constraint that the maximum character limit in Twitter is 140 [4]. The approaches such as Knowledge-based and usage of machine learning are two strategies to be used for analysis. By the analysis of the emotions in the domain-specific application, it is possible to identify the effect of the domain information in the classification of those emotions. They offer a new vector featured to classify the tweets based on polarity as positive, negative, and neutral with a score on a number scale [5].

In [6] the author has discussed the standard NLP libraries. The resources mainly include social networking sites that contain huge data and a set of libraries with a wide range of information. The obtained data is matched with the available libraries for each word contained and every word expresses a kind an emotion. Based on the number of those words falling in a category or two, the sentiment of the data is obtained. The key step is the selection of the buzzword in the data such as Election Campaign, World Health Issues, technical- Science Concepts, Inventions, Discoveries, and many more [7]. The usage of the Stanford NLP Library Cloud will handle each such word.

In [8], the author's main focus is on the sentimental sentence dictionary. Experiments show that we can achieve precision 84% for emotion recognition, and 6% precision emotional agent recognition. This method can identify eight types of emotions such as Happiness, Sadness, Love, Hatred, Surprise/shock, Uneasiness, and Temper along with the main agent that expresses the emotion. The dictionary is comprised of emotional statement patterns and the calculations of the stability are done based on these patterns, which helps in the removal of emotionless sentences but having emotional phrases.

In [9], the author introduces one of the conventional methods, i.e., the survey to analyze the sentiments. The data obtained is in such a form it suggests the type of emotion it contains and the parameters for measurement directly classifies the data thereby

making the further analysis easy. It may include ratings, multiple choices, etc., that simplifies the job of the classifier [10]. The analysis is carried out to understand the intensity of those emotions and the impact.

3 Methods Under Comparison for Sentimental Analysis

3.1 *Machine Learning*

We currently live in a data age. Due to the rapid increase in the data generated by the user on social media platforms such as Twitter, many options and new open doors are motivated for companies that end up in a track on customer reviews and their product reviews. Twitter is a microblogging social networking platform for people to publish their opinions on politics, products also certain sports, etc. These opinions help businesses, governments, and individuals. Hence, public opinion can be utilized as a useful source of tweets for data mining. Sentiment Analysis of the text obtained that expresses the polarity of the feedback about the entity (such as product, people, content, event, etc.) [11]. The purpose is to provide systematic details on the emotional analysis process in Twitter data through machine learning. Machine learning algorithms such as Naïve Bayes and Decision making are used for sentiment analysis in the proposed framework. Also some of the features like Term Frequency, negation, n-grams, Part-of-Speech and Term Presence [3]. These features enable us to discover the semantic positioning of words, phrases, sentences and that of documents. Semantic orientation is the polarity which may be either positive or negative. The machine can be trained using algorithms written for special purposes and based on the application of those studies, the results can be computed.

3.2 *Stanford NLP Libraries*

Stanford Core NLP provides technology tools to work with human language. It defines the originals of phrases, words, parts of their words, the names of organizations, people, etc., generalizing the chronology and numeric rates, identifying the structure of the sentence. It is based on phrases and syntax, like which phrases refer to the same components, feelings, having relationships, quotes that people say. The purpose of Stanford CoreNLP is that it is convenient to apply a set of linguistic analytics tools to a part of the text. CoreNLP is developed to be more flexible and expandable. You can change which devices you want to enable and disable as a single option. Many combine Stanford's NLP equipment, including Stanford CoreNLP Part-of-Speech (POS) tagger, Named Unit Recognition (NER), Parser, Coreline Resolution System, Sentiment Analysis, Bootstrap Pattern Learning, and Extra-Info Extraction Tools. In addition, the annotator pipeline contains additional custom or third-party

annotations. Analysis of Core NLP provides foundation building blocks for high-level and domain-specific text comprehension applications. It touches every aspect of NLP, e.g., co-reference resolution, negation handling, and word sense disambiguation, which add more difficulties since these are not solved problems in NLP [1]. The selection of the domain help finds the details with respect to the domain addressed and in a deeper sense using sophisticated core libraries rather than vague/naïve results.

3.3 *Sentimental Sentence Dictionary*

The rule-based emotion analysis method is proposed for opinion classification. Occasional information and the meaning of each sentence are separated according to the pattern of the sample. The semantic score is assigned to a sentence using sent-verdant in the sense obtained. The final meaning weight is calculated after each verbal inspection of each word is checked in the sentence. This decision will be made including sentence and word tonality scores. Results show that contextual information in the formation and review of the sentence is important for a feeling of perception and classification. The classification of the syntax level emotion works better than the word-level perception [12]. The limits are the dependence of lexicons and the absence of anomalies in the sense of the word. Experiments are conducted on three types of consumer review data. By the outcome, the proposed method is clear that consumer review datasets achieve averaging 86.6% at the rate of reaction and 97.8% accuracy without removing sound from the next level. However, this technique is highly précisised only for set words, processing a large set of words requires more time and complex techniques should be implemented in order to increase the level of processing texts.

4 Analysis Survey

The World Wide Web (WWW) has been created over the previous few years as a good repository of content and view data generated by users. The user expresses his view conveniently on social media such as Twitter, Facebook, etc. Social media, like Facebook, Twitter, etc. Many users can convey their views on a particular subject, regular communication, emotions, and opinions. There is no question that this constantly increasing character data is the wealthiest cause of any data decision process. The Sentiment Analysis Region has appeared to evaluate such information automatically. An analysis system with a visual component to compare consumer opinions of different products has been designed. This system is called Opinion Observer [13]. It aims at defining categorizing perspective data and typing its indications and polarity on the internet, i.e., advancing perspective favorably or wrongly. Summarizing all the customer reviews of a product forms a very important feature [14]. Sentiment Analysis is an issue with text-based assessment, but in contrast with traditional text-based

assessment, there are few difficult challenges that obviously express the need for an attempt to operate on these issues and are accessible to numerous other possibilities for potential studies on adverse leadership, concealed feelings, recognizance, ingenuity, and polysemy. However, in the increasing data rate, the request for automated data analysis techniques is high [15]. Private and public website of India is evaluated for accessibility [16]. Sports data are evaluated and compared with the SVM and RVM techniques for sentiment analysis [17].

5 Discussion

The comparative analysis based on parameters like Time Complexity, Space Complexity, Efficiency, and Precision is tabulated below.

The comparative analysis of the three techniques proposed in this paper in Table 1, that includes various fields. The machine learning technique has more time and space complexity when compared with the two others. The efficiency is high in both machine learning and Stanford NLP whereas the former has higher precision than the latter. The datasets are extrapolated and the graphical representation looks like the following, time and space complexity increases with increasing size of the text whereas the efficiency and precision are decreased. The horizontal and vertical axes for sample size “ n ” and parameters, respectively as shown in Figs. 1, 2, 3, and 4.

The comparison yields the result that the machine learning technique is more efficient and can be employed for large data, whereas the Stanford NLP and Sentimental sentence dictionary are best suitable for reducing the time and space complexities when it comes to high-performance systems.

Table 1 Comparative analysis of three sentimental analysis techniques

Parameters	Machine learning	Stanford NLP libraries	Sentimental sentence dictionary
Time complexity	More	Less	Less
Space complexity	More	Less	Moderate
Efficiency	High	High	Low
Precision	High	Low	Moderate

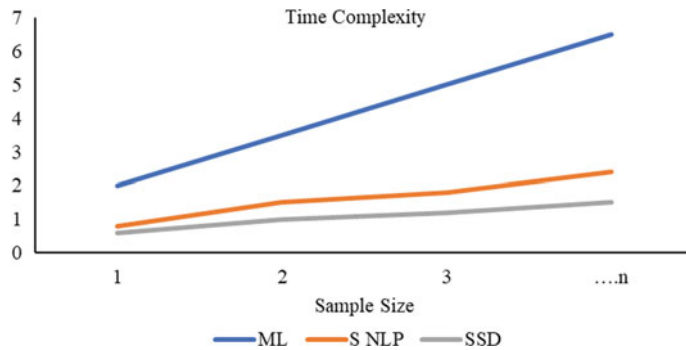


Fig. 1 Time complexity versus sample size

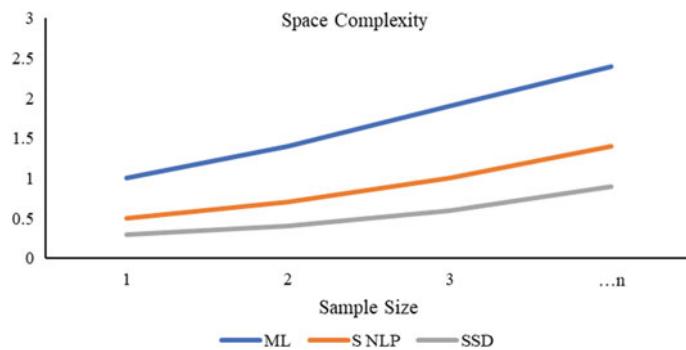


Fig. 2 Space complexity versus sample size

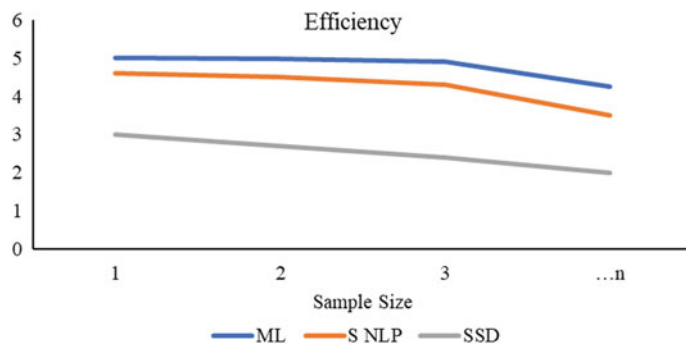


Fig. 3 Efficiency versus sample size

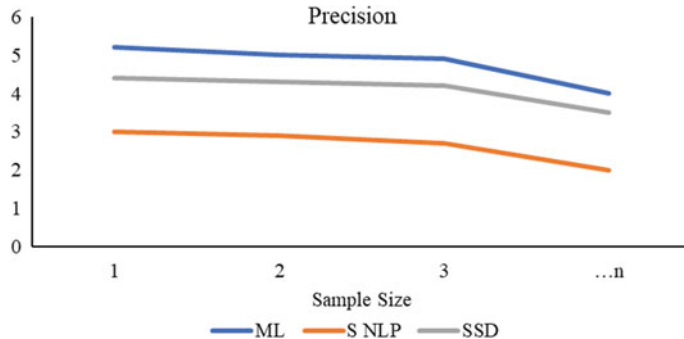


Fig. 4 Precision versus sample size

6 Conclusion

The technique of sentimental analysis is a prevailing new research directive that is important for deciding people's opinion due to a large number of real-world applications. Methodologies for document-level emotional analysis are one of the most important parts of the region. Lately, people have started expressing their views on various things on the web, which increases the requirement to analyze online content that is relevant to many of the real-world applications. There is a lot of research in the literature to find emotions from the input. Still, there is a wide range of improvements to these existing emotion analysis models. Existing techniques can be further improved by more semantic and general knowledge. Further work towards accepting diverse dataset and improving the precision is in the requirement for better results.

References

1. Liu, B.: Sentiment analysis and opinion mining. SoCTA, April 22 (2012)
2. Liu, B.: Sentiment analysis and subjectivity. In: Indurkhy, N., Damerau, F.J. (eds.) *Handbook of Natural Language Processing*, 2nd edn. SoCTA (2010)
3. Neethu, M.S., Rajasree, R.: Sentiment analysis in twitter using machine learning techniques. In: 2013 4th International Conference on Computing, Communications and Networking Technologies, ICCCNT 2013 (2013)
4. Gautam, G., Yadav, D.: Sentiment analysis of twitter data using machine learning approaches and semantic analysis. In: 2014 7th International Conference on Contemporary Computing, IC3 2014 (2014)
5. Ye, Q., Zhang, Z., Law, R.: Sentiment classification of online reviews to travel destinations by supervised machine learning approaches. *Expert Syst. Appl.* **36**, 6527–6535 (2009)
6. Kisan, H.S., Kisan, H.A., Suresh, A.P.: Collective intelligence & sentimental analysis of twitter data by using StandfordNLP libraries with software as a service (SaaS). In: 2016 IEEE International Conference on Computational Intelligence and Computing Research, ICCIC 2016 (2017)

7. Manning, C.D., Surdeanu, M., Bauer, J., Finkel, J., Bethard, S.J., McClosky, D.: The Stanford CoreNLP Natural Language Processing toolkit. In: Proceedings of 52nd Annual Meeting of the Association for Computational Linguistics: System Demonstrations, pp. 55–60 (2014)
8. Liu, D., Quan, C., Ren, F., Chen, P.: Sentiment and sentimental agent identification based on sentimental sentence dictionary. In: 2008 International Conference on Natural Language Processing and Knowledge Engineering, NLP-KE 2008 (2008)
9. Pak, A., Paroubek, P.: Twitter as a corpus for sentiment analysis and opinion mining. In: Proceedings of the Seventh Conference on International Language Resources and Evaluation (LREC'10), pp. 1320–1326 (2010)
10. Godbole, N., Srinivasaiah, M., Skiena, S.: Large-scale sentiment analysis for news and blogs. In: ICWSM'2007 (2007)
11. Bethard, S., Ogren, P., Becker, L.: ClearTK 2.0: design patterns for machine learning in UIMA. In: International Conference on Language Resources & Evaluation, pp. 3289–3293 (2014)
12. Socher, R., Perelygin, A., Wu, J.Y., Chuang, J., Manning, C.D., Ng, A.Y., Potts, C.: Recursive deep models for semantic compositionality over a sentiment treebank. In: Proceedings of the 2013 Conference on Empirical Methods in Natural Language Processing, pp. 1631–1642. Association for Computational Linguistics (2013)
13. Liu, B., Hu, M., Cheng, J.: Opinion observer: analyzing and comparing opinions on the web. SoCTA, May 10–14 (2005)
14. Hu, M., Liu, B.: Mining opinion features in customer reviews. SoCTA (2004)
15. Patil, H.P., Atique, M.: Sentiment analysis for social media: a survey. In: 2015 IEEE 2nd International Conference on Information Science and Security, ICISS 2015 (2016)
16. Rajendra A.B., Rajkumar, N., Prafulla, Naveenkumar, M.R.: Accessibility evaluation of private and public websites in India. In: Pant, M., et al. (eds.) Soft computing: theories and applications. Advances in Intelligent Systems and Computing, vol. 1053 (2018)
17. Athitya Kumaraguru, M., Vinod, V., Rajkumar N., Karthikeyan, S.: Parallel selective sampling for imbalance data sports activities. In: Pant, M., et al. (eds.) Soft computing: theories and applications. Advances in Intelligent Systems and Computing, vol. 1053 (2018)

An Approach to Select the Proper Combination within Positional and Non-positional Average Values of Features in Protein Classification



Suprativ Saha and Tanmay Bhattacharya

Abstract Protein classification is a vital field of research in Biological Data Mining. Selection of appropriate features with feature extraction procedure is an important part of this domain. These selective features are applied in any soft computing methodology to construct a classification model. Fuzzy ARTMAP is also a popular protein classification model which is used average molecular weight and isoelectric point as feature values. Weakness of these features was overcome by positional-average feature values. In this paper, four groups of feature extraction procedures with the combination of positional and non-positional average values of features are proposed which is applied in fuzzy ARTMAP model individually to classify unknown protein to its family. 497 unknown sequences of six different families are used to identify the best group among all on basic of classification accuracy as well as computational time. Finally, a statistical analysis of this experiment proved that combination of positional-average molecular weight and positional-average isoelectric point is provided a most significant result of classification when it was applied on fuzzy ARTMAP model with respect to better accuracy and computational time than others.

Keywords Molecular weight · Isoelectric point · Positional-average values · Non-positional-average value · Fuzzy ARTMAP model

1 Introduction

Bioinformatics includes the mix of PCs, programming devices, and databases with an end goal to address organic inquiries. Bioinformatics methodologies are regularly utilized for significant activities that create huge informational collections. Two sig-

S. Saha (✉)

Department of Computer Science and Engineering, Brainware University, Barasat, Kolkata 700125, India

e-mail: reach2suprativ@yahoo.co.in

T. Bhattacharya

Department of Information Technology, Techno India, Saltlake, Kolkata 700091, India
e-mail: dr.tb1029@gmail.com

nificant enormous scale exercises that utilization bioinformatics are genomics and proteomics. Genomics alludes to the investigation of genomes. A genome can be thought of as the total arrangement of DNA groupings that codes for the genetic material that is passed on from age to age [1]. Proteomics, then again, alludes to the investigation of the total arrangement of proteins or proteome. Notwithstanding genomics and proteomics, there are a lot more regions of science where bioinformatics is being connected (i.e., metabolomics, transcriptomics) [2]. Every one of these significant zones in bioinformatics intends to comprehend complex natural frameworks. In case of proteomics, protein sequence (a combination of 20 different amino acids) analysis is a vital field of research. Various data mining approaches are used to classify unknown protein sequences like neural network, fuzzy, rough set, etc. Selection of particular features, another important part of research, will be applied on data mining models to extract the information [3]. In this paper, different types of classification models are discussed in Sect. 2. Section 3 provides a brief knowledge regarding positional-average molecular weight and isoelectric point as the updated feature values of the fuzzy ARTMAP model are followed by the construction of separate group within combination of positional-average and non-positional-average feature values in Sect. 4. Section 5 provides an experimental analysis to identify the best group among four followed by the conclusion in Sect. 6.

2 Literature Review

A lot of classification models are proposed by various researchers on the basic of feature extraction procedure to classify unknown protein into its family. Classifier based on neural network [4] was proposed by different researchers with 90% accuracy. Here, ‘2-gram’ encoding method and ‘6-letter’ exchange group techniques are used to extract feature value which was enhanced from ‘2-gram’ to ‘n-gram’ by Zainuddin et al. [5]. Saha et al. [6] proposed the saturation point of ‘n-gram’ encoding method, which was fixed upto ‘5-gram’. This above fixation was also improved by using floating mean value in replace of standard mean value [7]. To improve accuracy, back-propagation technique [8] was proposed. Fuzzy ARTMAP model was proposed by Mohamed et al. [9], where molecular weight, isoelectric point, and hydropathy properties of sequence are used as features with 93% accuracy. Rank-based algorithm was applied on fuzzy ARTMAP to reduce CPU time by Mansoori et al. [10].

Cai et al. [11] developed rough set-based classifier with 97% accuracy which was improved using combination of all [12, 13] with 91% accuracy but low computational time. Spalding et al. [14] proposed string kernel-based model with 87.5% accuracy. String weighting scheme-based classifier was developed by Zaki et al. [15]. Fast Fourier transform-based classifier with 91% accuracy [16] was designed by Ali et al.. Tree-based classifier [17] was developed using TreeNN rules over neighborhood classifier and ROC method with 93% accuracy. Hidden Markov model-based clas-

sifier [18] with 94% accuracy was used for classification by executing three phases like training, decoding, and evolution.

Rahman et al. proposed structural analysis-based classifier [19] using structure comparison, sequence comparison, connectivity, cluster index, interactivity, and taxonomic with 98% accuracy. Caragea et al. [20] developed feature hashing-based classifier with 82.83% accuracy. SVM framework with genetic algorithm [21]-based hybrid classifier was proposed by Zhao et al. with 99.244% accuracy.

3 Positional-Average Molecular Weight & Positional-Average Isoelectric Point: The Feature Values of Protein Classification

Fuzzy ARTMAP [9, 10] is a popular classification model to classify unknown protein sequences into its family. This model involves various feature values like average molecular weight and average isoelectric point. In paper, Saha et al. [22] already described some weakness of the above features. If two protein sequences are considered with same length and same types of amino acids but positional combination of amino acids are different, in this case, value of average molecular weight and average isoelectric point value are same because of non-consideration of positional value of amino acids. These types of weakness are found in the features of traditional fuzzy ARTMAP model. This weakness will be overcame by using positional-average molecular weight [Eq. (3)] and positional-average isoelectric point [Eq. (4)] where position value of amino acid is multiplied with the molecular weight and isoelectric point of it, in place of traditional average molecular weight and isoelectric point value.

$$\text{aMolWt} = \frac{\sum_{i=1}^{\text{len}} \text{mol}_i}{\text{len}} \quad (1)$$

$$\text{aIsoEt} = \frac{\sum_{i=1}^{\text{len}} \text{iso}_i}{\text{len}} \quad (2)$$

$$\text{paMolWt} = \frac{\sum_{i=1}^{\text{len}} \text{mol}_i * i}{\text{len}} \quad (3)$$

$$\text{paIsoEt} = \frac{\sum_{i=1}^{\text{len}} \text{iso}_i * i}{\text{len}} \quad (4)$$

Equation (1) ‘aMolWt’, Eq. (2) ‘aIsoEt’, Eq. (3) ‘paMolWt’, and Eq. (4) ‘paIsoEt’ denote average molecular weight, average isoelectric point, positional-average molecular weight, and positional-average isoelectric point of protein sequence, respectively. ‘*i*’ indicates position value, and ‘len’ means the total length

Table 1 Average versus positional-average feature values of same length but different combination of protein sequence

Protein sequence	Avg. molecular weight	Avg. isoelectric point	Pos.-Avg. molecular weight	Pos.-Avg. isoelectric point
ARNCQG	121.48	6.47	412.12	21.35
ANRQCG	121.48	6.47	416.47	22.14

of a particular sequence. ‘mol,’ and ‘iso,’ point molecular weight and isoelectric point value of the amino acid.

Table 1 explains the advantage of uses of positional-average value than non-positional-average value of protein sequence to consider as features of fuzzy ARTMAP model. Here, it very much clear to observe that, in these two different protein sequences of table below, like ‘ARNCQG’ and ‘ANRQCG’ are same length and same types of amino acids are present. But combination of the amino acids are different which forms two different protein sequences. If previous methods are applied on it, then average molecular weight and average isoelectric point of two different protein sequences are same, i.e., 121.48 and 6.47, respectively. On the other hand, if positional-average molecular weight [Eq. (3)] and positional-average isoelectric point [Eq. (4)] are considered, then different results are produced for two different sequences. Positional-average molecular weight of the sequence ‘ARNCQG’ and ‘ANRQCG’ are 412.12 and 416.47, respectively. Positional-average isoelectric points of the sequence ‘ARNCQG’ and ‘ANRQCG’ are 21.35 and 22.14, respectively.

4 Problem Identification Along with Research Methodology

Nowadays, to develop protein classifier, i.e., to classify an unknown protein sequences into its families, is the most vital research. In continuation of this research, it is already observed that fuzzy ARTMAP model [9] also plays a vibrant role with various feature extraction procedures like average molecular weight, isoelectric point, hydropathy properties, etc. In this previous section, the weakness of this model and solution of it were already described. This solution also generates two different features’ extraction procedure which enhances the previous model of classification. Now problem is that, besides this solution, it also generates four combine groups of procedure to enhance fuzzy-based model. Group 1 is the combination of positional-average molecular weight [Eq. (3)] and positional-average isoelectric point [Eq. (4)]. Group 2 describes the combination of positional-average molecular weight [Eq. (3)] and non-positional-average isoelectric point [Eq. (2)]. Group 3 involves the combination of non-positional-average molecular weight [Eq. (1)] and positional-average isoelectric point [Eq. (4)]. Finally, Group 4 contains the combination of average molecular weight [Eq. (1)] and isoelectric point [Eq. (2)] which is already applied in previous model. Now, it is an important part of research to identify the best possible solution among these four groups which will apply on this model to classify unknown protein

sequences into its proper families with low computational time and high accuracy of classification.

It is obvious that, theoretically, Group 1 should be the proper approach in respect to the accuracy of the classification but, on the other hand, computational time also be another parameter to judge the classification techniques. To calculate the positional-average feature values, it should take more time than the calculation of non-positional value. In this respect, Group 1 may be or may not be the proper approach which will be applied on fuzzy ARTMAP model to classify unknown protein sequences. This contains a vital field of experimental research to choose the proper group which can increase the accuracy of classification with at least constant time of computation.

5 Experimental Result

To classify unknown protein sequences into its family, fuzzy ARTMAP model plays an important role. To execute this model, various types of features like average molecular weight and isoelectric point, etc., are used. In the previous chapter, some weaknesses of these features are identified and also an approach was proposed to solve it. Based on this proposed approach, four groups are already defined with the combination of positional-weighted and non-positional-weighted feature values. In this experiment, these four groups of features are used in fuzzy ARTMAP model separately to classify unknown protein sequences into its family. Every group contains only two features. It is right that, to classify unknown protein sequences using only two feature values is likely impossible. But it is also obvious that, these two features can reduce the classification result set, i.e., the set of possible families where the unknown sequences may belong. In this experiment, it is tried to identify that which group is provided the low size of result set along with at least same computational time.

In this paper, 497 protein sequences with six different families are used to identify one group among the four groups which can classify unknown sequences into proper family with high accuracy of classification. Table 2 provides the statistical analysis of the experiment. Here, six different protein families, i.e., ‘DsbB-like’, ‘FaeA-like’, ‘Marine Metagenome Family WH1’, ‘MiaE-like’, ‘PRP4-like’, and ‘SOCS box-like’ are used which are denoted by ‘F1’, ‘F2’, ‘F3’, ‘F4’, ‘F5’, and ‘F6’, respectively. ‘PAM_PA1_1’, ‘PAM_AI_1’, ‘AM_PA1_1’, and ‘AM_AI_1’ are used to identify positional-average molecular weight with positional-average isoelectric point in result set = 1 (Group 1), positional-average molecular weight with average isoelectric point in result set = 1 (Group 2), average molecular weight with positional-average isoelectric point in result set = 1 (Group 3), and average molecular weight with average isoelectric point in result set = 1 (Group 4), respectively. Result set = 1 means only one family is identified in the result set, i.e., most accurate classification. ‘PAM_PA1_2’, ‘PAM_AI_2’, ‘AM_PA1_2’, and ‘AM_AI_2’ are the same as above where result set = 2, i.e., two families are identified in the result set which is not an accurate classification but size of the result set is reduced from six to

Table 2 Summary report of statistical analysis of the experiment

two. This type of symbolization is sustained upto the value of the result set = 6 means all six families belong in the result set, i.e., sequence is not classified. [‘PAM_PA1_3’ to ‘PAM_PA1_6’, ‘PAM_AI_3’ to ‘PAM_AI_6’, ‘AM_PA1_3’ to ‘AM_PA1_6’, and ‘AM_AI_3’ to ‘AM_AI_6’].

This experimental analysis identifies that, Group 1 means features with the combination of positional-average molecular weight and positional-average isoelectric point, provides more accurate result of classification. In first part of the statistical analysis where result set is one, Group 1 can classify maximum number of sequences other than Group 2, 3, & 4. This trend is continued upto the result set is 3. After that, this trend goes to reverse from result set = 4 to result set is six. In the part of last where result set is 6, Group 1 provides least no. of sequences to be classified. It means a least no. of sequences are there which are unclassified. On the other hand, Group 4, i.e., combination of non-positional-average molecular weight and non-positional-average isoelectric point feature values provides maximum number of unclassified sequences. Group 2 and Group 4 cannot provide significant result in any part of the statistical analysis. From result set = 1 to result set = 6, Group 2 and Group 3 provide an average result which is not used in any conclude session. In the above scenario of the statistical analysis, it can be concluded that, if Group 1 is used in fuzzy ARTMAP model, it can provide more significant result of classification in respect to the accuracy. This experimental analysis identifies that, Group 1 means features with the combination of positional-average molecular weight and positional-average isoelectric point provide more accurate result of classification. In first part of the statistical analysis where result set is one, Group 1 can classify maximum number of sequences other than Group 2, 3, & 4. This trend is continued upto the result set is 3. After that, this trend goes to reverse from result set = 4 to result set is six. In the part of last where result set is 6, Group 1 provides least no. of sequences to be classified. It means a least no. of sequences are there which are unclassified. On the other hand, Group 4, i.e., combination of non-positional-average molecular weight and non-positional-average isoelectric point feature values provides maximum number of unclassified sequences. Group 2 and Group 4 cannot provide significant result in any part of the statistical analysis. From result set = 1 to result set = 6, Group 2 and Group 3 provide an average result which is not used in any conclude session. In the above scenario of the statistical analysis, it can be concluded that, if Group 1 is used in fuzzy ARTMAP model, it can provide more significant result of classification with respect to the accuracy.

Figure 1a-f represents a pictorial representation where a number of protein sequences of the six different families are present in every result set from one to six respect to Group 1 to Group 4. In Fig. 1a, it is clearly observed that, Group 1 category provides more significant result of classification than the other groups except for the family F3 (Marine Metagenome Family WH1). In respect to F3 family, Group 1, Group 2, and Group 3 provide more or less same results but for other families, lines for Group 1 belongs in the higher level than others. From this Fig. 1, it can be concluded that Group 1 (combination of positional-average molecular weight and positional-average isoelectric point) can help to get accurate classification, than other group, using fuzzy ARTMAP model. Figure 1b also provides the same results as like

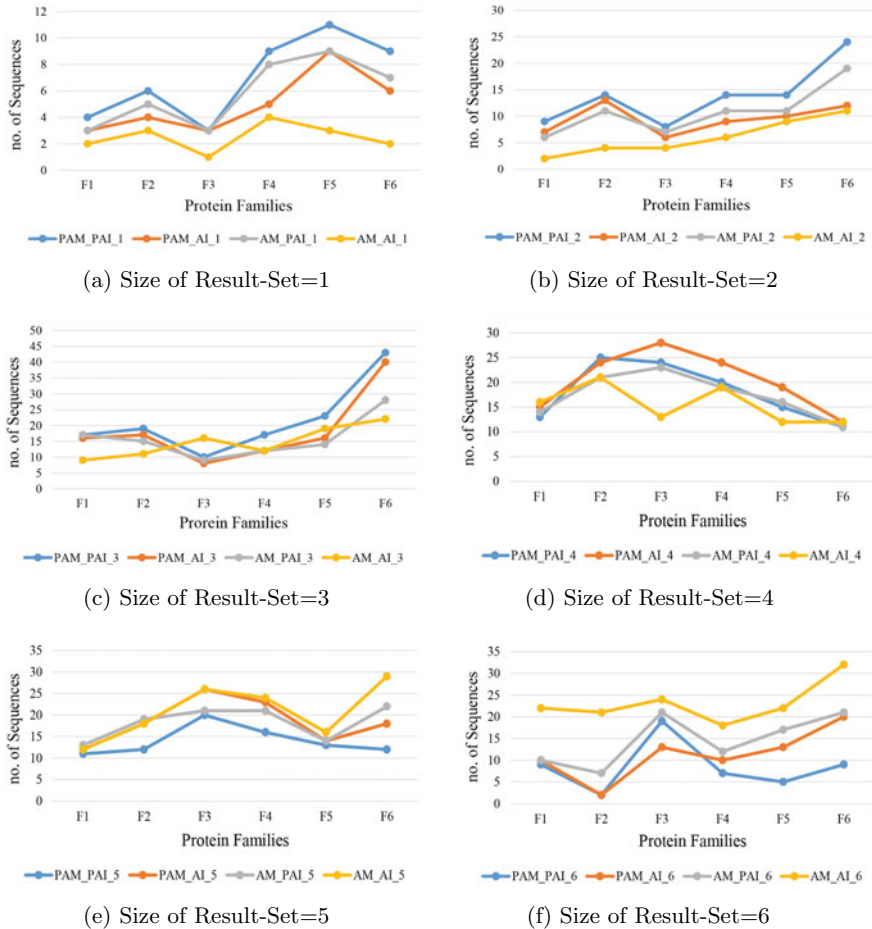


Fig. 1 Pictorial representation of the number of sequences presents in the different result sets (Result-set 1 to 6, respectively) after applying all groups of features

Fig. 1a. Here, line of Group 1 belongs in higher level than others means after using Group 1, features in the fuzzy ARTMAP model, it can reduce the value of result set from six to two, of maximum number of unknown sequences. In case of Group 2 and Group 3, for some families, Group 2 provides the better result or some cases Group 3 but every cases both belong in lower level on Group 1 and Group 4 belongs in last level in every cases. In Fig. 1b, same scenario is continued as like the Fig. 1b except family F3 (Marine Metagenome Family WH1). For F3, Group 4 provides the better result of classification but it can be considered an exceptional case. From Fig. 1d-f scenario goes to opposite one. Figure 1d line of Group 4 starts to lay in higher level means probability of classification is low for Group 4. After analysis of all above

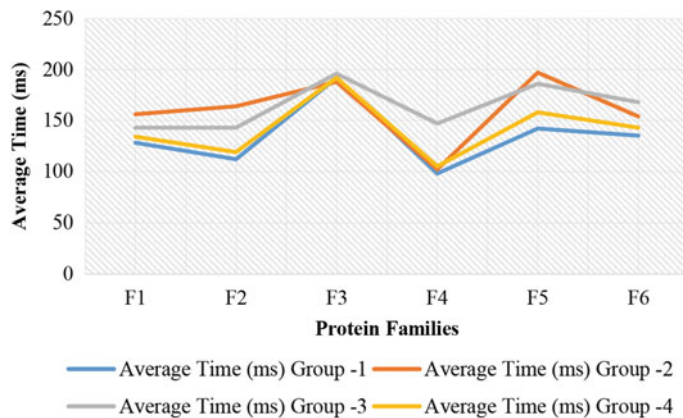


Fig. 2 Pictorial representation of computational time of every group of features respect to six different families

Table 3 Comparison of different techniques

Family name	Average time (ms)			
	Group-1	Group-2	Group-3	Group-4
F1	128	156	143	134
F2	112	164	143	119
F3	192	188	196	192
F4	98	102	147	105
F5	142	197	186	158
F6	135	154	168	143

figures, again it can be concluded that Group 1 always provides better significant result of classification with respect to accuracy (Fig. 2).

Now, in terms of computational time, Table 3 provides an experimental result that, how much time will be taken in average to classify unknown sequences into its family after using feature value of Group 1 to Group 4 into fuzzy ARTMAP model separately with respect to six individual families. This experimental result proves that for every family, Group 1 provides the low computational time than other groups. Figure 1a provides the graphical view of the above experimental result. Here, line of Group 1 is lied in the lower level of every cases means it takes low computational time for classification. After observing all the above scenario, it can be concluded that Group 1 provides the most significant result of classification with respect to both the accuracy and computational time.

6 Conclusion

Fuzzy ARTMAP is one of the important models to classify unknown protein into its family. Average molecular weight and average isoelectric point are used in this model as features. Based on the weakness of these features, positional-average molecular weight and isoelectric point are proposed and used in this model. Now, with the combination of positional-average and non-positional-average feature values, four groups of features are proposed here which were used in the fuzzy model separately. After the experimental analysis of all four proposed feature groups on 497 unknown protein sequences of six protein families, Group 1, i.e., the combination of positional-average molecular weight and positional-average isoelectric point provides more significant result of classification based on accuracy and computational time both. Finally, this feature group is used in fuzzy model to classify unknown protein sequence with more accurate and low time.

References

- Chauhan, R., Jangade, R., Rekapally, R.: Classification model for prediction of heart disease. In: SoCTA 2016. AISC, vol. 584. Springer, Singapore (2018)
- Chauhan, R., et al.: Predictive data analytics technique for optimization of medical databases. In: SoCTA 2017. AISC, vol. 742. Springer, Singapore (2019)
- Rajpurohit, J. et al.: Glossary of metaheuristic algorithms. *Int. J. Comput. Inf. Syst. Ind. Manage. Appl.* **9**, 181–205 (2017)
- Wang, J.T.L., Ma, Q.H., Shasha, D., Wu, C.H.: Application of Neural Networks to Biological Data Mining: A Case Study in Protein Sequence Classification, pp. 305–309. KDD, Boston, MA, USA (2000)
- Zainuddin, Z., et al.: Radial basic function neural networks in protein sequence classification. *Malays. J. Math. Sci.* **2**, 195–204 (2008)
- Saha, S., Bhattacharya, T.: An approach to find proper execution parameters of n-Gram encoding method for protein sequence classification. In: CCIS, Springer, vol. 1046, ICACDS-2019, Ghaziabad, India, pp. 294–303 (2019)
- Saha, S., Bhattacharya, T.: A novel approach to find the saturation point of n-gram encoding method for protein sequence classification involving data mining. In: LNNS, Springer, vol. 56, ICICC-2018, Delhi, pp. 101–108 (2018)
- Nageswara Rao, P.V., Uma Devi, T., Kaladhar, D., Sridhar, G., Rao, A.A.: A probabilistic neural network approach for protein superfamily classification. *J. Theor. Appl. Inf. Technol.* (2009)
- Mohamed, S., Rubin, D., Marwala, T.: Multi-class protein sequence classification using fuzzy ARTMAP. In: IEEE Conference, pp. 1676–1680 (2006)
- Mansoori, E.G., Zolghadri, M.J., Katebi, S.D., Mohabatkar, H., Boostani, R., Sadreddini, M.H.: Generating fuzzy rules for protein classification. *Iran. J. Fuzzy Syst.* **5**(2), 21–33 (2008)
- Cai, C.Z., Han, L.Y., Ji, Z.L., Chen, X., Chen, Y.Z.: SVM-Prot: web-based support vector machine software for functional classification of a protein from its primary sequence. *Nucleic Acids Res.* **31**, 3692–3697 (2003)
- Saha, S., Chaki, R.: Application of data mining in protein sequence classification. *Int. J. Database Manage. Syst. (IJDMS)* **4**(5) (2012)
- Saha, S., Chaki, R.: A brief review of data mining application involving protein sequence classification. In: AISC, Springer, ACITY 2012. Chennai, India, vol. 177, pp. 469–477 (2012)

14. Spalding, J.D., Hoyle, D.C.: Accuracy of string kernels for protein sequence classification. In: ICAPR 2005. LNCS, Springer, vol. 3686 (2005)
15. Zaki, N.M., Deri, S., Illias, R.M.: Protein sequences classification based on string weighting scheme. *Int. J. Comput. Internet Manage.* **13**(#1), 50–60 (2005)
16. Ali, A.F., Shawky, D.M.: A novel approach for protein classification using fourier transform. *Int. J. Eng. Appl. Sci.* **6**, 4 (2010)
17. Boujenfa, K., Essoussi, N., Limam, M.: Tree-kNN: a tree-based algorithm for protein sequence classification. *Int. J. Comput. Sci. Eng. (IJCSE)* **3**, 61–968 ISSN: 0975-3397 (2011)
18. Desai, P.: Sequence classification using hidden Markov models. <https://etd.ohiolink.edu/> (2005)
19. Rahman, M.M., Ul Alam, A., Abdullah-Al-Mamun, Mursalin, T.E.: A more appropriate protein classification using data mining. *J. Theor. Appl. Inf. Technol. (JATIT)*, pp. 33–43 (2010)
20. Caragea, C., Silvescu, A., Mitra, P.: Protein sequence classification using feature hashing. *Proteome Sci.* **10**(Suppl 1): S14 (2012) <https://doi.org/10.1186/1477-5956-10-S1-S14> (2012)
21. Zhao, X.-M., Huang, D.-S., Cheung, Y., Wang, H., Huang, X.: A novel hybrid GA/SVM system for protein sequences classification. In: IDEAL 2004. LNCS, Springer, vol. 3177, pp. 11–16 (2004)
22. Saha, S., Bhattacharya, T.: A new protein sequence classification approach using positional-average values of features. In: AISC, Springer, SoCTA2018. Jalandhar, India (2018)

Areca Nut Disease Detection Using Image Processing



A. B. Rajendra, N. Rajkumar, and P. D. Shetty

Abstract Neural networks and image processing techniques to identify and classify the importance of areca nuts in this research work. A back-propagation cellular network classifier was used to identify the significance of the areca nut. Areca nut is frequently affected with various pathogens, including crops, bacteria, viruses, and insect damage. The HSI system is used to portray the object color and the contrast curve increases the variations in brightness evenly across the image's dynamic spectrum. In the sector of areca nut advertising, Machine Vision Technology provides an alternative to replace manual sorting.

Keywords Areca nut · Disease detection · Classifier · Neural network

1 Introduction

Areca nut is one of India's major commercial plants. Areca nut, the astringent fruit of an areca palm, is often eaten with betel leaves [1]. For some Taiwanese, areca nut is a common and significant plant. While chewing areca nut is the source of oral disease, it is commonly called Taiwanese gum throughout Taiwan. Areca nut is typically grown with gentle IR flow on the mountainsides. Insects often infect areca nut. If the areca nut layer is harmed, the cost will decrease. It has only been arranged so far in Taiwan by traditional resources. The manual price and moment of sorting always affect the farmer's revenue [2].

The diseased and undiseased areca nuts are regarded for classification in the proposed work. Currently, human specialists have manually classified the diseased and undiseased areca nut (Fig. 1) [3].

A. B. Rajendra (✉) · P. D. Shetty

Department of Information Science and Engineering, Vidyavardhaka College of Engineering, Mysuru, Karnataka, India
e-mail: abrajendra@vvce.ac.in

N. Rajkumar

Accendere Knowledge Management Service Pvt. Ltd., New Delhi, India

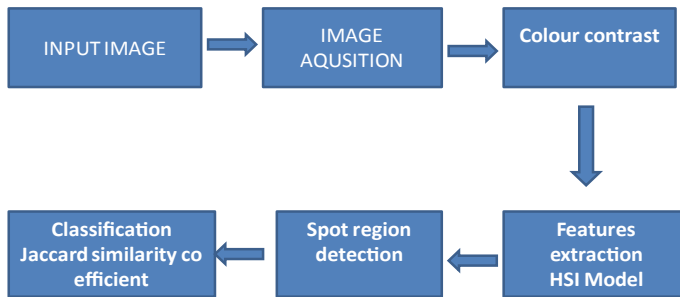


Fig. 1 Block diagram of stages

2 Related Work

Classification of diseased and undiseased areca nuts was determined using texture, local binary model characteristics, DFDF wavelets, GLCM, and GABOR. Areca nut is a section from a specified image using the Otsu technique in the suggested method. For classification, texture characteristics and a straightforward KNN classifier were used. The achievement level of LBP with histogram correlation was 92%. As a result, this technique has not accomplished outcomes. As a result, the texture features of Haer wavelets, GLCM and GABOR are obtained from each channel of HIS and YCbCr color methods which have provided a total of 14 features and dimensions of these features have been decreased to a subset of features with elevated uncertainty. For distinct texture features, the findings achieved are Haer wavelets with 92.30%, GLCM with 84.1 and 98% [1].

A novel technique is suggested in this article for areca nut in two color-based categories. The technique suggested consists of three steps. (i) Segmentation, (ii) Masking, (iii) Classification. The RGB image is transformed into a color room of YCBCR. The YCbCr image uses sigma trigger boundaries to effectively segment areca nut. The suggested technique effectively classifies CEARRON areca nuts such as api, bette, MFJFJ, and KFKK into two classes BN and NBN with the achievement level of 98.97 and 97.63%. They conclude by stating that the blue color element is usually ignored in the segmented area and that only red and yellow components are used to identify the areca nuts [4].

A solid algorithm for segmenting the food image from a context is provided using color images. They suggested a technique that has three measures. First, the computing elevated contrast gray quality picture from an ideal linear mixture of RGB color elements. Second, the global limit estimation using a statistical method. Third, the morphological procedure to complete the potential gaps described in the binary image section.

After testing the algorithm introduced in MATLAB on 45 images. The performance segmentation evaluated was 99.82% from the region under the receiving operating features (ROC) curve [5].

One of the most significant quality parameters for client preference assessment is the fruit shape. In addition, misshaped fruits are usually dismissed in accordance with the fruit sorting norm. This research was conducted to determine the quantitative fruit shape classification algorithm in kiwi fruit. Kiwi fruit physical characteristics such as assessment of external dimensions, mass, volume, and density have been evaluated. A simple method of assessment was used to detect fruit form based on an assessment of the exterior sizes of kiwi fruit. Short medium and large fruits were detected using the aspect ratio. Another ellipsoid proportion parameter was used for the detection of flat fruits. Here they are trying to assume that the aspect ratio and ellipsoid are used to determine ordinary and unshaped fruit efficiently. This technique can also be used and implemented with the same physical characteristics to other products [6].

A new model for grading oranges according to the surface features into three performance bands. Currently, this handling procedure in citrus packaging buildings is the non-automated phase. To acknowledge the radial color variety, a neural network qualifies for rotation invariant conversion. The current fruit inspection algorithm based on neural network classifies as shown to be near to fulfilling a potential commercial FJFDL grading machine necessity. A device, however, may involve a degree of profit to deal with the big collection of commercially accessible orange varieties. For instance, it may be necessary to adjust the device to specifically tiny or big oranges [7].

The development and execution of an optical detector to identify fruit color alterations by reflecting white light to evaluate fruit maturity in manufacturing and agricultural applications. Here, the electronic device was created using an Arduino Mega board that contains an Atmega 2560 micro printer for controlling the information link stream from picture sensors. Here, they present a prototype for estimating color and obtaining color quotes, created on the grounds of an RGB color sensor with a picture detector, used for color identification of mature guava fruit. Digitizing image is a useful color measurement technique because, unlike other color methods that use a single metric on a particular region, this technique can concentrate on required regions and prevent interacting with regions that might change the readings [8]. Private and public website of India is evaluated for accessibility [9]. Sports data are evaluated and compared with the SVM and RVM techniques for the sports data [10]. The same set of techniques which can help to evaluate the areca nut disease identification.

3 Problem Definition

Diseased and undiseased areca nut are regarded for classification in the proposed work. Currently, human experts have manually classified diseased and undiseased areca nut. This sorting is rather labor-consuming, time-consuming, and incompatible. In the segment of areca nut advertising, computer vision technology provides an alternative to replace manual sorting.

4 Background Process

Using image acquisition and Otsu algorithm, areca nut is segmented from a specified image in the proposed technique. RGB to HSI transformation and SRGB to studio color space transformation is used to obtain features such as three color features (i.e., mean gray level of the R, G, and B band image), main axis length, secondary axis length, region, etc. Results from each collection of features and discriminative subsets of HSI and lab color rooms are empirically chosen based on the mixture of features as shown in Fig. 2.

4.1 Segmentation

Areca nut segmentation [2] from the context is the first phase in the ranking of areca nut. The segmentation method subdivides an image into components or items that makeup it. The level of performance of this subdivision relies on the issue being fixed. The two methodologies used in segmentation are contrast enhancement and Otsu algorithm as shown in Fig. 3.

4.2 Feature Extraction

In the second step, geometric features such as the length of the principal axis, the secondary axis length, area, perimeter and compactness of the areca nut image, color features (i.e., the mean gray level of the areca nut image on the R, G and B bands), and defects area were used in the classification procedure. About 144 texture features are obtained from 6 HSI and lab color spaces color elements as shown in Fig. 4 [2].

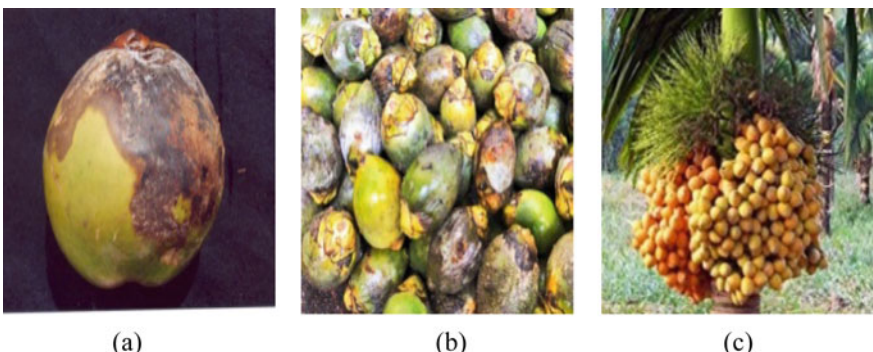
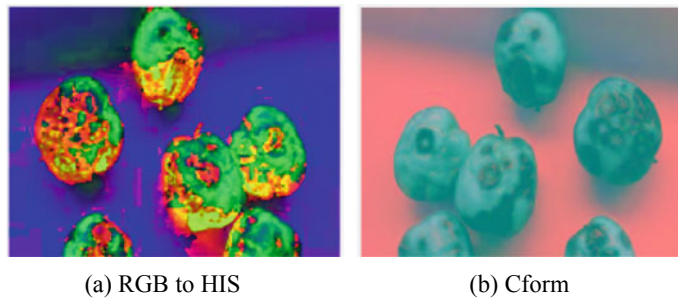


Fig. 2 Input images of diseased areca nut

**Fig. 3** Segmentation images**Fig. 4** Feature extraction

4.3 Spot Region Detection

In this phase, the objective is to use the clustering of k means to identify the diseased areca nut places. K means clustering seeks to divide n samples into k groups in which each observation corresponds to the cluster with the closest average, acting as a cluster prototype, likewise in our research k means segmentation uses each pixel as a function point with a room place, then arbitrarily locates the cluster nodes in multidimensional assessment room, the method goes on as shown in Fig. 5 [2].

5 Conclusion

In recent times, farmer's life have been made much simpler with the development of the crop illness detection system. With sophisticated classification methodologies used to identify and classify the illness with higher precision for different areca nut forests. With bare eyes, the areca nut that is diseased without any knowledge will be hard to define. In this research, the computer vision system was created to detect and classify the areca nuts as Excellent, Good, and Bad grades. The classification

Fig. 5 Spot region detection

system was established using the image processing methods, the DL algorithm, and the BPNN classifier.

The DL algorithm and image processing method can effectively segment the defect area. Three color features, six geometric features, and place spots were acquired. The following findings can be taken after studying different work performed on the forecast of areca nut illness.

1. Image processing: This phase includes capturing an areca nut image that requires to be screened for the illness.
2. Feature Extraction: Features such as areca nut form, color distinguished area, texture, etc., are obtained from the recorded image and contrasted to conventional information collection.
3. Spot Region Detection: K means clustering is implemented to the image using the extracted features and the diseased spots are identified.

References

1. Areca nut, https://en.wikipedia.org/wiki/Areca_nut
2. Huang, K.-Y.: Detection and classification of areca nuts with machine vision. *Comput. Math. Appl.* **64**, 739–746 (2012)
3. Suresha, M., Danti, A., Narasimhamurthy, S.K.: Classification of diseased areca nut based on texture features. *Int. J. Comput. Appl.* 1–6 (2014)
4. Danti, A., Suresha, : Segmentation and classification of raw areca nuts based on three sigma control limits. *Procedia Technol.* **4**, 215–219 (2012)
5. Mery, D., Pedreschi, F.: Segmentation of colour food images using a robust algorithm. *J. Food Eng.* **66**, 353–360 (2005)
6. Javadi, A., Hajiahmad, A.: Effect of a new combined implement for reducing secondary tillage operation. *Int. J. Agric. Biol.* **8**, 724–727 (2006)
7. Recce, M., Taylor, J., Piebe, A., Tropiano, G.: High speed vision-based quality grading of oranges. In: Proceedings of International Workshop on Neural Networks for Identification, Control, Robotics and Signal/Image Processing, pp. 136–144. IEEE Computer Society Press, Washington, DC

8. Filoteo-Razo, J.D., Estudillo-Ayala, J.M., Hernández-Garcia, J.C., Trejo-Durán, M., Muñoz-Lopez, A., Jauregui-Vázquez, D., Rojas-Laguna, R.: RGB color sensor implemented with LEDs. In: Kane, M.H., Jiao, J., Dietz, N., and Huang, J.-J. (Eds.) SPIE 9571, Fourteenth International Conference on Solid State Lighting and LED-based Illumination Systems, pp. 1–6 (2015)
9. Rajendra A.B., Rajkumar, N., Prafulla, Naveenkumar, M.R.: Accessibility Evaluation of Private and Public Websites in India. In: Pant M et al (eds.) Soft Computing: Theories and Applications. Advances in Intelligent Systems and Computing, vol. 1053 (2018)
10. Athitya Kumaragurum, M., Vinod, V., Rajkumar, N., Karthikeyan, S.: Parallel selective sampling for imbalance data sports activities. In: Pant M et al (eds.) Soft Computing: Theories and Applications. Advances in Intelligent Systems and Computing, vol. 1053 (2018)

Simulink Simulation for Predicting Thermodynamic Properties of Water–Lithium Bromide Solution Using ANN



Dheerendra Vikram Singh and Tikendra Nath Verma

Abstract The main aim of this work is software simulation for estimating thermodynamic properties (specific enthalpy and specific entropy) of water–lithiumbromide solution using artificial neural network under MATLAB Simulink environment. AI-Simulink simulator is developed by deploying extracted weights and bias from modeled artificial neural networks. Optimized performance is achieved with 2-10-2 ANN architecture which is validated on the basis of mean square error, coefficient of multiple determination (R^2), and absolute relative error.

Keywords ARS · ANN · Simulink

Nomenclature

- h Specific Enthalpy (kJ/kg)
 p Predicted
 s Specific entropy (kJ/kg K)
 T Temperature (°C)
 t Target

D. V. Singh (✉) · T. N. Verma
National Institute of Technology, Manipur, Imphal, India
e-mail: dheerendra.medi@gmail.com

1 Introduction

Waste heat energy operated ARS/AC cascade refrigeration system is attracting researchers because it can be run using low-temperature heat source or low-grade energy or renewable energy like solar, geothermal or biomass as well as it uses a combination of natural substances as a working fluid, which does not cause ozone depletion and global warming [1, 2]. Lack areas determination or exergetic optimization for those above systems, researchers are continuously developing new methodologies. Each methodology requires the thermodynamic properties (specific enthalpy and specific entropy) of water–lithium bromide solution. Estimation of thermodynamic properties (h and s) can be said to be the utmost thermodynamic properties for the energy and exergy analysis of an absorption refrigeration system/chillers/transformers. Many excellent procedures are available in the literature for predicting thermodynamic properties which required much knowledge of chemical science (like Fugacity in liquid solution, molar weight of salt and solution, universal gas constant, molar concentration, activity coefficient in liquid solution, chemical potential of salts and solution, etc.) and thermodynamic principles coupled with higher order differential or integral mathematical equations [3–8]. Engineering Equation Solver software is also available for the same which is based on the systematic evaluating procedure of Zhe et al. [6]. Some researchers have presented h - T - x graphs for predicting specific enthalpy of working fluids [7]. All procedures of predicting thermodynamic properties need calculating software that consumes electrical power or other software (EES) or accurate vision judgment to read-only specific enthalpy from any graph (h - T - x graph). To reduce that differential complexity and reduction, the use of computational electrical power for future mechanical and energy scientists, new computational intelligence method has been reviewed for extracting simple mathematical expressions for predicting the same. Artificial neural network is effectively suitable for tasks involving patchy or unspecific data sets, nonlinear, deficient information, and for highly intricate and imprecise problems, where humans brain usually take decision on an intuitional basis [9–14]. In this work, artificial intelligence approach has been decided to formulate simple artificial intelligent equations from validated ANN for estimating the thermodynamic properties of water–lithium bromide solution. Modeling and deployment of artificial neural network are performed under MATLAB/Simulink programming environment to see its higher computational ability.

2 Artificial Neural Network

Figure 1 illustrates how information is processed through a neuron. A neural network consists of a set of computational or processing units (cells or neurons) [9]. Similar to biological counterpart, a neuron is the processing element in the modeling of an artificial neural network which receives input information from the other element, the

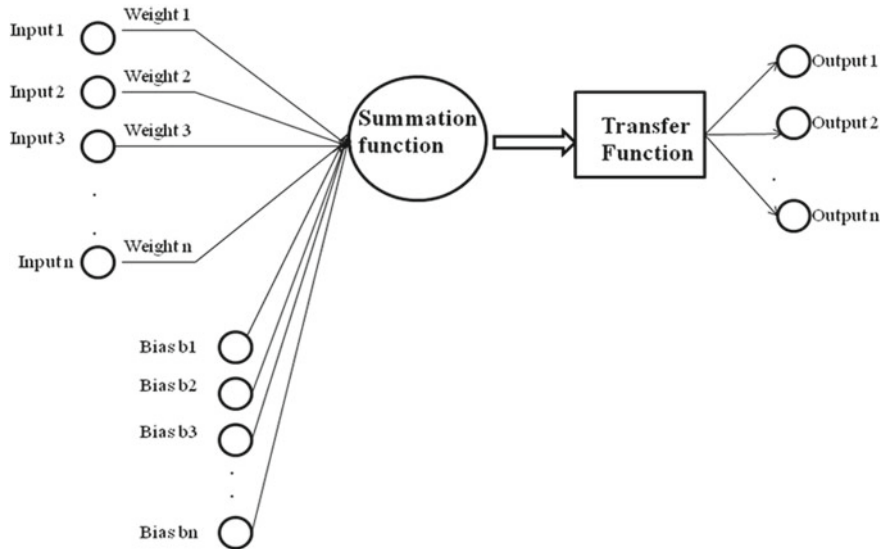


Fig. 1 ANN architecture

inputs are employed with weights and added the bias, the result is then transfigured (using transfer function) into the output.

3 MATLAB/Simulink Environment

The complexities of ANN modeling and weight and bias extraction have been kept to the minimum under MATLAB workspace environment/Simulink without compromising the extremely important attributes and exactness of the simulated model. MATLAB is high-level matrix laboratory-user-friendly programming language where users can define and write problem functions and formulate solutions using familiar mathematical notation. MATLAB workspace facilities Simulink library on the top which is a graphical mouse-friendly drag and drop program that allows the user to create the model, simulate, and examine the specific system.

4 Results and Analysis

Figure 2 illustrates a typical fully-connected neural network configuration. This configuration has one input layer, one hidden layer, and one output layer. The feed-forward artificial neural network with a back-propagation learning algorithm is used for the proposed work which is most popular among researchers. The input layer has

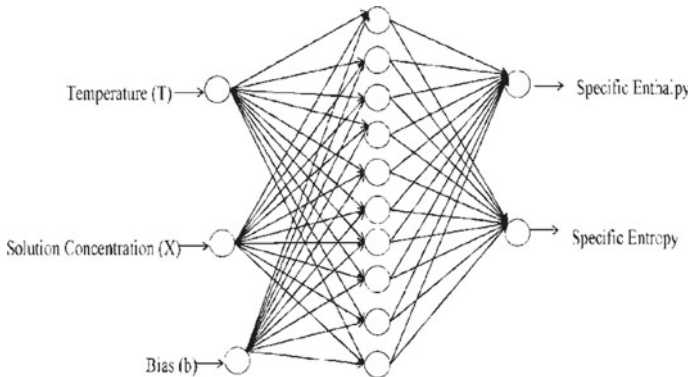


Fig. 2 Optimized 2-10-2 artificial neural network architecture

two inputs, temperature, and LiBr concentration, while the output layer predicts the specific enthalpy and specific entropy, respectively for the given input parameters. The algorithm uses Logistic Sigmoidal Transfer function as an activation function for the hidden layer and Tansigmoid Transfer function for the output layer.

Mathematical expressions of logsigmoid activation functions are expressed in Eq. (1) while tansigmoid in Eq. (2).

$$A_L(y) = \frac{1}{1 + e^{-y}} \quad (1)$$

$$A(y)_T = \left[\left(\frac{2}{1 + e^{-2y}} \right) - 1 \right]. \quad (2)$$

In the above equations, y is the sum of all weights used in modeling of the artificial neural network. Mathematical expressions of statistical methods are presented in Eq. (3) to Eq. (4).

$$RMS = \sqrt{\frac{\sum_{d,p(h/s)=1}^n (h/s_p - h/s_t)^2}{n}} \quad (3)$$

$$R^2 = 1 - \frac{\sum_{d,p(h/s)=1}^n (h/s_t - h/s_p)^2}{\sum_{d,p(h/s)=1}^n (h/s_t - h/s_{\bar{t}})^2} \quad (4)$$

4.1 Training and Validation of ANN

To train and test ANN, 440 input data patterns and corresponding targets are obtained from the past literature differential expressions work of Chua et al. [5]. In this analysis, 80% data has been used for training and remaining for testing the artificial neural network. Due to the asymptotic inherent of activation function, authors followed the principle of normalization. The input and output data patterns are in between the ranges from 0 to 1. Least value of RMSE is achieved with Levenberg–Marquardt (LM) using 2-10-2 neural network and behavior of root mean square error is presented in Fig. 3. In order to validate the artificial neural network, R^2 is achieved 0.99999 for specific enthalpy and 0.99993 for specific entropy. The regression curve is shown in Figs. 4 and 5 for specific enthalpy and specific entropy for the test data set,

Fig. 3 Pattern of mean square error based on 2-14-2 neural network architecture

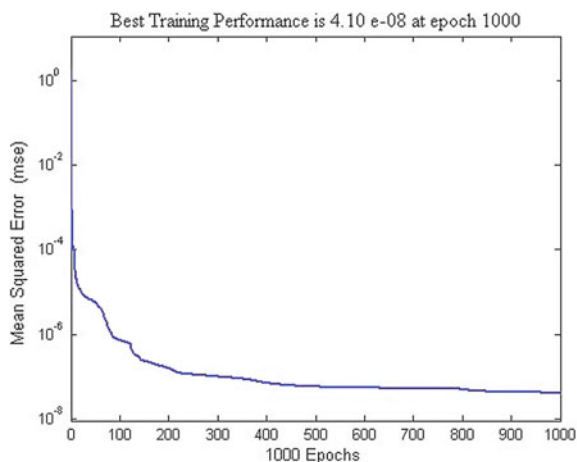


Fig. 4 Regression analysis— R^2 of actual specific enthalpy [5] versus from ANN

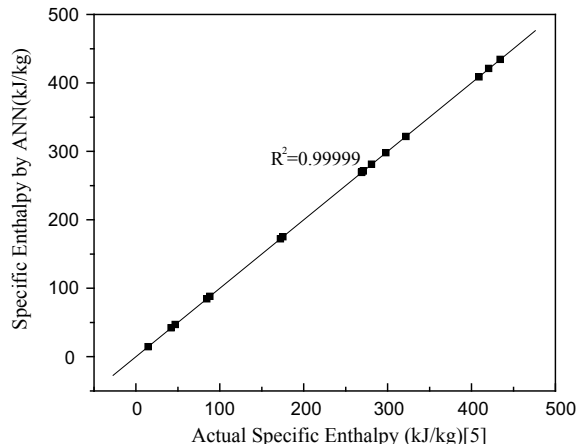
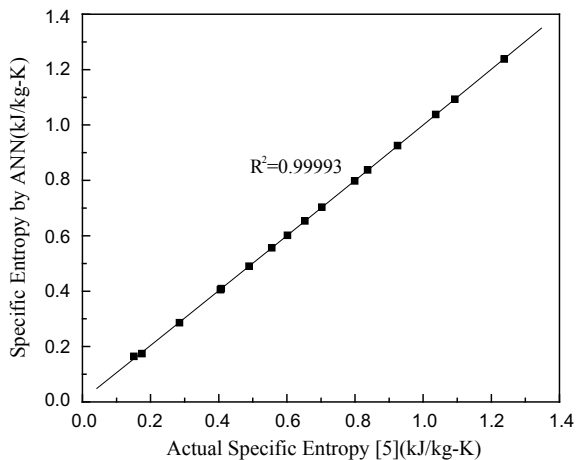


Fig. 5 Regression analysis— R^2 of actual specific entropy [5] versus from ANN



respectively. It is clearly observed that authors have achieved less value of Sum of the absolute relative errors. AI formulated linear and exponential equations are deployed in Simulink workspace using constant, display, and different function model blocks from library which is shown in Fig. 6. Simulator work space is reduced by creating simulator subsystem which makes it user-friendly for non-skill persons. Simulator metafile view is depicted in Fig. 6. All functional model blocks are contained by Subsystem_Combined model block. User can only pass the input information and press the run command. Thermodynamic properties will be displayed in display block. Table 1 shows another validation of above formulated mathematical expressions and Simulink Simulator on the basis of the absolute relative error. Specific enthalpy and entropy is reported from present and past published work on the same input parameters.

5 Conclusions

The aim of this paper is to present extraction linear and exponential mathematical expressions for estimating the thermodynamic properties of water–lithium bromide using an artificial neural network approach. These expressions reduce the need to follow complex differential mathematical expressions or read $h-T-x$ graphs or use of EES software for predicting the same. Mathematical expressions derived from the trained and validated artificial neural networks do not require artificial neural network programming dedicated software for predicting thermodynamic properties, every time we need to make a new prediction. These are free from any higher order differential or integral complexity which does not require electrical power because these can be solved on the calculator. Therefore, these mathematical expressions easily deployed in Simulink environment and developed AI-based simulator for predicting

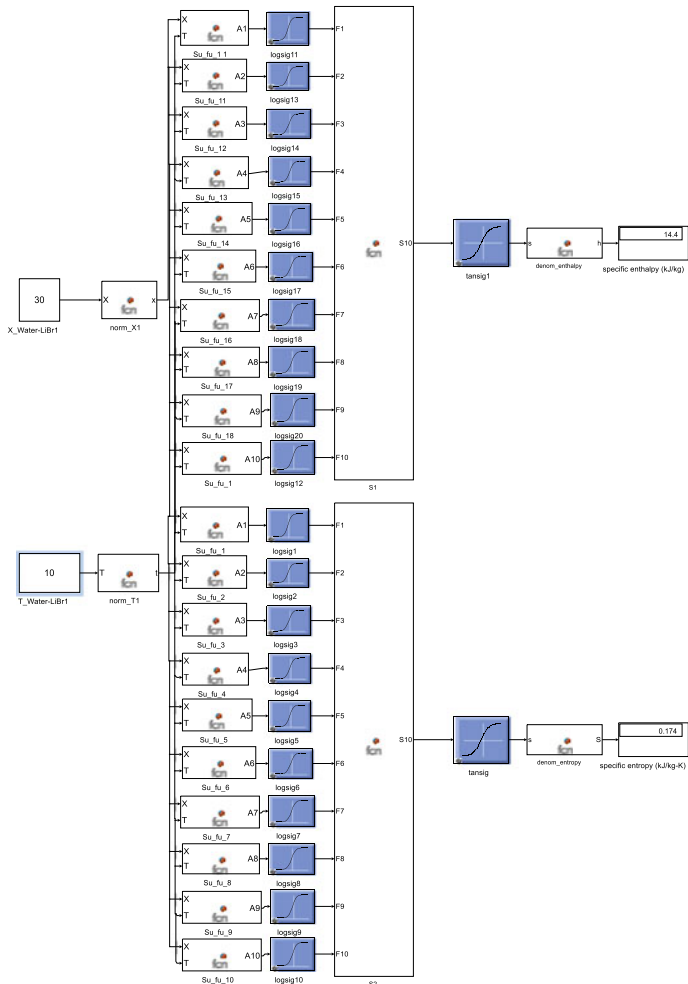


Fig. 6 Simlunkik model simulator metafile

the same. Developed subsystem simulator has facilitated by simple input enter system compared to any other simulator programming environment. These formulated expressions and simulator architectures are reported in the results sections.

Table 1 Validation of ANN predicted values to the past published work

Input parameters		Specific enthalpy (kJ/kg)		Absolute relative Error	Specific entropy (kJ/kg K)		Absolute relative error
x (%)	T (°C)	Actual [5]	ANN present work	[5]—Present Work	Actual [5]	Present work	[5]—present work
0	10	41.99	42.15	0.15	0.151	0.1518	0.0008
5	70	269.5	269.61	0.03	0.925	0.9248	0.0002
10	90	321.97	321.75	0.12	1.093	1.0929	1E–04
15	90	297.94	297.93	0.08	1.0372	1.037	0.0002
20	30	84.42	84.59	0.18	0.405	0.4048	0.0002
25	20	46.82	46.95	0.14	0.285	0.2856	0.0006
30	10	14.62	14.4	0.08	0.175	0.1748	0.0002
35	40	88.09	88.03	0.15	0.408	0.4086	0.0006
40	170	408.95	408.68	0.25	1.2381	1.2378	0.0003
45	80	172.36	172.07	0.01	0.602	0.6023	0.0003
50	130	280.93	281.06	0.1	0.837	0.8373	0.0003
55	80	175.35	175.18	0.08	0.4892	0.4895	0.0003
60	120	268.83	269.09	0.16	0.653	0.6529	1E–04
65	110	271.09	271.2	0.14	0.556	0.5567	0.0007
70	180	420.55	420.93	0.01	0.799	0.7988	0.0002
75	170	434.12	434.29	0.08	0.703	0.703	0

Absolute relative error = |Predicted Value – Actual Value|

References

- Li, Y., Hu, R.: Exergy-analysis based comparative study of absorption refrigeration and electric compression refrigeration in CCHP systems. *Appl. Therm. Eng.* **93**, 1228–1237 (2016)
- Chen, Y., Han, W., Jin, H.: Proposal and analysis of a novel heat-driven absorption–compression refrigeration system at low temperatures. *Appl. Energy* **185**(2), 2106–2116 (2017)
- Patek, J., Kalomfer, J.: Simple functions for fast calculation of selected thermodynamic properties of ammonia–water system. *Int. J. Refrig.* **18**(4), 228–234 (1995)
- Kaita, Y.: Thermodynamic properties of water–lithium–bromide solutions at high temperature. *Int. J. Refrig.* **24**, 374–390 (2001)
- Chua, H.T., Toh, H.K., Malek, A., Ng, K.C., Srinivasan, K.: Improved thermodynamic property fields of LiBr–H₂O solution. *Int. J. Refrig.* **23**, 412–429 (2000)
- <http://www.fchart.com/ees/>
- ASHRAE: Refrigerant properties. In: 2005 ASHRAE handbook, fundamentals, Chap. 20, pp. 20.68–20.69. ASHRAE, Atlanta (2005)
- Feurecker, G., Scharfe, J., Greiter, I., Frank, C.: Measurement of thermophysical properties of aqueous LiBr-solutions at high temperature and concentrations. In: Proceedings of the International Absorption Heat Pump Conference, New Orleans, Louisiana, vol. 31, pp. 493–499. AES (1994)

9. Foody, G.M.: Land cover classification by an artificial neural network with ancillary information. *Int. J. Geogr. Inform. Sci.* **9**(5), 542–547 (1995)
10. Krolikowska, M., Zawadzki, M., Skonieczny, M.: The influence of bromide-based ionic liquids on solubility of {LiBr (1) + water (2)} system. Experimental (solid + liquid) phase equilibrium data. Part 2. *J. Mol. Liquids* **265**, 316–326 (2018)
11. Bisio, G., Rubatto, G.: Energy saving and some environment improvements in coke-oven plants. *Energy* **3**, 247–265 (2000)
12. Verma, T.N., Nashine, P., Singh, D.V., Subhas Chandra Singh, T., Panwar, D.: ANN: prediction of an experimental heat transfer analysis of concentric tube heat exchanger with corrugated inner tubes. *Appl. Therm. Eng.* **120**, 219–227 (2017)
13. Xu, C.: Local and global Hopf bifurcation analysis on simplified bidirectional associative memory neural networks with multiple delays. *Math. Comput. Simul.* **149**, 69–90 (2018)
14. Islamoglu, Y.: A new approach for the prediction of the heat transfer rate of the wire-on-tube type heat exchanger use of an artificial neural network model. *Appl. Therm. Eng.* **23**(2), 243–249 (2003)

A New Bit Plane Specific Longest Repeating Pattern Test for Statistical Analysis of Bit Sequences



Bharat Lal Jangid and Ram Ratan

Abstract Most of the existing randomness tests treat whole bit sequence as a stream of bits in one-dimensional space for analysis. In this paper, a new bit plane specific statistical test for randomness analysis of bit sequences in two-dimensional space is presented. Primary focus of this test is to analyze the length of longest repeating pattern (LRP) in a binary random sequence. A random sequence is converted into matrix of $L \times L$ bytes. Then analysis of LRP is done for each row and column of each bit plane of the matrix. Experimentations are carried out on cipher data of four block ciphers, image data, and random alphabetic data of various sizes. It is observed that cipher data exhibits good randomness but image and random alphabetic data exhibits non-randomness in bit planes. The proposed test has the capability to capture the patterns by performing two-dimensional analysis in bit planes which may not be possible to capture by existing NIST statistical tests. It has been shown that sequences accepted as random by NIST suite are rejected by proposed LRP test.

Keywords Bit plane analysis · Chi-square goodness of fit · Cipher · Longest repeating pattern test · P -value · Randomness test · Statistical analysis

1 Introduction

Communications of sensitive information in the presence of adversary without compromise of confidentiality is a challenge. Cryptography is used to achieve confidentiality and integrity of sensitive data by means of ciphers (encryption/decryption) [1, 2]. The process of converting plain data into unintelligible form by using a secret key is called encryption and its reverse process is called decryption. Symmetric key cryptography and asymmetric key cryptography are two main types of cryptography. Same secret key is used to produce ciphertext by encryption as well as retrieving

B. L. Jangid (✉) · R. Ratan

Scientific Analysis Group, Defence R&D Organization, New Delhi, India

e-mail: bharatlal_ce@yahoo.com

R. Ratan

e-mail: ramratan_sag@hotmail.com

plain text from the ciphertext by decryption in symmetric key cryptography. It is further categorized into block cipher and stream cipher. There is a crucial role of Random Number Generators (RNGs) in symmetric key cryptography. Keystreams of stream ciphers are generated by the RNGs. The RNGs are further categorized into True Random Number Generators (TRNGs) and Pseudo Random Number Generators (PRNGs). Random sequences of TRNGs are produced by exploiting uncertainty associated with physical means/quantities [3]. PRNG is a deterministic algorithm that takes a seed as input to generate pseudo random sequence. It also has the capability to re-generate the same sequence if same seed is supplied as input [4–6]. PRNGs are widely used in stream ciphers. The most important characteristic of PRNG/TRNG is the randomness of output sequences.

A statistically independent bit sequence where “0” and “1” are uniformly distributed is called random bit sequence. An ideal random bit sequence can be generated by tossing an unbiased coin (one side of it is labeled as “0” and other with “1”). Any deviation of a bit sequence produced by RNG from random bit sequence may lead some clues for the statistical attack to recover the seed of the generator. Some essential statistical tests for analysis of randomness are discussed in [1, 7]. A suite consists of 15 statistical tests for analysis of randomness of bit sequences is developed by National Institute of Standard and Technology (NIST) [8]. Marsaglia also developed a suite of 12 statistical tests for randomness analysis of bit sequences which are also known as Diehard tests [9]. Duggan et al. developed a statistical test based on the concept of distance between consecutive pairs of random bits [10]. Ryabko et al. proposed randomness tests based on information-theoretic approach which uses data compression mechanism based on universal coding [11].

Presently, most of the existing statistical analysis of bit sequences treat whole sequence as a continuous bitstream (one-dimensional vector) for analysis. If a bitstream is converted into multi-dimensional space than its randomness must be exhibited in all dimensions.

In this paper, a bit plane specific longest repeating pattern statistical test is proposed. Primary focus of this test is to assess the desired maximum order complexity [12] of random sequence in two-dimensional space.

A bit sequence is converted into matrix of $L \times L$ bytes. After extracting eight bit planes of this matrix, row-vectors and column-vectors are generated by computing row-wise and column-wise length of longest repeating pattern, respectively, for each bit plane. Then chi-square (χ^2) goodness of fit test is used to compute P-value from above-said row-vectors and column-vectors of each bit plane to test deviation of length of longest repeating pattern from the expected value. The proposed statistical test has the capability to capture the patterns by performing two-dimensional analysis in bit planes which may not be possible to capture by existing NIST statistical tests. It has been shown that sequences accepted as random by NIST suite are rejected by the proposed test.

In Sect. 2, some background knowledge is discussed to understand the bit plane specific statistical analysis. In Sect. 3 proposed bit plane specific longest repeating pattern test for statistical analysis is discussed in detail. Experimental setup and results are discussed in Sects. 4 and 5. Final conclusion is discussed in Sect. 6.

2 Background

To understand the proposed statistical test for randomness analysis some background fundamentals of bit planes and χ^2 goodness of fit are briefly discussed here.

2.1 Bit Plane

Digital image processing has a vital role in bit plane terminology for various kinds of analysis [13]. Image is encoded as a matrix of $L \times M$ pixel values for storage in memory. Generally, eight bits are used by each pixel for a grayscale image. A matrix consists of least significant bits of each pixel is called Least Significant Bit (LSB) plane. Like this eight bit planes of $L \times M$ matrix can be extracted. Bit Plane 1 (BP₁) is LSB plane and BP₈ is Most Significant Bit (MSB) plane.

2.2 Chi-Square (χ^2) Goodness of Fit

Statistical hypothesis testing can be done by applying χ^2 goodness of fit [1, 7]. Primary goal of χ^2 goodness of fit is to find out deviation of practically observed statistical measure from expected value. Computed χ^2 can be defined as follows:

$$\chi_{\text{cal}}^2 = \sum_{j=1}^n (\text{Observed}_j - \text{Expected}_j)^2 / \text{Expected}_j \quad (1)$$

where Observed_j is observed statistical measure, Expected_j is expected statistical measure and n is number of observations. For a given value of n, the degree of freedom can be taken as n - 1. Computation of P-value from χ_{cal}^2 is defined as follow [8].

$$P_value = \text{igamma}((n - 1)/2, \chi_{\text{cal}}^2 / 2) \quad (2)$$

where “igamma” is called incomplete Gama-function which is defined as follows:

$$\text{igamma}(b, y) = 1 - (1/\Gamma(b)) \int_0^y e^{-z} z^{b-1} dz, \quad \text{where } \Gamma(b) = \int_0^\infty z^{b-1} e^{-z} dz \quad (3)$$

If P_value ≥ 0.01 then bit sequence is declared random at 1% level of significance [8].

3 Proposed Bit Plane Specific Statistical Test

A random sequence must exhibit randomness in all dimensions when a 1-D bit sequence is converted into multi-dimensional space. In this paper, a bit plane specific longest repeating pattern statistical test for randomness is proposed. The length of longest repeating pattern in a random sequence is called maximum order complexity of that sequence.

A matrix of $L \times L$ bytes is formulated from a random bit sequence of L^2 byte length. Total eight $L \times L$ bit matrices are generated after extracting eight bit planes of $L \times L$ bytes matrix. These eight matrices are taken as bit planes named BP₈, BP₇, BP₆, ..., BP₁, where BP₁ is LSB plane and BP₈ is MSB plane. To process these bit planes further, longest repeating pattern statistical test is presented as follows.

Bit Plane Specific Longest Repeating Pattern Statistical Test (LRP Test)

Bit plane specific longest repeating pattern statistical test focuses to assess the desired maximum order complexity of a random sequence in two-dimensional space by computing length of longest repeating pattern. Deviation of it may leads clues about patterns in bit sequence which may further help to cryptanalyst. Expected value of maximum order complexity is $E = 2 * \log(L)$ in a random sequence of length L bits [12]. The following are the steps to compute P -value for above-said test.

- i. **Input:** Eight bit planes (BP_8, BP_7, \dots, BP_1) of size $L \times L$ bit.
- ii. For each Bit Plane ($h=1$ to 8) do
 - For each Row ($i=1$ to L) do
 - Compute $Row_LRP_Length(h,i) =$ Length of longest repeating pattern in i^{th} row which occurs at least twice.
 - End do
 - For each Column ($i=1$ to L) do
 - Compute $Column_LRP_Length(h,i) =$ Length of longest repeating pattern in i^{th} column which occurs at least twice.
 - End do
 - End do
- iii. Expected value of length of longest repeating pattern is $E=2*\log(L)$.
- iv. For each Bit Plane ($h=1$ to 8) do
 - Compute $\chi_{cal_row}^2(h) = \sum_{n=1}^L [(Row_LRP_Length(h,n) - E)^2 / (E)]$.
 - Compute $\chi_{cal_column}^2(h) = \sum_{n=1}^L [(Column_LRP_Length(h,n) - E)^2 / (E)]$.
 - End do
 - v. For each Bit Plane ($h=1$ to 8) do
 - Compute $Pvalue_row(h) = igammac((L - 1)/2, \chi_{cal_row}^2(h)/2)$.
 - Compute $Pvalue_column(h) = igammac((L - 1)/2, \chi_{cal_column}^2(h)/2)$.
 - End do
 - vi. **Decision Criteria:** There is one P-value for row-wise measure and one for column-wise measure for each bit plane. For random data following condition must hold.
For each Bit Plane ($h=1$ to 8) do
 - $Pvalue_row(h) \geq 0.01$ and $Pvalue_column(h) \geq 0.01$ at 1% level of significance.
 - End do

4 Experimental Setup

MATLAB is used to implement the proposed statistical test described in Sect. 3. Three types of data sets are used for experimentation.

First one is an image data set, several images of fruit wallpapers of different sizes taken from [14] are used to demonstrate the performance of test on pattern data. Image shown in Fig. 1 is used to demonstrate the performance of test in this paper.

Another type of data set consists of random alphabetic sequences generated by BBS generator [6]. The BBS generator is cryptographically strong generator that is used to generate random bytes. The bytes corresponding to alphabets are stored and others are ignored to get random alphabetic sequence. Sample of generated sequence is as follows:

```
HOWJMEZPNFSSWJTFINRBFYQYWMYRIOOJXDQODCSQJUMCOWXPNEGO
QLBHWGVBDYEYDTQHMOEIXLBMAAZUDBHQMVDVHATQOFUYZKDLUCDCYS
MUWFQYLKYNLFPQPOXXGLCYXGUOTMEESTVCETZKFIHQBPJNYLZFIUC
QPJTBDKFGYOTXPGCICJYDXNELBYNZGMGMXTGLMPXEZKESFDSTJPBPQ
ERANLXYMSPIDJESJUNETYBNBTKFCYXOVMPAJOUSOYJOWFGSQGBMVZR
OEVHHSZRGLPOQYCUEZAKBFRPSLKWKTKZIEXWVKNNVXYEAYZMEND
MCPYEALHDRYUGTYTBTUBBACPHNDAMDOPRNZSEGXHONBOMVFFSU...
```

Third type of data set consists of cipher data generated by Advanced Encryption Standard (AES), Triple-Data Encryption Standard (3DES), IDEA and Blowfish block ciphers [15–18]. These Encryption schemes take above described image data set as an input to encrypt them and produce cipher data. Sample AES-encrypted cipher data in hexa-decimal format is as follows:

```
c0ad2ba38244faeda0033e9ade678890b136dc783c1a6ee8cd210a9b2482013586f3ec927d
e1c31b55345deba7f7670417e880f75f84dbf4ffeed1e143fdbdc798617a4a74d40681783c1
c8590a2471fc736996c74bf806644ce070a4614a158c4a958f01dda29b75e8b0d67352c95f5
c0d8da08907470c5ddcb2bb5545bb5355bd17a7650c8345de8a6d3daf3dce46b37d5963c38
d198a7b45c10c5f96383999f7f6b9252730fa0177e54aeb1ef34b7f9122272774df07a01673
```

Fig. 1 Fruits image



```
245b12f465322fbe24565a101a179c1a7890bcfbe90524c3b573635f647b4fbebdb898034d97
95050d757ceb55b9d2b614cbf86669416e1be8994da544cc2d228840c3ce9a79d3e8a5205f
62e6608ef62046006a6139077ddf48579f1597cf09c1ff8e2f9efcf7b2b571abcdee8d0f27a9e
a117c904613f6ff636a267d9d8f7fd04a7acbc2472f20b496e38ea6a050ee81b04e6a58e2a54
0a0737c14a1f8d941b48737574cf4d1878201799d0ce53de5f7d98599935dbe98c ...
```

All three type of data sets as described above have file size of 25×10^4 , 100×10^4 , 400×10^4 , 900×10^4 , 1600×10^4 and 2500×10^4 bytes for experimentation. But experimental results in this paper are presented on 25×10^4 bytes of each data set. The value of $L = 500$ (for $L \times L$ input data matrix) is taken. Ciphers data is taken from AES for presentation.

5 Experimental Results

Experimental results are demonstrated in the plots as shown in Fig. 2 for image, random alphabetic and cipher data. The X-axis represents bit planes (BP_1 , BP_2 , BP_3 , ..., BP_8), where BP_1 is LSB plane and BP_8 is MSB plane. Y-axis represents statistical measure (length of longest repeating pattern) of row or column. Each plot contains L linear graphs. Each graph is showing variation of length of longest repeating pattern with bit planes.

Figure 2a, d shows observed length of longest repeating pattern in rows and columns of fruit image as shown in Fig. 1. Figure 2b, e shows observed length of longest repeating pattern in rows and columns of random alphabetic data. Figure 2c, f shows plots of cipher data. Theoretically expected value of length of longest repeating pattern (maximum order complexity) is $2 * \log(L)$, which is 17.9316 for length $L = 500$. An observation can be made from Fig. 2a, b that length of longest repeating pattern in BP_1 and BP_2 is around the expected value but sharply departs from the expected value while proceeding towards BP_8 on the fruit image. In Fig. 2b, e, length of longest repeating pattern is around the expected value in BP_1 to BP_5 but raising from the expected value while proceeding towards BP_8 on random alphabetic data. It is 127 from BP_6 to BP_8 because of the patterns in extended ASCII values of the alphabets. *So it can be concluded that straightforward conversion of random alphabetic data into binary data is not desirable for production of random bit sequences.* Finally, it can be observed from Fig. 2c, f that length of longest repeating pattern in rows and columns is tightly close to expectations in all the bit planes of cipher data.

Values of computed chi-square for each bit plane are given in Table 1 for all three kind of data sets. Theoretically threshold χ_{tab}^2 with $L - 1$ degree of freedom (for $L = 500$) is 575.41 at 1% significance level. The condition of $\chi_{\text{cal}}^2 \leq \chi_{\text{tab}}^2$ must hold to accept the sequence as random [1]. It is noticed that value of χ_{cal}^2 is significantly large in bit planes nearer to MSB for both image as well as random alphabetic data set. But $\chi_{\text{cal}}^2 \leq \chi_{\text{tab}}^2$ for every bit plane of cipher data.

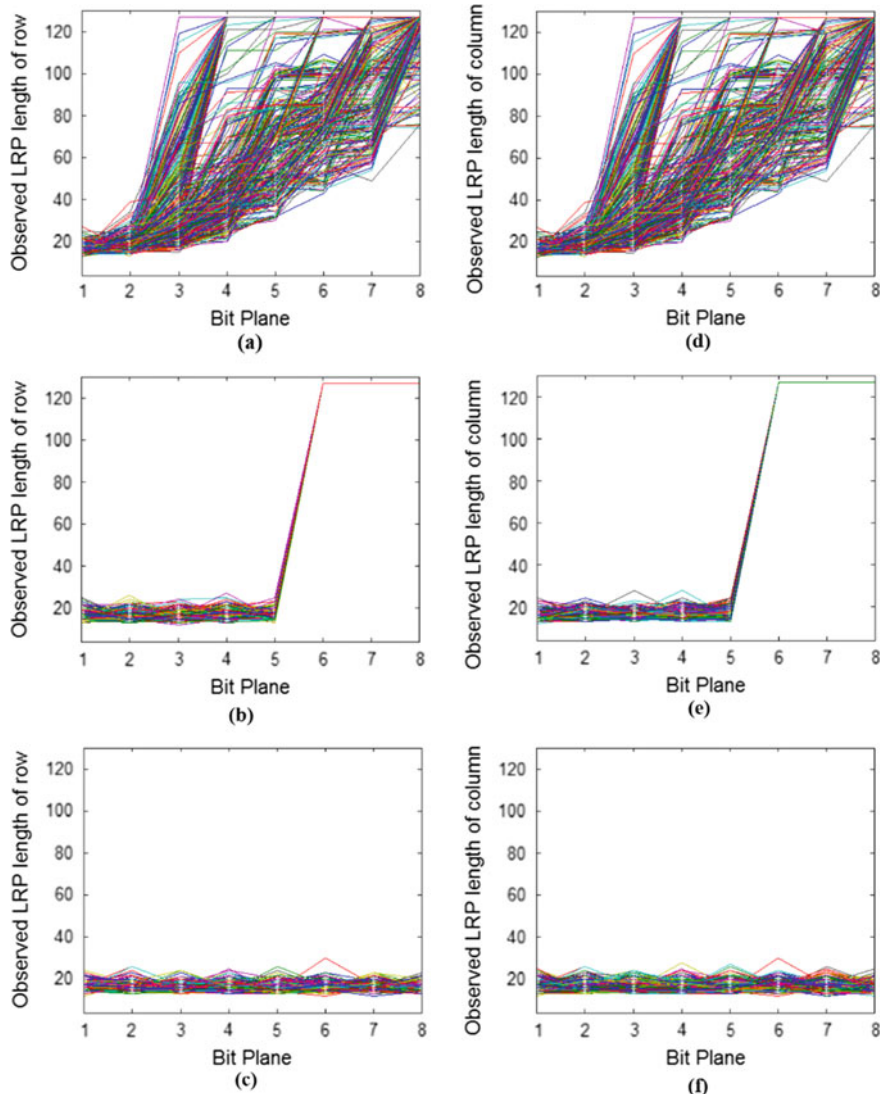


Fig. 2 **a–c** shows the observed length of longest repeating pattern in rows of image data, random alphabetic data and cipher data respectively. **d–f** shows observed length of longest repeating pattern in columns of image data, random alphabetic data and cipher data, respectively

Values of computed P -value for each bit plane are given in Table 2 for all three kinds of data sets. It is recommended that P -value must be more than 0.01 for a bit plane having randomness characteristics at 1% significance level. A sequence is declared random if all the bit planes exhibit randomness characteristics. An observation can be made that all the bit planes of AES-encrypted data sequence exhibit

randomness characteristics so that sequence is declared “Random”. Because of heavy patterns in bit planes of image as well as random alphabetic data these are declared “Non-random”.

An experimentation is also carried out on 100 samples of each type of data set of length 1000^2 bytes. Here 100 different images from [14] are encrypted by AES, 3DES, IDEA and Blowfish and corresponding cipher data are generated. All the samples are declared random as shown in Table 3.

5.1 Performance of LRP Test Over NIST Suite

The proposed statistical test has the capability to capture the patterns by performing two-dimensional analysis in bit planes which may not be possible to capture by existing NIST statistical tests [8]. To demonstrate the important capability of proposed statistical test over the NIST statistical test suite, 100 files of cipher data of AES each one has 10^6 bytes have been generated. Then introduced biasness in count of zeros in few columns as well as biasness in count of ones in other same number of columns of LSB bit plane of the generated data to compensate the biasness of zeros. Then these customized bit sequences are tested by both LRP test and NIST test suite. Details of P -values obtained for one input file are listed in Table 4 and consolidated results of 100 files are listed in Table 5.

It can be observed from Table 5 that all the 100 customized files are declared to be random by NIST suite but our proposed LRP test rejected all of them.

Table 1 Computed Chi-square values of each bit plane on three types of data sets

Bit plane	Image data		Random alphabetic data		Cipher data	
	Row	Column	Row	Column	Row	Column
BP1	195.57	186.65	193.45	193.62	184.81	192.45
BP2	340.68	318.43	200.09	187.21	178.4	185.09
BP3	20,103.48	17,234.68	173.8275	173.26	187.32	187.37
BP4	123474.9	292070.3	159.27	163.95	196.58	187.43
BP5	161,972.9	313,588.9	138.08	153.13	202.99	195.29
BP6	192,052.1	319,268.6	331,287.2	331,287.2	193.51	180.46
BP7	246,560.8	326,270.5	331,287.2	331,287.2	181.91	196.52
BP8	309,938.3	331,287.2	331,287.2	331,287.2	194.23	187.04

Table 2 Computed P -values of each bit plane on three types of data sets

Table 3 No. of samples out of 100 which are declared random on six types of data sets

	Image data set	Random alphabetic data set	AES cipher data set	3DES cipher data set	IDEA cipher data set	Blowfish cipher data set
No. of Random samples	0	0	100	100	100	100

Table 4 Comparison of computed *P*-values of both NIST suite and proposed LRP test for one input file

NIST test suite		<i>P</i>-value	Result
	Frequency	0.36445	Random
	Block frequency (on block size = 128 bits)	0.89885	Random
	Cusum-forward	0.15553	Random
	Cusum-reverse	0.98234	Random
	Runs	0.76310	Random
	Longest runs of ones	0.20375	Random
	Binary matrix rank	0.54023	Random
	Spectral DFT	0.89340	Random
	Non-overlapping templates (for template length = 9 bits and template = 000000001)	0.66728	Random
	Overlapping templates (for template length = 9 bits)	0.16596	Random
	Universal	0.08443	Random
	Approximate entropy (for block size = 10 bits)	0.15646	Random
	Random excursions (for state “+1” in cumulative sum)	0.68593	Random
	Random excursions variant (for state “-1” in cumulative sum)	0.87403	Random
	Linear complexity (for block length = 500 bits)	0.56783	Random
	Serial (for pattern length = 16)	0.09321	Random
Proposed LRP test		Row	Column
	BP1	1	0.0000023
	BP2	1	1
	BP3	1	1
	BP4	1	1
	BP5	1	1
	BP6	1	1
	BP7	1	1
	BP8	1	1

Table 5 Consolidated results of 100 customized files

	NIST suite	Proposed LRP test
No. of random files	100	0

6 Conclusion

A new bit plane specific LRP test has been proposed for randomness analysis of bit sequences in two-dimensional space. Primary focus of this test is to analyze the length of longest repeating pattern in a binary sequence. Experimentations have been done on image data, random alphabetic data and cipher data (AES, 3DES, IDEA, and Blowfish). Non-randomness of image and random alphabetic data is captured by bit plane specific LRP analysis. Cipher data demonstrated randomness characteristics in all bit planes and achieved 100% randomness. The proposed test has the capability to capture the patterns by performing two-dimensional analysis in bit planes which may not be possible to capture by existing NIST statistical test suite as demonstrated.

References

1. Menezes, A.J., Van Oorschot, P.C., Vanstone, S.A.: *Handbook of Applied Cryptography*, CRC Press (1996)
2. Stallings, W.: *Cryptography and network security: principles and practice*, 5th edn. Pearson, London (2010)
3. Lee, K., Lee, S., Seo, C., Yim, K.: TRNG (true random number generator) method using visible spectrum for secure communication on 5G network. *IEEE Access* **6**, 12838–12847 (2018)
4. Ankur, Divyanjali, Pareek, V.: A New Approach to Pseudorandom Number Generation. In: 2014 Fourth International Conference on Advanced Computing & Communication Technologies, pp. 290–295. IEEE Press, Orlando, FL, USA (2014)
5. Babaei, M., Farhad, M.: Introduction to secure PRNGs. *Int. J. Commun. Network Syst. Sci.* **4**(10), 616–621 (2011)
6. Blum, L., Blum, M., Shub, M.: A simple unpredictable pseudo-random number generator. *SIAM J. Comput.* **15**(2), 364–383 (1986)
7. Knuth, D.: *The Art of Computer Programming*. Addison-Wesley, Boston (1981)
8. Rukhin, A., Soto, J., Nechvatal, J., Smid, M., Barker, E., Leigh, S., Levenson, M., Vangel, M., Banks, D., Heckert, A., Dray, J.: A Statistical Test Suite for Random and Pseudorandom Number Generators for Cryptographic Applications. NIST Special Publication SP 800-22, Revision-1a, <http://www.nist.gov> (2010)
9. Marsaglia, G.: The Marsaglia random number CDROM including the diehard battery of tests of randomness. Department of Statistics, Florida State University, Tallahassee, FL, USA. <https://web.archive.org/web/20160125103112/http://stat.fsu.edu/pub/diehard/> (1995). Last accessed 10 Jan 2019
10. Duggan, M.J., Drew, J.H., Leemis, L.M.: A test of randomness based on the distance between consecutive random number pairs. In: Proceedings of the 2005 Winter Simulation Conference, pp. 741–748. IEEE Press, Orlando, FL, USA (2005)
11. Ryabko, B., Fionov, A., Monarev, V., Shokin, Y.: Using information theory approach to randomness testing. In: Krause, E., Shokin, Y., Resch, M., Shokina, N. (eds.) *Computational Science and High Performance Computing II. Notes on Numerical Fluid Mechanics and Multidisciplinary Design*, vol. 91, pp. 261–272. Springer, Berlin (2006)

12. Isik, L., Winterhof, A.: Maximum-order complexity and correlation measures. *Cryptography* **1**(1), 7 (2017). <https://doi.org/10.3390/cryptography1010007>. (last accessed 2019/10/01)
13. Ratan, R., Arvind: Bit-plane specific measures and its applications in analysis of ciphers. In: International Symposium on Signal Processing and Intelligent Recognition Systems, pp. 282–297. Springer, Singapore (2018)
14. Dataset of fruits wallpapers, https://wall.alphacoders.com/by_sub_category.php?id=159949&name=Fruit+Wallpapers&page=3. Last accessed 10 Jan 2019
15. Advanced Encryption Standard. Federal Information Processing Standards Publication 197 (2001)
16. Data Encryption Standard. Federal Information Processing Standards Publication 46-3 (1999)
17. Schneier, B.: Description of a new variable-length key, 64-bit block cipher (blowfish). In: Cambridge Security Workshop Proceedings, pp. 191–204. Springer, Berlin (1993)
18. Basu, S.: International data encryption algorithm (IDEA)—a typical illustration. *J. Global Res. Comput. Sci.* **2**(7), 116–118 (2011)

Intelligent Interference Minimization Algorithm for Optimal Placement of Sensors using BBO



Chandra Naik and D. Pushparaj Shetty

Abstract In wireless sensor networks, the performance metric such as energy conservation becomes paramount. One of the fundamental problems of energy drains is due to the interference of sensors during sensing, transmission, and receiving data. The issue of placing sensors on a region of interest to minimize the sensing and communication interference with a connected network is NP-complete. In order to overcome the existing problem, we have proposed a new work for interference minimization technique for optimal placement of sensors by employing biogeography-based optimization scheme. An efficient habitats representation, objective function derivation, migration, and mutation operators are adopted in the scheme. The simulations are performed to obtain the optimal position for sensor placement. Finally, the energy-saving of the network is compared with and without interference aware sensor nodes placement.

Keywords Sender interference · Receiver interference · Sensing interference · Wireless sensor networks · Biogeography-based optimization

1 Introduction

The progress of communication technology has led to the development of cost-effective, battery-powered, and multi-functional transceivers called sensors. Each sensor has sensing, processing, and communicating components. The collective settings of these sensor nodes form the wireless sensor networks (WSNs) [2].

The positions of sensor nodes in a network need not be pre-defined that allows the random deployment of sensors in hostile areas like disaster regions. The random

C. Naik (✉) · D. Pushparaj Shetty
Department of Mathematical and Computational Sciences, National Institute of Technology
Karnataka, Surathkal 575025, India
e-mail: chandra.nitk2017@gmail.com

D. Pushparaj Shetty
e-mail: prajshetty@nitk.edu.in

deployment scheme places sensors unevenly on the field of interest, some regions are highly dense, and some parts of regions are sparse. In the dense regions, maximum nodes are interfering during the sensing and transmitting of the data. One of the main reasons for the quick power drain is due to the interference of signals in the wireless media. This results in message drop and requires message retransmission, which in turn affects the energy efficiency of WSNs. In deterministic deployment, optimal sensor positions are determined in advance according to the design objectives. Optimal placement of sensors on a given set of potential locations in the field of interest with minimized interference is an NP-complete problem [5]. Many combinatorial real-world problems are solved using meta-heuristic algorithms, whenever exact solutions are not achievable, such as k -coverage and m -connectivity [10], optimal target coverage problem [9], clustering, and routing [19] in WSNs. There are many state-of-the-art metaheuristic algorithms adopted to solve different engineering problems. Spider monkey optimization (SMO) is enthused by fission–fusion behavior of spider monkey in the process of food search. It is proposed by Bansal et al. in 2014, and the model focuses on solving unconstrained optimization problems [18]. Teaching learning-based optimization (TLBO) mimics them teaching learning environment, proposed by Rao et al. in 2011. TLBO is highly used to solve mechanical and manufacturing design optimization problems [6]. Ensuff and Lansey in 2003 proposed shuffled frog leaping algorithm (SFLA), which is motivated by foraging behavior of frogs. Different variants of SFLA like [15] are proposed in improving efficiency of the algorithm.

In our study, we have employed biogeography-based optimization(BBO) which is also a meta-heuristic algorithm. This algorithm is designed on a study of the geographic distribution of living beings [13]. The geographic regions called habitat or island that are well suited for living beings are said to have a high habitat suitability index (HSI). The characteristics of habitat is determined by suitability index variables (SIVs). The high HSI habitat has a high emigration rate, whereas low HSI habitat has a high immigration rate. Therefore, low HSI habitats are more dynamic in their species distribution than high HSI habitats [17]. The BBO has the same features of genetic algorithm(GA), particle swarm optimization(PSO), and differential evolution(DE) in information sharing among neighbor solution, but in GA, solution dies after each generation. But BBO differ from ant colony optimization(ACO) because ACO generates a new set of solutions in each generation. The BBO is adopted in solving k -coverage and m -connectivity [5], clustering and routing [7, 11] problems in WSNs. In this work, we propose a BBO-based interference minimization sensor node placement algorithm and compare our algorithm with random deployment technique for energy efficiency.

The remaining part of this paper is organized as follows. Section 2 briefs related works on interference minimization problem of WSNs, Sect. 3 gives an overview of biogeography-based optimization algorithm. Section 4 presents assumptions on the system model and problem statement. The proposed BBO-based approach is described in Sect. 5 followed by results and discussion in Sect. 6. Finally, the paper concludes in Sect. 7.

2 Related Work

Many researchers have proposed variants of topology control-based interference minimization solutions in WSNs. The problem of minimizing maximum receiver interference of the network is proved to be NP-hard by Buchin [4]. Bilo and Proietti gave an optimal algorithm for minimizing the maximum sender interference [3]. Authors in [1] proposed an algorithm for minimizing maximum interference as well as total interference of the network. Authors in [12] proposed two new models SUM and MAX and presented algorithms for minimizing maximum and average node interference for WSN. The authors in [14] presented an algorithm which produces the best sender interference spanning tree for the input distribution of the nodes in the plane that gives minimum interference value for the WSN. Lou et al. proposed algorithm to minimize the total interference by assigning different power levels to each sensor node to form a connected graph [8]. All the above techniques are based on graph-theoretic modeling, and these techniques suffer from scalability problems.

3 Classical Biogeography-Based Optimization

Figure 1 represents species abundance in a single habitat, where λ and μ are immigration and emigration rates of species, respectively. The variables I and E are maximum immigration and emigration rates, respectively. The variable S_0 denotes equilibrium number of species at which immigration and emigration rates are equal. The maximum number of species that can live in a habitat is denoted by S_{\max} . In

Fig. 1 Species model of a single habitat in BBO

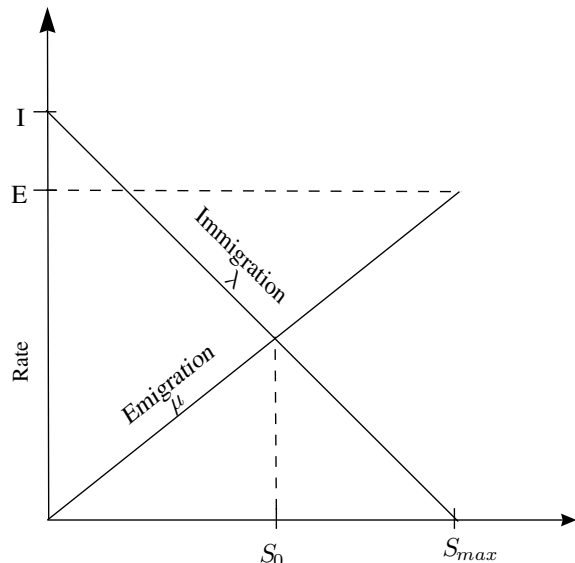


Fig. 2 Example of two candidate solution in BBO

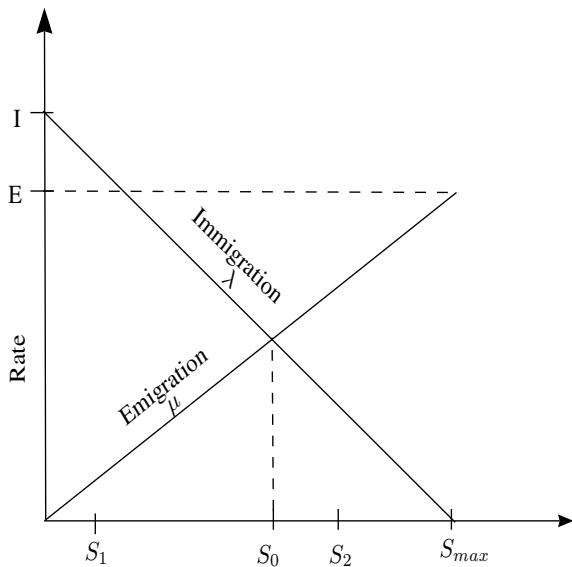


Fig. 2, S_1 represents a poor solution as compared with S_2 solution since S_2 is near to equilibrium solution S_0 . Therefore, S_1 solution immigration rate is higher, and the emigration rate is lower compared to S_2 solution [17].

The BBO algorithm is divided into migration and mutation phases as described below.

3.1 Migration Phase

In this phase, information is shared between habitats or vectors. A high HSI vector shares information with low HSI vector to obtain a better vector. The vectors are selected to exchange information (SIVs) using their immigration and emigration rates. Suppose the first habitat H_i is selected using immigration rate, and second habitat H_j is selected using emigration rate, then some SIVs are migrated from H_j to H_i .

3.2 Mutation Phase

The species in a habitat may undergo sudden changes due to natural calamity. The BBO employs SIV mutation to model these events. Each vector i is associated with a probability P_i to obtain mutation rate M_i . The value of the p_i is computed using λ_i and μ_i . The high p_i vector has less chance for mutation, and a low p_i vector has

a high chance for mutation [17]. The mutation rate is computed using the following formula,

$$M_i = M_{\max} * \left(\frac{1 - P_i}{P_{\max}} \right) \quad (1)$$

where M_{\max} is user-specified maximum mutation rate, P_i is mutation probability of i th species, P_{\max} is the maximum mutation probability, and M_i is the mutation rate of i th species.

4 Network Model and Problem Formulation

4.1 Network Model

In the proposed work, a network architecture is adopted, as shown in Fig. 3. It is a homogeneous network with nodes having equal energy, same sensing, and communicating capabilities. Initially, different potential positions for deploying sensors are identified randomly. After that, the given set of sensors are deployed in identified locations. The sensed data from sensors is transmitted directly or indirectly, as shown in Fig. 3.

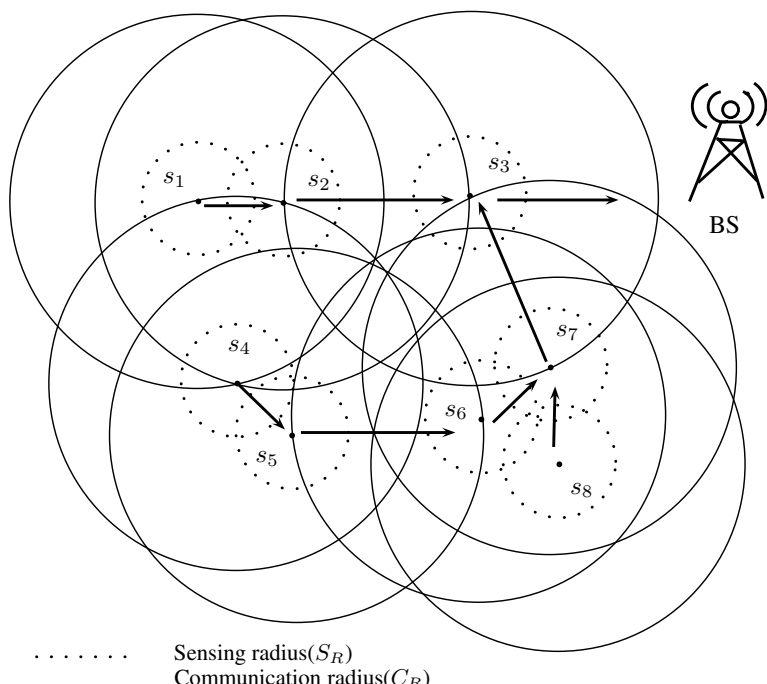


Fig. 3 An instance of network model

4.2 Problem Formulation

Our problem is modeled as a network with communication graph $G(V, E_1)$ and sensing graph $G(V, E_2)$. These graphs consist of vertex set V that represents n sensors and edge set E_1 and E_2 representing communication link and sensing link, respectively. The weight function $w: V \times V \rightarrow \mathbb{R}^+$ gives the Euclidean distance between sensors.

For each sensor node s , we construct a disk centering at s with radius equal to the communication range $C(s)$. The communication interference of a sensor node s is then defined as the number of communication disks that include node s (not counting the communication disk of s itself).

The **communication disk** of a vertex s is a circle centered at s and its communication range $C(s)$ as its radius, denoted by $D(s, C(s))$. Let S_R and C_R are the sensing radius and communication radius of each sensor, respectively. There are two types of transmission interference found in the literature, namely sender interference and receiver interference as detailed below [16]. In this work, we introduce a third type of interference called sensing interference.

Definition 4.1 The number of vertices which lie in s 's communication disk determines the **sender interference** of s , and is formally defined as follows:

$$I_s(s) = |\{t \in V \setminus \{s\}, t \in D(s, C(s))\}| \quad (2)$$

Definition 4.2 The **receiver interference** of a vertex s is the number of vertices having the vertex s in their communication disk, and is given as follows:

$$I_r(s) = |\{t \in V \setminus \{s\}, s \in D(t, C(t))\}| \quad (3)$$

Definition 4.3 For a node s , **sensing interference** is defined as the number of vertices having a distance less than $2 \times S_R$ from the vertex s as described below:

$$I_{\text{sense}}(s) = |\{t \in V \setminus \{s\}, \text{distance}(s, t) \leq 2 \times S_R\}| \quad (4)$$

Illustration 4.1 Consider an instance of a network model in Fig. 3. The sender, receiver, and sensing interferences are tabulated in Table 1, and their corresponding graph is shown in Fig. 4. Here, sender and receiver inferences are the same because the network consists of homogeneous sensor nodes. Consider 5 sensors to be deployed in any of the locations s_1, s_2, \dots, s_8 in Fig. 3. Let initial energy of each node be 5 J. Let sensing and communication radius of each node be 15 m and 30 m, respectively. Suppose sensing energy-loss(s_e) and communication energy-loss(c_e) of each node are

Fig. 4 Interference graph of Fig. 3

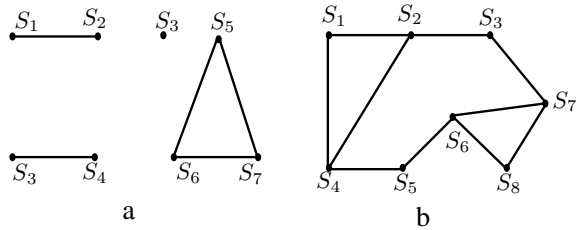


Table 1 Interference values of Fig. 3

	Sensors								Total
	s_1	s_2	s_3	s_4	s_5	s_6	s_7	s_8	
I_s	2 – 1	3 – 1	2 – 1	3 – 1	2 – 1	3 – 1	3 – 1	2 – 1	12
I_r	2 – 1	3 – 1	2 – 1	3 – 1	2 – 1	3 – 1	3 – 1	2 – 1	12
I_{sense}	1	1	0	1	1	2	2	2	10

0.015 J and 0.030 J, respectively. Consider a random nodes deployment in scenario 1, where 5 sensors are deployed in locations s_3 , s_5 , s_6 , s_7 , and s_8 in Fig. 3, and the corresponding sensing and receiver(sender) interferences are shown in Fig. 5a, b, respectively. The sensing and communication interferences involve in the total interference experienced by the given network and are computed as follows.

$$\text{Total}_{\text{interference}} = \text{Sensing}_{\text{interference}} + \text{Communication}_{\text{interference}}$$

$$\text{Total}_{\text{interference}} = I_{\text{sense}} + I_s + I_r$$

$$\text{Total}_{\text{interference}} = 6 + 7 + 7 = 20 \text{ from Table 2}$$

$$\text{Total}_{\text{interference}}^{\text{energy-loss}} = 6 \times 0.015 + 7 \times 0.030 + 7 \times 0.030 = 0.09 + 0.42 = 0.51 \text{ J.}$$

Consider an optimal nodes deployment in scenario 2, where 5 sensors are placed in locations s_2 , s_3 , s_5 , s_6 , and s_7 in Fig. 3, and the corresponding sensing and receiver(sender) interferences are shown in Fig. 6a, b, respectively.

$\text{Total}_{\text{interference}} = 2 + 3 + 3 = 8$ from Table 3. The total energy-loss of the network is due to interference that involves energy-loss of the sensing and communication interferences and is calculated as follows.

$$\text{Total}_{\text{interference}}^{\text{energy-loss}} = 2 \times 0.015 + 3 \times 0.030 + 3 \times 0.030 = 0.03 + 0.18 = 0.21 \text{ J.}$$

Fig. 5 Random nodes placement graph

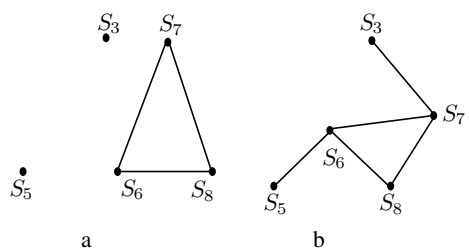
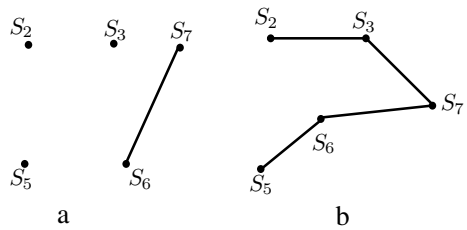


Table 2 Random nodes placement

	Sensors								Total
	s_1	s_2	s_3	s_4	s_5	s_6	s_7	s_8	
I_S	NP	NP	2 - 1	NP	2 - 1	3 - 1	3 - 1	2 - 1	7
I_R	NP	NP	2 - 1	NP	2 - 1	3 - 1	3 - 1	2 - 1	7
I_{sense}	NP	NP	0	NP	0	2	2	2	6

Fig. 6 Optimal nodes placement graph**Table 3** Optimal nodes placement

	Sensors								Total
	s_1	s_2	s_3	s_4	s_5	s_6	s_7	s_8	
I_S	NP	1 - 1	2 - 1	NP	1 - 1	2 - 1	2 - 1	NP	3
I_R	NP	1 - 1	2 - 1	NP	1 - 1	2 - 1	2 - 1	NP	3
I_{sense}	NP	0	0	NP	0	1	1	NP	2

The symbols ‘NP’, and ‘-’ indicates non-deployed sensor locations and subtract operation(preserves connectivity among sensors), respectively.

We observe that the computed total energy-loss interference for scenario 2 is far better than the scenario 1.

5 Proposed BBO-Based Algorithm

In this paper, we discuss an interference minimization BBO-based intelligent algorithm for m sensors deployment in a set of n potential position.

Let $S = \{s_1, s_2, s_3, \dots, S_m\}$ denote a set of sensors, and $P = \{p_1, p_2, p_3, \dots, p_n\}$ denote a set of candidate position. Our objective is to deploy a given set of sensors in a set of locations such that,

1. Minimize the sender interference for each node k , where $1 \leq k \leq m$.
2. Minimize the receiver interference for each node k , where $1 \leq k \leq m$.
3. Minimize the sensing interference for each node k , where $1 \leq k \leq m$.

5.1 Encoding of Habitats

Each habitat represented by an array of boolean values. The length of each habitat equals to the number of candidate positions. For a habitat, if the i th candidate position has chosen for a sensor node placement, then its entry value is 1; otherwise its value is 0.

5.2 Initialization of Habitats

Each habitat represents a selection of candidate positions to place sensors. The G th generation of i th habitat having n components are indicated as follows:

$$H_{i,G} = [SIV_{1,i,G}, SIV_{2,i,G}, SIV_{3,i,G}, \dots, SIV_{n,i,G}] \quad (5)$$

The habitat suitability index (HSI) measures the goodness of i th habitat as indicated below:

$$HSI_i = f([SIV_{1,i,G}, SIV_{2,i,G}, SIV_{3,i,G}, \dots, SIV_{n,i,G}]) \quad (6)$$

5.3 Derivation of Fitness Function

1. **Minimize sender interference (f_1)** To minimize the sender interference, we derive the first objective function as follows:

$$\text{Minimize } f_1 = \frac{1}{m} \sum_{v=1}^m I_{\text{Sender}}(v) \quad (7)$$

OR

$$\text{Maximize } f_1' = \frac{m}{\sum_{v=1}^m I_{\text{Sender}}(v)} \quad (8)$$

2. **Minimize receiver interference (f_2)** To minimize the receiver interference, we derive the second objective function as follows:

$$\text{Minimize } f_2 = \frac{1}{m} \sum_{v=1}^m I_{\text{Reciever}}(v) \quad (9)$$

OR

$$\text{Maximize } f_2' = \frac{m}{\sum_{v=1}^m I_{\text{Reciever}}(v)} \quad (10)$$

3. **Minimize sensing interference** (f_3) To minimize the sensing interference, we derive the third objective function as follows:

$$\text{Minimize } f_3 = \frac{1}{m} \sum_{v=1}^m I_{\text{Sense}}(v) \quad (11)$$

OR

$$\text{Maximize } f_3' = \frac{m}{\sum_{v=1}^m I_{\text{Sense}}(v)} \quad (12)$$

Based on individual objectives f_1' , f_2' , and f_3' , we devise the final fitness function F as follows:

$$\text{Maximize Fitness } F = w_1 \times f_1' + w_2 \times f_2' + w_3 \times f_3' \quad (13)$$

where w_i is weight, with $0 < w_i \leq 1$, $1 \leq i \leq 3$ and $w_1 + w_2 + w_3 = 1$. The objective is to find a better habitat having the highest fitness value.

5.4 Migration

In this process, habitats H_i and H_j are chosen randomly based on immigration rate λ_i and emigration rate μ_j , respectively. After the selection of habitats, a random number is generated between $(0, 1)$, and if the generated random number is less than λ_i , then migration is performed between habitats. To perform the migration, a $n/2$ th position selected in H_j and SIV are shifted from habitat H_j to habitat H_i from the selected position to last position of habitat H_j . This process guarantees a valid habitat generation.

5.5 Mutation

The mutation process involves the selection of a habitat based on mutation probability. After selecting the habitat, check for the first occurrence of the value 1 and changed to 0, and also check for the first occurrence of the value 0 and changed to 1. This process guarantees a valid habitat after mutation.

Algorithm 5.0 Interference minimization BBO based sensor node placement algorithm

Input: Set of m sensor nodes $S = \{s_1, s_2, s_3, \dots, s_m\}$, Set of m candidate positions $P = \{p_1, p_2, p_3, \dots, p_n\}$, and a number of habitats N_h

Output: Optimal sensor nodes placement positions

// Step 1: Habitat initialization

- 1: Initialize the habitats $H_i, \forall i, 1 \leq i \leq N_h$ with random values, such that first $n/2$ positions of H_i assigned with $m/2$ sensors; remaining $n/2$ positions assigned with remaining $m/2$ sensors to avoid uneven distribution

// Step 2: BBO algorithm starts

- 2: **while** !Termination **do**
- 3: Compute fitness of each habitat using Eq.(13)
- 4: Sort habitats from best to worst using their HSI/fitness values
- 5: Map habitat species count S_{count} for each habitat H_i [5]
- 6: For each habitat H_i , compute the immigration rate λ_i
- 7: and emmigration rate μ_i [5]

// Habitat migration

- 8: Select H_i based on highest immigration rate λ_i
- 9: Select H_j based on highest emmigration rate μ_j
- 10: Generate a random number $r_1, 0 < r_1 < 1$
- 11: **if** $r_1 < \lambda_i$ **then**
- 12: Select position $r_p = n/5$
- 13: **for** $k = r_p$ to n **do**
- 14: $H_i[k] = H_j[k]$
- 15: **end for**

16: // This process guarantees a valid habitat, after migration

- 17: **end if**
- 18: **// Habitat mutation**
- 19: Compute the mutation probability p_i of habitat using λ_i and μ_i [17]
- 20: Set user specified mutation rate $M_{max} = 0.2$
- 21: Compute mutation probability M_i for each habitat H_i using Eq.(1)
- 22: Select habitat H_i with maximum mutation rate M_i
- 23: **if** H_i is chosen **then**
- 24: Firstly, select the position with first occurrence of 1 and changed to 0
- 25: Secondly, select the position with first occurrence of 0 and changed to 1

// This process guarantees a valid habitat, after mutation

- 26: **end if**
- 27: **end while**
- 28: Sort the habitat according to their HSI values
- 29: **// check for communication connectivity**
- 30: **for** habitat = 1 to N_h **do**
- 31: **if** connected(habitat) **then**
- 32: $Best_{habitat} = habitat$
- 33: **break**
- 34: **end if**

35: Finally, $Best_{habitat}$ selected as the optimal sensor nodes placement positions

6 Results and Discussion

In our simulation, a set of 200 random potential positions are generated in a field of size 200×200 . The number of sensors to be placed in these locations is varied from 25 to 100 in steps of 25; The sensor sensing range and communication range are 15 m and 30m, respectively. The network is assumed to be homogeneous, and initial energy of each sensor node is 5J.

Energy drain on each communication and sensing interference considered as 0.030 J and 0.015 J, respectively. In this work, a set of 100 habitats are run through 100 generations. The mutation probability for habitat i is M_i , and the user-specified mutation rate is M_{\max} , which is set to 0.2. Figures 7 and 8 depicts the performance improvement of BBO-based interference aware sensor placement over non-interference aware

Fig. 7 Sensing interference between BBO-based scheme and random scheme

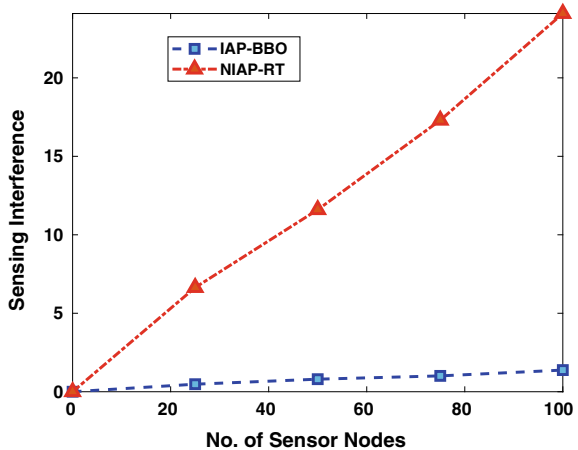


Fig. 8 Sender/Receiver interference between BBO-based scheme and random scheme

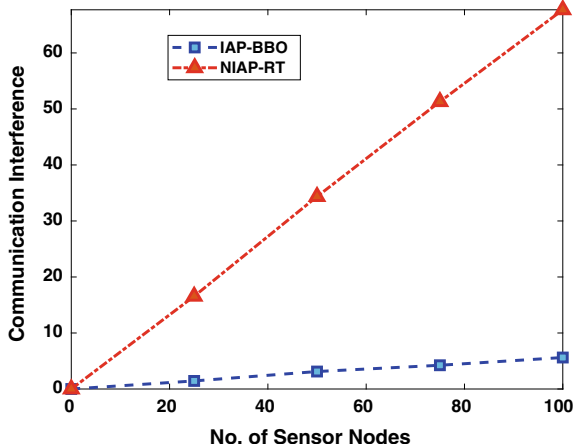


Fig. 9 Energy-saving between BBO-based scheme and random scheme

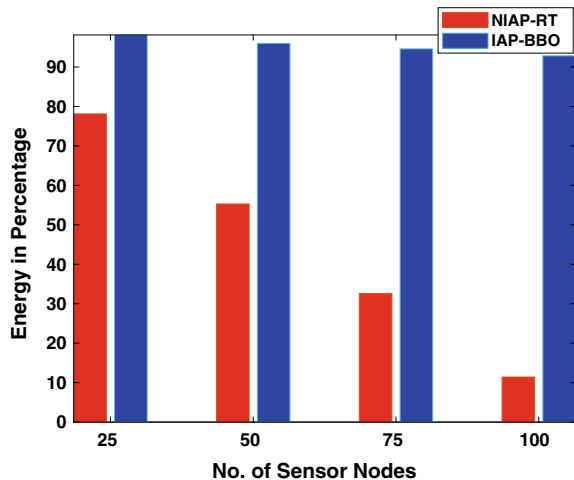
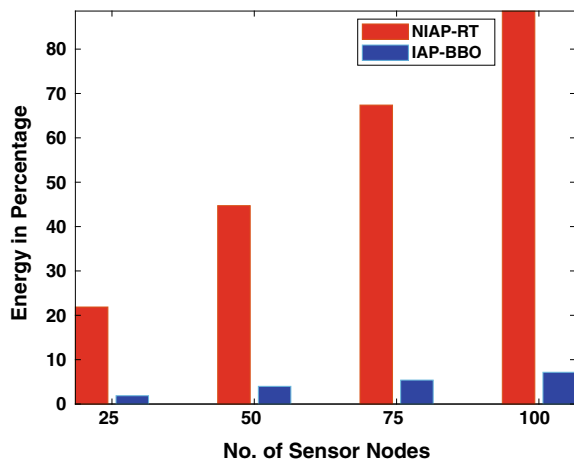


Fig. 10 Energy-loss between BBO-based scheme and random scheme



random sensor placement. In both the scenarios, the sensing and communication interferences are very low in BBO-based scheme compared to the random scheme. Figures 9 and 10 indicate performance comparison of total energy-saving and total energy-loss between BBO-based and random scheme, respectively. These graphs show that the percentage of energy-saving is high in the sparse network compared to dense networks. It is because the number of interfering nodes are low in sparse network as compared to the dense network.

7 Conclusion

In this work, an intelligent algorithm for finding optimal positions for deploying a set of given sensors is proposed. We adopted biogeography-based optimization technique to minimize the sensing and communication interference of the sensors before their deployment. An efficient habitat initialization, fitness calculation, migration, and mutation were designed in the proposed algorithm. For different network scenarios, results were obtained by varying potential positions and sensors. Finally, for energy-saving and energy-loss results were obtained with and without interference aware deployment of sensors. As future work, this could be explored with a fuzzy-based interference model or augmenting our model with target coverage constraint.

Acknowledgements The authors would like to acknowledge the support by the National Institute of Technology Karnataka, Surathkal, India, to carry out research.

References

1. Agrawal, P., Das, G.K.: Improved interference in wireless sensor networks. In: International Conference on Distributed Computing and Internet Technology, pp. 92–102. Springer, Berlin (2013)
2. Akyildiz, I.F., Su, W., Sankarasubramaniam, Y., Cayirci, E.: Wireless sensor networks: a survey. *Comput. Networks* **38**(4), 393–422 (2002)
3. Bilò, D., Proietti, G.: On the complexity of minimizing interference in ad-hoc and sensor networks. *Theor. Comput. Sci.* **402**(1), 43–55 (2008)
4. Buchin, K.: Minimizing the maximum interference is hard. arXiv preprint [arXiv:0802.2134](https://arxiv.org/abs/0802.2134) (2008)
5. Gupta, G.P., Jha, S.: Biogeography-based optimization scheme for solving the coverage and connected node placement problem for wireless sensor networks. *Wirel. Networks* **25**(6), 3167–3177 (2019)
6. Jagdeo, S., Umbarkar, A., Sheth, P.: Teaching–learning-based optimization on hadoop. In: Soft Computing: Theories and Applications, pp. 251–263. Springer, Berlin (2018)
7. Lalwani, P., Banika, H., Kumar, C.: Bera: a biogeography-based energy-saving routing architecture for wireless sensor networks. *Soft Comput.* **22**(5), 1651–1667 (2018)
8. Lou, T., Tan, H., Wang, Y., Lau, F.C.: Minimizing average interference through topology control. In: International Symposium on Algorithms and Experiments for Sensor Systems, Wireless Networks and Distributed Robotics, pp. 115–129. Springer, Berlin (2011)
9. Naik, C., Shetty, D.P.: A novel meta-heuristic differential evolution algorithm for optimal target coverage in wireless sensor networks. In: International Conference on Innovations in Bio-Inspired Computing and Applications, pp. 83–92. Springer, Berlin
10. Naik, C., Shetty, D.P.: Differential evolution meta-heuristic scheme for k-coverage and m-connected optimal node placement in wireless sensor networks. *Int. J. Comput. Inf. Syst. Ind. Manag. Appl.* **11**, 132–141 (2019)
11. Nomosudro, P., Mehra, J., Naik, C., Shetty D, P.: Ecabbo: energy-efficient clustering algorithm based on biogeography optimization for wireless sensor networks. In: 2019 IEEE Region 10 Conference (TENCON), pp. 826–832 (2019)
12. Panda, B., Shetty, D.P.: Strong minimum interference topology for wireless sensor networks. In: Advanced Computing, Networking and Security, pp. 366–374. Springer, Berlin (2011)
13. Rajpurohit, J., Sharma, T.K., Abraham, A., Vaishali, A.: Glossary of metaheuristic algorithms. *Int. J. Comput. Inf. Syst. Ind. Manag. Appl.* **9**, 181–205 (2017)

14. Rangwala, S., Gummadi, R., Govindan, R., Psounis, K.: Interference-aware fair rate control in wireless sensor networks. In: ACM SIGCOMM Computer Communication Review, vol. 36, pp. 63–74. ACM (2006)
15. Sharma, T.K., Pant, M.: Opposition-based learning embedded shuffled frog-leaping algorithm. In: Soft Computing: Theories and Applications, pp. 853–861. Springer, Berlin (2018)
16. Shetty, D.P., Lakshmi, M.P.: Algorithms for minimizing the receiver interference in a wireless sensor network. In: IEEE Distributed Computing, VLSI, Electrical Circuits and Robotics (DISCOVER), pp. 113–118. IEEE (2016)
17. Simon, D.: Biogeography-based optimization. *IEEE Trans. Evolution. Comput.* **12**(6), 702–713 (2008)
18. Swami, V., Kumar, S., Jain, S.: An improved spider monkey optimization algorithm. In: Soft Computing: Theories and Applications, pp. 73–81. Springer, Berlin (2018)
19. Tomar, M.S., Shukla, P.K.: Energy efficient gravitational search algorithm and fuzzy based clustering with hop count based routing for wireless sensor network. In: Multimedia Tools and Applications, pp. 1–22 (2019)

Classification of SOA-Based Cloud Services Using Data Mining Technique



Zeenat Parween and R. B. S. Yadav

Abstract Cloud computing model fulfills storage and computation requirements of users in the form of services that are based on Service-Oriented Architecture (SOA). Services in cloud computing are offered with different quality attributes such as flexibility, mobility, adaptation, migration, etc. In recent years, cloud computing has grown at a very fast pace offering a huge number of cloud services with various quality attributes but it still faces some issues. One of them is that there is a lack of approach which can classify a cloud service based on its quality attributes for the cloud users. In this paper, a new approach is presented to classify cloud services using data mining “Bayesian classification” technique. The proposed approach is evaluated empirically via experiments that are performed on cloud-based data set containing data for 20 services, where each service having ten quality attributes. Results show that the proposed approach successfully classifies the cloud service in one of three classes (best, good, and satisfactory). Further, the proposed research will help the users in selecting the services as per their desired class.

Keywords Service-oriented architecture · Cloud · Data mining · Classification · Quality

1 Introduction

Service-Oriented Architecture (SOA) is an architectural style that guides the creation and usage of services to enable the development of service-oriented enterprise applications [1]. SOA-based services are loosely coupled, coarse-grained and autonomous in nature [2, 3]. Cloud computing is used to provide software/platforms/hardware on a service request [4]. In cloud computing, different unlimited numbers of IT resources are dynamically scalable and are open as a service on the Internet [5]. Today, all major IT companies like Amazon EC2, Microsoft Azure, Google Apps, and IBM

Z. Parween (✉) · R. B. S. Yadav
Department of Computer Science and Mathematics, Magadh University,
Bodh Gaya, Bihar 824234, India
e-mail: zeenatparween@gmail.com

blue cloud offer cloud services [6, 7]. Users of clouds are able to access the services from anywhere through their mobile phones or laptops.

Today, cloud computing has enabled businesses to evolve in different forms such as Ecommerce, supply chain organizations and virtual enterprises [8, 9]. Users are given an enormous number of cloud-based services having different quality attributes [10, 11]. In this huge quantity of services, it becomes difficult for the service users to select a suitable service as per their desired requirements. Also, for the service providers, it becomes important to know the class of their offered services so that they can improve their services.

This gives rise to have a classification of these services which benefit both the service provider as well as the service user. Service provider is helped to know the class of the offered service which may help the service provider to improve the quality of the service. The service user is helped to select the service which has the highest probability to meet the requirements to truly benefit the user. Therefore, in this paper, a new approach has been proposed which classify the cloud services based on their quality.

The proposed research work investigates the “N” cloud-based divisions using Bayesian classification method. A dataset is considered for experiments which contain cloud services from different cloud service providers. These services are used by users to purchase their things using online shopping [12, 13]. The proposed classification method aims to categorize the services into one of the three classes (best, good, and satisfactory).

The remainder of the paper is organized as follows. The proposed approach is introduced in Sect. 2. Experiments and results are explained in Sect. 3 to illustrate the proposed approach. Related work is discussed in Sect. 4. Finally, the paper is concluded in Sect. 5.

2 Proposed Approach

The paper proposes a new approach that aims to classify the services into one of the classes (best, good, and satisfactory) based on the Bayesian classification method [14].

In general, the Bayesian classification method is used to predict the probability of class membership, i.e., the probability that a given tuple belongs to a particular class. It is referred to as class “Conditional Independence” [15, 16]. Bayesian classification is based on Bayes’ theorem which is given below:

$$P(H/X) = \frac{P(X/H)P(H)}{P(X)} \quad (1)$$

where H represents Hypothesis that X belongs to class C .

- $P(H/X)$ represents probability that H holds given the observed data sample X
 $P(X/H)$ represents probability of observing X given H holds
 $P(H)$ represents initial probability
 $P(X)$ represents that the sample data is observed
 X represents data tuple (X is data sample class label considered as unknown).

The Bayesian classifier [16] in the proposed approach works as follows:

1. A training dataset D of 20 cloud services is taken which has n -dimensional ($X = (x_1, x_2, \dots, x_n)$) depicting n -measurements for each tuple.
2. For m -classes (C_1, C_2, \dots, C_m) and a given X , the membership of X belonging to a class C_i is defined as the highest probability to be conditioned on X . For this, the following condition should hold:
Iff $P(C_i/X) > P(C_j/X)$, for $1 \leq j \leq m, j \neq i$, then $P(C_i/X)$ is the maximum probability for X to belong in C_i .
3. The computation of $P(X/C_i)$ become,

$$P(X/C_i) = \prod_{(k=1)}^n P(x_k/C_i) \quad (2)$$

4. In order to find the linguistic pattern (class label), $P(X/C_i)P(C_i)$ is calculated for each instance of class C_i . The Bayesian classifier assigns the linguistic pattern (class label) of service X in class instance C_i :
iff $P(X/C_i)P(C_i) > P(X/C_j)P(C_j)$ for $1 \leq j \leq m, j \neq i$.

3 Experiments and Analysis

Experiments are conducted on 20 cloud services (namely, A, B, C, ... T). Table 1 shows the training data set which contains ten quality attributes for each cloud service. Each cloud service has a specific class (best, good, and satisfactory) based on service quality attributes.

Next, let us consider a testing data set which contains the values for all ten quality attributes for service X . With the proposed approach, the class of service X needs to be determined by computing the probability.

S.No.	Cloud Service	Free Storage	Analytics	Security	Backup	Flexibility	Sharing	Mobility	Recovery	Auto Update	Migration	Class
1.	X	1	0	1	1	0	1	1	1	0	0	.

Here 1 represents YES and 0 represents NO in column 3 to 12

Table 1 Data set

S.No.	Cloud Service	Free Storage	Analytics	Security	Backup	Flexibility	Sharing	Mobility	Recovery	Auto Update	Migration	Class
1	A	1	1	1	1	1	1	1	1	1	1	1
2	B	1	1	1	1	1	1	1	1	1	1	1
3	C	0	1	1	1	1	0	1	1	0	1	2
4	D	0	1	1	1	1	0	1	1	1	1	2
5	E	0	1	1	1	1	0	1	1	0	1	3
6	F	1	0	1	1	0	1	1	1	1	0	3
7	G	0	1	1	1	1	0	1	1	0	1	3
8	H	1	1	1	1	1	1	1	1	1	1	1
9	I	0	0	1	1	1	0	1	1	0	1	1
10	J	0	0	1	1	1	1	1	1	0	1	2
11	K	1	0	1	1	0	1	1	1	1	0	2
12	L	0	1	1	1	1	0	1	1	0	1	3
13	M	1	1	1	1	1	1	1	1	1	1	1
14	N	0	0	1	1	1	0	1	1	0	1	1
15	O	0	0	1	1	1	1	1	1	0	1	2
16	P	1	1	1	1	1	1	1	1	1	1	2
17	Q	1	1	1	1	1	1	1	1	1	1	3
18	R	0	1	1	1	1	0	1	1	0	1	3
19	S	0	1	1	1	1	0	1	1	1	1	3
20	T	0	1	1	1	1	0	1	1	0	1	3

Here 1 represents YES and 0 represents NO in column 3 to 12,

1 for best, 2 for good and 3 for satisfactory in column 13

First, prior probability of each class (1 for best, 2 for good, and 3 for satisfactory) is computed as follows:

$$\text{Probability of best class} \quad P(1) = \frac{6}{20} = 0.3$$

$$\text{Probability of good class} \quad P(2) = \frac{6}{20} = 0.3$$

$$\text{Probability of satisfactory class} \quad P(3) = \frac{8}{20} = 0.4.$$

The probability using Bayesian classification for each quality attribute of the cloud services is computed as follows:

For attribute *free storage*

$$P(\text{free storage} = \text{yes}/\text{class} = 1) = 3/6 = 0.5$$

$$P(\text{free storage} = \text{yes}/\text{class} = 2) = 2/6 = 0.33$$

$$P(\text{free storage} = \text{yes}/\text{class} = 3) = 2/8 = 0.25$$

For attribute *analytics*

$$P(\text{analytics} = \text{no}/\text{class} = 1) = 1/6 = 0.17$$

$$P(\text{analytics} = \text{no}/\text{class} = 2) = 3/6 = 0.50$$

$$P(\text{analytics} = \text{no}/\text{class} = 3) = 1/8 = 0.125$$

For attribute *security*

$$P(\text{security} = \text{yes}/\text{class} = 1) = 6/6 = 1$$

$$P(\text{security} = \text{yes}/\text{class} = 2) = 6/6 = 1$$

$$P(\text{security} = \text{yes}/\text{class} = 3) = 8/8 = 1$$

For attribute *backup*

$$P(\text{backup} = \text{yes}/\text{class} = 1) = 6/6 = 1$$

$$P(\text{backup} = \text{yes}/\text{class} = 2) = 6/6 = 1$$

$$P(\text{backup} = \text{yes}/\text{class} = 3) = 8/8 = 1$$

For attribute *flexibility*

$$P(\text{flexibility} = \text{no}/\text{class} = 1) = 1/6 = 0.17$$

$$P(\text{flexibility} = \text{no}/\text{class} = 2) = 1/6 = 0.17$$

$$P(\text{flexibility} = \text{no}/\text{class} = 3) = 1/8 = 0.125$$

For attribute *sharing*

$$P(\text{sharing} = \text{yes}/\text{class} = 1) = 4/6 = 0.67$$

$$P(\text{sharing} = \text{yes}/\text{class} = 2) = 4/6 = 0.67$$

$$P(\text{sharing} = \text{yes}/\text{class} = 3) = 2/8 = 0.25$$

For attribute *mobility*

$$P(\text{mobility} = \text{yes}/\text{class} = 1) = 6/6 = 1$$

$$P(\text{mobility} = \text{yes}/\text{class} = 2) = 6/6 = 1$$

$$P(\text{mobility} = \text{yes}/\text{class} = 3) = 8/8 = 1$$

For attribute *recovery*

$$P(\text{recovery} = \text{yes}/\text{class} = 1) = 6/6 = 1$$

$$P(\text{recovery} = \text{yes}/\text{class} = 2) = 6/6 = 1$$

$$P(\text{recovery} = \text{yes}/\text{class} = 3) = 8/8 = 1$$

For attribute *auto update*

$$P(\text{auto update} = \text{no}/\text{class} = 1) = 2/6 = 0.333$$

$$P(\text{auto update} = \text{no}/\text{class} = 2) = 3/6 = 0.5$$

$$P(\text{auto update} = \text{no}/\text{class} = 3) = 5/8 = 0.625$$

For attribute *migration*

$$P(\text{migration} = \text{no}/\text{class} = 1) = 2/6 = 0.333$$

$$P(\text{migration} = \text{no}/\text{class} = 2) = 3/6 = 0.5$$

$$P(\text{migration} = \text{no}/\text{class} = 3) = 5/8 = 0.625$$

Using the above probabilities, the probability of all attributes for X and class 1 is calculated using Eq. (2):

$$\begin{aligned} P(X/\text{class} = \text{best}) &= P(\text{free storage} = \text{yes}/\text{class} = \text{best}) * P(\text{analytics} = \text{no}/\text{class} = \text{best}) \\ &\quad * P(\text{security} = \text{yes}/\text{class} = \text{best}) * P(\text{backup} = \text{yes}/\text{class} = \text{best}) \\ &\quad * P(\text{flexibilty} = \text{no}/\text{class} = \text{best}) * P(\text{sharing} = \text{yes}/\text{class} = \text{best}) \\ &\quad * P(\text{mobility} = \text{yes}/\text{class} = \text{best}) * P(\text{recovery} = \text{yes}/\text{class} = \text{best}) \\ &\quad * P(\text{autoupdate} = \text{no}/\text{class} = \text{best}) * P(\text{migration} = \text{no}/\text{class} = \text{best}) \\ &= 0.5 * 0.17 * 1 * 1 * 0.333 * 0.67 * 1 * 1 * 0.333 * 0.333 = 0.0021. \end{aligned}$$

Similarly, probabilities for X and other classes (2 and 3) are computed as follows:

$$P(X/\text{class} = \text{good}) = 0.333 * 0.5 * 1 * 1 * 0.17 * 0.67 * 1 * 1 * 0.5 * 0.5 = 0.0047$$

$$P(X/\text{class} = \text{satisfactory}) = 0.25 * 0.125 * 1 * 1 * 0.125 * 0.25 * 1 * 1 * 0.625 * 0.625 = 0.00038$$

For the service X ,

$$P(X/\text{class} = \text{best}) * P(C_i) = 0.0021 * 0.3 = 0.00063$$

$$P(X/\text{class} = \text{good}) * P(C_i) = 0.0047 * 0.3 = 0.00141$$

$$P(X/\text{class} = \text{satisfactory}) * P(C_i) = 0.00038 * 0.4 = 0.000152.$$

From the above values, it can be seen that $P(X/\text{class} = \text{good}) * P(C_i)$ is the maximum among all three probabilities. Therefore, after applying Bayesian classification, the class for the service X is good.

It may be concluded that the proposed approach successfully classifies a new cloud service (under consideration) into best/good/satisfactory class.

4 Related Work

Work done in [17] proposes a hybrid approach to enable dynamic web service discovery based on lightweight semantic descriptions using machine learning techniques. Authors in [18] propose a text mining approach to detect main concepts present in textual documentation of service. The research done in [19] deals with cloud data storage and analysis. In this paper, the class labels of unlabeled samples in large-scale datasets in cloud are predicted to reduce the burden of data owners and users. Authors in [20] have tested the authenticity of the data stored on the cloud server which a user accesses. In [21], fraud detection mechanism in the healthcare industry is implemented using data mining techniques. Bhardwaj et al. [22] propose a private cloud computing environment called Megh to host various IaaS and SaaS services for the users.

5 Conclusion

Cloud computing model offers cloud services having different values for different quality attributes. In this paper, Data mining Bayesian classification method is used for classifying these cloud services based on their quality attributes in one of three classes (best, good, and satisfactory). Experiments were performed on cloud-based data set containing data for ten quality attributes of 20 services. The proposed research will help the cloud users in selecting the services which fulfills their quality needs and also enable cloud-based stores to give more prominent precision and unwavering quality to the individuals to store their outstanding commodities within the crowded cloud.

References

1. Erl, T.: Service-Oriented Architecture: Concepts, Technology, and Design. Pearson Education India (2005)
2. Zhang, L.-J.: SOA and Web services. In: IEEE International Conference on Services Computing, 2006, SCC'06, pp. xxxvi–xxxvi (2006)
3. Laskey, K.B., Laskey, K.: Service oriented architecture. Wiley Interdiscip. Rev. Comput. Stat. **1**(1), 101–105 (2009)
4. Vaquero, L.M., Rodero-Merino, L., Morn, D.: Locking the sky: a survey on IaaS cloud security. J. Comput. **91**(1), 93,1/2011 1-26A (2011) (Springer Verlag)
5. Keith, J., Burkhard, N.: The future of cloud computing. Opportunities for European Cloud Computing Beyond. Expert group report. <http://cordis.europa.eu/fp7/ict/ssai/docs-cloudreport-final.pdf> (2010)
6. Takako, P., Estcio, G., Kelner, J., Sadok, D.: A survey on open-source cloud computing solutions. In: Teyssier, S. (ed.) WCGA—8th Workshop on Clouds, Grids and Applications, Gramado:28 May, 3–16 (2010)

7. Mahjoub, M., Mdhaffar, A., Halima, R.B, Jmaieli, M.: Comparative Study of the Current Cloud Computing Technologies and Offers (2011)
8. Sholler, D.: SOA User Survey: Adoption Trends and Characteristics, Gartner, September 26, p. 32 (2008)
9. Buyya, R., Yeo, C.S., Venugopal, S.: Market-oriented cloud computing: vision, hype, and reality for delivering IT services as computing utilities. In: Proceedings of the 2008 10th IEEE International Conference on High Performance (2008)
10. Tantik, E., Anderl, R.: Potentials of the asset administration shell of Industries 4.0 for service-oriented business models. *Procedia CIRP* **64**, 363–368 (2017)
11. Kem, O., Balbo, F., Zimmermann, A.: Traveler-oriented advanced traveler information system based on dynamic discovery of resources: potentials and challenges. *Transp. Res. Procedia* **22**, 635–644 (2017)
12. Stelly, C., Roussev, V.: SCARF: a container-based approach to cloud-scale digital forensic processing. *Digital Invest.* **22**, S39–S47 (2017)
13. Lu, Y., Ju, F.: Smart manufacturing systems based on Cyber-Physical Manufacturing Services (CPMS). *IFAC-Papers on Line* **50**(1), 15883–15889 (2017)
14. Kantardzic, M.: Data Mining—Concepts, Models, Methods, and Algorithms. IEEE Press, Wiley-Interscience (2003)
15. Cheeseman, P., Kelly, J., Self, M., Stutz, J., Taylor, W., Freeman, D.: Autoclass: A Bayesian classification system. In: Machine Learning Proceedings 1988, pp. 54–64. Morgan Kaufmann (1988)
16. Cheeseman, P.C., Self, M., Kelly, J., Taylor, W., Freeman, D., Stutz, J.C.: Bayesian classification. In: AAAI, vol. 88, pp. 607–611 (1988)
17. Shafiq, O., Alhajj, R., Rokne, J.G., Toma, I.: A hybrid technique for dynamic web service discovery. In: 2010 IEEE International Conference on Information Reuse & Integration, pp. 121–125. IEEE (2010)
18. Nisa, R., Qamar, U.: A text mining based approach for web service classification. *IseB* **13**(4), 751–768 (2015)
19. Zhu, Y., Li, X., Wang, J., Liu, Y., Qu, Z.: Practical secure naïve bayesian classification over encrypted big data in cloud. *Int. J. Found. Comput. Sci.* **28**(06), 683–703 (2017)
20. Mishra, N., Sharma, T.K., Sharma, V., Vimal, V.: Secure framework for data security in cloud computing. In: Soft Computing: Theories and Applications, pp. 61–71. Springer, Singapore (2018)
21. Pandey, P., Saroliya, A., Kumar, R.: Analyses and detection of health insurance fraud using data mining and predictive modeling techniques. In: Pant, M., Ray, K., Sharma, T., Rawat, S., Bandyopadhyay, A. (eds) Soft computing: theories and applications. Advances in Intelligent Systems and Computing, vol. 584. Springer, Singapore (2018)
22. Bhardwaj, T., Kumar, M., Sharma, S.C.: Megh: a private cloud provisioning various IaaS and SaaS. In: Soft Computing: Theories and Applications, pp. 485–494. Springer, Singapore (2018)

A Novel Clustering-Based Gene Expression Pattern Analysis for Human Diabetes Patients Using Intuitionistic Fuzzy Set and Multigranulation Rough Set Model



Swarup Kr Ghosh and Anupam Ghosh

Abstract In this article, we present an intuitionistic fuzzy set (IFS)-based gene expression pattern classification using multigranulation rough set theory for human diabetes patient. At the very beginning, the proposed scheme generates a soft-information structure from the microarray by IFS via multiple fuzzy membership functions with Yager generating function. The intuitionistic fuzzy set deals with the ambiguity between normal state and diabetic state from gene expression microarray via the hesitation degree while shaping the membership function. Thereafter, a multi-granulation rough set is utilized for the measurement of accuracy and roughness from expression pattern that has been deferentially expressed from normal state to diabetic state. Lastly, Rough-fuzzy C-means clustering has been applied on the datasets into two clusters such as diabetes or non-diabetes. The associations among human genes have also been identified which are correlated with diabetes (type-2). In addition, we have validated a measurement by F -score using diabetes gene expression NCBI database and achieved better performance in comparison with baseline methods.

Keywords Diabetes gene microarray · Rough set · Multigranulation · Intuitionistic fuzzy set · Rough-fuzzy c-means

1 Introduction

Diabetes identified as diabetes mellitus (DM) is an assembly of metabolic diseases considered as hyperglycemia subsequently from insufficiency in insulin emission, insulin action, or both [1, 2]. Basically diabetes is characterized into two major

S. K. Ghosh (✉)

Department of Computer Science and Engineering, Sister Nivedita University, Kolkata 700156, India

e-mail: swarupg1@gmail.com

A. Ghosh

Department of Computer Science and Engineering, Netaji Subhash Engineering College, Kolkata 700152, India

e-mail: anupam.ghosh@rediffmail.com

groups: type 1 and type 2. Microarrays extend the activity on expression level of the genes under unpredictable conditions [2, 3]. Microarray data or gene expression data are structured together as a matrix of expression values with rows and columns. Each record which can be a flat out incentive in the matrix represents as the articulation level of a gene under a condition. It can either be an absolute value (Affymetrix GeneChip) or a relative expression ratio (cDNA microarrays) [4, 5].

Various approaches and several techniques have been developed on gene expression data and disease classification. A pattern matching approach for clustering gene expression data had been described by Das et al. [4]. A density-based hierarchical clustering algorithm is proposed by Jiang et al. [5]. Knowledge encoding and classification by rough-fuzzy MLP on gene expression data had been proposed by Banerjee et al. [6]. A fuzzy soft set-based classification for gene expression data had been described by Kalaiselvi et al. [7]. A deep learning-based gene selection for cancer detection was proposed by Danaee et al., using stack denoising autoencoder [8], which require huge data for training purpose. Unsupervised learning-based clustering algorithms have been developed in the last two decades such as k-means or hard c-means (HCM), hierarchical clustering [9–11]. First overlapped clustering algorithm known as fuzzy c-means (FCM) algorithm was described by Dunn et al. [9, 10] and it has not produced good result for noisy data. Later, possibilistic c-means (PCM) algorithm was proposed by Krishnapuram and Keller [12], that utilized a possibilistic type of membership function to describe the degree of belongingness. However, sometimes coincident clusters are generated by PCM. The rough sets theory is a mathematical apparatus which manages the vague and imprecise data from uncertain and deficient information introduced by Pawlak [13]. A clustering approach using rough set, known as rough c-means (RCM) clustering was suggested by Lingras [14]. To handle uncertain and vague data, the hybridization of fuzzy set and rough sets serves a new mathematical model [15]. Several rough-fuzzy clustering algorithms, like rough-fuzzy c-means (RFCM) [16], rough-possibilistic c-means (RPCM), rough-fuzzy-possibilistic c-means (RFPCM) [11] described in literature.

Inspired from Intuitionistic fuzzy set theory [17] and rough-fuzzy c-means [16], we have proposed an intuitionistic fuzzy set-based clustering method in the domain of multigranulation rough set (called IFSMR) to handle high-dimensional and noisy data. The proposed clustering algorithm has been applied on microarray gene expression databases for human diabetes patient. The contributions of this paper can be summarized as follows:

- We have designed an efficient intuitionistic fuzzy set-based biomarker identification using multigranulation rough set in human diabetes (type-2) microarray gene expression data. The proposed model is used to better interpret the gene profiles in diabetes gene identification and provide an accurate judgment about diabetes in the treatment by a clinical expert without any subjective effort.
- A new intuitionistic fuzzy-rough sets multigranulation has been adopted for gene identification and used rough-fuzzy c-means clustering to minimizing the uncertainty of patterns selection and reduce the misclassification errors in microarray data classification.

- Experimental results and validation using F -score are demonstrated that the suggested model is efficient to identify genes from microarray database which are responsible for diabetes (type-2) in human body.

The rest of this paper is organized as follows: In Sect. 2, we brief preliminaries behind the proposed model. In Sect. 3, we present the designed scheme are described in details. In Sect. 4, we give empirical results and discussions. Conclusions and perspectives are given in Sect. 5.

2 Preliminaries

This section draws the general frameworks basic mathematical preliminaries of the proposed model and design issues of the proposed intuitionistic fuzzy set and multi-granulation rough set-based clustering (IFSMR) model to resolve clustering problem on gene expression data.

2.1 Construction of Intuitionistic Fuzzy Set

Let \mathbf{G} be a gene expression matrix of size $M \times N$, having $x \in \mathfrak{N}$ can be viewed as an array of fuzzy singletons [18, 19], where M and N are the number of sample and gene identifier, respectively. Each element in the array is the membership value of the corresponding gene expression value. In fuzzy set theory, a gene expression microarray \mathbf{G} is written as below:

$$\mathbf{X} = \left\{ \frac{\mu_X(x_{pq})}{x_{pq}}, p = 1, 2, \dots, M, q = 1, 2, \dots, N \right\} \quad (1)$$

where $\mu_X(x_{ij})$ denotes the membership of corresponding gene expression value x_{pq} with respect to the sample and gene identifier of matrix G . Here, ‘Triangular’ and ‘Gaussian’ membership functions have been used to quantify the highest vagueness from microarray. The triangular membership function computes fuzzy membership values using a given set of parameters. The triangular membership function $\mu_X(x; a, b, c)$ for each x over parameters $(a, b, c | a \leq b \leq c)$ is defined as

$$\mu_X(x; a, b, c) = \max \left(\min \left(\frac{x - a}{b - a}, \frac{c - x}{c - b} \right), 0 \right) \quad (2)$$

where $(a, b, c | a \leq b \leq c)$ are parameters. This function computes fuzzy membership values and it has a maximum value that is 1. Similarly, the ‘Gaussian’ membership function express as [18, 19]:

$$\mu_X(x; \sigma, c) = \exp \left\{ \frac{-(x - c)^2}{2\sigma^2} \right\} \quad (3)$$

where σ specifies the standard deviation and c is mean act as control parameter for the Gaussian function.

In order to construct intuitionistic fuzzy set (IFS), we derive it from a fuzzy set (FS) $\mu_X(x)|x \in X$. The intuitionistic fuzzy set (IFS) consists of both membership $\mu_X(x)$ and non-membership $\nu_X(x)$ functions [17]. An intuitionistic fuzzy set \mathbf{X} in \mathbf{G} is given as $\mathbf{X} = \{x, \mu_X(x), \nu_X(x)|x \in \mathbf{G}\}$ [17, 20], where $\mu_X(x) \rightarrow [0, 1]$, $\nu_X(x) \rightarrow [0, 1]$ represent membership and non-membership degrees of an element x in the set \mathbf{X} with respect to the constraint $[0 \leq x, \mu_X(x), \nu_X(x) \leq 1|x \in \mathbf{G}]$ If $\nu_X(x) = 1 - \mu_X(x) \forall x \in \mathbf{X}$, then \mathbf{X} turn into a fuzzy set. Atanassov has indicated the hesitation degree of an IFS $\pi_X(x)$ to be the lack of knowledge occurring to define a membership degree of each element x in set \mathbf{X} and it is defined as [17]:

$$\pi_X(x) = 1 - \mu_X(x) - \nu_X(x)|x \in \mathbf{G} \quad (4)$$

The membership values belong to the interval $[\mu_X(x), \mu_X(x) + \pi_X(x)|x \in \mathbf{G}]$ so , $0 \leq \pi_X(x) \leq 1$.

A continuous increasing and decreasing function $g(x) \rightarrow [0, 1]$ is called continuous increasing and decreasing intuitionistic fuzzy generator [20] if:

$$g(x) \leq (1 - x) \mid \forall x \in [0, 1] \text{ and } g(0) \leq 1; g(1) \leq 0 \quad (5)$$

The Yager generating function is utilized to define the intuitionistic fuzzy generator as [20]:

$$T(\mu(x)) = h^{-1}(h(1) - h(\mu(x))) \quad (6)$$

where $h(\cdot)$ is an increasing function such that $h : [0, 1] \rightarrow [0, 1]$. The Yager function is generated using Eq. (6) as:

$$h(x) = x^\alpha \quad (7)$$

Thus, Yager's intuitionistic fuzzy generator can be rewritten as [17]:

$$T(x) = (1 - x^\alpha)^{1/\alpha} \quad (8)$$

where $\alpha > 0$ and $T(1) = 0$, $T(0) = 1$, respectively. Thus, we can define IFS using Yager's intuitionistic fuzzy complement [17, 20] as:

$$\mathbf{X} = \{x, \mu_X(x), (1 - \mu_X(x)^\alpha)^{1/\alpha}|x \in \mathbf{G}\} \quad (9)$$

and the hesitation degree is determined as [17]:

$$\pi_X(x) = 1 - \mu_X(x) - (1 - \mu_X(x)^\alpha)^{1/\alpha}. \quad (10)$$

2.2 Rough Set Model for Microarray

Definition 1 Let $\mathbf{U}_1, \mathbf{U}_2$ be two universes of closer, and \mathbf{R} be a compatibility relation from U_1 to U_2 . The function $\mathbf{F} : \mathbf{U}_1 \rightarrow 2^v, u \mapsto \{v \in \mathbf{U}_2 | (u, v) \in \mathbf{R}\}$ is said to be mapping induced by \mathbf{R} [13].

The approximation space is defined from ordered triple $(\mathbf{U}_1, \mathbf{U}_2, \mathbf{R})$. The lower and upper approximations of $\mathbf{Z} \subseteq \mathbf{U}_2$ are given as follows [13]:

$$\underline{\Psi}_{\mathbf{F}}(\mathbf{Z}) = \{x \in \mathbf{U}_1 | \mathbf{F}(x) \subseteq \mathbf{Z}\} \text{ and } \overline{\Psi}_{\mathbf{F}}(\mathbf{Z}) = \{x \in \mathbf{U}_1 | \mathbf{F}(x) \cap \mathbf{Z} \neq \emptyset\}$$

The ordered set-pair $(\underline{\Psi}_{\mathbf{F}}(\mathbf{Z}), \overline{\Psi}_{\mathbf{F}}(\mathbf{Z}))$ is called a generalized rough set.

Definition 2 Let $(\mathbf{U}_1, \mathbf{U}_2, \mathbf{R})$ be multigranulation approximation space over two universes and $\mathbf{X} \in \mathbf{F}(\mathbf{U}_2)$. The optimistic lower approximation $\underline{\Psi}_{\sum_{i=1}^m \mathbf{R}_i}(\mathbf{X})$ and upper approximation $\overline{\Psi}_{\sum_{i=1}^m \mathbf{R}_i}(\mathbf{X})$ of fuzzy set X in $(\mathbf{U}_1, \mathbf{U}_2, \mathbf{R})$ are defined as follows [13, 15]:

$$\underline{\Psi}_{\sum_{i=1}^m \mathbf{R}_i}(\mathbf{X})(x) = \min\{\mathbf{X}(y) | \bigvee_{i=1}^m \mathbf{F}_i(x), y \in \mathbf{U}_2\}, x \in \mathbf{U}_1 \quad (11)$$

$$\overline{\Psi}_{\sum_{i=1}^m \mathbf{R}_i}(\mathbf{X})(x) = \max\{\mathbf{X}(y) | \bigvee_{i=1}^m \mathbf{F}_i(x), y \in \mathbf{U}_2\}, x \in \mathbf{U}_1 \quad (12)$$

where $\bigvee_{i=1}^m \mathbf{F}_i(x) = \mathbf{F}_1(x) \vee \dots \vee \mathbf{F}_m(x)$ and then $y \in \mathbf{F}_1(x) \vee \mathbf{F}_2(x)$.

Definition 3 Let $(\mathbf{U}, \mathbf{V}, \mathbf{R})$ be multigranulation approximation space over two universes. For any $\mathbf{X} \in \mathbf{F}(\mathbf{V})$ and α and β are parameters such that $0 < \beta \leq \alpha \leq 1$ [13, 16].

The accuracy ρ and the roughness σ of \mathbf{X} with respect to multigranulation approximation space over two universes are calculated as:

$$\rho_X(\alpha, \beta) = \frac{|\underline{\Psi}_{\sum_{i=1}^m \mathbf{R}_i}(\mathbf{X}_\alpha)|}{|\overline{\Psi}_{\sum_{i=1}^m \mathbf{R}_i}(\mathbf{X}_\beta)|} \text{ and } \sigma(\alpha, \beta) = 1 - \rho_X(\alpha, \beta) \quad (13)$$

The intuitionistic fuzzy-rough approximations positive regions $\text{POS}(C_j)$ and the boundary regions $\text{BOU}(C_j)$ can be expressed as:

$$x_i = \begin{cases} \text{POS}(C_j); & \text{if } x_i \in \underline{R}(\pi(x_i)) \\ \text{BOU}(C_j); & \text{if } x_i \in \overline{R}(\pi(x_i)) - \underline{R}(\pi(x_i)) \end{cases} \quad (14)$$

The new centroids are calculated based on positive and boundary regions using the bias field b_i as follows:

$$C_k = \frac{\sum_{x_i \in \text{POS}(C_k)} x_i b_i}{\sum_{x_i \in \text{POS}(C_k)} b_i^2} + \frac{\sum_{x_i \in \text{BOU}(C_k)} (\pi_{ij})^m x_i b_i}{\sum_{x_i \in \text{BOU}(C_k)} (\pi_{ij})^m x_i b_i^2}. \quad (15)$$

3 Proposed Methodology

The proposed clustering-based pattern analysis on microarray gene expression data determines some human genes and their expressions pattern that are correlated with diabetes patients. Basically, microarray gene databases consist of imprecise and vague information, hence it is very difficult to predict genes correlated with deadly diseases such as cancer or diabetes. Conventional clustering algorithm such as k-means, hierarchical-based clustering, fuzzy c-means, rough c-means algorithms are failed to achieve good accuracy in microarray databases due to ambiguous nature of data. Here, we have proposed an intuitionistic fuzzy set (IFS)-based clustering algorithm in the framework of multigranulation rough set (IFSMR) for the pattern analysis on microarray databases of human diabetes patients. The proposed work divides into three parts, firstly, fuzzify the microarray using IFS (Yager function) through the hesitant score calculation. Secondly, map microarray from fuzzy plane to multigranulation space under the closer of two universes which reduces the dimension of the data. Finally, apply rough-fuzzy c-means clustering algorithm of the data into two clusters, viz. diabetes and controlled through roughness and accuracy measurement. The schematic diagram of the proposed model is shown in Fig. 1.

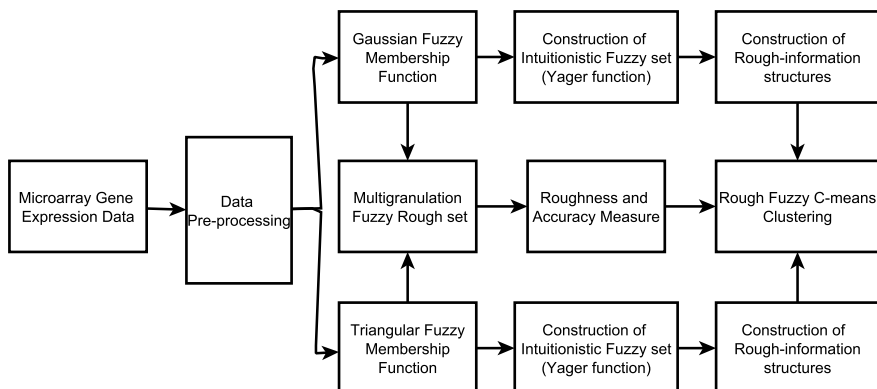


Fig. 1 Schematic diagram the proposed method

3.1 Preprocessing

Data preprocessing is a crucial step for the microarray gene expression data since it contains null values and outliers. To remove null value, we have utilized mean and hot-decking imputation in this article [21]. Outliers have been removed using some statistical methods like coefficient of variance (CV), and standard deviation. Finally, normalization has done on the matrix G as $G = \frac{x - x_{\min}}{x_{\max} - x_{\min}}$.

3.2 Conversion to Fuzzy and IFS Plane

Now, the process matrix G is converted into two fuzzy planes using triangular and Gaussian membership function separately using Eqs. (2) and (3), respectively [18, 19]. To construct IFS of the matrix \mathbf{X} as $\mathbf{X} = \{x, \mu_X(x), \nu_X(x) | x \in \mathbf{G}\}$, we calculate non-membership function $\nu_X(x) = 1 - \mu_X(x)$ and hesitant degree using Eq. (4) in this investigation. The gene expression microarray consists of more uncertain or vague information due to nature of the data. The Yager's IFS generating functions [Eqs. (7) and (8)] have been used to calculate Yager's IFS complement using Eq. (9) to handle such kind of uncertainty [17, 20]. Finally, we reduce the volume of data using Eq. (10), the generated IFS hesitant degree.

3.3 Multigranulation Rough-Fuzzy c-Means Clustering

In the next step of the proposed clustering model, we convert data into rough-fuzzy space such as lower and upper approximation, considering two universes of closer using Eqs. (11) and (12). Roughness and accuracy measurement are two crucial phases for the clustering to reduce the volume of the database. So, we have measured the accuracy (ρ_A) and roughness (σ) using Eq. (13). Sometimes clusters may overlap among each other for the fuzzy-based clustering. A cluster is illustrated by a fuzzy upper approximation and a fuzzy lower approximation known as rough-fuzzy c-means (RFCM) [13, 15, 16].

In order to cluster the microarray $\{x_1, x_2, \dots, x_n\}$ into two fuzzy clusters $\{c_0, c_1\}$, (where c_0 and c_1 refer the controlled state and diabetes state, respectively) the criterion for updating centroids in RFCM is summarized as follows [16]:

$$v_i = \begin{cases} \mathbf{S}_1, & \text{if } \underline{\mathbf{R}}(c_k) \neq \emptyset, \mathbf{BOU}(c_k) = \emptyset. \\ \mathbf{S}_2, & \text{if } \underline{\mathbf{R}}(c_k) = \emptyset, \mathbf{BOU}(c_k) \neq \emptyset. \\ \mathbf{w} \star \mathbf{S}_1 + \mathbf{w}' \star \mathbf{S}_2, & \text{if } \underline{\mathbf{R}}(c_k) \neq \emptyset, \mathbf{BOU}(c_k) \neq \emptyset. \end{cases} \quad (16)$$

$$\mathbf{S}_1 = \frac{1}{|\underline{R}(c_i)|} \sum_{x_k \in \underline{R}(c_i)} x_k, \quad \mathbf{S}_2 = \frac{1}{n_k} \sum_{x_i \in \text{BOU}(c_k)} (\mu_{ik})^m (x_k)$$

$$n_k = \sum_{x_i \in \text{BOU}(c_k)} (\mu_{ik})^m, \quad d_{il} = \|x_i - c_l\|, \quad d_{ik} = \|x_i - c_k\|$$

where μ_{ik} indicates the degree of belonging of i^{th} value to k^{th} ($k \in \{0, 1\}$) fuzzy cluster is determined by Eq. (17). The lower approximation of the cluster is represented by $\underline{R}(c_i)$. w and w' are the weight parameters such that $0 < w' < w < 1$, and $w' + w = 1$. These parameters control the importance of the approximation regions.

The fuzzy cluster is formulated as:

$$\mu_{ik} = \frac{1}{\sum_{l=1}^c \left(\frac{d_{ik}}{d_{il}} \right)^{2/m-1}} \quad (17)$$

where c represents the number of clusters and c_i indicates cluster i , $i = 2 \dots c$ (here, $i=2$ for proposed IFSMR method). The fuzzy membership value μ_{ik} calculates the membership degree of the object k which is the member of i cluster, and m denotes fuzzy coefficient. A new centroid is determined from Eq (15) and this process will continue till two approximations become empty.

Let μ_{ik} and μ_{lk} be the highest and second highest membership values of object k over two clusters. If $|\mu_{ik} - \mu_{lk}| > \theta$, object k belongs to the lower approximation of cluster i , otherwise, object k belongs to the boundary regions of both cluster i and cluster l for threshold θ [15, 16].

Furthermore, the fuzzy sets deal uncertainty whereas the rough set-based clustering deals with overlapping cluster problems. The object belongs to the lower approximation if it satisfies the threshold condition, otherwise it belongs to the boundary region. The objects of boundary region get second chance for fulfilling the threshold criteria. This process will continue until boundary region become empty [11, 15, 16].

The steps in the algorithm of intuitionistic fuzzy-rough c-means clustering algorithm is discussed as follows:

1. Initialize number cluster $k = 2$, k bias field $b_i = 1$, $\delta \in [0, 1]$, the stop condition.
2. Compute the initial cluster centroids using Eq. (16).
3. Determine the initial membership degree $\mathcal{U}^l = [u_{ij}]$ using Eqs. (2) and (3).
4. Calculate the highest membership degree for each expression value for all the centroids.
5. Compute the fuzzy-rough positive regions and boundary regions using Eqs. (11) and (12).
6. Update the new centroids \mathcal{U}^{l+1} using Eqs. (14) and (15) simultaneously.

7. Find the convergence distance (η) between \bigcup^{l+1} and \bigcup^l using $\bar{R}(\pi(x_j)) - R(\pi(x_j))$.
8. If($\eta \geq \delta$) then exit.

4 Experimental Results and Discussion

This section elaborates the experimental assessment and the results acquired for the proposed IFSMR method. The simulation of the proposed algorithm has been done over a diabetes (Type 2) gene expression datasets using *Matlab – 19a* on Processor Inter Core *i5 – 6200U* CPU 3.5 GHz with 16 GB of RAM and *Ubuntu 18.04-64 bits* Linux environment.

4.1 Description of Datasets

The effectiveness of our methods along with comparisons is demonstrated on two standard gene expression diabetes (type 2) databases which are taken from NCBI, viz. ‘type 2 diabetes: myotube (GDS3681)’ and ‘type 2 diabetes: pancreatic beta-cells (GDS3782)’. The samples’ organism of both the databases are homo sapiens and the gene expression values extracted from RNA and it has stored in tabular form. The database GDS3681 consists of 12625 genes and taken from 20 samples of which 10 samples are in disease state, i.e., diabetes (type 2) state and 10 samples are in normal state. The database GDS3782 contains 61359 number features set and taken of 20 samples of which 10 samples are in diabetes state and 10 samples are controlled state [22].

4.2 Performance Evaluation Metrics and Baseline Methods

To validate the result of the proposed IFSMR method we have used five performance measures such as accuracy, sensitivity, specificity, and *F*-Measure [23, 24] in this section. The calculation of these measures involves a number of true positive (TP), false positive (FP), true negative (TN), and false negative (FN) [23, 24]. We have considered three other clustering methods including fuzzy c-means (FCM) [9, 10], possibilistic c-means (PCM) [12], and rough-fuzzy c-means (RFCM) [16] as state-of-the-art methods in comparison with proposed IFSMR. All three state-of-the-art methods have been implemented on same gene expression databases.

4.3 Gene Clustering Analysis

The estimated accuracy across different gene expression results of the proposed IFSMR method along with three state-of-the-art methods, viz. FCM, PCM, and RFCM have been shown in Table 1 for two diabetes datasets taken average of each metric. The cluster analysis of the proposed method has been demonstrated in Fig. 2 for a subset of the database. Table 1 shows the classification accuracy with baseline methods for two diabetes databases (mean). From the simulation of the proposed method, approximately 105 and 122 genes have been selected from two databases respectively which are somewhat biologically significant with respect to their pattern. It is clear from Table 1 that F -score of the proposed method produces better result in comparison with three baseline methods. The F -score of the proposed IFSMR methods for two databases are 0.85 and 0.83, respectively. However, the RFCM method also produces good accuracy for two databases 0.90 and 0.86 which are close to the accuracy of the proposed methods as calculated 0.93 and 0.89.

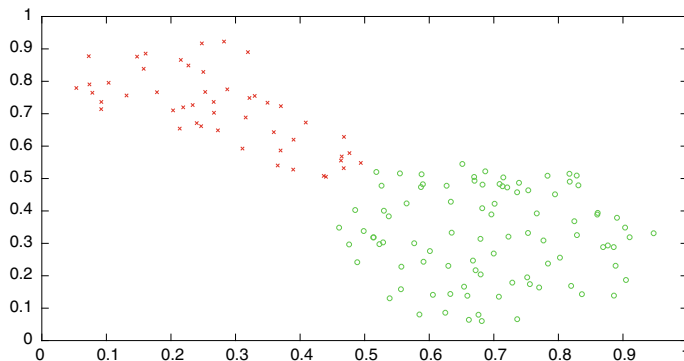


Fig. 2 Clustering result of the proposed method

Table 1 Accuracy measure (average) of two diabetes databases

Methods	Sensitivity	Specificity	Precision	Accuracy	F -score
FCM [9, 10]	0.825	0.913	0.769	0.877	0.796
PCM [12]	0.815	0.908	0.742	0.807	0.777
RFCM [16]	0.830	0.882	0.783	0.877	0.805
IFSMR	0.861	0.894	0.815	0.909	0.837

Bold face indicates the metrics of the proposed IFSMR model

4.4 Validation

For the effectiveness of the proposed method, we have validated of the first 50 gene sets with functional enrichment, called ‘GO-attributes’ with respect to their occurrences in the altered associations. The ‘GO-attributes’ for each gene has been determined corresponding to its p -value. A lower p -value illustrates that the genes belong to the enriched functional classes are biological significant, and hence, we have considered functional classes with p -values less than or equal to 5×10^{-5} ,

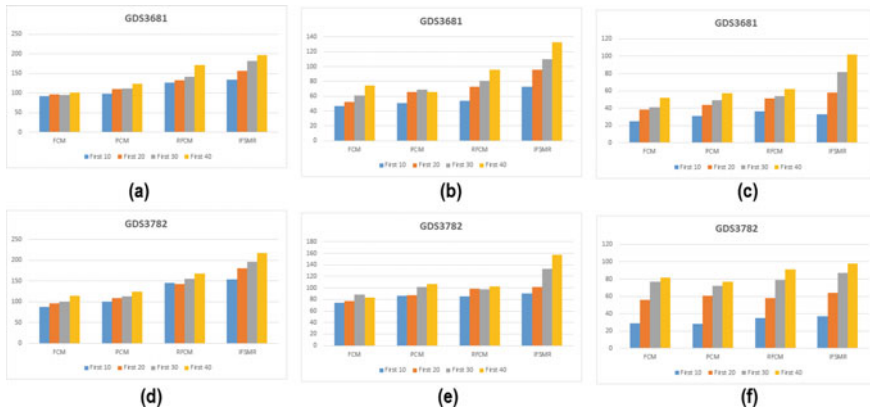


Fig. 3 Comparative analysis on number of functional enriched attributes of first 10 to first 40 gene sets: **a** p -value $\leq 5 \times 10^{-5}$ for database GDS3681, **b** p -value $\leq 5 \times 10^{-7}$ for database GDS3681, **c** p -value $\leq 5 \times 10^{-9}$ for database GDS3681, **d** p -value $\leq 5 \times 10^{-5}$ for database GDS3782, **e** p -value $\leq 5 \times 10^{-7}$ for database GDS3782, **f** p -value $\leq 5 \times 10^{-9}$ for database GDS3782

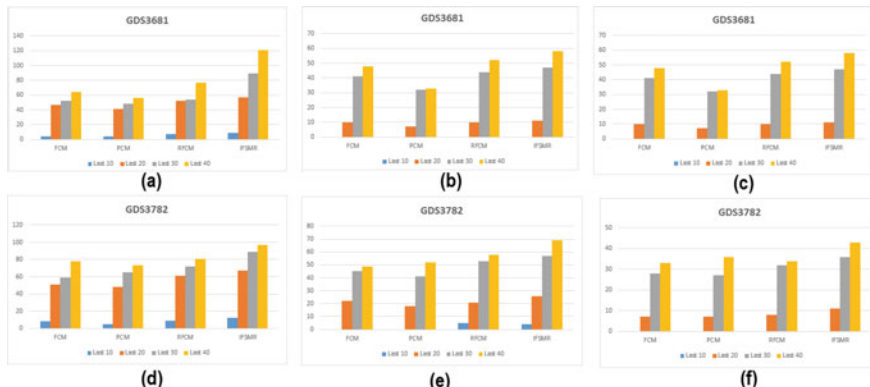


Fig. 4 Comparative analysis on number of functional enriched attributes of last 10 to last 40 gene sets: **a** p -value $\leq 5 \times 10^{-5}$ for database GDS3681, **b** p -value $\leq 5 \times 10^{-7}$ for database GDS3681, **c** p -value $\leq 5 \times 10^{-9}$ for database GDS3681, **d** p -value $\leq 5 \times 10^{-5}$ for database GDS3782, **e** p -value $\leq 5 \times 10^{-7}$ for database GDS3782, **f** p -value $\leq 5 \times 10^{-9}$ for database GDS3782

5×10^{-7} , and 5×10^{-9} . Figures 3 and 4 show the number of functional enriched attributes selected using proposed IFSMR method along with three baseline methods.

In order to demonstrate diabetes mediating gene correctly, we have computed the GO-attribute based on first 10, 20, 30, and 40 genes for two databases separately which is demonstrated in Fig. 3 and it illustrates that the proposed IFSMR method is more significant than other baseline methods. Similarly, we have computed the GO-attribute on last 10, 20, 30, and 40 genes in Fig. 4, which also describes that the proposed IFSMR method is more significant though RFCM sometimes is close to proposed method.

5 Conclusion

In microarray data analysis, proper gene selection is an important phase in determining the accurate categorization of gene expression pattern. Here, we propose an IFS-based gene expression microarray clustering in multigranulation rough set framework for human diabetes patient. It is utilized to predict different classes of genes or samples. The IFS provides more prominent flexibility to reduce the dimension of the data. The multigranulation rough set in fuzzy domain understands the uncertainty nature of the data for further clustering. The major drawback of rough set theory is to obstruct dealing with large data and computational overhead. The proposed method overcomes the issues in rough set to reduce the dimension of the data using IFS. The proposed scheme produces the best result as compared to the clustering-based state-of-the-art methods. The primary advantage of the suggested method is to reduce the computational cost via dimensional reduction using IFS.

In future, we will be working on more diabetes and cancer databases for the validation of the algorithm. We will also focus on gene-to-gene interaction on NCBI database and biochemical pathway analysis for the biological significance of the selected gene sets. We are also planning on finding any existence of relationship between diabetes genome and cancer genome.

References

1. Rebecca, T.L.: Prevalence of diabetic retinopathy within a national diabetic retinopathy screening service. *British J. Ophthal.* **99**(1), 64–68 (2015)
2. Hanson, R.L., Bogardus, C., Duggan, D.: A search for variants associated with young-onset type 2 diabetes in Americal Indians in 100K genotyping array. *Diabetes* **56**(12), 3045–3052 (2007)
3. Stekel, D.: *Microarray Bioinformatics*. Cambridge University Press, Cambridge (2006)
4. Das, R., Kalita, J., Bhattacharyya, D.K.: A pattern matching approach for clustering gene expression data. *Int. J. Data Mining Modeling Manage.* **3**(2) (2011)
5. Jiang, D., Peri, J., Zhang, A.: DHC: a density based hierarchical clustering methods for time series gene expression data. In: *IEEE International Symposium on Bioinformatics and Bioengineering* (2003)

6. Banerjee, M., Mitra, S., Banka, H.: Evolutionary rough feature selection in gene expression data. *IEEE Trans. Syst. Man Cybern. Part C: Appl. Rev.* **37** (2007)
7. Kalaiselvi, N., Inbarani, H.: A fuzzy soft set based classification for gene expression data. *IJSER* **3**, 1315–1321 (2014)
8. Danaee, P., Hendrix D.A.: A deep learning approach for cancer detection and relevant gene identification. In: Pacific Symposium on Biocomputing, pp. 219–229 (2017)
9. Dunn, J.C.: A fuzzy relative of the ISODATA process and its use in detecting compact well-separated clusters. *J. Cybern.* **3**(3), 32–57 (1973). :<https://doi.org/10.1080/01969727308546046> ISSN: 0022-0280
10. Bezdek, J.C.: *Pattern Recognition with Fuzzy Objective Function Algorithms*. ISBN 0-306-40671-3 (1981)
11. Maji, P., Pal, S.K.: Rough set based generalized fuzzy C-means algorithm and quantitative indices. *IEEE Trans. Syst. Man Cybern. Part B: Cybernet.* **37**(6), 1529–1540 (2007)
12. Krishnapuram, R., Keller, J.M.: The Possibilistic C-Means Algorithm: Insights and Recommendations. *IEEE Trans. Fuzzy Syst.* **4**(3), 385–393 (1996)
13. Pawlak, Z.: *Rough Sets: Theoretical Aspects of Reasoning About Data*. Kluwer Academic Publishers, Berlin (1991)
14. Lingras, P., West, C.: Interval set clustering of web users with rough K-means. *J. Intell. Inf. Syst.* **23**(1), 5–16 (2004)
15. Maji, P., Pal, S.K.: *Rough-Fuzzy Pattern Recognition: Applications in Bioinformatics and Medical Imaging*. Wiley-IEEE Computer Society Press, New Jersey (2012)
16. Maji, P., Pal, S.K.: RFCM: a hybrid clustering algorithm using rough and fuzzy sets. *Fundamenta Informaticae* **80**(4), 475–496 (2007)
17. Atanassov, K.: *Intuitionistic Fuzzy Sets: Theory and Applications*. Physica-Verlag, Heidelberg (1999)
18. Zadeh, L.A.: Fuzzy sets. *Inf. Comput.* **8**, 338–353 (1965)
19. Klir, G.J., Yuan, B.: *Fuzzy Sets and Fuzzy Logic: Theory and Applications*. Prentice-Hall PTR, Upper Saddle River, NJ (1995)
20. Montes, I., Pal, N.R., Janis, V., Montes, S.: Divergence measures for intuitionistic fuzzy sets. *IEEE Trans. Fuzzy Syst.* **23**(2), 444–456 (2014)
21. Little, R.J.A., Rubin, D.B.: *Statistical Analysis with Missing Data*, 2nd ed. Wiley, Hoboken (2002) (Computing Surveys **31**(3), 264–323 (1999))
22. Available <http://www.ncbi.nlm.nih.gov/geo>
23. Melin, P., Castillo, O.: A review on type-2 fuzzy logic applications in clustering, classification and pattern recognition. *Applied Soft Com.* **21**, 568–577 (2014)
24. Ghosh, S.K., Ghosh, A., Chakrabarti, A.: VEA: vessel extraction algorithm by active contour model and a novel wavelet analyzer for diabetic retinopathy detection. *Int. J. Image Graphics* **18**(2) (2018)

Investigation on HRV Signal Dynamics for Meditative Intervention



Dipen Deka and Bhabesh Deka

Abstract Heart rate variability (HRV) has been a very useful marker in unfolding the activity of the autonomic nervous system (ANS) for different actions and state of the human mind. With the continuous uprise in the meditation/yoga practitioners, for its well-known positive impacts on overall well-being, we have intended to find scientific evidences behind it. On that account, we have computed three nonlinear parameters, named increment entropy, fluctuation coefficient, and degree of dispersion to characterize the complex dynamical behaviour of HRV signal during meditation obtained from PhysioNet database. Further, time and frequency domain parameters are also evaluated to establish its correlation with nonlinear measures. The results from the analysis have demonstrated a decrease in the chaotic complexity and dynamics of the HRV signal during meditation, which can be used as a reliable tool in detecting diseases related to cardiology, endocrinology, and psychiatry.

Keywords HRV analysis · Autonomic nervous system · Meditation · Yoga · Increment entropy · Fluctuation · Dispersion

1 Introduction

The practice of meditation and yoga has proliferated worldwide due to its effectiveness in reducing stress, anxiety, and depression [1, 2]. This leads to enormous benefits in case of lifestyle diseases, like hypertension [1–3], diabetes [2], stress-related dis-

D. Deka

Department of Instrumentation Engineering, Central Institute of Technology, Kokrajhar, Assam 783370, India

e-mail: d.deka@cit.ac.in

URL: <http://www.cit.ac.in/departments/profile/ie/dipen-deka>

B. Deka (✉)

Department of Electronics and Communication Engineering, Tezpur University, Tezpur, Assam 784028, India

e-mail: bdeka@tezu.ernet.in

URL: <http://agnigarh.tezu.ernet.in/~bdeka>

orders [1, 4], etc. Meditation can be of many forms, such as mindfulness, controlled breathing, listening to some sound, imagination of a particular process, or some physical posture. The studies on the articles related to meditation/yoga have established the changes in the physiological states and the activity of the autonomic nervous system (ANS) due to its practice [1–3, 5–8]. Human cardiovascular system is controlled by complex phenomena including nervous and hormonal pathways besides external factors, under the influence of ANS. Two branches of ANS, namely the sympathetic nervous systems (SNS) and the parasympathetic nervous system (PNS) are activated under excited and resting states, respectively. Changes of any sort in the state of mind or action lead to a competition between these two nervous systems to prevail over each other. Their activation is rooted from the release of chemical messengers, called epinephrine and norepinephrine for SNS and the release of acetylcholine in case of PNS [9, 10]. These hormones are responsible for regulating the firing rates of sinoatrial (SA) and atrioventricular (AV) nodes which control the pumping rate of the heart (HR). This variation in the form of differences in the interbeat (RR) interval is represented by heart rate variability (HRV) signal [9, 11–13].

The works on HRV under meditation have been performed using three types of approaches: time domain, frequency domain, and nonlinear methods. In time domain methods, statistical parameters such as mean HR, standard deviation (SD) of normal-to-normal (NN) interval (SDNN), standard deviation of average NN interval (SDANN), number of adjacent intervals exceeding 50 ms (NN50), percentage of NN50 (pNN50), root mean square of successive differences between NN interval (RMSSD), and HRV triangular index (HTI) are derived to observe its changes due to meditation [6, 13, 14].

In frequency domain methods, the spectral powers are computed from the HRV signal, and the changes of powers in the different spectral bands are observed. The spectral bands of HRV signal are mainly divided into three ranges, very low-frequency (VLF), low-frequency (LF), and high-frequency (HF) ranges. VLF power (0.0033–0.04 Hz) indicates the activity of renin-aldosterone system and thermoregulation or vasomotor activity, LF power (0.04–0.15 Hz) indicates the baroreflex control due to the activity of SNS and PNS with major influence from SNS, and the HF power (0.15–0.40 Hz) indicates the vagal control associated with respiration due to the dominance of parasympathetic activity [7, 14].

In nonlinear dynamics analysis, the complexity, nonlinearity, and non-stationarity of the HRV signal are studied by various assessment parameters like entropy (Shannon entropy, approximate entropy, sample entropy), correlation dimension, Lyapunov exponents, Poincaré plots, recurrence plots, detrended fluctuation analysis (DFA), fractal dimension, and so on [7, 8, 11, 15–17].

The aim of this work is to capture reliable and deterministic changes in the HRV signal due to the practice of meditation. To this end, we have analysed the HRV signal using three nonlinear parameters, namely increment entropy, fluctuation coefficient, and degree of dispersion in addition to the conventional time and frequency parameters. Since the consistency in the change of parameters is an issue in many literature, the reliable conclusion on the effects of meditation is still naive. Motivated by the work of [18, 19] for their success in the quantification of the complexity of nonlinear

series, we have evaluated the increment entropy, fluctuation coefficient, and degree of dispersion for the HRV signal to study its dynamics during meditation. To the best of our knowledge, fluctuation coefficient and degree of dispersion have not been used earlier for HRV analysis to characterize meditative and non-meditative signals. Besides, the time and frequency methods are also applied to arrive at a firm conclusion. Through this work, we intend to give a precise yet computationally simple method for a detailed understanding of the effects of meditation on health and well-being. The organization of this paper is given as follows: Sect. 2 briefs the methods employed, and the results of the work using different approaches are discussed in Sect. 3. Finally, Sect. 4 gives the conclusion of the paper.

2 Materials and Methods

In this work, we have used the standard heart rate oscillations data from PhysioNet database "<https://www.physionet.org/physiobank/database/meditation/>" as mentioned by Peng et al. [20]. The database consists of the instantaneous HR of (i) four Kundalini yoga (Y1-Y4) practitioners for both pre- and during meditation, (ii) eight Chi meditators (C1-C8) for both pre- and during meditation, (iii) 11 normal healthy person (N1-N11) in sleeping condition, (iv) 14 subjects under metronomic breathing (M1-M14) in supine position, and (v) nine elite athletes (I1-I9) during their sleeping hours. For our analysis, we have applied time domain, frequency domain, and nonlinear techniques on selected HRV datasets, which is detailed in results and discussion Section.

2.1 Time Domain Parameters

From the RR intervals of the HR oscillations data, various statistical parameters are determined, which reflect the changes in the cardiac functionality before and during meditation. The differences between the values during and before meditation are compared using the statistical " t " test for level of significance, $\alpha < 0.05$. In this work, we have chosen mean HR (mHR), SDNN, NN50, pNN50, RMSSD, and HTI [10, 14] for analysis.

2.2 Frequency Domain Parameters

Frequency domain methods are based on power analysis from power spectral density (PSD) estimations by employing versatile transformation techniques [21, 22]. The power distributions in the spectral bands correspond to the selective activation of PNS or SNS. In this work, we have first sampled HRV signal at 4Hz using the

cubic spline interpolation technique as the HRV signal is not uniform in its period. The signal is then normalized, followed by a fast Fourier transform (FFT). Power distribution in different spectral bands is analysed to assess the effects of meditation. LF/HF ratio is also calculated which signifies the balance between the sympathetic and vagal actions [6, 9].

2.3 Nonlinear Dynamical Parameters

Increment Entropy. Increment entropy has originated from the idea of Shannon entropy, where each increment in the series is denoted by a two symbol codeword. First symbol of the word shows whether there is an increment or decrement, i.e. by + or - sign, and the second symbol gives the degree of increment as discussed in the work of [18].

From the HRV series, the successive differences (increments) were obtained. This increment series is then divided into $(N - m)$ vectors of m dimensions where N is the length of the original HRV series. Let us denote each element in the increment series $\{y(n)\}$ by words (w_n) , where $n = 1, 2, \dots, (N - m)$ and each w_n will have two letters s_n and q_n , where s_n gives the sign of increment and q_n , the degree of increment for resolution level r is given by

$$q_n = \begin{cases} 0, & \text{if } \text{std}(y) = 0 \\ \min(r, \frac{\|y(n)\| \times r}{\text{std}(y)}), & \text{otherwise} \end{cases} \quad (1)$$

Let $t(w_n)$ be the number of occurrences of n^{th} unique word, and the probability of occurrence of each unique word is given by

$$P(w_n) = \frac{t(w_n)}{N - m} \quad (2)$$

The increment entropy $H(m)$ for a series of dimension (m) and resolution level (r) is given by

$$H(m) = \sum_{n=1}^{(2r+1)^m} P(w_n) \log_2 P(w_n) \quad (3)$$

The $H(m)$ is computed for different values of m and r to compare the premeditation, meditation, and HRV series of other interventions.

Fluctuation Coefficient. The instability and fluctuation of short and coarse grained time series were rigorously analysed by Schiepek et al. [19] using simple mathematical operations. In this work, we have implemented the concept to evaluate the fluctuation coefficient, f for HRV time series in order to analyse its dynamics during meditation. Here, f gives the quantum of variations in the whole series by considering one segment at a time with the help of sliding window. The measurement

points within the window are divided based on the change in the slope and the rate of change $\{f(i)\}$ for different slopes are measured. Finally, the values of $\{f(i)\}$ in a window are summed up and divided by the maximum possible fluctuation for normalization. For an HRV series $\{x(i)\}$, window width (w) is appropriately chosen to determine the fluctuations. If RR interval for a sample $n(k)$ is $x(k)$ and the RR interval for a sample $n(k+1)$ is $x(k+1)$, the rate of change of RR interval for these two samples will be given by

$$Sl(k) = \frac{x(k+1) - x(k)}{n(k+1) - n(k)} \quad (4)$$

The fluctuation coefficient for a window of width, w is given by

$$f = \frac{\sum_{k=1}^w Sl(k)}{s.w} \quad (5)$$

where $s = \max\{x(i)\} - \min\{x(i)\}$.

Degree of Dispersion. For understanding the chaotic distribution of nonlinear data, Schiepek et al. [19] have computed the distribution measure. The degree of dispersion gives the deviations of series from an equally distributed series. At first, a window is chosen appropriately within which the HRV series data are sorted in ascending order. Then the deviations of the sorted data points from the equally distributed data within that same range of window are calculated. This window is slided to cover the whole length of the signal, and the dispersions of all the windows are summed to get the degree of dispersion. It is to be noted that the amount of shift and window size are properly chosen to avoid overlapping.

3 Results and Discussion

We have shown simulation results for the datasets of eight Chi and four Kundalini yoga meditators in case of both pre- and during meditation, in addition to randomly chosen single datasets for each normal, metronomic breathing subjects, and athletes, as our main intention is to investigate the effects of meditative interventions on the HRV signal complexity. Since these are standard meditative datasets used in the recent literatures for scientific investigation of the effect of meditation, we adopt the same in our study to maintain consistency with the existing works. All simulations are carried out in the MATLAB environment, and different linear and nonlinear HRV parameters are evaluated. Furthermore, to determine significant differences, “*t*” tests are conducted.

It has been observed from the computations that during meditation, mHR has increased for all the Kundalini yoga practitioners, whereas for some of the Chi meditators (C3, C5, and C7) it has decreased during meditation. It may also happen

Table 1 Time domain parameters for different meditators and other healthy subjects for premeditation, during meditation and supine/sleeping condition

Parameters	Y1 Med./Pre	Y2 Med./Pre	Y3 Med./Pre	Y4 Med./Pre	C1 Med./Pre	C3 Med./Pre	C5 Med./Pre	C7 Med./Pre	N1	M1
mHR (bpm)	93.94/63.79	96.09/64.71	82.66/64.71	88.93/45.92	68.50/64.17	69.15/89.25	67.83/77.45	81.2/85.22	62.29	76.80
SDNN (ms)	60.32/44.93	82.30/64.65	92.92/70.05	125.19/191	88.35/49.93	54.49/116.20	45.09/37.32	67.85/52.01	92.21	54.13
NN50	12/75	61/47	105/110	112/113	69/102	72/111	21/24	25/60	94	27
pNN50 (%)	2.61/23.18	12.75/14.82	25.78/34.10	25.24/49.61	20.13/31.28	20.86/24.87	6.19/6.20	6.15/14	30.20	7.03
RMSSTD (ms)	22.32/40.30	37.64/34.97	52.88/54.46	83.78/177.5	40.03/47.95	42.44/50.87	26.25/26.5	29.32/35.31	52.70	28.61
HTI	14.63/08.81	14.50/10.82	18.66/13.50	18.32/20	13.50/10.07	10.17/20.42	9.41/8.06	15.61/14.2	12.90	13.24

Table 2 Frequency domain parameters for different subjects under premeditation (pre), during meditation (med) and sleeping/supine condition

Spectral Para.	Y1 Med/Pre	Y2 Med/Pre	Y3 Med/Pre	Y4 Med/Pre	C1 Med/Pre	C2 Med/Pre	C3 Med/Pre	C4 Med/Pre	N1 Sleep	M1 Supine	I1 Sleep
VLF (dB)	1.22/1.23	1.81/0.666	1.58/0.87	1.37/0.763	1.115/1.052	0.916/1.25	0.818/1.388	1.112/0.751	0.721	0.765	2.37
LF (nu)%	31.21/31.34	69.21/70.15	44.34/73.52	58.83/56.53	39.33/59.81	43.76/81.21	28.05/37.93	47.92/71.43	50.04	48.23	68.41
HF (nu)%	68.79/68.66	30.79/29.85	55.66/26.48	41.17/43.47	60.67/40.19	56.24/18.79	71.95/62.07	52.08/28.57	49.96	51.77	31.59
LF/HF ratio	0.453/0.455	2.255/2.347	0.797/2.772	1.430/1.299	0.648/1.486	0.776/4.321	0.388/0.611	0.920/2.499	0.999	0.932	2.165

Table 3 Nonlinear parameters for different subjects under premeditation, during meditation and sleeping/supine condition

Nonlinear Parameters	Y1 Med/Pre	Y2 Med/Pre	Y3 Med/Pre	Y4 Med/Pre	C1 Med/Pre	C2 Med/Pre	C3 Med/Pre	C4 Med/Pre~	N1 Sleep	M1 Supine	II Sleep
IncrEn	Dimen = 2	5.23/1.88	5.78/26.023	5.434/5.943	4.392/4.764	2.585/5.752	3.196/3.645	6.118/6.108	5.861/5.761	5.372	6.002
	Resol. = 3	0.312/0.313	0.692/0.701	0.443/0.735	0.588/0.565	0.393/0.598	0.437/0.812	0.280/0.379	0.479/0.714	0.500	0.482
Fluct. Coeff.	Window width = 5	0.050/0.128	0.051/0.067	0.090/0.124	0.037/0.053	0.012/0.003	0.003/0.011	0.057/0.057	0.054/0.057	0.007	0.064~
	Window width = 10	0.053/0.131	0.055/0.072	0.095/0.120	0.062/0.081	0.090/0.125	0.070/0.011	0.095/0.069	0.076/0.102	0.084	0.080
Degree of Dispers.	Window width = 5	1.437/1.182	1.467/1.208	1.309/1.378	1.288/1.032	1.138/1.131	1.403/1.325	1.5/1.312	1.403/1.037	1.148	0.936~
	Window width = 10	0.839/0.630	0.895/0.654	0.586/0.863	1.173/0.715~	0.925/0.755	0.825/1.451	0.674/0.917	0.689/0.583	0.680	0.647

Table 4 Paired “*t*” test for mean values of HRV parameters during meditation and premeditation

Subjects	SDNN	RMSSD	HTI	LF/HF	IncrEn	Fluct. Coeff.	Degree of dispersion
Yoga Med (n = 4)	90 ± 26.6	49.6 ± 26.3	16.5 ± 5.2	1.23 ± 0.78	7.95 ± 0.76	0.057 ± 0.02	1.37 ± 0.09
Yoga Pre (n = 4)	92.8 ± 66.2	76 ± 67.32	13.3 ± 4.8	1.7 ± 1.01	8.1 ± 0.58	0.093 ± 0.04	1.2 ± 0.14
p value Med	0.40	0.18	0.06	0.22	0.35	0.045	0.055
Chi Med (n = 8)	66.4 ± 19.3	34.9 ± 9.8	14.2 ± 4.6	1.16 ± 0.94	7.9 ± 1.86	0.038 ± 0.03	1.34 ± 0.13
Chi Pre (n = 8)	128 ± 110.8	124.49 ± 162	14.4 ± 4.9	1.62 ± 1.30	7.9 ± 2.24	0.033 ± 0.02	1.24 ± 0.11
p value Chi	0.06	0.40	0.30	0.40	0.06	0.04	

because the Chi meditators are considerably new to this practice. Further, SDNN and HTI have increased for most of the meditators during meditation, whilst RMSSD and NN50 have decreased for majorities during meditation as compared to that before meditation. However, there is no such consistency in the trend of increase or decrease of the parameters due to meditative intervention except SDNN and HTI as shown in Table 1. It is to be noted that the readings of only C1, C3, C5, and C7 are shown in Table 1 as other Chi meditators are following the regular trend. However, all the datasets are considered for comparative analysis in Table 4.

It is noteworthy that for frequency domain analysis, VLF power is taken in absolute units, whereas LF and HF powers are taken in normalized units (nu) % by dividing with the factor (total power-VLF power) to avoid the effect of VLF power. It can be observed from Table 2 that during meditation, VLF power, LF power (nu), and LF/HF ratio decrease, whereas HF power (nu) increases in almost all cases of Chi or Kundalini yoga meditators. The increase in HF power and decrease in LF/HF ratio during meditation indicate the shift of sympathovagal balance towards the PNS. That may be the reason behind the peace of mind or reduction in anxiety for meditators. However, the changes in power are quite marginal.

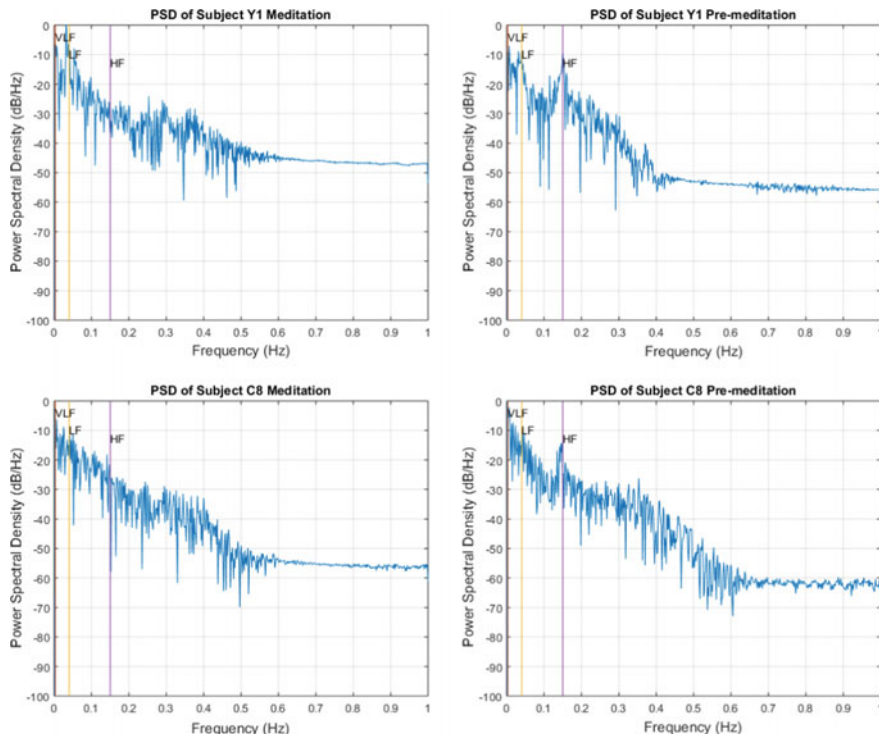


Fig. 1 Comparison of periodograms for subjects during meditation and premeditation

As the time and frequency-based measurements are unable to consistently provide significant results, which conforms to the works of [7, 23–25], we have evaluated nonlinear parameters in this work. It is observed that the non-stationary behaviour of HRV signal changes in a characteristic manner during meditation, as compared to that before meditation. This motivated us to evaluate the fluctuations and entropy over a sizeable window width. From the analysis of HRV dynamics, we have found a considerable decrease in the increment entropy during meditation for different dimensions except for one subject (Y1). For higher dimensions, the result is more consistent as shown in Table 3. After analysis with different m and r combinations, the value of $m = 3$ and $r = 4$ is found to be optimum for the HRV signals available. Again, fluctuation coefficients decrease during meditation, and degree of dispersion increases during meditation as compared to its values before meditation. It reflects the decrease in chaotic complexity during meditation. Interestingly, the sympathovagal balance for the subjects N1 and M1 is found to be shifted more towards the SNS, and chaotic complexity is much lesser than meditators as evident from the degree of dispersion measurements. The variations in the power spectral density (PSD) for Y1 and C8 have clearly shown the presence of peak in LF range before meditation and that in HF range during meditation as shown in Fig. 1.

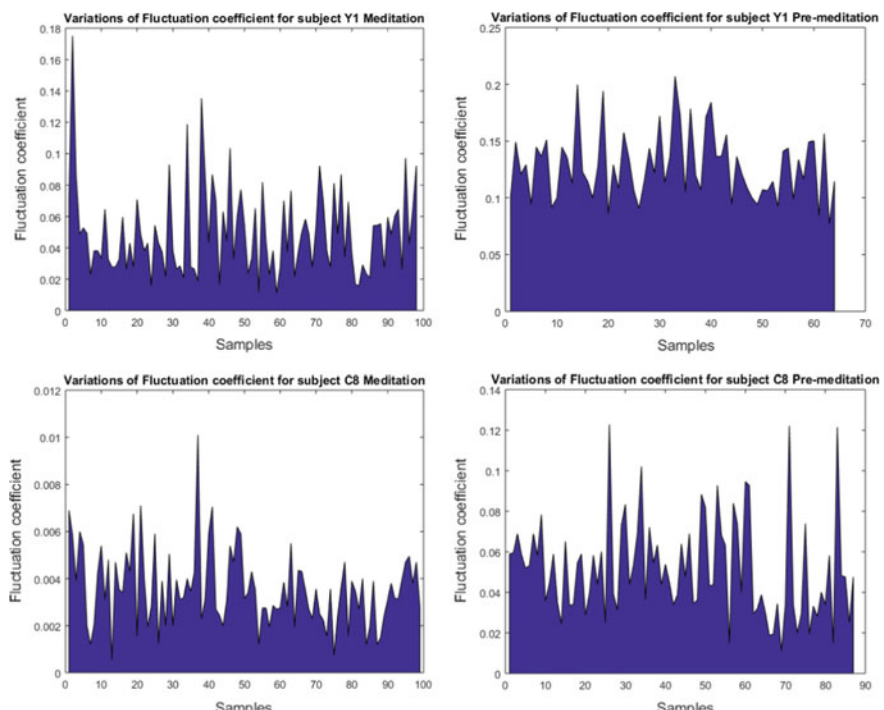


Fig. 2 Comparison of fluctuation coefficient graphs for subjects during meditation and pre-meditation

It is evident from Fig. 2 that the coefficient of fluctuation decreases during meditation. From the paired “*t*” ($\alpha < 0.05$) test for the chosen parameters, as shown in Table 4, a significant increase in the HTI and degree of dispersion are observed, whereas a significant decrease in fluctuation coefficient is observed.

4 Conclusion

It can be concluded that during meditation, SDNN and HTI increase significantly which reflects increased dynamic behaviour and hence better cardiac health. Again, we have found from frequency domain studies that the sympathovagal balance is tilted marginally towards the PNS during meditation, hinting prevalence of calmness. Further, the evaluation of the increment entropy, the degree of dispersion and fluctuation coefficients has clearly indicated that meditation reduces chaotic complexity. In terms of limitations, the small size of meditation datasets is a concern, as PhysioNet database is the only standard database available in the public domain. An extended examination on sufficient real-time data of meditators with long-term readings and detailed history of past and present diseases and drug interventions may provide useful outcomes in this area of research.

References

1. Bussing, A., Michalsen, A., Khalsa, S.B.S., Telles, S., Sherman, K.J.: Effects of yoga on mental and physical health: a short summary of reviews. *Evid. Based Complement. Alternat. Med.* **2012**(165410), 1–7 (2012)
2. Tyagi, A., Cohen, M.: Yoga and hypertension: a systematic review. *Altern. Ther. Health Med.* **20**, 32–59 (2014)
3. Tyagi, A., Cohen, M.: Yoga and heart rate variability: a comprehensive review of the literature. *Int. J. Yoga.* **9**, 97–113 (2016)
4. Li, A.W., Goldsmith, C.A.: The effects of yoga on anxiety and stress. *Altern. Med. Rev.* **17**, 21–35 (2012)
5. Lugo, J., Doti, R., Faubert, J.: The Fulcrum principle between parasympathetic and sympathetic peripheral systems: Auditory noise can modulate body’s peripheral temperature. In: Pant, M., Ray, K., Sharma, T., Rawat, S., Bandyopadhyay, A. (eds.) *Soft Computing: Theories and Applications. Advances in Intelligent Systems and Computing*, vol. 584, pp. 333–342. Springer, Singapore (2018)
6. Terathongkum, S., Pickler, R.H.: Relationships among heart rate variability, hypertension, and relaxation techniques. *J. Vasc. Nurs.* **22**(3), 78–82 (2004)
7. Kamath, C.: Analysis of heart rate variability signal during meditation using deterministic-chaotic quantifiers. *J. Med. Eng. Technol.* **37**(7), 436–448 (2013)
8. Goshvarpour, A., Goshvarpour, A.: Poincare indices for analyzing meditative heart rate signals. *Biomed J.* **38**(3), 229–234 (2015)
9. Singh, R.S., Saini, B.S., Sunkaria, R.K.: Power spectral analysis of short-term heart rate variability in healthy and arrhythmia subjects by the adaptive continuous morlet wavelet transform. *Appl. Med. Inform.* **39**(3–4), 49–66 (2017)

10. Malik, M., Camm, A.J., Bigger, J.T., Breithardt, G., Cerutti, S., Cohen, R.J.: Heart rate variability: standards of measurement, physiological interpretation, and clinical use. *Eur. Heart J.* **17**(3), 354–381 (1996)
11. Raghavendra, B.S., Dutt, D.N.: Nonlinear dynamical characterization of heart rate variability time series of meditation. *Int. J. Biomed. Biol. Eng.* **5**(9), 429–440 (2011)
12. Bhatt, A., Dubey, S.K., Bhatt, A.: Analytical study on cardiovascular health issues prediction using decision model-based predictive analytic techniques. In: Pant, M., Ray, K., Sharma, T., Rawat, S., Bandyopadhyay, A. (eds.) *Soft Computing: Theories and Applications. Advances in Intelligent Systems and Computing*, vol. 584, pp. 289–299. Springer, Singapore (2018)
13. Kleiger, R., Stein, P.K., Bigger, J.T.: Heart rate variability: measurement and clinical utility. *Ann. Noninvasive Electrocardiol.* **10**, 88–101 (2005)
14. Shaffer, F., Ginsberg, J.P.: An overview of heart rate variability metrics and norms. *Front. Public Health* **5**(258) (2017)
15. Vinutha, H.T., Raghavendra, B.R., Manjunath, N.K.: Effect of integrated approach of yoga therapy on autonomic functions in patients with type 2 diabetes. *Indian J. Endocrinol. Metab.* **19**(5), 653–657 (2018)
16. Yao, W., Zhang, Y., Wang, J.: Quantitative analysis in nonlinear dynamic complexity detection of meditative heart beats. *Phys. A* **512**, 1060–1068 (2018)
17. Goswami, D.P., Bhattacharya, D.K., Tibarewala, D.N.: Analysis of heart rate variability in meditation using normalized shannon entropy. *Int. J. Phys. Sci.* **14**(1), 61–67 (2010)
18. Liu, X., Jiang, A., Xu, N., Xue, J.: Increment entropy as a measure of complexity for time series. *Entropy* **18**(22), 1–14 (2016)
19. Schiepek, G., Strunk, G.: The identification of critical fluctuations and phase transitions in short term and coarse-grained time series—a method for the real-time monitoring of human change processes. *Biol. Cybern.* **102**, 197–207 (2010)
20. Peng, C., Mietus, J., Liu, Y., Khalsa, G., Douglas, P., Benson, H., Goldberger, A.: Exaggerated heart rate oscillations during two meditation techniques. *Int. J. Cardiol.* **70**(2), 101–107 (1999)
21. Peter, R., Sood, S., Dhawan, A.: Spectral parameters of HRV in yoga practitioners, athletes and sedentary males. *Indian J. Physiol. Pharmacol.* **59**(4), 380–387 (2015)
22. Bonello, J., Garg, L., Garg, G., Audu, E.: Effective data acquisition for machine learning algorithm in EEG signal processing. In: *Soft Computing: Theories and Applications. Advances in Intelligent Systems and Computing* (2018)
23. Bhaduri, A., Ghosh, D.: Quantitative assessment of heart rate dynamics during meditation: an ECG based study with multi-fractality and visibility graph. *Front. Physiol.* **7**(44), 1–10 (2016)
24. Jiang, S., Bian, C., Ning, X., Ma, Q.D.Y.: Visibility graph analysis on heartbeat dynamics of meditation training. *Appl. Phys. Lett.* **102**, 253–702 (2013)
25. Dey, A., Bhattacharya, D.K., Tibarewala, D., Dey, N., Ashour, A.S., Le, D.N., Gospodinova, E., Gospodinov, M.: Chinese-chi and Kundalini yoga meditations effects on the autonomic nervous system: comparative study. *Int. J. Interact. Multimedia Artif. Intell.* **3**(7), 87–95 (2016)

A Review on Deep Learning-Based Channel Estimation Scheme



Amish Ranjan, Abhinav Kumar Singh, and B. C. Sahana

Abstract In this review paper, we have tried to review the maximum amount of research work done till date on deep learning-based algorithms for channel estimation in different wireless systems of communication. Based on the numerical analysis of different papers, this review paper will prove that the DL-based approach is the new trend in channel estimation as it is highly outperforming the conventional schemes. In this paper, we have also tried to cover the basic concept of channel estimation.

Keywords Deep learning · Machine learning · Channel estimation · OFDM · MIMO

1 Introduction

Wireless communication technologies have been developed rapidly since the starting of the twenty-first century. The rate of data transfer has also been increased significantly, and as a result, the bandwidth becomes much wider in wireless communication systems. So, the quality of communication system has become a very important parameter today. Channel estimation has very high importance for any communication system as the degree to which the channel is estimated accurately determines the quality of the whole communication system [1].

A. Ranjan (✉) · A. K. Singh

University College of Engineering and Technology, VBU, Hazaribag, Jharkhand, India
e-mail: amishranjan347@gmail.com

A. K. Singh

e-mail: abhinav.bih7@gmail.com

B. C. Sahana

National Institute of Technology, Patna, India
e-mail: sahana@nitp.ac.in

In the past few years, there have been many researches on different conventional channel estimation schemes for different types of communication system [2]. Various channel estimation schemes are compared with respect to different parameters like signal-to-noise ratio (SNR), bit error rate (BER) [3], mean square error (MSE), etc., to find which scheme suited most for a particular type of communication system with the help of simulation. Some of the conventional channel estimation schemes along with the communication channel where they give best results are minimum mean square (MMSE) estimator and least square (LS) estimator for wireless orthogonal frequency division multiplexing (OFDM) systems [4], for a millimeter-wave multiple-input multiple-output (MIMO) system with analog-to-digital converters (ADCs) of one-bit, a modified expectation maximum (EM) channel estimator was suggested [5]. Similarly, maximum likelihood-based channel estimation has been suggested in microcellular OFDM uplinks in dispersive channels which are time-varying [6] and data-aided channel estimation scheme in large antenna system [7]. The new trend in channel estimation schemes is the application of deep learning algorithms. Deep learning is a part of machine learning that achieves flexibility and great power with the help of learning to represent the world as enclosed hierarchy of concept with each concept explained with respect to simpler concepts, and more abstract representations calculated in terms of less abstract one. One of the benefits of deep learning-based approach over conventional schemes is that it is more robust in nature. Deep learning outperforms other techniques if the data size is large. So, in our twenty-first century, wireless communication system where data rate and bandwidth are increasing significantly day by day, deep learning schemes emerges as a promising tool in the field of signal detection and channel estimation. In this paper, we will try our best to summarize maximum number of research work done in channel estimation on deep learning for various wireless communication schemes till date.

The rest of the paper is formatted as follows. The key concept of channel estimation theory is introduced in Sect. 2. Section 3 introduces the overview of different deep learning-based algorithms for channel estimation. Some open research challenges in this field are explained in Sect. 4. Finally, conclusions are presented in Sect. 5.

2 Channel Estimation Theory

In any communication system, the signal passes through a channel and it gets distorted as different types of noises are added to the signal. With an insight to properly decode the received signal, it is necessary to minimize the distortion and noise. To do that, the first step is to discern out the characteristic of the channel through which the signal has passed. This technique to characterize the channel is called “channel estimation.” The process for channel estimation is done in three basic steps. First one is to define properly and fix a mathematical model to find a correlation between the transmitted signal and the received signal using the channel matrix. In the second step, we transmit a known signal generally called pilot signal and detect the received

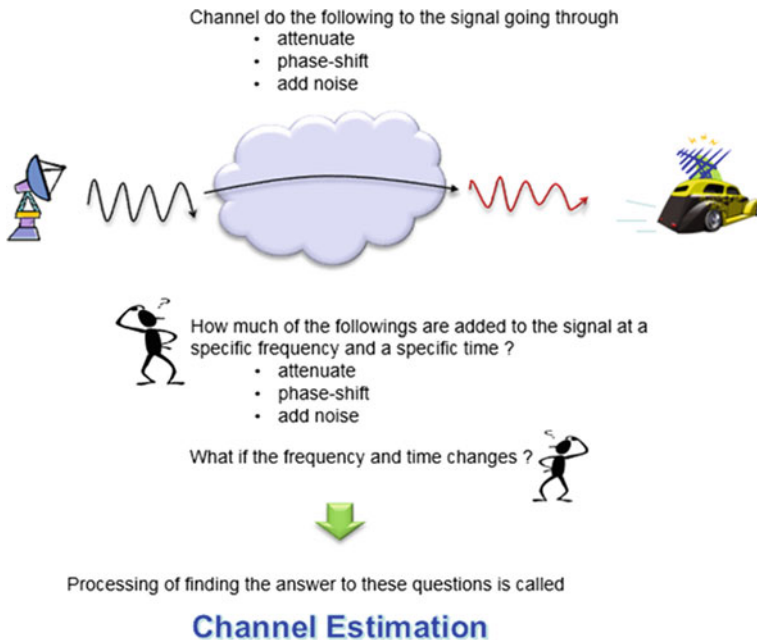


Fig. 1 Representation of channel estimation model

signal. And in the last step, by comparing both the signal, we can find out each and every element of channel matrix.

Stepwise general algorithm is illustrated as below

1. We send the set of predefined signals called pilot signals to the channel.
2. As these pilot signals go through the channel, it gets distorted due to noise.
3. We detect the received pilot signal at the receiver.
4. We compare the received signal with respect to the transmitted pilot signal and find a correlation between them.

A small representation of channel estimation is shown in Fig. 1.

3 The Overview of Different Deep Learning-Based Algorithms for Channel Estimation

Machine learning algorithms can be predominantly classified into two types. These are supervised learning and unsupervised learning [8, 9]. These categories are based on the data used in machine learning. The input data which is used in supervised learning is labeled and well known. The problem with unsupervised learning is it tries to find a hidden structure in unlabeled or untagged data. Since the data is untagged,

there is no error signal to evaluate a probable solution. Apart from these two primary categories, later, a third type of machine learning algorithm inspired by behavioral psychology emerged as a new category which is known as reinforcement learning [9]. In [10], four researchers presented an algorithm for channel estimation based on deep learning technique called ChannelNet. In this paper, the authors considered two-dimensional image of the time–frequency response of a fast-fading communication channel. The target was to find the response of the channel using well-defined data at specified locations of pilot signals. To achieve this, the authors suggested a technique called deep image processing techniques that are image super resolution (SR) and image restoration (IR) (Fig. 2).

The deep learning-based approach for channel estimation was suggested for an OFDM system. In this process, the authors suggested the frequency versus time grille of the channel response as a two-dimensional image which is well defined at the positions of pilot only. The authors considered channel grille with few pilots as low-resolution image and the channel which is estimated is considered as high-resolution image. To estimate the channel grille, the approach suggested that in the first phase, to enhance the low-resolution input, an image SR algorithm is used. After it, in the second phase, IR method is used to eliminate the noise effects. For SR and IR network, the author has used two recently developed convolution neural network (CNN)-based algorithms SRCNN and DnCNN [11]. SRCNN first finds approximate values of the high-resolution image, and after it, the resolution is improved using a three-layer convolutional network. In this whole work, the authors get motivation from [12], in which the considered image was channel matrix and then a denoising network was used for channel estimation. In this paper, the network was trained and the MSE was evaluated over an SNR range considering an only one antenna at the transmitter as well as the receiver. After simulation, the authors find the result that at low SNR values, the suggested ChannelNet algorithm has comparable performance with respect to ideal MMSE. It was observed that as long as the SNR is below 20 dB,

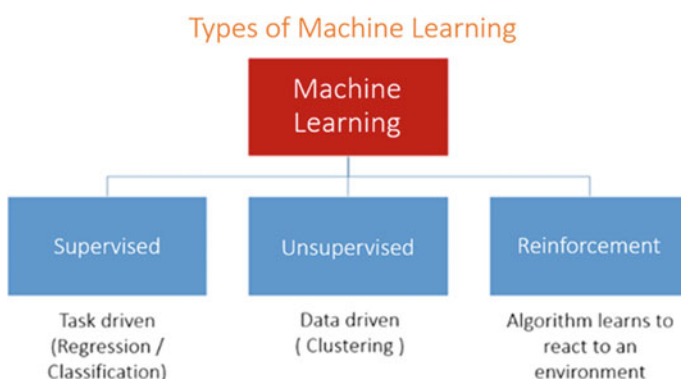


Fig. 2 Types of machine learning

the network is sufficient but if SNR value goes higher than 23 dB, the performance degrades and another network needs to be trained.

In paper [12], the authors performed DL-based channel estimation for beamspace mmWave massive MIMO systems. In this system, when there is a condition that the receiver is provided with the fixed count of radio frequency (RF) chains, the channel estimation becomes very challenging. To overcome this problem, authors suggested a learned denoising-based approximate message passing (LDAMP) network. This is a neural network and is capable to learn the structure of channel and can perform channel estimation from a very large number of training data. Based on the simulation results, the authors have successfully concluded that the LDAMP neural network significantly outperforms the conventional compressed sensing-based algorithm. To achieve this result, the authors considered the channel matrix as a two-dimensional image and then apply the LDAMP neural network in corporation with the denoising convolution neural network (DnCNN) [13]. The authors also compared the suggested network with the SD algorithm [14], sSCAMP algorithm [15], and the DAMP algorithm [16], and the results show that both the DAMP algorithm and the LDAMP network perform better than the SD and SCAMPI algorithms due to the power of denoisers.

In paper [17], authors designed a DL-based pilot design project for minimizing the MSE in the process of channel estimation for multiuser distributive MIMO systems. The authors designed a multilayered fully connected deep neural network (DNN) for optimizing the power allocation to each and every pilot sequence with an insight to reduce the MSE to minimum, where the power allocated to each pilot sequence is the corresponding weight. The authors compared the suggested scheme with other techniques that are exhaustive search-based pilot assignment (ESPA), average pilot power allocation (APPA), and random power pilot assignment (RPA), and the numerical results show that the suggested scheme gives the best MSE performance among them. The rest in decreasing order are SPA, RPA followed by APPA. However, some limitation of the suggested scheme by the authors reflects in elapsed time to find optimal pilot assignment where APPA takes the least time followed by RPA due to their low complexity. SPA takes the highest time, whereas the suggested scheme of the paper takes lower time than SPA.

In paper [18], the authors suggested to design a channel estimation scheme along with pilot design using a deep learning technique for multiuser MIMO systems. In this paper, the authors constructed a pilot designer, for which they used a two-layer neural network (TNN). They also designed a channel estimator by a deep neural network (DNN), and they both trained together to minimize the MSE for channel estimation. Successive interference cancelation (SIC) is also used to reduce the interference among multiple users. In the conventional method, based on linear minimum mean square error (LMMSE) for minimizing the MSE, to maintain the orthogonality in the channel matrix, the authors assumed the pilot length L to be larger than or at least up to the same count in respect to the number of all the antennas of all users M . But for a massive system, the value of M is very large, so accordingly the value of L has to be also very large. This reduces the spectral efficiency. In this paper, the main purpose of the authors is to overcome this problem by assuming the case $L < M$. Once the

author takes this case the system no longer remains linear. The numerical analysis shows that the suggested scheme gives far better performance than the conventional LMMSE-based channel estimator.

In [19], the authors suggested a DL-based technique of channel estimation for wireless energy transfer. In this paper, a deep autoencoder is used to develop a channel learning technique. Based on the gathered energy response from the receiver, it learns the channel state information (CSI) at the transmitter with an insight to minimize the MSE of the estimated channel. The problem in estimating the channel coefficient is considered as a phase betterment problem [20, 21], and the most popular technique to handle this problem is the Gerchberg–Saxton algorithm developed in [21]. However, due to global phase ambiguity issue, the presentation of Gerchberg–Saxton algorithm is not up to the mark to calculate the channel estimation. So, the authors try to overcome this problem, as a result, this paper gives a detailed study of channel estimation for the wireless energy transfer (WET) system. Numerical analysis proves that the suggested scheme learns CSI efficiently and also performs better than the conventional method in terms of the MSE in channel estimation as well as in terms of the gathered energy.

Paper [22] also proposes a channel estimation technique which is based on deep learning algorithm for a massive MIMO system, and in this paper also, the authors have taken the case where the pilot length is smaller than the number of transmitting antennas, as in the paper [18], but the estimation process adopted is different. Here, the authors have taken the estimation process in two stages. First stage is a DL-based pilot-aided channel estimation process. Second stage is a DL-based data-aided channel estimation [7]. Figure 3 shows an overview of different DL-based algorithm based on performance in MSE.

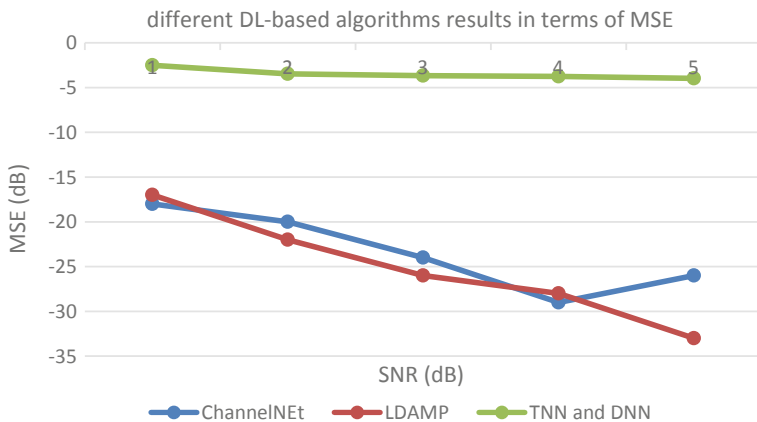


Fig. 3 Different DL-based algorithm results with respect to MSE

Table 1 List of various DL-based channel estimator used in different communication systems

S. no.	Reference number	DL-based algorithm	Communication system
1	[10]	ChannelNet	OFDM SISO
2	[12]	LDAMP	mm Wave massive MIMO
3	[17]	DNN	Multiuser distributive massive MIMO
4	[18]	TNN and DNN	Multiuser MIMO
5	[19]	Gerchberg-Saxton algorithm [21]	WET
6	[22]	TNN and DNN	Massive MIMO

4 Open Research Challenges

To compare the performance of DL-based algorithms, the main challenge is to have common benchmarks and open datasets [23]. Although this has certain rule in voice recognition, computer vision, and natural language processing fields, there is nothing comparable exists for communication systems. However, this domain is different from others as it deals with man-made signals that can be generated accurately or synthesized thus allowing the possibility of standardizing data rather than just taking some cases. To overcome this, it is most desirable to establish a data generating software on which researchers would be able to benchmark and compare their algorithms (Tables 1 and 2).

5 Conclusion

Throughout the study of different papers, we concluded that the different machine learning-based or deep learning-based channel estimator is always giving the comparable or even better results than the conventional channel estimator. Once the algorithm is trained with a different set of data, it outperforms the conventional method and gives better results within less time. However, it is also concluded that the performance and complexity are inversely proportional as it depends on the number of hidden layers used in the training scheme. The training time also increases with increase in the hidden layers (Table 3).

Table 2 Comparison of channel estimation method with respect to conventional method

S. no.	DL-based method	Compared with	Performance
1	ChannelNet	Ideal MMSE	Comparable up to SNR 20 dB in terms of MSE, after that performance degrades and required further training
2	LDAMP	SD and SCAMPI algorithms	Power efficiency of denoiser is better in suggested LDAMP algorithm than compared ones and gives better MSE with respect to a number of layers
3	DNN	ESPA, APPA and RPA	Performance and pilot allocation scheme are according to complexity where suggested gives better result in terms of MSE
4	TNN and DNN	LMMSE	Considerably outperforms the conventional LMMSE estimator in terms of MSE
5	Gerchberg–Saxton algorithm	No comparison	Uses deep autoencoder to outperform conventional method, also in terms of harvested energy, along with MSE

Table 3 List of abbreviation used in the paper

SNR	Signal-to-noise ratio
MSE	Mean square error
SER	Symbol error rate
MMSE	Minimum mean square error
LMMSE	Linear minimum mean square error
LS	Least square
OFDM	Orthogonal frequency division multiplexing
MIMO	Multiple-input multiple-output
ADCs	Analog-to-digital converters
SR	Image super-resolution
IR	Image restoration
SRCNN	Super-resolution convolution neural network
DnCNN	Denoising convolution neural network
RF	Radio frequency
LDAMP	Learned denoising-based approximation message Passing
APPA	Average pilot power allocation
ESPA	Exhaustive search-based pilot assignment
RPA	Random pilot assignment

References

1. Zhaoa, L., Zhang, P., Dong Q., Huang X., Zhao J. and Zeyu, Su.: Research of the Channel Estimation in Wireless Communication Systems ITM Web of Conferences, vol. 25, EDP Sciences (2019)
2. David, N., Wiese, T., Utschick, W.: Learning the MMSE channel estimator. IEEE Trans. Signal Process. **66**(11), 2905–2917 (2018)
3. Mo, J., Schniter, P., Prelicic, N.G., Robert W.H.: Channel estimation in millimeter wave MIMO systems with one-bit quantization. In: 48th Asilomar Conference on Signals, Systems and Computers, IEEE (2014)
4. Du, Z., Song, X., Cheng, J., Beaulieu, N.C.: Maximum likelihood-based channel estimation for macrocellular OFDM uplinks in dispersive time-varying channels. IEEE Trans. Wirel. Commun. **10**(1), 176–187 (2010)
5. Ma, J., Li, P.: Data-aided channel estimation in large antenna systems. IEEE Trans. Signal Process. **62**(12), 3111–3124 (2014)
6. Jiang, C., Zhang, H., Ren, Y., Han, Z., Chen, K.-C., Hanzo, L.: Machine learning paradigms for next-generation wireless networks. IEEE Wirel. Commun. **24**(2), 98–105 (2016)
7. Er, M.J., Zhou, Y.: Theory and novel applications of machine learning. InTech (2009)
8. Olutayo, O.O., Stanley, H.M.: Review of channel estimation for wireless communication systems. IETE Tech Rev. **29**(4), 282–298 (2012)
9. Han, S., Ahn, S., Oh, E., Hong, D.: Effect of channel-estimation error on BER performance in cooperative transmission. IEEE Trans. Veh. Technol. **58**(4), 2083–2088 (2008)
10. Soltani, M., Vahid, P., Ali, M., Hamid, S.: Deep learning-based channel estimation. IEEE Commun. Lett. **23**(4), 652–655 (2019)
11. Dong, C., Chen, C.L., He, K., Tang, X.: Image super-resolution using deep convolutional networks. IEEE Trans. Pattern Anal. Mach. Intell. **38**(2), 295–307(2015)

12. He, H.: Deep learning-based channel estimation for beamspace mmWave massive MIMO systems. *IEEE Wirel. Commun. Lett.* **7**(5), 852–855 (2018)
13. Kai, Z., Zuo, W., Chen, Y., Deyu, M., Lei, Z.: Beyond a gaussian denoiser: residual learning of deep cnn for image denoising. *IEEE Trans. Image Process.* **26**(7), 3142–3155 (2017)
14. Gao, X., Dai, L., Han, S., Chih-Lin, I., Wang, X.: Reliable beamspace channel estimation for millimeter-wave massive MIMO systems with lens antenna array. *IEEE Trans. Wirel. Commun.* **16**(9) 6010–6021 (2017)
15. Jie, Y., Wen, C.-K., Jin, S., Gao, F.: Beamspace channel estimation in mm wave systems via cosparse image reconstruction technique. *IEEE Trans. Commun.* **66**(10), 4767–4782 (2018)
16. Christopher, A.M., Maleki, A., Richard, G.B.: From denoising to compressed sensing. *IEEE Trans. Inf. Theory* **62**(9), 5117–5144 (2016)
17. Xu, J., Zhu, P., Li, J., You, X.: Deep learning based pilot design for multi-user distributed massive MIMO systems. *IEEE Wirel. Commun. Lett.* (2019)
18. Chun, C.-J., Kang, J.-M., Kim, I.-M.: Deep learning based joint pilot design and channel estimation for multiuser MIMO channels. [arXiv:1812.04120](https://arxiv.org/abs/1812.04120) (2018)
19. Kang, J.-M., Chun, C.-J., Kim, I.-M.: Deep-learning-based channel estimation for wireless energy transfer. *IEEE Commun. Lett.* **22**(11), 2310–2313 (2018)
20. Ying, S., Prabhu, B., Daniel, P.P.: Majorization-minimization algorithms in signal processing, communications, and machine learning. *IEEE Trans. Signal Process.* **65**(3), 794–816 (2016)
21. Ralph W.G.: A practical algorithm for the determination of phase from image and diffraction plane pictures. *Optik* **35**, 237–246 (1972)
22. Chun, C.-J., Kang, J.-M., Kim, I.-M.: Deep Learning Based Channel Estimation for Massive MIMO Systems. *IEEE Wirel. Commun. Lett.* (2019)
23. O’Shea, T., Jakob, H.: An introduction to deep learning for the physical layer. *IEEE Trans. Cognit. Commun. Netw.* **3**(4), 563–575 (2017)

Patient Diabetes Forecasting Based on Machine Learning Approach



Arvind Kumar Shukla

Abstract In current scenario, machine learning plays an important role for forecasting diseases. The patient should passes through number of tests for diseases detection. This paper deals with the forecast of diabetes. The main idea is to predict the diabetic cases and find the factors responsible for diabetics using classification method. In this paper, an attempt has been made to integrating cluster and classification, which will gives a capable categorization result with highest accuracy rate in diabetes prediction using medical data with machine learning algorithms (such as logistic regression algorithms) and methods.

Keywords Machine learning algorithm · Diabetes disease · Prediction · Python 3.7 · Scikit-learn · PyCharm

1 Introduction

Although diabetes has no cure, so it is important to detect whether a person have diabetes or not. Nowaday, diabetes is very harmful diseases. It is not only a disease but also an initiator of diverse types of diseases such as heart attack, heart problem, kidney failure, etc. For identifying process is that patient require to visit a diagnostic center, consult with doctor, and wait for a day or more to collect their reports. Besides, every time they would like to get their analysis report, they have to ravage their money in hopeless. But, by the use of machine learning processes, they able to find a answer to this problem, so we have to developed a system using data processing, by which we calculate and forecast whether the person has facing diabetes problem or not. Furthermore, forecasting the diabetes untimely leads to treating the patients before it becomes serious. Machine learning is able to extract information from large amount of diabetes-related facts. Because of that it has a major part in diabetes study and more than ever. In this study an attempt has been made to develop a method which may forecast the diabetic danger stage of a person with an exact correctness. Also, this

A. K. Shukla (✉)
IFTM University, Moradabad, India
e-mail: arvindshukla.india@gmail.com

study has focused on developing a system based on categorization method. Output has been confirmed using receiver operating characteristic curves in a susceptible manner. The created outfit strategy utilizes cast a ballot given by alternate calculations to deliver the last outcome. It additionally gets a more exact expectation of the malady. We utilized Python augmentation for information pre-processing and test investigation. Results demonstrate a noteworthy enhancement of exactness of the outfit strategy thinks about to other existing strategies. Information expository is a procedure of looking at and distinguishing the concealed examples from huge measure of information for result finding. In social insurance, by utilizing machine learning calculations for breaking down the therapeutic information to manufacture machine learning models to do the restorative determinations. Machine learning is a kind of computerized reasoning (AI) that empowers a framework to learn without anyone else and build up the information models to settle on choice by foreseeing the obscure information or name of the a given information [1, 2].

The machine learning calculations might be characterized into three classes (a) supervised learning, (b) unsupervised learning [3] and (c) semi-managed learning [4, 5]. Supervised learning is when the model is getting trained on a labeled dataset. Labeled dataset is one which has both input and output parameters. It is classified into two types: Classification: Where output is having defined labels (discrete value). And Regression: Here, The output is having continuous value.

Linear regression, nearest neighbor, Guassian Naive Bayes, decision trees, support vector machine (SVM), and random forest is the algorithms of supervised learning.

Unsupervised learning is a sort of realizing where we do not offer focus to our model while preparing, i.e., preparing model has just information parameter esteems. The model without anyone else's input needs to discover which way it can learn. Unsupervised learning can be arranged into:

Clustering: Broadly this technique is applied to group data based on different patterns, our machine model finds. For example, in above figure, we are not given output parameter value, so this technique will be used to group clients based on the input parameters provided by our data.

Association: This technique is a rule-based ML technique which finds out some very useful relations between parameters of a large dataset. For example, shopping stores use algorithms based on this technique to find out relationship between sale of one product with respect to others sale based on customer behavior. Once trained well, such models can be used to increase their sales by planning different offers.

K-means clustering, density-based spatial clustering of applications with noise (DBSCAN), balanced iterative reducing and clustering using hierarchies (BIRCH), and hierarchical clustering are example of unsupervised learning algorithm.

Semi-supervised learning as the name suggests its working lies between supervised and unsupervised techniques. We use these techniques when we are dealing with a data which is a little bit labeled and rest large portion of it is unlabeled. We can use unsupervised technique to predict labels and then feed these labels to supervised techniques. This technique is mostly applicable in case of image datasets where usually all images are not labeled.

The review is organized as follows: Sect. 2 provides the literature reviews. Section 3 defines the diabetes forecast system model. Section 4 provides the methodological approach adopted, and. Section 5 presents a discussion and providing conclusions.

2 Literature Review

This section deals with review of various research works that are associated with the proposed work.

Plis, Bunescu, Marling et al. clarify an answer that uses a conventional physiological model of blood glucose elements to create useful highlights for a support vector regression demonstrate that is prepared on patient particular information. His model beats diabetes specialists at foreseeing blood glucose levels and could be utilized to envision just about a fourth of hypoglycemic occasions 30 min ahead of time. Despite the fact that the comparing exactness is as of now only 42%, most false cautions are in close hypoglycemic districts and consequently patients reacting to these hypoglycemia alarms would not be hurt by mediation [6].

Dagliati, Marini et al. in this paper, the creators utilized logistic regression with stepwise component choice to foresee the beginning of retinopathy, neuropathy, or nephropathy, at various time situations, at 3, 5, and 7 years from the main visit at the hospital center for diabetes (not from the analysis). They take factors are sex, age, time from conclusion, weight file (BMI), glycated hemoglobin (HbA1c), hypertension, and smoking propensity. Last models, custom-made as per the intricacies, if exactness up to 0.838. Other factors were decided for each issue and time situation, prompting particular models simple to change over to the clinical practice. Machine learning methods to predict diabetes complications [7, 8].

Abdul et al. directed a study on information mining procedures on medicinal information for finding locally visit illnesses. The fundamental focal point of this study is to dissect the information digging procedures required for restorative information examination that is particularly used to find locally visit maladies, for example, heart lung disease, afflictions, bosom tumor utilizing order and relapse tree (CART) calculation, and the choice tree calculations, for example, ID3, C4.5 [9]. Zhao et al. displayed a framework for subcutaneous glucose concentration expectation. This proposed model may anticipate the sort one diabetes mellitus [10].

Srinivas et al. explain the uses of information mining strategies in human services and expectation of heart assaults. This examination utilized restorative profiles, for example, age, sex, circulatory strain, and glucose and anticipated the probability of patients getting a heart and kidney issues [11].

Agarwal et al. explain an execution examination of the aggressive learning calculations on Gaussian information for programmed group choice and furthermore contemplated and examined the execution of these calculations and randomized outcomes have been broke down on two-dimension Gaussian information with the

learning rate parameter kept straightforward for all calculations. Calculations utilized in their work incorporate grouping calculation, aggressive learning calculation, and recurrence touchy aggressive learning calculation. Managed learning machine calculations are utilized for arrangement of the Gaussian information [12].

Diwani et al. discussed the applications of data mining in health care. In this manuscript, further explained an overview of study on health care application using data mining methods. Data mining is a technology, used for knowledge discovery in databases and data representation. Moreover, the medical data in the form of text, and the digital medical images such as X-rays, magnetic resonance imaging are taken for syndrome analytical processing [13].

Durairaj et al. defined the possible use of classification-based data mining methods such as rule-based methods, decision tree algorithm, Naïve Bayes, and artificial neural network (ANN) to the considerable volume of healthcare data. In this research, medical problems have been investigated and evaluated such as heart disease and blood pressure [14].

Davis et al. explained individual sickness risk forecasting based on medical history. Manuscript also predicts every patient's maximum disease risks based on their own medical history data. Dataset are used for medical coding and collaborative assessment and recommendation engine information methods [7].

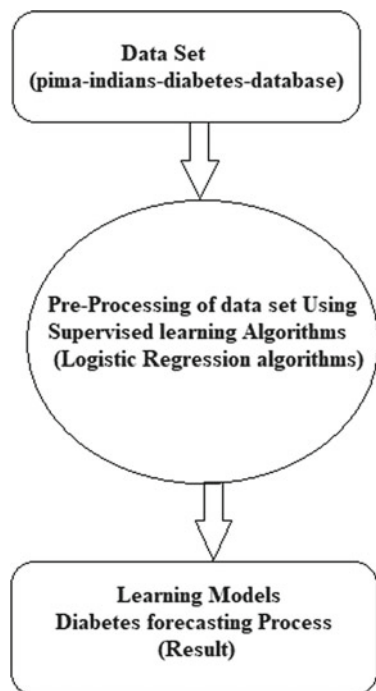
Alghamdi, Ehrman et al. clarify the capability of machine learning techniques for anticipating occurrence diabetes utilizing cardio respiratory wellness information. By examined forty-two statistic and clinical highlights for {32,555} patients of the FIT Project who were non-diabetic at pattern and took the pressure process test; at that point, they were followed up for a long time. The creators applying the random under-sampling procedure demonstrated no enhancement for the five characterization models. Here, the SMOTE techniques indicated imperative improvement on the expectation of all arrangement models forecast execution in accordance with the slow increment of the rates used. The results widely better the outcomes which are accounted for in different reports of the writing [8].

It is also observed that the machine learning algorithms put an important role in knowledge detection form the databases mainly in medical analysis with the medical dataset.

3 Diabetes Forecasting System Model

This section deals with the diabetes prediction system for diabetes diagnosis. Figure 1 shows the flowchart representation of the system model. Primarily, the diabetes dataset is given into the data pre-processing module. The pre-processing module removes the irrelevant features from the diabetes dataset and gives the pre-processed dataset with relevant features to the machine learning algorithm. Then, the machine learning algorithm develops a learning model from the pre-processed dataset. This learning model is known as knowledge learning model. Furthermore, the diabetes is predicted for a person's medical report or data using the learning model.

Fig. 1 Diabetes forecasting system model



With the help of system model, we will explain how to forecast whether a patient suffering from diabetes or not, it depends on information like blood pressure, body mass index (BMI), age, etc.

4 Investigational System and Method

4.1 Software Used

Python 3.7 software and the configuration of computer system 3 GB RAM, Intel (R) Core i3 CPU Processor, Windows 10, 32-bit operating system. For this study, The Pima Indians Diabetes Database can be used to train machine learning models to predict if a given patient has diabetes [<https://www.kaggle.com/uciml/pima-indians-diabetes-database>]. This dataset includes eight features of the patient such as number of time pregnant, plasma glucose concentration, blood pressure, skin fold thickness, insulin level, body mass index (BMI), diabetes pedigree function, age, and the results such as whether the person has diabetes (+ve) or not (-ve). By Python 3.7, Table 1 shows the description of dataset.

Table 1 Structure of diabetes dataset using Python (the datasets contain 768 data point, with nine features each)

Pregnancies	Blood pressure	Glucose	Skin thickness	Insulin	BMI	Diabetes pedigree function	Age	Outcome
6	148	72	35	0	33.67	0.637	50	1
1	84	85	28	0	26.63	0.361	31	0
8	184	183	1	1	23.34	0.688	32	1
1	89	89	23	93	28.13	0.177	21	0
0	40	137	35	168	43.1	2.299	33	1

4.2 Experimental Setup

Firstly, by importing pandas to read data from a diabetes .csv 768×9 file and operate it for further use. Here, NumPy [15] is used to convert our data into an appropriate format to feed our classification model. We will use Matplotlib for visualizations package. We will then import logistic regression algorithm from sklearn [16]. Algorithm will help us to construct our classification model. Table 1 shows the structure of diabetes datasets with its features.

The data has following texture that helps us to forecast whether a person is diabetic or not (Table 2).

We should likewise watch that the dataset is spotless (has no invalid qualities, etc.). The information has some missing qualities (see insulin = 0) in the examples in the past figure. For the model, we will utilize, (calculated relapse), estimations of 0 naturally infer that the model will just disregard these qualities. Preferably, we could supplant these 0 esteems with the mean an incentive for that feature.

Give us now a chance to investigate our informational collection to get a vibe of what it would appear that and get a few bits of knowledge about it. Let us begin

Table 2 Texture used in dataset

Pregnancies	Number of times pregnant
Glucose	Plasma glucose focus more than 2.5 h in an oral glucose resilience test
Blood pressure	Diastolic circulatory strain (mm Hg)
Skin thickness	Triceps skin overlap thickness (mm)
Insulin	2–2.5 h serum insulin (mu U/ml)
BMI	Body mass index [weight in kg/(height in m ²)]
Diabetes pedigree function	Diabetes family work (a capacity which scores probability of diabetes dependent on family history)
Age	Age in years
Outcome	Class variable (0 if—non-diabetic, 1 if—diabetic)

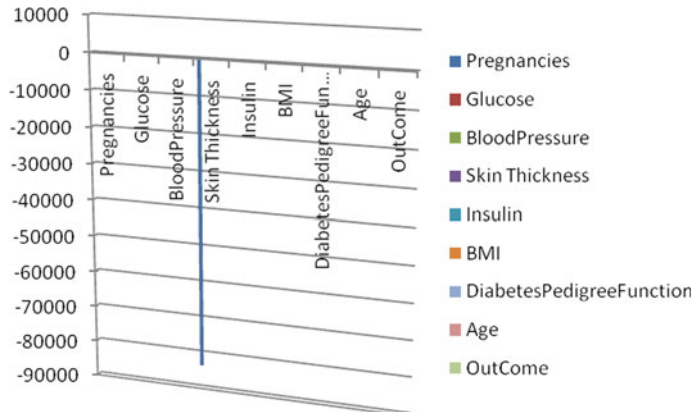


Fig. 2 Output of feature (and outcome) correlations

by discovering connection of each match of highlights (and the result variable), and imagine the relationships. Figure 2 shows the output of feature (and outcome) correlations, and Table 3 explains the output of characteristic and correlation.

It should be obvious from the above table, glucose level, age, BMI, and number of pregnancies all has impressive connection with the result variable. Likewise, see the relationship among the sets of highlights, similar to age and pregnancies, insulin, and skin thickness. Figure 3 demonstrates the numbers of individuals in the dataset are diabetic and what number of are not, utilizing the bar-plot of the equivalent.

It is likewise useful to imagine relations between a single variable and the result. Under, we will see the connection among age and result. We may also imagine different things to see. Figure 4 is a plot of the mean age for every one of the defer classes. We can see that the mean time of individuals having diabetes is higher.

4.3 Machine Learning Algorithms Used for Experimental Setup

Machine learning is used for calculations for that we should constantly part our information into a preparation set and test set. On the off chance that the quantity of examinations we are running is huge, at that point, we can isolate our information into three sections, to be specific—preparing set, improvement set, and test set. For our situation, we separate out a few information for manual cross-checking.

For the experimental study, we can gather record includes 768 patients out and out. To set up our model, we will use 668 records. We will use 100 records for testing, and the last 17 records to cross-check our model.

Table 3 Output of characteristic and correlation

	Pregnancies	Glucose	Blood pressure	Skin thickness	Insulin	BMI	Diabetes pedigree function	Age	Outcome
Pregnancies	1.00	0.0129459	0.141282	-83672	-0.07354	0.017683	-0.035523	0.544341	0.221898
Glucose	0.138955	1.000	0.15459	0.057328	0.335357	0.221071	0.138337	0.263514	0.466581
Blood pressure	0.151282	0.15559	1.000	0.207371	0.088933	0.281805	0.044265	0.239528	0.065068
Skin thickness	-0.084672	0.057528	0.207371	1.000	0.436783	0.392573	0.185928	-0.11397	0.074752
Insulin	-0.076535	0.331557	0.088933	0.436783	1.0000	0.197859	0.185071	-0.04263	0.130548
BMI	0.017783	0.225071	0.281805	0.392573	0.197859	1.0000	0.150647	0.037242	0.292695
Diabetes pedigree function	-0.035523	0.137337	0.041265	0.182928	0.185071	0.140647	1.000	0.037561	0.173844
Age	0.545341	0.265514	0.239528	-0.11397	-0.04256	0.036242	0.043561	98.190	0.238356
Out come	0.223898	0.136581	0.065068	0.074752	0.134548	0.292695	0.183844	0.258356	0.999

Fig. 3 Number of non-diabetic {0} and diabetic {1} people in the dataset

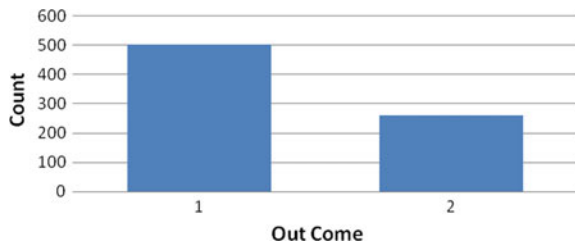
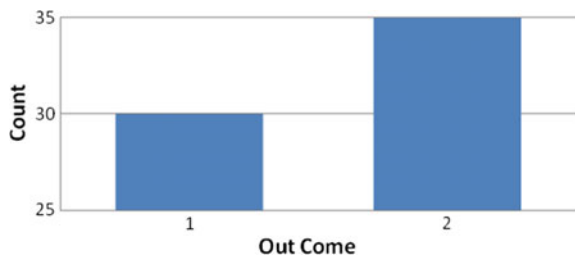


Fig. 4 Average age of non-diabetic and diabetic person in the given dataset



Furthermore, separate the name and features (for both getting ready and test dataset). Despite that we will similarly change over them into NumPy bunches [15] as our machine learning count process data in NumPy shows compose. As the last development before using machine learning, we will institutionalize our data sources.

Machine learning models frequently advantage generously from information standardization. It additionally makes it simpler for us to comprehend the significance of each component soon, when we will be taking a gander at the model weights. This study will standardize the information with the end goal that every factor has a zero mean and a standard deviation of one.

4.3.1 Estimating the Machine Learning Model

We would now be able to prepare our order display. We will be utilizing a straightforward machine learning model called calculated relapse. Since the model is promptly accessible in sklearn [16], the preparation procedure is very simple and we can do it in few lines of code. Initially, we make an example called diabetes check and afterward utilize the fit capacity to prepare the model.

To find the accuracy of the model, we use the following command

```
accuracy = diabetes_Check.score(test_Data, test_Label)
print {"accuracy = ", accuracy * 100, "%"}
here, print statement will shows the accuracy = 80.52%.
```

Understanding the ML model and out comes:

To show signs of improvement feeling of what is happening inside the calculated decline display, we may picture how our model uses the diverse highlights and which

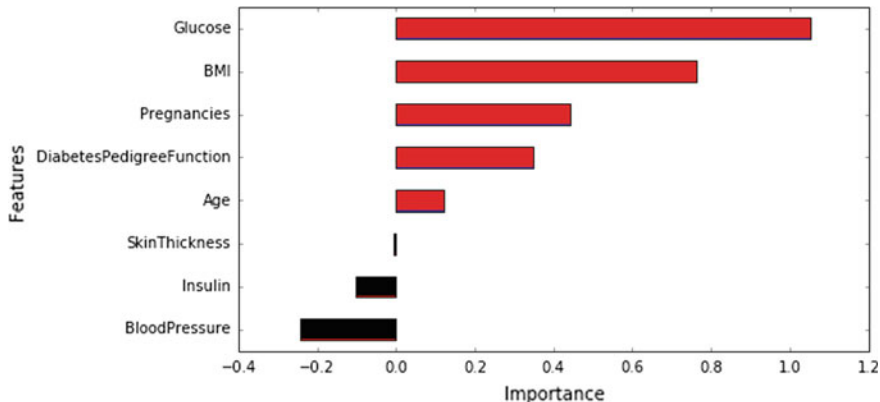


Fig. 5 Weight in the logistic regression demonstrates connecting to each one of the module factors

highlights have new significant impact. Figure 5 is the representation of the weights in the logistic regression shows identifying with each one of the part factors.

Figure 5 is the portrayal of the weights in the logistic regression exhibits identifying with each one of the park factors. Here, the glucose level, BMI, pregnancies, and diabetes family work incorporate essential impact on the model, exceptionally glucose level, and BMI. It regards see our machine learning model proportional what we have been requested from specialists our whole lives. A higher circulatory strain is connected with a man not being diabetic. Further, it is noticed that circulatory strain is more critical as a component than age, in light of the fact that the greatness is higher for a pulse. Regardless of whether age was more associated than BMI to the yield factors (as we saw amid information investigation), the model depends more on BMI. This may happen for a few reasons, including the data that the relationship caught by age is likewise caught by another variable, and though the data caught by BMI is not caught by new factors.

5 Discussion and Conclusion

In this investigation, an efficient exertion was made to recognize and audit machine learning and anticipating using the model—We will now utilize our unused information to perceive how expectations might be made and check the principal record to construct forecast. The essential part of display prediction probability 0.458 is the probability of the class being zero and the second segment 0.572 is the probability of the class being one. The combined likelihood will be enhanced by one. Our estimate characterized that the model predicts that the individual has diabetes. Information highlights bucketing should help, i.e., make new factors for circulatory strain in a specific range, glucose levels in a specific range, etc. Our framework models precision is 82.92%. We could likewise enhance the information cleaning, by supplanting

zero qualities with the mean esteem and what measurements specialists depend on the fundamentally to break down a diabetic patient and make new highlights in like manner. There are heaps of approaches to enhance the above model by applying semi-managed learning algorithms.

References

1. Sisodia, D., Sisodia, D.S.: Prediction of diabetes using classification algorithms. *Proc. Comput. Sci.* **132**, 1578–1585 (2018)
2. Darcy, A.D., Nitesh, V.C., Nicholas, B.: Predicting individual disease risk based on medical history. In: CIKM '08 Proceedings of the 17th ACM conference on Information and knowledge management, pp. 769–778 (2008)
3. Agarwal, C.C., Reddy, S.K.: Data Clustering, Algorithms and Applications. Chapman and Hall, CRC, Boca Raton (2014)
4. Marsland, S.: Machine Learning, an Algorithmic Perspective. Chapman and Hall, CRC Press, Boca Raton (2009)
5. Kavakiotis, I., Tsavos, O., Maglaveras, N., Vlahavas, I., Chouvarda, I.: Machine learning and data mining methods in diabetes research. *Comput. Struct. Biotechnol. J.* **15**, 104–116 (2017)
6. Plis, K., Bunescu, R., Marling, C., Jay, S., Schwartz, F.: A machine learning approach to predicting blood glucose levels for diabetes management. *Modern Artificial Intelligence for Health Analytics: Papers from the AAAI-14*, Association for the Advancement of Artificial Intelligence, pp. 35–39 www.aaai.org (2014)
7. Dagliat, A., Marini, S.: Machine learning methods to predict diabetes complications. *J. Diab. Sci. Technol.* **12**(3), 193229681770637 (2017)
8. Alghamdi, M., Al-Mallah, M., Keteyian, S., Brawner, C., Ehrman, J., Sakr, S.: Predicting diabetes mellitus using SMOTE and ensemble machine learning approach: the Henry Ford ExercIse Testing (FIT) project. <https://dx.doi.org/10.1371/journal.pone.0179805> (2017)
9. Mohd, A.K., Sateesh, K.P., Dash, G.N.: A survey of data mining techniques on medical data for finding locally frequent diseases. *Int. J. Adv. Res. Comput. Sci. Softw. Eng.* **3**(8), 149–153 (2013)
10. Chunhui, Z., Chengxia, Y.: Rapid model identification for online subcutaneous glucose concentration prediction for new subjects with type I diabetes. *IEEE Trans. Biomed. Eng.* **62**(5), 1333–1344 (2015)
11. Srinivas, K., Kavihta, R.B., Govrdhan, A.: Applications of data mining techniques in healthcare and prediction of heart attacks. *Int. J. Comput. Sci. Eng.* **2**(2), 250–255 (2010)
12. Agarwaal, V.K., Anil K.A.H.: Performance analysis of the competitive learning algorithms on gaussian data in automatic cluster selection. In: 2016 Second International Conference on Computational Intelligence and Communication Technology (2016)
13. Salim, D., Mishol, S., Daniel, S.K., et al.: Overview applications of data mining in health care: the case study of Arusha region. *Int. J. Comput. Eng. Res.* **3**(8), 73–77 (2013)
14. Durairaj, M., Ranjani, V.: Data mining applications in healthcare sector: a study. *Int. J. Sci. Technol. Res.* **2**(10), 31–35, 90 (2013)
15. NumPy is the fundamental package for scientific computing with Python <http://www.numpy.org/>
16. Simple and efficient tools for data mining and data analysis <http://scikit-learn.org/stable/>

Pose Invariant Face Recognition Using Principal Component Analysis



Akash Krishna Srivastava, H. Sneha, Diksha, and Koushlendra Kumar Singh

Abstract Facial recognition is a propitious field that has been actively studied and researched upon in the recent years. The main challenge in face recognition is the various poses exhibited by subject. It makes it difficult to accurately identify the individual based on facial recognition. The present work encompasses of a new frontalization algorithm and facial recognition using principal component analysis. The three-dimensional face geometry model has been used to produce better facial features. The Zhu-Ramanan detector has been used for detection of facial features. Principal component analysis is a statistical approach used for face recognition which involves dimensionality reduction. The proposed approach was validated on two different databases. Outcomes of the proposed approach clearly show the reduction in computational complexity of process of face recognition. The approach successfully recognizes faces up to $\pm 70^\circ$ yaw. It outperforms other methods for face recognition in terms of its efficiency to recognize faces.

Keywords Principal component analysis · Frontalization · Zhu-Ramanan detector

1 Introduction

Facial recognition is the process of identifying one or more people in images by analyzing and comparing patterns. Facial features like eyes, ears and nose play a vital role in designing algorithms for facial recognition. It is one of most intensively explored topics in biometric. Facial recognition software has improved a lot over the years delivering promising results in various conditions [1, 2].

The use of human face has significant applications in the law enforcement and non-law enforcement fields. The main advantage of this field over other biometric field is the entire process is non-contact/non-cooperativeness.

A. K. Srivastava · H. Sneha · Diksha · K. K. Singh (✉)
National Institute of Technology Jamshedpur, Jamshedpur, India
e-mail: kks04540@gmail.com

Despite the vast improvements of the technology over the years, it is still challenged by the wide variations in pose, illumination, expressions and aging effect. For practical applications, images are captured in different conditions which make it difficult to match with the images in the database which might have been taken in controlled environment. The proposed approach successfully solves the pose invariant challenge. The approach combats the pose problem which is matching of images in any pose from $+90^\circ$ of yaw to -90° degree of yaw with frontal gallery images. This is general setting used in pose invariant face recognition system.

Earlier proposed approaches have focused on synthesizing new facial views. This has been done by calculating 3D surface of the face appearing in image. Facial geometries based on 3D face models have been calculated in Morphable Models (MM) methods [3, 4]. Synthesis of face image can be done by 2D or 3D techniques. Ashraf et al. use 2D techniques to learn patch-wise warps between two images. Authors used the Lucas–Kanade optimization algorithm [5, 6]. There are some more methods of 2D face synthesis, e.g., face hallucination [7, 8]. Generic elastic models (GEMs) have been proposed for 3D modeling [8].

Face frontalization is sensitive to occlusion and has specularities (e.g., eyeglasses) [3]. Concept of symmetry has been applied to replace out-of-view facial regions [9].

Local feature analysis is an analytic method which recognizes face with local features. Eyes, ears, lips, etc., are treated as local feature, and it referred to local feature analysis kernels [10]. Principal component analysis is an appearance-based matching method. It is a statistical method based on eigenvectors [11].

The proposed manuscript gives an algorithm for face frontalization [9]. This related approach relies on high facial feature localization [11]. Facial recognition has been developed by projecting a new image in eigenface subspace. This is followed by classifying the person.

The present manuscript is divided into different sections. The proposed methodology has been explained in Sect. 2. Experiments are explained in Sect. 3. Results are discussed in Sect. 4.

2 Proposed Methodology

The proposed approach has been divided into two steps. Frontalization of face is performed in the first step, and the pose estimated is used in the next step. The second step performs facial recognition in which the query face is matched with the training database to produce the recognition result.

2.1 Face Frontalization

This section explains the method to synthesize frontal facing views of faces appeared in unconstrained photos. This work involves single 3D reference face geometry to



Fig. 1 An approach to face detection, pose estimation and landmark estimation

produce better aligned facial features in accordance with reference 3D model. The use of simple 3D face models for frontalization purpose is quite simple but proved to be effective (Fig. 1).

The frontalization process is illustrated in Fig. 2. Important visual features have been detected from a large set of features of detected face by using any simple and efficient detector [12]. This image is later cropped and rescaled according to the coordinate system. Compatibility issues have been avoided by keeping the dimensions and crop ratios for frontalization same as previously used for Labeled Faces in the Wild (LFW) [10].

Reference coordinate system is calculated with the frontal view of the given image. Detected facial feature points are aligned with the generic 3D model of a face. This 3D surface is considered as a proxy surface over here. The proxy surface is used for

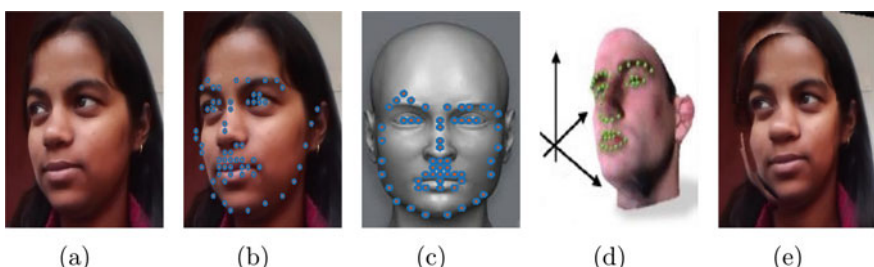


Fig. 2 Frontalization process. **a** Query image; **b** query image with facial features detected; **c** facial features in reference face photo; **d** 3D graphical model; **e** fitted image in 3D coordinates

obtaining the initial frontalized face by the rear projection of the appearance of query image to reference coordinate system. The final result consists of the superimposed frontalized face on query's face along with the parts of symmetry sides were the features are not clearly detected due to the pose of the query image.

The whole process of frontalization has been described in Fig. 2. Figure 2a is the given query image, and Fig. 2b describes the detected facial feature points on the query image. The detector used for query image has been used to localize the same facial features in a reference face photo, produced by rendering a textured 3D computer graphics model which can be seen in Fig. 2c. A projection matrix has been estimated by the 2D coordinates on the query and their corresponding 3D coordinates on the model which is then used to back-project query intensities to the reference coordinate system. This can be seen in Fig. 2e.

2.1.1 Frontalized View Generation

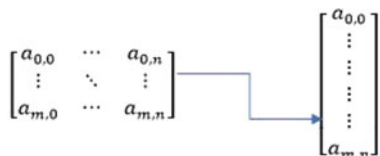
A method has been adopted for facial feature detection which attempts same feature points in both the images. The proposed approach first calculates the estimated projection matrix with the help of a model 3D struct and a 2D array having facial feature coordinates obtained with the same detector represented by the model 3D struct. So, points on the query image have been matched with points on 3D model (Figs. 3, 4 and 5).

2.1.2 Facial Feature Detection

Considerable research has been implemented in the field of face detection. However, it is still a challenge to obtain efficient estimation of head pose and facial landmarks [13]. Ambiguities due to latter lead to the founding stone of face detection [14]. There are several detectors available to carry out this process. The proposed system has been designed by the use of Zhu-Ramanan detector [13].

Earlier approaches used densely connected elastic graph [15], but this model used partial facial landmarks (1) [13]. Each tree is taken as a linear tree—structured pictorial structure taken as $T_m = (V_m, E_m)$, here m indicates mixture, $V_m \subseteq V$. Any pixel location for an image I let it be denoted by $l_i = (a_i, b_i)$. We sum a configuration of parts $L = l_i : i \in V$ as:

Fig. 3 Face images are assumed to be of size $M \times N$ which are then transformed to $MN \times 1$ dimensional space



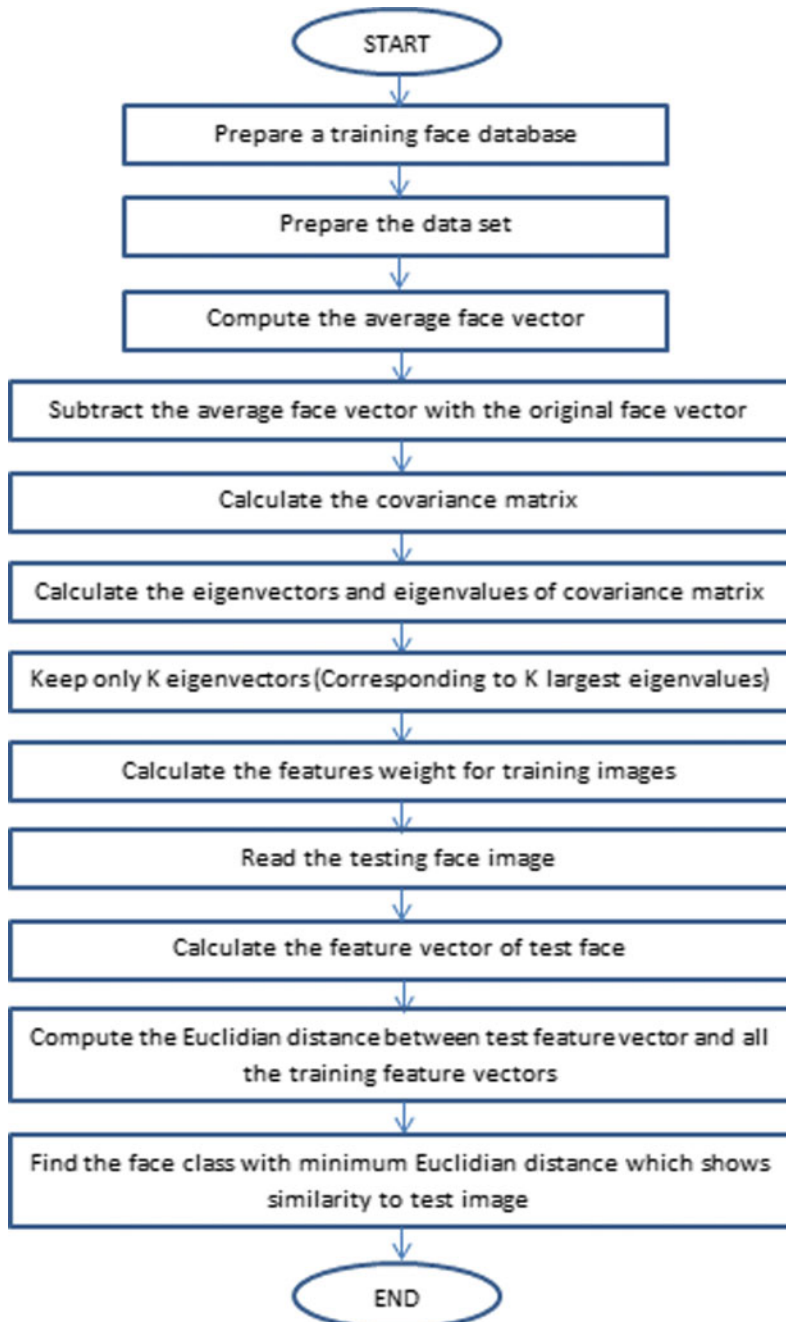


Fig. 4 Flowchart explaining the steps for the face recognition process

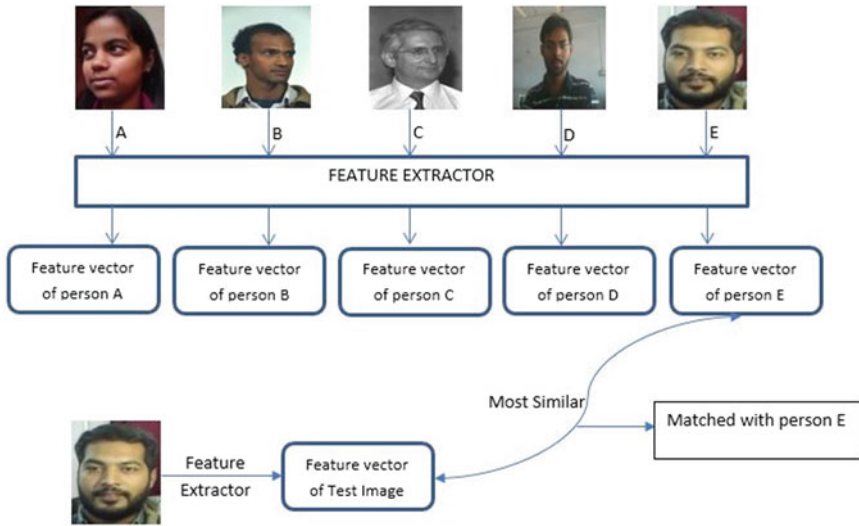


Fig. 5 PCA flowchart

$$S(I, L, m) = A'_m(I, L) + S'_m(L) + \alpha_m \quad (1)$$

$$A'_m(I, L) = \sum_{i \subseteq V_m} w_m^i \cdot \Phi(I, l_i) \quad (2)$$

$$S'_m(L) = \sum_{ij \subseteq E_m} a_{ij}^m dx^2 + b_{ij}^m dx + c_{ij}^m dy^2 + d_{ij}^m dy \quad (3)$$

Equation 2 has been used to sum up the appearance evidence for placing of a template w_i^m for part i , at location l_i for mixture m . Equation 3 scores the parts L and their mixture-specific spatial arrangement. The displacement of i th part relative to the j th part is considered as $dx = x_i - x_j$ and $dy = y_i - y_j$. Parameters (a, b, c, d) show the rest location and rigidity of spatial constraints between a pair of parts. The given equation can also be written as

$$S'_m(L) = -(L - \mu_m)^T \Lambda_m (L - \mu_m) + c \quad (4)$$

here, (μ, Λ) are re-parameterizations of the shape model (a, b, c, d) and C is any constant. α_m is a scalar bias associated with given mixture m .

2.1.3 Pose Estimation

Pose of an object in an input image has been estimated in this step. The image may be like stereo images, image sequence, etc. The synthetic rendered view of the model has been captured for which a reference projection matrix C_M is produced. $C_M = A_M[R_M T_M]$ here, A_M is the intrinsic matrix which includes the principal point and skew coefficient [16]. R_M is rotation matrix; T_M is the translation vector. R_M and T_M are extrinsic parameters.

Optical center is decided by origin of camera's coordinate. Plane of image is defined by its x - and y -axis [16]. To build the reference coordinate system, the rotation and translation (Fig. 2c) are selected so that the frontal view of the model can be produced.

Let I_R be the reference view for estimating the pose.

Let $P = (X; Y; Z)^T$ be the 3D point coordinates of P where P is the pixel of I_R for which:

$$P \sim C_M P \quad (5)$$

As shown already (Fig. 2b).

Let the detected facial feature points in the query image I_Q be denoted by $p_i = (x_i; y_i)^T$. Let detected facial feature points in the reference view (Fig. 2c) I_R be denoted by $p_i = (x_i; y_i)^T$. Equation 5 gives the coordinates $P_i = (X_i; Y_i; Z_i)^T$. These coordinates lie on the surface of the model. These coordinates are to be projected on P_i (Fig. 2d).

Hence, the generated correspondences are:

$$(p_i^T; P_i^T) = (x_i; y_i; X_i; Y_i; Z_i) \quad (6)$$

The above equation allows the estimation of the projection matrix M_Q for which:

$$M_Q \sim A_Q[R_Q T_Q] \quad (7)$$

Equation 7 thus further helps to calculate the approximation of camera for capture query image I_Q [16, 17].

2.1.4 Frontal Pose Synthesis

The initial frontalized view I_F is produced by the same proposed method as discussed in Sect. 2.1.3. For every pixel coordinate in the reference view $p_i = (x_i; y_i)^T$, Eq. 5 gives the coordinates $P_i = (X_i; Y_i; Z_i)^T$. Thus, in this way, we find the 3D location of the reference projected on the 2D surface by C_M . Bilinear interpolation has been used for sampling of intensities of query image at p . Figure 2e describes the result. Equation used is similar to Eq. 5

$$P \sim C_Q P. \quad (8)$$

2.2 Face Recognition

The previous section has introduced frontalization scheme, whereby face recognition can be accomplished by finding the Euclidean distance between projected input image and projection of all centered training images. PCA has been used for dimensional reduction in face recognition algorithms [7]. Depending on the field of application, PCA is also named the discrete Kosambi–Karhunen–Loeve transform (KLT) which chooses a dimensionality reduction method. This describes the face matching problem based on the proposed PCA-based face recognition system.

1. The first step is to obtain face images $I_1, I_2, I_3, I_4, \dots, I_M$ from the training set images. The input face image must be centered. The size of image is also same. Each image I_i is transformed into a vector. These vectors are stored into training set S , $S = T_1, T_2, T_3, \dots, T_n$.

In this paper, We create a set that contains each transformed image as a vector of size $MN \times 1$. The size of face images is $M \times N$ resulting in a point in $M \times N$ D space. Average face vector Ψ is calculated by Eq. 9 as follows

$$\Psi = \frac{\sum_{i=1}^M T_i}{M} \quad (9)$$

The average face vector is subtracted from the original faces and the result stored in the variable, $\Phi_i = T_i - \Psi$.

2. Covariance matrix C has been calculated as follows,

$$C = \frac{1}{M} \sum_{n=1}^M \Phi_n \Phi_n^T = AA^T \quad (10)$$

Here, $A = [\Phi_1 \Phi_2 \Phi_3, \dots, \Phi_M]$.

The covariance matrix C has a dimensionality of $M^2 \times N^2$, so one would have M^2 eigenface and eigenvalues.

For image of size, 512×512 that means we must compute a $262,144 \times 262,144$ matrix and calculate 262,144 eigenfaces. Computationally, this is not very efficient as most of those eigenfaces are not useful for our task. In general, PCA is used to reduce a large dimensionality of vector spaces.

TWO CASES ARISES:

Case 1: Compute the eigenvectors U_i of AA' .

Case 2: Compute the eigenvectors V_i of $A'A$.

AA' and $A'A$ have the same eigenvalues, and their eigenvectors are related as follows:

$$U_i = AV_i \quad (11)$$

AA' and $A'A$ have up to $M \times N$ and M eigenvalues and eigenvectors. The M eigenvalues of AA' (along with their corresponding eigenvectors) correspond to the M largest eigenvalues of $A'A$ (along with their corresponding eigenvectors). U_i is eigenvectors or eigenfaces.

As explained earlier, eigenfaces with low eigenvalues can be neglected, as they denote only a small part of characteristic features of the faces.

3. The next step is to project the training sample into the eigenface space. The feature weight for the training images can be calculated by the following formula:

$$\omega_i = u_i^T (T_i - \Phi) \quad (12)$$

where u_i is the i th eigenfaces and $i = 1, 2, 3, \dots, K$.

The weight is obtained as above which forms a vector as follows

$$\Omega_{test}^T = [\omega_1, \omega_2, \omega_3, \dots, \omega_k].$$

4. The fourth step is as follows:

- (a) Read the test image.
- (b) Calculation of feature vector of test image/face. The test image is transformed into its eigenface components. Then, input image is compared with mean image. The difference of images is multiplied with each eigenvectors. Every value would correspond to weight and would become a vector

$$\omega_{test} = u_i^T (T_{test} - \Phi).$$

where u_i is the i th eigenfaces and $i = 1, 2, 3, \dots, K$.

$$\Omega_{test}^T = [\omega_1, \omega_2, \omega_3, \dots, \omega_k].$$

- (c) Average distance between test feature vector and all training feature vectors has been calculated. Mathematically, recognition is finding the minimum Euclidean distance, between a testing point and a training point given in the following equation $\varepsilon_k = \sqrt{\|\Omega_{test} - \Omega_i\|^2}$ where $i = 1, 2, 3, \dots, K$. The Euclidean distance between two weight vectors thus provides a measurement of similarity between the corresponding images.
- (d) The face class with minimum Euclidean distance shows similarity to test image.

3 Experimental Evaluation

ORL [18] and color FERET [19] databases are used for validation of the proposed approach. ORL database has 10 images of 40 subjects taken under varying conditions of illumination, facial expression and facial details. All the subject images are taken in the same upright, frontal position in a dark background. Different sets of experiments

are conducted. The recognition technique is tested on its ability to recognize the subjects across different illumination conditions, different facial expressions and different facial details (glasses/no-glasses).

Color FERET [19] has images of 994 subjects collected at numerous angles. The proposed algorithm is tested on its capability to efficiently recognize the subjects in the images with variation in pose. The proposed approach is also evaluated against the other existing face recognition methods.

After the frontalization step described in Sect. 2.1, the frontalized images are cropped and resized to 180×200 pixels to have a consistent input to the recognition step described in Sect. 2.2.

4 Results

The effectiveness of the proposed approach is conducted in terms of frontalization and face recognition techniques. Experiments are conducted on two different datasets. First, the performance of the proposed approach of PIFR is briefly compared with the previous works for PIFR on color FERET [19]. Second, the proposed face recognition approach is compared with its single-task baselines to prove the importance of principal component analysis. PIFR is combined with different other factors which are also considered during experiments. Performance of the proposed approach is evaluated for different values of pose and illumination in the third set of experiments on ORL [18].

4.1 Comparison on Color FERET Dataset

200 color FERET images without any expression and normal illumination at seven different poses are given. Out of all, the images, 100 frontal images, are utilized as gallery images, and 100 images are used as probes. Table 1 shows the proposed method outperforming the other methods. It is evident from the evaluation that images whose pose vary by $\pm 30^\circ$ are the ones which are recognized most efficiently than for images up to $\pm 65^\circ$ degrees variation. The proposed method has shown cent percent accuracy for smaller invariance angles than for larger angles. Although the recognition rate of the proposed approach for $\pm 45^\circ$ lags behind other methods, its efficiency overshadows other approaches for $\pm 65^\circ$.

As shown in Figs. 7, 8 and 9, the frontalized results of images with angle up to $\pm 30^\circ$ of yaw are less distorted compared to the images with angle up to $\pm 65^\circ$ of yaw (Fig. 6).

The results of the images with pose angle greater than $\pm 45^\circ$ of yaw have distorted frontalized faces. For images with angle between $\pm 45^\circ$ and $\pm 65^\circ$, despite the distorted frontalized face result, the proposed face recognition technique excels better than the other methods. For images with pose angle greater than $\pm 65^\circ$, the

Table 1 Comparison of the proposed approach with the other existing methods

Methods	Gallery Size	-65	-45	-30	-15	+15	+30	+45	+65	Mean
VAM [5]	200	NA	90.50	98.00	98.50	97.50	97.00	91.90	NA	NA
MRFs +	200	92.00	98.50	99.50	100	99.50	99.00	99.50	91.00	97.38
MLBP [6]										
RR +	100	78.00	91.00	96.00	96.00	98.00	99.00	96.00	87.00	92.63
Gabor [20]										
Proposed Approach	100	96.00	98.50	99.00	100	100	100	98.00	96.50	98.50



Fig. 6 Image with angle of $\pm 15^\circ$ yaw

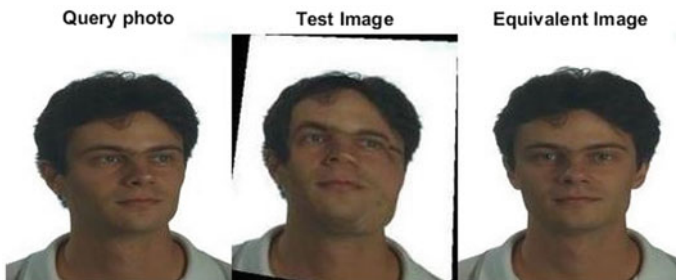


Fig. 7 Image with angle of $\pm 22.5^\circ$ yaw

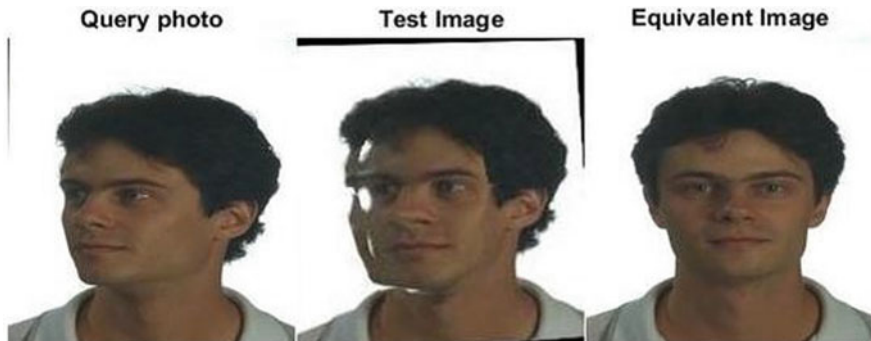


Fig. 8 Image with angle of $\pm 22.5^\circ$ yaw

distorted frontalized face is not suitable for face recognition technique due to lack of features. For images with angle greater than $\pm 65^\circ$, the proposed approach falls short of expectations.

The proposed approach represented by green line in Fig. 10. Surpasses the blue and maroon line which represent the previous approaches like VAAM [5], MRFs+MLBP [6], RR+Gabor [20]. The peak of all the lines is in the middle of the graph which shows that accuracy of query images is maximum for lower degree of variance than for higher degrees.

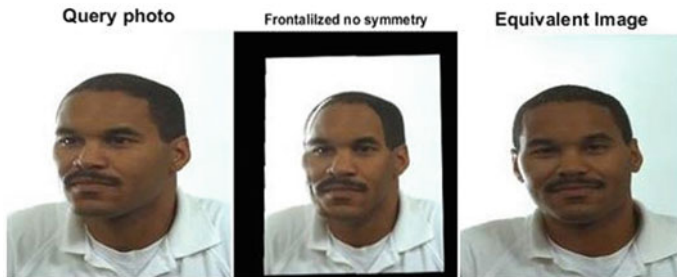


Fig. 9 Image with angle of $\pm 15^\circ$ yaw

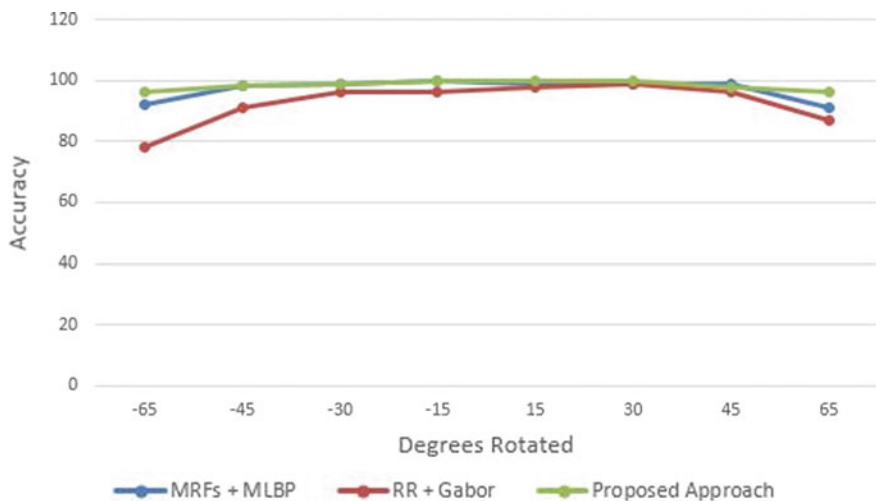


Fig. 10 Accuracy of various methods on degrees rotated

4.1.1 Evaluation of the Proposed Approach with Respect to Pose and Illumination

The performance of the proposed approach is compared with the existing algorithms under different conditions of pose and illumination. The experiments are performed over 10 images of 40 subjects each of ORL [18] face dataset. Recognition was carried out under widely varying conditions like the proposed frontalized view, scaled frontal view, subjects with spectacles, environment with varying illuminations, etc., while the training dataset covers limited views. The proposed approach shows higher accuracy

for unconstrained images than for images having some physical constraints like illumination, aging, facial expressions, etc. Lack of illumination in the environment brings down the recognition rate to 85%.

5 Conclusions

Face recognition is an exigent task if a large number of subjects exhibit different poses along with inevitable challenges of illumination, expression, etc. The proposed approach has two steps, frontalization and recognition. Frontalization is an approach which projects the frontal view of the image with the use of a facial feature detector. Recognition of the frontalized face is performed using principal component analysis which provides a practical solution which is well fitted for unrestrained environment. The proposed approach outperforms the previous approaches for face recognition in unconstrained environment. This approach gives promising results for images with up to $\pm 70^\circ$ yaw. Frontalization of images with angle greater than $\pm 70^\circ$ yaw gives a distorted image from which precise weighted eigenvectors cannot be determined for face recognition.

References

1. Ding, C., Choi, J., Tao, D., Davis, L.S.: Multi-directional multi-level dual-cross patterns for robust face recognition (2014). Available <http://arxiv.org/abs/1401.5311>
2. Tan, X., Triggs, B.: Enhanced local texture feature sets for face recognition under difficult lighting conditions. *IEEE Trans. Image Process.* **19**(6), 1635–1650 (2010)
3. Hassner, A., Harel, S., Paz, E., Enbar, R.: Effective Face Frontalization in Unconstrained Images. In: *IEEE Conference on Computer Vision and Pattern Recognition (CVPR)*, Boston (June, 2015)
4. Blanz, V., Scherbaum, K., Vetter, T., Seidel, H.: Exchanging faces in images. *Comput. Graphics Forum* **23**(3), 669–676 (2004)
5. Asthana, A., Marks, T.K., Jones, M.J., Tieu, K.H., Rohith, M.: Fully automatic pose-invariant face recognition via 3D pose normalization. In: *Proceedings of the IEEE International Conference on Computer Vision*, pp. 937–944 (Nov. 2011)
6. Arashloo, S.R., Kittler, J.: Efficient processing of MRFs for unconstrained-pose face recognition. In: *Proceedings of the IEEE 6th International Conference on Biometrics, Theory, Applications and Systems*, pp. 1–8 (Sept./Oct. 2013)
7. Wang, N., Tao, D., Gao, X., Li, X., Li, J.: A comprehensive survey to face hallucination. *Int. J. Comput. Vis.* **106**(1), 9–30 (2014)
8. Wang, N., Tao, D., Gao, X., Li, X., Li, J.: Transductive face sketchphoto synthesis. *IEEE Trans. Neural Netw. Learn. Syst.* **24**(9), 1364–1376 (2013)
9. Hassner, T.: Viewing real-world faces in 3D. In: *Proceedings of the International Conference on Computer Vision*, pp. 3607–3614. IEEE, New York (2013). Available www.openu.ac.il/home/hassner/projects/poses
10. Huang, G.B., Ramesh, M., Berg, T., Learned-Miller, E.: Labeled faces in the wild: a database for studying face recognition in unconstrained environments. University of Massachusetts, Amherst, TR 07-49 (2007)

11. Taigman, Y., Yang, M., Ranzato, M., Wolf, L.: Deepface: closing the gap to human-level performance in face verification. In: Proceedings of the Conference on Computer Vision Pattern Recognition, pp. 1701–1708 (2013)
12. Viola, P., Jones, M.: Robust real-time face detection. *Int. J. Comput. Vision* **57**(2), 137–154 (2004)
13. Zhu, X., Ramanan, D.: Face detection, pose estimation and landmark localization in the wild. In: Computer Vision and Pattern Recognition (CVPR) Providence, Rhode Island (2012). Available <http://www.ics.uci.edu/~xzhu/face/>
14. Zhao, W., Chellappa, R., Phillips, P., Rosenfeld, A.: Face recognition: a literature survey. *ACM Comput. Surveys* (2003)
15. Matthews, I., Baker, S.: Active appearance models revisited **60**(1), 135–164 (2004)
16. <https://in.mathworks.com/help/vision/ug/camera-calibration.html>
17. Hartley, R.I., Zisserman, A.: Multiple View Geometry in Computer Vision, 2nd edn. Cambridge University Press, ISBN:0521540518 (2004)
18. <http://www.cl.cam.ac.uk/research/dtg/attarchive/facedatabase.html>
19. <https://www.nist.gov/itl/iad/image-group/color-feret-database>
20. Li, A., Shan, S., Gan, W.: Coupled biasvariance tradeoff for crossspace face recognition. *IEEE Trans. Image Process.* **21**(1), 305–315 (2012)

An Autonomic Resource Allocation Framework for Service-Based Cloud Applications: A Proactive Approach



Tushar Bhardwaj, Himanshu Upadhyay, and Subhash Chander Sharma

Abstract The user's request changes dynamically in service-based cloud applications, which requires optimal amount of computing resources to meet service-level agreements (SLAs). The existing server-side resource allocation mechanisms have limitations in provisioning the required resources to handle the incoming load on the basis of user's requests. To overcome the aforementioned situation, cloud computing provides ample amount of computing resources to meet the SLAs. There are possibilities that cloud resources might not be properly utilized and might suffer over and under utilization. In this paper, the authors have proposed an autonomic resource allocation framework, that automatically provisions (allocate and de-allocate) the required computing resources as per the load. In this study, the proposed model leverages the linear regression model to predict the resources future usage and further leverage fuzzy logic controller to optimize the resource allocation process. The primary goal of this study is to improve the virtual resource utilization and response time with respect to the existing methods. Finally, the proposed model have been evaluated under real workload traces and results have shown that the proposed model minimize the SLA violation by at least 79% and cost by at least 28% as compared with other approaches.

Keywords Cloud computing · Service-based applications · Linear regression · Fuzzy logic controller

1 Introduction

“Cloud computing is a model for enabling convenient, on-demand network access to a shared pool of configurable computing resources (e.g. Networks, servers, storage, applications and services) that can be rapidly provisioned and released with minimal

T. Bhardwaj (✉) · H. Upadhyay
Applied Research Center, Florida International University, Miami, USA
e-mail: tushar.bhardwaj@fiu.edu

S. C. Sharma
Indian Institute of Technology Roorkee, Roorkee, India

management effort or service provider interaction” [1]. Cloud computing infrastructures create a virtual computing environment, providing service interfaces for their users to launch applications for importing/exporting virtual machine (VM) images with a variety of operating systems (OSs) [2].

In service-based cloud applications, the number of tasks/jobs per request changes drastically on the basis of its execution environment and behaviour of the application [3]. In practice, these requests need to be processed in real-time by the server-side mechanism so as to maintain the Quality-of-Service (QoS) [4]. Subsequently, the server-side may face two challenges: over-load and under-load conditions. The latter deals with the fact the number of requests is quite less as compared to the existing computing resources present in the server. Whereas, the former condition deals with the situation in which the number of user requests is too huge for the computing resources to handle [5].

Cloud computing, with its elasticity characteristics, can scale-out, scale-down, scale-up, and scale-in its computing resources on the basis of user requirement [6]. As the number of users increases on the cloud, load balancing, resource allocation and resource utilization have become the bottleneck for cloud service providers [7, 8]. It requires high computing and auto-scaling mechanisms so that the application may get processed in a minimum time frame for better performances [9].

In practical, a user submits the job through web interface to the cloud to get processed [10]. The job lands at the controller node, which checks the job (task) status (VIP or ordinary). After that, the controller node finds a suitable virtual machine (VM) for the job execution. If the VM is already executing other jobs (busy) then the upcoming jobs are stored in job queue and wait until VM has finished execution [11, 12]. Therefore, there is a need of an efficient resource allocation mechanisms that work at the controller layer to efficiently manage both the incoming tasks as well as the resources at the cloud. The current resource allocation mechanisms at server-side are inefficient in allocating the required computing resources to handle the workload of service-based cloud applications.

This study focuses on improving the utilization of virtual resources by efficient allocation and hence maintaining the response time for the application. Therefore, it is required to have a mechanism that scale-in and scale-out resources to meet the QoS parameters.

This paper presents an autonomous resource provisioning framework that dynamically allocates and de-allocates the computing resources as per the application’s requirements. The primary goal of this paper is to improve the virtual resource utilization and also maintain the response time as per the predefined SLAs between the client and the service provider. We have used the autonomic computing model that contains various phases that operates on a time interval basis. In this study, the proposed model leverages the linear regression model to predict the resources future usage and further leverage fuzzy logic controller to optimize the resource allocation process. The primary goal of this study is to improve the virtual resource utilization and response time with respect to the existing methods. Finally, the proposed model

has been evaluated under real workload traces and results have shown that the proposed model minimizes the SLA violation by at least 79% and cost by at least 28% as compared with other approaches.

The rest of the paper is structured as follows. Section 2 covers the literature survey that highlights the “resource allocation” mechanisms for “service-based” cloud services/applications. It covers the model, policy and objective metrics for the selected papers. Section 3 details the proposed autonomic resource allocation framework in detail. Section 4 presents the experimental setup and results analysis. Finally, Sect. 5 concludes the paper and highlights future work.

2 Literature Survey

This section showcases the work done in the area of dynamic resource allocation in cloud computing for service-based cloud applications. Table 1 comprises of the application type, model, policy and objective metrics from the related work.

In [13], the authors have presented a study that computes the response time and load of the virtual machine at every interval. This data is fed into the autonomic resource allocation module that leverages the linear regression model to predict and computes the number of virtual machines required to meet the SLAs. Authors in [14], presents the model that uses the simple heuristics for dynamic resource provisioning mechanism. The proposed model helps in reducing the scaling of virtual machines to a great deal and hence improves the response and execution time for ECG analysis applications. In [15], the authors have proposed a fuzzy logic based controller that computes the number of CPU cores required for a parallel scientific application. The study in [16], presents a heuristic approach that considers the response time and load on the VM at each monitoring interval to compute the number of virtual machines required. Authors in [17], have leveraged the queuing model to allocate the tasks to

Table 1 Papers related to dynamic resource allocation

References	Application type	Model	Policy	Objective metrics
[13]	Service-based	Linear regression	Proactive	Response time, load on VM
[14]	Service-based	Heuristic approach	Reactive	Response time
[15]	Parallel scientific	Fuzzy-based	Proactive	Response time, number of threads
[16]	Service-based	Heuristic approach	Reactive	Response time, load on VM
[17]	Service-based	Queuing model	Reactive	Response time
[18]	Service-based	Heuristic approach	Reactive	Response time, rejection percentage
[19]	Service-based	Heuristic approach	Reactive	Response time

the virtual machines on the basis of average response time. In [18], the authors have used the simple heuristic approach that computes the future resource requirements on the basis average response time. In [19], the authors propose a model on the basis of a heuristic approach that delivers the resources re-actively.

3 Autonomic Resource Allocation Framework

This section presents the proposed autonomic resource provisioning framework.

Cloud service provider handles many software and hardware modules. This paper proposed a framework, Fig. 1, for autonomic resource provisioning for service-based cloud applications [20]. The framework consists of the Software-as-a-service

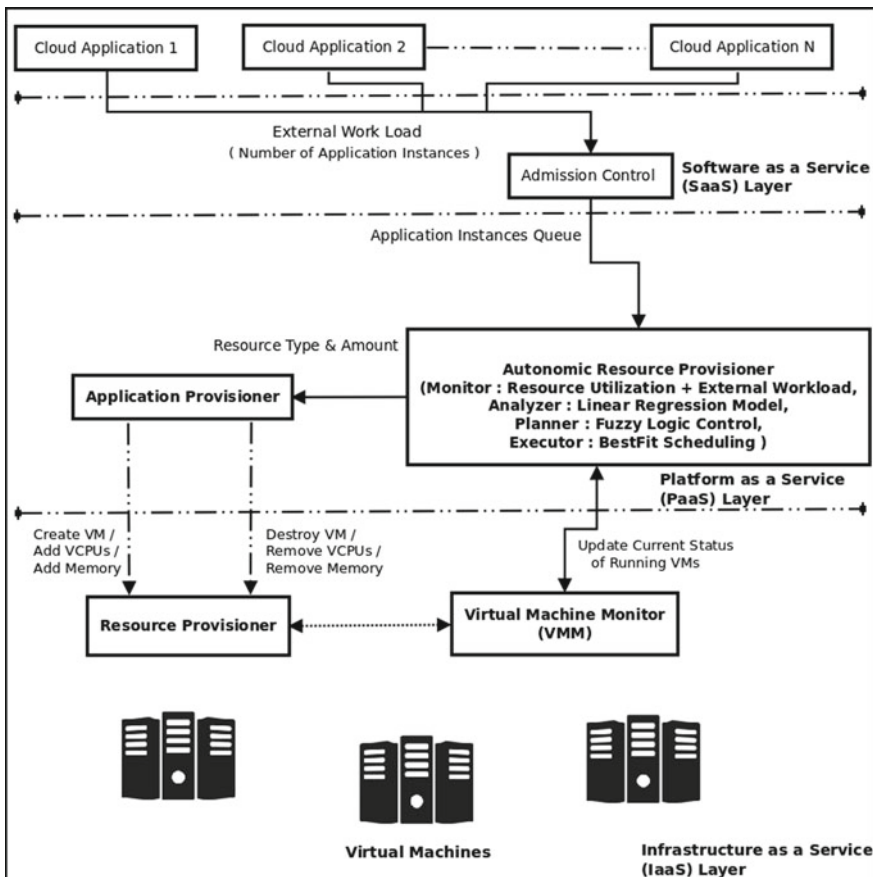


Fig. 1 High-level architecture of autonomic resource allocation framework

(SaaS) layers that encompass the “Admission Control Mechanism” which handles the incoming requests (job/task) from the service-based cloud applications. Subsequently, the control mechanism accepts and transfers the task/request with respect to the predefined SLAs to the Platform-as-a-service (PaaS) layer. PaaS layers leverage the “Application Provisioner” and “Autonomic Resource Provisioning Mechanism” [21, 22].

The application provisioner requests the Infrastructure-as-a-service (IaaS) layer for the required computing resources in terms of virtual machines. This layer comprises the cloud “data center” that provides the virtual resources which host the web-servers that handle the cloud applications via the internet.

The proposed model leverages the four iterative, functional, and step-wise concepts of “autonomous computing” provided by IBM research. The proposed autonomic resource allocation framework comprises of four distinct but inter-connected phases: “Monitor, Analyzer, Planner, and Executor”.

3.1 Mathematical Model

Let Data_n^r be the n th cloud application’s r th request. Each and every Data_n^r (request) is bound with the maximum deadline (time) DL_n^r .

The “load” of a Virtual Machine (VM) is computed in terms of “total length of tasks at time (Δt) on service queue of VM_i divided by the service rate of VM_i at time (Δt)”, Eq. (1) [7].

$$\text{Load[VM]} = \frac{\text{Total Length of Tasks } (T)}{\text{Processing speed of VM (mips)}} \quad (1)$$

The “total load of all the VMs at time interval (Δt)” is given by Eq. (2)

$$\text{Load}_{\text{total}}(\Delta t) = \sum_{i=0}^{\text{VM}_i(\Delta t)} \text{Load[VM, time}(\Delta t)] \quad (2)$$

Therefore, Eq. (3) gives the average load on VMs per interval.

$$\text{Load}_{\text{average}} = \frac{\text{Load}_{\text{total}}(\Delta t)}{\text{VM}_i(\Delta t)} \quad (3)$$

For a given task T , we have computed the system response time as per the Eq. (4).

$$\text{Response}_n^r = \text{FT}_n^r + \text{Waiting}_{\text{time}} \quad (4)$$

At each time interval, the total “response time” can be computed as the “sum of response time for each User_n ”, given by Eq. 5.

$$\text{Response}_{\text{total}}(\Delta t) = \sum_{i=0}^{\text{User}(\Delta t)} \text{Response}_n^r \quad (5)$$

The “average response time”, can be computed as the ratio of “total response time” Eq. (5) to “total number of users”, at each monitored time interval and given by Eq. (6).

$$\text{Response}_{\text{average}} = \frac{\text{Response}_{\text{total}}(\Delta t)}{\text{User}(\Delta t)} \quad (6)$$

When a User_n request fails to get processed as per the predefined SLA, then it is said to be get rejected. In this paper, we have computed the rejection percentage as the “ratio of number of User_n tasks processed according to SLA to the total number of requests per interval.”

$$\text{Delay}_n^r = \begin{cases} \text{FT}_n^r - \text{DL}_n^r & \text{FT}_n^r > \text{DL}_n^r \\ 0 & \text{otherwise} \end{cases} \quad (7)$$

As already mentioned, Delay_n^r shows the delay time given by Eq. (7).

To compute the occurrence of SLA violations, we compute delay time. If delay time is greater than zero, then it happens otherwise none, also given in Eq. (8).

$$\text{SLA}_{\text{violation}} = \begin{cases} \text{TRUE} & \text{Delay}_n^r > 0 \\ \text{FALSE} & \text{otherwise} \end{cases} \quad (8)$$

3.2 Monitor Phase

This is the first phase of the proposed resource allocation framework, which continuously monitors and collects the external load and the resource utilization on the virtual machine. In this paper, the authors have implemented the monitoring phase on each virtual machine (VM). It computes the load on each VM, over a given time interval (Eq. 1). In addition, it also monitors the VM for average response time (Eq. 7), and average rejection percentage (Eqs. 8 and 9) for at each interval.

3.3 Analysis Phase

The output from the “monitoring phase” acts as the inputs to this phase. The outputs are “requests arrival rate λ_i and average VM load (Load_i)” and it further analyzes

and predicts the optimal amount of the virtual resources required for the better performance of the cloud services in the “next time interval ($\Delta t + 1$)”. In this phase, we leverage the “linear regression model (LRM)” to forecast the “request arrival rate” and the “average VM load (Load_i)”. In general, for the given cloud service C_i at the time interval Δt , the linear regression model is presented by Eq. (9).

$$\text{Output}_{t+1} = \beta_1 + \beta_2 \times \text{Input}_t \quad (9)$$

In Eq. (9), the (t), is the “time interval indexes for the sample observation” and Output_t will be the value of the output, which can be “generalized” for both Load_{average} and requests arrival rate, respectively.

On the other hand, the Input_t is the timestamp that tells the actual value at which the given sample was captured. It has also been assumed that (n) is the total number of observed samples for “both performance metric parameters”. We have used “least square method” solve the linear regression equations and compute the values of β_1 and β_2 .

3.4 Planner Phase

The output values from the analysis phase are used by the planner phase to plan for the next iteration of the system. This phase has the capability to decide that a particular VM can handle the incoming real-time tasks or not. If the VM is unable to handle the incoming requests, then this phase initiates “a new instance” of that particular VM and re-schedule the incoming tasks to it.

This phase is bifurcated into two sub-phases. In the first phase, fuzzy controllers are leveraged to infer the number of VMs required by the application. To be precise, it computes the “degree of relevance” of the VM that affects the cloud service performances. The degree showcases the current requirement of more VMs for the application. In the second phase, the VM controller (on the basis of fuzzy controller) computes the “number of VM(s) required by the application” Fig. 2. All the decisions are made on the basis of performance metric parameters such as “average load (VMs), average response time (tasks), and the rejection percentage (tasks) over a monitored interval.”

3.5 Executor Phase

This phase is responsible for the execution of commands for VM initiation or termination from the planner phase. This phase contains all the details about the VM, such as (VM Id, host Id, data center) on which the VM is running.

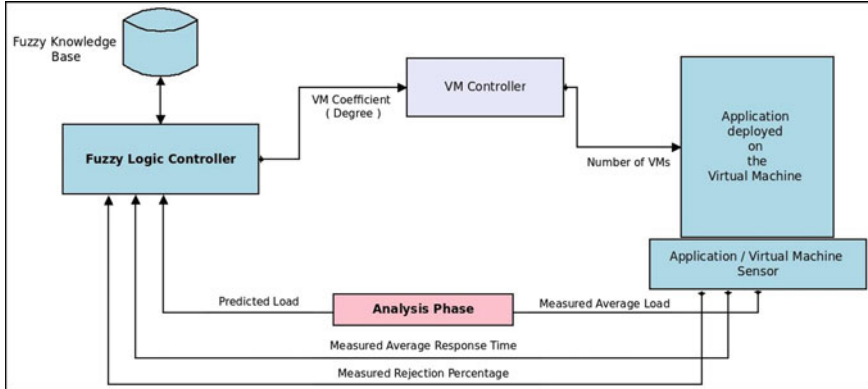


Fig. 2 Autonomic resource controller architecture

4 Simulation Setup and Results Analysis

This section highlights the experimental setup and result analysis of the proposed autonomic resource allocation model in detail. The cloud environment is setup using the Cloudsim [23] toolkit developed by the University of Melbourne. Cloud computing seems to be having an infinite number of computing resources, but practically, it is built on the top of a data center. Cloudsim helps in creating a configurable data center that consists of the list of blade servers.

On top of those mservers, host machines are created with specific host ID and PE (processing element); finally, this is added to the list of host machines. Each host machine is capable enough to create virtual machines depending upon each VMs' configuration. Each virtual machine has certain attributes such as Million instructions per second(MIPS), processing elements (PE), storage, etc. Therefore, to evaluate the proposed model, we leveraged the “real workload traces” for a server-based cloud application, ClarkNet traces [24]. There are certain distinct properties of this workload which makes the results more realistic and reliable for real-time cloud applications. Figure 3, showcases a sample of ClarkNet traces, which has been taken from “Metro Baltimore web server of Washington DC area, from August 1–31 1995.” Subsequently, the task/request which is called Cloudlet is being created with certain parameters such as TaskID, FileSize, Length, etc.

There is a broker in Cloudsim toolkit, which works similar to cloud controller, which sends the incoming requests/tasks to the specific VMs (on the basis of pre-defined scheduling policy). In this study, we have randomized the length of each Cloudlet on the basis of normal distribution.

In this paper, the proposed model has been evaluated under three scenarios with “response time, load on VM, and rejection percentage” as the QoS parameters. First, we refer this scenario as “MAPE (Response)”, in which the autonomic resource allocation in done on the basis of response time [13, 16, 25]. Second, the scenario is referred to as “MAPE (Processing)” that considers the load of the VM and allocates

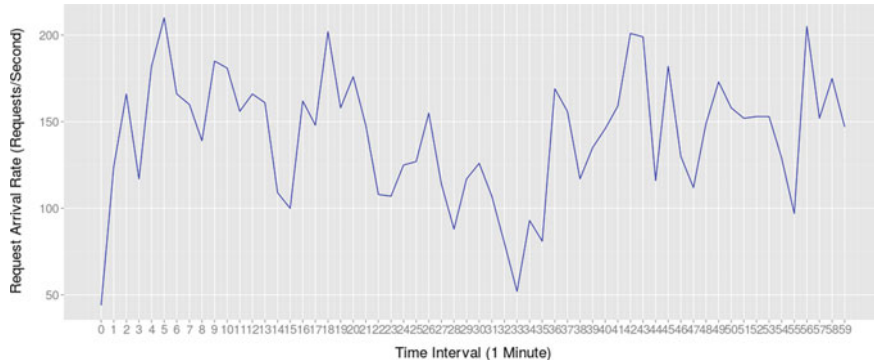


Fig. 3 Workload patterns: ClarkNet

resources accordingly [26, 27]. The last scenario, which is referred to as “MAPE (Rejection)” that allocates the resources on the basis of rejection percentage [19]. The reason behind selecting these models and comparing them with the proposed model is two-fold. First, all these models follow the control “MAPE” loop and secondly, all of these are proactive models for resource allocation.

The experimental results are computed and presented with respect to each of the performance metrics for resource utilization and QoS parameters.

Figure 4, showcase the “rejection percentage of SLA violation” with respect to the four models on the basis of ClarkNet real-time workloads for service-based cloud applications. The proposed model minimizes the SLA violation to a great deal with respect to the other approaches. Table 2, shows the average percentage rejection of SLA violation with respect to all compared approaches. It can be clearly observed that the proposed model gives 1.804421, whereas the MAPE (response), MAPE (processing) and MAPE (rejection) delivers 27.67964, 8.334668, 16.57139, respectively.

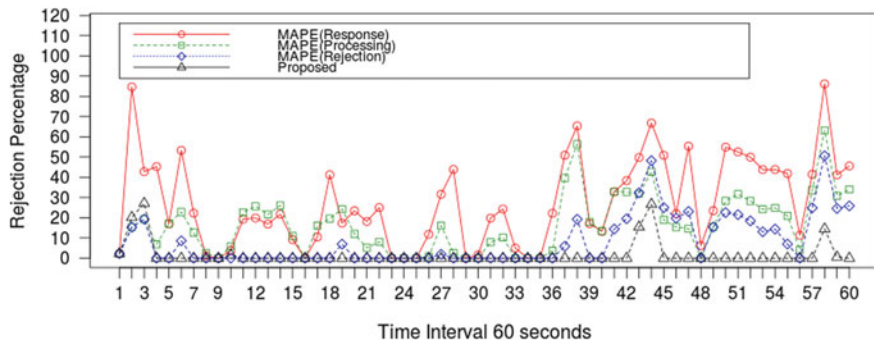


Fig. 4 Percentage of SLA violations

Table 2 Average of percentage of SLA violations

	Proposed	MAPE (response) [13, 16, 25]	MAPE (rejection) [19]	MAPE (processing) [26]
ClarkNet Workload	1.804421	27.67964	8.334668	16.57139

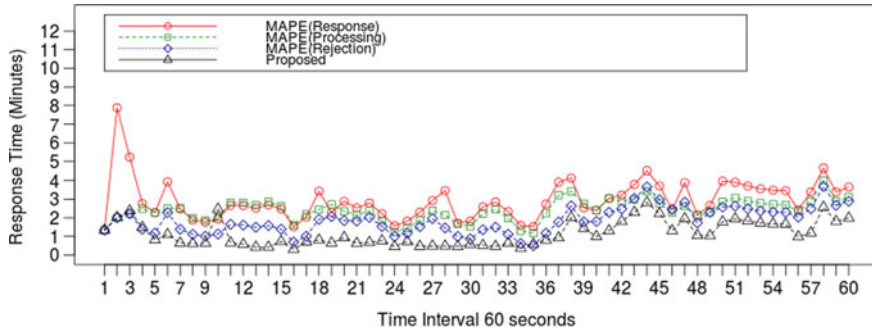
**Fig. 5** Average response time

Figure 5, showcase the response time variation at each time interval with respect to the four models on the basis of ClarkNet real-time workloads for service-based cloud applications. The proposed model delivers better finish time, which leads to improved response time with respect to the other resource allocation approaches. Table 3, showcases the comparative analysis of the average response time with respect to the four approaches. It can be clearly observed that the proposed model gives 1.153637 s of response time, whereas the MAPE (response), MAPE (rejection) and MAPE (processing) delivers 2.925818, 1.85217, 2.416054 s, respectively.

Figure 6, showcase the number of allocated VMs with respect to the four models on the basis of ClarkNet real-time workloads for service-based cloud applications. The proposed model delivers an adequate number of VMs at each interval. As observed from Fig. 3, the workload trace, at the 5th interval reaches 210 requests (approximately) and the proposed model initiates around 40 VMs to handle the incoming load. Table 4, shows the “average number of VMs allocated” for the four approaches. It can be clearly concluded that the proposed model uses 32 VMs, whereas the MAPE (response), MAPE (rejection) and MAPE (processing) uses 20, 26, 22 number of

Table 3 Average of response time

	Proposed	MAPE (response) [13, 16, 25]	MAPE (rejection) [19]	MAPE (processing) [26]
ClarkNet Workload	1.153637	2.925818	1.85217	2.416054

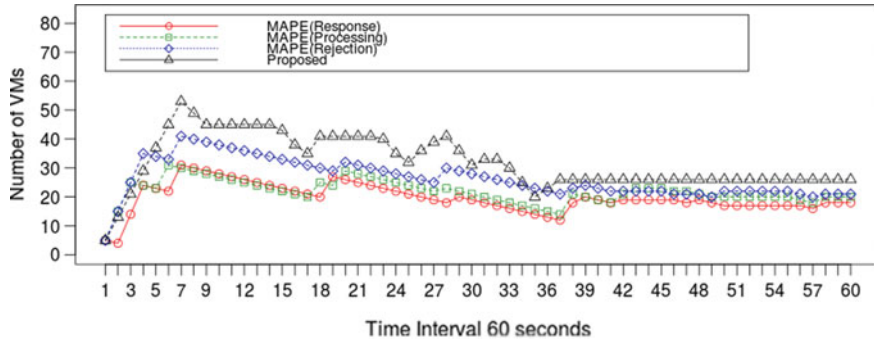


Fig. 6 Variations in number of allocated virtual machines (VMs)

Table 4 Average number of allocated VMs

	Proposed	MAPE (response) [13, 16, 25]	MAPE (rejection) [19]	MAPE (processing) [26]
ClarkNet Workload	32	20	26	22

VMs, respectively. It has been seen that the proposed autonomic resource allocation module leverages by far more VMs with respect to the rest of the compared approaches. But, the total cost justifies the performance of the proposed model even though it is using more number of VMs.

Figure 7 showcases the total cost for the allocated number of VMs with respect to the four models on the basis of ClarkNet real-time workloads for service-based cloud applications. The total cost is computed on the basis of virtual machine hours for each VM used by all the models.

Although, the proposed model initiates comparatively more “number of VMs” but it’s the amount of “virtual machine hours” and hence cost is less than other

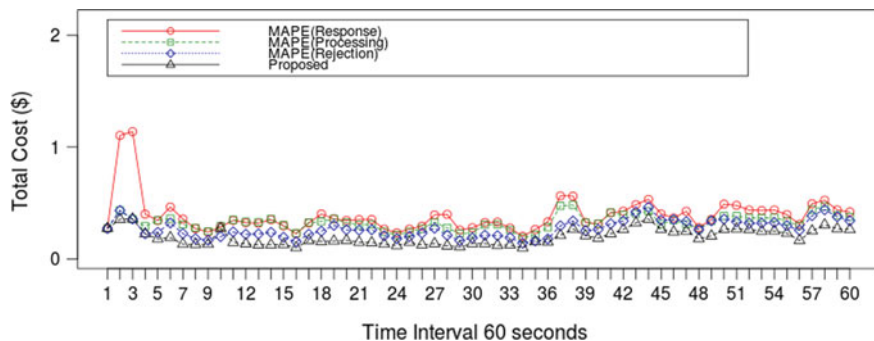


Fig. 7 Total cost variations

Table 5 Average of cost

	Proposed	MAPE (response) [13, 16, 25]	MAPE (rejection) [19]	MAPE (processing) [26]
ClarkNet Workload	0.1963491	0.3889213	0.271743	0.3278091

approaches. Table 5, shows the average cost for the four approaches. It can be clearly observed that the proposed model costs 0.1963491\$, whereas the MAPE (response), MAPE (rejection) and MAPE (processing) uses 0.3889213\$, 0.271743\$, 0.3278091\$, respectively.

5 Conclusions and Future Work

This paper highlights the limitations of the existing resource allocation mechanisms for autonomically adapting the resources with respect to the service-based cloud applications. To overcome this limitation, this paper presents an autonomic resource provisioning framework that allocates and de-allocates the computing resources at the server-side on with respect to the incoming load of the service-based cloud applications. The proposed model leverages the linear regression algorithm and fuzzy logic controller and takes “response time”, “rejection percentage” and “load on the virtual machine” as the fine-tuning parameter for decision-making. The results showcase that the proposed model efficiently allocates the computing resources (VMs) with respect to the load. The authors, in the future, will try to optimize the fuzzy logic rules and decision-making process using metaheuristic approaches.

References

1. Mell, P., Grance, T.: The NIST definition of cloud computing. <http://csrc.nist.gov/publications/nistpubs/800-145/SP800-145.pdf> (2011)
2. Ren, H., Lan, Y., Yin, C.: The load balancing algorithm in cloud computing environment. In: Proc. Conf. Computer Science and Network Technology, pp. 925–928 (2012)
3. Bhardwaj, T., Pandit, M.R., Sharma, T.K.: “A safer cloud”, data isolation and security by Tus-Man protocol. In: Proceedings of the Second International Conference on Soft Computing for Problem Solving (SocProS 2012). Advances in Intelligent Systems and Computing, vol. 236. Springer, New Delhi, 28–30 Dec 2012 (2014)
4. Bhanot, K., Peddoju, S.K., Bhardwaj, T.: A model to find optimal percentage of training and testing data for efficient ECG analysis using neural network. Int. J. Syst. Assur. Eng. Manag. (2015). <https://doi.org/10.1007/s13198-015-0398-7>
5. Bonatti, P.A., Festa, P.: On optimal service selection. In: Proceedings of the 14th International Conference on World Wide Web, ACM, pp. 530–538 (2005)
6. Zeng, L., Benatallah, B., Ngu, A.H., Dumas, M., Kalagnanam, J., Chang, H.: Qos-aware middleware for web services composition. IEEE Trans. Softw. Eng. **30**(5), 311–327 (2004)

7. Bhardwaj, T., Sharma, S.C.: Cloud-WBAN: an experimental framework for cloud-enabled wireless body area network with efficient virtual resource utilization. *Sustain. Comput. Inf. Syst.* **20**, 14–33 (2018)
8. Yu, T., Zhang, Y., Lin, K.-J.: Efficient algorithms for web services selection with end-to-end qos constraints. *ACM Trans. Web (TWEB)* **1**(1), 6 (2007)
9. Pandit, M.R., Bhardwaj, T., Khatri, V.: Steps towards web ubiquitous computing. In: Proceedings of the Second International Conference on Soft Computing for Problem Solving (SocProS 2012). Advances in Intelligent Systems and Computing, vol. 236. Springer, New Delhi, 28–30 Dec 2012 (2014)
10. Goudarzi, H., Pedram, M.: Maximizing profit in cloud computing system via resource allocation. In: Proceedings of IEEE Conference, International Conference on Distributed Computing System (ICDCSW), pp. 1–6 (2011)
11. Bhardwaj, T.: End-to-End data security for multi-tenant cloud environment. *J. Comput. Technol. Appl.* (2014). ISSN: 2229-6964
12. Ahn, Y.W., Cheng, A.M.K., Baek, J., Jo, M., Chen, H.H.: An auto-scaling mechanism for virtual resources to support mobile, pervasive, real-time healthcare applications in cloud computing. *IEEE Netw.* **27**, 62–68 (2013)
13. Pandey, S., Voorsluys, W., Niu, S., Khandoker, A., Buyya, R.: An autonomic cloud environment for hosting ECG data analysis services. *Future Gener. Comput. Syst.* **28**, 147–154 (2012)
14. Bhardwaj, T., Sharma, S.C.: An autonomic resource provisioning framework for efficient data collection in cloudlet-enabled wireless body area networks: a fuzzy-based proactive approach. *Soft Comput.* (2018)
15. Bhardwaj, T., Sharma, S.C.: Fuzzy logic-based elasticity controller for autonomic resource provisioning in parallel scientific applications: a cloud computing perspective. *Comput. Electr. Eng.* **70**, 1049–1073 (2018)
16. Bahrpeyma, F., Haghghi, H., Zakerolhosseini, A.: An adaptive RL based approach for dynamic resource provisioning in Cloud virtualized data centers. *Computing*, 1–26 (2015)
17. Bhardwaj, T., Sharma, S.C.: An efficient elasticity mechanism for server-based pervasive healthcare applications in cloud environment. In: 19th IEEE International Conference on High Performance Computing and Communications Workshops (HPCCWS), Bangkok, Thailand (2017)
18. Zheng, Z., Zhang, Y., Lyu, M.R.: Cloudrank: a qos-driven component ranking framework for cloud computing. In: 2010 29th IEEE Symposium on Reliable Distributed Systems, IEEE, pp. 184–193 (2010)
19. Kadarla, K., Sharma, S.C., Bhardwaj, T., Chaudhary, A.: A simulation study of response times in cloud environment for iot-based healthcare workloads. In: 14th IEEE International Conference on Mobile Ad Hoc and Sensor Systems (MASS-2017), pp. 678–683. <https://doi.org/10.1109/maсс.2017.85> (2017)
20. Bhardwaj, T., Kumar, M., Sharma, S.C.: Megh: a private cloud provisioning various IaaS and SaaS. In: Soft Computing: Theories and Applications. Advances in Intelligent Systems and Computing, vol. 584. Springer, Singapore (2016)
21. Bhardwaj, T., Sharma, S.C.: Internet of things: route search optimization applying ant colony algorithm and theory of computation. In: Proceedings of Fourth International Conference on Soft Computing for Problem Solving. Advances in Intelligent Systems and Computing, vol. 335. Springer, New Delhi (2015)
22. Bhardwaj, T., Sharma, T.K., Pandit, M.R.: Social engineering prevention by detecting malicious URLs using artificial bee colony algorithm. In: Proceedings of the Third International Conference on Soft Computing for Problem Solving. Advances in Intelligent Systems and Computing, vo. 258. Springer, New Delhi (2014)
23. Calheiros, R.N., Ranjan, R., Beloglazov, A., De Rose, C.A.F., Buyya, R.: Cloudsim: a toolkit for modeling and simulation of cloud computing environments and evaluation of resource provisioning algorithms. *Softw. Pract. Exp.* **41**, 23–50 (2011)
24. Clarknet-http-two weeks of http logs from the ClarkNet www server. <http://ita.ee.lbl.gov/html/contrib/ClarkNet-HTTP.html>. Accessed 10 Dec 17

25. Misra, S., Krishna, P.V., Kalaiselvan, K., Saritha, V., Obaidat, M.S.: Learning automata-based QoS framework for cloud IaaS. *IEEE Trans. Netw. Serv. Manage.* **11**(1), 15–24 (2014)
26. Calheiros, R.N., Ranjan, R., Buyya, R.: Virtual machine provisioning based on analytical performance and QoS. *Cloud Comput. Environ.* 295–304 (2011) <https://doi.org/10.1109/icpp.2011.17>
27. Sharma, T.K., Pant, M., Bhardwaj, T.: PSO ingrained artificial bee colony algorithm for solving continuous optimization problems. In: Proceedings of IEEE International Conference on Computer Applications and Industrial Electronics (ICCAIE), pp. 108–112, Malaysia (2011)

Index Point Detection and Semantic Indexing of Videos—A Comparative Review



Mehul Mahrishi and Sudha Morwal

Abstract Primarily used for fun and entertainment, videos are now a motivation behind social, commercial, and business activities. It is presumed that by 2025, about 75% of all Internet traffic will be of videos. In education, videos are a source of learning. Study Webs of Active Learning for Young Aspiring Minds (SWAYAM), National Programme on Technology Enhanced Learning (NPTEL), Massive Open Online Courses (MOOCs), Coursera, and many other similar platforms provide not only courseware but also beyond the curriculum contents apart from the conventional syllabi. Even at the junior level, Byju's and similar educational portals are witnessing an explosive growth in video contents. Despite that we are now able to extract semantic features from images, video sequences and besides being ubiquitous in nature, video lectures have a limitation of smooth navigation between topics. Through this paper, we want to throw light on existing automated video indexing approaches and their prerequisites that are recently proposed. We tried to analyze them based on some existing measures.

Keywords E-learning · Lecture videos · Video segmentation · Video indexing · Text similarity · Video analysis

1 Introduction

The augmented visualized digital content persuades the researchers to explore novel dimensions in terms of indexing and partitioning and thereby inducing a coherent structure of the video document. Automatic multimedia content generation of a captured video lecture is very old [1]. A survey at UC Berkeley states that up to 65% of students use videos for better understanding of topics, they missed in the class [2].

M. Mahrishi (✉) · S. Morwal
Swami Keshvanand Institute of Technology, Jaipur 302017, India
e-mail: mehul@skit.ac.in

S. Morwal
e-mail: sudha_morwal@yahoo.co.in

A video lecture comes with a limitation to waveringly access the concern topic. Adaptation of these videos is thus restricted especially for a lecture length of 60–90 min [3]. This review specially focuses on the literature that includes datasets of classroom lectures, online tutorials, open courseware, and similar resources with longer playback time. We conducted a formal study of steps and techniques for automatic video indexing and compared them on different criterion.

2 Motivation

Despite a lot of research in multimedia content analysis, major commercial giants like Google, Bing, etc., still rely on textual metadata [4]. The motivation behind this research is to provide proper video indexing to help the user to navigate between the topics in a video file and create a digital index for better information retrieval. Just as a textbook contains indexing on the basis of chapters and topics, through video indexing a reader can directly find locations where a particular topic is discussed in an educational video.

A video comprises a sequence of images and relative text information. Extraction of this textual information is very significant for effective video analysis and indexing. A user will see the indexed time stamps in the form of links of topics and subtopics within the video. Content wise browsing and switching of topics can be done just by clicking on the desired link.

A lot of work is done in relation to this which is not limited to extracting features, semantics, and related information from videos [5] and process like edge detection techniques [6], salient word ranking [7], etc.

3 Video Structure Analysis

Video structure analysis is a prerequisite and indispensably considered as the very first step in video analysis and automatic video indexing. It can be seen in Fig. 1 that a complete video clip is formed by combining a number of scenes which are actually a group of multiple shots.

The shortest unit of a video is an image frame. The figure shows only one instance of a video, i.e., one video clip. Likewise, there can be a number of clips comprising a complete video stream. A large portion of literature community has been devoted to the problem of segmentation of video into frames [8–12], shots [13–19] or scenes [20] on the basis of properties like color difference, edges detection, object association, histograms, motion cue, etc.

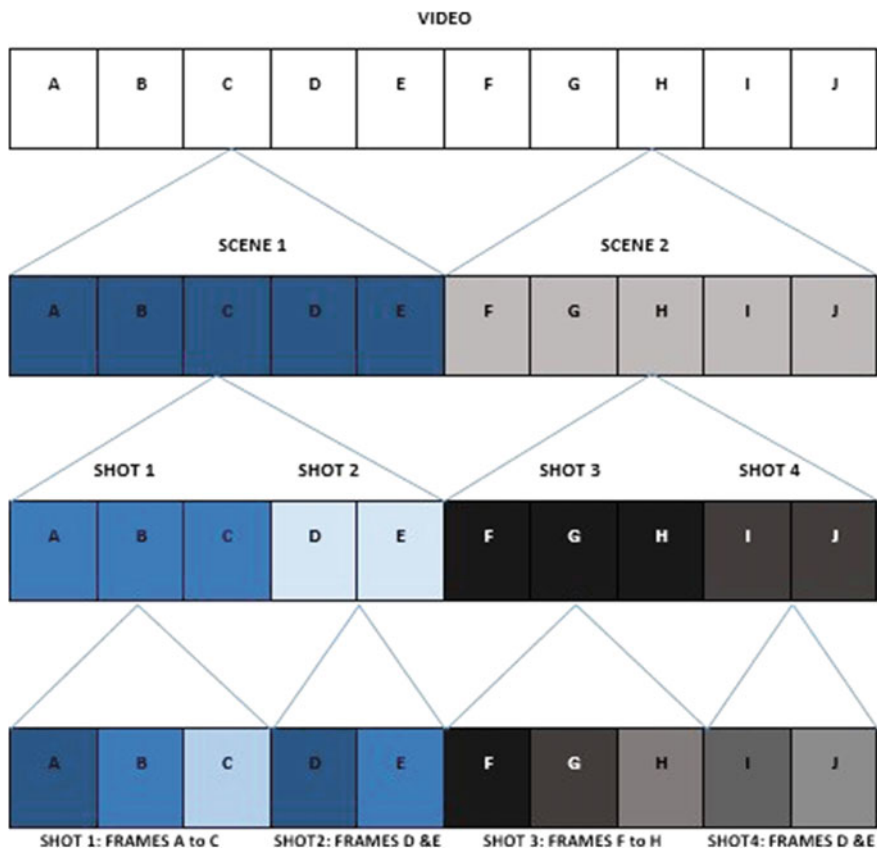


Fig. 1 Structure of video

4 Literature Review

4.1 Online Video Lecture

Rosalind Picard proposes affective video indexing in 1990, while defining effective computing [4]. Although affective annotations, like content annotation, will not be universal, they will still help reduce time searching for the right scene [21] (p. 11).

The idea of recording classroom lectures, presentations, and talks is longstanding [1, 22]. Similarly, the project NPTEL by MHRD, India [23], in which the transcribed files are given as .pdf files can be used to provide subtitles to the video (in English) and further for providing local language translations [24]. Hypervideo is another concept that applies the hypertext notion to a video but still they are manually indexed [25].

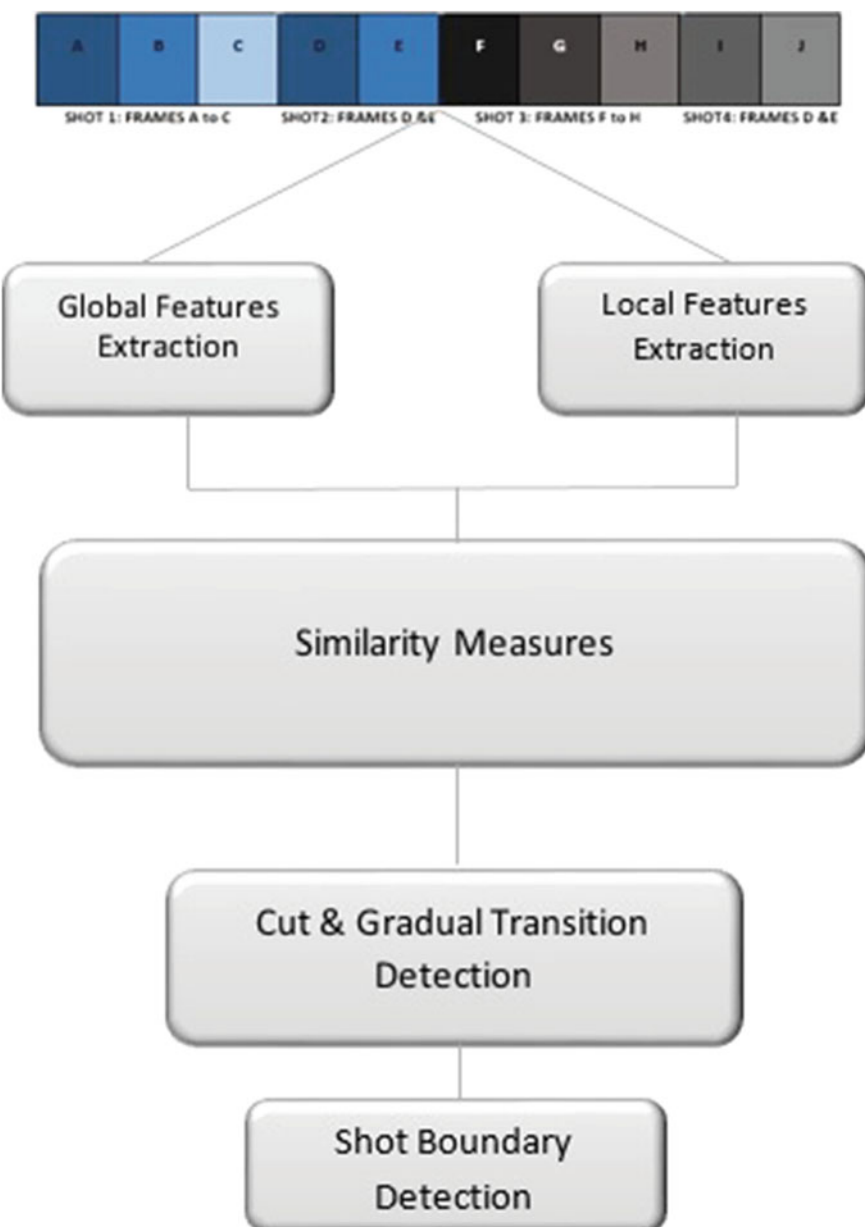


Fig. 2 Shot boundary detection framework

4.2 Video Segmentation

A video is a collection of sequence of scenes, which can be again decomposed into sequence of shots. For better segmentation of a video, accurate shot boundary detection is a must. More precise the boundary detection, greater is the indexing accuracy [26]. Figure 2 shows the steps involved in shot boundary detection. A shot can be defined as the longest continuous sequence instigated from a single camera take [20]. The content within a shot is continuous, and there is a strong content correlation among the frames.

Almost all approaches are detecting cut transitions, there are recent approaches that are focusing on detection of gradual transitions [27] and detecting the transition by amplitude, whereas in [14, 15, 28–32] distance of neighbor frames is computed to identify the CTs and generate the adaptive threshold for matching rate of frames for gradual transition identification. Tippaya et al. in multiple researches [8, 13, 33] use a rule-based classifier using one global threshold for only cut transition detection. In [34], Fourier transformation of the frame generated a salience map and then similarity measures are applied to detect abrupt change in the frames.

4.3 Text and Feature Extraction for Videos

The features can be classified as global features and local features, also called as descriptors. Image intensity or color histogram [16], pairwise pixel difference [17], edge [18] or combinations of different features called hybrid features [19] are few features of an image. Color histograms are the most common global feature of a video. They provide a good balance between accuracy and time [33]. Color histograms (CBH) are computed in RGB color space, whereas hue, saturation, and value (HSV) histograms encompass HSV color space. The HSV color space is more spontaneous because it describes a color in 3-D which in turn produces more robust detection results [29]. SIFT [30], SURF [13], Sobel edge detector [14], and MSER [35] are recently used, which employ histogram-based feature extraction techniques. CNN [15] and SVM [17] are learning-based classifiers.

4.4 Text Similarity

Most of the state-of-the-art algorithms are based on term-based text similarity which is the subset of string-based category. Density-based clustering (DBScan) [36] in which the density of a data object at a given point is considered as a measure of closeness. Euclidean distance matrices (EDMs) are a standard metric that contains squared distances between points [37]. Cosine similarity calculates the degree of similarity between two vectors, whereas the Jaccard coefficient calculates similarity

by calculating ratio between intersection and union of the objects [38]. Pearson correlation coefficient is very a popular method to determine vector similarity, on the other hand, the Kullback–Leibler divergence (KL divergence) defines similarity by calculating corresponding probability distribution [39].

4.5 Video Indexing

Words in a video may have different contexts at different locations. Sometimes, they are of great importance, whereas sometimes they only refer to a previous perspective [40]. It is therefore very important to recognize the significance of a word to the nature of its appearance. The standardized TREC conference series, supported by NIST, USA, updates the most popular TRECVID dataset every year [4, 41]. During our literature study, it was observed that TRECVID-2001 is the most popular dataset among researchers. Table 1 shows a comparative analysis and precision and recall comparison of different approaches based on the standard datasets used for the research. We observed that [15] is able to obtain a very substantial 95.3% recall and 98.6% precision using CNN with cosine similarity [28], suggested automated indexing of videos using OCR technology [6, 39, 42], worked on news dataset, and proposed a technique for automatic content recognition of the scenes. The limitation is that transcriptions are obtained through commercial tools, and news scenes will fall in one of the predefined six categories.

A video comprises either stills (frames) or moving images (video skims) [43]. These frames (specifically key frames) or video skims are joined by either a cut or a gradual effect. MMToC [7] obtained a ranking model for salient words. The words were extracted from both visual slides and speech for which speech transcripts were used. A cost function is formulated based on the ranked words. Dynamic programming optimization technique is used to generate the topic wise indexing of the video.

Lecture video segmentation based on the linguistic features of text [5] is somewhat similar to what we are proposing in our research. It extracts the text segments from the lecture videos and compares where the similarity among the text boundary is low. The major challenge faced by video indexing researchers is to differentiate between the context of the video, i.e., impact of the videos and descriptions that refers to the literal content of the video [44].

4.6 Learning in Video Analysis

Machine learning has an ability to automatically build a classifier by learning, from a historical dataset [45]. Feature extraction [46–48], video classification [6, 49–53], synchronization of video scenes [42, 54], and change in scene in a dynamic video [55] are the major applications where machine learning is already being used vigorously. Apart from this, deep learning has also left its footprints in scene detection, video

Table 1 Comparative analysis of approaches based on dataset used

Dataset	Year	Author	Approach	Feature extraction	Similarity measures	Recall (%)	Precision (%)
Random dataset	2018	Chongke Bi et al.	Dynamic mode decomposition	HSV Histogram	Amplitude	85.6	91.6
	2018	R. Shen et al.	Hybrid approach of HLFPN and keypoint matching	Global histogram	Histogram difference, speeded-up robust features (SURF)	72.39	86.56
	2016	Hannane et al.	SIFT-point distribution histogram	Difference of Gaussian by scale invariant feature transform (SIFT) algorithm	Euclidean distance	96.49	95.87
CC_Web_Video dataset	2015	Sangchul Kim et.al.	Combination of luminance and motion features	Global histogram	Chi-square distance method	97.36	92.61
TRECVID-2001	2017	Zhe Yang et al.	OTSU's method and dual Pauta criterion	HSV histogram	Cosine distance	94	96.9
	2017	J. Cao et al.	Support vector machine in compressed domain	3-class SVM classifier		93.3	98.3
	2017	Tippaya et al.	Multimodal visual feature-based	Speeded-up robust features (SURF) matching score color histogram	Cosine similarity	87.3	90.7
	2017	Thounaojam et al.	perceptual and semantic information	Gist Feature Extraction	Pearson correlation coefficient	95.6	85.2

(continued)

Table 1 (continued)

Dataset	Year	Author	Approach	Feature extraction	Similarity measures	Recall (%)	Precision (%)
	2017	Youssef et al.	Adaptive low rank and SVD updating	Block histograms	Euclidean norm	93	92
	2016	Shekar et.al.	Spectral residual saliency map	Spectral residual approach	Saliency map	95.65	88.55
	2016	Zongjie Li et al.	Multilevel difference of color histograms	HSV histogram	Euclidean distance	84	89
	2016	Rashmi et al.	Weighted edge information	Histogram	Sobel edge detector	86	85
	2016	D.M. Thounaojam et al.	Genetic algorithm and fuzzy logic	Color histogram	Histogram difference based on RGB intensity	93.1	88.7
	2016	Jingwei Xu et al.	Using convolutional neural networks	CNN	Cosine similarity	95.3	98.6
	2016	Zheng et al.	GPU accelerated	GPU block HSV histograms and GPU SURF	k-nearest neighbor (KNN) search on GPU	63.59	90.35
	2016	Hannane et al.	SIFT-point distribution histogram	Difference of Gaussian by scale invariant feature transform (SIFT) algorithm	Euclidean distance	98.7	91.3
	2015	Fang Liu	Two threshold method	HSV histogram	Image subsampling	93.4	95.2
	2015	Lee et al.	Graph theory	Color histograms with keypoint feature matching	Descriptor match and minmax cut algorithm	82.6	91.84

(continued)

Table 1 (continued)

Dataset	Year	Author	Approach	Feature extraction	Similarity measures	Recall (%)	Precision (%)
TRECVID-2002	2017	Youssef et al.	Adaptive low rank and SVD updating	Block histograms	Euclidean norm	92	93
	2016	Zheng et al.	GPU-Accelerated	GPU Block HSV Histograms	k-nearest neighbor (KNN) search on GPU	63.59	90.35
TRECVID-2005	2017	Youssef et al.	Adaptive Low Rank and SVD-Upditing	Block Histograms	Euclidean Norm	91	92
	2016	Zheng et al.	GPU accelerated	GPU block HSV histograms	k-nearest neighbor (KNN) search on GPU	63.59	90.35
Thailand Professional Golf Association Tournament	2015	S. Tipphaya et al.	SVM classifier	Color histogram	Chi-square distance method	97.09	97.79
	2015	S. Tipphaya et al.	Candidate segment selection and transition pattern analysis	Color histograms	Pearson's correlation coefficient (PCC)	97.54	95.83

segmentation, and concept detection [56]. CNN is used for obtaining global video-level descriptors, video classification, and retrieval [57–59], whereas limited research titles also exist that are working for automatic video indexing and summarizing [60].

5 Conclusion

Due to tremendous growth in the volume of video database, it is very important to browse the video directly through the content rather than accessing the entire video. Therefore, video indexing exhibits a wide spectrum and motivates the researchers worldwide. Through this research, we want to propose a review of existing research and steps involved in automatic text-based indexing method for topic wise segmentation of video lectures. We also tried to present some state-of-the-art algorithms and techniques which are in use through their comparison on standard datasets.

References

1. Abowd, G.D.: Classroom 2000: an experiment with the instrumentation of a living educational environment. *IBM Syst. J.* **38**, 508–530 (2000)
2. Harley, D., Henke, J., Lawrence, S., Mc-Martin, F., Maher, M., Gawlik, M., Muller, P.: Costs, culture, and complexity: an analysis of technology enhancements in a large lecture course, at UC Berkeley. *Cent. Stud. High. Educ.* (2003)
3. Tuna, T., et al.: Indexed captioned searchable videos: a learning companion for STEM coursework. *J. Sci. Educ. Technol.* **26**(1), 8299 (2017)
4. Yang, Z.-J.Z.: Exploiting web images for semantic video indexing via robust sample-specific loss. *IEEE Trans. Multimedia* **16**(6) (2014)
5. Lin, M., Nunamaker, J.J.F., Chau, M., Chen, H.: Segmentation of lecture videos based on text: a method combining multiple linguistic features, *J. System Sciences*, 2004. Proceedings of the 37th IEEE Annual Hawaii International Conference, p. 9(2004)
6. Percannella, G., Sorrentino, D., Vento, M.: Automatic indexing of news videos through text classification techniques. In: *Pattern Recognition and Image Analysis*, vol. 3687 of *Lecture Notes in Computer Science*, pp. 512–521. Springer, Berlin (2005)
7. Biswas, A., Gandhi, A., Deshmukh, O.: MM-TOC: a multi modal method for table of content creation in educational videos. In: *Proceedings of the 23rd ACM International Conference on Multi-media*, ACM, New York, NY, USA, pp. 621–630 (2015)
8. Tippaya, S., et al.: Video shot boundary detection based on candidate segment selection and transition pattern analysis. In: *IEEE International Conference on Digital Signal Processing (DSP)* (2015)
9. Sze, K.W., Lam, K.M., Qiu, G.: A new key frame representation for video segment retrieval. *IEEE Trans. Circuits Syst. Video Technol.* **15**(9), 11481155 (2005)
10. Truong, B.T., Venkatesh, S.: Video abstraction: a systematic review and classification. *ACM Trans. Multimedia Comput. Commun. Appl.* **3**(1), 3 (2007)
11. Besiris, D., Laskaris, N., Fotopoulou, F., Economou, G.: Key frame extraction in video sequences: a vantage points approach. In: *2007 IEEE 9th Workshop on Multimedia Signal Processing*, pp. 434–437 (2007)
12. Mukherjee, D.P., Das, S.K., Saha, S.: Key frame estimation in video using randomness measure of feature point pattern. *IEEE Trans. Circuits Syst. Video Technol.* **17**(5), 612–620 (2007)

13. Tippaya, S., et al.: Multi-modal visual features-based video shot boundary detection. *IEEE Access* **5**, 12563–12575 (2017)
14. Rashmi, B., et al.: Abrupt shot detection in video using weighted edge information. In: ICIA (2016)
15. Xu, J., et al.: Shot boundary detection using convolutional neural networks VCIP (2016)
16. Lin, G.S., Chang, M.-K., Chiu, S.-T.: Video-shot transition detection using spatio temporal analysis and fuzzy classification. In: Proceedings of the Circuits and Systems (2009)
17. Ling, X., Yuanxin, O., Huan, L., Zhang, X.: A method for fast shot boundary detection based on SVM. In: Proceedings of the Second International Congress on the Image and Signal Processing. CISP 08, pp. 445–449 (2008)
18. Lakshmi Priya, G.G., Dominic, S.: Edge strength extraction using orthogonal vectors for shot boundary detection. *Proc. Technol.* **6**, 247–254 (2012)
19. Ren, J., Jiang, J., Chen, J.: Shot boundary detection in MPEG videos using local and global indicators. *IEEE Trans. Circuits Syst. Video Technol.* **19**(8) (2009)
20. Huang, C.-L., Liao, B.-Y.: A robust scene change detection method for video segmentation circuits and systems for video technology. *IEEE Trans.* **1**(12), 1281–1288 (2001)
21. Picard, R.W.: Affective computing MIT, Media Laboratory Perceptual Computing Section. *Tech. Rep.* **321** (1995)
22. Ahanger, G., Little, T.D.: A survey of technologies for parsing and indexing digital video. *J. Vision Commun. Image Rep.* **7**(1), 28–43 (1996)
23. Project Document, National Programme on Technology Enhanced Learning (NPTEL) (2003–2007)
24. Krishnan, M.S., et al.: Text transcription of technical video lectures and creation of search able video index. *Metadata and Online Quizzes, Project Proposal* (2013)
25. Sauli, F., Cattaneo, A., vander Meij, H.: Hypervideo for educational purposes: a literature review on a multifaceted technological tool. *J. Technol. Pedagogy Educ.* (2017)
26. Lienhart, R.: Reliable dissolve detection. In: Proceedings of the SPIE Storage Retrieval Media Database, vol. 4315, 219–230 (2001)
27. Bi, C., et al.: Dynamic mode decomposition based video shot detection. *IEEE J. Transl. Content Mining* **6**, 2169–3536 (2018)
28. Yang, H., Siebert, M., Lhne, P., Sack, H., Meinel, C.: Lecture video indexing and analysis using video OCR technology. In: 7th International Conference on Signal Image Technology and Internet Based Systems (2011)
29. Liu, F., Wan, Y.: Improving the video shot boundary detection using the HSV color space and image subsampling 7th International Conference on Advanced Computational Intelligence (2015)
30. Hannane, R., Elboush, A.: An efficient method for video shot boundary detection and key frame extraction using SIFT-point distribution histogram. *Int. J. Multimedia Info. Retrieval* **5**(2), 89–104 (2016)
31. Thounaojam, D.M., et al.: A genetic algorithm and fuzzy logic approach for video shot boundary detection. *Comput. Intell. Neurosci.* (2016)
32. Shen, et al.: Automatic detection of video shot boundary in social media using a hybrid approach of HLFPN and key point matching. *IEEE Trans. Comput. Soc. Syst.* **5**(1) (2018)
33. Tippaya, S., et al.: A study of discriminant visual descriptors for sport video shot boundary detection. In: 10th Asian Control Conference (ASCC) (2015)
34. Shekar, B.H., et al.: Shot boundary detection using correlation based spectral residual saliency map. In: International Conference on Advances in Computing, Communications and Informatics (ICACCI) (2016)
35. Thounaojam, D.M., et al.: Shot boundary detection using perceptual and semantic information. *Int. J. Multimedia Inf. Retrieval* **6**(2), 167–174 (2017)
36. Ester, M., Kriegel, H.P., Sander, J., Xu, X.: A density-based algorithm for discovering clusters in large spatial databases with noise. In: International Conference on KDD (1996)
37. Dokmanic, I., et al.: Euclidean distance matrices: essential theory, algorithms, and applications. *IEEE Sign. Process. Maga.* **32**(6) (2015)

38. Yates, R.B., Neto, B.R.: *Modern Information Retrieval*. Addison-Wesley, New York (1999)
39. Huang, A.: Similarity measures for text document clustering. New Zealand Computer Science Research Student Conference (2008)
40. Lienhart, R., et al.: Automatic text segmentation and text recognition for video indexing. *Multimedia Syst.* **8**, 69–81 (2000)
41. Guidelines for TRECVID, October (2016)
42. Sahare, P., et al.: Review of text extraction algorithms for scene text and document images. *IETE Tech. Rev.* **34**(2), 144–164 (2017)
43. Truong, B.T., Venkatesh, S. : Video abstraction: a systematic review and classification. *ACM Trans. Multimedia Comput. Commun. Appl.* **3**, 1, Article 3 (2007)
44. Shrivakshan, G., Chandrasekar, C.: A comparison of various edge detection techniques used in image processing, *I. J. Comput. Sci. Issues* **9**, **5**, 269–276 (2012)
45. Samuel, A.L.: Some studies in machine learning using the game of checkers *IBM. J. Res. Development* **3**(3), 210229 (1959)
46. Diken, G., et al.: A review on feature extraction for speaker recognition under degraded conditions. *IEEE Techn. Rev.* pp. 321–332 (2016)
47. Kumar, R.: Speaker verification from short utterance perspective: a review. *IETE Tech. Rev.* (2017)
48. Adcock, J., et al.: TalkMiner: a lecture webcast search engine. MM10, October 25–29 (2010)
49. Camstra, F., Vinciarelli.: A Video segmentation and keyframe extraction. In: *Machine Learning for Audio, Image and Video Analysis, Advanced Information and Knowledge Processing*, pp. 413–430. Springer, London (2008)
50. Abdel-Mottaleb, M., et al.: CONIVAS: CONtent based Image and video access system. *ACM Multimedia* (1996)
51. Hearst, M.A.: TextTiling: A Quantitative Approach to Discourse Segmentation Technical Report. University of California at Berkeley, Berkeley, CA, USA (1993)
52. Sebastiani, F., et al.: Machine learning in automated text categorization. *ACM Comput. Surv.* **34**(1), pp. 1–47(2002)
53. Nandzik, J., et al.: CONTENTUS Technologies for Next Generation Multimedia Libraries Automatic Multimedia Processing for Semantic Search. Springer Science Business Media, LLC (2012)
54. Haberdar, H., Shah, S.K.: Change detection in dynamic scenes using local adaptive transform, *British Machine Vision Conference*, p. 6. BMVA Press (2013)
55. Haberdar, H., Shah, S.K.: Video synchronization as one-class learning 27th Conference on Image and Vision Computing New Zealand, pp. 469–474. ACM (2012)
56. Baraldi, L., et al.: A browsing and retrieval system for broadcast videos using scene detection and automatic annotation MM (2016)
57. Podlesnaya, A., et al.: Deep learning based semantic video indexing and retrieval. In: *Proceedings of SAI Intelligent Systems Conference (IntelliSys)*, pp. 359–372 (2016)
58. Yue-Hei Ng, J., et al.: Beyond short snippets: deep networks for video classification CVPR (open access) (2015)
59. Karpathy, A., et al.: Large-scale video classification with convolutional neural networks. In: *IEEE Conference on Computer Vision and Pattern Recognition* (2014)
60. Baraldi, L., et al.: Neural story: an interactive multimedia system for video indexing and re-use. In: *Proceedings of the 15th International Workshop on CBMI '17*, Article No. 21 Florence, Italy (2017)

Classification of Neuromuscular Disorders Using Machine Learning Techniques



Anuj Singh, Arun Vikram, M. P. Singh, and Sudhakar Tripathi

Abstract In this research, we have done the classification of Neuromuscular Disorders using different machine learning techniques. Neuromuscular disorders include the diseases that affect nerves and muscles and causes muscle numbness, weakness and twitching. The diseases have been classified into 16 groups on basis of enzyme classification scheme. Here we have discussed an approach to classify neuromuscular disorders using 42 different features (39 sequence annotations with enzyme class, mass and length of each genes) obtained from Uniprot Database. We have applied different machine learning algorithms like C5.0, Random Trees, Bayesian Net and Support Vector Machine (SVM) in which, the maximum accuracy of around 84.86% was obtained using SVM.

Keywords Bioinformatics · Machine learning · Classification tree · Predictive analytics

1 Introduction

Machine learning uses various statistical techniques enabling computer systems to improve the performance of a specific task automatically without being programmed. Machine learning when combined with data mining mostly focuses on exploratory data analysis. In data analytics, it helps to create complex models and algorithms for performing prediction. Commercially, this is called data analytics. It helps data

A. Singh (✉) · A. Vikram · M. P. Singh
NIT Patna, Bihar, India
e-mail: anujsingh.cse16@nitp.ac.in

A. Vikram
e-mail: arun.m.tech1628006@nitp.ac.in

M. P. Singh
e-mail: mps@nitp.ac.in

S. Tripathi
REC Ambedkarnagar, Akbarpur, UP, India
e-mail: stripathi.cse@nitp.ac.in

scientists, researchers, analysts and engineers in producing repeatable and reliable decisions and at the same time, discovering new facts.

As an interdisciplinary science, bioinformatics helps in interpreting biological data with the help of statistical methods and computer science. There is a lot of potential for machine learning in the field of Bioinformatics. It is derived from disciplines such as computer science, applied mathematics, and statistics to understand and organize related information. Deep learning, as a machine learning technique, uses automatic feature learning. So that, on basis of the dataset, the multiple features can be combined using the algorithm, into a more abstract set of features. This, subsequently, can be used to conduct further learning. In the present era, the biggest problem in bioinformatics is the conversion of large amount of data, provided by newly developed technologies to information. Machine learning could be a boon for this type of conversion. Neuromuscular disorder [1] is a very broad term that encompasses many diseases and ailments that impair the working of the muscles, either directly, being disorders of the voluntary muscle, or indirectly, being disorders of nerves or neuromuscular junctions [2].

Analysis of huge amount of biological datasets requires extracting facts from the data by generalizations. Protein structure prediction [3], classification of neuromuscular disorders, clustering of gene expression data, gene classification, statistical modeling of protein-protein interaction [3], etc. requires this type of analysis. One of the active areas of research in computational biology is the use of data mining techniques to solve biological problems. It can't be assumed that a particular disease can be caused by mutation of a particular gene because of two concurrent phenomenon known as phenotypic convergence and phenotypic divergence. In phenotypic convergence [4] one disease is caused by mutation of several genes. e.g.: Charcot-Marie-Tooth. In phenotypic divergence [4] one mutated gene could indicate multiple diseases. e.g.: lamin A/C.

Predictive analytics [5] deals with examination of the past historical data to reveal hidden pattern as well as provide new insights applying techniques from machine learning, artificial intelligence, statistics and modeling. These tools assist in process of prediction and extraction which help out the users in correct decision making. In this paper we have focused mainly on performing predictive analysis for classification of Neuromuscular Disorders using Machine learning models like C5.0 [6], Random Tree [7], Bayesian Net and SVM on SPSS Modeler [5].

2 Literature Survey

Electromyography plays a very essential role in medical diagnosis that indicate the type of abnormality and also expose disorders that are medically uncertain. Needle electromyography evaluates the neurophysiologic behavior of neuromuscular disorders [8]. Surface electromyography is not used on a large scale, because examination of Surface Electromyography by many research groups have produced poor results,

so it is not used generally. Entropy of surface electromyography was used to distinguish low-back pain from others without pain [9]. The study of entropy values from subject showed significant difference after the features of the surface electromyography signals are obtained, they can be classified. Various classification systems that are applying mainly classification of neuromuscular disorders were SVM [10] and c5.0 [6].

Electromyography is used for evaluating and also recording the electrical activity produced by human or some other living beings skeletal muscles. It is an electro diagnostic medicine technique. Electromyography is performed using electromyograph. Electromyograph detects the electric potential. Electric potential generated by human muscle cells when the cells are neurologically or electrically activated. The signals are resolve to predicts biomedical abnormalities or to consider the bio mechanics of human. Electromyography testing has a variety of biomedical and clinical applications. Electromyography is used as a diagnostics tool for finding neuromuscular disorders, or a tool for studying kinesiology. Electromyography signals are sometimes used to guide phenol injections into muscles. Electromyography are also used as a control signal for prosthetic hands, lower limbs and arms. Electromyography is performed with another electro diagnostic test that evaluate the conducting function of nerves, this is called a NCS [7]. Needle Electromyography Are indicated when there is pain in the limbs, spinal nerve compression, or worry about other neurological disorder. Electromyography based methods are not absolute for diagnosis in the initial stage of the disease. Electromyographic signal description is unfavorable in the diagnosis of neuromuscular disorders [8].

In paper [11], author present an impressive multi-classifier approach to increase the classification accuracy for diagnosis of neuromuscular disease. They used time domain and time-frequency domain appearance of MUAPs obtain from electromyogram signal. Authors have investigated time domain features and time frequency domain features. SVM and KNN classifier are used to guess class label for an inclined MUAP. Examination is carry out on clinical electromyogram database for the classification of disorders.

In paper [14], authors have used svm classifier and recorded surface electromyograms (sEMGs) for classification of Neuromuscular disorders. They had performed leave-one-out cross-validation deploying a binary classification schema for which the subjects were distinguished with 81.5% accuracy and a three-class classification with an accuracy of around 70.4%.

3 Research Methodology

3.1 Data Preparation

The list of genes were obtained from Musclegene [4] table, which is published annually in the month of December. With an aim to provide whosoever concerned

Table 1 Neuromuscular disorder groups

Id	Name	Description	Count
D1	Muscular dystrophies	Breakdown and weakening of skeletal muscles increases	24
D2	Congenital muscular dystrophies	Degenerative, genetic diseases affecting mostly voluntary muscles	10
D3	Congenital myopathies	Causes hypotonia and weakness of muscles	8
D4	Distal myopathies	Voluntary distal muscles become weak	2
D5	Other myopathies	Defect in functioning of muscle fibres	25
D6	Myotonic syndromes	Inherited disorders	4
D7	Ion channel muscle diseases	Caused by disturbed function of ion channel subunits	7
D8	Malignant hyperthermia	Muscle rigidity with rising body temperature	4
D9	Metabolic myopathies	Dysfunction of skeletal muscles	9
D10	Hereditary cardiomyopathies	Causes cardiac diseases in various age groups	40
D11	Congenital myasthenic syndromes	Physical exertion increasing the weakness of muscles	11
D12	Motor neuron diseases	Degeneration and death of motor neurons	16
D13	Hereditary ataxias	Progressive incoordination of gait	27
D14	Hereditary motor and sensory neuropathies	Neural development and degradation of neural tissue	30
D15	Hereditary paraplegias	Gait Disorders	14
D16	Other neuromuscular disorders	Uncategorized neuromuscular disorders	20

with Neuromuscular Disorders with a complete list of regularly updated monogenic muscle diseases. Till 2017, the diseases are classified into 16 groups as in Table 1. The dataset for sequence annotations of different human genes for the respective groups were obtained from Uniprot.

3.2 Tools

In this paper we have used SPSS Modeler Data Mining tool [5] to generate the Confusion Matrix. SPSS is a widely used Predictive Analytics tool from IBM [5]. 10 fold cross validation has been applied on our datasets for its manipulation. The list of genes for different Neuromuscular Disorders are obtained from musclegenetable [4].

Initially, Enzyme Class, Mass and Length corresponding to each gene were obtained from Uniprot Database. Then the Sequence Annotations corresponding to each of the genes were obtained from uniprot. Using SPSS Modeler, a modeler stream was created. Dataset is included in the modeled stream along with sequence annotations, that are selected as features and neuromuscular disorder groups were chosen as the target. We then applied C5.0 [12], Neural Net, Bayesian Net and Support vector machine algorithms on the modeler stream for analyzing the efficiency of the model.

3.3 Feature Selection

In order to reduce the large dimensionality of the dataset, feature selection was used. Feature Selection was done to improve prediction performance, make fast and more economical models, offer more awareness into the underlying processes [13, 16].

In this research, feature selection using following three methods was performed:-

- **Predictor Importance of Variables (PI)** basically describes the importance of each predictor in making a prediction. It is not related to the model accuracy. The relative importance of each predictor is used to estimate the model where the sum of the values for all selected predictors is 1.0.
- **Filter Methods** are those methods in which feature selection is done on the basis of their respective scores in different statistical tests. Here, F-Static test has been used since the features were continuous and the target was categorical.
- **Wrapper Methods** are those methods each subset of features of the original dataset is used to train a model and their performance is compared. On basis of the results that is obtained from the initial model, more features are added or removed from your subset mimicking a search problem. Thus the time complexity is often very high [15].

3.4 Confusion Matrix

In order to perform the validation process, a confusion matrix was created after generating a model using different learning techniques. A confusion matrix is basically used to describe the performance of a classifier on a set of test data for which the true values are known. It shows the experimental results of that model. For example TP or true positives indicate the number of samples with positive target value which have been predicted as positive correctly whereas FN shows the number of samples with positive target value which have been wrongly predicted as negatives. For a binary relation a confusion matrix consists of two rows and two columns that gives the number of true positives, false positives, false negatives, and true negatives. The Confusion matrix obtained for the C5.0 classification model has been shown in Table 2.

Table 2 Confusion Matrix

	D1	D2	D3	D4	D5	D6	D7	D8	D9	D10	D11	D12	D13	D14	D15	D16
D1	9	0	0	0	0	1	0	0	0	0	0	0	0	0	0	0
D2	0	8	0	0	1	0	2	0	0	0	0	0	0	0	0	0
D3	1	0	6	0	0	0	1	0	0	0	0	0	0	0	0	0
D4	0	0	0	2	0	0	0	0	0	0	0	0	0	0	0	0
D5	0	0	1	0	22	2	0	0	0	0	0	1	0	0	0	1
D6	0	0	1	1	33	1	1	0	0	0	0	1	0	1	0	0
D7	0	1	0	0	0	2	25	0	1	0	0	0	0	1	0	0
D8	0	0	0	1	1	0	11	0	0	0	0	0	0	0	0	0
D9	0	0	0	0	0	1	0	0	5	0	0	0	0	0	1	0
D10	0	0	1	0	0	1	0	0	0	2	0	0	0	0	0	0
D11	0	0	1	0	1	1	0	0	0	0	6	0	0	0	0	0
D12	0	0	0	1	1	2	1	1	0	0	1	17	0	0	0	0
D13	2	0	0	0	0	1	0	0	0	0	0	1	0	0	0	0
D14	1	1	1	0	1	1	1	0	0	0	0	0	19	0	0	0
D15	0	0	1	0	1	2	1	2	0	0	0	1	2	10	0	0
D16	0	0	0	0	1	2	2	3	0	2	0	1	0	1	0	4

3.5 Performance Evaluation

The different metrics used for measuring the performance of feature selection include Specificity, Sensitivity and Accuracy. The performance is measured by the quantity of True positive (TP), True Negative (TN), False Positive (FP), False Negative (FN).

- TP describes the count of true values that are correctly identified.
- FP describes the count of false values that are incorrectly identified as true.
- TN describes the count of false values that are correctly identified.
- FN describes the count of true values that are incorrectly identified as false.
- $TP + TN = \text{Number of correct instances or sum of diagonal elements of confusion matrix.} = (9 + 8 + 6 + 2 + 22 + 33 + 25 + 11 + 5 + 2 + 6 + 17 + 1 + 19 + 10 + 4) = 181$
- $TP + TN + FP + FN = \text{Total number of instances} = 251$
- Classification accuracy for C5.0 algorithm = $\frac{TP+TN}{TP+TN+FP+FN} = \frac{181}{251} = 71.71$

3.6 Evaluation Metrics

In order to evaluate the performance of the models, five evaluation metrics, which are the most commonly used metrics for the prediction accuracy, were used. We use the true positive, false positive, precision, recall and F-score metrics to measure the performance of the tests [17].

True Positive Rate: True positive rate, also called the sensitivity, is the proportion between the number of positive occurrence correctly identify as positive and total number of the real positive occurrence [17].

$$\text{True Positive Rate (TP Rate)} = \frac{TP}{TP + FN}$$

False Positive Rate: False positive proportion is the probability of falsely dismissing the null hypothesis for test. The false positive rate is the proportion of the number of negative occurrence incorrectly identify as positive and the total number of real negative occurrence [17].

$$\text{False Positive Rate (FP Rate)} = \frac{FP}{FP + TN}$$

Precision: Precision is defined as the fraction of relevant instances with all retrieved instances. Precision is used to test the relevance of the result set [17].

$$\text{Precision} = \frac{\text{Relevant Instance} \cap \text{Retrieved Instance}}{\text{Retrieved Instance}}$$

Table 3 Evaluation Metrics

Disorder	TP Rate	FP Rate	Precision	Recall	F-Score
Congenital Muscular dystrophies	0.90	0.80	0.69	0.90	0.78
Congenital Myasthenic syndromes	0.73	0.40	0.80	0.73	0.76
Congenital Myopathies	0.75	0.75	0.50	0.75	0.60
Distal Myopathies	1.00	1.00	0.40	1.00	0.57
Hereditary Ataxias	0.81	0.62	0.73	0.81	0.77
Hereditary Cardiomyopathies	0.83	0.70	0.67	0.83	0.74
Hereditary Motor & Sensory Neuropathies	0.83	0.67	0.71	0.83	0.77
Hereditary Paraplegias	0.79	0.70	0.61	0.79	0.69
Ion channel Muscle diseases	0.71	0.33	0.83	0.71	0.77
Malignant Hyperthermia	0.50	0.50	0.50	0.50	0.50
Metabolic Myopathies	0.67	0.25	0.86	0.67	0.75
Muscular Dystrophies	0.71	0.30	0.14	0.71	0.24
Myotonic Syndromes	0.25	0.25	0.50	0.25	0.33
Other Myopathies	0.76	0.45	0.79	0.76	0.78
Other Neuromuscular Disorders	0.50	0.00	1.00	0.50	0.67
Motor Neuron Diseases	0.25	0.14	0.66	0.25	0.36

Recall: Recall is the ration of relevant document that will successfully be retrieved from all the retrieved documents [17].

$$\text{Recall} = \frac{\text{Relevant Instance} \cap \text{Retrieved Instance}}{\text{Relevant Instance}}$$

F-score: F-score is the harmonic mean of preasion and recal [17].

$$F - \text{Score} = 2 * \frac{\text{Precision} * \text{Recall}}{\text{Precision} + \text{Recall}}$$

The Evaluation Metrics obtained corresponding to Confusion Matrix of Table 2 has been shown in Table 3.

Similarly, the evaluation metrics of other models (Random Forest, Bayesian Network, Support Vector Machine, CHAID) were calculated and tabulated in Table 4.

3.7 Results

In paper [9] authors have used wavelets and entropy matrices to classify neuromuscular disorders and achieved classification accuracy of around 57.74% using Decision

Table 4 Classification accuracy of different models

S. No.	Feature selection method	Features	C5.0	SVM	Random forest	Bayes Net	CHAID
1	Predictor Importance	All	71.71	84.86	63.75	71.71	31.47
2	Predictor Importance	18	65.34	62.15	58.57	60.16	31.47
3	Predictor Importance	7	61.35	45.42	54.18	43.42	25.9
4	Filter (F-Static)	13	52.59	40.24	43.82	41.04	29.48
5	Wrapper	12	55.16	42.35	42.24	40.49	25.9

tree, 61.44% using Random trees and 63.59% using SVM. Compared to that, during this research, classification accuracy of around 71.71% using Decision tree C5.0, 63.74% using Random trees, 64.94% using Bayesian Net and 84.86% using SVM.

In paper [14], authors had deployed a SVM based binary classification schema for which the subjects were distinguished with 81.5% accuracy and a three-class classification with an accuracy of around 70.4%.

In this research, the SVM based classification model gave the best performance with an accuracy of around 84.86%. Moreover, in other methods like entropy metrics, wavelets in the initial stages of the disease symptoms rarely undergo detection, while at a later stage, when the condition becomes critical, the symptoms are easily detectable. This is so because surface electromyography signals in NMD patients can change with the advancement of stage of the disease. Our approach to classify neuromuscular disorder is very less dependent on the stage of the disease. It gives much better true positive rate in the initial stages of the disease.

4 Conclusion and Future Work

In this paper, we have discussed the classification of Neuromuscular Disorders using machine learning methods. We have discussed an approach to classify neuromuscular disorders using 42 different features (39 sequence annotations with enzyme class, mass and length of each gene). Upon analysis using different machine learning techniques including C5.0, Bayesian Net, Random Trees and SVM Classification Algorithm, the best overall accuracy of around 84.86% was obtained using SVM.

As a further line of research, it would be more interesting to study the gene-gene interaction networks and other structure related feature to further boost the prediction performance. Thus, we may extend our approach to a hybrid one which applies PPI network for classification of neuromuscular disorders.

References

1. Pegoraro, E., Hoffman, E.P., Piva, L., Gavassini, B.F., Cagnin, S., Ermani, M., Bello, L., Soraru, G., Pacchioni, B., Bonifati, M.D., et al.: Spp1 genotype is a determinant of disease severity in duchenne muscular dystrophy. *Neurology*. WNL-0b013e318 207 (2010)
2. Sakellariou, A., Sanoudou, D., Spyrou, G.: Investigating the minimum required number of genes for the classification of neuromuscular disease microarray data. *IEEE Trans. Inf Technol. Biomed.* **15**(3), 349–355 (2011)
3. Syed, U., Yona, G.: Using a mixture of probabilistic decision trees for direct prediction of protein function. In: Proceedings of the Seventh Annual International Conference on Research in Computational Molecular Biology. ACM, pp. 289–300 (2003)
4. Kaplan, J.-C., Hamroun, D.: The 2015 version of the gene table of monogenic neuromuscular disorders (nuclear genome). *Neuromuscul. Disorders* **24**(12), 1123–1153 (2014)
5. Bruxella, J.M.D., Sadhana, S., Geetha, S.: Categorization of data mining tools based on their types. *Int. J. Comput. Sci. Mobile Comput.* **3**(3), 445–452 (2014)
6. Bujlow, T., Riaz, T., Pedersen, J.M.: A method for classification of network traffic based on c5. 0 machine learning algorithm. In: International Conference on Computing, Networking and Communications (ICNC), 2012. IEEE, pp 237–241 (2012)
7. Ham, J., Chen, Y., Crawford, M.M., Ghosh, J.: Investigation of the random forest framework for classification of hyperspectral data. *IEEE Trans. Geosci. Remote Sensing* **43**(3), 492–501 (2005)
8. Hogrel, J.-Y.: Clinical applications of surface electromyography in neuromuscular disorders. *Neurophysiol. Clin./Clini. Neurophysiol.* **35**(2–3), 59–71 (2005)
9. Istenic, R., Lenic, M., Kaplanis, P., Pattichis, C., Zazula, D.: Classification of neuromuscular disorders using wavelets and entropy metrics on surface electromyograms. In: Conference proceedings: Proceedings of the 7th WSEAS International Conference on Signal, Speech and Image Processing. Beijing, China, pp. 159–163 (2007)
10. Choi, S.B., Park, J.S., Chung, J.W., Yoo, T.K., Kim, D.W.: Multicategory classification of 11 neuromuscular diseases based on microarray data using support vector machine. In: Engineering in Medicine and Biology Society (EMBC), 2014 36th Annual International Conference of the IEEE. IEEE, pp. 3460–3463 (2014)
11. Kamali, T., Boostani, R., Parsaei, H.: A multi-classifier approach to muap classification for diagnosis of neuromuscular disorders. *IEEE Trans. Neural Syst. Rehabil. Eng.* **22**(1), 191–200 (2014)
12. Pandya, R., Pandya, J.: C5. 0 algorithm to improved decision tree with feature selection and reduced error pruning. *Int. J. Comput. Appl.* **117**(16), 18–21 (2015)
13. Li, T., Zhang, C., Ogihara, M.: A comparative study of feature selection and multiclass classification methods for tissue classification based on gene expression. *Bioinformatics* **20**(15), 2429–2437 (2004)
14. Kaplanis, P.A., Pattichis, C.S., Zazula, D.: Multiscale entropy-based approach to automated surface EMG classification of neuromuscular disorders. *Med. Biol. Eng. Comput.* **48**(8), 773–781 (2010)
15. Chandrashekhar, G., Sahin, F.: A survey on feature selection methods. *Comput. Electr. Eng.* **40**(1), 16–28 (2014)
16. Guyon, I., Elisseeff, A.: An introduction to variable and feature selection. *J. Mach. Learn. Res.* 1157–1182 (2003)
17. Chawla, N.V., Japkowicz, N., Kotcz, A.: Special issue on learning from imbalanced data sets. *ACM Sigkdd Explora. Newslett.* **6**(1), 1–6 (2004)

Comparative Study of the Ultrasonic and Infrared Person Counter



Ankit Saxena, Swapnesh Taterh, and Nishant Saxena

Abstract Nowadays, every organization is totally depend upon the technologies and the now working on the concept of the automation means, it means that every day work will perform by the machine automatically. So, the error chances may be less and the work will be done in effective manner as well as in short range of time. Some of daily task of any organization is to calculate the person who have entered or exit from the organization or any building. So, in this, we discuss about the person counter which is widely used by the organization for counter. We also define the methodology on which the principal of the counter works as well as we also discuss various technologies used to count the person count. In this paper, we also compare the technologies. This paper will provide the comparison on the ultrasonic and infrared sensor-based counter.

Keywords Infrared counter · Ultrasonic counter · Person counter · Study of counter · Comparison of various counters

1 Introduction

On the safety point of view of any building or any compound, it mandatory to know the count of the person who are presently present in it. Nowadays, many organizations are using person counter to count the number of persons who have entered or exit from the door. The counter is installed at the door of the building so that it can monitor the person count. As the visitor counter helps in determining the exact number of people in a room, it can be used in various places like seminar hall, hotels, cinema halls, mall and for security purposes. For the betterment of accuracy in these applications, we are currently using infrared and ultrasonic technologies. Both of these technologies have their own pros and cons.

A. Saxena (✉) · N. Saxena
Tula's Institute, Dehradun, India
e-mail: ankit.saxena5@yahoo.com

S. Taterh
Amity University, Jaipur, India

In the paper, we have discussed a door counter or a visitor counter, we have also discussed the two different mechanisms that it uses for its work. A visitor counter is an electronic device which, uses sensors, to count the no. of objects (here people) passing through it. And because of this, visitor counter is very helpful in making projects like—automatic room light controller, which turns ON or OFF the lights and fans of a room on the basis of people inside that room. Visitor counter is also used in places like seminar halls, hotels, malls and also for security purposes. In emergency situation, we have to know, with the help of counter, that how many people are currently present in the building so that we will be ready with the backup for them to avoid casualties.

2 Hardware Components for Counter

2.1 Arduino UNO R3 Board

Arduino is an open-source electronics platform based on easy-to-use hardware and software. It is an interactive board that receives various signals as input, it operates different operations based on the signal given to Arduino UNO R3 board. The board consists of 6 analog pins, 14 digital pins and a programmable with the Arduino IDE. Analog pins are used to get the basic input signals, whereas digital pins are connected to digital output. It has a 32 kb of flash memory to store the program that is coded for the operation (Fig. 1).

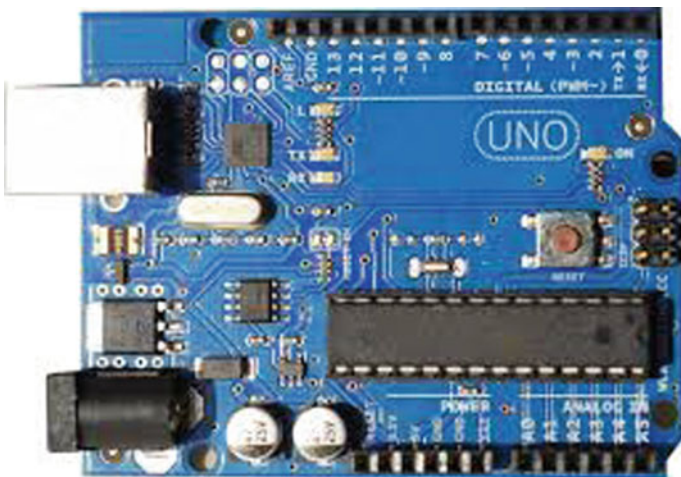


Fig. 1 Arduino board



Fig. 2 LCD display

2.2 *LCD Display*

LCD display liquid crystal display (LCD) screen is an electronic display module and finds a wide range of applications. The reason behind this is that LCDs are economical, easily programmable, have no limitation of displaying special and even custom characters, animation and so on. The output generated by Arduino is sent to the LCD for displaying the no. of the person currently present in room (Fig. 2).

2.3 *IR Sensor*

An infrared sensor is a device consists of two parts—an emitter, to emit IR rays, and a receiver, to collect the reflected rays. When an object intercepts these rays, then the object is detected. This information is then sent to the Arduino, which further process it to digital output (Fig. 3).

2.4 *Ultrasonic Sensor*

An ultrasonic sensor, same as a IR sensor, consists of the same two parts, an emitter and a receiver, both of these have the operation. But here, instead of IR rays, this sensor uses ultrasonic sound waves to detect the object (Fig. 4).

2.5 *Jumper Wires*

These are simply wires that have pins attach to both of their ends, this helps us in connecting two points without soldering (Fig. 5).

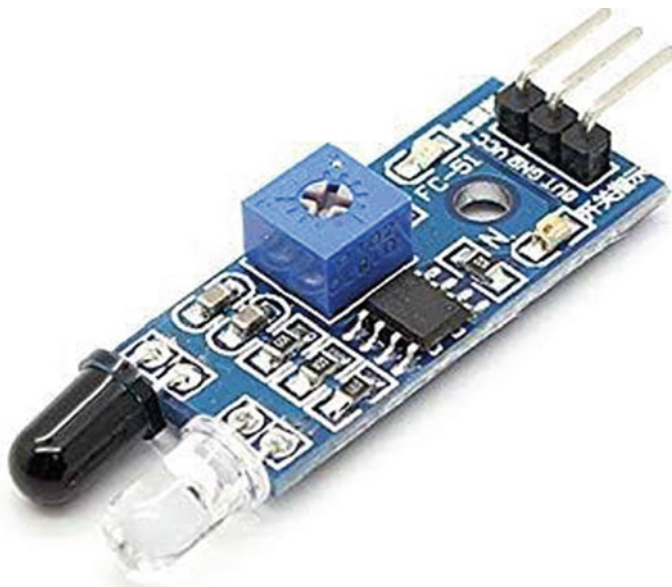


Fig. 3 IR sensor



Fig. 4 Ultrasonic sensor

Fig. 5 Jumper wires

2.6 Breadboard

Breadboard also is a solderless device. Pins of devices and jumpers are connected to the holes of breadboard so that these devices can be connected without any complex physical structures of wires (Fig. 6).

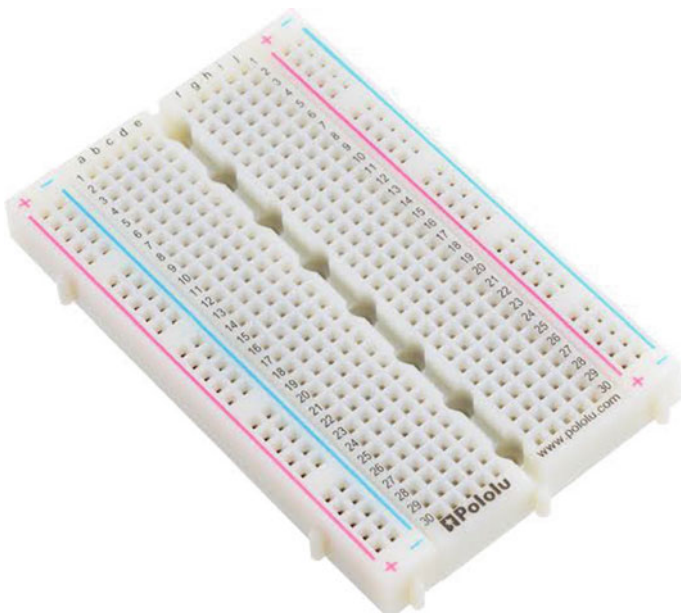
**Fig. 6** Bread board

Fig. 7 Arduino USB cable



2.7 *Arduino USB Cable*

This cable helps us to connect the Arduino board with a system so that code can be embedded in it (Fig. 7).

3 Circuit Diagram

The circuit diagram shows the model of a visitor counter. For connecting various elements in our circuit, a breadboard is used (Fig. 8).

4 Methodology

A visitor counter is an IoT-based project, so there are two possible approaches available for this. The first is using Arduino board. It is a microcontroller that can perform a single operation on a set of inputs, based on the code that is embedded in it. It is a cheap product, and it can only be controlled manually. The second approach include using a Raspberry pi. Raspberry pi has something called as a Raspberry OS which helps it to handle multiple operations at a time. It is quite expensive, but it gives us ability to connect to a network (WiFi or the Internet), which increases its reliability

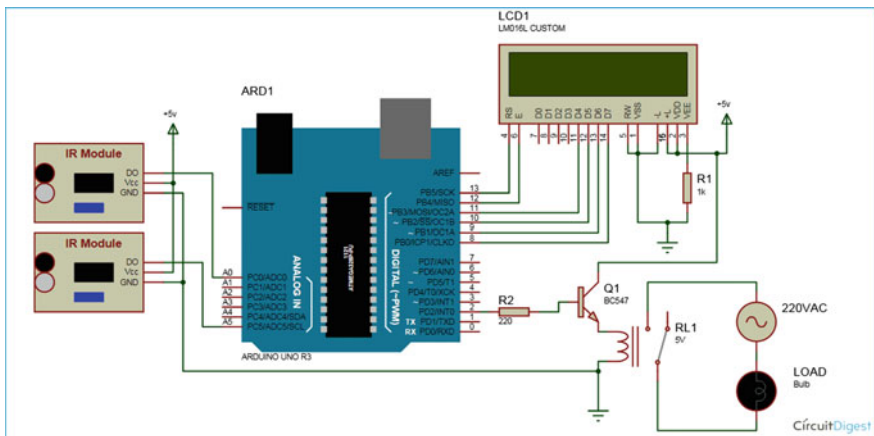


Fig. 8 Circuit diagram

as it can be controlled remotely. In this project, we have used Arduino as the brain of our visitor counter (Fig. 9).

Arduino board gets its input through a sensor, generally infrared or an ultrasonic sensor, which are placed at the entrance of our door. Both of these sensors consist of an emitter, which emit rays (IR rays in case of IR sensor and ultrasonic sound waves in ultrasonic sensor) and a receiver which collect those rays that are reflected back. These sensor detects an approaching person when the path of these rays are interrupted by a person, and it send signals to the Arduino board. Arduino takes these analog signals and operate on them, according to the manually written code in it, which is to program the Arduino board for performing the required operations.

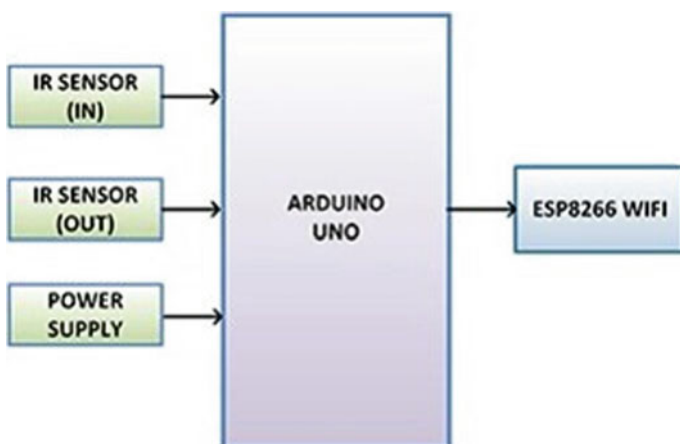


Fig. 9 Block diagram

By connecting the Arduino board with a system through its Arduino USB cable, an Arduino is programmed. The operations produces digital output, which either recognizes as an increment or a decrement in the no. of people already present in the room. These outputs then send to an LCD display, which shows the no. of people passes through the counter.

The circuit diagram shows the model of a visitor counter. For connecting various elements in our circuit, a breadboard is used.

5 Types of Counter

A visitor counter uses a sensor to get its inputs. There are generally two types of sensors that are used in this. First is infrared sensor (or passive Infrared sensor) and second is ultrasonic sensor. Both of these sensors have their pros and cons, and we are going to discuss them one by one.

5.1 *Infrared Sensor*

An infrared sensor is a distance sensor, meaning that it continuously calculates the distance of a person approaching in its field of view [1, 2]. It consists of two different parts—an emitter, which emits IR rays, and other is a receiver, which collect these rays when they get reflected back. The time between emission and receiving is simultaneously calculated, which is used in time of flight (TOF) equation and the distance of the approaching person is calculated.

$$D = (C * T)/2$$

where D = distance, C = speed of rays (here IR) and T = time.

IR sensors can be used in dark and can also be used in vacuum. Due to beam directionality (one way, vertically or horizontally), there is no leakage of data, but this also reduces its precision as the rays cannot detect a person that is not in its field of view (which is straight) [2] (Fig. 10).

IR rays also have a very low range of field, generally 100–500 cm, if more than that, it loses its accuracy. Also, as there is continuous emission and receiving happening, IR sensor have high power consumption (Fig. 11).

5.2 *Ultrasonic Sensor*

Ultrasonic sensor is also distance sensor. These sensor also have same two-parts as IR sensors—an emitter and a receiver, but the rays in action is ultrasonic sound waves

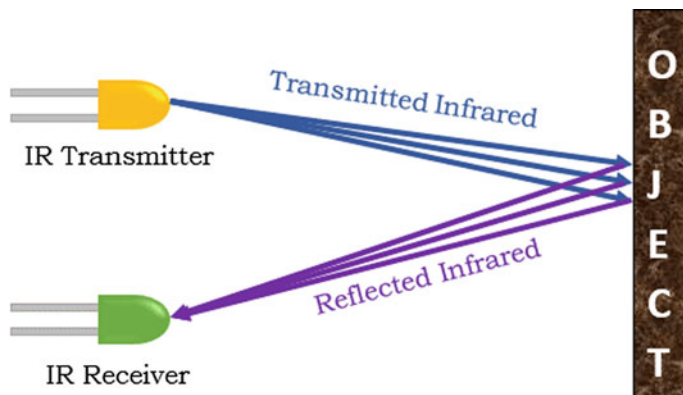


Fig. 10 IR sensor working principal

Comparison between actual distance and measured distance for infrared sensor

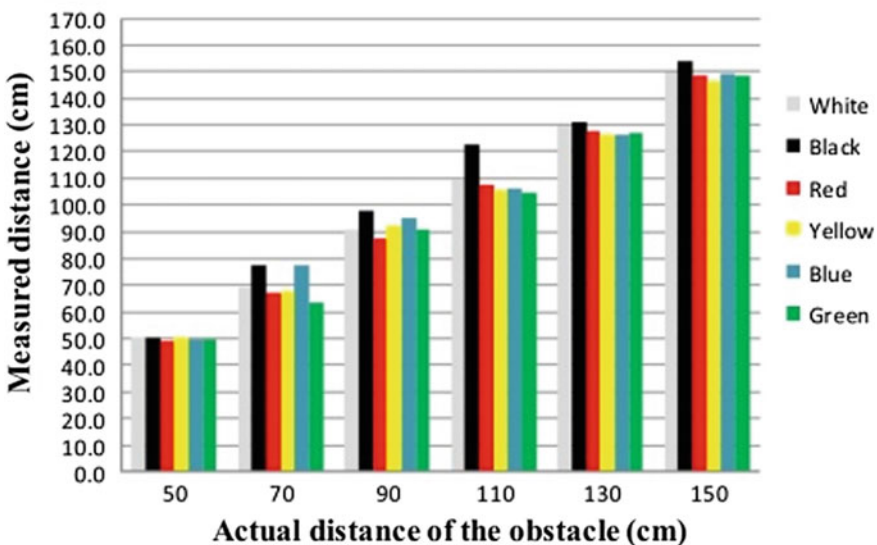


Fig. 11 Comparative graph for distance

[2]. With the same mechanism of calculating time of emission and receiving, distance is calculated with the help of TOF equation (but here C = speed of ultrasonic waves) [1].

Like IR sensor, ultrasonic sensor can be used in dark but cannot be used in vacuum. Its field of view is more than IR sensor, generally 20 cm–16.5 m, also as sound waves has the tendency to spread, ultrasonic sensor have also a large field-of-view area (Fig. 12).

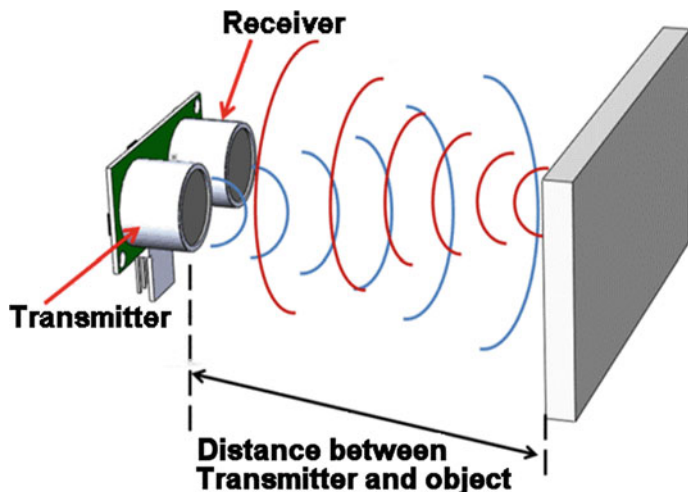


Fig. 12 Ultrasonic sensor working principal

It is a low cost option. But it also loses its accuracy because of change in environmental condition, like temperature, pressure and humidity. Sound absorbing materials also affect the precision of this sensor [2] (Fig. 13).

Comparison between actual value and measured value for ultrasonic sensor

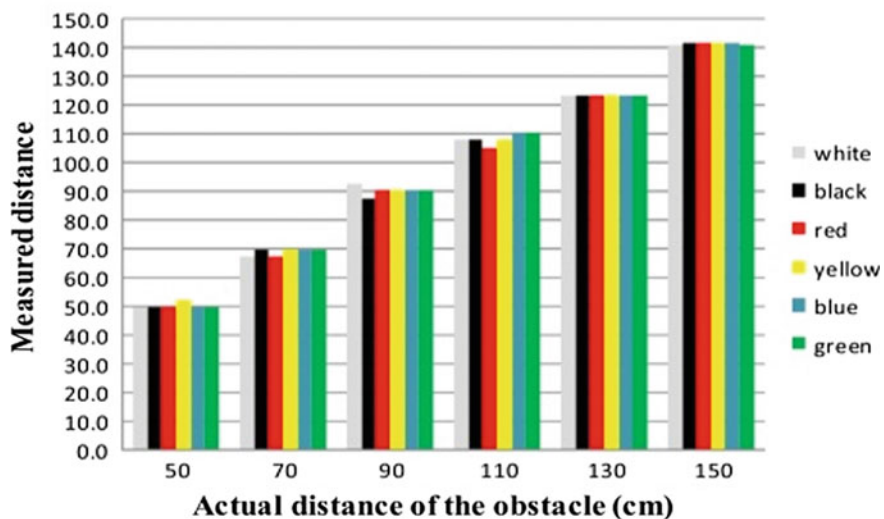


Fig. 13 Comparative graph for distance

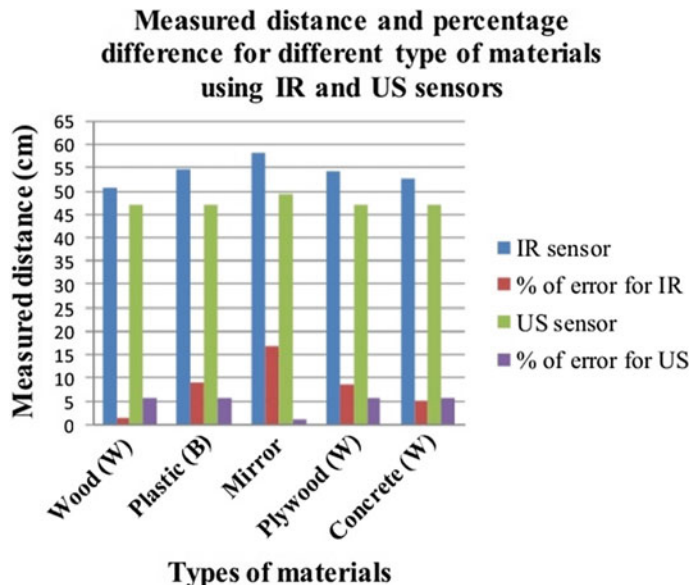


Fig. 14 Comparative graph for distance measurement between IR sensor and ultrasonic sensor

6 Conclusion

We have studied various papers relating this topic, visitor counter and papers which compare both IR and ultrasonic sensor. Also, in the graph below, we can see the error that both of these sensors give on different surfaces. In material, like wood and concrete, IR sensor has given less error than ultrasonic sensor, but that difference is relatively low. In material like plastic and mirror, the situation is opposite and the difference in error is too much (Fig. 14).

In the graphs below, a comparison between the actual and measured distance is given. And it clearly shows that in terms of range, IR sensor loses to ultrasonic sensor. Accuracy of both of these sensors can be degraded by environmental conditions, IR in hot climatic conditions, whereas ultrasonic sensor is in dense medium.

IR sensor is high priced and have power consumption, whereas an ultrasonic sensor is low cost and power efficient. So in the end, we conclude that an ultrasonic sensor is relatively better than an IR sensor for a visitor counter.

References

1. Mustapha, B., Zayegh, A., Begg, R.K.: Ultrasonic and infrared sensors performance in a wireless obstacle detection system. In: 2013 First International Conference on Artificial Intelligence, Modelling & Simulation, Victoria University, Australia

2. Carvalho, B.F., Silva, C.C.M., Silva, A.M., Buiati, F., Timóteo, R.: Evaluation of an Arduino-based IoT Person Counter. Laboratório LATITUDE—Faculdade de Tecnologia, Universidade de Brasília, Campus Darcy Ribeiro, Brasília, Brazil
3. Jothibasu, M., Aakash, B., Ebanesh, K.S., Vinayak, G.L.: Automatic room monitoring with visitor counter(ARM-VC). *Int. J. Innov. Technol. Explor. Eng. (IJITEE)* **8**(7) (2019). ISSN: 2278-3075
4. Chattoraj, S., Chakraborty, A.: Bidirectional visitor counter with automatic room light controller and Arduino as the master controller. *Int. J. Sci. Res. Publ.* **6**(7), 357 (2016). ISSN: 2250-3153
5. Rajani, A.B.R., Shalini, C.K., Vidyashree, H.N., Shilpashri, V.N.: Bidirectional visitor counter for smart power management. In: National conference on Engineering Innovations and Solutions (NCEIS—2018), *Int. J. Sci. Res. Comput. Sci. Eng. Inf. Technol.*
6. Van Groeningen, T., Driessen, H., Sohl, J., Voute, R.: An ultrasonic sensor for human presence detection to assist rescue work in large buildings. In: ISPRS Annals of the Photogrammetry, Remote Sensing and Spatial Information Sciences, vol. iv(4)/w7, 2018 3rd International Conference on Smart Data and Smart Cities, Delft, The Netherlands, 4–5 Oct 2018
7. Basaran, C., Yoon, J.-W., Son, S., Park, T.: Self-configuring indoor localization based on low-cost ultrasonic range sensors. *Sensors* **14**(10), 18728–18747 (2014)
8. Chen, Q., Gao, M., Ma, J., Zhang, D., Ni, L.M., Liu, Y.: MOCUS: moving object counting using ultrasonic sensor networks. *Int. J. Sens. Netw.* **3**(1) (2008)
9. Nikose, M., Gaikwad, K., Gamne, P., Bodke, A.: A survey on bidirectional visitor counter with automatic light and fan control for room. *Int. J. Adv. Res. Electr. Electron. Instrum. Eng.* **7**(3) (2018)

Fuzzy Logic Based Improved Control Design Strategy for MPPT of Solar PV Systems



Rahul Bisht, Newton Kumar, and Afzal Sikander

Abstract Nowadays renewable energy sources have significant contribution in electrical engineering. The solar photovoltaic (PV) systems are in great demand as a non-conventional energy source. The performance of solar PV system is highly affected by temperature and irradiance in the surroundings. This may also leads to change the maximum available power of PV system. To achieve maximum power, this paper contributes a new control design strategy for MPPT of solar PV systems. The concept of fuzzy logic is being employed to design suitable control law. The performance of designed controller is tested with wide range of environmental parameters change. It is observed that the obtained results not only provide the fast dynamics but also high accuracy in power is achieved.

Keywords Maximum power point tracking · Photovoltaic solar system · Fuzzy logic · Controller design · DC-DC converter

1 Introduction

In recent year, steady increase in greenhouse gas emission level, insufficient fossil fuel, and increasing energy demand have pushed research towards renewable energy which is an effective solution. The Sun is a primary source of energy and solar energy is free, clean and environment friendly. PV panel is one of the important technologies of solar energy. But solar panel has high cost, low conversion efficiency from sunlight to electricity (9–17%). PV panel voltage and current output is highly nonlinear due to change in environment condition. The PV panel output power depends on

R. Bisht · N. Kumar · A. Sikander (✉)

Department of Instrumentation and Control Engineering, Dr. B. R. Ambedkar National Institute of Technology, Jalandhar, Jalandhar, Punjab 144011, India
e-mail: afzals@nitj.ac.in

R. Bisht

e-mail: rahulbisht1706@gmail.com

N. Kumar

e-mail: kumar.newtonsingh@gmail.com

© Springer Nature Singapore Pte Ltd. 2020

M. Pant et al. (eds.), *Soft Computing: Theories and Applications, Advances in Intelligent Systems and Computing 1154, https://doi.org/10.1007/978-981-15-4032-5_97*

solar irradiance and temperature variation. It is clear from the following that when irradiance increases, the net output increases while increase in temperature results in decrease of output of PV panel [1].

$$\begin{aligned} I_P &= I_P(T_r)[1 + K_i(T - T_r)] \\ I_P(T_r) &= I \left(\frac{G}{G_o} \right) \end{aligned} \quad (1)$$

where, I_P is photo generated current (A), T_o and G_o are standard temperature and insolation respectively, T is atmospheric absolute temperature, K_i is temperature coefficient of short circuit current (A/K) and insolation is G (W/m^2).

Batteries are rated for voltage capacity and excessive voltage leads to permanent battery damage or reduce life span of battery and also may damage other directly connected electrical appliances. So various management approaches are effectively employed to charge battery efficiently [2–7]. It prevents battery overcharge to ensure long life span of battery. To charge battery efficiently it is required to charge at constant current or constant voltage. Many authors have studied the MPPT with different algorithms [8–11]. The author in [8] explains Hill climbing algorithm MPPT, but this algorithm fails under rapidly changing environment. The author Zaenal et al. [9] has studied PSO MPPT method. This application has slow speed of convergence and large search space, but it is better than P & O and it can be implemented for real application. The author [11] in 2014 explains Perturb and Observe MPPT method. This technique is cheap and easy to implement but its output oscillate across MPP which causes power loss. On the other hand, numbers of soft computing techniques are extensively employed in different field of applications [12–16]. The proposed system in this paper uses FLC algorithm which quickly respond to environment change and it does not required any knowledge about system parameter.

2 Photovoltaic System Description and Characteristics

PV panel consist several PV cells connected in series and parallel. Figure 1b shows basic solar equivalent circuit, it consist of two resistances and a diode. The value of R_{sh} should be large, so small leakage current passes through the parallel path [17]. The mathematical equations of one diode PV model are as follows.

$$I = I_{ph} - I_D - I_{sh}$$

Where

$$I_D = I_R \left[\exp \left(\frac{eI_P R_P}{nKT} \right) - 1 \right]$$

Then

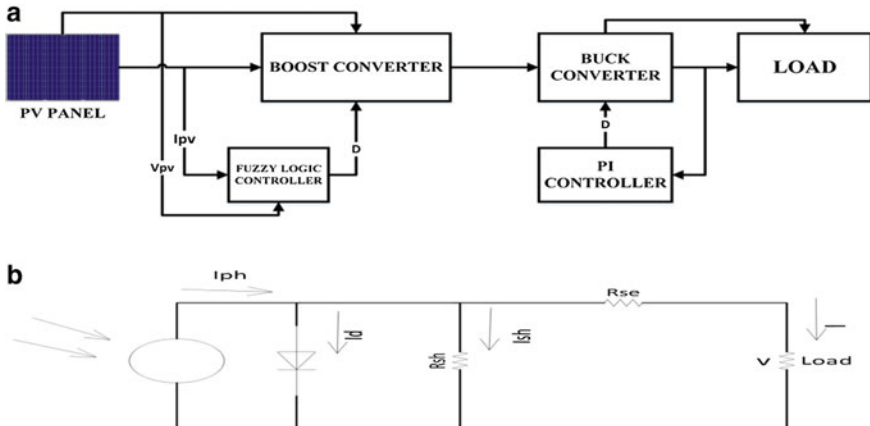


Fig. 1 a Block diagram of PV system with FLC and PI controller. b Circuit diagram of PV system

$$I = I_{ph} - I_R \left[\exp\left(\frac{eI_P R_P}{nKT}\right) - 1 \right] - \frac{V + I \times R_{se}}{R_{sh}} \quad (2)$$

where I_R is reverse saturated current, T is temperature (K) of PV panel, n is diode constant, K is Boltzmann's constant, e is an electron charge, I is load current and I_{ph} is PV generated current. Solar PV panels are sensitive to different environment conditions such as shading and cloud therefore two diode model is more accurate, it considers impact of shading and losses due to cell's internal resistance. It has more unknown parameters so it is more complicated and takes more computational time.

3 Proposed Methodology for Fuzzy Logic Controller of MPPT

Fuzzy logic computes “degree of truth” rather than the usual “True or false” (0 or 1). Here FLC controller determines duty cycle and has facility to determine MPP of panel. Tracking error $E(t)$ and change in error $CE(t)$ are the two inputs to the FLC. The following equation defines the value [4, 18, 19].

$$E(t) = \frac{P(i) - P(i-1)}{V(i) - V(i-1)}$$

And

$$CE(t) = E(t) - E(t-1) \quad (3)$$

where P_i is power, V_i represents photovoltaic voltage and P_{i-1} , V_{i-1} are the previous iteration voltage and power of PV panels. The flow chart of FLC is depicted in Fig. 2.

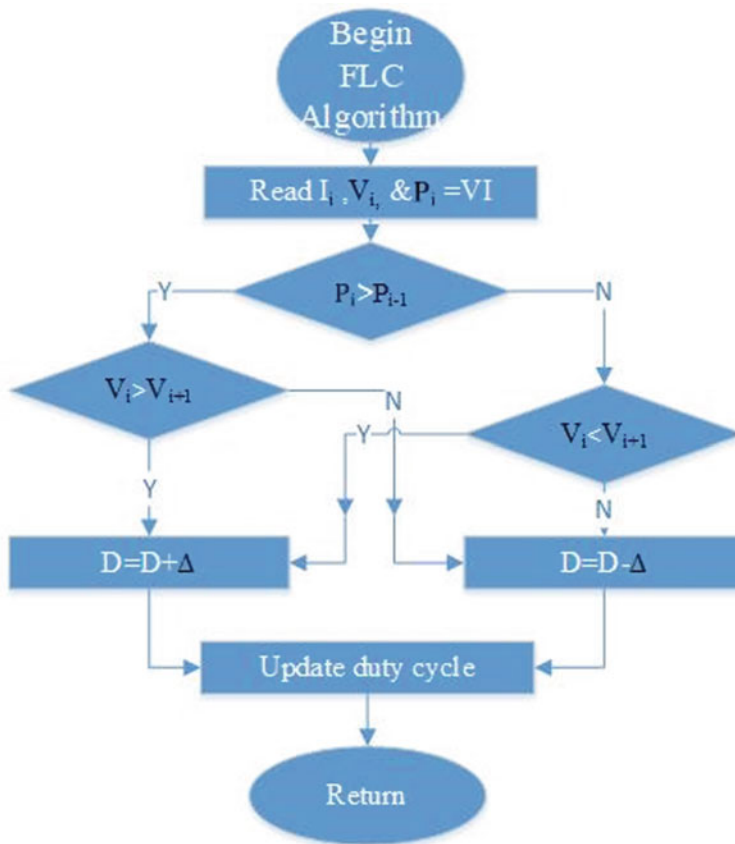


Fig. 2 Flow chart of FLC

4 DC-DC Converter Analysis

As its name implies, it is a device that converts one form of DC voltage to another and ensures less energy loss. The converter regulates the input voltage of PV solar panel and maintains maximum power. For maximum output power internal resistance is made equal to output resistance of panel by changing the value of D [20] which is given as

$$R_i = (1 - D)^2 R_{\text{Load}} \quad (4)$$

where R_i is input resistance, R_o output resistance and D is duty cycle. By varying ' D ' the R_i can easily change. Here FLC maintains duty cycle of PWM MOSFET of boost converter.

5 Boost Converter

It is a converter which gives output voltage more than input. It consists of an electronic switch, inductor diode and output capacitor. Boost converter works as step up transformer on the principle of law of conservation. When switch is closed, the diode is in reversed biased and when switch is open the diode is in forward biased. It is required to determine the duty cycle to calculate switch current [21, 22].

$$D = \frac{V_o - V_i}{V_i} \quad (5)$$

Inductor and capacitor value calculated as

$$\begin{aligned} \Delta I_L &= \frac{V_i \times D}{F_S \times L} \\ L &= \frac{V_i \times (V_o - V_i)}{\Delta I_L \times F_S \times V_o} \end{aligned} \quad (6)$$

where ΔI_L = Inductor ripple current, V_i = input minimum voltage, V_o = voltage, F_S = converter switching frequency, L = inductor, D = duty cycle.

$$C = \frac{I_o \times (V_o - V_i)}{\Delta V_C \times F_S \times V_o} \quad (7)$$

where C is capacitor, I_o is output current, ΔV_C is estimated output ripple voltage.

6 PI Controller for Buck Converter

To charge battery at constant level current-voltage PI controller regulates the Buck converter. In PI controller K_i eliminates steady state error and K_p reduce setup time. There are numerous tuning methods available to find suitable parameters of PI controller [23, 24]. Buck converter is an electronic device in which output voltage is less than input voltage [18]. Here output voltage of Buck converter and the reference voltage are compared which generates an error which is fed to the PI controller, and then resultant pulse of PI controls the D of buck converter and its parameters are calculated as given below

$$D = \frac{V_o}{V_i} \quad (8)$$

Inductor of buck converter

$$L = \frac{V_O(V_O - V_I)}{\Delta I_L \times F_S \times V_I} \quad (9)$$

Capacitor of buck converter

$$C = \frac{D \times I_L}{8 \times F_S \times \Delta V_C} \quad (10)$$

where ΔI_L = Inductor ripple current. V_O = voltage, ΔV_C is estimated output ripple voltage.

7 Performance Evaluation and Discussion

The PV MPPT Simulink model was prepared with the help of MATLAB software and results were observed in Simulink. This section exhibits the simulation results obtained under four conditions for a given system. Table 1 shows the parameter values used in the PV model [25] whereas Table 2 depicts the rule base for FLC in terms of error and change of error.

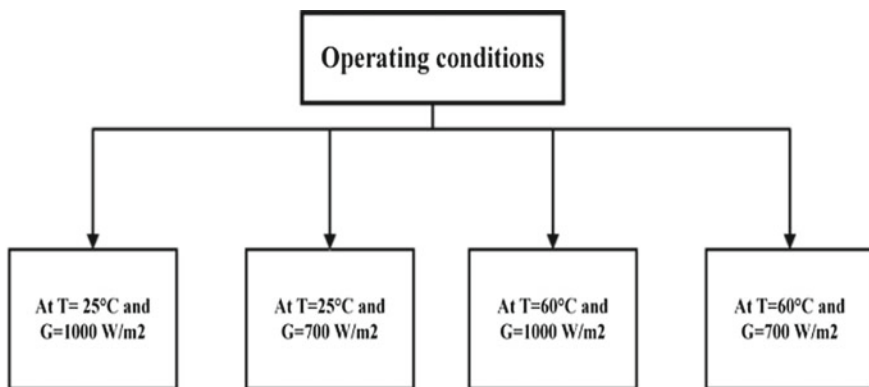
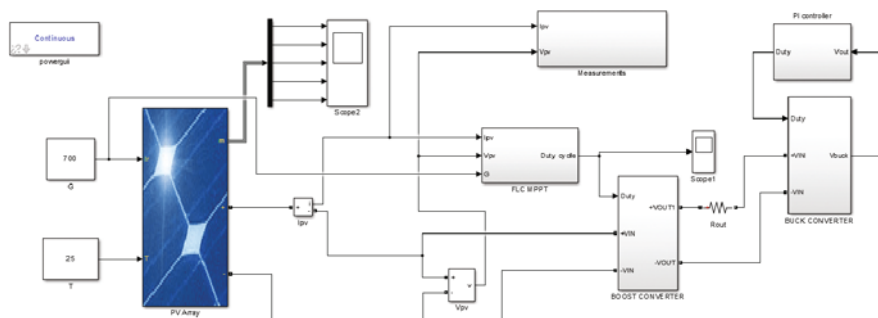
Figure 3 shows the four operating conditions for which proposed work has been compared with [25]. Figure 6 shows the response curve of P_{pv} , V_{pv} , and I_{pv} of the photovoltaic panel using proposed model depicted in Fig. 4 under four operating conditions. In this paper we have used FLC MPPT technique for PV system shown in Fig. 4. Apart from the mentioned operating conditions we have considered two cases: in first case, irradiance is increased step by step and temperature is considered constant then response is recorded which is shown in Fig. 7 while in second case, temperature is increased and irradiance is considered constant and response is recorded for the same shown in Fig. 9.

Table 1 Parameters used in model

Name of the Parameter	Value
V_{oc} (open circuit voltage)	24 V
I_{sc} (short circuit current)	5.1 A
V_{mpp} (voltage at MPP)	17.5 V
I_{mpp} (current at MPP)	4.8 A
Temperature coefficient of V_{oc} (%/°C)	-0.36099
Temperature coefficient of I_{sc} (%/°C)	0.102
Number of cells (N.cell)	20
C1	0.9
C2	0.2
C3	0.01
C4	0–0.5

Table 2 Rule base of FLC in terms of $E(t)$ and $CE(t)$

E/CE	PB	PM	PS	ZE	NS	NM	NB
PB	PB	PB	PB	PB	PB	PB	PB
PM	PB	PM	PM	PM	PM	PM	PM
PS	PB	PM	PS	PS	PS	PS	PS
ZE	PB	PM	PS	ZE	ZE	ZE	ZE
NS	PB	PM	PS	ZE	NS	NS	NS
NM	PB	PM	PS	ZE	NS	NM	NM
NB	PB	PM	PS	ZE	NS	NM	NB

**Fig. 3** Operating conditions of PV model**Fig. 4** Simulation model

In Fig. 8, I-V and P-V response are shown for case 1 while Fig. 10 shows the I-V and P-V response for case 2. Table 3 show the result obtained for four operating conditions and compares it with results obtained in [25].

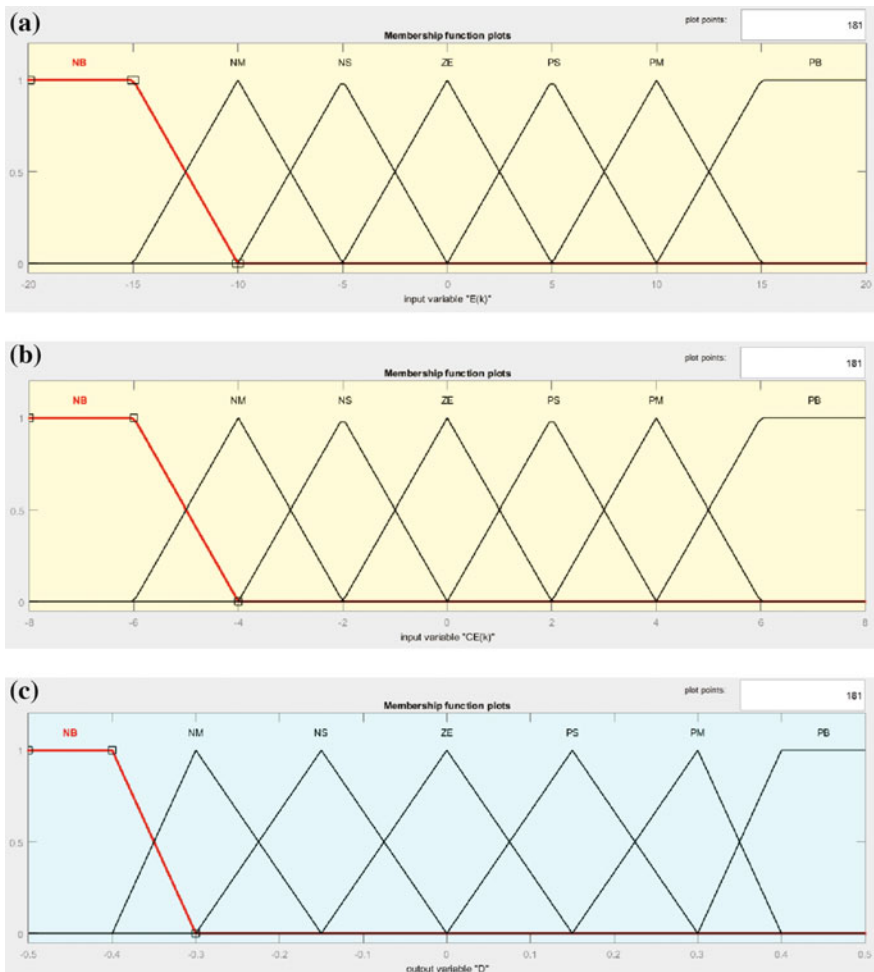


Fig. 5 Membership Functions for Input to FLC Error $E(t)$ and Change of error $CE(t)$ and output of FLC Duty cycle (D)

In Table 4, results are shown for both the cases using the proposed model and it can be seen that we obtained 99.93% of accuracy for $G = 800 \text{ W/m}^2$ and $T = 25^\circ\text{C}$ which is maximum out of all the cases.

8 Conclusion

This study presents an improved control design strategy for maximum power point tracking of PV systems. The proposed methodology is based on the concept of fuzzy

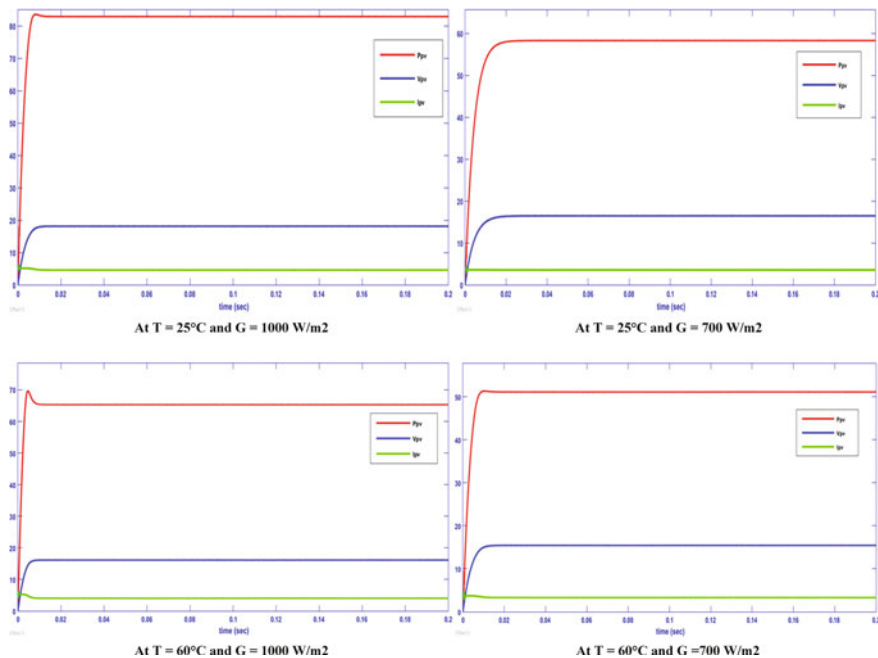


Fig. 6 PV response at different temperature and irradiance

Case 1: At constant $T = 25^\circ\text{C}$ and variable irradiance

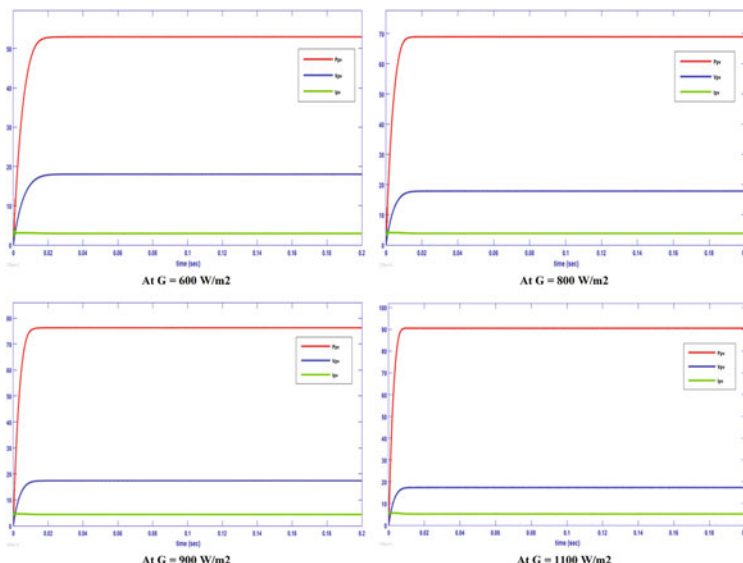


Fig. 7 PV response at variable irradiance

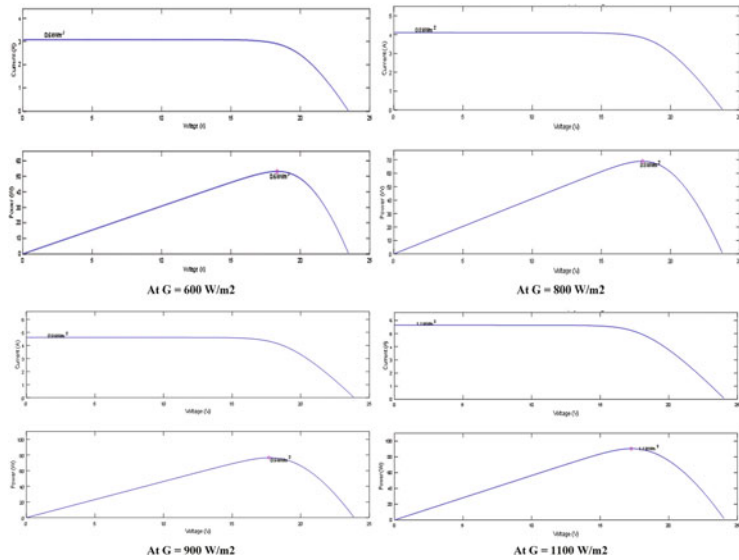


Fig. 8 I–V and P–V curve at different irradiance

Case 2: At constant irradiance $G = 1000 \text{ W/m}^2$ and variable temperature

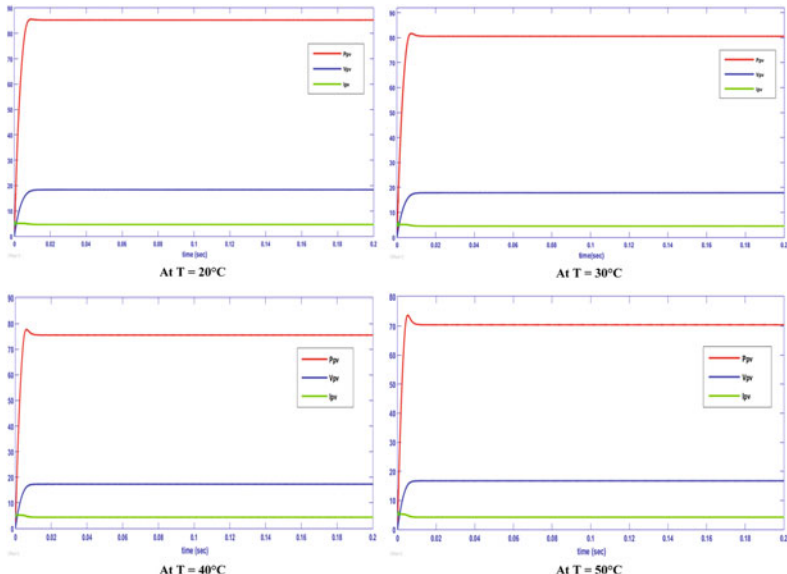


Fig. 9 PV response at different temperature

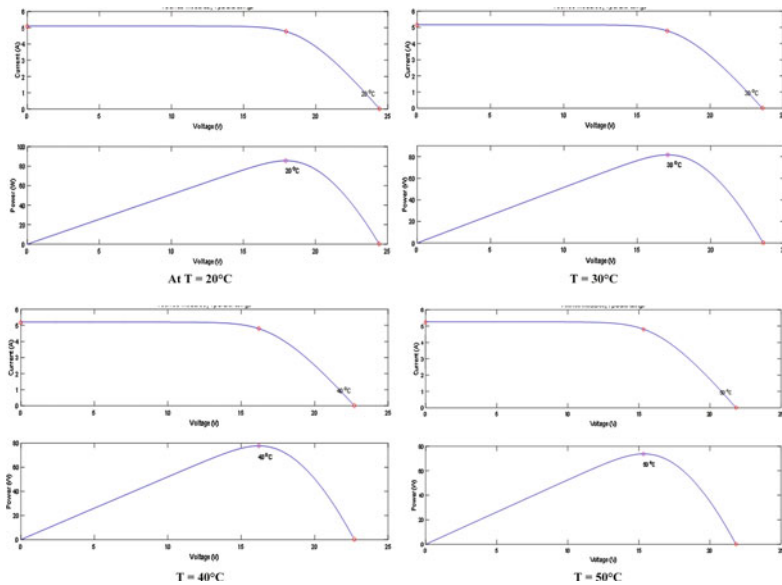


Fig. 10 P–V and I–V curve at different temperature

logic. The performance of the proposed controller is tested with numerical analysis. Numbers of cases have been taken into consideration with respect to temperature and irradiance variation. The analysis reveals that the obtained results of proposed controller are comparable. Additionally, an accuracy of 99.93%, in power, for $G = 800 \text{ W/m}^2$ and $T = 25^\circ\text{C}$ is achieved which is maximum out of all the cases. Further, the proposed method may be extended for fractional order controller.

Table 3 Comparison of responses

Conditions	T (°C)	G (W/m ²)	[25] (W)	P _{MPP} (W)	P _{PV} (W)	Accuracy (%)	I _{PV} (A)	V _{PV} (V)	V _{boost} (V)	DFLC
Condition 1	25	1000	79.7	84	82.87	98.65	4.56	18.15	33.26	0.399
Condition 2	25	700	63.3	61.2	51.7	84.75	3.58	14.44	26.25	0.399
Condition 3	60	1000	65.8	71	65.2	92.6	4.04	16.15	29.48	0.399
Condition 4	60	700	51.3	51	50.69	99.39	3.55	14.3	25.99	0.399

Table 4 PV response for both the cases

G (W/m ²)	P _{mpp} (W)	P _{pv} (W)	I _{pv} (A)	V _{pv} (V)	Accuracy (%)	D	V _{boost} (V)
<i>At constant T = 25 °C and variable irradiance</i>							
600	53.2	52.98	2.94	18.02	99.59	0.251	20.5
800	69	68.95	3.86	17.86	99.93	0.351	21.16
900	76.5	76.3	4.38	17.42	99.74	0.404	23.8 V
1100	90.52	90.43	5.22	17.32	99.90	0.451	32.76
<i>At constant irradiance G = 1000 W/m²</i>							
20	85.5	85.24	4.64	18.37	99.69	0.4004	22.8
30	81.7	80.56	4.51	17.86	98.64	0.4004	31.8
40	77.7	75.56	4.36	17.33	97.24	0.4004	30.9
50	73.7	70.46	4.21	16.73	95.60	0.4004	26.1

References

1. Vasantharaj, S., Vinodhkumar, G., Sasikumar, M.: Development of a fuzzy logic based, photovoltaic maximum power point tracking control system using boost converter. In: Proceedings of the Third International Conference on Sustainable Energy and Intelligent System (SEISCON 2012), VCTW, Tiruchengode, Tamilnadu, India, pp. 2–5 (2012)
2. Hua, C., Shen, C.: Control of DC/DC converters for solar energy system with maximum power tracking. In: Proceedings of the IECON'97 23rd International Conference on Industrial Electronics, Control, and Instrumentation, vol. 2, pp. 827–832 (1997)
3. Roy, C.P., Vijaybhaskar, C., Maity, T.: Modelling of fuzzy logic controller for variable step MPPT in photovoltaic system. Int. J. Res. Eng. Technol. **2**(8), 426–428 (2013)
4. Othman, A.M., El-arini M.M.M., Ghitas A., Fathy A.: Real world maximum power point tracking simulation of PV system based on fuzzy logic control. NRIAG J. Astron. Geophys. **1**(2), 186–194 (2012)
5. Jana, J., Bhattacharya, K.D., Saha H.: Design & implementation of MPPT algorithm for battery charging with photovoltaic panel using FPGA. IEEE, 1–5 (2014)
6. Singh, D., Yadav, R., Jyotsana.: Perturb and observe method MATLAB simulink and design of PV system using buck boost converter. Int. J. Sci. Eng. Technol. Res. (IJSETR) **3**(6) 235–239 (2014)
7. Suresh, H., Baskaran, A., Sudharsan, K.P., Vignesh, U., Viveknath, T., Sivraj, P., Vijith, K., Amrita Vishwa Vidyapeetham.: Efficient charging of battery and production of power from solar energy. In: Proceedings of the International Conference on Embedded Systems (ICES 2014). pp. 231–7 (2014)
8. Kjær, S.B.: Evaluation of the “hill climbing” and the “incremental conductance” maximum power point trackers for photovoltaic power systems. IEEE Trans. Energy Conv. **27**(4), 922–929 (2012)
9. Efendi, M.Z., Murdianto, F.D., Setiawan, R.E., Mubarak R.H.: Performance evaluation of MPPT using modified PSO algorithm for battery charge application. Int. Electron. Symp. Eng. Technol. Appl. (IES-ETA) (2018)
10. Subudhi, B., Pradhan, R.: A new adaptive maximum power point controller for a photovoltaic system. IEEE Trans. Sustain. Energy **10**(4), 1625–1632 (2019)

11. Latif, T., Hussain Syed, R.: Design of a charge controller based on sepic and buck topology using modified incremental conductance MPPT. In: Proceedings of the 8th International Conference on Electrical and Computer Engineering. Dhaka, Bangladesh; 20–22 December, 2014, vol. 27 (2012)
12. Agarwal, J., Parmar, G., Gupta, R., Sikander, A.: Analysis of grey wolf optimizer based fractional order PID controller in speed control of DC motor. *Microsyst. Technol.* **24**(12), 4997–5006 (2018)
13. Sikander, A., Thakur, P.: Reduced order modelling of linear time-invariant system using modified cuckoo search algorithm. *Soft. Comput.* **22**(10), 3449–3459 (2018)
14. Verma, P., Patel, N., Nair, C.K., Sikander A.: Design of PID controller using cuckoo search algorithm for buck-boost converter of LED driver circuit. In: proceedings of 2nd Annual Southern Power Electronics Conference (SPEC) pp. 1–6. IEEE, New Zealand (2016)
15. Sikander, A., Prasad, R.: New technique for system simplification using Cuckoo search and ESA. *Sadhana* **42**(9), 1453–1458 (2017)
16. Bhatt, R., Parmar, G., Gupta, R., Sikander, A.: Application of stochastic fractal search in approximation and control of LTI systems. *Microsyst. Technol.* **25**(1), 105–114 (2019)
17. Vimalarani, C., Kamaraj, N., Chitti Babu, B.: Improved method of maximum power point tracking of PV array using hybrid intelligent controller. *Elsevier J. OPTIK* **168**, 403–415 (2018). <https://doi.org/10.1016/j.jleo.2018.04.114>
18. Noman, A..M., Addoweesh, K.E., Mashaly, H.M. A fuzzy logic control method for MPPT of PV systems, pp. 875–377. IEEE (2012). 978-1-4673-2421-2/12
19. Taherbaneh, M., Menhaj, M.B.: A fuzzy-based maximum power point tracker for body mounted solar panels in LEO satellites. In: 2007 IEEE/IAS Industrial & Commercial Power Systems Technical Conference, pp. 1–6. IEEE (2007)
20. Kolsi, S., Samet, H., Ben, Amar M.: Design analysis of DC-DC converters connected to a photovoltaic generator and controlled by MPPT for optimal energy transfer throughout a clear day. *J. Power Energy Eng.* **2**, 27–34 (2014)
21. Texas Instruments: Application report SLVA372C; November 2009, Revised January 2014. pp. 1–8
22. Cho, S.Y., Lee, I.O., Moon, S., Moon, G.W., Kim, B.C., Kim, K.Y.: Constant Current Charging in Series-Series Compensated Nonradiative Wireless Power Link, 2792–2795. IEEE (2013)
23. Ahamad, N., Uniyal, S., Sikander, A., Singh, G.: A comparative study of PID controller tuning techniques for time delay processes. *UPB Sci. Bull. Series C Electr. Eng. Comput. Sci.* **81**(3), 129–142 (2019)
24. Dave Mitulkumar, R., Dave, K.C.: Analysis of boost converter using PI control algorithms. *Int. J. Eng. Trends Technol.* **3**, 71–73 (2012)
25. Yilmaz, U., Kircay, A., Borekci, S.: PV system fuzzy logic MPPT method and PI control as a charge controller. *Renewable Sustain. Energy Rev.* **81**, 994–1001 (2018)

Evaluation of Soil Physical, Chemical Parameter and Enzyme Activities as Indicator of Soil Fertility with SFM Model in IA–AW Zone of Rajasthan



Jyoti Sihag, Divya Prakash, and Parul Yadav

Abstract Soil fertility management of agricultural and waste land was a complicate process that involved multiple physical, chemical parameters and enzyme activities criteria. Field data was collected from two types of lands: agricultural and waste land. The variation in soil parameters was assessed using the deterioration index (DI). Soil laboratory analysis was performed following standard methods. Soil parameters considered were electrical conductivity (EC), pH, organic carbon (OC), organic matter (OM), nitrogen (N), potassium (K), phosphorus (P), zinc (Zn), copper (Cu), iron (Fe), manganese (Mn), sulphur (S), cation exchange capacity (CEC), soil contents, texture, calcium carbonate (CaCO_3), bulk density (BD), acid phosphatase activity (APA), alkaline phosphatase activity (ALPA), dehydrogenase activity (DHA) and urease activity (UA). The high status was observed in 70% FLS and 64% WLS soil for sulphur nutrient. Compared to reference site (FLS), overall deterioration index value was +53.53% observed for WLS of IA–AW zone. In WLS, positive DI value +72.32 and +57.14% was assessed for electrical conductivity and calcium carbonate, respectively. The increasing DI of dehydrogenase and sulphur nutrient –569.08 and –16.98% were analyzed for WLS in IA–AW zone. In this study, we are using a SFM model based on multi-criteria to identify exact soil fertility problem to sustainably achieve goals such as improvement of soil quality and agricultural production. This study can be applicable to make sustainability management of agricultural and waste land in IA–AW zone of Rajasthan. Soil fertility investigations of IA–AW zone are compulsory for efficient environmental management, soil ecology, and contribute to sustainable development of soil ecology and agricultural production.

J. Sihag

Amity School of Applied Sciences, Amity University Rajasthan, Jaipur, India

D. Prakash (✉)

Shobhit University Gangoh, Saharanpur, India

e-mail: divya1sharma1@gmail.com

P. Yadav

Amity University of Science and Instrumentation Centre, Amity University Rajasthan, Jaipur, India

Keywords SFM · IA–AW zone · Deterioration index · Soil fertility

1 Introduction

Farmers get their soil tested from ‘soil testing labs’ of government to increases their crop production. In these laboratories generally a few chemical parameters like pH, electrical conductivity, phosphorus and potassium are analyzed. In the absence of proper knowledge, the illiterate farmers use chemical fertilizers inefficient and wrongfully. In reality, the chemical fertilizers decrease the long term potential of soil. They also increase the problems like water pollution and soil pollution etc. [1]. Expanding of fertilizers in crops is strangling the sustainable development of agricultural economy. It is the important to estimate the soil fertility of farms for the sustainable management (both environmental and economical aspects) of IA-arid western zone. Generally, soil fertility term is used in soil science and it is including soil nutrients and soil organic carbon etc. [2]. Soil fertility cannot evaluate by some parameter because fertility of soil is comprehensive [3]. It can be determined by physical, chemical and biological parameters [4]. Nutrients levels of soil are varied from one land to another land. So, fertility of soil also changes. Soil fertility can be expressed as the ability of soil which behave like a suitable substrate for crops on which crops are grow easily because fertile soil has supply required nutrients, air and water to plants [5–7]. Health of soil is the capacity of agricultural production. Soil is a real, natural and dynamic body. And the soil is the foundation for most of terrestrial life [8].

In this study, we are discussing the soil fertility of IA–AW zone. In which Barmer and Jodhpur districts are laid. Jodhpur district is also known as Sun City, Gate way of Thar and the Blue city. According to geographical area, Barmer is the third and fifth largest district in Rajasthan and India, respectively. Total geographical area of IA-arid western zone is 51.237 km². The agriculture region covers 75.97% area of IA-arid western zone. Keeping in the mind the environment and economical development, study of fertility of waste land along with agriculture land is a better step. The percentile of waste land in studied zone is 24.02%. A lot of models are used in agriculture field [9]. In this study, SFM model can be used for better results in less time. It is capable in identifying soil problems like imbalanced nutrients and improving it with the help of bio-fertilizers because in most cases the leading factors in soil fertility is its nutrients status [10].

The main objective of this study was to determine the soil fertilization status of farmland and wasteland soil of IA-arid western zone. The soil fertility was evaluated by physical (soil contents, texture, bulk density) parameter, chemical (pH, electrical conductivity, organic matter, organic carbon, calcium carbonate, potassium, nitrogen, sulphur, phosphorus, cation exchange capacity) and enzyme activity (urease activity, acid phosphatase activity, alkaline phosphatase activity, dehydrogenase activity) with SFM model.

2 Materials and Methods

2.1 Study Area

The experiment was carried for IA-arid western (AW) zone of Rajasthan. The study zone stretches between $24^{\circ}58'$ and $27^{\circ}37'$ north latitude and $70^{\circ}5'$ – $73^{\circ}29'$ east longitude covering an approximate area of $51,237 \text{ km}^2$. Zone covers 4.72 million hectare area of the 'Thar' desert. All sample sites are located in IA-AW zone. In IA-AW zone, 38926.88 km^2 areas are covered by agriculture land while 12310.12 km^2 come in waste land. Soil samples of Agricultural and waste land were taken from different lands of Jodhpur district and Barmer, respectively. It is bounded in the west side by Pakistan, in the east by Pali and Jalore district, in north by Bikaner and northwest side touches Jaisalmer. Southern boundary of zone is shared by Gujrat. Nagaur lies on north-eastern side of zone. The south side of zone is covered by Jalore district (Fig. 1).

2.2 Climate and Vegetation

IA-arid western zone has arid climate which characterized by extremes of temperature with cold winter and hot summer season as well as high temperature in summer, high evaporation, extremely hot winds. Dust and thunder storms are very common. The average annual rainfall of the studied zone is 285 mm. During April to July, dust storms are easily seen in IA-arid western zone. Northerly and north westerly winds are common for IA-arid western zone. During summer months May–July, the wind speed is highest. The minimum temperatures often recorded below freezing point and maximum temperature are above 49°C for IA-AW zone. For studied zone,



Fig. 1 Location of study area in Rajasthan

average minimum and maximum temperature is 8°C and 40°C, respectively (Source: Government of Rajasthan Department of Agriculture).

The wild bushes, grasses, trees and thorny shrubs are found in natural vegetation of IA-AW zone. After the rain, grasses only survived for few months. In grasses mainly tantia (*Eleusine flagellifera*), bhurat (*Cenchrus biflorus*), gramma (*Penicum antidotale*), murath (*Panicum turgidum*), sewan (*Lasiurus sindicus*), anjan (*Cenchrus ciliaris*), munja (*Saccharum griffithii*) and murath (*Panicum turgidum*) etc. are found. In the studied zone mainly kair (*Capparis aphylla*), rohira (*Tecomella undulata*), khejri (*Prosopis cineraria*), peepal (*Ficus religiosa*), neem (*Azadirachta indica*), babool (*Vachellia nilotica*), kumat (*Acacia senegal*), phog (*Calligonum polygonoides*), jal (*Salvadora oleoides*), synia (*Crotalaria burhia*), datura (*Datura inoxia*), kheemp (*Leptadenia pyrotechnica*), ber (*Ziziphus mauritiana*), akra (*Calotropis procera*), thar (*Euphorbia caducifolia*), bui (*Aerna tomentosa*), vipeni (*Tephrosia purpuria*), dhamasa (*Fagonia cretica*) etc. are found. In IA-AW zone majorly rainfed crops like guar (*Cyamopsis tetragonoloba*), wheat (*Triticum aestivum*), mustard (*Brassica juncea*), til (*Sesamum indicum*), moong (*Vigna radiata*), chillies (*Capsicum spp.*), jower (*Sorghum*), bajra (*Pennisetum glaucum*), gram (*Cicer arietinum*), barley (*Hordeum vulgare*), cumin (*Cuminum cyminum*) and rape-seed (*Brassica napus*) are grown in this areas where irrigation water is available [11].

2.3 Soil Sampling

This study was conducted on farm land and waste land soil that is taken in IA-Arid Western Zone of Rajasthan province. Both type of soil was obtained from a depth of 0–30 cm from surface level. Farm land soil samples were taken from agricultural sites of Jodhpur district. From waste land of Barmer district, waste land soil samples were collected. The weight of soil was obtained 3 kg. Soil samples were air dried for chemical and physical analysis. But for enzyme activities analysis, soil sample were stored in refrigerator. After drying, soil samples were grinded by grinder. Then soil samples were sieved by 2 mm sieve to remove roots of plants and pebbles. The *Entisols* and *Aridisols* soil orders are present in IA-arid western zone of Rajasthan. In which, *calcids*, *cambids*, *salids*, *palids*, *torripsamments* and *quartzipsamments* soil groups are more dominant.

2.4 Method of Physico-chemical and Enzyme Activities

The soil physio-chemical methods and enzyme activities considered for the study are presented in Tables 1 and 2.

Table 1 Assessment of soil physico-chemical by following methods

Parameters	Methods or Instruments	References
Soil contents	Hydrometer method	Bishnoi and Brar [12]
BD	By density bottle	Mathur [13]
CaCO_3	Rapid titration method	Puri [14]
pH (1:2)	By glass electrode	Piper [15]
EC (1:2)	By conductivity meter	Piper [15]
N	Alkaline permanganate method	Subbiah and Asija [16]
P	Olsen method	Olsen et al. [17]
K	Flame photometer method	Black et al. [18]
S	By ammonium acetate-acetic acid method	Bishnoi and Brar [12]
OC	Wet digestion method	Walkley and Black's [19]
OM	OC multiply with 1.724	Kahle et al. [20]
Micro-nutrients	DTPA extractable method	Lindsay and Norvall [21]
CEC	By sodium acetate method	Chapman [22]

BD Bulk density; CaCO_3 Calcium carbonate; EC Electrical conductivity; N Nitrogen; P Phosphorus; K Potassium; S Sulphur; OC Organic carbon; OM Organic matter; CEC Cation exchange capacity

Table 2 Assessment of soil enzyme activities by following methods

Parameters	Methods	References
DHA	TTC reduction technique	Casida [23]
APA	PNP method	Tabatabai and Bremner [24]
ALPA	PNP method	Tabatabai and Bremner [24]
UA	Indophenol blue method	McGarity and Myers [25]

DHA Dehydrogenase activity; APA Acid phosphatase activity; ALPA Alkaline phosphatase activity; UA Urease activity

2.5 Statistical Analysis

The deterioration index value was calculated by the using of Microsoft excel 2007. The DI was calculated as the relative difference between values of individual soil property of reference site and compared site. Physico-chemical properties and enzyme activities of soil considered for DI were soil contents (sand, silt, clay), calcium carbonate, bulk density, pH, EC, OM, OC, N, P, K, Zn, Fe, Cu, Mn, S, CEC, DH, AP, ALP and urease. For waste land soil parameter, the deterioration index was assessed by an Eq. (1) and that was:

$$\text{Deterioration index} = [A_{\text{FLS}} - A_{\text{WLS}}]/A_{\text{FLS}} \times 100 \quad (1)$$

where, A_{FLS} was average value of soil property in FLS (farm land soil) and A_{WLS} was average value of soil property in WLS (waste land soil). In this study, FLS and WLS were reference and compared site, respectively. Negative sign of DI value suggest increasing order and positive sign of DI values suggest decreasing order of soil property in WLS as compared to FLS.

2.6 SFM Model

The soil fertility of IA-arid western zone was evaluated by the helping of soil fertility management (SFM) model [26]. SFM model has the specific objective of devising the best option in terms of management of soil fertility. The results of SFM model were helpful to determine and resolve quickly the problems in fertility of the soil. This model was not only just helping in increasing soil fertility of waste land rather than it was also utilized to manage fertility of farm land. The model was contributed to identifying problems or gaps in the soil fertility. Model that was based on physico-chemical and enzyme activities data was capable of supporting to fertility management.

3 Result and Discussions

3.1 Physical Parameter Evaluation of Farm Land Soil (FLS)

The mean data of soil physico-chemical parameters were shown in Table 1. Soil contents like sand, silt and clay were ranged from 75.06 to 87.90%, 2.10 to 18.34% and 10.03 to 14.25% for farmland soil of IA-AW zone. The mean values of sand, silt and clay content 78.44, 9.5 and 12.06%, respectively was determined. Same trends of sand, silt and clay were reported [27]. Almost similar trends of silt and clay content were observed for Jodhpur [28, 29]. The soil of farmland sites were categorized as loamy sand. Almost similar trends of texture were analyzed [27, 30, 31]. Some

different results of texture were also analyzed for Jodhpur [32, 33]. The calcium carbonate was varied from 1.9 to 6.92 percent in farm land soil. Mean calcium carbonate was 2.8 percent observed. For calcium carbonate, different trends were observed [27, 28]. The range of bulk density was assessed from 1.41 to 1.57 g/cc with a mean 1.52 g/cc. Results from this study, show some similarity in bulk density to those reported for Bap (Jodhpur) [34].

3.2 Physical Parameter Evaluation of Waste Land Soil (WLS)

Mean value for sand content of waste land soil samples was 94.04%. The mean values of clay and silt contents of soils were 2.36 and 8.60%, respectively. For wasteland soil samples: sand, silt and clay contents were varied from 90.02 to 98.36%, 2.36 to 9.97% and 1.09 to 9.84%, respectively. Almost similar trends of silt content were analyzed [28, 29]. The wasteland soil of IA-arid western zone was categorized as sand. Same trend of texture was assessed [29]. While different soil texture was observed for Barmer [35]. The range of bulk density was assessed from 1.49 to 1.58 g/cc with a mean 1.54 g/cc in WLS of IA-AW zone. A different trend of soil bulk density was measured [34]. The calcium carbonate of IA-AW zone was examined from 1.02 to 3.34%. Mean calcium carbonate was 1.2% calculated. For calcium carbonate, different results were analyzed [36].

3.3 Chemical Parameter Evaluation of Farm Land Soil (FLS)

For farmlands soils, pH value was ranged from 7.3 to 9.02 with mean value of 8.1 (Table 1). About 52% soil samples of surveyed areas were normal in nature. Remaining 30% and 18% soil of farmland were showed pH in moderately alkaline and strong alkaline range, respectively. Almost same trends of mean pH were observed for Jodhpur [29, 37–41]. The pH was assessed in normal range for 97.2% area of Jodhpur [42]. Different trends of pH were reported for Jodhpur [27, 30–33, 43–48]. The electrical conductivity of soil were ranged from 0.11 to 2.74 dS/m. Electrical conductivity (EC) was present in normal range for 46% FLS indicates that salinity was a not problems in these soil. Soils were found in critical (0.8–1.6 dS/m) and injurious (>2.5 dS/m) range for 34 and 20% FLS, respectively. The mean value of electrical conductivity 1.59 dS/m was observed for farmland soil of IA-AW zone. No salinity was examined in Jodhpur [48]. But normal electrical conductivity was examined for 97% area of Jodhpur [42]. Almost same trends of soil electrical conductivity was analyzed [28, 33, 37, 39, 40, 43, 48]. Different trends of EC were examined [29–32, 44, 46]. For FLS, organic carbon was varied from 0.16 to 0.78% with an average of 0.24%. In IA-AW, organic carbon was observed in low (<0.4%), medium (0.4–0.75%) and high (>0.75%) range for 87%, 10% and 3% farmland soil. Low to medium status of organic carbon was observed for Jodhpur [48]. Different

trends of organic carbon were reported [28–31, 33, 34, 38, 40, 44, 46]. Result from this study show similar trends to OC [37, 43, 47]. Similarly, organic matters were calculated from 0.27 to 1.34% with a mean of 0.41%. Similar trends of soil OM was assessed for Jodhpur [39, 47]. Soil nitrogen under studied varied from 170 to 582 kg/ha with a mean value 235 kg/ha. The nitrogen concentration in 90%, 6% and 4% farmland were assessed in low (<280 kg/ha), medium (280–560 kg/ha) and high (>560 kg/ha) range, respectively. Some different trends of nitrogen nutrient were assessed for Jodhpur [37, 38, 47]. Similar trends of N were examined [43]. Soil nitrogen and phosphorus concentrations were reported in low level for Jodhpur [42]. Similarly, low concentration of nitrogen was reported for Jodhpur [49, 50]. Phosphorus concentration of the soils was ranged from 4.5 to 61 kg/ha with mean value 21 kg/ha. Olsen phosphorus concentration was assessed in low and medium range for 30 and 45% FLS, respectively. High (>25 kg/ha) concentration of phosphorus was observed in 25% FLS. Low phosphorus concentration was observed for 71.6% Jodhpur area [42]. Different trends of soil phosphorus were observed for Jodhpur [31, 33, 38, 40, 41, 43, 44]. Concentration of soil potassium were varied from 87 to 672 kg/ha with mean value 487 kg/ha. Soil potassium was present in medium range for 73% FLS. Remaining 11% and 16% farm land soils were assessed potassium in low and high range, respectively. For Jodhpur, medium status of phosphorus and potassium was analyzed [49, 50].

In FLS, concentration of zinc and iron were varied from 0.25 and 4.1 ppm and 2.2 to 6.2 ppm, respectively. Average concentration of zinc and iron, 1.06 ppm and 4.7 ppm were found. The sufficient availability of iron (>4.5 ppm) and zinc (>0.6 ppm) nutrients was observed in 52% and 58% FLS, respectively. While remaining 48% and 42% FLS were found in deficient range for iron and zinc. Range of copper and manganese nutrient were found from 0.09 to 4.4 and 0.2 to 11.2 ppm in FLS, respectively. Mean concentration of copper and manganese, 0.86 ppm and 4.23 ppm were observed in farmland soil. Sufficient availability of copper and manganese nutrient were assessed in 72% and 79% FLS, respectively. While 28% and 21% farm land soil samples were found in deficient range for Cu and Mn nutrient, respectively. Almost similar deficiency of Zn, Cu and Mn were reported for FLS [48]. Deficiency of zinc, iron and manganese was observed in 31.25%, 27.5% and 15% FLS samples of Jodhpur, respectively [51]. Different trends of K, Zn, Cu and Mn were reported for Jodhpur [29]. Sulphur content was varied from 4.8 to 32.4 ppm with mean value of 21.2 ppm. Sulphur concentration in 70% FLS was observed in high (>20 ppm) range while 12% and 18% farmland soil assessed in low (<10 ppm) and medium (10–20 ppm) range, respectively. The mean value of S nutrient 21.2 ppm was examined in FLS. Cation exchange capacity of farmland soil was varied from 2.62 to 6.84 meq/100 g with mean value 4.50 meq/100 g. Result from this study show similar trends in CEC [28]. Some different results of CEC were assessed [27].

3.4 Chemical Parameter Evaluation of Waste Land Soil (WLS)

Soil pH was varied widely from 6.31 to 9.60 with an average value of 7.52. Soil pH was generally found in normal (natural) range for 68% WLS. Remaining 30% and 2% soil were showed pH in slightly acidic and strong alkaline range, respectively. Soil electrical conductivity was ranged from 0.14 to 3.63 dS/m with an average content of 0.44 dS/m. Electrical conductivity was found in normal (<0.8 dS/m) range for 90% WLS. While remaining 10% wasteland soil samples were showing EC above 2.5 dS/m. Almost same trends of pH and EC were reported [28, 37, 40]. Some different trends of electrical conductivity were also observed [29–31, 33, 36, 38, 42–44, 46]. Organic carbon and organic matter was varied from 0.07 to 0.59% and 0.12 to 1.02% with mean values of 0.12% and 0.20%, respectively. Results from this study show almost similar trends for organic carbon content [28, 29, 36, 38, 40, 41]. Different trends of organic carbon were reported [30, 31, 33, 35, 37, 43, 44, 46]. Soil organic carbon in 96% WLS was observed in low (<0.40%) range. In WLS, remaining 4% area was found in medium (0.40–0.75%) range of organic carbon. Different trend of soil OM was observed [46]. But, almost similar trends of organic matter were reported for Barmer [36]. Concentration of soil nitrogen were varied from 70 to 327 kg/ha with a mean value of 157 kg/ha. In this observation, nitrogen concentrations were observed in low and medium range for 95% and 5% WLS, respectively. Similar trends of soil nitrogen were observed [35, 43]. Very low concentrations of nitrogen nutrient and organic carbon were observed [49, 52]. Different results of nitrogen nutrient were reported [37, 38, 42, 46]. Concentration of nutrient phosphorus were found from 3 to 42 kg/ha with a mean value 17 kg/ha. Soil phosphorus concentration in 50% WLS was observed in low (<12.5 kg/ha) range. While 40% and 10% WLS samples were assessed in medium (12.5–25 kg/ha) and high (>25 kg/ha) range, respectively. Different trends of Soil P was reported [31, 33, 35, 38, 40, 41, 43]. The range of potassium nutrient was varied from 84 to 594 kg/ha with mean value 495 kg/ha. Potassium nutrient was analyzed in low, medium and high range for 18%, 68% and 14% WLS, respectively. Similar trends of iron and potassium was examined [35]. Medium availability of P and K was examined for Barmer [49, 50]. Soil P concentration were reported low to medium while K assessed in adequate [52].

The concentration of soil sulphur was varied from 2 to 40.2 ppm with a mean value of 24.8 ppm. High range of sulphur nutrient was assessed in 64% WLS. Sulphur was analyzed in low and medium range for 7% and 29% WLS samples, respectively. Cation exchange capacities of soil were varied from 1.07 to 4.20 meq/100 g. Mean value of cation exchange capacity was 3.07 meq/100 g observed. Micronutrient zinc and iron concentration were varied from 0.18 to 0.82 ppm and 2.0 to 6.84 ppm, respectively. For WLS, mean concentration of zinc and iron was observed 0.62 and 4.20 ppm, respectively. The sufficient availability of zinc (>0.6 ppm) and iron (>4.5 ppm) was assessed in 51% and 42%, respectively. Remaining 49% and

58% WLS were found deficiency of zinc and iron, respectively. For WLS, mean concentration of copper and manganese was observed 0.41 and 2.64 ppm, respectively. Micronutrient Cu and Mn concentration were varied from 0.03 to 0.87 ppm and 0.4 to 7.38 ppm, respectively. The sufficient availability of copper and manganese were observed in 66% and 47%, respectively. In WLS, 33% soil was showed deficiency (<0.2 ppm) of copper. Just like that, manganese was found in deficiency for 53% soil. For Barmer, different trends of iron and potassium were measured [29, 36]. Different trends of soil zinc, copper and manganese were reported [29, 36].

3.5 Enzyme Activities Evaluation of Farm Land Soil (FLS)

For farmland soil, mean acid phosphatase enzyme activity was $3.744 \mu \text{ mol PNP Sec}^{-1} \text{ g}^{-1}$. Range of acid phosphatase enzyme activity was varied from 2.543 to $4.945 \mu \text{ mol PNP Sec}^{-1} \text{ g}^{-1}$ for FLS of IA-AW zone. The enzyme activity of alkaline phosphatase was varied from 0.443 to $0.476 \mu \text{ mol PNP Sec}^{-1} \text{ g}^{-1}$ with a mean value of $0.459 \mu \text{ mol PNP Sec}^{-1} \text{ g}^{-1}$. Activity of acidic phosphatase enzyme has mainly observed in acid soil. Also this, acidic phosphatase enzyme activity is found in alkaline or neutral soil [53]. APA and ALPA have good relation with inorganic P fraction. The dehydrogenase enzyme activity in farm land soil was ranged from 0.72 to $1.234 \text{ p Kat g}^{-1}$. The average soil dehydrogenase enzyme activity $0.977 \text{ p Kat g}^{-1}$ was observed for farmland soil samples. The dehydrogenase enzyme activity has capable to measure microbial oxidative activity. Urease enzyme activities were varied from 0.022 to $0.193 \text{ NH}_4^+ - \text{N mg/gm dry soil/6 h}$. Mean value of urease enzyme activity was $0.0206 \text{ NH}_4^+ - \text{N mg/gm dry soil/6 h}$ observed in these soil samples.

3.6 Enzyme Activities Evaluation of Waste Land Soil (WLS)

The mean acid phosphatase enzyme activity was measured $2.937 \mu \text{ mol PNP Sec}^{-1} \text{ g}^{-1}$ within the range of $2.561\text{--}3.313 \mu \text{ mol PNP Sec}^{-1} \text{ g}^{-1}$. For waste land soil samples, the alkaline phosphatase enzyme activity was varied from 0.401 to $0.457 \mu \text{ mol PNP Sec}^{-1} \text{ g}^{-1}$. The mean value of alkaline phosphatase was $0.429 \mu \text{ mol PNP Sec}^{-1} \text{ g}^{-1}$ calculated in these soil samples. Soil pH has directly related to alkaline phosphatase enzyme activity [54]. Dehydrogenase enzyme activity was assessed from 5.707 to $7.367 \text{ p Kat g}^{-1}$ with mean value $6.537 \text{ p Kat g}^{-1}$. For WLS, data of urease enzyme activity was observed from 0.003 to $0.006 \text{ NH}_4^+ - \text{N mg/gm dry soil/6 h}$. The mean urease enzyme activity $0.004 \text{ NH}_4^+ - \text{N mg/gm dry soil/6 h}$ was calculated for waste land soils of IA-arid western zone. Urease enzyme activity has able to convert urea into carbon dioxide and ammonia (Tables 3 and 4).

Table 3 Mean data for physico-chemical parameters of FLS and WLS

Parameters	Mean data of FLS	Mean data of WLS
Sand (%)	78.44	94.04
Silt (%)	9.5	8.6
Clay (%)	12.06	2.36
Texture	Loamy sand	Sand
CaCO ₃ (%)	2.8	1.2
Bulk density (g/cc)	1.52	1.54
pH	8.1	7.52
EC (dS/m)	1.59	0.44
OC (%)	0.24	0.12
OM (%)	0.41	0.20
N (kg/ha)	235	157
P (kg/ha)	21	17
K (kg/ha)	487	495
Zn (ppm)	1.06	0.62
Fe (ppm)	4.7	4.2
Cu (ppm)	0.86	0.41
Mn (ppm)	4.23	2.64
S (ppm)	21.2	24.8
CEC (meq/100 g)	4.50	3.07

Table 4 Mean data for enzyme activity of FLS and WLS

Parameters	Mean of FLS	Mean of WLS
AP	3.744	2.937
ALP	0.459	0.429
DH	0.977	6.537
UA	0.0206	0.004

3.7 DI Value Between FLS and WLS

According to calculation in physico-chemical parameters and enzyme activities, positive DI values were calculated (except sand content, bulk density, potassium, sulphur and dehydrogenase) for wasteland soil of IA-AW zone. The negative DI –19.88% were estimated for sand content in WLS with respect to farmland soil. For silt and clay, respectively positive DI values +9.47% and +80.43% were observed in wasteland soil. From farmland soil to waste land, texture of soil varies from loamy sand to sand. The percentile of sand content in WLS was observed relatively more as compare to sand content of FLS. The decreasing DI of calcium carbonate +57.14% was examined for WLS. However, in case of soil bulk density, increasing DI –1.31% were observed for WLS.

Compared to FLS, waste land soils showed low mean pH values resulting positive DI value +7.16% was evaluated. The decreasing DI of electrical conductivity + 72.32% was observed for WLS. For organic carbon and organic matter, positive DI +50% and +51.21 percentile were analyzed in WLS samples. For nitrogen nutrient the positive DI +33.19% was estimated for WLS. In decreasing order, +19.04% DI value was observed for phosphorus in waste land soil. Compared to FLS, waste land soil was found high potassium concentration resulting increasing DI values – 1.64% was observed in waste land sites. In soil zinc and iron concentration, positive values of DI were +41.50% and +10.63% observed in WLS samples. In WLS, positive DI values of copper and manganese +52.32% and +37.58% were observed, respectively. Similarly, the positive DI of CEC +31.77% was analyzed for WLS with respect to FLS. The DI of sulphur nutrient, –16.98% was observed in WLS. The positive DI +21.55% were measured for acid phosphatase enzyme activity in WLS with respect to farm land soil. Similarly, in decreasing order +6.53% DI value was assessed for alkaline phosphatase in WLS. For urease enzyme activity the positive DI +80.58% was calculated for WLS. But in case of dehydrogenase enzyme activity, negative –569.08% DI value was observed for WLS.

3.8 Data Analysis by SFM Model

A Fertilization status of soil parameters data of IA–AW zone were analyzed with the help of SFM model. In this data, non fertile land data was separated from fertile soil data and were further analyzed. Data was further analyzed to observe positive and negative results. The positive value in those results show the deficiency of that nutrient in that zone and the negative value show the excess of nutrient.

[‘N: 206’, ‘OC: 0.42’, ‘P: 2.0’, ‘Zn: 0.22’, ‘Fe: 1.03’, ‘Cu: 0.17’]
[‘N: 100’, ‘OC: 0.23’, ‘P: 7.97’, ‘Zn: 0.09’, ‘Fe: 2.08’, ‘Cu: 0.05’, ‘Mn: 0.48’]
[‘N: 126’, ‘OC: 0.36’, ‘Fe: 0.31’, ‘Mn: 0.2’]
[‘N: 32’, ‘OC: 0.21’, ‘P: –8.0’, ‘K: 1’, ‘Zn: 0.33’, ‘Cu: 0.12’, ‘Mn: 0.73’]
[‘N: 53’, ‘OC: 0.39’, ‘K: 32’, ‘Zn: 0.42’, ‘Fe: 1.77’, ‘Cu: 0.09’, ‘Mn: 0.6’]

4 Conclusions

In The objective of this study was to identify soil fertility in IA–AW zone of Rajasthan, based on the soil properties. Fertilization status of collected soil samples from IA–AW zone were analyzed by chemical parameter (pH, EC, OC, OM, calcium carbonate, N, P, K, S, Zn, Fe, Cu, Mn, CEC), physical parameter (sand, silt, clay, bulk density) and biological parameters (enzyme activities like DHA, APA, ALPA, UA). Based on calculation of SFM model, agricultural land was observed in more fertile fertilization status as compared to WLS. According to data, the deficiency of nitrogen nutrient

was assessed for 90% FLS and 95% WLS. The deficiency of zinc and phosphorus concentration was observed in 49% and 50% waste land, respectively. The observation showed that, low status of organic carbon was found in 90% waste land soil of studied zone. The normal status of electrical conductivity was observed in 52% farm land and 90% waste land. In IA-arid western zone, positive DI +80.58% and +80.43% were found for urease enzyme activity and clay content, respectively.

SFM model suggested that nitrogen, potassium, zinc and phosphorus deficiency could be improved by bio-fertilizer like *Azotobacter*, *Acetobacter*, *Rhizobium*, *Azospirillum*, *B. subtilis*, *Saccharomyces*, *Bacillus megaterium*, *Bacillus edaphicus*, *Pseudomonas striata*, *Enterobacter*, *Bacillus circulans* and *Bacillus mucilaginosus* because use of bio-fertilizer has a unique and appreciable way to improve and sustainable soil fertility of waste land and agricultural land.

References

1. Sihag, J., Prakash, D., Yadav, P.: Comparative study of soil fertility based on SFM computational model for IB-INW and IC-HAPI zone. *Int. J. Mech. Prod. Eng. Res. Develop.* **9**(4), 499–508 (2019)
2. Desbiez, A., Matthewsa, R., Tripathi, B., Ellis-Jones, J.: Perceptions and assessment of soil fertility by farmers in the mid-hills of Nepal. *Agricu. Ecosyst. Environ.* **103**, 191–206 (2004)
3. Bautista-Cruz, A., Carrillo-Gonzalez, R., Arnaud-Vinas, M.R., Robles, C., De Leon-Gonzalez, F.: Soil fertility properties on *Agave Angustifolia* Haw Plantations. *Soil Tillage Res.* **96**, 342–349 (2007)
4. Abbott, L.K., Murphy, D.V. (eds.): *Soil Biological Fertility: A Key to Sustainable Land Use in Agriculture*. Springer, Berlin, Heidelberg, New York (2003)
5. Sihag, J., Prakash, D.: An Assessment of the soil fertilization status of IB-INW zone of Rajasthan. *Int. J. Mech. Prod. Eng. Res. Develop.* **9**(2), 137–150 (2019)
6. Izac, A.M.: Economic aspects of soil fertility management and agroforestry practices. CAB International 2003. In: Schroth, G., Sinclair, F.L. (eds.) *Trees, Crops and Soil Fertility*. 13–20 (2003)
7. Adjei-Nsiah, S., Kuyper, T.W., Leeuwis, C., Abekoe, M.K., Giller, K.E.: Evaluating sustainable and profitable cropping sequences with cassava and four legume crops: effects on soil fertility and maize yields in the forest/ savannah transitional agro-ecological zone of Ghana. *Field Crops Res.* **103**, 87–97 (2007)
8. Wilding, L.P., Lin, H.: Advancing the frontiers of soil science towards a geoscience. *Geoderma* **131**, 257–274 (2006)
9. Sihag, J., Prakash, D.: A Review: importance of various modeling techniques in agriculture/crop production. In: Ray, K., Sharma, T., Rawat, S., Saini, R., Bandyopadhyay, A. (eds.) *Soft Computing: Theories and Applications. Advances in Intelligent Systems and Computing* 742, 699–707 (2019)
10. Alfaia, S.S., Riberio, G.A., Nobre, A.D., Flavio, L., Luizao, J.: Evaluation of soil fertility in smallholder agroforestry systems and pastures in Western Amazonia. *Agric. Ecosyst. Environ.* **102**, 409–414 (2004)
11. Hussain, M.M.: Agro-climatic zones and economic development of Rajasthan. *Int. J. Hum. Soc. Sci. Inv.* **4**(2), 50–57 (2015)
12. Bishnoi, S.R., Brar, S.P.S.: *A Handbook on Soil Testing*, pp. 50–52. Communication Centre. Punjab Agricultural University, Ludhiana (1988)
13. Mathur, G.M.: Status, Availability and Transformation of Zinc in Irrigated North-West Plain Soils of Rajasthan. Ph.D. Thesis, Rajasthan Agriculture University, Bikaner (2001)

14. Puri, A.N.: A new method of estimating total carbonates in soils. Imp. Agric. Res. Inst. Pusa. Bull. 206–207 (1930)
15. Piper, C.S.: Soil and Plant Analysis. University of Adelaide, Adelaide, Australia (1950)
16. Subbiah, B.V., Asija, G.L.: A rapid procedure for the determination of available nitrogen in soils. Curr. Sci. **25**, 259–260 (1956)
17. Olsen, S.R., Cole, C.V., Watanabe, F.S., Dean, L.A.: Estimation of Available Phosphorus in Soils by Extraction with Sodium Bicarbonate. Washington: USDA Circular 939, US Government Printing Office (1954)
18. Black, C.A.: Methods of Soil Analysis, Part 2. American Society of Agronomy, Madison, WI, USA
19. Walkley, A., Black, I.A.: An examination of the Degtjareff method for determining soil organic matter and a proposed modification of the chromic acid titration method. Soil Sci. **37**, 29–38 (1934)
20. Kahle, P., Beuch, S., Boelcke, B., Leinweber, P., Schulten, H.: Cropping of Miscanthus in Central Europe: biomass production and influence on nutrients and soil organic matter. Euro. J. Agron. **15**, 171–184 (2001)
21. Lindsay, W.L., Norvell, W.A.: Development of a DTPA soil test for zinc, iron, manganese and copper. Soil Sci. Soc. Am. J. **42**(3), 421–428 (1978)
22. Chapman, H.D.: Cation-exchange Capacity. In: Black, C.A. (ed.) Method of Soil Analysis. Part 2: Chemical and Microbiological Properties, pp. 891–99.0 The American Society of Agronomy, Madison, Wisconsin (1965)
23. Casida Jr., L.E.: Microbial metabolic activity in soil as measured by dehydrogenase determinations. Appl. Environ. Microbiol. **34**(6), 630–636 (1977)
24. Tabatabai, M.A., Bremner, J.M.: Use of p-nitrophenyl Phosphate for assay of soil phosphatase assay. Soil Biol. Biochem. **1**, 371–376 (1969)
25. McGarity, J.W., Myers, M.G.: A survey of urease activity in soils of Northern New South Wales. Plant Soil **27**, 217–238 (1967)
26. Sihag, J., Prakash, D., Gupta, H.: Soil Fertilization Status Assessment for IC-HAPI Zone of Rajasthan with SFM Computational Model. In: Pant M., Sharma T., Verma O., Singla R., Sikander A. (eds) Soft Computing: Theories and Applications. Advances in Intelligent Systems and Computing, Springer, Singapore. 1053, 1425–1439 (2020)
27. Gandhi, A.P., Paliwal, K.V.: Effect of Different Quality Irrigation Waters and Soil Texture on the Yield and Uptake of Nutrients by Wheat. Proc. Indian Natn. Sci. Acad. B **41**, 440–451 (1975)
28. Chaudhary, D.R., Shukla, L.M.: Boron status of arid soils of Western Rajasthan in relation to their characteristics. J. Indian Soc. Soil Sci. **52**(2), 194–196 (2004)
29. Vyas, A.D., Vyas, M., Kalla, V.: Complex permittivity of soils of Western Rajasthan at microwave frequency. Solid State Phenom. **209**, 10–13 (2014)
30. Vyas, M., Vyas, A.: Diversity of *Arbuscular Mycorrhizal* Fungi associated with Rhizosphere of Capsicum Annum in Western Rajasthan. Int. J. Plant Animal Environ. Sci. **2**(3), 256–262 (2012)
31. Mathur, N., Singh, J., Bohra, S., Vyas, A.: Arbuscular mycorrhizal status of medicinal holophytes in saline areas of Indian Thar Desert. Int. J. Soil Sci. **2**(2), 119–127 (2007)
32. Joshi, D.C., Toth, T., Sari, D.: Spatial variability of electrical conductivity of soils irrigated with brackish water in the arid region of Rajasthan India. Ann. Arid Zone **45**(1), 9–17 (2006)
33. Tamboli, M., Vyas, A.: Mycorrhizae at polluted site of Western Rajasthan. Int. J. Plant Animal Environ. Sci. **2**(4), 206–212 (2012)
34. Singh, G., Sharma, R.: Effects of different land use changes and spatial variation in rainfall on soil properties and soil carbon storage in Western Rajasthan India. Ann. Adv. Agric. Sci. **1**(2), 43–53 (2017)
35. Mishra, B.K., Singh, B., Dubey, P.N., Joshi, A., Kant, K., Maloo, S.R.: Biochemical characteristics and microbial association of isabgol (*Plantago ovata* Forsk.) growing soils in Western arid region of India. African J. Microbiol. Res. **9**(10), 695–700 (2015)

36. Meena, M., D.P., J., Lowry, M.: Analysis of physico-chemical parameters of diesel oil contaminated soil collected from barmer. *Int. J. Basic Appl. Chem. Sci.* **3**(4), 15–19 (2013)
37. Kulloli, R.N., Mathur, M., Kumar, S.: Dynamics of top-down factors with relation to ecological attributes of an endangered species *Commiphora wightii*. *J. Appl. Nat. Sci.* **8**(3), 1556–1564 (2015)
38. Rao, A.V., Venkateswarlu, B.: Microbial ecology of the soils of Indian desert. *Agric. Ecosyst. Environ.* **10**(4), 361–369 (1983)
39. Verma, P., Kumar, V.S.K.: Inter correlation between soil properties and growth of *Azadirachta Indica* in various types of plantation of Jodhpur Region (Rajasthan, India). *Int. J. Plant Physiol. Bio-chem.* **4**(5), 120–125 (2012)
40. Verma, N., Tarafdar, J.C., Srivastava, K.K., Sharma, B.: Correlation of soil physico-chemical factors with AM fungal diversity in *Ailanthus Excelsa Roxb.* Under Different Agroecological Zones of Western Rajasthan. *Int. J. Life Sci.* **2**(4), 316–323 (2016)
41. Verma, N., Tarafdar, J.C., Srivastava, K.K., Sharma, B.: Arbuscular Mycorrhizal (AM) Diversity in *Acacia nilotica* subsp. *Indica* (Benth.) Brenan under Arid Agroecosystems of Western Rajasthan. *Int. J. Adv. Res. Biol. Sci.* **3**(3), 134–143 (2016)
42. Seth, S.P., Metha, K.N.: Fertility survey and soil test summaries of some districts of arid region of Rajasthan. *Ann.f Arid Zone* **II**(1), 61–68 (1963)
43. Aseri, G.K., Tarafdar, J.C.: Fluorescein diacetate: a potential biological indicator for arid soils. *Arid Land Res. Manag.* **20**(2), 87–99 (2006)
44. Mathur, N., Vyas, A.: Survival and establishment of exotic plant species in saline areas of Indian Thar desert by application of mycorrhizal technology. *Asian J. Plant Sci. Res.* **6**(3), 1–6 (2016)
45. Moghe, V.M., Mathur, G.M.: Status of boron in some arid-soils of Western Rajasthan. *Soil Sci. Plant Nutr.* **12**(3), 11–14 (1966)
46. Singh, K., Sharma, A., Chandra, S.: Comparative analysis of physico-chemical parameters of soil contaminated with petroleum hydrocarbons collected from semi-arid (Jaipur-Ajmer) and arid (Barmer) regions of Rajasthan with reference to Bioremediation. *J. Phytol. Res.* **30**(2), 89–99 (2017)
47. Tripathi, G., Bhardwaj, P.: Earthworm diversity and habitat preferences in arid regions of Rajasthan. *Zoos' Print J.* **19**(7), 1515–1519 (2004)
48. Yadav, B.K.: Micronutrient status of soils under legume crops in arid region of Western Rajasthan India. *Acad. J. Plant Sci.* **4**(3), 94–97 (2011)
49. Tewari, V.P., Singh, M.: Tree-crop interaction in the Thar sesert of Rajasthan (India). *Sci. et Changements Planet.* **17**(1), 326–332 (2006)
50. Singh, M., Arrawatia, M.L., Tewari, V.P.: Agroforestry for sustainable development in arid zones of Rajasthan. *Int. Tree Crops J.* **9**, 203–212 (1998)
51. Chawra, R.S.: Dynamics and Availability of Cationic Micronutrients in Soils of Different Physiographic Units of Arid Western Plain Zone (I-A) of Rajasthan. Ph.D. Thesis. Maharana Pratap University of Agriculture and Technology, Udaipur (2006)
52. Faroda, A.S., Joshi, N.L., Singh, R., Saxena, A.: Resource management for sustainable crop production in arid zone—a review. *Indian J. Agron.* **52**(3), 181–193 (2007)
53. Kumar, S., Chaudhuri, S., Maiti, S.K.: Soil phosphatase activity in natural and mined soil—a review. *Indian J. Environ. Prot.* **31**(11) (2011)
54. Sihag, J., Prakash, D., Yadav, P., Gupta, H.: Physico-chemical characteristics with enzyme activity of topsoil for farmlands management of Ajmer, Rajasthan. *Res. Rev. Int. J. Multidis.* **4**(3), 1547–1552 (2019)

Author Index

A

- Abhishek, Kumar, 47
Abuturab, Muhammad Rafiq, 745
Ajmeri, Moina, 143
Amirthagadeswari, K. S., 223
Anand, Ankush, 671
Anand Kumar, M., 579
Ankitdeshpandey, 755
Ansari, Irshad Ahmad, 197
Aravind Krishna, T., 223
Arunjyothi, B., 501
Arya, Rajeev, 173
Ateya, Ismail, 677
Azad, Chandrashekhar, 325

B

- Bandyopadhyay, Chandan, 57, 489, 639
Barai, Ankit K., 783
Baskaran, R., 209
Behera, Pratap Kumar, 381
Bhalerao, Siddharth, 197
Bhardwaj, Tushar, 1045
Bhattacharjee, Anirban, 57, 489
Bhattacharjya, Rajib Kumar, 295
Bhattacharya, Tanmay, 913
Bhatt, Chandradeep, 565
Biradar, Sujay, 185
Bisht, Rahul, 1093
Biswal, Laxmidhar, 639
Bordia, Bhavya, 579

C

- Chaitanya, A. Krishna, 849
Chakraborty, Falguni, 281

- Chandra, Prabhat Kumar, 47
Chatterjee, Ram, 103
Chaturvedi, Amrita, 649
Chethan, B. S., 793
Choudhary, Deepak, 1

D

- Dahiya, Sonika, 705
Dash, Ratnakar, 695
Dash, Stita Pragnya, 247
Deka, Bhabesh, 993
Deka, Dipen, 993
Desai, Veena, 309
Dhanush, P., 793
Dhanya, N. M., 153
Diksha, 1029
Dixit, Abhishek, 335

G

- Gaba, Nishchal, 705
Gaikar, Omkar, 403
Gangopadhyay, Sugata, 381
Gauri, Pratyush, 125
Gautam, Abhinav K., 869
Gautam, Jyoti, 235
Ghosh, Anupam, 979
Ghosh, Swarup Kr, 979
Giriprasad, M. N., 433
Gopal, Ram, 869
Gorre, Pradeep, 173
Gupta, Kumod Kumar, 455
Gupta, Namit, 165
Gupta, Rajendra Kumar, 335
Gururaj, H. L., 895

H

Hadsul, Dhanashree, 479
 Harikrishna, B., 501

I

Iyer, Brijesh, 37

J

Jain, Pooja, 783
 Jangid, Bharat Lal, 943
 Jatav, Chandrakant, 21
 Jauhar, Sunil Kumar, 209, 223
 Jha, Bharti, 413
 Jha, Saurabh, 325
 Jha, Vivekanand, 47
 Joshi, Shreya, 479

K

Kadam, Swapnali, 479
 Kalaivaani, P. T., 883
 Kalpana, V., 443
 Kandubothula, Vanaja, 813
 Kartheek, C. H., 849
 Karthi, R., 755
 Kashyap, Nithin, 895
 Kastwar, Adya, 357
 Kesava Durga Prasad, T., 859
 Korde, Aishwarya, 403
 Krishnadass, Sahil, 357
 Krishnamoorthy, Raja, 883
 Kulkarni, Amith A., 793
 Kulkarni, Sujata, 357
 Kumar, Anil, 197

Kumar, Avanish, 135
 Kumar, Dilip, 295, 467
 Kumari, Anchala, 367
 Kumar, Indrajeet, 565
 Kumar, Krishan, 135
 Kumar, Lokesh, 629
 Kumar, Mukesh, 629
 Kumar, Newton, 1093
 Kumar, Priyanka, 619
 Kumar, Rishi, 605
 Kumar, Sandeep, 173
 Kumar, Satyendra, 143
 Kumar, Tapan, 783
 Kumar, Vikas, 81
 Kundaram, Swathi S., 731
 Kundu, Sukhamay, 523
 Kushwaha, Ajay Kumar, 81, 115

L

Lal, Kanhaiya, 799

M

Mahajan, Asmita, 69
 Mahrishi, Mehul, 1059
 Mahto, Rajesh Kumar, 347
 Malali, Hari Raksha K., 895
 Mallika, H., 185
 Malsa, Nitima, 235
 Mani Sai Jyothi, P., 837
 Mehta, Ashok Kumar, 325
 Mishra, Ambarisha, 347
 Mishra, Priyanka, 257
 Mohammed Muddasir, N., 545
 Mohapatra, R. K., 695
 Mondal, Bappaditya, 57, 489
 Mohd, Noor, 565
 Morwal, Sudha, 1059
 Mukherjee, Diksha, 719
 Mukhopadhyay, Amit, 767
 Murali, Sariki, 391
 Mwangi, Waweru, 677

N

Nageswara Rao, P., 433
 Naik, Chandra, 955
 Nama, Sukanta, 593
 Nandan, Durgesh, 813, 825, 837, 849, 859
 Nandi, Debashis, 281
 Nath, Amitabha, 555
 Nikam, Sonam, 403
 Nishanth, N., 579
 Nivelkar, Mukta, 719

O

Ochieng, Nelson, 677

P

Pahadiya, Pallavi, 455
 Pahuja, Roop, 1
 Pandey, Abhishek, 103
 Pandey, Ajit Kumar, 659
 Pandey, Mrinal, 413
 Parvathi, M., 91
 Parween, Zeenat, 971
 Patel, Shaswat, 579
 Pathak, Ketki C., 731
 Pathik, Nikhlesh, 515
 Patidar, Nilesh, 165
 Patil, Yash, 357

Paulson, Albin, 719
 Pavankumar, S. P., 905
 Peeyusha, K. S., 905
 Pooja, G., 905
 Prakash, Divya, 1107
 Priyadarshini, 367
 Purohit, Kaustubh, 135
 Pushparaj Shetty, D., 955

R

Raghuveer, K., 545
 Rahaman, Hafizur, 57, 489, 639
 Rajan, M. Sunder, 869
 Rajeev Gandhi, B. G., 467
 Rajendra, A. B., 925
 Rajkumar, N., 925
 Raj, Utkarsh, 11
 Ramya, P. Sai, 825
 Raman, Rahul, 555
 Ranjan, Amish, 1007
 Rastogi, Akanksha, 69
 Ratan, Ram, 943
 Raushan, Ravi, 125
 Raut, Nitin B., 153
 Robert Rajkumar, S., 209
 Roy, Bidisha, 535
 Roy, Provas Kumar, 281
 Roy, Sankar Kumar, 605
 Rudra, Bhawana, 579
 Rukhande, Smita, 403

S

Saha, Apu Kumar, 593
 Sahana, B. C., 1007
 Saha, Suprativ, 913
 Saladi, Krishna, 859
 Sanyal, Banhi, 695
 Sarkar, Mitra Barun, 555
 Sasi Supritha Devi, Y., 859
 Satapathy, J. K., 247
 Saxena, Abhishek, 423
 Saxena, Ankit, 1081
 Saxena, Nishant, 1081
 Sen, Asim Kumar, 535
 Sequeira, A. H., 209, 223
 Sethi, Ridhi, 103
 Shah, Maharshi, 619
 Shankar, Ravi, 11, 391, 423
 Sharma, Nonita, 69
 Sharma, Priti, 869
 Sharma, Shashi Kumar, 565

Sharma, Subhash Chander, 1045
 Sharma, Sushmita, 593
 Sharma, Vikash Chandra, 29
 Shaw, Sourav, 479
 Shetty, P. D., 925
 Shinde, Sayali, 37
 Shreyas, S., 905
 Shrivastava, Prashant Kumar, 793
 Shukla, Arvind Kumar, 1017
 Shukla, Pragya, 515
 Sihag, Jyoti, 1107
 Sikander, Afzal, 1093
 Singh, Abhinav Kumar, 1007
 Singh, Aman Kumar, 629
 Singh, Anuj, 1071
 Singh, Ashutosh Kumar, 125
 Singh, Dheerendra Vikram, 933
 Singh, Koushrendra Kumar, 1029
 Singh, M. P., 1071
 Singh, Pooja, 235
 Singh, Santar Pal, 235
 Singh, Shashank Kumar, 649
 Si, Tapas, 767
 Sinha, Amit Kumar, 671
 Sneha , H., 1029
 Soni, Vishal, 629
 Srivastava , Akash Krishna, 1029
 Srivastava, Akriti, 269
 Srivastava, Arpita, 235
 Subhashini, K. R., 247
 Supraja, V., 433
 Sweta, Soni, 659, 799

T

Tarale, Snehal P., 309
 Taterh, Swapnesh, 1081
 Thakur, Hardeo Kumar, 103
 Thakur, Rahul, 413
 Thammegowda, C. S., 793
 Tiwari, Akhilesh, 335
 Tripathi, Sudhakar, 1071
 Tyagi, Rohit, 705

U

Upadhyay, B. B., 257, 269
 Upadhyay, Himanshu, 1045
 Upadhyay, Mayank, 135
 Upadhyaya, Yogendra Kumar, 115
 Uppada, Rajyalakshmi, 813

V

- Vadivel, S. M., [209](#), [223](#)
Varghese, Shajo, [719](#)
Venkat Sai Krishna, T., [185](#)
Verma, Sudhanshu, [21](#), [29](#)
Verma, Tikendra Nath, [933](#)
Vignesh, R., [173](#)
Vijaya Kishore, V., [443](#)
Vijay, Ritu, [455](#)

Vikram, Arun, [1071](#)

Vishruth, Y. S., [185](#)

Y

- Yadav, Hira Lal, [467](#)
Yadav, Parul, [1107](#)
Yadav, R. B. S., [971](#)